DIRECTORIO DE PROFESORES DEL CURSO: " INGENIERIA DE RESERVORIOS GEOTERMICOS ", DEL 7 DE SEPTIEMBRE AL 5 DE NOVIEMBRE.


COORDINADOR ACADEMICO:
DR. EDUARDO IGLESIAS RODRIGUEZ
INSTITUTO DE INVESTIGACIONES ELECTRICAS
JEFE DEL AREA DE YACIMIENTOS DEL DEPARTAMENTO
DE GEOTERMIA
APDO. POSTAL 475
CUERNAVACA, MORELOS
TEL: 91-731 438-11 EXT. 3210

DR. GERARDO HIRIART L.
JEFE DE LA OFICINA DE EVALUACION EN
MORELIA, MICHOACAN,
OKLAHOMA 85-6to. piso
COL. NAPOLES
MEXICO 18, D.F.
TEL: 91 451 304 53 (MORELIA, MICH.)
5430 52 48 (MEXICO)

DR. HEBER CINCO LEY
SUBJEFE DEL AREA DE
INGENIERIA DE RECURSOS DEL SUBSUELO
DIVISION DE ESTUDIOS DE POSGRADO
FACULTAD DE INGENIERIA
UNAM
MEXICO 20, D.F.
TEL: 550-87-12

DR. FRANCISCO CORDOVA M
PROFESOR EN EL DEPARTAMENTO DE
CIENCIAS MECANICAS DE LA UNIVERSIDAD
DE SONORA
HERMOSILLO, SONORA
TEL: 21046 EXT. 147 o 123

DR. FERNANDO SAMANIEGO
COORDINADOR DE LA SECCION DE INGENIERIA
ENERGETICA
CIRCUITO EXTERIOR
DIVISION DE ESTUDIOS DE POSTGRADO
FACULTAD DE INGENIERIA
UNAM
MEXICO 20, D.F.
TEL: 550-87-12

# EVALUACION DEL PERSONAL DOCENTE

**CURSO:** "INGENIERIA DE RESERVORIOS - GEOTERMICOS"

**FECHA:** DEL 7 DE SEPTIEMBRE AL 5 DE NOVIEMBRE DE 1981.

| | CONFERENCISTA | DOMINIO DEL TEMA | EFICIENCIA EN EL USO DE AYUDAS AUDIOVISUALES | MANTENIMIENTO DEL INTERES. (COMUNICACION CON LOS ASISTENTES, AMENIDAD, FACILIDAD DE EXPRESION). | PUNTUALIDAD | |
|---|---|---|---|---|---|---|
| 1. | DR. GERARDO HIRIART L. | | | | | |
| 2. | DR. JESUS RIVERA | | | | | |
| 3. | DR. JESUS RIVERA | | | | | |
| 4. | DR. HEBER CINCO-LEY | | | | | |
| 5. | DR. FRANCISCO CORDOBA | | | | | |
| 6. | DR. FERNANDO SAMANIEGO | | | | | |
| 7. | DR. ISMAEL HERRERA | | | | | |
| 8. | ING. ALFONSO ARAGON | | | | | |
| 9. | | | | | | |
| | ESCALA DE EVALUACION: 1 a 10 | | | | | |

# EVALUACION DE LA ENSEÑANZA



SU EVALUACION SINCERA NOS AYUDARA A MEJORAR LOS PROGRAMAS POSTERIORES QUE DISEÑAREMOS PARA USTED.

CURSO: "INGENIERIA DE RESERVORIOS GEOTERMICOS"

DEL 7 DE SEPTIEMBRE AL 5 DE NOVIEMBRE, 1981.

| | TEMA | ORGANIZACION Y DESARROLLO DEL TEMA | GRADO DE PROFUNDIDAD LOGRADO EN EL TEMA | GRADO DE ACTUALIZACION LOGRADO EN EL TEMA | UTILIDAD PRACTICA DEL TEMA | |
|---|---|---|---|---|---|---|
| 1 | FUNDAMENTOS DE HIDROLOGIA | | | | | |
| 2 | FUNDAMENTOS DE TERMODINAMICA | | | | | |
| 3 | CLASIFICACION DE LOS RESERVORIOS GEOTERMICOS | | | | | |
| 4 | FLUJO DE FLUIDOS Y CALOR EN MEDIO POROSO | | | | | |
| 5 | FLUJO DE FLUIDOS Y CALOR EN POZOS GEOTERMICOS | | | | | |
| 6 | PRUEBAS DE PRESION | | | | | |
| 7 | MODELOS MATEMATICOS DE SIMULACION | | | | | |
| 8 | ASPECTOS PRACTICOS DE PRODUCCION | | | | | |
| | | | | | | |
| | | | | | | |
| | ESCALA DE EVALUACION: 1 a 10 | | | | | |

1. ¿Qué le pareció el ambiente en la División de Educación Continua?

| MUY AGRADABLE | AGRADABLE | DESAGRADABLE |
|---|---|---|
| | | |

2. Medio de comunicación por el que se enteró del curso:

| PERIODICO EXCELSIOR ANUNCIO TITULADO DI VISION DE EDUCACIÓN CONTINUA | PERIODICO NOVEDADES ANUNCIO TITULADO DI VISION DE EDUCACIÓN CONTINUA | FOLLETO DEL CURSO |
|---|---|---|
| | | |

| CARTEL MENSUAL | RADIO UNIVERSIDAD | COMUNICACION CARTA, TELEFONO, VERBAL, ETC. |
|---|---|---|
| | | |

| REVISTAS TECNICAS | FOLLETO ANUAL | CARTELERA UNAM "LOS UNIVERSITARIOS HOY" | GACETA UNAM |
|---|---|---|---|
| | | | |

3. Medio de transporte utilizado para venir al Palacio de Minería:

| AUTOMOVIL PARTICULAR | METRO | OTRO MEDIO |
|---|---|---|
| | | |

4. ¿Qué cambios haría usted en el programa para tratar de perfeccionar el curso?

5. ¿Recomendaría el curso a otras personas?

| SI | NO |
|---|---|
| | |

# EVALUACION DEL CURSO



| | CONCEPTO | EVALUACION |
|---|---|---|
| 1 | APLICACION INMEDIATA DE LOS CONCEPTOS EXPUESTOS | |
| 2. | CLARIDAD CON QUE SE EXPUSIERON LOS TEMAS | |
| 3. | GRADO DE ACTUALIZACION LOGRADO CON EL CURSO | |
| 4. | CUMPLIMIENTO DE LOS OBJETIVOS DEL CURSO | |
| 5. | CONTINUIDAD EN LOS TEMAS DEL CURSO | |
| 6. | CALIDAD DE LAS NOTAS DEL CURSO | |
| 7. | GRADO DE MOTIVACION LOGRADO. CON EL CURSO | |

ESCALA DE EVALUACION DE 1 A 10

6. ¿Qué cursos le gustaría que ofreciera la División de Educación Continua?

7. La coordinación académica fue:

| EXCELENTE | BUENA | REGULAR | MALA |
|---|---|---|---|
| | | | |

8. Si está interesado en tomar algún curso <u>intensivo</u> ¿Cuál es el horario más conveniente para usted?

| LUNES A VIERNES DE 9 A 13 H. Y DE 14 A 18 H. (CON COMIDAS) | LUNES A VIERNES DE 17 A 21 H. | LUNES, MIERCOLES Y VIERNES DE 18 A 21 H. | MARTES Y JUEVES DE 18 A 21 H. |
|---|---|---|---|
| | | | |

| VIERNES DE 17 A 21 H. SABADOS DE 9 A 14 H. | VIERNES DE 17 A 21 H. SABADOS DE 9 A 13 Y DE 14 a 18 H. | O T R O |
|---|---|---|
| | | |

9. ¿Qué servicios adicionales desearía que tuviese la División de Educación Continua, para los asistentes?

10. Otras sugerencias:

# CALENDARIO DEL CURSO DE INGENIERIA DE RESERVORIOS GEOTERMICOS

| TEMA Y HORARIO | SEPTIEMBRE | | | | | OCTUBRE | | | | | NOV |
|---|---|---|---|---|---|---|---|---|---|---|---|
| | 1a SEMANA | 2a SEMANA | 3a SEMANA | 4a SEMANA | 5a SEMANA | 6a SEMANA | 7a SEMANA | 8a SEMANA | 9a SEMANA | | |
| I.- FUNDAMENTOS DE TERMODINAMICA. (9-11:30 hs.) | XXXXX | Dr. Jesús Pérez | | | | | | | | | |
| II.- FUNDAMENTOS DE HIDROLOGIA (12-14:30 hs.) | XXXXX | Dr. Francisco Hiriart | | | | | | | | | |
| III.- CLASIFICACION DE LOS RESERVORIOS GEOTERMICOS. (9-11:30 hs.) | | XX[16]XXX | Dr. Jesús Pérez | | | | | | | | |
| IV.- FLUJO DE FLUIDOS Y CALOR EN MEDIO POROSO. (12-14:30 hs.) | | XX[16]XXX | XXXXX | Dr. Manuel Lucero | | | | | | | |
| V PRUEBAS DE PRESION. (9-11:30 hs.) | | | XXXXX | XXXXX | Ing. Fernando Samaniego | | | | | | |
| VI.- FLUJO DE FLUIDOS Y CALOR EN POZOS GEOTERMICOS. (12-14:30 hs.) | | | | XXXXX | XXXXX | Dr. Francisco Pérez | | | | | |
| VII.- ASPECTOS PRACTICOS DE PRODUCCION. (9-11:30 hs.) | | | | | XXXXX | XXXXX | Ing. Alfonso Aragón | | | | |
| VIII.- MODELOS MATEMATICOS DE SIMULACION. (12-14:30 hs.) | | | | | | XXXXX | Dr. Ismael Herrera | | | | |
| IX.- PRACTICAS. (8 hs/Dia) | | | | Ing. Alfonso Aragón | | | [19][20]XXX | XXXXX | | XX[4][5] | |

SEPT. [16] DIA NACIONAL

OCT. [19][20] UN DIA PARA VIAJAR A LOS AZUFRES Y OTRO PARA CONOCERLO

NOV. [4][5] UN DIA PARA REGRESAR A MEXICO Y OTRO PARA LA GRADUACION

| TEMA | PROFESOR |
|---|---|
| I. FUNDAMENTOS DE HIDROLOGIA | Dr. Gerardo Hiriart L. |
| II. FUNDAMENTOS DE TERMODINAMICA | Dr. Jesús Rivera |
| III. CLASIFICACION DE LOS RESERVORIOS GEOTERMICOS | Dr. Jesús Rivera |
| IV. FLUJO DE FLUIDOS Y CALOR EN MEDIO POROSO | Dr. Heber Cinco Ley |
| V. FLUJO DE FLUIDOS Y CALOR EN POZOS GEOTERMICOS | Dr. Francisco Córdoba |
| VI. PRUEBAS DE PRESION | Dr. Fernando Samaniego |
| VII. MODELOS MATEMATICOS DE SIMULACION | Dr. Ismael Herrera |
| VIII. ASPECTOS PRACTICOS DE PRODUCCION | Ing. Alfonso Aragón |

Presented at the Fifth Workshop, Geothermal Reservoir Engineering, Stanford University, December 12-14, 1979

LBL-10299

# A PRELIMINARY SIMULATION OF LAND SUBSIDENCE AT THE WAIRAKEI GEOTHERMAL FIELD IN NEW ZEALAND

T. N. Narasimhan and K. P. Goyal

December 1979

Prepared for the U.S. Department of Energy
under Contract W-7405-ENG-48

LBL-10299

# A Preliminary Simulation of Land Subsidence At the Wairakei Geothermal Field in New Zealand

T. N. Narasimhan and K.P. Goyal

Earth Sciences Division
Lawrence Berkeley Laboratory
University of California,
Berkeley, California 94720

Several types of geothermal systems exist in nature but only hydrothermal convective systems are being exploited at the present time because of their proximity to the earth's surface and their amenability to utilization. Among the geothermal systems discovered to date, hot water systems are perhaps twenty times as common as vapor dominated systems (Muffler and White, 1972). Since the energy contents of liquid water is relatively less than that of pure steam, comparatively large volumes of geothermal liquids have to be produced for economic heat extraction. Such large scale production of geothermal fluids should generally be expected to cause significant reductions in pore fluid pressures leading to appreciable rock deformations and displacement at or near the ground surface. This phenomenon has already been observed over the Wairakei and Broadlands geothermal fields of New Zealand (Stilwell, et al., 1975 and Otway 1976). Since ground displacements may affect engineering structures related or unrelated to the operation of the geothermal field, it is important to be able to predict the pattern and magnitude of the deformations that may result from fluid production so that appropriate ameliorative actions could be taken in advance.

There are two fundamental processes which determine land displacements due to fluid withdrawal from underground systems. The first is the deformation of the reservoir (defined as the region which releases fluid from storage to compensate for the fluid being withdrawn; e.g., aquifers and aquitards) due to internally generated stresses resulting from changes in pore fluid pressures induced by fluid withdrawal. The second is the propagation of the deformation through the overburden to the ground surface. Overburden is defined as the region which does not release fluid from storage to compensate for the fluid withdrawn. It includes all material intervening between the top of the reservoir system and the land surface. The exact boundary between the reservoir and the overburden may be time dependent and difficult to define, yet from a computational standpoint this ambiguity in its location may not be too critical.

A most general approach to modeling land subsidence due to fluid withdrawal is to treat the entire region including the reservoir and the overburden as the total system. Within this system the fluid flow equation and the stress-deformation equation would be simultaneously solved with appropriate coupling between them. The stress-deformation will, in general, be three dimensional, with material properties being elastic or non-elastic in nature. In regard to geothermal subsidence, in as much as very limited field data is currently available, the aforesaid generalized approach appears to be too sophisticated and elaborate to justify the efforts involved in their implementation. Under the circumstances, alternative simplified approaches appear desirable.

One such simplified approach is to (a) decouple the reservoir and the overburden and (b) to consider only vertical deformation in the reservoir. In this context, the reservoir is taken to include the highly permeable zones as well as the less permeable but relatively more compressible zones which hold significant quantities of fluid in available storage. In contrast to this, the overburden is the zone which deforms without fluid release in response to deformation of the reservoir. The decoupling concept tacitly assumes that the overburden deformation does not induce any appreciable stress changes in the reservoir. The one dimensional consolidation assumption will be especially realistic in those systems in which the highly permeable, producing layers of the reservoir are more rigid than the less permeable fine grained layers which primarily conduct water in the vertical direction to the producing layers.

Results presented in this paper pertain solely to reservoir deformation according to the one-dimensional consolidation theory. It is assumed that the vertical displacements obtained at the interface of the reservoir and overburden are completely transmitted to the ground surface. The reservoir simulator, which combines a three dimensional flow field with one dimensional deformation is discussed elsewhere by Narasimhan and Witherspoon (1976). The purpose of the present study has been to make a preliminary study of the ground subsidence observed over the geothermal field at Wairakei, New Zealand and to find whether the field observations can be reasonably explained in terms of the well known geotechnical principles of consolidation. As the study is preliminary in nature, the geothermal system has been treated as an isothermal, liquid system.

The geology of the Wairakei field has been discussed by Grindley (1965), Healy (1965) and Grange (1937); reservoir engineering data has been compiled by Pritchett et al. (1978). The total subsidence observed at Wairakei is shown in Figure 1. It can be noted that the subsidence bowl is offset from the main production area. This subsidence pattern is possible if the Huka Falls formation (a relatively more compressible layer) is thicker in that region or alternatively the compressibility of the formation in the highly subsided zone is greater than in other areas. In our idealized model, we are using the first approach with a reasonable compressibility value of the Huka Falls formation. A plot of reservoir pressure drop versus subsidence at benchmark A97 (Figure 1) is shown in Figure 2. It can be noted that the drop in the reservoir pressure is linearly proportional to subsidence during early production times. However, in later periods, reservoir pressure seems to stabilize while subsidence continues. Such a behavior could be explained if one assumes that the deforming material passes from a state of preconsolidation to one of normal consolidation. Our preliminary model, then, studies the effect of heterogeneity and plasticity on the subsidence phenomenon.

For purposes of simulation we can idealize the system as consisting of the Waiora aquifer and the overlying Huka Falls (mudstone) aquitard. A Pumice overburden extends from the top of the Huka Falls to the ground surface. This idealized model is shown in Figure 3. The thickness of the overburden (holocene Pumice and Wairakei Breccia) is assumed to be 200 meters (Table 5.1, p. 30, Pritchett et al. 1978). The depth of the reservoir, including Huka Falls formation, is assumed to be 400 meters.

The maximum thickness of the Huka Falls formation is assumed to be 200 meters near the zone of maximum subsidence (Figure 5.21, p. 52, Pritchett et al. 1978). The reservoir is divided into six layers. The lowest layer which is 200 meters thick carries 100-level nodes. (By 100-level nodes we mean that the nodes in this layer are identified by numbers ranging from 100 - 199.) The other five layers, each 40 meters thick, lie over this layer and carry 200-300-400-500- and 600-level nodes. Figure 4 shows the numbers assigned to the 100-level nodes. In this three digit system, first digit represents the level while the number of node is represented by the other two. Thus the node 618 lies in the 600-level layer and is vertically above the nodes 118, 218, 318, 418 and 518. In horizontal plane its shape is exactly same as that of the node 118 (Figure 4). The sides AB and AC are each extended to 19.2 km and 27.15 km respectively with large size nodes to represent far away zones from the production area.

To model subsidence, we have used an idealized graded thickness of the Huka Falls formation of 40 m, 80m, 120 m, 160 m, and 200 meters (Figure 4). The maximum thickness of 200 meters over the nodes 138, 145 and 146 corresponds to the area of maximum subsidence (Figure 1). Node 107 is modeled as a production zone, indicative of the area of maximum discharge in Figure 1. To offset the subsidence bowl from the main production area, the thickness of the overburden is increased to 360 meters over the nodes 207 to 216. Rest of the volume elements represent the Wairora formation. Impermeable boundary conditions are imposed on the sides AB and AC. An initial potential of 600 meters of water is specified everywhere in the system. Material properties used in the model are follows:

Huka Falls Formation

Permeability = $10^{-14}$ $m^2$ (Mercer et al. 1975)
Coefficient of compressibility for virgin curve ($a_v$) = $5 \times 10^{-8}$ $m^2/N$
Coefficient of compressibility for swelling curve ($a_{vs}$) = $5 \times 10^{-9}$ $m^2/N$

Waiora Formation

Permeability = $8.5 \times 10^{-14}$ $m^2$
Coefficient of compressibility for virgin as well as swelling curve ($a_v = a_{vs}$) = $10^{-10}$ $m^2/N$
Relative density of the saturated soil = 2.

This model also assumes that the soil is preconsolidated. The preconsolidation pressure over and above hydrostatic pressure is about 225 meters of water. The properties used for the liquid are:

Viscosity = 0.2 centipoise,
Density = 940 $kg/m^3$,
Compressibility = $4.9 \times 10^{-10}$, $m^2/N$.

Total mass production for the Wairakei/Tauhara system as of December 31, 1976 was $2329 \times 10^9$ lbs (Pritchett, et al. 1978). This amounts to an average volumetric production rate of about 1.48 $m^3/sec$. Since our trianglular model (Figure 4) considers only one-eighth of the total area, the production rate is correspondingly reduced to about .185 $m^3/sec$. It

can be noted that this rate applies to both Wairakei and Tauhara fields. To consider only the area of maximum discharge (Figure 1), this amount should somewhat be reduced. In this study we have considered an average production rate of .1 $m^3$/sec. This amount is produced from the node 107 at the depth of 500 meters.

Subsidence produced under aforementioned conditions is shown in Figure 5. A comparison with Figure 1 shows that the results are qualitatively similar. Measured and calculated reservoir pressure drop vs. subsidence at the bench mark A97 and node 142 are shown in Figure 6. A qualitatively similar pattern is seen for the preconsolidated soil. This figure also shows the behavior of the normally consolidated soil which is quite different to that of the preconsolidated soil.

In summary, we developed and tested a preliminary model to explain subsidence in the Wairakei field and obtained results which are qualitatively similar to those measured at the site. The effect of preconsolidation stresses seems to be important to explain the changing slope of the reservoir pressure-subsidence relationship shown in Figure 2.

Acknowledgements

This work was supported by the Division of Geothermal Energy of the U.S. Department of Energy under contract No. W-7405-ENG-48.

References

Grange, L.I, The Geology of the Rotorua-Taupo Subdivision, Rotorua and Kaimanawa Divisions, DSIR Bulletin 37, 1937.

Grindley, G.W., The Geology, Structure, Exploitation of the Wairakei Field, Taupo, New Zealand, N.Z. Geol. Surv. Bull. 75, 131, 1965.

Healy, J., Geology of the Wairakei Geothermal Field, Proceedings, Eighth Commonwealth Mining and Metallurgical Congress, Australia and New Zealand, New Zealand Section, 1965.

Mercer, J.W., G.F. Pinder and I.G. Donaldson, A Galerkin-Finite Element Analysis of the Hydrothermal System at Wairakei, New Zealand. Journal of Geophysical Research, vol. 80, no. 17, pp. 2608-2621, 1975.

Muffler, L.J.P. and D.E. White, Geothermal Energy, The Science Teacher, vol. 39, No. 3, pp. 40-43, 1972.

Narasimhan, T.N. and P.A. Witherspoon, An Integrated Finite Difference Method for Analyzing Fluid Flow in Porous Media, Water Resources Res., vol. 12, p. 57, 1976.

Otway, P.M., Report on Results on Precise and Tilt Leveling. Broadlands Reinjection Project, 1968-1976. International Conference on the Geothermal Reservoir held at Wairakei, New Zealand, Aug. 29 - Sept. 3, 1976.

Pritchett, J.W., L.F. Rice and S.K. Garg, Reservoir Engineering Data: Wairakei Geothermal Field, New Zealand, vol. 1, SSS-R-78-3597-1, Systems, Science and Software, La Jolla, California, 1978.

Pritchett, J.W., S.K. Garg, D.H. Brownell, Numerical Simulation of Production and Subsidence at Wairakei, New Zealand, Report SGP-TR-20, Stanford Geothermal Program, Stanford, California, pp. 310-323, Dec. 1976.

Stilwell, W.B., W.K. Hall and J. Tawhai, Ground Movements in New Zealand Geothermal Fields, Proceedings of the Second United Nations Symposium on the Development and Use of Geothermal Resources, vol. 2, pp. 1427-1434, May 1975.

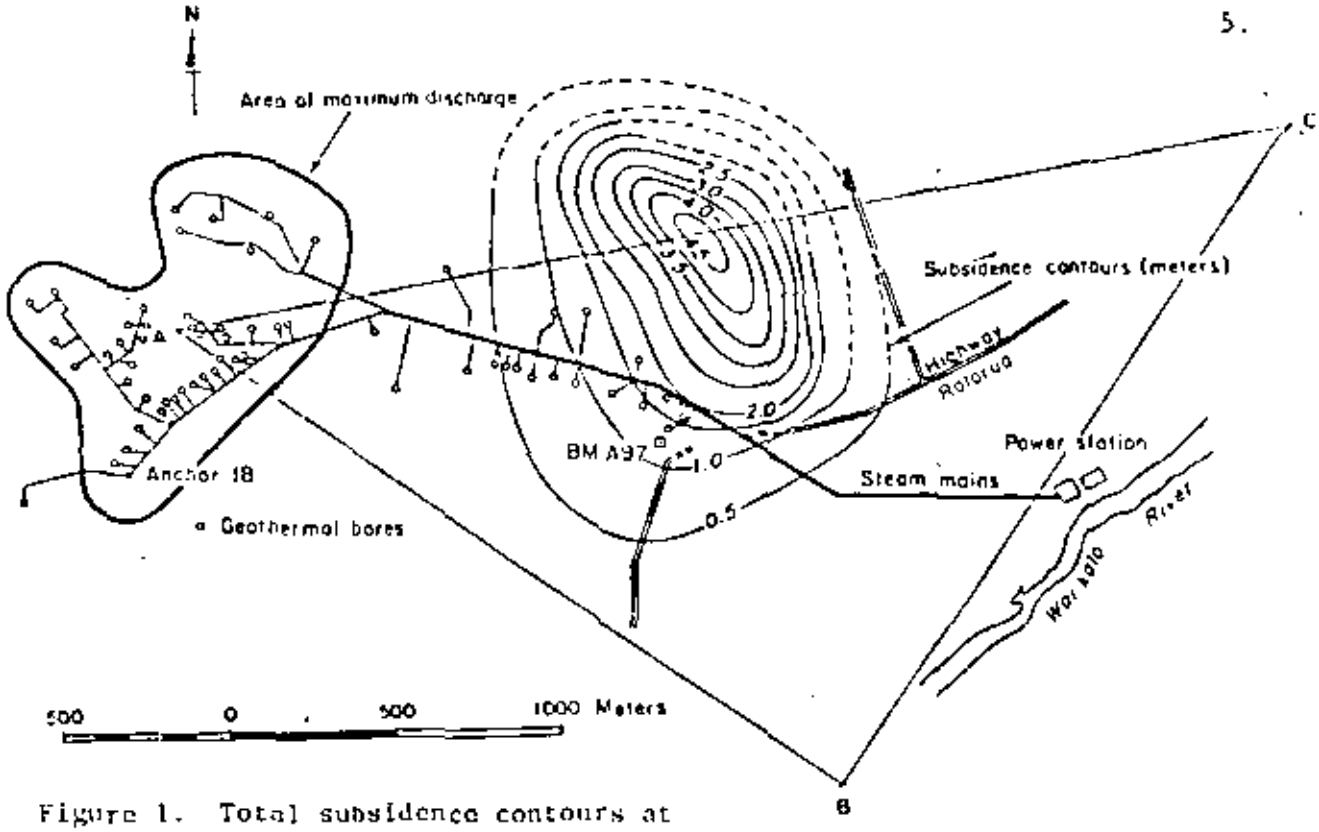


Figure 1. Total subsidence contours at Wairakei and the area of investigation ABC. (From Stilwell et al 1975)

XBL 7911-13203

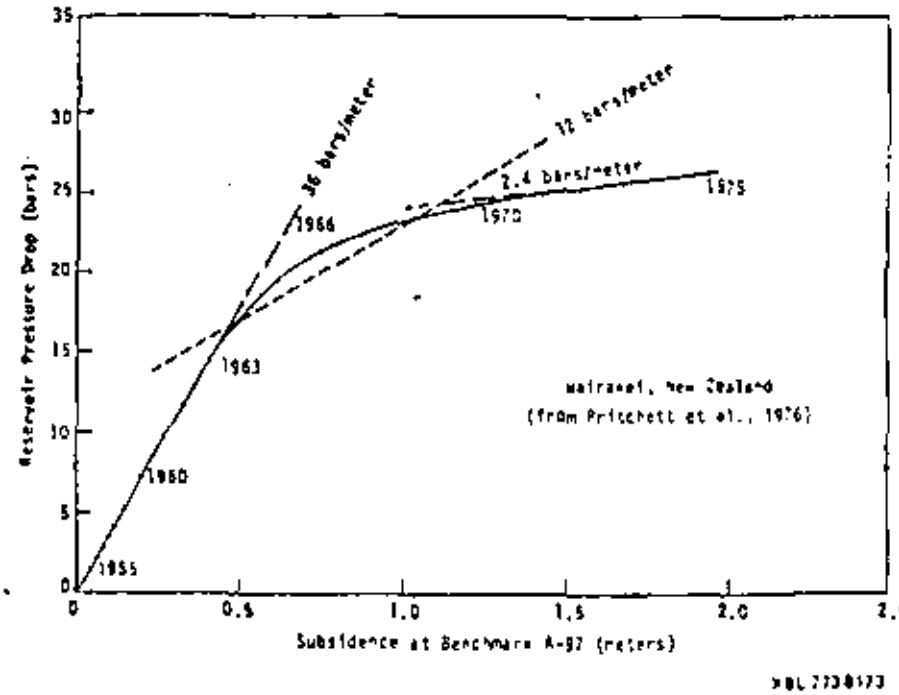


XBL 7708173

Figure 2. Reservoir pressure drop versus subsidence observed at the Wairakei geothermal field, New Zealand.

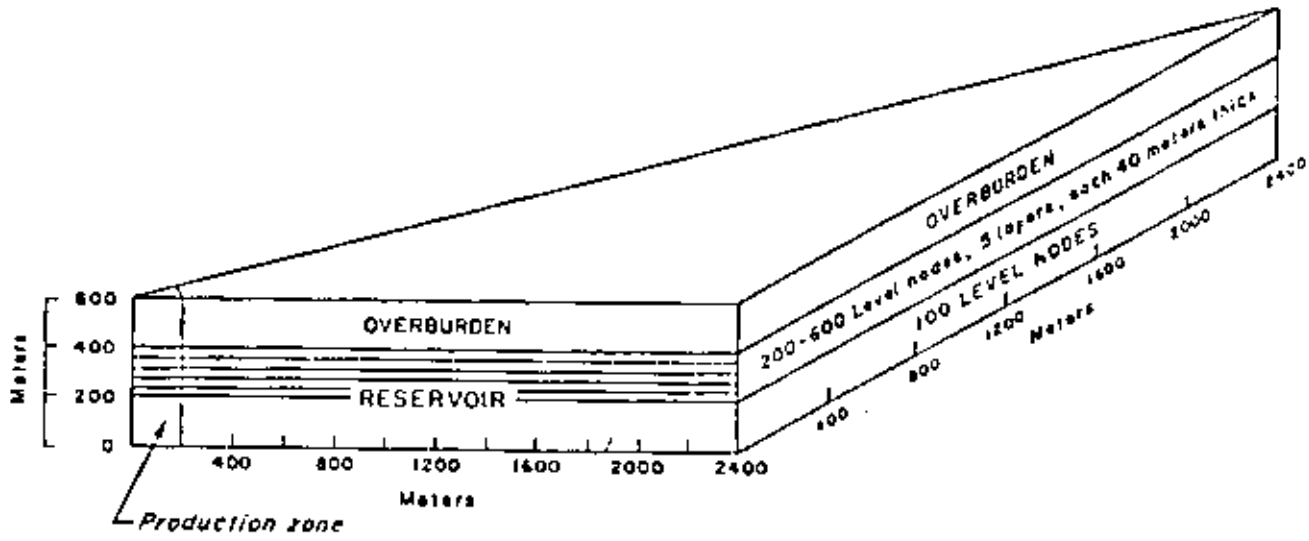


Figure 3. An idealized three-dimensional subsidence model of the Wairakei geothermal system. XBL 7911-13085

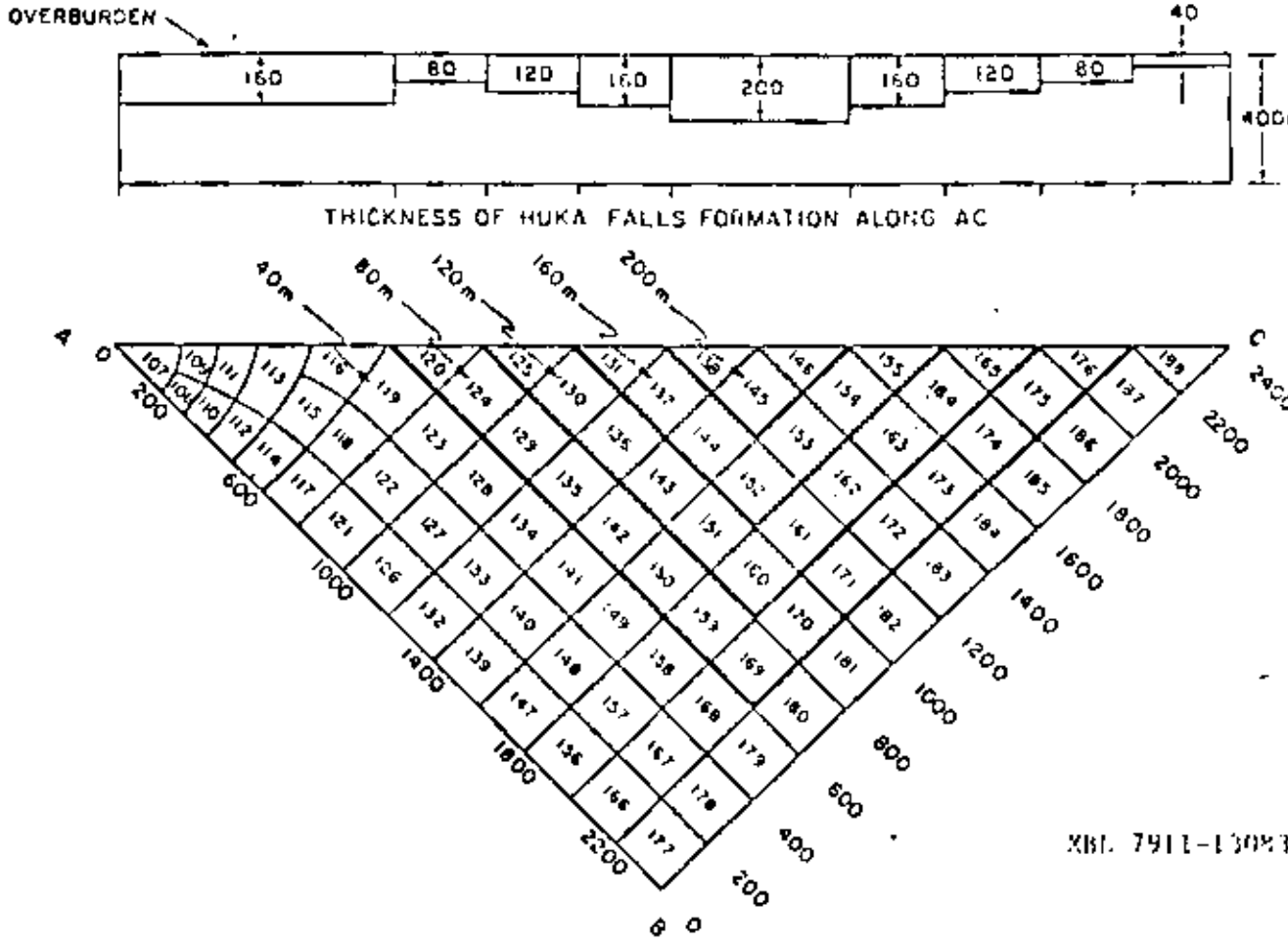


Figure 4. The thicknesses of the Huka Falls formation and the node numbers used in the model.

Figure 5. Subsidence contours in meters after 21 years of production.

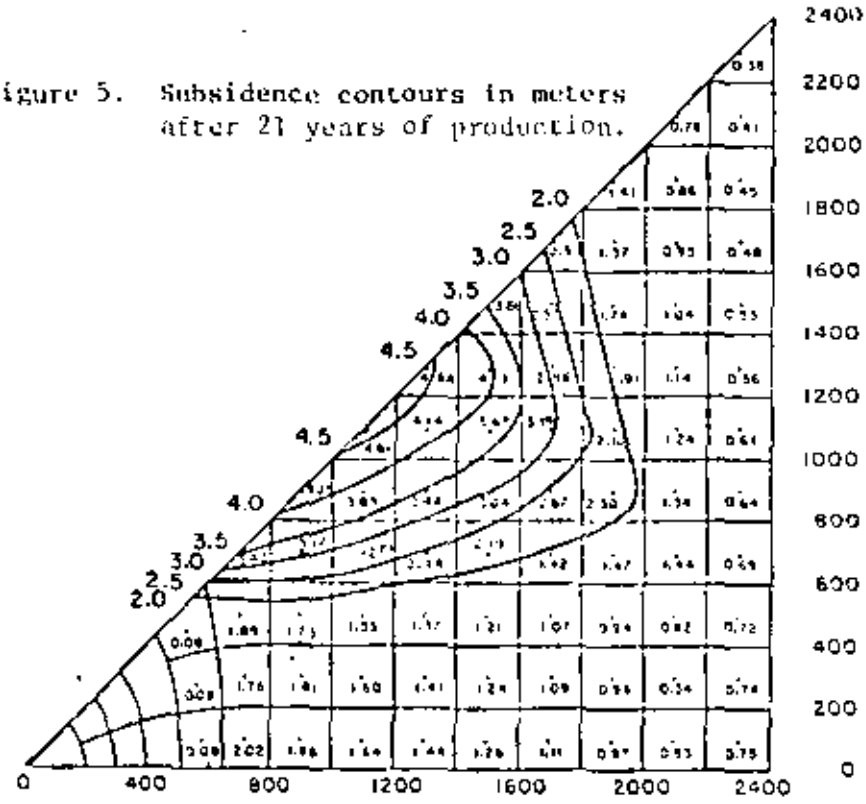


XBL 7911-13091

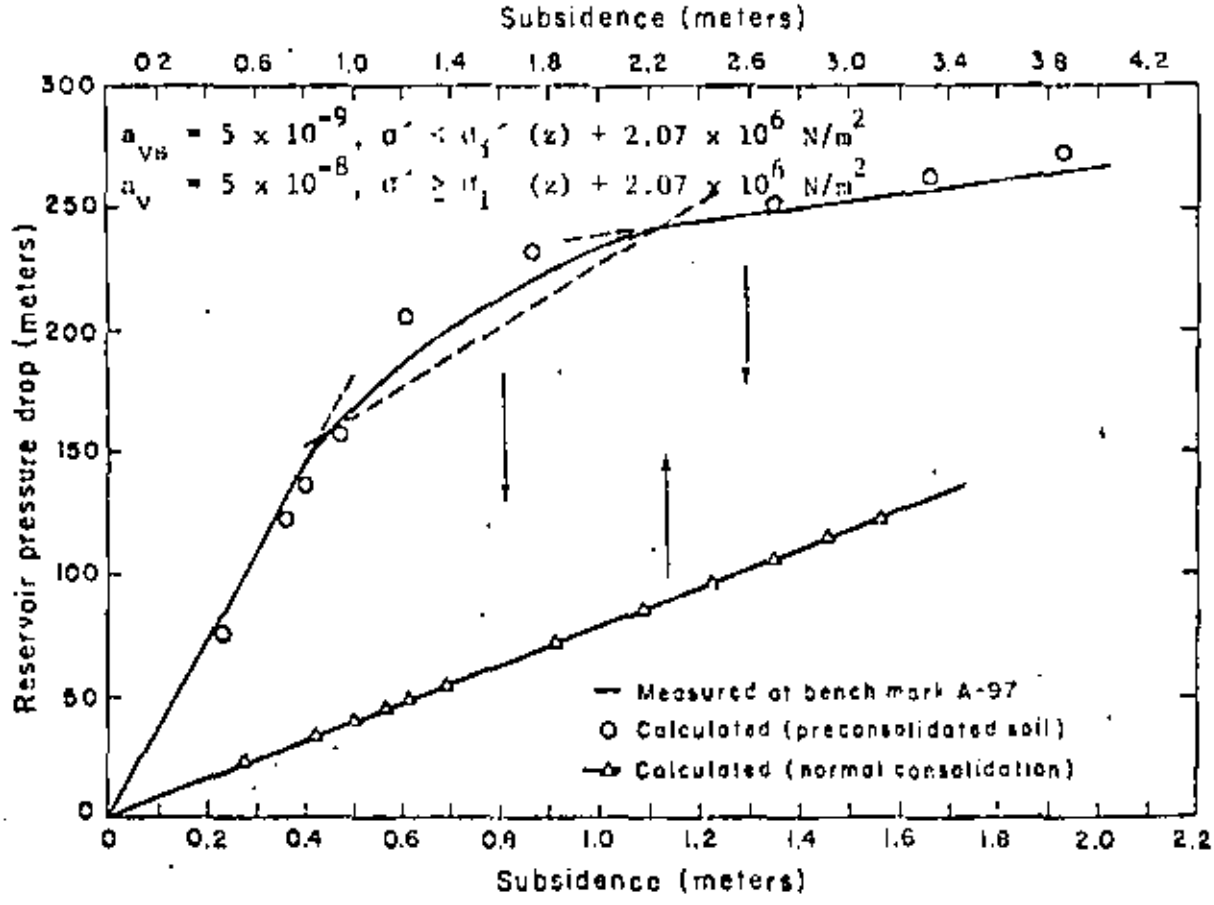


Figure 6. A comparison of the measured subsidence with that calculated at the node 142.

XBL 7911-13408

TECHNICAL INFORMATION DEPARTMENT
LAWRENCE BERKELEY LABORATORY
UNIVERSITY OF CALIFORNIA
BERKELEY, CALIFORNIA 94720

This report was done with support from the Department of Energy. Any conclusions or opinions expressed in this report represent solely those of the author(s) and not necessarily those of The Regents of the University of California, the Lawrence Berkeley Laboratory or the Department of Energy.

Reference to a company or product name does not imply approval or recommendation of the product by the University of California or the U.S. Department of Energy to the exclusion of others that may be suitable.

TECHNICAL INFORMATION DEPARTMENT
LAWRENCE BERKELEY LABORATORY
UNIVERSITY OF CALIFORNIA
BERKELEY, CALIFORNIA 94720

LBL-9056 Rev
UC-66b

# NUMERICAL MODEL OF TRANSIENT TWO-PHASE FLOW IN A WELLBORE

Constance W. Miller

October 1979

Prepared for the U. S. Department of Energy
under Contract W-7405-ENG-48

Printed in the United States of America
Available from
National Technical Information Service
U.S. Department of Commerce
5285 Port Royal Road
Springfield, VA 22161
Price Code: A03

LBL-9056 Revised

# NUMERICAL MODEL OF TRANSIENT TWO-PHASE FLOW IN A WELLBORE

Constance W. Miller

Earth Sciences Division
Lawrence Berkeley Laboratory
University of California
Berkeley, California 94720

Work supported by the Division of Geothermal Energy of the U. S. Department of Energy

TABLE OF CONTENTS

ABSTRACT

Transient two-phase flow in a geothermal well has been modelled with a finite-difference approximation. One-dimensional flow is assumed. The equations of mass, momentum, and energy are solved using a partially implicit method. Terms that would place a severe time restriction on the calculation are solved implicity, while other terms are solved explicitly for computational ease and efficiency. Homogenous flow of one component at thermodynamic equilibrium is assumed initially, but the extension of the model to include slip and a finite rate of condensation or evaporation or a noncondensible gas is given. The wellbore model includes heat and mass transfer and is coupled to a simple reservoir model. Using the model, the transient behavior of a single- or two-phase well during a well test was investigated. Results show that when the reservoir has a relatively large value of kh, as exists in a geothermal field, the slope of the log (pressure) vs. log (time) curve is not necessarily a unit slope when testing a homogenous reservoir. The early-time behavior of this curve is controlled by the interaction of the flow in the reservoir and that in the well, and can be used to determine near bore values of kh. Heat loss in the wellbore is shown to also affect the pressure vs. time plot in a well test. The time to reach the pseudo steady region increases when heat transfer is important, even in a relatively "warm" well, and the slope of the P vs. log t curve is no longer $q\mu/4\pi kh$ as derived in the petroleum literature.

## INTRODUCTION

For a complete analysis of a geothermal system, a model of the flow in the wellbore and in the reservoir is necessary. The equations governing the flow in these two cases are different, so reservoir models based on Darcy-type flow cannot be extended to predict the wellbore flow. Several numerical codes have been written to simulate the two phase flow of steam and water in a geothermal well (Sugiura and Faronq, 1979; Gould, 1974; Juprasert and Sanyal, 1977; Ryley, 1964; Elliot, 1975). Most of these models include the slip between the phases, using experimentally determined values of holdup and friction factors for each particular flow regime (such as annular or slug). However, the models reported in the geothermal cases all assume steady state flow. (There are several transient two phase codes, which will be considered below, that were developed for the nuclear energy industry.) The steady state models can be used to approximate downhole conditions from wellhead measurements given an equation of state that includes the effect of the non-dissolved gas and solids.

However, during well testing the steady-state models are not useful because transient changes in the well itself are important. At early times after a flow-rate change has been made in the well, the mass flow rate into the well does not equal the mass flow rate out because of wellbore storage. Under these circumstances, a steady-state model, which naturally assumes $\dot{m}_{in} = \dot{m}_{out}$, is not appropriate. Nevertheless, one might think that once wellbore storage is over, the steady state flow model could be used to determine downhole pressure changes, given the wellhead pressure measurements. At this point, the changes in pressure with time are usually small, so slight errors

in friction factor, slip, or heat transfer can produce relatively large errors in dP/dt. Also, many of the slip correlations used are based on water/air or oil/gas flow, whereas the flow of steam/water has interacting phases that should result in different effective values of holdup. Because of the unknown in these values, a two-phase flow model that includes transient effects is necessary for well-test analysis. Because the flow between the reservoir and the well is a function of the reservoir properties, a transient two-phase code could be used to determine near-bore values of $kh/\mu$, even when wellbore storage is important. During this early time, the error in the experimentally determined values of slip, friction factor, and heat-transfer coefficient are less important than at other times because dP/dt is large.

I have developed a transient two-phase numerical code for one-dimensional flow in the wellbore. The code has been coupled with a reservoir model of simple, one-phase, radial flow in a porous media. (Only flashing in the wellbore is being considered initially.) At early times, the flow in the reservoir is close to radial, so such a code could be used to predict the drawdown pressure curve for single-phase flow and for fluid that is flashing in the wellbore. I have obtained very interesting results with the model, which will be illustrated below. (Additional details are given in Miller, 1979.)

The model developed includes heat and mass transfer and has been written in a way so that very few, if any, iterations are needed at each time step. The effect of noncondensible gas can be included easily at a later stage by introducing a second continuity equation.

As mentioned above, transient multiphase codes have been developed for the nuclear energy industry (Liles and Reed, 1978: Harlow and Amsden,

1975; and Hirt and Romero, 1975). However, these codes usually require several iterations or the inversion of a nonsimple matrix, making them difficult to use efficiently. Some of the models are not designed to include the effect of more than one component. The model developed here solves transient homogeneous equilibrium flow. However, the basic solution procedure can be extended to include slip as well as nonequilbrium effects with few changes.

A description of the method is given below along with example calculations. This report is divided into three sections. The first section is a description of the working model, the second section describes how the model could be extended to include slip and nonequilibrium or a noncondensible gas, and the last section reports calculations of the flow in the wellbore.

## NUMERICAL MODEL

The problem is to solve the equations of mass, momentum, and energy for one-dimensional flow. The basic difference between the equations that model the wellbore and those that model the reservoir is that the Navior Stokes equation of momentum is used for the wellbore case instead of assuming Darcy-type flow. The nature of the flow changes when transients are important. For the fluid in the wellbore, the flow can be shown to be governed by a wave equation; in the reservoir, it is governed by a diffusion-like equation. In models developed for flow in porous media for a two-phase system, relative permeability curves are used to describe the flow of the gas and the liquid phases. The relative permeability curves take into account the interaction of the fluid with the rock and the interference of the phases with one another. However, for flow in a tube, the drag of one phase on the other is an important contribution to the flow, that is, the liquid phase can be

carried along by the gas. Only a negative relative permeability could account for this situation. In summary, using a porous media model to describe flow in a wellbore ignores the physics of fluid flow.

For a detailed theoretical description of the two-phase separated flow, six equations are necessary: two for mass, two for momentum, and two for energy. Additional relationships among the thermodynamic variables complete the set of equations. However, to solve this set of equations, interface interaction terms must be included, which are not well known. It is possible to approximate the fluid flow with fewer equations, while retaining the important characteristics of the flow. I have used empirical correlations to replace some of the equations. For the initial development of the model, I further reduced the equations to solve two phase homegeneous equilibrium flow.

The equations solved are:

$$\text{continuity,}\quad \frac{\partial}{\partial t}(\rho) + \frac{\partial}{\partial x}(\rho v) = 0 \tag{1}$$

$$\text{momentum,}\quad \frac{\partial}{\partial t}(\rho v) + \frac{\partial}{\partial x}(\rho v^2) + \frac{\partial P}{\partial x} + \rho g + \frac{f\rho v^2}{2D} = 0 \tag{2}$$

$$\text{and energy,}\quad \frac{\partial}{\partial t}(\rho e) + \frac{\partial}{\partial x}(\rho v e) + P\frac{dv}{dx} + 2H\frac{T_r - T_w}{r_w} = 0 \tag{3}$$

where $\rho$ and e are the mass-averaged values of density and energy, respectively, in the two-phase fluid. Only three equations are solved here instead of the original six. One momentum equation has been replaced with an experimentally determined correlation of the relative velocity, $v_r$, in terms of the other parameters in the flow. The correlation used above was $v_r = 0$, or that there is no slip. One continuity equation was eliminated by assuming the average density in the fluid can be expressed as a function of the average energy

and pressure or $\rho = fn(e,P)$. (An extension to nonequilibrium flow or to include a noncondensible gas will require a second continuity equation.) The assumption of thermodynamic equilibrium also implies that the temperature in the liquid and vapor are equal, thus eliminating one energy equation. The unknowns are $\rho$, e, P, and v; the four equations are mass, momentum, energy, and the equation of state.

The viscous term has been written as a friction factor times $\frac{1}{2}\rho v^2/D$. Such a term accounts for the frictional losses with the wall of the wellbore. When slip is taken into account, it also includes the frictional losses between the two phases.

My approach is to solve the equations using a finite-difference approximation with a partially implicit method. Terms that would impose very restrictive time steps, such as $\Delta t < \Delta x/a$, where a is the sound speed, are evaluated implicitly while the other terms are evaluated explicitly for ease and computational efficiency. The finite-differenced equations are:

$$\text{continuity,}\quad \frac{\rho_i^{\ell+1} - \rho_i^{\ell}}{\Delta t} + \frac{(\rho v)_{i+\frac{1}{2}}^{\ell+1} - (\rho v)_{i-\frac{1}{2}}^{\ell+1}}{\Delta x} = 0 \tag{4}$$

$$\text{momentum,}\quad \frac{(\rho v)_{i+\frac{1}{2}}^{\ell+1} - (\rho v)_{i+\frac{1}{2}}^{\ell}}{\Delta t} + \frac{\left[(\rho v^2)_{i+\frac{1}{2}} - (\rho v^2)_{i-\frac{1}{2}}\right]^{\ell}}{\Delta x} +$$

$$\frac{P_{i+1}^{\ell+1} - P_i^{\ell+1}}{\Delta x} + \rho_{i+\frac{1}{2}}^{\ell} g + \left[\frac{f(\rho v)^2_{i+\frac{1}{2}}}{2D}\right]^{\ell} = 0 \tag{5}$$

and energy,

$$\rho_i \frac{\left(e_i^{\ell+1} - e_i^{\ell+1}\right)}{\Delta t} + \rho v \frac{\left(e_i^{\ell} - e_{i-1}^{\ell}\right)}{\Delta x} + P_i^{\ell+1} \frac{\left(v_{i+\frac{1}{2}} - v_{i-\frac{1}{2}}\right)^{\ell}}{\Delta x}$$

$$+ 2H \frac{\left(T_r - T_w\right)^{\ell}}{r_w} = 0 \tag{6}$$

The energy equation has been written in a nonconserving form. The reason for this will be apparent in the solution procedure. The thermodynamic variables are computed at the nodal points (i, i+1, etc.), and the velocity is computed at the half-nodal points (i+½, etc.).

The solution procedure is to combine the four equations to give one expression for the new pressure. To use this method, the equation of state is used in the form of:

$$d\rho = \left(\frac{\partial \rho}{\partial P}\right)_e dP + \left(\frac{\partial \rho}{\partial e}\right)_P de$$

instead of $\rho = fn(P,e)$. The density change in time is written as:

$$\rho_i^{k+1} - \rho_i^{k} = \left(\frac{\partial \rho}{\partial P}\right)_i^{k} (P_i^{k+1} - P_i^{k}) + \left(\frac{\partial \rho}{\partial e}\right)_i^{k} (e_i^{k+1} - e_i^{k}) \quad , \tag{7}$$

the partial derivatives being evaluated at the old time levels. However, to eliminate large changes in the derivates, equation 7 is rewritten as:

$$\rho_i^{k+1} - \rho_i^{k} = \left(\frac{\partial \rho}{\partial P}\right)_i^{k} \left(P_i^{k+1} - P_i^{k}\right) + \left(\frac{1}{\rho} \frac{\partial \rho}{\partial e}\right)_i^{k} (\rho_i)^{*} \left(e_i^{k+1} - e_i^{k}\right) \quad . \tag{8}$$

The expression $(1/\rho)(\partial\rho/\partial e)$ varies approximately linearly while $(\partial\rho/\partial e)$ changes value abruptly. In addition, $\rho_i^{k} (e_i^{k+1} - e_i^{k})$ is solved for directly with the energy equation. Also at each calculation, the new value of $\rho_i^{k+1}$ is compared with the value of $\rho^{k+1}$, calculated from $\rho = fn(P^{k+1}, e^{k+1})$. If the difference is more than some specified percent, an iteration is necessary. The new pressure profile is recalculated with the partial derivatives in equation 7 as an average of the old and new values. The best average is to emphasize the value of $\partial\rho/\partial P$ at level $k+1$ because the system can self-correct any errors created when crossing the saturation line. When the fluid flashes, the derivative $\partial\rho/\partial P$ increases abruptly and then decreases slowly. If the

calculation provides an overexpansion of the fluid parcel when crossing the saturation line, then an average of the old and new derivatives at the next calculation can compensate for the overexpansion because of the decreasing value of $\partial\rho/\partial P$. If the fluid parcel underexpands when crossing the saturation line, no amount of averaging of the new and old derivatives can compensate. When condensing across the saturation line it is important not to overcondense, because the derivative $\partial\rho/\partial P$ is approximately constant. However, a slight error when crossing a saturation line for one particular fluid parcel produces little error in the net flow.

The four equations (4, 5, 6, 8) are combined in the following manner. The continuity equation is solved, using the expression for the new value of $(\rho v)^{\ell+1}$, which is given by the momentum equation. Equation 4 can be written in finite difference form:

$$\rho_i^{\ell+1} - \rho_i^{\ell} = -\frac{\Delta t}{\Delta x}\left[(\rho v)_{i+\frac{1}{2}}^{\ell+1} - (\rho v)_{i-\frac{1}{2}}^{\ell+1}\right] .$$

Then equation 5 is used to express $(\rho v)^{\ell+1}$ in terms of P:

$$\begin{aligned}\rho_i^{\ell+1} - \rho_i^{\ell} = -\frac{\Delta t}{\Delta x}\Bigg\{\Bigg[&(\rho v)_{i+\frac{1}{2}}^{\ell} - \frac{\Delta t}{\Delta x}(\rho v^2_{i+\frac{1}{2}} - \rho v^2_{i-\frac{1}{2}})^{\ell} \\ &- \frac{\Delta t}{\Delta x}(P_{i+1}^{\ell+1} - P_i^{\ell+1}) - \rho_{i+\frac{1}{2}}^{\ell} g\Delta t - \frac{f(\rho v^2)_{i+\frac{1}{2}}^{\ell}}{2D}\Delta t\Bigg] \\ -\Bigg[&(\rho v)_{i-\frac{1}{2}}^{\ell} - \frac{\Delta t}{\Delta x}(\rho v^2_{i-\frac{1}{2}} - \rho v^2_{i-\frac{3}{2}})^{\ell} \\ &- \frac{\Delta t}{\Delta x}(P_i^{\ell+1} - P_{i-1}^{\ell+1}) - \rho_{i-\frac{1}{2}} g\Delta t - \frac{f(\rho v^2)_{i-\frac{1}{2}}^{\ell}}{2D}\Delta t\Bigg]\Bigg\}\end{aligned} \qquad (9)$$

Equation 8 is used to write $\rho^{\ell+1}$ in terms of $P^{\ell+1}$ and the above equation is regrouped to give

$$\left[-2 - \frac{\Delta x}{\Delta t}^2 \left(\frac{\partial \rho}{\partial P}\right)_e\right] P_i^{k+1} + P_{i+1}^{k+1} + P_{i-1}^{k+1} = -\left(\frac{\Delta x}{\Delta t}\right)^2 \left(\frac{\partial \rho}{\partial P}\right)_e P_i^k$$

$$+ \frac{\Delta x}{\Delta t}\left[(\rho v)_{i+\frac{1}{2}} - (\rho v)_{i-\frac{1}{2}}\right]^k - (\rho_{i+\frac{1}{2}} - \rho_{i-\frac{1}{2}})^k g \Delta x \qquad (10)$$

$$- \frac{f \Delta x}{4R}\left[(\rho v^2)_{i+\frac{1}{2}} - (\rho v)^2_{i-\frac{1}{2}}\right]^k + \frac{1}{\nu}\left(\frac{\partial \rho}{\partial e}\right)^k \rho(e_i^{k+1} - e_i^k)\left(\frac{\Delta x}{\Delta t}\right)^2$$

$$- (\rho v^2_{i+\frac{1}{2}} - 2\rho v^2_{i-\frac{1}{2}} + \rho v^2_{i-\frac{3}{2}})^k.$$

The difference $\rho(e_i^{k+1} - e_i^k)$ is given by equation 6. Equation 10 can be written as $AP = x$, where A is a tridiagional matrix. The solution is straight-forward if the boundary conditions are specified.

The boundary conditions considered were: (1) specification of pressure and mass flow rate or velocity at either the wellhead or downhole; or (2) specification of pressure at both wellhead and downhole. The pressure must be specified at one of the boundaries. If the flow rate is measured, then $\partial(\rho v)/\partial t$ is known, and the pressure can be determined from the momentum equation:

$$\left(\frac{\partial P}{\partial x}\right)_b^{k+1} = -\frac{(\rho v^{k+1} - \rho v^k)_b}{\Delta t} - \frac{(\rho v_b^2 - \rho v_{b-1}^2)^k}{\Delta x}$$

$$- \rho_{b-1} g - \frac{(f \rho v^2)_b}{2D}$$

where b stands for the boundary.

Equation 10 is used to determine the new pressure profile. Once $P^{k+1}$ and $e^{k+1}$ are known, the density is calculated using equation 7, because this was the equation used to express $\rho$ in terms of P and e when the four equations

were combined. If one calculated the density at the new time level with $\rho = fn(P,e)$ instead of $d\rho = fn(dP, de)$, then two different expressions would be used and mass would not be conserved identically. However, as mentioned above, the two $\rho$'s are compared and an iteration is done if they are significantly different. This situation occurs when crossing the saturation line.

Once the new value of $\rho$ is known, the velocity is determined from either the continuity or the momentum equation. If the mass flow rate is being specified as a function of time, the velocity is best calculated by the continuity equation. Given $(\rho v)^{\ell+1}$, the velocity at position $\ell$ is

$$v_1^{\ell+1} = \left[(\rho v)_{i+1}^{\ell+1} + \frac{\Delta x}{\Delta t} \quad (\rho^{\ell+1} - \rho^{\ell})\right] / \rho^{\ell+1}$$

because $\rho v$ is known at the wellhead, the velocity can be calculated successively down the wellbore. If the pressure is given as a function of time at the top, it is easier to calculate the new velocity using the momentum equation, at least at the first node.

The wellbore model was connected to a reservoir model so that the drawdown pressure was consistent with the variable flow velocity into the well. The reservoir flow was assumed to be radial, homogeneous, and single phase. The fluid was allowed to flow into the wellbore over a finite length, h. (The effect of flashing in the well only was investigated initially. The intent was not to spend a great deal of effort on the reservoir itself but to at least use a model that would give a drawdown pressure consistent with the flow into the well.) When the initial transient changes take place in the well, the flow around the wellbore is almost radial. At a later stage, the simple reservoir model will be expanded to include flashing in the reservoir.

The equation solved in the reservoir was

$$\frac{\partial P}{\partial t} = \frac{k}{\mu c \phi} \left(\frac{1}{r} \frac{\partial}{\partial r} r \frac{\partial P}{\partial r}\right) \quad (11)$$

Equation 11 was solved at several different heights in the reservoir to allow flow into the wellbore over a finite height, making it possible to consider a layered reservoir system interacting with the well. Far from the wellbore, a constant pressure was assumed. At the well/formation boundary, mass had to be conserved.

The mass flow rate out of the reservoir and into the well must be equal. If the reservoir and the wellbore equations are combined, the matrix multiplying the pressure vector will no longer be tridiagonal, increasing the calculation time for each step. Instead, each set of equations was solved separately. The boundary condition at the reservoir/well interface was

$$(\mu v) = \frac{kh}{\mu} \mu \frac{2}{r_w} \left[\frac{P_r^{\ell}(1) - P_w^{\ell+1}}{r(1) - r_w}\right] .$$

The new pressure in the wellbore is solved first using the old value of the reservoir pressure. Then the new pressure in the reservoir is calculated by determining the fluid that flowed from the reservoir into the well over that time that is, the same derivative of $(\partial P/\partial r)$ was used in both calculations. Because this boundary condition for the reservoir flow is solved explicitly, there is a stability limit. The stability limit in terms of the radial spacing is (Zerzan, 1979, private communication.):

$$\left| \frac{(\Delta r_o + \Delta r_1) r_1 \Delta r_o + 2\alpha\Delta t \left[\frac{\Delta r_o}{\Delta r_1} r_{3/2} \pm \left(r_{1/2} + \frac{\Delta r_o}{\Delta r_1} r_{3/2}\right)\right]}{(\Delta r_o + \Delta r_1) r_1 \Delta r_o - 2\alpha\Delta t \, r_{1/2}} \right| \geq 1$$

where $\Delta r_o = r_1 - r_o$, $\Delta r_1 = r_2 - r_1$, and $r_{1/2} = (r_o + r_1)/2$ .

To account for the initial large changes near the bore, and the changes far away at later times, a variable radial grid was used. The finite differenced equation solved was:

$$\left(\frac{p^{\ell+1}_{r_i} - p^{\ell}_{r_i}}{\Delta t}\right) = \frac{\frac{k}{\mu c \phi}\left[r_{i+\frac{1}{2}}\left(\frac{p^{\ell+1}_{r_{i+1}} - p^{\ell+1}_{r_i}}{r_{i+1} - r_i}\right) - r_{i-\frac{1}{2}}\left(\frac{p^{\ell+1}_{r_i} - p^{\ell+1}_{r_{i-1}}}{r_i - r_{i-1}}\right)\right]}{\frac{1}{2}\left(r_{i+1} - r_{i-1}\right)}$$

The variable grid was calculated by using a logarithmic transformation

$$r(i) = \frac{\left(A^{N_i/\Delta N_o} - 1\right)}{\left(A^{1/\Delta N_o} - 1\right)} B + r(1) .$$

The quantity $N_i$ is just $i(\Delta N)$, and B, A, and $\Delta N_o$ are adjustable constants.

Once the new pressure is determined in the well, the change in the reservoir pressure is calculated as a function of r and at several different heights. The temperature of the fluid in the producing zone is assumed to be specified. However, the energy loss of the fluid in the wellbore itself must also be included.

One important difference between the well testing in a geothermal well and that done by the petroleum industry is the high temperature found in the geothermal reservoir. Because of this, it is important to include the heat transfer out of (or into) the wellbore from the surrounding rock in numerical models. Ramey (1962) estimated the heat loss from the wellbore as a function of time. This method is less valid when the flow rate is continually changing. To account for the heat transfer, I solved the conduction equation for the temperature in the rock. Again, I used a variable grid to allow for large changes near the wellbore and smaller changes further away. However, the grid variation is closer to the wellbore in this case, because the temperature

changes will be over a smaller spatial region than the pressure changes. The conduction equation solved for the temperature changes is similar to that of the pressure in the reservoir. However, the new temperature is solved for implicitly to avoid time step limitations imposed by the small grid spacing near the wellbore. The temperature far from the well was assumed to be the initial geothermal gradient. At the rock/wellbore boundary, the heat transfer was matched. When the energy equation in the fluid is solved, the heat transfer at the wall is

$$q = 2\pi r_w \Delta x \, H \, (T_r^k - T_w^k) \quad .$$

When the temperature in the reservoir is calculated, the boundary condition at the rock/well interface is:

$$k_r \frac{\partial T_r}{\partial r} = H \, (T_r^{k+1} - T_w^{k+1}) \quad .$$

The heat transfer is matched throughout the calculation except for the first time step for the energy in the fluid that is, the heat transfer into the reservoir for the calculation of the reservoir temperature at time $k+1$ is just the heat that will leave the fluid during the calculation for time $k+2$. The only heat transfer not matched is for the first calculation of the fluid energy, but usually $T_r = T_w$ for this case, so q will be zero. No stability problems were encountered because the temperature in the reservoir is solved implicitly, even at the boundary.

The model then solves for the transient flow in the wellbore, including heat loss to the surrounding rock. The simple reservoir model provides that the fluid flow into the well is consistent with the drawdown pressure. The assumption of no slip and thermodynamic equilibrium was made. However, the

extension of the model to nonslip and nonequilibrium flow, or to include non-condensible gases can be made.

EXTENSION OF NUMERICAL METHOD

To develop the initial numerical method, two-phase homogenous equlibrium flow was assumed. However, the method can be extended. First, to include slip in the flow, additional terms must be added to both the momentum and the energy equations. These terms account for the fluid accelerating or decelerating because of evaporation or condensation. For the momentum equation, the term that must be added is

$$\frac{\partial}{\partial x} \frac{(1-\alpha)\alpha\rho_\ell\rho_g v_r^2}{\rho_m}$$

where $\alpha$ is the volumetric quality and $\rho_m = (1-\alpha)\rho_\ell + \alpha\rho_g$. The average velocity is defined as

$$v_m = \frac{(1-\alpha)\rho_\ell v_\ell + (\alpha)\rho_g v_g}{\rho_m} .$$

The convection terms were evaluated explicitly in the basic model, so the addition of this term will not involve any modification of the method itself. The relative velocity is given usually by experimental measurements at present. It is specified as a function of void fraction and total flow rate. The main problem in adding the term is in choosing which correlations to use, since the scatter in different correlations can be large.

For the energy equation, the terms that must be included are:

$$\frac{\partial}{\partial x} \frac{(1-\alpha)\rho_\ell\alpha\rho_g v_r(e_g - e_\ell)}{\rho_m} .$$

because of the fluid changing velocity and

$$P \frac{\partial}{\partial x} \frac{\alpha(1-\alpha)\, v_r(\rho_\ell - \rho_g)}{\rho_m}$$

because of the volumetric expansion work when the fluid changes phase. Again the convection terms are evaluated explicity so they can be added very easily.

The more difficult problem is the extension of the method to allow for nonequilibrium flow or to include a noncondensible gas. The method in either case is similar so only the former case will be considered in detail. Condensation and evaporation do not take place instantaneously, but require a finite time. If this time is as long or longer than the pressure transients in the flow, nonequilibrium can be very important. Many well tests with flashing in the bore have pressure responses that seem to indicate a two-layer reservoir. These responses may be due to nonequilibrium effects in the wellbore and it is important in modelling these cases to understand if nonequilibrium could account for these pressure changes.

To include nonequilibrium, a second continuity equation must be used. The evaporation (or condensation) will be given by some rate term. However, inclusion of non-equilibrium will require some modification of the current method. The continuity equation needed is

$$\frac{\partial}{\partial t} \alpha\rho_g + \frac{\partial}{\partial x} \alpha\rho_g v_g = I$$

where I is the rate of evaporation or condensation. Now instead of $\rho_m = fn(e_m, P)$, the expression for the densities will be determined separately:

$$\rho_\ell = fn(e_\ell, P), \text{ and } \rho_g = fn(e_g, P)$$

where $e_\ell$ and $e_g$ are functions of temperature only. It will still be assumed

that $T_\ell = T_g$. Such an assumption means that a parcel of fluid can either condense or flash, but can not do both at the same time. Since the temperature of the two phases are equal, the mixture as a whole can be either above or below the saturation temperature. In a completely nonequilibrium situation, the temperature of the phases would differ. Although the approach used here assumes $T_\ell = T_g$, it does allow for the finite rate of flashing or condensation. This model is similar to that suggested by Liles and Reed (1978).

The individual equations of state can be combined to give

$$\nu_m = fn(T,P,\alpha).$$

Again the differential form of the equation of state will be used:

$$d\nu_m = \left.\frac{\partial \nu_m}{\partial T}\right|_{P,\alpha} dT + \left.\frac{\partial \nu_m}{\partial P}\right|_{T,\alpha} dP + \left.\frac{\partial \nu_m}{\partial \alpha}\right|_{T,P} d\alpha$$

The detail of writing $\partial\nu_m/\partial t$ in terms of $\partial P/\partial t$ is given in Appendix A. However, the general method is: (1) write $d\nu_\ell$ and $d\nu_g$ in terms of (dT, dP); (2) use the equation of energy to determine $\partial T/\partial t$ in terms of $\partial P/\partial t$ and $\partial\alpha/\partial t$; and (3) use the continuity equation to write $\partial\alpha/\partial t$ in terms of $\partial P/\partial t$. Using the equations for $\partial P/\partial t$, we can invert the tridiagonal matrix to solve for the new pressure.

Once the new pressure is known, the new void fraction, temperature, density, and average energy can be calculated from the expressions used to develop the equation

$$A\,P = B \qquad .$$

To consider the effect of noncondensible gases instead of nonequilibrium effects, the density is written as a function of P, T, S, where S is the saturation of the gas phase (noncondensible gas and steam). The average

density is

$$S\rho_g + (1 - S)\rho_k$$

where $\rho_g$, $\rho_k$ are the densities of the gas and liquid phases respectively. To determine S, a continuity equation conserving the noncondensible gas can be used. Then

$$\frac{\partial}{\partial t} Sx_g\rho_g = -\frac{\partial}{\partial x} Sx_g\rho_g v_g$$

where $x_g$ is the mass fraction of say $CO_2$ in the gas phase. The steam is assumed to be at the saturation density corresponding to the temperature of the phase. Then $\rho_g = \rho_{1g}/(1-x_g)$ where $\rho_{1g}$ is the density of the steam and is specified as a function of temperature only.

To solve the set of equations, it is necessary to specify an equation of state for the mixture. One set that is suggested by Iglesias (1979) is that

$$x_g = 1 - \frac{P_{1g}}{P}$$

and that $x_g$ can be determined by specifying the boiling curves of an $H_2O$ - $CO_2$ mixture. By specifying the equation of state, a complete set of equations will again exist, and the solution procedure is as specified above. The model is presently being updated to include these details.

## EXAMPLE CALCULATIONS

The numerical model has been used here to determine the early-time behavior of the wellbore flow for both single-phase and two-phase flow. Examples of the calculations are given below. Figure 1 is a plot of the pressure changes that propagate down the wellbore after a stepwise change in flow rate at the wellhead. In this figure, the calculations were done for a liquid-

filled well flowing under a positive head. The well is flowing steadily at one rate and then the rate is increased. At early times after the change, the increase in produced fluid is obtained from the well instead of from the reservoir. A pressure drop propagates down the well. After a certain amount of time, depending on the compressibility of the fluid, the pressure pulse interacts with the formation/well boundary. In the particular case plotted, the reservoir has a large value of $kh/\mu$, and it is capable of supplying more fluid for this pressure drop than the well could. This case results in a reverse pressure pulse, which propagates back up the well, cancelling part of the initial pressure drop. The pressure pulse oscillates until it is finally damped out by the interaction with the boundaries.

Figure 2 shows the same calculations for a flashed system. Again, the fluid is flowing slowly and then the flow rate was suddenly increased. The pressure pulse propagates down the well. However in this case, there is a brine/two-phase boundary. The dashed line in Figure 2 shows the approximate location of the flash point. (Obviously, as the flow rate is increased, the flash level drops.) When the pressure pulse reaches this boundary, the pulse is partly reflected and partly transmitted. The reflected pulse propagates back toward the surface. In the single-phase region, the propagation of the signal is much faster; oscillations are mainly in the two-phase region.

One can use the program to determine the pressure drawdown during the early time of a well test. It has been shown (Miller, 1979) that the initial slope of a log-log plot of pressure vs. time in well testing is not necessarily unity, as derived in the petroleum literature. As seen in the figures above there is a time delay until the downhole pressure registers the change made at the wellhead. Wellbore storage curves are derived assuming the fluid in

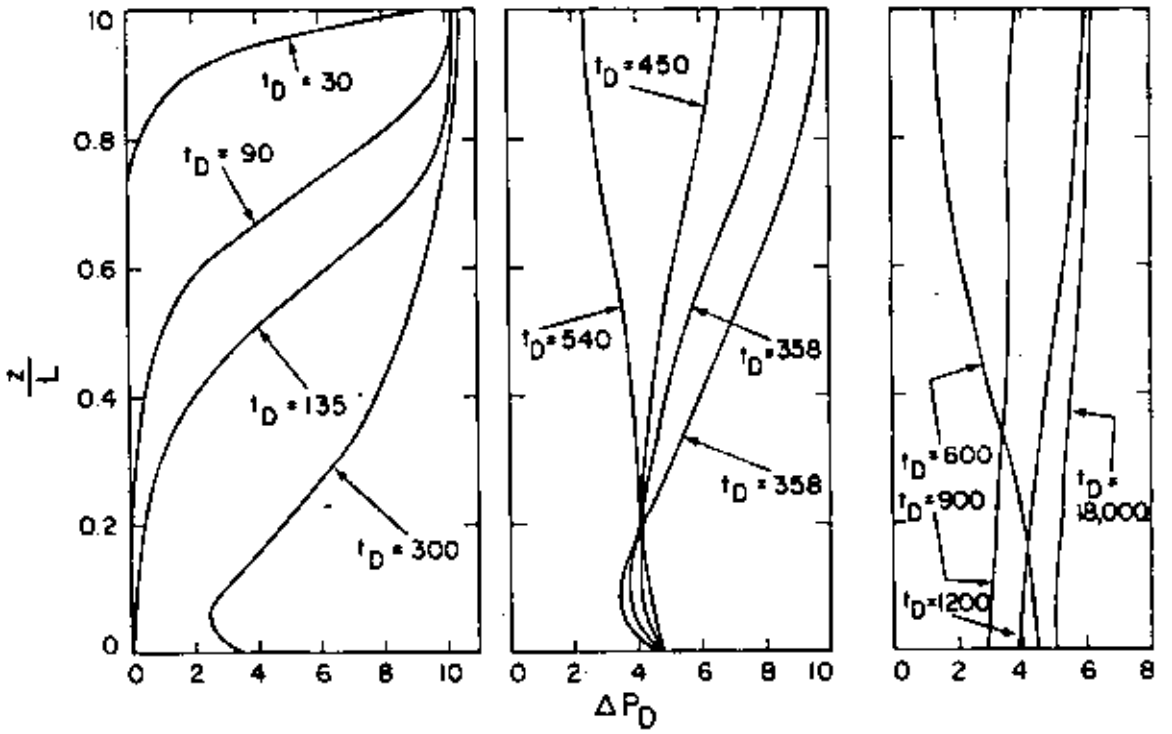


Figure 1. Propagation of pressure pulse down a wellbore as a function of time for a liquid-filled well. XBL 794-7404

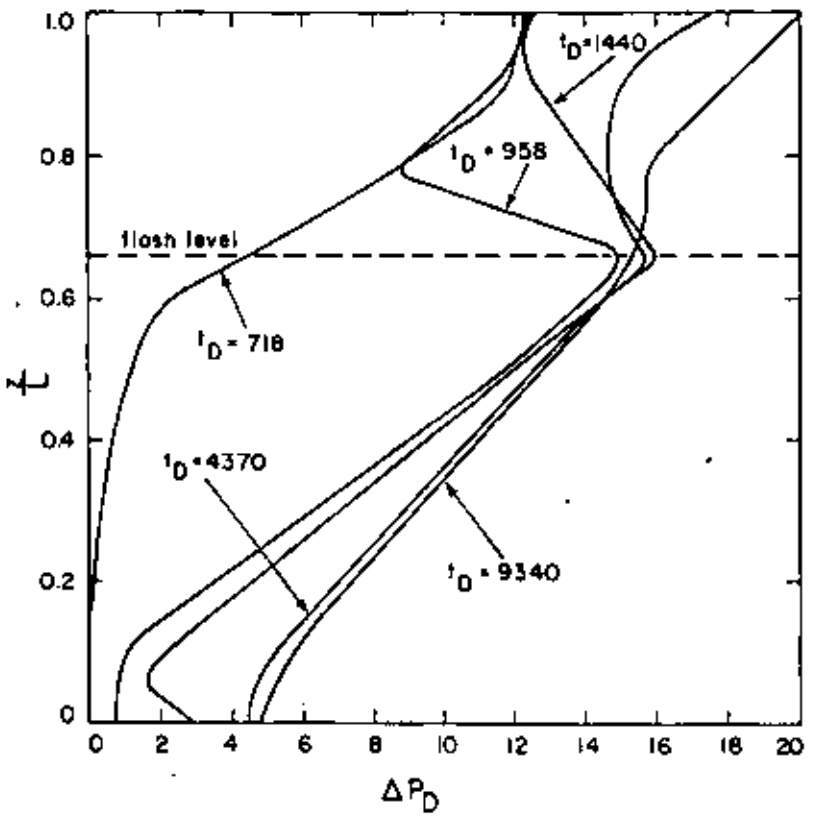


Figure 2. Propagation of pressure pulse down a wellbore in a two-phase well as a function of time. XBL 794-7403

the well responds as a well-mixed fluid. By being able to model the transient flow in the wellbore, it has been possible to calculate the expected drawdown in the well, taking into account the nonuniformities in the well. The results show that another nondimensional time $t_{RW}$ must also be determined in addition to the average wellbore storage coefficient $C_D$ (see Fig. 3). The plot shows calculations for flashed and unflashed wells. The parameter $t_{RW}$ is defined as

$$\left(\frac{\mu}{kh}\right) \frac{D^2}{8} \frac{1}{\rho} \left(\frac{\partial \rho}{\partial P}\right)_s$$

As $kh/\mu$ decreases, $t_{RW}$ increases, and the early-time behavior of the log P vs. log t approaches a one-to-one plot. As $kh/\mu$ increases, $t_{RW}$ decreases, and the slope of the log P vs. log t curve is steeper than unity.

The numerical model can also be used to determine the effect of heat loss to the rock surrounding the wellbore during a well test. The calculations shown are done for a well that has been flowing and is reasonably "warm". The assumed temperature profile is shown by the inset in Figure 4. The well has been flowing steadily, then the flow rate is decreased. Figure 4 compares the buildup curve and subsequent drawdown curve with and without heat transfer. The calculations show that even when the well has been flowing for several hours and the rock around the bore has been heated, heat transfer during a well test is still important and must be considered. When the well test data are plotted, the slope of the P vs. log t curve in the pseudo-steady region is significantly affected by the heat transfer. Also the time to reach the pseudo-steady region is longer when heat transfer is important.

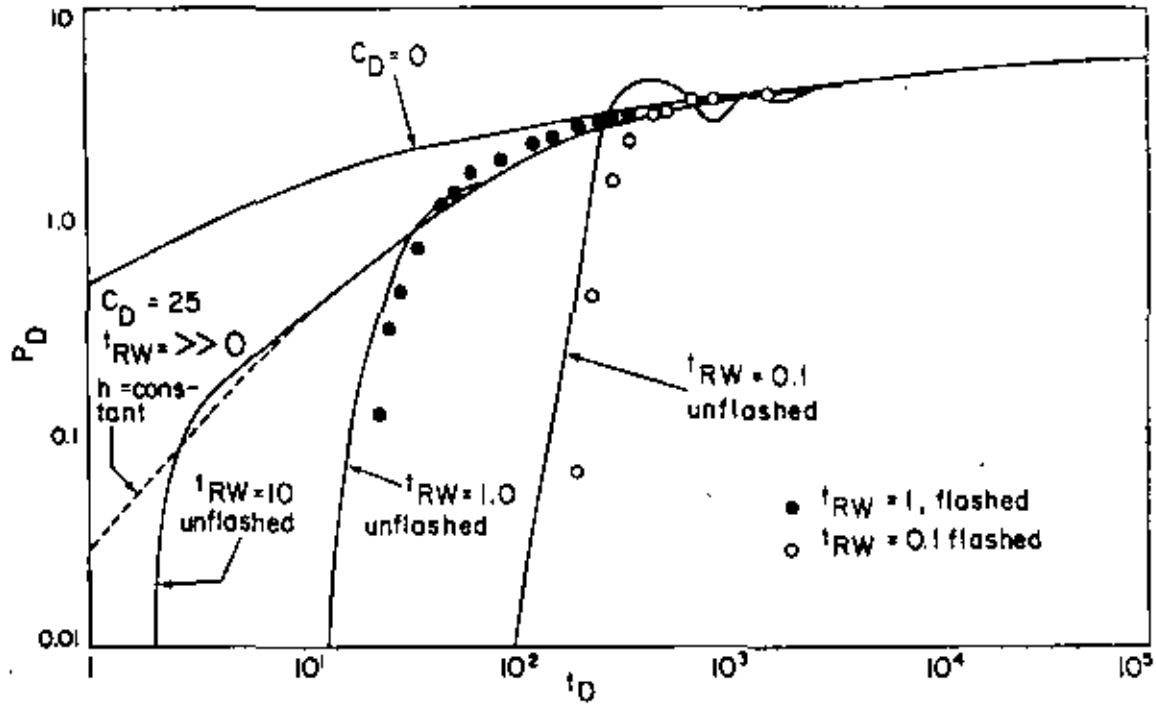


Figure 3. Nondimensional pressure vs. nondimensional time for different values of $C_D$ and different values of the parameter $t_{RW}$.
XBL 794-7402

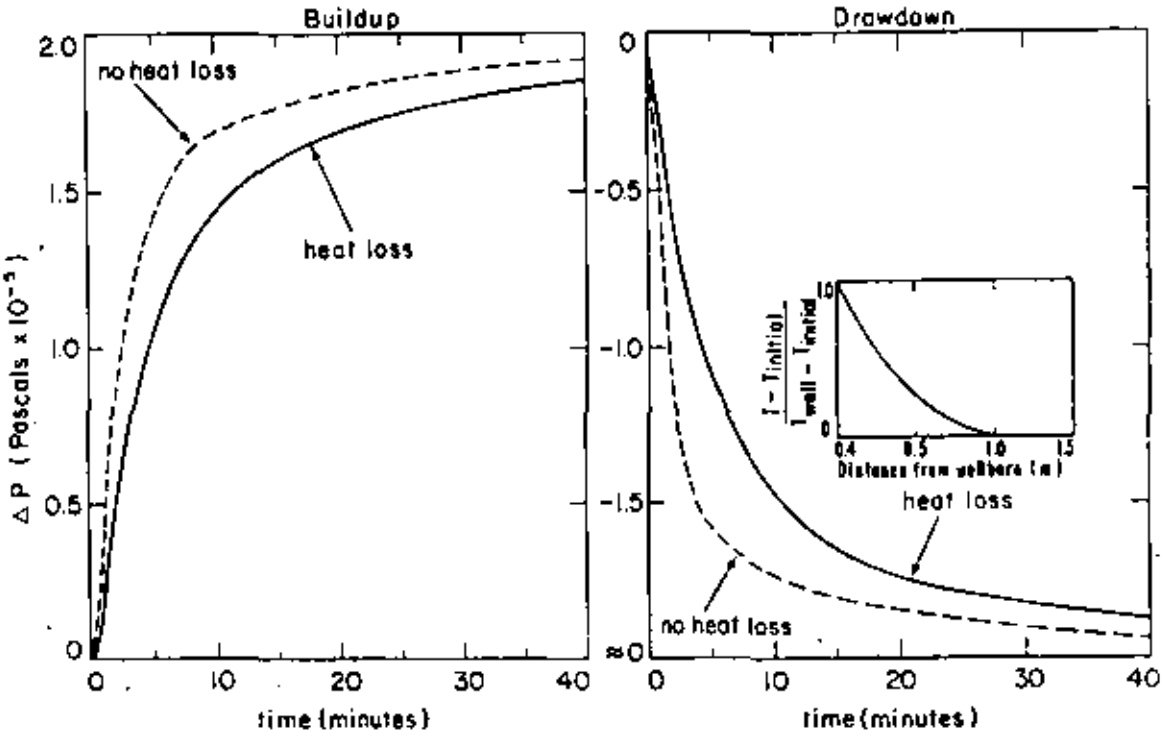


Figure 4. Effect of heat transfer on the buildup and drawdown well test.
XBL 794-7412

NOMENCLATURE

| | |
|---|---|
| a | Speed of sound |
| c | Reservoir compressibility |
| $C_D$ | Wellbore storage coefficient |
| D | Diameter of well |
| e | Specific energy |
| f | Friction factor |
| g | Gravity |
| h | Thickness of reservoir |
| H | Heat tranafer coefficient |
| I | Rate of evaporation or condensation |
| k | Permeability |
| $k_r$ | Conductivity of rock |
| $\dot{m}$ | Mass flow rate |
| P | Pressure |
| q | Volume flow rate |
| r | Radial direction |
| $r_w$ | Radius of well |
| S | Saturation |
| s | Specific entropy |
| t | Time |
| $T_r$ | Temperature of rock surrounding well |
| $T_w$ | Temperature of fluid in well |
| x | Axial direction |
| v | Velocity |
| $v_r$ | Relative velocity ($v_g - v_\ell$) |
| $\omega$ | volumetric quality (holdup) |
| $\rho$ | density |
| $\mu$ | Absolute viscosity |
| $\phi$ | Porosity |

Subscripts

| | |
|---|---|
| r | Reservoir |
| w | Well |
| $\ell$ | Liquid |
| m | Mixture |
| g | Gas |
| D | Non-dimensional parameter |

REFERENCES

Elliot, D.G., 1975, Comparison of brine production methods and conversion processes for geothermal electrical power generation: Environmental Quality Laboratory, California Institute of Technology, EQL Report #10.

Gould, T. L., 1974, Vertical two phase steam water flow in geothermal wells: Journal of Petroleum Technology, v. 26, p. 883-842.

Harlow, F. H. and Amsden, A. A., 1975, Numerical calculation of multiphase Fluid Flow: Journal of Computational Physics, v. 17, p. 19-52.

Hirt, C. W. and Romero, N. C., 1976, Application of a drift-flux model to flashing in straight pipes: Los Alamos, Los Alamos Scientific Laboratory, Report LA-6005-MA.

Iglesias, E. R., 1979, Approximate properties of $H_2O$-$CO_2$ mixture for geothermal reservoir and wellbore simulations: Lawrence Berkeley Laboratory LBL-9991 (in preparation).

Juprasat, S., and Sanyal, S. K., 1977, A numerical simulator for flow in geothermal wellbores: Geothermal Resources Council, Transactions, v.1, p. 159-161.

Liles, P. R., and Reed, W. H., 1978, A semi-implicit method for two-phase fluid dynamics: Journal of Computational Physics, v. 26, p. 390 - 407.

Miller, C. W., 1979, Wellbore storage in geothermal wells: presented at 1979 Annual Meeting of Society Petroleum Engineers, Las Vegas, Nevada, paper SPE 8203.

Ramey, H. J., Jr. 1962, Wellbore heat trasmission: Journal Petroleum Technology, v. 225, p. 427-435.

Ryley, D. J., 1964, Two-phase critical flow in geothermal steam wells: International Journal of Mechanical Science, v. 6, p. 273.

Sugiura, T., and Farouq, S. M., 1979, A comprehensive wellbore steam-water flow model for steam injection and geothermal applications: paper presented at 1979 California Regional Meeting of Society of Petroleum Engineers, Ventura, Ca., April 1979, SPE-7966.

APPENDIX A

To use the same numerical method that was developed for modelling the equilibrium flow, $\partial\rho_m/\partial t$ must be written in terms of $\partial P/\partial t$ only. In the non-equilibrium case, the number of independent variables has increased by one, and the average energy is no longer convenient to use as one of the independent variables. Now, temperature, pressure, and void fraction will be the independent variables. To be able to write the density change in time as a function of the pressure change only, the vapor continuity and the energy equations must be used to express $\partial\alpha/\partial t$ and $\partial T/\partial t$ in terms of $\partial P/\partial t$ respectively. After the new pressure is evaluated along the wellbore, the other independent and dependent variables can be calculated.

In the overall continuity equation (1), the convective term, $\partial(\rho_m v_m)/\partial x$, is evaluated by using the momentum equation as developed in the first section of this paper. The difficult part is expressing $\partial\rho_m/\partial t$ in terms of the three independent variables. The average density is $(1-\alpha)\rho_\ell + \alpha\rho_g$. The derivatives of $\rho_m$ with respect to T, P, and $\alpha$ are:

$$\left.\frac{\partial\rho_m}{\partial T}\right|_{P,\alpha} = (1-\alpha)\left.\frac{\partial\rho_\ell}{\partial T}\right|_{P,\alpha} + \alpha\left.\frac{\partial\rho_g}{\partial T}\right|_{P,\alpha},$$

$$\left.\frac{\partial\rho_m}{\partial P}\right|_{T,\alpha} = (1-\alpha)\left.\frac{\partial\rho_\ell}{\partial P}\right|_{T,\alpha} + \alpha\left.\frac{\partial\rho_g}{\partial P}\right|_{T,\alpha}, \text{ and}$$

$$\left.\frac{\partial\rho_m}{\partial\alpha}\right|_{T,P} = \rho_g - \rho_\ell$$

Then

$$\frac{\partial\rho_m}{\partial t} = \left[(1-\alpha)\frac{\partial\rho_\ell}{\partial T} + \alpha\frac{\partial\rho_g}{\partial T}\right]\frac{\partial T}{\partial t} + \left[(1-\alpha)\frac{\partial\rho_\ell}{\partial P} + \alpha\frac{\partial\rho_g}{\partial P}\right]\frac{\partial P}{\partial t} + (\rho_g - \rho_\ell)\frac{\partial\alpha}{\partial t}.$$

The continuity equation for the vapor component is rewritten to give $\partial\omega/\partial t$:

$$\rho_g \frac{\partial \omega}{\partial t} = -\omega \left( \frac{\partial \rho_g}{\partial T} \frac{\partial T}{\partial t} + \frac{\partial \rho_g}{\partial P} \frac{\partial P}{\partial t} \right) - \frac{\partial}{\partial x}(\omega \rho_g v_g) + I \qquad \text{(A1)}$$

where the term in the first parenthesis is just $\partial\rho_g/\partial t$.

The energy equation can be used to relate $\partial T/\partial t$ in terms of $\partial P/\partial t$. The average energy, $e_m$ is

$$\frac{1}{\rho_m} \left[ (1-\omega)\, \rho_\ell e_\ell + \omega \rho_g e_g \right]$$

and the derivative of $(\rho_m e_m)$ in terms of $\partial T/\partial t$, $\partial P/\partial t$, and $\partial\omega/\partial t$ is

$$\frac{\partial}{\partial t}(\rho_m e_m) = (1-\omega) \left\{ \left[ \frac{\partial}{\partial T} (\rho_\ell e_\ell) \right] \frac{\partial T}{\partial t} + \left[ \frac{\partial}{\partial P} (\rho_\ell e_\ell) \right] \frac{\partial P}{\partial t} \right\}$$

$$+ \omega \left\{ \left[ \frac{\partial}{\partial T} (\rho_g e_g) \right] \frac{\partial T}{\partial t} + \frac{\partial}{\partial P} \left[ (\rho_\ell e_\ell) \right] \frac{\partial P}{\partial t} \right\}$$

$$+ (\rho_g e_g - \rho_\ell e_\ell) \frac{\partial \omega}{\partial t} \qquad \text{(A2)}$$

However, the energy equation gives $\partial(\rho_m e_m)/\partial t$, which is:

$$-\frac{\partial}{\partial x} (\rho_m e_m v_m) - \frac{\partial}{\partial x} \left[ \frac{(1-\omega)\rho_\ell \omega \rho_g v_r (e_g - e_\ell)}{\rho_m} \right] - P \frac{\partial v_m}{\partial x}$$

$$- P \frac{\partial}{\partial x} \left[ \omega \frac{(1-\omega) v_r (\rho_\ell - \rho_g)}{\rho_m} \right] - \frac{2H\,(T - T_r)}{r_w} \quad . \qquad \text{(A3)}$$

All these terms are evaluated explicitly so they can be calculated directly. Then equation A2 can be solved for dT/dt by using equation A1 to express $\partial\omega/\partial t$ in terms of $\partial P/\partial t$ and $\partial T/\partial t$, and equation A3 is used to determine $\partial(\rho_m e_m)/\partial t$ in terms of known values. The resultant form is

$$A \frac{\partial T}{\partial t} = B \frac{\partial}{\partial t} (\rho_m e_m) + C \frac{\partial P}{\partial t} + D \; .$$

where

$$A = \left[ (1-\omega) \frac{\partial}{\partial T} (\rho_\ell e_\ell) + \omega \frac{\partial}{\partial T} (\rho_g e_g) - (\rho_g e_g - \rho_\ell e_\ell) \frac{\omega}{\rho_g} \frac{\partial \rho_g}{\partial T} \right]$$

$$B = 1,$$

$$C = \left[(1-\omega)\frac{\partial}{\partial P}(\rho_\ell e_\ell) + \omega\frac{\partial}{\partial P}(\rho_g e_g) - (\rho_g e_g - \rho_\ell e_\ell)\frac{\alpha}{\rho_g}\frac{\partial \rho_g}{\partial P}\right]$$

and

$$D = -(\rho_g e_g - \rho_\ell e_\ell)\left[-\frac{\partial}{\partial x}(\alpha \rho_g v_g) + I\right]$$

Since $\partial\rho_m/\partial t$ has been written in terms of $\partial P/\partial t$, one can evaluate the overall continuity equation for the new pressure. Once the new pressure is determined, the method is similar to that derived in the first section of the report.

U.S.GPO:1980-698-169/F-112

This report was done with support from the Department of Energy. Any conclusions or opinions expressed in this report represent solely those of the author(s) and not necessarily those of The Regents of the University of California, the Lawrence Berkeley Laboratory or the Department of Energy.

Reference to a company or product name does not imply approval or recommendation of the product by the University of California or the U.S. Department of Energy to the exclusion of others that may be suitable.

TECH[redacted], INFORMATION DEPARTMENT
LAWRENCE BERKELEY LABORATORY
UNIVERSITY OF CALIFORNIA
BERKELEY, CALIFORNIA 94720

Submitted to the Journal of Geophysical Research

LBL-10617
Preprint

# A PLAUSIBLE TWO-DIMENSIONAL VERTICAL MODEL OF THE EAST MESA GEOTHERMAL FIELD, CALIFORNIA, U.S.A.

K. P. Goyal and D. R. Kassoy

March 1980

Prepared for the U.S. Department of Energy
under Contract W-7405-ENG-48

# A PLAUSIBLE TWO-DIMENSIONAL VERTICAL MODEL OF THE EAST MESA GEOTHERMAL FIELD, CALIFORNIA, U.S.A.

K. P. Goyal
Earth Sciences Division
Lawrence Berkeley Laboratory
University of California
Berkeley, California 94720

and

D. R. Kassoy
Mechanical Engineering Department,
University of Colorado,
Boulder, Colorado, 80309.

A two-dimensional conceptual model of the East Mesa geothermal system is developed on the basis of the existing geological, geophysical geochemical, heat flux, and borehole logging data. A fault called the Mesa Fault is assumed to charge the reservoir, which is overlaid by a clay-rich cap. The mathematical model is based on the flow of liquid water in a saturated porous medium. To obtain temperature-depth distributions similar to those measured at the site, we assume that the liquid is convecting at a high Rayleigh number. In this approximation, liquid rises up the fault and spreads into the near regions of the reservoir isothermally. The cooling effect of the surface on the flow in the reservoir is confined to a thin layer adjacent to the cap-reservoir interface near the fault. This layer grows with the distance from the fault. Eventually, the full depth of the reservoir is cooled by the surface. Results are obtained for the velocities, pressures, and temperatures of the entire system (fault zone, aquifer and clay cap). Finally we compare the heat flux predicted for the surface to that measured at the site in shallow wells.

## INTRODUCTION

Liquid-dominated geothermal anomalies exist in the Imperial Valley of southern California at the Salton Sea, Brawley, East Mesa, Dunes, and Heber areas as shown in Figure 1. The East Mesa anomaly has been considered for development of its geothermal resources by the Bureau of Reclamation, Magma Power Company, and Republic Geothermal Inc., and this interest has produced a significant body of field data for this anomaly. The geological, geophysical, geochemical and borehole logging data is described in Black [1975], Bailey [1977] and several U.S. Bureau of Reclamation reports [1972, 1973, 1974, 1977]. A case history of the field is given by Davis and Sanyal [1979], and a thorough survey is contained in the work of Howard et al. [1978].

A conceptual model of the East Mesa anomaly was developed by Bailey [1977], based on the available field data. Goyal [1978] described a mathematical model for the system, based on saturated flow in porous media. A simplified version has been described in Goyal and Kassoy [1980]. Riney et al. [1979a] have described a closely related model.

In the present paper, we describe a two-dimensional vertical model of the East Mesa system that includes an impermeable clay cap ingnored in Goyal and Kassoy [1980]. Our preliminary goal is to show that the concept of fault-zone-controlled charging of a geothermal reservoir like that at East Mesa is plausible. To this end, we show that the shut-in well-bore temperature distributions with depth and near-surface heat flux patterns can be predicted with approximate quantitative accuracy. Of course, our simplified model, lacking many of the detailed features believed to exist at East Mesa, should not be thought of as the definitive description.

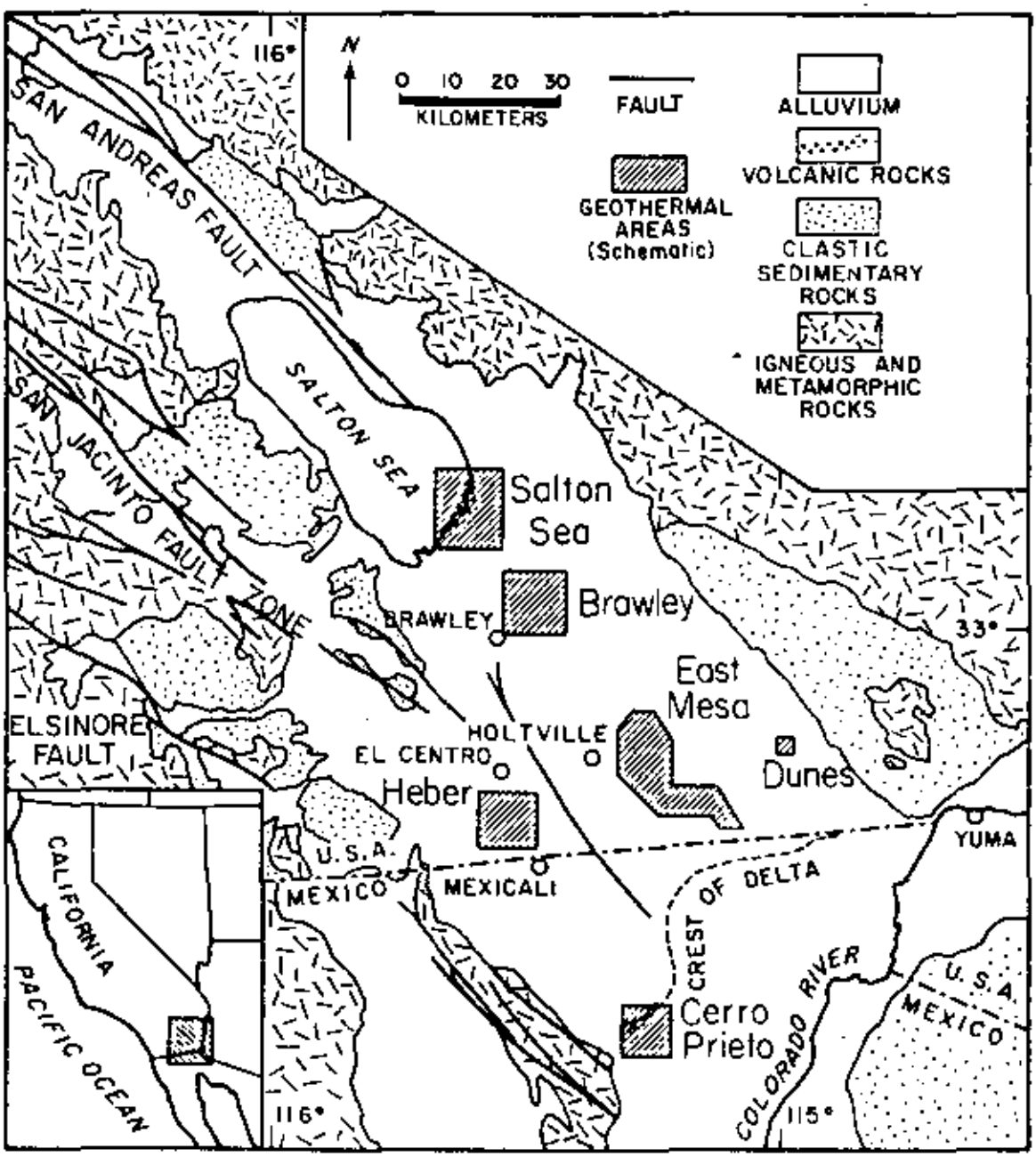


XBL 7912-13479

Figure 1. Geologic Map of the Imperial Valley, California, U.S.A. (Adapted from Elders et al. [1978].)

## EAST MESA FIELD DATA

The East Mesa geothermal anomaly is located on the northern flank of the Colorado River delta and on the east side of a deep sediment-filled structural basin called the Salton Trough. The basin contains three main rock groups. A lower sequence of mainly nonmarine sedimentary rocks of early to middle Tertiary age dominate the basal unit which unconformably overlies pre-Tertiary metamorphic and igneous rocks. The marine Imperial formation of Pliocene age comprises the beds of the middle sequence. The upper sequence consists predominantly of nonmarine deposits of late Tertiary and Quaternary age derived mainly from the Colorado River drainage area. This upper sequence accounts for most of the valley fill in the central part of the trough. Within its thick accumulations of the young valley fill, the sediments of the Imperial Valley comprise a vast water reservoir. The horizontal permeability of the sediments is much larger than the vertical permeability because of the presence of platey and ellipsoidal grains often aligned during sedimentation. The existence of the lenticular clays also reduces the vertical permeability.

The structure of the Imperial Valley is controlled by numerous strike-slip faults of the San Andreas and San Jacinto fault system. Three faults with no surface expressions [Rex, 1970; Babcock, 1971; and Combs and Hadley, 1973] have been inferred at the Mesa anomaly by indirect means such as resistivity surveys, oblique aerial infrared photography and microseismic activity (Figure 2). The Combs-Hadley fault is also called the Mesa fault [Combs and Hadley, 1977]. Howard et al. [1978] inferred two nearly parallel faults based on the seismic and well log data. The position of one of these faults is very close to that of the Mesa fault (Figure 3).

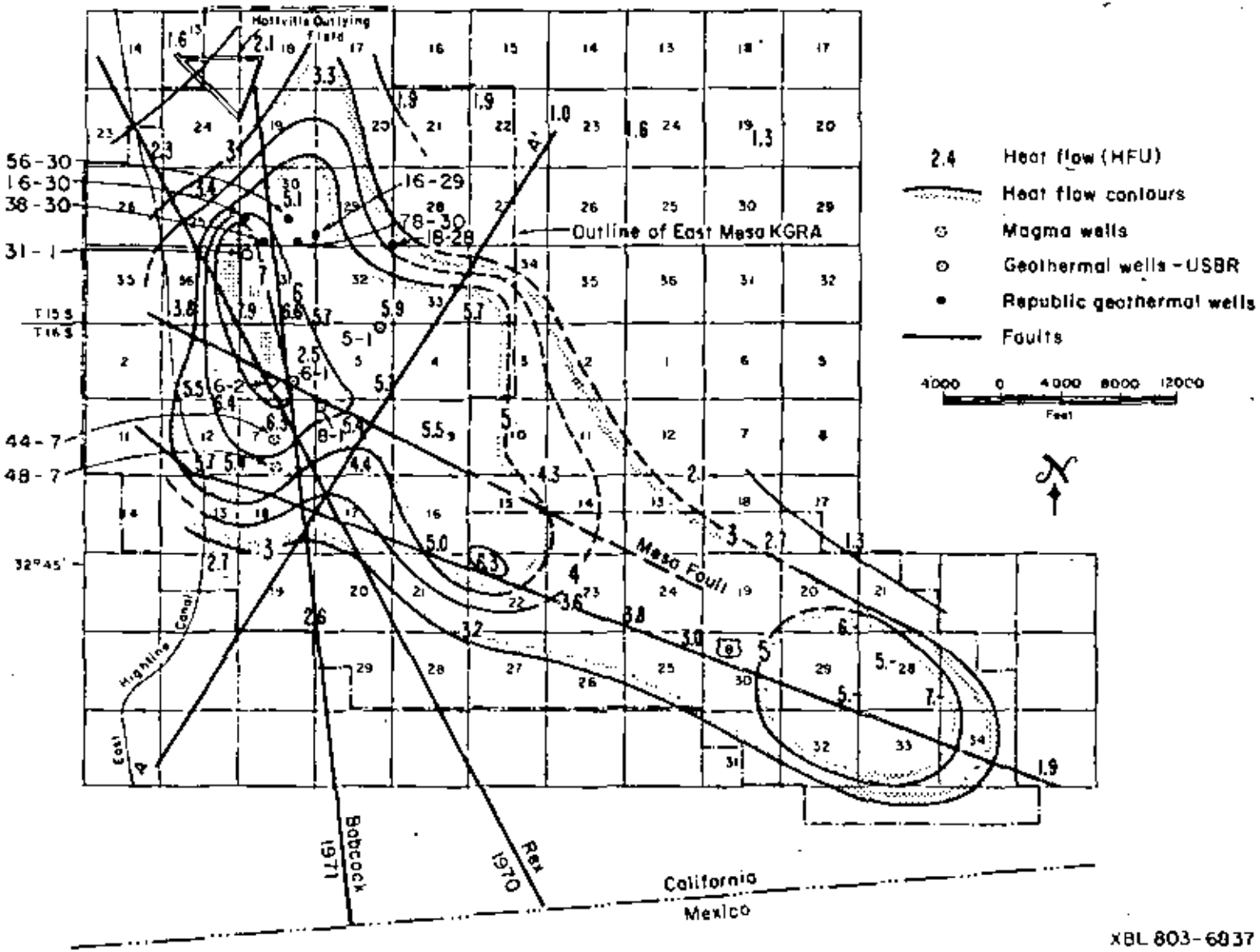


Figure 2. East Mesa KGRA (Known Geothermal Resource Areas) heat flow. (Adapted from U.S. Bureau of Reclamation Report, [1974].)

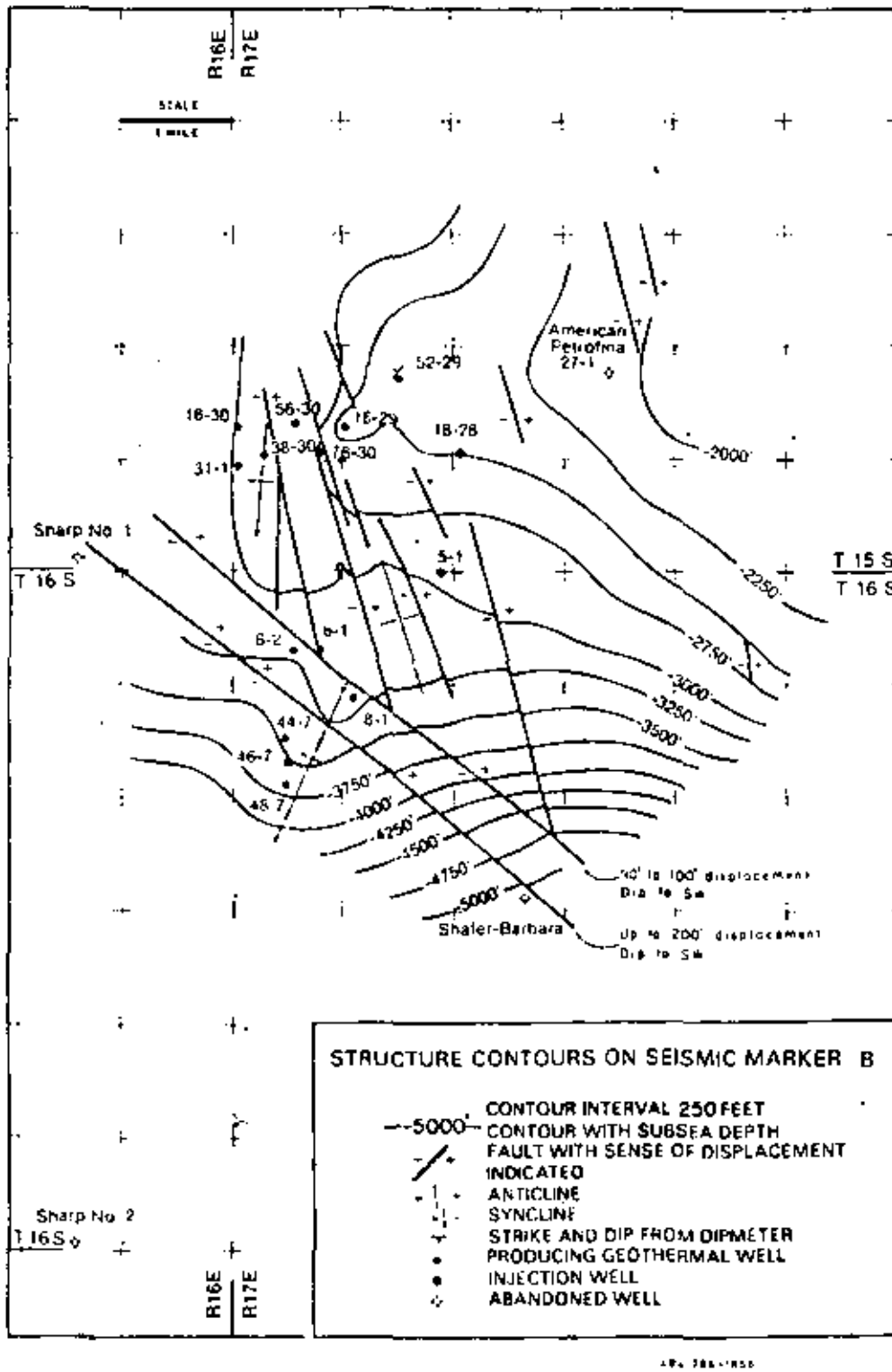


Figure 3. Location of faults on the basis of seismic and well log data. (Adapted from Howard et al. [1978].)

Electrical resistivity decreases with increasing temperature and increasing water salinity. Therefore, the combined effect of high salinity waters and high temperatures in a geothermal reservoir make electrical resistivity surveys a valuable tool in locating geothermal anomalies. Meidav and Furgerson [1971] made a detailed electrical resistivity study of the Imperial Valley at 305, 610 and 915 meters depth. Their results show a regional resistivity gradient which decreases northwestward from the southeast corner of the Imperial valley, near the Colorado River, to values about two orders of magnitude lower at the Salton Sea. Based on the resistivity surveys, the following conclusions can be derived: groundwater salinity increases with increasing distance from the Colorado River. Many of the faults in the Imperial Valley act as aquitards and restrict horizontal water movement. Resistivity lows are found at the East Mesa, Salton Sea, Heber, Brawley and Dunes geothermal anomalies.

Gravity studies of Biehler [1971] revealed the presence of a broad positive gravity anomaly throughout the Imperial Valley. It may be due to either an emplacement of high density crustal material beneath the trough axis or a thinner than average crust beneath the Imperial Valley. An increase in the density of the crustal material can be caused by clay diagenesis, cementation and/or thermal metamorphism. Some or all the above factors might be contributing to the gravity anomaly in the East Mesa area.

Combs and Hadley [1977] recorded microearthquakes associated with the East Mesa anomaly for five weeks during the summer of 1973 and defined a new right lateral strike-slip fault, called Mesa fault (Figure 2). The focal depths of the microearthquakes ranged from near surface to about 8 km. More than half of the located events have hypocenters

greater than 4 km which is approximately the depth to crystalline basement. This data shows that the fault is active both above and below the basement. A more recent microseismic study continuously conducted at East Mesa during the last 186 days of 1977 is described in Howard et al. [1978]. This latest study detected no local events within the East Mesa field for those six months, although a significant number of events with hypocenters located elsewhere in the Imperial Valley were recorded by the six-station instrument array positioned at East Mesa.

Areas of high near-surface heat flow are generally associated with active volcanism of geothermal areas (Bailey, 1977]. Figure 2 shows the heat flow contours and the locations of the test wells drilled in the East Mesa area by Republic Geothermal Inc., United States Bureau of Reclamation (USBR) and Magma Power Company. Republic Geothermal Inc. has drilled six wells to date, ranging in depth from 2.25 km to 2.77 km. Towards the south, the geothermal anomaly has been explored and assessed by USBR (five wells) and Magma Power Company (three wells). The position of the heat flow contours around Mesa fault confirms the hypothesis of Combs and Hadley [1977] that the Mesa fault acts as a conduit for rising geothermal fluids of the Mesa anomaly. Morrison et al. [1979] discovered a dipolar self-potential anomaly in the East Mesa field. Such anomalies are often associated with faults which are thought to serve as conduits for geothermal fluids, or with areas of high heat flow or vigorous subsurface fluid flow [Corwin et al., 1978]. The locations of the charging planes based on the self-potential study are shown in Figure 4. It can be noted in this figure that the charging plane A is located very near to Mesa fault and thus confirms the previously mentioned hypothesis.

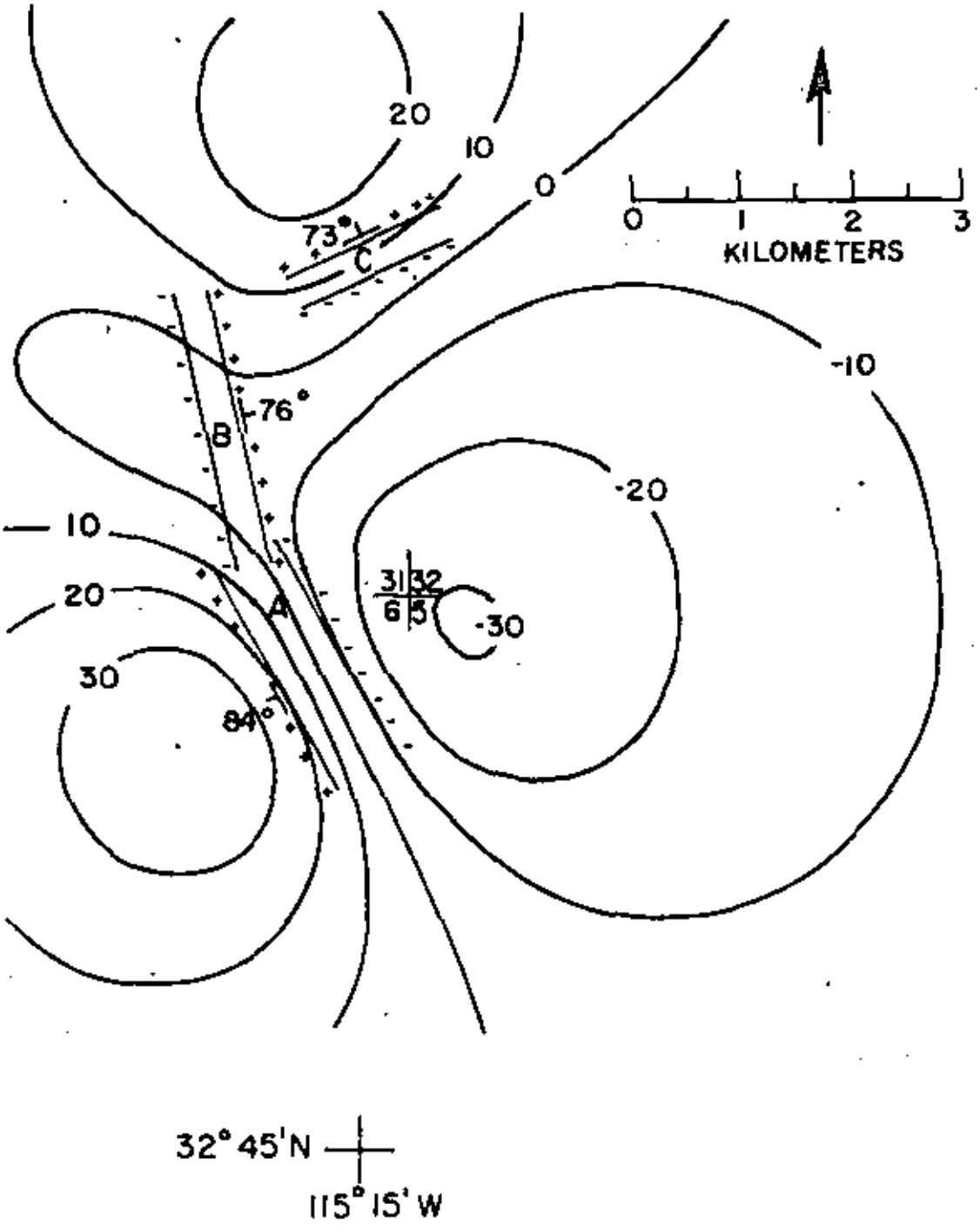


Figure 4. Self potential contours and inferred charging planes. (Adapted from Morrison et al. [1979].)

These charging planes range from about 300 to 600 m in width.

Borehole logging data indicate that the stratum in the upper 600 to 700 m is clay-dominated, below 2.1 km it is shale-dominated, and in the middle it is dominated by sands and sandstones. It is this part of the field that is considered to be a highly permeable zone consituting the geothermal reservoir. A plot of temperature versus depth in the wells shows three different gradients [Goyal, 1978]. Steep gradients in the upper 700-900 m are associated with vertical heat transfer by conduction. Presumably, the presence of large amounts of interbedded clays prevents vertical convection from occurring. Temperatures are less variable in the middle zone, which extends up to 1900-2100 m. Heat transfer in this zone is profoundly influenced by convection, which is possible in sandy zones of relatively high permeability. Steeper temperature gradients are seen below 1900-2100 m in Mesa Well 6-1. It would appear that the change in mode of heat transfer from convection to conduction at this depth is due to the presence of increasingly large amounts of shales in this zone. Figure 5 shows the temperature variations of the wells in the permeable zone of the anomaly. It can be seen that wells 6-1, 6-2, 8-1, 44-7, and 48-7 are the hottest in this area. Flat temperature profiles can be seen in wells 8-1, 48-7, and 44-7 between the depths 1200-1800 m, 1600-2100 m, and 1500-1850 m respectively. One could interpret these flat portions as zones that are strongly affected by fault zone flow.

## CONCEPTUAL MODEL

The conceptual model of the East Mesa geothermal system is shown in Figure 6. The basement complex of granite-metamorphic rocks is at a depth of about 4 km from the surface [Combs and Hadley, 1977]. The

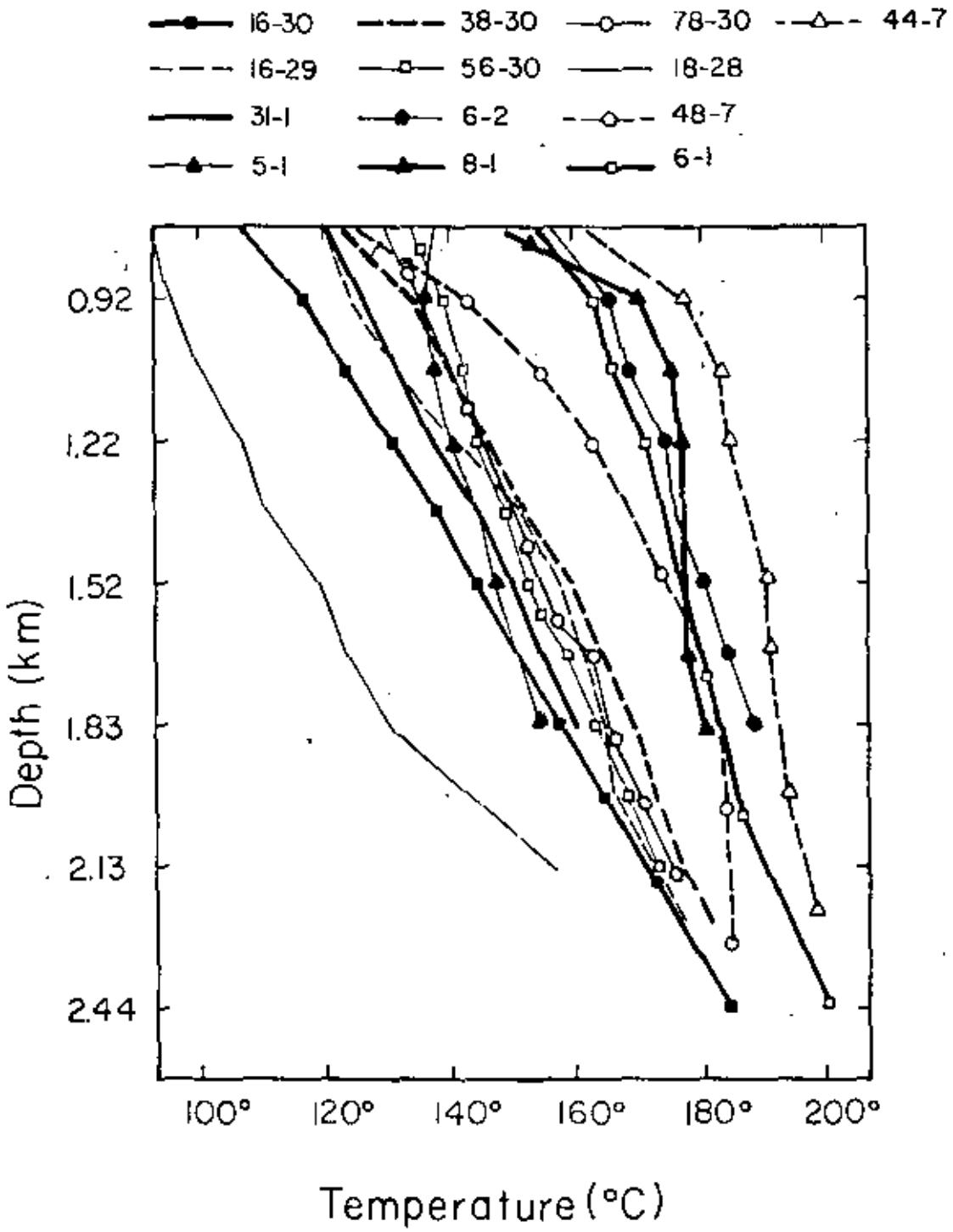


Figure 5. Temperature-depth profile for East Mesa wells below 800 meters depth.

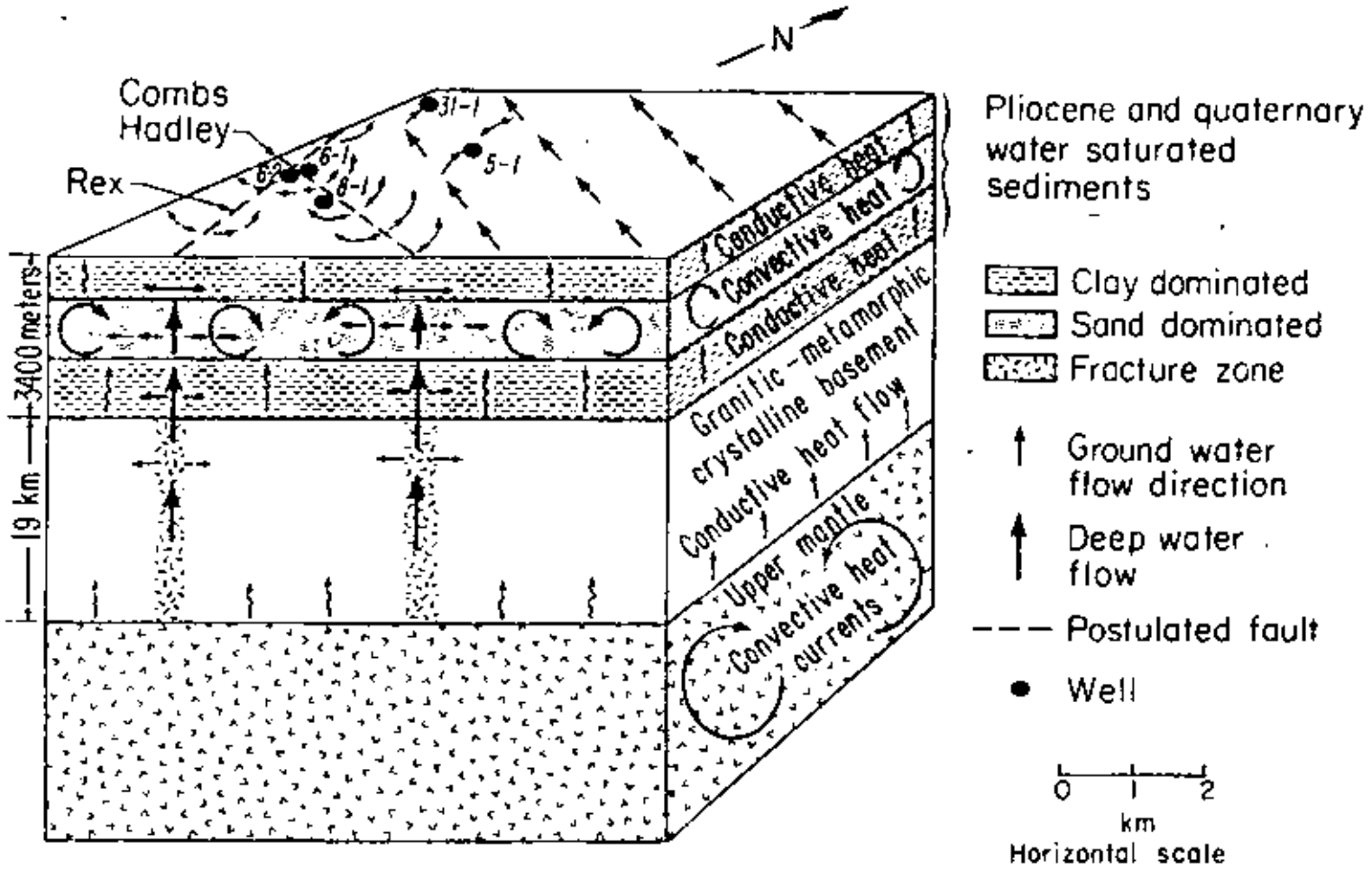


Figure 6. Conceptual model of the East Mesa anomaly. (Adapted from Bailey, [1977].)

basement complex is subjected to failure under adequate stresses. Fractures, once formed, would tend to be preserved in this high-strength rock. Nearly vertical tension fractures probably were the first to form during the evolution of the Salton Trough. These fractures would increase the vertical permeability much more than the horizontal permeability.

A shale-dominated zone overlies the basement. It is characterized by (1) steepening of the temperature profile in Mesa Well 6-1 below about 2100 meters depth, (2) an increase in percentage of shale and corresponding decrease in sands below 2200 m depth, and (3) marked change in salinities below 2200 m depth [Black, 1975]. This layer extends from the basement complex to about 1900-2200 m from the surface. Here the sediments are indurated by overburden and heat. They probably fracture, given any movement on the basement faults. The vertical permeability of these sediments is expected to be good near the fracture, but quite low away from it. The horizontal permeability in this layer is also thought to be only moderate because of the presence of clay and dirty sands.

Sands dominate the sedimentary zone from about 800 to 1900 m depth. Horizontal permeability in this zone is probably better than in the underlying material because of greater sand content and continuity and less compaction. Vertical permeability should be good near the fracture zones and in general should be better than in the underlying beds because of the greater amount of sand. Except near the fracture zones, relatively fresh water in this sand-dominated zone may be prevented from extensive mixing with more saline water in the sediments below by the restricted vertical permeability of the sediments in the lower zone.

The next 600 m or so of the sediments are dominated by clay. Fractures may form temporarily in these sediments with sudden differential motion, but under light loading, fractures in these beds would tend to close by slow flowage unless there are repeated fast movements. The vertical permeability is probably very low in these young sediments, but the numerous shallow wells in them indicate that their horizontal permeability is good.

The upper 200 m of the valley fill appears to have more sand and better porosity than the underlying zone. Vertical permeability is probably much higher than in the underlying zone. However, this zone and the underlying clay-dominated zone probably behave in similar ways when subjected to stress.

In summary, what vertical permeability exists in the lower four zones is due almost entirely to fractures, whereas, except in the vicinity of a fracture, horizontal flow in these zones is largely dependent upon intergranular permeability. The major source of fluid for southern Imperial Valley brines is the underflow from the Colorado River. This water percolates gradually into sediments and/or fractured basement rock over an area considerably larger than the anomaly itself. Heated at depth by an as yet undefined source, the liquid can rise in the high permeability fractured fault zone, convecting energy towards the surface. When a horizontal aquifer of relatively large permeability is intersected, reservoir charging will occur.

## MATHEMATICAL MODEL

The relative positions of the heat flux contours about the Mesa fault (Figure 2) tell us that the hot water rises up the fault and then spreads laterally losing heat to the surroundings. This idea is also

confirmed by the location of the charging plane A in Figure 4. If we consider a vertical front view at Section AA' of Figure 2, a two dimensional vertical model such as that given in Figure 7 would result. In this model, we have combined the upper two zones to represent a clay cap and the lower two zones to represent an aquifer. The fault is hypothesized to be a vertically oriented region of heavily fractured material of finite width ($2y_e'$). The vertical extent of the fault and its second horizontal dimension are large compared to its width. The fault extends downward through the clay-rich region (cap) of thickness $\ell'$, through the interbedded sediments of the reservoir for a distance L', and finally into the basement rock. It is postulated that the fault is charged at depth by liquid that has been heated in an extensive basement fractured system. The rate of charge cannot be obtained a priori without a global analysis of the entire convection process. The liquid rises up in the reservoir section of the fault. The presence of clays in the cap suppresses the vertical transport there. Water pushed out of the fault by the overpressure associated with convection is assumed to flow horizontally in the aquifer. The vertical transport should be less important, in large because of the presence of shaley layers associated with interbedding.

For mathematical purposes, the fracture zone is idealized as a vertical slab of porous medium. The adjacent aquifer is represented as a porous medium of lateral half width H' with horizontal permeability much larger than a vertical value of small absolute magnitude. The overlying clay cap is assumed to be impermeable. Spatially uniform temperature boundary conditions are imposed on the cold cap surface and at the hot

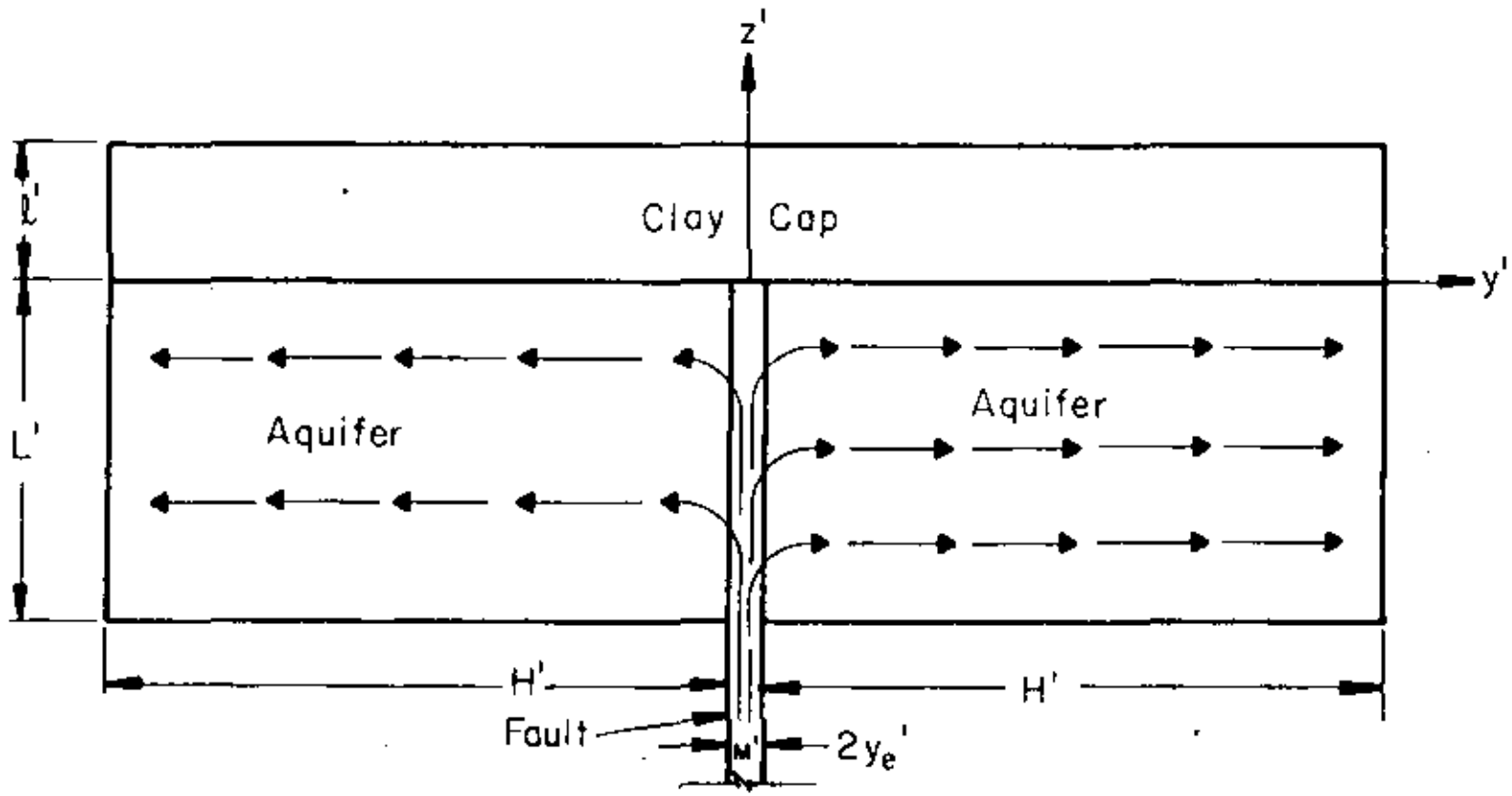


XBL 7811-6631

Figure 7. A two-dimensional mathematical model of the East Mesa anomaly.

bottom boundary of the reservoir. On the lateral boundary far from the fault ($H' \gg L' \gg y_e'$) the temperature distribution is assumed to be controlled by vertical conduction. The associated pressure distribution can be found once the density distribution is calculated. Finally, a horizontal mass flux is permitted in order to conserve matter.

A quasi-analytic theory is developed for high Rayleigh number convection of a liquid in a rigid porous medium. In this approximation liquid rises up the fault and spreads into the near regions of the reservoir adiabatically. The cooling effect of the cap in the reservoir is confined to a thin layer adjacent to the interface. The layer grows with distance from the fault. In the far field of the aquifer, the full depth of the reservoir is cooled by the surface.

A detailed derivation of the describing equations for a thermally active, saturated, and deformable porous material is given in Goyal (1978). The equations used here are obtained from that set by assuming that the flow is steady, the solid matrix is rigid, the fault medium is homogeneous and isotropic, liquid properties (except density) are constant, the thermal conductivities of the fault and aquifer media are constant and equal, the clay cap is impermeable, and that the vertical permeability in the aquifer is much smaller than the horizontal value, which is equal to that of the fault. Thus for all practical purposes vertical velocity in the aquifer is nearly zero. In addition, the Boussinesq approximation is invoked. The describing dimensional equations are:

Fault zone:

$$V'_{y'} + W'_{z'} = 0 \qquad (1)$$

$$v' = -\frac{K'}{\nu'} P'_{y'} \tag{2}$$

$$w' = \frac{K'}{\nu'} \{-(P' - P'_H)_{z'} + \alpha'(\rho' - \rho'_o)\} \tag{3}$$

$$C'_p \{v' T'_{y'} + w' T'_{z'}\} = \lambda'_m \{T'_{y'y'} + T'_{z'z'}\} \tag{4}$$

$$\rho' = \rho'_o [1 - \alpha'_e (T' - T'_o)] \tag{5}$$

Aquifer:

$$v'(z') = -\frac{K'}{\nu'} P'_{y'} \tag{6}$$

$$C'_p v' \theta'_{y'} = \lambda'_m (\theta'_{y'y'} + \theta'_{z'z'}) \tag{7}$$

Clay Cap:

$$\theta^{c'}_{y'y'} + \theta^{c'}_{z'z'} = 0 \tag{8}$$

where the variables are defined following equation (25). The solution of the above system is subjected to the following boundary and continuity conditions.

Boundary Conditions:

Fault Zone

$$w'(y',0) = 0 \qquad \text{impermeable upper boundary} \tag{9}$$

$$\int_{-y_{e'}}^{+y_{e'}} w'(y', -L')\, dy' = M', \qquad \text{input mass flow rate} \tag{10}$$

$$T'(y', -L') = T'_{max}, \qquad \text{hot lower boundary} \qquad (11)$$

$$T'_{y'}(0,z') = 0, \qquad \text{symmetry} \qquad (12)$$

Aquifer:

$$\theta'(y', -L') = T'_{max}, \qquad \text{hot lower boundary} \qquad (13)$$

$$\theta'(H', z') = T'_{ac} - (T'_{max} - T'_{ac}) \frac{z'}{L'}, \quad -L' \leq z' \leq 0, \text{ aquifer edge} \qquad (14)$$

where $T'_{ac}$ is the aquifer-clay cap interface temperature at the far field boundary and can be expressed as:

$$T'_{ac} = \frac{\lambda'_m \ell' T'_{max} + \lambda^{c'}_m L' T'_o}{\ell' \lambda'_m + L' \lambda^{c'}_m} \qquad (15)$$

Clay Cap:

$$\theta^{c'}(y', \ell') = T'_o, \qquad \text{cold upper boundary} \qquad (16)$$

$$\theta^{c'}_{y'}(0,z') = 0, \qquad \text{symmetry} \qquad (17)$$

$$\theta^{c'}(H', z') = T'_{ac} - (T'_{ac} - T'_o) \frac{z'}{\ell'}, \quad 0 \leq z' \leq \ell', \quad \text{clay cap edge} \qquad (18)$$

Continuity Conditions at the Fault-Aquifer Boundary:

$$T'(y'_e, z') = \theta'(y'_e, z') \qquad (19)$$

$$V'(\pm y'_e, z') = \pm v'(z') \qquad (20)$$

$$P'(y_e', z') = p'(y_e', z') \tag{21}$$

Continuity Conditions at the Fault-Clay Cap Boundary:

$$T'(y', 0) = \theta^{c'}(y', 0), \tag{22}$$

$$\lambda_m' T_{z'}'(y', 0) = \lambda_m^{c'} \theta_{z'}^{c'}(y', 0) \tag{23}$$

Continuity Conditions at the Aquifer-Clay Cap Boundary:

$$\theta'(y', 0) = \theta^{c'}(y', 0) \tag{24}$$

$$\lambda_m' \theta_{z'}'(y', 0) = \lambda_m^{c'} \theta_{z'}^{c'}(y', 0) \tag{25}$$

The dimensional variables are defined by:

$V'$ = horizontal Darcy mass flux in the fault per unit area, gm/cm$^2$-sec

$W'$ = vertical Darcy mass flux in the fault per unit area, gm/cm$^2$-sec

$K'$ = fault permeability and horizontal permeability in the aquifer, cm$^2$

$\nu'$ = kinematic viscosity, cm$^2$/sec

$P'$ = fault pressure, dynes/cm$^2$

$P_H'$ = cold hydrostatic pressure with respect to density $\rho_o'$, dynes/cm$^2$

$\rho_o'$ = density of the liquid at the ambient temperature $T_o'$, gm/cm$^3$

$\rho'$ = density of the liquid at the temperature $T'$, gm/cm$^3$.

$g'$ = acceleration due to gravity, cm/sec$^2$

$C_p'$ = specific heat of the liquid at constant pressure, cm$^2$/sec$^2$-$^\circ$K

$T'$ = fault temperature, $^\circ$K

$\lambda_m'$ = medium thermal conductivity of the fault and the aquifer, gm-cm/sec$^3$-$^\circ$K

$\alpha_e'$ = coefficient of thermal expansion of the liquid, /$^\circ$K.

$T_o'$ = ambient temperature, $^oK$

$v'$ = horizontal Darcy mass flux in the aquifer per unit area, $gm/cm^2$-sec

$p'$ = aquifer pressure, dynes/$cm^2$

$\theta'$ = aquifer temperature, $^oK$

$\theta^{c'}$ = clay cap temperature, $^oK$

$y_e'$ = semifault width, cm

$L'$ = depth of the reservoir, cm

$M'$ = mass flow rate per unit length in the direction perpendicular to the plane of paper, gm/cm-sec.

$T'_{max}$ = maximum temperature at the hot bottom boundary of the reservoir, $^oK$

$H'$ = width of the aquifer in the y'-direction, cm

$\ell'$ = thickness of the clay cap, cm

$\lambda_m^{c'}$ = medium thermal conductivity of the clay cap, gm-cm/$sec^3$-$^oK$.

In the fault, where the characteristic horizontal dimension and velocity component are much smaller than their vertical counterpart, the appropriate nondimensional variables can be defined as:

$$\bar{y} = y'/y_e', \quad y_e = y_e'/L', \quad z = z'/L'$$

$$\bar{V} = V'/y_e\, q_o'\, \rho_o', \quad W = W'/q_o'\, \rho_o', \quad T = T'/T_o' \tag{26}$$

$$\tau = (T'_{max} - T_o')/T_o', \quad P = (P' - P_H')/P_o'$$

Substitution of (26) into (1) to (5) leads to an inherent balance between the buoyancy, Darcy and pressure terms in the vertical momentum equation, if

$$q_o' = \frac{\alpha_e' \Delta T' \rho' K'}{\nu'} = \text{reference convection velocity}$$

$$p_o' = \rho_o' g' \alpha_e' L' \Delta T' = \text{reference convection pressure}$$

$$R = \frac{\rho_o' q_o' C_p' \Delta T'}{\lambda_m' (\Delta T'/L')} = \text{Rayleigh number} \qquad (27)$$

where $\Delta T' = T'_{max} - T'_o$

The non-dimensional equations, transformed boundary and continuity conditions relevant in the fault zone can be written as:

Fault Zone:

$$\bar{V}_{\bar{y}} + W_z = 0 \qquad (28)$$

$$y_e^2 \bar{V} = - P_{\bar{y}} \qquad (29)$$

$$W = - P_z + (T-1)/\tau \qquad (30)$$

$$\gamma^2(\bar{V}T_{\bar{y}} + WT_z) = T_{\bar{y}\bar{y}} + y_e^2 T_{zz} \qquad (31)$$

$$\gamma = y_e R^{\frac{1}{2}} \qquad (32)$$

$$W(\bar{y},0) = 0 \qquad (33)$$

$$W(\bar{y},-1) = M \qquad (34)$$

$$M = M'/M_o' \ , \ M_o' = 2y_e' \rho_o' q_o' \qquad (35a,b)$$

$$T(\bar{y},-1) = 1+\tau \qquad (36)$$

$$T_{\bar{y}}(0,z) = 0 \qquad (37)$$

$$T(\bar{y},0) = \theta^c(\bar{y},0) \qquad (38)$$

$$T_z(\bar{y},0) = \lambda\theta^c_z(\bar{y},0) \tag{39}$$

$$V(\pm 1,z) = \pm v(z) \tag{40}$$

where $\lambda$ is the ratio of the thermal conductivities of the cap and the aquifer. Equations (38) and (39) represent the continuity of temperature and heat flux at the boundary between clay cap and fault. In the aquifer, where the horizontal scale is measured by $\hat{y} = y'/H'$, the pressure $p = P$, the temperature $\theta = T$, and the velocity $v = V$, the appropriate system of equations is given by:

Aquifer:

$$v(z) = -p_{\hat{y}}/d \tag{41}$$

$$d\gamma^2 v(z)\theta_{\hat{y}} = y_e{}^2\theta_{\hat{y}\hat{y}} + d^2\theta_{zz} \tag{42}$$

where

$$H'/L' = d/y_e\,,\ d = O(1)\ \text{number} \tag{43a,b}$$

The magnitude of $H'$ with respect to the fault depth $L'$ in (43) is chosen to ensure a balance between the nondimensional aquifer velocity $v$ and the horizontal pressure gradient shown in (41). The number $d$, used in this study to define the location of the far-field boundary of the aquifer, will be determined by finding a location where the horizontal temperature gradient in the aquifer becomes vanishingly small. It may be emphasized that the horizontal motion exists at the far field boundary but the heat transfer is due to vertical conduction only. The nondimensional boundary and continuity conditions for the aquifer are:

$$\theta(\hat{y},0) = \theta^c(\hat{y},0) \tag{44}$$

$$\theta_z(\hat{y},0) = \lambda\theta^c_z(\hat{y},0) \tag{45}$$

$$\theta(\hat{y},-1) = 1+\tau \tag{46}$$

$$\theta\left(\hat{y} = \frac{y_e^2}{d}\ ,\ z\right) = T(\bar{y} = 1,\ z) \tag{47}$$

$$\theta(\hat{y} = 1,z) = 1 + \frac{\tau}{\lambda+\ell}\ (\ell - \lambda z),\ -1 \leq z \leq 0 \tag{48}$$

where $\ell = \ell'/L'$. Equations (44) and (45) represent the continuity of the temperature and the heat flux at the interface between the aquifer and the clay cap.

In the clay cap, where the temperature $\theta^c = \theta^{c'}/T'_o$, the energy equation, boundary, and continuity conditions are as follows:

$$y_e^2\ \theta^c_{\hat{y}\hat{y}} + d^2\theta^c_{zz} = 0 \tag{49}$$

$$\theta^c(\hat{y},\ell) = 1 \tag{50}$$

$$\theta^c_{\hat{y}}\ (0,z) = 0 \tag{51}$$

$$\theta^c(1,z) = 1 + \frac{\tau}{\lambda+\ell}\ (\ell-z),\ 0 \leq z \leq \ell \tag{52}$$

Temperature and heat flux continuity conditions between the fault and clay cap and also between aquifer and clay cap interfaces are already expressed in equations (38), (39), (44) and (45).

In order to proceed further we must consider the magnitude of the Rayleigh number and the parameter $\gamma$ associated with the East Mesa anomaly. The depth of the basement in this anomaly is about 4.15 km [Combs, 1977]. From well logs, one can assume the thickness of the clay cap ($\ell'$) to be 0.8 km. Thus the reservoir thickness ($L'$), consisting of both low and high permeability zones, equals to 3.35 km. The ratio ($\ell$) of cap thickness ($\ell'$)

to the reservoir depth (L') is thus equal to 0.238. The formation temperatures, based on Na-K-Ca geothermometry, are about 200°C ± 30°C [Bailey, 1977]. If the formation temperature ($T'_{max}$) is assumed to be 200°C, we find that the maximum temperature difference ($\Delta T'$) across the system is 175°C and the overheat ratio ($\tau$) is 0.587. The thermal conductivity of a geothermal reservoir depends on many factors such as its porosity, grain size, size distribution, physical properties of rocks and fluids, fluid saturation, temperature, and pressure. In the laboratory, the thermal conductivity of rock samples is found to increase with increasing liquid saturation [Somerton et al., 1974] and decreases with increasing temperatures [Martinez-Baez, 1978]. The thermal conductivities of the saturated sand stones were found to vary between $4 \times 10^{-3}$ to $6.4 \times 10^{-3}$ cal/cm-sec-°K in the Cerro Prieto geothermal field, Mexico [Martinez-Baez, 1978]. Besides being less than 50 km apart, East Mesa and Cerro Prieto fields both lie in the Colorado River delta stratigraphic system. Thus the physical properties of the sediments in the two systems are not expected to vary much and so we assume an average thermal conductivity ($\lambda'_m$) value of $4.91 \times 10^{-3}$ cal/cm-sec-°K for the reservoir part of the East Mesa system. Measured thermal conductivity values of unconsolidated sands, silts and clays in the upper 40 to 150 meters range from $2.48 \times 10^{-3}$ to $3.88 \times 10^{-3}$ cal/cm-sec-°K [Combs, 1972]. Thus an average thermal conductivity ($\lambda^{c}_{m}$') of $3.44 \times 10^{-3}$ cal/cm-sec-°K is assumed for the clay cap of the East Mesa system. This data leads to a thermal conductivity ratio ($\lambda$) of 0.7.

The permeability values obtained from the log analysis for the Republic geothermal wells ranged from 68.8 md to 941.3 md at a depth interval of 1524 m to 2134 m [Smith, 1979]. A drastic decrease in the permeability values was noted below this depth interval. Based on well test analysis, the permeabilities of the USBR wells ranged from 30 md to 84 md [Howard et al., 1978]. Thus we have assumed a representative value of 100 md ($K' = 10^{-9} cm^2$) for the permeability in the East Mesa area. If the thermodynamic variables evaluated at $T'_o = 298^oK$ are used in (27) and (35b) we find that

$q'_o = 0.43$ cm/day

$p'_o = 14.7$ atm

$R = 338.$

For a fault width of 230 m, as calculated later in this paper, we find from (35b) that $M_o' = 9.89 \times 10^5$ kg/day-km.

The local values of the above parameters may be 10 to 20 times higher if the local values of the physical properties are used. The Rayleigh number is also sensitive to the changes in permeability. The large values of R suggest that the energy transfer associated with liquid convection is far greater than that due to conduction. In this regard one may expect that fluid particles moving through the system will tend to behave isothermally unless affected by cooling associated with a relatively cold boundary.

It is possible to calculate the fault width based on energy transfer considerations as follows:

energy convected upward in the fault, per unit area $E'_{conv} = \rho' q'_o e'$

where e' is the internal energy of the liquid flowing in the fault. For an average temperature of 200°C in the fault, the convected energy is about $10^7$ cal/sec-km$^2$. In contrast, for a normal temperature gradient of 30°C/km, heat conducted through the clay cap is about $10^4$ cal/sec-km$^2$. Thus the convected energy is about 3 orders of magnitude larger than the purely conductive flux. The temperature drop experienced by the fluid in moving from Mesa well 6-2 to 5-1 is about 10% in the convection-dominated zone (Figure 5). Thus for a 10% energy loss to the surroundings, total heat lost through the cap is equal to $A_F' \times 10^6$ cal/sec where $A_F'$ is the area of fault in km$^2$. This quantity, when measured from the contours of Figure 2 is $4.88 \times 10^6$ cal/sec crossing an area of 110 km$^2$. Upon equating these quantities, one can then obtain the horizontal fault zone area ($A_F'$) of 4.88 km$^2$. Since the thermal activity of the Mesa field extends along the primary fault for about 21 km, a fault (fracture zone) width ($2y_e'$) of 230 m is suggested. Morrison et al. [1979] came up with a fault width of 300 to 600 m based on their self potential study. It may be noted that the Mesa well 44-7, located at the intersection of the Rex and Babcock faults (Figure 2) is the hottest in the field (Figure 5). This suggests that the Mesa fault is not the only fault contributing to this anomaly. Thus one should recognize that the suggested fault width is an order-of-magnitude estimate. Given the variable nature of input, a range $50 \text{ m} < y_e' < 150 \text{ m}$ might be appropriate. If the characteristic permeability were far smaller than $10^{-9}$cm$^2$, the fault zone area estimate would be far larger and thus not representative of the relatively localized anomalous properties of the Mesa field.

The parameter $\gamma$ is assumed to be an O(1) number because $y_e$ is considered small. For instance, a value of 0.034 is obtained for $y_e$ and 0.63

for Y if the previously discussed data of East Mesa is used. In the mathematical analysis, solutions are sought in the limit of large R with $Y = O(1)$, implying, of course, that $y_e$ is small.

Above the fault the cooling effect of the cap is confined to a thin thermal-boundary layer adjacent to the cap-fault interface, for a high Rayleigh number flow. The cooled boundary layer thickness increases as the fluid moves horizontally away from the fault. Beneath the boundary layer, the flow is isothermal. In the far field, the surface cooling effect influences the temperature distribution throughout the aquifer depth.

It can be noted from (29) that the horizontal pressure gradient in the fault is very small, $O(y_e^2)$. Thus the basic fault pressure is only a function of depth and can be calculated in terms of W or v. The horizontal aquifer velocity distribution v(z) can then be calculated explicitly from (41) because far-field pressure is known once (14) and (18) are specified. Upon decoupling the fluid mechanics from the thermal problem, the energy equations (42) and (49) can be solved for temperatures in the aquifer and the clay cap respectively, ensuring the continuity of the temperature and heat flux at the interface. To determine the temperatures, the fault aquifer system is divided into seven regions as shown in Figure 8. The solution procedure is similar to that used in Goyal and Kassoy [1980] to describe the capless system.

First we obtain the basic temperatures in the fault and near fault regions of the aquifer (regions 1 to 4). With the interface temperatures known, we then calculate the lowest-order temperatures in region 6 of the clay cap. To ensure the continuity of the heat flux at the interface, we then calculate the boundary layer temperature corrections in regions 1 and 3.

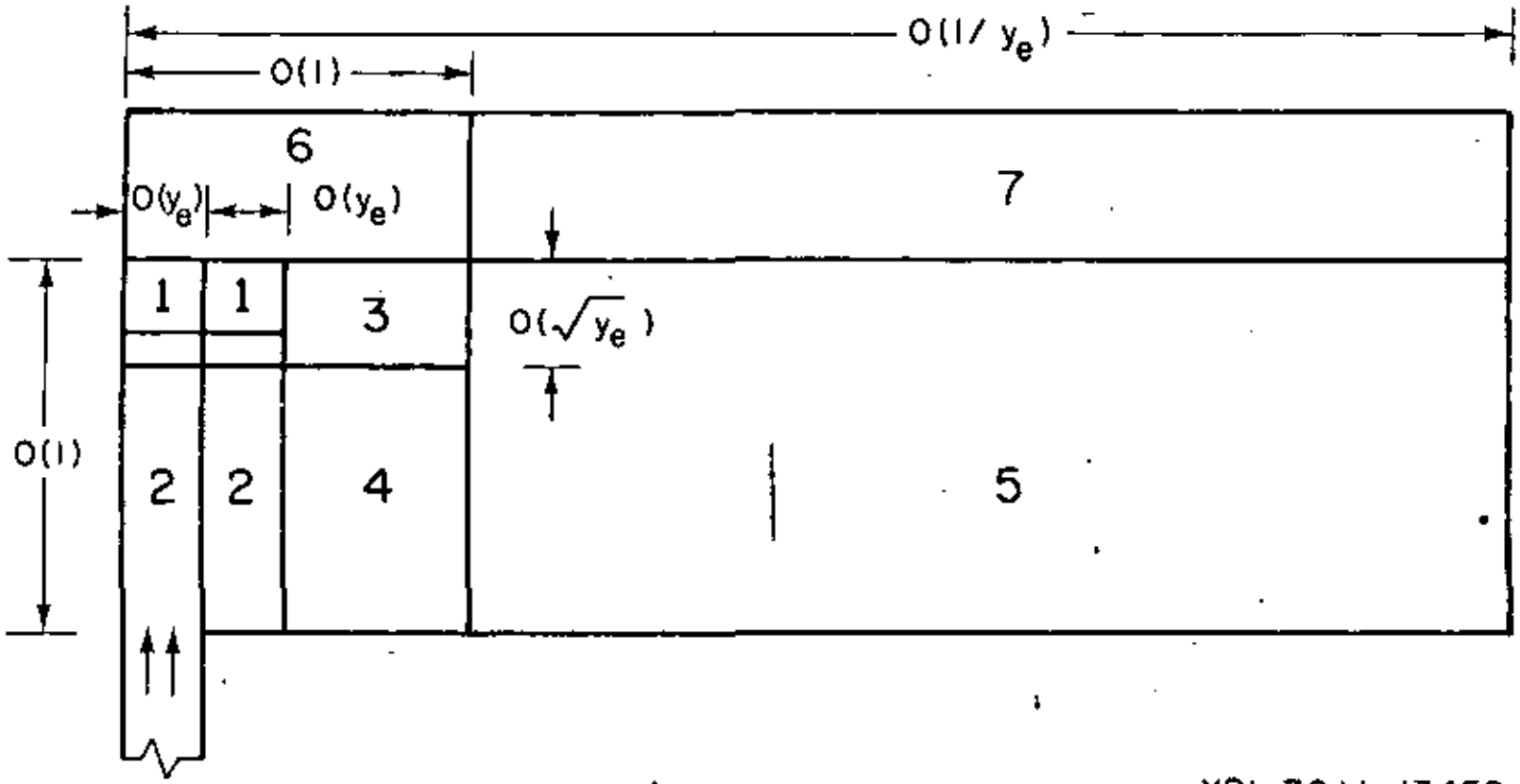


Figure 8. Seven different regions in the fault-aquifer system.

Temperatures in regions 5 and 7 are subsequently obtained for $\hat{y} \to 0$. With these known initial conditions, equations (42) and (49) are solved numerically in regions 5 and 7 for continuous heat flux and temperature at the interface.

## FAULT ZONE SOLUTION

The presence of the clay cap over the fault-aquifer system acts as an insulator that reduces the heat transfer to the surface relative to a capless system. The basic temperature of the hot liquid rising in the fault at a high Rayleigh number will remain at the supply temperature. Since the cooling can occur only through the cap, the lowest order temperatures in regions 1,2,3 and 4 of the aquifer are also expected to be equal to that in the fault. Once the temperatures in the fault zone are known, solutions for pressures and velocities in the fault and aquifer are calculated in a manner similar to Goyal and Kasaoy [1980]. In this case equations (29) and (30) are solved to obtain a relation between W and P to the lowest order. It turns out that to this order both P and W are functions of z only. A relation between aquifer velocity v and vertical fault velocity W can be obtained from the mass conservation equation (28). Finally, equations (41) and (48) can be used to determine a relation between fault pressure P and aquifer velocity v. It can be noted that equation (48) is used to determine the hydrostatic pressure at the far-field boundary of the field. Three relations thus obtained, can be used to form a second order ordinary differential equation in terms of W, and the equation can then be solved for boundary conditions (33) and (34). Once W is known, P and v can then be obtained from the relations mentioned above.

The basic solutions of the fault-aquifer system are:

$$T = 1 + \tau \tag{53}$$

$$\bar{V} = \bar{y} \left\{ a_2 \cosh \frac{z}{\sqrt{d}} + b_2 \sinh \frac{z}{\sqrt{d}} - \frac{\lambda}{\lambda+\ell} \right\} + O(y_e^2), \tag{54}$$

$$W = -a_2\sqrt{d} \sinh \frac{z}{\sqrt{d}} + b_2 \sqrt{d} \left(1 - \cosh \frac{z}{\sqrt{d}}\right) + \frac{\lambda z}{\lambda+\ell} + O(y_e^2) \tag{55}$$

$$P = d \left\{ a_2 \cosh \frac{z}{\sqrt{d}} + b_2 \sinh \frac{z}{\sqrt{d}} - \frac{\lambda}{\lambda+\ell} \right\} - \frac{\ell^2 - 2\ell z + \lambda z^2}{2(\lambda+\ell)} + O(y_e^2) \tag{56}$$

$$v(z) = a_2 \cosh \frac{z}{\sqrt{d}} + b_2 \sinh \frac{z}{\sqrt{d}} - \frac{\lambda}{\lambda+\ell} + O(y_e^2) \tag{57}$$

$$p = v(z)d(1-\hat{y}) - \frac{\ell^2 - 2\ell z + \lambda z^2}{2(\lambda+\ell)} + O(y_e^2) \tag{58}$$

where

$$a_2 = \frac{1 + \frac{\lambda}{\lambda+\ell} \cosh \frac{1}{\sqrt{d}}}{\sqrt{d} \sinh \frac{1}{\sqrt{d}}}, \quad b_2 = \frac{\lambda}{\sqrt{d}(\lambda+\ell)} \tag{59a,b}$$

It may be noted that $\left(- \frac{\ell^2 - 2\ell z + \lambda z^2}{2\lambda + 2\ell}\right)$ represents the pressure at the far field boundary of the aquifer and is consistent with the specified temperature field (48). It may also be observed that the temperatures given by (53) are only valid in regions 2 and 4 of figure 8. Once the fault temperature is known, one can calculate the basic temperatures in region 6 of the clay cap from the system of equations (91) to (95). The result is given by (96). The continuity of heat flux at the horizontal interface between the fault and the clay cap implies the necessity of a thermal boundary layer near the top of the fault. If the appropriately scaled variables

$$\bar{z} = \frac{z}{y_e} \quad \text{and} \quad \bar{w} = \frac{w}{y_e} \tag{60a,b}$$

are used in the basic fault-zone equations then the lowest order boundary layer system has the form:

$$\bar{v}_{o\bar{y}} + \bar{w}_{o\bar{z}} = 0 \tag{61}$$

$$P_{1\bar{y}} = 0 \tag{62}$$

$$\frac{T_o - 1}{\tau} - P_{1\bar{z}} = 0 \tag{63}$$

$$\gamma^2\left(\bar{v}_o T_{o\bar{y}} + \bar{w}_o T_{o\bar{z}}\right) = T_{o\bar{y}\bar{y}} + T_{o\bar{z}\bar{z}} \tag{64}$$

However, it can be seen that the lowest order fault temperature $T_o$ and pressure $P_o$ are constant and when matched with the outer solutions (53) and (56) one finds that

$$T_o = 1 + \tau \tag{65}$$

$$P_o = d\left(a_2 - \frac{\lambda}{\lambda+\ell}\right) - \frac{\ell^2}{2(\lambda+\ell)} \tag{66}$$

Equation (65) satisfies the energy equation (64) identically. The solution to the system of equations (61) to (63) is subjected to the following boundary, matching, and continuity conditions.

$$\bar{v}_o(\pm 1, \bar{z}) = \pm v_o(\bar{z}) \quad \text{[equation (84)]} \tag{67}$$

$$\bar{w}_o(\bar{y}, \bar{z} \to -\infty) = -\left(a_2 - \frac{\lambda}{\lambda+\ell}\right)\bar{z} \tag{68}$$

$$T_1(\bar{y}, \bar{z} \to -\infty) = \bar{z} \tag{69}$$

It may be noted that the matching conditions ($\bar{z} \to -\infty$) are obtained from the outer solutions (55) and (56) respectively. The solutions to this system for all values of $\bar{y}$ and $\bar{z}$ are equal to those expressed by the matching conditions (67) to (69). This occurs because the boundary layer is required to smooth a discontinuous derivative of T rather than the function itself. The describing system for the $O(y_e)$ terms is

$$\bar{v}_{1\bar{y}} + \bar{w}_{1\bar{z}} = 0 \qquad (70)$$

$$-\gamma^2 \left(a_2 - \frac{\lambda}{\lambda+\ell}\right) \bar{z} \frac{dT_1}{d\bar{z}} = \frac{d^2T_1}{d\bar{z}^2} \qquad (71)$$

The momentum equations in y and z directions can be used to show that $T_1$ is only a function of $\bar{z}$. The associated matching and boundary conditions for the system of equations (70) and (71) are

$$\bar{v}_1 (\pm 1, \bar{z}) = \pm v_1(\bar{z}) \qquad \text{[equation (89)]} \qquad (72)$$

$$\bar{w}_1(\bar{y}, \bar{z} \to -\infty) = -\frac{b_2 \bar{z}^2}{2\sqrt{d}} \qquad (73)$$

$$\frac{dT_1}{d\bar{z}} (\bar{y}, 0) = -\frac{\tau\lambda}{\ell} \qquad \text{[equation (96)]} \qquad (74)$$

$$T_1(\bar{y}, \bar{z} \to -\infty) = 0 \qquad (75)$$

It may be noted that (74) implies continuity of heat flux at the horizontal interface between fault and clay cap. The solutions to the system (70) to (75), when added to O(1) solutions (65) to (69) form the complete solutions for the boundary layer, as follows:

$$\bar{V} = \left(a_2 - \frac{\lambda}{\lambda+\ell}\right)\bar{y} + y_e \frac{b_2 \bar{y}\bar{z}}{\sqrt{d}} + O(y_e^2) \tag{76}$$

$$\bar{W} = -\left(a_2 - \frac{\lambda}{\lambda+\ell}\right)\bar{z} - y_e \frac{b_2 \bar{z}^2}{2\sqrt{d}} + O(y_e^2) \tag{77}$$

$$P = d\left(a_2 - \frac{\lambda}{\lambda+\ell}\right) - \frac{\ell^2}{2(\lambda+\ell)} + y_e\,\bar{z} + O(y_e^2) \tag{78}$$

$$T = 1 + \tau - ye\,\frac{\sqrt{\Pi\tau\lambda}}{2B\ell}\left[1 + \operatorname{erf}(B\bar{z})\right] + O(y_e^2) \tag{79}$$

where

$$B = \sqrt{\frac{\gamma^2}{2}\left(a_2 - \frac{\lambda}{\lambda+\ell}\right)} \tag{80}$$

The thermal boundary layer initiated at the top of the fault continues into the adjacent aquifer over a horizontal distance to scale $y_e'$. In this initial aquifer zone of water cooling, the relevant lowest order equation for the velocity and pressure field is

$$v_o(\bar{z}) = -\frac{p_{o\bar{y}}}{d} \tag{81}$$

the appropriate boundary and continuity conditions are

$$p_o(\bar{y} \to 0, \bar{z}) = P_o(\bar{y} = 1, \bar{z}) = d\left(a_2 - \frac{\lambda}{\lambda+\ell}\right) - \frac{\ell^2}{2(\lambda+\ell)} \quad \text{[equation (66)]} \tag{82}$$

$$p_o(1,\bar{z}) = \quad -\frac{\ell^2}{2(\lambda+\ell)} \tag{83}$$

The solution forms are

$$v_o(\bar{z}) = \left(a_2 - \frac{\lambda}{\lambda+\ell}\right) \tag{84}$$

$$p_o(\hat{y},\bar{z}) = (1-\hat{y})d\left(a_2 - \frac{\lambda}{\lambda+\ell}\right) - \frac{\ell^2}{2(\lambda+\ell)} \tag{85}$$

The aquifer momentum equation, describing $0(y_e)$ terms is

$$v_1(\bar{z}) = -\frac{p_{1\hat{y}}}{d} \tag{86}$$

The appropriate boundary and continuity conditions are

$$p_1(\hat{y} \to 0,\bar{z}) = p_1(\bar{y} = 1,\bar{z}) = \bar{z} \text{ , [ from equation (69) ]} \tag{87}$$

$$p_1(\hat{y} = 1,\bar{z}) = \frac{\ell\bar{z}}{(\lambda+\ell)} \tag{88}$$

The solutions to the system (86) to (88) when added to 0(1) solutions (84) and (85) give the following complete solutions in the aquifer boundary layer.

$$v(\bar{z}) = \left(a_2 - \frac{\lambda}{\lambda+\ell}\right) + y_e \frac{b_2}{\sqrt{d}}\bar{z} + 0(y_e^2) \tag{89}$$

$$p(\hat{y},\bar{z}) = d\left(a_2 - \frac{\lambda}{\lambda+\ell}\right)(1-\hat{y}) - \frac{\ell^2}{2(\lambda+\ell)} + y_e\left[b_2\sqrt{d}\,\bar{z}\,(1-\hat{y}) + \frac{\ell\bar{z}}{\lambda+\ell}\right] + 0(y_e^2) \tag{90}$$

It is observed that the boundary layer solutions [equations (89) and (90)] match with the outer solutions [equations (57) and (58)].

## TEMPERATURES IN THE CLAY CAP

The lowest-order energy equation, in the region 6 where the length scale is of $O(L')$, is given as follows:

$$\theta^c_{oyy} + \theta^c_{ozz} = 0 \tag{91}$$

where $y = y'/L'$ (92)

The appropriate boundary conditions are;

$$\theta^c_{oy}(0,z) = 0 \quad , \qquad \text{symmetry} \tag{93}$$

$$\theta^c_o(y,\ell) = 1 \quad , \qquad \text{cold top boundary} \tag{94}$$

$$\theta^c_o(y,0) = 1 + \tau, \quad y = 0\ (1)\ , \quad \text{bottom boundary} \tag{95}$$

where

$\theta^c_o(y \to \infty, z)$ is well behaved.

The symmetry condition in (93) implies that the complete temperature solution is given by the elementary form,

$$\theta^c_o(z) = 1 + \tau\left(1 - \frac{z}{\ell}\right) \tag{96}$$

The higher-order temperature distributions in the clay cap above the fault can be calculated in a manner similar to equations (91) to (96) if the higher-order interface temperatures are known. The interface temperature between clay cap and fault can be obtained from $O(y_e)$ terms of equation (79). The temperature solution in the clay cap for $|\bar{y}| \leq 1$ is given as follows,

$$\theta^c(y,z) = 1 + \tau\left(1 - \frac{z}{\ell}\right) - y_e \frac{\sqrt{\Pi\tau\lambda}}{2R\ell}\left(1 - \frac{z}{\ell}\right) + O(y_e^2) \tag{97}$$

The temperature in region 6 of the clay cap for all values of y, which is compatible with that in region 3 of the aquifer, can be written as:

$$\theta^c(y,z) = 1+\tau\left(1 - \frac{z}{\ell}\right) + y_e^{1/2}\sqrt{\frac{2}{\pi}}\frac{\tau\lambda}{R\ell}\,\theta_1^c\,(y,z) + O(y_e) \tag{98}$$

where $\theta_1^c$ is given by following Laplace equation and boundary conditions.

$$\theta^c_{1yy} + \theta^c_{1zz} = 0 \tag{99}$$

$$\theta^c_1(y,\ell) = 0 \tag{100}$$

$$\theta^c_1(y,0) = - y^{1/2} \tag{101}$$

$$\theta^c_1\ (y \to 0,\ z) = 0 \tag{102}$$

$\theta^c_1\ (y \to \infty,\ z)$ increases algebraically at most.

Equation (101) represents the interface temperature between aquifer region 3 and the clay cap. Equation (102) shows that the terms of $O\ (y_e^{1/2})$ disappear for $y \to 0$ as evident from (97).

The solution to the system of equations (99) to (102), obtained by using a Fourier sine integral transform with respect to y, is given as follows:

$$\theta^c_1\ (y,z) = -\frac{1}{2\ell}\left[\int_0^\infty \frac{\sin\frac{\pi}{\ell}(\ell-z)\ \zeta^{1/2}\,d\zeta}{\cosh\frac{\pi}{\ell}\left(|y-\zeta|\right) + \cos\frac{\pi}{\ell}\ (\ell-z)}\right.$$

$$- \int_0^{\infty} \frac{\sin \frac{\Pi}{\ell}(\ell-z)\, \zeta^{1/2} d\zeta}{\cosh \frac{\Pi}{\ell}(y+\zeta) + \cos \frac{\Pi}{\ell}(\ell-z)} \Bigg] \qquad (103)$$

A series solution, also obtained for the above system, can be written as

$$\theta_1^c(y,z) = \frac{1}{\ell} \sum_{n=1}^{\infty} \frac{1}{(-1)^n} \sin \frac{n\Pi}{\ell}(\ell-z) \int_0^{\infty} \zeta^{1/2} \left[ \exp\left\{ - \frac{n\Pi}{\ell}(|y-\zeta|) \right\} - \exp\left\{ - \frac{n\Pi}{\ell}(y+\zeta) \right\} \right] d\zeta \qquad (104)$$

An asymptotic solution for large values of y can be obtained directly from the system of equations (99) to (102). The same solution can also be developed by expanding (104) for $y \to \infty$. Substitution of such a solution in (98) results in the following expression for clay cap temperature:

$$\theta^c (y \to \infty, z) = 1 + \tau\left(1 - \frac{z}{\ell}\right) + y_e^{1/2} \sqrt{\frac{2}{\Pi}} \frac{\tau\lambda}{R\ell} \left[ -y^{1/2}\left(1 - \frac{z}{\ell}\right) + \frac{1}{24y^{3/2}} \left(-3z^2 + \frac{z^3}{\ell} + 2\ell z\right) + O\left(\frac{1}{y^{7/2}}\right) \right] + O(y_e) \qquad (105)$$

The temperatures in region 7 of the clay cap can be obtained by solving equation (49). Besides equation (50), another boundary condition is as follows.

$$\theta^c(\hat{y},0) = \theta_m(\hat{y}) \qquad (106)$$

where $\theta_m(\hat{y})$ is the interface temperature between the clay cap region 7 and region 5 of the aquifer. $\theta_m(\hat{y})$ is calculated numerically at each step of $(\hat{y})$ for continuous heat flux and temperature at the interface. The O(1) temperature solution in this region is:

$$\theta^c(\hat{y},z) = \theta_m(\hat{y}) + \frac{z}{\ell}\left[1-\theta_m(\hat{y})\right] \tag{107}$$

The temperatures in region 7 compatible with equation (105) can be obtained from (107) for small values of $\hat{y}$. The resulting expression is:

$$\theta^c(\hat{y}+0,\ z) = 1 + \tau\left(1-\frac{z}{\ell}\right) - \sqrt{\frac{2d\hat{y}}{\Pi}}\ \frac{\tau\lambda}{B\ell}\left(1-\frac{z}{\ell}\right) + O(\hat{y}) \tag{108}$$

## TEMPERATURE DISTRIBUTION IN THE AQUIFER

Once the velocity field in the aquifer is known the temperatures can be calculated from the energy equation. This must be done for five different regions shown in Figure 8. Since the effect of the surface cooling is limited to the boundary layer regions 1 and 3, the flow in regions 2 and 4 is isothermal. The solution structure in aquifer region 1 for $1 < \bar{y} < \infty$ appears to be more complex and will not be considered further because reasonable progress can be made without it. For all practical purposes, temperatures in aquifer region 1 can be assumed to be equal to those in fault region 1. The equation describing the thermal boundary layer in region 3 is:

$$\gamma^2\, v(z^*)\theta_y = y_e\ \theta_{yy} + \theta_{z^*z^*} \tag{109}$$

where

$$z^* = \frac{z}{y_e^{1/2}} \tag{110}$$

A similarity solution, compatible with equation (96) can be obtained for region 3. Elementary methods yield

$$\theta(y,z^*) = 1+\tau - \left(\frac{2yy_e}{\Pi}\right)^{1/2}\frac{\tau\lambda}{B\ell}\left[\sqrt{\frac{\Pi}{2}}\,B\eta\left\{1+\mathrm{erf}\left(\frac{B}{\sqrt{2}}\,\eta\right)\right\}\right.$$

$$+ e^{-\frac{B^2\eta^2}{2}}\Bigg] + O(y_e), \quad \eta = \frac{z^*}{y^{1/2}} \qquad (111a,b)$$

It is possible to obtain an analytical solution of (42) in region 5, when $\hat{y} \ll 1$, and $z \ll 1$ such that $\frac{z}{\hat{y}^{1/2}} = O(1)$, which can be matched with (111a). We find the form

$$\theta(\hat{y},z) = 1 + \tau - \sqrt{\frac{2d\hat{y}}{\Pi}}\frac{\tau\lambda}{B\ell}\left[\frac{Bz}{\hat{y}^{1/2}}\sqrt{\frac{\Pi}{2d}}\left\{1 + \text{erf}\left(\frac{B}{\sqrt{2d}}\frac{z}{\hat{y}^{1/2}}\right)\right\}\right. \qquad (112)$$

$$\left. + e^{-\frac{B^2z^2}{2d\hat{y}}}\right] + O(\hat{y})$$

by using coordinate expansion methods.

The energy equation in (42), parabolic to the lowest order, must be solved subject to the boundary conditions in equations (45), (46) and (106) and the initial condition $\theta(\hat{y} \to o,z) = 1 + \tau$ for $|z| > 0$ obtained from matching with region 4. The last formal condition at the far end of the aquifer, (48) is used to determine a value of d. Numerical integration by standard finite difference methods is carried out for assumed values of d until the solution at the far edge is within 1% of the real condition and the heat flux and temperatures at the interface are continuous. This approximation provides an engineering type estimate of the boundary location. At that point, convection of energy associated with the $\theta_{\hat{y}}$ - term in (42) is very small compared to the conduction term. Of course, in the formal mathematical sense, the purely conductive profile can be found only for $\hat{y} \to \infty$. From the mathematical viewpoint, the reduction of the full-elliptic problem in the far-field aquifer to the parabolic system in (42) permits a simplified numerical computation procedure. The fact that

the reduction can be developed in a formal, rational manner for the large Rayleigh number approximation shows that the imposition of the far-field boundary condition at an a priori specified location is fundamentally unsound. That means, in physical terms, that the thermal anomaly associated with the upward fault zone flow has a natural horizontal relaxation length, associated basically with the distance required to transfer out of the surface, heat in excess of that arising from the natural geothermal gradient $\Delta T'/(\ell'+L')$. A quantitative indication of this matter involves the evaluation of d.

It is found that d is different for different sets of parameters as listed in Table 1. It can be observed from this table that an increase in M, R, $\tau$ or $y_e$ increases d. Most notably, cases IV, I, V and VI in Table 1 show that d increases nearly linearly with growth in M, at least for $0.5 \leq M \leq 3$. It is clear that a longer aquifer is needed for the transition to the conduction temperature profile when any parameter except $\lambda$ in Table 1 is increased. In physical terms this result implies that the hot isothermal portions of the aquifer, maintained by horizontal convection effects, will be more extensive in systems of relatively larger mass flow, permeability, temperature difference, and fault size. An increase in $\lambda$ is associated with a decrease in d. Faster convergence to the far-field boundary condition occurs because of increased cap heat transfer. A reduction in cap heat transfer caused by an increase in cap thickness implies that a longer aquifer (or increase in d) is required to stabilize the temperatures, as confirmed by Table 1.

Table,1. Values of d for Different Sets of Parameters

| Case No. | d | ℓ | λ | M | R | τ | $y_e$ |
|---|---|---|---|---|---|---|---|
| I | 0.24 | 0.24 | 0.7 | 1 | 500 | 1 | 0.025 |
| II | 0.28 | 0.50 | 0.7 | 1 | 500 | 1 | 0.025 |
| III | 0.22 | 0.24 | 1.0 | 1 | 500 | 1 | 0.025 |
| IV | 0.14 | 0.24 | 0.7 | 0.5 | 500 | 1 | 0.025 |
| V | 0.49 | 0.24 | 0.7 | 2 | 500 | 1 | 0.025 |
| VI | 0.74 | 0.24 | 0.7 | 3 | 500 | 1 | 0.025 |
| VII | 0.18 | 0.24 | 0.7 | 1 | 338 | 1 | 0.025 |
| VIII | 0.50 | 0.24 | 0.7 | 1 | 1000 | 1 | 0.025 |
| IX | 0.24 | 0.24 | 0.7 | 1 | 500 | 0.6 | 0.025 |
| X | 1.04 | 0.24 | 0.7 | 1 | 500 | 1 | 0.05 |
| XI | 0.32 | 0.24 | 0.7 | 1 | 338 | 0.6 | 0.034 |

## RESULTS AND THEIR COMPARISON WITH THE FIELD DATA

The distribution with depth of the nondimensional aquifer velocity and of temperature in the aquifer and clay cap are shown in Figures 9 to 12. Parameters used in these plots are those calculated previously for the East Mesa anomaly. In Figure 9 we observe a significant distribution with depth of the velocity in the aquifer. This configuration is determined by the vertical distribution of the horizontal pressure gradient in the aquifer. The gradient near the top of the aquifer is relatively large because of the stagnation point effect near the top of the fault zone. It should be noted that this result has been obtained for an aquifer at constant horizontal permeability. One may speculate that a reduction in deep permeability will reduce the high velocity in the lower portion of the system. The dimensional value of the mass flow rate per unit area can be obtained by multiplying the nondimensional velocity of Figure 9 by $y_e\, q'_o \rho'_o$ .

Figure 10 shows the variation of the aquifer and clay cap temperatures with depth at several horizontal locations for the parameter set shown. The value $\hat{y} = 1$ represents the far end of the aquifer, which is located at $(d/y_e)L' = (9.41)(3.35\text{km}) = 31.5$ km. Even at $\hat{y} = 0.6$ (18.9 km) the temperature profile is nearly at the conduction value. The temperature decreases with distance from the fault at a given depth in the aquifer which is a result of heat loss through the clay cap. It may be noted that at 10% out in the aquifer, the bottom 60% of the reservoir is still within about 94% of the high temperature value. A qualitative comparison of Figures 5 and 10 implies that the hot wells, 48-7, 6-1, 6-2, 8-1, and 44-7, are located in or near the fractured fault zone. Relatively flat temperature profiles in Mesa wells 8-1, 44-7, and 48-7 below about 0.95 km can be interpreted as resulting from the near-fault zone flow. It is important to recognize that

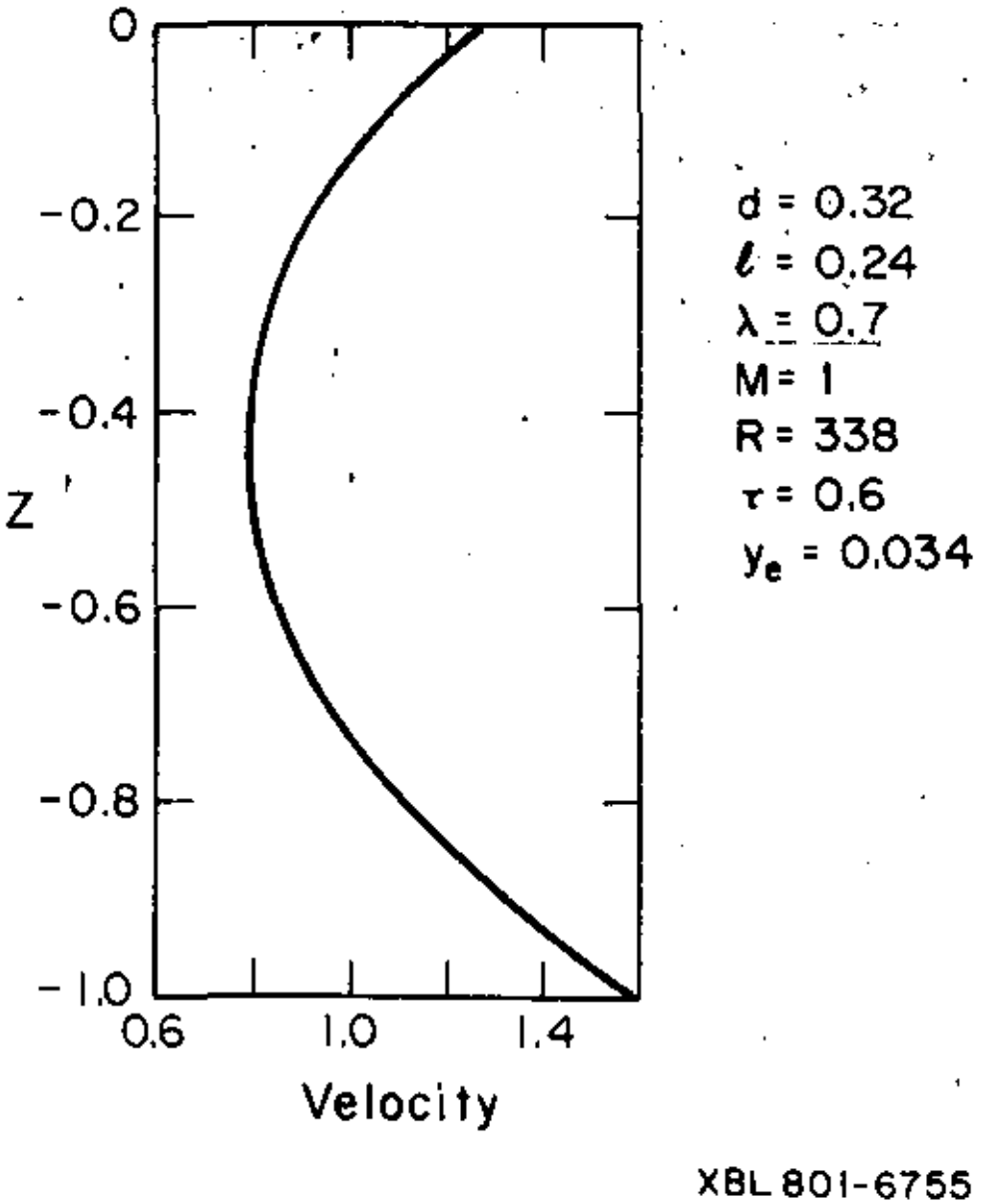


Figure 9. Horizontal velocities in the aquifer.

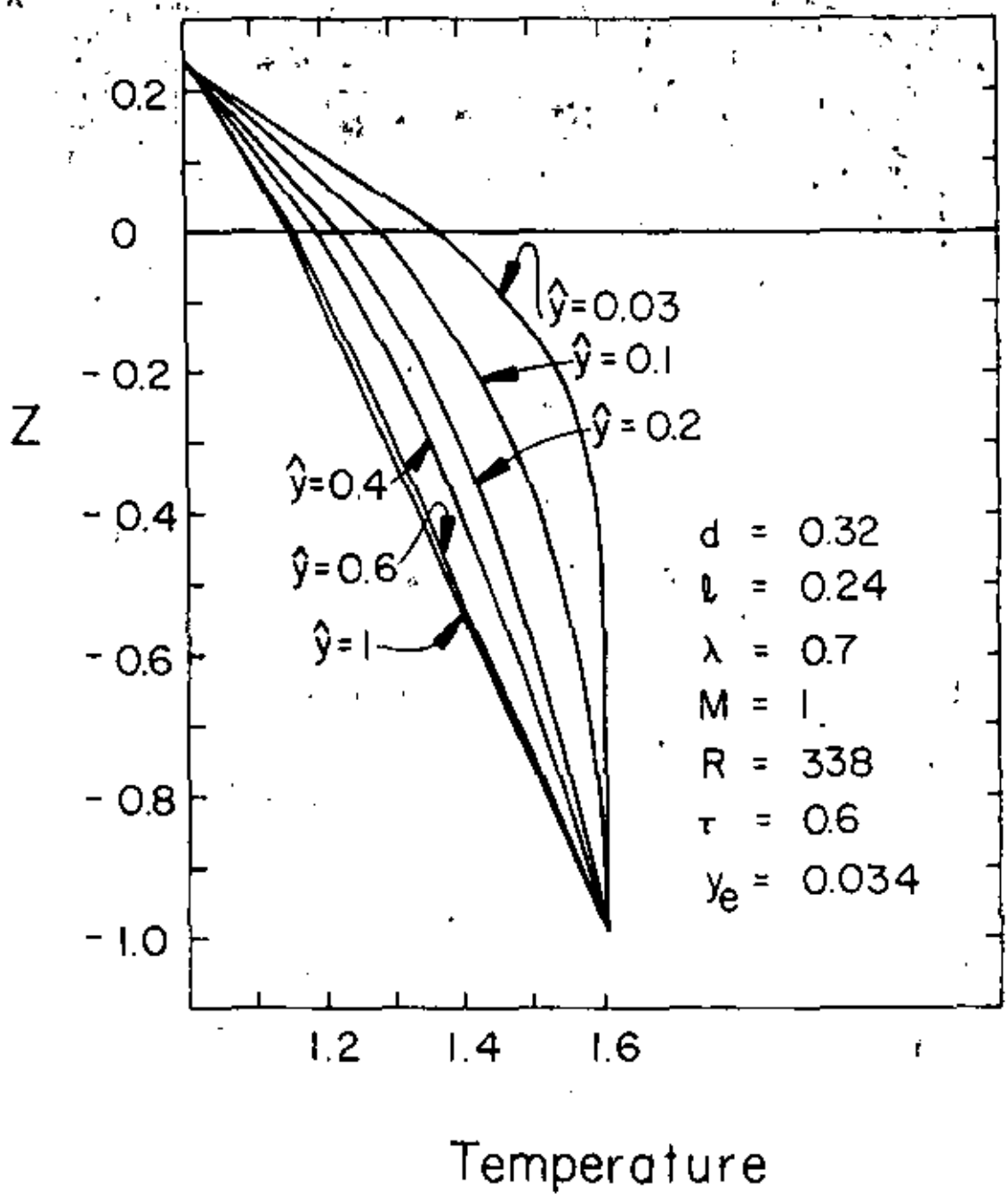


XBL 7811-6637A

Figure 10. Temperatures in the aquifer and clay cap for different values of $\hat{y}$.

these flat temperature profiles can occur in regions of purely horizontal flow as long as the bore is reasonably close to the hypothesized fault zone. One may observe from Figure 10 that even at $y_e = 0.1$ (3.15km) the lower part of the temperature profile is relatively flat. Temperature profiles for $y_e > 0.2$ (Figure 10) are similar to those of remaining wells in Figure 5, indicating that these wells are further away from the fracture zone. In particular well 18-28 is the farthest from any known fault zone. The nondimensional mass flux value M=1 corresponds to an input at the bottom of the fault of 11.44 kg/sec for each kilometer of horizontal extent. This value is quite similar to the estimate used by Riney et al., [1979a] in a recent study of the northwest lobe of the Mesa system. The isotherms corresponding to the temperatures of Figure 10 are shown in Figure 11. It is apparent in this figure that the horizontal temperature gradient decreases as the liquid moves away from the fault and becomes negligibly small near the far end. The near-fault isotherm values are calculated from the boundary layer solutions of regions 1, 3, and 6.

The temperature gradients at the cap surface are shown in Figure 12. The discontinuity in the curve arises because the solutions in aquifer regions 3 and 5 and clay cap regions 6 and 7 have been calculated to different orders of accuracy in the asymptotic analysis. It is found that an increase in M, R, $\tau$, and $y_e$ enhances the temperature gradients at the surface while an increase in $\ell$ and $\lambda$ decreases the temperature gradients there, as expected. In Figure 12 we see that the fault zone convection process enhances the surface heat flux by a factor of about 4 above the background conductive value. A similar ratio can also be obtained from Figure 2 where the near-fault heat transfer is about 8 heat flow units (HFU) compared to the background value of 1.5 to 2.0 HFU.

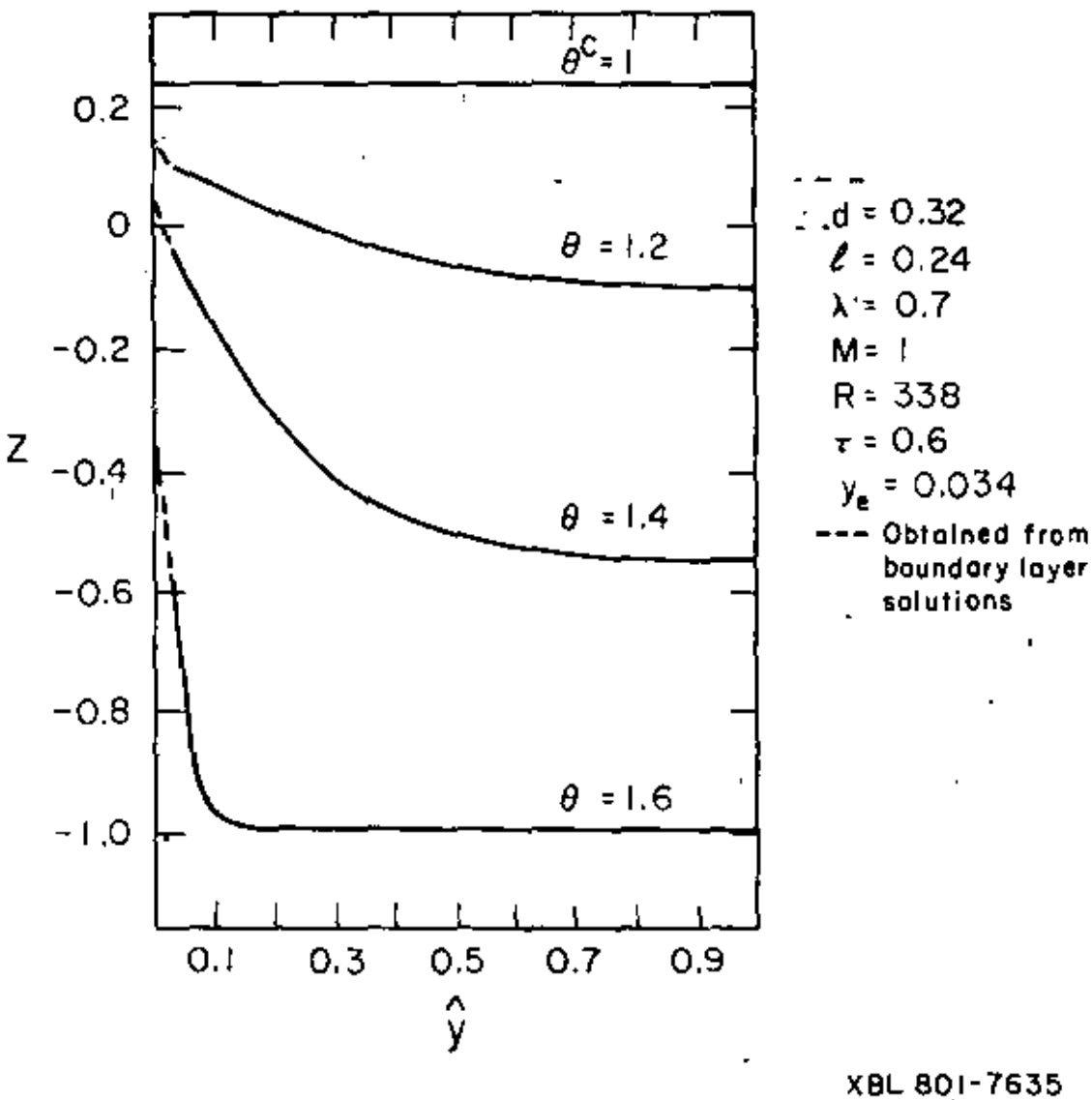


Figure 11. Isotherms in the aquifer and the clay cap.

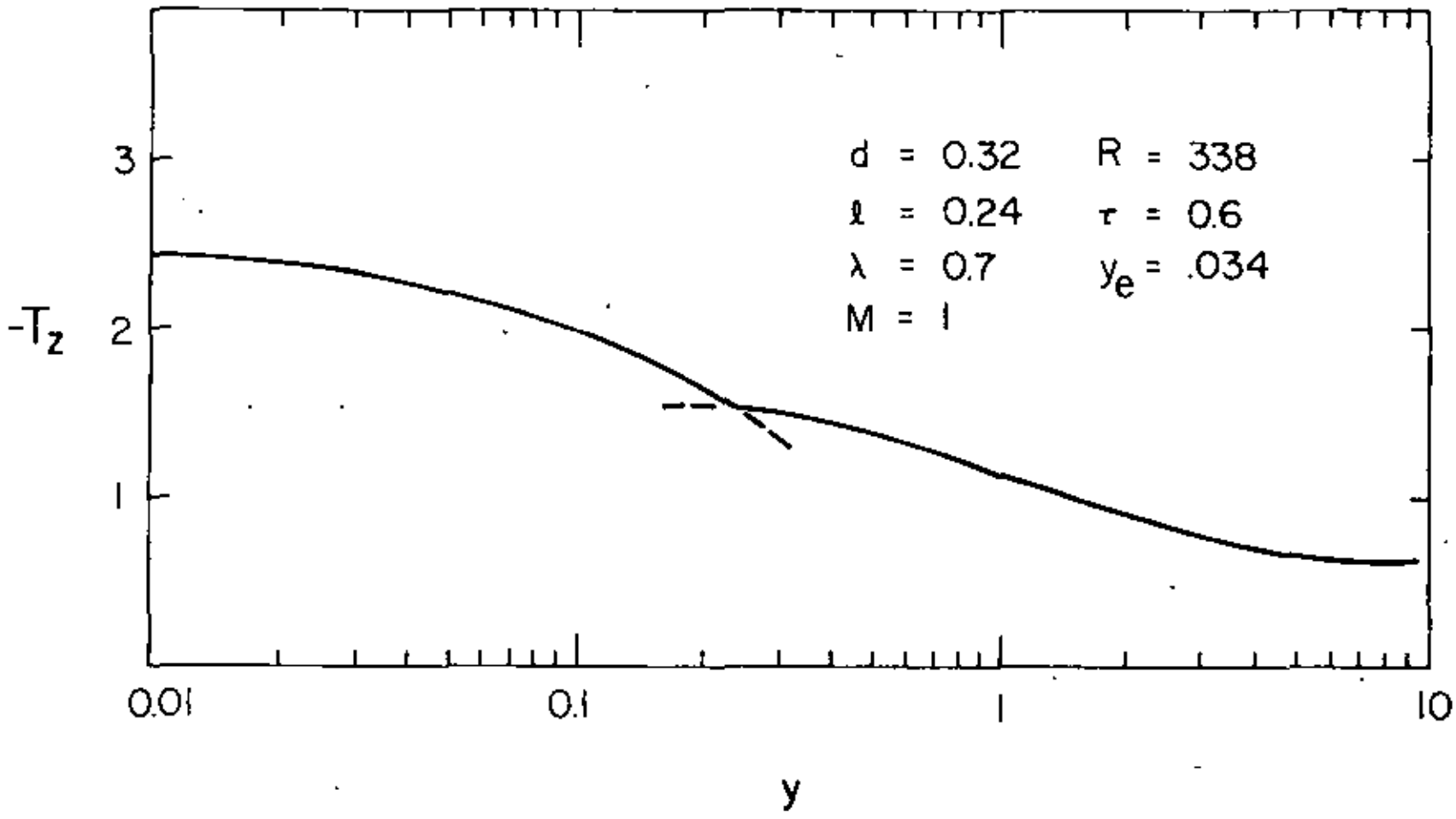


XBL 7811-6633A

Figure 12. Surface temperature gradients along the length of the aquifer.

Heat flux contours measured in the proximity of the East Mesa wells are shown in Figure 13. A plot of heat flux versus distance along three lines ①, ② and ③ of Figure 13 is given in Figure 14. The surface heat flux predicted from the theory is also shown in Figure 14 along with the related parameters. This comparison shows that heat flux in field observations is somewhat larger than predicted. The discrepancy can arise for a variety of reasons. In this analysis we have considered the reservoir to be a zone of constant horizontal permeability while the field data shows the existence of two distinct zones of permeability (Figure 6). For a given mass input M we would expect more hot liquid to pass through the upper, more permeable section, thus increasing the surface heat flux. Liquid transport properties are assumed to be constant in our model. However, to some extent the decrease of viscosity with depth (temperature) compensates for the actual decrease in permeability deep in the system. The actual mass flow rate in the field may be different than $9.89 \times 10^5$ kg/day-km used in Figure 14. It is clear on physical grounds that a larger mass flux would increase the surface heat flux. This is verified theoretically by the solution in (98). Most significantly, the planar geometrical configuration used in the model, representing flow up to a vertical narrow fault and into adjacent aquifers, is not an accurate representation of the localized northwest lobe from which the data in Figure 14 is obtained. In all probability, an axisymmetric model, like that used by Riney et al. [1979b] would be more compatible with the local system. Also, it appears that the Rex and Babcock faults (Figures 2 and 13), as well as the Mesa fault contribute to the anomaly. This seems reasonable since the hottest wells, 44-7 and 48-7, lie near the intersection of the Rex and Babcock faults (Figures 2 and 13). In retrospect it seems that the

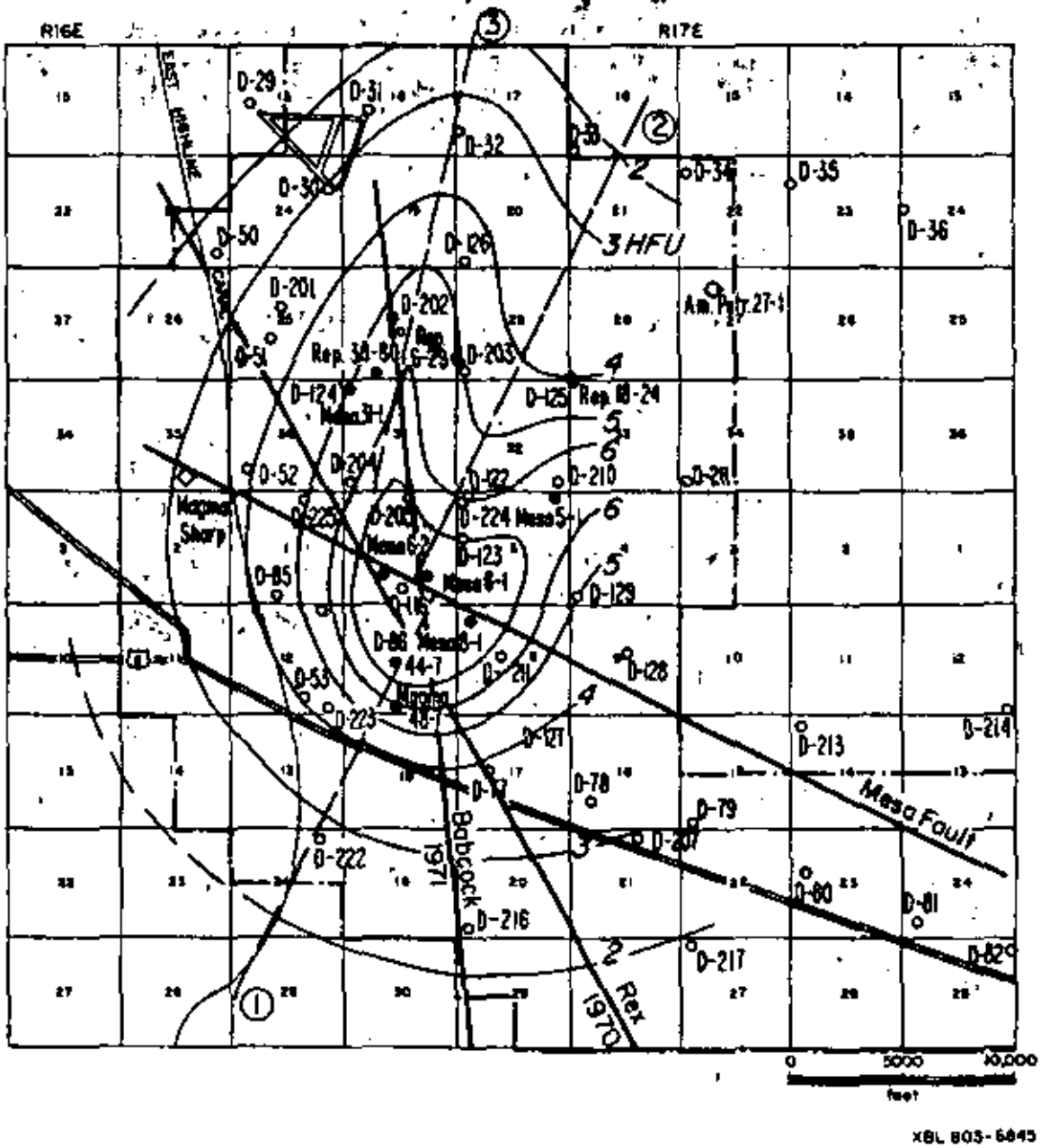


Figure 13. Heat flow contours measured in the proximity of East Mesa wells. (Adapted from Pearson, [1976].)

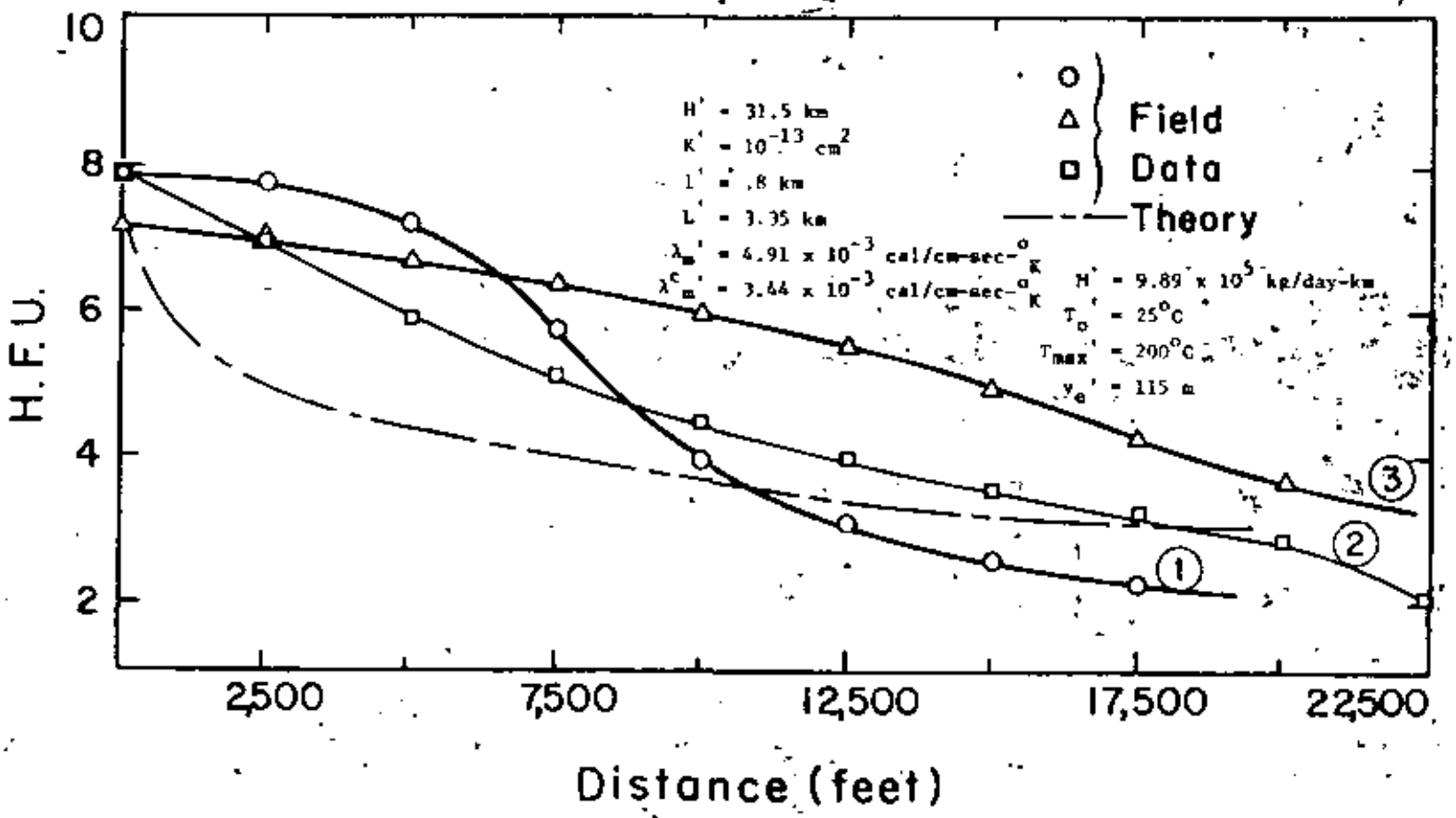


XBL 792-7366

Figure 14. A comparison of the calculated surface heat flux to that measured in the field along lines ①, ② and ③ of Figure 13.

the mass input value were not chosen in a way that would specifically encourage the predicted results to agree with the field measurements. In particular, no special distributions of temperature or heat flux on the upper or lower boundaries were considered in order to improve the agreement. Nor was an attempt made in this model to manipulate the permeability distributions in the aquifer. That we obtain results reasonably similar to the observations without iterating these constraints suggests that the conceptual model is physically plausible.

In a related study by Riney et al. [1979a], described in more detail in Riney et al. [1979b], a conceptual model similar to that used here is developed for the Mesa system. The mathematical model is based on a cylindrical, axisymmetric geometry with fracture zone-type upflow localized near the center. The effects of variable fluid properties and spatially-dependent material properties (permeability and porosity), are included. At the aquifer bottom, the temperature decreases slowly with increasing radial distance from the origin. Other boundary conditions are like those employed in the present work, although the location of the far-field boundary at a radial distance of 10 km is selected a priori. A finite difference technique based on line-successive overrelaxation is used to develop solutions. The computations are carried out for a mass input, obtained from an overall energy balance, of 16.9 kg/sec. at 469.26°K. A variable-size grid, basically 5 cells high and 13 cells long, is used in the computation. Results are presented for a variety of spatial distributions of the vertical and horizontal permeability. It was found that intrusion of deep cold water from the far-field boundary could occur if there was adequate vertical permeability in the system. In this case, there was inflow in the

deep section and outflow in the shallow section such that the net mass flux at the far boundary was just equal to the input value. This partial convective circulation cell results from the propensity of a system with a hot bottom temperature, highest near the axis, cold top, and open side boundary to develop a natural convection mode. Cheng and Lau [1974] have considered a related problem. The associated prediction of an inverted temperature profile at depth is not compatible with known field data. It was concluded that only a very minimal vertical permeability, 0.3-0.5 millidarcy, relative to a maximum horizontal value of 90 md was needed to model the Mesa system. This conforms with the known geological structure in the area. The flow pattern in this case involves outflow through the aquifer depth. Vertical permeability reduction leads to the suppression of the natural convection mode. An excellent reproduction of the surface heat flux pattern was obtained by carefully tailoring the spatial distribution of vertical and horizontal permeability. In general the results obtained are qualitatively similar to those found in the present work. It is reasonable to conclude that fault zone controlled charging of a geothermal reservoir is at least plausible if not a fact.

## SUMMARY

A conceptual model of fault-zone-controlled charging of a geothermal reservoir, based on data from the Fast Mesa system, has been developed. The mathematical model is based on flow in a liquid-saturated porous medium. A two-dimensional, vertical, planar geometry is considered. The problem formulation is based on perturbation methods and asymptotic procedures valid in the limit of large Rayleigh number and small values of

the nondimensionalized fault width. Both analytical and numerical methods are employed to develop solutions for the velocities, pressures, and temperatures in the field. There is better than qualitative agreement between predictions of variation of temperature-depth profiles with distance from the fault, and surface heat flux patterns with the associated field data. It is shown that flat temperature profiles at depth can be associated with purely horizontal water motion (Darcy flow rate of about 0.01 cm/day near to hypothesized faults) rather than only with the more rigorous upflow itself. Although the model used here lacks the various elements of reality discussed earlier, the comparison of prediction and field data is quite reasonable. We are led to believe that the model is a plausible generic type that may be useful in considering other systems as well. In particular, we believe that improved interpretation of field data may be possible by utilizing some of the physical ideas presented here.

Acknowledgment: This work was supported by the Assistant Secretary for Resource Application, Office of the Division of Geothermal Energy of the U. S. Department of Energy under Contract W-7405-ENG-48 administered by Lawrence Berkeley Laboratory as part of the Laboratory's Geothermal Reservoir Engineering Management Program ("GREMP"). Manuscript development was supported in part (for D. R. Kassoy) by the U. S. Geological Survey Extramural Geothermal Program through Grant #14-08-001-0628.

## REFERENCES

Bailey, T. P., A hydrogeological and subsurface study of Imperial Valley geothermal anomalies, Imperial Valley, California: Report CUMER77-4 p. 101, Geological Sciences, University of Colorado, Boulder, 1977.

Biehler, S., Gravity studies in the Imperial Valley in cooperative geological-geophysical-geochemical investigations of geothermal resources in the Imperial Valley of California, Final Report, Contract No. 14-06-300-2194 United States Bureau of Reclamation, pp. 29-42, University of California, Riverside, 1971.

Black, H. T., A subsurface study of the Mesa Geothermal Anomaly, Imperial Valley, California: CUMER 75-5, p. 58, Geological Sciences, University of Colorado, Boulder, 1975.

Cheng, P. and K. H. Lau, Steady State free convection in an unconfined geothermal reservoir, J. Geophysical Res., 79,(29), 4425-4431, 1974.

Combs, J., Thermal studies in cooperative investigations of geothermal resources in the Imperial Valley Area and their potential value for desalting of water and other purposes, UCR/TCPP 72-33, pp. B-1 to B-23, University of California, Riverside, 1972.

Combs, J., Seismic refraction and basement temperature investigation of the East Mesa Known Geothermal Resources Area, Southern California: Transactions, vol. 1, pp. 45-47, Geothermal Resources Council, 1977.

Combs, J., and D. Hadley, Microearthquake investigation of the Mesa Geothermal Anomaly, Imperial Valley, California, Geophysics, 42, (1) 17-33, 1977.

Corwin, R. F., H. F. Morrison, S. Diaz, C., and J. Rodriguez B., Self potential studies at the Cerro Prieto Geothermal Field, in Proceedings of the First Symposium on the Cerro Prieto Geothermal Field, Baja California, Mexico, held at San Diego California, LBL-7098,,Lawrence

Berkeley Laboratory, Berkeley, California, pp. 204-210, 1978.

Davis, D. G., and S. K. Sanyal, Case history report on East Mesa and Cerro Prieto Geothermal Fields, LA-7889-MS (informal report), Los Alamos Scientific Laboratory, Los Alamos, New Mexico, 1979.

Elders, W. A., J. R. Hoagland, E. R. Olson, S. D. McDowell, And P. Collier, A comprehensive study of samples from geothermal reservoirs, UCR/IGPP-78/26, University of California, Riverside, pp. 264, December 1978.

Goyal, K. P., Heat and mass transfer in a saturated porous medium with applications to geothermal reservoirs, Ph. D. thesis, Mechanical Engineering Department, University of Colorado, Boulder, p. 294, 1978.

Goyal, K. P., and D. R. Kassoy, Fault zone controlled charging of a liquid dominated geothermal reservoir: J. Geophysical Res. 85(B4) pp. 1867-1875, 1980.

Howard, J., J. A. Apps, S. Benson, N. E. Goldstein, A. N. Graf, J. Haney, D. Jackson, S. Juprasert, E. Majer, D. McEdwards, T. V. McEvilly, T. N. Narasimhan, B. Schechter, R. Schroeder, R. Taylor, P. Van de Kamp and T. Wolery, Geothermal resource and reservoir investigations of U.S. Bureau of Reclamation leaseholds at East Mesa, Imperial Valley, California, LBL-7094, Lawrence Berkeley Laboratory, Berkeley, California, p. 305, October 1978.

Martinez Baez, L. F., Thermal conductivity of core samples from the Cerro Prieto Geothermal Field: Experimental results and an improved prediction method, in Proceedings of the First Symposium on Cerro Prieto Geothermal Field, Baja, California, Mexico, held at San Diego, California, LBL-7098, Lawrence Berkeley Laboratory, Berkeley, California, pp. 342-351, 1978.

Meidav, T., and R. B. Furgerson, Electrical resistivity for geothermal exploration in the Imperial Valley, in Cooperative geological-geophysical-geochemical investigations of geothermal resources in the Imperial Valley of California, Final report Contract no. 14-06-300 2194, U. S. Bureau of Reclamation, pp. 43-83, University of California, Riverside, 1971.

Morrison, H. F., R. F. Corwin, R. Harding, and G. Demonlly, Interpretation of self potential data from geothermal areas, semi-annual technical progress report, USGS Contract #14-08-0001-16546, University of California, Berkeley, 1979.

Pearson, R. O., Planning design of East Mesa geothermal test facilities (Phase 1B), vol. 1 of TRW Inc. Final Report, Energy Research and Development Administration (Department of Energy) contract no. E(04-3)-1140, 1976.

Riney, T. D., J. W. Pritchett, L. F. Rice, and S. K. Garg, A preliminary model of the East Mesa hydrothermal system, in Proceedings Fifth Workshop Geothermal Reservoir Engineering, SGP-TR-40, Stanford University, Stanford, California, pp. 211-214, 1979a.

Riney, T. D., J. W. Pritchett, L. F. Rice, and S. K. Garg, Integrated model of the shallow and deep hydrothermal systems in the East Mesa Area, Imperial Valley, California, Semi-Annual Tech. Report #1, SSS-R-79-3995, Systems, Science and Software Inc., Box 1620, La Jolla, California, 92038, 1979b.

Smith, J. L., Geology and commercial development of the East Mesa Geothermal Field, Imperial Valley, California, in Geology and Geothermics of the Salton Trough, Geological Society of America, 92nd Annual Meeting, San Diego, W. A. Elders, editor, pp. 86-94, 1979.

Somerton, W. H., and A. H. El-Shaarani, High temperature behavior of rocks associated with geothermal type reservoirs, Paper No. SPE 4897, presented at the 44th Annual California Regional Meeting of the Society of Petroleum Engineers of AIME San Francisco, California, April 4-5, 1974.

U.S. Bureau of Reclamation, Geothermal resource investigations, Imperial Valley, California: Developmental Concepts, p. 57, Washington D.C., U.S. Department of the Interior, Bureau of Reclamation, January 1972.

U.S. Bureau of Reclamation, Geothermal resource investigations, Imperial Valley, California: Special report, Test Well Mesa 6-1, p. 44, Washington D.C. U.S. Department of the Interior, Bureau of Reclamation, February 1973.

U.S. Bureau of Reclamation, Geothermal resource investigations, Imperial Valley, California: Status report, p. 63, Washington D.C., U.S. Department of the Interior, Bureau of Reclamation, November 1974.

U.S. Bureau of Reclamation, Geothermal resource investigations, Imperial Valley California: Status report, p. 99, Washington D.C., U.S. Department of the Interior, Bureau of Reclamation, 1977.

This report was done with support from the Department of Energy. Any conclusions or opinions expressed in this report represent solely those of the author(s) and not necessarily those of The Regents of the University of California, the Lawrence Berkeley Laboratory or the Department of Energy.

Reference to a company or product name does not imply approval or recommendation of the product by the University of California or the U.S. Department of Energy to the exclusion of others that may be suitable.

TECHNICAL INFORMATION DEPARTMENT
LAWRENCE BERKELEY LABORATORY
UNIVERSITY OF CALIFORNIA
BERKELEY, CALIFORNIA 94720

Presented at the Sixth Annual Workshop on Geothermal Reservoir Engineering, Stanford Geothermal Program, Stanford University, Stanford, CA, December 16-18, 1980

LBL-11835

# EFFECT OF MEASURED WELLHEAD PARAMETERS AND WELL SCALING ON THE COMPUTED DOWNHOLE CONDITIONS IN CERRO PRIETO WELLS

K.P. Goyal, C.W. Miller, and M.J. Lippmann

December 1980

Prepared for the U.S. Department of Energy under Contract W-7405-ENG-48

# EFFECT OF MEASURED WELLHEAD PARAMETERS AND WELL SCALING ON THE COMPUTED DOWNHOLE CONDITIONS IN CERRO PRIETO WELLS

K. P. Goyal, C. W. Miller and M. J. Lippmann
Earth Sciences Division, Lawrence Berkeley Laboratory,
University of California, Berkeley, California 94720

## INTRODUCTION

The primary objective of modeling a geothermal system is to be able to predict with some confidence the energy production capacity and longevity of the field under various production and injection scenarios. To achieve this goal, a modeler needs to construct a comprehensive mathematical model based on available data and validate this model against the production history of the field. This, in turn, requires the data associated with the evolution of the field due to its exploitation. Typically, the information related to the variations in the mass flow rate, enthalpy, pressure, temperature and fluid saturation as a function of time is used to validate the model. The production data is routinely measured at the wellhead whereas most reservoir models compute the changes in the temperature, pressure, enthalpy, fluid velocity and other physical properties of the fluid at the sandface. To validate any model, wellhead data must be corrected to reflect the downhole conditions. In this paper, we shall confine ourselves to the discussion of computing bottomhole pressures from the measured wellhead data by using a wellbore model. Several wellbore models which compute wellhead conditions from the given bottomhole data have been cited in the literature. (Sanyal, et al., 1979; Aydelotte, 1980; Gould, 1974). Such calculations are of interest in predicting the conditions under which an optimum production could be obtained from a given well. This approach does not suit us since our primary goal is to study the evolution of the field due to production. The following paragraphs are devoted to the discussion of the wellbore model and its describing equations, comparison between the computed and measured pressures and the effect of measured wellhead parameters on the downhole pressures in the well. Finally a wellbore model with multiple inside diameters is discussed and the effect of well scaling on the bottom hole pressures is studied.

## WELLBORE MODEL

The steady state computer program WELFLO used in this study calculates the bottomhole conditions if the wellhead conditions such as mass flow rate, pressure and enthalpy (or dryness fraction) are prescribed. The length of open interval and heat loss from the well bore are also considered in the program. However, the effect of the radial pressure gradient responsible for inflow to the well is not taken into account. The total mass inflow to the well is assumed to be distributed evenly throughout the open interval. Also, in-place internal energy in the open interval is assumed constant. The equations, describing a transient two-phase flow through a well are discussed in Miller (1979). The steady-state equations

of mass, momentum and energy as obtained from that set for a constant diameter well are as follows:

$$\frac{\partial}{\partial x}(\rho u) = 0 \tag{1}$$

$$\frac{\partial P}{\partial x} = -\rho g - \frac{f\rho u^2}{2D_i} - \frac{\partial}{\partial x}(\rho u^2) - \frac{\partial}{\partial x}\left[\frac{(1-\alpha)\alpha\rho_\ell\rho_g(u_r^2)}{\rho}\right] \tag{2}$$

$$\rho u \frac{\partial e}{\partial x} = -P\frac{\partial u}{\partial x} - \frac{\partial}{\partial x}\left[\frac{(1-\alpha)\alpha\rho_\ell\rho_g u_r(e_g - e_\ell)}{\rho}\right] - P\frac{\partial}{\partial x}\left[\frac{(1-\alpha)\alpha u_r(\rho_\ell - \rho_g)}{\rho}\right] + \frac{4H}{D_i}(T_{res} - T_w) \tag{3}$$

The above equations describe average fluid properties over the cross section and thus do not satisfy the no-slip boundary condition at the wall of the well. The slip is given as a function of flow regime. The limits of these regions (bubble, slug, transition and mist) that were used are defined in Orkiszewski (1967). Slip for these regions is discussed in Orkiszewski, (1967) and Wallis (1969). The program uses an overall friction factor as described in Chisholm (1973). Empirical relations, correlating steam tables for the properties of water and wet steam are used in the program (Miller, 1978). These relations are accurate to within 5% of the steam table values.

## MEASURED AND COMPUTED PRESSURES IN WELL M90

An attempt was made to calculate the pressures at various depths in the bore and then to compare them with those measured in the Cerro Prieto wells. Figure 1 shows the measured and computed pressures in well M-90 for the given wellhead conditions. The well is of uniform diameter. Calculated pressure profiles for two different wellhead pressures are shown in the figure. One of them is for the measured wellhead pressure of 37.4 kg/cm$^2$ gauge. The computed pressures are lower than those measured throughout the depth of the well with a maximum difference of about 11% at a depth of 1380 meters. The second calculated profile is for the wellhead pressure of 39.5 kg/cm$^2$-gauge which is obtained by extending the measured pressure profile to the surface. The maximum pressure difference in this case is only about 6%. It was observed from the computer output that a two-phase slug flow regime existed throughout the well and thus a drastic change in pressure gradient is not likely near the wellhead. In other words, one would expect a wellhead pressure of 39.5 kg/cm$^2$ gauge at the wellhead if the pressures measured in the well are correct. Or alternatively, if the measured wellhead pressure of 37.4 kg/cm$^2$ gauge is correct, then the measured downhole pressures should be in error. This

shows that there exists a discrepancy between the pressures measured at the wellhead and those in the well. As in any other field work or experimentation, such discrepancies do arise as a direct result of human errors, instrumental errors or both. The computed and measured profiles for M-90 are in good agreement. However, it must be emphasized that even a 5% error in the calculation can lead to a large absolute error. For M-90, 5% error is about 70 psi. A comparison between the measured and computed pressures in the Cerro Prieto well M-51 was also made. It was found that computed pressures were within 6-7% of those measured in the well.

## EFFECT OF HEAT LOSS AND OPEN INTERVAL ON COMPUTED DOWNHOLE PRESSURE

The effect of heat loss from the wellbore to the surroundings on the well pressure was also studied by considering that a linear temperature profile (assumed to approximate the natural geothermal gradient) exists in the reservoir at a distance ($R_1$) of 1 m and 5 m from the well. A hyperbolic profile was then fitted between the well and the geothermal gradient to obtain the temperature gradient at the well. It was found that the maximum pressure drop associated with heat loss for $R_1$ = 1 m was about 2.5% while negligibly small for $R_1$ = 5 m in well M-90. Thus, for all practical purposes, steady state heat transfer from Cerro Prieto production wells can be neglected. Gould (1974) also arrived at the same conclusion for high production wells. To study the effect of the thickness of open interval on the bottom hole pressures, we varied the thickness from 10 m to 160 m in the well M-90. It was found that an increase of only about 0.5% occurred in the bottom hole pressures for an open interval of 160 m. Thus, for all the cases discussed hereafter, we assume that the heat loss from the well is negligibly small, and that the depth of the open interval is equal to the distance between two nodes in the finite difference mesh.

## EFFECTS OF WELLHEAD PARAMETERS

As noted, a possibility exists that the measured wellhead parameters such as pressure, mass flow rate, dryness fraction, enthalpy, etc., may be in error by a few percent. Thus, it seems appropriate to find the effect of such errors on the calculated downhole pressures in the well. We varied three important wellhead parameters (mass flow rate, pressure, and enthalpy) within $\pm$20% of their measured value in well M-90 and calculated the change on the bottom hole pressures.

Table 1 shows bottom hole pressures (BHP) for different mass flow rates in well M-90. For a 20% increase in mass flow rate at the wellhead, the bottom hole pressure increased by about 6.5% the for a 20% decrease in flow rate there is about 5% decrease in BHP. The difference between wellhead and downhole pressure is not affected significantly by the mass flow rate. However, it maybe noted that the wellbore model is independent of the reservior.

Table 2 shows the effect of wall head pressures (WHP) on the BHP in well M-90. It may be observed that a 20% increase in WHP results in an increase of about 25% in BHP while a 20% decrease in

the WHP leads to about 18% decrease in BHP. The error in the WHP in this case shows up directly in the BHP.

Effect of enthalpy on BHP is shown in Table 3. It may be observed that an enthalpy increase of 20% reduces BHP by about 14% but a corresponding decrease leads to an increase of about 70% in BHP. An increase in enthalpy results in more steam and lighter fluid giving rise to lower pressures at the bottom of the well as shown in Table 3. BHP is not affected as much by an increase in enthalpy as it does by decreasing the same. This may be attributed to the fact that a decrease in the enthalpy results in a denser, heavier fluid giving rise to higher pressures at the bottom of the well. Effect of flowing dryness fraction at the wellhead on BHP was also studied. It was found that a variation in enthalpy affects the downhole pressures more than a corresponding change in the dryness fraction. The fluid enthalpies at Cerro Prieto wells are calculated by using dryness fraction and steam properties at the separator pressure. Thus, it is advisable to compute BHP by using dryness fraction rather than enthalpy to avoid the possibility of a compounding error.

## EFFECTS OF WELLBORE DIAMETER AND SCALING

In addition to the measured wellhead data, the inside diameter of the well is needed to calculate the BHP. A study was done to find its effect on the calculated bottom hole pressures. Table 4 shows the calculated BHP in M-90 for various inside radii. The BHP was 41% more for 12 cm inside diameter and 150% more for 8 cm diameter compared to that for 16.3 cm diameter. Thus, in the 8 cm diameter case, a reduction of 76% in area leads to a much higher increase (150%) in the downhole pressure. This figure may be unrealistic since a large reduction in the area is assumed throughout the wellbore. In any event, it is clear that the effect of inside diameter on the BHP is considerable. Some Cerro Prieto wells do have large scale deposits. For example, well M-30, which, as of 1976, had scaling in excess of 60 mm at a depth of 1,500 meters. Similar scale deposits were also observed in many other wells in the field. Thus, to obtain reasonable values for downhole pressures, it is necessary to have a computer program which accounts for variations in the wellbore diameters. Using the control volume concept, the following equations of mass, momentum and energy were derived for a finite volume in which the diameter change occurred.

$$(\rho A u)_{\ell} + g\Big|_{up} = (\rho A u)_{\ell} + g\Big|_{down} \qquad (4)$$

$$(PA_{av} - \rho A \frac{\Delta x}{2} g + \rho A u^2)_{\ell + g} - \frac{f \rho u^2 \pi D_i \Delta x}{16} \Bigg|_{up}$$

$$= (PA_{av} + \rho A \frac{\Delta x}{2} g + \rho A u^2)_{\ell + g} + \frac{f \rho u^2 \pi D_i \Delta x}{16} \Bigg|_{down} \quad (5)$$

$$[\rho A u (e + \frac{u^2}{2}) + PAu]_{\ell + g} \Big|_{up} = [\rho A u (e + \frac{u^2}{2} + g\Delta x) + PAu]_{\ell + g} \Big|_{down} \quad (6)$$

In deriving the above equations, we have neglected energy dissipation due to friction and eddy losses. In these equations 'up' stands for the upstream side and 'down' for the downstream side. Subscript $\ell$ stands for liquid and g for steam. Given the conditions at point 'up', the parameters at point 'down' could be calculated. Figure 2 shows the computed and calculated pressures in the Cerro Prieto well M-91. The inside diameter of the well changes at a depth of about 1940 meters. It was found from the computer output that a two phase slug flow exists in the well above 900 metres and a single phase liquid water flows below 950m. A change in the pressure gradient at about 900-1000 m depth is noticed. It is clear from the figure that there is an excellent agreement between the measured and computed pressures. The percentage difference in BHP is less than 1%.

Well M-39 of Cerro Prieto field was also selected to show the effect of multiple inside casing diameters on downhole pressures (Figure 3). Production data for June 1976 was used to compute downhole pressures. Pressures calculated using the actual casing diameters are highest among all the cases shown. Pressure gradient between 1000 m to 1100 m depth change in response to changes in inside casing diameters. Higher pressure gradients below 1200 meters indicate single phase liquid flow. The computed pressures for the uniform inside diameters of 0.2012 m and 0.2736 m, as shown in Figure 3, are lower than those obtained using the actual diameters. In fact, bottom hole pressures decrease by 31.6% and 67.8% for the internal diameter of 0.2012 m and 0.2736 m, respectively. Pressures calculated assuming a uniform diameter of 0.177 m were very close to those computed using the actual casing diameter. This indicates that the gravity effect dominates the pressures more than the inertia effect when there is single phase liquid flow. Unfortunately, no data for measured downhole pressures were available to compare with these computed pressures. These results indicate that the computed downhole pressure may be significantly in error if actual inside casing diameters are not taken into account.

Figure 4 shows the effect of size and position of the scale deposits or of a liner of 200 m length on the pressure distributions in the Cerro Prieto well M-51. Pressures are larger for thicker scale deposits since one would require higher pressures to push the fluid through a small opening. A liner of small diameter set near the wellhead needs higher bottom hole pressure compared to the one set near the bottom of the well bore. This is due to the pressure propagation in the well bore. A similar profile was measured in test 11-3 of the well BR-11 where solid scale deposits up to 2 inches thick were found in the liner (Gould, 1974).

## CONCLUSIONS

We have found that calculated downhole pressures are quite sensitive to measured well head conditions and well inside diameter data. The parameters to be measured, in order of decreasing accuracy, are well inside diameter, wellhead pressure, dryness fraction and mass flow rate. Based on the data presented we consider that LBL's computer program WELFLO calculates reasonable downhole conditions provided that accurate data is provided.

## ACKNOWLEDGEMENTS

We want to thank the Coordinadora Ejecutiva de Cerro Prieto of CFE for making available the data used in this study. This work was performed under the auspices of the U. S. Department of Energy, Division of Geothermal Energy, under contract No. W-7405-ENG-48.

## NOMENCLATURE

$A_{up(down)}$ = inside area of the well at upstream (downstream) side, $m^2$
$A_{av}$ = average area of the well = $(A_{up} + A_{down})/2$, $m^2$
$D_i$ = inside diameter of the well, m
$e$ = internal energy, of the steam-water mixture, J/kg
$e_{\ell(g)}$ = internal energy of water (steam), J/kg
$f$ = coefficient of friction in the two-phase flow
$g$ = gravitational acceleration, $m/sec^2$
$H$ = film heat transfer coefficient in the well, $J/sec\text{-}m^2\text{-}°K$
$P$ = pressure in the well at any cross section, Pascals
$T_{res}$ = reservoir temperature, °K
$T_w$ = well temperature, °K
$u$ = mass averaged velocity in x-direction, m/sec
$u_{\ell(g)}$ = velocity of water (steam) in the well, m/sec
$u_r$ = slip velocity = velocity of steam - velocity of water, m/sec
$x$ = coordinate axis passing through the center of the well, upward positive, m
$\alpha$ = saturation of steam
$\Delta x$ = interval between two nodes in the finite difference scheme, m
$\rho$ = density of the steam-water mixture, $Kg/m^3$
$\rho_{\ell(g)}$ = density of water (steam) in the well, $kg/m^3$

REFERENCES

Aydelotte, S. R.,, "Transient Well Testing in Two-Phase Geothermal Reservoirs", Lawrence Berkeley Laboratory, LBL-10562, GREMP-8, UC-66a, p. 139, 1980.

Chisholm, D., "Pressure Gradients Due to Friction During the Flow of Evaporating Two Phase Mixtures in Smooth Tubes and Channels", Int. Journal Heat Mass Transfer, Vol. 16, pp. 347-358, 1973.

Gould, T. L., "Vertical Two Phase Steam-Water Flow in Geothermal Wells", Jour. Pet. Tech. pp. 833-842, August 1974.

Miller, C. W., Unpublished research, 1978.

Miller, C. W., "Numerical Model of Transient Two-Phase Flow in a Wellbore", Lawrence Berkeley Laboratory, LBL-9056, Rev. p. 31, 1979.

Orkiszewski, J., "Predicting Two Phase Pressure Drops in Vertical Pipe", Jour. Pet. Tech. pp. 829-838, June 1967.

Sanyal, S. K., S. Brown, L. Pandriana, and S. Juprasert. "Sensitivity Study of Variables Affecting Fluid Flow in Geothermal Wells" in Proceedings Fifth Workshop, Geothermal Reservoir Engineering Stanford University, SGP-TR-40, pp. 197-204, 1979.

Wallis, G. B., "One-Dimensional Two Phase Flow", McGraw-Hill Inc. U.S.A. p. 408, 1969.

TABLE 1: Effect of mass flow rate on the bottom hole pressures (B.H.P.) in the Cerro Prieto well M-90

| PERCENTAGE CHANGE | MASS FLOW RATE (Tonnes/hr) | B.H.P. ($Kg/cm^2$-g) | % DIFF B.H.P. |
|---|---|---|---|
| +20% | 195.60 | 95.6146 | +6.5 |
| +15% | 187.45 | 94.0685 | +4.8 |
| +10% | 179.30 | 92.6014 | +3.184 |
| + 5% | 171.15 | 91.1352 | +1.57 |
| 0% | 163.00 | 89.7122 | 0 |
| - 5% | 154.85 | 88.3324 | -1.52 |
| -10% | 146.70 | 86.996 | -2.99 |
| -15% | 138.55 | 85.9179 | -4.18 |
| -20% | 130.40 | 84.9890 | -5.2 |

TABLE 2: Well head pressures and corresponding bottom hole pressures (B.H.P.) in the Cerro Prieto well M-90

| PERCENTAGE CHANGE | WELLHEAD PRESSURE ($Kg/cm^2$-g) | B.H.P. ($Kg/cm^2$-g) | % DIFF B.H.P. |
|---|---|---|---|
| +20% | 47.40 | 112.776 | +25.42 |
| +15% | 45.43 | 107.047 | +19.10 |
| +10% | 43.45 | 101.205 | +12.66 |
| + 5% | 41.48 | 95.2621 | + 6.12 |
| 0% | 39.5 | 89.7122 | 0% |
| - 5% | 37.53 | 84.9074 | - 5.29 |
| -10% | 35.55 | 80.6937 | - 9.94 |
| -15% | 33.58 | 77.0025 | -14.00 |
| -20% | 31.6 | 73.7173 | -17.63 |

TABLE 3: Effect of well head enthalpy on the downhole pressures in the Cerro Prieto well M-90

| PERCENTAGE CHANGE | ENTHALPY (Kcal/kg) | B.H.P. ($Kg/cm^2$-g) | % DIFF B.H.P. |
|---|---|---|---|
| +20% | 387.60 | 77.1392 | -13.85 |
| +10% | 355.30 | 77.6372 | -13.31 |
| + 5% | 339.15 | 80.4552 | -10.20 |
| 0% | 323.00 | 89.7122 | 0 |
| - 5% | 306.85 | 111.342 | +23.83 |
| -10% | 290.70 | 131.156 | +45.67 |
| -15% | 274.55 | 146.203 | +62.252 |
| -20% | 258.40 | 153.316 | +70.09 |

TABLE 4: Effect of well inside diameter on the bottom hole pressures in the Cerro Prieto well M-90

| INSIDE RADIUS (m) | AREA ($m^2$) | % AREA CHANGE ($m^2$) | B.H.P. ($Kg/cm^2$-gauge) | % DIFF B.H.P. |
|---|---|---|---|---|
| 0.08172 | $2.098 \times 10^{-2}$ | 0 | 89.7122 | 0 |
| 0.06 | $1.13097 \times 10^{-2}$ | -46.1 | 127.071 | 41.17 |
| 0.04 | $5.0265 \times 10^{-3}$ | -76.04 | 225.592 | 149.74 |

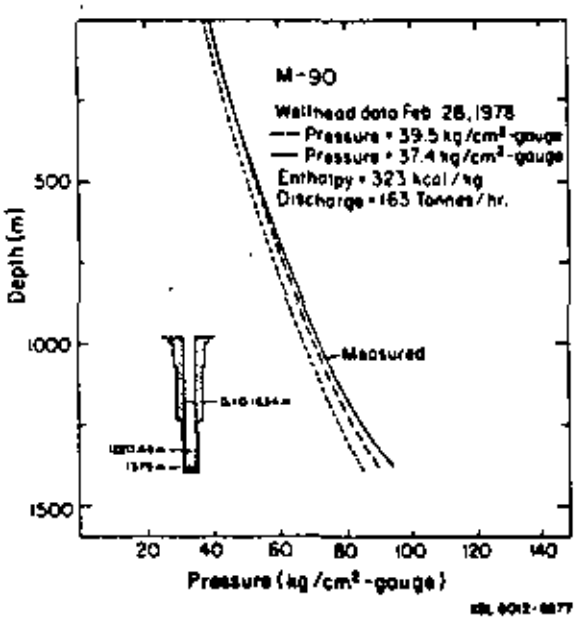


Figure 1. Measured and calculated pressures in the Cerro Prieto well M-90.

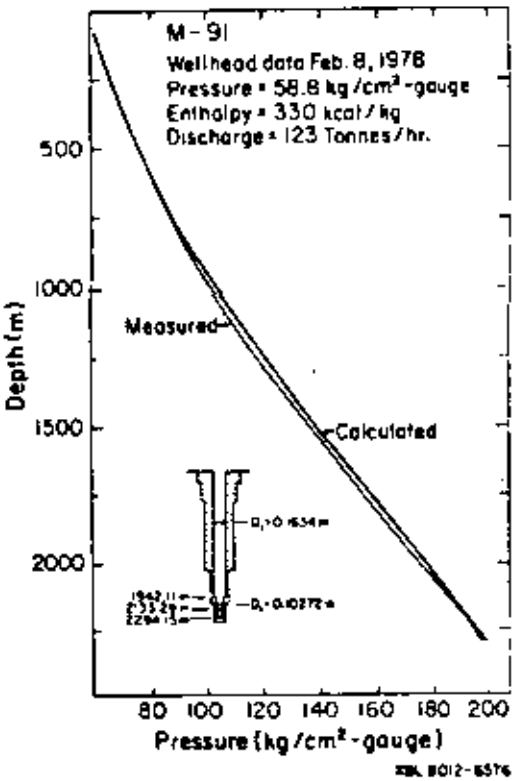


Figure 2. Computed and measured pressures in the Cerro Prieto well M-91.

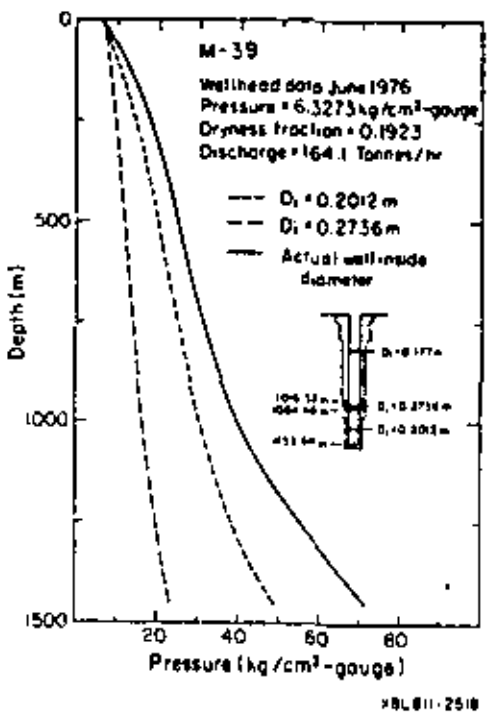


Figure 3. Effect of inside diameter on the calculated pressures for the Cerro Prieto well M-39.

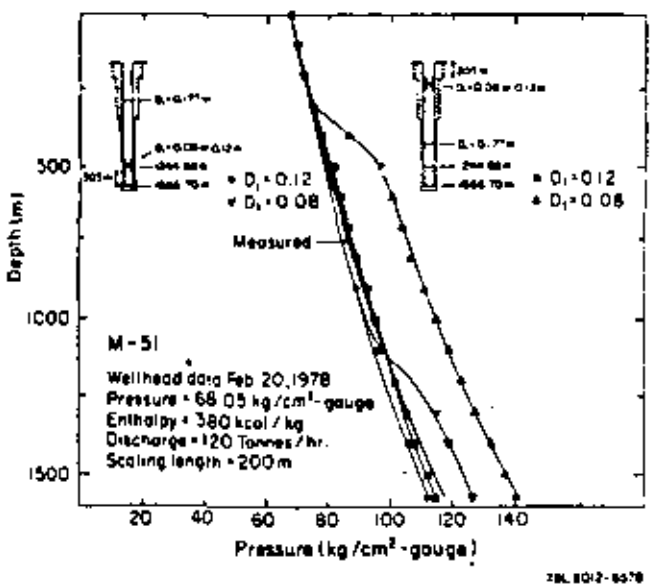


Figure 4. Effect of size and location of scaledeposits on the pressures in the well.

This report was done with support from the Department of Energy. Any conclusions or opinions expressed in this report represent solely those of the author(s) and not necessarily those of The Regents of the University of California, the Lawrence Berkeley Laboratory or the Department of Energy.

Reference to a company or product name does not imply approval or recommendation of the product by the University of California or the U.S. Department of Energy to the exclusion of others that may be suitable.

TECHNICAL INFORMATION DEPARTMENT
LAWRENCE BERKELEY LABORATORY
UNIVERSITY OF CALIFORNIA
BERKELEY, CALIFORNIA 94720

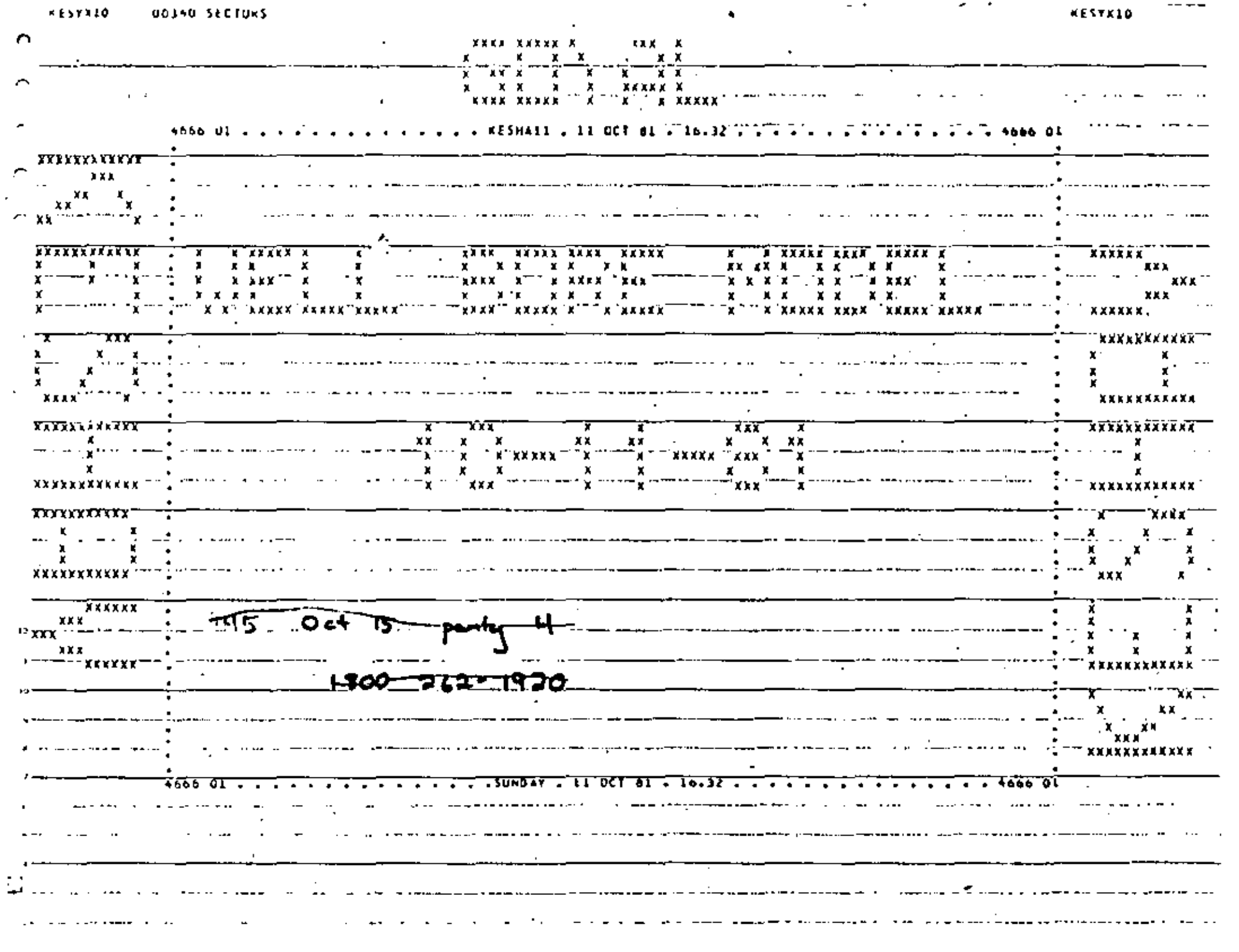
4666 01 KESH411 11 OCT 81 16.32 4666 01
115 Oct 15 party 4
1800 262 1920
4666 01 SUNDAY 11 OCT 81 16.32 4666 01

```
      1.  0000000B      PROGRAM WELFLO (INPUT,OUTPUT)     C6=OUTPUT,FILM)
      2.  0015448B      DIMENSION PZ(200),EI(200),RTI(200),DEP(10)
      3.  0015448B      DIMENSION RHO(200),V(200)
      4.  0015448B      DIMENSION THES(25,200),T(200)
      5.  0015448B      DIMENSION FXI(200),SL(200)
      6.  0015448B      DIMENSION UFG(200),UFT(200)
      7.  0015448B      COMMON/ALL/DX,LENGTH,NNODES,RI,RRM(10),RMAX(10),FFLOW(10),AL(10),
                       1NMAX
      8.  0015448B      COMMON/PROPFL/RHOL(200),RHOG(200),QUAL(200),SLIPR(200),DUMMY(200)
      9.  0015448B      COMMON/INFS/PO,N,AREA(10),XOUT
     10.  0015448B      COMMON/PROP/KH(30),PTOTAL
     11.  0015448B      COMMON/CONDUC/HCOEFF,CONDUC
     12.  0015448B      COMMON/CGS////PDGE(200)
     13.  0015448B      COMMON/KFSHAV/AWELL,PWELL,MONTH,YEAR,DOTM,PPTOP,HH
     14.  0015448B      COMMON/KESHAV1/IFLAG
     15.  0015448B      REAL KH,LENGTH,KL,KTOTAL,MU
     16.  0015448B    910 FORMAT(1H0,4X,*CONSTANT FLOW RATE OUT (TON/HOUR) **,F10.4,/,5X,
                      1*WELLHEAD PRESSURE (PSIG) **,E12.5,/,5X,*WELL DEPTH (M) **,
                      2F10.1,/,4X,* AMBIENT TEMPERATURE (C) **,F8.3,/,5X,*BOTTOMHOLE
                      3TEMPERATURE(C)**,F8.3,/)
     17.  0015448B    915 FORMAT(1H0,4X,*SPECIFIED ENTHALPY(KCAL/KG)**,F8.3,/)
     18.  0015448B    925 FORMAT(1H0,4X,*SPECIFIED WELLHEAD DRYNESS FRACTION**,F8.6,/)
     19.  0015448B    100 FORMAT(2A5,A1)
     20.  0015448B    150 FORMAT(5X ,A5,9X,A5,4(5X,I5))
     21.  0015448B    200 FORMAT(1H1,4X ,*WELL    NUMBER      MONTH      DAY      YEAR*)
     22.  0015448B    920 FORMAT(1H0,4X,*RADIUS(M)   LENGTH(M)      FLOW(KG/M2-SEC)      DEP
                      1TH      SHARE()*)
     23.  0015448B    400 FORMAT(8F10.5)
     24.  0015448B    500 FORMAT(4F15.5,5X,I5)
     25.  0015448B    300 FORMAT(I10,7F10.5)
     26.  0015448B    350 FORMAT(5X,*HCOEFF**,F10.5)
                      C*****************************************
                      C
                      C     THE FLOWING PARAMETERS MUST BE SPECIFIED
                      C        (1) RADIUS IS THE INNER RADIUS OF THE WELL IN METERS
                      C        (2) LENGTH IS THE DEPTH OF THE WELL IN METERS
                      C        (3) P100 IS THE PRESSURE AT WELLHEAD IN PASCALS (NOT THE SEPAR
                      C         ATOR PRESSURE)
                      C        (4) FLOW IS THE TOTAL MASS FLOW RATE IN METRIC TON/HOUR
                      C            (A) XOUT IS THE FLOWING QUALITY, DETERMINE FROM THE
                      C                GAS MASS FLOW/TOTAL MASS FLOW OR USE THE ENTHALPY
                      C                WHERE XOUT IS (ENTHALPY AT WELLHEAD - SATURATED LIQUID
                      C                ENTHALPY AT WELLHEAD PRESSURE)/(SATAURATED VAPOR ENTHALPY-
                      C                SATURATED LIQUID ENTHALPY ALL AT WELLHEAD PRESSURE)
                      C        (5) IF SOME HEAT LOSS IS DESIRED THEN SPECIFY THE MINIMUM
                      C            GEOTHERMAL TEMPERATURE AND THE MAXIMUM GEOTHERMAL TEMPRATU
                      C            RE IN DEGREES C.
                      C            IT IS ALSO NECESSARY TO SET HCOEFF TO A VALUE GREATER THAN
                      C            0.
                      C            THE HEAT LOSS IS CONTROLLED BY A TEMPRATURE DISTRIBUTION
                      C            THAT IS ASSUMED
                      C        (6) THE NUMBER OF STEPS DOWN THE WELLBORE IS SPECIFIED BY
                      C            VARIABLE MAX WHICH IS THE NUMBER OF INTERVALS PLUS 1
                      C
                      C*****************************************************************
     27.  0015448B      CONDUC=1.8
                      C     RI IS THE DISTANCE TO THE LINEAR TEMPERATURE PROFILE IN METERS.
```

```
                0170308        A1=5.
                          C    *****CHOICE******OR GIVEN XDOT USE IFLAG=1**********************
                          C    IFLAG=1
     29.        0170128        MAX=25
     30.        0170318        TM1=25.0
     31.        0170348        HCOEFF=0.0
     32.        0170358        PI= 4.*ATAN(1.)
                          C ***************************************************************
     33.        0170408        LAY1=30
     34.        0170428        LAY2=60
     35.        0170438        NNODES=21
     36.        0170448        K1=.1E-10
     37.        0170458        A1=K1/10.
     38.        0170468        NMAX=30
                          C    CALL MODESG(NNODE,5,8H COVAL  )
     39.        0170478        DO1 I1=1,NMAX
     40.        0170518        READ 100,A=ELL,I=ELL,MONTH,DAY,YEAR
     41.        0170628        IF(EOF(5LINPUT)).NE.0) GO TO 2
     42.        0170648        PRINT 200
     43.        0170708        PRINT 150,A=ELL,I=ELL,MONTH,DAY,YEAR
                          C    NNMAX ARE THE NUMBER OF THE SECTIONS WITH VARIABLE DIAMETERS
     44.        0171008        IF(IFLAG.EQ.1) GO TO 4
     45.        0171018        GO TO 10
     46.        0171028      4 READ 300,NNMAX,LENGTH,DOTM,PPTOP,XDOT,TMAX,DX
     47.        0171158        GO TO 11
     48.        0171158     10 READ 300,NNMAX ,LENGTH,DOTM,PPTOP,HH,TMAX,DX
                          C    INPUT FOR THE LOWEST SECTION FIRST AND TOP SECTION LAST.
     49.        0171308     11 DO 1 I=1,NNMAX
     50.        0171328      3 READ 400,R=R(I),AL(I)
                          C    IF(NNMAX.EQ.3) NNODES=8
                          C    IF(NNMAX.EQ.2) NNODES=16
     51.        0171448        DO 4 I=1,NNMAX
     52.        0171458        AREA(I)=PI*R(I)*R(I)
     53.        0171468      4 FFLO(I)=DOTM/(AREA(I)*3.6)
     54.        0171528        KTOTAL=0.
     55.        0171538        DO 5 I=1,NNODES
     56.        0171558        KH(I)=K1
     57.        0171598        IF(I.GT.LAY1) KH(I)=2.*K1
     58.        0171628        IF (I.GT.LAY2) KH(I)=4.*K1
     59.        0171668        KTOTAL=KTOTAL+KH(I)
     60.        0171678      5 CONTINUE
     61.        0171729        PRINT 920
     62.        0171768        DEP(1)=0.
     63.        0171768        NNMAX1=NNMAX-1
     64.        0171778        DO 3 I=1,NNMAX1
     65.        0172028        KK=NNMAX-I+1
     66.        0172038      6 DEP(I+1)=DEP(I)+AL(KK)
     67.        0172078        SUM=0.
     68.        0172078        DO 6 I=1,NNMAX
     69.        0172118        SUM=SUM+AL(I)
     70.        0172178      6 HMAX(I)=SUM/DX+1.52
     71.        0172188        DO 7 KK=1,NNMAX
     72.        0172178        I=NNMAX-KK+1
     73.        0172208      7 PRINT 500,R=R(I),AL(I),FFLOW(I),DEP(KK),HMAX(I)
                          C    PRINT 350,HCOEFF
     74.        0172418        PTOP=PPTOP*0.068951E+05
     75.        0172428        PTOP=PTOP*1.0135E+05
     76.        0172448        RADIUS=R(1)
```

```
                                                CALL GPIDENT(*MAKE,RADIUS)
    74.   0172A5E       PRINT 910,ODIE,PPIOP,LENGTH,TMIA,TMAX
    75.   0172A06       IF(IFLAG.EQ.1)GO TO 12
    80.   0172A1A       RHO=PI196.5
    81.   0172A19       PRINT 915,RHO
    82.   0172A3F       GO TO 13
    83.   0172A08   12  PRINT 925,RHOI
    84.   0172A58   13  CALL INITIAL (PPIOP,TMAX,TMIN,P2,E,V,T,RHO2,TRES,RT,MAXT,
                      1PRIC,SLOPI
    85.   0172A7A       CALL SPRINT (P2,E,RHO2,V,T,Z)
    86.   0173018   1   CONTINUE
    87.   0173018   2   CONTINUE
                  C     CALL EXITGIZMODE)
    88.   017304A       STOP
    89.   0173058       END
>         CAUTION  ----------STATEMENT NUMBER 350 WAS NEVER USED
```

TABLE OF STATEMENT NUMBERS

| NUMBER | USE | ADDRESS | SOURCE PROGRAM REFERENCES |
|---|---|---|---|
| 1 | END OF DO | 0173019 | 86L 39E |
| 2 | EXECUTABLE | 0173044 | 87L 41J |
| 3 | END OF DO | 0171124 | 50L 49E |
| 4 | END OF DO | 0171469 | 53L 51E |
| 5 | END OF DO | 0171704 | 60L 55E |
| 6 | END OF DO | 0172124 | 70L 68E |
| 7 | END OF DO | 0172204 | 73L 71E |
| 8 | END OF DO | 0172018 | 66L 64E |
| 9 | EXECUTABLE | 0171038 | 46L 44J |
| 10 | EXECUTABLE | 0171148 | 48L 46J |
| 11 | EXECUTABLE | 0171309 | 47L 47J |
| 12 | EXECUTABLE | 0172F19 | 83L 79J |
| 13 | EXECUTABLE | 0172F94 | 84L 82J |
| 100 | FORMAT | LR = 30 | 40R 19L |
| 150 | FORMAT | LR = 60 | 43R 20L |
| 200 | FORMAT | LR = 50 | 42R 21L |
| 300 | FORMAT | LR = 40 | 48R 46R 25L |
| 350 | (UNUSED) | LR = 22 | 20L |
| 400 | FORMAT | LR = 60 | 50R 23L |
| 500 | FORMAT | LR = 70 | 73R 24L |
| 910 | FORMAT | LR = 50 | 76R 16L |
| 915 | FORMAT | LR = 41 | 81R 17L |
| 920 | FORMAT | LR = 74 | 61R 22L |
| 925 | FORMAT | LR = 44 | 83R 18L |

TABLE OF NAMES ENCOUNTERED

| NAME | TYPE | MAIN USE | BLOCKS | ADDRESS | SOURCE PROGRAM REFERENCES |
|---|---|---|---|---|---|
| AL | R | ARRAY | /ALL/ | 0000474 | 73U 69U 66U 50S 7U |
| AREA | R | ARRAY | /AREA/ | 0000029 | 53U 52S 9U |
| ATAN | R | STANDARD | | | 12U |

| | | | | | | | | | | | | | | | |
|---|---|---|---|---|---|---|---|---|---|---|---|---|---|---|---|
| AAE | R | VARIABLE | /KESHAV/ | 0000004 | 43U | 40S | 1[illegible] | | | | | | | | |
| CONDUC | R | VARIABLE | /CONDUC/ | 0000014 | 27S | 11D | | | | | | | | | |
| DAY | R | VARIABLE | | 0175203 | 43U | 40S | | | | | | | | | |
| DEP | R | ARRAY | | 0145044 | 73U | 66S | 66U | 62S | 2D | | | | | | |
| DOTM | R | VARIABLE | /KESHAV/ | 0000044 | 78U | 53U | 48S | 46S | 13D | | | | | | |
| DX | R | VARIABLE | /ALL/ | 0000004 | 70U | 48S | 46S | 7D | | | | | | | |
| E | R | ARRAY | | 0141744 | 85P | 84P | 2D | | | | | | | | |
| FOR | R | EXTERNAL | | | 41U | | | | | | | | | | |
| FFLOW | R | ARRAY | /ALL/ | 0000304 | 73U | 53S | 7D | | | | | | | | |
| FRIC | R | ARRAY | | 0157000 | 84P | 5D | | | | | | | | | |
| GMLU | R | EXTERNAL | | | 77U | | | | | | | | | | |
| H | R | VARIABLE | /MESH/ | 0000014 | 60S | 9D | | | | | | | | | |
| HCOEFF | R | VARIABLE | /CONDUC/ | 0000004 | 31S | 11D | | | | | | | | | |
| HH | R | VARIABLE | /KESHAV/ | 0000064 | 81U | 80U | 48S | 13D | | | | | | | |
| I | I | VARIABLE | | 0175224 | 73U | 72S | 70U | 69U | 68I | 66U | 65U | 64I | 60U | 59U | 58U |
| | | | | | 57U | 57S | 57U | 56U | 55I | 53U | 52U | 51I | 50U | 50S | 49I |
| IFLAG | I | VARIABLE | /KESHAV1/ | 0000003 | 77U | 44U | 14D | | | | | | | | |
| II | I | VARIABLE | | 0175179 | 86U | 40S | 39I | | | | | | | | |
| INITIAL | I | EXTERNAL | | | 84U | | | | | | | | | | |
| INPUT | | FILE | | | 90U | 48U | 46U | 40U | | | | | | | |
| IWELL | I | VARIABLE | /KESHAV/ | 0000013 | 43U | 40S | 13D | | | | | | | | |
| KH | R | ARRAY | /PROP/ | 0000004 | 59U | 59S | 57S | 56S | 15D | 10D | | | | | |
| KK | I | VARIABLE | | 0175244 | 73U | 73S | 72U | 71I | 66U | 65S | | | | | |
| KTURAL | R | VARIABLE | /PROP/ | 0000344 | 59S | 59U | 54S | 15D | 10D | | | | | | |
| KZ | R | VARIABLE | | 0156774 | 56U | 57U | 56U | 37S | 37U | 36S | 15D | | | | |
| LAY1 | I | VARIABLE | | 0175174 | 57U | 33S | | | | | | | | | |
| LAY2 | I | VARIABLE | | 0175114 | 56U | 34S | | | | | | | | | |
| LENGTH | R | VARIABLE | /ALL/ | 0000014 | 75U | 48S | 46S | 15D | 7D | | | | | | |
| MAXT | I | VARIABLE | | 0175123 | 84P | 77P | 29S | | | | | | | | |
| MMAX | I | ARRAY | /ALL/ | 0000164 | 71U | 70S | 7D | | | | | | | | |
| MONTH | I | VARIABLE | /KESHAV/ | 0000024 | 43U | 40S | 13D | | | | | | | | |
| NMAX | I | VARIABLE | | 0175164 | 56U | 39U | 39N | 38S | | | | | | | |
| NMAX | I | VARIABLE | /ALL/ | 0000543 | 73U | 72U | 71N | 68U | 68N | 65U | 63U | 51N | 50U | 49U | 49N |
| | | | | | 48S | 46S | 7D | | | | | | | | |
| NNMAX1 | I | VARIABLE | | 0175238 | 64U | 64N | 63S | | | | | | | | |
| NNODES | I | VARIABLE | /ALL/ | 0000024 | 60U | 55U | 55N | 35S | 7D | | | | | | |
| OUTPUT | | FILE | | | 83U | 81U | 78U | 73U | 61U | 43U | 42U | | | | |
| PI | R | VARIABLE | | 0175148 | 52U | 32S | | | | | | | | | |
| PPTOP | R | VARIABLE | /KESHAV/ | 0000054 | 79U | 74U | 48S | 46S | 13D | | | | | | |
| PTOP | R | VARIABLE | | 0175264 | 84P | 75S | 75U | 74S | | | | | | | |
| PZ | R | ARRAY | | 0020544 | 85P | 84P | 2D | | | | | | | | |
| RADIUS | R | VARIABLE | | 0175274 | 77P | 76S | | | | | | | | | |
| RHOZ | R | ARRAY | | 0015444 | 85P | 84P | 3D | | | | | | | | |
| RRW | R | ARRAY | /ALL/ | 0000044 | 76U | 73U | 52U | 50S | 7D | | | | | | |
| RT | R | ARRAY | | 0155164 | 84P | 77P | 2D | | | | | | | | |
| SI | R | VARIABLE | /ALL/ | 0000014 | 24S | 7D | | | | | | | | | |
| SLIP | R | ARRAY | | 0153674 | 84P | 5D | | | | | | | | | |
| SPRINT | R | EXTERNAL | | | 85U | | | | | | | | | | |
| SUP | R | VARIABLE | | 0175254 | 70U | 69S | 69U | 67S | | | | | | | |
| T | R | ARRAY | | 0145274 | 85P | 84P | 4D | | | | | | | | |
| TMAX | R | VARIABLE | | 0175214 | 84P | 78U | 48S | 46S | | | | | | | |
| TMIN | R | VARIABLE | | 0175134 | 84P | 78U | 30S | | | | | | | | |
| TRES | R | ARRAY | | 0023644 | 84P | 4D | | | | | | | | | |
| U | R | ARRAY | | 0150574 | 85P | 84P | 3D | | | | | | | | |
| XDOT | R | VARIABLE | /MESH/ | 0000144 | 83U | 46S | 9D | | | | | | | | |
| YEAR | R | VARIABLE | /KESHAV/ | 0000034 | 43U | 40S | 13D | | | | | | | | |

1 LIST OF VARIABLE AND ARRAY NAMES IN ADDRESS ORDER IN EACH BLOCK

BLOCK LENGTH

| | | | | | | | | | | | |
|---|---|---|---|---|---|---|---|---|---|---|---|
| *LOCAL | 6451 | 0015444 | RHO2 | 0020548 | P2 | 0023648 | TRES | 0141746 | E | 0145048 | DEP |
| | | 0145142 | RT | 0145478 | T | 0150576 | V | 0153678 | SLIP | 0156778 | KL |
| | | 0157303 | FRIC | 0162108 | UFG | 0165208 | UF | 0171116 | LAY2 | 0175128 | MAXT |
| | | 0175135 | TMIN | 0175148 | PI | 0175158 | LAY1 | 0175168 | NMAX | 0175178 | II |
| | | 0175208 | DAY | 0175218 | TMAX | 0175228 | J | 0175238 | NNMAX1 | 0175248 | KK |
| | | 0175258 | SUM | 0175268 | PTOP | 0175278 | RADIUS | | | | |
| /ALL/ | 45 | 0000048 | DX | 0000018 | LENGTH | 0000028 | NNODES | 0000038 | RI | 0000048 | RRM |
| | | 0000068 | MMAX | 0000308 | FFLOW | 0000428 | AL | 0000548 | NNMAX | | |
| /PROPEL/ | 1000 | 0000001 | PHDL | 0003108 | RHOG | 0006208 | QUAL | 0011308 | SLIPR | 0014408 | DUMMY |
| /MES/ | 13 | 0000008 | MU | 0000018 | H | 0000028 | AREA | 0000148 | XDOT | | |
| /PROP/ | 31 | 0000004 | KH | 0000368 | KTOTAL | | | | | | |
| /CONDIF/ | 2 | 0000008 | HDIFF | 0000018 | CONDUC | | | | | | |
| /IGS////// | 200 | 0000024 | Z400X | | | | | | | | |
| /RESAV/ | 7 | 0000008 | ARELL | 0000018 | IWELL | 0000028 | MONTH | 0000038 | YEAR | 0000048 | DDTM |
| | | 0000058 | PPTOP | 0000068 | MM | | | | | | |
| /RFSHAV1/ | 1 | 0000008 | IFLAG | | | | | | | | |

AMOUNT OF STORAGE USED BY SUBPROGRAM

| | | | |
|---|---|---|---|
| (BLOCK COMMON AREA) | 1249 = 0024238 | | |
| LOCAL STORAGE AREA | 6451 = 0153038 | | |
| I/O BITS + BUFFERS | 1367 = 0015437 | | |
| FORMAT STATEMENTS | 66 = 0001024 | | |
| CONSTANTS | 24 = 0000308 | | |
| ENTRY CODE | 6 = 0000068 | | |
| EXECUTABLE CODE | 1274 = 0002368 | | |
| ACTUAL ARGUMENTS | 33 = 0000418 | | |
| TEMPORARY STORAGE | 3 = 0000038 | | |
| TOTAL (LESS COMMON) | 8024 = 0175308 | | |

ABBREVIATIONS USED ABOVE (THESE ARE KEYED TO THE SOURCE LISTING LINE NUMBER)

| | | | |
|---|---|---|---|
| A | USED IN FORTRAN ASSIGN STATEMENT | P | ARGUMENT IN CALL OR FUNCTION CALL |
| B | OCTAL ADDRESS RELATIVE TO PROGRAM | R | FORMAT USED IN A READ STATEMENT |
| D | DEFINED IN DECLARATIVE STATEMENT | S | STORED SO CONTENTS MAY BE CHANGED |
| F | STATEMENT NUMBER ENDING A DO LOOP | T | STATEMENT NUMBER USED IN A TRACE |
| I | INDEX OF A DO OR IMPLIED DO LOOP | U | NAME USED IN EXECUTABLE STATEMENT |
| J | STATEMENT NUMBER USED IN TRANSFER | W | FORMAT USED IN A WRITE STATEMENT |
| L | SOURCE LINE OF A STATEMENT NUMBER | LR | LONGEST RECORD PRODUCED BY FORMAT |
| N | NAME USED AS A DO LOOP PARAMETER | * | (R=7) NAME DECLARED BUT NOT USED |

7600 COMPILATION -- FNF4 LEVEL 5.24 11 OCT 81 16.25.50

```
GRID                    **SUBROUTINE GRID (RT,MAXT,R    S)**                    PAGE    1

    1.  0000000         SUBROUTINE GRID (RT,MAXT,RADIUS)
    2.  0000004         DIMENSION RT(1)
    3.  0000006         AK=1.0
    4.  000000C         DN=0.1
    5.  0000012         DN=0.04
    6.  0000018         RT(1)=RADIUS
    7.  000001E         DO 60 I=1,MAXT
    8.  0000028         RT(I) = 3.*(AK**(I-1)*DN/DN0)-1.)/(AK**(1./DN0)-1.) * RT(1)
    9.  0000105     60  CONTINUE
   10.  0000128         RETURN
   11.  0000134         END


TABLE OF STATEMENT NUMBERS

NUMBER     USE                    ADDRESS     SOURCE PROGRAM REFERENCES

    60     END OF DO              0000323     9L      7E

TABLE OF NAMES ENCOUNTERED

NAME  TYPE  MAIN USE   BLOCKS      ADDRESS     SOURCE PROGRAM REFERENCES

AK      R   VARIABLE               0001014     8U      3S
DN      R   VARIABLE               0001008     8U      5S
DN0     R   VARIABLE               0000FA8     8U      4S
I       I   VARIABLE               0000778     8U      7I
MAXT    I   VARIABLE   ARGUMENT    NO.  2      7U      7N      8U
RADIUS  R   VARIABLE   ARGUMENT    NO.  3      6U      8U
RT      R   ARRAY      ARGUMENT    NO.  1      6S      8U      6S      2D      1D

LIST OF VARIABLE AND ARRAY NAMES IN ADDRESS ORDER IN EACH BLOCK

 BLOCK     LENGTH

/LOCAL/        *      0000FA8 DN0          0000778 I          0001008 DN          0001014 AK

AMOUNT OF STORAGE USED BY SUBPROGRAM    ABBREVIATIONS USED ABOVE (THESE ARE KEYED TO THE SOURCE LISTING LINE NUMBER)

LOCAL STORAGE AREA      4 = 0000048     A  USED IN FORTRAN  ASSIGN STATEMENT     P  ARGUMENT IN CALL OR FUNCTION CALL
CONSTANTS               5 = 0000058     B  OCTAL ADDRESS RELATIVE TO PROGRAM     R  FORMAT USED IN A  READ  STATEMENT
ENTRY CODE             18 = 0000228     D  DEFINED IN  DECLARATIVE STATEMENT     S  STORED SO CONTENTS MAY BE CHANGED
EXECUTABLE CODE        30 = 0000368     E  STATEMENT NUMBER ENDING A DO LOOP     T  STATEMENT NUMBER USED IN A  TRACE
TEMPORARY STORAGE       9 = 0000118     I  INDEX OF A DO  OR IMPLIED DO LOOP     U  NAME USED IN EXECUTABLE STATEMENT
TOTAL (LESS COMMON)    66 = 0001028     J  STATEMENT NUMBER USED IN TRANSFER     W  FORMAT USED IN A  WRITE STATEMENT
                                        L  SOURCE LINE OF A STATEMENT NUMBER     LR LONGEST RECORD PRODUCED BY FORMAT
                                        N  NAME USED AS A  DO LOOP PARAMETER     *  (R-7) NAME DECLARED  BUT NOT USED

7600 COMPILATION -- FNF4 LEVEL 5.24     11 OCT 81 15.25.50
```

```
      SUBROUTINE INITIAL (PTOP,TMAX,TMIN,P2,E,V,T,RHO2,TRES,RT,MAXT,
     1X,IC,SLIP)
      DIMENSION P2(1),E(1),V(1),T(1),RHO2(1),TRES(MAXT,1)
      DIMENSION X(IC(1),SLIP(1)
      DIMENSION UFG(200),UF(200)
      DIMENSION PP1(200),PP2(200),PP3(200),PPN(200),PP5(200)
      DIMENSION T(MP(200),NT(1)
      COMMON/ALL/G,LENGTH,NNODES,FI,RR(10),MMAX(10),FFLO(10),AL(10),
     1N,MX
      COMMON/PES/MU,M,AA(10),XDOT
      COMMON/PP/NP(30),RTOTAL
      COMMON/CONDIF/HCOEFF,CONDUC
      COMMON/PROFIL/RHOL(200),RHOG(200),QUAL(200),SLIPR(200),DUMMY(200)
      REAL LHS,LENGTH,MTOTAL,MU ,LHSENGY,LHSFLOW
 1002 FORMAT(1X,*I=*,I5,1X,*RHOL(I)=*,E10.4,1X,*RHOG(I)=*,E10.4,1X,
     1*RHO2(I)=*,E10.4,1X,*P2(I)=*,E10.4,/,4X,*V(I)=*,E10.4,1X,
     2*QUAL(I)=*,E10.4,1X,*SLIP(I)=*,E10.4,1X,*UFG(I)=*,E10.4)
 1001 FORMAT(1X,*I=*,I5,5X,*EI=*,E10.4,5X,*RHO2EVL=*,E10.4,5X,*DUMMY=*,
     1A12/)
 1004 FORMAT(4X,2(5,E10.4)
 1005 FORMAT(4X,* FIRST ITERATION*,5X,*I=*,I5,5X,*E(I)=*,E12.6,5X,
     1*ERR=*,E12.6,/)
 1006 FORMAT(4X,*SECOND ITERATION*,5X,*I=*,I5,5X,*E(I)=*,E12.6,5X,
     1*ERR =*,E12.6,/)
      PI=4.*ATAN(1.)
C     CONST=0.1
      G=7.8
      MAX=MMAX(NN*MX)
      FLO=FFLO(NN*MX)
      RADIUS=RR(NN*MX)
      CALL TUP(PTOP,M,RHOL(MAX),RHOG(MAX),UFG(MAX),UF(MAX),XDOT,T(MAX))
      INDEX=0
      RATIO=(1.-XDOT)/XDOT*(RHOG(MAX)/RHOL(MAX))
      QUAL(MAX)=1./(1.+RATIO)
      SLIP1=2.*1.
    5 RHO2(MAX)=(1.-QUAL(MAX))*RHOL(MAX)*QUAL(MAX)*RHOG(MAX)
      V(MAX)=FLO/RHO2(MAX)
      CALL FRICSLIP(T(MAX),RHOL(MAX),RHOG(MAX),QUAL(MAX),FRIC(MAX),
     1SLIP(MAX),V(MAX),RADIUS,MU,SLIPR(MAX),DUMMY(MAX),I)
      QUALO=QUAL(MAX)
      QUAL(MAX)=1./(1.+RATIO*SLIPR(MAX))
      INDEX=INDEX+1
      IF (INDEX.GT.15) GO TO 10
      IF (ABS((QUALO-QUAL(MAX))/QUAL(MAX)).GT.0.01) GO TO 5
   10 CONTINUE
      QUALX=1./(1.+(1.-QUAL(MAX))/QUAL(MAX))*(RHOL(MAX)/RHOG(MAX)))
      E(MAX)=UF(MAX)+QUALX*UFG(MAX)
      PRINT 1009,QUAL(MAX),QUALX,XDOT,T(MAX),UF(MAX),UFG(MAX)
 1009 FORMAT(4X,*SATURATION=*,E12.4,4X,*DRYNESS FRACTION  IN PLACE=*,E12
     1.4,/,4X,*FLOWING DRYNESS FRACTION=*,E12.4,4X,* FLOWING WELL HEAD
     2TEMPERATURE(C)= *,F10.5,/,4X,*SATURATED LIQUID ENERGY(J/KG)= *,E12
     3.4,4X,*ENERGY DIFFERENCE(J/KG)=*,E12.4,/)
      RHO2(MAX)=EQUES(PTOP,E(MAX),T(MAX),RHOL(MAX),RHOG(MAX),QUAL(MAX)
     1,UFG(MAX),UF(MAX))
      P2(MAX)=PTOP
      V(MAX)=FLO/RHO2(MAX)
      I=MAX
```

```
                0032406         DUT=VI*MAXI*RHO2(MAX)
                0032414         VAVE=(VI*MAXI+VI*MAXI+1)*0.5
                      C         TO GET SLIP AND FRICTION AGAIN AT TOP.
   47.          0032424         CALL FRICSLP(TI(MAX),RHOL(MAX),RHOG(MAX),QUAL(MAX),FRIC(MAX),
                               1SLIP(MAX),VAVE,RADIUS,MU,SLIPR(MAX),DUMMY(MAX),I)
   48.          0032550         RHO2(MAX)=(1.-QUAL(MAX))*RHOL(MAX)+QUAL(MAX)*RHOG(MAX)
   49.          0032616         DO 21 II=1,NN*AX
   50.          0032648         II=NNMAX-II+1
   51.          0032658         IF(III.EQ.1) GO TO 20
   52.          0032678         FLO=FFLO(III)
   53.          0032718         RADIUS=RR(III)
   54.          0032728         AAVE=(AREA(III)+AREA(II+1))/2.
                      C         TO CALCULATE THE PRESSURE AND ENERGY AT THE SECTION WHERE THE
                      C         DIAMETERS CHANGE FOR A FINITE VOLUME.
                      C         ITERATIONS TO OBTAIN VALUES FOR VARIOUS PARAMETERS AT THE SECTION
                      C         WHERE DIAMETER CHANGED.
   55.          0032758         I=I-1
   56.          0032778         EE(I)=E(I+1)
   57.          0033018         PZ(I)=PZ(I+1)
   58.          0033028         SLIP(I)=SLIP(I+1)
   59.          0033048         DO 23 KK=1,10
   60.          0033069         RHO2(I)=SOUFS(PZ(I),E(I),TI(I),RHOL(I),RHOG(I),QUAL(I),UFG(I),UF(I)
                               1)
   61.          0033218         VI(I)=FLO/RHO2(I)
   62.          0033228         CALL FRICSLP(TI(I),RHOL(I),RHOG(I),QUAL(I),FRIC(I),SLIP(I),VI(I),RAD
                               1IUS,MU,SLIPR(I),DUMMY(I),I)
   63.          0033368         IF(QUAL(I).LT.1.E-06 .OR.QUAL(I).GT.1.) GO TO 29
   64.          0033478         IF(SLIP(I).LT.1.E-06) GO TO 51
   65.          0033448         VL1=SLIP(I)/(SLIPR(I)-1.)
   66.          0033478         VG1=SLIP(I)*VL1
   67.          0033518         GO TO 31
   68.          0033528      29 IF(QUAL(I).GT.1.) GO TO 32
   69.          0033548         VL1=V(I)
   70.          0033558         VG1=0.
   71.          0033568         GO TO 31
   72.          0033608      32 VG1=V(I)
   73.          0033618         VL1=0.
   74.          0033628         GO TO 31
   75.          0033638      51 VL1=V(I)
   76.          0033648         VG1=VI(I)
                      C31       IF(V(I).LT.V(I+1)) DEDDY=CONST*V(I+1)*V(I+1)*.5*RHO2(I+1)*AREA(II
                      C        1+1)
                      C         IF(V(I).GE.V(I+1)) DEDDY=CONST*V(I)*V(I)*.5*RHO2(I)*AREA(II)
   77.          0033658      31 DRAG1=F*FRIC(I)*RHO2(I)*VI(I)*VI(I)*PI*RADIUS*DX/8.
   78.          0033748         LHSFLOW=AREA(II)*(RHOG(I)*QUAL(I)*VG1*VG1+RHOG(I)*(1.-QUAL(I))*VL1
                               1*VL1- RHO2(I)*DX*G*.5)-DRAG1
                      C        1*VL1- RHO2(I)*DX*G*.5)-DRAG1 -DEDDY
   79.          0034138         PZ(I)=(RHSFLOW-LHSFLOW)/AAVE
  (79) - CAUTION ----------------------------------------RHSFLOW IS NOT SET ABOVE
   80.          0034158         PRESEN1= AREA(II)*PZ(II)+(VG1*QUAL(I)+VL1*(1.-QUAL(I)))
   81.          0034248         AKISEN1= .5*AREA(II)*(RHOG(I)*VG1*VG1*VG1*QUAL(I)+RHOL(I)*VL1*VL1
                               1*VL1*(1.-QUAL(I)))
   82.          0034348         ALHS3= AREA(II)*RHOL(I)*RHOG(I)*QUAL(I)*(1.-QUAL(I))*SLIP(I)*UFG(I
                               1)/RHO2(I)
   83.          0034438         LHSENGY=PRESEN1+AKIKEN1+ALHS3
                      C         LHSENGY=AREA(II)*(QUAL(I)*VG1*(VG1*VG1*.5*RHOG(I)*PZ(I))+(1.-QUAL
                      C        1I))*VL1*(PZ(I)+.5*VL1*VL1*RHOL(I))*RHOL(I)*RHOG(I)*QUAL(I)*(1.-QUA
                      C        2L(I))*SLIP(I)*UFG(I)/RHO2(I))
```

```
      0014468  23   E(I)=(RHSENGY-LHSENGY)/(FLOW*AREA(
                C     PRINT 1000,KK,LHSENGY,E(I),PZ(I),RHOZ(I),QUAL(I),SLIP(I),UFG(I)
                C 23  PRINT 1000,I,SLIP(I),VL(I),VG(I),ACHS,AK(NEN),PRESN(I),AREA(I),AAVE
                C     THE VALUES AT THE NEXT NODE OF THE VARIABLE SECTION ARE CALCULATED
                C     UP TO HERE.
> (84) - CAUTION  ------------------------------------------RHSENGY IS NOT SET ABOVE
   85.  0014578       24 I=I-1
   86.  0014608        SLIP(I)=SLIP(I+1)
   87.  0014618        ALENG=LENGTH-DX*(NNODES)
   88.  0014648        TL=P(I)-(TMAX-(TMAX-TMIN)/ALENG)*DX*(I-1-NNODES)
   89.  0014748        IF (I.LE.NODFSITEMP(I)-TMAX+5.
   90.  0015018        PZ(I)=PZ(I+1)+RHOZ(I+1)*G*DX+FRIC(I+1)*(FLOW*FLOW/RHOZ(I+1))*DX/(
                     14.*RADIUS)
   91.  0015148        E(I)=E(I+1)
   92.  0015158        DO 15 J = 1,10
   93.  0015208        RHOZ(I)=FQUAL(PZ(I),E(I),T(I),RHOL(I),RHOG(I),QUAL(I),UFG(I),UF(I)
                     1)
   94.  0015318        RAVE=(RHOZ(I)+RHOZ(I+1))/2.
   95.  0015358        IF (I.LE.NNODES) VIN=(FLOW/RHOZ(I))*XH(I)/XTOTAL
   96.  0015448        IF(I.GT.NNODES) VIN=0.
   97.  0015518        V(I)=(V(I+1)*RHOZ(I+1)-VIN*RHOZ(I))/RHOZ(I)
   98.  0015548        DUDM=V(I)*RHOZ(I)
   99.  0015648        IF(I.LE.NNODES) DUDM=(DUDM+V(I+1)*RHOZ(I+1))/2.
  100.  0015658        VAVE=(V(I)+V(I+1))*0.5
  101.  0015698        CALL FRICSLP(I,II,RHOL(I),RHOG(I),QUAL(I),FRIC(I),SLIP(I),V(I),
                     1RADIUS,MU,SLIPS(I),DUMMY(I),I)
  102.  0015818        IF (I.GT.MAX) DUDM=DUDM*0.5
  103.  0015858        PZ(I)=PZ(I+1)+RAVE*G*DX
  104.  0015918        PZ(I)=PZ(I)+FRIC(I)*RAVE*VAVE*VAVE*DX/(4.*RADIUS)-((RHOZ(I)+
                     1RHOZ(I+1)*V(I)*V(I)*0.5-(RHOZ(I+1)*RHOZ(I+1))*(V(I+1)**2)*0.5)
> (104) - CAUTION  ------------------------------------------PZ APPEARED TO LEFT OF PREVIOUS =
  105.  0015951P       IP=I+1
  106.  0016128        PZ(I)=PZ(I)-((1.-QUAL(IP))*QUAL(IP)*RHOL(IP)*RHOG(IP)*SLIP(IP)**2/RHOZ(
                     1IP) -(1.-QUAL(IP))*QUAL(IP)*RHOG(IP)*RHOL(IP)*SLIP(IP)**2/RHOZ(IP))
  107.  0016528        DUDM=E(I)
  108.  0016538        E(I)=E(I+1)+(PZ(I)*(V(IP)-V(I)))/DUDM
                C     E(I)=(E(I+1)+(PZ(I)*(1.-RHOZ(I+1)/RHOZ(I)))/RHOZ(I+1)
  109.  0016628        E(I)=E(I)-((1.-QUAL(I))*QUAL(I)*RHOL(I)*RHOG(I)*SLIP(I)*UFG(I))/RHO
                     1Z(I)-(1.-QUAL(IP))*QUAL(IP)*RHOG(IP)*RHOL(IP)*SLIP(IP)*UFG(IP)/RHO
                     2Z(IP))/DUDM
> (109) - CAUTION  ------------------------------------------E APPEARED TO LEFT OF PREVIOUS =
  110.  0016798        E(I)=E(I)-PZ(I)*((QUAL(I)*(1.-QUAL(I))*SLIP(I)*(RHOL(I)-RHOG(I))/
                     1RHOZ(I)-QUAL(IP)*(1.-QUAL(IP))*SLIP(IP)*(RHOL(IP)-RHOG(IP))/
                     2RHOZ(IP))/DUDM
                C     CHECKING ***********************************************
> (110) - CAUTION  ------------------------------------------E APPEARED TO LEFT OF PREVIOUS =
  111.  0016918        PKETERM=PZ(I)*(V(IP)-V(I))
  112.  0016958        GAMMAIP=PZ(I)*(QUAL(IP)*(1.-QUAL(IP))*SLIP(IP)*(RHOL(IP)-RHOG(IP))
                     1)/RHOZ(IP)
  113.  0017448        GAMMAI=PZ(I)*(QUAL(I)*(1.-QUAL(I))*SLIP(I)*(RHOL(I)-RHOG(I))
                     1)/RHOZ(I)
  114.  0017558        WEIP=(RHOL(IP)*RHOG(IP)*QUAL(IP)*(1.-QUAL(IP))*SLIP(IP)*UFG(IP))/
                     1RHOZ(IP)
  115.  0017648        RHOZEVM=DUDM*E(IP)
  116.  0017658        RHOZEVM=RHOZEVM+WEIP+PKETERM+GAMMAIP-GAMMAI
  117.  0017778        WEI=(RHOL(I)*RHOG(I)*QUAL(I)*(1.-QUAL(I)))*SLIP(I)*UFG(I))/
                     1RHOZ(I)
  118.  0018018        RHOZEVL=RHOZEVM+WEI
```

```
.19.   0040308        ENER= RHOZEVL/DOT=
120.   0040048        IF(QUAL(I).LT. 1.E-06 .OR.QUAL(I).GT.1.) GO TO 53
121.   0040118        IF(SLIP(I).LT.1.E-06) GO TO 151
122.   0040198        IF(I.GT.1) GO TO 153
123.   0040158        VL=SLIP(I)/(SLIPR(I)-1.)
124.   0040208        VG=SLIP(I)*VL
125.   0040228        GO TO 152
126.   0040238   151  VL=V(I)
127.   0040248        VG=V(I)
128.   0040258        GO TO 152
129.   0040268   53   IF(QUAL(I).GT.1.) GO TO 54
130.   0040308        VL=V(I)
131.   0040318        VG=0.
132.   0040328        IF(E(I).LT.UF(I)) UF(I)=E(I)
133.   0040368        GO TO 152
134.   0040358   54   VG=V(I)
135.   0040408        VL=0.
136.   0040418   152  UG=UF(I)+UFG(I)
137.   0040448        RHS4=AREA(I)*(RHOG(I)*VG*QUAL(I)*UG+RHOL(I)*VL*(1.-QUAL(I))*UF(I)
                     1)
138.   0040558        RHS5=AZERO(I)*(RHOG(I)*RHOG(I)*QUAL(I)*VL-QUAL(I)*SLIP(I)*UFG(I)
                     1)/RHOZ(I)
139.   0040668        ENER2=(RHS4-RHS5)/(FLOW*AREA(I))
140.   0040738        RHS4=RHS4/AREA(I)
141.   0040758        RHS5=RHS5/AREA(I)
142.   0040768        IF(I.EQ.4).AND.J.EQ.10) GO TO 154
143.   0041048        GO TO 155
144.   0041048   154  PRINT 1002,I,RHOL(I),RHOG(I),RHOZ(I),P2(I),V(I),QUAL(I),SLIP(I),
                     1UFG(I)
145.   0041138        PRINT 1000,J,PRETOP,GAMMAP,GAMMAI,WEIP,RHOZEVR,RHOZEVN,ENER,E(I)
146.   0041468        PRINT 1000,I,UF(I),ENER1,UG,FLOW,VL,VG,RHS4,RHS5
147.   0041638        PRINT 1003,I,WEI,RHOZEVL,DUMMY(I)
148.   0041738   153  IF(I.LE.(NNODES-1)) E(I)=E(I+1)
                C     CHECKING DONE **********************************************
149.   0041778        IF (I.LE.(NNODES-1)) E(I)=E(I+1)
150.   0042028        E(I)=0.5*(E(I)+EOLD)
151.   0042048   15   CONTINUE
152.   0042078        RHOZ(I)=EQOFS(P2(I),E(I),T(I),RHOL(I),RHOG(I),QUAL(I),UFG(I),UF(I)
                     1)
153.   0042228        IF(I.LE.(NNODES-1)) VIN=(FLOW/RHOZ(I))*KH(I)/KTOTAL
154.   0042318        IF(I.GT.(NNODES-1)) VIN=0.
155.   0042358        V(I)=(V(I+1)*RHOZ(I+1)-VIN*RHOZ(I))/RHOZ(I)
156.   0042408        CALL FRICSLIP(T(I),RHOL(I),RHOG(I),QUAL(I),FRIC(I),SLIP(I),VI(I),
                     1RADIUS,MU,SLIPP(I),DUMMY(I),I)
                C     IF(I.LE.(NNODES-1) GO TO 56
                C     GO TO 57
                C56   PRINT 1004,I,NNODES,KH(I),KTOTAL,FLOW,VIN,V(I),V(I+1),RHOZ(I),
                C     1RHOZ(I+1)
157.   0042548        IF(I.EQ. 1) GO TO 22
158.   0042558        IF(I.EQ.MMAX(J)-1)) GO TO 24
159.   0042608        GO TO 20
160.   0042618   22   IF(I.GT.1) GO TO 20
161.   0042628        GO TO 21
                C     USE THE KNOWN VALUES AT THE SECTION TO CALCULATE NEW PARAMETERS.
162.   0042638   24   IF(QUAL(I).LT.1.E-06 .OR.QUAL(I).GT.1.) GO TO 33
163.   0042708        IF(SLIP(I).LT.1.E-06) GO TO 52
164.   0042728        VL=SLIP(I)/(SLIPR(I)-1.)
165.   0042758        VG=SLIP(I)*VL
```

```
    6.  0042778          GO TO 34
  167.  0043098      33  IF(QUAL(I).GT.1.) GO TO 37
  168.  0043278          VL=V(I)
  169.  0043038          VG=0.
  170.  0043048          IF(E(I).LT.UF(I)) UF(I)=E(I)
  171.  0043108          GO TO 34
  172.  0043188      37  VG=V(I)
  173.  0043128          VL=0.
  174.  0043138          GO TO 34
  175.  0043148      52  VL=V(I)
  176.  0043158          VL=V(I)
  177.  0043168      34  DRAG2=FRIC(I)*RHO2(I)*V(I)*V(I)*PI*RADIUS*DX/8.
  178.  0043258          AAVE=(AREA(I)+AREA(I-1))/2.
  179.  0043318          RHSFLOW=AREA(I)*(RHOG(I)*QUAL(I)*VG*VG*RHOL(I)*(1.-QUAL(I
                        1))*VL*VL+(1.-RHO2(I))*G*DX/32.)-DRAG2*P2(I)*AAVE
  180.  0043508          UG=UF(I)+UFG(I)
  181.  0043538          PRESEN2=AREA(I)*P2(I)*(QUAL(I)*VG*(1.-QUAL(I))*VL)
  182.  0043628          AKINEN2=(AREA(I)*.5*(QUAL(I)*RHOG(I)*VG*VG*VG*(1.-QUAL(I))*RHOL(I)
                        1*VL*VL*VL)
  183.  0043728          AINTEN2=AREA(I)*(QUAL(I)*RHOG(I)*VG*UG*(1.-QUAL(I))*RHOL(I)*VL*
                        1UF(I))
  184.  0044038          GRAVITY=FLOW*AREA(I)*G*DX
  185.  0044068          RHSENGY= PRESEN2+AKINEN2+AINTEN2+GRAVITY
  186.  0044128          RHS4=AREA(I)*(RHOG(I)*VG*QUAL(I)*UG*RHOL(I)*VL*(1.-QUAL(I))*UF(I)
                        1)
  187.  0044228          RHS5=AREA(I)*(1.*RHOL(I)*RHOG(I)*QUAL(I)*(1.-QUAL(I))*SLIP(I)*UFG(I)
                        1)/RHO2(I)
  188.  0044318          ENERL=(RHS4-RHS5)/(FLOW*AREA(I))
  189.  0044358          PRINT 1005,I,E(I),ENERL
                C     /  RHSENGY=AREA(I)*(QUAL(I)*VG*(RHOG(I)*UG+P2(I))*RHOG(I)*.5*VG*VG)
                C     1+(1.-QUAL(I))*VL*(RHOL(I)*UF(I)+P2(I))*RHOL(I)*.5*VL*VL)+
                C     2G*DX*(RHOG(I)*VG*QUAL(I)+RHOL(I)*VL*(1.-QUAL(I))))
                C     PRINT 1000,I,E(I),ENERL,PRESEN2,AKINEN2,AINTEN2,RHS4,GRAVITY,
                C    1RHSENGY
                C     PRINT 1000,I,SLIP(I),VL,VG,UFG(I),RHOL(I),RHOG(I),RHO2(I),RHS5
  190.  0044458      21  CONTINUE
  191.  0044478          CALL FRICSLP(T(I),RHOL(I),RHOG(I),QUAL(I),FRIC(I),SLIP(I),V(I),
                        1RADIUS,MU,SLIP(I),DUMMY(I),I)
                C         DO 28 I=1,MAX
                C28       PRINT 1000,I,P2(I),E(I),RHO2(I),QUAL(I),V(I),RHOL(I),RHOG(I),SLIP
                C         (I)
  192.  0044558          DO 45 J=1,MAX
  193.  0044578          ALENG=LENGTH-(NNODES)*DX
  194.  0044678          TEMP(J)=TMAX-(TMAX-TMIN)/ALENG*DX*(J-1-NNODES)
  195.  0044728          IF (J.LE.NNODES) TEMP(J)=TMAX+5.
  196.  0044778      45  CONTINUE
  197.  0045018          DO 46 J=1,5
  198.  0045038          I=MAX
  199.  0045038          DO 30 III=1,NNMAX
  200.  0045078          II=NNMAX-III+1
  201.  0045108          FLOW=FFLOW(II)
  202.  0045118          RADIUS=RRW(II)
  203.  0045138          IF(II.EQ.1) GO TO 47
  204.  0045158          AAVE=(AREA(II)+AREA(II+1))/2.
                C         TO CALCULATE THE PRESSURE AND ENERGY AT THE SECTION WHERE THE
                C         DIAMETERS CHANGE(SECOND TIME).
                C         TO CALCULATE THE PRESSURE AND ENERGY AT THE SECTION WHERE THE
                C         DIAMETERS CHANGE FOR A FINITE VOLUME.
```

```
                C     ITERATIONS TO OBTAIN VALUES FOR     JUS PARAMETERS AT THE SECTION
                C     WHERE DIAMETER CHANGES.
  205.  0045208       I=I-1
  206.  0045228       DO 26 KK=1,10
  207.  0045248       RHOZ(I)=EQOFS(PZ(I),E(I),T(I),RHOL(I),RHOG(I),QUAL(I),UFG(I),UF(I
                     1)
  208.  0045378       V(I)=FLOW/RHOZ(I)
  209.  0045408       CALL FRICSLP(I(I),RHOL(I),RHOG(I),QUAL(I),FRIC(I),SLIP(I),V(I),RAD
                     1IUS,*U,SLIPM(I),DUMMY(I),I)
  210.  0045548       IF(QUAL(I).LT.1.E-06 .OR.QUAL(I).GT.1.) GO TO 38
  211.  0045608       IF(SLIP(I).LT.1.E-06) GO TO 56
  212.  0045628       VL1=SLIP(I)/(SLIP(I)-1.)
  213.  0045658       VG1=SLIP(I)*VL1
  214.  0045678       GO TO 39
  215.  0045708    38 IF(QUAL(I).GT.1.) GO TO 42
  216.  0045728       VL1=V(I)
  217.  0045738       VG1=0.
  218.  0045748       GO TO 39
  219.  0045768    42 VG1=V(I)
  220.  0045778       VL1=0.
  221.  0046008    56 VL1=V(I)
  222.  0046028       VGL=V(I)
                C39   IF(V(I).LT.V(I+1)) DEDDY=CONST*V(I+1)*V(I+1)*.5*RHOZ(I+1)*AREA(I
                C     1+1)
                C     IF(V(I).GE.V(I+1)) DEDDY=CONST*V(I)*V(I)*.5*RHOZ(I)*AREA(I)
  223.  0046038    3  DRAG1=F4(C(I)*RHOZ(I)*V(I)*V(I)*P(*RADIUS*DX/8.
  224.  0046128       LHSFLO=AREA(I)*(RHOG(I)*QUAL(I)*VG1*VG1*RHOG(I)*(1.-QUAL(I))*VL1
                     1*VL1- RHOZ(I)*DX*G*.5)-DRAG1
                C     1*VL1- RHOZ(I)*DX*G*.5)-DRAG1-DEDDY
  225.  0046318       PZ(I)=(RHSFLOW-LHSFLOW)/AAVE
                C     LHSENGY=AREA(I)*(QUAL(I)*VG1*(VG1*VG1*.5*RHOG(I)*PZ(I))*(1.-QUAL(
                C    1I))*VL1*(PZ(I)+.5*VL1*VL1*RHOL(I))*RHOL(I)*RHOG(I)*QUAL(I)*(1.-QUA
                C    2L(I))*SLIP(I)*UFG(I)/RHOZ(I))
  226.  0046338       ALHS1= AREA(I)*PZ(I)*(VG1*QUAL(I)+VL1*(1.-QUAL(I)))
  227.  0046428       ALHS2= .5*AREA(I)*(RHOG(I)*VG1*VG1*VG1*QUAL(I)+RHOL(I)*VL1*VL1*VL
                     1I*(1.-QUAL(I)))
  228.  0046528       ALHS3= AREA(I)*RHOL(I)*RHOG(I)*QUAL(I)*(1.-QUAL(I))*SLIP(I)*UFG(I
                     1)/RHOZ(I)
  229.  0046618       LHSENGY=ALHS1+ALHS2+ALHS3
  230.  0046644    26 E(I)=(RHSENGY-LHSENGY)/(FLOW*AREA(I))
                C26   PRINT 1000,KK,PZ(I),ALHS1,LHSENGY,E(I),AREA(I),FLOW,RHOZ(I),
                C     1SLIP(I)
                C     THE VALUES AT THE NEXT NODE OF THE VARIABLE SECTION ARE CALCULATED
                C     UP TO HERE.
                C     NEW VALUES AT THE SAME SECTION ARE ALREADY CALCULATED(SECOND TIME)
  231.  0046758    47 I=I-1
  232.  0046768       DO 148 K=1,10
  233.  0047008       RHOZ(I)=EQOFS(PZ(I),E(I),T(I),RHOL(I),RHOG(I),QUAL(I),UFG(I),UF(I
                     1)
  234.  0047138       RAVE=(RHOZ(I)+RHOZ(I+1))/2.
  235.  0047158       PAVE=(PZ(I)+PZ(I+1))/2.
  236.  0047208       FAVE=(FRIC(I)+FRIC(I+1))/2.
  237.  0047238       IF (I.LE.(NNODES)) VIN=(FLOW/RHOZ(I))*RH(I)/RTOTAL
  238.  0047338       IF (I.GT.(NNODES)) VIN=0.
  239.  0047378       IM=I-1
  240.  0047398       IF (IM.EQ.0) IM=1
  241.  0047428       V(I)=(RHOZ(I)*(I)*V(I)*V(I)-VIN*RHOZ(I))/(0.5*(RHOZ(I)+RHOZ(IM)))
  242.  0047508       VAVE=(V(I)+V(I+1))/2.
```

```
 243.  0047528      CALL FRICSLP(TLI),RHOL(I),RHOG(I),QUA.    ,FRIC(I),SLIP(I),VI(I)
                   1RADIUS,PI,SLIP(I),DUMMY(I),I)
                C  CHANGED DOTM FROM "VA,E"RAVE TO V(I) X RHO2(I) ON 10.26.80.
 244.  0047668      DOTM=V(I)*RHO2(I)
                C  FOLLOWING LINE TO PREVENT PROGRAM FROM BLOWING.
 245.  0047678      IF(I.LE.(NODES-1) DOTM=(DOTM+V(I+1)*RHO2(I+1))/2.
 246.  0047768      P2(I)=P2(I+1)+RAVE*G*DX
 247.  0050018      PP1(I)=P2(I)+FAVE*RAVE*VAVE*VAVE*DX/(4.*RADIUS)
                C  PP2(I)=(FLOW)**2/RHO2(I)
 248.  0050108      PP2(I)=V(I)*V(I)*RHO2(I)
 249.  0050128      PP3(I)=V(I+1)*V(I+1)*RHO2(I+1)
 250.  0050148      P2(I)=PP1(I)-(PP2(I)-PP3(I))
 251.  0050178      IP=I+1
 252.  0050208      PP4(I)=(1.-QUAL(I))*QUAL(I)*RHOL(I)*RHOG(I)*SLIP(I)**2/RHO2(I)
 253.  0050268      PP5(I)=(1.-QUAL(IP))*QUAL(IP)*RHOG(IP)*RHOL(IP)*SLIP(IP)**2/RHO2(I
                   1P)
 254.  0050368      P2(I)=P2(I)-(PP4(I)-PP5(I))
 255.  0050428      IF (I.EQ.MAX) IP=I
 256.  0050468      E(I)=E(I+1)+FAVE*(V(I)-V(I))/DOTM
 257.  0050528      IF (I.EQ.MAX) DOTM=DOTM*0.5
 258.  0050568      E(I)=E(I+1)-(1.-QUAL(I))*QUAL(I)*RHOL(I)*RHOG(I)*SLIP(I)*UFG(I)/RHO
                   12(I)-(1.-QUAL(IP))*QUAL(IP)*RHOG(IP)*RHOL(IP)*SLIP(IP)*UFG(IP)/RHO
                   22(IP))/DOTM
 259.  0050778      QUALAP=(QUAL(IP)+QUAL(IP))*0.5
 260.  0051008      QUALAM=(QUAL(I)+QUAL(I))*0.5
 261.  0051038      SLIPAP=(SLIP(IP)+SLIP(IP))*0.5
 262.  0051048      SLIPAM=(SLIP(I)+SLIP(I))*0.5
 263.  0051068      RHOLAP=(RHOL(IP)+RHOL(IP))*0.5
 264.  0051078      RHOLAM=(RHOL(I)+RHOL(I))*0.5
 265.  0051118      RHOGAP=(RHOG(IP)+RHOG(IP))*0.5
 266.  0051138      RHOGAM=(RHOG(I)+RHOG(I))*0.5
 267.  0051168      DORJ=(RHO2(IP)+RHO2(IP))*0.5
 268.  0051218      DORI=(RHO2(I)+RHO2(I))*0.5
                C  FRIENGY=FAVE*VAVE*VAVE*DX/(4.*RADIUS)
 269.  0051248      E(I)=E(I)+FAVE*(QUALAP*(1.-QUALAP)*SLIPAP*(RHOLAP-RHOGAP)/
                   1DORJ-QUALAM*(1.-QUALAM)*SLIPAM*(RHOLAM-RHOGAM)/DORI)/DOTM
                C  E(I)=E(I)+FRIENGY
                C  CHECKING ***************************************************
                C  UG=UF(I)+UFG(I)
                C  IF(SLIP(I).LT.1.E-06) GO TO 149
                C  IF(I.EQ.1) GO TO 148
                C  VL=SLIP(I)/(SLIPH(I)-1.)
                C  VG=SLIP(I)*VL
                C  GO TO 150
                C149  VL=V(I)
                C  VG=V(I)
                C150  RHS=AREA(I)*(RHOG(I)*VG*QUAL(I)*UG+RHOL(I)*VL*(1.-QUAL(I))*UF(I)
                C     1)
                C     RHS=AREA(I)*(RHOL(I)*RHOG(I)*QUAL(I)*(1.-QUAL(I))*SLIP(I)*UFG(I)
                C     1)/RHO2(I)
                C  ENER=(RHS-RHSS)/(FLOW*AREA(I))
                C  PRINT 1000,K,P2(I),E(I),ENER,VL,VG,RHO2(I),DOTM
                C  CHECKING DONE **********************************************
 270.  0051478      IF (ABS(TEMP(I)-T(I)).LT.1.E-7) GO TO 1193
 271.  0051538      RSTAR=(RADIUS*T(I)-TEMP(I)*RI)/(TEMP(I)-T(I))
 272.  0051618  1193 CONTINUE
 273.  0051628      IF (HCOEFF.EQ.0.) GO TO 1140
 274.  0051638      TRES(I,J)=RT(I)*HCOEFF*(RADIUS-RSTAR)/(RT(I)-RSTAR)*HCOEFF+CONDU
```

```
                                  1C)
  275.  0051668                   E(I)=E(I)+CONDUC*4.*(TRES(I,I)*DX/(RHOZ(I)*(RADIUS*RSTAR)*RADIUS*(V
                                  1(I+1)-V(I)))
  276.  0052148    1148 CONTINUE
  277.  0052158         IF (I.LE.(NNODES-1)) E(I)=E(I+1)
  278.  0052218     148 CONTINUE
                  C      PRINT 1000,I,SLIP(I),QUAL(I),FLOW,RHS4,RHS5,ENER,E(I)
  279.  0052238    1000 FORMAT(4X,I5,8E12.6 )
  280.  0052338         IF(I.EQ.1) GO TO 41
  281.  0052258         IF(I.EQ.MMAX(I-1)) GO TO 25
  282.  0052278         GO TO 47
  283.  0052308     41  IF(I.GT.1) GO TO 47
  284.  0052328         GO TO 30
                  C      USE THE KNOWN VALUES AT THE SECTION TO CALCULATE NEW PARAMETERS.
  285.  0052338     25  IF(QUAL(I).LT.1.E-06 .OR.QUAL(I).GT.1.) GO TO 43
  286.  0052408         IF(SLIP(I).LT.1.E-06) GO TO 55
  287.  0052428         VL=SLIP(I)*V(I)/(SLIP(I-1)
  288.  0052458         VG=SLIP(I)*VL
  289.  0052478         GO TO 49
  290.  0052508     43  IF(QUAL(I).GT.1.) GO TO 44
  291.  0052528         VL=V(I)
  292.  0052538         VG=0.
  293.  0052548         IF(E(I).LT.UF(I)) UF(I)=E(I)
  294.  0052608         GO TO 49
  295.  0052608     44  VG=V(I)
  296.  0052628         VL=0.
  297.  0052638         GO TO 49
  298.  0052648     55  VG=V(I)
  299.  0052658         VL=V(I)
  300.  0052668     49  DRAG2=FRIC(I)*RHOZ(I)*V(I)*V(I)*PI*RADIUS*DX/8.
  301.  0052758         AAVE=(AREA(I)+AREA(I-1))/2.
  302.  0053018         RHSFLOW=AREA(I)*(RHOG(I)*QUAL(I)*VG*VG*RHOL(I)*(1.-QUAL(I
                       1))*VL*VL )+(RHOZ(I)*G*DX)/2.)+DRAG2 +P2(I)*(AREA(I)-AREA(I-1))*.5
  303.  0053228         UG=UF(I)+UFG(I)
  304.  0053248         RHSENGY=AREA(I)*(QUAL(I)*VG*(RHOG(I)*UG+P2(I)+RHOG(I)*.5*VG*VG)
                       1+(1.-QUAL(I))*VL*(RHOL(I)*UF(I)+P2(I)+RHOL(I)*.5*VL*VL)+
                       2G*DX*(RHOG(I)*VG*QUAL(I)+RHOL(I)*VL*(1.-QUAL(I))))
                  C      RHS1=AREA(I)*P2(I)*(QUAL(I)*VG+(1.-QUAL(I))*VL)
                  C      RHS2=.5*AREA(I)*(RHOG(I)*QUAL(I)*VG*VG+VG*(1.-QUAL(I))*RHOL(I)*
                  C     1VL*VL+VL*VL)
                  C      RHS3=G*DX*(RHOG(I)*VG*QUAL(I)+(1.-QUAL(I))*RHOL(I)*VL)*AREA(I)
  305.  0053578         RHS4=AREA(I)*(RHOG(I)*VG*QUAL(I)*UG+RHOL(I)*VL*(1.-QUAL(I))*UF(I)
                       1)
  306.  0053718         RHS5=AREA(I)*(RHOL(I)*RHOG(I)*QUAL(I)*(1.-QUAL(I))*SLIP(I)*UFG(I)
                       1)/RHOZ(I)
  307.  0054038         ENER=(RHS4-RHS5)/(FLOW*AREA(I))
                  C      RHS6=RHS1+RHS2+RHS3+RHS4
                  C      PRINT 1000,I,RHS1,RHS2,RHS3,RHS4,RHS5,RHSENGY,ENER ,E(I)
  308.  0054108         IF(J.EQ.5) PRINT 1006,I,E(I),ENER
  309.  0054228     30  CONTINUE
  310.  0054248    1006 FORMAT (//,4X,'NEXT ITERATION',/)
  311.  0054268      46 CONTINUE
                  C      GETTING FINAL VALUES OF PZ AND E AT EACH NODE.
  312.  0054278         I=MAX
  313.  0054308         DO 35 II=1,NNMAX
  314.  0054338         I=NNMAX-II+1
  315.  0054348         FLOW=FFLOW(I)
  316.  0054358         RADIUS=RRW(I)
```

```
                0054370        LCHECK=MMAX(I)-1
                0054408     45 I=I-1
  319.          0054448        RHO2(I)=EOQFS(P2(I),T(I),T(I),RHOC(I),RHOG(I),QUAL(I),UFG(I),UF(I)
                              1)
  320.          0054578        IF(I.LE.(NNODES-1)) VIN=(FLOW/RHO2(I))*K(I)/KTOTAL
  321.          0054668        IF(I.GT.(NNODES-1)) VIN=0.
  322.          0054724        V(I)=(V(I+1)*RHO2(I+1)-VIN*RHO2(I))/RHO2(I)
  323.          0054758        IF(I.EQ.LCHECK) V(I)=(FLOW-VIN*RHO2(I))/RHO2(I)
  324.          0055038        IF(I.EQ.1) GO TO 36
  325.          0055068        IF(I.GT.(MMAX(I)-1)) GO TO 48
  326.          0055078        GO TO 35
  327.          0055108     36 IF(I.GT.1) GO TO 48
  328.          0055118     35 CONTINUE
                         C     DO 27 J=1,MAX
                        C27   PRINT 1000,I,P2(I),E(I),RHO2(I),QUAL(I),V(I),RHOL(I),RHOG(I)
  329.          0055158        DO 40 J = 1,MAXT
  330.          0055178        DO 50 I = 1,MART
  331.          0055228        IF (49951(C*P(J)-T(J))).LT.0.05) GO TO 1590
  332.          0055278        RSTAR=(RADIUS*T(J)-TEMP(J)*R1)/(TEMP(J)-T(J))
  333.          0055448        IF (HCOEFF.EQ.0.) GO TO 1590
  334.          0055528        TRES(I,J)=T(J)*HCOEFF*((RADIUS*RSTAR))/((RT(I)-RSTAR)*HCOEFF+CONDU
                              1C)
  335.          0055618        TRES(I,J)=((TRES(I,J)*(RADIUS-RSTAR))/(RT(I)-RSTAR)
  336.          0055628        GO TO 50
  337.          0055638     1590 TRES(I,J)=T(J)
  338.          0055678     50 CONTINUE
  339.          0055728     40 CONTINUE
  340.          0055758        RETURN
  341.          0055778        END
                CAUTION ----------STATEMENT NUMBER 1004 WAS NEVER USED
                CAUTION ----------STATEMENT NUMBER 1001 WAS NEVER USED
```

ABLE OF STATEMENT NUMBERS

| UMBER | USE | ADDRESS | SOURCE PROGRAM REFERENCES | | | |
|---|---|---|---|---|---|---|
| 5 | EXECUTABLE | 0031368 | 35J | 28L | | |
| 10 | EXECUTABLE | 0031738 | 36L | 34J | | |
| 15 | END OF DO | 0042058 | 191L | 92E | | |
| 20 | EXECUTABLE | 0034579 | 160J | 159J | 85L | 51J |
| 21 | END OF DO | 0044458 | 190L | 161J | 49E | |
| 22 | EXECUTABLE | 0042818 | 140L | 157J | | |
| 23 | END OF DO | 0034474 | 64L | 59E | | |
| 24 | EXECUTABLE | 0042648 | 167L | 158J | | |
| 25 | EXECUTABLE | 0052348 | 235L | 281J | | |
| 26 | END OF DO | 0048658 | 230L | 206E | | |
| 29 | EXECUTABLE | 0053528 | 68L | 63J | | |
| 30 | END OF DO | 0054228 | 309L | 284J | 199E | |
| 31 | EXECUTABLE | 0033668 | 77L | 74J | 71J | 67J |
| 32 | EXECUTABLE | 0033608 | 72L | 68J | | |
| 33 | EXECUTABLE | 0043008 | 167L | 162J | | |
| 34 | EXECUTABLE | 0043178 | 177L | 174J | 171J | 166J |
| 35 | END OF DO | 0055198 | 326L | 326J | 313E | |
| 36 | EXECUTABLE | 0055118 | 327L | 324J | | |

```
   37      EXECUTABLE      0043118   172L   167J
   38      EXECUTABLE      0045708   215L   210J
   39      EXECUTABLE      0046045   221L   216J   214J
   40      END OF DO       0055738   331L   329E
   41      EXECUTABLE      0052118   283L   280J
   42      EXECUTABLE      0045768   219L   215J
   43      EXECUTABLE      0052508   290L   285J
   44      EXECUTABLE      0052618   295L   290J
   45      END OF DO       0044778   196L   192E
   46      END OF DO       0054258   311L   197E
   47      EXECUTABLE      0046758   283J   282J   231L   203J
   48      EXECUTABLE      0054438   327J   325J   310L
   49      EXECUTABLE      0052678   300L   297J   294J   289J
   50      END OF DO       0055708   338L   336J   330E
   51      EXECUTABLE      0013638    75L    69J
   52      EXECUTABLE      0043148   175L   163J
   53      EXECUTABLE      0040268   129L   120J
   54      EXECUTABLE      0040378   134L   129J
   55      EXECUTABLE      0052548   298L   286J
   56      EXECUTABLE      0046018   221L   211J
  148      END OF DO       0052218   278L   232E
  151      EXECUTABLE      0040238   126L   121J
  152      EXECUTABLE      0040428   136L   133J   128J   125J
  153      EXECUTABLE      0041738   148L   143J   122J
  154      EXECUTABLE      0041058   144L   142J
 1000      FORMAT          LR =105   279L   146W   145W
 1001      FORMAT          LR = 15   310L
 1002      FORMAT          LR = 85   144W    13L
 1003      FORMAT          LR = 76   147W    14L
 1004      FORMAT          LR = 94    15L
 1005      FORMAT          LR = 77   189W    16L
 1006      FORMAT          LR = 77   308W    17L
 1009      FORMAT          LR = 91    40L    39J
 1146      EXECUTABLE      0052158   276L   273J
 1193      EXECUTABLE      0051628   272L   270J
 1590      EXECUTABLE      0055638   337L   333J   331J
```

TABLE OF NAMES ENCOUNTERED

```
NAME    TYPE  MAIN USE   BLOCKS    ADDRESS    SOURCE PROGRAM REFERENCES
AAVE      R   VARIABLE             0056628   301S   225U  2045   179U   178S    79U   54S
ABS       R   STANDARD                       331U   270U   35U
ABSTENZ   R   VARIABLE             0067178   185U   183S
ACOSENS   R   VARIABLE             0056705    83U    81S
ACOSENZ   R   VARIABLE             0067161   185U   182S
ALENG     R   VARIABLE             0056738   194U   193S    86U    87S
ALHS1     R   VARIABLE             0057219   229U   226S
ALHS2     R   VARIABLE             0057229   229U   227S
ALHS3     R   VARIABLE             0056718   229U   228S    83U    82S
AREA      R   ARRAY      /AREA/    0000028   307U   306U   305U   304U   302U   301U   230U   228U   227U   226U   224U
                                             204U   198U   187U   186U   184U   183U   182U   181U   179U   178U   141U
                                             140U   139U   136U   137U    84U    82U    81U    80U    78U    54U    80
ATAN      R   STANDARD                       180U
CONDUC    N   VARIABLE   /CONDUIF/ 0000018   334U   275U   274U   LOD
DDRI      R   VARIABLE             0057368   269U   268S
DDRJ      R   VARIABLE             0057358   269U   267S
```

```
DDTM     R VARIABLE               006657B   269U   258U   2575   [illegible]   256U   2455   245U   2445   119U   115U   110U
                                            109U   108U   1025   102U   995    99U    985    455
DRAG1    R VARIABLE               006635B   224U   2235   78U    775
DRAG2    R VARIABLE               006714B   302U   3005   179U   1775
DUMMY    R ARRAY     /PROPFL/     001449B   243P   243U   209P   209U   191P   156P   156U   147U   101P   101U   62P
                                            62U    47P    47U    30P    30U    11D
DX       R VARIABLE  /ALL/        000000B   304U   302U   300U   275U   247U   246U   224U   223U   194U   193U   184U
                                            179U   177U   104U   103U   90U    88U    87U    78U    77U    7D
F        R ARRAY     ARGUMENT  NO.   5      319P   319U   308U   293U   2775   277U   2755   275U   2695   269U   2585
                                            259U   2565   256U   233P   233U   2305   207P   207U   189U   170U   152P
                                            152U   1505   150U   1495   149U   1485   148U   145U   132U   115U   1105
                                            110U   1095   109U   1085   108U   107U   93P    93U    915    91U    845
                                            60P    60U    565    56U    41P    41U    385    2D     1D
ENER     R VARIABLE               006705B   308U   3075   145U   1195
ENERI    R VARIABLE               006713B   189U   1885   146U   1395
EOLD     R VARIABLE               006642B   150U   1075
EQUFS    R EXTERNAL                         319U   233U   207U   152U   93U    60U    41U
FAVE     R VARIABLE               006725B   247U   2365
FFLOW    R ARRAY     /ALL/        000030B   315U   201U   52U    21U    7D
FLOW     R VARIABLE               006653B   321U   320U   3155   307U   237U   230U   208U   2015   188U   184U   153U
                                            146U   139U   95U    90U    84U    61U    525    43U    29U    215
FRIC     R ARRAY     ARGUMENT  NO.  12      300U   243P   243U   236U   223U   209P   209U   191P   191U   177U   156P
                                            156U   104U   101P   101U   90U    77U    62P    62U    47P    47U    30P
                                            30U    3D     1D
FRICSLP  R EXTERNAL                         243U   209U   191U   156U   101U   62U    47U    30U
G        R VARIABLE               006652B   304U   302U   246U   224U   184U   179U   103U   90U    78U    195
GAMMAI   R VARIABLE               006634B   145U   116U   1135
GAMMAIP  R VARIABLE               006677B   145U   116U   1125
GRAVITY  R VARIABLE               005720B   185U   1845
H        R VARIABLE  /MES/        000001B   23P    8D
HCOEFF   R VARIABLE  /CONDIF/     000000B   334U   333U   274U   273U   10D
I        I VARIABLE               006656B   338U   337U   335U   3315   3301   327U   325U   323U   322U   321U   320U
                                            319U   3185   316U   3125   308U   306U   305U   304U   303U   302U   300U
                                            299U   298U   295U   293U   291U   290U   288U   287U   286U   285U   283U
                                            281U   277U   275U   274U   271U   270U   269U   268U   266U   264U   262U
                                            260U   258U   257U   256U   255U   254U   253U   252U   251U   250U   249U
                                            248U   247U   246U   245U   244U   243P   243U   242U   241U   239U   238U
                                            237U   236U   235U   234U   233U   2315   231U   230U   228U   227U   226U
                                            225U   224U   223U   222U   221U   219U   216U   215U   213U   212U   211U
                                            210U   209P   209U   208U   207U   2055   205U   1985   189U   187U   186U
                                            183U   182U   181U   180U   179U   177U   176U   175U   172U   170U   168U
                                            167U   165U   164U   163U   162U   160U   158U   156P   156U   155U   154U
                                            153U   152U   150U   149U   148U   147U   146U   145U   144U   142U   138U
                                            137U   136U   134U   132U   130U   129U   127U   126U   124U   123U   122U
                                            121U   120U   117U   113U   112U   111U   110U   109U   108U   107U   106U
                                            105U   104U   103U   102U   101P   101U   100U   99U    98U    97U    96U
                                            95U    94U    93U    91U    90U    89U    88U    86U    855    85U    84U
                                            82U    81U    80U    79U    78U    77U    76U    75U    72U    69U    68U
                                            66U    65U    64U    63U    62P    62U    61U    60U    58U    57U    56U
                                            56U    555    55U    47P    445    30P
II       I VARIABLE               006661B   325U   324U   317U   316U   315U   3145   307U   306U   305U   304U   302U
                                            301U   281U   280U   230U   228U   227U   226U   224U   204U   202U   201U
                                            2005   188U   187U   186U   184U   183U   182U   181U   179U   178U   158U
                                            157U   141U   140U   139U   138U   137U   84U    82U    81U    80U    78U
                                            54U    53U    52U    505
III      I VARIABLE               006660B   328U   3185   314U   3131   309U   2035   203U   200U   1991   190U   515
                                            51U    50U    491
IM       I VARIABLE               006726B   2405   240U   2395
```

| | | | | | | | | | | | | | | | |
|---|---|---|---|---|---|---|---|---|---|---|---|---|---|---|---|
| INDEX | I | VARIABLE | | 00b6459 | 340 | 335 | 33 | 245 | | | | | | | |
| IP | I | VARIABLE | | 0066741 | 2750 | 2670 | 2650 | 2630 | 2610 | 2590 | 2580 | 2555 | 2530 | 2515 | 11 |
| | | | | | 1140 | 1120 | 1110 | 1100 | 1090 | 1080 | 1060 | 1040 | 1055 | | |
| J | I | VARIABLE | | 0066748 | 3390 | 3370 | 3350 | 3340 | 3320 | 3310 | 3305 | 3291 | 3110 | 3080 | 1995 |
| | | | | | 1971 | 1960 | 1950 | 1955 | 1950 | 1940 | 1921 | 1510 | 1450 | 1420 | 935 |
| | | | | | 921 | | | | | | | | | | |
| K | I | VARIABLE | | 00b7238 | 2780 | 2335 | 2321 | | | | | | | | |
| KM | R | ARRAY | /PROP/ | 0000004 | 3200 | 2370 | 1530 | 950 | 120 | 90 | | | | | |
| KK | I | VARIABLE | | 0066639 | 2300 | 2075 | 2061 | 840 | 605 | 591 | | | | | |
| KTOTAL | R | VARIABLE | /PROP/ | 0000368 | 3200 | 2370 | 1530 | 950 | 120 | 90 | | | | | |
| LCHECK | I | VARIABLE | | 0067378 | 3230 | 3175 | | | | | | | | | |
| LENGTH | R | VARIABLE | /ALL/ | 0000018 | 1930 | 870 | 120 | 70 | | | | | | | |
| LHSENGY | R | VARIABLE | | 0000008 | 2300 | 2295 | 840 | 835 | 120 | | | | | | |
| LHSFLUX | R | VARIABLE | | 0031018 | 2750 | 2245 | 790 | 785 | 120 | | | | | | |
| MAX | I | VARIABLE | | 0066418 | 3390 | 3290 | 3298 | 3120 | 2570 | 2550 | 1980 | 1960 | 1920 | 1928 | 1020 |
| | | | | | 480 | 470 | 460 | 450 | 440 | 430 | 420 | 410 | 390 | 380 | 370 |
| | | | | | 350 | 320 | 310 | 300 | 290 | 280 | 270 | 260 | 250 | 230 | 205 |
| MAXT | I | VARIABLE | ARGUMENT | NO. 11 | 3380 | 3300 | 3308 | 20 | 10 | | | | | | |
| MMAX | I | ARRAY | /ALL/ | 0000168 | 3250 | 3170 | 2810 | 1560 | 200 | 70 | | | | | |
| MU | R | VARIABLE | /PFS/ | 0000058 | 2438 | 2098 | 1918 | 1568 | 1018 | 628 | 478 | 308 | 120 | 80 | |
| MMAX | I | VARIABLE | /ALL/ | 0000548 | 3280 | 3140 | 3130 | 3138 | 3090 | 2000 | 1990 | 1998 | 1900 | 500 | 490 |
| | | | | | 498 | 220 | 210 | 200 | 70 | | | | | | |
| NNODES | I | VARIABLE | /ALL/ | 0000028 | 3210 | 3200 | 2770 | 2450 | 2380 | 2370 | 1950 | 1940 | 1930 | 1540 | 1530 |
| | | | | | 1440 | 1480 | 990 | 980 | 950 | 890 | 880 | 870 | 70 | | |
| OUTPUT | | FILE | | | 3080 | 1890 | 1470 | 1460 | 1450 | 1440 | 390 | | | | |
| PAVE | R | VARIABLE | | 0067248 | 2690 | 2560 | 2355 | | | | | | | | |
| PI | R | VARIABLE | | 0066519 | 3000 | 2230 | 1770 | 770 | 185 | | | | | | |
| PP1 | R | ARRAY | | 0000018 | 2500 | 2475 | 50 | | | | | | | | |
| PP2 | R | ARRAY | | 0003118 | 2500 | 2485 | 50 | | | | | | | | |
| PP3 | R | ARRAY | | 0025718 | 2500 | 2495 | 50 | | | | | | | | |
| PP4 | R | ARRAY | | 0006218 | 2540 | 2525 | 50 | | | | | | | | |
| PP5 | R | ARRAY | | 0011318 | 2540 | 2535 | 50 | | | | | | | | |
| PRESENT | R | VARIABLE | | 0066678 | 830 | 805 | | | | | | | | | |
| PRESENZ | R | VARIABLE | | 0067158 | 1850 | 1815 | | | | | | | | | |
| PRETERM | R | VARIABLE | | 0066478 | 1450 | 1180 | 1115 | | | | | | | | |
| PTUP | R | VARIABLE | ARGUMENT | NO. 1 | 420 | 418 | 410 | 238 | 230 | 10 | | | | | |
| P2 | R | ARRAY | ARGUMENT | NO. 4 | 3148 | 3190 | 3040 | 3020 | 2545 | 2540 | 2505 | 2470 | 2465 | 2460 | 2350 |
| | | | | | 2538 | 2330 | 2260 | 2255 | 2078 | 2070 | 1810 | 1790 | 1528 | 1520 | 1440 |
| | | | | | 1130 | 1120 | 1110 | 1100 | 1060 | 1065 | 1060 | 1045 | 1040 | 1035 | 1030 |
| | | | | | 938 | 930 | 905 | 900 | 800 | 795 | 608 | 600 | 575 | 570 | 425 |
| | | | | | 20 | 10 | | | | | | | | | |
| QUAL | R | ARRAY | /PROPEL/ | 0006208 | 3148 | 3190 | 3060 | 3050 | 3040 | 3020 | 2900 | 2850 | 2600 | 2540 | 2580 |
| | | | | | 2530 | 2520 | 2438 | 2430 | 2338 | 2330 | 2280 | 2270 | 2260 | 2240 | 2150 |
| | | | | | 2100 | 2098 | 2090 | 2078 | 2078 | 1918 | 1870 | 1860 | 1830 | 1820 | 1810 |
| | | | | | 1790 | 1670 | 1620 | 1568 | 1560 | 1520 | 1520 | 1440 | 1380 | 1370 | 1290 |
| | | | | | 1200 | 1170 | 1140 | 1130 | 1120 | 1100 | 1090 | 1060 | 1018 | 1010 | 938 |
| | | | | | 930 | 820 | 810 | 800 | 780 | 680 | 630 | 628 | 620 | 608 | 600 |
| | | | | | 480 | 478 | 470 | 418 | 410 | 390 | 370 | 350 | 325 | 310 | 308 |
| | | | | | 300 | 280 | 265 | 110 | | | | | | | |
| QUALAM | R | VARIABLE | | 0066468 | 2690 | 2605 | | | | | | | | | |
| QUALAP | R | VARIABLE | | 0057278 | 2630 | 2595 | | | | | | | | | |
| QUALU | R | VARIABLE | | 0066378 | 350 | 315 | | | | | | | | | |
| QUALX | R | VARIABLE | | 0066408 | 390 | 380 | 375 | | | | | | | | |
| RADIUS | R | VARIABLE | | 0066549 | 3350 | 3340 | 3320 | 3165 | 3000 | 2750 | 2740 | 2710 | 2470 | 2438 | 2230 |
| | | | | | 2098 | 2025 | 1918 | 1770 | 1568 | 1040 | 1018 | 900 | 770 | 628 | 535 |
| | | | | | 428 | 308 | 225 | | | | | | | | |
| RATIO | R | VARIABLE | | 0068559 | 320 | 280 | 255 | | | | | | | | |
| RAVE | R | VARIABLE | | 0066758 | 2478 | 2460 | 2345 | 1040 | 1030 | 945 | | | | | |

```
RHO      R ARRAY    /PROPEL/   0003100   319P  319U  306U  305U  304U  302U  266U  265U  258U  253U  25
                                          243P  243U  233P  233U  228U  227U  224U  209P  209U  207P  207
                                          191P  187U  186U  183U  182U  179U  156P  156U  152P  152U  144U
                                          138U  137U  117U  114U  113U  112U  110U  109U  106U  101P  101U
                                           93P   93U   82U   81U   78U   62P   62U   60P   60U   48U   47P
                                           47U   41P   41U   37U   30P   30U   28U   25U   23P   23U   11D
RHOGAM   R VARIABLE                0006418   269U  266S
RHOGAP   R VARIABLE                0067348   269U  265S
RHOL     R ARRAY    /PROPEL/   0000008   319P  319U  306U  305U  304U  302U  264U  263U  258U  253U  252U
                                          243P  243U  233P  233U  228U  227U  224U  209P  209U  207P  207U
                                          191P  187U  186U  183U  182U  179U  156P  156U  152P  152U  144U
                                          138U  137U  117U  114U  113U  112U  110U  109U  106U  101P  101U
                                           93P   93U   82U   81U   78U   62P   62U   60P   60U   48U   47P
                                           47U   41P   41U   37U   30P   30U   28U   25U   23P   23U   11D
RHOLAM   R VARIABLE                0067318   269U  264S
RHOLAP   R VARIABLE                0067328   269U  263S
RHO2     R ARRAY    ARGUMENT   NO.  8   323U  322U  320U  319S  306U  302U  300U  275U  268U  267U  258U
                                          253U  252U  249U  248U  245U  244U  241U  237U  234U  233S  228U
                                          224U  223U  208U  207S  187U  179U  177U  155U  153U  152S  144U
                                          138U  117U  114U  113U  112U  110U  109U  106U  104U   99U   98U
                                           97U   95U   94U   93S   90U   82U   78U   77U   61U   60S   48S
                                           45U   43U   41S   29U   28S   20    10
RHO2EVL  R VARIABLE                0067048   147U  119U  118S
RHO2EVR  R VARIABLE                0067018   145U  116U  115S
RHO2EVS  R VARIABLE                0067028   145U  118U  116S
RHSENGY  R VARIABLE                0066728   304S  230U  185S   84U
RHSFLOW  R VARIABLE                0066648   302S  225U  179S   79U
RHS4     R VARIABLE                0067118   307U  305S  188U  186S  146U  140S  140U  139U  137S
RHS5     R VARIABLE                0067128   307U  306S  188U  187S  146U  141S  141U  139U  138S
RR       R ARRAY    /ALL/      0000048   316U  202U   53U   22U   7D
RSTAR    R VARIABLE                0066508   335U  334U  332S  275U  274U  271S
RT       R ARRAY    ARGUMENT   NO. 10   335U  334U  274U   6D   1D
RL       R VARIABLE /ALL/      0000034   332U  271U   7D
SLIP     R ARRAY    ARGUMENT   NO. 13   306U  288U  287U  286U  262U  261U  258U  253U  252U  243P  243U
                                          228U  213U  212U  211U  209P  209U  191P  191U  187U  165U  164U
                                          163U  156P  156U  144U  138U  124U  123U  121U  117U  114U  113U
                                          112U  110U  109U  106U  101P  101U   86S   86U   82U   66U   65U
                                           64U   62P   62U   58S   58U   47P   47U   30P   30U   27S   3D
                                           1D
SLIPAM   R VARIABLE                0067318   269U  262S
SLIPAP   R VARIABLE                0067308   269U  261S
SLIPR    R ARRAY    /PROPEL/   0011308   287U  243P  243U  212U  209P  209U  191P  164U  156P  156U  123U
                                          101P  101U   65U   62P   62U   47P   47U   32U   30P   30U   11D
T        R ARRAY    ARGUMENT   NO.  7   337U  334U  332U  331U  319P  319U  274U  271U  270U  243P  243U
                                          233P  233U  209P  209U  207P  207U  191P  191U  156P  156U  152P
                                          152U  101P  101U   93P   93U   62P   62U   60P   60U   47P   47U
                                           41P   41U   39U   30P   30U   23P   23U   2D    1D
TEPP     R ARRAY                   0014418   332U  331U  271U  270U  195S  194S   89S   88S   6D
TMAX     R VARIABLE ARGUMENT   NO.  2   196U  194U   89U   88U   1D
TMIN     R VARIABLE ARGUMENT   NO.  3   194U   89U   1D
TOP      R EXTERNAL                        23D
TKES     R ARRAY    ARGUMENT   NO.  9   337S  335S  335U  334S  275U  274S   2D    1D
UF       R ARRAY                   0022618   319P  319U  305U  304U  303U  293S  293U  233P  233U  207P  207U
                                          186U  183U  180U  170S  170U  152P  152U  146U  137U  136U  132S
                                          132U   93P   93U   60P   60U   41P   41U   39U   38U   23P   23U
                                           4D
UFG      R ARRAY                   0017518   319P  319U  306U  303U  258U  233P  233U  228U  207P  207U  187U
                                          180U  152P  152U  144U  138U  136U  117U  114U  109U   93P   93U
```

| | | | | | | | | | | | | | | |
|---|---|---|---|---|---|---|---|---|---|---|---|---|---|---|
| | | | | | 820 | 60P | 60U | 4P | 41U | 39U | 38U | 23P | 23U | 4D |
| UG | R | VARIABLE | | 0067104 | 305U | 304U | 303S | 186U | 183U | 180S | 146U | 137U | 136S | |
| V | R | ARRAY | ARGUMENT | NO. 6 | 325S | 322S | 322U | 300U | 297U | 298U | 295U | 291U | 275U | 256U |
| | | | | | 244U | 245U | 244U | 243P | 243U | 242U | 241S | 241U | 223U | 222U |
| | | | | | 219U | 216U | 209P | 209U | 208S | 191P | 191U | 177U | 176U | 175U |
| | | | | | 164U | 156P | 156U | 155S | 155U | 144U | 134U | 130U | 127U | 126U |
| | | | | | 108U | 104U | 101P | 101U | 100U | 99U | 98U | 97S | 97U | 77U |
| | | | | | 75U | 72U | 69U | 62P | 62U | 61S | 46U | 45U | 43S | 30P |
| | | | | | 29S | 20 | 10 | | | | | | | |
| VAVE | R | VARIABLE | | 0066368 | 247U | 242S | 104U | 100S | 47P | 46S | | | | |
| VG | R | VARIABLE | | 0067078 | 305U | 304U | 302U | 298S | 295S | 292S | 288S | 186U | 183U | 182U |
| | | | | | 179U | 175S | 172S | 169S | 165S | 146U | 137U | 134S | 131S | 127S |
| VGL | R | VARIABLE | | 0066658 | 227U | 226U | 224U | 222S | 219S | 217S | 213S | 81U | 80U | 78U |
| | | | | | 72S | 70S | 66S | | | | | | | |
| VIN | R | VARIABLE | | 0066444 | 323U | 322U | 321S | 320S | 241U | 238S | 237S | 155U | 154S | 153S |
| | | | | | 96S | 95S | | | | | | | | |
| VL | R | VARIABLE | | 0067068 | 305U | 304U | 302U | 299S | 296S | 291S | 288U | 287S | 186U | 183U |
| | | | | | 181U | 179U | 176S | 173S | 168S | 165U | 164S | 146U | 137U | 135S |
| | | | | | 126S | 124U | 123S | | | | | | | |
| VLL | R | VARIABLE | | 0066648 | 227U | 226U | 224U | 221S | 220S | 216S | 213U | 212S | 81U | 80U |
| | | | | | 75S | 73S | 69S | 66U | 65S | | | | | |
| WEI | R | VARIABLE | | 0067034 | 147U | 118U | 117S | | | | | | | |
| WEIP | R | VARIABLE | | 0067008 | 145U | 116U | 114S | | | | | | | |
| XDOT | R | VARIABLE | /MFS/ | 0000148 | 39U | 25U | 23P | 8D | | | | | | |

LIST OF VARIABLE AND ARRAY NAMES IN ADDRESS ORDER IN EACH BLOCK

| BLOCK | LENGTH | | | | | | | | |
|---|---|---|---|---|---|---|---|---|---|
| *LOCAL | 1670 | 0000008 LHSENGY | 0000018 PP1 | 0003118 PP2 | 0006218 PP4 | 0011318 PP5 |
| | | 0014418 TEMP | 0017518 UFG | 0022618 UF | 0025718 PP3 | 0031018 LHSFLOW |
| | | 0066148 GAMMAI | 0066358 DRAG1 | 0066368 VAVE | 0066378 QUALO | 0066408 QUALX |
| | | 0066418 MAX | 0066428 EOLD | 0066438 RHOGAM | 0066448 VIN | 0066458 INDEX |
| | | 0066468 QUALAM | 0066478 PRETERM | 0066508 HSTAR | 0066518 PI | 0066528 G |
| | | 0066538 FLOW | 0066548 RADIUS | 0066558 RATIO | 0066568 E | 0066578 DQTM |
| | | 0066588 III | 0066618 T1 | 0066628 AAVE | 0066638 KK | 0066648 VL1 |
| | | 0066658 VG1 | 0066668 RHSFLOW | 0066678 PRESENI | 0066708 AKINENI | 0066718 ALHS3 |
| | | 0066728 RHSENGY | 0066738 ALENG | 0066748 J | 0066758 HAVE | 0066768 IP |
| | | 0066778 GAMMAIP | 0067008 WEIP | 0067018 RHOZEVR | 0067028 RHOZEVM | 0067038 WEI |
| | | 0067048 RHOZEVL | 0067058 ENER | 0067068 VL | 0067078 VG | 0067108 UG |
| | | 0067118 RHS4 | 0067128 RHS5 | 0067138 ENER1 | 0067148 DRAG2 | 0067158 PRESEN2 |
| | | 0067168 AKINEN2 | 0067178 AINTEN2 | 0067208 GRAVITY | 0067218 ALHS1 | 0067228 ALHS2 |
| | | 0067238 K | 0067248 PAVE | 0067258 FAVE | 0067268 IN | 0067278 QUALAP |
| | | 0067288 SLIPAP | 0067318 SLIPAM | 0067328 RHOLAP | 0067338 RHOLAM | 0067348 RHOGAP |
| | | 0067358 DORJ | 0067368 DORI | 0067378 LCHECK | | |
| /ALL/ | 45 | 0000008 DX | 0000018 LENGTH | 0000028 NNODES | 0000038 RI | 0000048 RRM |
| | | 0000168 NMAX | 0000308 FFLOW | 0000428 AL | 0000548 NNMAX | |
| /PROPEL/ | 1000 | 0000008 RHOL | 0000108 RHOG | 0000208 QUAL | 0001308 SLIPR | 0014408 DUMMY |
| /MFS/ | 13 | 0000008 MU | 0000018 M | 0000028 AREA | 0000148 XDOT | |
| /PROP/ | 31 | 0000008 RM | 0000368 KTOTAL | | | |
| /CONDIF/ | 2 | 0000008 HCOEFF | 0000018 CONDUC | | | |

AMOUNT OF STORAGE USED BY SUBPROGRAM

(BLOCK COMMON AREA) 1091 - 0321035

ABBREVIATIONS USED ABOVE (THESE ARE KEYED TO THE SOURCE LISTING LINE NUMBER)

& USED IN FORTRAN ASSIGN STATEMENT  # ARGUMENT IN CALL OR FUNCTION CALL

| | | | | | |
|---|---|---|---|---|---|
| LOCAL STORAGE AREA | 1470 | = 0012068 | B | OCTAL ADDRESS RELATIVE TO PROGRAM | R FORMAT USED IN A READ STATEME |
| FORMAT STATEMENTS | 74 | = 0001128 | D | DEFINED IN DECLARATIVE STATEMENT | S STORED SO CONTENTS MAY BE CHANGED |
| CONSTANTS | 15 | = 0000178 | E | STATEMENT NUMBER ENDING A DO LOOP | T STATEMENT NUMBER USED IN A TRACE |
| ENTRY CODE | 381 | = 0005758 | I | INDEX OF A DO OR IMPLIED DO LOOP | U NAME USED IN EXECUTABLE STATEMENT |
| EXECUTABLE CODE | 1343 | = 0024778 | J | STATEMENT NUMBER USED IN TRANSFER | W FORMAT USED IN A WRITE STATEMENT |
| ACTUAL ARGUMENTS | 61 | = 0000758 | L | SOURCE LINE OF A STATEMENT NUMBER | LR LONGEST RECORD PRODUCED BY FORMAT |
| TEMPORARY STORAGE | 9 | = 0000118 | N | NAME USED AS A DO LOOP PARAMETER | * (R=7) NAME DECLARED BUT NOT USED |
| TOTAL (LESS COMMON) | 3552 | = 0067408 | | | |

7600 COMPILATION -- MNF4 LEVEL 5.24 11 OCT 81 16.25.50

```
      SUBROUTINE FRICSPLT,RHOF,RHOG,QUAL,FRIC,SLIP,V,RADIUS,MU,SLIPR,DU
     1MMY,II
      REAL MU,LM,L1,LS
      G=9.8
      K=1
      SIGMA=(-0.12*T+75.7)*1.E-3
      AAA=247.9/(T+133.15)
      MU=(241.**(10.1**AAA))*1.E-07
      RHON=(1.-QUAL)*RHOF+QUAL*RHOG
      IF (QUAL.LT.1.E-6) GO TO 65
   15 CONTINUE
      SLIPO=SLIP
      IF (QUAL.LT.1.).AND.(QUAL.GT.0.)) GO TO 16
      SLIP=0.
      DUMMY=LHSINGLPHASE
      GO TO 65
   16 VELVOL=V*(1.-QUAL)*((RHOF-RHOM)/RHOM)*SLIP
  215 FORMAT(1X,*LS=*,F10.4,5X,*LM=*,F10.4,5X,*VGD=*,F10.4)
  210 FORMAT(1X,8X,*,15.1X,*SLIP=*,F8.4,1X,*SLIPO=*,F8.4,1X,*SLIPMIN=*
     1,F8.4,/,9X,*SLIPMAX=*,F8.4,1X,*VELLIQ=*,F8.4,1X,*VELGAS=*,F8.4,
     21X,*DUMMY=*,A12,/)
  220 FORMAT(1X,*X=*,I5.5X,*SLIP=*,F10.4,5X,*SLIPO=*,F10.4,5X,*VELLIQ=*
     1,F10.4,5X,*VELGAS=*,F10.4)
      VELGAS=VELVOL/(1.-QUAL)*SLIP
      VELLIQ=VELGAS-SLIP
      IF(K.EQ.1) GO TO 62
C     PRINT 215,LS,LM,VGD
C     PRINT 210,K,SLIP,SLIPO,SLIPMIN,SLIPMAX,VELLIQ,VELGAS,DUMMY
C     GO TO 63
C62   PRINT 220,K,SLIP,SLIPO,VELLIQ,VELGAS
      IF(VELLIQ.LT.0.01 GO TO 61
      FLOWRT=VELGAS*QUAL/VELVOL
      VGD=VELGAS*QUAL*(RHOF/(G*SIGMA))**0.25
      DIAM=2.*RADIUS
      LM=1.071-0.7277*VELVOL*VELVOL/DIAM
      IF (LM.LT.0.13) LM=0.13
      LS=(0.36*VGD*VELLIQ*(1.-QUAL))/(VELGAS*QUAL)
      IF (QUAL.GT.0.) GO TO 46
      PRINT 1000,VELGAS,QUAL,SLIP,VELVOL,V
 1000 FORMAT (1X,*SOMETHING HAS GONE WRONG*,I5,5X,5F12.5)
   46 CONTINUE
      LM=75.*84.*(VGD*VELLIQ*(1.-QUAL))/(VELGAS*QUAL))**0.75
      IF (FLOWRT.LE.LBI GO TO 20
C     SLIPS=0.35*SQRT(G*DIAM)/(1.-QUAL)
C     ABOVE EXPRESSION FOR SLIPS WAS CHANGED AS FOCCUS ON 10.15.80.
      SLIPS=1.35*SQRT(G*DIAM)+0.2*VELVOL
C     FOLLOWING LINE WAS INSERTED ON 5.1.81,BUT WAS NOT USED BECAUSE IT
C     GAVE POOR CONVERGENCE.
C     SLIPS=SLIPS/(1.-QUAL)
C     SLIPS=0.35*SQRT(G*DIAM)+0.7*VELLIQ
      IF (VGD.LE.LS) GO TO 30
      IF ((VGD.GT.LS).AND.(VGD.LE.LM)) GO TO 40
      GO TO 50
   20 CONTINUE
      IF ((QUAL.GE.1.).OR.(QUAL.LT.0.).OR.(RHOF.LT.0.).OR.(RHOF.LE.RHOG)
     1.OR.(SIGMA.LT.0.)) GO TO 100
      SLIP=(1.-QUAL)**1.5*1.53*(G*(RHOF-RHOG)*SIGMA/RHOF**2)**0.25
```

```
 41.  0002048        DUMMY=UNUSABLE
 42.  0002058        GO TO 40
 43.  0002068     30 SLIP=SLIPS
 44.  0002078        DUMMY=UNSLUG
 45.  0002118        GO TO 50
 46.  0002128     40 RATIO=(LM-VGO)/(LM-LS)
 47.  0002168        SLIP=(1.-RATIO)*SLIPS
 48.  0002208        DUMMY=LOWTRANSITION
 49.  0002228        GO TO 60
 50.  0002238     50 SLIP=0.
 51.  0002248        DUMMY=UNMIST
 52.  0002258        GO TO 60
 53.  0002278     61 SLIP=3.56*QUAL**3*(1.-QUAL)**.3333
 54.  0002358        DUMMY=10HNEGVELLIQ
 55.  0002368     60 CONTINUE
 56.  0002408        IF(K.EQ.1) GO TO 26
 57.  0002418        IF(SLIP.LT.SLIPMIN) SLIPMIN=SLIP
(57) - CAUTION ----------SLIPMIN IS NOT SET ABOVE
 58.  0002458        IF(SLIP.GT.SLIPMAX) SLIPMAX=SLIP
(58) - CAUTION ----------SLIPMAX IS NOT SET ABOVE
 59.  0002478        K=K+1
 60.  0002508        IF (K.LT.101 GO TO 15
 61.  0002518        IF(K.GE.10 .AND. ABS(SLIP-SLIPO) .GT. .001) GO TO 25
 62.  0002608        GO TO 65
 63.  0002608     26 K=K+1
 64.  0002628        SLIPMIN=SLIP
 65.  0002638        SLIPMAX=SLIP
 66.  0002638        GO TO 15
 67.  0002658     25 SLIP=(SLIPMIN+SLIPMAX)/2.
 68.  0002678        DUMMY=7HIMPOSED
 69.  0002708        VELVOL=V*(1.-QUAL)*((RHOF-RHOM)/RHOM)*SLIP
 70.  0003008        VELGAS=VELVOL+(1.-QUAL)*SLIP
 71.  0003038        VELLIQ=VELGAS-SLIP
                C     PRINT 215,LS,LM,VGO
                C     PRINT 210,K,SLIP,SLIPO,SLIPMIN,SLIPMAX,VELLIQ,VELGAS,DUMMY
 72.  0003048     65 CONTINUE
 73.  0003058        GAMMA=SQRT(RHOF/RHOG)
 74.  0003118        REYN=(RHOM*V)*2.*RADIUS/MU
 75.  0003148        IF (V.LT.1.E-4) GO TO 10
 76.  0003178        IF (REYN.LT.2000.) FCOEFF=64./REYN
 77.  0003238        IF (REYN.GT.2000.) FCOEFF=0.18/(REYN)**0.2
                CCCC  DETERMINE BCOEFF
 78.  0003308        RHOV=RHOM*V
 79.  0003318        IF ((GAMMA.LE.9.5).AND.(RHOV.LE.500.)) BCOEFF=4.8
 80.  0003418        IF ((GAMMA.LE.9.5).AND.(RHOV.GT.500.).AND.(RHOV.LT.1900.)) BCOEFF=
                   12400./RHOV
 81.  0003528        IF ((GAMMA.LE.9.5).AND.(RHOV.GE.1900.)) BCOEFF=55./SQRT(RHOV)
 82.  0003638        IF ((GAMMA.GT.9.5).AND.(GAMMA.LT.28.).AND.(RHOV.LE.600.)) BCOEFF
                   1=520./(GAMMA*SQRT(RHOV))
 83.  0003778        IF ((GAMMA.GT.9.5).AND.(GAMMA.LT.28.).AND.(RHOV.GT.600.)) BCOEFF
                   1=21./GAMMA
 84.  0004108        IF (GAMMA.GE.28.) BCOEFF=15000./(GAMMA*GAMMA*SQRT(RHOV))
 85.  0004178        IF (QUAL.LT.1.E-7) GO TO 5
                C     IF (VELLIQ.LT.1.E-7) GO TO 10
                C     SLIPR IS CALCULATED HERE AND THIS STATEMENT IS EXECUTED FOR CASES.
 86.  0004218        SLIPR=(SLIP/VELLIQ)+1.
 87.  0004238        IF (VELLIQ.LT.1.E-7) SLIPR=1.
 88.  0004268        QUAX=1./11.*((1.-QUAL)/QUAL)*(RHOF/RHOG)*(1./SLIPR))
```

```
    89.  0004368        > IF (QUAL.LT.1.E-7) QUAL=0.
    90.  0004478          DELP=RHOJ*FL.*(CA*MA**2-1.)*(8COEFF*QUAL*(1.-QUAL)+QUAL*QUAL)
    91.  0004528          FRIC=FCOEFF*DELP/RHOF
    92.  0004568          IF (SLIP.GE.0.) RETURN
    93.  0004608      200 FORMAT(4X,*SLIP=*,E12.5,10X,*QUAL=*,E12.5)
    94.  0004608          PRINT 200,SLIP,QUAL
    95.  0004658          RETURN
    96.  0004678       10 FRIC=0.
    97.  0004678          RETURN
    98.  0004728      100 PRINT 1000,(SLIP,QUAL,RHOF,RHOG,SIGMA)
    99.  0005028          SLIP=0.
   100.  0005028          RETURN
   101.  0005058          END
>          CAUTION ----------DUMMY ARGUMENT E WAS NEVER USED
>          CAUTION ----------STATEMENT NUMBER 215 WAS NEVER USED
>          CAUTION ----------STATEMENT NUMBER 220 WAS NEVER USED
>          CAUTION ----------STATEMENT NUMBER 210 WAS NEVER USED
```

$\Delta P = \rho_L \frac{\Delta P_{TP}}{\Delta P_{LO}}$

TABLE OF STATEMENT NUMBERS

| NUMBER | USE | ADDRESS | SOURCE | PROGRAM | REFERENCES |
|---|---|---|---|---|---|
| 5 | EXECUTABLE | 0004378 | 89L | 85J | |
| 10 | EXECUTABLE | 0004678 | 96L | 75J | |
| 15 | EXECUTABLE | 0000258 | 66J | 60J | 9L |
| 16 | EXECUTABLE | 0000369 | 19L | 11J | |
| 20 | EXECUTABLE | 0001528 | 38L | 33J | |
| 25 | EXECUTABLE | 0002058 | 67L | 61J | |
| 26 | EXECUTABLE | 0002618 | 63L | 56J | |
| 30 | EXECUTABLE | 0002078 | 43L | 35J | |
| 40 | EXECUTABLE | 0002138 | 46L | 36J | |
| 46 | EXECUTABLE | 0001168 | 31L | 28J | |
| 50 | EXECUTABLE | 0002248 | 50L | 37J | |
| 60 | EXECUTABLE | 0002408 | 55L | 52J | 49J 45J 42J |
| 61 | EXECUTABLE | 0002278 | 53L | 21J | |
| 65 | EXECUTABLE | 0003058 | 72L | 62J | 14J |
| 100 | EXECUTABLE | 0004728 | 98L | 39J | |
| 200 | FORMAT | LR = 65 | 94W | 93L | |
| 210 | (UNUSED) | LR = 71 | 17L | | |
| 215 | (UNUSED) | LR = 56 | 16L | | |
| 220 | (UNUSED) | LR = 96 | 18L | | |
| 1000 | FORMAT | LR = 98 | 98W | 30L | 29W |

TABLE OF NAMES ENCOUNTERED

| NAME | TYPE | MAIN USE | BLOCKS | ADDRESS | SOURCE | PROGRAM | REFERENCES |
|---|---|---|---|---|---|---|---|
| AAA | R | VARIABLE | | 0010728 | 70 | 65 | |
| ABS | R | STANDARD | | | 61U | | |
| BCOEFF | R | VARIABLE | | 0011078 | 90U | 84S | 83S 82S 81S 80S 79S |
| DELP | R | VARIABLE | | 0011118 | 91U | 90S | |
| DIAM | R | VARIABLE | | 0011028 | 34U | 25U | 24S |
| DUMMY | R | VARIABLE | ARGUMENT NO. 11 | | 68S | 54S | 51S 48S 44S 41S 13S 10 |

```
                SUBROUTINE SPLINT(PZ,T,RHOZ,Y,T,
                DIMENSION PZ(1),T(1),RHOZ(1),Y(1),T(1),Y(200),A(8),P(2),Q(2)
                COMMON/ALL/DX,LENGTH,NNODES,R1,RRW(10),AMAX(10),PFLOW(10),ALL(10),
               1N,MAX
                COMMON/PROPEL/PHOL(200),RHOG(200),QUAL(200),SLIPR(200),DUMMY(200)
                COMMON/IGSZZZZ/MODE(200)
                COMMON/RESHAV/MWELL,IWELL,MONTH,YEAR,DOTM,PPTOP,HH
                REAL LENGTH
                PRINT 4020
                PRINT 4050
                MAX=MAX(NNMAX)
                RADIUS=RRW(NNMAX)
                DO 10 I=1,MAX
   10           Y(I)=LENGTH-(I-1)*DX
                MM=Y(1)/100.+1.02
                YF=100.**MM
                DO 810 I=1,MAX
                M=MAX-(I-1)
C               PZ(M)=PZ(M+1)-1.0172E-05-1.0315
                RHE=(1.-QUAL(M))*RHOL(M)+QUAL(M)*RHOG(M)
                SLIPRZ=SQRT(PHOL(M)/RHOZ(M))
  810           PRINT 1050,M,Y(M),PZ(M),P(M),RHOZ(M),V(M),T(M),QUAL(M),DUMMY(M)
 1050 FORMAT(2X,I3,F8.1,8X,E12.6,10X,F10.2,10X,F8.2,12X,E12.5,5X,F8.4,2X
               1,F8.4,5X,A12)
                K=1
                IF(K.EQ.1) RETURN
C               SUBROUTINE OBJCTG SETS UP THE DISPLAY AREA IN COMPUTER FRAME
C               COORDINATES WHILE SUBJEG DOES IN LOCAL(WORLD) COORDINATES.
C               CHANGE CHARACTER SIZE,F IS NUMBER OF TIMES NORMAL SIZE FOR CHARA
C               CTERS.
                CALL MODESG(Z*MODE,6,8H COYAL  )
                CALL SETSMG(Z*MODE,45,2.0)
C               SUBROUTINE SETS*G SETS A SINGLE VALUE IN THE MODE SET ARRAY.
                CALL OBJCTG(Z*MODE,0.,0.,100.,100.)
                CALL SUBJEG(Z*MODE,0.,0.,100.,100.)
C               TO LABEL DEPTH ON THE Y-AXIS
                CALL SETSMG(Z*MODE,46,90.)
                CALL LEGNDG(Z*MODE,1.,50.,9,8HDEPTH(M))
                CALL SETS*G(Z*MODE,46,0.)
                P(1)=10.
                P(2)=15.
                Q(1)=12.
                Q(2)=12.
                IPAT=1777B
                CALL DASHG(Z*MODE,2,P,Q,IPAT,0,0.,0.)
                CALL LEGNDG(Z*MODE,17.,2(1),20,20HPRESSURE(KG/CM2-ABS))
                P(1)=55.
                P(2)=60.
                IPAT=3478
                CALL DASHG(Z*MODE,2,P,Q,IPAT,0,0.,0.)
                CALL LEGNDG(Z*MODE,65.,Q(1),10,10HSATURATION)
                P(1)=35.
                P(2)=43.
                Q(1)=97.
                Q(2)=97.
                IPAT=37B
C               Q NOT CHANGED SINCE NOTATIONS ARE PRODUCED AT THE SAME HEIGHT.
```

```
> ...  CAUTION ----------  -----DUMMY ARGUMENT RR WAS NEVER USED
> ...  CAUTION ----------  ----------SLIPR2 WAS SET BUT NEVER USED
> ...  CAUTION ----------  ----------RRE WAS SET BUT NEVER USED
```

TABLE OF STATEMENT NUMBERS

| NUMBER | USE | ADDRESS | SOURCE PROGRAM REFERENCES |
|---|---|---|---|
| 10 | END OF DO | 0003378 | 13L 12E |
| 810 | END OF DO | 0003566 | 20L 16E |
| 1050 | FORMAT | LR +135 | 22L 20W |
| 4020 | FORMAT | LR + 70 | 81L 8W |
| 4050 | FORMAT | LR +131 | 88L 9W |
| 5000 | FORMAT | LR + 97 | 82L 50W |
| 5001 | FORMAT | LR + 67 | 83L 52W |
| 5002 | FORMAT | LR + 59 | 84L 54W |

TABLE OF NAMES ENCOUNTERED

| NAME | TYPE | MAIN USE | BLOCKS | ADDRESS | SOURCE PROGRAM REFERENCES |
|---|---|---|---|---|---|
| AMELL | R | VARIABLE | /KESHAV/ | 0000001 | 50U 6D |
| DASHG | R | EXTERNAL | | | 77U 70U 60U 48U 41U 36U |
| OUTP | R | VARIABLE | /KESHAV/ | 0000048 | 52U 6D |
| DUMMY | R | ARRAY | /PROPEL/ | 0014431 | 20U 4D |
| DX | R | VARIABLE | /ALL/ | 0000004 | 13U 3D |
| E | R | ARRAY | ARGUMENT | NO. 2 | 20U 2D 1D |
| GMTOG | R | EXTERNAL | | | 61U |
| HH | R | VARIABLE | /KESHAV/ | 0000068 | 54U 6D |
| I | I | VARIABLE | | 0013420 | 20U 19S 17U 16I 13U 12I |
| IA | I | ARRAY | | 0000008 | 55P 54S 53P 52S 51P 50S 2D |
| IPAT | I | VARIABLE | | 0013464 | 77P 72S 70P 69S 60P 59S 48P 47S 41P 40S 36P 39S |
| IRELL | I | VARIABLE | /KESHAV/ | 0000018 | 50U 6D |
| K | I | VARIABLE | | 0013439 | 23U 22S |
| LABELG | I | EXTERNAL | | | 76U 68U 65U 62U |
| LEGNDG | I | EXTERNAL | | | 55U 53U 51U 49U 42U 37U 29U |
| LENGTH | R | VARIABLE | /ALL/ | 0000014 | 13U 7D 3D |
| M | I | VARIABLE | | 0013536 | 20U 19U 18U 18U 17S |
| MAX | I | VARIABLE | | 0013458 | 77P 70P 60P 20U 17U 16N 12U 12N 10S |
| MM | I | VARIABLE | | 0013474 | 15U 14S |
| MMAX | I | ARRAY | /ALL/ | 0000164 | 10U 3D |
| MODFSG | I | EXTERNAL | | | 24U |
| MONTH | I | VARIABLE | /KESHAV/ | 0000029 | 50U 6D |
| NNMAX | I | VARIABLE | /ALL/ | 0000548 | 11U 10U 3D |
| OBJECTG | R | EXTERNAL | | | 57U 26U |
| OUTPUT | | FILE * | | | 20U 9U 8U |
| P | R | ARRAY | | 0000108 | 44P 44S 43S 41P 39S 38S 36P 32S 31S 2D |
| PAGEG | R | EXTERNAL | | | 79U |
| PPTOP | R | VARIABLE | /KESHAV/ | 0000054 | 52U 6D |
| PZ | R | ARRAY | ARGUMENT | NO. 1 | 60P 60U 20U 2D 1D |
| Q | R | ARRAY | | 000012H | 49P 48P 46S 45S 42P 41P 37P 36P 34S 33S 2D |
| QUAL | R | ARRAY | /PROPEL/ | 0006208 | 77P 20U 19U 4D |

| | | | | | | | | | | | | | |
|---|---|---|---|---|---|---|---|---|---|---|---|---|---|
| RA | R VARIABLE | | 0013518 | 54U | 13S | | | | | | | | |
| RHOU | R ARRAY | /PROPEL/ | 0003104 | 18U | 4D | | | | | | | | |
| RHOL | R ARRAY | /PROPEL/ | 0000004 | 14U | 18U | 4D | | | | | | | |
| RHO2 | R ARRAY | ARGUMENT NO. 3 | | 20U | 19U | 2D | 1D | | | | | | |
| RRE | R VARIABLE | | 0013508 | 16S | | | | | | | | | |
| RRW | R ARRAY | /ALL/ | 0000048 | 11U | 3D | | | | | | | | |
| RSETMG | R EXTERNAL | | | 76U | | | | | | | | | |
| SETSMG | R EXTERNAL | | | 75U | 74U | 73U | 67U | 64U | 63U | 56U | 30U | 28U | 25U |
| SLIPR2 | R VARIABLE | | 0013448 | 19S | | | | | | | | | |
| SORT | R STANDARD | | | 19U | | | | | | | | | |
| SUBJEC | R EXTERNAL | | | 71U | 66U | 58U | 27U | | | | | | |
| T | R ARRAY | ARGUMENT NO. 5 | | 7DP | 7DU | 2DU | 2D | 1D | | | | | |
| V | R ARRAY | ARGUMENT NO. 4 | | 2DU | 2D | 1D | | | | | | | |
| Y | R ARRAY | | 0013148 | 77P | 7DP | 6DP | 2DU | 14U | 13S | 2D | | | |
| YEAR | R VARIABLE | /RESHAV/ | 0000038 | 5DU | 6D | | | | | | | | |
| YM | R VARIABLE | | 0013528 | 71P | 66P | 58P | 15S | | | | | | |
| ZMODE | R ARRAY | /IGS/ZZ/ | 0000008 | 79P | 78P | 77P | 76P | 75P | 74P | 73P | 71P | 70P | 68P | 67P |
| | | | | 66P | 65P | 64P | 63P | 62P | 61P | 60P | 58P | 57P | 56P | 55P |
| | | | | 53P | 51P | 49P | 48P | 42P | 41P | 37P | 36P | 30P | 29P | 28P |
| | | | | 27P | 26P | 25P | 24P | 5D | | | | | | |

LIST OF VARIABLE AND ARRAY NAMES IN ADDRESS ORDER IN EACH BLOCK

| BLOCK | LENGTH | | | | | | | | |
|---|---|---|---|---|---|---|---|---|---|
| .LOCAL. | 222 | 0000008 IA | 0000108 P | 0000128 Q | 0000148 Y | 0013428 I | | | |
| | | 0013438 K | 0013448 SLIPR2 | 0013458 MAX | 0013468 IPAT | 0013478 MM | | | |
| | | 0013508 RRE | 0013518 RADIUS | 0013528 YM | 0013538 M | | | | |
| /ALL/ | 45 | 0000008 DX | 0000018 LENGTH | 0000028 NNODES | 0000038 RL | 0000048 RRW | | | |
| | | 0000168 MMAX | 0000308 FFLOW | 0000428 AL | 0000548 NNMAX | | | | |
| /PROPEL/ | 1000 | 0000004 RHOL | 0003104 RHOU | 0006208 QUAL | 0011308 SLIPR | 0014408 DUMMY | | | |
| /IGS/ZZ/ | 200 | 0000008 ZMODE | | | | | | | |
| /RESHAV/ | 7 | 0000008 AWELL | 0000018 IWELL | 0000028 MONTH | 0000038 YEAR | 0000048 DOTM | | | |
| | | 0000058 PPTIP | 0000068 MM | | | | | | |

AMOUNT OF STORAGE USED BY SUBPROGRAM

| | | |
|---|---|---|
| BLOCK COMMON AREA | 1252 | = 0023448 |
| LOCAL STORAGE AREA | 222 | = 0003368 |
| FORMAT STATEMENTS | 55 | = 0000678 |
| CONSTANTS | 61 | = 0000758 |
| ENTRY CODE | 26 | = 0000328 |
| EXECUTABLE CODE | 181 | = 0002658 |
| ACTUAL ARGUMENTS | 200 | = 0003104 |
| TEMPORARY STORAGE | 3 | = 0000038 |
| TOTAL (LESS COMMON) | 748 | = 0013548 |

ABBREVIATIONS USED ABOVE (THESE ARE KEYED TO THE SOURCE LISTING LINE NUMBER)

| | | | |
|---|---|---|---|
| A | USED IN FORTRAN ASSIGN STATEMENT | P | ARGUMENT IN CALL OR FUNCTION CALL |
| B | OCTAL ADDRESS RELATIVE TO PROGRAM | R | FORMAT USED IN A READ STATEMENT |
| D | DEFINED IN DECLARATIVE STATEMENT | S | STORED SO CONTENTS MAY BE CHANGED |
| F | STATEMENT NUMBER ENDING A DO LOOP | T | STATEMENT NUMBER USED IN A TRACE |
| I | INDEX OF A DO OR IMPLIED DO LOOP | U | NAME USED IN EXECUTABLE STATEMENT |
| J | STATEMENT NUMBER USED IN TRANSFER | W | FORMAT USED IN A WRITE STATEMENT |
| L | SOURCE LINE OF A STATEMENT NUMBER | LR | LONGEST RECORD PRODUCED BY FORMAT |
| N | NAME USED AS A DO LOOP PARAMETER | * | (R-7) NAME DECLARED BUT NOT USED |

7600 COMPILATION -- MNF4 LEVEL 5.24 11 OCT 81 16.25.50

```
                0000008       FUNCTION EQOFS(P,L,T,RHOF,RHOG,QUA  ,UFG,UF)
     2.         0000008       DIMENSION D(4),EEE(2),H(4)
     3.         0000038       DATA D/10.2487,-0.016775,0.4645E-4,-0.741E-7/
     4.         0000068       DATA D/5.6337,0.054453,0.000595,0.2355E-3/
                      C       DATA EEE/4.19L-11,2.10E-3/
     5.         0000088       PRP=P/1.E3
     6.         0000148       Y=ALOG(PRP)
     7.         0000178       T273=D(1)+D(2)*Y+D(3)*Y*Y+D(4)*Y*Y*Y
     8.         0000248       T273=CAPLT273)
     9.         0000278       TSAT=T273-273.0
    10.         0000308       UF=TSAT*(1.E3*(4.17+5.7E-6*(TSAT-90)**2)-1
    11.         0000358       IF (E.LT.UF) GO TO 10
    12.         0000378       UFGA=B(1)+B(2)*T273+B(3)*T273**2+B(4)*T273**3
    13.         0000458       UFG=1.E3*EXP(UFGA)
                      C       TP=TSAT-20.0
    14.         0000508       Z=TSAT
    15.         0000528       RHOF=1005.5442-0.235083*Z-0.23698E-2*Z*Z+(0.4588-0.1472E-2*Z
                             1+0.13348E-4*Z*Z)*P/1.E6
                      C       KN=EEE(1)*TP**3+EEE(2)
                      C       RHOG=(P*KN)/T273
                      C       FOLLOWING 4 LINES ARE ADDED AND UPPER 2 ARE DELETED ON 10.15.80.
    16.         0000658       K=61,52
    17.         0000668       RHOG=P/(R*T273)
    18.         0000708       DO 5 I=1,15
    19.         0000728     5 RHOG=(P/(R*(T273))+1.58VE06*RHOG**2/T273**3.04
    20.         0001048       T=TSAT
    21.         0001058       QUALX=(E-UFT/UFG
    22.         0001108       QUAL=1.741.+(RHOG/RHOF)*((1.-QUALX)/QUALX))
    23.         0001168       EQOFS=QUAL*RHOG*(1.-QUAL)*RHOF
    24.         0001218       RETURN
                      C       ITERATIONS ARE INTENSIONALLY REPEATED BELOW AS T APPEARS IN ALL
                      C       OF THEM.
                      C       TEMPERATURES CALCULATED ARE THE ACTUAL TEMPERATURES NOT
                      C       SATURATION TEMPERATURES.
    25.         0001248    10 T=E/4170
    26.         0001258       UFG=0.
    27.         0001268       T=E/(4.17**4.5E-6*(T-60.)**2)
    28.         0001328       T=T/1.E3
    29.         0001338       T=E/(4.17**4.5E-6*(T-60.)**2)
    30.         0001368       T=T/1.E3
    31.         0001378       EQOFS=1005.5442-0.235083*T-0.23698E-2*T*T+(0.4588-0.1472E-2*T
                             1+0.13348E-4*T*T)*P/1.E6
    32.         0001518       QUAL=0.
    33.         0001528       RHOF=EQOFS
    34.         0001538       RHOG=10.
    35.         0001548       RETURN
    36.         0001608       END
```

TABLE OF STATEMENT NUMBERS

| NUMBER | USE | ADDRESS | SOURCE PROGRAM REFERENCES |
|---|---|---|---|
| 5 | END OF DO | 0000728 | 19L 18F |

EXECUTABLE 0001243 256 111

TABLE OF NAMES ENCOUNTERED

| NAME | TYPE | MAIN USE | BLOCKS | ADDRESS | SOURCE PROGRAM REFERENCES | | | | | | | | | |
|---|---|---|---|---|---|---|---|---|---|---|---|---|---|---|
| ALOG | R | STANDARD | | | 60 | | | | | | | | | |
| B | R | ARRAY | | 0000008 | 120 | 35 | 20 | | | | | | | |
| D | R | ARRAY | | 0000348 | 70 | 45 | 20 | | | | | | | |
| E | R | VARIABLE | ARGUMENT NO. 2 | | 290 | 270 | 250 | 210 | 110 | 10 | | | | |
| EQDFS | R | VARIABLE | | 0000128 | 350 | 330 | 315 | 235 | 10 | | | | | |
| EXP | R | STANDARD | | | 130 | 80 | | | | | | | | |
| F | I | VARIABLE | | 0003078 | 161 | | | | | | | | | |
| P | R | VARIABLE | ARGUMENT NO. 1 | | 310 | 190 | 170 | 150 | 50 | 10 | | | | |
| PKP | R | VARIABLE | | 0003068 | 6P | 55 | | | | | | | | |
| QUAL | R | VARIABLE | ARGUMENT NO. 6 | | 325 | 230 | 230 | 225 | 10 | | | | | |
| QUALX | R | VARIABLE | | 0003168 | 220 | 220 | 215 | | | | | | | |
| R | R | VARIABLE | | 0003108 | 190 | 170 | 165 | | | | | | | |
| RHDF | R | VARIABLE | ARGUMENT NO. 4 | | 335 | 230 | 220 | 155 | 10 | | | | | |
| RHDG | R | VARIABLE | ARGUMENT NO. 5 | | 345 | 230 | 220 | 195 | 190 | 175 | 10 | | | |
| T | R | VARIABLE | ARGUMENT NO. 3 | | 310 | 305 | 300 | 295 | 290 | 285 | 280 | 275 | 270 | 255 | 205 |
| | | | | | 10 | | | | | | | | | |
| TSAT | R | VARIABLE | | 0003158 | 200 | 140 | 100 | 100 | 95 | | | | | |
| T273 | R | VARIABLE | | 0003148 | 190 | 170 | 120 | 90 | 85 | 8P | 75 | | | |
| UF | R | VARIABLE | ARGUMENT NO. 8 | | 210 | 110 | 105 | 10 | | | | | | |
| UFG | R | VARIABLE | ARGUMENT NO. 7 | | 265 | 210 | 135 | 10 | | | | | | |
| UFGA | R | VARIABLE | | 0003138 | 130 | 125 | | | | | | | | |
| Y | R | VARIABLE | | 0003118 | 70 | 70 | 65 | | | | | | | |
| Z | R | VARIABLE | | 0003128 | 150 | 150 | 145 | | | | | | | |

LIST OF VARIABLE AND ARRAY NAMES IN ADDRESS ORDER IN EACH BLOCK

| BLOCK | LENGTH | | | | | | | | | |
|---|---|---|---|---|---|---|---|---|---|---|
| LOCAL | 20 | 0000008 B | 0000048 D | 0000108 EEE | 0000128 EQDFS | 0003068 PKP | | | | |
| | | 0003078 F | 0003108 R | 0003118 Y | 0003128 Z | 0003138 UFGA | | | | |
| | | 0003148 T273 | 0003158 TSAT | 0003168 QUALX | | | | | | |

AMOUNT OF STORAGE USED BY SUBPROGRAM

| | | |
|---|---|---|
| LOCAL STORAGE AREA | 20 | = 0000024R |
| CONSTANTS | 23 | = 0000027B |
| ENTRY CODE | 49 | = 0000061A |
| EXECUTABLE CODE | 103 | = 0001474 |
| ACTUAL ARGUMENTS | 6 | = 0000006B |
| TEMPORARY STORAGE | 6 | = 0000006H |
| TOTAL (LESS COMMON) | 207 | = 0003178 |

ABBREVIATIONS USED ABOVE (THESE ARE KEYED TO THE SOURCE LISTING LINE NUMBER)

| | | | |
|---|---|---|---|
| A | USED IN FORTRAN ASSIGN STATEMENT | P | ARGUMENT IN CALL OR FUNCTION CALL |
| B | OCTAL ADDRESS RELATIVE TO PROGRAM | R | FORMAT USED IN A READ STATEMENT |
| D | DEFINED IN DECLARATIVE STATEMENT | S | STORED SO CONTENTS MAY BE CHANGED |
| E | STATEMENT NUMBER ENDING A DO LOOP | T | STATEMENT NUMBER USED IN A TRACE |
| I | INDEX OF A DO OR IMPLIED DO LOOP | U | NAME USED IN EXECUTABLE STATEMENT |
| J | STATEMENT NUMBER USED IN TRANSFER | W | FORMAT USED IN A WRITE STATEMENT |
| L | SOURCE LINE OF A STATEMENT NUMBER | LR | LONGEST RECORD PRODUCED BY FORMAT |
| N | NAME USED AS A DO LOOP PARAMETER | * | (R=7) NAME DECLARED BUT NOT USED |

```
TUP                    **SUBROUTINE TUP(PTOP,H,RHOL,RHOG     UF,XDOT,Z)**                    PAGE    1

      1.  0000004B        SUBROUTINE TUP(PTOP,H,RHOL,RHOG,UF     ,XDOT,Z)
      2.  0000008B        DIMENSION B(4),EE(2),A(4)
      3.  0000008B        COMMON/KCSHAV1/IFLAG
      4.  0000008B        DATA B/10.2987,-0.0187735,0.4645E-4,-0.41E-7/
      5.  0000008B        DATA D/5.0317,0.054953,0.000595,0.23554E-3/
                    C     DATA EE/4.19E-11,2.16E-3/
      6.  0000008B        PKP=PTOP/1.E3
      7.  0000138B        Y=ALOG(PKP)
      8.  0000160B        T273=B(1)+B(2)*Y+B(3)*Y*Y+B(4)*Y*Y*Y
      9.  0000238B        T273=EXP(T273)
     10.  0000268B        TSAT=T273-273.0
     11.  0000278B        UF=TSAT*(1.E-3*(4.17+5.7E-6*(TSAT-90)**2) )
     12.  0000348B        UFGA=D(1)+D(2)*T273+D(3)*T273**2+D(4)*T273**3
     13.  0000428B        UFG=1.E-3*EXP(UFGA)
                    C     TP=TSAT-20.0
     14.  0000458B        Z=TSAT
     15.  0000478B        RHOL=1005.5D+2-0.23508D+2-0.2369E-2*Z*Z+10.4588-0.1472E-2*Z
                         1+0.133*E-4*Z*Z)*PTOP/1.E6
                    C     RK=EE(1)*TP**3+EE(2)
                    C     RHOG=(PTOP*RK)/T273
                    C     FOLLOWING 4 LINES ARE ADDED AND UPPER 2 ARE DELETED ON 10.15.80.
     16.  0000628B        R=461.52
     17.  0000638B        RHOG=PTOP/(R*T273)
     18.  0000658B        DO 5 I=1,15
     19.  0000678B      5 RHOG=(PTOP/(R*T273))+1.589E06*RHOG**2/T273**3.04
     20.  0001018B        HF=UF*PTOP/RHOL
     21.  0001048B        HG=UF*UFG*PTOP/RHOG
     22.  0001068B        IF(IFLAG.EQ.1) H=HF+XDOT*(HG-HF)
     23.  0001158B        IF(IFLAG.NE.1) XDOT=(H-HF)/(HG-HF)
     24.  0001238B   1000 FORMAT(4X,6E15.4)
     25.  0001238B        RETURN
     26.  0001258B        END
          CAUTION ----------------------------------------STATEMENT NUMBER 1000 WAS NEVER USED
```

TABLE OF STATEMENT NUMBERS

| NUMBER | USE | ADDRESS | SOURCE PROGRAM REFERENCES |
|---|---|---|---|
| 5 | END OF DO | 000067B | 19L 19E |
| 1000 | (UNUSED) | LR - 44 | 24L |

TABLE OF NAMES ENCOUNTERED

| NAME | TYPE | MAIN USE | BLOCKS | ADDRESS | SOURCE PROGRAM REFERENCES |
|---|---|---|---|---|---|
| BLOC | R | STANDARD | | | 7U |
| B | R | ARRAY | | 0000008 | 12U 4S 20 |
| D | R | ARRAY | | 0000048 | 8U 5S 20 |
| EXP | R | STANDARD | | | 13U 9U |
| H | R | VARIABLE | ARGUMENT NO. 2 | | 23U 22S 1D |
| HF | R | VARIABLE | | 0002458 | 23U 22U 20S |
| HG | R | VARIABLE | | 0002428 | 23U 22U 21S |

| | | | | | | | | | | | |
|---|---|---|---|---|---|---|---|---|---|---|---|
| I | V | VARIABLE | | 0002364 | 16I | | | | | | |
| IFLAG | I | VARIABLE | /FRESHAV1/ | 0000004 | 23U | 22U | 3D | | | | |
| PKP | R | VARIABLE | | 0002354 | 7P | 6S | | | | | |
| PTOP | R | VARIABLE | ARGUMENT NO. 1 | | 21U | 20U | 19U | 17U | 15U | 6U | 1D |
| R | R | VARIABLE | | 0002378 | 19U | 17U | 16S | | | | |
| KMOG | R | VARIABLE | ARGUMENT NO. 4 | | 21U | 19S | 18U | 17S | 1D | | |
| KMOL | R | VARIABLE | ARGUMENT NO. 3 | | 20U | 15S | 1D | | | | |
| TSAT | R | VARIABLE | | 0002448 | 14U | 11U | 11U | 10S | | | |
| T273 | R | VARIABLE | | 0002434 | 14U | 17U | 12U | 10U | 9S | 8P | 8S |
| UF | R | VARIABLE | ARGUMENT NO. 6 | | 21U | 20U | 11S | 1D | | | |
| UFG | R | VARIABLE | ARGUMENT NO. 5 | | 21U | 13S | 1D | | | | |
| UFGA | R | VARIABLE | | 0002418 | 13P | 12S | | | | | |
| XDOT | R | VARIABLE | ARGUMENT NO. 7 | | 23S | 22U | 1D | | | | |
| Y | R | VARIABLE | | 0002403 | 8U | 8U | 7S | | | | |
| Z | R | VARIABLE | ARGUMENT NO. 8 | | 15U | 15U | 14S | 1D | | | |

LIST OF VARIABLE AND ARRAY NAMES IN ADDRESS ORDER IN EACH BLOCK

| BLOCK | LENGTH | | | | | | | | | | |
|---|---|---|---|---|---|---|---|---|---|---|---|
| .LOCAL. | 19 | 0000008 | B | 0000048 | D | 0000108 | EEE | 0002350 | PKP | 0002368 | I |
| | | 000237B | R | 0002408 | Y | 0002418 | UFGA | 0002428 | HG | 0002438 | T273 |
| | | 0002448 | TSAT | 0002458 | HF | | | | | | |
| /FRESHAV1/ | 1 | 0000008 | IFLAG | | | | | | | | |

AMOUNT OF STORAGE USED BY SUBPROGRAM

| | | |
|---|---|---|
| (BLOCK COMMON AREA) | 1 | = 0000018 |
| LOCAL STORAGE AREA | 19 | = 0000238 |
| FORMAT STATEMENTS | 2 | = 0000028 |
| CONSTANTS | 17 | = 0000218 |
| ENTRY CODE | 40 | = 0000508 |
| EXECUTABLE CODE | 77 | = 0001198 |
| ACTUAL ARGUMENTS | 6 | = 0000068 |
| TEMPORARY STORAGE | 5 | = 0000058 |
| TOTAL (LESS COMMON) | 166 | = 0002468 |

ABBREVIATIONS USED ABOVE (THESE ARE KEYED TO THE SOURCE LISTING LINE NUMBER)

| | | | |
|---|---|---|---|
| A | USED IN FORTRAN ASSIGN STATEMENT | P | ARGUMENT IN CALL OR FUNCTION CALL |
| B | OCTAL ADDRESS RELATIVE TO PROGRAM | R | FORMAT USED IN A READ STATEMENT |
| D | DEFINED IN DECLARATIVE STATEMENT | S | STORED SO CONTENTS MAY BE CHANGED |
| F | STATEMENT NUMBER ENDING A DO LOOP | T | STATEMENT NUMBER USED IN A TRACE |
| I | INDEX OF A DO OR IMPLIED DO LOOP | U | NAME USED IN EXECUTABLE STATEMENT |
| J | STATEMENT NUMBER USED IN TRANSFER | W | FORMAT USED IN A WRITE STATEMENT |
| L | SOURCE LINE OF A STATEMENT NUMBER | LR | LONGEST RECORD PRODUCED BY FORMAT |
| N | NAME USED AS A DO LOOP PARAMETER | * | (R-7) NAME DECLARED BUT NOT USED |

7600 COMPILATION -- FNF4 LEVEL 5.24 11 OCT 81 16.25.50

FL REQUIRED TO LOAD 57300
FL REQUIRED TO RUN 44400
INITIAL TRANSFER TO ACLFLG = 22032

LOAD ERRORS.

PROGRAM ERROR DETECTED

UNSATISFIED EXTERNALS, SEE END OF LOAD MAP.

BLOCK ASSIGNMENTS.

| BLOCK | ADDRESS | LENGTH | FILE |
|---|---|---|---|
| /ALL/ | 100 | 55 | |
| /PAUSEL/ | 155 | 1750 | |
| /MFS/ | 2125 | 15 | |
| /PROP/ | 2142 | 37 | |
| /CONSOL/ | 2201 | 2 | |
| /IGS2222/ | 2203 | 310 | |
| /RESHAV/ | 2513 | 7 | |
| /RESHAV1/ | 2522 | 1 | |
| ACLFLG | 2523 | 17530 | LGO |
| GPIO | 22253 | 102 | LGO |
| INITIAL | 22355 | 6740 | LGO |
| PRICSLP | 31315 | 1112 | LGO |
| SPACNT | 32427 | 1359 | LGO |
| FUNCS | 34003 | 317 | LGO |
| TOP | 34322 | 246 | LGO |
| /JOCOM./ | 34570 | 27 | |
| ENTER. | 34617 | 22 | RNFALIB |
| INTRI. | 34641 | 40 | RNFALIB |
| INTRO. | 34701 | 33 | RNFALIB |
| INPUTS | 34734 | 122 | RNFALIB |
| OUTPUTS | 35056 | 65 | RNFALIB |
| /.JCOMP./ | 35143 | 1 | |
| QSNTN* | 35144 | 54 | RNFALIB |
| VTOA* | 35220 | 147 | RNFALIB |
| ALOG | 35367 | 6 | FTNALIB |
| ALOG. | 35375 | 63 | FTNALIB |
| ATAN | 35460 | 6 | FTNALIB |
| ATAN. | 35466 | 60 | FTNALIB |
| CIO* | 35546 | 13 | FTNALIB |
| EMDJ* | 35561 | 2 | FTNALIB |
| EXP | 35563 | 54 | FTNALIB |
| EXP | 35637 | 6 | FTNALIB |
| EXP. | 35645 | 73 | FTNALIB |
| /OH.IO./ | 35740 | 171 | |
| /FCL.C./ | 36131 | 26 | |

LOAD MAP.
BLOCK ASSIGNMENTS.

| BLOCK | ADDRESS | LENGTH | FILE |
|---|---|---|---|
| /ULTMNT/ | 36157 | 1 | |
| /QUOSFL/ | 36160 | 2 | |
| /QASAFLG/ | 36162 | 1 | |
| /STP.END/ | 36163 | 1 | |
| FO*SYS* | 36164 | 662 | FTN4LIB |
| /QDVERC1/ | 37046 | 1 | |
| FDPUTL* | 37047 | 16 | FTN4LIB |
| GETELL* | 37063 | 43 | FTN4LIB |
| SQRT | 37130 | 6 | FTN4LIB |
| SORT. | 37136 | 32 | FTN4LIB |
| SYSAID* | 37170 | 1 | FTN4LIB |
| SYS* | 37171 | 34 | FTN4LIB |
| SYS*1ST | 37225 | 62 | FTN4LIB |
| #TH* | 37307 | 30 | FTN4LIB |
| #1** | 37337 | 66 | FTN4LIB |
| IOFLAG. | 37425 | 3 | FNF4LIB |
| OFDOSY* | 37430 | 32 | FNF4LIB |
| FTN5LIB | 37462 | 1 | FTN4LIB |
| COMIO* | 37463 | 60 | FTN4LIB |
| ENCODE* | 37543 | 144 | FTN4LIB |
| F.CHSX* | 37707 | 41 | FTN4LIB |
| FLIP** | 37750 | 156 | FTN4LIB |
| FLTOUT* | 40126 | 314 | FTN4LIB |
| F*SAP* | 40442 | 406 | FTN4LIB |
| F.OPEN | 41050 | 120 | FTN4LIB |
| F.*FADF | 41170 | 170 | FTN4LIB |
| F.WRITF | 41360 | 122 | FTN4LIB |
| GETEP. | 41502 | 60 | FTN4LIB |
| INCU** | 41562 | 262 | FTN4LIB |
| INPC* | 42044 | 234 | FTN4LIB |
| KOOL** | 42300 | 536 | FTN4LIB |
| KRAKER* | 43036 | 435 | FTN4LIB |
| OUTCUM* | 43473 | 242 | FTN4LIB |
| OUTC* | 43735 | 155 | FTN4LIB |
| KOU* | 44112 | 23 | FTN4LIB |
| UZERO.. | 44135 | 2 | FTN4LIB |
| #FD* | 44137 | 17 | FTN4LIB |
| LOKUSX | 44156 | 161 | SYSLIB |

UNSATISFIED EXTERNALS.

| EXTERNAL | REFERENCES | | | | | | | |
|---|---|---|---|---|---|---|---|---|
| SUBJCG | SPRINT | 33060 | 33162 | 33202 | 33214 | | | |
| LABFLG | SPRINT | 33172 | 33200 | 33206 | 33225 | | | |
| OPTOG | SPRINT | 33170 | | | | | | |
| OBJCTG | SPRINT | 33056 | 33160 | | | | | |
| SETSNG | SPRINT | 33054 | 33066 | 33174 | 33204 | 33221 | | |
| | | 33062 | 33156 | 33176 | 33217 | 33223 | | |
| *QUESG | SPRINT | 33052 | | | | | | |
| LEGNOG | SPRINT | 33064 | 33100 | 33110 | 33122 | 33134 | 33144 | 33154 |
| DASHG | SPRINT | 33076 | 33106 | 33120 | 33166 | 33212 | 33227 | |

| EXTERNAL | REFERENCES | |
|---|---|---|
| *SETMG | SPRINT | 33231 |
| PAGEG | SPRINT | 33233 |

WELL NUMBER MONTH DAY YEAR
0 -0 -0 -0

| ROUGHNESS | LENGTH(M) | FLOW(KG/M2-SEC) | DEPTH | NMAX(I) |
|---|---|---|---|---|
| .07000 | 600.00000 | 214.31954 | 0. | 61 |

CONSTANT FLOW RATE OUT (TON/HOUR) = 20.0000
WELLHEAD PRESSURE (PSIG) = .11503E+03
WELL DEPTH (M) = 600.000
AMBIENT TEMPERATURE (C) = 26.000
BOTTOMHOLE TEMPERATURE(C)= 240.000

SPECIFIED ENTHALPY(KCAL/KG)= 199.960

SATURATION= .4591E+00 DRYNESS FRACTION IN PLACE= .3083E-01
FLOWING DRYNESS FRACTION= .4746E-01 FLOWING WELL HEAD TEMPERATURE(C)= 175.50875
SATURATED LIQUID ENTHALPY(J/KG)= .7342E+06 ENERGY DIFFERENCE(J/KG)= .1651E+07

I= 61 RHOL(I)= .8727E+03 RHOG(I)= .6790E+01 RHO2(I)= .5526E+03 P2(I)= .1339E+07
V(I)= .3951E+00 QUAL(I)= .3697E+00 SLIP(I)= .5867E+00 UFG(I)= .1786E+07
10 .951261E+05 .360112E+06 .286876E+06 .335683E+07 .179239E+09 .182785E+09 .825239E+06 .825239E+06
61 .817125E+06 .825239E+06 .250332E+07 .218320E+03 .392429E+00 .979149E+00 .182784E+09 .261866E+07
I= 61 <L(I)= .2614E+07 RHO2FVL= .1402E+09 DUMMY= SLUG

THE STEADY STATE DISTRIBUTION OF THE PRESSURE IN THE WELL IS

| I | DEPTH(M) | PRESSURE(PASCALS) | ENERGY(J/KG) | DENSITY(KG/M3) | VELOCITY(M/SEC) | TEMP | SATURATION | PHASE STATE |
|---|---|---|---|---|---|---|---|---|
| 61 | 0. | .9013776+06 | 796251.67 | 129.66 | .16838E+01 | 175.5087 | .8591 | SLUG |
| 60 | 10.0 | .9148846+06 | 796999.13 | 135.22 | .16145E+01 | 176.1452 | .8528 | SLUG |
| 59 | 20.0 | .9289466+06 | 797776.83 | 141.30 | .15451E+01 | 176.8000 | .8459 | SLUG |
| 58 | 30.0 | .9436156+06 | 798586.71 | 147.96 | .14755E+01 | 177.4747 | .8383 | SLUG |
| 57 | 40.0 | .9588536+06 | 799439.50 | 155.31 | .14057E+01 | 178.1715 | .8299 | SLUG |
| 56 | 50.0 | .9756336+06 | 800334.89 | 163.46 | .13356E+01 | 178.8925 | .8206 | SLUG |
| 55 | 60.0 | .9939406+06 | 801281.93 | 172.55 | .12653E+01 | 179.6405 | .8102 | SLUG |
| 54 | 70.0 | .1009776+07 | 802288.90 | 182.76 | .11945E+01 | 180.4187 | .7985 | SLUG |
| 53 | 80.0 | .1028866+07 | 803366.85 | 194.33 | .11234E+01 | 181.2309 | .7853 | SLUG |
| 52 | 90.0 | .1048746+07 | 804529.29 | 207.56 | .10518E+01 | 182.0818 | .7701 | SLUG |
| 51 | 100.0 | .1070176+07 | 805793.74 | 222.83 | .97976E+00 | 182.9768 | .7526 | SLUG |
| 50 | 110.0 | .1093256+07 | 807183.14 | 240.66 | .90716E+00 | 183.9230 | .7320 | SLUG |
| 49 | 120.0 | .1118176+07 | 808726.00 | 261.77 | .83402E+00 | 184.9290 | .7077 | SLUG |
| 48 | 130.0 | .1145386+07 | 810469.76 | 287.12 | .76039E+00 | 186.0060 | .6785 | SLUG |
| 47 | 140.0 | .1175316+07 | 812465.70 | 318.09 | .68635E+00 | 187.1682 | .6426 | SLUG |
| 46 | 150.0 | .1206426+07 | 814796.57 | 356.67 | .61211E+00 | 188.4346 | .5979 | SLUG |
| 45 | 160.0 | .1240206+07 | 817578.05 | 405.75 | .53807E+00 | 189.8306 | .5409 | SLUG |
| 44 | 170.0 | .1278236+07 | 820979.36 | 469.62 | .46489E+00 | 191.3911 | .4666 | SLUG |
| 43 | 180.0 | .1355346+07 | 839276.84 | 365.28 | .59787E+00 | 193.7055 | .5857 | SINGLPH |
| 42 | 190.0 | .1429176+07 | 836208.68 | 635.97 | .34329E+00 | 196.1965 | .2706 | BUBBLE |
| 41 | 200.0 | .1503136+07 | 839308.68 | 868.01 | .25152E+00 | 197.2757 | 0. | SINGLPH |
| 40 | 210.0 | .1568226+07 | 839308.90 | 868.07 | .25150E+00 | 197.2757 | 0. | SINGLPH |
| 39 | 220.0 | .1673316+07 | 839308.92 | 868.13 | .25148E+00 | 197.2757 | 0. | SINGLPH |
| 38 | 230.0 | .1756416+07 | 839309.06 | 868.19 | .25147E+00 | 197.2757 | 0. | SINGLPH |
| 37 | 240.0 | .1843526+07 | 839309.20 | 868.25 | .25145E+00 | 197.2758 | 0. | SINGLPH |
| 36 | 250.0 | .1928646+07 | 839309.34 | 868.31 | .25143E+00 | 197.2758 | 0. | SINGLPH |
| 35 | 260.0 | .2013756+07 | 839309.50 | 868.37 | .25141E+00 | 197.2758 | 0. | SINGLPH |
| 34 | 270.0 | .2098866+07 | 839309.66 | 868.42 | .25140E+00 | 197.2759 | 0. | SINGLPH |

| | | | | | | | | |
|---|---|---|---|---|---|---|---|---|
| 33 | 290. | .7154[illegible]E+07 | 839309.82 | 868.48 | .25138E+00 | 197.2759 | 0. | SINGLPHA |
| 32 | 2[illegible] | .7226[illegible]E+07 | 839309.99 | 868.54 | .25136E+00 | 197.2760 | 0. | SINGLPHA |
| 31 | 300. | .7295[illegible]E+07 | 839310.17 | 868.60 | .25135E+00 | 197.2760 | 0. | SINGLPHA |
| 30 | 310. | .7363[illegible]E+07 | 839310.36 | 868.66 | .25133E+00 | 197.2760 | 0. | SINGLPHA |
| 29 | 320. | .7429[illegible]E+07 | 839310.55 | 868.72 | .25131E+00 | 197.2761 | 0. | SINGLPHA |
| 28 | 330. | .7496[illegible]E+07 | 839310.75 | 868.78 | .25130E+00 | 197.2761 | 0. | SINGLPHA |
| 27 | 340. | .7563[illegible]E+07 | 839310.96 | 868.83 | .25128E+00 | 197.2762 | 0. | SINGLPHA |
| 26 | 350. | .7629[illegible]E+07 | 839311.17 | 868.89 | .25126E+00 | 197.2762 | 0. | SINGLPHA |
| 25 | 360. | .7696[illegible]E+07 | 839311.39 | 868.95 | .25124E+00 | 197.2763 | 0. | SINGLPHA |
| 24 | 370. | .7763[illegible]E+07 | 839311.61 | 869.01 | .25123E+00 | 197.2763 | 0. | SINGLPHA |
| 23 | 380. | .7830[illegible]E+07 | 839311.85 | 869.07 | .25121E+00 | 197.2764 | 0. | SINGLPHA |
| 22 | 390. | .7896[illegible]E+07 | 839312.08 | 869.13 | .25119E+00 | 197.2764 | 0. | SINGLPHA |
| 21 | 400. | .7963[illegible]E+07 | 839312.08 | 869.19 | .23922E+00 | 197.2764 | 0. | SINGLPHA |
| 20 | 410. | .8029[illegible]E+07 | 839312.08 | 869.24 | .22724E+00 | 197.2764 | 0. | SINGLPHA |
| 19 | 420. | .8096[illegible]E+07 | 839312.08 | 869.30 | .21527E+00 | 197.2764 | 0. | SINGLPHA |
| 18 | 430. | .8163[illegible]E+07 | 839312.08 | 869.36 | .20329E+00 | 197.2764 | 0. | SINGLPHA |
| 17 | 440. | .8229[illegible]E+07 | 839312.08 | 869.42 | .19132E+00 | 197.2764 | 0. | SINGLPHA |
| 16 | 450. | .8296[illegible]E+07 | 839312.08 | 869.48 | .17935E+00 | 197.2764 | 0. | SINGLPHA |
| 15 | 460. | .8363[illegible]E+07 | 839312.08 | 869.54 | .16738E+00 | 197.2764 | 0. | SINGLPHA |
| 14 | 470. | .8429[illegible]E+07 | 839312.08 | 869.60 | .15542E+00 | 197.2764 | 0. | SINGLPHA |
| 13 | 480. | .8496[illegible]E+07 | 839312.08 | 869.65 | .14345E+00 | 197.2764 | 0. | SINGLPHA |
| 12 | 490. | .8563[illegible]E+07 | 839312.08 | 869.71 | .13149E+00 | 197.2764 | 0. | SINGLPHA |
| 11 | 500. | .8629[illegible]E+07 | 839312.08 | 869.77 | .11953E+00 | 197.2764 | 0. | SINGLPHA |
| 10 | 510. | .8696[illegible]E+07 | 839312.08 | 869.83 | .10757E+00 | 197.2764 | 0. | SINGLPHA |
| 9 | 520. | .8763[illegible]E+07 | 839312.08 | 869.89 | .95609E-01 | 197.2764 | 0. | SINGLPHA |
| 8 | 530. | .8829[illegible]E+07 | 839312.08 | 869.95 | .83652E-01 | 197.2764 | 0. | SINGLPHA |
| 7 | 540. | .8896[illegible]E+07 | 839312.08 | 870.01 | .71697E-01 | 197.2764 | 0. | SINGLPHA |
| 6 | 550. | .8963[illegible]E+07 | 839312.08 | 870.06 | .59744E-01 | 197.2764 | 0. | SINGLPHA |
| 5 | 560. | .9029[illegible]E+07 | 839312.08 | 870.12 | .47792E-01 | 197.2764 | 0. | SINGLPHA |
| 4 | 570. | .9096[illegible]E+07 | 839312.08 | 870.18 | .35841E-01 | 197.2764 | 0. | SINGLPHA |
| 3 | 580. | .9163[illegible]E+07 | 839312.08 | 870.24 | .23893E-01 | 197.2764 | 0. | SINGLPHA |
| 2 | 590. | .9229[illegible]E+07 | 839312.08 | 870.30 | .11946E-01 | 197.2764 | 0. | SINGLPHA |
| 1 | 600. | .9296[illegible]E+07 | 839312.08 | 870.36 | -.14956E-13 | 197.2764 | 0. | SINGLPHA |

```
16.25.  KESHALL.  11 OCT 81   24002   RKY30# V0   KESHAV  I              466502 GOYAL
16.25.  KESHALL.  *KESHAV,7,500,466502,GOYAL
16.25.44. KESHALL.  *ESHALO 56998 16.25.50  11 OCT 81  VIA KESHALO
16.25.47. KESHALL.  COPY,I*PUT,LP,CONTROL/BA,DEN=OFF.
16.25.50. KESHALL.  FLS=0200  FLL=0000K  LCM BUFFERS=0054K  TOTAL LCM=0074K
16.25.50. KESHALL.   CONTROL DISK 2
16.25.50. KESHALL.  COPY COMPLETE.
16.25.50. KESHALL. LANURAGE STEPPED DIAMETERSFINITE VOLUME
16.25.50. KESHALL.*NULOUUT
16.25.50. KESHALL. *PSS.
16.25.50. KESHALL. SEL=70000.
16.25.50. KESHALL.  FLS=0600  FLL=0000K  LCM BUFFERS=0014K  TOTAL LCM=0074K
16.25.50. KESHALL.  FLS=0700  FLL=0000K  LCM BUFFERS=0014K  TOTAL LCM=0104K
16.25.50. KESHALL. ANFN,PL=13300.
16.25.50. KESHALL.   ZZZZSY* DISK 2
16.25.50. KESHALL.   OUTPUT  DISK 2
16.25.51. KESHALL.   LGO     DISK 2
16.25.51. KESHALL.  CORE USED = 0n060JB OCTAL WORDS
16.25.51. KESHALL.  TIME USED =   0.018 CPU SECONDS
16.25.51. KESHALL.   ZZZZSY* UNLOADED      1 BLD, BS= 0040B,FS=0000038
16.25.52. KESHALL. LINK,E=LGO,X,ED.
16.25.52. KESHALL.   ZZZZLS DISK 1
16.25.52. KESHALL.   ZZZZLS RETURNED      0 BLD, BS= 0040B,FS=0000008
16.25.54. KESHALL.   OVGMAP  DISK 1
16.25.54. KESHALL.         1 LOAD ERRORS), SEE MAP.
16.25.54. KESHALL.   OVGMAP  UNLOADED      1 BLD, BS= 0040B,FS=0000018
16.25.54. KESHALL.   LGO     UNLOADED      1 BLD, BS= 0040B,FS=0000128
16.25.54. KESHALL.   MAGNETS UNLOADED      1 BLD, BS= 0010B,FS=0000078
16.25.54. KESHALL.   FTN4LIB UNLOADED      1 BLD, BS= 0100B,FS=0001008
16.25.54. KESHALL.   SYSLIB  UNLOADED      1 BLD, BS= 0110B,FS=0001108
16.25.54. KESHALL.  LOAD COMPLETE. LINK 4.4.
16.25.54. KESHALL.    TIME---       104 MSEC.
16.25.54. KESHALL.    MEMORY-      LOAD     57300,  EXECUTE     45000.
16.25.54. KESHALL.  FLS=0+5K  FLL=0500K  LCM BUFFERS=0046K  TOTAL LCM=0113K
16.25.54. KESHALL.        BEGIN PROGRAM HELFLD    USING -
16.25.54. KESHALL.          FTN4 LIBRARY VERSION 3.4
16.25.54. KESHALL.          FTN4 LIBRARY 7600-VSN2/810CB.17.30
16.25.55. KESHALL.     STOP
16.25.55. KESHALL.       1.329 CP SECONDS EXECUTION TIME
16.25.55. KESHALL.       4.226 COMPUTING UNITS USED
16.25.55. KESHALL.   LINK    RETURNED      1 BLD, BS= 0012B,FS=0000128
16.25.55. KESHALL.   MAGNETS RETURNED      1 BLD, BS= 0010B,FS=0000078
16.25.55. KESHALL.   FTN4LIB RETURNED      1 BLD, BS= 0100B,FS=0001008
16.25.55. KESHALL.   SYSLIB  RETURNED      1 BLD, BS= 0110B,FS=0001108
16.25.55. KESHALL. STOP.
16.25.55. KESHALL.   OUTPUT* QUEUED PR      2 BLD, BS= 0020B,FS=0000358
16.25.55. KESHALL.  *J JR14Z9F   Ahe5028 110CT81D2 N 000015          GOYAL
16.25.55. KESHALL.  ..........................
16.25.55. KESHALL.  SECTORS TRANSFERRED       300
16.25.55. KESHALL.  MR4 DISK SECTORS          290
16.25.55. KESHALL.  CP SECONDS               2.048
16.25.55. KESHALL.  SYSTEM SECONDS           0.121
16.25.55. KESHALL.  OLD BLDS                    11
16.25.55. KESHALL.  LCM BUFFER LOADS            13
16.25.55. KESHALL.  ITO CUS                      1
16.25.55. KESHALL.  KWORDS XFERRED              74
16.25.55. KESHALL.  CIO CALLS                  239
16.25.55. KESHALL.  STAGING CUS                  0
16.25.55. KESHALL.  ..........................
16.25.55. KESHALL.  TOTAL JOB CUS               15
16.25.55. KESHALL.  CUST + OVERHEAD  =         1.01
16.25.55. KESHALL.  ..........................
```

**********
**********
**********

KESYX10 KESYX10

B I L L B O A R D  WRITEUPS SUBSET BRYNENS WAS LAST CHANGED SEP 30
DOCUMENTATION WAS LAST CHANGED SEP 14 - SEE
THE HANDBOOK SUBSET CHANGES FOR DETAILS.

OCT 7 TERMINALS FOR RENT
ONE ADM-3A (CN11), TWO VISTAR SATELLITE (CP11), AND ONE TTY MODEL 43 (HARDCOPY)
ARE AVAILABLE IN COMPUTER CENTER 2ST RENT-A-TERMINAL SERVICE, ED BOYON (x6218)

OCT 01 PSS DISK HARDWARE FAILURE
PSS SUBSETS CREATED OR REPLACED BETWEEN 0700 AND 0900 ON SEPT 30 WERE LOST DUE
TO A HARDWARE FAILURE.

SEP 16 VAX DEVELCON CODES CHANGING
THE DEVELCON ACCESS CODES AND THE DECNET NODE NAMES FOR THE PROGRAM DEVELOP-
MENT MACHINE AND THE NUMERICAL MODELING MACHINE WILL BE CHANGED ON MON SEPT 28
FROM VMS1 AND VMS2 TO PDM AND NMM, RESPECTIVELY. THIS IS PART OF AN EFFORT TO
MAKE NAMING CONVENTIONS THROUGHOUT THE COMPUTER CENTER NETWORK MORE CONSISTENT.

SEP 14 GRAFPAC WRITEUP UPDATED
THE WRITEUPS SUBSET GRAFPAC WAS UPDATED TODAY TO INCLUDE DOCUMENTATION ON HOW
TO USE GRAFPAC ON VAX/VMS. THE NEW DOCUMENT IS 30 PAGES LONGER THAN THE OLD
ONE. TO GET A COPY, EXECUTE THESE CONTROL CARDS -

LIBCOPY,WRITEUPS,OUT,GRAFPAC.
DISPOSE,OUT=PR,PA=LF. (USE PA=LF AT BRY ONLY)

THE CONSULTANTS' OFFICE (BLDG. 50A, RM. 1245) IS OPEN WEEKDAYS FROM 9 - 5.

TO CALL A CONSULTANT DIAL X, 5981, (415) 486 5981, OR FTS 451 5981

CURSO: INGENIERIA DE RESERVORIOS GEOTERMICOS.

MATERIA: FLUJO DE FLUIDOS Y CALOR EN MEDIO POROSO.

PROF. DR. HEBER CINCO LEY

SEPTIEMBRE, 1981.

(6) ... Dr. Heber Cinco

# THE APPLICATION OF THE LAPLACE TRANSFORMATION TO FLOW PROBLEMS IN RESERVOIRS

A. F. VAN EVERDINGEN, SHELL OIL CO., HOUSTON, AND W. HURST, PETROLEUM CONSULTANT, HOUSTON, MEMBERS AIME

## ABSTRACT

For several years the authors have felt the need for a source from which reservoir engineers could obtain fundamental theory and data on the flow of fluids through permeable media in the unsteady state. The data on the unsteady state flow are composed of solutions of the equation

$$\frac{\partial^2 P}{\partial r^2} + \frac{1}{r}\frac{\partial P}{\partial r} = \frac{\partial P}{\partial t}$$

Two sets of solutions of this equation are developed, namely, for "the constant terminal pressure case" and "the constant terminal rate case." In the constant terminal pressure case the pressure at the terminal boundary is lowered by unity at zero time, kept constant thereafter, and the cumulative amount of fluid flowing across the boundary is computed, as a function of the time. In the constant terminal rate case a unit rate of production is made to flow across the terminal boundary (from time zero onward) and the ensuing pressure drop is computed as a function of the time. Considerable effort has been made to compile complete tables from which curves can be constructed for the constant terminal pressure and constant terminal rate cases, both for finite and infinite reservoirs. These curves can be employed to reproduce the effect of any pressure or rate history encountered in practice.

Most of the information is obtained by the help of the Laplace transformations, which proved to be extremely helpful for analyzing the problems encountered in fluid flow. The application of this method simplifies the more tedious mathematical analysis employed in the past. With the help of Laplace transformations some original developments were obtained (and presented) which could not have been easily foreseen by the earlier methods.

## INTRODUCTION

This paper represents a compilation of the work done over the past few years on the flow of fluid in porous media. It concerns itself primarily with the transient conditions prevailing in oil reservoirs during the time they are produced. The study is limited to conditions where the flow of fluid obeys the diffusivity equation. Multiple-phase fluid flow is not considered.

A previous publication by Hurst[1] shows that when the pressure history of a reservoir is known, this information can be used to calculate the water influx, an essential term in the material balance equation. An example is offered in the literature by Old[2] in the study of the Jones Sand, Schuler Field, Arkansas. The present paper contains extensive tabulated data (from which work curves can be constructed), which data are derived by a more rigorous treatment of the subject matter than available in an earlier publication.[1] The application of this information will enable those concerned with the analysis of the behavior of a reservoir to obtain quantitatively correct expressions for the amount of water that has flowed into the reservoirs, thereby satisfying all the terms that appear in the material balance equation. This work is likewise applicable to the flow of fluid to a well whenever the flow conditions are such that the diffusivity equation is obeyed.

## DIFFUSITY EQUATION

The most commonly encountered flow system is radial flow toward the well bore or field. The volume of fluid which flows per unit of time through each unit area of sand is expressed by Darcy's equation as

$$v = \frac{K}{\mu}\frac{\partial P}{\partial r}$$

where K is the permeability, $\mu$ the viscosity and $\partial P/\partial r$ the pressure gradient at the radial distance r. A material balance on a concentric element AB, expresses the net fluid traversing the surfaces A and B, which must equal the fluid lost from within the element. Thus, if the density of the fluid is expressed by $\rho$, then the weight of fluid per unit time and per unit sand thickness, flowing past Surface A, the surface nearest the well bore, is given as

$$2\pi r\rho\,\frac{K}{\mu}\frac{\partial P}{\partial r} = \frac{2\pi K}{\mu}\left(\rho r\frac{\partial P}{\partial r}\right)$$

The weight of fluid flowing past Surface B, an infinitesimal distance $\delta r$, removed from Surface A, is expressed as

$$\frac{2\pi K}{\mu}\left[\rho r\frac{\partial P}{\partial r} + \frac{\partial\left(\rho r\frac{\partial P}{\partial r}\right)}{\partial r}\delta r\right]$$

Manuscript received at office of Petroleum Branch January 13, 1947. Paper presented at the AIME Annual Meeting in San Francisco, February 16-17, 1948.

[1] References are given at end of paper.

The difference between these two terms, namely,

$$-\frac{2\pi K}{\mu}\frac{\partial\left(\rho r\frac{\partial P}{\partial r}\right)}{\partial r}\delta r,$$

is equal to the weight of fluid lost by the element AB, or

$$-2\pi f r\frac{\partial \rho}{\partial T}\delta r$$

where f is the porosity of the formation.

This relation gives the equation of continuity for the radial system, namely,

$$\frac{K}{\mu}\frac{\partial\left(\rho r\frac{\partial P}{\partial r}\right)}{\partial r}=f r\frac{\partial \rho}{\partial T} \quad \ldots\ldots \text{(II-1)}$$

From the physical characteristics of fluids, it is known that density is a function of pressure and that the density of a fluid decreases with decreasing pressure due to the fact that the fluid expands. This trend expressed in exponential form is

$$\rho=\rho_a e^{-c(P_a-P)} \quad \ldots\ldots\ldots \text{(II-2)}$$

where P is less than $P_a$, and c the compressibility of the fluid. If we substitute Eq. II-2 in Eq. II-1, the diffusivity equation can be expressed using density as a function of radius and time, or

$$\left(\frac{\partial^2 \rho}{\partial r^2}+\frac{1}{r}\frac{\partial \rho}{\partial r}\right)\frac{K}{f\mu c}=\frac{\partial \rho}{\partial T} \quad \ldots \text{(II-3)}$$

For liquids which are only slightly compressible, Eq. II-2 simplifies to $\rho \cong \rho_a[1-c(P_a-P)]$ which further modifies Eq. II-3 to give

$$\left(\frac{\partial^2 P}{\partial r^2}+\frac{1}{r}\frac{\partial P}{\partial r}\right)\frac{K}{f\mu c}=\frac{\partial P}{\partial T}$$

Furthermore, if the radius of the well or field, $R_a$, is referred to as a unit radius, then the relation simplifies to

$$\frac{\partial^2 P}{\partial r^2}+\frac{1}{r}\frac{\partial P}{\partial r}=\frac{\partial P}{\partial t} \quad \ldots\ldots \text{(II-4)}$$

where $t=KT/f\mu cR_a^2$ and r now expresses the distance as a multiple of $R_a$, the unit radius. The units appearing in this paper are always used in connection with Darcy's equation, so that the permeability K must be expressed in darcys, the time T in seconds, the porosity f as a fraction, the viscosity $\mu$ in centipoises, the compressibility c as volume per volume per atmosphere, and the radius $R_a$ in centimeters.

## LAPLACE TRANSFORMATION

In all publications, the treatment of the diffusivity equation has been essentially the orthodox application of the Fourier-Bessel series. This paper presents a new approach to the solution of problems encountered in the study of flowing fluids, namely, the Laplace transformation, since it was recognized that Laplace transformations offer a useful tool for solving difficult problems in less time than by the use of Fourier-Bessel series. Also, original developments have been obtained which are not easily foreseen by the orthodox methods.

If $P_{(t)}$ is a pressure at a point in the sand and a function of time, then its Laplace transformation is expressed by the infinite integral

$$\bar{P}_{(p)}=\int_0^\infty e^{-pt}P_{(t)}\,dt \quad \ldots\ldots \text{(III-1)}$$

where the constant p in this relationship is referred to as the operator. If we treat the diffusivity equation by the process implied by Eq. III-1, the partial differential can be transformed to a total differential equation. This is performed by multiplying each term in Eq. II-4 by $e^{-pt}$ and integrating with respect to time between zero and infinity, as follows:

$$\int_0^\infty e^{-pt}\left(\frac{\partial^2 P}{\partial r^2}+\frac{1}{r}\frac{\partial P}{\partial r}\right)dt=\int_0^\infty e^{-pt}\frac{\partial P}{\partial t}dt \quad \text{(III-2)}$$

Since P is a function of radius and time, the integration with respect to time will automatically remove the time function and leave P a function of radius only. This reduces the left side to a total differential with respect to r, namely,

$$\int_0^\infty e^{-pt}\frac{\partial^2 P}{\partial r^2}dt=\frac{\partial^2\int_0^\infty(e^{-pt}P\,dt)}{\partial r^2}=\frac{d^2\bar{P}_{(p)}}{dr^2} \quad \text{etc.}$$

and Eq. III-2 becomes

$$\frac{d^2\bar{P}_{(p)}}{dr^2}+\frac{1}{r}\frac{d\bar{P}_{(p)}}{dr}=\int_0^\infty e^{-pt}\frac{dP}{dt}dt$$

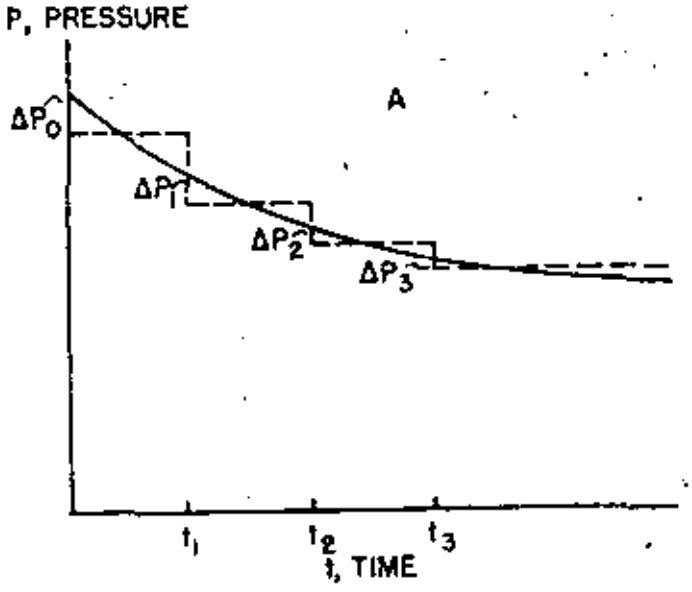


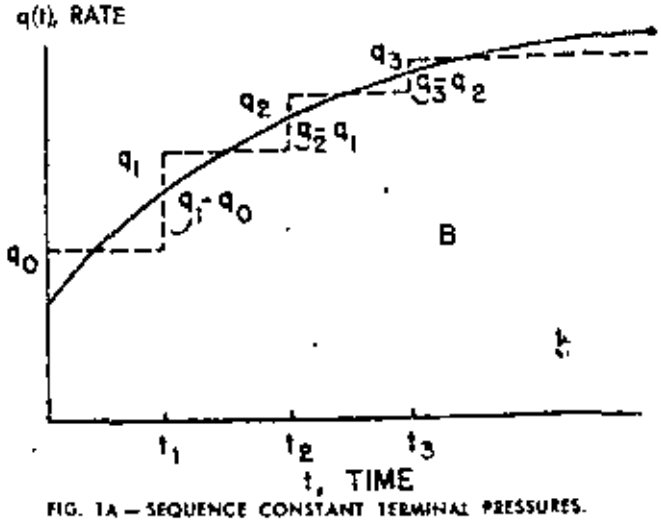


FIG. 1A — SEQUENCE CONSTANT TERMINAL PRESSURES.
1B — SEQUENCE CONSTANT TERMINAL RATES.

Furthermore, if we consider that $P_{(t)}$ is a cumulative pressure drop, and that initially the pressure in the reservoir is everywhere constant so that the cumulative pressure drop $P_{(t=0)}=0$, the integration of the right hand side of the equation becomes

$$\int_0^\infty e^{-pt} \frac{dP}{dt}\, dt = e^{-pt} P_{(t)} \Big|_0^\infty + p \int_0^\infty e^{-pt} P_{(t)}\, dt$$

$$= p \int_0^\infty e^{-pt} P_{(t)}\, dt$$

As this term is also a Laplace transform, Eq. III-2 can be written as a total differential equation, or

$$\frac{d^2\bar{P}_{(p)}}{dr^2} + \frac{1}{r}\frac{d\bar{P}_{(p)}}{dr} = p\bar{P}_{(p)} \quad \ldots\ldots \text{(III-3)}$$

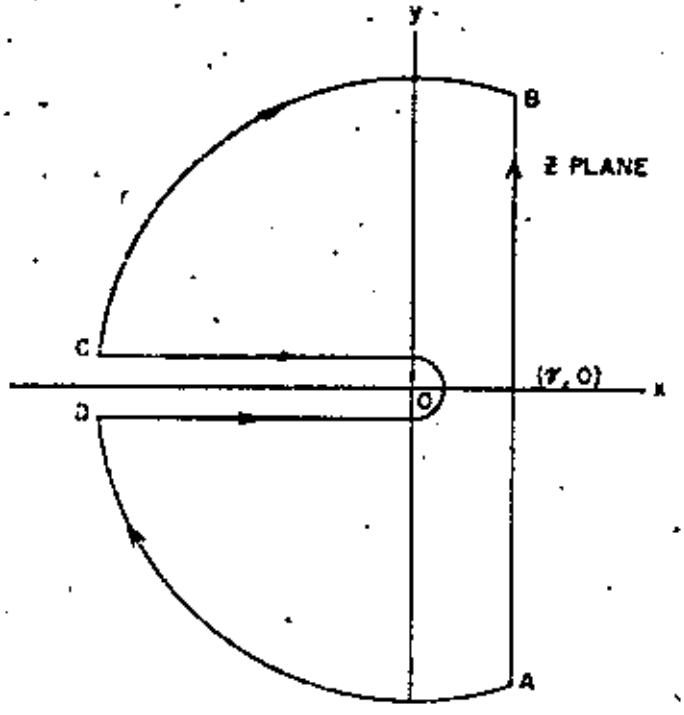


FIG. 2 — CONTOUR INTEGRATION IN ESTABLISHING THE CONSTANT TERMINAL RATE CASE FOR INFINITE EXTENT.

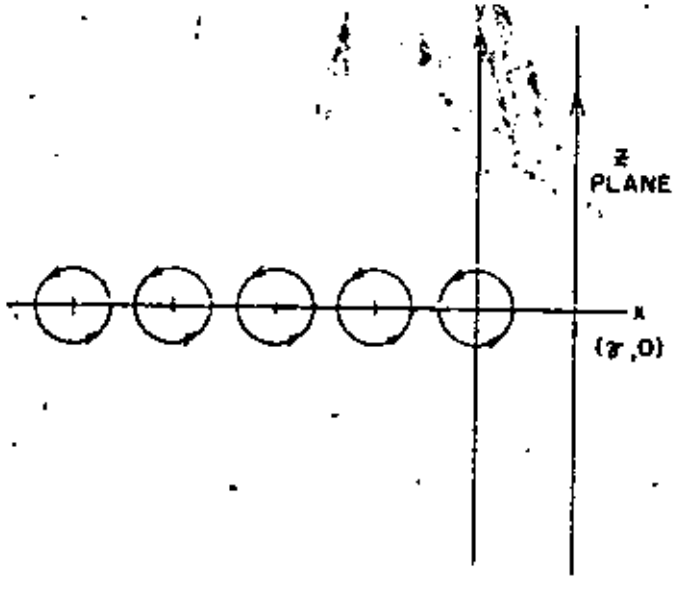


FIG. 3 — CONTOUR INTEGRATION IN ESTABLISHING THE CONSTANT TERMINAL RATE CASE FOR LIMITED RESERVOIR.

The next step in the development is to reproduce the boundary condition at the well bore or field radius, $r = 1$, as a Laplace transformation and introduce this in the general solution for Eq. III-3 to give an explicit relation

$$\bar{P}_{(p)} = f_{(p,r)}$$

By inverting the term on the right by the Mellin's inversion formula, or other methods, we obtain the solution for the cumulative pressure drop as an explicit function of radius and time.

## ENGINEERING CONCEPTS

Before applying the Laplace transformation to develop the necessary work-curves, there are some fundamental engineering concepts to be considered that will allow the interpretation of these curves. Two cases are of paramount importance in making reservoir studies, namely, the constant terminal pressure case and the constant terminal rate case. If we know the explicit solution for the first case, we can reproduce any variable pressure history at the terminal boundary to determine the cumulative influx of fluid. Likewise, if the rate of fluid influx varies, the constant terminal rate case can be used to calculate the total pressure drop. The constant terminal pressure and the constant terminal rate case are not independent of one another, as knowing the operational form of one, the other can be determined, as will be shown later.

### *Constant Terminal Pressure Case*

The constant terminal pressure case is defined as follows: At time zero the pressure at all points in the formation is constant and equal to unity, and when the well or reservoir is opened, the pressure at the well or reservoir boundary, $r = 1$, immediately drops to zero and remains zero for the duration of the production history.

If we treat the constant terminal pressure case symbolically, the solution of the problem at any radius and time is given by $P = P_{(r,t)}$. The rate of fluid influx per unit sand thickness under these conditions is given by Darcy's equation

$$q_{(T)} = \frac{2\pi K}{\mu}\left(r\frac{\partial P}{\partial r}\right)_{r=1} \quad \ldots\ldots \text{(IV-1)}$$

If we wish to determine the cumulative influx of fluid in absolute time T, and having expressed time in the diffusivity equation as $t = KT/\phi\mu cR_w^2$, then

$$Q_{(T)} = \int_0^T q_{(T)}\, dT = \frac{2\pi K}{\mu} \times \frac{\phi\mu cR_w^2}{K} \int_0^t \left(\frac{\partial P}{\partial r}\right)_{r=1} dt$$

$$= 2\pi\phi cR_w^2\, Q_{(t)} \quad \ldots\ldots \text{(IV-2)}$$

where

$$Q_{(t)} = \int_0^t \left(\frac{\partial P}{\partial r}\right)_{r=1} dt \quad \ldots \text{(IV-3)}$$

In brief, knowing the general solution implied by Eq. IV-3, which expresses the integration in dimensionless time, t, of the pressure gradient at radius unity for a pressure drop of one atmosphere, the cumulative influx into the well bore or into the oil-bearing portion of the field can be determined by Eq. IV-2. Furthermore, for any pressure drop, $\Delta P$, Eq. IV-2 expresses the cumulative influx as

$$Q_{(T)} = 2\pi\phi cR_w^2\, \Delta P\, Q_{(t)} \quad \ldots\ldots \text{(IV-4)}$$

per unit sand thickness.*

* The set of symbols now introduced and the symbols reported in Hurst's earlier paper on water-drive are related as follows:

$C(s' \theta/R') = Q_{(t)}$ and $\bar{C}(s' \theta/R') = \int_0^t Q_{(t)}\, dt$ where $s' \theta/R' = t$

When an oil reservoir and the adjoining water-bearing formations are contained between two parallel and sealing faulting planes, the flow of fluid is essentially parallel to these planes and is "linear." The constant terminal pressure case can also be applied to this case. The basic equation for linear flow is given by

$$\frac{\partial^2 P}{\partial x^2} = \frac{\partial P}{\partial t} \quad \ldots\ldots\ldots \text{(IV-5)}$$

where now $t = KT/f\mu c$ and $x$ is the absolute distance measured from the plane of influx extending out into the water-bearing sand. If we assume the same boundary conditions as in radial flow, with $P = P(x,t)$ as the solution, then by Darcy's law, the rate of fluid influx across the original water-oil contact per unit of cross-sectional area is expressed by

$$q_{(T)} = \frac{K}{\mu}\left(\frac{\partial P}{\partial x}\right)_{x=0} \quad \ldots\ldots \text{(IV-6)}$$

The total fluid influx is given by

$$Q_{(T)} = \int_0^T q_{(T)}\, dT = \frac{K}{\mu}\cdot\frac{f\mu c}{K}\int_0^t \left(\frac{\partial P}{\partial x}\right)_{x=0} dt$$
$$= f\,c\,Q_{(t)} \quad \ldots\ldots\ldots \text{(IV-7)}$$

where $Q_{(t)}$ is the generalized solution for linear flow and is equal to

$$Q_{(t)} = \int_0^t \left(\frac{\partial P}{\partial x}\right)_{x=0} dt \quad \ldots \text{(IV-8)}$$

Therefore, for any over-all pressure drop $\Delta P$, Eq. IV-7 gives

$$Q_{(T)} = fc\Delta P\, Q_{(t)} \quad \ldots\ldots\ldots \text{(IV-9)}$$

per unit of cross-sectional area.

### *Constant Terminal Rate Case*

In the constant terminal rate case it is likewise assumed that initially the pressure everywhere in the formation is constant but that from the time zero onward the fluid is withdrawn from the well bore or reservoir boundary at a unit rate. The pressure drop is given by $P = P_{(r,t)}$ and at the boundary of the field, where $r = 1$, $(\partial P/\partial r)_{r=1} = -1$. The minus sign is introduced because the gradient for the pressure drop relative to the radius of the well or reservoir is negative. If the cumulative pressure drop is expressed as $\Delta P$, then

$$\Delta P = q_{(t)}\, P_{(r,t)} \quad \ldots\ldots\ldots \text{(IV-10)}$$

where $q_{(t)}$ is a constant relating the cumulative pressure drop with the pressure change for a unit rate of production. By applying Darcy's equation for the rate of fluid flowing into the well or reservoir per unit sand thickness

$$q_{(T)} = \frac{-2\pi K}{\mu}\left(\frac{\partial \Delta P}{\partial r}\right)_{r=1} = \frac{-2\pi K\, q_{(t)}}{\mu}\left(\frac{\partial P_{(r,t)}}{\partial r}\right)_{r=1}$$

which simplifies to $q_{(t)} = \dfrac{q_{(T)}\mu}{2\pi K}$. Therefore, for any constant rate of production the cumulative pressure drop at the field radius is given by

$$\Delta P = \frac{q_{(T)}\mu}{2\pi K} P_{(t)} \quad \ldots\ldots\ldots \text{(IV-11)}$$

Similarly, for the constant rate of production in linear flow, the cumulative pressure drop is expressed by

$$\Delta P = \frac{q_{(T)}\mu}{K} P_{(t)} \quad \ldots\ldots\ldots \text{(IV-12)}$$

where $q_{(T)}$ is the rate of water encroachment per unit area of cross-section, and $P_{(t)}$ is the cumulative pressure drop at the sand face per unit rate of production.

### *Superposition Theorem*

With these fundamental relationships available, it remains to be shown how the constant pressure case can be interpreted for variable terminal pressures, or in the constant rate case, for variable rates. The linearity of the diffusivity equation allows the application of the superposition theorem as a sequence of constant terminal pressures or constant rates in such a fashion that it reproduces the pressure or production history at the boundary, $r = 1$. This is essentially Duhamel's principle, for which reference can be made to transient electric circuit theory in texts by Karman and Biot,[4] and Bush.[5] It has been applied to the flow of fluids by Muskat,[6] Schilthuis and Hurst,[7] in employing the variable rate case in calculating the pressure drop in the East Texas Field.[8]

The physical significance can best be realized by an application. Fig. 1-A shows the pressure decline in the well bore or a field that has been flowing and for which we wish to obtain the amount of fluid produced. As shown, the pressure history is reproduced as a series of pressure plateaus which represent a sequence of constant terminal pressures. Therefore, by the application of Eq. IV-4, the cumulative fluid produced in time $t$ by the pressure drop $\Delta P_n$, operative since zero time, is expressed by $Q_{(T)} = 2\pi fcR^2\, \Delta P_n\, Q_{(t)}$. If we next consider

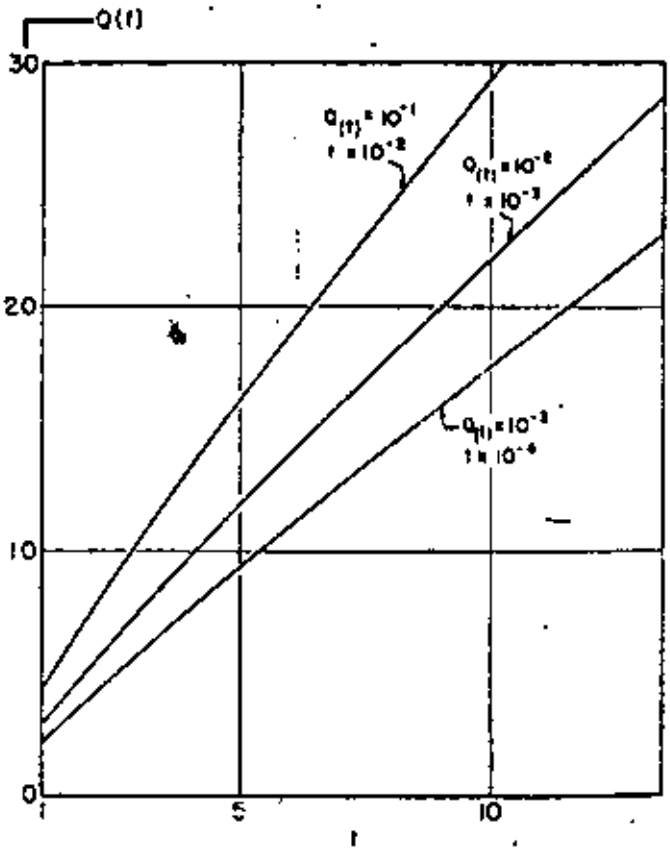


FIG. 4 — RADIAL FLOW, CONSTANT TERMINAL PRESSURE CASE, INFINITE RESERVOIR, CUMULATIVE PRODUCTION VS. TIME.

the pressure drop $\Delta P_n$ which occurs in time $t_n$ and treat this as a separate entity, but take cognizance of its time of inception $t_n$, then the cumulative fluid produced by this increment of pressure drop is $Q_{(t)} = 2\pi fcR_s^2 \Delta P_n Q_{(t-t_n)}$. By superimposing all these effects of pressure changes, the total influx in time t is expressed as

$$Q_{(t)} = 2\pi fcR_s^2 [\Delta P_0 Q_{(t)} + \Delta P_1 Q_{(t-t_1)} + \Delta P_2 Q_{(t-t_2)} + \Delta P_3 Q_{(t-t_3)} + \ldots] \quad . \quad (IV\text{-}13)$$

when $t > t_n$. To reproduce the smooth curve relationship of Fig. 1-A, these pressure plateaus can be taken as infinitesimally small, which give the summation of Eq. IV-13 by the integral

$$Q_{(t)} = 2\pi fcR_s^2 \int_0^t \frac{\partial \Delta P}{\partial t'} Q_{(t-t')}\, dt' \quad . \quad . \quad . \quad (IV\text{-}14)$$

By considering variable rates of fluid production, such as shown in Fig. 1-B, and reproducing these rates as a series of constant rate plateaus, then by Eq. IV-11 the pressure drop in the well bore in time t, for the initial rate $q_0$ is $\Delta P_0 = q_0 P_{(t)}$. At time $t_1$, the comparable increment for constant rate is expressed as $q_1 - q_0$, and the effect of this increment rate on the corresponding increment of pressure drop is $\Delta P_1 = (q_1 - q_0) P_{(t-t_1)}$. Again by superimposing all of these effects, the determination for the cumulative pressure drop is expressed by

$$\Delta P = q_{(0)} P_{(t)} + [q_{(t_1)} - q_{(0)}] P_{(t-t_1)} + [q_{(t_2)} - q_{(t_1)}] P_{(t-t_2)} + [q_{(t_3)} - q_{(t_2)}] P_{(t-t_3)} + \ldots \quad . \quad (IV\text{-}15)$$

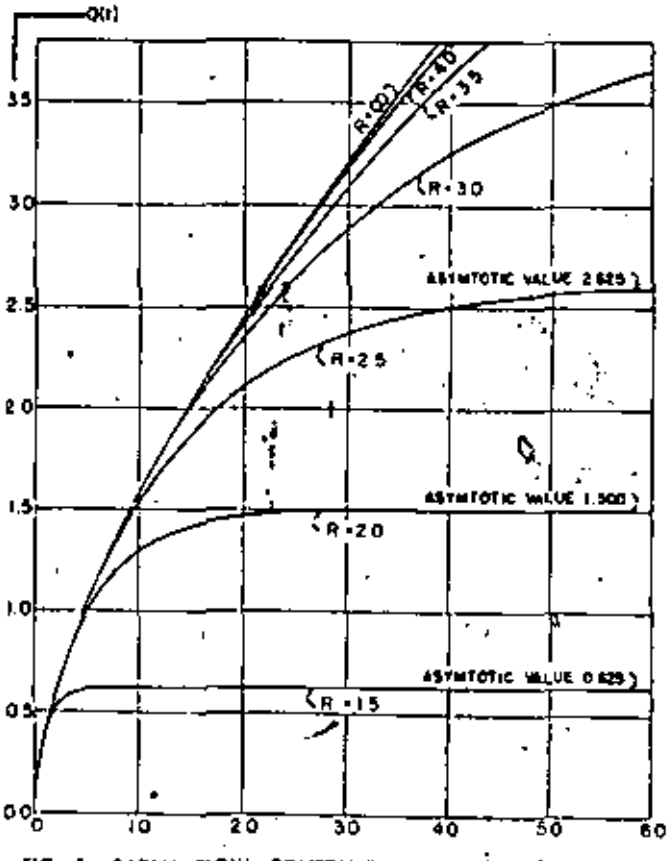


FIG. 3 — RADIAL FLOW, CONSTANT TERMINAL PRESSURE CASE, CUMULATIVE PRODUCTION VS. TIME FOR LIMITED RESERVOIRS.

If the increments are infinitesimal, or the smooth curve relationship applies, Eq. IV-15 becomes

$$\Delta P = q_{(0)} P_{(t)} + \int_0^t \frac{dq_{(t')}}{dt'} P_{(t-t')}\, dt' \quad . \quad (IV\text{-}16)$$

If $q_{(0)} = 0$, Eq. IV-16 can also be expressed as

$$\Delta P = \int_0^t q_{(t')} P'_{(t-t')}\, dt' \quad . \quad . \quad . \quad . \quad (IV\text{-}17)$$

where $P'_{(t)}$ is the derivative of $P_{(t)}$ with respect to t.

Since Eqs. IV-13 and IV-15 are of such simple algebraic forms, they are most practical to use with production history in making reservoir studies. In applying the pressure or rate plateaus as shown in Fig. 1, it must be realized that the time interval for each plateau should be taken as small as possible, so as to reproduce within engineering accuracy the trend of the curves. Naturally, if an exact interpretation is desired, Eqs. IV-14 and IV-16 apply.

## FUNDAMENTAL CONSIDERATIONS

In applying the Laplace transformation, there are certain fundamental operations that must be clarified. It has been stated that if $P_{(t)}$ is a pressure drop, the transformation for $P_{(t)}$ is given by Eq. III-1, as

$$\overline{P}_{(p)} = \int_0^\infty e^{-pt} P_{(t)}\, dt$$

To visualize more concretely the meaning of this equation, if the unit pressure drop at the boundary in the constant terminal pressure case is employed in Eq. III-1, its transform is given by

$$\overline{P}_{(p)} = \int_0^\infty e^{-pt} 1\, dt = \frac{-e^{-pt}}{p} 1 \Bigg|_0^\infty = \frac{1}{p} \quad . \quad (V\text{-}1)$$

The Laplace transformations of many transcendental functions have been developed and are available in tables, the most complete of which is the tract by Campbell and Foster.[4] It is therefore often possible after solving a total differential such as Eq. III-3 to refer to a set of tables and transforms and determine the inverse of $\overline{P}_{(p)}$ or $P_{(t)}$. It is frequently necessary to simplify $\overline{P}_{(p)}$ before an inversion can be made. However, Mellin's inversion formula is always applicable, which requires analytical treatment whenever used.

There are two possible simplifications for $\overline{P}_{(p)}$ when time is small or time is large. This is evident from Eq. III-3, where p can be interpreted by the operational calculus as the operator d/dt. Therefore, if we consider this symbolic relation, then if t is large, p must be small, or inversely, if t is small, p will be large. To understand this, if $\overline{P}_{(p)}$ is expressed by an involved Bessel relationship, the substitution for p as a small or large value will simplify $\overline{P}_{(p)}$ to give $P_{(t)}$ for the corresponding times.

Mellin's inversion formula is given on page 71 of Carslaw and Jaeger:[5]

$$P_{(t)} = \frac{1}{2\pi i} \int_{\gamma-i\infty}^{\gamma+i\infty} e^{\lambda t} \bar{P}_{(\lambda)} \, d\lambda$$

where $\bar{P}_{(\lambda)}$ is the transform $\bar{P}_{(t)}$. Where this report is concerned with pressure drops, the above can be written as

$$P_{(t_1)} - P_{(t_2)} = \frac{1}{2\pi i} \int_{\gamma-i\infty}^{\gamma+i\infty} (e^{\lambda t_1} - e^{\lambda t_2}) \bar{P}_{(\lambda)} \, d\lambda. \quad (V\text{-}2)$$

The integration is in the complex plane $\lambda = x + iy$, along a line parallel to the y-axis, extending from minus to positive infinity, and a distance $\gamma$ removed from the origin, so that all poles are to the left of this line, Fig. 2. The reader who has a comprehensive understanding of contour integrals will recognize that this integral is equal to the integration around a semi-circle of infinite radius extending to the left of the line $x = \gamma$, and includes integration along the "cuts," which joins the poles to the semi-circle. Since the integration along the semi-circle in the second and third quadrant is zero for radius infinity and $t>0$, this leaves the integration along the "cuts" and the poles, where the latter, as expressed in Eq. V-2, are the residuals.

Certain fundamental relationships in the Laplace transformations are found useful:[7]

*Theorem A* — If $\bar{P}_{(p)}$ is the transform of $P_{(t)}$ then

$$\int_0^\infty e^{-pt} \frac{dP_{(t)}}{dt} dt = e^{-pt} P_{(t)} \Big|_0^\infty + p \int_0^\infty e^{-pt} P_{(t)} \, dt$$

$$= p \bar{P}_{(p)} - P_{(t=0)}$$

or the transform of $\frac{dP_{(t)}}{dt} = p \bar{P}_{(p)} - P_{(t=0)}$, provided $e^{-pt} P_{(t)}$ approaches zero as time approaches infinity.

*Theorem B* — The transform of $\int_0^\infty P_{(t')} \, dt'$ is expressed by

$$\int_0^\infty e^{-pt} \int_0^t P_{(t')} \, dt' \, dt = \frac{-e^{-pt}}{p} \int_0^t P_{(t')} \, dt' \Big|_0^\infty + \frac{1}{p} \int_0^\infty e^{-pt} P_{(t)} \, dt$$

$$= \frac{\bar{P}_{(p)}}{p}$$

or the transform of the integration $P_{(t')}$ with respect to $t'$ from zero to $t$ is $\bar{P}_{(p)}/p$, if $e^{-pt} \int_0^t P_{(t')} \, dt'$ is zero for time infinity.

*Theorem C* — The transform for $e^{\pm ct} P_{(t)}$ is equal to

$$\int_0^\infty e^{-pt} e^{\pm ct} P_{(t)} \, dt = \int_0^\infty e^{-(p \mp c)t} P_{(t)} \, dt = \bar{P}_{(p \mp c)}$$

if $p - c$ is positive.

*Theorem D* — If $\bar{P}_1(p)$ is the transform of $P_1(t)$, and $\bar{P}_2(p)$ is the transform of $P_{2(t)}$, then the product of these two transforms is the transform of the integral

$$\int_0^t P_{1(t')} P_{2(t-t')} \, dt'$$

This integral is comparable to the integrals developed by the superimposition theorem, and of appreciable use in this paper.

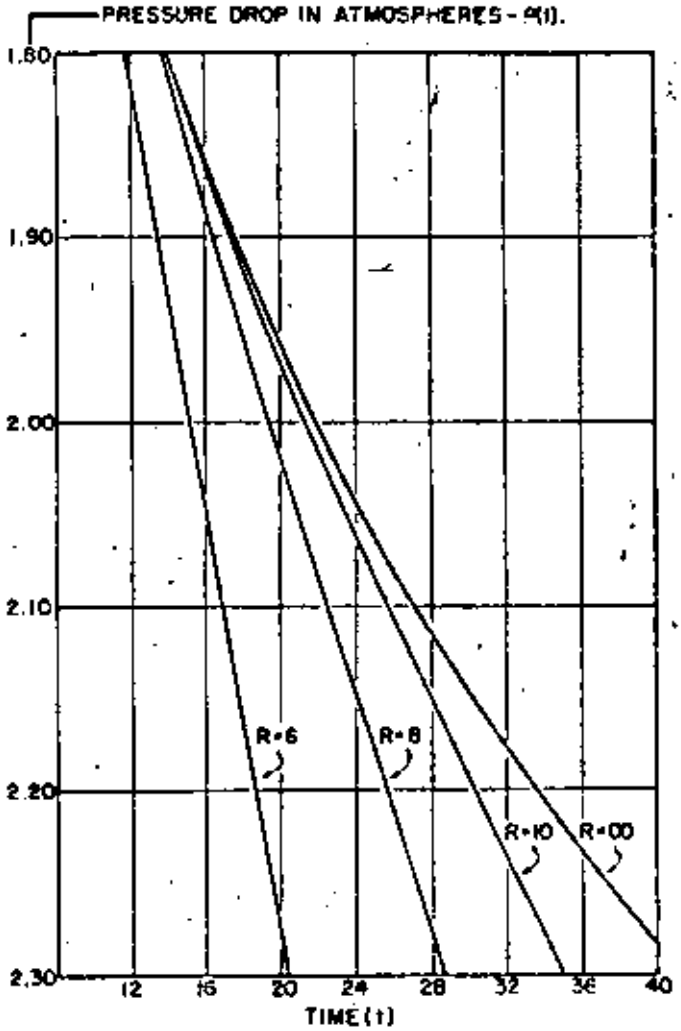


FIG. 6 — RADIAL FLOW, CONSTANT TERMINAL RATE CASE, PRESSURE DROP VS. TIME, P(t) VS. t

## CONSTANT TERMINAL PRESSURE AND CONSTANT TERMINAL RATE CASES, INFINITE MEDIUM

The analytics for the constant terminal pressure and rate cases have been developed for limited reservoirs[4,5] when the exterior boundary is considered closed or the production rate through this boundary is fixed. In determining the volume of water encroached into the oil-bearing portion of reservoirs, few cases have been encountered which indicated that the sands in which the oil occurs are of limited extent. For the most part, the data show that the influx behaves as if the water-bearing parts of the formations are of infinite extent, because within the productive life of oil reservoirs, the rate of water encroachment does not reflect the influence of an exterior boundary. In other words, whether or not the water sand is of limited extent, the rate of water encroachment is such as if supplied by an infinite medium.

Computing the water influx for an infinite reservoir with the help of Fourier-Bessel expansions, an exterior boundary can be assumed so far removed from the field radius that the production for a considerable time will reflect the infinite case. Unfortunately, the poor convergence of these expansions invalidates this approach. An alternative method consists of using increasing values for exterior radius, evaluating the water influx for each radius separately, and then drawing the envelope of these curves, which gives the infinite case, Fig. 5. In such a procedure, each of the branch curves reflects a water reservoir of limited extent. Inasmuch as the drawing of an envelope does not give a high degree of accuracy, the solutions for the constant terminal pressure and constant terminal rate cases for an infinite medium are presented here, with values for $Q_{(t)}$ and $P_{(t)}$ calculated directly.

The constant terminal pressure case was first developed by Nicholson[11] by the application of Green's function to an instantaneous circular source in an infinite medium. Goldstein[12] presented this solution by the operational method, and Smith[13] employed Carslaw's contour method in its development. Carslaw and Jaeger[14,15] later gave the explicit treatment of the constant terminal pressure case by the application of the Laplace transformation. The derivation of the constant terminal rate case is not given in the literature, and its development is presented here.

### *The Constant Rate Case*

As already discussed, the boundary conditions for the constant rate case in an infinite medium are that (1) the pressure drop $P_{(r,t)}$ is zero initially at every point in the formation, and (2) at the radius of the field ($r = 1$) we have $\left(\frac{\partial P}{\partial r}\right)_{r=1} = -1$ at all times.

A reference to a text on Bessel functions, such as Karman and Biot,[5] pp. 61-63, shows that the general solution for Eq. III-3 is given by

$$\bar{P}_{(r,p)} = A\, I_o\,(r\sqrt{p}) + B\, K_o\,(r\sqrt{p}) \quad . \quad \text{(VI-1)}$$

where $I_o\,(r\sqrt{p})$ and $K_o(r\sqrt{p})$ are modified Bessel functions of the first and second kind, respectively, and of zero order. A and B are two constants which satisfy a second order differential equation. Since $\bar{P}(r,p)$ is the transform of the pressure drop at a point in the formation, and because at a point not yet affected by production the absolute pressure equals the initial pressure, it is required that $\bar{P}(r,p)$ should approach zero as r becomes large. As shown in Karman and Biot,[5] $I_o(r\sqrt{p})$ becomes increasingly large and $K_o(r\sqrt{p})$ approaches zero as the argument $(r\sqrt{p})$ increases. Therefore, to obey the initial condition, the constant A must equal zero and (VI-1) becomes

$$\bar{P}_{(r,p)} = B\, K_o(r\sqrt{p}) \quad . \quad . \quad . \quad . \quad . \quad \text{(VI-2)}$$

To fulfill the second boundary condition for unit rate of production, namely $(\partial P/\partial r)_{r=1} = -1$, the transform for unity gives

$$\left(\frac{\partial \bar{P}}{\partial r}\right)_{r=1} = -\frac{1}{p} \quad . \quad . \quad . \quad . \quad \text{(VI-3)}$$

by Eq. V-1. The differentiation of the modified Bessel function of the second kind, Watson's Bessel Functions,[16] W.B.F., p. 79, gives $K_o'(z) = -K_1(z)$. Therefore, differentiation Eq.

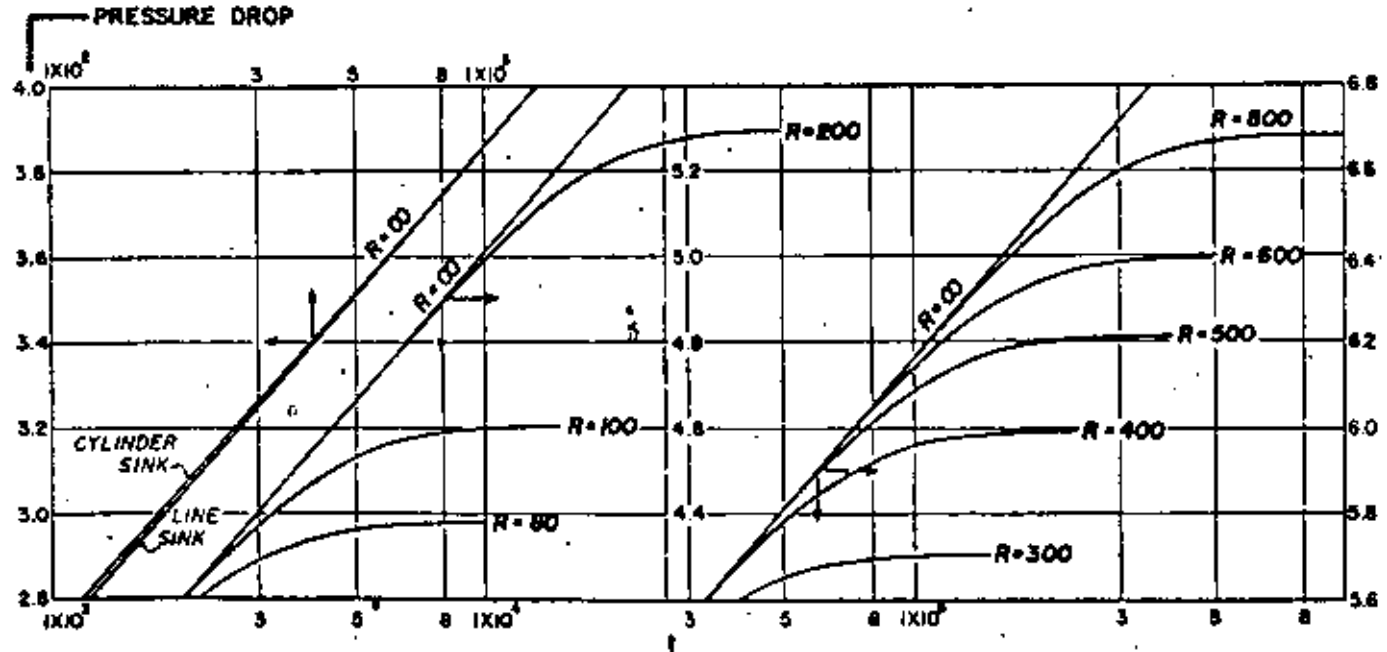


FIG. 7 — RADIAL FLOW, CONSTANT TERMINAL RATE CASE, CUMULATIVE PRESSURE DROP VS. TIME P(t) VS. t

VI-2, with respect to r at r = 1, gives

$$\left(\frac{\partial \bar{P}}{\partial r}\right)_{r=1} = -B\sqrt{p}\ K_1(\sqrt{p})$$

and since

$$\left(\frac{\partial \bar{P}}{\partial r}\right)_{r=1} = -\frac{1}{p}$$

the constant $B = 1/p^{3/2} K_1(\sqrt{p})$. Therefore, the transform for the pressure drop for the constant rate case in an infinite medium is given by

$$\bar{P}_{(r,p)} = \frac{K_0(r\sqrt{p})}{p^{3/2}K_1(\sqrt{p})} \quad \ldots\ldots \text{(VI-4)}$$

To determine the inverse of Eq. VI-4 in order to establish the pressure drop at radius unity, we can resort to the simplification that for small times the operator p is large. Since

$$K_0(z) = \sqrt{\frac{\pi}{2z}}\, e^{-z} \quad \ldots\ldots \text{(VI-5)}$$

for z large, W.B.F., p. 202, then

$$\bar{P}_{(1,p)} = \frac{1}{p^{3/2}} \quad \ldots\ldots \text{(VI-6)}$$

The inversion for this transform is given in Campbell and Foster, Eq. 516, as

$$P_{(1,t)} = \frac{2}{\sqrt{\pi}}\, t^{1/2} \quad \ldots\ldots \text{(VI-7)}$$

In brief, Eq. VI-7 states that when $t = KT/fscR_e^2$ is small, which can be caused by the boundary radius for the field, $R_e$ being large, the pressure drop for the unit rate of production approximates the condition for linear flow.

To justify this conclusion, the treatment of the linear flow equation, Eq. IV-5, by the Laplace transformation gives

$$\frac{d^2 \bar{P}_{(x,p)}}{dx^2} = p\bar{P}_{(x,p)} \quad \ldots\ldots \text{(VI-8)}$$

for which the general solution is the expression

$$\bar{P}_{(x,p)} = Ae^{-x\sqrt{p}} + Be^{+x\sqrt{p}} \quad \ldots \text{(VI-9)}$$

By repeating the reasoning already employed in this development, the transform for the pressure drop at $x = 0$ gives

$$\bar{P}(0\sqrt{p}) = 1/p^{3/2}$$

which is identical with (VI-6) with p the operator of $t = KT/fsc$.

The second simplification for the transform (VI-4) is to consider p small, which is equivalent to considering time, t, large. The expansions for $K_0(z)$ and $K_1(z)$ are given in Carslaw and Jaeger,* p. 248.

$$K_0(z) = -I_0(z)\left\{\log\frac{z}{2} + \gamma\right\} + \left(\frac{z}{2}\right)^2 + \frac{\left(1+\frac{1}{2}\right)\left(\frac{z}{2}\right)^4}{(2!)^2} + \frac{\left(1+\frac{1}{2}+\frac{1}{3}\right)\left(\frac{z}{2}\right)^6}{(3!)^2} + \cdots \quad \text{(VI-10)}$$

$$K_n(z) = -(-1)^{n+1} I_n(z)\left\{\log\frac{z}{2} + \gamma\right\} + \frac{1}{2}(-1)^n \sum_{r=0}^{\infty} \frac{\left(\frac{z}{2}\right)^{n+2r}}{r!\,(n+r)!}\left[\sum_{m=1}^{r}\frac{1}{m} + \sum_{m=1}^{n+r}\frac{1}{m}\right] + \frac{1}{2}\sum_{r=0}^{n-1}(-1)^r \left(\frac{z}{2}\right)^{n-2r}\frac{(n-r-1)!}{r!} \quad \ldots \text{(VI-11)}$$

where $\gamma$ is Euler's constant 0.57722, and the logarithmic term consists of natural logarithms. When z is small

$$K_0(z) \cong -\left[\log\frac{z}{2} + \gamma\right] \quad \ldots \text{(VI-12)}$$

$$K_1(z) \cong 1/z \quad \ldots\ldots \text{(VI-13)}$$

Therefore, Eq. VI-4 becomes

$$\bar{P}_{(1,p)} = \frac{-\log p}{2p} + \frac{(\log 2 - \gamma)}{p} \quad \ldots \text{(VI-14)}$$

The inversion for the first term on the right is given by Campbell and Foster, Eq. 892, and the inverse of the second term by

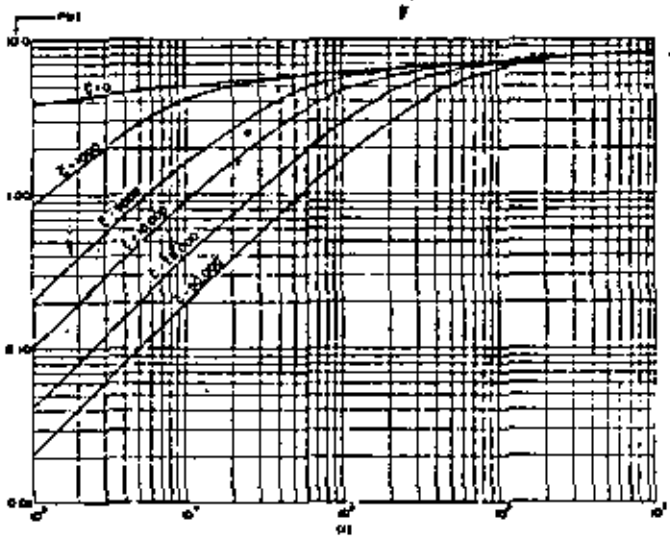

FIG. 8 — CONSTANT RATE OF PRODUCTION IN THE STOCK TANK ADJUSTING FOR THE UNLOADING OF FLUID IN THE ANNULUS, $P_D$ VERSUS $\tau$ where $\tau = c/2\pi fcR_e^2$, AND c is the VOLUME OF FLUID UNLOADED FROM THE ANNULUS, CORRECTED TO RESERVOIR CONDITIONS, PER ATMOSPHERE BOTTOM-HOLE PRESSURE DROP, PER UNIT SAND THICKNESS.

Eq. V-1. Therefore, the pressure drop at the boundary of the field when t is large is given by

$$P_{(1,t)} = \frac{1}{2}\left[\log 4t - \gamma\right] = \frac{1}{2}\left[\log t + 0.80907\right] \quad \ldots \text{(VI-15)}$$

The solution given by Eq. VI-15 is the solution of the continuous point source problem for large time t. The relationship has been applied to the flow of fluids by Bruce,** Elkins,** and others, and is particularly applicable for study of interference between flowing wells.

The point source solution originally developed by Lord Kelvin and discussed in Carslaw* can be expressed as

$$P_{(r,t)} = \frac{1}{2}\int_{\frac{1}{4t}}^{\infty} \frac{e^{-n}}{n}\, dn = \frac{1}{2}\left\{-\mathrm{Ei}\left(-\frac{1}{4t}\right)\right\} \quad \ldots \text{(VI-16)}$$

often referred to as the logarithmic integral or the Ei-function. Its values are given in Tables of Sine, Cosine, and Exponential Integrals, Volumes I and II, Federal Works Agency, W.P.A., City of New York. For large values of the time, t, Eq. VI-16 reduces to $P_{(r,t)} = \frac{1}{2}\left[\log 4t - \gamma\right]$ which is Eq. VI-15, and this relation is accurate for values of $t > 100$.

By this development it is evident that the point source solution does not apply at a boundary for the determination of the pressure drop when t is small. However, when the radius, $R_e$, is small, such as a well radius, even small values of the absolute time, T will give large values of the dimensionless time t, and the point source solution is applicable. On the other hand, in considering the pressure drop at the periphery of a field (in which case $R_e$ can have a large numerical value) the value of t can be easily less than 100 even for large values of absolute time, T. Therefore, for intermediate times, the rigorous solution of the constant rate case must be used, which we will now proceed to obtain.

To develop the explicit solution for the constant terminal rate case, it is necessary to invert the Laplace transform, Eq. VI-4, by the Mellin's Inversion formula. The path of integration for this transform is described by the "cut" along the negative real axis, Fig. 2, which gives a single valued function on each side of the "cut." That is to say that Path AB required by Eq. V-2 is equal to the Path AD and CB, both of which are described by a semi-circle of radius infinity. Since its integration is zero in the second and third quadrant, this leaves the integration along Paths DO and OC equal to AB. The integration on the upper portion of the "cut" can be obtained by making $\lambda = u' e^{+i\pi}$, which yields

$$\frac{1}{2\pi i}\int_{-\infty}^{0} \frac{(e^{\lambda t_1} - e^{\lambda t_2})\, K_o(\sqrt{\lambda}\, r)}{\lambda\, K_1(\sqrt{\lambda})}\, d\lambda =$$

$$\frac{1}{\pi i}\int_{0}^{\infty} \frac{(e^{-u't_1} - e^{-u't_2})\, K_o(u\, e^{\frac{i\pi}{2}} r)\, du}{u'\, e^{i\pi}\, K_1(u\, e^{\frac{i\pi}{2}})} \quad \ldots \quad \text{(VI-17)}$$

Carslaw and Jaeger' (page 249) shows that modified Bessel functions of the first and second kind of arguments $z\, e^{\pm \frac{i\pi}{2}}$ can be expressed by the regular Bessel functions as complex values, as follows:

$$I_o(z\, e^{\pm \frac{i\pi}{2}}) = J_o(z)$$

$$K_o(z\, e^{\pm \frac{i\pi}{2}}) = \mp \frac{\pi i}{2}\{J_o(z) \pm i\, Y_o(z)\}$$

$$I_1(z\, e^{\pm \frac{i\pi}{2}}) = \pm i\, J_1(z) \quad \ldots \quad \text{(VI-18)}$$

and

$$K_1(z\, e^{\pm \frac{i\pi}{2}}) = -\frac{\pi}{2}[J_1(z) \mp i\, Y_1(z)]$$

The substitution of the corresponding values for $K_o(u\, e^{i\pi/2} r)$ and $K_1(u\, e^{i\pi/2})$ from Eq. VI-18 in Eq. VI-17 gives the integration along the upper portion of the negative real "cut" as

$$\frac{1}{\pi}\int_{0}^{\infty} \frac{(e^{-u't_1} - e^{-u't_2})\,[Y_1(u)\, J_o(ur) - J_1(u)\, Y_o(ur)]\, du}{u'[J_1^2(u) + Y_1^2(u)]} \quad \text{(VI-19)}$$

where the imaginary term has been dropped.

Likewise, the integration along the under portion of the negative real "cut" is expressed by $\lambda = u' e^{-i\pi}$ and

$$\frac{1}{2\pi i}\int_{0}^{-\infty} \frac{(e^{\lambda t_1} - e^{\lambda t_2})\, K_o(\sqrt{\lambda}\, r)\, d\lambda}{\lambda\, K_1(\sqrt{\lambda})}$$

$$= -\frac{1}{\pi i}\int_{0}^{\infty} \frac{(e^{-u't_1} - e^{-u't_2})\, K_o(u\, e^{-i\pi/2} r)\, du}{u'\, e^{-i\pi/2}\, K_1(u\, e^{-i\pi/2})}$$

Using Eq. VI-18, yields the relationship

$$\frac{1}{\pi}\int_{0}^{\infty} \frac{(e^{-u't_1} - e^{-u't_2})\,[Y_1(u)\, J_o(ur) - J_1(u)\, Y_o(ur)]\, du}{u'\,[J_1^2(u) + Y_1^2(u)]} \quad \text{(VI-20)}$$

The integration along Paths DO and OC is the sum of the relations VI-19 and VI-20, or

$$P_{(r,\,t_1)} - P_{(r,\,t_2)} =$$

$$\frac{2}{\pi}\int_{0}^{\infty} \frac{(e^{-u't_1} - e^{-u't_2})\,[Y_1(u)\, J_o(ur) - J_1(u)\, Y_o(ur)]\, du}{u'[J_1^2(u) + Y_1^2(u)]}$$

Initially, that is at time zero, the cumulative pressure drop at any point in the formation is zero, $P_{(r,\,t=0)} = 0$. Hence, the pressure drop since zero time equals:

$$P_{(r,t)} = \frac{2}{\pi}\int_{0}^{\infty} \frac{(1 - e^{-u't})\,[J_1(u)\, Y_o(ur) - Y_1(u)\, J_o(ur)]\, du}{u'[J_1^2(u) + Y_1^2(u)]} \quad \text{(VI-21)}$$

which is the explicit solution of the constant terminal rate case for an infinite medium.

To determine the cumulative pressure drop for a unit rate of production at the well bore or field radius, (where $r = 1$) then Eq. VI-21 changes to

$$P_{(1,\,t)} = \frac{2}{\pi}\int_{0}^{\infty} \frac{(1 - e^{-u't})\,[J_1(u)\, Y_o(u) - Y_1(u)\, J_o(u)]\, du}{u'\,[J_1^2(u) + Y_1^2(u)]} \quad \text{(VI-22)}$$

By the recurrence formula given in W.B.F., p. 77

$$J_1(u)\, Y_o(u) - J_o(u)\, Y_1(u) = \frac{2}{\pi u} \quad \ldots \quad \text{(VI-23)}$$

Equation VI-22 simplifies to

$$\boxed{P_{(t)} = \frac{4}{\pi^2}\int_{0}^{\infty} \frac{(1 - e^{-u't})\, du}{u'\,[J_1^2(u) + Y_1^2(u)]}} \quad \ldots \quad \text{(VI-24)}$$

*Constant Terminal Pressure Case*

As already shown, the transform of the pressure drop in an infinite medium is $\bar{P}_{(r,p)} = B\, K_o(\sqrt{p}\, r)$. In the constant terminal pressure case it is assumed that at all times the pressure drop at $r = 1$ will be unity, which is expressed as a transform by Eq. V-1

$$\bar{P}_{(1,p)} = 1/p$$

By solving for the constant B at $r = 1$ in the above formula, we find $B = 1/p\, K_o(\sqrt{p})$, so that the transform for the pressure at any point in the reservoir is expressed by

$$\bar{P}_{(r,p)} = \frac{K_o(\sqrt{p}\, r)}{p\, K_o(\sqrt{p})} \quad \ldots \quad \text{(VI-25)}$$

The comparable solution of VI-25 for a cumulative pressure drop can be developed as before by considering the paths of Fig. 2, with a pole at the origin, to give the solution

$$P_{(r,\,t)} - P_{(r,\,0)} = \frac{2}{\pi} \int_0^\infty \frac{(e^{-u^2 t_1} - e^{-u^2 t_2})\,[J_0(u)\;Y_0(ur) - Y_0(u)\;J_0(ur)]}{u^2[J_0^2(u) + Y_0^2(u)]}\,du \quad \ldots \quad (VI\text{-}26)$$

If we are interested in the cumulative fluid influx at the field radius, $r = 1$, then the relationship Eq. IV-3 applies, or

$$Q_{(t)} = \int_0^t \left(\frac{\partial P}{\partial r}\right)_{r=1} dt \quad \ldots \quad (IV\text{-}3)$$

The determination of the transform of the gradient of the pressure drop at the field's edge follows from Eq. VI-25,

$$\left(\frac{\partial \bar{P}_{(r,\,p)}}{\partial r}\right)_{r=1} = -\frac{K_1(\sqrt{p})}{p^{1/2}\,K_0(\sqrt{p})}$$

since $K_0'(z) = -K_1(z)$. Since the pressure drop $P_{(r,\,t)}$ corresponds to the difference between the initial and actual pressure, the transform of the gradient of the actual pressure at $r = 1$ is given by

$$\left(\frac{\partial \bar{P}}{\partial r}\right)_{r=1} = \left(\frac{-\partial \bar{P}_{(r,\,p)}}{\partial r}\right)_{r=1}$$

or

$$\left(\frac{\partial \bar{P}}{\partial r}\right)_{r=1} = \frac{K_1(\sqrt{p})}{p^{1/2}\,K_0(\sqrt{p})}$$

which corresponds to the integrand of Eq. IV-3. Further, from the definition given by Theorem B, namely, that if $\bar{P}(p)$ is the transform of $P_{(t)}$ then the transform of $\int_0^t P_{(t)}\,dt'$ is given by $\bar{P}(p)/p$ and the Laplace transform for $Q_{(t)}$ is expressed by

$$\bar{Q}_{(p)} = \frac{K_1(\sqrt{p})}{p^{3/2}\,K_0(\sqrt{p})} \quad \ldots \quad (VI\text{-}27)$$

The application of the Mellin's inversion formula to Eq. VI-27 follows the paths shown in Fig. 2, giving

$$Q_{(t)} = \frac{4}{\pi^2} \int_0^\infty \frac{(1 - e^{-u^2 t})\,du}{u^3\,[J_0^2(u) + Y_0^2(u)]} \quad \ldots \quad (VI\text{-}28)$$

With respect to the transform $\bar{Q}_{(p)}$, there is the simplification that for time small, p is large, or Eq. VI-27 reduces to

$$\bar{Q}_{(p)} = 1/p^{3/2} \quad \ldots \quad (VI\text{-}29)$$

and the inversion is as before

$$Q_{(t)} = \frac{2}{\sqrt{\pi}}\,t^{1/2} \quad \ldots \quad (VI\text{-}30)$$

which is identical to the linear flow case. For all other values of the time, Eq. VI-28 must be solved numerically.

### *Relation Between $\bar{Q}(p)$ and $\bar{P}(p)$*

It is evident from the work that has already gone before, that the Laplace transformation and the superimposition theorem offer a basis for interchanging the constant terminal pressure to the constant terminal rate case, and vice versa. In any reservoir study the essential interest is the analyses of the flow either at the well bore or the field boundary. The purpose of this work is to determine the relationship between $Q(t)$, the constant terminal pressure case, and $P(t)$, the constant terminal rate case, which explicitly refer to the boundary $r = 1$. Therefore, if we conceive of the influx of fluid into a

TABLE I — *Radial Flow, Constant Terminal Pressure and Constant Terminal Rate Cases for Infinite Reservoirs*

| $t_D$ | $Q_{(t)_D}$ | $P_{(t)_D}$ | $t$ | $Q_{(t)}$ |
|---|---|---|---|---|
| 1.0(10)$^{-4}$ | 0.112 | 0.112 | 1.8(10)$^{3}$ | 4.136(10)$^{2}$ |
| 5.0 " | 0.278 | 0.229 | 2.0 " | 5.515 " |
| 1.0(10)$^{-3}$ | 0.404 | 0.315 | 2.5 " | 6.466 " |
| 1.5 " | 0.520 | 0.378 | 3.0 " | 7.350 " |
| 2.0 " | 0.606 | 0.424 | 4.0 " | 9.757 " |
| 2.5 " | 0.686 | 0.466 | 5.0 " | 11.89 " |
| 3.0 " | 0.756 | 0.502 | 6.0 " | 13.55 " |
| 4.0 " | 0.886 | 0.564 | 7.0 " | 15.98 " |
| 5.0 " | 1.020 | 0.615 | 8.0 " | 18.05 " |
| 6.0 " | 1.140 | 0.656 | 9.0 " | 19.88 " |
| 7.0 " | 1.241 | 0.702 | 1.0(10)$^{4}$ | 21.56 " |
| 8.0 " | 1.350 | 0.738 | 1.5 " | 3.148(10)$^{3}$ |
| 9.0 " | 1.460 | 0.772 | 2.0 " | 4.079 " |
| 1.0 | 1.570 | 0.802 | 2.5 " | 4.994 " |
| 1.5 | 2.032 | 0.927 | 3.0 " | 5.891 " |
| 2.0 | 2.462 | 1.020 | 4.0 " | 7.654 " |
| 2.5 | 2.858 | 1.101 | 5.0 " | 9.342 " |
| 3.0 | 3.209 | 1.169 | 6.0 " | 11.00 " |
| 4.0 | 3.807 | 1.275 | 7.0 " | 12.66 " |
| 5.0 | 4.341 | 1.362 | 8.0 " | 14.32 " |
| 6.0 | 4.846 | 1.436 | 9.0 " | 15.96 " |
| 7.0 | 5.340 | 1.500 | 1.0(10)$^{5}$ | 17.60 " |
| 8.0 | 5.814 | 1.556 | 1.5 " | 2.578(10)$^{4}$ |
| 9.0 | 6.281 | 1.604 | 2.0 " | 3.388 " |
| 1.0(10)$^{1}$ | 7.417 | 1.651 | 2.5 " | 4.088 " |
| 1.5 " | 1.066 | 1.829 | 3.0 " | 4.717 " |
| 2.0 " | 1.3249(30)$^{1}$ | 1.950 | 4.0 " | 5.867 " |
| 2.5 " | 1.456 " | 2.047 | 5.0 " | 7.008 " |
| 3.0 " | 1.681 " | 2.147 | 6.0 " | 9.113 " |
| 4.0 " | 2.063 " | 2.252 | 7.0 " | 10.51 " |
| 5.0 " | 2.452 " | 2.338 | 8.0 " | 11.99 " |
| 6.0 " | 2.860 " | 2.476 | 9.0 " | 13.26 " |
| 7.0 " | 3.228 " | 2.560 | 1.0(10)$^{6}$ | 14.62 " |
| 8.0 " | 3.599 " | 2.618 | 1.5 " | 2.126(10)$^{5}$ |
| 9.0 " | 3.942 " | 2.672 | 2.0 " | 2.761 " |
| 1.0(10)$^{2}$ | 4.301 " | 2.723 | 2.5 " | 3.427 " |
| 1.5 " | 5.988 " | 2.921 | 3.0 " | 4.064 " |
| 2.0 " | 7.548 " | 3.064 | 4.0 " | 5.313 " |
| 2.5 " | 9.138 " | 3.173 | 5.0 " | 6.544 " |
| 3.0 " | 10.58 " | 3.252 | 6.0 " | 7.761 " |
| 4.0 " | 13.49 " | 3.408 | 7.0 " | 8.965 " |
| 5.0 " | 16.21 " | 3.516 | 8.0 " | 10.16 " |
| 6.0 " | 18.97 " | 3.608 | 9.0 " | 11.34 " |
| 7.0 " | 21.60 " | 3.684 | 1.0(10)$^{7}$ | 12.52 " |
| 8.0 " | 24.23 " | 3.750 | | |
| 9.0 " | 26.77 " | 3.809 | | |
| 1.0(10)$^{3}$ | 29.31 " | 3.860 | | |

TABLE I — *Continued*

| $t_D$ | $Q_{(t)_D}$ | | $t$ | $Q_{(t)}$ |
|---|---|---|---|---|
| 1.5(10)$^{7}$ | 1.8329(10)$^{7}$ | | 1.5(10)$^{10}$ | 1.17(10)$^{10}$ |
| 2.0 " | 2.309 " | | 2.0 " | 1.35 " |
| 2.5 " | 2.761 " | | 2.5 " | 1.52 " |
| 3.0 " | 3.217 " | | 3.0 " | 2.29 " |
| 4.0 " | 4.010 " | | 4.0 " | 3.02 " |
| 5.0 " | 4.780 " | | 5.0 " | 3.75 " |
| 6.0 " | 5.538 " | | 6.0 " | 4.47 " |
| 7.0 " | 6.288 " | | 7.0 " | 5.19 " |
| 8.0 " | 7.032 " | | 8.0 " | 5.89 " |
| 9.0 " | 7.771 " | | 9.0 " | 6.59 " |
| 1.0(10)$^{8}$ | 8.507 " | | 1.0(10)$^{11}$ | 7.29 " |
| 1.5 " | 1.2198(10)$^{8}$ | | 1.5 " | 1.08(10)$^{11}$ |
| 2.0 " | 1.587 " | | 2.0 " | 1.42 " |
| 2.5 " | 1.949 " | | | |
| 3.0 " | 2.305 " | | | |
| 4.0 " | 3.009 " | | | |
| 5.0 " | 3.705 " | | | |
| 6.0 " | 4.396 " | | | |
| 7.0 " | 5.082 " | | | |
| 8.0 " | 5.764 " | | | |
| 9.0 " | 6.443 " | | | |
| 1.0(10)$^{9}$ | 7.118 " | | | |
| 1.5 " | 1.054 " | | | |

TABLE II — *Constant Terminal Pressure Case Radial Flow, Limited Reservoirs*

| $R = 1.5$ $a_1 = 2.8899$ $a_2 = 0.2402$ | | $R = 2.0$ $a_1 = 1.3666$ $a_2 = 4.6159$ | | $R = 2.5$ $a_1 = 0.8662$ $a_2 = 3.0475$ | | $R = 3.0$ $a_1 = 0.6250$ $a_2 = 2.3041$ | |
|---|---|---|---|---|---|---|---|
| $t$ | $Q_{(t)}$ | $t$ | $Q_{(t)}$ | $t$ | $Q_{(t)}$ | $t$ | $Q_{(t)}$ |
| $5.0(10)^{-5}$ | 0.226 | $5.0(10)^{-5}$ | 0.224 | $1.0(10)^{-4}$ | 0.108 | $2.0(10)^{-4}$ | 0.745 |
| 6.0 " | 0.264 | 7.5 " | 0.318 | 1.5 " | 0.305 | 4.0 " | 0.484 |
| 7.0 " | 0.298 | $1.0(10)^{-4}$ | 0.404 | 2.0 " | 0.498 | 6.0 " | 0.833 |
| 8.0 " | 0.334 | 1.25 " | 0.536 | 2.5 " | 0.691 | 8.0 " | 1.163 |
| 9.0 " | 0.373 | 1.50 " | 0.667 | 3.0 " | 0.884 | 1.0 | 1.494 |
| $1.0(10)^{-4}$ | 0.395 | 1.75 " | 0.853 | 3.5 " | 0.978 | 1.20 | 1.769 |
| 1.1 " | 0.411 | 2.00 " | 0.997 | 4.0 " | 1.072 | 1.40 | 1.965 |
| 1.2 " | 0.431 | 2.25 " | 1.024 | 4.5 " | 1.162 | 1.60 | 2.163 |
| 1.3 " | 0.444 | 2.50 " | 1.074 | 5.0 " | 1.254 | 1.80 | 2.361 |
| 1.4 " | 0.461 | 2.75 " | 1.115 | 5.5 " | 1.343 | 2.00 | 2.557 |
| 1.5 " | 0.471 | 3.00 " | 1.161 | 6.0 " | 1.434 | 2.20 | 2.754 |
| 1.6 " | 0.486 | 3.25 " | 1.205 | 6.5 " | 1.524 | 2.40 | 2.950 |
| 1.7 " | 0.497 | 3.50 " | 1.247 | 7.0 " | 1.614 | 2.60 | 3.147 |
| 1.8 " | 0.507 | 3.75 " | 1.288 | 7.5 " | 1.704 | 2.80 | 3.343 |
| 1.9 " | 0.517 | 4.00 " | 1.327 | 8.0 " | 1.794 | 3.00 | 3.540 |
| 2.0 " | 0.525 | 4.25 " | 1.365 | 8.5 " | 1.884 | 3.20 | 3.736 |
| 2.1 " | 0.533 | 4.50 " | 1.401 | 9.0 " | 1.974 | 3.40 | 3.933 |
| 2.2 " | 0.541 | 4.75 " | 1.436 | 9.5 " | 2.064 | 3.60 | 4.129 |
| 2.3 " | 0.548 | 5.00 " | 1.469 | 1.0 | 2.154 | 3.80 | 4.326 |
| 2.4 " | 0.554 | 5.50 " | 1.535 | 1.1 | 2.334 | 4.20 | 4.719 |
| 2.5 " | 0.559 | 6.00 " | 1.597 | 1.2 | 2.514 | 4.60 | 5.112 |
| 2.6 " | 0.565 | 6.50 " | 1.656 | 1.3 | 2.694 | 5.00 | 5.505 |
| 2.8 " | 0.574 | 7.00 " | 1.713 | 1.4 | 2.874 | 5.40 | 5.898 |
| 3.0 " | 0.582 | 7.50 " | 1.768 | 1.5 | 3.054 | 5.80 | 6.291 |
| 3.2 " | 0.588 | 8.00 " | 1.820 | 1.6 | 3.234 | 6.20 | 6.684 |
| 3.4 " | 0.594 | 9.00 " | 1.920 | 1.7 | 3.414 | 6.60 | 7.077 |
| 3.6 " | 0.599 | 1.00 | 2.015 | 1.8 | 3.594 | 7.00 | 7.470 |
| 3.8 " | 0.603 | 1.1 | 2.200 | 2.0 | 3.954 | 7.80 | 8.256 |
| 4.0 " | 0.606 | 1.2 | 2.380 | 2.2 | 4.314 | 8.60 | 9.042 |
| 4.5 " | 0.613 | 1.3 | 2.560 | 2.4 | 4.674 | 9.40 | 9.828 |
| 5.0 " | 0.617 | 1.4 | 2.740 | 2.6 | 5.034 | 10.20 | 10.61 |
| 6.0 " | 0.621 | 1.5 | 2.920 | 2.8 | 5.394 | 11.00 | 11.40 |
| 7.0 " | 0.623 | 1.6 | 3.100 | 3.0 | 5.754 | 11.80 | 12.19 |
| 8.0 " | 0.624 | 1.7 | 3.280 | 3.2 | 6.114 | 12.60 | 12.98 |
| | | 1.8 | 3.460 | 3.4 | 6.474 | 13.40 | 13.77 |
| | | 2.0 | 3.820 | 3.6 | 6.834 | 14.20 | 14.56 |
| | | 2.5 | 4.720 | 4.0 | 7.554 | 15.80 | 16.13 |
| | | 3.0 | 5.620 | 4.5 | 8.454 | 17.80 | 18.11 |
| | | 4.0 | 7.420 | 5.0 | 9.354 | 19.80 | 20.09 |
| | | 5.0 | 9.220 | 6.0 | 11.15 | 23.80 | 24.05 |
| | | | | 7.0 | 12.95 | 27.80 | 28.02 |
| | | | | 8.0 | 14.75 | 31.80 | 32.00 |
| | | | | 9.0 | 16.55 | | |
| | | | | 10.0 | 18.35 | | |

TABLE II — *Continued*

| $R = 3.5$ $a_1 = 0.4851$ $a_2 = 1.6374$ | | $R = 4.0$ $a_1 = 0.3935$ $a_2 = 1.6267$ | | $R = 4.5$ $a_1 = 0.3296$ $a_2 = 1.3084$ | | $R = 5.0$ $a_1 = 0.2823$ $a_2 = 1.1892$ | | $R = 6.0$ $a_1 = 0.2182$ $a_2 = 0.9025$ | |
|---|---|---|---|---|---|---|---|---|---|
| $t$ | $Q_{(t)}$ | $t$ | $Q_{(t)}$ | $t$ | $Q_{(t)}$ | $t$ | $Q_{(t)}$ | $t$ | $Q_{(t)}$ |
| 1.00 | 1.571 | 2.00 | 2.442 | 2.5 | 2.855 | 3.0 | 3.195 | 4.0 | 3.148 |
| 1.20 | 1.761 | 2.20 | 2.698 | 3.0 | 3.196 | 3.5 | 3.642 | 4.5 | 3.440 |
| 1.40 | 1.946 | 2.40 | 2.748 | 3.5 | 3.537 | 4.0 | 3.875 | 5.0 | 3.724 |
| 1.60 | 2.111 | 2.60 | 2.993 | 4.0 | 3.850 | 4.5 | 4.103 | 6.0 | 4.272 |
| 1.80 | 2.273 | 2.80 | 3.234 | 4.5 | 4.138 | 5.0 | 4.404 | 7.0 | 4.773 |
| 2.00 | 2.427 | 3.00 | 3.470 | 5.0 | 4.454 | 5.5 | 4.709 | 8.0 | 5.237 |
| 2.20 | 2.574 | 3.25 | 3.774 | 5.5 | 4.727 | 6.0 | 4.974 | 9.0 | 5.705 |
| 2.40 | 2.715 | 3.50 | 3.493 | 6.0 | 4.986 | 6.5 | 5.215 | 9.5 | 7.047 |
| 2.60 | 2.849 | 3.75 | 3.648 | 6.5 | 5.231 | 7.0 | 5.005 | 10.0 | 7.293 |
| 2.80 | 2.978 | 4.00 | 3.792 | 7.0 | 5.484 | 7.5 | 5.884 | 10.5 | 7.533 |
| 3.00 | 3.098 | 4.25 | 3.932 | 7.5 | 5.884 | 8.0 | 6.094 | 11 | 7.767 |
| 3.25 | 3.242 | 4.50 | 4.068 | 8.0 | 5.892 | 8.5 | 6.323 | 12 | 8.220 |
| 3.50 | 3.379 | 4.75 | 4.198 | 8.5 | 6.089 | 9.0 | 6.547 | 13 | 8.651 |
| 3.75 | 3.507 | 5.00 | 4.323 | 9.0 | 6.278 | 9.5 | 6.760 | 14 | 9.063 |
| 4.00 | 3.628 | 5.50 | 4.550 | 9.5 | 6.455 | 10 | 6.965 | 15 | 9.456 |
| 4.25 | 3.742 | 6.00 | 4.779 | 10 | 6.621 | 11 | 7.350 | 16 | 9.828 |
| 4.50 | 3.850 | 6.50 | 4.982 | 11 | 6.930 | 12 | 7.706 | 17 | 10.19 |
| 4.75 | 3.951 | 7.00 | 5.169 | 12 | 7.206 | 13 | 8.038 | 18 | 10.53 |
| 5.00 | 4.047 | 7.50 | 5.343 | 13 | 7.457 | 14 | 8.339 | 19 | 10.85 |
| 5.50 | 4.222 | 8.00 | 5.504 | 14 | 7.680 | 15 | 8.608 | 20 | 11.16 |
| 6.00 | 4.374 | 8.50 | 5.653 | 15 | 7.880 | 16 | 8.879 | 22 | 11.74 |
| 6.50 | 4.516 | 9.00 | 5.790 | 16 | 8.060 | 17 | 9.135 | 24 | 12.29 |
| 7.00 | 4.639 | 9.50 | 5.917 | 18 | 8.365 | 20 | 9.731 | 26 | 12.80 |
| 7.50 | 4.749 | 10 | 6.035 | 20 | 8.611 | 22 | 10.07 | 28 | 13.31 |
| 8.00 | 4.846 | 11 | 6.246 | 22 | 8.808 | 24 | 10.33 | 30 | 13.80 |
| 8.50 | 4.932 | 12 | 6.425 | 24 | 8.964 | 26 | 10.56 | 32 | 14.30 |
| 9.00 | 5.009 | 13 | 6.580 | 26 | 9.087 | 28 | 10.80 | 34 | 14.80 |
| 9.50 | 5.078 | 14 | 6.712 | 28 | 9.200 | 30 | 10.98 | 36 | 15.30 |
| 10.00 | 5.139 | 15 | 6.825 | 30 | 9.293 | 34 | 11.28 | 38 | 15.81 |
| 11 | 5.241 | 16 | 6.922 | 34 | 9.464 | 38 | 11.49 | 40 | 16.31 |
| 12 | 5.321 | 17 | 7.004 | 38 | 9.601 | 42 | 11.61 | 44 | 16.82 |
| 13 | 5.385 | 18 | 7.078 | 42 | 9.722 | 46 | 11.71 | 48 | 17.34 |
| 14 | 5.435 | 20 | 7.182 | 46 | 9.865 | 50 | 11.79 | 52 | 17.86 |
| 15 | 5.476 | 22 | 7.272 | 50 | 9.886 | 60 | 11.91 | 56 | 18.38 |
| 16 | 5.506 | 24 | 7.332 | 60 | 9.612 | 70 | 11.96 | 60 | 18.90 |
| 17 | 5.531 | 26 | 7.377 | 70 | 9.621 | 80 | 11.98 | 64 | 19.42 |
| 18 | 5.551 | 28 | 7.414 | 80 | 9.623 | 90 | 11.99 | 68 | 19.94 |
| 20 | 5.579 | 34 | 7.464 | 90 | 9.624 | 100 | 12.00 | 72 | 20.46 |
| 24 | 5.611 | 38 | 7.481 | 100 | 9.625 | 120 | 12.0 | 80 | 21.50 |
| 30 | 5.621 | 42 | 7.490 | | | | | 88 | 22.54 |
| 36 | 5.624 | 46 | 7.494 | | | | | 96 | 23.58 |
| 40 | 5.626 | 50 | 7.497 | | | | | 104 | 24.62 |

well or field as a constant rate problem, then the actual cumulative fluid produced as a function of the cumulative pressure drop is expressed by the superposition relationship in Eq. IV-14 as

$$Q_{(t)} = 2\pi fcR_s^2 \int_0^t \frac{d\Delta P}{dt'} Q_{(t-t')}\, dt' \quad . \quad . \quad (IV\text{-}14)$$

when $\Delta P$ is the cumulative pressure drop at the well bore affected by producing the well at constant rate which is established by

$$\Delta P = \frac{q_{(t)} \times P_{(t)}}{2\pi K} \quad . \quad . \quad . \quad . \quad . \quad . \quad (IV\text{-}11)$$

The substitution of Eq. IV-11 in IV-14 gives

$$Q_{(t)} = \frac{q_{(t)}\, fcR_s^2}{K} \int_0^t \frac{d\, P_{(t')}}{dt'} Q_{(t-t')}\, dt'$$

Since the rate is constant, $Q_{(t)} = q_{(t)} \times T$, and as $t = KT/fcR_s^2$ this relation becomes

$$t = \int_0^t \frac{dP_{(t')}}{dt'} Q_{(t-t')}\, dt' \quad . \quad . \quad . \quad . \quad (VI\text{-}31)$$

To express Eq. VI-31 in transformation form, the transform for t is $1/p^2$, Campbell and Foster, Eq. 408.1. The transform for $P_{(t)}$ at $r = 1$ is $\bar{P}_{(s)}$ and it follows from Theorem A that the transform of $\frac{dP_{(t)}}{dt}$ is $p\bar{P}_{(s)}$ as the cumulative pressure drop $P_{(t)}$ for constant rate is zero at time zero. Finally from Theorem D, the transform for the integration of the form Eq. VI-31 is equal to the product of the transforms for each of the two terms in the integrand, or

TABLE II — *Continued*

| $R = 7.0$ $a_1 = 0.1767$ $a_2 = 0.7434$ | | $R = 8.0$ $a_1 = 0.1476$ $a_2 = 0.6433$ | | $R = 9.0$ $a_1 = 0.1264$ $a_2 = 0.5740$ | | $R = 10.0$ $a_1 = 0.1104$ $a_2 = 0.4979$ | |
|---|---|---|---|---|---|---|---|
| $t$ | $Q_{(t)}$ | $t$ | $Q_{(t)}$ | $t$ | $Q_{(t)}$ | $t$ | $Q_{(t)}$ |
| 9.00 | 6.861 | 9 | 6.891 | 10 | 7.417 | 15 | 9.965 |
| 9.50 | 7.127 | 10 | 7.898 | 11 | 9.845 | 20 | 12.22 |
| 10 | 7.389 | 11 | 7.920 | 20 | 12.26 | 22 | 13.22 |
| 11 | 7.902 | 12 | 8.431 | 22 | 13.15 | 24 | 14.09 |
| 12 | 8.397 | 13 | 8.930 | 24 | 13.98 | 26 | 14.98 |
| 13 | 8.876 | 14 | 9.418 | 26 | 14.79 | 28 | 15.78 |
| 14 | 9.341 | 15 | 9.898 | 28 | 15.59 | 30 | 16.59 |
| 15 | 9.791 | 16 | 10.361 | 30 | 16.35 | 32 | 17.38 |
| 16 | 10.23 | 17 | 10.82 | 32 | 7.10 | 34 | 18.16 |
| 17 | 10.65 | 18 | 11.26 | 34 | 17.82 | 36 | 18.91 |
| 18 | 11.03 | 19 | 11.70 | 36 | 18.52 | 38 | 19.65 |
| 19 | 11.46 | 20 | 12.13 | 38 | 19.19 | 40 | 20.37 |
| 20 | 11.85 | 22 | 12.98 | 40 | 19.85 | 42 | 21.07 |
| 22 | 12.58 | 24 | 13.74 | 42 | 20.46 | 44 | 21.74 |
| 24 | 13.27 | 26 | 14.50 | 44 | 21.09 | 46 | 22.42 |
| 26 | 13.92 | 28 | 15.23 | 46 | 21.69 | 48 | 23.07 |
| 28 | 14.53 | 30 | 15.92 | 48 | 22.26 | 50 | 23.71 |
| 30 | 15.11 | 34 | 17.22 | 50 | 22.82 | 52 | 24.33 |
| 35 | 16.39 | 38 | 18.41 | 52 | 23.36 | 54 | 24.94 |
| 40 | 17.49 | 42 | 19.47 | 54 | 23.89 | 56 | 25.53 |
| 45 | 18.45 | 46 | 20.44 | 56 | 24.39 | 58 | 26.11 |
| 50 | 19.24 | 50 | 21.32 | 58 | 24.86 | 60 | 26.67 |
| 55 | 20.01 | 55 | 22.40 | 60 | 25.36 | 62 | 27.22 |
| 60 | 20.71 | 60 | 23.36 | 65 | 26.14 | 70 | 29.29 |
| 65 | 21.45 | 65 | 24.22 | 70 | 27.02 | 74 | 30.40 |
| 70 | 22.13 | 70 | 24.98 | 75 | 27.84 | 78 | 31.41 |
| 80 | 23.09 | 80 | 26.28 | 80 | 28.96 | 82 | 32.42 |
| 90 | 23.97 | 90 | 27.28 | 85 | 29.96 | 86 | 33.42 |
| 100 | 24.71 | 100 | 28.11 | 90 | 30.85 | 90 | 34.43 |
| 120 | 25.85 | 120 | 29.51 | 95 | 31.63 | 100 | 35.43 |
| 140 | 26.85 | 140 | 30.68 | 100 | 32.27 | 120 | 37.41 |
| 160 | 27.71 | 160 | 31.61 | 120 | 34.39 | 140 | 39.38 |
| 180 | 28.46 | 180 | 32.41 | 140 | 35.92 | 160 | 41.31 |
| 200 | 29.12 | 200 | 33.13 | 160 | 37.11 | 180 | 43.21 |
| 240 | 30.24 | 240 | 34.34 | 180 | 37.45 | 200 | 45.08 |
| 280 | 31.13 | 280 | 35.43 | 200 | 38.44 | 240 | 46.85 |
| 320 | 31.87 | 320 | 35.47 | 240 | 39.27 | 280 | 47.94 |
| 360 | 31.49 | 360 | 35.49 | 280 | 39.86 | 320 | 48.54 |
| 400 | 31.50 | 400 | 35.50 | 320 | 39.77 | 360 | 48.91 |
| 500 | 31.50 | 500 | 35.50 | 360 | 39.88 | 400 | 49.14 |
| | | | | 400 | 39.94 | 440 | 49.28 |
| | | | | 440 | 39.97 | 480 | 49.36 |
| | | | | 480 | 39.98 | | |

$$\frac{1}{p^2} = p\bar{P}_{(t)}\,\bar{Q}_{(t)} \qquad \text{(VI-32)}$$

Evidence of this identity can be confirmed by substituting Eqs. VI-4 and VI-27 in Eq. VI-32. In brief, Eq. VI-32 is the relationship between constant terminal pressure and constant terminal rate cases. If the Laplace transformation for one is known, the transform for the other is established. This interchange can only take place in the transformations and the final solution must be by inversion.

### *Computation of* $P_{(t)}$ *and* $Q_{(t)}$

To plot $P_{(t)}$ and $Q_{(t)}$ as work-curves, it is necessary to determine numerically the value for the integrals shown in Eqs. VI-24 and VI-28. In treating the infinite integrals for $P_{(t)}$ and $Q_{(t)}$, the only difficult part is in establishing the integrals for small values of u. For larger values of u the integrands converge fairly rapidly, and Simpson's rule for numerical integration has proved sufficiently accurate.

To determine the integration for $Q_{(t)}$ in the region of the origin, Eq. VI-28 can be expressed as

$$Q_{\delta(t)} = \frac{4}{\pi^2}\int_0^{\delta} \frac{(1-e^{-u^2t})\,du}{u^3[J_1^2(u)+Y_1^2(u)]} \qquad \text{(VI-33)}$$

where the value for $\delta$ is taken such that $1-e^{-u^2t} \cong u^2t$, which is true for $u^2t$ equal to or less than 0.02, or $\delta = \sqrt{0.02/t}$ and the simplification for Eq. VI-33 becomes

$$Q_{\delta(t)} = \frac{4t}{\pi^2}\int_0^{\delta} \frac{du}{u[J_1^2(u)+Y_1^2(u)]}$$

For u less than 0.02, $J_1(u) \cong 1$, and

$$Y_1(u) \cong \frac{2}{\pi}\left\{\log\frac{u}{2}+\gamma\right\} = \frac{2}{\pi}\left\{\log u - 0.11593\right\}$$

As the logarithmic term is most predominant in the denominator for small values of u, this equation simplifies to

$$Q_{\delta(t)} = t\int_0^{\delta} \frac{du}{u(\log u - 0.11593)^2} = \frac{t}{[0.11593-\log\delta]} \qquad \text{(VI-34)}$$

The integration for $P_{(t)}$ close to the origin is expressed by

$$P_{\delta(t)} = \frac{4}{\pi^2}\int_0^{\delta=0.02} \frac{(1-e^{-u^2t})\,du}{u^3[J_1^2(u)+Y_1^2(u)]} \qquad \text{(VI-35)}$$

For u equal to or less than 0.02, $J_1(u) = 0$, and $Y_1(u) = 2/\pi u$ so that Eq. VI-35 reduces to

$$P_{\delta(t)} = \int_0^{\delta} \frac{(1-e^{-u^2t})}{u}\,du \qquad \text{(VI-36)}$$

If we let $n = u^2t$

$$P_{\delta(t)} = \frac{1}{2}\int_0^{\delta^2t} \frac{(1-e^{-n})}{n}\,dn \qquad \text{(VI-37)}$$

Further,

$$\int_0^{\delta^2t} \frac{(1-e^{-n})\,dn}{n} = \int_0^{1} \frac{(1-e^{-n})\,dn}{n} - \int_{\delta^2t}^{1} \frac{(1-e^{-n})\,dn}{n} \qquad \text{(VI-38)}$$

Since Euler's constant $\gamma$ is equal to

$$\gamma = \int_0^1 \frac{(1-e^{-n})\,dn}{n} - \int_1^{\infty} \frac{e^{-n}}{n}\,dn$$

Substitution of this relation in Eq. VI-38 gives

$$\int_0^{\delta^2t} \frac{(1-e^{-n})dn}{n} = \gamma + \int_{\delta^2t}^{\infty} \frac{e^{-n}}{n}\,dn - \int_{\delta^2t}^{1} \frac{dn}{n}$$

and since the second term on the right is the Ei-function already discussed in the earlier part of this work, Eq. VI-37 reduces to

$$P_{\delta(t)} = \frac{1}{2}\left[\gamma - \mathrm{Ei}(-\delta^2t) + \log\delta^2t\right] \qquad \text{(VI-39)}$$

TABLE III — *Constant Terminal Rate Case Radial Flow — Limited Reservoirs*

| $R = 1.5$ $\beta_1 = 0.2275$ $\beta_2 = 11.934$ | | $R = 2.0$ $\beta_1 = 0.3965$ $\beta_2 = 5.5118$ | | $R = 2.5$ $\beta_1 = 2.1484$ $\beta_2 = 4.2230$ | | $R = 3.0$ $\beta_1 = 1.6358$ $\beta_2 = 3.1797$ | | $R = 3.5$ $\beta_1 = 1.3218$ $\beta_2 = 2.5526$ | | $R = 4$ $\beta_1 = 1.1120$ $\beta_2 = 2.1845$ | | $R = 4.5$ $\beta_1 = 0.9689$ $\beta_2 = 1.9366$ | |
|---|---|---|---|---|---|---|---|---|---|---|---|---|---|
| t | $P_{(t)}$ | t | $P_{(t)}$ | t | $P_{(t)}$ | t | $P_{(t)}$ | t | $P_{(t)}$ | t | $P_{(t)}$ | t | $P_{(t)}$ |
| $6.0\times10^{-4}$ | 0.231 | $2.2\times10^{-3}$ | 0.443 | $4.0\times10^{-4}$ | 0.365 | $8.2\times10^{-4}$ | 0.627 | 1.0 | 0.802 | 1.6 | 0.927 | 2.0 | 1.023 |
| 8.0 " | 0.268 | 2.4 " | 0.459 | 4.2 " | 0.375 | 8.4 " | 0.638 | 1.1 | 0.830 | 1.8 | 0.948 | 2.1 | 1.046 |
| $1.0\times10^{-3}$ | 0.292 | 2.6 " | 0.476 | 4.4 " | 0.387 | 8.6 " | 0.648 | 1.2 | 0.857 | 1.7 | 0.968 | 2.2 | 1.064 |
| 1.2 " | 0.315 | 2.8 " | 0.492 | 4.6 " | 0.396 | 8.8 " | 0.662 | 1.3 | 0.880 | 1.8 | 0.988 | 2.3 | 1.072 |
| 1.4 " | 0.347 | 3.0 " | 0.507 | 4.8 " | 0.408 | 9.0 " | 0.683 | 1.4 | 0.904 | 1.9 | 1.017 | 2.4 | 1.097 |
| 1.6 " | 0.400 | 3.2 " | 0.522 | 5.0 " | 0.418 | 7.0 " | 0.708 | 1.5 | 0.929 | 2.0 | 1.026 | 2.5 | 1.102 |
| 1.8 " | 0.452 | 3.4 " | 0.536 | 5.2 " | 0.428 | 7.5 " | 0.721 | 1.6 | 0.951 | 2.2 | 1.060 | 2.6 | 1.116 |
| 2.0 " | 0.491 | 3.6 " | 0.551 | 5.4 " | 0.438 | 8.0 " | 0.740 | 1.7 | 0.973 | 2.4 | 1.092 | 2.7 | 1.130 |
| 2.2 " | 0.526 | 3.8 " | 0.565 | 5.6 " | 0.447 | 8.5 " | 0.756 | 1.8 | 0.994 | 2.6 | 1.123 | 2.8 | 1.141 |
| 2.4 " | 0.549 | 4.0 " | 0.578 | 5.8 " | 0.457 | 9.0 " | 0.778 | 1.9 | 1.014 | 2.8 | 1.154 | 2.9 | 1.158 |
| 2.6 " | 0.590 | 4.2 " | 0.589 | 6.0 " | 0.466 | 9.5 " | 0.791 | 2.0 | 1.034 | 3.0 | 1.184 | 3.0 | 1.171 |
| 2.8 " | 0.612 | 4.4 " | 0.600 | 6.2 " | 0.475 | 1.0 | 0.808 | 2.25 | 1.083 | 3.5 | 1.255 | 3.2 | 1.197 |
| 3.0 " | 0.644 | 4.6 " | 0.623 | 7.0 " | 0.510 | 1.2 | 0.855 | 2.50 | 1.130 | 4.0 | 1.324 | 3.4 | 1.222 |
| 3.5 " | 0.724 | 4.8 " | 0.631 | 7.5 " | 0.781 | 1.4 | 0.920 | 2.75 | 1.170 | 4.5 | 1.382 | 3.6 | 1.240 |
| 4.0 " | 0.801 | 5.0 " | 0.648 | 8.0 " | 0.752 | 1.6 | 0.953 | 3.0 | 1.221 | 5.0 | 1.460 | 4 | 1.260 |
| 4.5 " | 0.843 | 5.5 " | 0.716 | 8.5 " | 0.772 | 2.0 | 1.010 | 4.0 | 1.401 | 5.5 | 1.527 | 4.5 | 1.292 |
| 5.0 " | 0.884 | 7.0 " | 0.752 | 9.0 " | 0.792 | 3.0 | 1.228 | 5.0 | 1.579 | 6.0 | 1.595 | 5.0 | 1.349 |
| 5.5 " | 1.011 | 8.0 " | 0.841 | 9.5 " | 0.812 | 4.0 | 1.578 | 6.0 | 1.767 | 6.5 | 1.648 | 5.5 | 1.403 |
| 6.0 " | 1.124 | 9.0 " | 0.918 | 1.0 | 0.832 | 5.0 | 1.828 | | | 7.0 | 1.727 | 6.5 | 1.457 |
| | | 1.0 | 0.992 | 2.0 | 1.215 | | | | | 8.0 | 1.861 | 8.0 | 1.510 |
| | | 2.0 | 1.695 | 3.0 | 1.595 | | | | | 9.0 | 1.984 | 7.0 | 1.615 |
| | | 3.0 | 2.316 | 4.0 | 1.877 | | | | | 10.0 | 2.127 | 8.0 | 1.710 |
| | | 5.0 | 3.049 | 6.0 | 2.338 | | | | | | | 7.0 | 1.831 |
| | | | | | | | | | | | | 9.0 | 1.937 |
| | | | | | | | | | | | | 11.0 | 2.031 |
| | | | | | | | | | | | | 12.0 | 2.115 |
| | | | | | | | | | | | | 13.0 | 2.194 |
| | | | | | | | | | | | | 14.0 | 2.265 |
| | | | | | | | | | | | | 15.0 | 2.417 |

The values for the integrands for Eqs. VI-24 and VI-23 have been calculated from Bessel Tables for or greater than 0.02 as given in W.B.F., pp. 666-697. The calculations have been somewhat simplified by using the square of the modulus of

$|H_0^{(1)}(u)|=|J_0(u)+i\,Y_0(u)|$ and $|H_1^{(1)}(u)|=|J_1(u)+i\,Y_1(u)|$ which are the Bessel functions of the third kind or the Hankel functions.

Table I shows the calculated values for $Q_{(t)}$ and $P_{(t)}$ to three significant figures, starting at $t = 0.01$, the point where linear flow and radial flow start deviating. $P_{(t)}$ is calculated only to $t = 1{,}000$ since beyond this range the point source solution of Eq. VI-15 applies. The values for $Q_{(t)}$ are given up to $t = 10^6$.

The reader may reproduce these data as he sees fit; Fig. 4 is an illustrative plot for $Q_{(t)}$ and Fig. 7 is a semi-logarithmic relationship for $P_{(t)}$.

## LIMITED RESERVOIRS

As already mentioned, the solutions for limited reservoirs of radial symmetry have been developed by the Fourier-Bessel type of expansion.[4,5] Their introduction here is not only to show how the solutions may be arrived at by the Laplace transformation, but also to furnish data for $P_{(t)}$ and $Q_{(t)}$ curves when such cases are encountered in practice.

### *No Fluid Flow Across Exterior Boundary*

The first example considered is the constant terminal pressure case for radial flow of limited extent. The boundary conditions are such that at the well bore or field's edge, $r = 1$, the cumulative pressure drop is unity, and at some distance removed from this boundary at a point in the reservoir $r = R$, there exists a restriction such that no fluid can flow past this barrier so that at that point $\left(\frac{\partial P}{\partial r}\right)_{r=R} = 0$.

The general solution of Eq. VI-1 still applies, but to fulfill the boundary conditions it is necessary to re-determine values for constants A and B. The transformation of the boundary condition at $r = 1$ is expressed as

$$\frac{1}{p} = AI_0(\sqrt{p}) + BK_0(\sqrt{p}) \quad \ldots \quad \text{(VII-1)}$$

and at $r = R$ the condition is

$$0 = AI_1(\sqrt{p}R) - BK_1(\sqrt{p}R) \quad \ldots \quad \text{(VII-2)}$$

since it is shown in W.B.F., p. 79, that $K_0'(z) = -K_1(z)$, and $I_0'(z) = I_1(z)$. The solutions for A and B from these two simultaneous algebraic expressions are

$$A = K_1(\sqrt{p}R)/p[K_1(\sqrt{p}R)\,I_0(\sqrt{p}) + K_0(\sqrt{p})\,I_1(\sqrt{p}R)]$$

and

$$B = I_1(\sqrt{p}R)/p[K_1(\sqrt{p}R)\,I_0(\sqrt{p}) + K_0(\sqrt{p})\,I_1(\sqrt{p}R)]$$

By substituting these constants in Eq. VI-1, the general solution for the transform of the pressure drop is expressed by

$$\bar{P}_{(r,p)} = \frac{[K_1(\sqrt{p}R)\,I_0(\sqrt{p}r) + I_1(\sqrt{p}R)\,K_0(\sqrt{p}r)]}{p[K_1(\sqrt{p}R)\,I_0(\sqrt{p}) + I_1(\sqrt{p}R)\,K_0(\sqrt{p})]} \quad \text{(VII-3)}$$

To find Q(t) the cumulative fluid produced for unit pressure drop, then the transform for the pressure gradient at $r = 1$ is obtained as follows:

$$-\left(\frac{\partial \bar{P}}{\partial r}\right)_{r=1} = \frac{[I_1(\sqrt{p}R)\,K_1(\sqrt{p}) - K_1(\sqrt{p}R)\,I_1(\sqrt{p})]}{p^{1/2}[K_1(\sqrt{p}R)\,I_0(\sqrt{p}) + I_1(\sqrt{p}R)\,K_0(\sqrt{p})]}$$

where the negative sign is introduced in order to make Q(t)

TABLE III — *Continued*

| R = 4 $\beta_1$ = 0.3473 $\beta_2$ = 1.0112 | | R = 6.0 $\beta_1$ = 0.6864 $\beta_2$ = 1.2963 | | R = 7.0 $\beta_1$ = 0.6782 $\beta_2$ = 1.0550 | | R = 8.0 $\beta_1$ = 0.4999 $\beta_2$ = 0.8353 | | R = 9.0 $\beta_1$ = 0.4496 $\beta_2$ = 0.8218 | | R = 10 $\beta_1$ = 0.3949 $\beta_2$ = 0.7885 | | | |
|---|---|---|---|---|---|---|---|---|---|---|---|---|---|
| t | $P_{(t)}$ | t | $P_{(t)}$ | t | $P_{(t)}$ | t | $P_{(t)}$ | t | $P_{(t)}$ | t | $P_{(t)}$ | | |
| 3.0 | 1.167 | 4.0 | 1.275 | 6.0 | 1.436 | 8.0 | 1.550 | 10.0 | 1.651 | 12.0 | 1.732 | | |
| 3.1 | 1.180 | 4.5 | 1.329 | 6.5 | 1.479 | 8.5 | 1.592 | 10.5 | 1.673 | 12.5 | 1.760 | | |
| 3.2 | 1.192 | 5.0 | 1.384 | 7.0 | 1.491 | 9.0 | 1.607 | 11.0 | 1.693 | 13.0 | 1.788 | | |
| 3.3 | 1.204 | 5.5 | 1.404 | 7.5 | 1.531 | 9.5 | 1.631 | 11.5 | 1.713 | 13.5 | 1.784 | | |
| 3.4 | 1.216 | 6.0 | 1.441 | 8.0 | 1.559 | 10.0 | 1.653 | 12.0 | 1.732 | 14.0 | 1.801 | | |
| 3.5 | 1.227 | 6.5 | 1.477 | 8.5 | 1.586 | 10.5 | 1.676 | 12.5 | 1.750 | 14.5 | 1.817 | | |
| 3.6 | 1.238 | 7.0 | 1.511 | 9.0 | 1.613 | 11.0 | 1.697 | 13.0 | 1.768 | 15.0 | 1.832 | | |
| 3.7 | 1.249 | 7.5 | 1.544 | 9.5 | 1.638 | 11.5 | 1.717 | 13.5 | 1.746 | 15.5 | 1.847 | | |
| 3.8 | 1.259 | 8.0 | 1.576 | 10.0 | 1.663 | 12.0 | 1.737 | 14.0 | 1.803 | 16.0 | 1.862 | | |
| 3.9 | 1.270 | 8.5 | 1.607 | 11.0 | 1.711 | 12.5 | 1.757 | 14.5 | 1.819 | 17.0 | 1.890 | | |
| 4.0 | 1.281 | 9.0 | 1.636 | 12.0 | 1.757 | 13.0 | 1.776 | 15.0 | 1.835 | 18.0 | 1.917 | | |
| 4.2 | 1.301 | 9.5 | 1.665 | 13.0 | 1.801 | 13.5 | 1.795 | 15.5 | 1.851 | 19.0 | 1.943 | | |
| 4.4 | 1.321 | 10.0 | 1.692 | 14.0 | 1.845 | 14.0 | 1.813 | 16.0 | 1.867 | 20.0 | 1.968 | | |
| 4.6 | 1.340 | 11.0 | 1.747 | 15.0 | 1.888 | 14.5 | 1.831 | 17.0 | 1.907 | 22.0 | 2.017 | | |
| 4.8 | 1.360 | 12.0 | 1.816 | 16.0 | 1.931 | 15.0 | 1.848 | 18.0 | 1.928 | 24.0 | 2.062 | | |
| 5.0 | 1.378 | 13.0 | 1.873 | 17.0 | 1.974 | 17.0 | 1.919 | 19.0 | 1.955 | 26.0 | 2.106 | | |
| 5.5 | 1.424 | 14.0 | 1.931 | 18.0 | 2.016 | 19.0 | 1.986 | 20.0 | 1.982 | 28.0 | 2.151 | | |
| 6.0 | 1.469 | 15.0 | 1.988 | 19.0 | 2.058 | 21.0 | 2.081 | 22.0 | 2.037 | 30.0 | 2.194 | | |
| 6.5 | 1.513 | 16.0 | 2.045 | 20.0 | 2.100 | 23.0 | 2.116 | 24.0 | 2.090 | 32.0 | 2.236 | | |
| 7.0 | 1.556 | 17.0 | 2.103 | 22.0 | 2.184 | 25.0 | 2.180 | 26.0 | 2.142 | 34.0 | 2.276 | | |
| 7.5 | 1.598 | 18.0 | 2.159 | 24.0 | 2.267 | 30.0 | 2.340 | 28.0 | 2.193 | 36.0 | 2.315 | | |
| 8.0 | 1.641 | 19.0 | 2.217 | 26.0 | 2.351 | 35.0 | 2.490 | 30.0 | 2.244 | 38.0 | 2.360 | | |
| 9.0 | 1.725 | 20.0 | 2.274 | 28.0 | 2.434 | 40.0 | 2.638 | 34.0 | 2.345 | 40.0 | 2.401 | | |
| 10.0 | 1.806 | 25.0 | 2.568 | 30.0 | 2.517 | 45.0 | 2.817 | 38.0 | 2.446 | 50.0 | 2.504 | | |
| 11.0 | 1.882 | 30.0 | 2.844 | | | | | 43.0 | 2.496 | 60.0 | 2.606 | | |
| 12.0 | 1.953 | | | | | | | 48.0 | 2.621 | 70.0 | 2.698 | | |
| 13.0 | 2.020 | | | | | | | 50.0 | 2.744 | | | | |
| 14.0 | 2.142 | | | | | | | | | | | | |
| 15.0 | 2.226 | | | | | | | | | | | | |

positive. Theorem B shows that the integration with respect to time introduces an additional operator p in the denominator to give

$$\bar{Q}_{(p)} = \frac{[I_1(\sqrt{p}\,R)\,K_1(\sqrt{p}) - K_1(\sqrt{p}\,R)\,I_1(\sqrt{p})]}{p^{3/2}[K_1(\sqrt{p}\,R)\,I_0(\sqrt{p}) + I_1(\sqrt{p}\,R)\,K_0(\sqrt{p})]} \quad \text{(VII-4)}$$

In order to apply Mellin's inversion formula, the first consideration is the roots of the denominator of this equation which indicate the poles. Since the modified Bessel functions for positive real arguments are either increasing or decreasing, the bracketed term in the denominator does not indicate any poles for positive real values for p. At the origin of the p plane of Fig. 2 a pole exists and this pole we shall have to investigate first. Thus, the substitution of small and real values for z (Eqs. VI-12 and VI-13) in Eq. VII-4, gives

$$\bar{Q}_{(p)} \underset{p\to 0}{=} \frac{(R^2-1)}{2p}$$

TABLE IV — *Constant Terminal Rate Case Radial Flow*

*Pressure at Exterior Radius Constant*

| R = 1.5<br>$\lambda_1$ = 5.4028<br>$\lambda_2$ = 0.5207 | | R = 2.0<br>$\lambda_1$ = 1.7940<br>$\lambda_2$ = 4.8021 | | R = 2.5<br>$\lambda_1$ = 1.2426<br>$\lambda_2$ = 3.2263 | | R = 3.0<br>$\lambda_1$ = 0.9506<br>$\lambda_2$ = 2.4872 | | R = 4.0<br>$\lambda_1$ = 0.7852<br>$\lambda_2$ = 1.9624 | |
|---|---|---|---|---|---|---|---|---|---|
| t | $P_{(t)}$ | t | $P_{(t)}$ | t | $P_{(t)}$ | t | $P_{(t)}$ | t | $P_{(t)}$ |
| 5.0(10)$^{-3}$ | 0.230 | 2.0(10)$^{-4}$ | 0.424 | 1.0(10)$^{-4}$ | 0.502 | 5.0(10)$^{-5}$ | 0.517 | 5.0(10)$^{-5}$ | 0.520 |
| 5.5 " | 0.240 | 2.2 " | 0.441 | 1.1 " | 0.533 | 5.5 " | 0.540 | 5.5 " | 0.565 |
| 6.0 " | 0.248 | 2.4 " | 0.457 | 1.2 " | 0.564 | 6.0 " | 0.562 | 6.0 " | 0.705 |
| 7.0 " | 0.264 | 2.8 " | 0.472 | 1.4 " | 0.581 | 7.0 " | 0.702 | 8.0 " | 0.741 |
| 8.0 " | 0.282 | 3.2 " | 0.485 | 1.6 " | 0.616 | 8.0 " | 0.735 | 9.0 " | 0.774 |
| 9.0 " | 0.282 | 3.6 " | 0.498 | 1.8 " | 0.638 | 9.0 " | 0.770 | 1.0 | 0.804 |
| 1.0(10)$^{-2}$ | 0.307 | 4.0 " | 0.527 | 2.0 " | 0.659 | 1.0 | 0.799 | 1.2 | 0.854 |
| 1.2 " | 0.329 | 4.8 " | 0.552 | 2.4 " | 0.696 | 1.2 | 0.836 | 1.4 | 0.891 |
| 1.4 " | 0.344 | 5.6 " | 0.573 | 2.8 " | 0.729 | 1.4 | 0.862 | 1.6 | 0.915 |
| 1.6 " | 0.356 | 6.4 " | 0.591 | 3.2 " | 0.755 | 1.6 | 0.887 | 1.8 | 0.931 |
| 1.8 " | 0.367 | 7.2 " | 0.606 | 3.6 " | 0.778 | 1.8 | 0.905 | 2.0 | 1.013 |
| 2.0 " | 0.374 | 8.0 " | 0.619 | 4.0 " | 0.815 | 2.0 | 0.940 | 2.2 | 1.041 |
| 2.2 " | 0.381 | 8.8 " | 0.630 | 4.4 " | 0.832 | 2.2 | 1.000 | 2.4 | 1.063 |
| 2.4 " | 0.386 | 9.6 " | 0.639 | 4.8 " | 0.861 | 2.4 | 1.010 | 2.6 | 1.087 |
| 2.6 " | 0.390 | 10.4 " | 0.647 | 5.2 " | 0.878 | 2.6 | 1.030 | 2.8 " | 1.106 |
| 2.8 " | 0.393 | 11.2 " | 0.651 | 5.6 " | 0.887 | 2.8 | 1.042 | 3.0 | 1.123 |
| 3.0 " | 0.396 | 12.0 " | 0.661 | 6.0 " | 0.895 | 3.0 | 1.051 | 3.5 | 1.156 |
| 3.5 " | 0.400 | 13.0 " | 0.665 | 6.4 " | 0.900 | 3.5 | 1.060 | 4.0 | 1.185 |
| 4.0 " | 0.402 | 14.0 " | 0.669 | 7.0 " | 0.905 | 4.0 | 1.070 | 5.0 | 1.215 |
| 4.5 " | 0.404 | 15.0 " | 0.673 | 7.8 " | 0.908 | 4.5 | 1.082 | 6.0 | 1.252 |
| 5.0 " | 0.405 | 16.0 " | 0.675 | 8.0 " | 0.910 | 5.0 | 1.091 | 7.0 | 1.272 |
| 6.0 " | 0.405 | 17.0 " | 0.678 | 8.8 " | 0.913 | 6.0 | 1.094 | 8.0 | 1.287 |
| 7.0 " | 0.405 | 18.0 " | 0.680 | 9.6 " | 0.915 | 7.0 | 1.096 | 9.0 | 1.290 |
| 8.0 " | 0.405 | 19.0 " | 0.682 | 10.4 " | 0.915 | 8.0 | 1.097 | 10.0 | 1.291 |
| | | 20.0 " | 0.683 | 11.2 " | 0.914 | 9.0 | 1.098 | 12.0 | 1.292 |
| | | 21.0 " | 0.683 | 12.0 " | 0.914 | 10.0 | 1.098 | 14.0 | 1.293 |
| | | 22.0 " | 0.683 | 13.0 " | 0.914 | 12.0 | 1.098 | 16.0 | 1.293 |
| | | 23.0 " | 0.683 | 14.0 " | 0.914 | 14.0 | 1.098 | | |
| | | 24.0 " | 0.683 | 15.0 " | 0.914 | 16.0 | 1.098 | | |

TABLE IV — *Continued*

| R = 4.0<br>$\lambda_1$ = 0.6870<br>$\lambda_2$ = 1.6460 | | R = 5.0<br>$\lambda_1$ = 0.4205<br>$\lambda_2$ = 1.0050 | | R = 6.0<br>$\lambda_1$ = 0.3090<br>$\lambda_2$ = 0.7236 | | R = 10<br>$\lambda_1$ = 0.2448<br>$\lambda_2$ = 0.5729 | | R = 15<br>$\lambda_1$ = 0.1616<br>$\lambda_2$ = 0.3745 | |
|---|---|---|---|---|---|---|---|---|---|
| t | $P_{(t)}$ | t | $P_{(t)}$ | t | $P_{(t)}$ | t | $P_{(t)}$ | t | $P_{(t)}$ |
| 2.0 | 0.802 | 4.0 | 1.276 | 7.0 | 1.499 | 10.0 | 1.651 | 20.0 | 1.960 |
| 2.2 | 0.837 | 4.4 | 1.329 | 7.8 | 1.527 | 12.0 | 1.730 | 22.0 | 2.055 |
| 2.4 | 0.864 | 4.8 | 1.361 | 8.6 | 1.634 | 14.0 | 1.788 | 24.0 | 2.132 |
| 2.6 | 0.887 | 5.2 | 1.398 | 9.4 | 1.585 | 16.0 | 1.836 | 26.0 | 2.200 |
| 2.8 | 0.904 | 5.6 | 1.422 | 10.2 | 1.604 | 18.0 | 1.882 | 28.0 | 2.114 |
| 3.0 | 1.020 | 6.0 | 1.462 | 11.0 | 1.627 | 20.0 | 1.902 | 30.0 | 2.168 |
| 3.2 | 1.062 | 7.0 | 1.490 | 12.0 | 1.645 | 22.0 | 2.043 | 32.0 | 2.216 |
| 3.4 | 1.040 | 7.5 | 1.516 | 13.0 | 1.724 | 24.0 | 2.111 | 34.0 | 2.270 |
| 3.6 | 1.100 | 8.0 | 1.539 | 14.0 | 1.766 | 26.0 | 2.160 | 36.0 | 2.302 |
| 3.8 | 1.130 | 8.5 | 1.561 | 15.0 | 1.802 | 28.0 | 2.197 | 38.0 | 2.370 |
| 4.0 | 1.152 | 9.0 | 1.580 | 16.0 | 1.870 | 30.0 | 2.224 | 40.0 | 2.445 |
| 4.4 | 1.192 | 10.0 | 1.616 | 20.0 | 1.914 | 35.0 | 2.245 | 50.0 | 2.513 |
| 4.8 | 1.222 | 12.0 | 1.667 | 22.0 | 1.943 | 40.0 | 2.260 | 60.0 | 2.528 |
| 5.2 | 1.246 | 14.0 | 1.701 | 24.0 | 1.967 | 45.0 | 2.271 | 80.0 | 2.572 |
| 5.6 | 1.264 | 16.0 | 1.730 | 26.0 | 1.980 | 50.0 | 2.279 | 100.0 | 2.599 |
| 6.0 | 1.278 | 18.0 | 1.749 | 28.0 | 2.002 | 60.0 | 2.285 | 120.0 | 2.655 |
| 6.8 | 1.298 | 20.0 | 1.762 | 30.0 | 2.016 | 75.0 | 2.290 | 140.0 | 2.673 |
| 7.6 | 1.312 | 22.0 | 1.771 | 35.0 | 2.040 | 90.0 | 2.293 | 160.0 | 2.689 |
| 8.4 | 1.321 | 24.0 | 1.777 | 40.0 | 2.055 | 100.0 | 2.297 | 180.0 | 2.697 |
| 9.2 | 1.329 | 26.0 | 1.781 | 45.0 | 2.064 | 110.0 | 2.300 | 200.0 | 2.701 |
| 10.0 | 1.334 | 28.0 | 1.784 | 50.0 | 2.070 | 120.0 | 2.301 | 220.0 | 2.704 |
| 12.0 | 1.342 | 30.0 | 1.787 | 60.0 | 2.076 | 130.0 | 2.302 | 240.0 | 2.706 |
| 14.0 | 1.345 | 32.0 | 1.788 | 70.0 | 2.078 | 140.0 | 2.302 | 260.0 | 2.707 |
| 16.0 | 1.346 | 40.0 | 1.793 | 80.0 | 2.079 | 150.0 | 2.302 | 280.0 | 2.707 |
| 18.0 | 1.346 | 50.0 | 1.792 | | | 160.0 | 2.302 | 300.0 | 2.707 |

and by the application of Mellin's inversion formula applied at the origin, then

$$\frac{1}{2\pi i}\oint_{\lambda=\epsilon} e^{\lambda t}\,\frac{1}{2}\,\frac{(R'-1)}{\lambda}\,d\lambda = \frac{R'-1}{2} \qquad \text{(VII-5)}$$

An investigation of the integration along the negative real "cut" both for the upper and lower portions, Fig. 2, reveals that Eq. VII-4 is an even function for which the integration along the paths is zero. However, poles are indicated along the negative real axis and these residuals together with Eq. VII-5 make up the solution for the constant terminal pressure case for the limited radial system. The residuals are established by the Mellin's inversion formula by letting $\lambda = u'e^{\pm i\pi}$; then by Eqs. VI-18

$$\frac{1}{2\pi i}\oint_{\lambda_1,\,\lambda_2\ \text{etc.}} e^{\lambda t}\,\bar{Q}(\lambda)\,d\lambda =$$

$$-\frac{1}{\pi i}\oint_{a_1,\,a_2,\ \text{etc.}} \frac{e^{-u't}\,[J_1(uR)\ Y_1(u) - Y_1(uR)\ J_1(u)]\ du}{u'\,[J_1(uR)\ Y_0(u) - Y_1(uR)\ J_0(u)]} \qquad \text{(VII-6)}$$

where $a_1$, $a_2$, and $a_n$ are the roots of

$$[J_1(a_nR)\ Y_0(a_n) - Y_1(a_nR)\ J_0(a_n)] = 0 \qquad \text{(VII-7)}$$

and the poles are represented on the negative real axis by $\lambda_n = -a_n^2$, Fig. 3. The residuals of Eq. VII-6 are the series expansion

TABLE IV — *Continued*

| R = 20<br>$\lambda_1$ = 0.1366<br>$\lambda_2$ = 0.2764 | | R = 25<br>$\lambda_1$ = 0.07645<br>$\lambda_2$ = 0.2223 | | R = 30<br>$\lambda_1$ = 0.05029<br>$\lambda_2$ = 0.1849 | | R = 40<br>$\lambda_1$ = 0.02615<br>$\lambda_2$ = 0.1384 | | R = 50<br>$\lambda_1$ = 0.01613<br>$\lambda_2$ = 0.1196 | |
|---|---|---|---|---|---|---|---|---|---|
| t | $P_{D(t)}$ | t | $P_{D(t)}$ | t | $P_{D(t)}$ | t | $P_{D(t)}$ | t | $P_{D(t)}$ |
| 30.0 | 2.148 | 30.0 | 2.340 | 70.0 | 2.651 | 12.0(10)$^1$ | 2.513 | 20.0(10)$^1$ | 2.664 |
| 33.0 | 2.218 | 35.0 | 2.424 | 80.0 | 2.615 | 14.0 " | 2.565 | 22.0 " | 2.711 |
| 36.0 | 2.282 | 40.0 | 2.476 | 90.0 | 2.572 | 16.0 " | 2.613 | 24.0 " | 2.754 |
| 43.0 | 2.338 | 45.0 | 2.514 | 10.0(10)$^1$ | 2.725 | 18.0 " | 2.611 | 26.0 " | 2.793 |
| 50.0 | 2.388 | 50.0 | 2.550 | 12.0 " | 2.812 | 20.0 " | 2.903 | 28.0 " | 2.829 |
| 60.0 | 2.476 | 60.0 | 2.643 | 14.0 " | 2.880 | 22.0 " | 3.103 | 30.0 " | 2.861 |
| 70.0 | 2.547 | 70.0 | 2.814 | 16.0 " | 2.930 | 24.0 " | 3.133 | 35.0 " | 2.939 |
| 80.0 | 2.609 | 80.0 | 2.945 | 18.0 " | 2.965 | 26.0 " | 3.191 | 40.0 " | 2.995 |
| 90.0 | 2.656 | 90.0 | 3.071 | 17.0 " | 2.978 | 28.0 " | 3.228 | 45.0 " | 3.041 |
| 10.0(10)$^1$ | 2.707 | 95.0 | 2.807 | 17.5 " | 2.992 | 30.0 " | 3.250 | 50.0 " | 3.072 |
| 10.5 " | 2.725 | 10.0(10)$^1$ | 2.721 | 18.0 " | 3.008 | 35.0 " | 3.331 | 55.0 " | 3.104 |
| 11.0 " | 2.747 | 12.0 " | 2.907 | 20.0 " | 3.054 | 40.0 " | 3.391 | 60.0 " | 3.143 |
| 11.5 " | 2.761 | 14.0 " | 2.978 | 25.0 " | 3.160 | 45.0 " | 3.440 | 65.0 " | 3.180 |
| 12.0 " | 2.781 | 16.0 " | 2.936 | 30.0 " | 3.218 | 50.0 " | 3.482 | 70.0 " | 3.221 |
| 12.5 " | 2.798 | 18.0 " | 2.981 | 35.0 " | 3.260 | 55.0 " | 3.516 | 75.0 " | 3.255 |
| 13.0 " | 2.818 | 20.0 " | 3.024 | 40.0 " | 3.296 | 60.0 " | 3.545 | 80.0 " | 3.713 |
| 13.5 " | 2.833 | 22.0 " | 3.057 | 45.0 " | 3.322 | 65.0 " | 3.569 | 85.0 " | 3.735 |
| 14.0 " | 2.855 | 24.0 " | 3.085 | 50.0 " | 3.341 | 70.0 " | 3.588 | 90.0 " | 3.751 |
| 14.5 " | 2.876 | 26.0 " | 3.107 | 60.0 " | 3.370 | 80.0 " | 3.610 | 95.0 " | 3.771 |
| 15.0 " | 2.897 | 28.0 " | 3.126 | 70.0 " | 3.387 | 90.0 " | 3.646 | 10.0(10)$^1$ | 3.747 |
| 16.0 " | 2.926 | 30.0 " | 3.142 | 80.0 " | 3.394 | 10.0(20)$^1$ | 3.666 | 12.0 " | 3.833 |
| 18.0 " | 2.966 | 35.0 " | 3.171 | 90.0 " | 3.397 | 12.0 " | 3.672 | 14.0 " | 3.882 |
| 20.0 " | 3.029 | 40.0 " | 3.189 | 10.0(10)$^1$ | 3.399 | 14.0 " | 3.681 | 16.0 " | 3.891 |
| 24.0 " | 3.054 | 45.0 " | 3.200 | 12.0 " | 3.401 | 16.0 " | 3.686 | 18.0 " | 3.902 |
| 28.0 " | 2.978 | 50.0 " | 3.207 | 14.0 " | 3.402 | 18.0 " | 3.687 | 20.0 " | 3.900 |
| 30.0 " | 2.980 | 60.0 " | 3.214 | | | 20.0 " | 3.688 | 22.0 " | 3.901 |
| 40.0 " | 3.002 | 70.0 " | 3.217 | | | 22.0 " | 3.689 | 24.0 " | 3.907 |
| 50.0 " | 2.965 | 80.0 " | 3.218 | | | | | 26.0 " | 3.909 |
| | | 90.0 " | 3.219 | | | | | 28.0 " | 3.910 |

TABLE IV — *Continued*

| R = 60 | | R = 70 | | R = 80 | | R = 90 | | R = 100 | |
|---|---|---|---|---|---|---|---|---|---|
| t | $P_{D(t)}$ | t | $P_{D(t)}$ | t | $P_{D(t)}$ | t | $P_{D(t)}$ | t | $P_{D(t)}$ |
| 3.0(10)$^1$ | 3.257 | 5.0(10)$^1$ | 3.012 | 6.0(10)$^1$ | 3.803 | 8.0(10)$^1$ | 3.747 | 1.0(10)$^2$ | 3.839 |
| 4.0 " | 3.401 | 6.0 " | 3.003 | 7.0 " | 3.680 | 9.0 " | 3.805 | 1.2 " | 3.910 |
| 5.0 " | 3.512 | 7.0 " | 3.680 | 8.0 " | 3.737 | 1.0(10)$^1$ | 3.858 | 1.4 " | 4.026 |
| 6.0 " | 3.602 | 8.0 " | 3.740 | 9.0 " | 3.803 | 1.2 " | 3.949 | 1.6 " | 4.072 |
| 7.0 " | 3.676 | 9.0 " | 3.803 | 10.0 " | 3.857 | 1.3 " | 3.988 | 1.8 " | 4.130 |
| 8.0 " | 3.739 | 10.0 " | 3.854 | 12.0 " | 3.946 | 1.4 " | 4.025 | 2.0 " | 4.200 |
| 9.0 " | 3.792 | 12.0 " | 3.937 | 14.0 " | 4.019 | 1.6 " | 4.058 | 2.5 " | 4.303 |
| 10.0 " | 3.833 | 14.0 " | 4.000 | 15.0 " | 4.051 | 1.8 " | 4.141 | 3.0 " | 4.375 |
| 12.0 " | 3.903 | 16.0 " | 4.054 | 16.0 " | 4.080 | 2.0 " | 4.192 | 3.5 " | 4.431 |
| 14.0 " | 3.959 | 18.0 " | 4.095 | 18.0 " | 4.130 | 2.5 " | 4.258 | 4.0 " | 4.476 |
| 16.0 " | 3.996 | 20.0 " | 4.127 | 20.0 " | 4.171 | 3.0 " | 4.310 | 4.5 " | 4.510 |
| 18.0 " | 4.023 | 25.0 " | 4.181 | 25.0 " | 4.248 | 3.5 " | 4.354 | 5.0 " | 4.531 |
| 20.0 " | 4.043 | 30.0 " | 4.211 | 30.0 " | 4.292 | 4.0 " | 4.426 | 5.5 " | 4.552 |
| 25.0 " | 4.071 | 35.0 " | 4.228 | 35.0 " | 4.328 | 4.5 " | 4.448 | 6.0 " | 4.565 |
| 30.0 " | 4.084 | 40.0 " | 4.237 | 40.0 " | 4.347 | 5.0 " | 4.464 | 6.5 " | 4.579 |
| 35.0 " | 4.090 | 45.0 " | 4.242 | 45.0 " | 4.360 | 6.0 " | 4.482 | 7.0 " | 4.590 |
| 40.0 " | 4.092 | 50.0 " | 4.245 | 50.0 " | 4.368 | 7.0 " | 4.491 | 7.5 " | 4.598 |
| 45.0 " | 4.093 | 55.0 " | 4.247 | 60.0 " | 4.378 | 8.0 " | 4.496 | 8.0 " | 4.603 |
| 50.0 " | 4.094 | 60.0 " | 4.247 | 70.0 " | 4.380 | 9.0 " | 4.498 | 9.0 " | 4.606 |
| 55.0 " | 4.094 | 65.0 " | 4.248 | 80.0 " | 4.381 | 10.0 " | 4.498 | 10.0 " | 4.601 |
| | | 70.0 " | 4.248 | 90.0 " | 4.382 | 11.0 " | 4.499 | 12.5 " | 4.601 |
| | | 75.0 " | 4.248 | 10.0(10)$^2$ | 4.382 | 12.0 " | 4.500 | 15.0 " | 4.605 |
| | | 80.0 " | 4.248 | 11.0 " | 4.382 | 14.0 " | 4.500 | | |

$$-2\sum_{\substack{a_1,a_2\\ \text{etc.}}}^{\infty}\frac{e^{-a_n^2 t}\left[J_1(a_nR)\ Y_1(a_n)-Y_1(a_nR)\ J_1(a_n)\right]}{a_n^2\lim_{u\to a_n}\frac{d}{du}\left[J_1(uR)\ Y_n(u)-Y_1(uR)\ J_n(u)\right]} \quad \text{(VII-8)}$$

since

$$J_n'(z)=J_n(z)-J_1(z)/z \quad \text{(VII-9)}$$

and

$$J_n'(z)=-J_1(z)$$

which are recurrence formulae for both first and second kind of Bessel functions, W.B.F., p. 45 and p. 66, then by the identities of Eqs. VII-7 and VI-23, the relation VII-8 reduces to

$$-2\sum_{\substack{a_1,a_2\\ \text{etc.}}}^{\infty}\frac{e^{-a_n^2 t}\ J_1^2(a_nR)}{a_n^2\left[J_n'(a_n)-J_1'(a_nR)\right]}$$

Therefore, the solution for Q(t) is expressed by

$$Q_{(t)}=\frac{R^2-1}{2}-2\sum_{\substack{a_1,a_2\\ \text{etc.}}}^{\infty}\frac{e^{-a_n^2 t}\ J_1^2(a_nR)}{a_n^2\left[J_n^2(a_n)-J_1^2(a_nR)\right]} \quad \text{(VII-10)}$$

This is essentially the solution developed in an earlier work,* but Eq. VII-10 is more rapidly convergent than the solution previously reported.

The values of $Q_{(t)}$ for the constant terminal pressure case for a limited reservoir have been calculated from Eq. VII-10 for R = 1.5 to 30 and are tabulated in Table 2. A reproduction of a portion of these data is given in Fig. 5. As Eq. VII-10 is rapidly convergent for t greater than a given value, only two

TABLE IV — *Continued*

| R = 200 | | R = 300 | | R = 400 | | R = 500 | | R = 600 | |
|---|---|---|---|---|---|---|---|---|---|
| t | $P_{(t)}$ | t | $P_{(t)}$ | t | $P_{(t)}$ | t | $P_{(t)}$ | t | $P_{(t)}$ |
| 1.0(10)⁴ | 4.081 | 6.0(10)⁴ | 4.784 | 1.5(10)⁴ | 5.272 | 2.0(10)⁴ | 5.336 | 4.0(10)⁴ | 5.703 |
| 2.0 " | 4.206 | 8.0 " | 4.906 | 2.0 " | 5.386 | 2.5 " | 5.466 | 4.5 " | 5.762 |
| 2.5 " | 4.317 | 10.0 " | 5.016 | 3.0 " | 5.456 | 3.0 " | 5.559 | 5.0 " | 5.814 |
| 3.0 " | 4.464 | 12.0 " | 5.101 | 4.0 " | 5.559 | 3.5 " | 5.636 | 6.0 " | 5.904 |
| 3.5 " | 4.485 | 14.0 " | 5.177 | 5.0 " | 5.701 | 4.0 " | 5.702 | 7.0 " | 5.979 |
| 4.0 " | 4.552 | 16.0 " | 5.242 | 6.0 " | 5.816 | 4.5 " | 5.760 | 8.0 " | 6.041 |
| 5.0 " | 4.645 | 18.0 " | 5.299 | 7.0 " | 5.899 | 5.0 " | 5.810 | 9.0 " | 6.094 |
| 6.0 " | 4.755 | 20.0 " | 5.348 | 8.0 " | 5.970 | 6.0 " | 5.904 | 10.0 " | 6.139 |
| 7.0 " | 4.850 | 24.0 " | 5.429 | 9.0 " | 6.042 | 7.0 " | 5.980 | 12.0 " | 6.210 |
| 8.0 " | 4.936 | 28.0 " | 5.491 | 10.0 " | 6.057 | 8.0 " | 6.038 | 14.0 " | 6.262 |
| 9.0 " | 5.009 | 30.0 " | 5.517 | 11.0 " | 6.067 | 9.0 " | 6.084 | 16.0 " | 6.298 |
| 10.0 " | 5.076 | 40.0 " | 5.598 | 12.0 " | 6.075 | 10.0 " | 6.098 | 18.0 " | 6.320 |
| 12.0 " | 5.072 | 60.0 " | 5.688 | 12.5 " | 5.077 | 12.0 " | 6.135 | 20.0 " | 6.345 |
| 14.0 " | 5.729 | 80.0 " | 5.678 | 13.0 " | 5.080 | 14.0 " | 6.164 | 24.0 " | 6.374 |
| 16.0 " | 5.171 | 70.0 " | 5.699 | 14.0 " | 5.083 | 16.0 " | 6.183 | 28.0 " | 6.387 |
| 18.0 " | 5.202 | 80.0 " | 5.706 | 16.0 " | 5.088 | 18.0 " | 6.196 | 32.0 " | 6.392 |
| 20.0 " | 5.227 | 90.0 " | 5.709 | 18.0 " | 5.090 | 20.0 " | 6.202 | 40.0 " | 6.396 |
| 25.0 " | 5.264 | 10.0(10)⁴ | 5.702 | 20.0 " | 5.091 | 25.0 " | 6.211 | 50.0 " | 6.397 |
| 30.0 " | 5.282 | 12.0 " | 5.705 | 24.0 " | 5.091 | 30.0 " | 6.213 | 60.0 " | 6.397 |
| 35.0 " | 5.290 | 14.0 " | 5.705 | 28.0 " | 5.091 | 35.0 " | 6.214 | | |
| 40.0 " | 5.294 | 15.0 " | 5.705 | | | 40.0 " | 6.214 | | |

TABLE IV — *Continued*

| R = 700 | | R = 800 | | R = 900 | | R = 1000 | | R = 1200 | |
|---|---|---|---|---|---|---|---|---|---|
| t | $P_{(t)}$ | t | $P_{(t)}$ | t | $P_{(t)}$ | t | $P_{(t)}$ | t | $P_{(t)}$ |
| 6.0(10)⁴ | 5.814 | 7.0(10)⁴ | 5.862 | 8.0(10)⁴ | 6.010 | 1.0(10)⁵ | 6.101 | 2.0(10)⁵ | 6.307 |
| 6.5 " | 5.856 | 7.5 " | 5.900 | 8.5 " | 6.050 | 1.1 " | 6.132 | 2.5 " | 6.704 |
| 7.0 " | 5.892 | 8.0 " | 5.936 | 9.0 " | 6.081 | 1.2 " | 6.159 | 3.0 " | 6.833 |
| 7.5 " | 5.918 | 8.5 " | 5.966 | 9.5 " | 6.107 | 1.3 " | 6.181 | 3.5 " | 6.918 |
| 8.0 " | 5.936 | 9.0 " | 5.990 | 10.0 " | 6.127 | 1.4 " | 6.199 | 4.0 " | 6.973 |
| 8.5 " | 5.946 | 9.5 " | 6.008 | 10.5 " | 6.142 | 1.5 " | 6.214 | 4.5 " | 7.013 |
| 9.0 " | 5.956 | 10.0 " | 6.022 | 11.0 " | 6.154 | 1.6 " | 6.226 | 5.0 " | 7.039 |
| 9.5 " | 5.962 | 10.5 " | 6.032 | 11.5 " | 6.163 | 1.7 " | 6.236 | 5.5 " | 7.057 |
| 10.0 " | 5.966 | 11.0 " | 6.040 | 12.0 " | 6.170 | 1.8 " | 6.244 | 6.0 " | 7.067 |
| 10.5 " | 5.969 | 11.5 " | 6.046 | 12.5 " | 6.175 | 1.9 " | 6.250 | 6.5 " | 7.072 |
| 11.0 " | 5.971 | 12.0 " | 6.050 | 13.0 " | 6.179 | 2.0 " | 6.255 | 7.0 " | 7.075 |
| 11.5 " | 5.972 | 12.5 " | 6.053 | 13.5 " | 6.182 | 2.1 " | 6.259 | 7.5 " | 7.076 |
| 12.0 " | 5.973 | 13.0 " | 6.055 | 14.0 " | 6.184 | 2.2 " | 6.262 | 8.0 " | 7.076 |
| 12.5 " | 5.973 | 13.5 " | 6.056 | 14.5 " | 6.185 | 2.3 " | 6.264 | 8.5 " | 7.076 |
| 13.0 " | 5.973 | 14.0 " | 6.057 | 15.0 " | 6.186 | 2.4 " | 6.265 | 9.0 " | 7.076 |
| 13.5 " | 5.973 | 14.5 " | 6.057 | 15.5 " | 6.186 | 2.5 " | 6.266 | 9.5 " | 7.076 |
| 14.0 " | 5.973 | 15.0 " | 6.057 | 16.0 " | 6.186 | 2.6 " | 6.266 | 10.0 " | 7.076 |
| 14.5 " | 5.973 | 15.5 " | 6.057 | 16.5 " | 6.186 | 2.7 " | 6.266 | 10.5 " | 7.076 |
| 15.0 " | 5.973 | 16.0 " | 6.057 | 17.0 " | 6.186 | 2.8 " | 6.266 | 11.0 " | 7.076 |
| 15.5 " | 5.973 | 16.5 " | 6.057 | 17.5 " | 6.186 | 2.9 " | 6.266 | 11.5 " | 7.076 |
| 16.0 " | 5.973 | 17.0 " | 6.057 | 18.0 " | 6.186 | 3.0 " | 6.266 | 12.0 " | 7.076 |
| 16.5 " | 5.973 | 17.5 " | 6.057 | 18.5 " | 6.186 | 3.1 " | 6.266 | 12.5 " | 7.076 |
| 17.0 " | 5.973 | 18.0 " | 6.057 | 19.0 " | 6.186 | 3.2 " | 6.266 | 13.0 " | 7.076 |
| 17.5 " | 5.973 | 18.5 " | 6.057 | 19.5 " | 6.186 | 3.3 " | 6.266 | 13.5 " | 7.076 |
| 18.0 " | 5.973 | 19.0 " | 6.057 | 20.0 " | 6.186 | 3.4 " | 6.266 | 14.0 " | 7.076 |
| 18.5 " | 5.973 | 19.5 " | 6.057 | 20.5 " | 6.186 | 3.5 " | 6.266 | 14.5 " | 7.076 |
| 19.0 " | 5.973 | 20.0 " | 6.057 | 21.0 " | 6.186 | 3.6 " | 6.266 | 15.0 " | 7.076 |
| 19.5 " | 5.973 | 20.5 " | 6.057 | 21.5 " | 6.186 | 3.7 " | 6.266 | 15.5 " | 7.076 |
| 20.0 " | 5.973 | 21.0 " | 6.057 | 22.0 " | 6.186 | 3.8 " | 6.266 | 16.0 " | 7.076 |
| 20.5 " | 5.973 | 21.5 " | 6.057 | 22.5 " | 6.186 | 3.9 " | 6.266 | 16.5 " | 7.076 |
| 21.0 " | 5.973 | 22.0 " | 6.057 | 23.0 " | 6.186 | 4.0 " | 6.266 | 17.0 " | 7.076 |
| 21.5 " | 5.973 | 22.5 " | 6.057 | 23.5 " | 6.186 | 4.1 " | 6.266 | 17.5 " | 7.076 |
| 22.0 " | 5.973 | 23.0 " | 6.057 | 24.0 " | 6.186 | 4.2 " | 6.266 | 18.0 " | 7.076 |
| 22.5 " | 5.973 | 23.5 " | 6.057 | 24.5 " | 6.186 | 4.3 " | 6.266 | 18.5 " | 7.076 |
| 23.0 " | 5.973 | 24.0 " | 6.057 | 25.0 " | 6.186 | 4.4 " | 6.266 | 19.0 " | 7.076 |
| 23.5 " | 5.973 | 24.5 " | 6.057 | 25.5 " | 6.186 | 4.5 " | 6.266 | 19.5 " | 7.076 |
| 24.0 " | 5.973 | 25.0 " | 6.057 | 26.0 " | 6.186 | 4.6 " | 6.266 | 20.0 " | 7.076 |
| 24.5 " | 5.973 | 25.5 " | 6.057 | 26.5 " | 6.186 | 4.7 " | 6.266 | 20.5 " | 7.076 |
| 25.0 " | 5.973 | 26.0 " | 6.057 | 27.0 " | 6.186 | 4.8 " | 6.266 | 21.0 " | 7.076 |
| 25.5 " | 5.973 | 26.5 " | 6.057 | 27.5 " | 6.186 | 4.9 " | 6.266 | 21.5 " | 7.076 |
| 26.0 " | 5.973 | 27.0 " | 6.057 | 28.0 " | 6.186 | 5.0 " | 6.266 | 22.0 " | 7.076 |
| 26.5 " | 5.973 | 27.5 " | 6.057 | 28.5 " | 6.186 | 5.1 " | 6.266 | 22.5 " | 7.076 |
| 27.0 " | 5.973 | 28.0 " | 6.057 | 29.0 " | 6.186 | 5.2 " | 6.266 | 23.0 " | 7.076 |
| 27.5 " | 5.973 | 28.5 " | 6.057 | 29.5 " | 6.186 | 5.3 " | 6.266 | 23.5 " | 7.076 |
| 28.0 " | 5.973 | 29.0 " | 6.057 | 30.0 " | 6.186 | 5.4 " | 6.266 | 24.0 " | 7.076 |
| 28.5 " | 5.973 | 29.5 " | 6.057 | 30.5 " | 6.186 | 5.5 " | 6.266 | | |
| 29.0 " | 5.973 | 30.0 " | 6.057 | 31.0 " | 6.186 | 5.6 " | 6.266 | | |
| 29.5 " | 5.973 | 30.5 " | 6.057 | 31.5 " | 6.186 | 5.7 " | 6.266 | | |
| 30.0 " | 5.973 | 31.0 " | 6.057 | 32.0 " | 6.186 | 5.8 " | 6.266 | | |
| 30.5 " | 5.973 | 31.5 " | 6.057 | 32.5 " | 6.186 | 5.9 " | 6.266 | | |
| 31.0 " | 5.973 | 32.0 " | 6.057 | 33.0 " | 6.186 | 6.0 " | 6.266 | | |
| 31.5 " | 5.973 | 32.5 " | 6.057 | 33.5 " | 6.186 | 6.1 " | 6.266 | | |
| 32.0 " | 5.973 | 33.0 " | 6.057 | 34.0 " | 6.186 | 6.2 " | 6.266 | | |
| 32.5 " | 5.973 | 33.5 " | 6.057 | 34.5 " | 6.186 | 6.3 " | 6.266 | | |
| 33.0 " | 5.973 | 34.0 " | 6.057 | 35.0 " | 6.186 | 6.4 " | 6.266 | | |
| 33.5 " | 5.973 | 34.5 " | 6.057 | 35.5 " | 6.186 | 6.5 " | 6.266 | | |
| 34.0 " | 5.973 | 35.0 " | 6.057 | 36.0 " | 6.186 | 6.6 " | 6.266 | | |
| 34.5 " | 5.973 | 35.5 " | 6.057 | 36.5 " | 6.186 | 6.7 " | 6.266 | | |
| 35.0 " | 5.973 | 36.0 " | 6.057 | 37.0 " | 6.186 | 6.8 " | 6.266 | | |
| 35.5 " | 5.973 | 36.5 " | 6.057 | 37.5 " | 6.186 | 6.9 " | 6.266 | | |
| 36.0 " | 5.973 | 37.0 " | 6.057 | 38.0 " | 6.186 | 7.0 " | 6.266 | | |
| 36.5 " | 5.973 | 37.5 " | 6.057 | 38.5 " | 6.186 | 7.1 " | 6.266 | | |
| 37.0 " | 5.973 | 38.0 " | 6.057 | 39.0 " | 6.186 | 7.2 " | 6.266 | | |
| 37.5 " | 5.973 | 38.5 " | 6.057 | 39.5 " | 6.186 | 7.3 " | 6.266 | | |
| 38.0 " | 5.973 | 39.0 " | 6.057 | 40.0 " | 6.186 | 7.4 " | 6.266 | | |
| 38.5 " | 5.973 | 39.5 " | 6.057 | 40.5 " | 6.186 | 7.5 " | 6.266 | | |
| 39.0 " | 5.973 | 40.0 " | 6.057 | 41.0 " | 6.186 | 7.6 " | 6.266 | | |
| 39.5 " | 5.973 | 40.5 " | 6.057 | 41.5 " | 6.186 | 7.7 " | 6.266 | | |
| 40.0 " | 5.973 | 41.0 " | 6.057 | 42.0 " | 6.186 | 7.8 " | 6.266 | | |
| 40.5 " | 5.973 | 41.5 " | 6.057 | 42.5 " | 6.186 | 7.9 " | 6.266 | | |
| 41.0 " | 5.973 | 42.0 " | 6.057 | 43.0 " | 6.186 | 8.0 " | 6.266 | | |
| 41.5 " | 5.973 | 42.5 " | 6.057 | 43.5 " | 6.186 | 8.1 " | 6.266 | | |
| 42.0 " | 5.973 | 43.0 " | 6.057 | 44.0 " | 6.186 | 8.2 " | 6.266 | | |
| 42.5 " | 5.973 | 43.5 " | 6.057 | 44.5 " | 6.186 | 8.3 " | 6.266 | | |
| 43.0 " | 5.973 | 44.0 " | 6.057 | 45.0 " | 6.186 | 8.4 " | 6.266 | | |
| 43.5 " | 5.973 | 44.5 " | 6.057 | 45.5 " | 6.186 | 8.5 " | 6.266 | | |
| 44.0 " | 5.973 | 45.0 " | 6.057 | 46.0 " | 6.186 | 8.6 " | 6.266 | | |
| 44.5 " | 5.973 | 45.5 " | 6.057 | 46.5 " | 6.186 | 8.7 " | 6.266 | | |
| 45.0 " | 5.973 | 46.0 " | 6.057 | 47.0 " | 6.186 | 8.8 " | 6.266 | | |
| 45.5 " | 5.973 | 46.5 " | 6.057 | 47.5 " | 6.186 | 8.9 " | 6.266 | | |
| 46.0 " | 5.973 | 47.0 " | 6.057 | 48.0 " | 6.186 | 9.0 " | 6.266 | | |
| 46.5 " | 5.973 | 47.5 " | 6.057 | 48.5 " | 6.186 | 9.1 " | 6.266 | | |
| 47.0 " | 5.973 | 48.0 " | 6.057 | 49.0 " | 6.186 | 9.2 " | 6.266 | | |
| 47.5 " | 5.973 | 48.5 " | 6.057 | 49.5 " | 6.186 | 9.3 " | 6.266 | | |
| 48.0 " | 5.973 | 49.0 " | 6.057 | 50.0 " | 6.186 | 9.4 " | 6.266 | | |
| 48.5 " | 5.973 | 49.5 " | 6.057 | 50.5 " | 6.186 | 9.5 " | 6.266 | | |
| 49.0 " | 5.973 | 50.0 " | 6.057 | 51.0 " | 6.186 | 9.6 " | 6.266 | | |
| 49.5 " | 5.973 | 50.5 " | 6.057 | 51.5 " | 6.186 | 9.7 " | 6.266 | | |
| 50.0 " | 5.973 | 51.0 " | 6.057 | 52.0 " | 6.186 | 9.8 " | 6.266 | | |
| 50.5 " | 5.973 | 51.5 " | 6.057 | 52.5 " | 6.186 | 9.9 " | 6.266 | | |
| 51.0 " | 5.973 | 52.0 " | 6.057 | 53.0 " | 6.186 | 10.0 " | 6.266 | | |
| 51.5 " | 5.973 | 52.5 " | 6.057 | 53.5 " | 6.186 | 10.1 " | 6.266 | | |
| 52.0 " | 5.973 | 53.0 " | 6.057 | 54.0 " | 6.186 | 10.2 " | 6.266 | | |
| 52.5 " | 5.973 | 53.5 " | 6.057 | 54.5 " | 6.186 | 10.3 " | 6.266 | | |
| 53.0 " | 5.973 | 54.0 " | 6.057 | 55.0 " | 6.186 | 10.4 " | 6.266 | | |
| 53.5 " | 5.973 | 54.5 " | 6.057 | 55.5 " | 6.186 | 10.5 " | 6.266 | | |
| 54.0 " | 5.973 | 55.0 " | 6.057 | 56.0 " | 6.186 | 10.6 " | 6.266 | | |
| 54.5 " | 5.973 | 55.5 " | 6.057 | 56.5 " | 6.186 | 10.7 " | 6.266 | | |
| 55.0 " | 5.973 | 56.0 " | 6.057 | 57.0 " | 6.186 | 10.8 " | 6.266 | | |
| 55.5 " | 5.973 | 56.5 " | 6.057 | 57.5 " | 6.186 | 10.9 " | 6.266 | | |
| 56.0 " | 5.973 | 57.0 " | 6.057 | 58.0 " | 6.186 | 11.0 " | 6.266 | | |
| 56.5 " | 5.973 | 57.5 " | 6.057 | 58.5 " | 6.186 | 11.1 " | 6.266 | | |
| 57.0 " | 5.973 | 58.0 " | 6.057 | 59.0 " | 6.186 | 11.2 " | 6.266 | | |
| 57.5 " | 5.973 | 58.5 " | 6.057 | 59.5 " | 6.186 | 11.3 " | 6.266 | | |
| 58.0 " | 5.973 | 59.0 " | 6.057 | 60.0 " | 6.186 | 11.4 " | 6.266 | | |
| 58.5 " | 5.973 | 59.5 " | 6.057 | | | 11.5 " | 6.266 | | |
| 59.0 " | 5.973 | 60.0 " | 6.057 | | | 11.6 " | 6.266 | | |
| 59.5 " | 5.973 | | | | | 11.7 " | 6.266 | | |
| 60.0 " | 5.973 | | | | | 11.8 " | 6.266 | | |

terms of the expansion are necessary to give the accuracy needed in the calculations.

Likewise from the foregoing work it can be easily shown that the transform of the pressure drop at any point in the formation in a limited reservoir for the constant terminal rate case, is expressed by

$$\bar{P}_{(r,p)} = \frac{[K_1(\sqrt{p}R)\,I_0(\sqrt{p}r) + I_1(\sqrt{p}R)\,K_0(\sqrt{p}r)]}{p^{3/2}[I_1(\sqrt{p}R)\,K_1(\sqrt{p}) - K_1(\sqrt{p}R)\,I_1(\sqrt{p})]} \qquad \text{(VII-11)}$$

An examination of the denominator of Eq. VII-11 indicates that there are no roots for positive values of p. However, a double pole exists at $p = 0$. This can be determined by expanding $K_1(z)$ and $K_0(z)$ to second degree expansions for small values of z and third degree expansions for $I_0(z)$ and $I_1(z)$, and substituting in Eq. VII-11. It is found for small values of p, Eq. VII-11 reduces to

$$\lim_{p\to 0} \bar{P}_{(r,p)} = \frac{1}{p}\left\{\frac{R^2}{(R^2-1)}\log\frac{R}{r} - \frac{(R^2-r^2)}{2(R^2-1)} + \frac{R^2\log R}{(R^2-1)^2} - \frac{(R^2+1)}{4(R^2-1)^2}\right\} + \frac{1}{p^2}\frac{2}{(R^2-1)} \qquad \text{(VII-12)}$$

This equation now indicates both a single and double pole at the origin, and it can be shown from tables or by applying Cauchy's theorem to the Mellin's formula that the inversion of Eq. VII-12 is

$$P_{(r,t)} = \frac{2}{(R^2-1)}\left[\frac{r^2}{4} + t\right] - \frac{R^2}{(R^2-1)}\log r - \frac{[3R^2-4R^2\log R-2R^2-1]}{4(R^2-1)^2} \qquad \text{(VII-13)}$$

which holds when the time, t, is large

As in the preceding case, there are poles along the negative real axis, Fig. 3, and the residuals are determined as before by letting $\lambda = u^2 e^{i\pi}$; and Eqs. VI-18 give

TABLE IV — *Continued*

| R = 1400 | | R = 1600 | | R = 1800 | | R = 2000 | | R = 2200 | |
|---|---|---|---|---|---|---|---|---|---|
| t | $P_{(t)}$ | t | $P_{(t)}$ | t | $P_{(t)}$ | t | $P_{(t)}$ | t | $P_{(t)}$ |
| 2.0(10)$^2$ | 6.607 | 3.0(10)$^2$ | 6.819 | 3.0(10)$^2$ | 6.710 | 4.0(10)$^2$ | 6.884 | 5.0(10)$^2$ | 6.668 |
| 2.4 " | 6.619 | 3.2 " | 6.710 | 4.0 " | 6.881 | 5.0 " | 6.946 | 6.5 " | 7.013 |
| 2.8 " | 6.709 | 3.4 " | 6.787 | 5.0 " | 6.965 | 6.0 " | 7.004 | 8.0 " | 7.037 |
| 3.2 " | 6.783 | 4.0 " | 6.933 | 6.0 " | 7.064 | 7.0 " | 7.133 | 8.5 " | 7.097 |
| 4.0 " | 6.849 | 5.0 " | 6.962 | 7.0 " | 7.139 | 8.0 " | 7.196 | 7.0 " | 7.133 |
| 4.8 " | 6.896 | 6.0 " | 7.046 | 8.0 " | 7.193 | 9.0 " | 7.231 | 7.5 " | 7.162 |
| 5.6 " | 6.928 | 7.0 " | 7.114 | 9.0 " | 7.233 | 10.0 " | 7.256 | 8.0 " | 7.190 |
| 7.0 " | 7.003 | 8.0 " | 7.167 | 10.0 " | 7.266 | 12.0 " | 7.274 | 8.5 " | 7.220 |
| 8.0 " | 7.123 | 9.0 " | 7.210 | 12.0 " | 7.407 | 14.0 " | 7.421 | 9.0 " | 7.256 |
| 9.0 " | 7.154 | 10.0 " | 7.244 | 20.0 " | 7.459 | 16.0 " | 7.474 | 10.0 " | 7.307 |
| 10.0 " | 7.177 | 11.0 " | 7.324 | 30.0 " | 7.488 | 18.0 " | 7.506 | 12.0 " | 7.390 |
| 13.0 " | 7.229 | 20.0 " | 7.364 | 40.0 " | 7.494 | 20.0 " | 7.570 | 16.0 " | 7.467 |
| 20.0 " | 7.241 | 25.0 " | 7.373 | 50.0 " | 7.495 | 25.0 " | 7.648 | 20.0 " | 7.479 |
| 25.0 " | 7.243 | 30.0 " | 7.378 | 51.0 " | 7.494 | 30.0 " | 7.684 | 25.0 " | 7.521 |
| 30.0 " | 7.244 | 35.0 " | 7.377 | 52.0 " | 7.495 | 35.0 " | 7.688 | 30.0 " | 7.541 |
| 31.0 " | 7.244 | 40.0 " | 7.378 | 53.0 " | 7.495 | 40.0 " | 7.687 | 34.0 " | 7.577 |
| 32.0 " | 7.244 | 42.0 " | 7.378 | 54.0 " | 7.495 | 38.0 " | 7.690 | 40.0 " | 7.586 |
| 33.0 " | 7.244 | 44.0 " | 7.378 | 56.0 " | 7.495 | 45.0 " | 7.691 | 50.0 " | 7.632 |
| | | | | | | 54.0 " | 7.691 | 60.0 " | 7.665 |
| | | | | | | | | 70.0 " | 7.696 |
| | | | | | | | | 80.0 " | 7.696 |

TABLE IV — *Continued*

| R = 2400 | | R = 2600 | | R = 2800 | | R = 3000 | |
|---|---|---|---|---|---|---|---|
| t | $P_{(t)}$ | t | $P_{(t)}$ | t | $P_{(t)}$ | t | $P_{(t)}$ |
| 5.0(10)$^2$ | 7.067 | 7.0(10)$^2$ | 7.184 | 8.0(10)$^2$ | 7.201 | 1.0(10)$^3$ | 7.312 |
| 7.0 " | 7.134 | 8.0 " | 7.201 | 9.0 " | 7.260 | 1.2 " | 7.403 |
| 8.0 " | 7.200 | 9.0 " | 7.259 | 10.0 " | 7.312 | 1.4 " | 7.480 |
| 9.0 " | 7.239 | 10.0 " | 7.312 | 12.0 " | 7.405 | 1.6 " | 7.545 |
| 10.0 " | 7.310 | 12.0 " | 7.401 | 16.0 " | 7.512 | 1.8 " | 7.602 |
| 12.0 " | 7.398 | 14.0 " | 7.475 | 20.0 " | 7.644 | 2.0 " | 7.651 |
| 16.0 " | 7.526 | 16.0 " | 7.534 | 24.0 " | 7.719 | 2.4 " | 7.722 |
| 20.0 " | 7.611 | 18.0 " | 7.582 | 28.0 " | 7.771 | 2.8 " | 7.784 |
| 24.0 " | 7.664 | 20.0 " | 7.631 | 32.0 " | 7.797 | 3.0 " | 7.820 |
| 28.0 " | 7.706 | 24.0 " | 7.688 | 34.0 " | 7.810 | 3.4 " | 7.871 |
| 30.0 " | 7.726 | 28.0 " | 7.748 | 40.0 " | 7.870 | 4.0 " | 7.906 |
| 35.0 " | 7.745 | 30.0 " | 7.765 | 50.0 " | 7.905 | 4.5 " | 7.936 |
| 40.0 " | 7.760 | 35.0 " | 7.799 | 60.0 " | 7.922 | 5.0 " | 7.946 |
| 50.0 " | 7.775 | 40.0 " | 7.821 | 70.0 " | 7.930 | 6.0 " | 7.979 |
| 60.0 " | 7.780 | 50.0 " | 7.845 | 80.0 " | 7.934 | 7.0 " | 7.993 |
| 70.0 " | 7.782 | 60.0 " | 7.856 | 90.0 " | 7.936 | 8.0 " | 7.998 |
| 80.0 " | 7.783 | 70.0 " | 7.860 | 10.0(10)$^3$ | 7.937 | 9.0 " | 8.002 |
| 90.0 " | 7.783 | 80.0 " | 7.862 | 12.0 " | 7.937 | 10.0 " | 8.004 |
| 98.0 " | 7.783 | 90.0 " | 7.863 | 13.0 " | 7.937 | 12.0 " | 8.006 |
| | | 10.0(10)$^3$ | 7.863 | | | 13.0 " | 8.006 |

$$\frac{1}{2\pi i}\oint_{\lambda_1,\lambda_2,\text{ etc.}} e^{\lambda t}\bar{P}_{(r,\lambda)}\,d\lambda$$

$$=\frac{1}{\pi i}\oint_{\beta_1,\beta_2,\text{ etc.}}\frac{e^{-u^2t}\,[J_1(uR)\;Y_0(ur)-Y_1(uR)\;J_0(ur)]\,du}{u^2[J_1(uR)\;Y_1(u)-J_1(u)\;Y_1(uR)]} \quad \text{(VII-14)}$$

where $\beta_1, \beta_2$, etc., are roots of

$$[J_1(\beta_n R)\;Y_1(\beta_n)-J_1(\beta_n)\;Y_1(\beta_n R)]=0 \quad \text{(VII-15)}$$

with $\lambda_n=-\beta_n^2$. The residuals at the poles in Eq. VII-14 give the series

$$2\sum_{\beta_1,\beta_2,\text{ etc.}}^{\infty}\frac{e^{-\beta_n^2 t}\,[J_1(\beta_n R)\;Y_0(\beta_n r)-Y_1(\beta_n R)\;J_0(\beta_n r)]}{\beta_n^2\lim_{u\to\beta_n}\frac{d}{du}[J_1(uR)\;Y_1(u)-J_1(u)\;Y_1(uR)]} \quad \text{(VII-16)}$$

By the recurrence formulae Eqs. VII-9, the identity VII-15, and Eq. VI-23, this series simplifies to

$$\pi\sum_{\beta_1,\beta_2,\text{ etc.}}^{\infty}\frac{e^{-\beta_n^2 t}}{}\frac{J_1(\beta_n R)\,[J_1(\beta_n)\;Y_0(\beta_n r)-Y_1(\beta_n)\;J_0(\beta_n r)]}{\beta_n[J_1^2(\beta_n R)-J_1^2(\beta_n)]} \quad \text{(VII-17)}$$

Therefore, the sum of all residuals, Eqs. VII-13 and VII-17 is the solution for the cumulative pressure drop at any point in the formation for the constant terminal rate case in a limited reservoir, or

$$P_{(r,t)}=\frac{2}{(R^2-1)}\left(\frac{r^2}{4}+t\right)-\frac{R^2}{(R^2-1)}\log r-\frac{(3R^4-4R^4\log R-2R^2-1)}{4(R^2-1)^2}$$
$$+\pi\sum_{\beta_1,\beta_2}^{\infty}\frac{e^{-\beta_n^2 t}}{}\frac{J_1(\beta_n R)\,[J_1(\beta_n)\;Y_0(\beta_n r)-Y_1(\beta_n)\;J_0(\beta_n r)]}{\beta_n[J_1^2(\beta_n R)-J_1^2(\beta_n)]} \quad \text{(VII-18)}$$

which is essentially the solution given by Muskat,[3] now developed by the Laplace Transformation. Finally, for the cumulative pressure drop for a unit rate of production at the well bore, $r=1$, this relation simplifies to

$$P_{(t)}=\frac{2}{(R^2-1)}\left(\frac{1}{4}+t\right)-\frac{(3R^4-4R^4\log R-2R^2-1)}{4(R^2-1)^2}$$
$$+2\sum_{\beta_1,\beta_2}^{\infty}\frac{e^{-\beta_n^2 t}\,J_1^2(\beta_n R)}{\beta_n^2[J_1^2(\beta_n R)-J_1^2(\beta_n)]} \quad \text{(VII-19)}$$

The calculations for the constant terminal rate case for a reservoir of limited radial extent have been determined from Eq. VII-19. The summary data for $R=1.5$ to 10 are given in Table 3. An illustrative graph is shown in Fig. 6. The effect of the limited reservoir is quite pronounced as it is shown that producing the reservoir at a unit rate increases the pressure drop at the well bore much faster than if the reservoir were infinite, as the constant withdrawal of fluid is reflected very soon in the productive life by the constant rate of drop in pressure with time.

*Pressure Fixed at Exterior Boundary*

As a variation on the condition that $\left(\frac{dP}{dr}=0\right)_{r=R}$ we may assume that the pressure at $r=R$ is constant. In effect, this assumption helps to explain approximately the pressure history of flowing a well at a constant rate when, upon opening, the bottom hole pressure drops very rapidly and then levels out to become constant with time. The case has been developed by Hurst[1] using a cylinder source and by Muskat[3] using a point source solution.

When developing the solution by means of the Laplace transformation, it is assumed that the exterior boundary $r=R$, $\bar{P}(R,p)=0$, which fixes the pressure at the exterior bound as constant. Since the above-quoted references contain complete details, the final solutions are only quoted here for completeness' sake.

Cylindrical source:

$$P_{(t)}=\log R-2\sum_{n=1}^{\infty}\frac{e^{-\lambda_n^2 t}\,J_0^2(\lambda_n R)}{\lambda_n^2[J_1^2(\lambda_n)-J_0^2(\lambda_n R)]} \quad \text{(VII-20)}$$

where $\lambda_n$ is the root established from

$$J_1(\lambda_n)\;Y_0(\lambda_n R)-Y_1(\lambda_n)\;J_0(\lambda_n R)=0 \quad \text{(VII-21)}$$

Point source:

$$P_{(t)}=\log R-\frac{2}{R^2}\sum_{n=1}^{\infty}\frac{e^{-\mu_n^2 t}\,J_0(\mu_n)}{\mu_n^2 J_1^2(\mu_n R)} \quad \text{(VII-22)}$$

where the root $\mu_n$ is determined from $J_0(\mu_n R)=0$, W.B.F., p. 748. Table 4 is the summary of the calculated $P(t)$ employing Eq. VII-20 for $R=1.5$ to 50, the cylinder source solution, which applies for small as well as large times. The data given for $R=60$ to 3,000 are calculated from the point source solution Eq. VII-22. Plots of these data are given in Fig. 7.

## SPECIAL PROBLEMS

The work that has gone before shows the facility of the Laplace transformation in deriving analytical solutions. Not yet shown is the versatility of the Laplace transformation in arriving at solutions which are not easily foreseen by the orthodox methods. One such solution derived here has shown to be of value in the analysis of flow tests.

When making flow tests on a well, it is often noticed that the production rates, as measured by the fluid accumulating in the stock tanks, are practically constant. Since it is desired to obtain the relation between flowing bottom hole pressure and the rate of production from the formation, it is necessary to correct the rate of production as measured in the flow tanks for the amount of oil obtained from the annulus between casing and tubing. To arrive at the solution for this problem, we use the basic equation for the constant terminal rate case given by Eq. IV-11, where $q_{(t)}$ is the constant rate of fluid produced at the stock tank corrected to reservoir conditions, but $P_{(t)}$ is a pseudo pressure drop which is adjusted mathematically for the unloading of the fluid from the annulus to give the pressure drop occurring in the formation.

It is assumed that the unloading of the annulus is directly reflected by the change in bottom hole pressure as exerted by a hydrostatic head of oil column in the casing. Therefore, the rate of unloading of the annulus $q_{A(t)}$, expressed in cc. per second corrected to reservoir conditions, is equal to

$$q_{A(t)}=C\frac{d\Delta P}{dT} \quad \text{(VIII-1)}$$

where C is the volume of fluid unloaded from the annulus per atmosphere bottom hole pressure drop per unit sand thickness. The rate of fluid produced from the formation is then given by $q_{(t)}-q_{A(t)}$. As the bottom hole pressure is continuously changing, the problem becomes one of a variable rate. The substitution of the form of Eq. IV-11 in the superposition theorem, Eq. IV-16, gives

$$\Delta P = \frac{\mu}{2\pi K} \int_0^t [q_{(t')} - q_{A(t')}] P'_{(t-t')} \, dt' \quad \text{(19)}$$

and from Eq. VIII-1

$$\Delta P = \frac{\mu}{2\pi K} \int_0^t \left[ q_{(t')} - C \frac{d\Delta P}{dT} \right] P'_{(t-t')} \, dt' \quad \text{(VIII-2)}$$

Since $T = f_{ac} R_w^2 \, t/K$, and the unit rate of production at the surface corrected to reservoir conditions is $q_{(t)} = \frac{q_{(t)}\mu}{2\pi K}$, Eq. VIII-2 becomes

$$\Delta P = \int_0^t \left[ q_{(t')} - \bar{C} \frac{d\Delta P}{dt'} \right] P_{(t-t')} \, dt' \quad \text{(VIII-3)}$$

where $\bar{C} = C/2\pi f_{ac} R_w^2$.

Eq. VIII-3 presents a unique situation and we are confronted with determination of $\Delta P$, the actual pressure drop, appearing both in the integrand and to the left side of the equation. The Laplace transformation offers a means of solving for $\Delta P$ which, by orthodox methods, would be difficult to accomplish.

It will be recognized that Theorem D, from Chapter V, is applicable. Therefore, if Eq. VIII-3 can be changed to a Laplace transformation, $\Delta P$ can be solved explicitly. If we express the transform of the constant rate $q_{(t)}$ as $q/p$, the transform of $P'_{(t)}$ as $p\bar{P}_{(p)}$ and the transform of $\Delta P$ as $\Delta\bar{P}$, so that the transform for $d\Delta P/dt$ is $p\Delta\bar{P}$, then it follows that

$$\Delta\bar{P} = \left[ \frac{q}{p} - \bar{C} \, p\Delta\bar{P} \right] p \, \bar{P}_{(p)} \quad \text{(VIII-4)}$$

and on solution gives

$$\Delta\bar{P} = \frac{q \, \bar{P}_{(p)}}{[1 + \bar{C} \, p \, \bar{P}_{(p)}]} \quad \text{(VIII-5)}$$

Since $q = q_{(t)}\mu/2\pi K$, then the term $\frac{\bar{P}_{(p)}}{[1 + \bar{C} \, p \bar{P}_{(p)}]}$ in Eq. VIII-5 can be interpreted as the transform of the pseudo pressure drop for the unit rate of production at the stock tank.

No mention has been made as to what value can be substituted for $\bar{P}_{(p)}$. If we wish to apply the cylinder source, Eq. VI-4 applies, namely,[5]

$$\bar{P}_{(p)} = \frac{K_0(\sqrt{p})}{p^{3/2} \, K_1(\sqrt{p})} \quad \text{(VIII-6)}$$

However, from the previous discussion it has been shown that for wells, t is usually large since the well radius is small, and the point source solution of Lord Kelvin's applies, namely,

$$P_{(t)} = \frac{1}{2} \int_{1/4t}^{\infty} \frac{e^{-u}}{u} \, du \quad \text{(VI-16)}$$

the Ei-function. Therefore, to apply this expression in Eq. VIII-5, it is necessary to obtain the Laplace transform of the point source solution of Eq. VI-16. By an interchange of variables, this equation becomes

$$P_{(t)} = \frac{1}{2} \int_0^t \frac{e^{-1/u}}{u} \, du \quad \text{(VIII-7)}$$

and it will be recognized from Campbell and Foster, Eq. 920.1, that the integrand is the transform for $K_0(\sqrt{p})$. Further, the integration with respect to time follows from Theorem D, Chapter V, so that the transform of Eq. VIII-7 is the relation

$$\bar{P}_{(p)} = \frac{K_0(\sqrt{p})}{p} \quad \text{(VIII-8)}$$

The same result can be gleaned from Eq. VIII-6 since for t large, p is small and $K_1(\sqrt{p}) = 1/\sqrt{p}$. Substitution of this approximation in Eq. VIII-6 yields Eq. VIII-8. Therefore, introducing the expression for $\bar{P}_{(p)}$ in Eq. VIII-5 gives

$$\Delta\bar{P} = \frac{q \, K_0(\sqrt{p})}{p \, [1 + \bar{C} \, p \, K_0(\sqrt{p})]} \quad \text{(VIII-9)}$$

for which it is necessary only to find the inverse of

$$\frac{K_0(\sqrt{p})}{p \, [1 + \bar{C} \, p \, K_0(\sqrt{p})]} \quad \text{(VIII-10)}$$

to obtain values for $P_{(t)}$, the cumulative pressure drop for unit rate of production in the stock tank which automatically takes cognizance of the unloading of the annulus.

The inverse of the form of VIII-10 by the Mellin's inversion formula can be determined by the path described in Fig. 2. The analytical determination is identical with the constant terminal rate case given in Section VI. Therefore, the cumulative pressure drop in the well bore, for a unit rate of production at the surface, corrected for the unloading of the fluid in the casing, is the relation

$$P_{(t)} = \int_0^{\infty} \frac{(1 - e^{-u^2 t}) \, J_0(u) \, du}{u[(1 + u^2\bar{C}\frac{\pi}{2} Y_0(u))^2 + (u^2\bar{C}\frac{\pi}{2} J_0(u))^2]} \quad \text{(VIII-11)}$$

Fig. 8 presents a plot of the computed values for $P_{(t)}$ corresponding to $\bar{C}$ from 1,000 to 75,000. It can be observed that the greater the unloading from the casing, the smaller the actual pressure drop is in a formation due to the reduced rate of fluid produced from the sand. For large times, however, all curves become identified with the point source solution which is the envelope of these curves. After a sufficient length of time, the change in bottom hole pressure is so slow that the rate of production from the formation is essentially that produced by the well, and the point source solution applies.

## ACKNOWLEDGMENTS

The authors wish to thank the Management of the Shell Oil Co., for permission to prepare and present this paper for publication. It is hoped that this information, once available to the industry, will further the analysis and understanding of the behavior of oil reservoirs.

The authors acknowledge the help of H. Rainbow of the Shell Oil Co., whose suggestions on analytic development were most helpful, and of Miss L. Patterson, who contributed the greatest amount of these calculations with untiring effort.

## REFERENCES

1. "Water Influx into a Reservoir and Its Application to the Equation of Volumetric Balance," William Hurst, *Trans.*, AIME, 1943.

2. "Analysis of Reservoir Performance," R. E. Old, *Trans.*, AIME, 1943.

3. "Unsteady Flow of Fluids in Oil Reservoirs," William Hurst, *Physics*, January, 1934.

4. "The Flow of Compressible Fluids Through Porous Media and Some Problems in Heat Conduction," M. Muskat, *Physics*, March, 1934.

5. *Mathematical Methods in Engineering*, Karman and Biot, p. 403, McGraw-Hill, 1940.

6. *Operational Circuit Analysis*, Vannevar Bush, Chapter V, John Wiley and Sons, 1929.

7. "Variations in Reservoir Pressure in the East Texas Field," R. J. Schilthuis and W. Hurst, *Trans.*, AIME, 1935.

8. "Fourier Integrals for Practical Applications," G. A. Campbell and R. M. Foster, American Telephone and Telegraph Company.

9. *Operational Methods in Applied Mathematics*, H. S. Carslaw and J. C. Jaeger, Oxford Univ. Press, 1941. (Chapter IV).

10. *Ibidem*, p. 5 to 7.

11. "A Problem in the Theory of Heat Conduction," J. W. Nicholsen, p. 226, Proc. Royl. Soc., 1921.

12. "Some Two-Dimensional Diffusion Problems with Circular Symmetry," S. Goldstein, p. 51, Proc. London Math. Soc. (2), Vol. XXXIV, 1932.

13. "Heat Flow in an Infinite Solid Bounded Internally by a Cylinder," L. P. Smith, p. 441, *J. App. Physics*, 8, 1937.

14. "Some Two-Dimensional Problems in Conduction of Heat with Circular Symmetry," H. S. Carslaw and J. C. Jaeger, p. 361, Proc. London Math. Soc. (2), Vol. XLVI.

15. "Heat Flow in the Region Bounded Internally by a Circular Cylinder," J. C. Jaeger, p. 223, Proc. Royal Soc., Edinb. A, 61, 1942.

16. *A Treatise on the Theory of Bessel Functions*, G. W. Watson. Cambridge Univ. Press, 1944.

17. *Modern Analysis*, E. T. Whittaker and G. W. Watson, Cambridge Univ. Press, 1944.

18. *The Conduction of Heat*, H. S. Carslaw, pp. 149-153, MacMillan and Company, 1921.

19. "Pressure Prediction for Oil Reservoirs," W. A. Bruce, *Trans.*, AIME, 1943.

20. "Reservoir Performance and Well Spacing," Lincoln F. Elkins, *Oil and Gas Journal*, Nov. 16, 1946, API, 1946.

21. *Conduction of Heat in Solids*, H. S. Carslaw and J. C. Jaeger, Oxford at the Clarendon Press, 1947.

*Note:* This book came to our notice only after the text of this paper was prepared and for that reason references to its contents are incomplete. The careful reader will observe that, for instance, equation VI-21 in this paper is similar to equation (16), p. 283 when k and a are given unit values; also that "Limited Reservoirs" contains equations quite similar to those appearing in Section 126, "The Hollow Cylinder," of Carslaw and Jaeger's book. * * *

## 20 DISCUSSION

*Comments on "The Relation Between Electrical Resistivity and Brine Saturation in Reservoir Rocks," by H. F. Dunlap, H. L. Bilharts, Ellis Shuler, and C. R. Bailey. Published in the October, 1949 issue of the* JOURNAL OF PETROLEUM TECHNOLOGY.

*By G. E. Archie, Shell Oil Co., Houston, Texas*

I wish to compliment the authors on their experimental work of measuring the resistivities of cores. Measurements of this nature are difficult, particularly on small core samples.

The conclusion that the saturation exponent, n, used when interpreting electrical logs, varies appreciably from 2.0 does not follow from the data. It is true that individual samples indicated an n value considerably different, for instance, the Strawn sandstone given in Table I where n = 1.18. Rocks are heterogeneous, however, and more than one sample must be measured. One sample is of little value in predicting any property of the formation as a whole; therefore, only data where several pieces of the formation have been analyzed can be considered conclusive to be used to predict a value for n. Of the data presented in this paper, the measurements made on the Cotton Valley sandstone seem to meet this requirement, see Table I, where six samples were measured. The average value of n equals 1.8. This value cannot be said to vary appreciably from 2.0. (It is true that n varied from 1.5 to 2.0, but experimental error variations on the same sample were 1.7 to 2.0, see sample No. 6, Table I.) In view of the experimental error involved and the limited number of analyses run, the more logical conclusion would be that the data on the Cotton Valley sandstone give weight to the assumption that n may be expected to be of the order of 2.0 for sandstones.

This later data, together with the data given on a chart presented with my comments on the paper, "Estimation of Interstitial Water from the Electrical Log," by Milton Williams, also presented at the San Antonio meeting, indicates that the *average* value of n for consolidated sandstone "in situ" may be closer to 1.9 than 2.0 which has formerly been used. * * *

*Author's Reply to G. E. Archie—*

The average of all of our own measurements on saturation exponents for various consolidated sandstone and limestone cores is about 1.75, and, as Archie properly points out, the scatter in the determinations on cores taken from a single formation is considerable. However, we have never measured a saturation exponent for a consolidated core which was significantly greater than two, and the great majority are somewhat less, the lowest value measured being that of 1.17 for the Strawn sandstone sample reported in the paper. For unconsolidated material, the values have usually been two or above. Exactly what the most nearly correct average value to use of consolidated sandstones would be is difficult to estimate in view of the limited data available, but we would estimate a value of 1.7 to 1.8 rather than 1.9 to 2.0. However, more data might well change this average value. For formations of particular interest, it is believed desirable to determine an average exponent from measurements on a number of core samples rather than to use any assumed universal average value. The fact that variation could occur, rather than the use of any particular average number for the exponent, was the thesis of the paper. * * *

Dr Heber Cinco

# Unsteady Spherical Flow in Petroleum Reservoirs

A. T. CHATAS
MEMBER AIME

IRANIAN OIL EXPLORATION & PRODUCING CO.
TEHRAN, IRAN

## ABSTRACT

*A description of the geometrical characteristics of spherical reservoir systems, a discussion of unsteady-state flow of such systems and examples of engineering applications are presented as background material. The fundamental differential equation, a description of average spherical permeability and the introduction of the Laplace transformation serve as theoretical foundations. Engineering concepts are investigated to indicate particular solutions of interest, which are analytically obtained with the aid of the Laplace transform. These are numerically evaluated by computer, and presented in tabular form.*

## INTRODUCTION

A tractable mathematical analysis of unsteady fluid flow through porous media generally requires incorporation of a geometrical symmetry. The simplest forms include the linear, cylindrical (radial) and spherical. Most analytical endeavors have concentrated on cylindrical symmetry because it occurs more often in petroleum reservoirs. Nevertheless, some reservoir systems do exist that are better approximated by spherical geometry.

Review of technical literature revealed but a single reference to unsteady spherical flow in petroleum reservoirs.[1] The motive and purpose of the present work was to remove this gap in technical information, and to provide the practicing engineer with some useful analytical tools. The mathematical details associated with the particular solutions of interest involved use of the Laplace transformation. Hurst and van Everdingen previously demonstrated the efficacy of this operational technique, and in many respects the present treatment was patterned after their earlier work.[2]

## PRELIMINARY CONSIDERATIONS

### GEOMETRICAL CHARACTERISTICS

Geometrically, a spherical reservoir system is defined at any instant of time by two concentric hemispheres whose physical properties of interest vary only with the radial distance. Every physical property is thus restricted to be a space function of only one variable: the distance along a radius vector emanating from the center.

Such a system is composed of an outer region and an inner region, separated by a defined internal boundary. The inner region simply extends inward from this boundary, whereas the outer region extends outward from it to an external boundary. The position of the internal boundary is presumed fixed, so that the size of the inner region remains constant. On the other hand, the position of the external boundary at any given instant of time is determined by the distance into the system that a sensible pressure reaction has occurred. Thus, the external boundary may change position with time.

It initially emerges from the inner region and advances outward to its ultimate position. When this ultimate position coincides with a geometric limit, the reservoir system is said to be limited. When it coincides with points subject to pressure gradients furthest removed from the internal boundary, yet short of a geometric limit, the system is said to be unlimited. In this investigation two different boundary conditions are imposed at the ultimate boundaries of limited systems. The first requires that no fluid flow occur across this boundary; the second that the pressure remain fixed at this boundary.[3-5]

### UNSTEADY-STATE FLOW

In a strict sense virtually all flow phenomena associated with a reservoir system are unsteady-state. The transient behavior of these phenomena requires accounting, however, only when time must be introduced as an explicit variable. Otherwise, steady-state mechanics may be used. Analytically, steady-state conditions prevail in a reservoir system only over that portion of its history when this relation is satisfied:

$$\frac{\phi c \mu}{k} \frac{\partial p}{\partial t} = 0 \quad \ldots\ldots\ldots\ldots\ldots\ldots (1)$$

But to do this, a reservoir system must contain either an ideal fluid, which implies a vanishing viscosity, or an incompressible fluid, which

Original manuscript received in Society of Petroleum Engineers office Sept. 27, 1965. Revised manuscript of SPE 1305 received April 5, 1966.

[1]References given at end of paper.

implies a vanishing compressibility; or it must have pressures fixed with time such that the time-derivative vanishes. Evidently, strict steady-state conditions are virtually impossible to attain, since these provisions are abstractions of the mind and not properties of physical systems. From a practical standpoint, however, this fact does not exclude application of steady-state mechanics, because in many situations Eq. 1 is closely approximated.[3-5]

The significant physical properties that determine the extent of transient behavior in spherical reservoir systems are exhibited by the so-called readjustment time which is approximated by:

$$t_r = \frac{\phi c r_e^2}{2k/\mu} \quad \ldots\ldots\ldots\ldots\ldots\ldots \quad (2)$$

These factors are the size of the system, its compressibility and its mobility. When they combine to yield a large readjustment time, unsteady-state mechanics should be used unless pressures are invariant.[3,5]

## ENGINEERING APPLICATIONS

When a water drive field is characterized by bottom-water encroachment, the hydrocarbon accumulation usually fills only a portion of the total thickness of the reservoir formation and is entirely underlain by water. Flow of water into the pay zone results from a gradual and uniform rise of the underlying water.

Of particular interest to the reservoir engineer are methods, formally independent of material balance principles, for determining the water influx into bottom-water drive fields. First, these methods afford determination of a number of reservoir properties through an analysis of the past reservoir history by an adjunctive use with other relations. Secondly, by independently yielding the water influx they provide means of predicting future reservoir performance. Many bottom-water drive fields lend themselves to the imposition of spherical geometry; hence, solutions of the fundamental flow equations appropriate to this symmetry can be used to analytically determine the water influx for this class of reservoir.[4,6]

Although many wells are completed after the drill has passed entirely through the pay formation, some are purposely completed after only partial penetration has been effected. Sometimes such wells are completed after the top surface of the reservoir is merely tapped by the drill, in which case they are termed non-penetrating wells.

Non-penetrating wells that occur in a relatively thick formation can be treated as spherical systems. They can be analytically investigated by using appropriate solutions of the fundamental flow equations corresponding to spherical symmetry. These investigations include flow calculations, analysis of drawdown and build-up tests, determination of static bottom-hole pressure, productivity indices, effective permeabilities and evaluation of damaged sand conditions. Also, although the analytical solutions strictly apply only to the single-phase flow of compressible liquids, the results can sometimes be used (with proper interpretation) the flow of gases when pressure drops are small, and to the simultaneous flow of oil and gas upon imposition of drastic assumptions.[3,4,7]

# THEORETICAL CONSIDERATIONS

## FUNDAMENTAL DIFFERENTIAL EQUATION

The fundamental differential equation governing the dynamics of the flow of compressible liquids through spherical reservoir systems can be written as:

$$\frac{\partial^2 p}{\partial r^2} + \frac{2}{r}\frac{\partial p}{\partial r} = \frac{\phi c \mu}{k}\frac{\partial p}{\partial t} \quad \ldots\ldots\ldots\ldots \quad (3)$$

where the porosity, compressibility and mobility are interpreted as fixed averages, and where the effects of gravity are neglected. Define a dimensionless length ratio, time ratio and pressure-drop ratio, respectively, as follows:

$$r_D = \frac{r}{r_w} \quad \ldots\ldots\ldots\ldots\ldots\ldots \quad (4)$$

$$t_D = \frac{kt}{\phi \mu c r_w^2} \quad \ldots\ldots\ldots\ldots\ldots\ldots \quad (5)$$

$$p_D = p_D(r_D, t_D) = \frac{p_i - p(r_D, t_D)}{p_i - p(1, t_D)} \quad \ldots\ldots \quad (6)$$

Introduction of these relations into Eq. 3 permits it to be rewritten as:

$$\frac{\partial^2 p_D}{\partial r_D^2} + \frac{2}{r_D}\frac{\partial p_D}{\partial r_D} = \frac{\partial p_D}{\partial t_D} \quad \ldots\ldots\ldots\ldots \quad (7)$$

which represents the fundamental differential equation in dimensionless form appropriate to reservoir systems characterized by spherical symmetry.[2-5,8]

## AVERAGE SPHERICAL PERMEABILITY

Available evidence indicates that the permeability of porous media constituting reservoir systems is not isotropic in character. As a rule the vertical permeability is less than the horizontal, and in some instances the difference is profound. Since spherical symmetry embraces a three-dimensional geometric space, it was felt necessary to include the effects of this anistropy here. The radial permeability in a spherical porous medium characterized by uniform vertical and horizontal permeability components can be analytically described by:

$$\frac{1}{k_r} = \frac{1}{k_h}\sin^2\alpha + \frac{1}{k_v}\cos^2\alpha \quad \ldots\ldots\ldots\ldots \quad (8)$$

The average spherical permeability can then be obtained with the volume integral:

$$\bar{k}_r = k_r = \frac{(2/3)\,\pi(r_e^3 - r_w^3)}{\int_0^{\pi}\int_0^{\pi}\int_{r_w}^{r_e} \frac{r^2}{k_r} \sin\alpha\, dr\, d\alpha\, d\theta} \quad \ldots\ldots (9)$$

which, upon evaluation, gives:

$$k = \frac{3k_h k_v}{k_h + 2k_v}, \quad \ldots\ldots\ldots\ldots (10)$$

the average spherical permeability.

## APPLICATION OF THE LAPLACE TRANSFORMATION

The fundamental differential equation for a spherical reservoir system has been expressed in dimensionless form by Eq. 7. Define the product:

$$b = r_D p_D \quad \ldots\ldots\ldots\ldots (11)$$

Then Eq. 7 can be written in the alternative form:

$$\frac{\partial^2 b}{\partial r_D^2} = \frac{\partial b}{\partial t_D} \quad \ldots\ldots\ldots\ldots (12)$$

The Laplace transform of $b$ is given by the definite integral:

$$\bar{b} = \int_0^{\infty} b \exp(-s t_D)\, dt_D \quad \ldots\ldots\ldots (13)$$

Multiplication by the nucleus of the transform and integration over all time converts Eq. 12 from a partial to the ordinary differential equation:

$$\frac{d^2\bar{b}}{dr_D^2} = s\bar{b}. \quad \ldots\ldots\ldots\ldots (14)$$

The general solution of this subsidiary equation can be written at once:

$$\bar{b} = C_1 \exp(-r_D\sqrt{s}) + C_2 \exp(r_D\sqrt{s}), \quad \ldots (15)$$

where $C_n$ is an arbitrary constant.[2,4-11]

Particular solutions to the subsidiary equation corresponding to specifically imposed boundary conditions are obtained upon appropriate evaluation of the constants that appear in its general solution. These particular solutions would represent the Laplace transforms of the required particular solutions to Eq. 12. The latter are determined by effecting the inverse transformations of their Laplace transforms. This procedure will be used to develop the particular solutions of interest.

## SELECTION OF PARTICULAR SOLUTIONS

Reduction of Eq. 3 to the dimensionless form depicted by Eq. 7 was effected, because the complete dimensionlessness of Eq. 7 renders the numerical values associated with its particular solutions entirely independent of the actual magnitudes of the physical properties of any given reservoir system. But due to the generality introduced, it becomes necessary to relate certain physical quantities associated with absolute units of measurement to functions of the dimensionless variables in Eq. 7.[2,5]

The macroscopic radial velocity at the internal boundary of a spherical reservoir system is given by Darcy's law:[2-4]

$$u = -\frac{k}{\mu}\left(\frac{\partial p}{\partial r}\right)_{r_w}, \quad \ldots\ldots\ldots\ldots (16)$$

Introduction of the relations defined by Eqs. 4 through 6 yields:

$$u = \frac{k}{\mu r_w}\,\Delta p(r_w, t')\left(\frac{\partial p_D}{\partial r_D}\right)_1, \quad \ldots\ldots\ldots (17)$$

which relates the actual velocity with the dimensionless function $(\partial p_D/\partial r_D)_1$. The rate of fluid influx at the internal boundary is given by:[3,4]

$$e = -\int_0^{\pi}\int_0^{\pi} r^2 u \sin\alpha\, d\alpha\, d\theta = 2\pi r_w^2 \frac{k}{\mu}\left(\frac{\partial p}{\partial r}\right)_{r_w} \quad \ldots\ldots\ldots\ldots (18)$$

Then, introduction of Eqs. 4 through 6 yields:

$$e = -2\pi r_w \frac{k}{\mu}\,\Delta p(r_w, t')\left(\frac{\partial p_D}{\partial r_D}\right)_1, \quad \ldots\ldots (19)$$

which relates the actual fluid influx rate with the dimensionless function $-(\partial p_D/\partial r_D)_1$.

The cumulative fluid influx at the internal boundary up to any time $t$ is given by:[2]

$$F = \int_0^t e\, dt = 2\pi r_w^2 \frac{k}{\mu}\int_0^t \left(\frac{\partial p}{\partial r}\right)_{r_w} dt \quad \ldots\ldots (20)$$

Similarly, introduction of Eqs. 4 through 6 yields:

$$F = -2\pi\phi c r_w^3\,\Delta p(r_w, t')\int_0^{t_D}\left(\frac{\partial p_D}{\partial r_D}\right)_1 dt_D \quad \ldots (21)$$

which relates the actual cumulative fluid influx with the time integral of the dimensionless function $-(\partial p_D/\partial r_D)_1$. Upon proper interpretation, Eqs. 17, 19 and 21 can be used to determine the fluid flow and pressure behavior in a spherical reservoir system, and also to indicate the appropriate choice of particular solutions to Eq. 7. Two distinct cases arise: the so-called pressure and rate cases.[2,5]

### *The Pressure Case*

The pressure case presumes knowledge of the pressure conditions at the internal boundary of a reservoir system and permits determination of the fluid flow behavior. Consider a spherical reservoir system characterized by dimensionless properties. Let this system be charged to a unit dimensionless pressure, and at zero time let the pressure at the internal boundary vanish and remain zero. This

condition represents the distinctive feature of the pressure case. The problem then remains to determine the dimensionless rate and cumulative fluid influx at the internal boundary as functions of dimensionless time. This dimensionless description of the fluid flow behavior and its translation into absolute units of measurement constitutes the pressure case.[2,5]

Under the precepts of the pressure case, the dimensionless fluid influx rate is defined by:

$$e_D = e_D(1, t_D) = -\left(\frac{\partial p_D}{\partial r_D}\right)_1 , \quad . \quad . \quad . \quad . \quad . \quad . \quad . \quad . \quad (22)$$

and the dimensionless cumulative fluid influx by:

$$F_D = F_D(1, t_D) = -\int_0^{t_D} \left(\frac{\partial p_D}{\partial r_D}\right)_1 dt_D \quad . \quad . \quad . \quad . \quad . \quad (23)$$

Symbolically, the actual velocity, rate and cumulative fluid influx may now be expressed in terms of $e_D$ and $F_D$ as follows:

$$v = u(r_w, t) = -\frac{k}{\mu r_w} \Delta p(r_w, 0)\, e_D(1, t_D) . \quad . \quad (24)$$

$$e = e(r_w, t) = 2\pi r_w \frac{k}{\mu} \Delta p(r_w, 0)\, e_D(1, t_D) . \quad . \quad (25)$$

$$F = F(r_w, t) = 2\pi \phi c r_w^3 \Delta p(r_w, 0) F_D(1, t_D) . \quad . \quad (26)$$

Eqs. 24 through 26 express the facets of fluid flow behavior in terms of field data and the dimensionless functions $e_D$ and $F_D$. By application of the superposition principle (Duhamel's theorem) these functions can also be used to treat time-varying pressure histories.

### *The Rate Case*

The rate case presumes knowledge of the fluid flow conditions at the internal boundary and permits determination of the pressure behavior. Consider a dimensionless spherical reservoir system charged to a unit dimensionless pressure, and from zero-time onward let a unit dimensionless fluid influx rate be imposed. This condition, which expressed analytically is:

$$-\left(\frac{\partial p_D}{\partial r_D}\right)_1 = 1 , \quad . \quad . \quad . \quad . \quad . \quad . \quad . \quad . \quad . \quad . \quad . \quad (27)$$

for all time $t_D$, represents the distinctive feature of the rate case. The problem here is to determine the dimensionless pressure drop distribution in the system, and the pressure drop at the internal boundary under the conditions prescribed by Eq. 27. This dimensionless description of pressure behavior and its translation into absolute units of measurement constitutes the rate case.[2,5]

Under the precepts of the rate case, the actual pressure distribution in the system is given by:

$$p(r, t) = p_i - \frac{q\mu}{2\pi k r_w} p_D(r_D, t_D) . \quad . \quad . \quad . \quad . \quad . \quad (28)$$

Similarly, the actual pressure at the internal boundary is given by:

$$p = p(r_w, t) = p_i - \frac{q\mu}{2\pi k r_w} p_D(1, t_D) \quad . \quad . \quad . \quad (29)$$

These symbolic relations express the pressure behavior in terms of field data and the dimensionless functions $p_D(t_D, t_D)$ and $p_D(1, t_D)$. Likewise, by application of the superposition principle, these functions can be used to treat time-varying rate histories.

## DESCRIPTION OF PARTICULAR SOLUTIONS

### UNLIMITED SYSTEM

By definition the external boundary of an unlimited system continuously recedes from the internal boundary without reaching a geometric limit. Under these conditions the product $r_D p_D$ vanishes and Eq. 15 becomes:

$$\bar{b} = C_1 \exp(-r_D\sqrt{s}) . \quad . \quad . \quad . \quad . \quad . \quad . \quad . \quad . \quad . \quad . \quad (30)$$

The precepts of the pressure case require that a dimensionless pressure drop of unity be maintained at the internal boundary, and since the Laplace transform of unity is $1/s$, it follows that:

$$\bar{b} = \frac{1}{s} \exp\left[-\sqrt{s}\,(r_D - 1)\right] , \quad . \quad . \quad . \quad . \quad . \quad . \quad (31)$$

which is the subsidiary equation appropriate to the pressure case for an unlimited system. The dimensionless fluid influx rate $e_D$ can be rewritten in terms of $b$:

$$e_D = -\left(\frac{\partial p_D}{\partial r_D}\right)_1 = -\left(\frac{\partial b}{\partial r_D} - b\right)_1 \quad . \quad . \quad . \quad . \quad . \quad (32)$$

Then the Laplace transform of $e_D$, utilizing Eqs. 31 and 32, is:

$$\bar{e}_D = \frac{1}{\sqrt{s}} + \frac{1}{s} , \quad . \quad . \quad . \quad . \quad . \quad . \quad . \quad . \quad . \quad . \quad . \quad (33)$$

whose inverse transformation can be written at once as:

$$e_D = 1 + (\pi t_D)^{-1/2} , \quad . \quad . \quad . \quad . \quad . \quad . \quad . \quad . \quad . \quad . \quad (34)$$

which is the dimensionless fluid influx rate of an unlimited system. The Laplace transform of $F_D$ (dimensionless cumulative fluid influx) is simply:

$$\bar{F}_D = \frac{\bar{e}_D}{s} = \frac{1}{s^{3/2}} + \frac{1}{s^2} , \quad . \quad . \quad . \quad . \quad . \quad . \quad . \quad . \quad (35)$$

whose inverse transformation can likewise be

written at once as:

$$F_D = t_D + 2\left(\frac{t_D}{\pi}\right)^{1/2} \quad \ldots\ldots\ldots\ldots (36)$$

which is the dimensionless cumulative fluid influx of an unlimited system.[9,11,13,14]

The precepts of the rate case require that a dimensionless rate of unity be maintained at the internal boundary, which can be written in terms of $b$ as:

$$-\left(\frac{\partial p_D}{\partial r_D}\right)_1 = -\left(\frac{\partial b}{\partial r_D} - b\right)_1 = 1 \quad \ldots\ldots (37)$$

Using Eq. 30 it follows that:

$$b = \frac{\exp\left[-\sqrt{s}\,(r_D - 1)\right]}{s\,(1 + \sqrt{s})} \quad \ldots\ldots\ldots (38)$$

which is the subsidiary equation appropriate to the rate case for an unlimited system. The inverse transformation is available from integral transform tables. This result divided by $r_D$ yields:

$$p_D(r_D, t_D) = \frac{1}{r_D}\left[\operatorname{erfc}\left(\frac{r_D - 1}{2\sqrt{t_D}}\right) - \exp(r_D + t_D - 1)\operatorname{erfc}\left(\frac{r_D - 1}{2\sqrt{t_D}} + \sqrt{t_D}\right)\right] \quad \ldots (39)$$

which is the dimensionless pressure-drop distribution of an unlimited system. Upon placing $r_D$ at unity, Eq. 39 reduces to:

$$p_D = 1 - \exp(t_D)\operatorname{erfc}(t_D^{1/2}). \quad \ldots\ldots\ldots (40)$$

which is the dimensionless pressure drop at the internal boundary of an unlimited system.[2,9,11,13,14]

At this juncture some significant observations can be made. First, the least upper bound of the dimensionless pressure drop is unity. Consequently, under the conditions of constant rate the pressure drop at the internal boundary of an unlimited spherical system can never exceed a fixed finite value. Secondly, the greatest lower bound of the dimensionless rate is also unity. Hence, the rate engendered by a single pressure drop imposed at zero time at the internal boundary of an unlimited spherical system can never be less than a fixed non-vanishing value. In either situation, it appears that an unlimited spherical reservoir system approaches steady-state conditions as dimensionless time assumes excessively large values. This property, strangely enough, is not enjoyed by unlimited linear or cylindrical (radial) systems.[2,5]

## LIMITED SYSTEM WITH CLOSED EXTERNAL BOUNDARY

In a limited reservoir system the external boundary eventually coincides with a geometric limit. At this limit, a system with a closed external boundary can sustain no fluid flow across it. Hence, the normal pressure derivative there must vanish. Introduction of this condition into Eq. 15 gives:

$$\bar{b} = C_1\left[\exp(-r_D\sqrt{s}) + \left(\frac{r_D'\sqrt{s}+1}{r_D'\sqrt{s}-1}\right)\exp\sqrt{s}\,(r_D - 2r_D')\right] \quad \ldots\ldots\ldots (41)$$

Under the precepts of the pressure case and by subsequent conversion to hyperbolic functions, Eq. 41 becomes:

$$\bar{b} = \frac{\sinh[\sqrt{s}(r_D' - r_D)] - \sqrt{s}\,r_D'\cosh[\sqrt{s}(r_D' - r_D)]}{s\{\sinh[\sqrt{s}\,(r_D' - 1)] - \sqrt{s}\,r_D'\cosh[\sqrt{s}\,(r_D' - 1)]\}} \quad \ldots\ldots\ldots (42)$$

which is the subsidiary equation appropriate to the pressure case for a closed limited system. The Laplace transform of $e_D$, using Eqs. 32 and 42, is:

$$\bar{e}_D = \frac{\sqrt{s}(r_D' - 1)\cosh[\sqrt{s}(r_D' - 1)] + (s r_D' - 1)\sinh[\sqrt{s}\,(r_D' - 1)]}{s\{\sqrt{s}\,r_D'\cosh[\sqrt{s}\,(r_D' - 1)] - \sinh[\sqrt{s}\,(r_D' - 1)]\}} \quad \ldots\ldots\ldots (43)$$

The inverse transformation of the relation may be obtained with the aid of Mellin's inversion theorem, and is given by the following integral in the complex plane:

$$e_D = \frac{1}{2\pi i}\lim_{\delta\to\infty}\int_{\gamma-i\delta}^{\gamma+i\delta}\exp(z\,t_D)\,\bar{e}_D\,dz \quad \ldots (44)$$

which for the function at hand may be evaluated by converting it to a closed contour integral and then applying the calculus of residues. Thus, by virtue of Cauchy's integral formula:

$$\frac{1}{2\pi i}\lim_{\delta\to\infty}\int_{\gamma-i\delta}^{\gamma+i\delta} e^{zt_D}\bar{e}_D\,dz = \frac{1}{2\pi i}\int_c e^{zt_D}\bar{e}_D\,dz = R_0 + \sum_{n=1}^{\infty} R_n \quad \ldots (45)$$

where $R_0$ is the residue corresponding to the singularity at the origin and $R_n$ the residues corresponding to the other singular points. Evaluation of Eq. 45 yields the dimensionless fluid influx rate for a closed limited spherical system, as follows:

$$e_D = \frac{2}{(r_D' - 1)}\sum_{n=1}^{\infty}\frac{w_n^2 r_D'^2 + (r_D' - 1)^2}{w_n^2 r_D'^2 - (r_D' - 1)}\exp\left[-\frac{w_n^2 t_D}{(r_D'^2 - 1)}\right], \quad \ldots\ldots\ldots (46)$$

where $w_n$ are the roots of the equation:

$$\frac{\tan w}{w} = \frac{r_D'}{(r_D' - 1)} \quad \ldots\ldots\ldots (47)$$

The Laplace transform of $F_D$ is:

$$\bar{F}_D = \frac{\bar{e}_D}{s}$$

$$= \frac{\sqrt{s}(r_D'-1)\cosh\sqrt{s}(r_D'-1) + (sr_D'-1)\sinh\sqrt{s}(r_D'-1)}{s^2[\sqrt{s}\,r_D'\cosh\sqrt{s}(r_D'-1) - \sinh\sqrt{s}(r_D'-1)]} \quad \ldots\ldots\ldots\ldots\ldots\ldots\ldots\ldots (48)$$

By virtue of previous arguments, the inverse transformation of Eq. 48 yields the dimensionless cumulative fluid influx for a closed limited system:

$$F_D = R_0 + \sum_{n=1}^{\infty} R_n = \frac{1}{3}(r_D'^3 - 1) - 2(r_D'-1)\sum_{n=1}^{\infty} \frac{1}{w_n^2}\left[\frac{w_n^2 r_D' + (r_D'-1)^2}{w_n^2 r_D' - (r_D'-1)}\right] e^{-\frac{w_n^2 t_D}{(r_D'-1)^2}} \quad \ldots\ldots\ldots\ldots\ldots\ldots\ldots\ldots (49)$$

where $w_n$ are also the roots of Eq. 47.[2,10,11,13-18]

Under the precepts of the rate case, Eq. 41 becomes, upon conversion to hyperbolic functions:

$$\bar{b} = \frac{\sqrt{s}\,r_D'\cosh\left|\sqrt{s}\,(r_D'-r_D) - \sinh\sqrt{s}(r_D'-r_D)\right.}{s[\sqrt{s}(r_D'-1)\cosh\sqrt{s}(r_D'-1) + (sr_D'-1)\sinh\sqrt{s}(r_D'-1)]} \quad \ldots\ldots\ldots\ldots\ldots\ldots\ldots\ldots (50)$$

which is the subsidiary equation appropriate to the rate case for a closed limited system. As before, the inverse transformation of Eq. 50 is given by the sum of the residues, and since $b$ is $r_D p_D$, there follows:

TABLE 1 — UNLIMITED SYSTEM

| Dimensionless Time ($t_D$) | Dimensionless Rate ($e_D$) | Dimensionless Influx ($F_D$) | Dimensionless Pressure-Drop ($p_D$) | Dimensionless Time ($t_D$) | Dimensionless Rate ($e_D$) | Dimensionless Influx ($F_D$) | Dimensionless Pressure-Drop ($p_D$) |
|---|---|---|---|---|---|---|---|
| 0.001 | 18.84124 | 0.03668 | 0.03471 | | | | |
| 0.002 | 13.61566 | 0.05246 | 0.04853 | 60.0 | 1.07284 | 68.7 | 0.92595 |
| 0.003 | 11.30065 | 0.06480 | 0.05892 | 70.0 | 1.06743 | 79.4 | 0.93103 |
| 0.004 | 9.92062 | 0.07536 | 0.06755 | 80.0 | 1.06309 | 90.1 | 0.93512 |
| 0.005 | 8.97885 | 0.08479 | 0.07504 | 90.0 | 1.05947 | 100.7 | 0.93851 |
| 0.006 | 8.28366 | 0.09340 | 0.08174 | 100.0 | 1.05642 | 111.0 | 0.94139 |
| 0.007 | 7.74336 | 0.10141 | 0.08782 | 200.0 | 1.03989 | 216.0 | 0.95703 |
| 0.008 | 7.30783 | 0.10893 | 0.09343 | 300.0 | 1.03257 | 320.0 | 0.96408 |
| 0.009 | 6.94708 | 0.11605 | 0.09865 | 400.0 | 1.02821 | 423.0 | 0.96835 |
| 0.01 | 6.64190 | 0.12284 | 0.10354 | 500.0 | 1.02523 | 525.0 | 0.97131 |
| 0.02 | 4.98942 | 0.17958 | 0.14152 | 600.0 | 1.02303 | 628.0 | 0.97352 |
| 0.03 | 4.25735 | 0.22544 | 0.16894 | 700.0 | 1.02132 | 730.0 | 0.97526 |
| 0.04 | 3.82095 | 0.26568 | 0.19098 | 800.0 | 1.01995 | 832.0 | 0.97668 |
| 0.05 | 3.52313 | 0.30231 | 0.20962 | 900.0 | 1.01881 | 934.0 | 0.97787 |
| 0.06 | 3.30329 | 0.33640 | 0.22589 | 1,000.0 | 1.01784 | 1,036.0 | 0.97888 |
| 0.07 | 3.13244 | 0.36854 | 0.24036 | 2,000.0 | 1.01262 | 2,050.0 | 0.98453 |
| 0.08 | 2.99471 | 0.39915 | 0.25345 | 3,000.0 | 1.01030 | 3,062.0 | 0.98714 |
| 0.09 | 2.88063 | 0.42851 | 0.26540 | 4,000.0 | 1.00892 | 4,071.0 | 0.98874 |
| 0.10 | 2.78412 | 0.45682 | 0.27642 | 5,000.0 | 1.00798 | 5,080.0 | 0.98984 |
| 0.20 | 2.26157 | 0.70463 | 0.35621 | 6,000.0 | 1.00728 | 6,087.0 | 0.99067 |
| 0.30 | 2.03006 | 0.91804 | 0.40798 | 7,000.0 | 1.00674 | 7,094.0 | 0.99132 |
| 0.40 | 1.89206 | 1.11365 | 0.44639 | 8,000.0 | 1.00631 | 8,101.0 | 0.99185 |
| 0.50 | 1.79788 | 1.29788 | 0.47684 | 9,000.0 | 1.00595 | 9,107.0 | 0.99229 |
| 0.60 | 1.72837 | 1.47406 | 0.50198 | 10,000.0 | 1.00564 | 10,113.0 | 0.99267 |
| 0.70 | 1.67434 | 1.64407 | 0.52330 | 20,000.0 | 1.00399 | 20,160.0 | 0.99473 |
| 0.80 | 1.63078 | 1.80925 | 0.54175 | 30,000.0 | 1.00326 | 30,195.0 | 0.99566 |
| 0.90 | 1.59471 | 1.97047 | 0.55798 | 40,000.0 | 1.00282 | 40,226.0 | 0.99623 |
| 1.0 | 1.56419 | 2.12838 | 0.57242 | 50,000.0 | 1.00252 | 50,252.0 | 0.99662 |
| 2.0 | 1.39894 | 3.59577 | 0.66380 | 60,000.0 | 1.00230 | 60,276.0 | 0.99690 |
| 3.0 | 1.32574 | 4.95441 | 0.71266 | 70,000.0 | 1.00213 | 70,299.0 | 0.99713 |
| 4.0 | 1.28209 | 6.25676 | 0.74460 | 80,000.0 | 1.00199 | 80,319.0 | 0.99731 |
| 5.0 | 1.25231 | 7.52313 | 0.76765 | 90,000.0 | 1.00188 | 90,339.0 | 0.99746 |
| 6.0 | 1.23033 | 8.76395 | 0.78534 | 100,000.0 | 1.00178 | 100,357.0 | 0.99759 |
| 7.0 | 1.21324 | 9.98541 | 0.79946 | 200,000.0 | 1.00126 | 200,505.0 | 0.99829 |
| 8.0 | 1.19947 | 11.19154 | 0.81109 | 300,000.0 | 1.00103 | 300,618.0 | 0.99860 |
| 9.0 | 1.18806 | 12.38514 | 0.82088 | 400,000.0 | 1.00089 | 400,714.0 | 0.99878 |
| 10.0 | 1.17841 | 13.56825 | 0.82927 | 500,000.0 | 1.00080 | 500,798.0 | 0.99891 |
| 20.0 | 1.12616 | 25.04626 | 0.87624 | 600,000.0 | 1.00073 | 600,874.0 | 0.99900 |
| 30.0 | 1.10301 | 36.18039 | 0.89770 | 700,000.0 | 1.00067 | 700,944.0 | 0.99908 |
| 40.0 | 1.08921 | 47.13650 | 0.91060 | 800,000.0 | 1.00063 | 801,009.0 | 0.99914 |
| 50.0 | 1.07979 | 57.97885 | 0.91943 | 900,000.0 | 1.00059 | 901,070.0 | 0.99919 |
| | | | | 1,000,000.0 | 1.00056 | 1,001,128.0 | 0.99923 |

$$p(r_D,t_D)=$$

$$\frac{[3r_D'+(r_D'-1)^2]\left[\frac{1}{6}(r_D'-r_D)^2(2r_D'+r_D)+r_Dt_D\right]-\frac{1}{2}(r_D'-1)^2\left[\frac{1}{5}(r_D'-1)^2+r_D'\right]r_D}{(r_D'-1)\left[\frac{1}{5}(r_D'-1)^4+2r_D'(r_D'-1)^2+3r_D'^2\right]r_D}$$

$$-\frac{2(r_D'-1)^2}{r_D}\sum_{n=1}^{\infty}\frac{\left[\frac{r_D'w_n}{r_D'-1}\cos\left(w_n\frac{r_D'-r_D}{r_D'-1}\right)-\sin\left(w_n\frac{r_D'-r_D}{r_D'-1}\right)\right]e^{-\frac{w_n^2t_D}{(r_D'-1)^2}}}{w_n^2[w_nr_D'\cos w_n+(r_D'^2+1)\sin w_n)}\times, \quad \ldots\ldots\ldots\ldots\ldots\ldots\ldots\ldots (51)$$

where $w_n$ are here the roots of:

$$\frac{\sin w}{w}-\frac{1}{w^2}=\frac{r_D'}{(r_D'-1)^2} \quad \ldots\ldots\ldots\ldots (52)$$

The expression embodied by Eq. 51 represents the dimensionless pressure-drop distribution for a closed limited spherical system. Upon placing $r_D$ at unity and simplifying, there follows at once the dimensionless pressure-drop at the internal boundary:

$$p_D=$$

$$\frac{[(r_D'-1)^2+3r_D']\left[\frac{1}{6}(r_D'-1)^2(2r_D'+1)+t_D\right]-\frac{1}{2}(r_D'-1)^2\left[\frac{1}{5}(r_D'-1)^2+r_D'\right]}{(r_D'-1)\left[\frac{1}{5}(r_D'-1)^4+2(r_D'-1)^2r_D'+3r_D'^2\right]}$$

$$-2(r_D'-1)\sum_{n=1}^{\infty}\frac{[w_n^2r_D'^2+(r_D'-1)^2]}{w_n^2[w_n^2r_D'^2+(r_D'^2+r_D'+1)(r_D'-1)^2]}\times e^{-\frac{w_n^2t_D}{(r_D'-1)^2}}, \quad \ldots\ldots\ldots\ldots\ldots (53)$$

where $w_n$ are still the roots of Eq. 52.

## LIMITED SYSTEM WITH OPEN EXTERNAL BOUNDARY

It will be recalled that a limited reservoir system is characterized by the arrestment of growth of the external boundary when the latter coincides with the geometric limit of the system. For the case of an open boundary it is presumed that at this limit ($r_D'$) the system suffers no pressure drop. Introduction of this condition into Eq. 15 gives:

$$\bar{b}=C_1[\exp(-r_D\sqrt{s})-\exp(r_D-2r_D)\sqrt{s}] \quad \ldots (54)$$

Under the precepts of the pressure case and conversion to hyperbolic functions, Eq. 54 becomes:

$$\bar{b}=\frac{\sinh\sqrt{s}\,(r_D'-r_D)}{s\,\{\sinh\sqrt{s}\,(r_D'-1)\}} \quad \ldots\ldots\ldots (55)$$

which is the subsidiary equation appropriate to the pressure case for an open limited system. The Laplace transform of $e_D$ using Eq. 55, is:

$$\bar{e}_D=\frac{1}{s}+\frac{\cosh\sqrt{s}\,(r_D'-1)}{\sqrt{s}\,[\sinh\sqrt{s}\,(r_D'-1)]} \quad \ldots\ldots (56)$$

The inverse transformation is available from integral tables in the form:

$$e_D=1+\frac{1}{(r_D'-1)}\,\theta_4\left[\frac{1}{2}\middle|\frac{\pi t_D}{(r_D'-1)^2}\right], \quad \ldots (57)$$

and upon expanding the Theta function this becomes:

$$e_D=\frac{r_D'}{r_D'-1}+\frac{2}{r_D'-1}\sum_{n=1}^{\infty}\exp\left[-\frac{n^2\pi^2t_D}{(r_D'-1)^2}\right], \quad \ldots (58)$$

which is the dimensionless rate for an open limited system. As before, the Laplace transforms of $F_D$ is:

$$\bar{F}_D=\frac{\bar{e}_D}{s}=\frac{1}{s^2}+\frac{\cosh\sqrt{s}\,(r_D'-1)}{s^{3/2}\,[\sinh\sqrt{s}\,(r_D'-1)]}, \quad \ldots (59)$$

whose inverse transformation was obtained with the aid of the Faltung convolution theorem as:

$$F_D=\frac{r_D't_D}{r_D'-1}+\frac{1}{3}(r_D'-1)-\frac{2(r_D'-1)}{\pi^2}\sum_{n=1}^{\infty}\frac{1}{n^2}\exp\left[-\frac{n^2\pi^2t_D}{(r_D'-1)^2}\right], \quad \ldots (60)$$

the dimensionless cumulative fluid influx for an open limited system.[9-11,13-20]

Under the precepts of the rate case, Eq. 54 becomes:

$$\bar{b}=\frac{\sinh\sqrt{s}\,(r_D'-r_D)}{s[\sqrt{s}\cosh\sqrt{s}\,(r_D'-1)+\sinh\sqrt{s}\,(r_D'-1)]}, \quad \ldots (61)$$

which is the subsidiary equation appropriate to the rate case for a limited system with a fixed pressure at the external boundary. The inverse transformation of Eq. 61 was again obtained by Mellin's inversion theorem, as previously explained. Thus, the pressure-drop distribution is given by:

## TABLE 2 — LIMITED SYSTEMS
### Closed External Boundary

| Time ($t_D$) | Rate ($q_D$) | Influx ($F_D$) | Pressure Drop ($p_D$) |
|---|---|---|---|
| **Dimensionless External Radius $r_D' = 2$** | | | |
| 0.07 | 3.1324 | 0.3685 | 0.2404 |
| 0.08 | 2.9947 | 0.3992 | 0.2534 |
| 0.09 | 2.8806 | 0.4285 | 0.2654 |
| 0.10 | 2.7839 | 0.4568 | 0.2764 |
| 0.20 | 2.2411 | 0.7040 | 0.3567 |
| 0.30 | 1.9342 | 0.9120 | 0.4120 |
| 0.40 | 1.6858 | 1.0927 | 0.4591 |
| 0.50 | 1.4713 | 1.2503 | 0.5033 |
| 0.60 | 1.2844 | 1.3879 | 0.5467 |
| 0.70 | 1.1212 | 1.5080 | 0.5897 |
| 0.80 | 0.9788 | 1.6128 | 0.6326 |
| 0.90 | 0.8544 | 1.7044 | 0.6755 |
| 1.0 | 0.7459 | 1.7843 | 0.7184 |
| 2.0 | 0.1916 | 2.1921 | 1.1469 |
| 3.0 | 0.0491 | 2.2970 | 1.5755 |
| 4.0 | 0.0127 | 2.3240 | 2.0041 |
| 5.0 | 0.0033 | 2.3309 | 2.4327 |
| 6.0 | 0.0008 | 2.3327 | 2.8612 |
| 7.0 | 0.0002 | 2.3332 | 3.2898 |
| 8.0 | 0.0001 | 2.3333 | 3.7184 |
| 9.0 | 0.0000 | 2.3333 | 4.1469 |
| 10.0 | 0.0000 | 2.3333 | 4.5755 |
| **Dimensionless External Radius $r_D' = 3$** | | | |
| 0.2 | 2.2616 | 0.7046 | 0.3562 |
| 0.3 | 2.0301 | 0.9180 | 0.4080 |
| 0.4 | 1.8920 | 1.1136 | 0.4464 |
| 0.5 | 1.7972 | 1.2978 | 0.4769 |
| 0.6 | 1.7261 | 1.4739 | 0.5021 |
| 0.7 | 1.6688 | 1.6435 | 0.5236 |
| 0.8 | 1.6199 | 1.8079 | 0.5425 |
| 0.9 | 1.5764 | 1.9677 | 0.5595 |
| 1.0 | 1.5363 | 2.1233 | 0.5750 |
| 2.0 | 1.2114 | 3.4891 | 0.7012 |
| 3.0 | 0.9586 | 4.5692 | 0.8171 |
| 4.0 | 0.7586 | 5.4239 | 0.9325 |
| 5.0 | 0.6004 | 6.1004 | 1.0479 |
| 6.0 | 0.4751 | 6.6356 | 1.1633 |
| 7.0 | 0.3760 | 7.0591 | 1.2787 |
| 8.0 | 0.2975 | 7.3944 | 1.3941 |
| 9.0 | 0.2354 | 7.6598 | 1.5095 |
| 10.0 | 0.1863 | 7.8698 | 1.6249 |
| 20.0 | 0.0180 | 8.5899 | 2.7787 |
| 30.0 | 0.0017 | 8.6593 | 3.9325 |
| 40.0 | 0.0002 | 8.6659 | 5.0864 |
| 50.0 | 0.0000 | 8.6666 | 6.2402 |
| 60.0 | 0.0000 | 8.6667 | 7.3941 |
| **Dimensionless External Radius $r_D' = 4$** | | | |
| 0.7 | 1.6743 | 1.644 | 0.5233 |
| 0.8 | 1.6308 | 1.809 | 0.5418 |
| 0.9 | 1.5946 | 1.970 | 0.5580 |
| 1.0 | 1.5640 | 2.128 | 0.5724 |
| 2.0 | 1.3869 | 3.592 | 0.6655 |
| 3.0 | 1.2755 | 4.921 | 0.7234 |
| 4.0 | 1.1780 | 6.147 | 0.7734 |
| 5.0 | 1.0878 | 7.279 | 0.8216 |
| 6.0 | 1.0049 | 8.325 | 0.8693 |
| 7.0 | 0.9283 | 9.291 | 0.9170 |
| 8.0 | 0.8576 | 10.184 | 0.9646 |
| 9.0 | 0.7922 | 11.008 | 1.0122 |
| 10.0 | 0.7318 | 11.770 | 1.0599 |
| 20.0 | 0.3311 | 16.822 | 1.5361 |
| 30.0 | 0.1498 | 19.110 | 2.0122 |
| 40.0 | 0.0678 | 20.144 | 2.4884 |
| 50.0 | 0.0307 | 20.613 | 2.9646 |
| 60.0 | 0.0139 | 20.825 | 3.4408 |
| 70.0 | 0.0063 | 20.921 | 3.9170 |
| 80.0 | 0.0028 | 20.964 | 4.3932 |
| 90.0 | 0.0013 | 20.984 | 4.8694 |
| 100.0 | 0.0006 | 20.993 | 5.3456 |
| 200.0 | 0.0000 | 21.000 | 10.1076 |

| Time ($t_D$) | Rate ($q_D$) | Influx ($F_D$) | Pressure Drop ($p_D$) |
|---|---|---|---|
| **Dimensionless External Radius $r_D' = 5$** | | | |
| 1.0 | 1.5642 | 2.128 | 0.5724 |
| 2.0 | 1.3986 | 3.596 | 0.6638 |
| 3.0 | 1.3216 | 4.953 | 0.7133 |
| 4.0 | 1.2673 | 6.246 | 0.7479 |
| 5.0 | 1.2203 | 7.490 | 0.7764 |
| 6.0 | 1.1766 | 8.688 | 0.8024 |
| 7.0 | 1.1348 | 9.843 | 0.8273 |
| 8.0 | 1.0946 | 10.958 | 0.8518 |
| 9.0 | 1.0558 | 12.033 | 0.8761 |
| 10.0 | 1.0184 | 13.070 | 0.9004 |
| 20.0 | 0.7103 | 21.621 | 1.1424 |
| 30.0 | 0.4954 | 27.585 | 1.3843 |
| 40.0 | 0.3455 | 31.744 | 1.6262 |
| 50.0 | 0.2410 | 34.646 | 1.8682 |
| 60.0 | 0.1680 | 36.669 | 2.1101 |
| 70.0 | 0.1172 | 38.080 | 2.3520 |
| 80.0 | 0.0818 | 39.064 | 2.5940 |
| 90.0 | 0.0570 | 39.751 | 2.8359 |
| 100.0 | 0.0398 | 40.230 | 3.0778 |
| 200.0 | 0.0000 | 41.333 | 5.5068 |
| **Dimensionless External Radius $r_D' = 6$** | | | |
| 2.0 | 1.3989 | 3.596 | 0.6638 |
| 3.0 | 1.3255 | 4.954 | 0.7127 |
| 4.0 | 1.2807 | 6.256 | 0.7449 |
| 5.0 | 1.2477 | 7.520 | 0.7687 |
| 6.0 | 1.2201 | 8.753 | 0.7881 |
| 7.0 | 1.1951 | 9.961 | 0.8051 |
| 8.0 | 1.1714 | 11.144 | 0.8207 |
| 9.0 | 1.1487 | 12.304 | 0.8356 |
| 10.0 | 1.1265 | 13.441 | 0.8501 |
| 20.0 | 0.9283 | 23.683 | 0.9903 |
| 30.0 | 0.7650 | 32.123 | 1.1298 |
| 40.0 | 0.6304 | 39.078 | 1.2693 |
| 50.0 | 0.5195 | 44.810 | 1.4089 |
| 60.0 | 0.4281 | 49.534 | 1.5484 |
| 70.0 | 0.3528 | 53.426 | 1.6879 |
| 80.0 | 0.2907 | 56.634 | 1.8275 |
| 90.0 | 0.2396 | 59.277 | 1.9670 |
| 100.0 | 0.1974 | 61.455 | 2.1065 |
| 200.0 | 0.0285 | 70.191 | 3.5019 |
| 300.0 | 0.0041 | 71.453 | 4.8972 |
| 400.0 | 0.0006 | 71.636 | 6.2926 |
| 500.0 | 0.0001 | 71.662 | 7.6879 |
| 600.0 | 0.0000 | 71.666 | 9.0833 |
| 700.0 | 0.0000 | 71.666 | 10.4786 |
| 800.0 | 0.0000 | 71.667 | 11.8740 |
| **Dimensionless External Radius $r_D' = 7$** | | | |
| 3.0 | 1.3257 | 4.95 | 0.7127 |
| 4.0 | 1.2820 | 6.26 | 0.7446 |
| 5.0 | 1.2519 | 7.52 | 0.7678 |
| 6.0 | 1.2289 | 8.76 | 0.7857 |
| 7.0 | 1.2099 | 9.98 | 0.8004 |
| 8.0 | 1.1933 | 11.18 | 0.8131 |
| 9.0 | 1.1780 | 12.37 | 0.8244 |
| 10.0 | 1.1636 | 13.54 | 0.8348 |
| 20.0 | 1.0354 | 24.52 | 0.9255 |
| 30.0 | 0.9223 | 34.30 | 1.0133 |
| 40.0 | 0.8216 | 43.01 | 1.1010 |
| 50.0 | 0.7318 | 50.76 | 1.1887 |
| 60.0 | 0.6518 | 57.68 | 1.2765 |
| 70.0 | 0.5806 | 63.83 | 1.3642 |
| 80.0 | 0.5172 | 69.31 | 1.4519 |
| 90.0 | 0.4607 | 74.20 | 1.5396 |
| 100.0 | 0.4104 | 78.55 | 1.6273 |
| 200.0 | 0.1290 | 102.86 | 2.5045 |
| 300.0 | 0.0406 | 110.51 | 3.3817 |
| 400.0 | 0.0127 | 112.91 | 4.2598 |
| 500.0 | 0.0040 | 113.66 | 5.1361 |
| 600.0 | 0.0012 | 113.90 | 6.0133 |
| 700.0 | 0.0004 | 113.97 | 6.8905 |
| 800.0 | 0.0001 | 113.99 | 7.7677 |
| 900.0 | 0.0000 | 114.00 | 8.6449 |
| 1,000.0 | 0.0000 | 114.00 | 9.5221 |

TABLE 2—LIMITED SYSTEMS (continued)

| Time ($t_D$) | Rate ($q_D$) | Influx ($F_D$) | Pressure Drop ($p_D$) |
|---|---|---|---|
| **Dimensionless External Radius $r_D$ = 8** | | | |
| 4.0 | 1.2821 | 6.26 | 0.7446 |
| 5.0 | 1.2523 | 7.52 | 0.7678 |
| 6.0 | 1.2302 | 8.76 | 0.7854 |
| 7.0 | 1.2128 | 9.98 | 0.7996 |
| 8.0 | 1.1983 | 11.19 | 0.8115 |
| 9.0 | 1.1859 | 12.38 | 0.8216 |
| 10.0 | 1.1747 | 13.56 | 0.8306 |
| 20.0 | 1.0860 | 24.85 | 0.8971 |
| 30.0 | 1.0078 | 35.31 | 0.9361 |
| 40.0 | 0.9354 | 45.02 | 1.0148 |
| 50.0 | 0.8681 | 54.04 | 1.0735 |
| 60.0 | 0.8056 | 62.40 | 1.1322 |
| 70.0 | 0.7477 | 70.12 | 1.1910 |
| 80.0 | 0.6939 | 77.37 | 1.2497 |
| 90.0 | 0.6440 | 84.06 | 1.3084 |
| 100.0 | 0.5976 | 90.26 | 1.3671 |
| 200.0 | 0.2832 | 132.37 | 1.9542 |
| 300.0 | 0.1342 | 152.34 | 2.5412 |
| 400.0 | 0.0637 | 161.80 | 3.1283 |
| 500.0 | 0.0302 | 166.29 | 3.7154 |
| 600.0 | 0.0143 | 168.41 | 4.3025 |
| 700.0 | 0.0068 | 169.42 | 4.8896 |
| 800.0 | 0.0032 | 169.90 | 5.4767 |
| 900.0 | 0.0015 | 170.13 | 6.0638 |
| 1,000.0 | 0.0007 | 170.24 | 6.6508 |
| 2,000.0 | 0.0000 | 170.33 | 12.5218 |
| **Dimensionless External Radius $r_D$ = 9** | | | |
| 5.0 | 1.2523 | 7.52 | 0.7678 |
| 6.0 | 1.2303 | 8.76 | 0.7853 |
| 7.0 | 1.2132 | 9.99 | 0.7995 |
| 8.0 | 1.1993 | 11.19 | 0.8112 |
| 9.0 | 1.1877 | 12.38 | 0.8211 |
| 10.0 | 1.1776 | 13.57 | 0.8296 |
| 20.0 | 1.1094 | 24.98 | 0.8848 |
| 30.0 | 1.0539 | 35.70 | 0.9271 |
| 40.0 | 1.0015 | 46.04 | 0.9684 |
| 50.0 | 0.9518 | 55.83 | 1.0096 |
| 60.0 | 0.9045 | 65.11 | 1.0508 |
| 70.0 | 0.8596 | 73.92 | 1.0920 |
| 80.0 | 0.8169 | 82.30 | 1.1332 |
| 90.0 | 0.7763 | 90.27 | 1.1745 |
| 100.0 | 0.7378 | 97.84 | 1.2157 |
| 200.0 | 0.4433 | 155.64 | 1.6278 |
| 300.0 | 0.2663 | 190.37 | 2.0398 |
| 400.0 | 0.1600 | 211.24 | 2.4519 |
| 500.0 | 0.0962 | 223.79 | 2.8640 |
| 600.0 | 0.0578 | 231.32 | 3.2761 |
| 700.0 | 0.0347 | 235.85 | 3.6882 |
| 800.0 | 0.0209 | 238.57 | 4.1003 |
| 900.0 | 0.0125 | 240.21 | 4.5124 |
| 1,000.0 | 0.0075 | 241.19 | 4.9245 |
| 2,000.0 | 0.0000 | 242.67 | 9.0455 |
| **Dimensionless External Radius $r_D$ = 10** | | | |
| 6.0 | 1.2303 | 8.76 | 0.7853 |
| 7.0 | 1.2132 | 9.99 | 0.7995 |
| 8.0 | 1.1995 | 11.19 | 0.8112 |
| 9.0 | 1.1880 | 12.38 | 0.8210 |
| 10.0 | 1.1783 | 13.57 | 0.8295 |
| 20.0 | 1.1196 | 25.02 | 0.8797 |
| 30.0 | 1.0783 | 36.01 | 0.9174 |
| 40.0 | 1.0399 | 46.60 | 0.9477 |
| 50.0 | 1.0027 | 56.81 | 0.9728 |
| 60.0 | 0.9669 | 66.66 | 1.0028 |
| 70.0 | 0.9325 | 76.15 | 1.0329 |
| 80.0 | 0.8992 | 85.31 | 1.0629 |
| 90.0 | 0.8672 | 94.14 | 1.0929 |
| 100.0 | 0.8362 | 102.66 | 1.1229 |
| 200.0 | 0.5816 | 172.78 | 1.4232 |
| 300.0 | 0.4045 | 221.56 | 1.7235 |
| 400.0 | 0.2813 | 255.48 | 2.0238 |
| 500.0 | 0.1956 | 279.07 | 2.3241 |
| 600.0 | 0.1361 | 295.49 | 2.6244 |
| 700.0 | 0.0947 | 306.90 | 2.9247 |
| 800.0 | 0.0659 | 314.85 | 3.2250 |
| 900.0 | 0.0458 | 320.37 | 3.5253 |
| 1,000.0 | 0.0319 | 324.22 | 3.8256 |
| 2,000.0 | 0.0008 | 332.77 | 6.8287 |
| 3,000.0 | 0.0000 | 332.99 | 9.8317 |
| 4,000.0 | 0.0000 | 333.00 | 12.8347 |

| Time ($t_D$) | Rate ($q_D$) | Influx ($F_D$) | Pressure Drop ($p_D$) |
|---|---|---|---|
| **Dimensionless External Radius $r_D$ = 20** | | | |
| 30.0 | 1.1030 | 36.2 | 0.8977 |
| 40.0 | 1.0892 | 47.1 | 0.9106 |
| 50.0 | 1.0796 | 58.0 | 0.9199 |
| 60.0 | 1.0724 | 68.7 | 0.9270 |
| 70.0 | 1.0664 | 79.4 | 0.9328 |
| 80.0 | 1.0611 | 90.1 | 0.9378 |
| 90.0 | 1.0562 | 100.7 | 0.9423 |
| 100.0 | 1.0516 | 111.2 | 0.9465 |
| 200.0 | 1.0088 | 214.2 | 0.9851 |
| 300.0 | 0.9681 | 313.0 | 1.0229 |
| 400.0 | 0.9291 | 407.9 | 1.0604 |
| 500.0 | 0.8916 | 498.9 | 1.0979 |
| 600.0 | 0.8557 | 586.2 | 1.1354 |
| 700.0 | 0.8212 | 670.1 | 1.1729 |
| 800.0 | 0.7881 | 750.5 | 1.2104 |
| 900.0 | 0.7563 | 827.7 | 1.2479 |
| 1,000.0 | 0.7259 | 901.8 | 1.2854 |
| 2,000.0 | 0.4610 | 1,496.9 | 1.6604 |
| 3,000.0 | 0.3187 | 1,891.2 | 2.0355 |
| 4,000.0 | 0.2111 | 2,152.4 | 2.4105 |
| 5,000.0 | 0.1400 | 2,325.7 | 2.7856 |
| 6,000.0 | 0.0929 | 2,440.5 | 3.1606 |
| 7,000.0 | 0.0616 | 2,516.7 | 3.5357 |
| 8,000.0 | 0.0408 | 2,567.1 | 3.9107 |
| 9,000.0 | 0.0270 | 2,600.6 | 4.2858 |
| 10,000.0 | 0.0179 | 2,622.7 | 4.6608 |
| 20,000.0 | 0.0000 | 2,666.3 | 8.4113 |
| **Dimensionless External Radius $r_D$ = 30** | | | |
| 80.0 | 1.0631 | 90.1 | 0.9351 |
| 90.0 | 1.0595 | 100.7 | 0.9385 |
| 100.0 | 1.0564 | 111.3 | 0.9414 |
| 200.0 | 1.0281 | 215.9 | 0.9680 |
| 300.0 | 1.0254 | 319.1 | 0.9724 |
| 400.0 | 1.0133 | 421.0 | 0.9840 |
| 500.0 | 1.0014 | 521.7 | 0.9954 |
| 600.0 | 0.9895 | 621.3 | 1.0068 |
| 700.0 | 0.9780 | 719.7 | 1.0177 |
| 800.0 | 0.9665 | 816.9 | 1.0290 |
| 900.0 | 0.9552 | 913.0 | 1.0401 |
| 1,000.0 | 0.9439 | 1,007.9 | 1.0517 |
| 2,000.0 | 0.8388 | 1,898.3 | 1.1623 |
| 3,000.0 | 0.7453 | 2,689.4 | 1.2733 |
| 4,000.0 | 0.6622 | 3,392.4 | 1.3846 |
| 5,000.0 | 0.5884 | 4,017.0 | 1.4957 |
| 6,000.0 | 0.5228 | 4,572.0 | 1.6068 |
| 7,000.0 | 0.4646 | 5,065.2 | 1.7179 |
| 8,000.0 | 0.4128 | 5,503.4 | 1.8290 |
| 9,000.0 | 0.3668 | 5,892.7 | 1.9401 |
| 10,000.0 | 0.3259 | 6,238.6 | 2.0513 |
| 20,000.0 | 0.1000 | 8,153.6 | 3.1624 |
| 30,000.0 | 0.0307 | 8,739.1 | 4.2736 |
| 40,000.0 | 0.0094 | 8,919.7 | 5.3847 |
| 50,000.0 | 0.0029 | 8,975.1 | 6.4959 |
| 60,000.0 | 0.0009 | 8,992.1 | 7.6070 |
| 70,000.0 | 0.0003 | 8,997.3 | 8.7182 |
| 80,000.0 | 0.0001 | 8,998.9 | 9.8293 |
| 90,000.0 | 0.0000 | 8,999.4 | 10.9405 |
| 100,000.0 | 0.0000 | 8,999.6 | 12.0516 |
| **Dimensionless External Radius $r_D$ = 40** | | | |
| 100.0 | 1.0564 | 111.0 | 0.9414 |
| 200.0 | 1.0398 | 216.0 | 0.9570 |
| 300.0 | 1.0320 | 320.0 | 0.9653 |
| 400.0 | 1.0262 | 422.0 | 0.9715 |
| 500.0 | 1.0210 | 525.0 | 0.9769 |
| 600.0 | 1.0160 | 627.0 | 0.9820 |
| 700.0 | 1.0110 | 728.0 | 0.9871 |
| 800.0 | 1.0060 | 829.0 | 0.9925 |
| 900.0 | 1.0011 | 929.0 | 0.9972 |
| 1,000.0 | 0.9962 | 1,029.0 | 1.0019 |
| 2,000.0 | 0.9485 | 2,001.0 | 1.0488 |
| 3,000.0 | 0.9031 | 2,927.0 | 1.0957 |
| 4,000.0 | 0.8598 | 3,808.0 | 1.1425 |
| 5,000.0 | 0.8186 | 4,647.0 | 1.1894 |
| 6,000.0 | 0.7794 | 5,446.0 | 1.2363 |
| 7,000.0 | 0.7421 | 6,207.0 | 1.2832 |
| 8,000.0 | 0.7066 | 6,931.0 | 1.3301 |
| 9,000.0 | 0.6727 | 7,620.0 | 1.3769 |
| 10,000.0 | 0.6405 | 8,277.0 | 1.4238 |
| 20,000.0 | 0.3920 | 13,339.0 | 1.8926 |
| 30,000.0 | 0.2400 | 16,436.0 | 2.3613 |
| 40,000.0 | 0.1472 | 18,333.0 | 2.8301 |
| 50,000.0 | 0.0901 | 19,494.0 | 3.2988 |
| 60,000.0 | 0.0552 | 20,208.0 | 3.7676 |
| 70,000.0 | 0.0338 | 20,644.0 | 4.2363 |
| 80,000.0 | 0.0207 | 20,911.0 | 4.7051 |
| 90,000.0 | 0.0127 | 21,075.0 | 5.1739 |
| 100,000.0 | 0.0078 | 21,175.0 | 5.6426 |
| 200,000.0 | 0.0000 | 21,333.0 | 10.3302 |

# TABLE 2—LIMITED SYSTEMS (continued)

| Dimensionless Functions | | | |
|---|---|---|---|
| Time ($t_D$) | Rate ($q_D$) | Influx ($F_D$) | Pressure Drop ($p_D$) |
| **Dimensionless External Radius $r_D$ = 50** | | | |
| 200.0 | 1.0399 | 216.0 | 0.9570 |
| 300.0 | 1.0325 | 320.0 | 0.9641 |
| 400.0 | 1.0280 | 423.0 | 0.9693 |
| 500.0 | 1.0246 | 525.0 | 0.9732 |
| 600.0 | 1.0217 | 626.0 | 0.9765 |
| 700.0 | 1.0190 | 730.0 | 0.9795 |
| 800.0 | 1.0164 | 831.0 | 0.9823 |
| 900.0 | 1.0139 | 933.0 | 0.9850 |
| 1,000.0 | 1.0113 | 1,034.0 | 0.9880 |
| 2,000.0 | 0.9865 | 2,031.0 | 1.0120 |
| 3,000.0 | 0.9622 | 3,007.0 | 1.0360 |
| 4,000.0 | 0.9383 | 3,958.0 | 1.0600 |
| 5,000.0 | 0.9155 | 4,884.0 | 1.0840 |
| 6,000.0 | 0.8930 | 5,789.0 | 1.1080 |
| 7,000.0 | 0.8710 | 6,671.0 | 1.1320 |
| 8,000.0 | 0.8496 | 7,531.0 | 1.1560 |
| 9,000.0 | 0.8287 | 8,370.0 | 1.1800 |
| 10,000.0 | 0.8083 | 9,188.0 | 1.2040 |
| 20,000.0 | 0.6301 | 16,364.0 | 1.4440 |
| 30,000.0 | 0.4912 | 21,931.0 | 1.6840 |
| 40,000.0 | 0.3828 | 26,269.0 | 1.9240 |
| 50,000.0 | 0.2984 | 29,638.0 | 2.1640 |
| 60,000.0 | 0.2326 | 32,299.0 | 2.4040 |
| 70,000.0 | 0.1813 | 34,397.0 | 2.6440 |
| 80,000.0 | 0.1413 | 35,967.0 | 2.8840 |
| 90,000.0 | 0.1106 | 37,272.0 | 3.1240 |
| 100,000.0 | 0.0862 | 38,201.0 | 3.3640 |
| 200,000.0 | 0.0072 | 41,278.0 | 5.7641 |
| 300,000.0 | 0.0006 | 41,642.0 | 8.1641 |
| 400,000.0 | 0.0000 | 41,664.0 | 10.5641 |
| 500,000.0 | 0.0000 | 41,666.0 | 12.9641 |
| **Dimensionless External Radius $r_D$ = 60** | | | |
| 300.0 | 1.0326 | 320.0 | 0.9641 |
| 400.0 | 1.0282 | 423.0 | 0.9684 |
| 500.0 | 1.0252 | 525.0 | 0.9717 |
| 600.0 | 1.0228 | 626.0 | 0.9745 |
| 700.0 | 1.0209 | 730.0 | 0.9765 |
| 800.0 | 1.0192 | 832.0 | 0.9784 |
| 900.0 | 1.0176 | 934.0 | 0.9801 |
| 1,000.0 | 1.0160 | 1,035.0 | 0.9818 |
| 2,000.0 | 1.0035 | 2,046.0 | 0.9969 |
| 3,000.0 | 0.9873 | 3,030.0 | 1.0137 |
| 4,000.0 | 0.9732 | 4,019.0 | 1.0276 |
| 5,000.0 | 0.9594 | 4,985.0 | 1.0395 |
| 6,000.0 | 0.9457 | 5,937.0 | 1.0513 |
| 7,000.0 | 0.9323 | 6,874.0 | 1.0632 |
| 8,000.0 | 0.9190 | 7,802.0 | 1.0811 |
| 9,000.0 | 0.9060 | 8,714.0 | 1.0950 |
| 10,000.0 | 0.8931 | 9,614.0 | 1.1089 |
| 20,000.0 | 0.7739 | 17,935.0 | 1.2478 |
| 30,000.0 | 0.6708 | 25,165.0 | 1.3867 |
| 40,000.0 | 0.5813 | 31,393.0 | 1.5256 |
| 50,000.0 | 0.5036 | 36,808.0 | 1.6645 |
| 60,000.0 | 0.4363 | 41,499.0 | 1.8034 |
| 70,000.0 | 0.3780 | 45,564.0 | 1.9422 |
| 80,000.0 | 0.3275 | 49,086.0 | 2.0811 |
| 90,000.0 | 0.2838 | 52,137.0 | 2.2200 |
| 100,000.0 | 0.2458 | 54,781.0 | 2.3589 |
| 200,000.0 | 0.0590 | 67,879.0 | 3.7478 |
| 300,000.0 | 0.0141 | 71,044.0 | 5.1367 |
| 400,000.0 | 0.0034 | 71,766.0 | 6.5256 |
| 500,000.0 | 0.0008 | 71,943.0 | 7.9145 |
| 600,000.0 | 0.0002 | 71,986.0 | 9.3034 |
| 700,000.0 | 0.0000 | 71,996.0 | 10.6921 |
| 800,000.0 | 0.0000 | 72,000.0 | 12.0812 |
| **Dimensionless External Radius $r_D$ = 70** | | | |
| 700.0 | 1.0213 | 730.0 | 0.9753 |
| 800.0 | 1.0198 | 832.0 | 0.9769 |
| 900.0 | 1.0185 | 934.0 | 0.9785 |
| 1,000.0 | 1.0174 | 1,036.0 | 0.9799 |
| 2,000.0 | 1.0079 | 2,048.0 | 0.9906 |
| 3,000.0 | 0.9989 | 3,052.0 | 1.0005 |
| 4,000.0 | 0.9899 | 4,046.0 | 1.0093 |
| 5,000.0 | 0.9811 | 5,027.0 | 1.0180 |
| 6,000.0 | 0.9723 | 6,000.0 | 1.0268 |
| 7,000.0 | 0.9636 | 6,976.0 | 1.0355 |
| 8,000.0 | 0.9550 | 7,936.0 | 1.0443 |
| 9,000.0 | 0.9465 | 8,884.0 | 1.0530 |
| 10,000.0 | 0.9380 | 9,829.0 | 1.0618 |
| 20,000.0 | 0.8575 | 18,800.0 | 1.1492 |
| 30,000.0 | 0.7838 | 27,002.0 | 1.2367 |
| 40,000.0 | 0.7165 | 34,498.0 | 1.3241 |
| 50,000.0 | 0.6549 | 41,351.0 | 1.4116 |
| 60,000.0 | 0.5987 | 47,615.0 | 1.4991 |
| 70,000.0 | 0.5472 | 53,341.0 | 1.5865 |
| 80,000.0 | 0.5002 | 58,575.0 | 1.6740 |
| 90,000.0 | 0.4572 | 63,359.0 | 1.7615 |
| 100,000.0 | 0.4179 | 67,732.0 | 1.8489 |
| 200,000.0 | 0.1707 | 93,296.0 | 2.7236 |
| 300,000.0 | 0.0692 | 106,570.0 | 3.5982 |
| 400,000.0 | 0.0280 | 111,168.0 | 4.4728 |
| 500,000.0 | 0.0113 | 113,042.0 | 5.3475 |
| 600,000.0 | 0.0045 | 113,807.0 | 6.2221 |
| 700,000.0 | 0.0018 | 114,118.0 | 7.0968 |
| 800,000.0 | 0.0007 | 114,245.0 | 7.9714 |
| 900,000.0 | 0.0003 | 114,297.0 | 8.8460 |
| 1,000,000.0 | 0.0001 | 114,318.0 | 9.7207 |
| 2,000,000.0 | 0.0000 | 114,333.0 | 18.4617 |

| Dimensionless Functions | | | |
|---|---|---|---|
| Time ($t_D$) | Rate ($q_D$) | Influx ($F_D$) | Pressure Drop ($p_D$) |
| **Dimensionless External Radius $r_D$ = 80** | | | |
| 900.0 | 1.0188 | 934.0 | 0.9779 |
| 1,000.0 | 1.0178 | 1,036.0 | 0.9791 |
| 2,000.0 | 1.9108 | 2,050.0 | 0.9875 |
| 3,000.0 | 1.0047 | 3,057.0 | 0.9944 |
| 4,000.0 | 0.9987 | 4,059.0 | 1.0009 |
| 5,000.0 | 0.9927 | 5,055.0 | 1.0060 |
| 6,000.0 | 0.9868 | 6,045.0 | 1.0117 |
| 7,000.0 | 0.9809 | 7,028.0 | 1.0185 |
| 8,000.0 | 0.9750 | 8,006.0 | 1.0244 |
| 9,000.0 | 0.9692 | 8,978.0 | 1.0303 |
| 10,000.0 | 0.9634 | 9,945.0 | 1.0361 |
| 20,000.0 | 0.9073 | 19,295.0 | 1.0947 |
| 30,000.0 | 0.8545 | 28,102.0 | 1.1533 |
| 40,000.0 | 0.8048 | 36,396.0 | 1.2119 |
| 50,000.0 | 0.7579 | 44,207.0 | 1.2705 |
| 60,000.0 | 0.7138 | 51,564.0 | 1.3291 |
| 70,000.0 | 0.6723 | 58,493.0 | 1.3877 |
| 80,000.0 | 0.6331 | 65,018.0 | 1.4463 |
| 90,000.0 | 0.5963 | 71,163.0 | 1.5049 |
| 100,000.0 | 0.5616 | 76,950.0 | 1.5634 |
| 200,000.0 | 0.3081 | 119,176.0 | 2.1496 |
| 300,000.0 | 0.1697 | 142,333.0 | 2.7353 |
| 400,000.0 | 0.0933 | 155,096.0 | 3.3213 |
| 500,000.0 | 0.0512 | 162,112.0 | 3.9072 |
| 600,000.0 | 0.0281 | 165,967.0 | 4.4931 |
| 700,000.0 | 0.0155 | 168,084.0 | 5.0791 |
| 800,000.0 | 0.0085 | 169,248.0 | 5.6650 |
| 900,000.0 | 0.0047 | 169,887.0 | 6.2510 |
| 1,000,000.0 | 0.0026 | 170,238.0 | 6.8369 |
| 2,000,000.0 | 0.0000 | 170,666.0 | 12.6963 |
| **Dimensionless External Radius $r_D$ = 90** | | | |
| 1,000.0 | 1.0178 | 1,036.0 | 0.9789 |
| 2,000.0 | 1.0119 | 2,050.0 | 0.9864 |
| 3,000.0 | 1.0075 | 3,060.0 | 0.9916 |
| 4,000.0 | 1.0033 | 4,065.0 | 0.9965 |
| 5,000.0 | 0.9991 | 5,066.0 | 1.0006 |
| 6,000.0 | 0.9949 | 6,063.0 | 1.0047 |
| 7,000.0 | 0.9907 | 7,056.0 | 1.0088 |
| 8,000.0 | 0.9866 | 8,045.0 | 1.0129 |
| 9,000.0 | 0.9824 | 9,029.0 | 1.0170 |
| 10,000.0 | 0.9783 | 10,010.0 | 1.0212 |
| 20,000.0 | 0.9381 | 19,590.0 | 1.0623 |
| 30,000.0 | 0.8995 | 28,776.0 | 1.1035 |
| 40,000.0 | 0.8625 | 37,585.0 | 1.1446 |
| 50,000.0 | 0.8270 | 46,031.0 | 1.1858 |
| 60,000.0 | 0.7930 | 54,129.0 | 1.2269 |
| 70,000.0 | 0.7603 | 61,895.0 | 1.2681 |
| 80,000.0 | 0.7291 | 69,341.0 | 1.3092 |
| 90,000.0 | 0.6991 | 76,480.0 | 1.3504 |
| 100,000.0 | 0.6703 | 83,326.0 | 1.3915 |
| 200,000.0 | 0.4402 | 138,050.0 | 1.8031 |
| 300,000.0 | 0.2890 | 173,987.0 | 2.2146 |
| 400,000.0 | 0.1905 | 197,575.0 | 2.6261 |
| 500,000.0 | 0.1253 | 213,137.0 | 3.0378 |
| 600,000.0 | 0.0824 | 223,370.0 | 3.4491 |
| 700,000.0 | 0.0541 | 230,097.0 | 3.8607 |
| 800,000.0 | 0.0356 | 234,519.0 | 4.2722 |
| 900,000.0 | 0.0234 | 237,425.0 | 4.6837 |
| 1,000,000.0 | 0.0154 | 239,335.0 | 5.0952 |
| 2,000,000.0 | 0.0000 | 243,000.0 | 9.2104 |
| **Dimensionless External Radius $r_D$ = 100** | | | |
| 1,000.0 | 1.0178 | 1,036.0 | 0.9789 |
| 2,000.0 | 1.0123 | 2,050.0 | 0.9853 |
| 3,000.0 | 1.0090 | 3,061.0 | 0.9874 |
| 4,000.0 | 1.0058 | 4,068.0 | 0.9930 |
| 5,000.0 | 1.0028 | 5,073.0 | 0.9964 |
| 6,000.0 | 0.9997 | 6,074.0 | 1.0000 |
| 7,000.0 | 0.9967 | 7,072.0 | 1.0030 |
| 8,000.0 | 0.9936 | 8,067.0 | 1.0060 |
| 9,000.0 | 0.9906 | 9,059.0 | 1.0090 |
| 10,000.0 | 0.9876 | 10,048.0 | 1.0120 |
| 20,000.0 | 0.9578 | 19,775.0 | 1.0420 |
| 30,000.0 | 0.9290 | 29,208.0 | 1.0720 |
| 40,000.0 | 0.9010 | 38,358.0 | 1.1020 |
| 50,000.0 | 0.8739 | 47,232.0 | 1.1320 |
| 60,000.0 | 0.8476 | 55,839.0 | 1.1620 |
| 70,000.0 | 0.8221 | 64,187.0 | 1.1920 |
| 80,000.0 | 0.7974 | 72,283.0 | 1.2220 |
| 90,000.0 | 0.7733 | 80,136.0 | 1.2520 |
| 100,000.0 | 0.7501 | 87,753.0 | 1.2820 |
| 200,000.0 | 0.5525 | 152,377.0 | 1.5820 |
| 300,000.0 | 0.4158 | 199,972.0 | 1.8820 |
| 400,000.0 | 0.2995 | 235,018.0 | 2.1820 |
| 500,000.0 | 0.2210 | 260,815.0 | 2.4820 |
| 600,000.0 | 0.1630 | 279,849.0 | 2.7820 |
| 700,000.0 | 0.1203 | 293,918.0 | 3.0820 |
| 800,000.0 | 0.0887 | 304,287.0 | 3.3820 |
| 900,000.0 | 0.0655 | 311,928.0 | 3.6820 |
| 1,000,000.0 | 0.0483 | 317,558.0 | 3.9820 |
| 2,000,000.0 | 0.0000 | 333,333.0 | 6.9820 |

TABLE 3 — LIMITED SYSTEMS
Open External Boundary

| Time ($t_D$) | Rate ($q_D$) | Influx ($F_D$) | Pressure Drop ($p_D$) |
|---|---|---|---|
| | **Dimensionless External Radius $r'_D = 2$** | | |
| 0.07 | 3.1324 | 0.3685 | 0.2404 |
| 0.08 | 2.9947 | 0.3992 | 0.2534 |
| 0.09 | 2.8807 | 0.4285 | 0.2654 |
| 0.10 | 2.7843 | 0.4568 | 0.2764 |
| 0.20 | 2.2786 | 0.7052 | 0.3558 |
| 0.30 | 2.1036 | 0.9[illegible]8 | 0.4048 |
| 0.40 | 2.0386 | 1.1294 | 0.4370 |
| 0.50 | 2.0144 | 1.3319 | 0.4582 |
| 0.60 | 2.0054 | 1.5328 | 0.4723 |
| 0.70 | 2.0020 | 1.7331 | 0.4817 |
| 0.80 | 2.0007 | 1.9333 | 0.4878 |
| 0.90 | 2.0003 | 2.1333 | 0.4919 |
| 1.00 | 2.0001 | 2.3333 | 0.4947 |
| 2.00 | 2.0000 | 4.3333 | 0.4999 |
| 3.00 | 2.0000 | 6.3333 | 0.5000 |
| | **Dimensionless External Radius $r'_D = 3$** | | |
| 0.2 | 2.2616 | 0.7046 | 0.3562 |
| 0.3 | 2.0301 | 0.9180 | 0.4080 |
| 0.4 | 1.8921 | 1.1137 | 0.4464 |
| 0.5 | 1.7984 | 1.2979 | 0.4768 |
| 0.6 | 1.7302 | 1.4742 | 0.5019 |
| 0.7 | 1.6788 | 1.6445 | 0.5230 |
| 0.8 | 1.6393 | 1.8103 | 0.5412 |
| 0.9 | 1.6087 | 1.9727 | 0.5568 |
| 1.0 | 1.5849 | 2.1323 | 0.5704 |
| 2.0 | 1.5072 | 3.6638 | 0.6407 |
| 3.0 | 1.5006 | 5.1664 | 0.6597 |
| 4.0 | 1.5001 | 6.6666 | 0.6648 |
| 5.0 | 1.5000 | 8.1667 | 0.6661 |
| 6.0 | 1.5000 | 9.6667 | 0.6665 |
| 7.0 | 1.5000 | 11.1667 | 0.6666 |
| | **Dimensionless External Radius $r'_D = 4$** | | |
| 0.7 | 1.6743 | 1.6441 | 0.5233 |
| 0.8 | 1.6308 | 1.8093 | 0.5418 |
| 0.9 | 1.5948 | 1.9705 | 0.5580 |
| 1.0 | 1.5643 | 2.1284 | 0.5724 |
| 2.0 | 1.4078 | 3.5988 | 0.6625 |
| 3.0 | 1.3582 | 4.9773 | 0.7054 |
| 4.0 | 1.3416 | 6.3258 | 0.7272 |
| 5.0 | 1.3361 | 7.6641 | 0.7383 |
| 6.0 | 1.3343 | 8.9992 | 0.7440 |
| 7.0 | 1.3336 | 10.3331 | 0.7469 |
| 8.0 | 1.3334 | 11.6666 | 0.7484 |
| 9.0 | 1.3334 | 13.0000 | 0.7492 |
| 10.0 | 1.3333 | 14.3333 | 0.7496 |
| 20.0 | 1.3333 | 27.6667 | 0.7500 |
| | **Dimensionless External Radius $r'_D = 5$** | | |
| 1.0 | 1.5642 | 2.1284 | 0.5724 |
| 2.0 | 1.3992 | 3.5958 | 0.6638 |
| 3.0 | 1.3289 | 4.9558 | 0.7121 |
| 4.0 | 1.2924 | 6.2646 | 0.7422 |
| 5.0 | 1.2729 | 7.5462 | 0.7618 |
| 6.0 | 1.2623 | 8.8133 | 0.7748 |
| 7.0 | 1.2567 | 10.0725 | 0.7833 |
| 8.0 | 1.2536 | 11.3275 | 0.7890 |
| 9.0 | 1.2519 | 12.5802 | 0.7927 |
| 10.0 | 1.2510 | 13.8316 | 0.7952 |
| 20.0 | 1.2500 | 26.3333 | 0.7999 |
| 30.0 | 1.2500 | 38.8333 | 0.8000 |
| | **Dimensionless External Radius $r'_D = 6$** | | |
| 2.0 | 1.3989 | 3.5958 | 0.6638 |
| 3.0 | 1.3259 | 4.9545 | 0.7126 |
| 4.0 | 1.2832 | 6.2573 | 0.7444 |
| 5.0 | 1.2557 | 7.5258 | 0.7669 |
| 6.0 | 1.2375 | 8.7718 | 0.7834 |
| 7.0 | 1.2252 | 10.0028 | 0.7957 |
| 8.0 | 1.2170 | 11.2236 | 0.8050 |
| 9.0 | 1.2115 | 12.4377 | 0.8119 |
| 10.0 | 1.2077 | 13.6471 | 0.8172 |
| 20.0 | 1.2001 | 25.6663 | 0.8324 |
| 30.0 | 1.2000 | 37.6667 | 0.8333 |
| 40.0 | 1.2000 | 49.6667 | 0.8333 |

| Time ($t_D$) | Rate ($q_D$) | Influx ($F_D$) | Pressure Drop ($p_D$) |
|---|---|---|---|
| | **Dimensionless External Radius $r'_D = 7$** | | |
| 3.0 | 1.3257 | 4.9544 | 0.7127 |
| 4.0 | 1.2822 | 6.2568 | 0.7446 |
| 5.0 | 1.2527 | 7.5234 | 0.7676 |
| 6.0 | 1.2315 | 8.7649 | 0.7851 |
| 7.0 | 1.2157 | 9.9881 | 0.7988 |
| 8.0 | 1.2039 | 11.1977 | 0.8098 |
| 9.0 | 1.1950 | 12.3969 | 0.8187 |
| 10.0 | 1.1882 | 13.5883 | 0.8258 |
| 20.0 | 1.1681 | 25.3283 | 0.8531 |
| 30.0 | 1.1668 | 37.0000 | 0.8566 |
| 40.0 | 1.1667 | 48.6666 | 0.8571 |
| 50.0 | 1.1667 | 60.3333 | 0.8571 |
| | **Dimensionless External Radius $r'_D = 8$** | | |
| 4.0 | 1.2821 | 6.2568 | 0.7446 |
| 5.0 | 1.2523 | 7.5233 | 0.7676 |
| 6.0 | 1.2305 | 8.7640 | 0.7853 |
| 7.0 | 1.2136 | 9.9857 | 0.7944 |
| 8.0 | 1.2003 | 11.1925 | 0.8109 |
| 9.0 | 1.1897 | 12.3873 | 0.8205 |
| 10.0 | 1.1811 | 13.5725 | 0.8285 |
| 20.0 | 1.1479 | 25.1652 | 0.8653 |
| 30.0 | 1.1435 | 36.8157 | 0.8730 |
| 40.0 | 1.1429 | 48.0472 | 0.8746 |
| 50.0 | 1.1429 | 59.4761 | 0.8749 |
| 60.0 | 1.1429 | 70.9048 | 0.8750 |
| 70.0 | 1.1429 | 82.3333 | 0.8750 |
| | **Dimensionless External Radius $r'_D = 9$** | | |
| 5.0 | 1.2523 | 7.5231 | 0.7676 |
| 6.0 | 1.2303 | 8.7640 | 0.7853 |
| 7.0 | 1.2133 | 9.9854 | 0.7995 |
| 8.0 | 1.1996 | 11.1917 | 0.8111 |
| 9.0 | 1.1884 | 12.3855 | 0.8209 |
| 10.0 | 1.1790 | 13.5690 | 0.8292 |
| 20.0 | 1.1384 | 25.0925 | 0.8717 |
| 30.0 | 1.1274 | 36.4008 | 0.8838 |
| 40.0 | 1.1255 | 47.6633 | 0.8874 |
| 50.0 | 1.1251 | 58.9159 | 0.8884 |
| 60.0 | 1.1250 | 70.1665 | 0.8888 |
| 70.0 | 1.1250 | 81.4166 | 0.8889 |
| 80.0 | 1.1250 | 92.6667 | 0.8889 |
| | **Dimensionless External Radius $r'_D = 10$** | | |
| 6.0 | 1.2303 | 8.764 | 0.7853 |
| 7.0 | 1.2132 | 9.985 | 0.7994 |
| 8.0 | 1.1995 | 11.192 | 0.8111 |
| 9.0 | 1.1881 | 12.385 | 0.8209 |
| 10.0 | 1.1785 | 13.568 | 0.8293 |
| 20.0 | 1.1306 | 25.063 | 0.8747 |
| 30.0 | 1.1169 | 36.286 | 0.8906 |
| 40.0 | 1.1128 | 47.431 | 0.8965 |
| 50.0 | 1.1116 | 58.551 | 0.8987 |
| 60.0 | 1.1113 | 69.665 | 0.8995 |
| 70.0 | 1.1112 | 80.777 | 0.8998 |
| 80.0 | 1.1111 | 91.889 | 0.8999 |
| 90.0 | 1.1111 | 103.000 | 0.9000 |
| | **Dimensionless External Radius $r'_D = 20$** | | |
| 30.0 | 1.1030 | 36.180 | 0.8977 |
| 40.0 | 1.0892 | 47.137 | 0.9106 |
| 50.0 | 1.0799 | 57.980 | 0.9193 |
| 60.0 | 1.0732 | 68.743 | 0.9261 |
| 70.0 | 1.0682 | 79.449 | 0.9312 |
| 80.0 | 1.0645 | 90.112 | 0.9351 |
| 90.0 | 1.0616 | 100.741 | 0.9382 |
| 100.0 | 1.0595 | 111.346 | 0.9406 |
| 200.0 | 1.0531 | 216.843 | 0.9486 |
| 300.0 | 1.0527 | 322.122 | 0.9495 |
| 400.0 | 1.0526 | 427.386 | 0.9497 |
| 500.0 | 1.0526 | 532.649 | 0.9499 |
| 600.0 | 1.0526 | 637.912 | 0.9500 |

$$p_D(r_D, t_D) = \frac{r_D'-r_D}{r_D' r_D} + \frac{2(r_D'-1)}{r_D} \sum_{n=1}^{\infty} \times \frac{\exp\left[-\frac{\omega_n^2 t_D}{(r_D'-1)^2}\right] \sin\left[\omega_n\left(\frac{r_D'-r_D}{r_D'-1}\right)\right]}{\omega_n[r_D'(r_D'-1)+\omega_n^2]\cos\omega_n} \quad \ldots\ldots\ldots\ldots\ldots\ldots\ldots\ldots (62)$$

where $\omega_n$ are the roots of the equation:

$$\frac{\tan w}{w} = -\frac{1}{r_D'-1} \quad \ldots\ldots\ldots\ldots (63)$$

Upon placing $r_D$ at unity in Eq. 62 and simplifying, the dimensionless pressure drop is obtained:

$$p_D = \frac{r_D'-1}{r_D'} - 2(r_D'-1) \sum_{n=1}^{\infty} \frac{\exp\left[-\frac{\omega_n^2 t_D}{(r_D'-1)^2}\right]}{r_D'(r_D'-1)+\omega_n^2}, \quad \ldots (64)$$

which is the concluding result.[9-11,17]

## NUMERICAL COMPUTATION OF PARTICULAR SOLUTIONS

Nine particular solutions to Eq. 7 obtained with the aid of the Laplace transformation were numerically computed. Specifically, these included the functions defined by Eqs. 34, 36, 40, 46, 49, 53, 58, 60 and 64.

The numerical computations were carried out with the aid of IBM 1401 and 1620 computer systems. Programming was in FORTRAN. The functions for

TABLE 3 — LIMITED SYSTEMS (Continued)

| Time ($t_D$) | Rate ($q_D$) | Influx ($F_D$) | Pressure Drop ($p_D$) |
|---|---|---|---|
| | Dimensionless Functions | | |
| | Dimensionless External Radius $r_D'$ = 30 | | |
| 80.0 | 1.0631 | 90.093 | 0.9351 |
| 90.0 | 1.0595 | 100.705 | 0.9385 |
| 100.0 | 1.0564 | 111.284 | 0.9414 |
| 200.0 | 1.0411 | 216.001 | 0.9576 |
| 300.0 | 1.0365 | 319.838 | 0.9629 |
| 400.0 | 1.0351 | 423.406 | 0.9649 |
| 500.0 | 1.0347 | 526.891 | 0.9656 |
| 600.0 | 1.0345 | 630.351 | 0.9660 |
| 700.0 | 1.0345 | 733.803 | 0.9662 |
| 800.0 | 1.0345 | 837.252 | 0.9664 |
| 900.0 | 1.0345 | 940.701 | 0.9665 |
| 1,000.0 | 1.0345 | 1,044.149 | 0.9667 |
| | Dimensionless External Radius $r_D'$ = 40 | | |
| 100.0 | 1.0564 | 111.28 | 0.9414 |
| 200.0 | 1.0399 | 215.96 | 0.9570 |
| 300.0 | 1.0330 | 319.56 | 0.9646 |
| 400.0 | 1.0295 | 422.67 | 0.9686 |
| 500.0 | 1.0278 | 525.51 | 0.9708 |
| 600.0 | 1.0267 | 628.22 | 0.9721 |
| 700.0 | 1.0262 | 730.86 | 0.9729 |
| 800.0 | 1.0259 | 833.47 | 0.9734 |
| 900.0 | 1.0258 | 936.05 | 0.9737 |
| 1,000.0 | 1.0257 | 1,038.63 | 0.9739 |
| 2,000.0 | 1.0256 | 2,064.28 | 0.9750 |
| | Dimensionless External Radius $r_D'$ = 50 | | |
| 200.0 | 1.0399 | 215.96 | 0.9570 |
| 300.0 | 1.0326 | 319.54 | 0.9641 |
| 400.0 | 1.0283 | 422.58 | 0.9688 |
| 500.0 | 1.0256 | 525.27 | 0.9718 |
| 600.0 | 1.0239 | 627.74 | 0.9739 |
| 700.0 | 1.0227 | 730.06 | 0.9754 |
| 800.0 | 1.0219 | 832.29 | 0.9764 |
| 900.0 | 1.0214 | 934.46 | 0.9771 |
| 1,000.0 | 1.0211 | 1,036.58 | 0.9776 |
| 2,000.0 | 1.0204 | 2,057.15 | 0.9794 |
| 3,000.0 | 1.0204 | 3,077.56 | 0.9800 |
| | Dimensionless External Radius $r_D'$ = 60 | | |
| 300.0 | 1.0326 | 319.54 | 0.9641 |
| 400.0 | 1.0282 | 422.57 | 0.9684 |
| 500.0 | 1.0253 | 525.23 | 0.9716 |
| 600.0 | 1.0232 | 627.65 | 0.9740 |
| 700.0 | 1.0216 | 729.89 | 0.9758 |
| 800.0 | 1.0205 | 831.99 | 0.9772 |
| 900.0 | 1.0196 | 933.99 | 0.9783 |
| 1,000.0 | 1.0189 | 1,035.91 | 0.9792 |
| 2,000.0 | 1.0171 | 2,053.52 | 0.9822 |
| 3,000.0 | 1.0170 | 3,070.51 | 0.9829 |
| 4,000.0 | 1.0169 | 4,087.46 | 0.9833 |

| Time ($t_D$) | Rate ($q_D$) | Influx ($F_D$) | Pressure Drop ($p_D$) |
|---|---|---|---|
| | Dimensionless Functions | | |
| | Dimensionless External Radius $r_D'$ = 70 | | |
| 700.0 | 1.0213 | 730.0 | 0.9753 |
| 800.0 | 1.0200 | 832.0 | 0.9767 |
| 900.0 | 1.0190 | 934.0 | 0.9781 |
| 1,000.0 | 1.0181 | 1,036.0 | 0.9795 |
| 2,000.0 | 1.0150 | 2,052.0 | 0.9838 |
| 3,000.0 | 1.0146 | 3,066.0 | 0.9848 |
| 4,000.0 | 1.0145 | 4,081.0 | 0.9853 |
| 5,000.0 | 1.0145 | 5,095.0 | 0.9857 |
| 6,000.0 | 1.0145 | 6,110.0 | 0.9857 |
| | Dimensionless External Radius $r_D'$ = 80 | | |
| 900.0 | 1.0188 | 934.0 | 0.9779 |
| 1,000.0 | 1.0179 | 1,036.0 | 0.9794 |
| 2,000.0 | 1.0137 | 2,051.0 | 0.9847 |
| 3,000.0 | 1.0129 | 3,064.0 | 0.9862 |
| 4,000.0 | 1.0127 | 4,077.0 | 0.9868 |
| 5,000.0 | 1.0127 | 5,090.0 | 0.9872 |
| 6,000.0 | 1.0127 | 6,102.0 | 0.9875 |
| 7,000.0 | 1.0127 | 7,115.0 | 0.9875 |
| | Dimensionless External Radius $r_D'$ = 90 | | |
| 1,000.0 | 1.0178 | 1,036.0 | 0.9789 |
| 2,000.0 | 1.0131 | 2,051.0 | 0.9850 |
| 3,000.0 | 1.0118 | 3,063.0 | 0.9870 |
| 4,000.0 | 1.0114 | 4,074.0 | 0.9878 |
| 5,000.0 | 1.0113 | 5,086.0 | 0.9883 |
| 6,000.0 | 1.0112 | 6,097.0 | 0.9886 |
| 7,000.0 | 1.0112 | 7,108.0 | 0.9889 |
| 8,000.0 | 1.0112 | 8,120.0 | 0.9889 |
| | Dimensionless External Radius $r_D'$ = 100 | | |
| 1,000.0 | 1.0178 | 1,036.0 | 0.9789 |
| 2,000.0 | 1.0128 | 2,051.0 | 0.9846 |
| 3,000.0 | 1.0111 | 3,062.0 | 0.9874 |
| 4,000.0 | 1.0105 | 4,073.0 | 0.9885 |
| 5,000.0 | 1.0102 | 5,083.0 | 0.9891 |
| 6,000.0 | 1.0101 | 6,094.0 | 0.9894 |
| 7,000.0 | 1.0101 | 7,104.0 | 0.9897 |
| 8,000.0 | 1.0101 | 8,114.0 | 0.9899 |
| 9,000.0 | 1.0101 | 9,124.0 | 0.9900 |

the unlimited system were computed first over the dimensionless time range 0.001 to 1,000,000. Then tables of the trigonometric relations described by Eqs. 47, 52 and 63 were developed from which the roots $w_n$ (with $n = 6$) were obtained. Finally, numerical values of the functions for limited systems were computed over the range of external radii ($r_D'$) 2 to 100. The range of dimensionless time ($t_D$) for these functions was chosen to begin with the points of divergence from the unlimited system envelope and to end with steady-state values. These numerical results are included in tabular form to foster practical application of this work.

## NOMENCLATURE

$C_1, C_2$ = arbitrary constants
$F$ = cumulative fluid influx
$F_D$ = dimensionless cumulative fluid influx
$\bar{F}_D$ = Laplace transform of $F_D$
$R_0$ = residue of singularity at origin
$R_n$ = residues of singularities at $z_n$
$b$ = dimensionless product of pressure drop and radial distance
$\bar{b}$ = Laplace transform of $b$
$c$ = compressibility
$e$ = rate of fluid influx or fluid rate
$e_D$ = dimensionless rate of fluid influx
$\bar{e}_D$ = Laplace transform of $e_D$
$k$ = permeability
$k_h$ = horizontal permeability
$k_r$ = radial permeability in spherical system
$k_v$ = vertical permeability
$n$ = element of domain of positive integers
$p$ = pressure
$p_i$ = initial pressure
$p_D$ = dimensionless pressure drop
$r$ = radial distance, length of radius vector of sphere
$r_e$ = radius of external boundary
$r_w$ = radius of internal boundary
$r_D$ = dimensionless radial distance
$r_D'$ = dimensionless radius of external boundary
$s$ = Laplace transform parameter, = complex variable
$t$ = time
$t_r$ = readjustment time
$t_D$ = dimensionless time
$t'$ = maximum time
$u$ = macroscopic velocity in porous media
$w$ = arbitrary real variable
$z$ = complex variable
$\alpha$ = colatitude angle, spherical coordinates
$\gamma$ = abscissa of convergence
$\delta$ = arbitrary parameter
$\theta$ = longitudinal angle, spherical coordinates
$\theta_4$ = Jacobian theta function, also denoted by $\theta_0$ or $\theta$
$\mu$ = viscosity
$\phi$ = porosity
$\Delta p$ = cumulative pressure drop


## ACKNOWLEDGMENTS

Grateful acknowledgment is made to A. S. Odeh of Mobil Oil Co.'s Field Research Laboratories who reviewed this work, critically checked the mathematics and offered some valuable criticisms. The author wishes to express his appreciation to Deno Ladas of IBM Corp. for his help in programming the analytic functions and to William Chichester, for his help in their computation. Thankful acknowledgment is also made to H. L. Smith of the U. S. Corps of Engineers for his practical suggestions and encouragement to publish this paper.


## REFERENCES


1. Hurst, W.: "Water Influx Into a Reservoir and Its Application to the Equation of Volumetric Balance", *Trans.*, AIME (1943) Vol. 151, 57.
2. Hurst, W. and van Everdingen, A. F.: "The Application of the Laplace Transformation to Flow Problems in Reservoirs", *Trans.*, AIME (1949) Vol. 186, 305.
3. Muskat, M.: *The Flow of Homogeneous Fluids Through Porous Media*, J. W. Edwards, Ann Arbor (1946).
4. Muskat, M.: *Physical Principles of Oil Production*, McGraw-Hill Book Co., New York, N. Y. (1949).
5. Chatas, A. T.: "A Practical Treatment of Nonsteady-State Flow Problems in Reservoir Systems", *Pet. Eng.* (May, June and Aug., 1953) 25.
6. Muskat, M.: "The Performance of Bottom-Water Drive Reservoirs", *Trans.*, AIME (1947) Vol. 170, 81.
7. Hurst, W.: "The Skin Effect and Its Impediment to Fluid Flow into a Wellbore", *Pet. Eng.* (Oct., 1953) Vol. 25, B-6.
8. Eisenhart, L. P.: *An Introduction to Differential Geometry with the Use of the Tensor Calculus*, Princeton U. Press, Princeton, N. J. (1947).
9. Churchill, R. V.: *Modern Operational Mathematics in Engineering*, McGraw-Hill Book Co., New York, N.Y. (1944).
10. Widder, D. V.: *The Laplace Transform*, Princeton U. Press, Princeton, N. J. (1946).
11. Carslaw, H. S. and Jaeger, J. C.: *Operational Methods in Applied Mathematics*, Dover, New York (1963).
12. Bush, V.: *Operational Circuit Analysis*, John Wiley & Sons, Inc., New York, N. Y. (1929).
13. Abramowitz, M. and Stegun, I. A.: *Handbook of Mathematical Functions*, U. S. Government Printing Office, Washington, D. C. (1964).
14. Erdelyi, A. *et al.*: *Tables of Integral Transforms*, McGraw-Hill Book Co., New York, N.Y. (1954) Vol. 1.
15. Hildebrand, F. B.: *Advanced Calculus for Engineers*, Prentice-Hall, Inc., Inglewood Cliffs, N. J. (1948).
16. Murnaghan, F. D.: *Introduction to Applied Mathematics*, Dover, New York (1963).
17. Churchill, R. V.: *Introduction to Complex Variables and Applications*, McGraw-Hill Book Co., New York, N. Y. (1948).
18. Korn, G. A. and Korn, T. M.: *Mathematical Handbook for Scientists and Engineers*, McGraw-Hill Book Co., New York, N. Y. (1961).
19. Erdelyi, A. *et al.*: *Higher Transcendental Functions*, McGraw-Hill Book Co., New York, N.Y. (1953) Vol. II.
20. Carslaw, H. S. and Jaeger, J. C.: *Conduction of Heat in Solids*, Oxford U. Press, Oxford, England (1959).

Dr. Heber Cinco

[Reprinted from the Journal of the Institute of Petroleum, Vol. 48, No. 467, pp. 365–379, November 1962.]

# THEORY OF UNSTEADY-STATE INFLUX OF WATER IN LINEAR RESERVOIRS*

By FRANK G. MILLER†

*Symbols*

$x$ = distance from oil reservoir (measured in aquifer)
$L$ = length of aquifer
$b$ = width of aquifer
$h$ = thickness of aquifer
$u$ = microscopic velocity
$\bar{u}$ = average microscopic velocity
$Q$ = volumetric rate of flow
$A$ = bulk cross-sectional area transverse to direction of flow
$q$ = macroscopic velocity
$\phi$ = fractional porosity
$s$ = distance
$\theta$ = time
$\gamma$ = mass density
$k$ = absolute permeability
$\mu$ = viscosity
$P$ = pressure
$\Delta P$ = pressure drop
$\bar{P}$ = mean pressure
$T$ = absolute temperature
$x_e$ = unit length
$\sigma = \frac{k}{\phi\mu c}$
$\psi$ = a function of $x$ and $\theta$

Dimensionless quantities (defined in context):

$\Delta P$ = dimensionless pressure drop
$t$ = dimensionless time
$Q_D$ = dimensionless volumetric rate of flow
$Q_C$ = dimensionless cumulative influx
$\left(\frac{\Delta P}{Q_D}\right)$ = dimensionless pressure function
$\left(\frac{Q_D}{\Delta P}\right)$ = dimensionless flow function
$F(t)$ = function of $t$

## INTRODUCTION

This report describes the theoretical behaviour of linear systems of oil reservoirs and adjoining high-pressure aquifers under conditions of transient flow of fluids. The present work augments that of van Everdingen and Hurst[1] and Chatas.[2] They dealt almost entirely with radial flow, giving little attention to linear flow.

The structure or configuration of oil reservoir–aquifer systems is seldom, if ever, known with a high degree of precision. Geological evidence would indicate generally that the geometry is neither strictly radial nor strictly linear. If it is one or the other the equations developed either in the cited work or in this paper would describe the flow behaviour without qualification. Although the true performance of systems of mixed geometry can usually be estimated better with ideal radial-flow equations than with ideal linear-flow equations, there are many instances when the latter are the more appropriate. Of further importance, the linear equations would be expected to yield the more conservative estimates of oil recovery.

Van Everdingen and Hurst, with regard to linear systems, indicate briefly a method of solving problems pertaining to infinite aquifers. They do not treat linear aquifers of finite length. Chatas' work on linear systems also relates only to aquifers of infinite length. He offers solutions to four problems which differ from one another by the boundary conditions at the outflow end of the aquifer adjacent to the oil reservoir: constant pressure, constant volumetric rate of flow, pressure an arbitrary function of time, and volumetric rate of flow an arbitrary function of time. In all four the pressure initially is uniformly high throughout the aquifer. No numerical examples are presented.

An excellent review of steady- and unsteady-state flow in reservoirs has been published recently.[3] It summarizes the status of knowledge on the subject and provides an extensive bibliography. The review includes unsteady-state compressible-liquid flow. The treatment does not go beyond that given by the foregoing investigators, however.

In the present study the concept of unsteady-state fluid flow in porous media is discussed. Problems on the unsteady-state flow of water in linear aquifers of both finite and infinite length are solved. The pressure distribution within finite and infinite aquifers is determined as a function of time for conditions of a constant pressure or a constant volumetric rate of flow at the outflow end, which is represented by the original plane of contact of the water in the aquifer and the oil in the oil reservoir. The relationship at this terminal plane between volumetric rate of flow and time is determined for the constant and variable pressure cases. The relationship between pressure and time is determined for the constant and variable rate cases. For convenience in application, results are plotted in dimensionless form where practicable. Numerical examples are offered.

The present work is intended to fill a need in petroleum literature for further data on the theoretical flow behaviour of linear systems of oil reservoirs and adjoining high pressure aquifers.

* MS received 21 February 1962. † Dept of Petroleum Engineering, Stanford University, Stanford, California.

## SIMPLIFIED GEOMETRY OF FLUID-CONNECTED OIL RESERVOIRS AND AQUIFERS

*Linear Systems*

Fig 1 is a schematic plan view of a linear oil reservoir–aquifer system of the kind discussed in this paper. The right-hand boundary of the aquifer at $x = L$ would be either a finite or an infinite distance from the oil reservoir, depending on the particular problem under study. Initially the vertical plane of contact of the reservoir oil and aquifer water would be

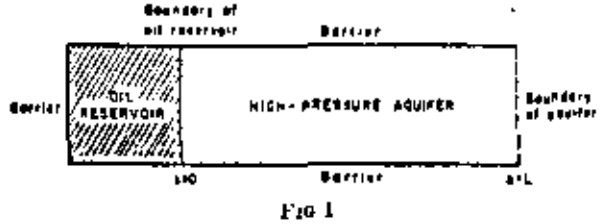


FIG 1

SCHEMATIC DRAWING OF A LINEAR RESERVOIR SYSTEM

at $x = 0$. In an actual system in the field, the parallel barriers along the top and bottom of the figure and the one at the left-hand side could be impermeable vertical fault zones. The sand or other porous rock comprising the solid matrix of the system would be homogeneous and its thickness constant.

At time zero, just before oil producing operations are begun, the oil reservoir would be filled with evenly distributed liquid oil undersaturated with gas and immobile interstitial water. Also at this time the water in the aquifer and the fluids in the oil reservoir would be at a uniformly high pressure. The temperature of the fluids in the system as a whole would be assumed the same at all points and independent of time.

Oil producing operations would cause water to move into the oil reservoir under conditions of unsteady-state flow. The nature of this flow phenomenon is discussed in the next main section of this report. In the subsequent theoretical analyses the oil is considered to remain undersaturated with gas throughout the oil-productive life of the reservoir. Because of the homogeneity of the reservoir rock and the even distribution of the oil-reservoir fluids initially, proper well control would result in the production of oil only. The volumetric rate of oil production in the calculations is assumed equivalent to the volumetric rate of flow of water at $x = 0$. This assumption introduces an error that could be corrected through application of appropriate formation-volume-factor data. Such a refinement would be unwarranted, however, because significantly greater errors would be likely to occur as a result of treating any actual reservoir as if its geometry was idealized linear-flow-system geometry.

The pressure or flow conditions specified at $x = 0$ and the length of the aquifer, whether finite or infinite, cause the differences among the oil-production problems discussed.

*Radial Systems*

In comparison to Fig 1, the oil reservoir of a radial system would be circular instead of rectangular. Radius $r_w$ at the periphery of the circle would represent the initial vertical, cylindrical surface of contact between the oil in the oil reservoir and the water in the aquifer. The outer boundary of the aquifer at $r_e$ would be a circle concentric with the initial oil–water contact. As in the linear system, the thickness of the porous rock comprising the aquifer would be considered constant and its thickness uniform. Reservoir temperature, initial reservoir pressure, and fluid properties and their distribution also would be considered similarly.

Radial systems received most of the attention of van Everdingen and Hurst, and Chatas. Differences among the reservoir problems investigated by them may be attributed to variations in the pressure and flow conditions imposed at $r_w$, and to the finite or infinite size of the aquifer.

These systems may be construed to represent oil reservoirs within circular aquifers or single wells within closed oil reservoirs. In the former, the boundary of the oil reservoir is the outflow face of the aquifer. In the latter, the wall of the well is the outflow face of the oil reservoir. In both instances the oil reservoir is assumed circular.

## CONCEPT OF UNSTEADY-STATE SINGLE-PHASE FLOW IN POROUS MEDIA

*Microscopic and Macroscopic Velocities*

In ordinary fluid-flow problems the boundaries of the flow channel or conduit can almost always be described mathematically. With a few possible exceptions, the geometry of the pore channels within porous media cannot be so described. Problems relating to flow through porous media are solved, therefore, by techniques differing from those commonly used in other branches of fluid mechanics.

The basic law of flow applied generally to porous oil-reservoir rocks is Darcy's law, which was established experimentally more than a century ago. This law states that the macroscopic velocity of the fluid in the direction of flow at any particular point within the porous medium is proportional to the instantaneous gradient in fluid head or flow potential at the point.

Fig 2 is a schematic diagram of porous medium through which a single-phase fluid is flowing. The path of flow of a particular fluid particle moving through the system is shown. At one point its velocity is $v_m$. This is its microscopic velocity at this point at the instant of time represented by the diagram. The instantaneous direction of movement

is indicated by the arrow tangent to the path of flow. Microscopic velocities are true velocities. They apply to all points within the fluid occupying the pore space. Their values at arbitrarily selected points cannot be

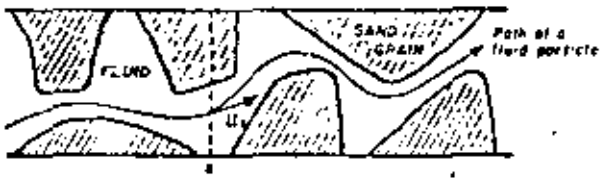


FIG 2

PATH OF A FLUID PARTICLE IN A MACROSCOPICALLY-LINEAR FLOW SYSTEM

When particle is at X its microscopic velocity is $u_x$

calculated, however, without mathematical definition of the geometry of the pore channels. Even if such definition could be developed, it would probably be so complicated as to make calculation of the microscopic velocity impractical.

Macroscopic velocities, in contrast to microscopic velocities, are not true velocities. They are of great practical importance, however, and can be calculated without knowledge of pore-channel geometry. Macroscopic velocity is defined as the volumetric rate of flow per unit of bulk area transverse to the macroscopic direction of flow and is referred to a point in the system. The macroscopic direction of flow is the statistical average direction of movement of the fluid particles in the neighbourhood of the point in question.

Referring again to Fig 2, the total bulk cross-sectional area perpendicular to the plane of the paper would be uniform in the direction of the axis because the flow is specified to be macroscopically linear. Therefore, in the sense of macroscopic flow behaviour, all sections transverse to the $X$ axis are equi-potential surfaces. If the flow is from left to right as shown and if $Q$ is the volumetric rate at $x$, then by definition $Q/A$ is the macroscopic velocity $q$ at this section. This velocity would have the same magnitude and direction at all points of the transverse area. The direction would be parallel to and in the positive direction of the $X$ axis. Generally, in non-linear systems the macroscopic velocity is not the same at all points of equipotential surfaces. It is defined more precisely therefore as $dQ/dA$.

In accordance with the described concept of macroscopic flow, the solid matrix of the porous medium and the fluid occupying the pore channels are envisioned together as a composite conductor of fluids, the rate of flow being proportional at any point to the gradient in the flow potential. This is the concept underlying Darcy's law.

Macroscopic and microscopic velocities may be related. The microscopic velocity $u_x$ (Fig 1) would have components $u_x$, $u_y$, and $u_z$ in the directions of the co-ordinate axes. If the section at $x$ is a statistically average section the area presented to flow would be $A\phi$. As the net flow is in the positive $X$ direction only, the mean value of $u_x$, designated $\bar{u}_x$, would be equal to $u_x$ itself at all fluid-occupied points.

No net flow normal to the $X$ axis means also that $\bar{u}_y$ and $\bar{u}_z$ would each be zero. All components of $u_x$ in the negative directions of the $Y$ and $Z$ axes would cancel respectively all components in the positive directions of these axes. Thus the volumetric rate of flow $Q$, at $x$, would be $A\phi\bar{u}_x$. From the definition of macroscopic velocity the volumetric rate of flow at $x$ is equivalent to $qA$. Hence,

$$q = \bar{u}\phi \quad . \quad . \quad . \quad . \quad . \quad (1)$$

in which the subscript $x$ has been dropped.

*Distinction of States of Fluid Motion*

A moving single-phase fluid would be in a state of steady motion if its properties and the forces acting on it at any given point in the flow system are independent of time. Otherwise it would be in a state of unsteady motion.

Considering streamline motion as is the case in Darcy-law flow, the fluid-particle velocity $u$, would be a function of the distance along the path of flow $s$ and time $\theta$. A small change in $u$, may be expressed therefore by the equation

$$du = \left(\frac{\partial u}{\partial s}\right)_\theta ds + \left(\frac{\partial u}{\partial \theta}\right)_s d\theta \quad . \quad .$$

in which the subscript of $u$ has been dropped. Dividing through by $d\theta$ and noting that $ds/d\theta$ and $u$ are equivalent yields the following expression for the total acceleration $du/d\theta$ of the fluid particle

$$\frac{du}{d\theta} = u\left(\frac{\partial u}{\partial s}\right)_\theta + \left(\frac{\partial u}{\partial \theta}\right)_s \quad . \quad . \quad (3)$$

The first term on the right is the convectional acceleration. It pertains to the rate of change of velocity with distance at a particular instant. The second term on the right is the local acceleration. It pertains to the rate of change of velocity with time at a particular place. The sum of these two terms is the total acceleration at a particular instant and place.

Fundamentally, the flow is steady if the local acceleration is zero and unsteady if the local acceleration is not zero. The convectional acceleration may be zero or finite for either state of flow.

Considering the macroscopic point of view, mass velocity may be defined as macroscopic velocity times fluid density, $q\rho$, or as mass per unit area per unit time referred to a point. Thus mass rate is $Aq\rho$ in a rectilinear flow system. It would be a function of $x$, and $\theta$ and could be treated in the same manner as $v$ in equation (3). The velocity indicated by $dx/d\theta$ would

be equivalent to $\delta$ in equation (1). Hence the total rate of change of $A\phi\gamma$ with time would be given by

$$\frac{d(A\phi\gamma)}{d\theta} = \frac{\partial(A\phi\gamma)}{\partial x}\frac{q}{\phi} + \frac{\partial(A\phi\gamma)}{\partial\theta} \quad . \quad . \quad (4)$$

If the mass rate is to be an absolute constant, each of the two terms of the right-hand member of equation (4) must be zero. The partial derivative in the first one represents the instantaneous rate of change of mass rate with distance $x$. As there can be no accumulation of mass in any part of the system, this derivative would be zero. As the rate must be fixed at all cross-sections transverse to the flow the second derivative would also be zero.

If the mass rate is not constant and instantaneously is $A\phi\gamma$ at $x$ and $A\phi\gamma + \frac{\partial(A\phi\gamma)}{\partial x}\delta x$ at $x + \delta x$ a short distance downstream from $x$, the rate of depletion of mass in the element would be $-\frac{\partial(A\phi\gamma)}{\partial x}\delta x$. Since the instantaneous mass of fluid in the element is $A \cdot \delta x \cdot \phi\gamma$, this rate of depletion would be given also by $-\frac{\partial}{\partial\theta}(A\phi\gamma) \cdot \delta x$. Equating these two values of the instantaneous rate of depletion and cancelling the $A$'s and $\delta x$'s results in

$$\frac{\partial(q\gamma)}{\partial x} = -\phi\frac{\partial\gamma}{\partial\theta} \quad . \quad . \quad . \quad (5)$$

which is the basic continuity relation for rectilinear, macroscopic flow. Taking the $A$'s out from under the differential operators in the right-hand member of equation (4), and then substituting $-\phi\frac{\partial\gamma}{\partial\theta}$ for $\frac{\partial(q\gamma)}{\partial x}$ and performing the indicated differentiation results in

$$\frac{d(A\phi\gamma)}{d\theta} = A\gamma\frac{\partial q}{\partial\theta} \quad . \quad . \quad . \quad (6)$$

It follows that a steady mass rate of flow depends on $\left(\frac{\partial q}{\partial\theta}\right)_x$ being zero. As the $A$'s cancel out, equation (6) also discloses that the total rate of change of the mass velocity with time vanishes if the local time rate of change of the macroscopic velocity is zero. Thus the term $\frac{\partial q}{\partial\theta}$ has the same significance with respect to mass velocity in macroscopic flow as the term $\frac{\partial u}{\partial\theta}$ has with respect to fluid-particle velocity in microscopic flow.

The study reported here relates to the unsteady-state flow of water in the aquifer of linear oil-reservoir aquifer systems. The continuity relation (equation (5)) is the starting point of the analysis. As the flow is unsteady $\frac{\partial\gamma}{\partial\theta} \neq 0$.

## FUNDAMENTAL DIFFERENTIAL EQUATION DESCRIBING FLOW IN LINEAR SYSTEMS

Assuming the flow to take place in horizontal planes, and introducing Darcy's law, equation (5) becomes

$$\frac{\partial}{\partial x}\left(\frac{k\gamma}{\mu}\frac{\partial P}{\partial x}\right) = \phi\frac{\partial\gamma}{\partial\theta} \quad . \quad . \quad . \quad (7)$$

Noting that the isothermal coefficient of fluid compressibility is defined by $c = \frac{1}{\gamma}\left(\frac{\partial\gamma}{\partial P}\right)_T$ and assuming that $c$ is constant over a range of pressure, $P - P_0$, integration leads to the density–pressure relationship: $\gamma = \gamma_0 e^{c(P-P_0)}$. Substituting for $\gamma$ in equation (7), performing the indicated differentiation, and assuming permeability $k$ and viscosity $\mu$ to be independent of $x$ yields the fundamental flow equation sought

$$\frac{\partial^2 P}{\partial x^2} + c\left(\frac{\partial P}{\partial x}\right)^2 = \frac{\phi\mu c}{k}\frac{\partial P}{\partial\theta} \quad . \quad . \quad . \quad (8)$$

As the second term of the left-hand member of equation (8) is negligible,[3] the equation to be solved may be written

$$\frac{\partial P}{\partial\theta} = \frac{k}{\phi\mu c}\frac{\partial^2 P}{\partial x^2} \quad . \quad . \quad . \quad . \quad (9)$$

Significantly, the derivation of equation (9) does not account for compression of the porous medium itself as a result of increased intergranular stress caused by reduced fluid pressure. If this phenomenon is considered, one should also consider the effect of this compression on the porosity and permeability distribution in the porous medium. This leads to complications considered unnecessary in view of the limited accuracy of basic field data.

Solutions of equation (9) would evidently express $P$ as a function of $x$ and $\theta$. Thus, initial and boundary conditions must be specified. Once the pressure distribution in the aquifer is known as a function of time, the volumetric rate of flow at $x = 0$ at particular times may be determined from direct applications of Darcy's law: $Q = \frac{Ak}{\mu}\left(\frac{\partial P}{\partial x}\right)_{x=0}$; $\theta = \theta_1, \theta_2, \ldots, \theta_n$, where $A$, the bulk area presented to flow, is the product of the width $b$ of the aquifer and its thickness $h$. This is the technique used in the ensuing calculations.

## PRESSURE DISTRIBUTION IN THE AQUIFER

Solutions of the fundamental differential equation, expressing $P$ as a function of $x$ and $\theta$, are developed in this section. Four sets of initial and boundary conditions are treated. In each instance the solution developed satisfies the differential equation and these conditions as stated.

Referring to Fig 1, the flow of water in the aquifer

is from right to left in all problems investigated. The same values are assigned to the constants pertaining to the aquifer sand and water in all numerical examples presented here and in subsequent sections. These values are $k = 500$ md, $\phi = 0.200$, $\mu = 0.300$ cP, and $c = 3.00 \times 10^{-6}$ (vol/vol)/psi.

In the mathematical analyses the coefficient $\frac{k}{\phi\mu c}$ (equation (9)) is for convenience set equal to the single factor $a$.

*Constant-rate Case—Infinite Aquifer*

This problem may be stated

$$\frac{\partial P}{\partial \theta} = a\frac{\partial^2 P}{\partial x^2} \quad \ldots\ldots\ldots \quad (10)$$

$$\left.\begin{array}{lll} \theta = 0: & P = P_f & ;\ x \geq 0 \\ \theta > 0: & \left\{\begin{array}{ll} \dfrac{\partial P}{\partial x} = \dfrac{Q\mu}{bhk} & ;\ x = 0 \\ \lim\limits_{x\to\infty} P(x, \theta) = P_f & ;\ x \to \infty \end{array}\right. \end{array}\right\} \quad (11)$$

Equation (10) describes the flow at any point in the aquifer. Relations (11) express the initial and boundary conditions. Volumetric rate of flow $Q$ in the present instance is a constant.

Using $P = P_f - \phi(x, \theta)$ and then expressing the statement of the problem in terms of $\phi$ instead of $P$ causes it to take the form of a heat-conduction problem which has been solved with the Laplace-transform method to determine temperature as a function of distance and time.[4] The result applied to the present fluid-flow problem states pressure as a function of distance and time.

$$P = P_f - \frac{Q\mu}{bhk}\left[2\sqrt{\frac{a\theta}{\pi}}\exp\left(-\frac{x^2}{4a\theta}\right) - x\,\mathrm{erfc}\left(\frac{x}{2\sqrt{a\theta}}\right)\right] \quad (12)$$

in which exp symbolizes exponential and erfc complementary error function: thus,

$$\left.\begin{array}{l} \exp y = e^y \\ \mathrm{erfc}\, y = 1 - \mathrm{erf}\, y \\ \mathrm{erf}\, y = \dfrac{2}{\sqrt{\pi}}\displaystyle\int_0^y e^{-y^2}\,dy \end{array}\right\} \quad (13)$$

where erf symbolizes error function.[5]

Equation (12) is the pressure-distribution equation sought. Data for plotting Fig 3 were obtained with it by setting the initial pressure $P_f$ equal to 4200 psia, and the constant water-influx rate, $Q/L$, equal to $1.00 \times 10^{-2}$ (bbl)/sq ft. The equation then was solved for three different values of $\theta$: 1, 20, and 50 years. Numerical values of the complementary error function were obtained from tables.[5]

*Constant-rate Case—Finite Aquifer*

The initial and boundary conditions for this problem may be stated

$$\left.\begin{array}{lll} \theta = 0: & P = P_f & ;\ x \geq 0 \\ \theta > 0: & \left\{\begin{array}{ll} \dfrac{\partial P}{\partial x} = \dfrac{Q\mu}{bhk} & ;\ x = 0 \\ \dfrac{\partial P}{\partial x} = 0 & ;\ x = L \end{array}\right. \end{array}\right\} \quad (14)$$

The solution may be developed by the separation-of-variables method or by the Laplace-transform method.[6] Utilizing the first of these a new variable $\phi(x, \theta)$ is introduced such that

$$P = \phi - \frac{Q\mu}{bhkL}\left[\frac{(L-x)^2}{2} + a\theta\right] \quad (15)$$

In terms of $\phi$ the differential equation is the same as equation (10) except $P$ is replaced with $\phi$. The initial and boundary conditions are

$$\left.\begin{array}{lll} \theta = 0: & \phi = P_f - \dfrac{Q\mu}{bhkL}\dfrac{(L-x)^2}{2} & ;\ x \geq 0 \\ \theta > 0: & \left\{\begin{array}{ll} \dfrac{\partial \phi}{\partial x} = 0 & ;\ x = 0 \\ \dfrac{\partial \phi}{\partial x} = 0 & ;\ x = L \end{array}\right. \end{array}\right\} \quad (16)$$

After the solution developed in terms of $\phi$ is transformed back into terms of $P$, through equation (15), it becomes the desired pressure-distribution equation

$$P = P_f - \frac{Q\mu}{bhk}\left[\frac{(L-x)^2}{2L} - \frac{L}{6} + \frac{a\theta}{L}\right] + \frac{2Q\mu L}{bhk\pi^2}\sum_{n=1}^{\infty}\left(\frac{1}{n^2}\right)\exp\left(-\frac{n^2\pi^2 a\theta}{L^2}\right)\cos\frac{n\pi x}{L} \quad (17)$$

The pressure distribution curves of Fig 4 were plotted using equation (17) and the same numerical values for the initial pressure and constant water-influx rate as were used in Fig 3. In contrast to Fig 3 the curves pertain to times of 0.5, 1.0, 2.5, and 5.0 years, respectively. The length of the aquifer is specified as 10 miles.

*Constant-pressure Case—Infinite Aquifer*

The initial and boundary conditions for this problem may be stated

$$\left.\begin{array}{lll} \theta = 0: & P = P_f & ;\ x \geq 0 \\ \theta > 0: & \left\{\begin{array}{ll} P = P_s = \text{constant} & ;\ x = 0 \\ \lim\limits_{x\to\infty} P = P_f & ;\ x = \infty \end{array}\right. \end{array}\right\} \quad (18)$$

If a new variable $\phi(x, \theta)$ is introduced such that

$$P = P_s + (P_f - P_s)\phi \quad \ldots \quad (19)$$

the statement of the problem in terms of $\phi$ takes the form of a heat-conduction problem that has been

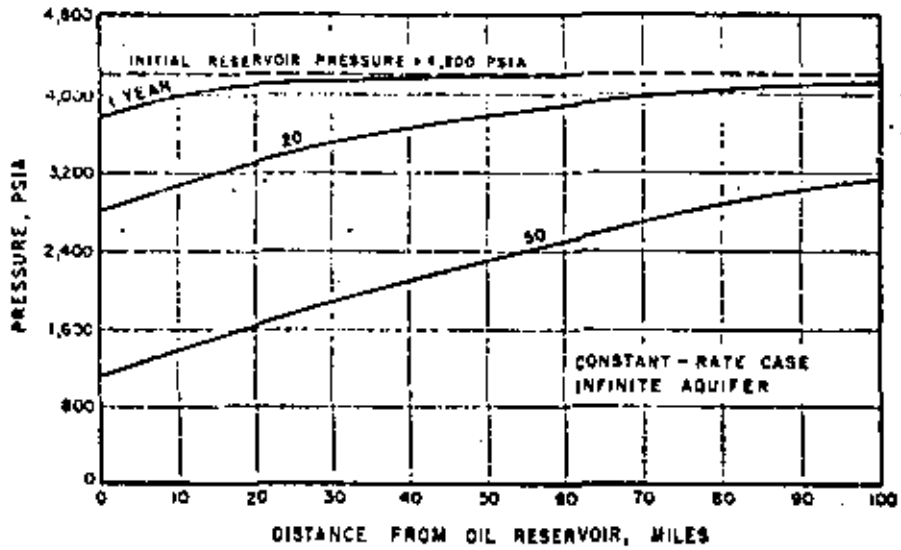


FIG 3

PRESSURE DISTRIBUTION IN THE AQUIFER AT VARIOUS TIMES FOR A CONSTANT VOLUMETRIC RATE OF WATER INFLUX AT BOUNDARY OF OIL RESERVOIR AND AN INFINITE AQUIFER

Permeability: 500 mD Porosity: 0·200 Viscosity of water: 0·300 cP
Compressibility of water: $3{\cdot}00 \times 10^{-6}$ (vol/vol)/psi
Influx rate: $1{\cdot}00 \times 10^{-3}$ (bd)/sq ft of cross-section at boundary of oil reservoir

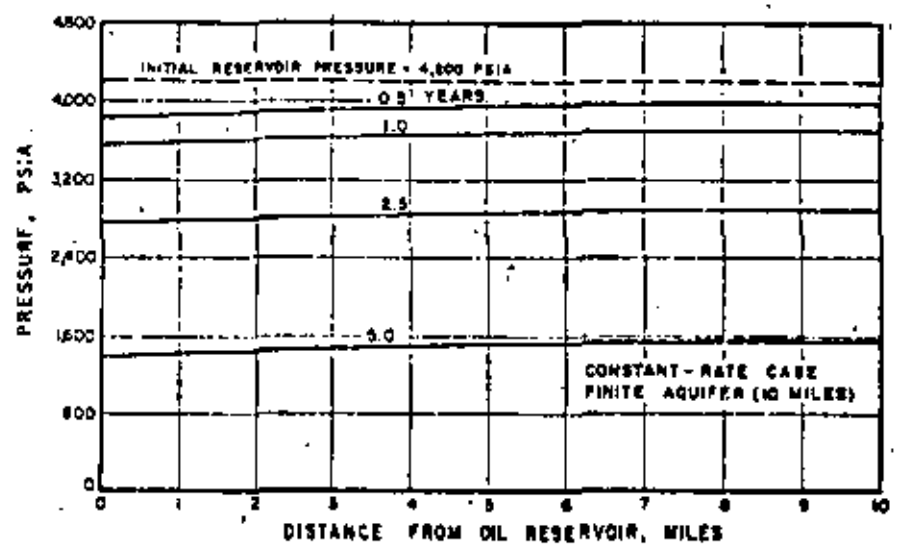


FIG 4

PRESSURE DISTRIBUTION IN THE AQUIFER AT VARIOUS TIMES FOR A CONSTANT VOLUMETRIC RATE OF WATER INFLUX AT BOUNDARY OF OIL RESERVOIR AND AN AQUIFER 10·0 MILES LONG

Permeability: 500 mD Porosity: 0·200 Viscosity of water: 0·300 cP
Compressibility of water: $3{\cdot}00 \times 10^{-6}$ (vol/vol)/psi
Influx rate: $1{\cdot}00 \times 10^{-3}$ (bd)/sq ft of cross-section at boundary of oil reservoir

solved through application of Fourier integrals to determine temperature as a function of time and distance.[7] In terms of the present fluid-flow problem and the original variables, the pressure-distribution equation would be

$$P = P_i + (P_f - P_i)\,\mathrm{erf}\,\frac{x}{2\sqrt{a\theta}} \quad . \quad (20)$$

Fig 5 was plotted using the same numerical values for $P_f$ and $a$ as in the foregoing cases. The constant pressure at $x = 0$ was specified as 1050 psia. The curves represent distributions for $\theta = 1$, 10, and 50 years, respectively.

original variables, the pressure-distribution equation would be

$$P = P_i + (P_f - P_i)\frac{4}{\pi}\sum_{n=1}^{\infty}\left(\frac{1}{2n-1}\right)\exp\left[-\frac{(2n-1)^2\pi^2 a\theta}{4L^2}\right]\sin\frac{(2n-1)\pi x}{2L} \quad (22)$$

Fig 6 was plotted using the same numerical values for $P_f$, $P_i$, and $a$ as were used in plotting Fig 5. The length of the aquifer, $L$, was specified to be 10·0 miles. The curves represent values of $\theta$ of 1, 3, 6, and 12 months respectively.

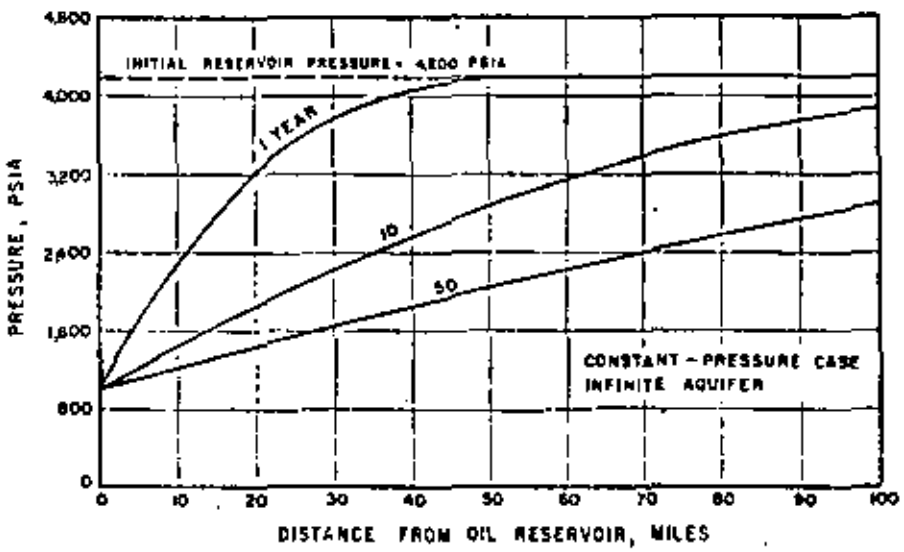


Fig 5

PRESSURE DISTRIBUTION IN THE AQUIFER AT VARIOUS TIMES FOR A CONSTANT PRESSURE AT BOUNDARY OF OIL RESERVOIR AND AN INFINITE AQUIFER

Permeability: 500 md  Porosity: 0·200  Viscosity of water: 0·300 cP
Compressibility of water: $3{\cdot}60 \times 10^{-6}$ $(\mathrm{vol}_i/\mathrm{vol})_i$psi
Constant pressure: 1050 psi at boundary of oil reservoir

*Constant-pressure Case—Finite Aquifer*

The initial and boundary conditions of the problem may be

$$\left.\begin{array}{lll} \theta = 0: & P = P_f & ;\ x \geq 0 \\ \theta > 0: & P = P_i = \text{constant} & ;\ x = 0 \\ & \dfrac{\partial P}{\partial x} = 0 & ;\ x = L \end{array}\right\} \quad (21)$$

If the variable $\psi$ as defined by equation (10) is introduced, the statement of the problem when expressed in terms of $\psi$ takes the form of a heat-conduction problem which has been solved with the separation-of-variables method to determine the relationship of temperature, distance, and time.[7] Expressed in terms of the present fluid-flow problem and the

## DIMENSIONLESS PRESSURE AND FLOW FUNCTIONS

*Definitions*

The properties of the aquifer sand and water symbolized by $k, \phi, \mu$, and $c$ change from system to system. A very great deal of graphing would be necessary to show their effects individually on unsteady state flow behaviour. This difficulty, plus that which would be brought about by showing in addition the effect of changes in boundary conditions and time, have led to the adoption of dimensionless groups of variables for graphing purposes.[8]

In the present work the groups used are the same as those of the cited reference:

M M

Dimensionless pressure differential, $\Delta P = \frac{P_i - P_r}{P_i}$

Dimensionless time $t = \frac{\alpha\theta}{x_e^2}$

Dimensionless volumetric rate of flow, $Q_D = \frac{Q\mu}{hkP_i}$

Dimensionless cumulative influx, $Q_c = \int_0^t Q_D\, dt$

Dimensionless pressure function, $\Delta P/Q_D$

Dimensionless flow function, $Q_c/\Delta P$

The quantity $x_e$ in the expression for dimensionless time $t$ represents unit length. It is introduced merely to make the expression dimensionless.

time zero and $P_r$ at times greater than zero. If the water influx rate $Q$ is fixed, $P_r$ must decrease with time. In the constant-rate cases $\Delta P$ is considered therefore as a dimensionless cumulative drop in pressure and its determination is of primary concern. If $P_r$ is a constant for time $\theta > 0$, $\Delta P$ would also be fixed. The influx rate would decrease continuously. Hence, in the constant-pressure cases the cumulative influx is the element to be determined.

The dimensionless ratio $\Delta P$ is not to be misconstrued as pertaining in any way to a pressure differential over a length of porous medium. Instead, it is to be recognized as pertaining to the time rate of change of the difference between initial and final pressures at a particular place, namely, at $x = 0$.

The constant-rate-case curves of Fig 7 show

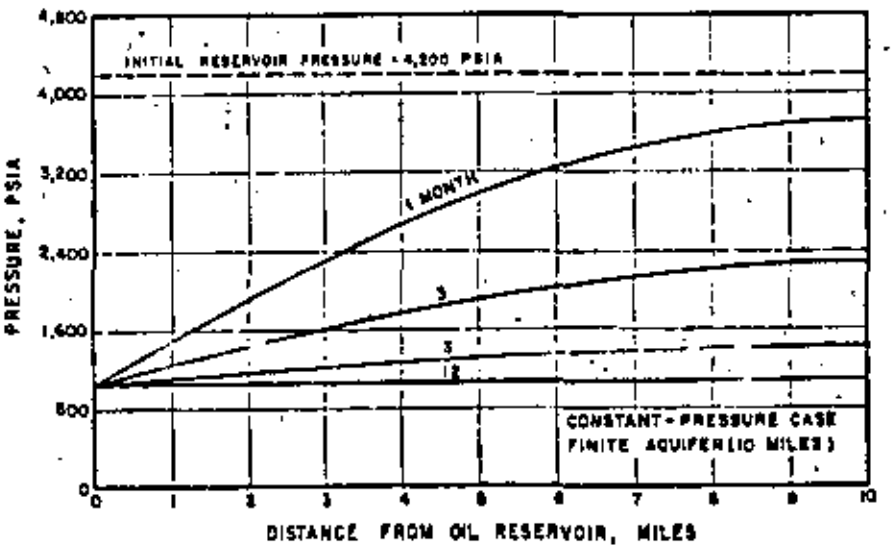


FIG 6

PRESSURE DISTRIBUTION IN THE AQUIFER AT VARIOUS TIMES FOR A CONSTANT PRESSURE AT BOUNDARY OF OIL RESERVOIR AND AN AQUIFER 10·0 MILES LONG

Permeability: 500 mD Porosity: 0·200 Viscosity of water: 0·300 cP
Compressibility of water: 3·60 × $10^{-6}$ (vol/vol)/psi

*Relationships with Dimensionless Time*

*Graphical Representation.* Considering the foregoing constant-rate cases, practical considerations indicate that desired information on oil-reservoir performance could be gained if a relationship is established between volumetric rate of influx of water, oil-reservoir pressure, time, and length of aquifer. A relationship of this kind based on the above-defined dimensionless groups and applicable to all constant-rate-case linear systems would be of major importance in simplifying their analysis. A similar relationship applicable to all constant-pressure-case linear systems would be of equal importance.

All the curves of Fig 7 refer in their entirety to conditions at the water-influx boundary ($x = 0$, Fig 1). The fluid pressure at this boundary is $P_r$ at

dimensionless cumulative pressure drop per unit dimensionless volumetric rate, $\Delta P/Q_D$, plotted on log–log graph paper, as a function of dimensionless time $t$ for aquifers of different length. It is a simple matter to estimate for any particular system the reduction in oil-reservoir pressure corresponding to a given fixed rate of oil production and a given time of operation, assuming, of course, that the time is short enough for the calculated reduction to be less than the initial pressure minus the pre-assigned final pressure.

The maximum cumulative influx of water or cumulative oil production (assuming enough oil is available for displacement) is limited by the minimum value specified for $P_r$. The bubble-point pressure of the liquid reservoir oil at reservoir temperature would probably be selected as this minimum. If the minimum is used in calculating $\Delta P/Q_D$ and the result

entered on Fig 7, the corresponding dimensionless time $t$ may be read off directly. The product of this time and the dimensionless flow rate is the maximum cumulative influx.

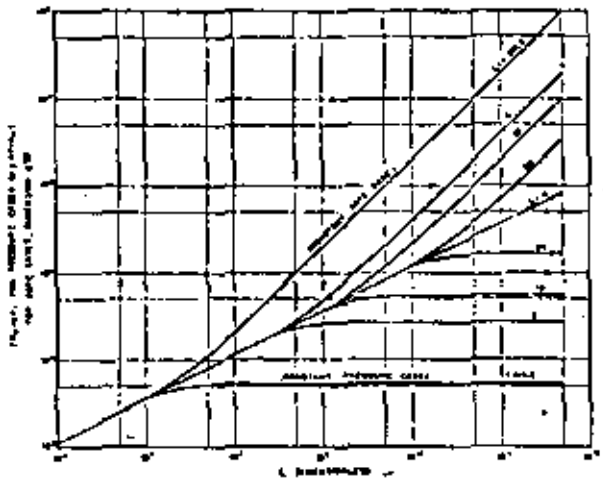

FIG 7

VARIATION OF PRESSURE FUNCTION AND FLOW FUNCTION WITH DIMENSIONLESS TIME FOR AQUIFERS OF DIFFERENT LENGTH

Evidently the slopes of the constant-rate curves relating to finite aquifers become and remain equal to unity when $t$ is large enough. Under these conditions $\frac{d}{dt}\left(\frac{\Delta P}{Q_D}\right) = \text{constt.}$, or $\frac{Q_c}{\Delta P} = \text{const.}$ As $P_f$ is fixed, this leads to the foregoing obvious result, namely, that $Q_c$ attains its maximum magnitude when $P_e$ attains its minimum.

The constant-pressure-case curves of Fig 7 show dimensionless cumulative influx of water per unit dimensionless pressure drop, $Q_c/\Delta P$, plotted as a function of dimensionless time $t$ for aquifers of different length. For any particular system these curves may be used to estimate the cumulative influx corresponding to a fixed pre-assigned pressure maintained at the water-influx boundary over a given period of time.

All the constant-pressure-case curves except the one for which $L = \infty$ eventually become and remain horizontal. When they are horizontal $\frac{d}{dt}\left(\frac{Q_c}{\Delta P}\right) = 0$ or $Q_D = 0$. When $Q_D = 0$ the fluid pressure must be the same at all points of the aquifer and equal to fixed pressure $P_i$ at $x = 0$. Thus the minimum value of $t$ required for the maximum cumulative influx is the value of $t$ at which the curve becomes horizontal.

The curve representing $L = \infty$ applies to both the constant-rate and constant-pressure families of curves. Its equation, as well as the equations of the other curves of both families, are derived in the next part of this paper.

As indicated by the figure, aquifers of finite length behave the same as aquifers of infinite length during the early stages of water influx regardless of whether the pressure or the rate is constant at $x = 0$. If the aquifer is 10·0 miles long, for example, it will behave the same as an infinite aquifer, for either type of boundary condition, until dimensionless time $t$ exceeds about $1{\cdot}00 \times 10^{0}$.

Fig 8 shows the constant-rate-case family of curves of Fig 7 plotted on ordinary arithmetic graph paper. Fig 9 shows the constant-pressure-case curves plotted similarly. It also includes curves for $L = 20{\cdot}0$, 50·0, 80·0, and 120 miles.

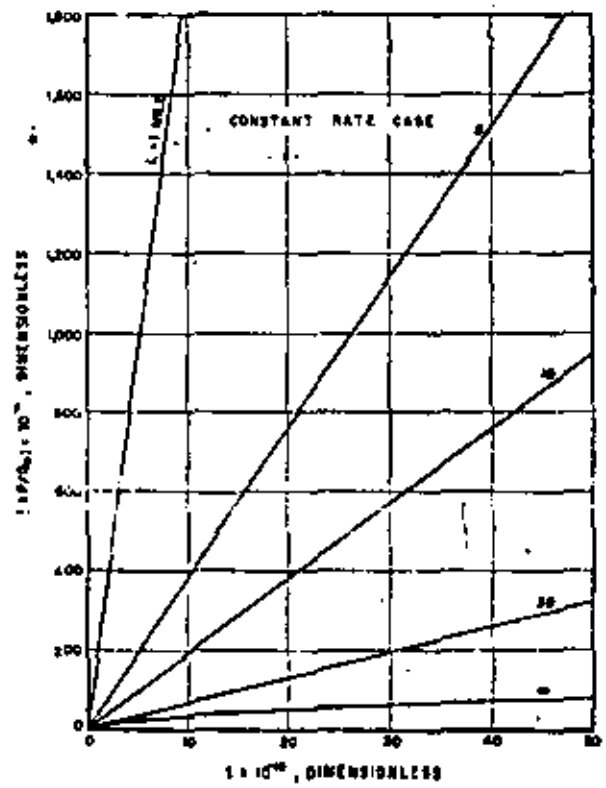


FIG 8

VARIATION OF PRESSURE FUNCTION WITH DIMENSIONLESS TIME FOR AQUIFERS OF DIFFERENT LENGTH—CONSTANT-RATE CASE

*Equations of Constant-rate Cases.* When $P_i$ is substituted for $P$ and zero for $x$, equation (12) pertaining to infinite aquifers takes the form

$$P_e = P_i - \frac{Q_t}{bhk}\left(2\sqrt{\frac{\alpha t}{\pi}}\right) \quad . \quad (23)$$

In terms of the dimensionless pressure function and dimensionless time this may be written

$$\frac{\Delta P}{Q_D} = \frac{2x_e}{b}\sqrt{\frac{t}{\pi}} \quad . \quad . \quad . \quad (24)$$

Equation (24) is the equation of the curve representing $L = \infty$ on Figs 7 and 8; $x_e$ and $b$ are each unity in this equation and in subsequent equations.

In the constant-rate cases $Q_D = Q_c/t$. If this substitution is made for $Q_D$, equation (24) becomes

$$\frac{\Delta P}{Q_c} = \frac{2x_e}{b\sqrt{\pi t}} \quad . \quad . \quad . \quad (25)$$

When $P_e$ is substituted for $P$ and zero for $x$, equation (17) pertaining to finite aquifers takes the form

$$P_e = P_f - \frac{Q_x}{bhk}\left(\frac{L}{3} + \frac{a\theta}{L}\right) + \frac{2Q_\mu L}{bhk\pi^2}\left(\sum_{n=1}^{n=\infty}\frac{1}{n^2}\right)\exp\left(-\frac{n^2\pi^2 a\theta}{L^2}\right) \quad . \quad (26)$$

In terms of the dimensionless pressure function and dimensionless time this may be written

$$\frac{\Delta P}{Q_D} = \frac{1}{b}\left(\frac{L}{3} + \frac{x_e^2}{L}\right) - \frac{2L}{\pi^2 b}\sum_{n=1}^{n=\infty}\left(\frac{1}{n^2}\right)\exp\left(-\frac{n^2\pi^2 x_e^2 t}{L^2}\right) \quad . \quad (27)$$

or

$$\frac{\Delta P}{Q_D} = F(t) \quad . \quad . \quad . \quad . \quad (28)$$

which is the equation of the constant-rate-case curves in Figs 7 and 8 for finite aquifers. Equation (28) in terms of $Q_c$ may be written

$$\frac{\Delta P}{Q_c} = \frac{F(t)}{t} \quad . \quad . \quad . \quad . \quad (29)$$

*Equations of Constant-pressure Cases.* Equations expressing the relationship of the dimensionless flow function and dimensionless time are necessary in order to plot the constant-pressure-case curves of Figs 7 and 8. Derivation of such equations begins with differentiation of the pressure-distribution equation to determine $\left(\frac{\partial P}{\partial x}\right)_{x=0}$ for substitution in Darcy's law.

Differentiating equation (20) with respect to $x$ and then setting $x$ equal to zero gives for infinite aquifers:

$$\left(\frac{\partial P}{\partial x}\right)_{x=0} = \frac{P_f - P_e}{\sqrt{\pi a\theta}} \quad . \quad . \quad (30)$$

According to Darcy's law the left-hand member of equation (30) is equal to $\left(\frac{Q_\mu}{bhk}\right)$. Hence,

$$\frac{Q}{bh} = \frac{k}{\mu}\frac{P_f - P_e}{\sqrt{\pi a\theta}} \quad . \quad . \quad . \quad (31)$$

or in terms of the dimensionless quantities $Q_D$, $\Delta P$, and $t$

$$Q_D = \frac{b \cdot \Delta P}{x_e\sqrt{\pi t}} \quad . \quad . \quad . \quad . \quad (32)$$

Integrating over dimensionless time $t$, this becomes a relationship between the dimensionless flow function and dimensionless time,

$$\frac{Q_c}{\Delta P} = \frac{2b}{x_e}\sqrt{\frac{t}{\pi}} \quad . \quad . \quad . \quad . \quad (33)$$

Equation (33) is the equation of the curve representing $L = \infty$ on Figs 7 and 8. As $b$ and $x_e$ are each unity, the right-hand member is the same numerically

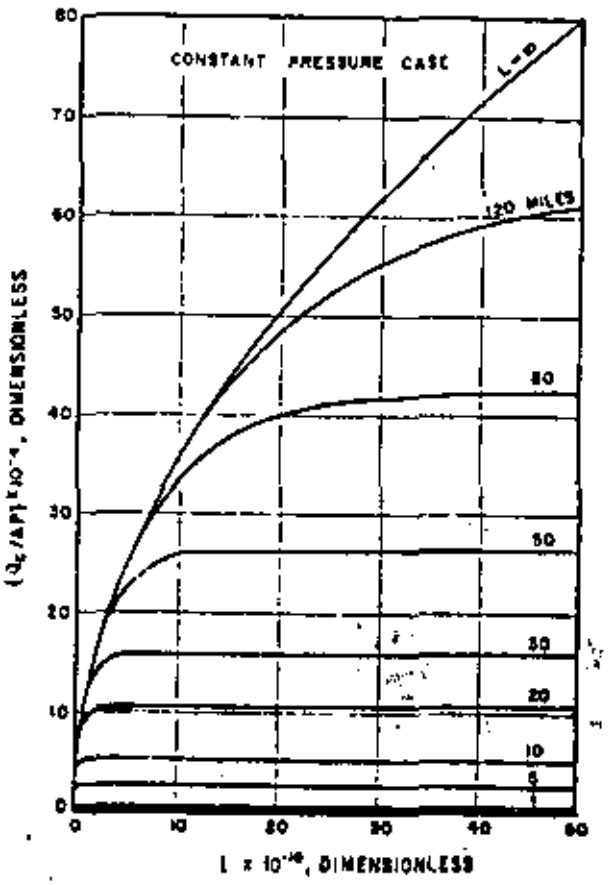


FIG 9

VARIATION OF FLOW FUNCTION WITH DIMENSIONLESS TIME FOR AQUIFERS OF DIFFERENT LENGTH—CONSTANT PRESSURE CASE

as the right-hand member of equation (21). For this reason the $L = \infty$ curve of Fig 7 applies to both the constant-rate and constant-pressure cases.

Transformation of equation (33) back to the original variables gives the cumulative influx per unit of bulk area transverse to the direction of flow at $x = 0$:

$$\left(\frac{1}{bh}\right)\int_0^\theta Q d\theta = 2\alpha\phi(P_f - P_e)\sqrt{\frac{a\theta}{\pi}} \quad . \quad (34)$$

Differentiating equation (22) with respect to $x$ and then setting $x$ equal to zero gives

$$\left(\frac{\partial P}{\partial x}\right)_{x=0} = \frac{2(P_f - P_e)}{L}\sum_{n\ \mathrm{odd}}^{n=\infty}\exp\left(-\frac{n^2\pi^2 a\theta}{4L^2}\right) \quad (35)$$

Considering Darcy's law this may be written

$$\left(\frac{Q}{bh}\right) = \frac{2k(P_f - P_e)}{\mu L} \sum_{n\,\text{odd}}^{\infty} \exp\left(-\frac{n^2\pi^2\alpha\theta}{4L^2}\right) \quad (36)$$

or in terms of $Q_D$, $\Delta P$, and $t$,

$$\left(\frac{Q_D}{\Delta P}\right) = \frac{2b}{L} \sum_{n\,\text{odd}}^{\infty} \exp\left(-\frac{n^2\pi^2 x_e^2 t}{4L^2}\right). \quad (37)$$

Integrating term by term, over dimensionless time $t$ results in

$$\int_0^t Q_D\,dt = \frac{8bL \cdot \Delta P}{\pi^2 x_e^2}\left[\sum_{n\,\text{odd}}^{\infty}\left(\frac{1}{n^2}\right) - \sum_{n\,\text{odd}}^{\infty}\left(\frac{1}{n^2}\right)\exp\left(-\frac{n^2\pi^2 x_e^2 t}{4L^2}\right)\right]. \quad (38)$$

The first summation within the brackets on the right is equivalent[1] to $\frac{\pi^2}{8}$ and the left-hand member is equivalent to $Q_c$. Therefore, in terms of the dimensionless flow function, equation (38) may be written

$$\left(\frac{Q_c}{\Delta P}\right) \quad \frac{bL}{x_e^2}\left[1 - \frac{8}{\pi^2}\sum_{n\,\text{odd}}^{\infty}\left(\frac{1}{n^2}\right)\exp\left(-\frac{n^2\pi^2 x_e^2 t}{4L^2}\right)\right] \quad (39)$$

Equation (39) is the equation of the constant-pressure-case curves of Figs 7 and 9 relating to finite aquifers. Transformation of this equation back to the original variables gives the cumulative influx per unit of bulk area transverse to the direction of flow at $x = 0$:

$$\frac{1}{bh}\int_0^\theta Q\,d\theta = \phi c L(P_f - P_e)\left[1 - \frac{8}{\pi^2}\sum_{n\,\text{odd}}^{\infty}\left(\frac{1}{n^2}\right)\exp\left(-\frac{n^2\pi^2\alpha\theta}{4L^2}\right)\right] \quad (40)$$

*Applications*

Oil-reservoir performance curves are shown in Figs 10–13. They could be developed through application of Figs 7–9 or through direct substitution in the foregoing equations.

Equation (23) is the equation of the pressure-decline curves of Fig 10: $P_f$ is 4200 psia, and the constant values of $\left(\frac{Q}{bh}\right)$ are $0.500 \times 10^{-2}$, $0.750 \times 10^{-2}$, and $1.00 \times 10^{-2}$ (bbl)/ft². The cumulative-influx curves were developed by plotting $\left(\frac{1}{bh}\right)\int_0^\theta Q\,d\theta$ expressed in (bbl/ft²) against $\theta$ expressed in years. The maximum-influx rate has been chosen arbitrarily to correspond to $P_e = 0$.

Equation (26) is the equation of the pressure-decline curves of Fig 11. The initial pressure, final pressure, and constant rates are the same as those used in Fig 10, and the cumulative-influx curves were plotted in the same manner.

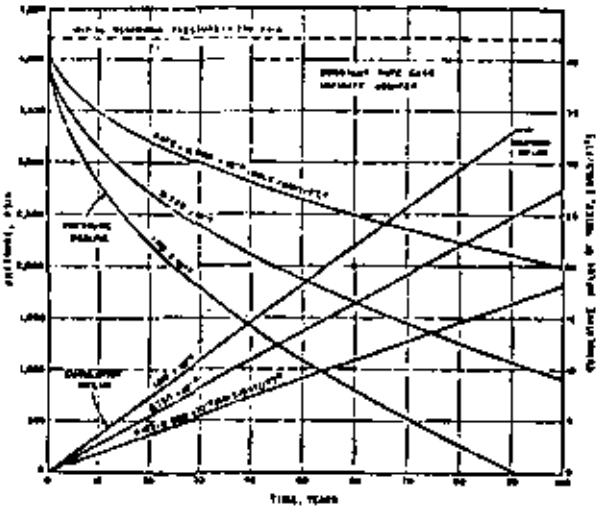

FIG 10

RESERVOIR PRESSURE AND CUMULATIVE INFLUX OF WATER AS FUNCTIONS OF TIME FOR VARIOUS CONSTANT RATES AND AN INFINITE AQUIFER

Permeability: 500 md
Porosity: 0·200
Viscosity of water: 0·300 cP
Compressibility of water: $3.00 \times 10^{-6}$ (vol/vol)/psi

Equation (31) is the equation of the rate curves of Fig 12: $P_f$ is 4200 psia, and the constant values of $P_e$ are 2000, 2800, and 3600 psia. The cumulative-influx curves were developed by plotting $\left(\frac{1}{bh}\right)\int_0^\theta Q\,d\theta$ as determined from equation (34), expressed in (bbl/ft²), against $\theta$ expressed in years.

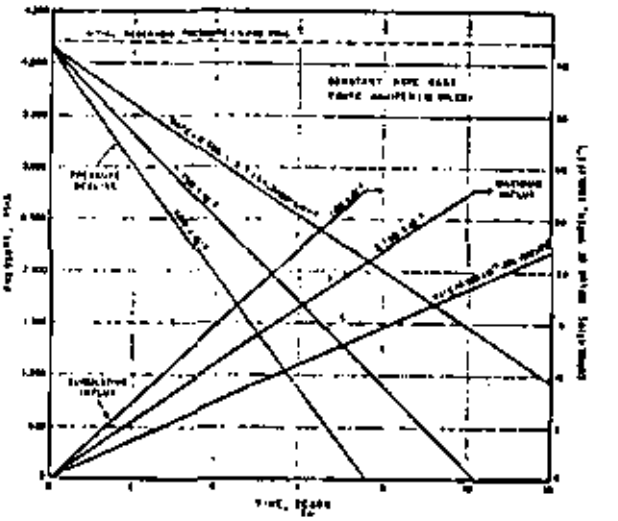

FIG 11

RESERVOIR PRESSURE AND CUMULATIVE INFLUX OF WATER AS FUNCTIONS OF TIME FOR VARIOUS CONSTANT RATES OF INFLUX AND AN AQUIFER 100 MILLS LONG

Permeability: 500 md
Porosity: 0·200
Viscosity of water: 0·300 cP
Compressibility of water: $3.00 \times 10^{-6}$ (vol/vol)/psi

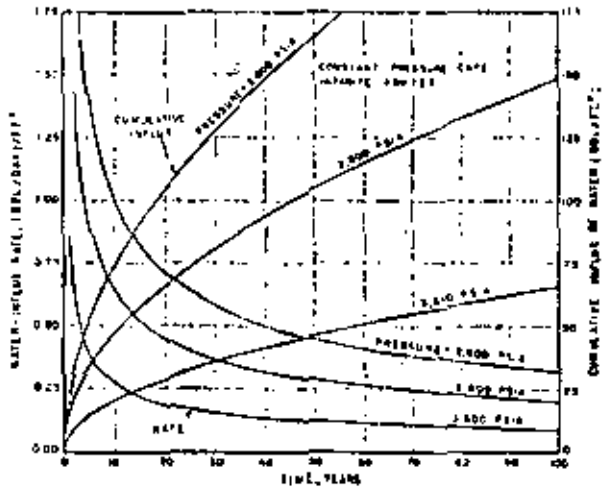

FIG 12

RATE OF INFLUX OF WATER AND CUMULATIVE INFLUX OF WATER AS FUNCTIONS OF TIME FOR VARIOUS CONSTANT PRESSURES AT THE BOUNDARY OF THE OIL RESERVOIR AND FOR AN INFINITE AQUIFER

Permeability: 500 mD
Porosity: 0·200
Viscosity of water: 0·300 cP
Compressibility of water: 3·60 × $10^{-6}$ (vol/vol)/psi

Equation (30) is the equation of the rate curves of Fig 13. The initial pressures, $P_i$, and the three constant values of $P_s$ are the same as those used in Fig 12. The cumulative influx curves were developed by plotting $\left(\frac{1}{bh}\right)\int_0^\theta Q d\theta$ as determined from equation (40), expressed in (brl/ft²), against $\theta$ expressed in years.

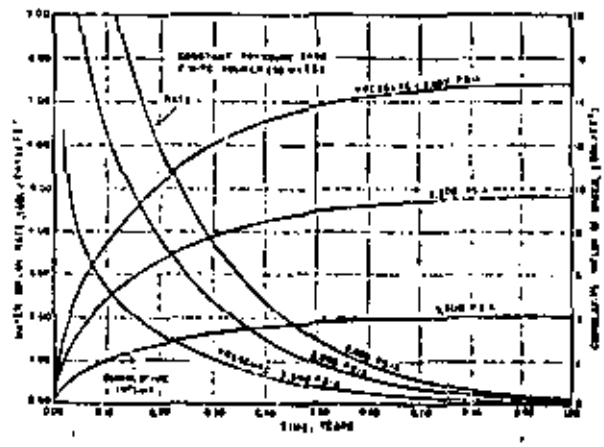

FIG 13

RATE OF INFLUX OF WATER AND CUMULATIVE INFLUX OF WATER AS FUNCTIONS OF TIME FOR VARIOUS CONSTANT PRESSURES AT THE BOUNDARY OF THE OIL RESERVOIR AND FOR AN AQUIFER 10·0 MILES LONG

Permeability: 500 mD
Porosity: 0·200
Viscosity of water: 0·300 cP
Compressibility of water: 3·60 × $10^{-6}$ (vol/vol)/psi

## EFFECT OF WATER-INFLUX RATE ON CUMULATIVE OIL RECOVERY

*Constant-rate Cases*

If equations (24) and (25) are combined and $t$ eliminated, the resulting relationship between $Q_c$, $Q_D$, and $\Delta P$, for infinite aquifers, is found to be

$$Q_c = \frac{\pi}{4}\frac{b^2}{x_c^2}\frac{(\Delta P)^2}{Q_D} \quad . \quad . \quad . \quad (41)$$

A pre-assigned initial pressure $P_i$ at time zero and final pressure $P_f$ at time $\theta_M$, at $x = 0$, cause the resulting relationship of $Q_c$ and $Q_D$ to apply only at

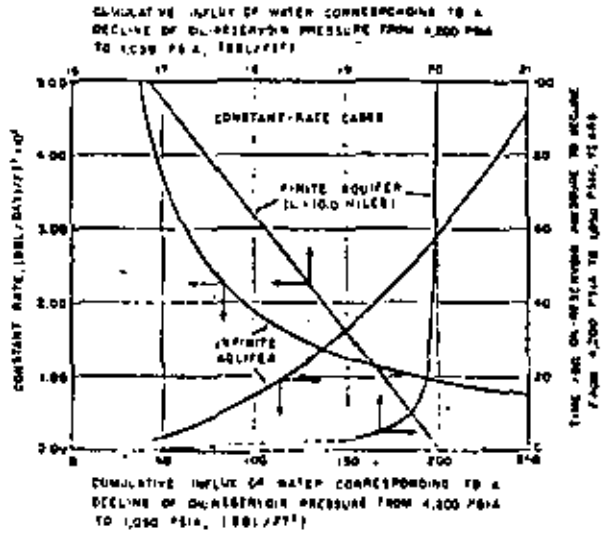

FIG 14

EFFECT OF RATE OF INFLUX OF WATER ON THE CUMULATIVE INFLUX CORRESPONDING TO A DECLINE OF OIL RESERVOIR PRESSURE FROM 4200 psia TO 1050 psia FOR SYSTEMS HAVING 10·0 MILES AND INFINITE AQUIFERS

Permeability: 500 mD
Porosity: 0·200
Viscosity of water: 0·300 cP
Compressibility of water: 3·60 × $10^{-6}$ (vol/vol)/psi

the instant $t = t_M$. At this instant $Q_c$ would be greater for a relatively low constant rate $Q_D$ than for a relatively high one. The instant in question is variable. Equation (24) with $t = t_M$ results if $Q_D$ in equation (41) is replaced with $Q_D t_M$. Thus one finds that reductions in $Q_D$ cause $t_M$ to be greater and increases in $Q_D$ cause $t_M$ to be smaller.

The infinite-aquifer curve of Fig 14 depicting the relationship between constant rate of influx and cumulative influx, for a fixed pre-assigned cumulative pressure drop, was developed from equation (41) after it was transformed back to the original variables. The curve shows $\left(\frac{Q}{bh}\right)$ as a function of $\left(\frac{Q_0}{bh}\right)$ for $P_i = 4200$ psia and $P_s = 1050$ psia. The infinite-aquifer curve portraying the relationship between time and cumulative influx, for the same pre-assigned

fixed cumulative pressure drop, was developed from equation (25) after $t$ was replaced by $t_M$ and it was transformed back to the original variables.

These curves indicate that the cumulative influx from infinite aquifers, corresponding to a fixed cumulative pressure drop, may be increased markedly by reducing the constant rate. If, for example, the rate is decreased from $1.62 \times 10^{-2}$ to $1.15 \times 10^{-2}$ bbl/ft², the cumulative influx, according to the figure, would increase from about 117 to 165 bbl/ft². The required time would be increased, however, from 20 to 40 years. In this instance a 29 per cent reduction in the rate would cause a 41 per cent increase in the cumulative and a 100 per cent increase in the time.

This phenomenon may be explained theoretically. Constant rate $Q_D$ determines the pressure distribution in the aquifer at any time. The distribution existing at time $t_M$ when final pressure $P_f$ is approached at $x = 0$ reflects the volume of water that has crossed the section at $x = 0$ and entered the oil reservoir. At that time pressure $P$ at some particular transverse section, at $x_s$, back in the aquifer would approach pressure $P_f$. If the mean value of the pressure over the distance from $x = 0$ to $x = x_s$ is represented by $\bar{P}$, and if the isothermal coefficient of compressibility of the water, represented by $\frac{1}{\gamma}\left(\frac{\partial \gamma}{\partial P}\right)_T$, is essentially constant over the pressure range from $P_i$ to $P_f$, the cumulative influx would be given by $bhx_s\phi[e^{c(P_i - \bar{P})} - 1]$. Thus the cumulative influx would increase with increasing $x_s$ and with decreasing $\bar{P}$. The foregoing analysis pertaining to Fig 14 reveals that relatively low constant rates of influx either cause $x_s$ to increase or $\bar{P}$ to decrease, or both. Tests of individual problems may be made with equation (12).

It can be shown readily that the summation term of equation (26) is negligible if $L \geq 10.0$ miles and $0 \geq 1.00$ years. When these conditions are specified the dimensionless time as determined from equation (27) would be given by

$$t = \left(\frac{b \cdot \Delta P}{Q_D} - \frac{L}{3}\right)\frac{L}{x_e^2} \quad . \quad . \quad (42)$$

Substitution of $Q_C/Q_D$ for $t$ in this equation yields the following relationship between $Q_C$, $Q_D$, and $\Delta P$:

$$Q_C = \frac{bL \cdot \Delta P}{x_e^2} - \frac{L^2 Q_D}{3x_e^2} \quad . \quad . \quad (43)$$

Cumulative pressure drop $\Delta P$ is fixed by the preassigned value of $P_f$ at $x = 0$ at time $t = t_M$. Hence $Q_C$ would be greater at this time for relatively low values of $Q_D$ than for relatively high ones, and the relationship between the two would be linear. The finite-aquifer curve of Fig 14 showing the relationship between cumulative influx and rate of influx, for a given $\Delta P$, was developed from equation (43) after transforming it back to the original variables. As in the case of the infinite aquifer this curve shows $\left(\frac{Q}{bh}\right)$ as a function of $\left(\frac{q}{bh}\right)$ for $P_i = 4200$ psia and $P_f = 1050$ psia.

As the summation term in equation (27) may be neglected, equation (29) with $t$ replaced by $t_M$ can be put in the form

$$Q_C = \frac{3bL \cdot \Delta P \cdot t_M}{L^2 + 3x_e^2 t_M} \quad . \quad . \quad (44)$$

which also would have been obtained as a result of letting $t = t_M$ in equation (42) and then dividing through by $t_M$. The resulting equation, after being transformed back to the original variables, was used to plot the finite-aquifer relationship portrayed on Fig 14 between time and cumulative influx, for a fixed cumulative pressure drop.

The finite-aquifer curves of Fig 14 disclose that relatively small reductions in the rate of influx in the range from $5.00 \times 10^{-2}$ to about $1.00 \times 10^{-2}$ (bd) ft² are quite effective in increasing the cumulative influx, for the fixed cumulative pressure drop. Reductions in rate below about $1.00 \times 10^{-2}$ (bd)/ft² cause no significant change in the cumulative influx. If the time taken for the pressure at $x = 0$ to drop from 4200 to 1050 psia is increased from 20 to 100 years, the increase in cumulative influx approximates only about 4 per cent.

*Constant-pressure Cases*

If equations (32) and (33) are combined and $t$ eliminated, the resulting relationship between $Q_C$, $Q_D$, and $\Delta P$ for the infinite aquifer is found to be

$$Q_C = \frac{2b^2(\Delta P)^2}{x_e^2 Q_D} \quad . \quad . \quad . \quad (45)$$

In this case $\Delta P$ is a fixed constant independent of time. The relationship between $Q_C$ and $Q_D$ applies therefore at all times $0 \leq t \leq t_M$.

The relationship between $Q_D$ and $t$ expressed by equation (32) is also established by the choice of $\Delta P$. Thus there can be only one $Q_C$ and $t_M$. This line of reasoning applies equally well to finite aquifers. One concludes that in the constant-pressure cases the cumulative influx and the corresponding required time are fixed by the choice of $\Delta P$.

## SUPERPOSITION CONCEPT

*Principles*

Physically, it is not feasible or perhaps even possible to drop the pressure instantaneously and substantially at $x = 0$ and then maintain the lower pressure over a long period of time. Thus the theoretical constant-pressure cases have no real oilfield

counterpart. Similarly, it is not feasible to effect instantaneously and thereafter maintain a constant volumetric rate of influx so that the theoretical constant-rate cases also have no field counterpart.

Under normal oilfield conditions the pressure and volumetric rate at $x = 0$ would change gradually. The superposition concept or theorem provides the means for mathematical analysis of changing-pressure or changing-rate cases, through utilization of the equations already developed.

Let the ratio $\left(\frac{P_x}{P_i}\right)$ be the ratio of the pressure $P_x$ at $x = 0$ at dimensionless time $t$ to the pressure $P_i$ at this section at time zero. Consider that this ratio is a continuously decreasing function of $t$ when plotted over the interval $0 \leq t \leq t_M$. Consider further that the $t$ axis (abscissa) is divided into $M$ equal increments, the time being $t_1$ at the end of the first increment, $t_2$ at the end of the second, and so on to $t_M$ at the end of the $M$th increment.

To apply the superposition concept the continuous relationship of $\left(\frac{P_x}{P_i}\right)$ and $t$ must be replaced by a matching step-function relationship of these two variables. For this purpose assume that the pressure ratio is reduced by an amount $\Delta P_0$ at time zero and maintained at the lower value to $t_1$. Let $(1 - \Delta P_0)$ be equivalent to the average pressure ratio as determined from the true pressure ratio-time curve, over the first increment of time $(t_1 - 0)$. Similarly, let the pressure ratio be further reduced at time $t_1$ by an amount $\Delta P_1$ and let $1 - \Delta P_0 - \Delta P_1$ be equivalent to the average pressure ratio over the time increment $(t_2 - t_1)$. If this process is continued until it includes the last increment of time $(t_M - t_{M-1})$, and if the equal increments of time are small enough, the resulting step function will match closely the true pressure ratio–time curve.

The pressure decrement $\Delta P_0$ imposed at time zero affects the flow over the time interval $(t_M - 0)$. Similarly, $\Delta P_1$, $\Delta P_2$, . . . $\Delta P_{M-1}$ are effective over the intervals $(t_M - t_1)$, $(t_M - t_2)$, . . . $(t_M - t_{M-1})$, respectively. The constant pressure-case equations developed earlier (equations (33) and (30)), expressing cumulative influx as a function of time, may be put in the form

$$Q_c = \Delta P \cdot f(t) \quad . \quad . \quad . \quad (46)$$

Considering equation (46) and the foregoing step function, the superposition concept indicates that the cumulative influx obtained under conditions of continuously decreasing pressure at $x = 0$ would be given by

$$\begin{aligned} Q_c = {} & \Delta P_0 f(t_M) + \Delta P_1 f(t_M - t_1) \\ & + \Delta P_2 f(t_M - t_2) + \ldots + \\ & \Delta P_{M-1} f(t_M - t_{M-1}) \quad . \quad . \quad . \quad . \quad (47) \end{aligned}$$

Since $\Delta t = t_1 - 0 = t_2 - t_1 = \ldots$ = constant and

$$\left.\begin{aligned} t_M - t_1 &= (M-1)\Delta t \\ t_M - t_2 &= (M-2)\Delta t \\ &\ldots\ldots\ldots\ldots \\ t_M - t_{M-1} &= [M-(M-1)]\Delta t \end{aligned}\right\} \quad (48)$$

the cumulative influx would be given by

$$Q_c = \Delta P_0 f(t_M) + \sum_{\tau=\Delta t}^{\tau=t_M} \Delta P(\tau) f(t_M - \tau) \quad (49)$$

Noting that

$$\Delta P(\tau) = \frac{\Delta P(\tau)}{\Delta \tau} \Delta \tau \quad . \quad . \quad . \quad (50)$$

and letting $\Delta \tau \to 0$, equation (49) may be written in the integral form

$$Q_c = \Delta P_0 f(t_M) + \int_0^{t_M} \frac{dP}{d\tau} f(t_M - \tau)\, d\tau \quad (51)$$

Equation (51) is one form of Duhamel's integral.[4]

Suppose dimensionless volumetric rate of flow instead of dimensionless pressure ratio is treated in the foregoing manner. Let $Q_D$ be an increasing function of $t$ and again let the $t$ axis be divided into $M$ equal increments, each equal to $\Delta t$. The constant-rate case equations (equations (24) and (28)) indicate that the cumulative pressure drop as a function of time may be put in the form

$$\Delta P = Q_D f(t) \quad . \quad . \quad . \quad (52)$$

It follows that the changing-rate case equation parallel to equation (47) for the changing-pressure case would be, according to the superposition concept,

$$\begin{aligned} \Delta P = {} & Q_{D0} f(t_M) + \Delta Q_{D1} f(t_M - t_1) \\ & + \Delta Q_{D2} f(t_M - t_2) + \ldots \\ & + (\Delta Q_D)_{M-1} f(t_M - t_{M-1}) \quad . \quad . \quad (53) \end{aligned}$$

in which $Q_{D0}$ is the initial rate, $\Delta Q_{D1}$ the increase in rate at $t_1$, $\Delta Q_{D2}$ the increase in rate at $t_2$, and so on to the final increase $(\Delta Q_D)_{M-1}$ at $t_{M-1}$, effective over the last increment of time, $(t_M - t_{M-1})$. Equation (53) may be put in the form

$$\Delta P = Q_{D0} f(t_M) + \sum_{\tau=\Delta t}^{\tau=t_M} \Delta Q_D(\tau) f(t_M - \tau) \quad . \quad (54)$$

or in the form of a Duhamel integral

$$\Delta P = Q_{D0} f(t_M) + \int_0^{t_M} \frac{dQ_D}{d\tau} f(t_M - \tau)\, d\tau \quad . \quad (55)$$

*Numerical Example*

Referring to Fig 15, the rate–time relationship was imposed. The initial rate $Q_0$ is $0{\cdot}250 \times 10^{-3}$ (bd)/ft², and at the beginning of each of the next 12 quarters ($\Delta\theta$) this rate is increased by an amount equal to the initial value. Therefore, if $Q_0$ is expressed in (brl/qtr)/ft² the cumulative influx at the end of the $n$th quarter, expressed in brl/ft², would be $\sum_{m=1}^{n} m\, Q_0 \Delta\theta$. The

# Unsteady-State Linear Flow Equations

**Constant Flow Rate**

$\Delta p = \alpha \frac{q \mu L}{k b h} F_{1/2}(t_D)$ — Acuífero Infinito

$\Delta p = \alpha \frac{q \mu L}{k b h} F_1(t_D)$ — Acuífero Finito limitado con frontera impermeable

$\Delta p = \alpha \frac{q \mu L}{k b h} F_0(t_D)$ — Acuífero Finito con Cilindro Externo a Presión Constante

$\alpha$ = Factor de conversión de unidades.

| Darcy | SI | Inglés |
|---|---|---|
| $\alpha = 1$ | $\alpha = 1$ | 887.2 |
| $\beta = 1$ | $\beta = 1$ | 0.00633 |

$$t_D = \frac{\beta k t}{\phi \mu c_t L^2}$$

**Constant Pressure**

$W_e = \phi b h L c_t \Delta p F_{1/2}(t_D)$ — Acuífero infinito

$W_e = \phi b h L c_t \Delta p F_0(t_D)$ — Acuífero finito sin frontera impermeable

$W_e = \phi b h L c_t \Delta p F_1(t_D)$ — Acuífero finito con frontera externa a presión constante.

$$F_0(t_D) = 1 - \frac{8}{\pi^2} \sum_{n\,odd}^{\infty} \left(\frac{1}{n^2}\right) \exp\left(-\frac{n^2 \pi^2 t_D}{4}\right)$$

$$F_{1/2}(t_D) = 2\sqrt{\frac{t_D}{\pi}}$$

$$F_1(t_D) = \left(t_D + \frac{1}{3}\right) - \frac{2}{\pi^2} \sum_{n=1}^{\infty} \left(\frac{1}{n^2}\right) \exp\left(-\frac{n^2 \pi^2 t_D}{\blacksquare}\right)$$

49 Pet E. 270.A

$F_0 = F_1 = F_{1/2} = 2\sqrt{t_D/\pi}$ for $t_D \leq 0.25$

For $t_D \geq 2.5$ $\quad F_0 = 1$

$F_1 = t_D - \frac{1}{3}$

Principio de Superposición.

Aplicaciones

a) Fracturas

b) Entrada de agua.

$$\frac{\partial^2 p}{\partial r^2} + \frac{1}{r}\frac{\partial p}{\partial r} = \frac{\phi\mu c}{k}\frac{\partial p}{\partial t}$$

$$y = \frac{\phi\mu c r^2}{4kt} \Rightarrow \frac{\partial p}{\partial r} = \frac{\partial p}{\partial y}\frac{\partial y}{\partial r} = \frac{\partial p}{\partial y}\left(2\frac{\phi\mu c r}{4kt}\right)$$

$$\frac{1}{r}\frac{\partial}{\partial r}\left(r\frac{\partial p}{\partial r}\right) = \frac{1}{r}\,2\frac{\phi\mu c r}{4kt}\frac{\partial}{\partial y}\left(2\frac{\phi\mu c r^2}{4kt}\frac{\partial p}{\partial y}\right)$$

$$= \frac{\phi\mu c}{2t}\frac{\partial}{\partial y}\left(y\frac{\partial p}{\partial y}\right)$$

$$\frac{\partial p}{\partial t} = \frac{\partial p}{\partial y}\frac{\partial y}{\partial t} = \frac{\partial p}{\partial y}\left(-\frac{\phi\mu c r^2}{4kt^2}\right)$$

$$\frac{4}{r^2}\,y\,\frac{\partial}{\partial y}\left(y\frac{\partial p}{\partial y}\right) = -\frac{\phi\mu c}{k}\,\frac{\phi\mu c r^2}{4kt^2}\,\frac{\partial p}{\partial t}$$

$$y\frac{\partial}{\partial y}\left(y\frac{\partial p}{\partial y}\right) = -y^2\frac{\partial p}{\partial y}$$

$$y\frac{\partial^2 p}{\partial y^2} + \frac{\partial p}{\partial y} = -y\frac{\partial p}{\partial y} \qquad \therefore\ y\frac{\partial^2 p}{\partial y^2} + \frac{\partial p}{\partial y}(1+y) = 0$$

$$q = +\frac{8L^2}{\pi^2} \sum_{n=1,3,5,\ldots}^{\infty} \frac{1}{n^2} \left(1 - e^{-\frac{n^2\pi^2 kt}{4\rho c L^2}}\right)$$

ضعف الطبقة

$$q = 2 \frac{k \Delta T}{L} \sum_{n=1,3,5,\ldots}^{\infty} \frac{8}{n^2\pi^2} e^{-\frac{n^2\pi^2 kt}{4\rho c L^2}}$$

cumulative-influx curve therefore may be plotted readily.

The figure pertains to a finite aquifer. The constant-rate case equation is equation (26), but as the rate is increasing this equation must be used with equation (53) to calculate the pressure at any time.

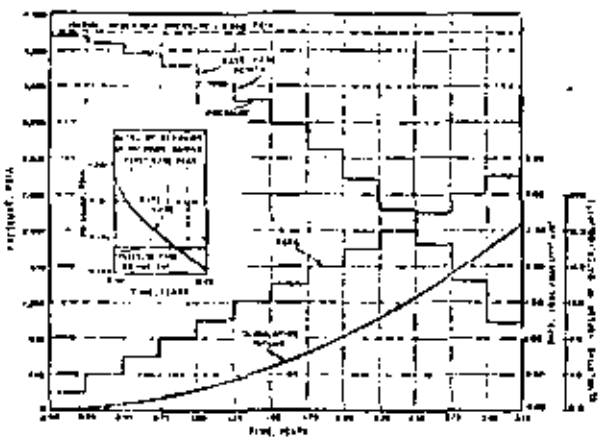

FIG 15

OIL RESERVOIR PERFORMANCE DETERMINED THROUGH APPLICATION OF THE SUPERPOSITION CONCEPT

The rate-time step function was pre-assigned and the corresponding cumulative-influx relationship calculated. This relationship was then used in determining both the rate-case and pressure-case pressure-time functions. Length of aquifer 4 miles.

Permeability, 200 mD
Porosity, 0.25
Viscosity of water, 0.300 cP
Compressibility of water, $3.00 \times 10^{-6}$ (vol/vol)/psi

Since the increases in rate $(Q_1 - Q_0)$ at $\theta_1$, $(Q_2 - Q_1)$ at $\theta_2$, $(Q_3 - Q_2)$ at $\theta_3$ and so on to $(Q_{M-1} - Q_{M-2})$ at $\theta_{M-1}$ are each equal to $Q_0$, the pressure $P_M$ at time $\theta_M$ may be calculated with the equation

$$P_M = P_i - \frac{Q_0 \alpha}{bkh}\left[\frac{ML}{3} + \frac{n}{L}\sum_{m=1}^{M} m \cdot \Delta\theta - \frac{2L}{\pi^2}\sum_{n=1}^{\infty}\sum_{m=1}^{M}\left(\frac{1}{n^2}\right)\exp\left(-\frac{n^2\pi^2\alpha}{L^2}(n-\Delta\theta)\right)\right] \quad (56)$$

Pressure-time data calculated with equation (56) are shown as small circles on Fig 15 and are identified as "rate-case points." The detailed behaviour of the "rate case" curve that would join two such points, *e.g.* the ones for $\theta = 0$ and $\theta = 0.25$ years, is shown in the inset on the figure.

Data for the pressure-case equivalent or pressure step-function was determined through application of equation (40), and the known cumulative influx at the end of each quarter as fixed by the initially imposed rate–time relationship.

If the bracketed term of equation (40) is symbolized by $f(0)$ or $f(n - \Delta\theta)$, that equation leads to the expression

$$\left(\frac{1}{bh}\right)\int_0^{n\Delta\theta} Q d\theta = \phi c L \sum_{m=1}^{n} \delta P_m f[(n-m)\Delta\theta] \quad (57)$$

The pressure drop $\delta P_0$ for the first increment of time may be calculated directly by setting $n = 1$. When this pressure drop is known, the drop for the second increment, $\delta P_1$ may be calculated by setting $n = 2$. Continuation of this process until it includes the last increment of time provides necessary data for plotting the pressure step-function.

A fundamental consequence of the superposition concept is that actual oilfield water-drive problems involving continuous changes in rate and pressure may be treated on an established theoretical basis.

## CONCLUSION

States of single-phase fluid motion in porous media are examined in this report. The theory of unsteady state influx of water in linear systems of oil reservoirs and fluid-connected aquifers is described in detail. Aquifers of both finite and infinite length are treated. Constant-rate-case and constant-pressure-case problems are stated analytically and solved. Results are plotted in easily usable graphical form, and numerical examples are worked out wherever practicable. The superposition concept in its relation to the problems discussed is explained. Its applicability to oilfield problems is indicated.

This paper should fill a need in petroleum literature for a theoretical dissertation on the subject of water influx in linear reservoirs. It should find application in engineering analyses of such reservoirs. Finally, it should be useful to practising engineers researchers studying this subject.

## ACKNOWLEDGMENTS

The author wishes to express his appreciation to the management of Socony-Mobil Oil Co. Inc. for permission to publish this paper. Helpful discussions with many engineers of Mobil Oil Co. de Venezuela during the period 1 July 1959 to 1 March 1960 are gratefully acknowledged. Special thanks are due to Carlos F. Gonzales for his assistance with the calculations.

*References*

1 van Everdingen, A. F., and Hurst, W. *Petrol. Trans. Amer. Inst. min. Engrs.* 1949, 186, 305.
2 Chatas, A. T. *Petrol. Engr.* 1953, 25 (5), B42; 25 (6), B31; 25 (9), B44.
3 Kurz, D. L., *et al.* "Handbook of Natural Gas Engineering," p. 400.
4 Churchill, R. V. "Modern Operational Mathematics in Engineering." New York: McGraw-Hill, 1944, p. 197.
5 "Tables of the Error Function and Its Derivative." Washington: U.S. Dept of Commerce, National Bureau of Standards, Applied Mathematics, Series 41, 22 Oct 1951.
6 Carslaw, H. S., and Jaeger, J. C. "Conduction of Heat in Solids," second edn. London: Oxford University Press, 1959, p. 112.
7 Churchill, R. V. "Fourier Series and Boundary Value Problems." New York: McGraw-Hill, 1941, p. 111, 123.
8 von Karman, T., and Biot, M. A. "Mathematical Methods in Engineering." New York: McGraw-Hill, 1940, p. 326, 403.

Dr. Heber Cinco

Reference: J. Pet. Tech., (May 1966) 637-642.

25

# The Flow of Real Gases Through Porous Media

R. AL-HUSSAINY
JUNIOR MEMBER AIME
H. J. RAMEY, JR.*
F. B. CRAWFORD
MEMBERS AIME

TEXAS A&M U.
COLLEGE STATION, TEX.

## ABSTRACT

*The effect of variations of pressure-dependent viscosity and gas law deviation factor on the flow of real gases through porous media has been considered. A rigorous gas flow equation was developed which is a second order, non-linear partial differential equation with variable coefficients. This equation was reduced by a change of variable to a form similar to the diffusivity equation, but with potential-dependent diffusivity. The change of variable can be used as a new pseudo-pressure for gas flow which replaces pressure or pressure-squared as currently applied to gas flow.*

*Substitution of the real gas pseudo-pressure has a number of important consequences. First, second degree pressure gradient terms which have commonly been neglected under the assumption that the pressure gradient is small everywhere in the flow system, are rigorously handled. Omission of second degree terms leads to serious errors in estimated pressure distributions for tight formations. Second, flow equations in terms of the real gas pseudo-pressure do not contain viscosity or gas law deviation factors, and thus avoid the need for selection of an average pressure to evaluate physical properties. Third, the real gas pseudo-pressure can be determined numerically in terms of pseudo-reduced pressures and temperatures from existing physical property correlations to provide generally useful information. The real gas pseudo-pressure was determined by numerical integration and is presented in both tabular and graphical form in this paper. Finally, production of real gas can be correlated in terms of the real gas pseudo-pressure and shown to be similar to liquid flow as described by diffusivity equation solutions.*

*Application of the real gas pseudo-pressure to radial flow systems under transient, steady-state or approximate pseudo-steady-state injection or production have been considered. Superposition of the linearized real gas flow solutions to generate variable rate performance was investigated and found satisfactory. This provides justification for pressure build-up testing. It is believed that the concept of the real gas pseudo-pressure will lead to improved interpretation of results of current gas well testing procedures, both steady and unsteady-state in nature, and improved forecasting of gas production.*

## INTRODUCTION

In recent years a considerable effort has been directed to the theory of isothermal flow of gases through porous media. The present state of knowledge is far from being fully developed. The difficulty lies in the non-linearity of partial differential equations which describe both real and ideal gas flow. Solutions which are available are approximate analytical solutions, graphical solutions, analogue solutions and numerical solutions.

The earliest attempt to solve this problem involved the method of successions of steady states proposed by Muskat.[1] Approximate analytical solutions[2] were obtained by linearizing the flow equation for ideal gas to yield a diffusivity-type equation. Such solutions, though widely used and easy to apply to engineering problems, are of limited value because of idealized assumptions and restrictions imposed upon the flow equation. The validity of linearized equations and the conditions under which their solutions apply have not been fully discussed in the literature. Approximate solutions are those of Heatherington *et al.*,[3] MacRoberts[4] and Janicek and Katz.[5] A graphical solution of the linearized equation was given by Cornell and Katz.[6] Also, by using the mean value of the time derivative in the flow equation, Rowan and Clegg[7] gave several simple approximate solutions. All the solutions were obtained assuming small pressure gradients and constant gas properties. Variation of gas properties with pressure has been neglected because of analytic difficulties, even in approximate analytic solutions.

Green and Wilts[8] used an electrical network for simulating one-dimensional flow of an ideal gas. Numerical methods using finite difference equations and digital computing techniques have been used extensively for solving both ideal and real gas equations. Aronofsky and Jenkins[9] and Bruce *et al.*[10] gave numerical solutions for linear and radial gas flow. Douglas *et al.*[11] gave a solution for a square drainage area. Aronofsky[12] included the effect of slippage on ideal gas flow. The most important contribution to the theory of flow of ideal gases through porous media was the conclusion reached by Aronofsky and Jenkins[9] that solutions for the liquid flow case[13] could be used to generate approximate solutions for constant rate production of ideal gases.

An equation describing the flow of real gases has been solved for special cases by a number of investigators using numerical methods. Aronofsky and Ferris[14] considered linear flow, while Aronofsky and Porter[15] considered radial gas flow. Gas properties were permitted to vary as linear functions of pressure. Recently, Carter[16] proposed an empirical correlation by which gas well behavior can be estimated from solutions of the diffusivity equation using instantaneous values of pressure-dependent gas

Original manuscript received in Society of Petroleum Engineers office June 29, 1965. Revised manuscript of SPE 1243A received Feb. 21, 1966. Paper was presented at SPE Annual Fall Meeting held in Denver, Colo., Oct. 3-6, 1965.

*Presently on the faculty at Stanford U.

[1]References given at end of paper.

properties evaluated at an average pressure also defined empirically. Carter gave a limited number of numerical solutions as a basis, and suggested some relations which might give a better correlation. However, the proposed relations were not evaluated in the mentioned work. Solutions have been presented by Eilerts *et al.*[25,26] for flow of gas-condensate fluids in linear and radial systems.

It has been observed that as the gas flow velocity increases, departure from Darcy's law occurs.[1-3] Such flow is termed non-Darcy, or turbulent flow. Flow is transitional, and not truly turbulent. A gas flow equation including a quadratic velocity term to account for turbulence near the producing well has been solved by Swift and Kiel[27] and Tek *et al.*[28] for ideal gases. Eilerts *et al.*[25,26] and Carter[29,30] also included non-Darcy flow in their solutions for real gases. An approximate solution including non-Darcy flow has been presented by Rowan and Clegg.[31]

Two other calculational procedures appear in the works of Roberts[32] and Kidder[33] for solving the one-dimensional flow equation for an ideal gas. Roberts used a stepwise forward integration in time by joining together a sequence of solutions for linearized differential equations. Kidder, applying perturbation technique and using the well-known Boltzmann transformation in the theory of diffusion, gave an exact analytic solution for gas flow in a semi-infinite porous medium. Kidder's solution is very similar to a more general one reported by Polubarinova-Kochina[34] on the movement of ground water.

In summary, only a limited number of solutions for flow of real gases are available, and these are not of general utility. Furthermore, methods of analyzing gas reservoir performance in current use are generally based on solutions for the flow of ideal gases *under the assumption of small pressure gradients*. These methods fail to describe the behavior of low permeability and high pressure reservoirs.

## FLOW OF REAL GASES

The following concerning the flow of real gases through porous media is drawn from an analogy with the theory of heat conduction in solids.[35] Variation of gas physical properties with the pressure correspond to that of temperature-dependent properties in the theory of heat conduction.

The mechanism of fluid flow through a porous medium is governed by the physical properties of the matrix, geometry of flow, PVT properties of the fluid and pressure distribution within the flow system. In deriving the flow equations and establishing the solutions, the following assumptions are made. The medium is homogeneous, the flowing gas is of constant composition and the flow is laminar and isothermal. Assumption of laminar flow can be removed, but will be used to simplify the presentation.

The principle of conservation of mass for isothermal fluid flow through a porous medium is expressed by the well-known continuity equation:

$$\nabla\cdot[\rho\, v] = \phi\,\frac{\partial \rho}{\partial t} \quad \ldots\ldots\ldots\ldots\ldots\ldots (1)$$

The velocity vector in Eq. 1 is given by Darcy's law for laminar flow as:

$$v = -\frac{k(p)}{\mu(p)}\nabla p \quad \ldots\ldots\ldots\ldots\ldots\ldots (2)$$

Substituting Eq. 2 in Eq. 1 yields:

$$\nabla\cdot\left[\rho\,\frac{k(p)}{\mu(p)}\,\nabla p\right] = \phi\,\frac{\partial \rho}{\partial t} \quad \ldots\ldots\ldots\ldots\ldots\ldots (3)$$

For real gases:

$$\rho = \frac{M}{RT}\left[\frac{p}{z(p)}\right] \quad \ldots\ldots\ldots\ldots\ldots\ldots (4)$$

Density can be eliminated from Eq. 3 to yield:

$$\nabla\cdot\left[\frac{k(p)}{\mu(p)z(p)}\,p\nabla p\right] = \phi\,\frac{\partial}{\partial t}\left[\frac{p}{z(p)}\right] \quad \ldots\ldots\ldots\ldots\ldots\ldots (5)$$

Eq. 5 is one form of the fundamental non-linear partial differential equation describing isothermal flow of real gases through porous media.

The pressure-dependent permeability for gas was expressed by Klinkenberg[36] as:

$$k(p) = k_l\left(1 + \frac{b}{p}\right) \quad \ldots\ldots\ldots\ldots\ldots\ldots (6)$$

where $k_l$ = effective permeability to liquids; and $b$ = the slope of a linear plot of $k(p)$ vs $\frac{1}{p}$.

However, the dependency of permeability on pressure is usually negligible for pressure conditions associated with gas reservoirs, as pointed out by Aronofsky.[36] In a subsequent paper, Aronofsky and Ferris[37] indicated that variations of gas properties with pressure are more important than variations of permeability with pressure. Therefore, liquid permeability can be used for gas flow, and the following equation is correct for all practical purposes:

$$\nabla\cdot\left[\frac{p}{\mu(p)z(p)}\,\nabla p\right] = \frac{\phi}{k}\,\frac{\lambda}{\partial t}\left[\frac{p}{z(p)}\right] \quad \ldots\ldots\ldots\ldots (7)$$

Eq. 7 can be expanded to many different forms. For example, Eq. 7 can be rearranged to point out explicitly the real gas diffusivity

$$\frac{k}{\phi\mu(p)c_t(p)}$$

Since

$$\rho\nabla p = \frac{1}{2}\,\nabla p^2 \quad \ldots\ldots\ldots\ldots\ldots\ldots (8)$$

Eq. 7 becomes, after some rearrangement:

$$\nabla^2 p^2 - \frac{d[\ln \mu(p)z(p)]}{dp^2}(\nabla p^2)^2 = \frac{2\phi\mu(p)z(p)}{k}\,\frac{\lambda}{\partial t}\left[\frac{p}{z(p)}\right] \quad \ldots\ldots\ldots\ldots (9)$$

From the definition of the isothermal compressibility of gas:

$$c_t(p) = \frac{1}{\rho}\,\frac{d\rho}{dp} = \frac{z(p)}{p}\,\frac{d}{dp}\left(\frac{p}{z(p)}\right) = \frac{1}{p} - \frac{1}{z(p)}\,\frac{dz(p)}{dp} \quad \ldots\ldots\ldots\ldots (10)$$

Thus:

$$\frac{\partial}{\partial t}\left[\frac{p}{z(p)}\right] = \frac{pc_t(p)}{z(p)}\,\frac{\partial p}{\partial t} \quad \ldots\ldots\ldots\ldots (11)$$

Combining Eqs. 9 and 11:

Permeability can be considered an important function of pressure for a well-consolidated sand as used by Eilerts.[25,26] This case can be handled, as will be shown later in this paper.

$$\nabla^2 p - \frac{d[\ln \mu(p)z(p)]}{dp}(\nabla p)^2 = \frac{\phi\mu(p)c_t(p)}{k}\frac{\partial p}{\partial t} \quad \ldots (12)$$

If it is assumed that viscosity and gas law deviation factors change slowly with pressure change, the pressure differential of $[\ln \mu(p)z(p)]$ becomes negligible. On the other hand, the assumption that pressure gradients are small will permit omission of terms of order $(\nabla p)^2$. In either event, Eq. 12 can be simplified to:

$$\nabla^2 p = \frac{\phi\mu(p)c_t(p)}{k}\frac{\partial p}{\partial t} \quad \ldots (13)$$

Eq. 13 is similar in form to the diffusivity equation. However, the diffusivity is a function of pressure, even for a perfect gas. In this form, the close analogy with liquid flow found by Jenkins and Aronofsky[8, 9] is emphasized. *However, the assumption that pressure gradients are small everywhere in the flow system cannot be justified in many important cases.* The assumption of small pressure gradients is implicit in *all* of the pressure build-up and drawdown methods currently in use which are based upon ideal gas flow solutions or liquid flow analogies. We return, then, to the rigorous Eq. 7.

Eq. 7 can be transformed to a form similar to that of Eq. 13 *without assuming small pressure gradients*, by making a scale change in pressure. Define a new pseudo-pressure $m(p)$ as follows:

$$m(p) = 2\int_{p_b}^{p} \frac{p}{\mu(p)z(p)}\,dp \quad \ldots (14)$$

where $p_b$ is a low base pressure. The variable $m(p)$ has the dimensions of pressure-squared per centipoise. Since $\mu(p)$ and $z(p)$ are functions of pressure alone for isothermal flow, this is a unique definition of $m(p)$. It follows that:

$$\frac{\partial m(p)}{\partial t} = \frac{\partial m(p)}{\partial p}\frac{\partial p}{\partial t} = \left(\frac{2p}{\mu(p)z(p)}\right)\frac{\partial p}{\partial t} \quad \ldots (15)$$

and

$$\frac{\partial m(p)}{\partial x} = \left(\frac{2p}{\mu(p)z(p)}\right)\frac{\partial p}{\partial x} \quad \ldots (16)$$

with similar expressions for $\frac{\partial m(p)}{\partial y}$ and $\frac{\partial m(p)}{\partial z}$.

Therefore, Eq. 7 can be rewritten in terms of the variable $m(p)$ using the definition of $c_t(p)$ given by Eq. 10 as:

$$\nabla\cdot[\nabla m(p)] = \frac{\phi\mu(p)c_t(p)}{k}\frac{\partial m(p)}{\partial t} \quad \ldots (17)$$

or

$$\nabla^2 m(p) = \frac{\phi\mu(p)c_t(p)}{k}\frac{\partial m(p)}{\partial t} \quad \ldots (18)$$

Comparison of Eqs. 13 and 18 shows that the form of the diffusivity equation is preserved in terms of the new variable $m(p)$. However, Eq. 18 is still *non-linear* because diffusivity is a function of potential. The gas law deviation factor $z$ does not appear in the equation, but is involved in $m(p)$ and $c_t(p)$. Eq. 18 does not involve the assumptions of small pressure gradients, nor that of slow variation of $[\mu(p)z(p)]$.

The importance of Eq. 18 deserves emphasis. It is a fundamental partial differential equation which describes the flow of real gases. To the authors' knowledge, this equation has not been presented previously in connection with gas flow. Equations of this type have been called quasi-linear flow equations.[8, 9] The real importance lies in the extreme utility of this form of the equation. As will be shown, the form of the equation suggests a powerful engineering approach to the flow of real gases.

To solve Eq. 18, it is necessary to convert the usual initial and boundary conditions into terms of the new pseudo-pressure $m(p)$. Important considerations are as follows.

The gas mass flux is:

$$v_\rho = \frac{q}{A}\rho = \frac{-Mk}{RT}\frac{p}{\mu(p)z(p)}\nabla p \quad \ldots (19)$$

In terms of $m(p)$, the mass flux is:

$$\frac{q}{A}\rho = \frac{-Mk}{2RT}\nabla m(p) \quad \ldots (20)$$

The usual boundary conditions are either specification of pressure or the gas flux across bounding surfaces. When pressure is fixed, $m(p)$ can be determined from Eq. 14. If flux is specified, the boundary conditions can be determined from Eq. 20. If the outer boundary is impermeable, then:

$$\frac{dm(p)}{dn} = 0 \quad \ldots (21)$$

where $n$ is the direction normal to the boundary.

Steady-state flow occurs when pressure distribution and fluid velocity are independent of time. Eq. 18 reduces to:

$$\nabla^2 m(p) = 0 \quad \ldots (22)$$

which is Laplace's equation. Thus, previous solutions of the Laplace equation can be used if $m(p)$ is used as the potential.

Steady-state flow can rarely be obtained in reality because gas wells usually produce gas from a limited, finite reservoir or drainage volume. There can be no flow across the outer boundary. Thus, pressure must decline as production continues. True steady-state would require pressure to remain constant at the outer boundary, which implies flow across the outer boundary. Production of a bounded reservoir at constant production is an important problem, which will be considered later in this paper.

## REAL GAS PSEUDO-PRESSURE

To obtain generally useful solutions for Eq. 18, the proper physical properties for natural gases must be specified. Fortunately, all required physical properties have been correlated as functions of pseudo-reduced pressures and temperatures for many gases met in field work. It should be emphasized that the concept of the real gas pseudo-pressure is not limited to use of specific gas property correlations. Pseudo-reduced pressure and temperature are defined, respectively, as:

$$p_{pr} = \frac{p}{p_{pc}} \quad \ldots (23)$$

and

$$T_{pr} = \frac{T}{T_{pc}} \quad \ldots (24)$$

where $p_{pc}$ is the pseudo-critical pressure and $T_{pc}$ is the pseudo-critical temperature. Real gas law deviation factors $z(p)$ have been presented by Standing and Katz.[10] Vis-

cosities of natural gases have been correlated by Carr *et al.*[3] as the ratio of viscosity at any pressure to that at one atmosphere. Thus:

$$\frac{\mu(p)}{\mu_1} = f(p_{pr}, T_{pr}) \quad \ldots \quad (25)$$

Compressibilities of natural gases have been correlated by Trube[4] as reduced compressibilities, the product of compressibility and pseudo-critical pressure. That is:

$$c_{pr} = c(p) \cdot p_{pc} = f(p_{pr}, T_{pr}) \quad \ldots \quad (26)$$

Substitution of Eqs. 23 to 25 in Eq. 14 yields:

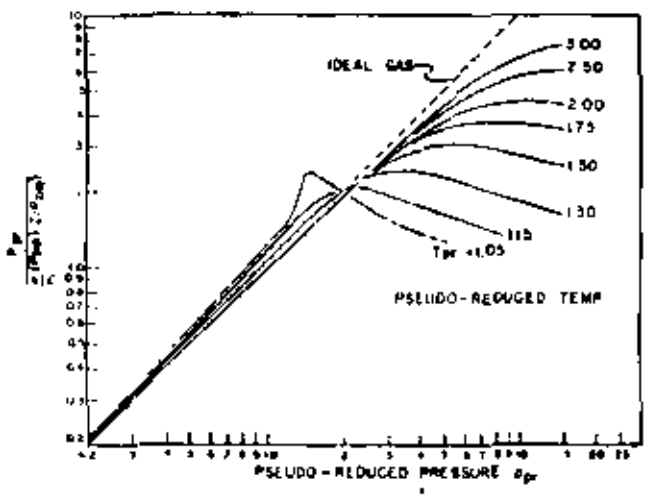


FIG. 1 RATIO OF PSEUDO-REDUCED PRESSURE TO VISCOSITY-GAS DEVIATION FACTOR PRODUCT AS PSEUDO-REDUCED PRESSURE

$$m(p) = \int_{(p_{pr})_a}^{p_{pr}} \frac{p_{pr}}{(\mu_1/\mu)z(p_{pr})}\, dp_{pr} \quad \ldots \quad (27)$$

The integral can be evaluated generally from reduced properties correlations.

## EVALUATION OF REAL GAS PSEUDO-PRESSURE

To establish the relationship between $p_{pr}$ and $m(p)$, the integral must be evaluated numerically for various isotherms. The lower limit of the integration $(p_{pr})_a$ can be set arbitrarily. A value of 0.20 was chosen. Selected isotherms from pseudo-reduced temperatures of 1.05 to 3.0 were used.

Fig. 1 presents the argument of the integral in Eq. 27 vs pseudo-reduced pressure for various pseudo-reduced temperatures. The dashed line represents the ideal gas case with both viscosity ratio and gas law deviation factor equal to unity. The magnitude of gross variations of gas properties with pressure and temperature is apparent.

Fig. 2 presents $m(p)$ integrals as functions of pseudo-reduced pressures and temperatures. The integrals were evaluated by means of the Trapezoidal rule using an IBM 709 digital computer. Values of the integrals are also presented in Table 1. Interpolation between the curves or between the values presented in the table can be performed easily.

Use of Fig. 2 or Table 1 is limited to gases containing small amounts of contaminants for which changes in viscosity and gas law deviation factor can be handled by appropriate changes in the pseudo-critical properties, as suggested by Carr *et al.*[3] However, useful charts can be prepared for gases containing large amounts of contaminants if complete properties are known. See Robinson

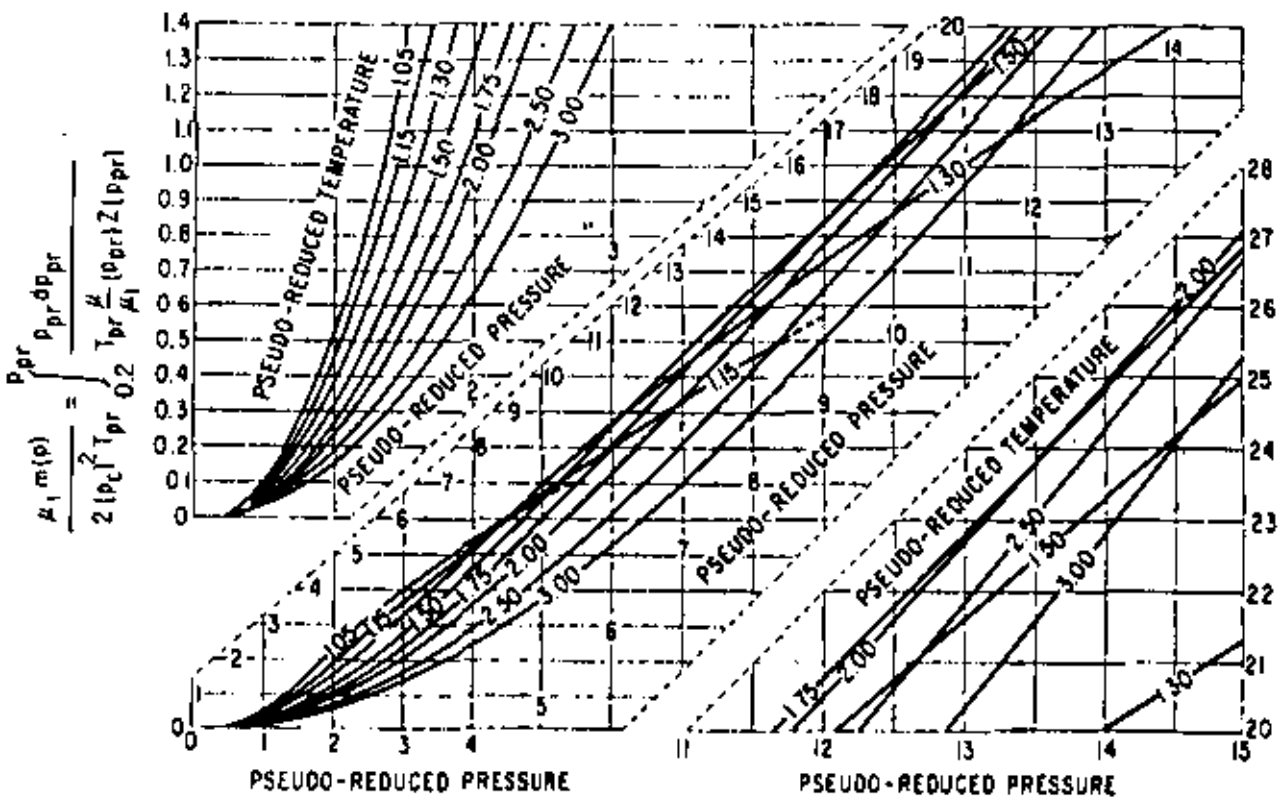


FIG. 2 REAL GAS PSEUDO-PRESSURE INTEGRALS AS PSEUDO-REDUCED PRESSURE

*et al*[11] for density data for gases containing large amounts of contaminants.

In general, it is useful to prepare a chart of $m(p)$ in units of psi-squared per centipoise vs pressure in psi for any given reservoir to aid engineering use of the real gas pseudo-pressure. The $m(p)$ can be computed readily for *any* specific gas and reservoir temperature if density and viscosity are known as functions of pressure. The integration can be performed using the Trapezoidal rule or graphical integration. More sophisticated integrations are usually not required.

The $m(p)$ values in Fig. 2 and Table 1 are presented as a convenience because it is necessary to assume many gases do follow the existing correlations because of lack of specific data. It is emphasized that the concept of the real gas potential is *general* and is *not* limited to use of the $m(p)$ values presented herein. If viscosity and density data are available for a specific gas, it should be used in preference to Fig. 2 and Table 1 to prepare $m(p)$ plots for the specific gas.

## TRANSIENT FLOW

### CONSTANT-RATE PRODUCTION

As has been described in the introduction of this paper, Eq. 7 has been solved for specific flow cases under appropriate boundary and initial conditions by a number of authors using finite difference solutions. We seek a general solution which can be used for engineering purposes without the aid of a digital computer. Eq. 18 and the work of Aronofsky and Jenkins[5] provide a basis for an approach. For radial flow of *ideal* gas, the continuity equation leads to:

$$\frac{\partial^2 p^2}{\partial r^2} + \frac{1}{r}\frac{\partial p^2}{\partial r} = \frac{\phi \mu c_g(p)}{k}\frac{\partial p^2}{\partial t} \quad \ldots\ldots (28)$$

where $c_g(p)$ for an ideal gas is the reciprocal of the pressure. Several features of Eq. 28 are noteworthy. First,

TABLE 1—$\int_0^{p_{pr}} \frac{p_{pr}\,dp_{pr}}{\mu_g z}$ $\frac{\mu_g m(p)}{2(p_{pc})(T_{pc})}$ $T_{pr} = \frac{T}{T_{pc}}$ $(p_{pr})$ $z$ $(p_{pr})$

| Pseudo Reduced Pressure $p_{pr}$ | Values of Integral for Pseudo Reduced Temperature $T_{pr}$ of | | | | | | | |
|---|---|---|---|---|---|---|---|---|
| | 1.05 | 1.10 | 1.30 | 1.50 | 1.75 | 2.00 | 2.50 | 3.00 |
| 0.20 | 0.0257 | 0.0229 | 0.0198 | 0.0170 | 0.0145 | 0.0126 | 0.0100 | 0.0083 |
| 0.40 | 0.0623 | 0.0553 | 0.0477 | 0.0409 | 0.0348 | 0.0303 | 0.0241 | 0.0200 |
| 0.60 | 0.1102 | 0.0971 | 0.0839 | 0.0716 | 0.0609 | 0.0530 | 0.0421 | 0.0349 |
| 0.80 | 0.1698 | 0.1483 | 0.1283 | 0.1091 | 0.0927 | 0.0807 | 0.0640 | 0.0532 |
| 1.00 | 0.2418 | 0.2103 | 0.1810 | 0.1532 | 0.1303 | 0.1132 | 0.0898 | 0.0747 |
| 1.20 | 0.3264 | 0.2835 | 0.2419 | 0.2037 | 0.1734 | 0.1505 | 0.1194 | 0.0993 |
| 1.40 | 0.4238 | 0.3678 | 0.3111 | 0.2608 | 0.2221 | 0.1927 | 0.1529 | 0.1271 |
| 1.60 | 0.5326 | 0.4631 | 0.3889 | 0.3246 | 0.2763 | 0.2397 | 0.1902 | 0.1580 |
| 1.80 | 0.6546 | 0.5691 | 0.4755 | 0.3954 | 0.3358 | 0.2915 | 0.2312 | 0.1920 |
| 2.00 | 0.7903 | 0.6855 | 0.5707 | 0.4734 | 0.4004 | 0.3483 | 0.2761 | 0.2292 |
| 2.20 | 0.9484 | 0.8126 | 0.6734 | 0.5579 | 0.4707 | 0.4098 | 0.3248 | 0.2695 |
| 2.40 | 1.1444 | 0.9503 | 0.7838 | 0.6484 | 0.5457 | 0.4738 | 0.3773 | 0.3129 |
| 2.60 | 1.3671 | 1.0980 | 0.9020 | 0.7449 | 0.6253 | 0.5461 | 0.4335 | 0.3594 |
| 2.80 | 1.5828 | 1.2546 | 1.0277 | 0.8473 | 0.7114 | 0.6209 | 0.4932 | 0.4090 |
| 3.00 | 1.7924 | 1.4191 | 1.1606 | 0.9558 | 0.8025 | 0.7001 | 0.5566 | 0.4616 |
| 3.20 | 1.9959 | 1.5883 | 1.3001 | 1.0703 | 0.8983 | 0.7840 | 0.6235 | 0.5173 |
| 3.40 | 2.1926 | 1.7595 | 1.4457 | 1.1906 | 0.9988 | 0.8724 | 0.6940 | 0.5760 |
| 3.60 | 2.3821 | 1.9321 | 1.5966 | 1.3164 | 1.1047 | 0.9653 | 0.7679 | 0.6378 |
| 3.80 | 2.5649 | 2.1071 | 1.7524 | 1.4474 | 1.2146 | 1.0624 | 0.8454 | 0.7025 |
| 4.00 | 2.7424 | 2.2841 | 1.9128 | 1.5838 | 1.3298 | 1.1636 | 0.9264 | 0.7701 |
| 4.20 | 2.9147 | 2.4619 | 2.0791 | 1.7253 | 1.4498 | 1.2687 | 1.0111 | 0.8407 |
| 4.40 | 3.0833 | 2.6399 | 2.2473 | 1.8712 | 1.5744 | 1.3777 | 1.0994 | 0.9143 |
| 4.60 | 3.2486 | 2.8173 | 2.4186 | 2.0214 | 1.7034 | 1.4904 | 1.1912 | 0.9907 |
| 4.80 | 3.4066 | 2.9937 | 2.5935 | 2.1758 | 1.8370 | 1.6068 | 1.2863 | 1.0700 |
| 5.00 | 3.5633 | 3.1680 | 2.7710 | 2.3341 | 1.9751 | 1.7268 | 1.3844 | 1.1522 |
| 5.20 | 3.7169 | 3.3401 | 2.9504 | 2.4957 | 2.1169 | 1.8504 | 1.4864 | 1.2373 |
| 5.40 | 3.8679 | 3.5094 | 3.1320 | 2.6612 | 2.2626 | 1.9778 | 1.5915 | 1.3253 |
| 5.60 | 4.0165 | 3.6766 | 3.3153 | 2.8308 | 2.4123 | 2.1091 | 1.6998 | 1.4159 |
| 5.80 | 4.1628 | 4.0876 | 3.5001 | 3.0043 | 2.5658 | 2.2442 | 1.8114 | 1.5093 |
| 6.00 | 4.3068 | 4.0876 | 3.6866 | 3.1815 | 2.7230 | 2.3834 | 1.9264 | 1.6056 |
| 6.20 | 4.4478 | 4.2464 | 3.8744 | 3.3622 | 2.8838 | 2.5264 | 2.0447 | 1.7049 |
| 6.40 | 4.5865 | 4.4026 | 4.0637 | 3.5464 | 3.0482 | 2.6734 | 2.1664 | 1.8071 |
| 6.60 | 4.7228 | 4.5564 | 4.2540 | 3.7339 | 3.2161 | 2.8243 | 2.2914 | 1.9123 |
| 6.80 | 4.8565 | 4.7078 | 4.4453 | 3.9246 | 3.3875 | 2.9792 | 2.4197 | 2.0204 |
| 7.00 | 4.9878 | 4.8566 | 4.6375 | 4.1184 | 3.5623 | 3.1381 | 2.5513 | 2.1315 |
| 7.20 | 5.1166 | 5.0030 | 4.8305 | 4.3152 | 3.7405 | 3.3010 | 2.6862 | 2.2455 | |
| 7.40 | 5.2430 | 5.1469 | 5.0242 | 4.5149 | 3.9220 | 3.4680 | 2.8244 | 2.3624 |
| 7.60 | 5.3670 | 5.2884 | 5.2185 | 4.7175 | 4.1068 | 3.6391 | 2.9659 | 2.4823 |
| 7.80 | 5.4886 | 5.4275 | 5.4134 | 4.9228 | 4.2948 | 3.8143 | 3.1107 | 2.6051 |
| 8.00 | 5.6078 | 5.5642 | 5.6088 | 5.1308 | 4.4860 | 3.9936 | 3.2589 | 2.7309 |
| 8.25 | 5.7570 | 5.7386 | 5.8322 | 5.3911 | 4.7170 | 4.2060 | 3.4387 | 2.8866 |
| 8.50 | 5.9035 | 5.9102 | 6.0564 | 5.6532 | 4.9500 | 4.4205 | 3.6208 | 3.0446 |
| 8.75 | 6.0474 | 6.0793 | 6.2813 | 5.9170 | 5.1849 | 4.6372 | 3.8052 | 3.2049 |
| 9.00 | 6.1887 | 6.2458 | 6.5069 | 6.1824 | 5.4217 | 4.8560 | 3.9919 | 3.3675 |
| 9.25 | 6.3275 | 6.4098 | 6.7331 | 6.4494 | 5.6603 | 5.0769 | 4.1809 | 3.5324 |
| 9.50 | 6.4638 | 6.5713 | 6.9599 | 6.7179 | 5.9007 | 5.2998 | 4.3722 | 3.6996 |
| 9.75 | 6.5977 | 6.7303 | 7.1873 | 6.9879 | 6.1429 | 5.5247 | 4.5658 | 3.8691 |
| 10.00 | 6.7292 | 6.8869 | 7.4153 | 7.2594 | 6.3868 | 5.7516 | 4.7617 | 4.0408 |
| 10.50 | 6.9870 | 7.1928 | 7.8727 | 7.8054 | 6.8781 | 6.2114 | 5.1599 | 4.3882 |
| 11.00 | 7.2373 | 7.4909 | 8.3314 | 8.3552 | 7.3736 | 6.6792 | 5.5662 | 4.7406 |
| 11.50 | 7.4803 | 7.7814 | 8.7911 | 8.9085 | 7.8731 | 7.1548 | 5.9804 | 5.0977 |
| 12.00 | 7.7161 | 8.0645 | 9.2518 | 9.4652 | 8.3765 | 7.6382 | 6.4024 | 5.4594 |
| 12.50 | 7.9449 | 8.3403 | 9.7134 | 10.0252 | 8.8837 | 8.1293 | 6.8321 | 5.8255 |
| 13.00 | 8.1668 | 8.6090 | 10.1758 | 10.5883 | 9.3945 | 8.6280 | 7.2694 | 6.1958 |
| 13.50 | 8.3820 | 8.8707 | 10.6390 | 11.1544 | 9.9089 | 9.1342 | 7.7142 | 6.5702 |
| 14.00 | 8.5907 | 9.1256 | 11.1029 | 11.7234 | 10.4268 | 9.6478 | 8.1664 | 6.9485 |
| 14.50 | 8.7931 | 9.3739 | 11.5674 | 12.2951 | 10.9481 | 10.1686 | 8.6258 | 7.3306 |
| 15.00 | 8.9894 | 9.6157 | 12.0325 | 12.8695 | 11.4727 | 10.6965 | 9.0923 | 7.7163 |

the second degree pressure gradient term $(dp/dr)^2$ does not appear for an ideal gas. Second, Eq. 28 has the form of the diffusivity equation, but the diffusivity is proportional to pressure. Viscosity is a function of temperature, but not of pressure for an ideal gas. Aronofsky and Jenkins found that for constant rate production of an ideal gas from a closed radial system, the pressure at the producing well could be correlated as a function of a dimensionless time based on a compressibility evaluated at the initial pressure. The correlation was slightly sensitive to the production rate, but not sensitive enough to affect engineering accuracy.

Aronofsky and Jenkins demonstrated that production of ideal gas from a closed radial system could be approximated very closely from the solutions for transient liquid flow of van Everdingen and Hurst.[4] Matthews[5] later pointed out the application of this conclusion to pressure build-up analysis for gas wells as a liquid case analog.

For radial flow of a real gas, Eq. 18 becomes:

$$\frac{\partial^2 m(p)}{\partial r^2} + \frac{1}{r}\frac{\partial m(p)}{\partial r} = \frac{\phi \mu(p) c_g(p)}{k}\frac{\partial m(p)}{\partial t} \quad \ldots \quad (29)$$

The close analogy between Eqs. 28 and 29 suggests that the real gas pseudo-pressure $m(p)$ should correlate as a function of a dimensionless time based on viscosity and compressibility evaluated at the initial pressure, if the variation of the viscosity-compressibility product with $m(p)$ for a real gas is similar to the variation of compressibility for an ideal gas $(1/p)$ with pressure squared. Fig. 3 shows the comparison.

In view of the close resemblance between $(\mu c_g)$ vs $m(p)$ for the real gas, and $p^{-1}$ vs $p^2$ for the ideal gas, it is reasonable to expect solutions for the flow of real gases to correlate as functions of a dimensionless time based on initial values of viscosity and compressibility. That is, let:

$$t_a = \frac{kt}{\phi(\mu c_g)_i r_w^2} \quad \ldots \quad (30)$$

Further, define a dimensionless real gas pseudo-pressure drop $m_a(r_a, t_a)$:

$$m_a(r_a, t_a) = \frac{\pi k h T_{sc}}{q_{sc} p_{sc} T}\,[m(p_i) - m(r, t)] \quad \ldots \quad (31)$$

where $r_a = r/r_w$. The dimensionless real gas pseudo-pressure drop is thus analogous to the van Everdingen-Hurst[4] dimensionless pressure drop $p_a(r_a, t_a)$.

Fig. 4 shows the comparison between $p_a(t_a)$ for the liquid flow solutions and $m_a(t_a)$ obtained from Eilerts *et al.*[6] solutions for the radial flow of natural gases. The solid line represents the liquid case, while points shown are computed from the Eilerts *et al.* solutions. As can be seen, the comparison is excellent for the entire range of flow considered by Eilerts *et al.* for both natural gases and condensate gases. The transient flow data computed by Carter[7] correlate just as well. The Eilerts *et al.* data are a severe test of the linearization of the real gas flow equation, because production included a tenfold range in production rate, and almost complete depletion over a pressure range from 10,000 to 1,000 psi. Carter's results covered a range from 4,700 to 1,160 psia, and a more restricted range of flow rate.

The $m_a(t_a)$ correlation (Fig. 4) is actually not as good as it appears. Although it is quite good at times before the boundary effect is felt, at long times there may be a considerable difference between $m_a(t_a)$ and $p_a(t_a)$ values

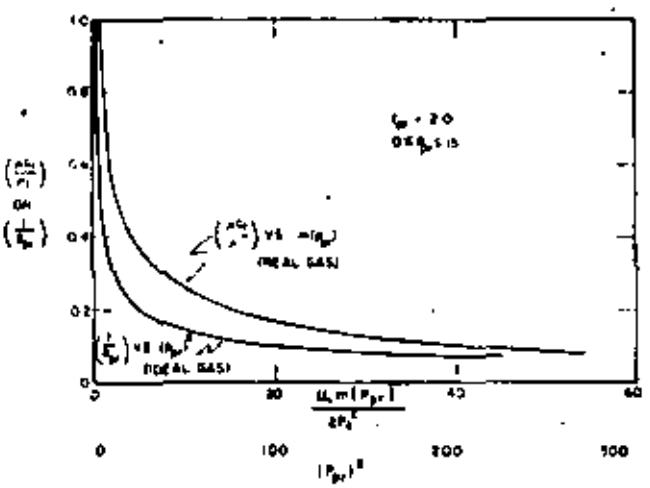


Fig. 4—$p_a(t_a)$ and $m_a(t_a)$ vs $t_a$ for a Closed, Radial Reservoir Produced at Constant Rate.

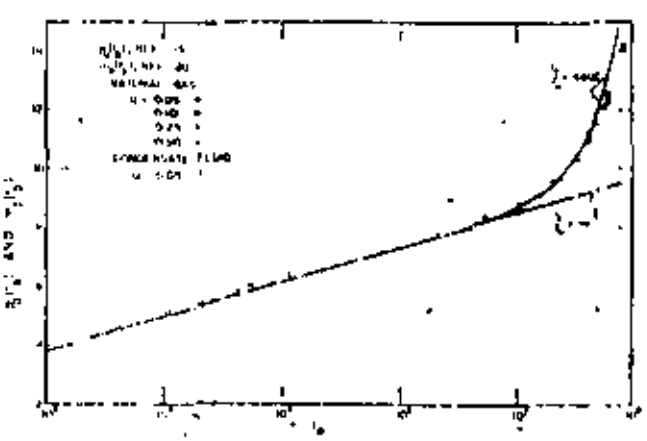

Fig. 3—Pressure-Dependent Diffusivity Terms vs Pressure for Ideal and Real Gas Flow.

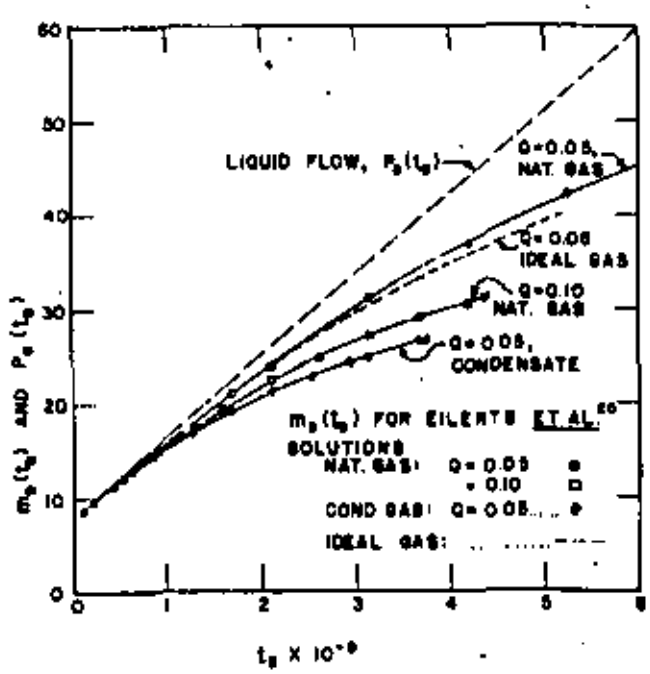


Fig. 5—$m_a(t_a)$ and $p_a(t_a)$ vs $t_a$ for Radial Flow of Liquid, Ideal Gas and Real Gases.

(Fig. 5). Also shown on Fig. 5 are the Aronofsky-Jenkins' ideal gas flow results. It is clear that both the ideal and real gas cases lead to dimensionless pressure drops which are lower than the liquid case—and which are flow-rate dependent. Another important difference is illustrated by the case $Q = 0.05$. The ideal gas line terminates at the point where the well pressure is zero. The real gas solutions terminate at a well pressure of 10 per cent of the initial pressure. Although not shown on Fig. 5, the production times for the real gas cases to reach a limiting production pressure are about two and a half times that required for the ideal gas flow cases. Clearly, production forecasts based on the ideal gas solutions will be far too conservative.

Another important observation can be made from Fig. 5 by comparing the real gas solutions for natural gas and condensate for a flow rate $Q$ of 0.05. Although the natural gas line is close to the liquid case, the condensate line is far below the liquid case line. The terminal producing pressure is reached earlier for the condensate line than for the natural gas line. This indicates the importance of gas property variations upon the results. That is, no single set of $m_D(t_D)$ correlations could be expected to apply to all real gases at long production times. It is also clear from Fig. 5 that the real gas results tend to approach the liquid case results as flow rate decreases, and at small production times.

Aronofsky and Jenkins introduced the concept of a transient drainage radius $r_s$. This term should not be confused with the dimensionless radial coordinate $r_D$. From the Aronofsky-Jenkins definition of the transient drainage radius, we write for real gas flow:

$$\ln\frac{r_s}{r_w} = \frac{\pi khT_{sc}}{q_{sc}p_{sc}\bar{T}}\left[m(\bar{p}) - m(p_w)\right] = m_D(p_w) - \bar{m}_D(\bar{p}) \quad \ldots\ldots\ldots\ldots (32)$$

The Eilerts *et al.*[7] results can also be correlated as transient drainage radii vs dimensionless time. The results are presented in Fig. 6, and agree with the Aronofsky-Jenkins results and the liquid flow results almost exactly. Actually, the correlation of the real gas flow solutions in terms of the transient drainage radius (Fig. 6) is a much better correlation than the correlation in terms of $m_D(t_D)$ (Figs. 4 and 5). The drainage radius correlation is excellent for all values of production time. Thus, Eq. 32 provides the most useful engineering approach to the transient flow of real gases. As recommended by Jenkins and Aronofsky for ideal gas flow, the transient drainage radius for real gas flow can be found from:[7]

$$\ln\frac{r_s}{r_w} = p_D(t_D) - 2s_s\left(\frac{r_w}{r_e}\right)^2 \quad \ldots\ldots\ldots\ldots (33)$$

and the $m(\bar{p})$ can be found from the materials balance:

$$\left(\frac{p}{z}\right)_i - \left(\frac{\bar{p}}{\bar{z}}\right) = \frac{Tp_{sc}q_{sc}t}{\pi hr_e^2\phi T_{sc}} = \frac{1}{2}\int_{m(\bar{p})}^{m(p_i)} (pc_t)\,dm(p) \approx \frac{(pc_t)_{avg}}{2}\left[m(p_i) - m(\bar{p})\right] \quad \ldots (34)$$

Eqs. 32 through 34 are not strictly a solution to Eq. 18. They represent an excellent engineering approximation which applies for a wide range of conditions. The method appears to be every bit as good as the Jenkins-Aronofsky result for ideal gas flow.

Fig. 6 shows that at long production times $r_s$ takes the constant value 0.472 $r_e$. This is similar to the Aronofsky-Jenkins finding for ideal gas. Substitution of long-time values for $p_D(t_D)$ in Eq. 33 also leads to this conclusion. Thus, Eq. 32 becomes similar in form to the liquid case pseudo-steady-state equation at times long enough that the outer boundary effect is controlling. The fact that $r_s$ eventually becomes constant at 0.472 $r_e$ does not mean the physical drainage radius stabilizes about half-way out in the reservoir. The entire reservoir volume is being drained, as can be seen by inspection of any of the Eilerts *et al.*[7] production figures.

The Eilerts *et al.* solutions have provided an excellent set of information to test the linearization of the real gas flow solutions for production. Eilerts *et al.* specified that the effective permeability was a function of pressure (assuming pressure drop would result in condensation and reduction of effective permeability). Effective permeability can thus be taken within the $m(p)$ integral. Correlations in Figs. 4 through 6 do include a pressure-dependent permeability. Thus, if an approximation of the effect of pressure drop upon liquid condensation and reduction in permeability near the wellbore can be made, the performance can be estimated from:

$$\ln\frac{r_s}{r_w} = \frac{\pi hT_{sc}}{q_{sc}p_{sc}\bar{T}}\left[m'(\bar{p}) - m'(p_w)\right] \quad \ldots\ldots (35)$$

where

$$m'(p) = 2\int_{p_w}^{p}\frac{kp\,dp}{\mu z} \quad \ldots\ldots\ldots (36)$$

and $k$ is a known function of pressure.

The usefulness of considering $k$ a function of pressure to handle condensate flow might be open to question. Nevertheless, it is clearly indicated that variation of $k$ as a function of pressure can be included in the real gas pseudo-pressure.

Correlation of the Eilerts *et al.*[7] data presented previously involves calculation of $m(p)$ and determination of relationships between the Eilerts *et al.* nomenclature and that used in this paper. (Necessary relationships are in the Appendix).

Eilerts *et al.*[7] also determined performance with a steady-state, non-Darcy flow region near the producing well. As a result, a steady-state skin effect can also be introduced to yield the following approximation for the radial flow of real gases during production:

$$\frac{\pi khT_{sc}}{q_{sc}p_{sc}\bar{T}}\left[m(\bar{p}) - m(p_w)\right] = \ln\frac{r_s}{r_w} + s + Dq_{sc} \quad \ldots (37)$$

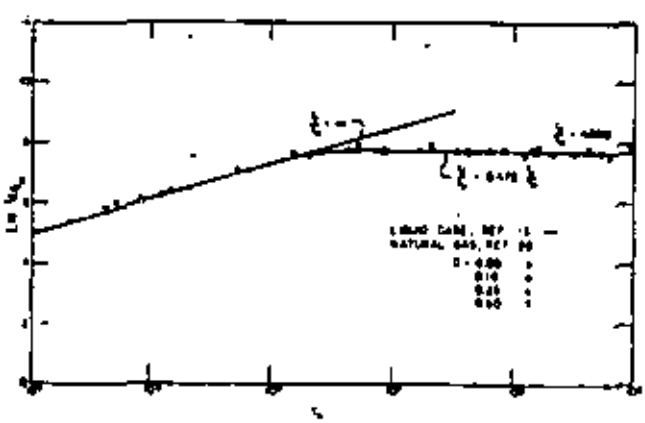

FIG. 6—JENKINS ARONOFSKY DRAINAGE RADIUS VS $t_D$ FOR A CLOSED RADIAL RESERVOIR PRODUCED AT CONSTANT RATE.

where $s$ is the skin effect and $D$ is the non-Darcy flow coefficient.

## CONSTANT RATE INJECTION

All of the preceding discussion of real and ideal gas transient flow deals with *production* only. *Injection* results, as was clearly shown by Aronofsky and Jenkins[5] for radial ideal gas flow, cannot be linearized in as simple a fashion. Aronofsky and Jenkins correlated injection well pressures for radial flow of an ideal gas as functions of a dimensionless time based on gas compressibility evaluated at the initial formation pressure before injection. The dimensionless pressure rise at a given dimensionless time was generally greater than that for a liquid case, and increased with injection rate. Aronofsky and Jenkins showed that injection case results were very close to the liquid case for low injection rates. Although injection is of practical importance in itself, the major utility of injection case correlations is in application of the principle of superposition to generate variable rate production cases, including the important pressure build-up case.

Superposition, as it has been applied to gas well testing, requires that dimensionless times for both injection and production be based on the same gas physical property evaluation. Although superposition could be based on different dimensionless times for injection and production, the added complexity of such a procedure does not appear justified. Thus, an obvious question is will injection solutions correlate closer to the liquid case if dimensionless times are based on physical properties evaluated at a pressure above the initial, low formation pressure?

We rule out the scheme of using a point evaluation at the existing injection pressure because this would yield a result not usable for forecasting. That is, it would be necessary to know the injection pressure-time history before it could be calculated. An obvious possibility is to evaluate physical properties at the final, elevated injection pressure, as in the case of superposition applied to reservoir production or build-up, at the initial formation pressure before production was started. This idea is fundamentally the basis for all gas well pressure build-up applications currently in use.

In brief, correlations for injection based on an elevated pressure are no better (or worse) than those based on physical properties evaluated at the initial, low formation pressure. This is true for *both* the ideal and real gas flow cases. Fig. 7 presents the dimensionless real gas potential rise for the Ehlers *et al.*[6] injection case (their Fig. 8) correlated vs dimensionless times based on both the initial low formation pressure and the final injection pressure. The dashed line presents the liquid flow solution. Two facts are apparent: the slopes of the correlations are similar, and correlations based on final injection pressure are no worse than those based on initial, low formation pressure. From the Jenkins-Aronofsky studies of ideal gas flow, we can also conclude that the difference between the injection case correlations and the liquid case become smaller as injection rate decreases; in any case, the differences aren't large.

Fig. 7 can lead to another idea. Correlation based on a dimensionless time evaluated with physical properties about half-way between the extremes might be quite good. This idea follows immediately from the *theorem of the mean*. That is, if flowing fluid physical properties vary monotonically with potential, the proper result is limited by those evaluated at the extreme values of physical properties. Friedmann[7] proved that results must lie between those evaluated at the extremes of physical properties whether physical properties are monotonic functions or not. The injection problem has been the subject of much investigation in the fields of heat transmission and ground-water movement (Friedmann,[7] Storm[11] and Polubarinova-Kochina[12]). As has been shown by these authors, it cannot always be assumed that evaluation at an average property will yield good results. Sometimes the answer will vary from one extreme to the other.

## SUPERPOSITION OF LINEARIZED SOLUTIONS

Superposition is rigorously correct only for linear partial differential equations. Nevertheless, the extremely close check between the linearized real gas solutions correlated on the basis of the $m_d(t_D)$, as given by Eq. 31, and a $t_D$ given by Eq. 30, and the liquid flow solutions of van Everdingen and Hurst, indicates the possibility that superposition might be quite good for matching an *increasing* rate production schedule. An increasing rate

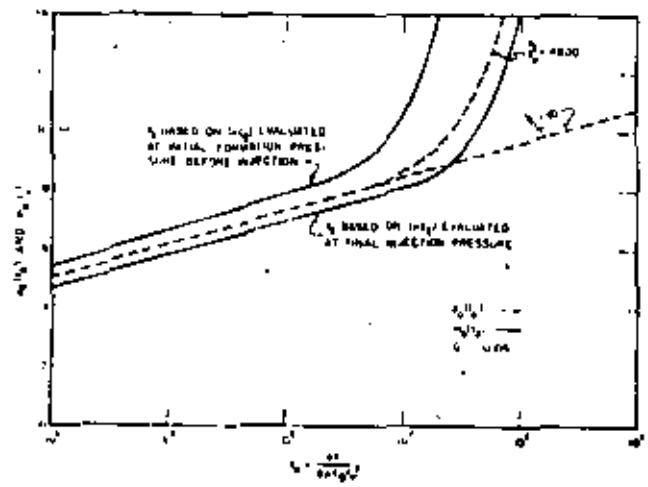

FIG. 7—$m_D(t_D)$ VS $t_D$ FOR INJECTION OF A REAL GAS (CORRELATION OF EHLERS *et al.*[6] DATA).

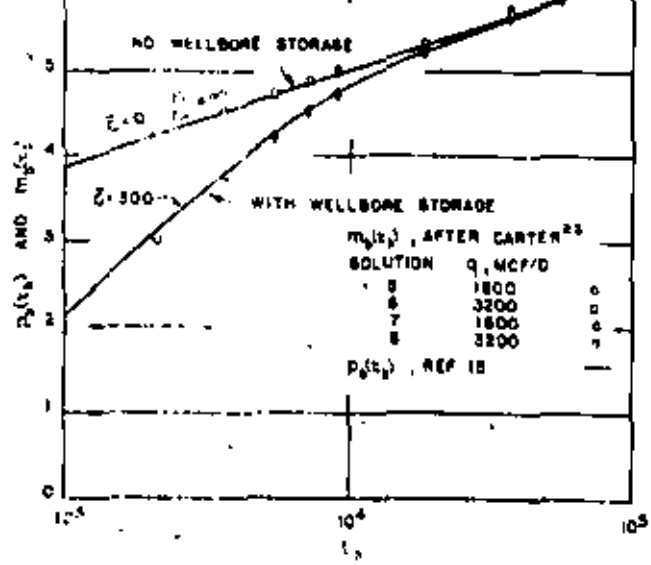


FIG. 8—$p_D(t_D)$ AND $m_D(t_D)$ VS $t_D$ FOR CONSTANT RATE PRODUCTION WITH WELLBORE STORAGE.

schedule would require superposition of positive incremental rates. However, the real gas flow solutions do depend slightly upon production rate. Thus, the only way that the application of the principle of superposition (as an acceptable approximation) to real gas flow can be established is by comparison with finite-difference solutions of variable-rate, real gas flow problems.

Such a comparison can be made for an increasing production rate schedule from data for real gas flow published by Carter.[24] Carter studied the effect of wellbore storage on gas production. For his solutions, it was assumed that the surface flow rate was held constant, but 0.02965 Mcf was withdrawn from the wellbore per psi pressure drop in the wellbore. This resulted in the sand face flow rate increasing as a function of time toward the constant surface flow rate. This case is almost exactly analogous to the wellbore unloading case presented by van Everdingen and Hurst[6] in their Eq. VIII-11. The wellbore storage constant $\overline{C}$ for Carter's solutions can be determined from Eq. 6 presented by Ramey.[9] The value of $\overline{C}$ for Carter's solutions does vary slightly with pressure, but a value of 300 is quite good. Fig. 8 presents a comparison between the $m_p(t_D)$ obtained from Carter's solutions, both with and without wellbore storage, and the van Everdingen-Hurst $p_D(t_D)$ solutions for the liquid flow case. As can be seen, the comparison with constant rate liquid flow *without* storage is excellent. This was previously shown for the Ehlers *et al.*[8] solutions. Of more interest, the comparison between the liquid flow case *with* wellbore storage and Carter's two solutions with wellbore storage are also excellent. This establishes that superposition of the linearized real gas flow solutions for an increasing flow rate should be a very good approximation—at least before outer boundary effects are controlling.

Although superposition in an increasing production rate schedule appears quite good, it is not apparent that a *decreasing* rate schedule is susceptible to superposition. This results because the dimensionless real gas injection pressure increases do not correlate with the liquid case as well as do production data. Even for transient injection of an ideal gas,[9] the resulting dimensionless pressure rise appears to depend upon injection rate, but does approach the liquid case solution as injection rate decreases. The fact that injection results do approach the liquid case as injection rate approaches zero suggests that superposition of small *positive* incremental rates (injections) would be feasible. Again, the possibility can only be checked by comparison with finite-difference solutions.

Fortunately, both Carter[24] and Dykstra[41] have presented finite-difference solutions for decreasing flow-rate production. Dykstra's data provide an excellent set for comparison of finite-difference solutions with superposition of the linearized solutions. Fig. 9 presents a comparison of Dykstra's computed flowing pressures with those obtained by superposition of linearized real gas flow solutions. The line is Dykstra's result, while points represent results of superposition using only four or five incremental rate changes to represent a rapidly changing flow rate. The flow rate is shown by the dashed line. For the example shown, the permeability was 0.25 md, thickness was 179 ft, initial pressure 6,150 psia and flow rate declined quadratically as a function of time from 6,556 to 2,500 Mcf/D by 50 days' producing time. Superposition was accomplished using dimensionless times based on the *initial* pressure and the $m_p(p_i)$ taken equal to the liquid case $p_i(t_{Di})$ values. The maximum difference between Dykstra's result and those computed by superposition was 20 psi out of a drawdown of 2,150 psi—a difference of 0.9 per cent. The 50-day production period was long enough that initial rate changes were influenced by the outer boundary. Thus, we conclude that superposition can be used to reproduce variable-rate drawdown data with acceptable accuracy.

The previous remarks concerning superposition of incremental rate *increases* are, of course, directly applicable to pressure build-up testing. Although insufficient comparisons between finite-difference build-up solutions and superposition solutions for the real gas flow case have been made to completely explore this problem, it does appear that build-up theory can be used with good accuracy. An interesting test of pressure build-up can be made by comparison of Dykstra's[41] solutions with superposition solutions. Because Dykstra's cases involved a variable-rate production period, permeability was low and pressure gradients high, it is believed that a fairly extreme test results. Fig. 10 presents the build-up following the drawdown of Fig. 9. As can be seen, the

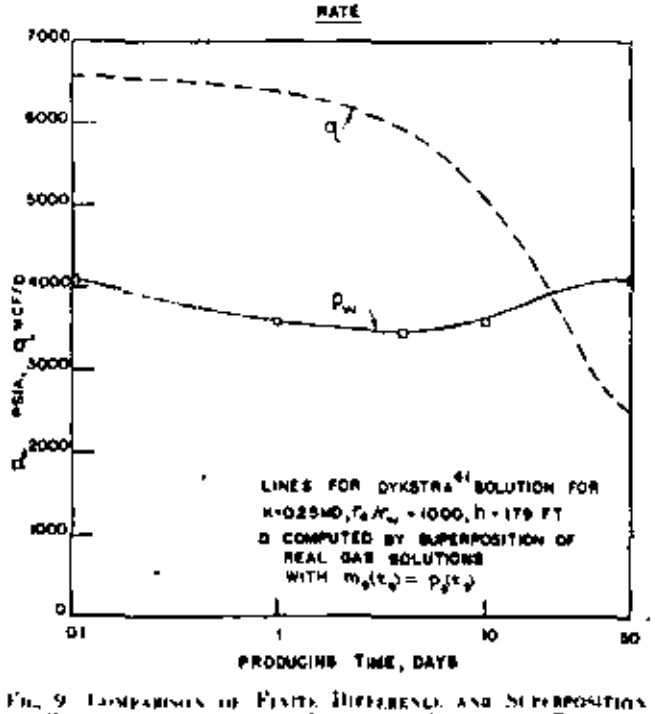


Fig. 9 Comparison of Finite Difference and Superposition Flowing Pressures for a Decreasing Production Rate.

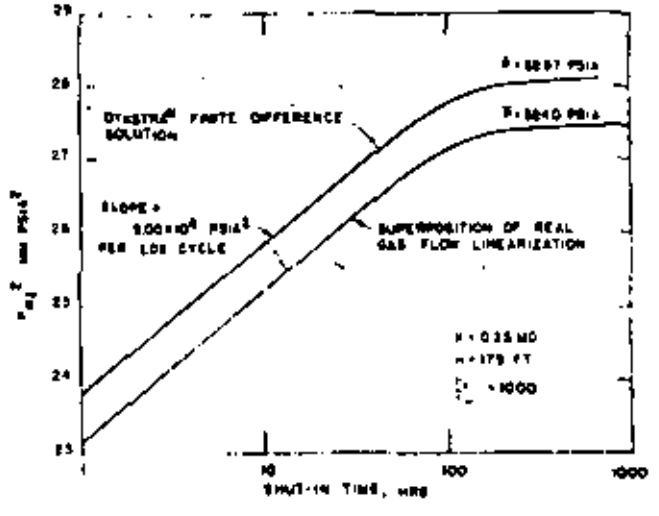


Fig. 10 Comparison of Finite Difference and Superposition Build-up Pressures for a Real Gas.

superposition result yields a similar build-up curve of identical slope, but about 60 psi below Dykstra's finite-difference solutions. Again, the percentage difference is small; the final static pressure is about 1.1 per cent too low. It appears that superposition of the real gas flow linearization will always yield a pressure build-up static pressure that is too low, but as good or better than results of current methods. Furthermore, field application would be to the field measured data—the real solution—which would tend to correct for this error. We conclude that pressure-build-up analysis based on superposition can be done for real gas flow with acceptable accuracy, but that further study of pressure build-up for real gas flow is desirable.

## STEADY-STATE AND PSEUDO-STEADY-STATE FLOW

Radial gas flow at constant production rate will be considered. A horizontal homogeneous porous medium of constant thickness $h$ with impermeable upper and lower boundary, and a well of radius $r_w$ located in the center of a radial reservoir, constitutes the flow system. The outer radius $r_e$ represents either the real boundary or the radius of drainage. Two cases will be considered: (1) constant pressure at $r_e$, and (2) no flow across $r_e$.

### CONSTANT PRESSURE AT OUTER BOUNDARY

The steady-state equation for a real gas in axisymmetrical coordinates can be written from Eq. 22 as:

$$\frac{1}{r}\frac{d}{dr}\left[r\frac{dm(p)}{dr}\right] = 0 \quad \ldots\ldots\ldots (38)$$

The boundary conditions for two concentric cylinders of radii $r_w$ and $r_e$ are:

$$r = r_w : m(p) = m(p_w) \quad \ldots\ldots\ldots (39)$$

$$r = r_e : m(p) = m(p_e) \quad \ldots\ldots\ldots (40)$$

Integrating Eq. 38 and using the boundary conditions, the steady-state pressure distribution in the system is:

$$m(p_r) = m(p_w) + \frac{q_{sc} p_{sc} T}{\pi k h T_{sc}} \left(\ln \frac{r}{r_w}\right) \quad \ldots (41)$$

Eq. 41 can be evaluated for $p = \bar{p}$ at $r = r_e$, and rearranged to provide an equation analogous to the normal radial flow equation:

$$q_{sc} = \frac{\pi k h T_{sc} [m(p_e) - m(p_w)]}{T p_{sc} \ln \frac{r_e}{r_w}} \quad \ldots\ldots (42)$$

Both Eqs. 41 and 42 are in darcy, or cgs units. Thus, the $m(p)$ have the units of sq atm/cp.

### NO FLOW ACROSS OUTER BOUNDARY

As was shown previously by Eq. 32 and Fig. 6 at long times, a flow equation for the closed outer boundary, constant mass rate production, radial flow case can be written:

$$\ln \frac{r_e}{r_w} = \ln \frac{0.472 r_e}{\bar{r}_w} = \frac{\pi k h T_{sc}}{q\, p_{sc} T} [m(\bar{p}) - m(p_w)] \quad \ldots (43)$$

Since the $m(\bar{p})$ values were determined from a materials balance, the $\bar{p}$ argument represents the average pressure which would yield the proper average density, or the static pressure following a complete pressure build-up. It is *not* a volumetric average pressure. Eq. 43 coupled with the normal material balance for a bounded drainage volume provides a useful means to couple production rate and gas recovery.

In the case of liquid flow, an equation similar to Eq. 43 can be derived using the concept of pseudo-steady-state flow. That is, a condition is eventually reached for constant rate liquid production when the rate of pressure decline becomes constant everywhere in the reservoir. This condition is expressed mathematically by setting the Laplacian of the pressure equal to a constant (other than zero). Although it can be shown that the Laplacian of pressure-squared for an ideal gas, or the Laplacian of the real gas pseudo-pressure cannot be equal to a constant rigorously, a flow condition similar to pseudo-steady-state does appear to exist for both ideal and real gas flow, for all practical purposes. The existence of such a condition is suggested by Eq. 43. Fig. 11 presents an interesting inspection of the pressure behavior during the period that Eq. 43 applies for one of the Eilerts *et al.*[39] cases. Also shown is the $p_w(t_a)$ for comparison with the liquid case. As was seen previously in Fig. 5, the $m_w(t_a)$ does not change at a constant rate during this period. Although it matches the liquid case solution at early times, eventually the $m_w(t_a)$ drops below the liquid case solution. The most interesting feature of Fig. 11, however, is that the $m_w(r_w, t_a)$ for all radial locations are *eventually* parallel. Thus, the $m(p)$ profile is essentially independent of time. This condition can be described approximately by setting the Laplacian of $m(p)$ equal to a constant. As shown in Refs. 39 and 42, this leads to an equation similar to Eq. 32, but in terms of an average $\bar{m}(p)$ rather than $m(\bar{p})$. Although it can be shown that these two averages tend to be equivalent for practical ranges of conditions, it does not appear worthwhile to show the development here. In any event, Eq. 32 describes the long-time flow behavior of closed radial systems with remarkable accuracy.

Another consequence of inspection of Fig. 11 is that the $m(p)$ distribution can be obtained readily. For ex-

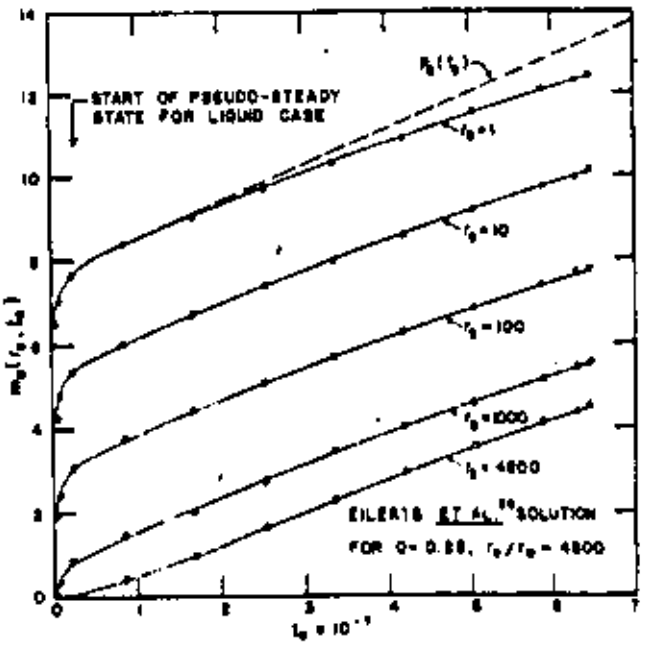


FIG. 11 $m_w(r_w, t_a)$ VS $t_a$ FOR CONSTANT RATE PRODUCTION OF A REAL GAS FROM A CLOSED, RADIAL RESERVOIR.

ample, the following equation also describes flow reasonably well:

$$\ln\left(\frac{r_e}{r_w}\right) = \frac{\pi kh}{q}\left[m(p_i) - m(p_{wf})\right] \quad \ldots \quad (44)$$

## DISCUSSION AND CONCLUSIONS

The purpose of the preceding was to describe fundamental considerations which can be used successfully to analyze the flow of real gases. The concept of the real gas pseudo-pressure promises a considerable simplification and improvement in all phases of gas well testing analysis and gas reservoir calculations. Such applications will be described in useful engineering form in a companion paper.

Several remarks concerning the real gas pseudo-pressure are in order. No claim of originality can be made for the substitution we have called the *real gas pseudo-pressure*. Carslaw and Jaeger[5] reviewed application of a similar transformation which was used in solution of heat conduction problems as early as 1894 and the early 1930's. Recently, McMordie[6] pointed out the utility of this sort of transformation in heat conduction problems. There have even been numerous mentions of the use of a transformation similar to the $m(p)$ function in connection with flow through porous media. In 1949, Muskat[7] used the same transformation in a discussion of the theory of potentiometric models. In 1953, Leibenzon[8] used the transformation, and Russian authors refer to it as the Leibenzon transformation. In 1951, Fay and Prats[9] discussed use of a similar transformation in connection with transient liquid flow. In 1955, Atkinson and Crawford[10] evaluated numerically a similar function but with constant viscosity. In 1962, Carter[11] used a gas mobility term $M(p)$, which was defined as:

$$M(p) = \frac{kh\rho}{T\mu z} \quad .$$

Clearly, the $m(p)$ function is proportional to the pressure integral of Carter's $M(p)$. In 1963, Hurst *et. al.*[12] used a similar integral, but with constant viscosity. To our knowledge, however, this paper represents the first application of the real gas pseudo-pressure to linearization of transient real gas flow. Perhaps the most surprising fact is that the realization of the utility of this concept has been so long in coming.

In the original draft of this paper and the companion paper,[13,14] we called the $m(p)$ function the *real gas potential*. It was stated in those papers that the $m(p)$ transformation was not a true potential. Carslaw and Jaeger[5] termed a similar substitution in heat conduction an *effective potential*, while Muskat[7] called the transformation a *potential* as a matter of convenience. We feel that the $m(p)$ transformation will be an important function in gas reservoir engineering, and it is important that the function be given a suitable name. If we were to name the transformation as Russian authors have, we would call it the Muskat transformation. In the belief that the name should be reasonably descriptive and brief, the term real gas pseudo-pressure was finally selected. This name was originally suggested to us by M. Prats, with Shell Development Co.

It appears that the following conclusions are justified. The transformation called the real gas pseudo-pressure in this paper reduces a rigorous partial differential equation for the flow of real gas in an ideal system to a form similar to the diffusivity equation, but with potential-dependent diffusivity. Because the variation of the diffusivity of real gas with pressure was similar to that of an ideal gas, it was possible to correlate finite difference solutions for the ideal radial production of real gas from a bounded system with the liquid flow solutions of van Everdingen and Hurst, and the ideal gas solutions of Aronofsky and Jenkins. This correlation avoids the assumption of small pressure gradients in the reservoir and offers generally useful solutions for the radial flow of real gas.

An investigation of the injection of real gas into a bounded radial system also gave a reasonable correlation —but not as good a correlation as production data. The correlation was as good as, or better than, the correlation of ideal gas flow results made by Aronofsky and Jenkins.

An investigation of the possibility of superposition of the linearized results indicated that superposition can be used as an acceptible engineering approximation to generate variable rate flow of real gases in a radial system. Pressure build-up for real gas flow was thus justified for the first time. (No justification for pressure build-up for the non-linear problem of ideal gas flow has yet been presented.)

Accurate and simple equations can be written to describe unsteady flow of real gases which properly consider variation of gas physical properties.

## NOMENCLATURE

$\nabla$ = grad
$\nabla\cdot$ = divergence
$\nabla^2$ = Laplacian operator
$A$ = area, sq cm
$b$ = slope of a straight line in a plot of $k(p)$ vs $1/p$
$c_g(p)$ = real gas compressibility defined by Eq. 10
$h$ = thickness, cm
$k(p)$ = effective permeability, darcies
$M$ = molecular weight
$m(p)$ = real gas pseudo-pressure defined by Eq. 14
$p$ = pressure, atm
$q$ = flow rate, cm³/sec
$r$ = radius, cm
$R$ = gas constant
$t$ = time, sec
$T$ = temperature, °K
$v$ = velocity, cm/sec
$V$ = pore volume, cm³
$x, y, z$ = direction notation
$z(p)$ = gas deviation factor, a function of pressure at constant temperature
$\rho$ = density, gm/cm³
$\mu(p)$ = real gas viscosity, a function of pressure at constant temperature, cp
$\mu_i$ = viscosity at atmospheric pressure, cp
$n$ = normal distance scale
$\phi$ = hydrocarbon porosity, fraction

SUBSCRIPTS

$e$ = external boundary
$l$ = liquid
$pc$ = pseudo-critical
$r$ = radius
$sc$ = standard conditions
$w$ = internal boundary, the well

## ACKNOWLEDGMENTS

The authors wish to acknowledge financial support of the Texas A&M U., the Texas Engineering Experiment Station of Texas A&M and the Texas Petroleum Research Committee. This paper represents a composite of research effort conducted over a period of time by several agencies. Crawford first evaluated the $m(p)$ function during the post decade. Use of the $m(p)$ function and a more recent evaluation of the function were described by Al-Hussainy.* The authors also wish to acknowledge the encouragement in the course of this study by R. L. Whiting. Portions of this work were done by Al-Hussainy in partial fulfillment of graduate degree requirements in petroleum engineering at Texas A&M U. Finally, and sincerely, the authors wish to acknowledge the numerous helpful suggestions made by the reviewers of the original draft of this paper.

## REFERENCES

1. Muskat, M.: *The Flow of Homogeneous Fluids*, J. E. Edwards, Inc., Ann Arbor, Mich. (1946).
2. Katz, D. L., Cornell, D., Kobayashi, R., Poettmann, F., Vary, J. A., Elenbaas, J. R. and Weinaug, C. F.: *Handbook of Natural Gas Engineering*, McGraw-Hill Book Co., Inc., New York, N. Y. (1959).
3. Heatherington, C. R., MacRoberts, D. T. and Huntington, R. L.: "Unsteady Flow of Gas Through Porous Media", *Trans.*, AIME (1952) **146**, 186.
4. MacRoberts, D. T.: "Effect of Transient Conditions in Gas Reservoirs", *Trans.*, AIME (1951) **186**, 36.
5. Hancock, E. D. and Katz, D. L.: "Applications of Unsteady State Gas Flow Calculations", paper presented at Research Conference on Flow of Natural Gas Reservoirs, U. of Michigan Ann Arbor, Mich. (June 30, 1955).
6. Cornell, D. and Katz, D. L.: "Pressure Gradients in Natural Gas Reservoirs", *Trans.*, AIME (1953) **198**, 61.
7. Rowan, G. and Clegg, M. W.: "An Approximate Method for Transient Radial Flow", *Soc. Pet. Eng. Jour.* (Sept., 1962) 225.
8. Green L. and Wilde, C. H.: "Nonsteady Flow of Gas Through a Porous Wall", *Proc.*, First U. S. National Congress Applied Mechanics, J. E. Edwards, Inc., Ann Arbor, Mich. (1952) 777.
9. Aronofsky, J. S. and Jenkins, R.: "Unsteady Flow of Gas Through Porous Media: One-dimensional Case", *Proc.*, First U. S. National Congress Applied Mechanics, J. E. Edwards, Inc., Ann Arbor, Mich. (1952) 763.
10. Deakins, R. and Aronofsky, J. S.: "Unsteady Radial Flow of Gas Through Porous Media", *Jour. Appl. Mech.* (1954) **20**, 210.
11. Brice, C. D., Poettmann, D. W., Rachford, H. H. and Rice, J.: "Calculations of Unsteady State Gas Flow Through Porous Media", *Trans.*, AIME (1953) **198**, 79.
12. Douglas, J., Jr., Peaceman, D. W. and Rachford, H. H.: "Calculation of Unsteady-State Gas Flow in a Square Reservoir", *Trans.*, AIME (1955) **204**, 190.
13. Aronofsky, J. S.: "Effect of Gas Slip on Unsteady Flow of Gas Through Porous Media", *Jour. Appl. Phys.* (1954) **25**, 48.
14. Aronofsky, J. S. and Jenkins, R.: "A Simplified Analysis of Unsteady Radial Gas Flow", *Trans.*, AIME (1954) **201**, 149.
15. van Everdingen, A. F. and Hurst, W.: "The Application of the LaPlace Transformation to Flow Problems in Reservoirs", *Trans.*, AIME (1949) **186**, 305.
16. Aronofsky, J. S. and Ferdi, O. D.: "Transient Flow of Non-ideal Gases in Porous Media – One-dimensional Case", *Jour. Appl. Phys.* (1951) **25**, 289.
17. Aronofsky, J. S. and Porter, J. D.: "Unsteady Radial Flow of Gas Through Porous Media: Variable Viscosity and Compressibility", *Jour. Appl. Mech.* (1956) **23**, 128.
18. Carter, R. D.: "Solutions of Unsteady-State Radial Gas Flow", *Jour. Pet. Tech.* (May, 1962) 549.
19. Elkins, C. K.: "Integration of Partial Differential Equation for Transient Linear Flow of Gas Condensate Fluids in Porous Structures", *Soc. Pet. Eng. Jour.* (Dec., 1964) 291.
20. Elkins, C. K., Sumner, E. F. and Potts, N. L.: "Integration of Partial Differential Equation for Transient Radial Flow of Gas Condensate Fluids in Porous Structures", *Soc. Pet. Eng. Jour.* (June, 1967) 141.
21. Swift, G. W. and Kiel, O. G.: "The Prediction of Gas Well Performance Including the Effect of Non-Darcy Flow", *Jour. Pet. Tech.* (July, 1962) 791.
22. Tek, M. R., Coats, K. H. and Katz, D. L.: "The Effect of Turbulence on the Flow of Natural Gas Through Porous Reservoirs", *Jour. Pet. Tech.* (July, 1962) 799.
23. Carter, R. D.: Supplemental Appendix to "Determination of Stabilized Gas Well Performance from Short Flow Tests", *ADI Doc. No. 7171*, Library of Congress, Washington, D. C.
24. Rowan, G. and Clegg, M. W.: "An Approximate Method for Non-Darcy Radial Gas Flow", *Soc. Pet. Eng. Jour.* (June, 1964) 96.
25. Roberts, R. C.: "Unsteady Flow of Gas Through a Porous Medium", *Proc.*, First U. S. National Congress Applied Mechanics, J. E. Edwards, Inc., Ann Arbor, Mich. (1952) 773.
26. Kibler, R. E.: Unsteady Flow of Gas Through a Semi-Infinite Porous Medium", *Jour. Appl. Mech.* (1957) **24**, 329.
27. Polubarinova Kochina, P. Ya.: *Theory of Ground Water Movement*, Princeton U. Press, Princeton, N. J. (1962).
28. Carslaw, H. S. and Jaeger, J. C.: *Conduction of Heat in Solids*, 2nd Ed., Oxford U. Press, London, England (1959) 11.
29. Klinkenberg, L. J.: "The Permeability of Porous Media to Liquids and Gases", *Drill. and Prod. Prac.*, API (1941) 200.
30. Fay, C. H. and Crats, M.: "The Application of Numerical Methods to Cycling and Flooding Problems", *Proc.*, Third World Petroleum Congress, Section II (1951) 555.
31. Standing, M. B. and Katz, D. L.: "Density of Natural Gases", *Trans.*, AIME (1942) **146**, 140.
32. Carr, N. L., Kobayashi, R. and Burrows, D. B.: "Viscosity of Hydrocarbons Under Pressure", *Trans.*, AIME (1954) **201**, 264.
33. Trube, A. S.: "Compressibility of Natural Gases", *Trans.*, AIME (1957) **210**, 69.
34. Robinson, D. B., Macrygeorgos, C. A. and Govier, G. W.: "The Volumetric Behavior of Natural Gases Containing Hydrogen Sulfide and Carbon Dioxide", *Trans.*, AIME (1960) **219**, 51.
35. Matthews, C. S.: "Analysis of Pressure Build-Up and Flow Test Data", *Jour. Pet. Tech.* (Sept., 1961) 862.
36. Friedmann, N. E.: "Quasilinear Heat Flow", *Trans.*, ASME (April, 1958) 635.
37. Storm, M. L.: "Heat Conduction in Simple Metals", *Jour. Appl. Phys.* (July, 1951) **22**, No. 7, 192.
38. McMordie, R. K.: "Steady-State Conduction With Variable Thermal Conductivity", *Trans.*, ASME (Feb., 1962) 92.
39. Al-Hussainy, R.: "Flow of Real Gases Through Porous Media", MS Thesis, Texas A&M U. (Jan., 1965).
40. Ramey, H. J., Jr.: "Non-Darcy Flow and Wellbore Storage Effects in Pressure Buildup and Drawdown of Gas Wells", *Jour. Pet. Tech.* (Feb., 1965) 223.
41. Dykstra, H.: "Calculated Pressure Build-up for a Low Permeability Gas-Condensate Well", *Jour. Pet. Tech.* (Nov., 1961) 1131.
42. Al-Hussainy, R., Ramey, H. J., Jr. and Crawford, P. B.: "The Theory of the Real Gas Potential", Paper No. 1243-A, presented at SPE Annual Fall Meeting, Denver, Colo. (Oct. 3-6, 1965).
43. Muskat, M.: "The Theory of Potentiometric Models", *Trans.*, AIME (1939) **179**, 216.
44. Leibenzon, L. S.: "Subsurface Hydraulics of Water, Oil and Gas", *Publ. Acad. Sci.*, collected works, U.S.S.R. (1953) **2**.
45. Atkinson, D. D. and Crawford, P. B.: "Generalized Pressure Distribution and Gas Mass in Pipe Lines", *Pet. Prod. Tech.*, AIME Conference Proc. of 1956, Miscellaneous Publication of the Texas Engineering Experiment Station (Sept., 1956) 59.
46. Hurst, W., Goodson, W. C. and Lease, R. E.: "Aspects of Gas Deliverability", *Jour. Pet. Tech.* (June, 1963) 668.
47. Al-Hussainy, R. and Ramey, H. J., Jr.: "Application of the Real Gas Potential", Paper No. 1243-B, presented at the SPE Annual Fall Meeting, Denver, Colo. (Oct. 3-6, 1965).

## APPENDIX

## CORRELATION OF EILERTS *ET AL.*[7] SOLUTIONS

Eilerts *et al.*[7] solved the following equation numerically (in their nomenclature):

$$\frac{\partial}{\partial U}\left[\kappa(P)\frac{\partial P}{\partial U}\right] = \phi\mu c\frac{\partial}{\partial U}\left[\frac{P}{Z(P)}\right] \quad \ldots \quad (A\text{-}1)$$

where

$$\kappa \equiv \kappa(P, K(p)) \equiv k(p_i)K(P), \quad c(p) \equiv z(p_i)Z(P), \quad \mu(p)$$
$$\mu(p_i)\,\mu(P), \quad \phi(p) \equiv \phi(p_i)f_\phi(p)\varepsilon(p)$$

and

$$\kappa(p) = \kappa(p_i)H(P) \quad \ldots \quad (A\text{-}2)$$

Dimensionless time is defined as:

$$U \equiv \frac{p\,k(p_i)}{2\phi_i(p_i)\mu_i c_i r_w^2}\,t \quad \ldots \quad (A\text{-}3)$$

and the dimensionless radius:

$$U \equiv \ln\frac{r}{r_w} \quad \ldots \quad (A\text{-}4)$$

In terms of the $m(p)$ function, and using the dimensionless variables Eq. A-2, the flow equation takes the form:

$$\frac{1}{r_D}\frac{\partial}{\partial r_D}\left[r_D\frac{\partial m(P)}{\partial r_D}\right] = \frac{\phi_i(p_i)\mu(P)c_t\,\partial P}{p\,k(p_i)K(P)\,\partial t} \quad (A\text{-}5)$$

where

$$m(P) \equiv 2\int_0^P \frac{P}{\mu Z}\,dP \quad \ldots \quad (A\text{-}6)$$

Let the coefficient on the left side of Eq. A-5 be evaluated at the initial conditions, and define:

$$r_D \equiv \frac{r}{r_w} \quad \ldots \quad (A\text{-}7)$$

$$t_D \equiv \frac{k(p_i)p_i}{\phi_i\mu(p_i)C_t(P_i)r_w^2}\,t \equiv \frac{2U}{C_t(P_i)\left(\frac{r_b}{r_w}\right)^2} \quad (A\text{-}8)$$

Notice that $\mu(P)$ and $K(P)$ are equal to one at the initial $P_i$. Hence, Eq. A-5 takes the form:

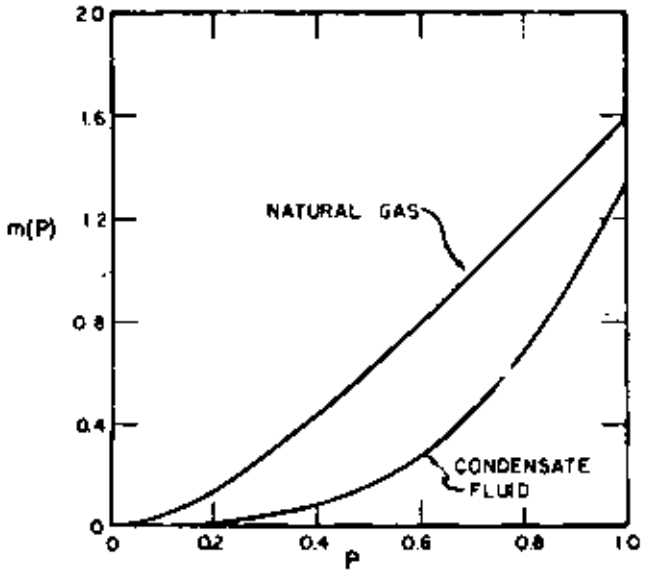


FIG. 12 — $m(P)$ vs $P$ FOR THE EILERTS *ET AL.*[7] GASES.

$$\frac{1}{r_D}\frac{\partial}{\partial r_D}\left[r_D\frac{\partial m(P)}{\partial r_D}\right] = \frac{\partial m(P)}{\partial t_D} \quad \ldots \quad (A\text{-}9)$$

The flow rate at the producing face as given by Eilerts *et al.*[7] is:

$$Q \equiv 2\Pi(P)\frac{\partial P}{\partial U} \equiv 2\frac{\partial m(P)}{\partial U} \quad \ldots \quad (A\text{-}10)$$

and the closed boundary:

$$\frac{\partial m(P)}{\partial U} \equiv 0 \quad \ldots \quad (A\text{-}11)$$

Thus, in terms of the dimensionless real gas pseudo-pressure drop:

$$m_i(r_w, t_D) = \frac{2}{Q}\Delta m(P) \quad \ldots \quad (A\text{-}12)$$

The $m(P)$ for the Eilerts *et al.* natural gas and condensate fluid are shown in Fig. 12. The large difference between physical properties of the two fluids is apparent.

***

Appendix A

# Solutions for Radial Flow of Fluids of Small and Constant Compressibility

## Constant Rate, Infinite Reservoir Case

The initial value problem represented by this case is presented in Chapter 2. In summary, the mathematical problem which we must solve is:

$$\frac{\partial^2 p}{\partial r^2}+\frac{1}{r}\frac{\partial p}{\partial r}=\frac{\phi\mu c}{k}\frac{\partial p}{\partial t}. \quad . \quad . \quad . \quad . \quad . \quad . \quad (A.1)$$

Boundary and initial conditions:

(1) $p = p_i$ at $t = 0$ for all $r$.

(2) $\left(r\frac{\partial p}{\partial r}\right)_{r_w} = \frac{q\mu}{2\pi kh}$ for $t > 0$.

(3) $p \to p_i$ as $r \to \infty$ for all $t$.

As mentioned in the text, several slightly different approaches to the solution of this problem have appeared in the literature. We have chosen to present the approach of Polubarinova-Kochina[1] because it is quite straightforward. We are indebted to H. J. Ramey, Jr., for calling this approach to our attention.

To develop the solution, we first replace the second boundary condition by the condition

$$\lim_{r\to 0} r\frac{\partial p}{\partial r}=\frac{q\mu}{2\pi kh}, \quad \text{for } t > 0.$$

This boundary condition is the "line-source" approximation to the original boundary condition. It has been shown to yield identical results (from a practical standpoint) with those obtained from solution of the problem with the original, less-tractable condition (see Mueller and Witherspoon[6]).

Fundamental to the solution is the use of the Boltzmann Transformation,

$$y = \frac{\phi\mu c r^2}{4kt} \quad . \quad . \quad . \quad . \quad . \quad . \quad . \quad . \quad . \quad . \quad (A.2)$$

Substitution of Eq. A.2 into the differential Eq. A.1 and accompanying boundary conditions gives

$$y\frac{d^2p}{dy^2}+\frac{dp}{dy}(1+y) = 0, \quad . \quad . \quad . \quad (A.3)$$

with

(1) $p \to p_i$ as $y \to \infty$,

(2) $\lim_{y\to 0} 2y\frac{dp}{dy}=\frac{q\mu}{2\pi kh}$.

To solve Eq. A.3 let $p' = \frac{dp}{dy}$.

Then Eq. A.3 becomes

$$y\frac{dp'}{dy} + (1 + y)\,p' = 0. \quad . \quad . \quad . \quad . \quad . \quad . \quad (A.4)$$

Separation of the variables and integration yield

$$\ln p' = -\ln y - y + C$$

or

$$p' = \frac{dp}{dy} = \frac{C_1}{y}e^{-y}. \quad . \quad . \quad . \quad . \quad . \quad . \quad . \quad . \quad (A.5)$$

$C$ and $C_1$ are constants of integration.

From boundary condition (2) above,

$$\lim_{y\to 0} 2y\frac{dp}{dy} = \frac{q\mu}{2\pi kh}.$$

Comparison of this expression with Eq. A.5 shows that

$$\lim_{y\to 0} 2y\frac{dp}{dy} = \frac{q\mu}{2\pi kh} = \lim_{y\to 0} 2C_1 e^{-y}.$$

Thus,

$$C_1 = \frac{q\mu}{4\pi kh} \quad . \quad . \quad . \quad . \quad . \quad . \quad . \quad . \quad . \quad (A.6)$$

Eq. A.5 now becomes

$$\frac{dp}{dy} = \frac{q\mu}{4\pi kh}\frac{e^{-y}}{y},$$

which can be integrated to yield

$$p = \frac{q\mu}{4\pi kh}\int^{y}\frac{e^{-y}}{y}dy + C_2. \quad . \quad . \quad . \quad . \quad (A.7)$$

The lower limit of the integral in Eq. A.7 can be assigned arbitrarily. We choose $y = \infty$ and obtain

ed drainage volume with a centrally located well which produces at constant rate. We must now obtain the inverse Laplace transform of Eq. A.15.

Examination of Eq. A.15 in the complex plane indicates that there is a pole of order two at the origin and simple poles along the negative real axis. These are the only singularities of the function.

We first determine the behavior of $\bar{P}$ at small values of $s$. Inversion of this equation will give the behavior of $\Delta p_D$ at large values of $t_{Dw}$. The behavior at small values of $s$ is established by introducing small argument, asymptotic expansions for the Bessel functions and examining Eq. A.15 in the limit as $s \to 0$. The details of this manipulation are somewhat tedious; however, the final result is

$$\lim_{s\to 0} \bar{P} = \frac{1}{s}\left\{\frac{r_{eD}^2}{r_{eD}^2-1}\ln\frac{r_{eD}}{r_D} - \frac{r_{eD}^2-r_D^2}{2(r_{eD}^2-1)} + \frac{r_{eD}^2 \ln r_{eD}}{(r_{eD}^2-1)^2} - \frac{(r_{eD}^2+1)}{4(r_{eD}^2-1)}\right\} + \frac{1}{s^2}\,\frac{2}{r_{eD}^2-1} \quad \ldots \quad (A.16)$$

Consultation of standard Laplace transform tables shows that the inverse of Eq. A.16 is

$$\Delta p_D = \frac{2}{r_{eD}^2-1}\left[\frac{r_D^2}{4} + t_{Dw}\right] - \frac{r_{eD}^2}{r_{eD}^2-1}\ln r_D - \frac{3r_{eD}^4 - 4r_{eD}^4 \ln r_{eD} - 2r_{eD}^2 - 1}{4(r_{eD}^2-1)^2} \quad \ldots \quad (A.17)$$

Eq. A.17 is valid for large values of time, $t_{Dw}$. This equation is the "long-time behavior" section of Eq. 2.34 of the text.

To find the behavior for early values of time, we must apply the Cauchy Residue Theorem. The version of that theorem which we shall apply here is as follows.

Denote by $F(s)$ the Laplace Transform of $f(t)$. Let

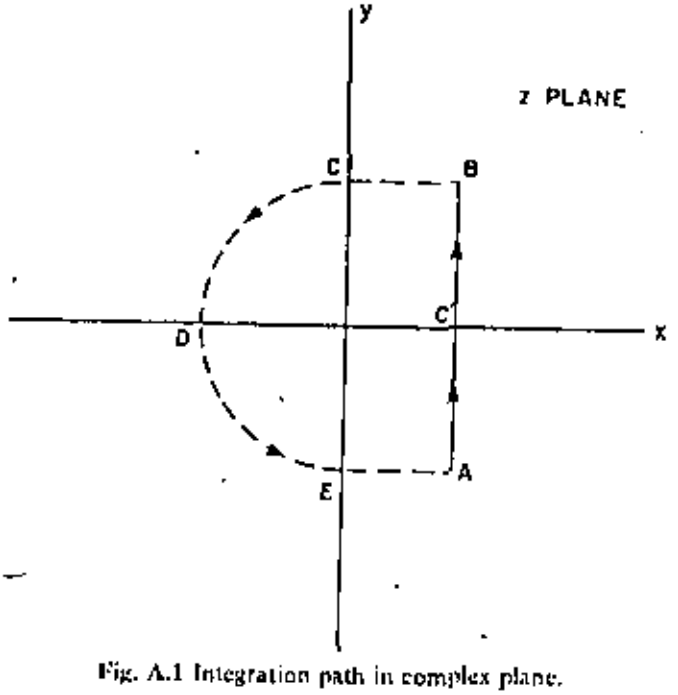


Fig. A.1 Integration path in complex plane.

$F(z)$ be the corresponding function of a complex variable. Suppose that $F(z)$ is analytic except for a finite number of poles, all of which are to the left of some line $x = C'$. Also, suppose that $F(z)$ tends uniformly to zero along the semi-circle CDE and the segments BC and EA of Fig. A.1. Then $f(t) = \Sigma \text{Residue } (e^{zt} F(z); a_n)$ where the points $a_n$ are the poles of $F(z)$.

Since we have already found the contribution of the double pole at the origin, we must determine the residues at the poles along the negative real axis. We set $z = u^2 e^{i\pi}$. From Eq. A.15 we obtain

$$\text{Res}\left\{e^{tz+z}\bar{P}(z)\right\} = \frac{1}{2\pi i}\oint e^{tz+z}\bar{P}(z)\,dz =$$

$$\frac{1}{\pi i}\oint \frac{e^{-u^2 t+u}\left[J_1(ur_{eD})Y_0(ur_D) - Y_1(ur_{eD})J_0(ur_D)\right]}{u^2\left[J_1(ur_{eD})Y_1(u) - J_1(u)Y_1(ur_{eD})\right]}\,du \quad \ldots \quad (A.18)$$

The singularities (poles) are the roots $\alpha_n$ of the denominator of Eq. A.18, or

$$J_1(\alpha_n r_{eD})\,Y_1(\alpha_n) - J_1(\alpha_n)\,Y_1(\alpha_n r_{eD}) = 0 \quad \ldots \quad (A.19)$$

The residues at the $\alpha_n$ are given by

$$2\sum_{n=1}^{\infty} \frac{e^{-\alpha_n^2 t_{Dw}}}{\alpha_n^2 \lim_{u\to\alpha_n}\frac{d}{du}} \cdot \frac{\left[J_1(\alpha_n r_{eD})\,Y_0(\alpha_n r_D) - Y_1(\alpha_n r_{eD})\,J_0(\alpha_n r_D)\right]}{\left[J_1(ur_{eD})\,Y_1(u) - J_1(u)\,Y_1(ur_{eD})\right]}, \quad \ldots \quad (A.20)$$

or

$$\pi\sum_{n=1}^{\infty}\left[\left(e^{-\alpha_n^2 t_{Dw}} J_1^2(\alpha_n r_{eD})\left[J_1(\alpha_n)\,Y_0(\alpha_n r_D) - Y_1(\alpha_n)\,J_0(\alpha_n r_D)\right]\right) \div \left(\alpha_n\left[J_1^2(\alpha_n r_{eD}) - J_1^2(\alpha_n)\right]\right)\right] \quad \ldots \quad (A.21)$$

By adding these exponential terms (which die out at large values of time) to the large time solution, Eq. A.17, we obtain the complete solution given below.

$$p(r,t) = p_i - \frac{q\mu}{2\pi kh}\left\{\frac{2}{r_{eD}^2-1}\left(\frac{r_D^2}{4} + t_{Dw}\right) - \frac{r_{eD}^2 \ln r_D}{r_{eD}^2-1} - \frac{(3r_{eD}^4 - 4r_{eD}^4 \ln r_{eD} - 2r_{eD}^2 - 1)}{4(r_{eD}^2-1)^2} + \pi\sum_{n=1}^{\infty} \frac{e^{-\alpha_n^2 t_{Dw}} J_1^2(\alpha_n r_{eD})\left[J_1(\alpha_n)\,Y_0(\alpha_n r_D) - Y_1(\alpha_n)\,J_0(\alpha_n r_D)\right]}{\alpha_n\left[J_1^2(\alpha_n r_{eD}) - J_1^2(\alpha_n)\right]}\right\} \quad \ldots \quad (A.22)$$

which is Eq. 2.34 of the text. Note that we used the definition of $\Delta p_D$ (Eq. A.10) in obtaining Eq. A.22.

### Constant Rate, Constant Pressure Outer Boundary Case

The mathematical statement of this problem is as follows.

$$\frac{\partial^2 p}{\partial r^2} + \frac{1}{r}\frac{\partial p}{\partial r} = \frac{\phi\mu c}{k}\frac{\partial p}{\partial t},$$

with

(1) $p = p_i = p_r$ at $t = 0$, for all $r$.

(2) $\left(r\frac{\partial p}{\partial r}\right)_{r_w} = \frac{q\mu}{2\pi kh}$, for $t > 0$.

(3) $p\,|_{r_e} = p_i$, for all $t$.

If we recast the problem in terms of the dimensionless variables of Eq. A.10, we obtain

$$\frac{\partial^2 \Delta p_D}{\partial r_D^2} + \frac{1}{r_D}\frac{\partial \Delta p_D}{\partial r_D} = \frac{\partial \Delta p_D}{\partial t_{Dw}},$$

with

(1) $\Delta p_D = 0$, at $t_{Dw} = 0$ for all $r_D$.

(2) $\left.\frac{\partial \Delta p_D}{\partial r_D}\right|_1 = -1$, for $t_{Dw} > 0$.

(3) $\Delta p_D = 0$ at $r_D = r_{eD}$, for all $t_{Dw}$.

Application of the Laplace transform to the above gives

$$\frac{d^2\bar{P}}{dr_D^2} + \frac{1}{r_D}\frac{d\bar{P}}{dr_D} = s\bar{P}, \quad \ldots\ldots \quad (A.23)$$

with

$$\left.\begin{array}{ll} (1) & \dfrac{d\bar{P}}{dr_D} = -\dfrac{1}{s} \\ (2) & \bar{P}\,|_{r_{eD}} = 0 \end{array}\right\} \quad \ldots\ldots \quad (A.24)$$

Again, Eq. A.14 is a general solution of the differential equation and the conditions (Eq. A.24) must be used to evaluate the constants $A$ and $B$. In this case

$$A\sqrt{s}\,I_1(\sqrt{s}) - B\sqrt{s}\,K_1(\sqrt{s}) = -\frac{1}{s},$$

$$A\,I_0(r_{eD}\sqrt{s}) + B\,K_0(r_{eD}\sqrt{s}) = 0.$$

Solving for $A$ and $B$ and substituting into Eq. A.14 yields

$$\bar{P} = \frac{I_0(r_{eD}\sqrt{s})\,K_0(r_D\sqrt{s}) - K_0(r_{eD}\sqrt{s})\,I_0(r_D\sqrt{s})}{s^{3/2}\left[I_1(\sqrt{s})\,K_0(r_{eD}\sqrt{s}) + K_1(\sqrt{s})\,I_0(r_{eD}\sqrt{s})\right]}, \quad \ldots\ldots \quad (A.25)$$

which is the transformed solution to our problem.

Proceeding as with the bounded circular reservoir case we find that the only singularities of Eq. A.25 in the complex plane are simple poles at the origin and along the negative real axis. At the origin

$$\bar{P} = \frac{1}{s}(\ln r_{eD} - \ln r_D) \quad \ldots\ldots \quad (A.26)$$

and, therefore, for large time

$$\Delta p_D = \ln r_{eD} - \ln r_D \quad \ldots\ldots \quad (A.27)$$

To obtain the complete solution we again need to find the singularities along the negative real axis. Those interested in the details are referred to Carslaw and Jaeger.[4]

Finally, we obtain the following expression for the pressure behavior at the well.

$$p_{wf} = p_i - \frac{q\mu}{2\pi kh}\left[\ln r_{eD} - 2\sum_{n=1}^{\infty} \frac{e^{-\beta_n^2 t_{Dw}}\,J_0^2(\beta_n r_{eD})}{\beta_n^2\left[J_1^2(\beta_n) - J_0^2(\beta_n r_{eD})\right]}\right], \quad \ldots\ldots \quad (A.28)$$

where $\beta_n$ is a root of

$$J_1(\beta_n)\,Y_0(\beta_n r_{eD}) - Y_1(\beta_n)\,J_0(\beta_n r_{eD}) = 0.$$

Eq. A.28 is identical with Eq. 2.38 of the text.

In Ref. 4 of Chapter 8 a slightly different form of Eq. A.28 is employed to provide a basis for pressure fall-off analysis prior to reservoir fillup in the unit mobility ratio case. This form is based on the vanishingly small wellbore radius ($r_w \to 0$) assumption. The pressure fall-off equation which is obtained is of the form

$$p_{ws} = p_i + b_1 e^{-\beta_1 \Delta t}.$$

Since only the first term in the series expansion has been retained, this expression is valid for large values of shut-in time only.

### References


1. Polubarinova-Kochina, P. Ya.: *Theory of Ground Water Movement*, Translated from the Russian by J. M. R. DeWeist, Princeton University Press, Princeton, N.J. (1962) 549.

2. Collins, R. E.: *Flow of Fluids Through Porous Materials*, Reinhold Publishing Corp., New York (1961).

3. van Everdingen, A. F. and Hurst, W.: "The Application of the Laplace Transformation to Flow Problems in Reservoirs", *Trans.*, AIME (1949) 186, 305-324.

4. Carslaw, H. S. and Jaeger, J. C.: *Conduction of Heat in Solids*, Oxford at the Clarendon Press (1959) 89.

5. Mueller, Thomas D. and Witherspoon, Paul A.: "Pressure Interference Effects Within Reservoirs and Aquifers", *J. Pet. Tech.* (April, 1965) 471-474.

DIVISION DE EDUCACION CONTINUA
FACULTAD DE INGENIERIA U.N.A.M.

CURSO: "INGENIERIA DE RESERVORIOS GEOTERMICOS"

# FLUJO DE FLUIDOS Y CALOR EN MEDIO POROSO.

PROF: DR. HEBER CINCO LEY

SEPTIEMBRE, 1981.

SOCIETY OF PETROLEUM ENGINEERS OF AIME
6200 North Central Expressway
Dallas, Texas 75206

1

PAPER NUMBER SPE-5521

THIS PRESENTATION IS SUBJECT TO CORRECTION

# Two-Phase, Two-Dimensional Simulation of a Geothermal Reservoir and the Wellbore System

By

Robert M. Toronyi, Member SPE-AIME, Scientific Software Corp. and S. M. Farouq Ali, Member SPE-AIME, Pennsylvania State U.



## ABSTRACT

A numerical mathematical model for simulating production from a two-phase geothermal reservoir was developed and tested. The simulation is rather unique, in that it consists of two coupled models, a reservoir model and a wellbore model. The reservoir model was a two-dimensional areal or cross-sectional, unsteady state description of the flow of mass and heat within an anisotropic, heterogeneous porous medium, containing a single component, two-phase fluid. The wellbore model was a one-dimensional, steady state description of the flow of a homogeneous, two-phase mixture. A totally implicit solution scheme was employed.

The simulator was used to investigate the effects of various levels of porosity, permeability, and initial pressure and liquid phase saturation distributions upon production.

The numerical simulator was tested for a wide variety of conditions, and was found to be stable for large time steps.

Based upon the numerical results, the behavior of two-phase geothermal reservoir was classified into three types, depending on the initial liquid saturation. Wellhead steam quality was higher than the bottomhole quality, in the runs conducted. It was found that superheated regions formed more readily in reservoirs of low porosity and permeability.

## INTRODUCTION

A geothermal system occurs as a heat anomaly, which can be explained as follows. The earth's interior is hotter than its surface, and this difference produces a temperature gradient which in turn provides a measure of the heat flow rate. The average heat flux for the earth is 1.5 $\mu cal/cm^2$ - sec (1). A geothermal system involves a flux which is one and one-half to five times higher than the average (2). Consequently, a geothermal system occurs as an anomaly in terms of heat flow. A high heat flux, along with surface seeps, is indicative of a geothermal system.

Since the main mode of heat transfer within a geothermal fluid reservoir is convection, the reservoir itself is called a hydrothermal convection system. Hydrothermal convection systems have been classified into two types based upon the physical state of the dominant pressure-controlling

phase, i.e. hot water systems and vapor-dominated sytems (1). In hot water systems, fluids exist within the reservoir mostly in the liquid state and generally produce from 70 to 90% of their total mass as water at the surface.

Vapor dominated systems generally produce dry to superheated steam, and fluids exist within the reservoir mostly in the vapor state. Surface manifestations will usually take the form of fumaroles, mud pots, mud volcanoes, turbid pools, and acid leached ground. Only three known areas in the world exist as this type of system. These are the Geysers field in California, the Larderello field in Italy, and the Matsukawa field in Japan. The pressures of vapor dominated systems are below hydrostatic. Also, the initial pressures and temperatures in vapor dominated systems are very close to the temperature and pressure relating to the maximum enthalpy of saturated steam, i.e., 236°C and 31.8 kg/cm$^2$. An explanation for this behavior has been given by James (3) and White, Muffler, and Truesdell (4).

Only during the last decade have reservoir engineering principles been used to study production aspects of geothermal systems. In that time relatively few models have been developed that simulate the production from a geothermal reservoir containing both a liquid and a vapor phase.

In fact, only three models have assumed the presence of a two-phase fluid within a geothermal reservoir. One of these models, developed by Donaldson (5) was a steady state, one-dimensional description of two-phase flow within porous media, but did not simulate production. The other two models, that of Whiting and Ramey (6) and that of Brigham and Morrow (7), were lumped parameter formulations. Thus, the objective of this work is to develop a model that simulates production from a two-phase geothermal reservoir in greater detail than has previously been done. Specifically, the simulation consists of two models, one for the reservoir and the other for the wellbore. The reservoir model is a two-dimensional areal or cross-sectional, unsteady state description of the flow of mass and heat within an anisotropic, heterogeneous porous medium containing a single component, two-phase fluid; while the wellbore model is a one-dimensional, steady state description of the flow of a homogeneous, two-phase mixture. The two models are then coupled together by treating the wellbore block as a point sink within the reservoir and by viewing the reservoir pressure and quality as inlet conditions for the wellbore.

## MATHEMATICAL MODELS OF GEOTHERMAL SYSTEMS

Models of geothermal systems can be thought of as being concerned either with the formation and stability of a geothermal system or with the production of fluids from a geothermal reservoir. Shown in Figure 1 is a diagrammatic representation of models relating to geothermal systems.

The fundamental formulation of a free convection problem in porous media, henceforth called the Fundamental Problem, is given in the AGU monograph on terrestrial heat flow, by Elder (8). Laboratory models and theoretical studies dealing with the physical processes of geothermal systems derive from this formulation in varying degrees of complexity. Constant temperature as well as no-flow boundary conditions, are employed in this formulation. For scaled model studies, Prandtl and Rayleigh numbers, and the aspect ratio can be used to define the system. Additionally, heat and fluid discharge can be characterized by the Nusselt and discharge numbers, respectively.

Wooding (9) first related the Fundamental Problem to a geothermal system, using classical perturbation methods.

Donaldson (10) carried out a mathematical study of the Fundamental Problem, but instead used finite difference techniques for its solution. He also solved a variation of the Fundamental Problem where the planar region was a two-layer system consisting of an upper permeable layer and an underlying impermeable layer. In a more complex formulation (11), he represented the planar region by three permeable channels, surrounded by impermeable rock. The model was studied further (12), taking account of the various permeabilities upon the Nusselt and discharge numbers.

The Fundamental Problem and the studies resulting from it consider only a single phase fluid. The only study that has been done that considers a two-phase fluid is by Donaldson (12). In the study a mathematical treatment was undertaken of the steady flow of water within a one-dimensional vertical channel (heated from below). A most interesting finding of Donaldson from a reservoir engineering standpoint was the sudden change in fluid saturations at interfaces of permeability reduction and at points of flow rate change. Donaldson's formulation in a sense is a specific case of a more general model considered in this paper.

Model studies relating to the production of fluids from geothermal reservoirs center

on fluid flow in the reservoir and in the wellbore. Thus, a further breakdown of model studies can be based on whether the model concerns itself with fluid flow in the reservoir or with fluid flow in the wellbore.

Reservoir Mechanics

Ramey, Kruger, and Raghavan (13) have pointed out factors which affect boiling in porous media. They state that vapor pressure data obtained from flat interfaces may not be appropriate in porous media due to the effect of capillarity which bends an interface between two phases. Works by Cady (14) and Bilhartz (15) have tried to validate this effect under conditions similar to geothermal reservoirs.

Evaporation and condensation of a liquid and its vapor within a porous medium greatly increase the heat transfer capacity of the rock. This behavior, first introduced by Grover, Cotter, and Erickson (16), has been called the heat pipe concept. White, Muffler, and Truesdell (4) suggested a vapor dominated reservoir exists as a heat pipe, i.e., it transfers heat at high rates by evaporating the liquid in warm parts and condensing the vapors in the cooler parts of the reservoir. Gomaa and Somerton (17) have studied the effect of vapor saturation on thermal conductivities of rock and have confirmed the heat pipe phenomenon.

Reservoir models of thermal processes are based upon a mass balance and an energy balance. The most detailed of these reservoir models is a distributed parameter system, i.e., the independent variables are parameterized with respect to both spatial and temporal variables. Models offering less detail but which have wider use are lumped parameter systems, i.e., the independent variables are parameterized only with respect to time.

The conservation of mass can be applied to the phases making up the system, or to the components making up the phases. In the former case, an interphase mass transfer term is to be included. The energy balance is made upon the entire system, but it has been based either upon internal energies or enthalpies. Coats (18) has formulated the energy balance for a steamflooding model in terms of internal energies, while Shutler (19) has formulated the energy balance for a steamflooding model in terms of enthalpies. Differing solution methods validate the need for these two formulations.

All but one of the reservoir models of geothermal systems that have been published in the literature are lumped parameter formulations. The most wellknown is by Whiting and Ramey (6). Their model consists of a conservation of mass balance upon the single component, water, and a conservation of energy balance using internal energies.

Brigham and Morrow (7), in an attempt to take into account the large spatial variation of the independent variables, found by Cady (14) for vapor-containing reservoirs, developed three lumped parameter models based on vapor liquid distribution. For each model it was assumed that there was no influx of mass into the reservoir. The resulting equations developed for each model were solved in a trial-and-error process for a given increment of depletion.

The only distributed parameter model that has been published is by Mercer (20). This model was developed for an areal study of a hot-water dominated field. The model consists of a single phase mass balance and the energy balance. The time term was approximated by finite difference techniques, while spatial terms were approximated by mixing isoparametric quadrilateral elements in a finite element technique. The model was successfully used to match temperature and pressure distributions in a hot water field in Wairakei, New Zealand.

Wellbore Models

Wellbore models used in reservoir studies have as their basis the steady state, one-dimensional balances of mass, momentum, and energy. Wallis (21) gives these equations for homogeneous equilibrium flow. In the petroleum literature these same equations have been solved assuming the two-phase to be homogeneous for steam injection down a wellbore by Pacheco and Farouq Ali (22), and others.

James (23) has developed one of three wellbore models published in the literature where flashing is assumed to occur within the wellbore. For this type of flow James has split up the wellbore into two sections. From the sandface up to the point where the pressure drops below the saturation pressure, the flashpoint, James solves the mass and momentum equations for a single phase fluid. From the flashpoint up to the wellhead, James solves the mass balance and the momentum balance under a homogeneity assumption for two-phase flow, along with a third empirical equation which couples the sandface enthalpy with the wellhead pressure. The empirical equation was derived from a bean (or choke) performance on flowing geothermal wells in the Wairakei field in New Zealand and is functionally identical to equations used on oil field wellbores.

The second wellbore model where flashing is assumed to occur in the wellbore, originally

done by Elder (8), was later modified by Nathenson (24). Again they split the wellbore into two sections.

The third and most detailed wellbore model has been developed by Gould (25). Gould's two-phase flow model differs from the homogeneous models discussed previously in that it considers the flow of each phase separately. This means that instead of solving the momentum balance for average viscosities and densities, empirical approximations based upon the morphology of flow are used for the acceleration, frictional, and gravitational terms.

Rumi (26) has proposed a wellbore model for the single phase flow of steam vapor. He formulates his problem in terms of a conservation of energy equation neglecting the potential energy term, a conservation of momentum equation neglecting gravity, a mass balance, an equation of state, and an equation for entropy production. By assuming isothermal flow, these equations are reduced to a single equation which relates flow rate with pressure.

## MATHEMATICAL DEVELOPMENT

The production of fluids from a two-phase geothermal system is envisioned as follows. A two-phase, single component mixture of steam and water is assumed to be contained within a porous reservoir. The reservoir is closed to flow of mass and heat. Specifically, the no-flow mass boundary condition corresponds to a reservoir which is not surrounded by an aquifer and thus is not subject to a water drive. The no-flow heat boundary condition corresponds to the case where the heat gain and the heat loss for the reservoir is small compared to the forced convective heat transfer generated by production. A well is assumed to be drilled into the reservoir from the surface of the earth and thus serves as a conduit for the flow of fluids from the reservoir up to the surface. Production is then accomplished by expansion of the fluids within the reservoir at the wellbore. The wellbore model herein developed assumes the flow of a homogeneous mixture of steam and water. This assumption has proven to be adequate for the high flow rates encountered in geothermal reservoirs.

### Reservoir Model

The physical system representing the reservoir is considered to be a two-dimensional, anisotropic, heterogeneous porous rock of rectilinear geometry. The rock is saturated with a single component fluid, water, existing either in the liquid state or the vapor state. The capillary pressure existing between these two phases is neglected. It is recognized that in cross-sectional simulations in particular, capillary pressure would influence fluid saturation distributions.

The conservation of mass with a point sink term applied to the single component, water, over a differential volumetric element of the reservoir yields:

$$-\hat{\nabla}\cdot(\eta_w\rho_w\hat{v}_w+\eta_g\rho_g\hat{v}_g)-Q=\frac{\partial}{\partial t}(\phi\eta_w\rho_wS_w+\phi\eta_g\rho_gS_g) \quad (1)$$

The relative permeabilities are assumed to be independent of the direction of the medium and to be unique functions of the liquid phase saturation; they are assumed to be independent of temperature. Thus the extension of Darcy's Law for multiphase flow is given as:

$$\hat{v}_w=\frac{-\bar{k}k_{rw}}{\mu_w}(\hat{\nabla}P-\gamma_w\hat{\nabla}\xi) \quad (2)$$

and

$$\hat{v}_g=\frac{-\bar{k}k_{rg}}{\mu_g}(\hat{\nabla}P-\gamma_g\hat{\nabla}\xi) \quad (3)$$

where

$$\bar{k}=\begin{pmatrix}k_x & 0\\ 0 & k_y\end{pmatrix}$$

The relative permeabilities assumed in this study are variations of a functional form proposed by Corey (30) for a drainage displacement process. The drainage assumption implies that the wetting phase saturation is decreasing. For a two-phase, single component fluid this means that the process of vaporization will predominate condensation.

$$k_{rw}=\frac{(S_w-S_{w_i})^4}{(1-S_{w_i})^4} \quad (4)$$

$$k_{rg} = \left[1 - \frac{(S_w - S_{w_i})}{(S_{w_m} - S_{w_i})}\right]^2 \left[1 - \frac{(S_w - S_{w_i})^2}{(S_{w_i} - 1)^2}\right] \quad (5)$$

where

$$S_{w_i} = .05 \text{ and } S_{w_m} = .95$$

Since a single component fluid is assumed to exist within the rock, the mass fraction of water in each phase is taken to be one, that is

$$\eta_w = 1$$

$$\eta_g = 1 \quad (6)$$

Substitution of Equations (2) and (3) and (6) into Equation (1) results in:

$$\hat{\nabla} \cdot \left[\frac{\bar{k} k_{rw} \rho_w}{\mu_w} (\hat{\nabla} P - \gamma_w \hat{\nabla} \xi) + \frac{\bar{k} k_{rg} \rho_g}{\mu_g} (\hat{\nabla} P - \gamma_g \hat{\nabla} \xi)\right] - Q = \frac{\partial}{\partial t} (\phi \rho_w S_w + \phi \rho_g S_g) \quad (7)$$

The conservations of energy with a heat sink made over a differential volumetric reservoir element based on enthalpies yields:

$$\hat{\nabla} \cdot (\bar{\kappa} \hat{\nabla} T) - \hat{\nabla} \cdot (\eta_w \rho_w h_w \hat{v}_w + \eta_g \rho_g h_g \hat{v}_g) - Q_h = \frac{\partial}{\partial t} \left[\phi (\eta_w \rho_w h_w S_w + \eta_g \rho_g h_g S_g) + (1 - \phi) \rho_r h_r\right] \quad (8)$$

This equation assumes constant rock density, constant specific heat of rock, instantaneous thermal equilibrium between the reservoir rock and the two fluid phases, and anisotropic behavior of thermal conductivity similar to that of permeability, i.e., orthogonal principal axes are congruent with the coordinate axis.

Again by assuming a single component fluid and Darcy's Law, substitution of Equations (2), (3) and (6) into Equation (8) yields:

$$\hat{\nabla} \cdot (\bar{\kappa} \hat{\nabla} T) - \hat{\nabla} \cdot \left[\frac{\bar{k} k_{rw} \rho_w h_w}{\mu_w} (\hat{\nabla} P - \gamma_w \hat{\nabla} \xi) + \frac{\bar{k} k_{rg} \rho_g h_g}{\mu_g} (\hat{\nabla} P - \gamma_g \hat{\nabla} \xi)\right] - Q_h = \frac{\partial}{\partial t} \left[(\phi \rho_w h_w S_w + \phi \rho_g h_g S_g) + (1 - \phi) \rho_r h_r\right] \quad (9)$$

The temperatures and pressures within the reservoir are then connected by the saturated pressure relationship for steam:

$$T = 115.1 \; P^{.225} \quad (10)$$

Substituting Equation (10) into Equation (9) results in:

$$\hat{\nabla} \cdot (\bar{\kappa} \frac{\partial T}{\partial P} \hat{\nabla} P) - \hat{\nabla} \cdot \left[\frac{\bar{k} k_{rw} \rho_w h_w}{\mu_w} (\hat{\nabla} P - \gamma_w \hat{\nabla} \xi) + \frac{\bar{k} k_{rg} \rho_g h_g}{\mu_g} (\hat{\nabla} P - \gamma_g \hat{\nabla} \xi)\right] - Q_h = \frac{\partial}{\partial t} \left[(\phi \rho_w h_w S_w + \phi \rho_g h_g S_g) + (1 - \phi) \rho_r h_r\right] \quad (11)$$

Auxiliary Relations

The vapor and liquid phase saturations are related by

$$S_g + S_w = 1 \quad (12)$$

The density, viscosity, and enthalpy for both water and steam are assumed to be functionally dependent on pressure and temperature at saturated conditions as follows:

$$\mu_g = 10^{-4}[82.2516 + .17815\ T + 6.59 \cdot 10^{-5}\ T^2 - \rho_g\ (31.45 - .05253\ T)] \quad (13)$$

$$\mu_w = 2.185\ /(0.04012\ T + 5.154 \cdot 10^{-6}\ T^2 - 1.0) \quad (14)$$

$$h_w = 91.0\ P^{.2574} \quad (15)$$

$$h_g = 1119\ P^{.01267} \quad (16)$$

$$\rho_w = 1.0/(.0158682 + .7475 \cdot 10^{-6}\ T + 15.111 \cdot 10^{-9}\ T^2) \quad (17)$$

$$\rho_g = .002473007\ P^{.9588} \quad (18)$$

The porosity of the rock is assumed to be a function of both space and pressure. The functional form assumed separates the effects of space and pressure in the following manner:

$$\phi = \phi_r(x, y) \cdot \phi_p(P) \quad (19)$$

where

$\phi_p = [1 + C_r\ (P - P_o)]$

$P_o$ = pressure at assumed reference point

$C_r$ = rock compressibility

## Wellbore Model

The wellbore (as shown in Figure 2) is considered to be a one-dimensional, vertical duct of constant diameter, through which a two-phase mixture of steam and water undergoes steady flow. The two-phase fluid is assumed to be a homogeneous mixture in which the phases are in thermal equilibrium with each other. In particular the frictional pressure drop of the two-phase mixture is determined by Martinelli-Nelson (27) two-phase multipliers. The Martinelli correlation balances frictional shear stresses versus pressure drop under a separated flow hypothesis. This correlation was made on the horizontal flow of boiling water. In a geothermal wellbore, vertical, flashing flow of water occurs. This then implies that the body forces and inertial forces are assumed small compared to frictional forces.

The equations describing a homogeneous, two-phase fluid undergoing steady, one-dimensional equilibrium flow over a differential element are a conservation of mass

$$\omega = \rho_m\ u\ a = \text{constant}, \quad (20)$$

a conservation of momentum

$$\frac{\omega}{g_c}\ \frac{du}{dZ} = 144\ a\ \frac{dP}{dZ} - P\ \tau_w - a\ \rho_m\ \frac{g}{g_c}, \quad (21)$$

and an energy balance

$$\frac{dq_e}{dZ} - \frac{1}{J_c}\ \frac{dW_e}{dZ} = \omega\ \frac{d}{dZ}\left[h_m + \frac{u^2}{2g_c J_c} + \frac{gZ}{g_c J_c}\right] \quad (22)$$

Here Z is taken in the direction of the flow and is thus positive upwards.

The rate of work of viscous and pressure forces is neglected, thus

$$\frac{dW_e}{dZ} = 0$$

So rearranging Equation (22) results in:

$$\frac{1}{\omega}\frac{dq_e}{dZ} = \frac{d}{dZ}\left[h_m + \frac{u^2}{2g_c J_c} + \frac{gZ}{g_c J_c}\right] \quad (23)$$

Equations (20), (21), and (23) are the equations that Pacheco and Farouq Ali (22) used in their study of steam injection. The treatment employed in this work is similar to their work except for the handling of friction and heat loss. The method consists of eliminating the mass balance equation by substituting it into the momentum and energy balances. Further algebraic and functional relations are then applied to the resulting two balances in order to produce a pair of differential equations in pressure and quality, which are as follows:

$$\frac{1}{\omega}\frac{dq_e}{dZ} - \frac{g}{J_c g_c} = \left[\frac{\partial h_m}{\partial P} + \frac{\Gamma^2 v_m}{J_c g_c}\frac{\partial v_m}{\partial P}\right]\frac{dP}{dZ} + \left[\frac{\partial h_m}{\partial X} + \frac{\Gamma^2 v_m}{J_c g_c}\frac{\partial v_m}{\partial X}\right]\frac{dX}{dZ} \quad (24)$$

$$\left[\frac{\Gamma^2 v_m}{g_c}\frac{\partial v_m}{\partial P} + 144\, v_m\right]\frac{dP}{dZ} + \frac{\Gamma^2 v_m}{g_c}\frac{\partial v_m}{\partial X}\frac{dX}{dZ} = -\frac{2\theta_f f v_m^2 \Gamma^2}{D g_c} - \frac{g}{g_c} \quad (25)$$

Auxiliary Relations

In order to solve these differential equations, auxiliary relations are needed for the friction factor, the two-phase multiplier, and the heat loss.

The Fanning friction factor is determined from one of three equations which are correlated with the Reynolds number and the relative roughness of the pipe as follows (Welty, Wicks and Wilson, (28) and Sommerfeld (29)):

for laminar flow (Re < 2100)

$$f = \frac{16}{Re} \quad (26)$$

for turbulent flow

$$\left(\frac{D/e}{Re\sqrt{f}} > .01\right)$$

$$\frac{1}{\sqrt{f}} = 4.0 \log_{10}\left(\frac{D}{e}\right) + 2.28 \text{ (Nikuradze)}, \quad (27)$$

and for transition flow

$$\frac{1}{\sqrt{f}} = 4.0 \log_{10}\left(\frac{D}{e}\right) + 2.28 - 4.0 \log_{10}\left(4.67\,\frac{D/e}{Re\sqrt{f}} + 1.0\right) \text{Colebrook)} \quad (28)$$

The Reynolds number used in this study was

$$Re = \frac{D\,\Gamma}{6.7197 \times 10^{-4}\,\mu_m}$$

where the viscosity, $\mu$, is determined from one of three equations depending on the value of the volumetric concentration of the vapor, $\beta$ (21).

For $5\% < \beta < 95\%$, the viscosity, $\mu_m$, was chosen by an average of steam and water viscosities weighted with respect to quality as follows:

$$\mu_m = X\,\mu_g + (1 - X)\,\mu_w \quad (29)$$

For $\beta < 5\%$, the mixture is assumed to be an emulsion of gas bubbles whose viscosity is assumed to be

$$\mu_m = \mu_w\,(1 + \beta) \quad (30)$$

For $\beta > 95\%$, the mixutre is assumed to be a mist whose viscosity is assumed to be

$$\mu_m = \mu_g (1 + \beta) \tag{31}$$

The two-phase multiplier, $\theta_f$, was determined by using Thom's (30) update of the Martinelli-Nelson (27) correlation. The curve fit of the tabulated values given by Wallis (21) is as follows:

$$\theta_f = .108547 \cdot 10^{3} X - .93493 \cdot 10^{-3} P + 2.10933 X^{5} - .307153 \cdot 10^{-2} X^{4} \cdot P + 1.5943 \tag{32}$$

Heat flow from the wellbore was assumed to take place at a steady state rate from the wellbore to the formation and at an unsteady state rate within the formation. The heat loss from the wellbore was given by:

$$\frac{dq_e}{dZ} = - 2\pi r_{c_1} U (T - T_{ho})/3600 \tag{33}$$

The overall heat transfer coefficient is composed of the resistance of the casing and the resistance of the cement, where the film coefficient at the inside casing wall has been neglected Willhite (32).

The heat loss from the wellbore into the formation at the cement formation interface has been given by Ramey (33) as

$$\frac{dq_e}{dZ} = \frac{-2\pi k_e (T_{ho} - T_e)}{3600 F(t)} \tag{34}$$

where F(t) is the transient heat conduction function.

Now Equations (24) and (25) along with the boundary conditions describe the flow within the wellbore.

The reservoir model gives as its solution the pressure and water saturation at the wellbore. The wellbore quality is given by

$$X = \frac{1 - S_w}{S_w \left(\frac{v_g}{v_w}\right) - 1 + 1} \tag{35}$$

Hence, using the reservoir pressure and liquid phase saturation given by the reservoir model, the reservoir quality can be determined by Equation (35). The reservoir pressure and the quality calculated from Equation (35) are then used as boundary conditions for the wellbore model.

## SOLUTION METHOD

The reservoir model and the wellbore model both involve nonlinear equations, which were solved numerically, employing a finite difference scheme and a fouth order Runge-Kutta method, respectively.

Basically the solution procedure involves solving the two partial differential equations of the reservoir model simultaneously for a given production rate. The solution is then obtained in terms of pressure (or temperature) and liquid phase saturation which are used to calculate the quality of steam at the wellbore. The calculated quality and the pressure used to calculate it serve as boundary conditions for the simultaneous solution of the differential equations of the wellbore model. The wellbore model then gives as its solution the wellhead quality and pressure.

### Finite Difference Representation

The partial differential equation corresponding to the mass balance Equation (7), written for two-dimensional rectilinear coordinates, after substitution of Equation (14), is discretized, using centered difference approximation to represent spatial derivatives, and a backward difference for the time derivative, obtaining:

$$TM^{n+1}_{wx_{i+\frac{1}{2},\,j}} \left(P^{n+1}_{i+1,\,j} - P^{n+1}_{i,\,j}\right) - TM^{n+1}_{wx_{i-\frac{1}{2},\,j}} \left(P^{n+1}_{i,\,j} - P^{n+1}_{i-1,\,j}\right) + TM^{n+1}_{gx_{i+\frac{1}{2},\,j}} \left(P^{n+1}_{i+1,\,j} - P^{n+1}_{i,\,j}\right) - TM^{n+1}_{gx_{i-\frac{1}{2},\,j}} \left(P^{n+1}_{i,\,j} - P^{n+1}_{i-1,\,j}\right) + TM^{n+1}_{wy_{i,\,j+\frac{1}{2}}} \left(P^{n+1}_{i,\,j+1} - P^{n+1}_{i,\,j}\right) - TM^{n+1}_{wy_{i,\,j+\frac{1}{2}}} -$$

$$TM^{n+1}_{wy_{i,\,j-\frac{1}{2}}}\left(P^{n+1}_{i,\,j}-P^{n+1}_{i,\,j-1}\right)+$$

$$TM'^{\,n+1}_{wy_{i,\,j-\frac{1}{2}}}+TM^{n+1}_{gy_{i,\,j+\frac{1}{2}}}$$

$$\left(P^{n+1}_{i,\,j+1}-P^{n+1}_{i,\,j}\right)-TM'^{\,n+1}_{gy_{i,\,j+\frac{1}{2}}}-$$

$$TM^{n+1}_{gy_{i,\,j-\frac{1}{2}}}\left(P^{n+1}_{i,\,j}-P^{n+1}_{i,\,j-1}\right)+$$

$$TM'^{\,n+1}_{gy_{i,\,j-\frac{1}{2}}}$$

$$-\frac{q^{n+1}_{T_{i,\,j}}}{\Delta x\Delta y\chi}=\frac{1}{\Delta t}\left\{\left[\phi\rho_w S_w\right]^{n+1}_{i,\,j}-\left[\phi\rho_w S_w\right]^{n}_{i,\,j}+\right.$$

$$\left.\left[\phi\rho_g\,(1-S_w)\right]^{n+1}_{i,\,j}-\left[\phi\rho_g\,(1-S_w)\right]^{n}_{i,\,j}\right\} \tag{36}$$

If saturation dependent terms are assumed to be highly nonlinear, then only those terms that are functions of saturation need to be taken at the (n + 1) time level. Hence the following temporal evaluation is performed.

$$TM^{n+1}_{wx}=M^{n}_{wx}k^{n+1}_{rw}\qquad TM^{n+1}_{gx}=M^{n}_{gx}k^{n+1}_{rg}$$

$$TM'^{\,n+1}_{wy}=\frac{\Delta y\,g}{144\,g_c}\,\rho^{n}_{w}k^{n+1}_{rw}\,M^{n}_{wy}$$

$$TM^{n+1}_{wy}=M^{n}_{wy}k^{n+1}_{rw}\qquad TM^{n+1}_{gy}=M^{n}_{gy}k^{n+1}_{rg}$$

$$TM'^{\,n+1}_{gy}=\frac{\Delta y\,g}{144\,g_c}\,\rho^{n}_{g}k^{n+1}_{rg}\,M^{n}_{gy}$$

where

$$M^{n}_{wx}=\frac{6.328\,k_x}{\Delta x^2}\left(\frac{\rho_w}{\mu_w}\right)^{n}\qquad M^{n}_{gx}=\frac{6.328\,k_x}{\Delta x^2}\left(\frac{\rho_g}{\mu_g}\right)^{n}$$

$$M^{n}_{wy}=\frac{6.328\,k_y}{\Delta y^2}\left(\frac{\rho_w}{\mu_w}\right)^{n}\qquad M^{n}_{gy}=\frac{6.328\,k_y}{\Delta y^2}\left(\frac{\rho_g}{\mu_g}\right)^{n}$$

In regards to spatial evaluation, the interblock transmissibility values are required at positions between grid points. Since the independent variables are only known at the grid points themselves, a suitable average of adjacent grid point values has to be devised. A linear average of adjacent grid points in the direction of the difference was used for the pressure dependent terms. For the saturation dependent terms, a weighted average of adjacent grid points was used based upon fluid potentials. Both of these averages have been implemented with success in other models reported in the literature: Letkeman and Ridings (34), MacDonald and Coats (35), and Diaz and Farouq Ali (36). The secondary parameter, permeability, was evaluated by means of a harmonic average of adjacent grid point values, which has been shown by the author (Toronyi and Farouq Ali, 37) to be correct from geometric and deterministic considerations.

Hence, an interblock transmissibility is exemplified by the following:

$$TM^{n+1}_{wx_{i+\frac{1}{2},\,j}}=M^{n}_{wx_{i+\frac{1}{2},\,j}}\,k^{n+1}_{rw_{i+\frac{1}{2},\,j}}$$

where

$$M^{n}_{wx_{i+\frac{1}{2},\,j}}=\frac{6.328}{\Delta x^2}\left\{\frac{2\,k_{x_{i,\,j}}\,k_{x_{i+1,\,j}}}{k_{x_{i,\,j}}+k_{x_{i+1,\,j}}}\right\}\cdot$$

$$\frac{1}{2}\left[\left(\frac{\rho_w}{\mu_w}\right)^{n}_{i+1,\,j}+\left(\frac{\rho_w}{\mu_w}\right)^{n}_{i,\,j}\right]$$

and

$$k^{n+1}_{rw_{i+\frac{1}{2},\,j}} = (1 - w_{xf})\, k^{n+1}_{rw_{i,\,j}} + w_{xf}\, k^{n+1}_{rw_{i+1,\,j}}$$

such that,

$$w_{xf} = 1 \quad \text{if} \quad \Phi^{n}_{w_{i,\,j}} < \Phi^{n}_{w_{i+1,\,j}}$$

$$w_{xf} = 0 \quad \text{if} \quad \Phi^{n}_{w_{i,\,j}} \geq \Phi^{n}_{w_{i+1,\,j}}$$

where

$$\Phi^{n}_{w_{i,\,j}} = P^{n}_{i,\,j} - \frac{y^{*}g}{144\,g_c}\,\rho^{n}_{w_{i,\,j}}$$

$y^{*}$ = distance from a datum level

The position of the well coincides with a grid point. A constant mass flow rate is assumed for the well. Hence, for the partial differential equation corresponding to the mass balance, the mass sink is defined as follows:

$$\text{for } i = K,\ j = L \quad q^{n+1}_{T_{i,\,j}} = \omega/8.64 \cdot 10^{4}$$

$$\text{for } i \neq K,\ j \neq L \quad q^{n+1}_{T_{i,\,j}} = 0$$

where $(x_K, y_L)$ corresponds to the location of the wellbore.

The partial differential equation corresponding to the energy balance, Equation (11), written in two-dimensional rectilinear coordinates, after substitution of Equation (12) is as follows:

$$\frac{\partial}{\partial x}\left[\kappa_x \frac{\partial T}{\partial P}\frac{\partial P}{\partial x}\right] + \frac{\partial}{\partial y}\left[\kappa_y \frac{\partial T}{\partial P}\frac{\partial P}{\partial y}\right] + \frac{\partial}{\partial x}\left[\frac{k_{rw}k_x\rho_w h_w}{\mu_w}\frac{\partial P}{\partial x}\right] + \frac{\partial}{\partial y}\left[\frac{k_{rw}k_y\rho_w h_w}{\mu_w}\left(\frac{\partial P}{\partial y} - \frac{\rho_w g}{144 g_c}\right)\right] +$$

$$\frac{\partial}{\partial x}\left[\frac{k_{rg}k_x\rho_g h_g}{\mu_g}\frac{\partial P}{\partial x}\right] + \frac{\partial}{\partial y}\left[\frac{k_{rg}k_y\rho_g h_g}{\mu_g}\left(\frac{\partial P}{\partial y} - \frac{\rho_g g}{144 g_c}\right)\right] - Q_h$$

$$= \frac{\partial}{\partial t}\left[\phi(S_w\rho_w h_w) + \phi(1 - S_w)\rho_g h_g + (1 - \phi)\rho_r h_r\right] \tag{37}$$

where again the y-direction is assumed to be coincident with the vertical direction.

Similarly to the mass balance, a centered difference approximation is used to represent the spatial derivatives and a backward difference is used for the time derivative. This results in:

$$V^{n}_{x_{i+\frac{1}{2},\,j}}\left(P^{n+1}_{i+1,\,j} - P^{n+1}_{i,\,j}\right) -$$

$$V^{n}_{x_{i-\frac{1}{2},\,j}}\left(P^{n+1}_{i,\,j} - P^{n+1}_{i-1,\,j}\right)$$

$$+ V^{n}_{y_{i,\,j+\frac{1}{2}}}\left(P^{n+1}_{i,\,j+1} - P^{n+1}_{i,\,j}\right) -$$

$$V^{n}_{y_{i,\,j-\frac{1}{2}}}\left(P^{n+1}_{i,\,j} - P^{n+1}_{i,\,j-1}\right)$$

$$+ TE^{n+1}_{wx_{i+\frac{1}{2},\,j}}\left(P^{n+1}_{i+1,\,j} - P^{n+1}_{i,\,j}\right) -$$

$$TE^{n+1}_{wx_{i-\frac{1}{2},\,j}}\left(P^{n+1}_{i,\,j} - P^{n+1}_{i-1,\,j}\right)$$

$$+ TE^{n+1}_{gx_{i+\frac{1}{2},\,j}}\left(P^{n+1}_{i+1,\,j} - P^{n+1}_{i,\,j}\right) -$$

$$TE^{n+1}_{gx_{i-\frac{1}{2},\,j}}\left(P^{n+1}_{i,\,j} - P^{n+1}_{i-1,\,j}\right)$$

$$+ TE^{n+1}_{wy_{i,j+\frac{1}{2}}} \left( P^{n+1}_{i,j+1} - P^{n+1}_{i,j} \right) -$$

$$TE'^{n+1}_{wy_{i,j+\frac{1}{2}}} - TE^{n+1}_{wy_{i,j-\frac{1}{2}}}$$

$$\left( P^{n+1}_{i,j} - P^{n+1}_{i,j-1} \right) + TE'^{n+1}_{wy_{i,j-\frac{1}{2}}}$$

$$+ TE^{n+1}_{gy_{i,j+\frac{1}{2}}} \left( P^{n+1}_{i,j+1} - P^{n+1}_{i,j} \right) -$$

$$TE'^{n+1}_{gy_{i,j+\frac{1}{2}}} - TE^{n+1}_{gy_{i,j-\frac{1}{2}}}$$

$$\left( P^{n+1}_{i,j} - P^{n+1}_{i,j-1} \right) + TE'^{n+1}_{gy_{i,j-\frac{1}{2}}}$$

$$- \frac{q^{n+1}_h}{\Delta x \Delta y X} = \frac{1}{\Delta t}$$

$$\left[ (\phi S_w \rho_w h_w)^{n+1}_{i,j} - (\phi S_w \rho_w h_w)^{n}_{i,j} \right] + \frac{1}{\Delta t}$$

$$\left[ \left[ \phi (1 - S_w) \rho_g h_g \right]^{n+1}_{i,j} - \left[ \phi (1 - S_w) \rho_g h_g \right]^{n}_{i,j} \right]$$

$$+ \frac{1}{\Delta t} \left[ \left[ (1 - \phi) \rho_r h_r \right]^{n+1}_{i,j} - \left[ (1 - \phi) \rho_r h_r \right]^{n}_{i,j} \right]$$

(38)

where

$$V_x = 24 \kappa_x \frac{\partial T}{\partial P} \qquad V_y = 24 \kappa_y \frac{\partial T}{\partial P}$$

$$TE_{wx} = h_w TM_{wx} \qquad TE_{wy} = h_w TM_{wy}$$

$$TE'_{wy} = h_w TM'_{wy} \qquad TE_{gx} = h_g TM_{gx}$$

$$TE_{gy} = h_g TM_{gy} \qquad TE'_{gy} = h_g TM'_{gy}$$

Again assuming that saturation dependent terms are highly nonlinear, then only those terms that are functions of saturation need to be taken at the (n + 1) time level. Hence the following temporal evaluation is performed:

$$V^n_x = \frac{24 \kappa_x}{\Delta x^2} \left. \frac{\partial T}{\partial P} \right|^n \qquad V^n_y = \frac{24 \kappa_y}{\Delta y^2} \left. \frac{\partial T}{\partial P} \right|^n$$

$$TE^{n+1}_{wx} = O^n_{wx} k^{n+1}_{rw} \qquad TE^{n+1}_{wy} = O^n_{wy} k^{n+1}_{rw}$$

$$TE'^{n+1}_{wy} = \frac{\Delta y g}{144 g_c} (\rho_w h_w)^n k^{n+1}_{rw} M^n_{wy}$$

$$TE^{n+1}_{gx} = O^n_{gx} k^{n+1}_{rg} \qquad TE^{n+1}_{gy} = O^n_{gy} k^{n+1}_{rg}$$

$$TE'^{n+1}_{gy} = \frac{\Delta y g}{144 g_c} (\rho_g h_g)^n k^{n+1}_{rg} M^n_{gy}$$

where

$$O^n_{wx} = \frac{6.328 k_x}{\Delta x^2} \left( \frac{\rho_w h_w}{\mu_w} \right)^n$$

$$O^n_{gx} = \frac{6.328 k_x}{\Delta x^2} \left( \frac{\rho_g h_g}{\mu_g} \right)^n$$

$$O^n_{wy} = \frac{6.328 k_y}{\Delta y^2} \left( \frac{\rho_w h_w}{\mu_w} \right)^n$$

$$O^n_{gy} = \frac{6.328 k_y}{\Delta y^2} \left( \frac{\rho_g h_g}{\mu_g} \right)^n$$

In regards to spatial evaluation, the interblock, thermal transconductivity values are formed by using a linear average of adjacent grid point values in the direction of the difference for the pressure dependent terms and by employing a harmonic average of adjacent grid point values for the thermal conductivity. Hence an interblock, thermal transconductivity is exemplified by the following:

$$Y^n_{x_{i+\frac{1}{2},j}} = \frac{24}{\Delta x^2}\left[\frac{2\kappa_{x_{i,j}}\kappa_{x_{i+1,j}}}{\kappa_{x_{i,j}}+\kappa_{x_{i+1,j}}}\right] \cdot \frac{1}{2}\left[\left.\frac{\partial T}{\partial P}\right|^n_{i+1,j} + \left.\frac{\partial T}{\partial P}\right|^n_{i,j}\right]$$

The interblock, thermal transmissibilities are formed similar to the interblock mass transmissibilities, i.e., a linear average of pressure dependent terms, a harmonic average of permeability, and a weighted average with respect to fluid potentials for the saturation dependent terms. Hence an interblock, thermal transmissibility is exemplified by the following:

$$TE^{n+1}_{gy_{i,j-\frac{1}{2}}} = O^n_{gy_{i,j-\frac{1}{2}}} k^{n+1}_{rg_{i,j-\frac{1}{2}}}$$

where

$$O^n_{gy_{i,j-\frac{1}{2}}} = \frac{6.328}{\Delta y^2}\left[\frac{2k_{y_{i,j}}k_{y_{i,j-1}}}{k_{y_{i,j}}+k_{y_{i,j-1}}}\right] \cdot \frac{1}{2}\left[\left(\frac{\rho_g h_g}{\mu_g}\right)^n_{i,j} + \left(\frac{\rho_g h_g}{\mu_g}\right)^n_{i,j-1}\right]$$

and

$$k^{n+1}_{rg_{i,j-\frac{1}{2}}} = (1 - s_{yb})\, k^{n+1}_{rg_{i,j}} + s_{yb}\, k^{n+1}_{rg_{i,j-1}}$$

such that

$$s_{yb} = 1 \text{ if } \Phi^n_{g_{i,j}} < \Phi^n_{g_{i,j-1}}$$

$$s_{yb} = 0 \text{ if } \Phi^n_{g_{i,j}} \geq \Phi^n_{g_{i,j-1}}$$

where

$$\Phi^n_{g_{i,j}} = P^n_{i,j} - \frac{y^* g}{144 g_c}\rho^n_{g_{i,j}}$$

$y^*$ - distance below a datum level

The heat sink term is given by

$$q_h = h_w q_T + (h_g - h_w)\, q_g \qquad (39)$$

The steam production rate is determined by the fractional flow of the steam phase within the block containing the wellbore as follows:

$$q_g = \sigma_g q_T \qquad (40)$$

where

$$\sigma_g = \frac{k_{rg}}{k_{rg} + \lambda k_{rw}} \quad \text{and} \quad \lambda = \frac{\mu_g}{\mu_w}\frac{\rho_w}{\rho_g}$$

Substituting Equation (40) into Equation (39) and differencing results in:

$$q^{n+1}_{h_{i,j}} = \left[h^n_w + \frac{\left(h^n_g - h^n_w\right) k^{n+1}_{rg}}{k^{n+1}_{rg} + \lambda^n k^{n+1}_{rw}}\right]_{i,j} q^{n+1}_{T_{i,j}} \qquad (41)$$

All terms in Equation (36) can be placed on one side of the equation and be defined to be the mass residual $R_{m_{i,j}}$; similarly, all terms in Equation (38) can be placed on one side of the equation and be defined as the energy residual $R_{E_{i,j}}$.

The no-flow boundary conditions are represented by zero fluid transmissibilities on the bounding surfaces, and zero flow velocities on the same surfaces, for mass and heat, respectively.

Initially, a pressure and saturation distribution is specified throughout the reser-

vair such that gravitational equilibrium is maintained.

Newtonian Formulation

Since Equations (36) and (38) in residual form are defined at every grid point, a system of 2·I·J nonlinear algebraic equations needs to be solved for each time step. Since each grid point is coupled to at most four adjacent grid points, the equations have at most five unknown grid point values for each independent variable, or ten unknowns per equation. These remarks can be summarized by representing the system of equations vectorially as follows:

$$\hat{R}(z) = 0 \qquad (42)$$

where

$$\hat{R} = (R_{m_{1,1}}, \ldots, R_{m_{I,J}}, \ldots, R_{m_{I-1,1}}, \ldots, R_{m_{I,J}}, \ldots, R_{E_{I,1}}, \ldots, R_{E_{I,J}}, \ldots, R_{E_{I-1,1}}, \ldots, R_{E_{I,J}})$$

and

$$\hat{z} = \left(P^{n+1}_{i,j-1}, P^{n+1}_{i-1,j}, P^{n+1}_{i,j}, P^{n+1}_{i+1,j}, P^{n+1}_{i,j+1}, S^{n+1}_{w_{i,j-1}}, S^{n+1}_{w_{i-1,j}}, S^{n+1}_{w_{i,j}}, S^{n+1}_{w_{i+1,j}}, S^{n+1}_{w_{i,j+1}}\right)$$

Such a system of nonlinear equations can be solved by means of a Newton-Raphson technique (Remson, Hornberger, and Molz (38)). The Newton-Raphson method applied to a set of nonlinear equations involves approximating the equation by a truncated Taylor's series expansion about an assumed solution to the set of equations. The result is a set of linear equations which can then be solved by matrix techniques. The method is repeated until the solution of the linearized equations agrees with the assumed solution within a certain tolerance. The Newton-Raphson method applied to Equation (42) results in:

$$\left[\delta \hat{z}^{(K+1)} \cdot \hat{\nabla}_z\right] \hat{R}(\hat{z}^{(K)}) = -\hat{R}(\hat{z}^{(K)}) \qquad (43)$$

where

$$\delta \hat{z}^{(K+1)} = \hat{z}^{(K+1)} - \hat{z}^{(K)} \quad K = 1, 2, \ldots$$

$$\hat{\nabla}_z = \left(\frac{\partial}{\partial P^{n+1}_{i,j-1}}, \frac{\partial}{\partial P^{n+1}_{i-1,j}}, \ldots, \frac{\partial}{\partial S^{n+1}_{w_{i,j+1}}}\right)$$

The method of solution proceeds by the following inductive argument. A trial solution, $z^{(0)}$, is assumed, which for the reservoir model is the initial condition. The vector function, $R(z^{(0)})$ and the dyadic, $\nabla_z R(z^{(0)})$, are then calculated. Note that the determinant of the dyadic is the Jacobian of R(z). The variables $\delta z^{(1)}$ are then solved for in Equation (43). If

$$|\delta z^{(1)}| < \epsilon$$

where $\epsilon$ is sufficiently small, then the trial solution, $z^{(0)}$, is assumed the true solution and the method is completed. If

$$|\delta z^{(1)}| > \epsilon$$

then a new guess is made by using the following relation:

$$z^{(1)} = z^{(0)} + \delta z^{(1)}$$

and the process is repeated. The process is terminated when

$$|\delta z^{(K+1)}| < \epsilon$$

and the solution is accepted as

$$z^{(K+1)} = z^{(K)}$$

A direct method was employed for the solution of the linear equations at each iteration.

Mathematical Checks

Mathematical checks were used in stability studies and the debugging of the reservoir model. Since the reservoir model can be viewed as a distributed parameter system, its reduction to a lumped parameter form gives a means for analyzing the stability of the model. The lumped parameter form of Equation (7) and (9)

can be obtained by integrating out all spatial variation and is as follows:

$$\frac{d}{dt}\left[ < \phi\rho_w' S_w > + < \phi\rho_g S_g > \right] = -Q \quad (44)$$

$$\frac{d}{dt}\left[ < \phi\rho_w h_w S_w > + < \phi\rho_g h_g S_g > + < (1-\phi)\rho_r h_r > \right] = -Q_h \quad (45)$$

In terms of systems theory, Q and $Q_h$ are the forcing functions for these equations (Porter (39)), and hence the manner in which the system responds is related to the nature of the forcing function. Thus, the effect of discretization of both time and space upon the system is influenced by the forcing function. These combined effects are measured by means of a dimensionless throughput defined as follows:

$$N_{TP} = \frac{q_T \Delta t}{m_p}$$

where

$m_p$ = total mass per cell containing the well

$\Delta t$ = time step size

$q_T$ = total mass production rate

A similar measure of stability has been developed by Todd, O'Dell, and Hirasaki, (40). A number of numerical stability studies were performed on the reservoir model; it was found that the maximum stable $N_{TP}$ ranged from about 1.0 to 33, for the various initial conditions and areal and cross-sectional models.

The lumped parameter model can be reduced further, resulting in dimensionless ratios that serve as measures for the accuracy of the model. By integrating out the temporal variation in Equations (44) and (45), the following relations are formed:

$$N_m = 1 \quad (46)$$

$$N_E = 1 \quad (47)$$

where

$$N_m = \frac{-\int_{t_0}^{t_1} Q\, dt}{\Delta_t[< \phi\rho_w S_w > + < \phi\rho_g S_g >]}$$

$$N_E = \frac{-\int_{t_0}^{t_1} Q_h\, dt}{\Delta_t[< \phi\rho_w h_w S_w > + < \phi\rho_g h_g S_g > + <(1-\phi)\rho_r h_r >]}$$

and the operator $\Delta_t$ is defined as $\Delta_t X = X_{t_1} - X_{t_0}$ for time levels $t_1$ and $t_0$. If the solution to the finite difference representation is to be correct, it must satisfy Equations (46) and (47).

## Wellbore Model

The wellbore model is represented by a system of mathematical equations in terms of two independent variables, pressure and quality. A solution is sought for this system in terms of the spatial parameter, Z. In particular, a solution is sought for the wellhead, $Z = Z_H$. Hence, the simultaneous solution of the two differential Equations (24) and (25), which relate the independent variables with space, suffices to solve the system. These equations can be placed in matrix form as follows:

$$\begin{pmatrix} K_1 & K_3 \\ K_2 & K_4 \end{pmatrix} \begin{pmatrix} dP/dZ \\ dX/dZ \end{pmatrix} = \begin{pmatrix} L_1 \\ L_2 \end{pmatrix} \quad (48)$$

where

$$K_1 = \frac{\partial h_m}{\partial P} + \frac{\Gamma^2 v_m}{J_c g_c}\frac{\partial v_m}{\partial P}$$

$$K_2 = 144 v_m + \frac{\Gamma^2 v_m}{g_c}\frac{\partial v_m}{\partial P}$$

$$K_3 = \frac{\partial h_m}{\partial X} + \frac{\Gamma^2 v_m}{g_c J_c}\frac{\partial v_m}{\partial X}$$

$$K_4 = \frac{\Gamma^2 v_m}{g_c}\frac{\partial v_m}{\partial X}$$

$$L_1 = \frac{1}{\omega}\frac{dq_e}{dZ} - \frac{g}{g_c J_c}$$

$$L_2 = -2\frac{\theta_f f v_m^2 \Gamma^2}{g_c D} - \frac{g}{g_c}$$

Equation (48) can be rearranged into the following form:

$$\begin{pmatrix} dP/dZ \\ dX/dZ \end{pmatrix} = \begin{pmatrix} K_1 & K_3 \\ K_2 & K_4 \end{pmatrix}^{-1} \begin{pmatrix} L_1 \\ L_2 \end{pmatrix} = \begin{pmatrix} H_1 \\ H_2 \end{pmatrix} \quad (49)$$

Having obtained the differential equations in this form, the Runge-Kutta method can be applied. The step size, Z, is chosen so that the positions of the wellhead and the borrom of the hole are coincident with the grid points. From the reservoir model and Equation (35), the bottomhole pressure and quality can be obtained, which in this case are the boundary conditions for the set of differential equations given in Equation (49).

The computer flow chart for the entire reservoir-wellbore simulation model is shown in Figures 3 and 4.

## DISCUSSION OF RESULTS

In order to gain insight into the problem of production from a two-phase geothermal reservoir, simulations were performed for various values of porosity, permeability, and intial pressure and saturation distributions. In particular, for the areal formulation five different levels of initial liquid phase saturation were used: 1.0, 0.80, 0.60, 0.40, and 0.20. For the cross-sectional formulation five different levels of initial liquid phase saturation were also used: 0.50, 0.40, 0.30, 0.20, and 0.10. In both formulations two different levels of initial pressure, 650 and 450 psia, two levels of porosity, 0.05 and 0.35, and two levels of permeability, 1.0 and 0.10 darcies, were employed.

Results of these simulations will be discussed in detail in another paper. A few examples of the results obtained, and the main conclusions derived will be stated here.

For the simulation runs, a 6 x 6 grid system was employed for the reservoir model. In order to better determine the effects of the secondary parameters, the reservoir was assumed to be homogeneous and isotropic. The rock density and the coefficient of rock compressibility were assumed constant at the values of 160 $lbm/ft^3$ and $5 \cdot 10^{-6}$ $psi^{-1}$ respectively. All computer runs were conducted using double precision arithmetic on an IBM 370/168. The convergence tolerance, $\varepsilon$, employed was $10^{-9}$. The typical range of the mass residual was $10^{-12}$ to $10^{-15}$, and the typical range of the energy residual was $10^{-9}$ to $10^{-11}$. The range in percent error associated with both incremental and cumulative mass balance numbers and energy balance numers was $10^{-9}$ to $10^{-10}$.

The wellbore model was not varied throughout the simulation runs. Its parameters were held constant and are given in Table 1. Step-size, Z, smaller than 10 ft. demonstrated solutions which differed by no more than $10^{-5}$ parts in 1.0 from solutions for $\Delta Z$ equal to 10 ft.

### Stability Analysis

The stability or time discretization effect of the reservoir model was tested in both cross-sectional and areal formulations. The difference in the two forms is that in the areal formulation the gravitational force was neglected. In particular, stability was tested by noting the sensitivity of the model to time step size. As has been mentioned in the previous chapter, the reservoir model is ultimately sensitive to the nature of the forcing function or in this case to the mass rate of production per unit volume of reservoir. Hence the measure employed here in analyzing the stability of the model was the dimensionless mass throughput $N_{TP}$.

For a particular initial saturation and pressure distribution, computer runs of the reservoir model were made progressively increasing time step size. A series of runs was terminated when the model produced physically unrealistic solutions or convergence could not be attained. The last time step size employed was used to calculate the maximum dimensionless throughput. Basically, the determination of this maximum dimensionless throughput to an accuracy of two decimal places was a trial-and-error procedure.

Table 2 shows results of an areal study with various initial saturation and pressure distributions. It is seen that generally the maximum dimensionless throughput increases with increasing initial pressure, except for an initial saturation level of 1.0. For all levels of initial pressure the initial saturation level of 0.20 attained the larges $N_{TP}$. Similar trends were observed for cross-sectional studies, but the trends were not as consistent, and the values of $N_{TP}$ were smaller than those for the areal simulations, possibly because of the added effect of gravity.

The effect of dimensionless throughput as a measure stability was also tested, varying the production rate. Close agreement of throughputs was obtained at low initial saturation levels, but at higher levels disparity appeared. This indicates that thermal effects, e.g. flashing, may dominate the stability of the system at high liquid saturations.

The effects of porosity and permeability on reservoir performance are exemplified for a cross-sectional formulation at an initial pressure of 650 psia. Shown in Figures 4 to 7 are plots of bottomhole pressure versus fraction of mass produced for the four different cases resulting from testing two levels of porosity and permeability. In comparison to the higher porosity level, the lower porosity level produces very little bottomhole pressure decline, which can be seen by comparing Figures 4 and 5 and Figures 6 and 7. This result coincides with the finding of Brigham and Morrow (7), who also found that low porosity produced small pressure decline. The lower permeability level produces a larger pressure decline than the higher level, but this decline is not as drastic as for porosity. This follows from comparing Figures 5 and 7 and Figures 4 and 6.

In comparison to the areal simulations, the addition of a gravitational force in the

cross-sectional formulation hastens the development of a superheated region in the reservoir. The level of initial pressure does not change the shape of the pressure decline curves, but does effect the advent of a superheated region. The higher level of initial pressure develops a superheated region before the lower level. Again in regards to the development of a superheated region, the lower porosity level developed a superheated region before the higher porosity level. Also, the lower permeability level developed a superheated region before the higher permeability level. This appears to agree with the results of Donaldson (5), who found that saturation changes were effected by permeability.

In the cross-sectional formulation, the smaller the initial liquid phase saturation level, the smaller the pressure decline, the shape of which is concave upward as can be seen in Figures 4 through 7. In the areal formulation, initial saturation levels larger than 0.40 demonstrated smaller pressure decline for a given amount of mass produced than the 0.40 level. Their shapes were concave downward.

For initial liquid phase saturations lower than 0.50, bottomhole quality increased as production proceeded, except for the case where both the lower level of porosity and permeability occurred, e.g. Figures 4A and 5A. Larger initial liquid phase saturations tended to decrease the bottomhole quality or increase it very slightly as production proceeded.

In the areal formulation, bottomhole quality demonstrated similar behavior, except for the initial saturation of 0.40.

The initial pressure level does not seem to alter the shape of the bottomhole quality curves.

Figures 8 and 8A present examples of the reservoir liquid phase saturation and pressure distributions, respectively, for a selected set of conditions for the cross-sectional formulation. The node indicated by a "+" is the production block.

In an areal formulation the most significant effect was that of the initial liquid phase saturation level upon the saturation distribution. Permeability and porosity levels did not alter this effect. For initial liquid phase saturation levels of 0.40 and smaller, the lowest liquid phase saturation about the wellbore existed at the wellbore grid point and the superheated region formed around the wellbore grid point. In contrast, for initial liquid phase saturation levels above 0.40, the highest liquid phase saturation existed at the wellbore grid point and the superheated region formed away from the wellbore.

## Wellhead Pressure and Quality

Wellhead pressure and quality were determined for every time step in all simulation runs until negative wellhead pressures were obtained. Negative wellhead pressure was interpreted to mean that the mass flow rate was too large to be physically attained. Figures 9 and 9A depict an example of the wellhead and bottomhole quality variation with production.

Wellhead quality was always found to be greater than bottomhole quality, while wellhead pressure was always less than bottomhole pressure. Neither wellhead pressure nor wellhead quality was always monotonic with respect to mass fraction produced. Further, bottomhole quality and pressure variations were often not reflected in wellhead variations.

The pressure drop, i.e., the difference in bottomhole and wellhead pressures, generally increased in time for initial liquid phase saturation levels less than 0.30 while it generally decreased in time for initial liquid phase saturation levels larger than 0.40. The larger level of initial pressure, 650 psia, for a given level of initial saturation gave a larger pressure drop than the smaller level of initial pressure, 450 psia.

For the initial pressure level of 650 psia, pressure drop ranged from 100 to 250 psia for initial liquid phase saturation levels larger than 0.30 and ranged from 100 to 350 psia for initial liquid phase saturation levels smaller than 0.30. For the initial pressure level of 450 psia, pressure drop ranged from 100 to 200 psia for initial liquid phase saturation levels larger than 0.30 and ranged from 100 to 300 psia for initial saturation levels below 0.30.

The quality rise, i.e., the difference in bottomhole and wellhead quality, for a given level of initial saturation was larger for an initial pressure level of 450 psia than for 650 psia, but only in the order of $10^{-3}$. Generally, initial quality rise ranged from 0.010 to 0.062, while final quality rise ranged from 0.014 to 0.123. The quality rise also generally increased with respect to mass fraction produced, but there were cases in which quality rise decreased for initial liquid phase saturation levels larger than 0.40.

## Theories and Implications

From the foregoing discussion of results, theories and implications of the production behavior of two-phase geothermal reservoirs may be deduced.

Three types of production behavior can be enumerated, based on the nature of the bottomhole pressure and steam quality variations.

For reservoirs of initial liquid phase saturations below 0.40, bottomhole quality increases with time and larger slopes of the bottomhole pressure decline curve are attained at the onset of production than later in the producing life of the reservoir. Since the initial vapor phase saturation is larger than the liquid phase saturation, this type may be called a vapor dominated system. For reservoirs of initial liquid phase saturations larger than 0.60, large slopes of the bottomhole pressure decline curve are attained near the end of the producing life of the reservoir and bottomhole quality decreases or increases very little with time. Since the initial liquid phase saturation is larger than the vapor phase saturation, this type may be called a liquid dominated system. Reservoirs of initial liquid phase saturations between 0.40 and 0.60 exhibit no uniform production behavior, so these reservoirs may be considered to be mixed domination systems.

This classification system may be considered as an extension of a classification of hydrothermal convection systems proposed by White (1). White classified geothermal reservoirs as hot water systems if water was the dominant pressure-controlling phase and as vapor dominated systems if steam was the dominant pressure-controlling phase. Hence, by considering the production behavior of two-phase geothermal reservoirs, a refinement of White's classification system can be made in terms of the initial liquid phase saturation.

Tight reservoir rock, as well as rock which has low permeability and porosity, develops a superheated region more quickly during its production life than rock which has a large permeability of porosity. Furthermore, the smaller the porosity of the reservoir rock, the smaller the pressure decline within the reservoir, and hence super-heated steam is generated with little loss in reservoir energy, i.e., reservoir pressure. Since porosity and permeability are known to decrease with depth, the chances of finding and producing these types of reservoirs are improved by drilling deeper into the earth. Also, proposed projects which involve the injection of water into hot rock in order to generate steam have a greater chance of developing superheated steam if the reservoir has small porosity and permeability.

### Utility of the Model Developed

In the light of the preceding theories and discussion, the model developed herein is useful in engineering the production behavior of two-phase geothermal reservoirs. Due to its distributed parameter form, the model can monitor fluid distributions and, hence, production behavior as no other model to date has done. Also, the reservoir model can handle very large time step sizes and still remain stable, in view of the implicit simultaneous solution scheme employed.

In particular, the model can predict the formation of superheated regions whose locations aid in the production of dry or higher quality steam. The model is able to take into account vaporization and condensation which can generate varied production and saturation behavior as discussed previously. The model also can utilize the heterogeneous and anisotropic nature of the reservoir rock and their resulting effect upon production. Further, since the incorporation of two-phase multipliers enables the wellbore model to handle any type of flow regime, the simulator is able to monitor wellhead behavior.

## CONCLUSIONS

The following conclusions and observations are derived on the basis of the present study:

1. Both areal and cross-sectional formulations produced stable solutions under large time step sizes.

2. Production behavior of two-phase geothermal reservoirs was classified into three types in terms of the initial liquid phase saturation. These are a vapor dominated system, i.e., initial liquid phase saturations below 0.40, a liquid dominated system, i.e., initial liquid phase saturations larger than 0.60, and a mixed domination system, i.e., initial liquid phase saturations between 0.40 and 0.60.

3. Superheated regions within the reservoirs formed more quickly for reservoirs of low porosity and permeability.

4. Wellhead quality was always found to be greater than the bottomhole quality, although the maximum quality rise was small.

## ACKNOWLEDGEMENT

The authors are indibted to Mr. Charles R. Faust, U.S. Geological Survey, for helpful suggestions.

## REFERENCES

1. White, D.E.: "Characteristics of Geothermal Resources," Geothermal Energy, Paul Kruger and Carel Otte, ed., Standford University Press, Stanford, California (1973) 69-94.
2. Muffler, L.J.P.: "Geothermal Resources," U.S. Geol. Surv. Prof. Pap. No. 820, D.H. Brobst and W.P. Pratt, ed., United States Government Printing Office, Washington, (1973) 251-261.
3. James, R.C.: "Wairakei and Larderello: Geothermal Power Systems Compared," N.Z.

J. Sci. (December, 1968) 11, 706-719.

4. White, D.E., Muffler, L.J.P. and Truesdell, A.H.: "Vapor-dominated Hydrothermal Systems compared with Hot-water Systems," Econ. Geol. (January-February, 1971) 66, 75-87.
5. Donaldson, I.G.: "A Possible Model for Hydrothermal Systems and Methods of Studying Such a Model," paper 2580 presented at 3rd Australasian Conference on Hydraulics and Fluid Mechanics, Sidney, Australia, November 25-29, 1968
6. Whiting, R.L. and Ramey, H.J., Jr.: "Applications of Material and Energy Balances to Geothermal Steam Procution," J. Pet. Tech. (July, 1969) 21, 893-900.
7. Brigham, W.E. and Morrow, W.B.: "P/Z Behavior for Geothermal Steam Reservoirs," paper SPE 4899 presented at SPE - AIME 44th Annual California Regional Meeting, San Francisco, California, April 4-5, 1974.
8. Elder, J.W.: "Physical Processes in Geothermal Areas," Terrestrial Heat Flow, W. Lee, ed., American Geophysical Union, Washington (1965), 211-239.
9. Wooding, R.A.: "Steady State Free Thermal Convection of Liquid in a Saturated Permeable Medium," J. Fluid Mech. (May, 1957) 2, 273-285.
10. Donaldson, I.G.: "Temperature Gradients in the Upper Layers of the Earth's Crust due to Convective Water Flows," J. Geophys. Res. (August, 1962) 67, 3449-3459.
11. Donaldson, I.G.: "The Flow of Steam/Water Mixtures through Permeable Beds: A Simple Simulation of a Natural Undisturbed Hydrothermal Region," N.Z. J. Sci. (March, 1968) 11, 3-23.
12. Donaldson, I.G.: "The Simulation of Geothermal Systems with a Simple Convective Model," Geothermics, Special Issue 2 (1970) 2 part 1, 649-654.
13. Ramey, H.J., Jr., Kruger, P. and Raghavan, R.: "Explosive Stimulation of Hydrothermal Reservoirs," Geothermal Energy, Paul Kruger and Carel Otte, ed., Standford University Press, Stanford, California (1973) 231-249.
14. Cady, G.V.: "Model Studies of Geothermal Fluid Production," Ph.D. Thesis, Stanford University, Stanford, California (November, 1969).
15. Billhartz, H.L., Jr.: "Fluid Production from Geothermal Steam Reservoirs," M.S. Report, Stanford University, Stanford, California (Spring, 1971).
16. Grover, G.M., Cotter, T.P. and Erickson, G.F.: "Structure of Very High Conductance," J. App. Phys. (June, 1964) 35, 1990-1991.
17. Gomaa, E.E. and Somerton, W.H.: "Thermal Behavior of Multifluid-saturated Formations Part II: Effect of Vapor Saturation-Heat Pipe Concept and Apparent Thermal Conductivity," paper SPE 4896-B presented at SPE - AIME 44th Annual California Regional Meeting, San Francisco, California, April 4-5, 1974.
18. Coats, K. H., George, W.D., Chu, C. and Marcum, B.E.: "Three-dimensional Simulation of Steamflooding," paper SPE 4500 presented at SPE - AIME 48th Annual Fall Meeting, Las Vegas, Nevada, September 30 - October 3, 1973.
19. Shutler, N.D.: "Numerical, Three-phase Simulation of the Two-dimensional Steamflood Process," Soc. Pet. Eng. J. (December, 1970) 10, 405-417.
20. Mercer, J.W., Jr.: "Finite Element Approach to the Modeling of Hydrothermal Systems," Ph.D. Thesis, University of Illinois, Urbana-Champaign, Illinois (1973).
21. Wallis, G.B.: One-dimensional Two-phase Flow, McGraw-Hill, Inc., New York (1969).
22. Pacheco, E.F. and Farouq Ali, S.M.: "Wellbore Heat Losses and Pressure Drop in Steam Injection," J. Pet. Tech. (February, 1972) 24, 139-144.
23. James, R.C.: "Factors Controlling Borehole Performance," Geothermics, Special Issue 2 (1970) 2 part 2, 1502-1515.
24. Nathenson, M.: "Flashing Flow in Hot Water Geothermal Wells," U.S. Geological Survey Open File Report (1974).
25. Gould, T.L.: "Vertical Two-phase Steam-Water Flow in Geothermal Wells," presented at the National AICHE Meeting, Tulsa, Oklahoma, March 10-13, 1974.
26. Rumi, O.: Some Considerations on the Flow-Rate Pressure Curve of the Steam Wells of Larderello," Geothermics (March, 1972) 1, 13-23.
27. Martinelli, R.C. and Nelson, D.B.: "Prediction of Pressure Drop during Forced-Circulation Boiling of Water," Trans. ASME (1948) 70, 695-702.
28. Welty, J.R., Wicks, C.E. and Wilson, R.E.: Fundamentals of Momentum, Heat and Mass Transfer, John Wiley and Sons, Inc., New York (1969).
29. Sommerfeld, J.T., "Equation for Fluid Friction Factor," Hydrocarbon Processing (July, 1967) 46, 135-136.
30. Thom, J.R.S.: "Prediction of Pressure Drop During Forced Circulation Boiling of Water," Intern. J. Heat Mass Transfer, (July, 1964) 1, 709-724.
31. Corey, A.T.: "The Interrelation between Gas and Oil RElative Permeabilities," Producers Monthly (November, 1954) 19, 38-41.
32. Willhite, G.P.: "Overall Heat Transfer Coefficients in Steam and Hot Water Injection Wells," J. Pet. Tech. (May, 1967) 19, 607-615.
33. Ramey, H.J.: "Wellbore Heat Transmission," J. Pet. Tech. (April, 1962) 14, 427-435.
34. Letkeman, J.P. and Ridings, R.L.: "A Numerical Coning Model," Soc. Pet. Eng. J. (December, 1970) 10, 418-424.

35. MacDonald, R.C. and Coats, K.H." "Methods for Numerical Simulation of Water and Gas Coning," Soc. Pet. Eng. J. (December, 1970) 10, 425-436.
36. Diaz, J.M., and Farouq Ali, S.M.: "Simulation of Hot Water Stimulation of Heavy Oil Formations, presented at the 44th National Meeting of AICLE, Tulsa, Feb., 1974.
37. Toronyi, R.M. and Farouq Ali, S.M.: "Determining Interblock Transmissibility in Reservoir Simulators," J. Pet. Tech. (January, 1974) 26, 77-78.
38. Remson, I., Hornberger, G.M. and Molz, F.J.: Numerical Methods in Subsurface Hydrology, Wiley-Interscience, New York (1971).
39. Porter, W.A.: Modern Foundations of Systems Engineering, The MacMillan Co. New York (1966).
40. Todd, M.R., O'Dell, P.M. and Hirasaki, G.J.: "Methods for Increased Accuracy in Numerical Reservoir Simulators," Soc. Pet. Eng. J. (December, 1972) 12, 515-530.

NOMENCLATURE

$C_r$ = rock compressibility, $in^2/lbf$

D = pipe diameter, ft

$J_c$ = mechanical equivalent of heat, 778 ft-lbf/BTU

$N_E$ = energy balance number, dimensionless

$N_m$ = mass balance number, dimensionless

$N_{TP}$ = dimensionless throughput, dimensionless

P = pressure, $lbf/in^2$

Q = mass rate of production per unit volume of reservoir, $lbm/ft^3$-day

$Q_h$ = rate of heat loss per unit volume of reservoir, $BTU/ft^3$-day

Re = Reynolds number, dimensionless

$R_E$ = energy residual, $BTU/ft^3$-day

$R_m$ = mass residual, $lbm/ft^3$-day

S = phase saturation (volume fraction), dimensionless

T = temperature, °F

TE = thermal transmissibility, $in^2$-BTU/lbf-$ft^3$-day

TM = mass transmissibility, $in^2$-lbm/lbf-$ft^3$-day

U = heat transfer coefficient, BTU/hr-$ft^2$-°F

$W_e$ = rate of work, ft-lbf/sec

X = quality (mass fraction of steam), dimensionless

Z = linear wellbore coordinate, ft

a = pipe area, $ft^2$

e = pipe roughness, dimensionless

f = Fanning friction factor, dimensionless

g = acceleration due to gravity, $ft/sec^2$

$g_c$ = gravitational conversion factor, 32.17 lbm-ft/lbf-$sec^2$

h = specific enthalpy, BTU/lbm

k = absolute permeability, darcy

$k_r$ = relative permeability, dimensionless

$\hat{n}$ = normal vector

q = heat flux, $BTU/ft^2$-hr

$q_e$ = heat transfer rate, BTU/sec

$q_g$ = mass production rate of vapor, lbm/day

$q_h$ = reservoir heat transfer rate, BTU/day

$q_T$ = mass production rate of both liquid and vapor, lbm/day

$q_w$ = mass production rate of liquid, lbm/day

r = radius, ft

s, w = weighting parameters

t = time, day

u = velocity of fluid mixture within wellbore, ft/sec

v = darcy (reservoir) velocity, ft/day

x, y = rectangular reservoir coordinates, ft

$\Gamma$ = mass flux, lbm/sec-$ft^2$

$\phi$ = fluid potential, $lbf/in^2$

$\alpha$ = thermal diffusivity, $ft^2/day$

$\beta$ = volumetric fraction of vapor within wellbore, dimensionless

$\gamma$ = $\frac{\rho g}{144 g_c}$, lbf/ft-in$^2$

$\eta$ = mass fraction, dimensionless

$\theta_f$ = two-phase multiplier, dimensionless

$\kappa$ = thermal conductivity, BTU/ft-hr-°F

$\lambda$ = viscosity ratio, dimensionless

$\mu$ = viscosity, centipoise

$\nu$ = specific volume, ft$^3$/lbm

$\xi$ = vertical coordinate, ft

$\rho$ = desnity, lbm/ft$^3$

$\tau$ = wall shear stress, lbf/ft$^2$

$\phi$ = effective rock porosity, dimension less

$\chi$ = reservoir thickness, ft

$\omega$ = mass flow rate, lbm/sec

Subscripts

$c_i$ = inner casing

f = forward

g = vapor

h = heat

ho = hole

I = number of nodes in x-coordinate direction of reservoir grid system

J = number of nodes in y-coordinate direction of reservoir grid system

K, L = wellbore location indices

m = mixture

M = number of nodes in wellbore grid system

n = time position index

o = base or reference point

p = pressure

r = rock

s = vapor

T = total

w = liquid

x, y = reservoir coordinate directions

Superscripts

$\langle\ \rangle$ = average

o = initial

$\bar{\ }$ = matrix

$\vec{\ }$ = vector

TABLE 1 - WELLBORE MODEL PARAMETERS EMPLOYED IN SIMULATION RUNS

| | | | |
|---|---|---|---|
| $\alpha$ | = | 0.96 | $ft^2/day$ |
| $\kappa_{cem}$ | = | 0.51 | BTU/hr-ft-$^oF$ |
| $\kappa_{cas}$ | = | 25.0 | BTU/hr-ft-$^oF$ |
| $\kappa_e$ | = | 1.0 | BTU/hr-ft-$^oF$ |
| $r_{c_o}$ | = | 0.2916 | ft |
| $r_{c_i}$ | = | 0.26525 | ft |
| $r_{ho}$ | = | 0.4073 | ft |
| e | = | $0.15 \cdot 10^{-3}$ | dimensionless |
| well depth | = | $14.0 \cdot 10^2$ | ft |
| $\Delta Z$ | = | 10.0 | ft |
| $\omega$ | = | 555.56 | lbm/sec ($2 \cdot 10^5$ lbm/hr) |

TABLE 2 - RESULTS OF A STABILITY STUDY UNDER AN AREAL FORMULATION

| Initial Liq. Sat. $S_w^o$ | Initial Pressure $P^o$ (psia) | Max. Dimensionless Throughput Max $N_{TP}$ |
|---|---|---|
| 0.20 | 250 | 24.81 |
| 0.40 | 250 | 6.85 |
| 0.60 | 250 | 7.30 |
| 0.80 | 250 | 7.30 |
| 1.00 | 250 | 6.80 |
| 0.20 | 450 | 33.06 |
| 0.40 | 450 | 16.17 |
| 0.60 | 450 | 19.36 |
| 0.80 | 450 | 9.89 |
| 1.00 | 450 | 5.30 |
| 0.20 | 650 | 33.47 |
| 0.40 | 650 | 27.81 |
| 0.60 | 650 | 6.70 |
| 0.80 | 650 | 11.72 |
| 1.00 | 650 | 3.53 |

where

Cell Size: $\chi$ = 1000 ft
$\Delta_x$ = 100 ft
$\Delta_y$ = 10 ft

Production Rate: $q_T = 4.8 \cdot 10^6$ lbm/day

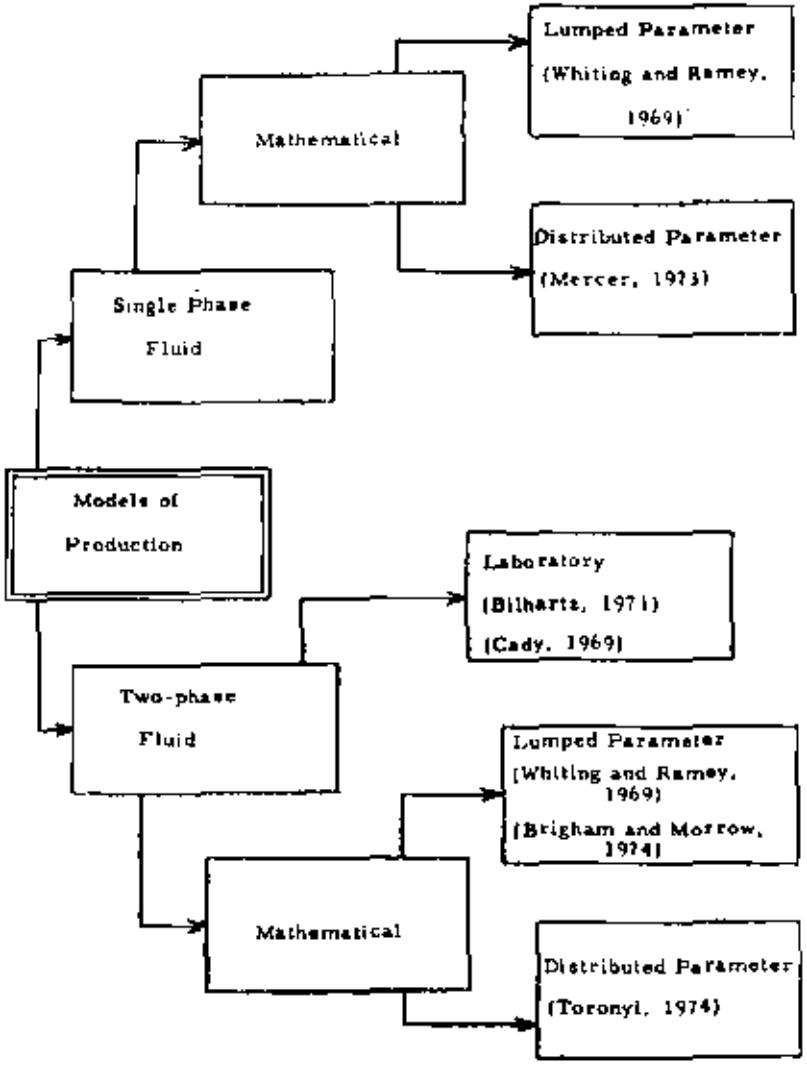


Fig. 1 - Diagrammatical representation of models relating to geothermal systems.

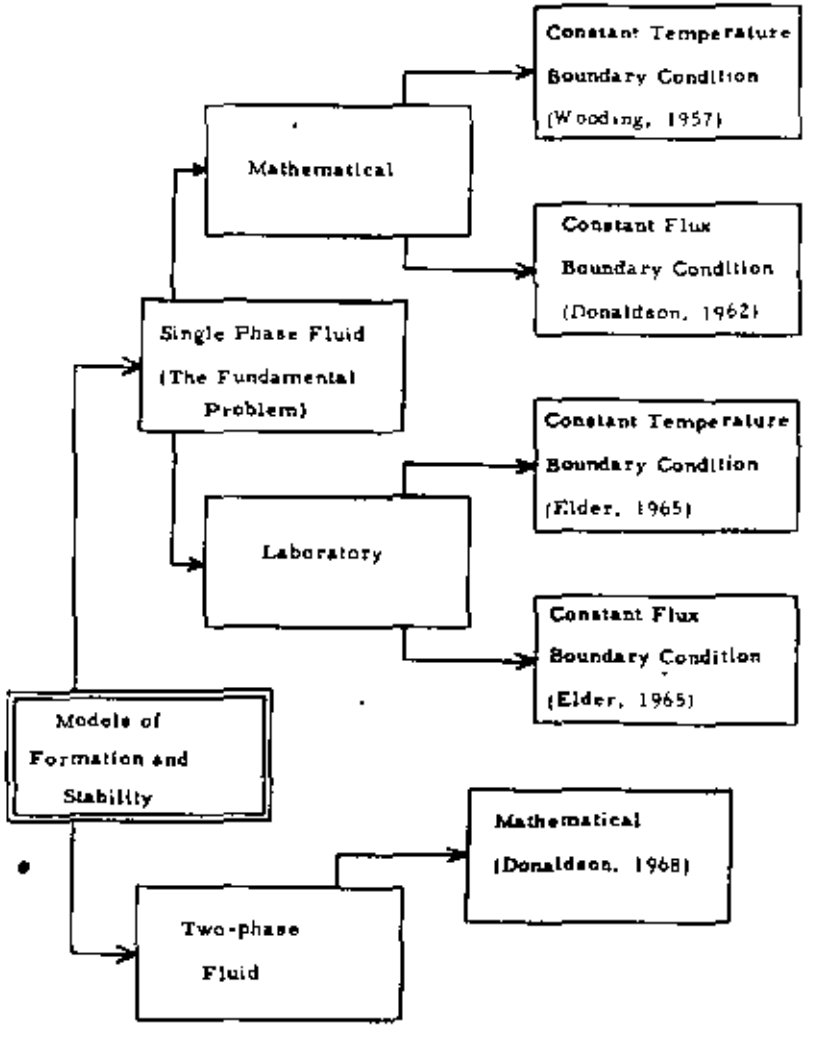


Fig. 1 - (Con't.)

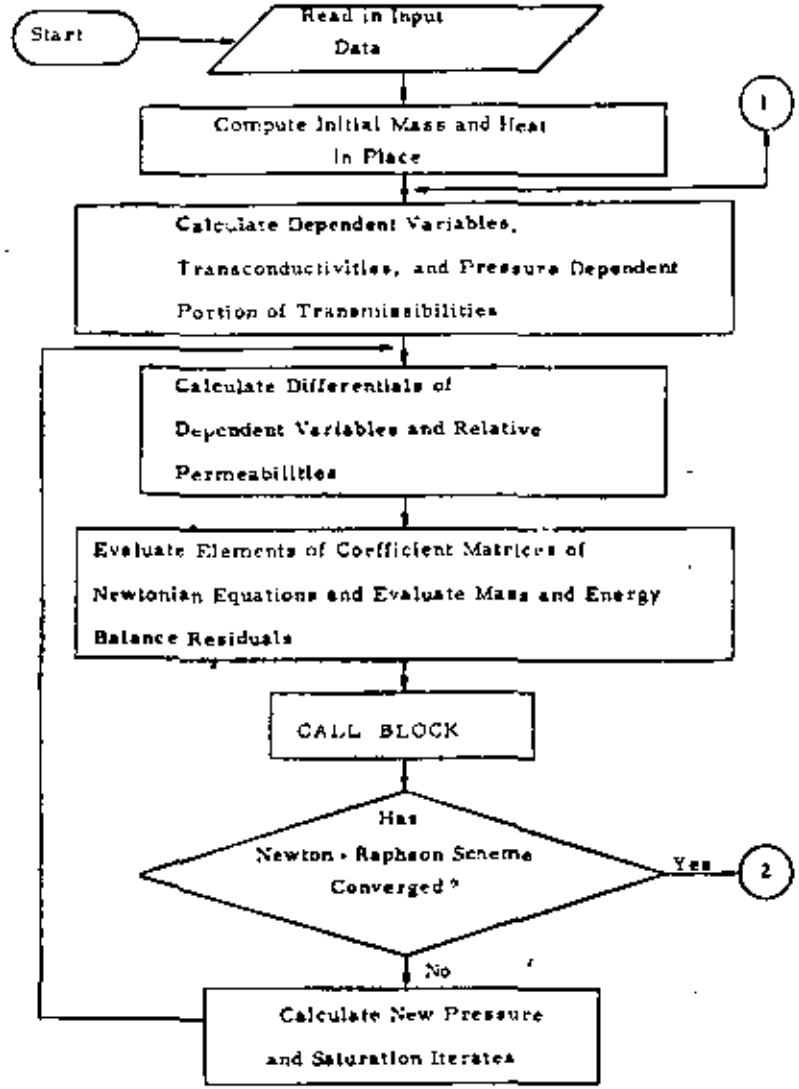


Fig. 2 - Flow chart for the main program of the computational procedure.

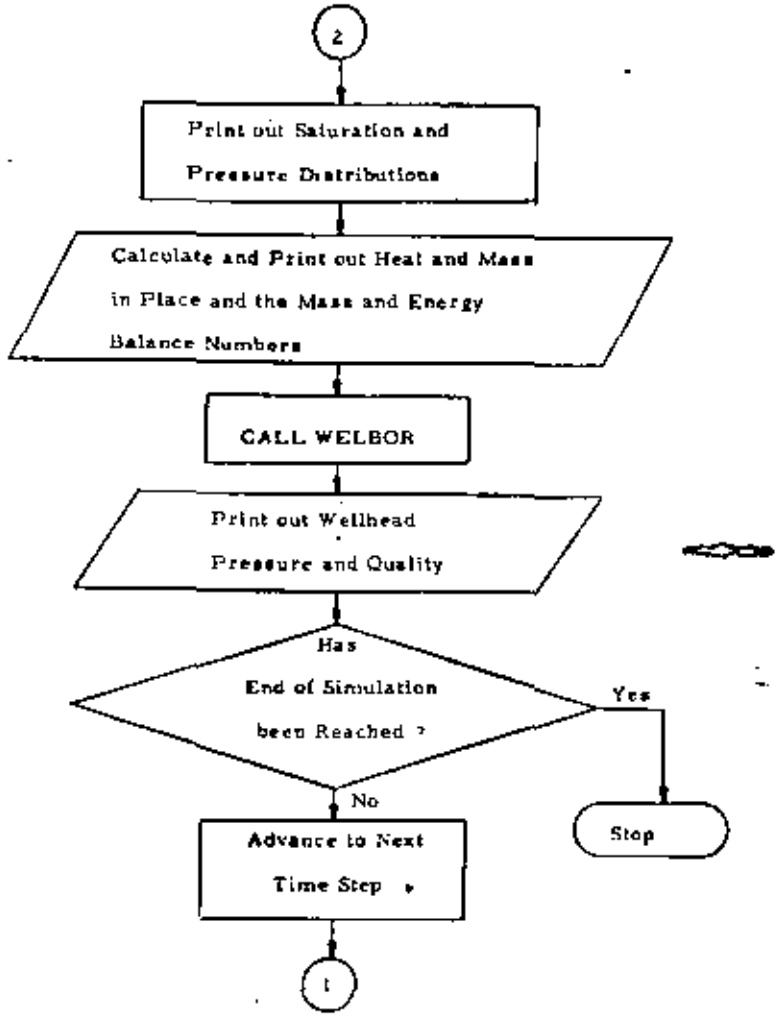


Fig. 2 - (Con't.)

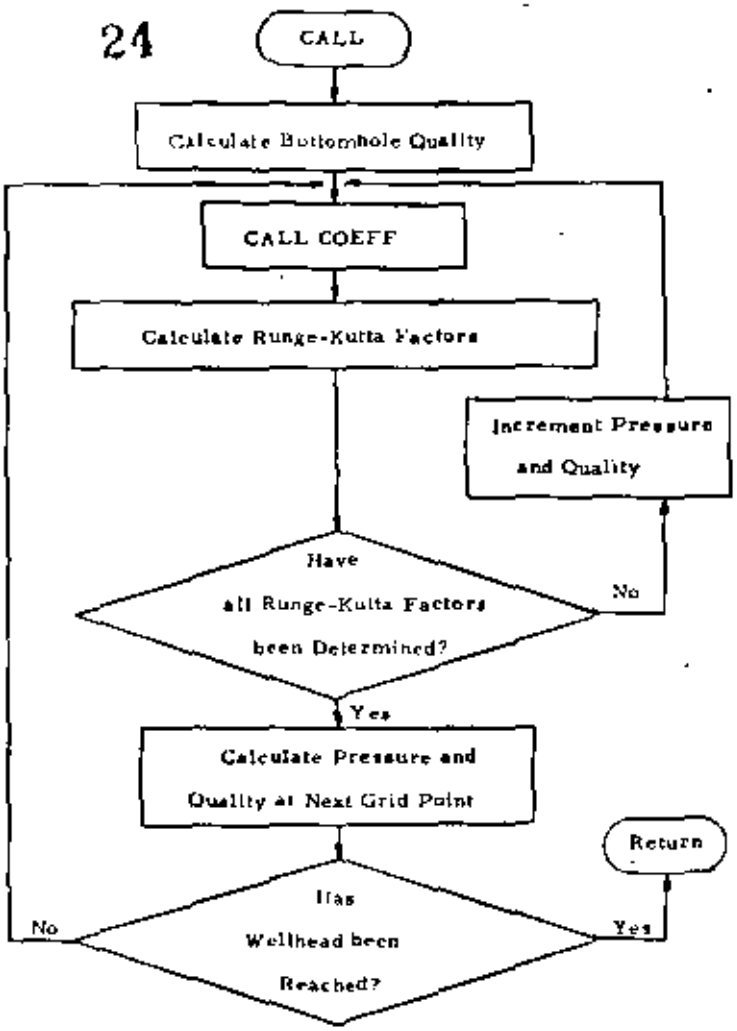


Fig. 3 - Flow chart for subroutine WILHOM of the computational procedure.

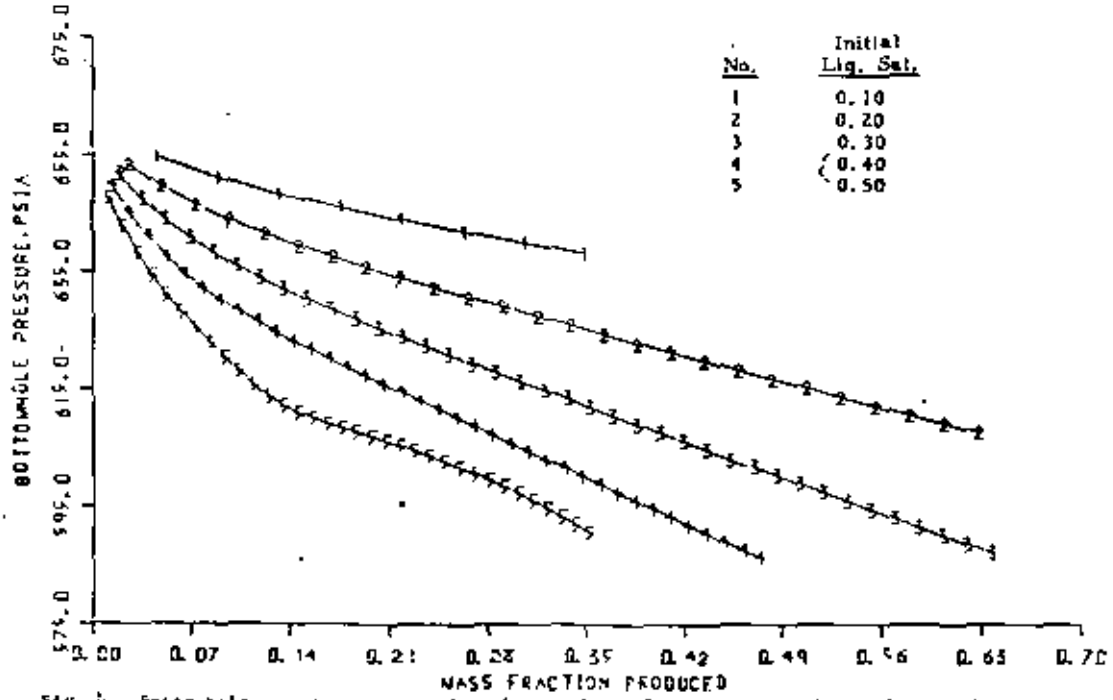


Fig. 4 - Bottomhole pressure vs mass fraction produced for a cross-sectional formulation of a reservoir having permeability = 1.0 darcies, porosity = 0.05, and initial pressure = 650 psia.

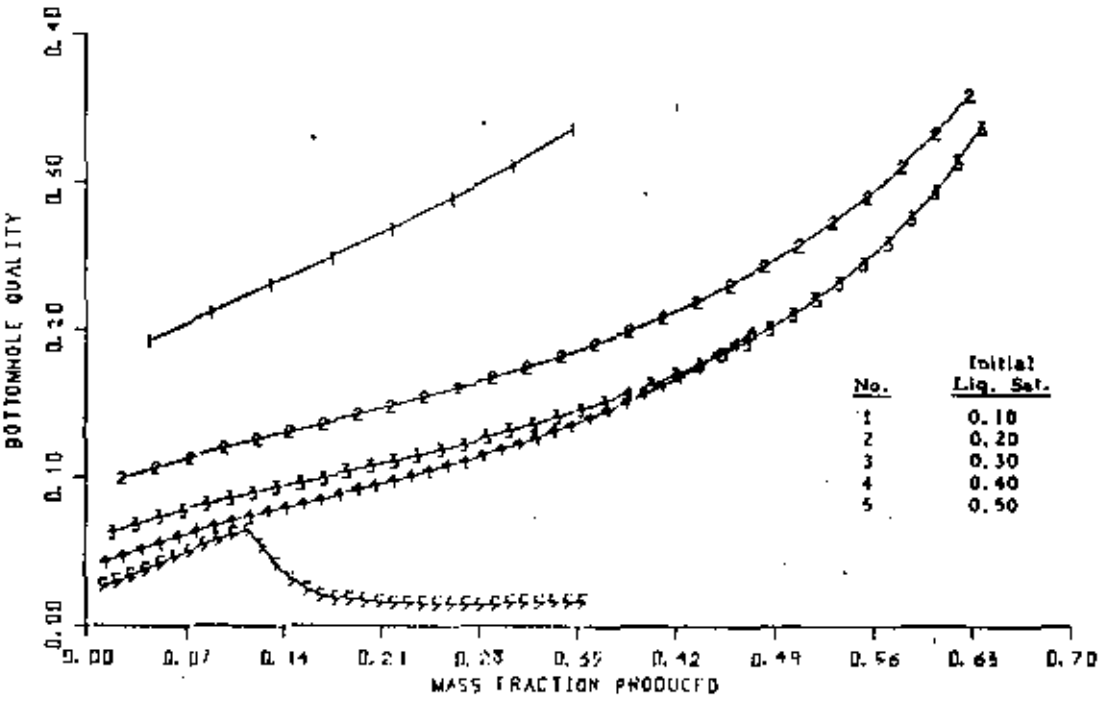


Fig. 4A - Bottomhole quality vs mass fraction produced for a cross-sectional formulation of a reservoir having permeability = 1.0 darcies, porosity = 0.05, and initial pressure = 650 psia.

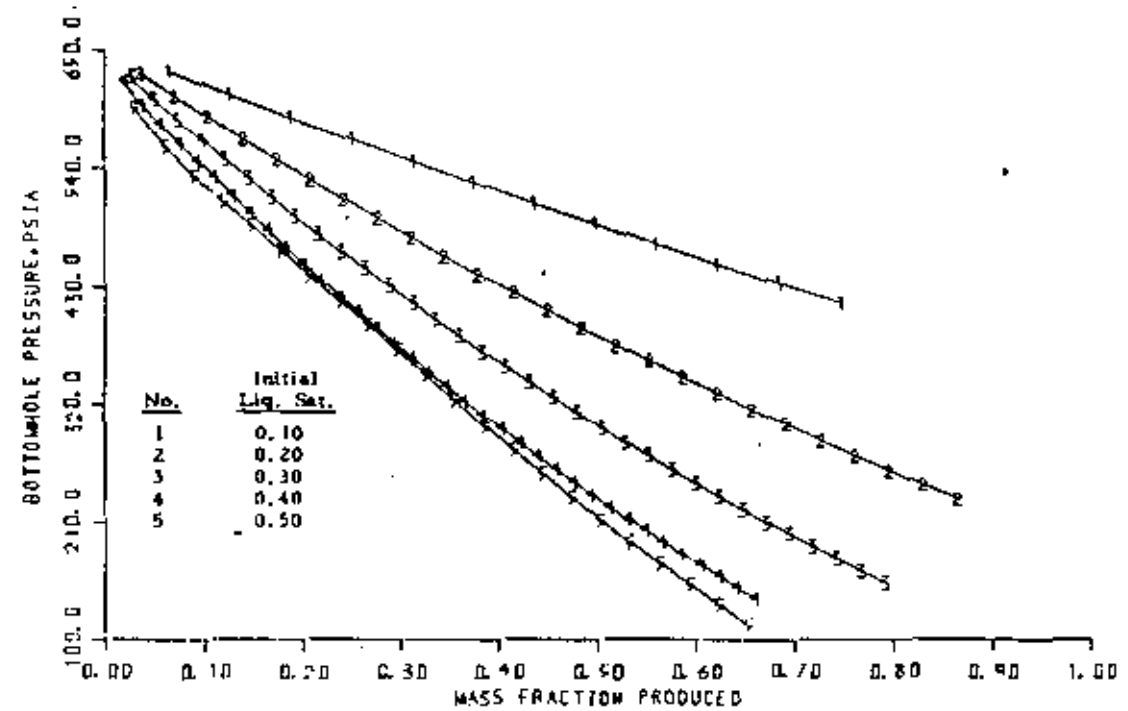


Fig. 5 - Bottomhole pressure vs mass fraction produced for a cross-sectional formulation of a reservoir having permeability = 1.0 darcies, porosity = 0.35, and initial pressure = 650 psia.

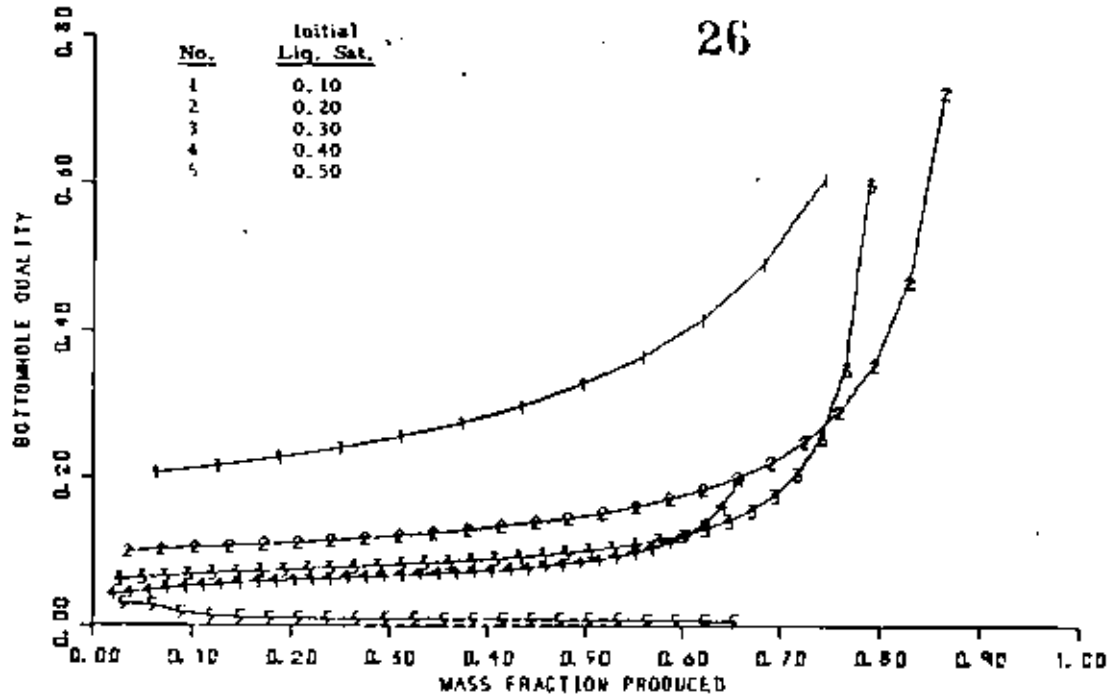


Fig. 5A - Bottomhole quality vs mass fraction produced for a cross-sectional formulation of a reservoir having permeability = 1.0 darcies, porosity = 0.35, and initial pressure = 650 psia.

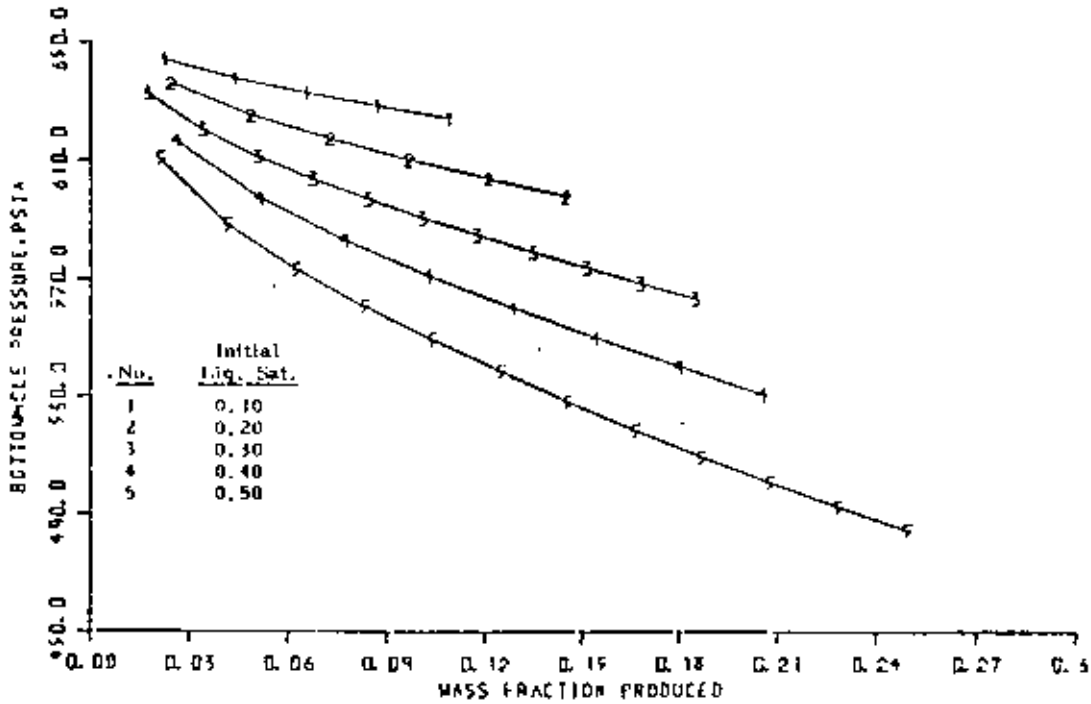


Fig. 6 - Bottomhole pressure vs mass fraction produced for a cross-sectional formulation of a reservoir having permeability = 0.10 darcies, porosity = 0.05, and initial pressure = 650 psia.

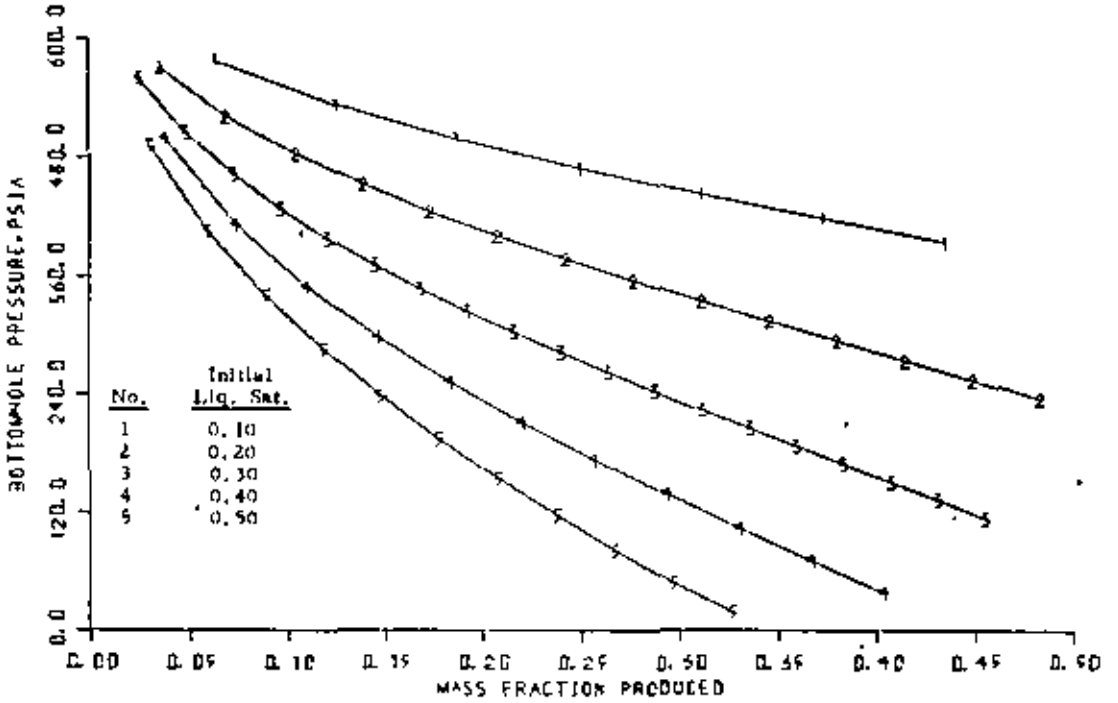


Fig. 7 - Bottomhole pressure vs mass fraction produced for a cross-sectional formulation of a reservoir having permeability = 0.10 darcies, porosity = 0.25, and initial pressure = 600 psia.

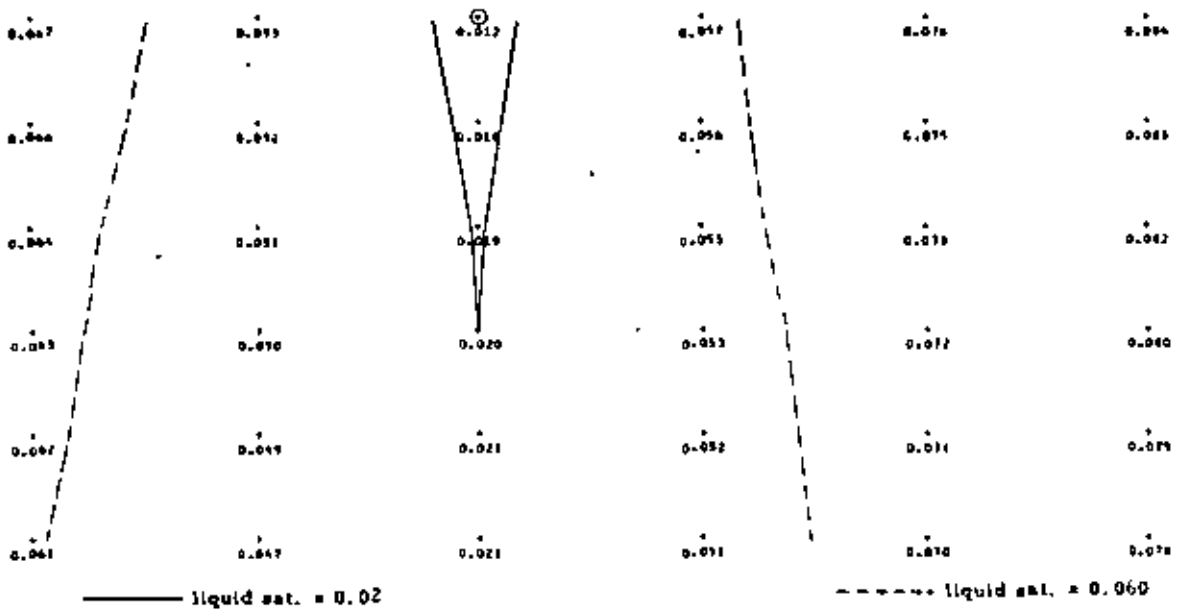


Fig. 8 - Liquid phase saturation distribution where mass fraction produced = 0.37 for a cross-sectional formulation of a reservoir having permeability = 0.10 darcies, porosity = 0.25, initial pressure = 600 psia, and initial liquid phase saturation = 0.10.

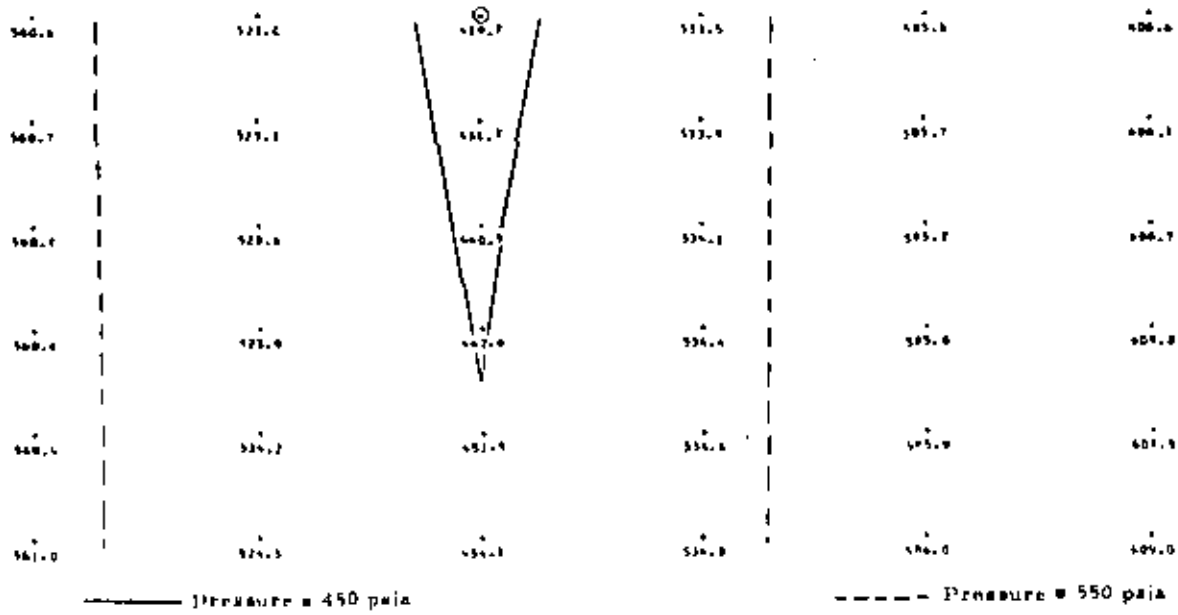


Fig. 8A - Pressure distribution where mass fraction produced = 0.37 for a cross-sectional formulation of a reservoir having permeability = 0.10 darcies, porosity = 0.35, initial pressure = 650 psia, and initial liquid phase saturation = 0.10.

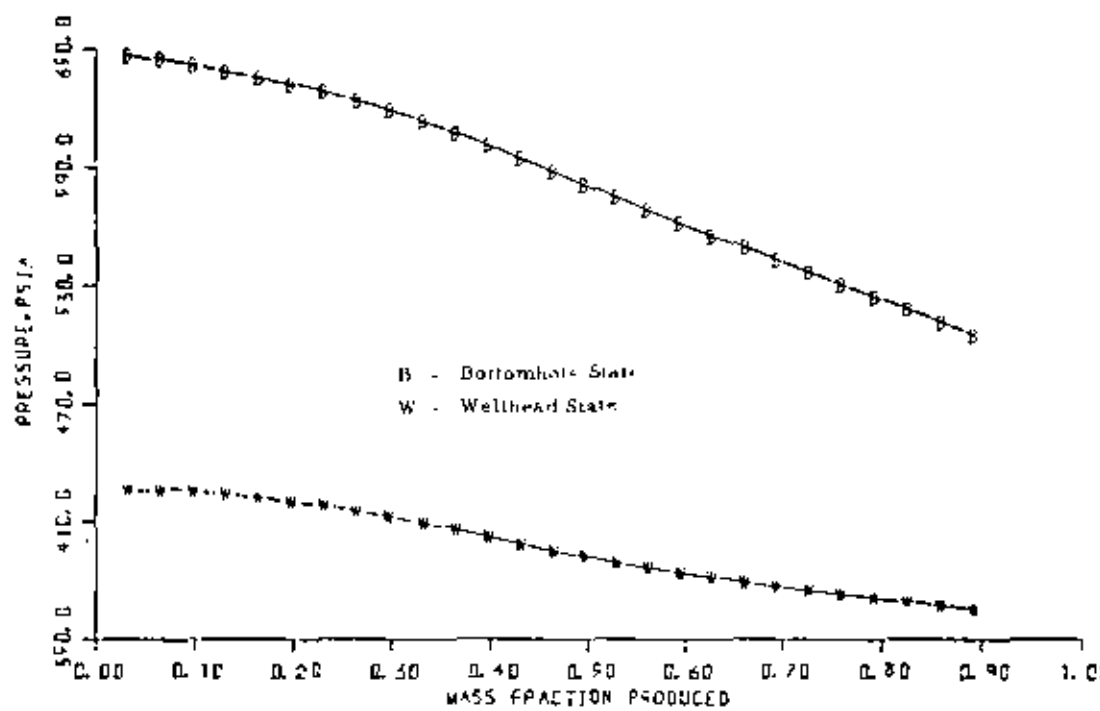


Fig. 9 - Pressure vs mass fraction produced for an areal formulation of a reservoir having permeability = 1.0 darcies, porosity = 0.05, initial pressure = 650 psia, and initial liquid phase saturation = 0.90.

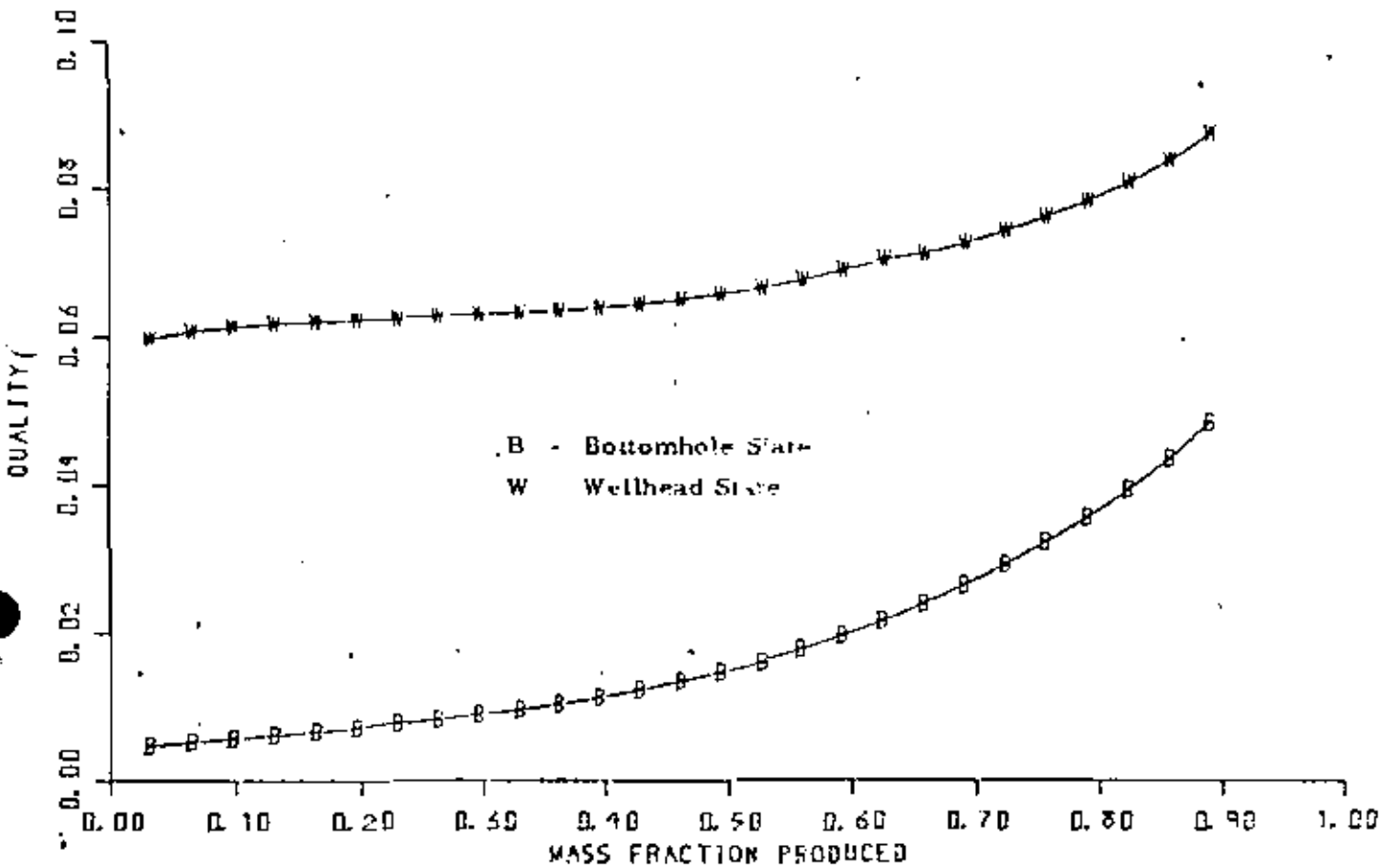


Fig. 9A - Quality vs mass fraction produced for an areal formulation of a reservoir having permeability = 1.0 darcies, porosity = 0.05, initial pressure = 650 psia, and initial liquid phase saturation = 0.80.

30 DR. HEBER CINCO LEY H. Cinco

SPE

Society of Petroleum Engineers of AIME

SPE 7479

# PRESSURE TRANSIENT ANALYSIS FOR TWO-PHASE (LIQUID WATER/STEAM) GEOTHERMAL RESERVOIRS

by S. K. Garg, Systems, Science and Software



This paper was presented at the 53rd Annual Fall Technical Conference and Exhibition of the Society of Petroleum Engineers of AIME, held in Houston, Texas, Oct. 1-3, 1978. The material is subject to correction by the author. Permission to copy is restricted to an abstract of not more than 300 words. Write 6200 N. Central Expy., Dallas, Texas 75206.

## ABSTRACT

A new diffusivity equation for two-phase (liquid water/steam) flow in geothermal reservoirs is derived. The geothermal reservoir may either be initially two-phase or may evolve into a two-phase system during production. Solutions of the diffusivity equation for a continuous line source are presented; the solutions imply that the plot of bottomhole pressure versus log10t (t = time) should be a straight line. The slope of the straight line is inversely proportional to the total kinematic mobility (defined in the text). Comparison of the theory with a limited number of computer simulated drawdown histories shows excellent agreement.

## INTRODUCTION

In petroleum engineering and groundwater hydrology, well tests are routinely conducted to diagnose the well's condition and to estimate formation properties. Analysis of well test data may be made to yield quantitative information regarding (1) formation permeability, storativity and porosity, (2) the presence of barriers and leaky boundaries, (3) the condition of the well (i.e., damaged or stimulated), (4) the presence of major fractures close to the well, and (5) the mean formation pressure. Well testing procedures (and the quality of information obtained) depend on the age of the well. During temporary completion, testing involves producing the reservoir using a temporary plumbing system (e.g., Drill Stem Testing); and the estimates obtained for the formation parameters are not very accurate. After completion, testing is usually performed in the hydraulic mode. In hydraulic testing, one or more wells are produced at controlled rates and changes in pressure within the producing well itself or nearby observation wells (interference tests) are monitored.

A major concern of well testing is the interpretation of pressure transient data. Much of the existing literature (see Matthews and Russell[1] and Ramey[2] for reviews) deals with isothermal single-phase (water/oil) and isothermal two-phase (oil with gas in solution, free gas) systems. There is, in general, a lack of a methodology for the analysis of nonisothermal reservoir systems, either single or two-phase (liquid water/steam). Geothermal reservoirs commonly involve nonisothermal two-phase (water/steam) flow during well testing. In this paper, we present a theoretical framework for analyzing multiphase pressure transient data in geothermal systems.

References and illustrations at end of paper.

## TWO-PHASE (LIQUID WATER/STEAM) FLOW IN GEOTHERMAL SYSTEMS

We consider a fully penetrating well located in an infinite reservoir of thickness H. We will neglect any variations in either formation or fluid properties in the vertical direction (this is a common assumption in pressure transient analysis). The geothermal system may either be two-phase prior to production, or may evolve into a two-phase system as a result of fluid production. In the latter case, a boiling front will propagate outwards from the wellbore. The boiling front may be treated as a constant pressure boundary (p=saturation pressure corresponding to the local reservoir temperature).

For the sake of simplicity, let us consider a reservoir which is initially two-phase everywhere. Furthermore, it is convenient to assume that the pressure (and hence temperature) is uniform throughout the system. In radial geometry, the pressure response is governed by the following diffusivity equation (see Appendix for a derivation of equation (1)):

$$\frac{\partial p}{\partial t} - \frac{(k/\nu)_T}{\phi \rho C_T}\left[\frac{1}{r}\frac{\partial p}{\partial r} + \frac{\partial^2 p}{\partial r^2}\right] = 0 \quad \ldots\ldots \quad (1)$$

We are interested in solutions of equation (1) for the case of flow into a centrally located well at a constant mass rate of production M. Mathematically, we have at $r = r_w$

$$r\left.\frac{\partial p}{\partial r}\right|_{r=r_w} = -\frac{M}{2\pi H (k/\nu)_T} \quad \ldots\ldots \quad (2)$$

For the sake of mathematical convenience, the boundary condition at $r=r_w$ is replaced by the "line source"

approximation, i.e.,

$$\lim_{r\to 0} r\frac{\partial p}{\partial r} = -\frac{M}{2\pi H}(k/\nu)_T \quad \ldots\ldots\ldots (3)$$

The "line source" boundary condition yields identical results (from a practical viewpoint) with those obtained with the original condition.[1,3] We also require that initially (t=0) the reservoir is at a uniform pressure $p_i$, and that at $r=\infty$ (for all t) we have

$$\lim_{r\to\infty} p(r,t) = p_i \quad \ldots\ldots\ldots (4)$$

The solution for equation (1) subject to the boundary conditions (3) and (4) can be written as follows[4]

$$p(r,t) = p_i + \frac{M}{4\pi H (k/\nu)_T} Ei\left\{-\frac{r^2 \phi\rho C_T}{4t (k/\nu)_T}\right\} . \quad (5)$$

Equation (5) implies that the pressure at the wellbottom $p_w(t)$ is

$$p_w(t) = p_i + \frac{M}{4\pi H (k/\nu)_T} Ei\left[-\frac{r_w^2 \phi\rho C_T}{4t (k/\nu)_T}\right] . \quad (6)$$

For $[4t (k/\nu)_T/\phi r_w^2 \rho C_T] > 100$, equation (6) yields the approximate solution:[1]

$$p_w(t) = p_i - \frac{1.15 M}{2\pi H (k/\nu)_T}\left\{\log_{10}\left[\frac{t (k/\nu)_T}{\phi r_w^2 \rho C_T}\right] + 0.351\right\} \quad \ldots\ldots\ldots (7)$$

Equation (7) implies that a plot of $p_w$ versus $\log_{10} t$ should be a straight line. Let m be the slope of this straight line; then we have

$$(k/\nu)_T = \frac{1.15 M}{2\pi H m} \quad \ldots\ldots\ldots (8)$$

Substituting from equation (8) into equation (7), we obtain for compressibility $C_T$

$$\frac{1}{C_T} = \frac{\phi r_w^2 \rho}{t(k/\nu)_T} \text{ Antilog}_{10}\left[\frac{p_i - p_w(t)}{m} - 0.351\right] . \quad (9)$$

PROPAGATING FLASH-FRONT

Theoretical considerations for the case when a flash front propagates into an initially single-phase reservoir are much more complex than those outlined above for the purely two-phase case. In this instance, the reservoir is two-phase for $r < R$ ($R = R(t)$ denotes the location of the flash-front) and is single phase for $r > R$. The flow behavior in these two regimes is governed by

$$\frac{\partial p_j}{\partial t} - \left[\frac{(k/\nu)_T}{\phi\rho C_T}\right]_j \frac{1}{r}\frac{\partial}{\partial r}\left[r\frac{\partial p_j}{\partial r}\right] = 0 \quad \ldots\ldots (10)$$

where j=1 and 2 denote the two-phase and single-phase regions, respectively. The definitions for the various quantities in equation (10) for the two-phase region (j=1) have already been given. In the single-phase region (j=2), we have:

$$[(k/\nu)_T]_2 = k\rho_\ell/\mu_\ell$$

$$\rho_2 = \rho_\ell$$

$$(C_T)_2 = ((1-\phi)/\phi)\, C_m + C_f$$

Note that with the above definitions, equation (10) (in the single-phase region) reduces to the usual diffusivity equation for the isothermal flow of a liquid of small and constant compressibility.

We will assume that the reservoir is initially at a uniform pressure $p_i$ and temperature $T_i$. We will, furthermore, require the fluid flow to be isothermal in the single-phase region ($r > R$); in practice, this implies no severe restriction as temperature changes in single-phase flow are usually very small. The boundary conditions at the wellbore and at infinity are:

$$\lim_{r\to 0} r\frac{\partial p_1}{\partial r} = -\frac{M}{2\pi H [(k/\nu)_T]_1} \quad \ldots\ldots (11a)$$

$$\lim_{r\to\infty} p_2(r,t) = p_i \quad \ldots\ldots (11b)$$

In addition to the boundary conditions (11), we need to satisfy continuity conditions on mass flow and pressure at the flash-front ($r=R$). Mathematically, we have at $r=R$:

$$\left[(k/\nu)_T \frac{\partial p}{\partial r}\right]_1 = \left[(k/\nu)_T \frac{\partial p}{\partial r}\right]_2 \quad \ldots\ldots (12a)$$

$$p_1 = p_2 = p_s(T_i) \quad \ldots\ldots (12b)$$

To develop a solution for equations (10) subject to the boundary conditions (11) and (12), we note that these equations are similar to the equations for melting and freezing with cylindrical symmetry presented by Carslaw and Jaeger.[4] The solution for the present case can, therefore, be obtained by following the general approach of Carslaw and Jaeger. We have thus:

$$0 < r < R: \quad p = p_s + \frac{M}{4\pi H [(k/\nu)_T]_1}\left[Ei\left(-\frac{r^2}{4t}\left[\frac{\phi\rho C_T}{(k/\nu)_T}\right]_1\right) + Ei(-\lambda^2)\right] \quad (13a)$$

$$r > R: \quad p = p_i + \frac{p_s - p_i}{Ei\left(-\lambda^2 \left|(k/\nu)_T/\phi\rho C_T\right|_1 / \left|(k/\nu)_T/\phi\rho C_T\right|_2\right)} \times Ei\left(-\frac{r^2}{4t}\left[\frac{\phi\rho C_T}{(k/\nu)_T}\right]_2\right) \quad \ldots\ldots (13b)$$

where

$$R = 2\lambda \left[ \left\{ \frac{(k/\nu)_T}{\phi\rho\, C_T} \right\}_1 t \right]^{1/2} \qquad \ldots\ldots\ldots \quad (13c)$$

and $\lambda$ is the root of

$$[(k/\nu)_T]_2 \frac{p_s - p_i}{Ei\left(-\lambda^2 \left\{(k/\nu)_T/\phi\rho C_T\right\}_1 / \left\{(k/\nu)_T/\phi\rho C_T\right\}_2\right)} \times \exp\left(-\lambda^2 \left\{(k/\nu)_T/\phi\rho C_T\right\}_1 / \left\{(k/\nu)_T/\phi\rho C_T\right\}_2\right) = \frac{M}{4\pi H} \exp(-\lambda^2) \qquad \ldots\ldots\ldots \quad (13d)$$

Equation (13a) yields the following expression for well-bottom pressure $p_w(t)$

$$p_w(t) = p_s + \frac{M}{4\pi H [(k/\nu)_T]_1} \left[ Ei\left( -\frac{r_w^2}{4t} \left[ \frac{\phi\rho\, C_T}{(k/\nu)_T} \right]_1 \right) - Ei(-\lambda^2) \right] \qquad \ldots\ldots\ldots\ldots \quad (14)$$

For $4t\,[(k/\nu)_T]_1/r_w^2[\phi\rho C_T]_1 > 100$, equation (14) can be approximated as follows:

$$p_w(t) = p_s - \frac{M\, Ei(-\lambda^2)}{4\pi H\,[(k/\nu)_T]_1} - \frac{1.15\, M}{2\pi H[(k/\nu)_T]_1} \left\{ \log_{10}\left[ t\, \frac{[(k/\nu)_T]_1}{r_w^2(\phi\rho C_T)_1} \right] + 0.351 \right\} \qquad \ldots\ldots\ldots\ldots\ldots\ldots \quad (15)$$

Equation (15), like equation (7), implies that a plot of $p_w$ versus $\log_{10}t$ should be a straight line and that $[(k/\nu)_T]_1$ is given by equation (8).

## NUMERICAL RESULTS

In order to test the validity of the preceding theory, the Systems, Science and Software ($S^3$) reservoir simulator MUSHRM[5] was exercised in one-dimensional radial configuration to generate a series of drawdown histories. All of the cases described below were simulated using a 50 zone ($\Delta r_1 = \Delta r_2 = \ldots = \Delta r_{11} = 1$m (3.281 feet); $\Delta r_{12} = 1.2\,\Delta r_{11}$, $\Delta r_{13} = 1.2\,\Delta r_{12}$, .... $\Delta r_{50} = 1.2\,\Delta r_{49}$) radial grid.

The reservoir rock is assumed to be a sandstone with the following properties (unless otherwise indicated):

$\rho_R = 2.65\ 10^3$ kg/m$^3$ (165.4 lbm/ft$^3$)

$\phi = 0.2$

$C_m = 0$ MPa$^{-1}$ (0 psi$^{-1}$)

$K_R = 5.25$ W/m.K (3.03 Btu/h.ft$^2$.°F/ft)

$C_R = 1$ kJ/kg.K (0.239 Btu/lbm °F)

$k = 0.1\ \mu m^2$ (≈ 0.1 darcy)

$S_{\ell r} = 0.3$

$S_{gr} = 0.05$.

Relative permeabilities $R_\ell$ and $R_g$ are represented by the Corey equations and the mixture (rock-liquid-vapor) thermal conductivity is approximated by Budiansky's formula.[5] The mass withdrawal rate is assumed to be 0.14 kg/s.m (0.094 lbm/s.ft.).

In the numerical examples discussed here, the effect of mass withdrawal is represented by a volumetric sink term in the well-block (radial extent r = 0 to $r = \Delta r_1$). For purposes of comparison with the analytical results presented earlier, it is necessary to define an equivalent radius $r_w$ at which the calculated well-block pressure is equal to the actual flowing pressure due to a continuous line source/sink.

In the numerical simulation of reservoir behavior, it is often necessary to employ well-blocks (i.e., a grid block containing a well) with dimensions much larger than the wellbore radius. Naturally, the pressure calculated for the well-block will be, in general, different from the actual flowing bottomhole pressure. Van Poolen, et al.[6] stated that the calculated pressure for a well-block should be the average pressure in the portion of the reservoir represented by the block. Assuming steady-state single-phase flow in the well-block (but not in the reservoir as a whole), this implies that the calculated well-block pressure should be equal to the actual flowing pressure at a radius $r_w$,

$$\ln\frac{r_w}{r_0} = \frac{R^2 \ln(R/r_0)}{R^2 - r_0^2} - \frac{1}{2} \qquad \ldots\ldots\ldots \quad (16a)$$

where $r_0$ is the actual well radius and R is the radius of the grid block. For $R \gg r_0$, equation (16a) simplifies to

$$r_w = R \exp(-1/2) \qquad \ldots\ldots\ldots\ldots \quad (16b)$$

$$\approx 0.6065\ R$$

Equations (16a) and (16b), strictly speaking, hold only for a well located in the center of a radial grid block. For rectangular grid blocks (with dimensions $\Delta x$, $\Delta y$), equation (16b) is usually replaced by the following expression

$$\frac{r_w}{\sqrt{\Delta x\ \Delta y}} = \frac{0.6065}{\sqrt{\pi}} \qquad \ldots\ldots\ldots\ldots \quad (17)$$

Assuming $\Delta x = \Delta y$, equation (17) yields

$$\frac{r_w}{\Delta x} = 0.342. \qquad (33)$$

Peaceman[7] examined the grid pressures obtained in the numerical solution of steady incompressible single-phase flow into a single well located in the center of a square grid block ($\Delta x = \Delta y$) and concluded that the well-block pressure should be equal to the actual flowing pressure at a radius of 0.2 $\Delta x$ (and not at the radius given by equation (17)).

In an attempt to evaluate the significance of Peaceman's results for numerical simulation, Garg, et al.[8] analyzed the numerical solution of steady incompressible single-phase flow into a single well located in both radial and rectangular grid blocks. It is found that the equivalent radius depends, among other things, on the shape of the grid block (radial or rectangular) and the type of mesh (uniform or stretch) employed. Thus, for example, use of uniform radial mesh yields $r_w/R \simeq 0.5615$ in the limit $N \to \infty$, where N denotes the number of grid blocks.

Garg, et al.[8] also compared the numerical solution for transient, slightly compressible (water) single-phase flow into a single well with the line-source solution for the diffusivity equation (see, e.g., Matthews and Russell[1]). It was concluded that the equivalent radius (i.e., the radius at which the actual flowing pressure is equal to the calculated well-block pressure) is approximated by 0.56 R. In this work, we will, therefore, assume that $r_w$ in transient single-phase flow (and also approximately in transient two-phase flow) is given by 0.56 R.

Figures 1-5 show five examples for the case when the reservoir initially boiling everywhere, was produced at a constant rate. As can be seen, the drawdown data closely fit a straight line; furthermore, the values of $(k/v)_T$ computed from the slope of the straight line are in excellent agreement with the actual values in the well-blocks (see Tables 1-5 for the actual values). Note that the actual values (Tables 1-5) vary over a range; this variation is the result of slow changes (except at very early times not considered in drawing the straight line) in steam saturation in the computational well-block as a result of continued production. Figure 3 (drawdown history c) and Table 3 present an especially interesting case; in this case the liquid, initially immobile, becomes mobile for $t > \sim 2\ 10^5$s due to condensation in the well-block. The condensation is caused by a drop in pressure (and hence temperature); in drawing the straight line the pressure data for $t > \sim 2\ 10^5$s was ignored. If the computation had been carried for times sufficiently greater than $t > 2\ 10^5$s, one would see another straight line segment (with a different slope).

Table 6 compares the compressibility $C_T$ values inferred from the slope of the straight line and equation (9) with the actual values. The agreement is quite good for Cases b, c and d. In Cases a and e, the inferred values are quite a bit larger than the actual values; this disagreement is not really surprising in view of the extremely large changes in $(k/v)_T$ very early times (see Tables 1 and 5). Large values $(k/v)_T$ at very early times lead to relatively small pressure drops compared to those implied by the straight line. Stated somewhat differently, at early times, equation (7) with constant $(k/v)_T$ cannot be used to calculate the well-block pressure in Cases a and e.

Figures 6 and 7 show two additional drawdown histories generated by MUSHRM. In these examples, the reservoir was initially single-phase (liquid) everywhere. In the case shown in Figure 6, a flash-front starts propagating outward from the wellbore at $t \sim 0$; it takes, however a finite time for conditions to stabilize in the two-phase region. For $t > 5\ 10^3$s the data lie on a straight line; and the kinematic mobility calculated from the slope of this straight line agrees quite well with the actual range of values. Figure 7 presents a more interesting case; in this instance the liquid water does not start flashing at the instant the production starts. Thus, we have a short time of single-phase flow followed by a propagating flash-front. The two-phase part of the drawdown curve has a relatively long flat part; this part of the curve is associated with boiling only in the computational well-block. Since the flow behavior in the two-phase region is primarily governed by the location of the flash-front, it follows that a failure to adequately resolve the location of the flash-front in numerical simulations (as it happens when the two-phase flow is restricted to one or two computational zones) would lead to physically meaningless results. In other words, the flat part of the curve in Figure 7 is a purely numerical phenomenon and has no physical significance. A straight line is again seen to fit the late-time data; once again the computed value of $(k/v)_T$ is in good agreement with the actual range of values. We have also examined the numerical solutions (Figures 6 and 7) for flash-front velocities; the flash-front position, as a function of time is given by (within numerical precision) $R(t) = A\ t^{1/2}$ where A is constant. The latter observation is in agreement with equation (13c).

## CONCLUDING REMARKS

The analytical solutions for two-phase flow discussed in the preceding sections provide a potentially powerful tool for the analysis of pressure transient data from multiphase geothermal systems. Determination of the total kinematic mobility only requires the measurement of mass flow rate M and the bottomhole pressures $p_w$. The mass flow rate M can be measured at the well-head provided there is no loss of the produced fluid to the non-producing formations as the fluid travels through the wellbore to the well-head. Practical techniques exist for measuring the needed variables. It should be noted that the present analysis does not require separate measurements for liquid and vapor phase mass flow rates. Such data, if available, may be combined with the analysis of the preceding sections to yield additional information regarding relative permeabilities, etc.

## NOMENCLATURE

$C_f$ = isothermal liquid compressibility

$C_m$ = formation compressibility

$C_R$ = heat capacity of the rock matrix

$C_T$ = total compressibility, equation (A.12b)

$h$ = enthalpy of liquid/vapor mixture

$= (1-Q)\ h_\ell + Q\ h_g$

$h_\ell (h_g)$ = liquid (vapor) enthalpy

$h_{g\ell}$ = heat of vaporization $= h_g - h_\ell$

$h_R$ = enthalpy of rock matrix

H = formation thickness

k = absolute permeability

$K_R$ = thermal conductivity of the rock grain

m = slope of $p_w$ versus $\log_{10} t$ straight line

M = mass production rate

p = pressure

$p_i$ = initial reservoir pressure

$p_s(T_i)$ = saturation pressure at $T = T_i$

$p_w$ = well-bottom pressure

Q = steam quality = $S\,\rho_g/\rho$

r = radius

$r_w$ = wellbore radius

R(t) = instantaneous position of the flash-front

$R_\ell(R_g)$ = relative liquid (vapor) permeability

S = vapor volume fraction

$S_{\ell r}(S_{gr})$ = residual liquid (vapor) saturation

t = time

$(k/\nu)_g$ = kinematic mobility for the vapor = $k\,R_g\rho_g/\mu_g$

$(k/\nu)_\ell$ = kinematic mobility for the liquid = $k\,R_\ell\rho_\ell/\mu_\ell$

$(k/\nu)_T$ = total kinematic mobility = $(k/\nu)_\ell + (k/\nu)_g$

$\mu_\ell(\mu_g)$ = liquid (vapor) dynamic viscosity

$\rho$ = mixture (liquid and vapor) density = $(1-S)\,\rho_\ell + S\rho_g$

$\rho_\ell(\rho_g)$ = liquid (vapor) density

$\rho_R$ = rock grain density

$\phi$ = porosity

ACKNOWLEDGMENTS

This work was performed under Systems, Science and Software IR&D research project No. 93102-06. I would like to thank my colleagues Dr. T. R. Blake, Mr. J. W. Pritchett, Dr. M. H. Rice and Dr. T. D. Riney for many helpful discussions.

REFERENCES

1. Matthews, C. S. and Russell, D. G.: Pressure Buildup and Flow Tests in Wells, Society of Petroleum Engineers of AIME, Monograph No. 1, Dallas, Texas (1967).

2. Ramey, H. J., Jr.: "Pressure Transient Analysis for Geothermal Wells", Proceedings Second United Nations Symposium on the Development and Use of Geothermal Resources, San Francisco, California Volume 3 (May 1975), 1749-1757.

3. Mueller, T. D. and Witherspoon, P. A.: "Pressure Interference Effects within Reservoirs and Aquifers", Journal of Petroleum Technology (April 1965), 471-474.

4. Carslaw, H. S. and Jaeger, J. C.: Conduction of Heat in Solids, Oxford University Press, London, 2nd Edition (1959), 294-296.

5. Garg, S. K., Pritchett, J. W., Rice, M. H. and Riney, T. D.: "U.S. Gulf Coast Geopressured Geothermal Reservoir Simulation", Systems, Science and Software, La Jolla, California, Report SSS-R-77-3147 (1977).

6. Van Poolen, H. K., Breitenbach, E. A. and Thurnau, D. H.: "Treatment of Individual Wells and Grids in Reservoir Modeling", Journal of Petroleum Technology (December 1968), 341-346.

7. Peaceman, D. W.: "Interpretation of Well-Block Pressures in Numerical Reservoir Simulation", paper SPE 6893 presented at Society of Petroleum Engineers 52nd Annual Fall Meeting, Denver, Colorado, October 9-12, 1977.

8. Garg, S. K., Pritchett, J. W., Brownell, D. H., Jr. and Riney, T. D.: "U.S. Gulf Coast Geopressured Geothermal Reservoir Simulation - Year 2", Systems Science and Software, La Jolla, California, Report SSS-R-78-3639 (1978).

9. Donaldson, I. G.: "The Flow of Steam Water Mixtures through Permeable Beds: A Simple Simulation of a Natural Undisturbed Hydrothermal Region", New Zealand Journal of Science, Volume 11 (1968), 3-23.

10. Mercer, J. W., Jr., Faust, C. and Pinder, G. F.: "Geothermal Reservoir Simulation", Proceedings NSF/RANN Conference on Research for the Development of Geothermal Energy Resources, Jet Propulsion Laboratory/California Institute of Technology, Pasadena, California (1974), 256-267.

11. Brownell, D. H., Jr., Garg, S. K. and Pritchett, J. W.: "Governing Equations for Geothermal Reservoirs", Water Resources Research, Volume 13 (1977), 929-934.

12. Garg, S. K. and Pritchett, J. W.: "On Pressure-Work, Viscous Dissipation and the Energy Balance Relation for Geothermal Reservoirs", Advances in Water Resources, Volume 1 (1977), 41-47.

13. Moench, A. F. and Atkinson, P. G.: "Transient Pressure Analysis in Geothermal Steam Reservoirs with an Immobile Vaporizing Liquid Phase - Summary Report", Proceedings Third Stanford Workshop on Geothermal Reservoir Engineering, Stanford, California (1977), 64-69.

## APPENDIX: DERIVATION OF DIFFUSIVITY EQUATION FOR TWO-PHASE (LIQUID WATER/STEAM) FLOW IN POROUS MEDIA

The balance equations for two-phase flow in porous media have previously been discussed by Donaldson,[9] Mercer, et al.,[10] Brownell, et al.[11] and Garg and Pritchett.[12] For the present application, the most general form of the balance laws will not be required. In particular, we will assume that (1) the rock porosity depends only upon the fluid pressure, (2) the rock matrix, the liquid and the vapor are in local thermal equilibrium and that heat conduction is negligible, (3) the liquid and the vapor are in local pressure equilibrium such that the capillary pressure is negligible, and (4) the fluid flow is governed by Darcy's law. The second assumption implies that we need consider only the mixture (rock, liquid, vapor) energy balance.

With these assumptions, the balance equations for mass and energy in radial geometry can be written as follows[12]

Mass (Liquid and Vapor)

$$\frac{\partial}{\partial t}(\phi\rho) - \frac{1}{r}\frac{\partial}{\partial r}\, r\left|(k/\nu)_T \frac{\partial p}{\partial r}\right| = 0 \quad \ldots \quad (A.1)$$

Energy (Rock, Liquid and Vapor)

$$\frac{\partial}{\partial t}\left[(1-\phi)\rho_R h_R + \phi\rho h - \phi p\right] - \frac{1}{r}\frac{\partial}{\partial r}\left|r[(k/\nu)_\ell h_\ell + (k/\nu)_g h_g]\frac{\partial p}{\partial r}\right| = 0 \quad \ldots \quad (A.2)$$

The first term in equation (A.1) can be expanded and rewritten in the following form:

$$\frac{\partial}{\partial t}(\phi\rho) = \rho\frac{\partial\phi}{\partial t} + \phi\left|\left(\frac{\partial\rho}{\partial p}\right)_h \frac{\partial p}{\partial t} + \left(\frac{\partial\rho}{\partial h}\right)_p \frac{\partial h}{\partial t}\right|$$

On noting that[5]

$$\frac{\partial\phi}{\partial t} = (1-\phi)\, C_m \frac{\partial p}{\partial t} \quad \ldots \quad (A.3)$$

we obtain

$$\frac{\partial(\phi\rho)}{\partial t} = \phi\rho\left\{\left(\frac{1-\phi}{\phi}\right) C_m \frac{\partial p}{\partial t} + \frac{1}{\rho}\left(\frac{\partial\rho}{\partial p}\right)_h \frac{\partial p}{\partial t} + \frac{1}{\rho}\left(\frac{\partial\rho}{\partial h}\right)_p \frac{\partial h}{\partial t}\right\} \quad \ldots \quad (A.4)$$

We will now proceed to express $\partial h/\partial t$ in terms of $\partial h/\partial r$, $\partial p/\partial t$ and $\partial p/\partial r$.

For geothermal applications, it will suffice to assume that

$$h_R = c_R T \quad \ldots \quad (A.5a)$$

where T is the common local temperature of the rock matrix and the pore fluids. Under the steam dome (i.e., two-phase regime), temperature T is a unique function of fluid pressure p.

$$T = T(p) \quad \ldots \quad (A.5b)$$

Combining equations (A.5a) and (A.5b) and differentiating w.r.t. t, we have

$$\frac{\partial h_R}{\partial t} = c_R \frac{dT}{dp}\frac{\partial p}{\partial t} \quad \ldots \quad (A.6)$$

Substituting for $\partial/\partial t\,(\phi\rho)$ from equation (A.1), for $\partial\phi/\partial t$ from equation (A.3), and for $\partial h_R/\partial t$ from equation (A.6) into equation (A.2), we obtain:

$$\left|-(1-\phi)\, C_m\rho_R h_R + (1-\phi)\,\rho_R c_R \frac{dT}{dp} - \phi - (1-\phi)\, C_m p\right| \times \frac{\partial p}{\partial t} + \phi\rho\frac{\partial h}{\partial t} = \left|(k/\nu)_\ell h_\ell + (k/\nu)_g h_g - (k/\nu)_T h\right| \frac{1}{r}\frac{\partial}{\partial r}\left(r\frac{\partial p}{\partial r}\right) + \frac{\partial p}{\partial r}\left|\frac{\partial}{\partial r}[(k/\nu)_\ell h_\ell + (k/\nu)_g h_g - (k/\nu)_T h] + (k/\nu)_T\frac{\partial h}{\partial r}\right| \quad \ldots \quad (A.7)$$

We next note that in practical geothermal applications, the last two terms in the brackets on the left hand side of equation (A.7) ($\phi$ and $(1-\phi)\, C_m p$) are liable to be negligible compared to the first two terms. Also, we have

$$h_\ell - h = -Q h_{g\ell}$$
$$h_g - h = (1-Q) h_{g\ell} \quad \ldots \quad (A.8)$$

Substitution of equation (A.8) in equation (A.7) yields:

$$\phi\rho\frac{\partial h}{\partial t} = (1-\phi)\rho_R h_R\left|C_m - \frac{1}{T}\frac{dT}{dp}\right|\frac{\partial p}{\partial t} + h_{g\ell}\,(k/\nu)_T\left[\frac{(k/\nu)_g}{(k/\nu)_T} - Q\right]\frac{1}{r}\frac{\partial}{\partial r}\left(r\frac{\partial p}{\partial r}\right) + \frac{\partial p}{\partial r}\left\{\frac{\partial}{\partial r}\left[h_{g\ell}\,(k/\nu)_T\left(\frac{(k/\nu)_g}{(k/\nu)_T} - Q\right)\right] + (k/\nu)_T\frac{\partial h}{\partial r}\right\} \quad \ldots \quad (A.9)$$

Combining equations (A.1), (A.4) and (A.9) we obtain:

$$\phi\rho\left[\left(\frac{1-\phi}{\phi}\right) C_m + \frac{1}{\rho}\left(\frac{\partial\rho}{\partial p}\right)_h + \frac{1}{\rho^2}\left(\frac{\partial\rho}{\partial h}\right)_p \left(\frac{1-\phi}{\phi}\right) \rho_R h_R \right] C_m$$

$$- \frac{1}{T}\frac{dT}{dp}\Big]\Big\{\frac{\partial p}{\partial t} - (k/\nu)_T \Big[1$$

$$- \frac{1}{\rho}\left(\frac{\partial\rho}{\partial h}\right)_p h_{g\ell}\left[\frac{(k/\nu)_g}{(k/\nu)_T} - Q\right]\Big] \frac{1}{r}\frac{\partial}{\partial r}\left(r\frac{\partial p}{\partial r}\right)$$

$$+ \frac{\partial p}{\partial r}\Big\{-\frac{\partial}{\partial r}(k/\nu)_T + \frac{1}{\rho}\left(\frac{\partial\rho}{\partial h}\right)_p (k/\nu)_T \frac{\partial h}{\partial r}$$

$$+ \frac{1}{\rho}\left(\frac{\partial\rho}{\partial h}\right)_p \frac{\partial}{\partial r}\Big[h_{g\ell}(k/\nu)_T\left(\frac{(k/\nu)_g}{(k/\nu)_T}\right.$$

$$\left. - Q\right)\Big]\Big\} = 0 \quad \ldots\ldots\ldots \quad (A.10)$$

An examination of the numerical solution for equations (A.1) and (A.2) with a constant rate of mass production (e.g., Cases 1-5 discussed elsewhere in this paper) reveals the following important points:

1. The total kinematic mobility $(k/\nu)_T$ increases with increasing distance r from the wellbore.

2. In the vicinity of the wellbore, we have

$$\left|(k/\nu)_T\left[1 - \frac{1}{\rho}\left(\frac{\partial\rho}{\partial h}\right)_p h_{g\ell}\left[\frac{(k/\nu)_g}{(k/\nu)_T} - Q\right]\right]\frac{1}{r}\frac{\partial}{\partial r}\left(r\frac{\partial p}{\partial r}\right)\right|$$

$$>> \left|\frac{\partial p}{\partial r}\Big\{-\frac{\partial}{\partial r}(k/\nu)_T + \frac{1}{\rho}\left(\frac{\partial\rho}{\partial h}\right)_p (k/\nu)_T \frac{\partial h}{\partial r}\right.$$

$$+ \frac{1}{\rho}\left(\frac{\partial\rho}{\partial h}\right)_p \frac{\partial}{\partial r}\Big[h_{g\ell}(k/\nu)_T\left(\frac{(k/\nu)_g}{(k/\nu)_T}\right.$$

$$\left.\left. - Q\right)\Big]\Big\}\right| \quad \ldots\ldots\ldots \quad (A.11)$$

This strong inequality does not, however, hold for radial distances greater than a few borehole radii.

3. Both the radial terms in equations (A.10) are maximum (in an absolute sense) near the wellbore, and fall off rapidly with increasing radial distance r.

4. The radial terms in equation (A.10) are of opposite signs.

We now replace equation (A.10) by the following diffusivity equation:

$$\phi\rho\, C_T \frac{\partial p}{\partial t} - (k/\nu)_T \frac{1}{r}\frac{\partial}{\partial r}\left(r\frac{\partial p}{\partial r}\right) = 0 \quad \ldots \quad (A.12a)$$

where

$$C_T = \Big[\left(\frac{(1-\phi)}{\phi} C_m + \frac{1}{\rho}\left(\frac{\partial\rho}{\partial p}\right)_h + \frac{(1-\phi)}{\phi}\frac{1}{\rho^2}\left(\frac{\partial\rho}{\partial h}\right)_p \rho_R h_R\right] C_m$$

$$- \frac{1}{T}\frac{dT}{dp}\Big]\Big\{/\Big\{1 - \frac{1}{\rho}\left(\frac{\partial\rho}{\partial h}\right)_p h_{g\ell}[(k/\nu)_g/(k/\nu)_T$$

$$- Q]\Big\} \quad (A.12b)$$

Note that $(k/\nu)_T$ in equation (A.12a) represents the value of the total kinematic mobility in the vicinity of the borehole. The approximations involved in deriving equation (A.12a) (i.e., (1) neglecting the second radial term in equation (A.10) and (2) replacing $(k/\nu)_T$ by its value near the wellbore) are strictly speaking valid only in the immediate neighborhood of the borehole. Even though equation (A.12a) is not expected to apply at large radii, its use should not cause large errors in the computed response since pressures change only very slowly at large radial distances from the borehole.

The diffusivity equation (A.12a) forms the basis for our analysis of two-phase flow in geothermal systems. Unlike in single-phase isothermal flow, the total compressibility $C_T$ in two-phase flow (c.f., equation (A.12b)) has no simple interpretation; consequently its determination from well-tests, in the absence of data regarding rock thermomechanical properties and detailed knowledge regarding the thermodynamic state of the produced fluid, may have only limited practical utility.

We shall now briefly consider a geothermal steam reservoir with an immobile vaporizing liquid phase in the pores. In this case, we have

$$(k/\nu)_\ell = 0, \quad (k/\nu)_T = (k/\nu)_g = k_g\rho_g/\mu_g \quad . \quad (A.13)$$

where $k_g = kR_g$. Substituting from equation (A.13) into equation (A.12) and rearranging terms, we obtain:

$$\frac{\partial p}{\partial t} - \frac{k_g}{\phi\,\mu_g\, C_T'}\frac{1}{r}\frac{\partial}{\partial r}\left(r\frac{\partial p}{\partial r}\right) = 0 \quad \ldots\ldots \quad (A.14)$$

where

$$C_T' = \frac{\rho\, C_T}{\rho_g} \quad \ldots\ldots\ldots\ldots \quad (A.15a)$$

$$C_T = \Big[\left(\frac{(1-\phi)}{\phi} C_m + \frac{1}{\rho}\left(\frac{\partial\rho}{\partial p}\right)_h + \frac{(1-\phi)}{\phi}\frac{1}{\rho^2}\left(\frac{\partial\rho}{\partial h}\right)_p \rho_R h_R\right] C_m$$

$$- \frac{1}{T}\frac{dT}{dp}\Big]\Big\{/\Big\{1 - \frac{1}{\rho}\left(\frac{\partial\rho}{\partial h}\right)_p h_{g\ell}\,(1-Q)\Big\} \quad (A.15b)$$

We note that equation (A.14) is identical (albeit with a different definition for the total compressibility) to the diffusivity equation for isothermal single-phase reservoir systems; this fact provides the fundamental justification for the application of classical single-

phase procedures to determine the steam-phase permeability of a geothermal steam reservoir with an immobile vaporizing liquid phase (see, e.g., Moench and Atkinson[13]).

TABLE 1

ACTUAL $(k/\nu)_i$ ($i = \ell, g, T$) AND VAPOR SATURATION (S) VALUES IN THE WELL-BLOCK FOR SIMULATED DRAWDOWN HISTORY (a)

| Time s | | Vapor Saturation (S) | $10^8\ (k/\nu)_\ell$ s | $10^8\ (k/\nu)_g$ s | $10^8\ (k/\nu)_T$ s |
|---|---|---|---|---|---|
| 0 | | 0.050 | 79.85 | 0 | 79.85 |
| 0.576 | $10^4$ | 0.163 | 37.26 | 0.22 | 37.48 |
| 0.1296 | $10^5$ | 0.169 | 35.43 | 0.26 | 35.69 |
| 0.3456 | $10^5$ | 0.175 | 34.00 | 0.29 | 34.29 |
| 0.7056 | $10^5$ | 0.178 | 33.12 | 0.31 | 33.43 |
| 0.14256 | $10^6$ | 0.181 | 32.36 | 0.33 | 32.69 |
| 0.35856 | $10^6$ | 0.185 | 31.52 | 0.36 | 31.88 |
| 0.71856 | $10^6$ | 0.187 | 30.96 | 0.37 | 31.33 |
| 0.100656 | $10^7$ | 0.188 | 30.69 | 0.38 | 31.07 |

TABLE 2

ACTUAL $(k/\nu)_i$ ($i = \ell, g, T$) AND VAPOR SATURATION (S) VALUES IN THE WELL-BLOCK FOR SIMULATED DRAWDOWN HISTORY (b)

| Time s | | Vapor Saturation (S) | $10^8\ (k/\nu)_\ell$ s | $10^8\ (k/\nu)_g$ s | $10^8\ (k/\nu)_T$ s |
|---|---|---|---|---|---|
| 0 | | 0.350 | 6.71 | 3.48 | 10.19 |
| 0.504 | $10^4$ | 0.400 | 3.59 | 4.90 | 8.49 |
| 0.1224 | $10^5$ | 0.402 | 3.49 | 4.90 | 8.39 |
| 0.3384 | $10^5$ | 0.404 | 3.41 | 4.88 | 8.29 |
| 0.6984 | $10^5$ | 0.404 | 3.39 | 4.84 | 8.23 |
| 0.14184 | $10^6$ | 0.405 | 3.37 | 4.79 | 8.16 |
| 0.35784 | $10^6$ | 0.405 | 3.34 | 4.74 | 8.08 |
| 0.71784 | $10^6$ | 0.406 | 3.30 | 4.71 | 8.01 |
| 0.100584 | $10^7$ | 0.406 | 3.29 | 4.69 | 7.98 |

TABLE 3

ACTUAL $(k/\nu)_i$ (i = ℓ, g, T) AND VAPOR SATURATION (S) VALUES IN THE WELL-BLOCK FOR SIMULATED DRAWDOWN HISTORY (c)

| Time s | | Vapor Saturation (S) | $10^8\ (k/\nu)_\ell$ s | $10^8\ (k/\nu)_g$ s | $10^8\ (k/\nu)_T$ s |
|---|---|---|---|---|---|
| 0 | | 0.702 | 0 | 23.02 | 23.02 |
| 0.432 | $10^4$ | 0.731 | 0 | 22.26 | 22.26 |
| 0.1152 | $10^5$ | 0.734 | 0 | 22.13 | 22.13 |
| 0.3312 | $10^5$ | 0.734 | 0 | 21.99 | 21.99 |
| 0.6912 | $10^5$ | 0.729 | 0 | 21.89 | 21.89 |
| 0.14112 | $10^6$ | 0.714 | 0 | 21.80 | 21.80 |
| 0.35712 | $10^6$ | 0.662* | 0* | 19.12* | 19.12* |
| 0.71712 | $10^6$ | 0.624 | 0.02 | 16.58 | 16.60 |
| 0.100512 | $10^7$ | 0.623 | 0.02 | 16.53 | 16.55 |

*Liquid slightly mobile

TABLE 4

ACTUAL $(k/\nu)_i$ (i = ℓ, g, T) AND VAPOR SATURATION (S) VALUES IN THE WELL-BLOCK FOR SIMULATED DRAWDOWN HISTORY (d)

| Time s | | Vapor Saturation (S) | $10^8\ (k/\nu)_\ell$ s | $10^8\ (k/\nu)_g$ s | $10^8\ (k/\nu)_T$ s |
|---|---|---|---|---|---|
| 0 | | 0.160 | 35.38 | 0.10 | 35.48 |
| 0.720 | $10^4$ | 0.298 | 10.84 | 0.96 | 11.80 |
| 0.144 | $10^5$ | 0.301 | 10.47 | 0.97 | 11.44 |
| 0.360 | $10^5$ | 0.305 | 10.02 | 0.99 | 11.01 |
| 0.720 | $10^5$ | 0.308 | 9.68 | 1.01 | 10.69 |
| 0.144 | $10^6$ | 0.309 | 9.58 | 1.00 | 10.58 |
| 0.360 | $10^6$ | 0.312 | 9.27 | 1.00 | 10.27 |
| 0.720 | $10^6$ | 0.314 | 9.00 | 1.01 | 10.01 |
| 0.1008 | $10^7$ | 0.315 | 8.87 | 1.01 | 9.88 |

TABLE 5

ACTUAL $(k/\nu)_i$ (i = l, g, T) AND VAPOR SATURATION (S) VALUES IN THE WELL-BLOCK FOR SIMULATED DRAWDOWN HISTORY (a)

| Time s | | Vapor Saturation (S) | $10^8\ (k/\nu)_g$ s | $10^8\ (k/\nu)_o$ s | $10^8\ (k/\nu)_T$ s |
|---|---|---|---|---|---|
| 0 | | 0.050 | 34.49 | 0 | 34.49 |
| 0.720 | $10^4$ | 0.236 | 19.21 | 0.45 | 19.66 |
| 0.144 | $10^5$ | 0.241 | 18.50 | 0.47 | 18.97 |
| 0.360 | $10^5$ | 0.246 | 17.62 | 0.50 | 18.12 |
| 0.720 | $10^5$ | 0.250 | 16.94 | 0.53 | 17.47 |
| 0.144 | $10^6$ | 0.254 | 16.42 | 0.54 | 16.96 |
| 0.360 | $10^6$ | 0.256 | 16.01 | 0.56 | 16.57 |
| 0.720 | $10^6$ | 0.259 | 15.56 | 0.57 | 16.13 |
| 0.1008 | $10^7$ | 0.261 | 15.35 | 0.58 | 15.93 |

TABLE 6

COMPARISON OF ACTUAL ($C_{fact}$) AND INFERRED ($C_{finf}$) COMPRESSIBILITIES

| Drawdown Case | Time s | | $C_{fact}$ $MPa^{-1}$ $(10^{-2}psi^{-1})$ | $C_{finf}$ $MPa^{-1}$ $(10^{-2}psi^{-1})$ | $C_{finf}/C_{fact}$ |
|---|---|---|---|---|---|
| a | 0.14256 | $10^6$ | 1.80 (1.24) | 6.83 (4.70) | 3.79 |
| b | 0.14184 | $10^6$ | 0.286 (0.197) | 0.305 (0.211) | 1.07 |
| c | 0.6912 | $10^5$ | 0.309 (0.213) | 0.399 (0.275) | 1.29 |
| d | 0.144 | $10^6$ | 1.99 (1.37) | 2.91 (2.00) | 1.46 |
| e | 0.144 | $10^6$ | 3.75 (2.59) | 8.79 (6.06) | 2.34 |

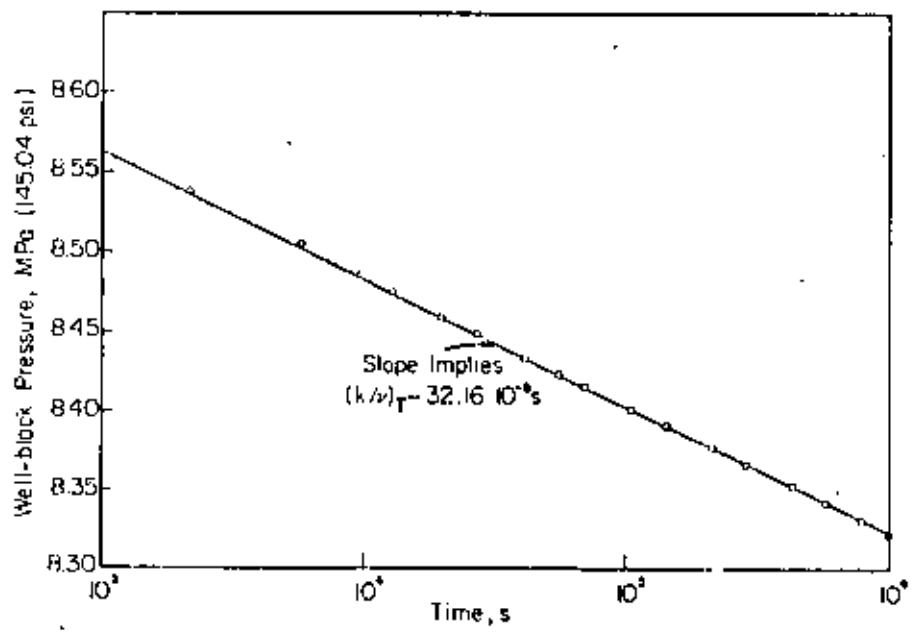


FIG. 1 – SIMULATED DRAWDOWN HISTORY (a). RESERVOIR IS INITIALLY TWO-PHASE EVERYWHERE ($p_i$=8.5991 MPa = 1247.2 psi, S=0.05). SEE TABLE 1 FOR ACTUAL $(k/\nu)_T$ VALUES.

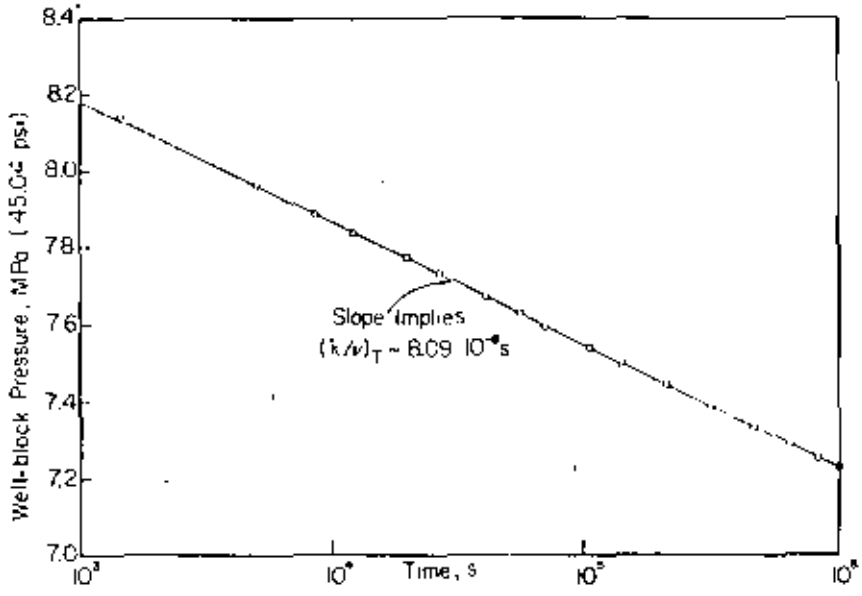


FIG. 2 - SIMULATED DRAWDOWN HISTORY (B). RESERVOIR IS INITIALLY TWO-PHASE EVERYWHERE (P=8.5991 MPA ~ 1247.2 PSI, S=0.55). SEE TABLE 2 FOR ACTUAL $(k/\nu)_T$ VALUES.

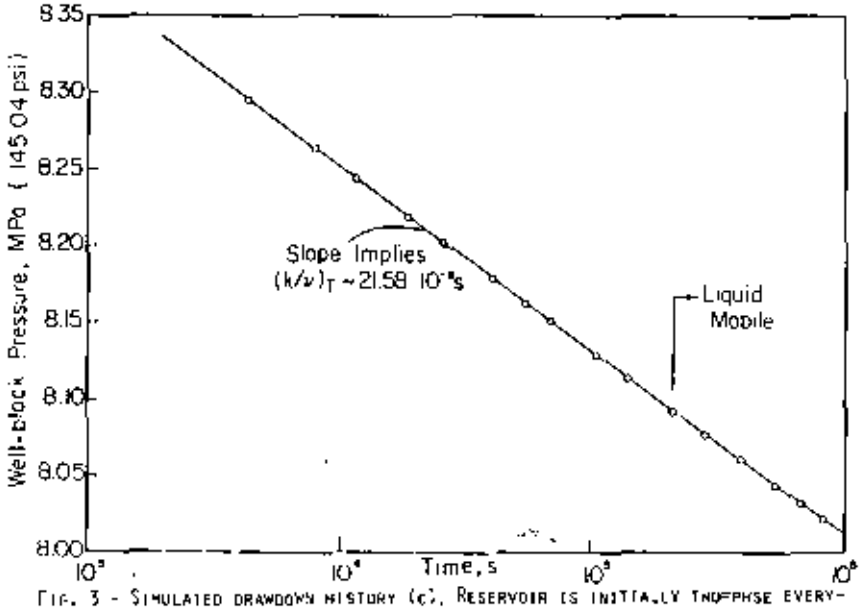


FIG. 3 - SIMULATED DRAWDOWN HISTORY (C). RESERVOIR IS INITIALLY TWO-PHASE EVERYWHERE (P=8.5991 MPA ~ 1247.2 PSI, S=0.7015). SEE TABLE 3 FOR ACTUAL $(k/\nu)_T$ VALUES

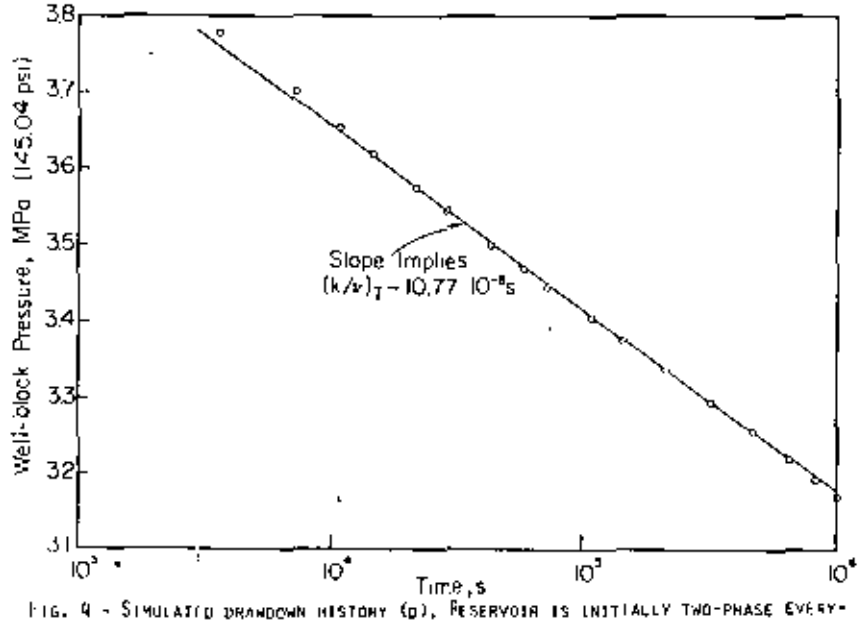


FIG. 4 - SIMULATED DRAWDOWN HISTORY (D). RESERVOIR IS INITIALLY TWO-PHASE EVERYWHERE (P=5.9808 MPA ~ 577.4 PSI, S=0.1604). SEE TABLE 4 FOR ACTUAL $(k/\nu)_T$ VALUES.

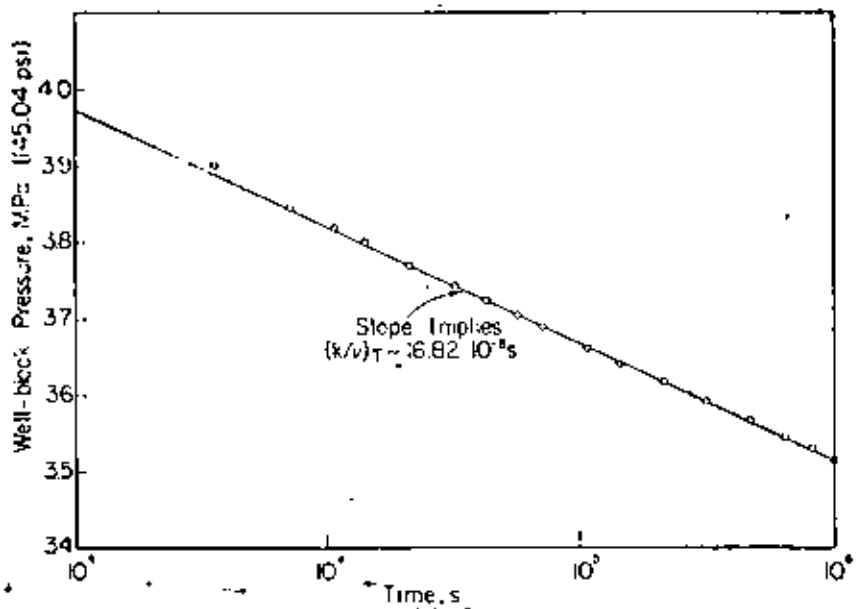


FIG. 5 - SIMULATED DRAWDOWN HISTORY (E). RESERVOIR IS INITIALLY TWO-PHASE EVERYWHERE (P=3.9808 MPa ~ 577.4 PSI, S=0.0.05). SEE TABLE 5 FOR ACTUAL $(k/\nu)_T$ VALUES.

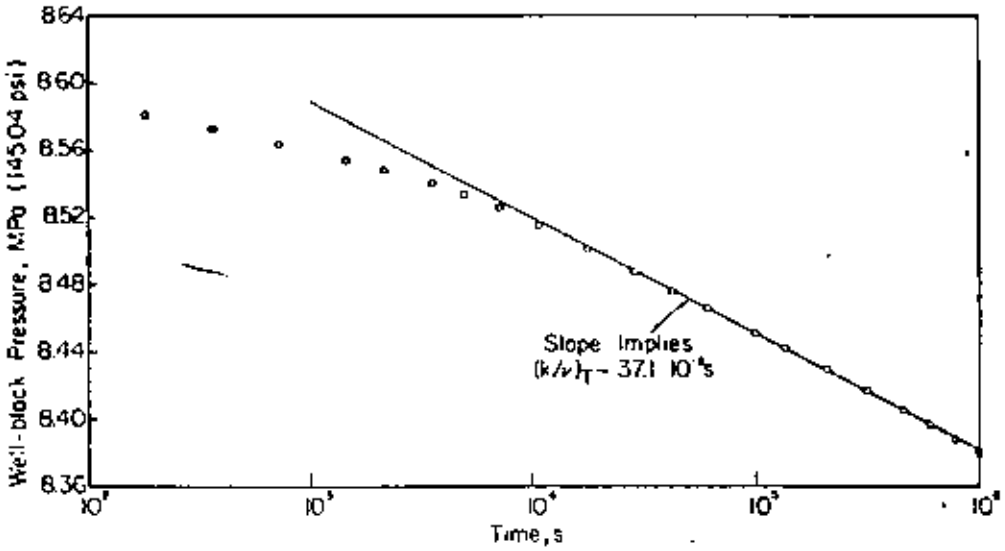


FIG. 6 - SIMULATED DRAWDOWN HISTORY (F). RESERVOIR IS INITIALLY SINGLE-PHASE (LIQUID) EVERYWHERE (P=8.62 MPa ~ 1250.2 PSI, T=573.15K=572°F). ACTUAL RANGE OF $(k/\nu)_T$ VALUES FOR POINTS LYING ON THE STRAIGHT LINE IS $(36.1\text{-}42.3)\ 10^{-8}$s.

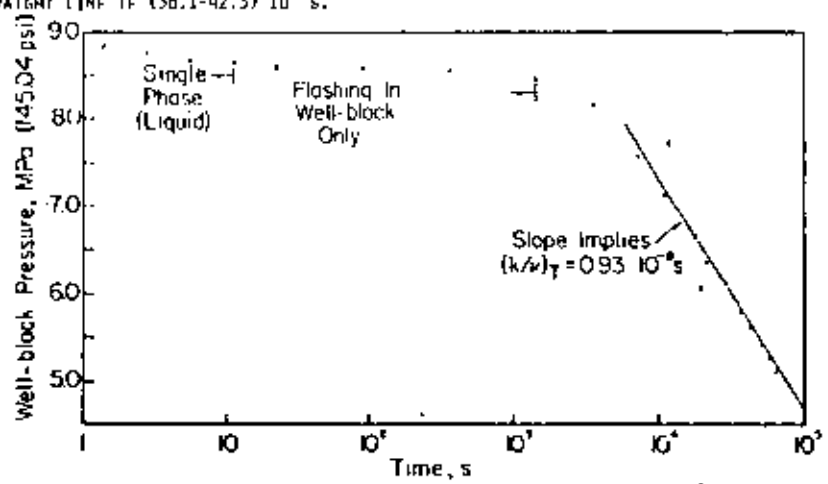


FIG. 7 - SIMULATED DRAWDOWN HISTORY (G). RESERVOIR IS INITIALLY SINGLE-PHASE EVERYWHERE (P=9.000 MPa ~ 1305.3 PSI, T = 573. 15K=572°F). ABSOLUTE PERMEABILITY k FOR THIS CASE IS 0.01 $\mu m^2$ (~ 0.01 DARCY) AND THE ACTUAL RANGE OF $(k/\nu)_T$ VALUES FOR POINTS LYING ON THE STRAIGHT LINE IS $(0.93\text{-}1.15)\ 10^{-8}$s.

# Mathematical Modeling of Geothermal Systems

CHARLES R. FAUST*
JAMES W. MERCER
*U.S. Geological Survey, National Center, Reston, Virginia 22092, USA*

## ABSTRACT

Simulation of geothermal systems yields estimates of recoverable energy, helps determine optimum management techniques, and aids in refining descriptions of reservoir geometry, boundary conditions, and rock properties. To develop an appropriate mathematical model, the continuity equations for mass, momentum, and energy in porous media are reduced to two nonlinear, partial differential equations in which the dependent variables are fluid pressure and enthalpy. These equations include the effects of phase changes and are applicable to both hot-water and vapor-dominated geothermal systems. The equations are solved by a numerical method that combines a Galerkin-finite element approximation in space and finite-difference approximation in time. This method yields results which compare favorably with an analytical solution for the one-dimensional steady vertical flow of hot water in a porous medium. Simulations of more realistic hypothetical problems involving transient, two-phase, two-dimensional (horizontal) flow suggest that this approach is promising for the modeling of natural geothermal systems.

## INTRODUCTION

Most geothermal reservoirs are complex hydrothermal systems controlled by single and multiphase fluid flow, thermodynamics, and the influx of mass and energy. Such systems have many characteristics in common with petroleum reservoirs and ground-water systems. Consequently, some of the engineering methods used in these related fields are applicable to geothermal reservoir engineering.

One of the most promising techniques that has been widely utilized in hydrogeology and petroleum reservoir engineering is mathematical modeling. For the purpose of this discussion we define a geothermal model as: (1) a set of equations which describe the physical processes active in a geothermal reservoir, and (2) the numerical solution of these equations for a given set of reservoir properties, subject to boundary and initial conditions. Since these equations and boundary conditions are generally complicated, the numerical approach is designed for solution on a digital computer.

The application of such geothermal models should play an important role in many aspects of geothermal reservoir engineering. For the preliminary evaluation of potential reservoirs they provide estimates of reserves and future productivity. At the production stage these models are particularly useful for determining the optimal location, spacing, and production rates of wells. As additional performance data become available during operation, the data base of the model can be increased and predictions of future productivity and reserves refined.

The purpose of this paper is to outline the basis of the geothermal model that we have developed and to consider some hypothetical examples in order to demonstrate its applicability to multiphase fluid flow and energy transport in porous media.

## MATHEMATICAL MODEL

The development of our mathematical model for geothermal systems consists of two parts: (1) the formulation of the continuity equations of mass, momentum and energy for each phase, and (2) the reduction of this system of equations to two nonlinear partial differential equations. The derivation of these equations is given by Mercer, Faust, and Pinder (1974); only the final equations and constitutive assumptions are presented in this paper.

The final equations which serve as the basis of our numerical model are posed in terms of the unknown dependent variables, fluid pressure and enthalpy. They are given by:

$$\nabla\cdot\left\{\frac{\bar{k}k_{rl}\rho_l}{\mu_l}\cdot(\nabla p-\rho_l\bar{g})\right\}+\nabla\cdot\left\{\frac{\bar{k}k_{rw}\rho_w}{\mu_w}\cdot(\nabla p-\rho_w\bar{g})\right\}+q_l+q_w=\left\{\rho\frac{d\phi}{dp}+\phi\left(\frac{\partial\rho}{\partial p}\right)_h\right\}\frac{\partial p}{\partial t}+\phi\left(\frac{\partial\rho}{\partial h}\right)_p\frac{\partial h}{\partial t} \quad (1)$$

and

$$\nabla\cdot\left\{\frac{\bar{k}k_{rl}\rho_l h_l}{\mu_l}\cdot(\nabla p-\rho_l\bar{g})\right\}+\nabla\cdot\left\{\frac{\bar{k}k_{rw}\rho_w h_w}{\mu_w}\cdot(\nabla p-\rho_w\bar{g})\right\}+\nabla\cdot\left\{\bar{K}_m\cdot\left[\left(\frac{\partial T}{\partial p}\right)_h\nabla p+\left(\frac{\partial T}{\partial h}\right)_p\nabla h\right]\right\}+q_w h_w=q_l h_l \quad (2)$$

*Also of the Department of Geosciences, Pennsylvania State University, University Park, Pennsylvania 16802, (PhD candidate, Geology)

$$+\left\{\rho_s h_s \frac{\partial b}{\partial p} + \phi h_s \left(\frac{\partial \rho}{\partial p}\right)_h \right. \quad (3)$$

$$\left. - (1-\phi)\rho_r C_r \left(\frac{\partial T}{\partial p}\right)_h \right\} \frac{\partial p}{\partial t} + \left\{\phi h_s \left(\frac{\partial \rho}{\partial h}\right)_p \right.$$

$$\left. + (1-\phi)\rho_r C_r \left(\frac{\partial T}{\partial h}\right)_p + \phi\rho \right\} \frac{\partial h}{\partial t}$$

where,

$\bar{k}$ = local intrinsic permeability tensor, $[L^2]$
$k_s(k_w)$ = relative permeability for steam (water), dimensionless
$\rho_s(\rho_w)$ = average steam (water) density, $[ML^{-3}]$
$\mu_s(\mu_w)$ = dynamic viscosity, $[ML^{-1}t^{-1}]$
$p$ = pressure, $[ML^{-1}t^{-2}]$
$\bar{g}$ = gravitational acceleration, $[Lt^{-2}]$
$q_s(q_w)$ = mass source term, $[ML^{-3}t^{-1}]$
$\phi$ = porosity, dimensionless
$h_s(h_w)$ = enthalpy of saturated steam (water), $[L^2t^{-2}]$
$\bar{K}_m$ = thermal dispersion tensor for the medium, $[ML t^{-3}T^{-1}]$
$T$ = temperature, $[T]$
$\rho_r$ = average rock-grain density, $[ML^{-3}]$
$h_r$ = rock enthalpy, $[L^2t^{-2}]$
$C_r$ = rock specific heat, $[L^2t^{-2}T^{-1}]$.

Average fluid density, $\rho$, is defined by:

$$\rho = S_s\rho_s + S_w\rho_w, \quad (3)$$

where $S$ = saturation, dimensionless, and $S_w + S_s = 1.0$. Finally, the total enthalpy of the mixture, $h$, is defined by:

$$h = \frac{S_s\rho_s h_s + S_w\rho_w h_w}{\rho} \quad (4)$$

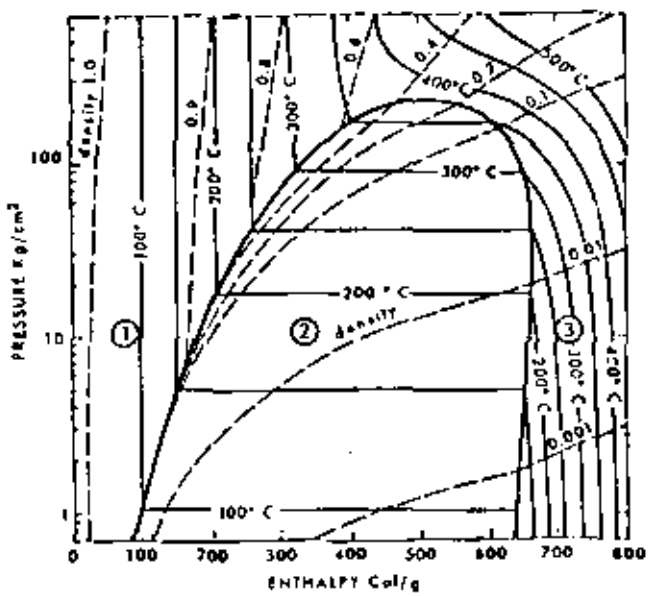


Figure 1. Pressure-enthalpy diagram (equation of state) for pure water and vapor showing three thermodynamic regions below the critical point (apex of parabola): (1) compressed water, (2) two-phase steam-water, and (3) superheated steam (after White, Muffler, and Truesdell, 1971).

The pressure-enthalpy approach is one of several possible approaches. For hot-water geothermal systems (region 1 in Fig. 1), pressure and temperature may be used as unknowns (Mercer, 1973). Toronyi (1974) formulated a two-phase model in terms of fluid pressure and water saturation (this approach is restricted to the saturated vapor-pressure curve, region 2 in Fig. 1). Brownell, Garg, and Pritchett (1975) and T. J. Lasseter (oral commun., 1974) have suggested a method valid in all three regions of Figure 1 which uses fluid density and internal energy as the unknown variables. Fluid pressure and enthalpy have been chosen as unknowns in this study because they define the thermodynamic state of the system (valid in all three regions of Fig. 1), and they are commonly obtained in field situations.

In developing Equations (1) and (2) the following assumptions were made: (1) the reservoir is treated as a porous medium; (2) capillary pressure is negligible—that is, the local pressures in the water and steam phases are equal; and (3) local thermal equilibrium exists among all three phases—rock, steam, and water. As can be seen from Figure 1, consideration of the thermodynamic equation of state for water allows total density, saturated steam density, saturated water density, saturated steam enthalpy, saturated water enthalpy, water saturation, and temperature to be expressed as functions of fluid pressure and enthalpy. For this study, these relationships are expressed as regression equations using data from Meyer et al. (1968). The regression equations were obtained using an enthalpy range of $2.09 \times 10^9$ to $3.175 \times 10^{10}$ ergs/gm, a pressure range of $1.0 \times 10^6$ to $1.75 \times 10^8$ dynes/cm$^2$, and a temperature range of 50 to 350°C. Additional relationships needed to express other parameters in Equations (1) and (2) include (Mercer, Faust, and Pinder, 1974): (1) Porosity as a function of pressure alone; (2) average rock-grain density treated as constant; (3) rock enthalpy considered as a function of temperature; (4) viscosities considered as functions of temperature; (5) relative permeability treated as a function of saturation; and (6) thermal dispersion treated as a property of the medium. (For this paper thermal dispersion and permeability are considered constants.)

Implicit in the above development is the assumption that the geothermal fluid may be treated as a pure aqueous system. For geothermal fields with high salinity this assumption is not valid. Unfortunately, to properly account for transport of chemical species, chemical data such as kinetic reaction rates are required which, in general, are not available. Furthermore, the additional partial differential equations which must be included in such a formulation would produce a model which might be uneconomical to use.

A possible method of avoiding these difficulties for the higher salinity, hot-water systems does exist. For this approach the thermodynamic equation of state for pure water would be modified to account for a mean dissolved-solids concentration of the particular geothermal reservoir. This approximation would account for the thermodynamics of the fluid, but would not account for fluid-solid interactions. Using a mean concentration and the corresponding modified equation of state would require no significant changes in the mathematical model presented in this paper.

## NUMERICAL MODEL

The numerical model used to solve Equations (1) and (2) combines a Galerkin-finite element approximation for

the spatial solution with a finite difference approximation in time. This method is well documented (Zienkiewicz, 1971) and details of this approach applied to equations similar to (1) and (2) are given in Mercer (1970). Only a brief summary of the method is presented here.

The partial differential Equations (1) and (2) are transformed to approximate integral equations using the Galerkin criterion. The integral equations are solved simultaneously using the finite-element method. In this approach the dependent variables, $p$ and $h$, are approximated using piecewise polynomials, and the problem reduces to determining the coefficients of the polynomials.

To apply the finite-element method, the region of interest is divided into subdomains called "finite elements," which are connected at "nodal points." Although the model is designed for higher-order elements, linear elements are employed for the one-dimensional problems discussed in this paper, and linear quadrilateral elements are used for the two-dimensional problem. Linear polynomials are therefore utilized, and enthalpy are determined at the node points.

For transient (time-dependent) problems, it is a common practice to approximate the time derivative by finite-differences techniques. For the examples presented in this paper we use a backward-difference approximation. The solution proceeds through time using the pressure and enthalpy values at the preceding time-step as initial conditions for the current time-step.

The Galerkin-finite element method offers several advantages. Since the shapes of the finite elements can be arbitrary, this approach yields good approximations of external and internal boundaries. For linear problems involving sharp fronts the finite-element method has been shown to yield better solutions (less numerical dispersion) than finite-difference methods (Price, Cavendish and Varga, 1968). It is also possible to represent coefficients of the partial differential equations which vary in space (for example, permeability and density) as piecewise functions over each element (Pinder, Frind, and Papadopulos, 1973). The selection of the Galerkin-finite element approach for our geothermal model was based upon these considerations.

## APPLICATIONS

### One-Dimensional, Steady-State, Vertical Flow

An analytical solution for the steady-state, one-dimensional vertical flow of water and heat in a porous medium is available (Bredehoeft and Papadopulos, 1965; Donaldson, 1968). Since this problem involves compressed water, in the above references the equations are formulated in terms of pressure and temperature. The boundary conditions are: at the top of the system (depth, $z = 0$), temperature is $T_1$ and pressure is $p_1$; at the base ($z = h$), temperature is $T_2$ and a mass flow rate per unit area is specified as $Q$. Assuming constant permeability, $k$, thermal conductivity, $K_m$, and heat capacity of water, $C_w$, the analytical solution for temperature is:

$$T = T_1 + (T_2 - T_1)\left\{\frac{1 - \exp\left(\frac{C_w Qz}{K_m}\right)}{1 - \exp\left(\frac{C_w Qh}{K_m}\right)}\right\} \qquad (5)$$

Other data used in this problem include: a thickness of 3.0 km; $T_1 = 116°C$; $T_2 = 224°C$; $p_1 = 3.0 \times 10^7$ dynes/cm$^2$; $C_w = 3.2 \times 10^7$ ergs/gm·°C; and $K_m = 3.2 \times 10^5$ ergs/cm·sec·°C. The mass flow rate per unit area, $Q$, varies from $3.0 \times 10^{-5}$ to $3.0 \times 10^{-7}$ gm/sec·cm$^2$. Since our model is designed to treat transient problems, an arbitrary set of initial conditions was used and the problem was simulated through time until a steady-state solution was obtained.

Donaldson (1968) defines a fraction, $C_w Q/K_m$, which indicates the relative importance of convection in comparison with conduction. For a given reservoir thickness, this ratio increases as convection becomes more dominant. Figure 2 shows results calculated using the vertical, one-dimensional form of the pressure-enthalpy model compared with the results of the analytical solution for several values of the ratio $C_w Q/K_m$. As may be seen in Figure 2 the comparison is very good, with the maximum error being only 0.4°C.

On the basis of this example, the geothermal model presented in this paper appears to be valid for hot-water geothermal systems (subject to the assumptions used in the model and the example). This example does not verify this approach for the more complicated vapor-dominated systems. To test our model for two-phase flow problems we have compared our results with other available numerical results. A report on this aspect of the study is in preparation. In the remainder of this paper we shall discuss several hypothetical two-phase flow examples, concentrating on the problem of conversion from a hot-water reservoir to a two-phase reservoir.

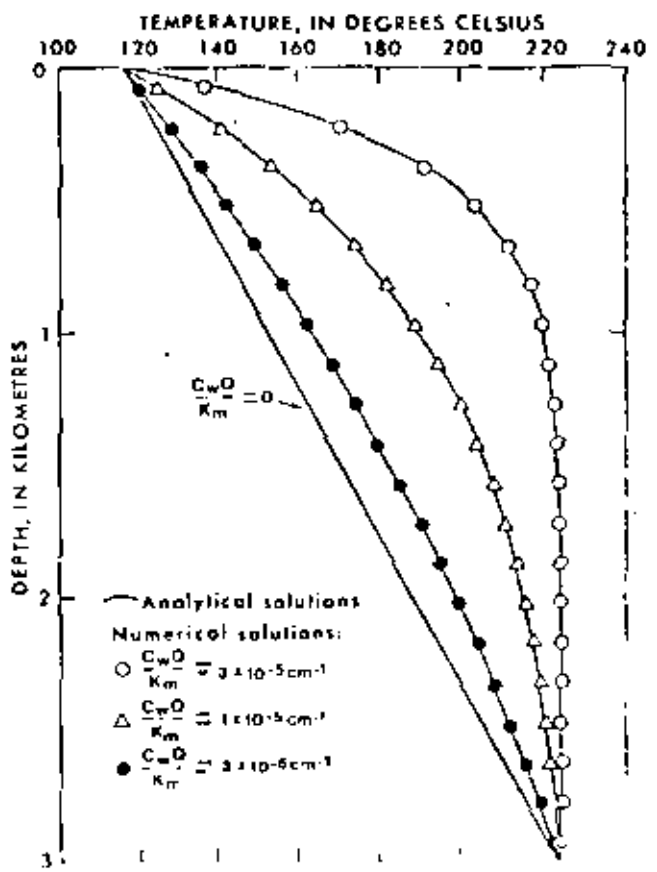


Figure 2. Computed temperature with depth for the one-dimensional, vertical flow of compressed water

## Multiphase Horizontal Flow

Two one-dimensional examples are presented to demonstrate some characteristics of multiphase horizontal flow in geothermal systems. Figure 3 is a geologic section of a hypothetical geothermal reservoir for which the flow system can be approximated by a one-dimensional model. The reservoir is assumed to be closed to the flow of both energy and mass at the boundaries. This assumption is unrealistic in that some mass leakage does occur in most geothermal reservoirs and conductive heat leakage is always present. Although our model is designed to account for these more realistic boundary conditions, for the purpose of the following examples these simple boundary conditions are sufficient. Additionally, to allow one-dimensional treatment, it is assumed that the reservoir is elongate and contains a line of wells centrally located within the reservoir and parallel to the elongation.

In this one-dimensional problem we consider a vertical slice 0.5 km thick and perpendicular to the elongation. Furthermore, on the basis of symmetry about the line of wells, it is only necessary to examine flow in half the vertical slice. This system is represented by 10 elements (each 0.2 km long) with a sink in the first element (on the left).

Equations (1) and (2) are reduced to their one-dimensional form without the gravity terms (since flow is horizontal). The reservoir property data and initial conditions are given in Figure 3. Additional property data for the reservoir are: $K_m = 3.2 \times 10^5$ ergs/cm·sec·°C, $\rho_r = 2.5$ gm/cm$^3$, $C_r = 1.01 \times 10^7$ ergs/gm·°C, and porosity is considered constant. Additionally, water and steam viscosity equations are given by Meyer et al. (1968), modified for cgs system:

$$\mu_w = 10^{-4}\{241.4 \times 10^{[247.8/(T+133.15)]}\} \quad (6)$$

$$\mu_s = 10^{-4}(0.407\,T + 80.4) \quad (7)$$

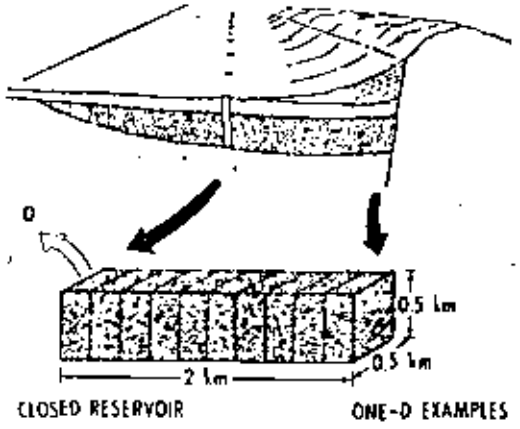


Figure 3. Idealized geological section of a hypothetical geothermal reservoir for one-dimensional, horizontal analysis.

The relative permeabilities for steam and water are essentially unknown, and are assumed to be a variation of those given by Corey (1954) for a drainage displacement process, that is, vaporization dominates condensation:

$$k_{rw} = \frac{(S_w - S_{wr})^4}{(1 - S_{wr})^4} \quad (8)$$

$$k_{rs} = \left[1 - \frac{(S_w - S_{wr})}{(S_{ws} - S_{wr})}\right]^2 \left[1 - \frac{(S_w - S_{wr})^2}{(S_w - 1)^2}\right] \quad (9)$$

where $S_{wr} = 0.05$ and $S_{ws} = 0.95$. Finally, in the two-phase region, the heat sink term is a function of the mobilities of each phase. That is, the amount of heat lost to the well is defined as,

$$q_h = q_s h_s + q_w h_w \quad (10)$$

and total mass lost to the well as,

$$q_m = q_s + q_w. \quad (11)$$

The steam production rate is determined by the fractional flow of the steam phase as follows:

$$q_s = \alpha_s q_m, \quad (12)$$

where

$$\alpha_s = k_{rs} \Big/ \left(k_{rs} + \frac{\mu_s \rho_w}{\mu_w \rho_s} k_{rw}\right)$$

Since $k_{rs}$, $h_w$, and $q_m$ are known, $q_s$ is calculated using (12), $q_w$ is calculated using (11), and $q_h$ is calculated using (10).

**Example 1.** This example was designed to demonstrate the behavior of an initially hot-water geothermal reservoir which develops a two-phase zone under the influence of production. Two graphs are given in Figure 4. In the upper one, pressure values at various times are plotted against distance from the center of the reservoir (left boundary of the model). The specified times represent the duration of exploitation. In this example the pressure drops rapidly in the early stages of production and at the end of one month the first element has become two-phase. When this occurs the pressure continues to drop rapidly in the rest of the reservoir, but changes only slightly in the element containing the sink. This is expected since once an element becomes two-phase the pressure is maintained by the formation of steam. After three years of exploitation the pressures in the entire reservoir have lowered to a point just slightly above the value where it would become two-phase. At this stage mass extraction results in reduced water saturations in elements near the sink, and pressures drop very slowly.

Water saturations for each element at the end of five years of exploitation are shown in the lower graph of Figure 4. It may be seen that a substantial portion of the reservoir is still single-phase (indicated by the shaded area). This may be an artifact resulting from the numerical method. It is also noticed that a slight oscillation in the saturation distribution occurs. The oscillation is not physically significant, but is due to the numerical approximation.

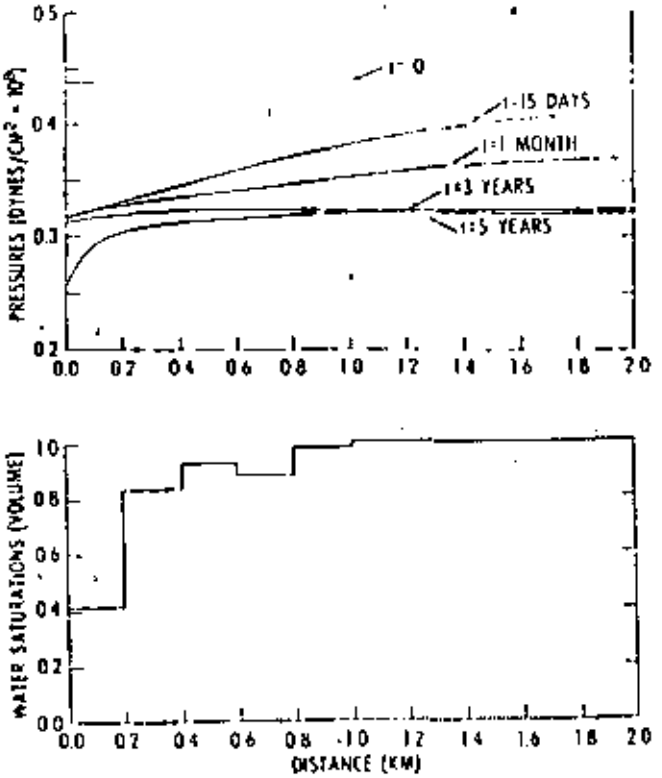


Figure 4. *Top:* computed pressure versus distance for various times. *Bottom:* computed water saturation versus distance after five years of exploitation (shaded area indicates water saturation of 1.0).

For problems such as this example where both single- and two-phase regions exist, it is necessary to take special precautions in order to reduce mass and energy balance errors. Discontinuities in the derivatives of the thermodynamic properties occur at the boundary between these regions. These derivatives appear as coefficients in the partial differential equations and are a major source of mass and energy balance errors. For problems involving both regions, it was not possible to represent these coefficients as functions over each element. Instead, the coefficients were treated as constants over each element and were calculated on the basis of the average element pressure and enthalpy values.

Mass and energy balance errors also occur when an element changes from single- to two-phase. These errors are reduced by checking (at the end of each time step) to determine if an element has become two-phase. If such a change has occurred, the exact time (during the time step) at which the phase change took place is linearly interpolated by using the saturation pressure and the pressures and times at the beginning and end of the time step. To calculate the saturation pressure, this method takes advantage of the fact that during a time step, pressure decreases at a nearly constant enthalpy in the compressed-water region. Once the time at which the phase change occurred is calculated, it is used to compute a new time increment. The program then returns to the previous time step and using the new time increment recomputes pressures, enthalpies treating the "phase change" element as being in the compressed water region. For subsequent time steps, the "phase-change" element is assumed to be two-phase. This procedure is repeated each time an element becomes two-phase, and if several elements change during the same time step, the element which converted first is used to compute the new time increment.

**Example 2.** The permeability of a geothermal reservoir strongly affects the productivity of wells; that is in low-permeability zones wells go "dry" rapidly. In order to examine the effect of reservoir permeability, a series of one-dimensional problems was solved using a range of permeabilities typical of geothermal reservoir rocks (see Figure 3). For this example a reservoir with an initial water saturation of 25% was specified.

In Figure 5, water saturation distributions are shown for a range of permeabilities from $2.5 \times 10^{-11}$ to $2.5 \times 10^{-9}$ cm². As anticipated, the reservoirs with lower permeabilities present sharp saturation fronts. The significance of the permeability effect is also demonstrated by Figure 6. In this figure the permeability of the system is plotted against the production time required to reduce the water saturation to 2.0% in the first element (the element including the sink). For reservoirs with low permeability the volume of the sink element dominates the time required to reach 2.0% water saturation, that is, mass is being removed from the sink element instead of from the entire reservoir. Whereas in

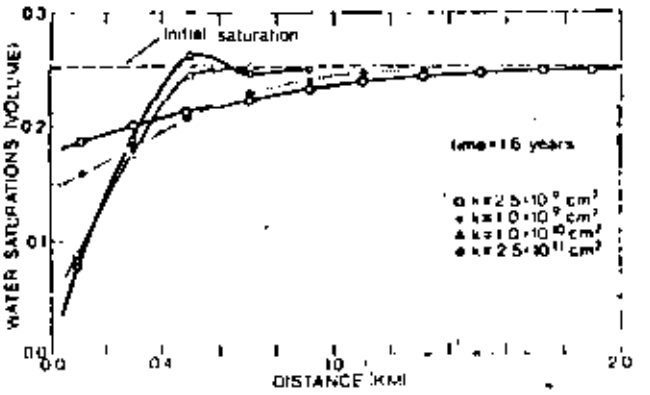


Figure 5. Computed water saturation versus distance for various permeabilities.

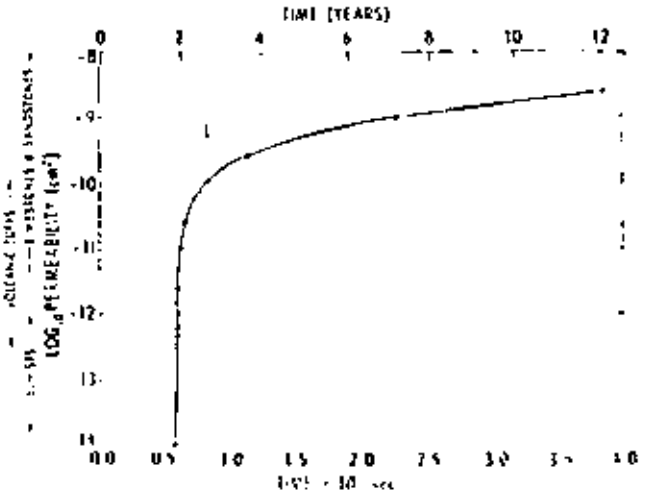


Figure 6. Permeability versus exploitation time to reach a water saturation of 0.02 in the sink element.

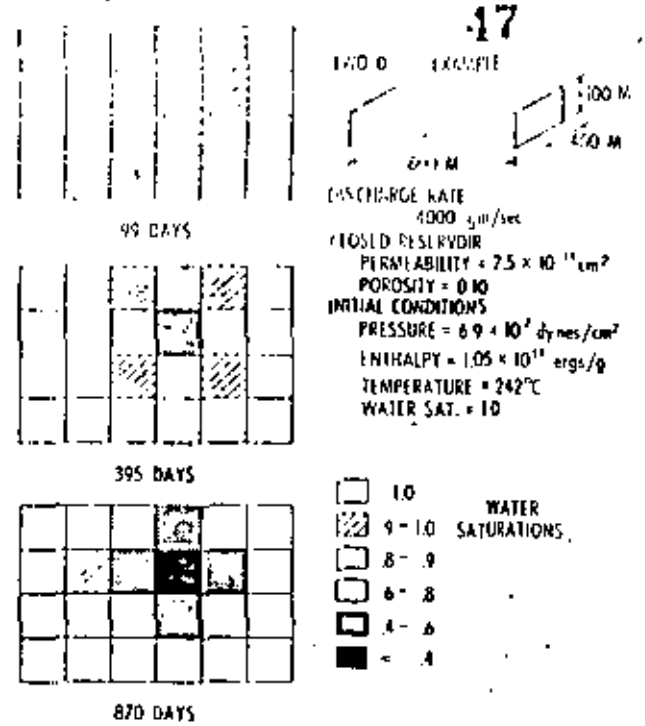


Figure 7. Two-dimensional, two-phase geothermal reservoir analysis showing water saturation distribution for various times.

reservoirs with relatively high permeabilities, fluid is allowed to flow to the sink element and maintain the water saturation longer.

## Two-Dimensional Horizontal Flow

As an example of two-phase, horizontal flow in two dimensions, a small hypothetical geothermal reservoir is considered. The dimensions, initial conditions and certain properties of the reservoir are specified in Figure 7. Other reservoir properties are: $K_m = 3.2 \times 10^5$ ergs/cm·sec·°C, $\rho_r = 2.5$ gm/cm$^3$ and $C_r = 1.01 \times 10^7$ ergs/gm·°C. Viscosities and relative permeabilities are given by the formulas presented for the earlier examples, and porosity is assumed to vary according to:

$$\phi = \phi_i(x, y)[1 + \beta(p - p_i)] \qquad (13)$$

where $i$ indicates an initial value and $\beta$ is the vertical compressibility. For this problem $\beta = 7.25 \times 10^{-11}$ cm$^2$/dyne. The boundary conditions are no-flow.

The two-dimensional (horizontal) form of Equations (1) and (2) are solved using an element configuration which consists of 35 nodes and 24 elements which are 0.1 km square. The reservoir is initially a hot-water system, but develops a two-phase zone in the vicinity of the sink (the element in the fourth column and third row). The three diagrams in Figure 7 show how the two-phase front changes with time. Figure 8 shows the pressure and temperature distribution after 870 days of exploitation (this corresponds with the final saturation distribution in Fig. 7). Note that the pressures and temperatures in the compressed-water region are essentially the same everywhere, and are slightly above the values that would cause conversion to a steam-water mixture. Since the boundary conditions are no flow, continued exploitation would result in decreased pressures and eventually the entire reservoir would become two-phase.

At the end of 870 days approximately 0.15 mass fraction was produced resulting in $3.6 \times 10^{21}$ ergs of heat removed. Using a fully implicit time step, the overall mass and energy balances had less than 1.0% error.

## CONCLUSIONS

In this paper we have outlined the important characteristics of a model that has been developed for geothermal reservoir simulation. The mathematical model consists of two nonlinear partial differential equations with fluid pressure and enthalpy as the dependent variables. The complex form of the partial differential equations requires numerical solution, and for this purpose a Galerkin-finite element method has been utilized. This model is valid for compressed water, two-phase mixtures and superheated steam; thus, it permits the simulation of both hot-water and vapor-dominated hy-

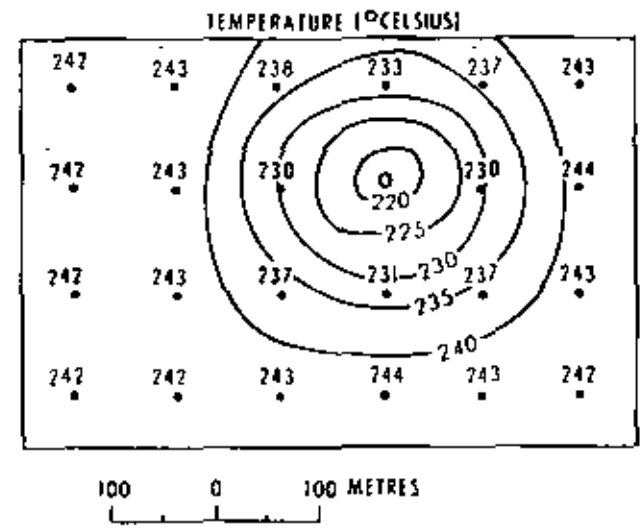


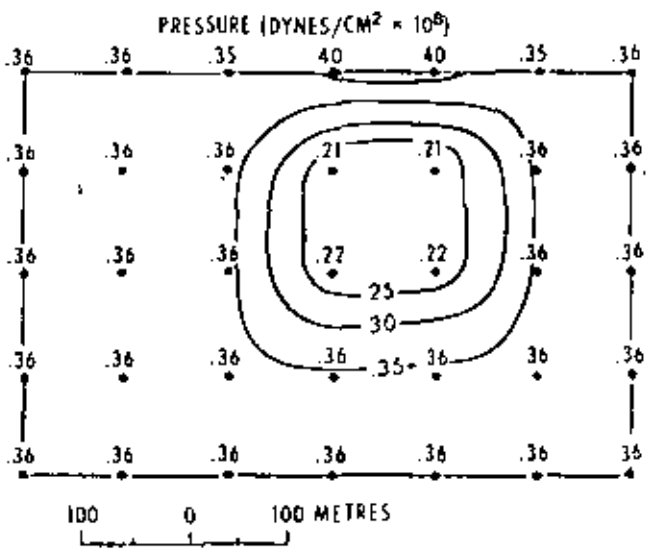


Figure 8. *Top:* temperature distribution for the two-dimensional example after 870 days of exploitation. *Bottom:* pressure distribution for the two dimensional example after 870 days of exploitation.

drothermal systems, as well as the conversion from a hot-water system to a two-phase system.

Several examples have been discussed in order to demonstrate the nature of heat transport and multiphase fluid flow in porous media. For the compressed-water region, the model was verified using an analytical solution for one-dimensional, vertical, steady-state flow. For the two-phase region, the model was verified qualitatively, since results are in accord with observed and expected behavior of geothermal systems.

In the formulation of the mathematical model, several simplifying assumptions were made (for example, negligible capillary pressure and local thermal equilibrium). For some geothermal reservoirs these assumptions are reasonable approximations. For other reservoirs where the assumptions are not valid, the proposed model could serve as a point of departure for a more sophisticated model.

It is evident that the modeling of geothermal systems is a difficult task and that several challenging problems have yet to be adequately considered. Among these are: multiphase flow and heat transport in fractured media, multiphase flow and heat transport in saline systems, three-dimensional simulation of geothermal reservoirs, coupled well-bore and reservoir models, and management models of geothermal reservoirs. In addition, experience with the model described in this paper indicates that further research is needed to determine the most suitable numerical techniques for application to geothermal reservoir engineering.

## REFERENCES CITED


Bredehoeft, J. D., and Papadopulos, I. S., 1965, Rates of vertical groundwater movement estimated from the earth's thermal profile: Water Resources Research, v. 1, no. 2, p. 325.

Brownell, D. H., Jr., Garg, S. K., and Pritchett, J. W., 1975, Computer simulation of geothermal reservoirs: Ventura, California, 45th Annual California Regional Meeting of the Soc. Petroleum Engineers, paper SPE5381.

Corey, A. T., 1954, The interrelation between gas and oil relative permeabilities: Producers Monthly, v. 19, p. 38.

Donaldson, I. G., 1968, The flow of steam water mixtures through permeable beds; a simple simulation of a natural undisturbed hydrothermal region: New Zealand Jour. Sci., v. 11, no. 1, p. 3.

Mercer, J. W., 1973, Finite element approach to the modeling of hydrothermal systems [Ph.D. Thesis]: Urbana-Champaign, University of Illinois.

Mercer, J. W., Faust, C., and Pinder, G. F., 1974, Geothermal reservoir simulation: Proceedings of National Science Foundation Conference on Research for the Development of Geothermal Energy Resources, Pasadena, California, p. 256.

Meyer, C. A., McClintock, R. B., Silvestri, G. J., and Spencer, R. C., 1968, 1967 ASME steam tables: New York, American Soc. Mechanical Engineers, 328 p.

Pinder, G. F., Frind, E. O., and Papadopulos, S. S., 1973, Functional coefficients in the analysis of ground water flow: Water Resources Research, v. 9, no. 1, p. 222.

Price, H. S., Cavendish, J. C., and Varga, R. S., 1968, Numerical methods of higher-order accuracy for diffusion-convection equations: Soc. Petroleum Engineers Jour., v. 8, no. 3, p. 293.

Toronyi, R. M., 1974, Two-phase, two-dimensional simulation of a geothermal reservoir and the wellbore system [Ph.D. Thesis]: University Park, Pennsylvania State Univ.

White, D. E., Muffler, L. P. J., and Truesdell, A. H., 1971, Vapor dominated hydrothermal systems compared with hot-water systems: Economic Geology, v. 66, p. 75.

Zienkiewicz, O. C., 1971, The finite element method in engineering science: London, McGraw-Hill, 521 p.

# SIMULATION OF HEAT TRANSPORT IN FRACTURED, SINGLE-PHASE GEOTHERMAL RESERVOIRS

William G. Gray, Kevin O'Neill and George F. Pinder
Water Resources Program
Department of Civil Engineering
Princeton University
Princeton, N. J. 08540

Although many geothermal reservoirs depend upon fracture permeability to obtain adequate mass flows, relatively little research effort has been directed toward fractured reservoir simulation. This paper outlines the mathematical apparatus necessary to develop a numerical simulator for a fractured, single-phase geothermal reservoir. It is assumed that the fracturing is extensive and well-distributed (though not necessarily uniform) so that it is reasonable to consider a superficial discharge through the fractures as well as the pores. While mass and heat transport are of course coupled in a system of this kind, we have subdivided the ensuing discussion into mass flow and heat flow for clarity of presentation.

## Mass Flow Equation

Analytical solutions for the pressure distributions in porous blocks of various shapes and sizes show that the pressure in the interior of a typical block reaches 95% of the value of an initial "step" input imposed on the block surface in a time which is very short relative to the length of time typically required for overall, macroscopic system changes. In addition, recent modeling analyses and examination of pertinent field data by Closmann (1975) support the point of view that for most purposes one may consider both pore and fracture flow fields to be characterized by a single pressure variable. A net flow of mass may exist between one flow regime and the other, but this will be such as to maintain the near equality of pressure. Application of accepted space-averaging techniques (Gray and Lee, 1976) to a point mass balance equation provides the following mass conservation equation:

$$\frac{\partial}{\partial t}(\rho_w \varepsilon_w) = -\nabla\cdot[\rho_w \mathbf{v}_{w\text{-}w}] + S_m = -\nabla\cdot[\rho_f \mathbf{v}_{f\text{-}f} + \rho_p \mathbf{v}_{p\text{-}p}] + S_m \qquad (1)$$

where $\rho_w$ is the averaged density of all (pore plus fracture) water,

$\rho_f$ is the density of fracture water,

$\rho_p$ is the density of pore water,

$\epsilon_w$ is the void fraction occupied by all water,

$v_f$ is the superficial discharge through the fracture (vector),

$v_p$ is the superficial discharge through the pores (vector), and

$S_m$ is the mass source or sink strength, that is, mass entering or leaving per unit time per unit volume of total medium.

The lefthand side of (1) may be expanded as

$$\frac{\partial}{\partial t}(\rho_w c_w) = \rho_w \frac{\partial c_w}{\partial t} + c_w \frac{\partial \rho_w}{\partial t} \tag{2}$$

$$- \rho_w \alpha_p \frac{\partial p}{\partial t} + \rho_w \alpha_T \frac{\partial T_w}{\partial t} + \epsilon_w \rho_w \beta_p \frac{\partial p}{\partial t} + \epsilon_w \rho_w \beta_T \frac{\partial T_w}{\partial t}$$

where $\epsilon_f$ is the void fraction of the fractures,

$\epsilon_p$ is the void fraction of the pores,

$p$ is the incremental fluid pressure,

$T_f$ is the local average fluid temperature in the fractures,

$T_{pm}$ is the local average temperature of the porous medium, and

$T_w$ is the locally averaged temperature of all water defined as

$$T_w = \epsilon_f T_f + \epsilon_p T_{pm} \tag{3}$$

The parameters $\alpha_p$, $\alpha_T$, $\beta_p$ and $\beta_T$ are empirical coefficients defined through the relations:

$$\frac{\partial \epsilon_w}{\partial t} = \alpha_p \frac{\partial p}{\partial t} + \alpha_T \frac{\partial T_w}{\partial t} \tag{4a}$$

$$\frac{\partial \rho_w}{\partial t} = \rho_w \beta_p \frac{\partial p}{\partial t} + \rho_w \beta_T \frac{\partial T_w}{\partial t} \tag{4b}$$

Superficial fracture and pore discharges may be expressed in terms of incremental pressure gradients, as

$$\underset{\sim}{v}_f = -\left(\frac{\underset{=}{k}}{\mu}\right)_f \cdot \underset{\sim}{\nabla} p \tag{5a}$$

$$\underset{\sim}{v}_p = -\left(\frac{\underset{=}{k}}{\mu}\right)_p \cdot \underset{\sim}{\nabla} p \tag{5b}$$

where $\mu$ is the fluid viscosity,

$\underset{=}{k}_f$ is the fracture permeability (tensor), and

$\underset{=}{k}_p$ is the pore permeability (tensor)

Under certain conditions $\underset{=}{k}_f$ may be considered to be a function of $\underset{\sim}{v}_f$.

Substitution of equations (2) through (5) into (1) yields the following expression for the conservation of all fluid mass:

$$\rho_w(\alpha_p + \epsilon_w\beta_p)\ \frac{\partial p}{\partial t} + \rho_w(\alpha_T + \epsilon_w\beta_T)\ \frac{\partial T_w}{\partial t} \tag{6}$$

$$= \underset{\sim}{\nabla} \cdot \left[\left(\rho\frac{\underset{=}{k}}{\mu}\right)_f + \left(\rho\frac{\underset{=}{k}}{\mu}\right)_p\right] \cdot \nabla p + S_m$$

In addition to the explicit coupling of this equation to the temperature equations through the second term on the lefthand side, temperature dependence also enters implicitly through the changing value of $\mu$.

Heat Flow

The governing equations for heat flow are provided by space averaging of conservation of energy equations written in terms of temperature. For the fracture system, this results in

$$\rho_f c\varepsilon_f\ \frac{\partial T_f}{\partial t} + \rho_f c \underset{\sim}{v}_f \cdot \underset{\sim}{\nabla} T_f - \underset{\sim}{\nabla} \cdot \underset{=}{D}_f \cdot \underset{\sim}{\nabla} T_f$$

$$= h(T_{pm} - T_f) + c\, S_{\sigma,f}(T_{\sigma,f} - T_f) \tag{7a}$$

and for the porous medium

$$(\rho c\varepsilon)_{pm} \frac{\partial T_{pm}}{\partial t} + \rho_p c v_p \cdot \nabla T_{pm} - \nabla \cdot \underline{\underline{D}}_{pm} \cdot \nabla T_{pm}$$

$$= h(T_f - T_{pm}) + c\, S_{m,p}(T_{s,pm} - T_{pm}) \qquad (7b)$$

where $(\rho c\varepsilon)_{pm} \equiv \rho_p c_p + \rho_s c_s \varepsilon_s$,

$\rho_s$ is the rock density,

$c_s$ is the specific heat of the rock,

$\varepsilon_s$ is the volume fraction of the rock,

$c$ is the specific heat of water,

$\underline{\underline{D}}_f$ is the tensor coefficient of dispersion for the fractures,

$\underline{\underline{D}}_{pm}$ is the tensor coefficient of dispersion for the porous medium,

$h$ is a porous medium-fracture heat transfer coefficient relating the time rate of heat transport between those regimes, per volume of the medium, to the temperature difference between the two. $T_{s,f}$ and $T_{s,pm}$ are source or sink temperatures of fracture and pore fluids, respectively. (For withdrawal, the sink temperature is the reservoir fluid temperature and the last terms in 7 vanish).

$S_{m,f}$ is the fracture mass source or sink strength,

$S_{m,p}$ is the pore mass source of sink strength, and

$S_m = S_{m,f} + S_{m,p}$ and the ratio of the two components can be determined using the permeabilities of the two systems.

The superficial velocities in (7) must, of course, be computed using the pressure field through equations (5) and (6). Equations (5), (6), and (7) provide five equations in the five dependent variables $T_{pm}$, $T_f$, $p$, $v_f$ and $v_p$. These equations have been solved successfully for a variety of hypothetical problems for which analytical solutions exist. The numerical simulator uses isoparametric Hermitean finite elements (Van Genuchten, et al, 1977) to solve in three space dimensions, and a time-centered difference scheme to solve in time.

Figures 1 and 2 show results for an additional fully coupled, one-dimensional, transient test case, subject to the following conditions:

at $x = 0$ $\quad T_{pm} = T_f = 40^{\circ}C$

$t > 0$ $\quad p = 0$

at $x = 100cm$ $\quad T_{pm} = T_f = 0$

$p = -1.0 \times 10^5$ dyne/cm$^2$

$\frac{1}{\mu} = 5.38 \times 10^2 + (T-150) \times 3.8 - (T-150)^3 \times 2.6 \times 10^{-5}$ cm.sec/g for $0<T<300^{\circ}C$

(Mercer et al, 1975)

$c_f = 0.02$, $\epsilon_p = 0.2$, $\alpha_p = 1.0 \times 10^{-10}$cm$^2$/dyne, $\alpha_T = 0$

$\frac{k_f}{\epsilon_f} = 10^{-7}$cm$^2$, $\frac{k_{pm}}{\epsilon_p} = 3.0 \times 10^{-8}$cm$^2$, $\beta_p = 5.0 \times 10^{-11}$cm$^2$/dyne

$\beta_T = 5.0 \times 10^{-4}/^{\circ}C$

$\rho_s = 2.5$g/cm$^3$, $c_s = 0.2$cal/g.$^{\circ}$C, $D_f = 5.0 \times 10^{-4}$cal/$^{\circ}$C.cm.sec,

$D_{pm} = 3.0 \times 10^{-3}$cal/$^{\circ}$C cm.sec.

The initial temperature distribution for both fractures and porous medium is displayed on each figure. As expected, a non-zero value of $h$ retards translation of the fracture temperature front, increases translation of the porous medium front, and increases dispersion of both. As the fronts progress, the pressure gradient (not shown) decreases from the initial, essentially isothermal value, due primarily to the decrease in fluid viscosity with rising temperature.

## References


Closmann, P. J., "An Aquifer Model for Fissured Reservoirs," Society of Petroleum Engineers Journal, October 1975, 385-398.

Gay, W. G. and P. C. Y. Lee, "On the Theorems for Local Volume Averaging of Multiphase Systems," International Journal of Multiphase Flow, in press 1976.

Mercer, W. M., G. F. Pinder, and I. G. Donaldson, "A Galerkin Finite Element Analysis of the Hydrothermal System at Wairakei, New Zealand," Journal of Geophysical Research, June 1975, 2608-2621.

Van Genuchten, M. T., G. F. Pinder, and E. O. Frind, "Simulation of Two-dimensional Contaminant Transport with Isoparametric Hermitean Finite Elements," Water Resources Research, In press 1976.

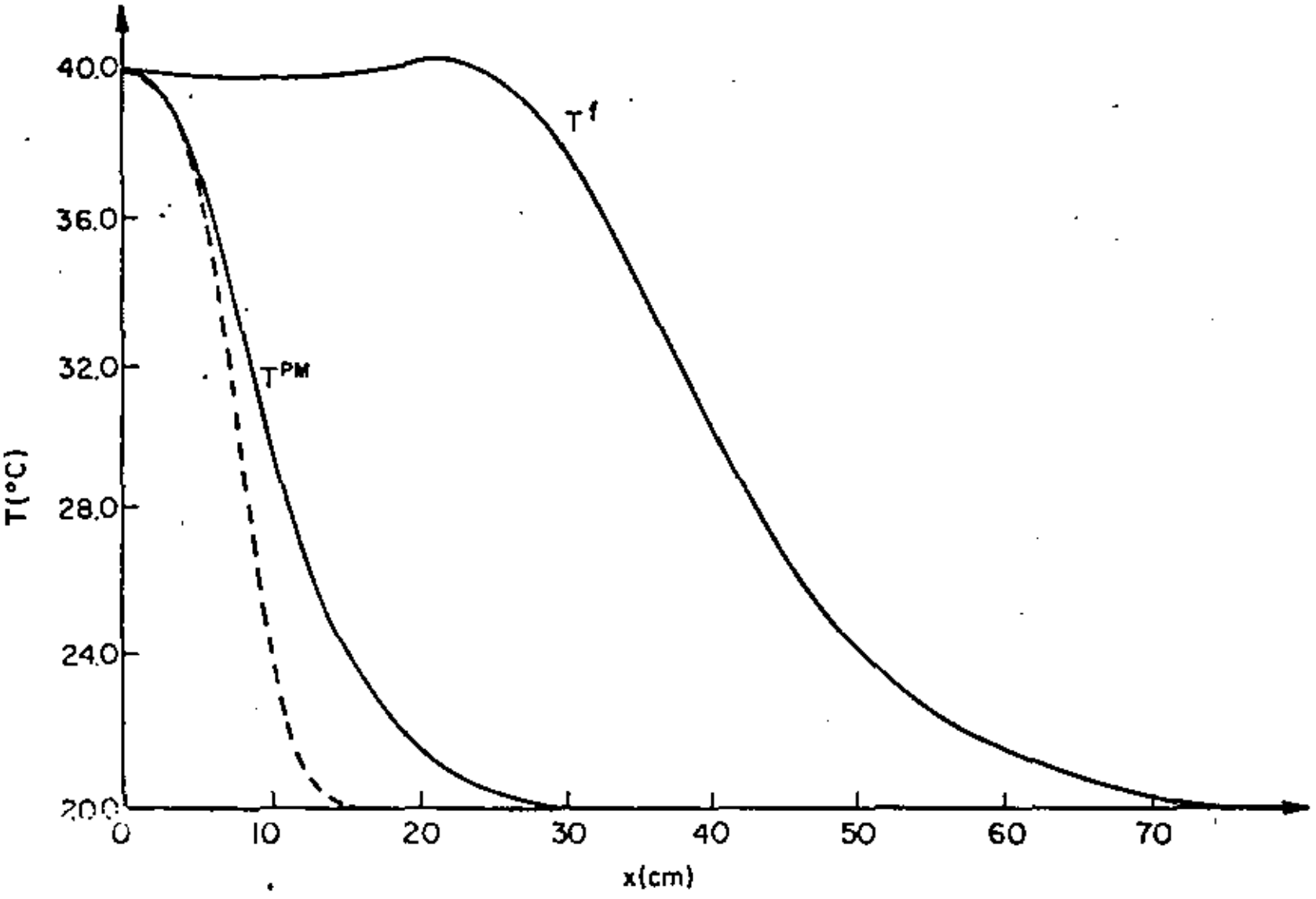


h = 0
$t = 3.0 \times 10^3$ sec
DASHED LINE SHOWS INITIAL TEMPERATURE
FIGURE 1

FIGURE 2

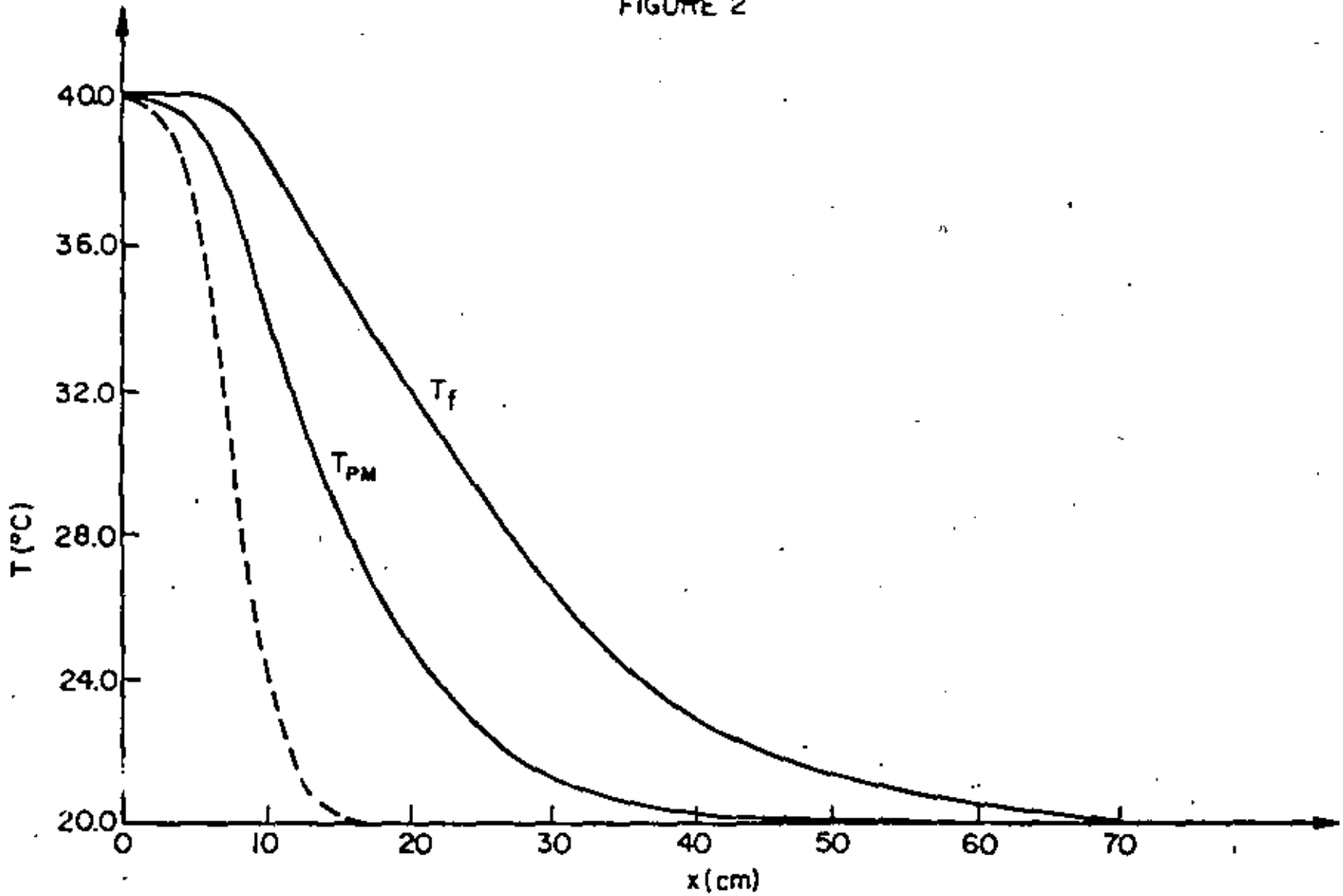


$h = 2.0 \times 10^{-5}$ CAL/cm$^2$ sec °C

$t = 5.25 \times 10^3$ sec

DASHED LINE SHOWS INITIAL TEMPERATURE

SPE 6892

# GEOTHERMAL RESERVOIR MODELLING

by

K. H. Coats
INTERCOMP Resource Development
and Engineering, Inc.



This paper was presented at the 52nd Annual Fall Technical Conference and Exhibition of the Society of Petroleum Engineers of AIME held in Denver, Colorado, Oct. 9-12, 1977. The material is subject to correction by the author. Permission to copy is restricted to an abstract of not more than 300 words. Write 6200 N. Central Expy., Dallas, Texas 75206.

## ABSTRACT

This paper describes and partially evaluates an implicit, three-dimensional geothermal reservoir simulation model. The evaluation emphasizes stability or time-step tolerance of the implicit finite-difference formulation. In several illustrative multiphase flow problems, the model stably accommodated time steps corresponding to grid block saturation changes of 80-100% and grid block throughput ratios the order of $10^8$. This compares to our experience of limits of 3 to 10% saturation change and roughly 20,000 throughput ratio with semi-implicit oil and geothermal reservoir models.

The illustrative applications shed some light on practical aspects of geothermal reservoir behavior. Applications include single- and two-phase single-well behavior, fractured-matrix reservoir performance and well test interpretation, and extraction of energy from fractured hot dry rock. Model stability allows inclusion of formation fractures and wellbores as grid blocks.

An analytical derivation is presented for a well deliverability reduction factor which can be used in simulations using large grid blocks. The factor accounts for reduced deliverability due to hot water flashing and steam expansion accompanying pressure decline near the well.

References and illustrations at end of paper.

## INTRODUCTION

This paper describes a numerical model for simulating geothermal well or reservoir performance. The model is considerably more general than any described in the literature to date. It treats transient, three-dimensional, single- or two-phase fluid flow in normal heterogeneous or fractured-matrix formations. Both conductive and convective heat flow are accounted for and fluid states in the reservoir can range from undersaturat liquid to two-phase steam-water mixtures to superheated steam. Aquifer water influx and heat source/sink terms necessary in simulating free convection cells are included in the model formulation.

The primary purpose of the work described here was evaluation of the capability of an implicit model formulation. Our experience with semi-implicit simulation of petroleum and geothermal reservoirs has shown time step restrictions related to conditional stability. In multiphase flow problems, the maximum tolerable time step size generally corresponds to a maximum of 3 to 10 percent saturation change in any grid block in one time step. In some steamflood and geothermal simulations, we have found this to result in very small time steps and correspondingly high computing costs. This work was performed with the hope that the implicit model formulation would give unconditional stability with no time step restriction other than that imposed by time truncation error.

Calculated results are presented for a variety of geothermal well and reservoir illustrative problems. Emphasis in connection with these results is placed on the stability or time step tolerance of the model. However, the applications are also intended to shed some light on practical aspects of geothermal reservoir behavior.

Following description of the implicit model formulation, the paper presents applications including single-well deliverability under two-phase flow conditions, depletion of a fractured-matrix formation with boiling, drawdown test interpretation in single-phase, fractured-matrix formations, and heat extraction from artificially fractured hot dry rock. An analytical expression is derived to represent the effective transient productivity index of a well which experiences hot water flashing due to pressure drawdown from an exterior radius where steam saturation may be zero or small.

We have applied the model extensively in simulation of natural convection cells with zero porosity (hard rock) grid block definition above and below the formation. This definition eliminates the erroneous imposition of constant temperature boundaries at the top and bottom of the convection cell common in many reported studies of natural convection. Another application simulated development over geologic time of a superheated (Geyser's type) reservoir from an early time of magma or heat source intrusion beneath an initial normal gradient cold water aquifer. These natural convection type applications are omitted here due to the significant length of the paper. Some of this convection work is reported in a recent paper [1].

## MODEL DESCRIPTION

The model consists of two equations expressing conservation of mass of $H_2O$ and conservation of energy. These equations account for three-dimensional, single- or two-phase fluid flow, convective and conductive heat flow in the reservoir and conductive heat transfer between the reservoir and overlying and underlying strata. The phase configuration at any time can vary spatially through the formation from single-phase undersaturated water to two-phase steam-water mixture to single-phase superheated steam.

The equations represent water influx from an aquifer extending beyond the reservoir grid using the Carter-Tracy [2] or simpler approximations. Heat source and sink terms in the equations are useful in imposing temperature and/or heat flux boundary conditions in simulation of natural convection. The model equations do not account for the presence of inert gases or for varying concentration and precipitation of dissolved salts.

The model applies to reservoir grids including one-dimensional, two-dimensional radial-z, x-z or x-y and three-dimensional, either x-y-z Cartesian or r-θ-z cylindrical. In the r-z and r-θ-z case, the wellbore of a well at r = 0 can be included in the grid, resulting in enhanced stability and accuracy as discussed below. The r-z grid can be used in simulating a sector of a fractured-matrix reservoir with the horizontal and vertical fractures represented by grid blocks. The grid can include blocks of zero porosity representing hard rock, with no pressure calculated, and blocks of 100% porosity representing either fractures or wellbores.

The mass balance on $H_2O$ combines in a single equation the steam-phase and liquid water-phase mass balance equations. This combination was proposed in our early steamflood work [3] to eliminate difficulties in handling the mass transfer term. The energy balance is the First Law of Thermodynamics applied to each grid block. The grid block is an open system with fixed boundaries. With potential and kinetic energy terms ignored, the energy balance states that (enthalpy flow rate in) - (enthalpy flow rate out) = rate of gain of internal energy in the grid block. For some reason, considerable confusion exists in the literature regarding this energy balance. Enthalpy is U + pv where U is internal energy. Many modelling papers ignore the pv term, in which case the energy balance erroneously becomes (net flow rate of internal energy into the grid block = rate of gain of internal energy in the block). A recent paper [4] uses an erroneous energy balance stating (net flow rate of enthalpy into the grid block = rate of gain of enthalpy in the block).

The two model equations are*

$$\Delta[T_w(\Delta p_w - \gamma_w \Delta z) + T_g(\Delta p_g - \gamma_g \Delta z)] - q = \frac{V}{\Delta t}\overline{\delta}(\phi\rho_w S_w + \phi\rho_g S_g) \qquad (1a)$$

$$\Delta[T_w H_w(\Delta p_w - \gamma_w \Delta z) + T_g H_g(\Delta p_g - \gamma_g \Delta z)] + \Delta(T_c \Delta T) - q_{HL} - q_H = \frac{V}{\Delta t}\overline{\delta}(\phi\rho_w S_w U_w + \phi\rho_g S_g U_g) + (1-\phi)(\rho C_p)_R T \qquad (1b)$$

For a given grid block (i,j,k), all terms in these equations are single-valued functions of $(T, S_g, p)_{i,j,k}$ and $(T, S_g, p)$ in the six neighboring grid blocks (i±1,j,k), (i,j±1,k), (i,j,k±1). Thus, transposing the right-hand sides, we can write Equations (1) simply as

*See Nomenclature for definition of terms.

$$F_1(\underline{x}) = 0$$
$$F_2(\underline{x}) = 0 \qquad (2)$$

where $\underline{x}$ represents the vector of the above listed 21 unknowns.

Following the totally implicit procedure described by Blair and Weinaug [5], we apply the Newton-Raphson iterative method to (2) as

$$F_1(\underline{x}) \doteq F_1(\underline{x}^\ell) + \sum_{i=1}^{21} (\partial F_1/\partial x_i)^\ell \delta x_i = 0$$
$$F_2(\underline{x}) \doteq F_2(\underline{x}^\ell) + \sum_{i=1}^{21} (\partial F_2/\partial x_i)^\ell \delta x_i = 0 \qquad (3)$$

where we temporarily use $x_i$ to denote the 21 unknowns and superscript $\ell$ denotes latest iterate value. The operator $\delta$ in Equations (1) denotes change over time step while $\delta$ in Equations (3) denotes change over the coming iteration. The approximation $\delta x_i \doteq x_{i,n+1} - x_i^\ell$ becomes increasingly exact as we near convergence.

The partial derivatives in Equations (3) are all evaluated at latest iterate values of $x_i$. The functions $F_1$, $F_2$ involve three different types of terms: right-hand sides (accumulation terms), sink/source terms and interblock flow terms. Differentiation of accumulation terms is straightforward. The heat loss term and its derivative is evaluated as described in Reference [3]. The well injection/production terms and their derivatives are evaluated as described in some detail below. The interblock flow terms are evaluated as follows: Relative permeabilities and enthalpies are evaluated at upstream grid block conditions, interblock $\rho/p$ and $\gamma$ values are evaluated as arithmetic averages of their values in the two grid blocks. Water phase pressure $p_w$ is expressed as $p - P_c$ where $p$ is gas pressure and capillary pressure $P_c$ is a single-valued function of $S_g$.

For all $N_x N_y N_z$ grid blocks taken together, Equations (3) are $2N_xN_yN_z$ equations in $3N_xN_yN_z$ unknowns, ($\delta T$, $\delta S_g$, $\delta p$) for each grid block. Only two of these three unknowns in each block are independent. If the block contains undersaturated water or superheated steam, $\delta S_g = 0$ and $\delta T$, $\delta p$ are the block's two unknowns. If the block is saturated, two-phase, then temperature $T = T_s(p)$ and $\delta T$ is $(dT/dp)_s \delta p$ where subscript $s$ denotes the saturated condition.

Equations (3) can be written for each grid block in the form

$$\Delta(T_{11}\Delta P_1) + \Delta(T_{12}\Delta P_2) + R_1 = C_{11}P_1 + C_{12}P_2$$
$$\Delta(T_{21}\Delta P_1) + \Delta(T_{22}\Delta P_2) + R_2 = C_{21}P_1 + C_{22}P_2 \qquad (4)$$

where $P_1$ is either $\delta T$ or $\delta S_g$ and $P_2$ is $\delta p$. The terms $R_1$, $R_2$ are $F_1(\underline{x}^\ell)$, $F_2(\underline{x}^\ell)$, respectively, in Equations (3). The $\Delta(T\Delta P)$ type terms are not true Laplacians but rather are, as illustrated by the x-direction component

$$\Delta_x(T_x\Delta_x P) = T^+_{xi}P_{i+1} + T^0_{xi}P_i + T^-_{xi}P_{i-1}$$

where the center term $T^0_{xi}$ can be combined with the appropriate $C_{ij}$ in Equation (4) and need not be stored. More simply, Equation (4) can be written

$$\Delta(T\Delta\underline{P}) + \underline{R} = C\underline{P} \qquad (5)$$

where T and C are the 2 x 2 matrices $T_{ij}$, $C_{ij}$ and $\underline{R}$ and $\underline{P}$ are column vectors. We use reduced band width direct solution [6] to solve Equation (5) for $P_1$, $P_2$ and obtain new iterate values as $p^{\ell+1} = p^\ell + \delta p$. Convergence is defined by

$$\text{Max}|\delta p_{ijk}| \leq \epsilon_p$$
$$\text{Max}|\delta T_{ijk}| \leq \epsilon_T \qquad (6)$$
$$\text{Max}|\delta S_{gijk}| \leq \epsilon_S$$

where MAX denotes maximum over all grid blocks. We generally use tolerances of .1 psia, 1°F, 1% saturation and have not found sensitivity of results to tighter tolerances.

## PVT TREATMENT

At saturated conditions, $U_w$, $U_g$, $\rho_w$, $\rho_g$ are evaluated as single-valued functions of temperature from the Steam Tables [7]. $U_w$ is assumed a single-valued function of temperature for undersaturated water. Density of undersaturated water is calculated as

$$\rho_w \doteq \rho_{ws}(T)[1 + c_w(T)(p - p_s(T))] \qquad (7)$$

where subscript s denotes saturation condition. The "compressibility" $c_w(T)$ is derived as follows. The Steam Tables [7] include a tabulation of $(v - v_s)$ for undersaturated water as a function of temperature and pressure, where v is specific volume, cubic feet per pound. The tabular values are fit well by the expression

$$v = v_s - s(T)(p - p_s(T))$$

where s(T) is dependent only upon temperature as:

| T, °F | s(T) x $10^5$ |
|---|---|
| < 200 | .0054 |
| 300 | .0072 |
| 400 | .0109 |
| 500 | .0205 |
| 600 | .065 |
| 660 | .355 |

This equation can be written

$$\frac{1}{\rho_w} = \frac{1}{\rho_{ws}(T)} - \frac{s(T)\rho_{ws}(T)}{\rho_{ws}(T)}(p - p_s(T))$$

Since $s(T)\rho_{ws}(T)(p - p_s(T))$ is small in comparison to 1 (except at temperatures approaching 700°F), this equation can be written as Equation (7) where $c_w(T)$ is $s(T)\rho_{ws}(T)$.

For superheated steam, internal energy $U_g$ and density $\rho_g$ are approximated by

$$U_g \cong U_{gs}(p) + C_{psteam}(T - T_s(p)) \quad (8)$$

$$\rho_g \cong \rho_{gs}(p)\frac{T_s(p) + 460}{T + 460} \quad (9)$$

where specific heat $C_{psteam}$ is constant. Equation (9) is accurate in proportion to the constancy of steam z-factor from p, $T_s(p)$ to p, T. Water and steam phase viscosities are evaluated as single-valued functions of temperature equal to their respective saturated values. Enthalpies are

$$H_w = U_w + 144/778.2\ p/\rho_w$$

$$H_g = U_g + 144/778.2\ p/\rho_g \quad (10)$$

The model uses steam phase pressure as the pressure variable in all PVT relationships.

Porosity is calculated from

$$\phi = \phi_o(1 + c_r(p - p_o)) \quad (11)$$

where $\phi_o$ is porosity at pressure $p_o$ and $c_r$ is constant. Reservoir thermal conductivity may vary with spatial position, but is treated as independent of pressure, temperature and saturation. Formation rock heat capacity may vary with position but is independent of temperature. Overburden thermal conductivity and heat capacity are constants.

## IMPLICIT AND SEMI-IMPLICIT ALLOCATIONS OF WELL RATE AMONG LAYERS

Numerical simulation of most reservoir processes encounters the problem of representing production rates from wells located in grid blocks of large areal dimensions. The reservoir grid system consists of NZ vertical layers with the layers numbered from top to bottom as k = 1, k = 2, . . ., k = NZ. A producing well located in areal block (i, j) is perforated or open to flow in layers $k = k_1, k_1 + 1, \ldots, k_2$. For example, NZ might be 8 and a well open in layers 3-7, ($k_1 = 3$, $k_2 = 7$). The wellbore radius is denoted by $r_w$. The grid blocks penetrated by the well are of dimensions $\Delta x$, $\Delta y$, $\Delta z_k$ where $\Delta x$ and $\Delta y$ are the areal dimensions. Assuming (a) $\Delta x \cong \Delta y$, b) the well is located areally near the center of the grid block, (c) steady- or semi-steady-state radial flow in each grid block $\Delta x$, $\Delta y$, $\Delta z_k$ open to the well, (d) no vertical crossflow between open layers, we can derive from Darcy's law for single-phase flow of a unit mobility fluid ($k_r/\mu = 1$)

$$Q_k \cong \frac{2\pi(k\Delta z)_k}{\ln(r_e/r_w) + S}(p_k - p_{wbk}) \equiv PI_k(p_k - p_{wbk}) \quad (12)$$

where

- $Q_k$ = rate of radial flow of a unit mobility fluid in layer k from grid block to the wellbore, cubic feet/day,
- $k_k$ = absolute permeability of layer k, md x 0.00633,
- $\Delta z_k$ = layer thickness, feet,
- $S$ = skin factor,
- $r_e$ = $\sqrt{\Delta x \cdot \Delta y/\pi}$ = equivalent radius feet,
- $p_k$ = pressure in grid block i,j,k at $r = r_e$, psia,
- $p_{wbk}$ = flowing wellbore pressure opposite layer k, psia.

In practice, for the case where $r_e >> r_w$, we assume $p_k$ equal to the average grid block pressure calculated in the simulator and, for more rigor, replace S by S - 1/2 or S - 1/4 for steady- or semi-steady-state flow. $PI_k$ denotes the coefficient in Equation (12), a layer productivity index in units of cubic feet/day-psi. All pressures $p_k$, $p_{wbk}$ refer to points vertically centered in the thickness $\Delta z_k$.

In the geothermal reservoir case treated here, $\bar{q}$ denotes the well target or desired production rate, and $\bar{p}_{wb}$ denotes the minimum flowing wellbore pressure in layer $k_t$. If no tubing is in the well, then $k_t$ would normally be specified as $k_1$, the uppermost open layer. If tubing is in the perforated casing, then a minimum (bottomhole tubing) wellbore pressure may be specified at any layer, $k_1 \leq k_t \leq k_2$.

$p_{wb}$ denotes the actual flowing wellbore pressure at the center of layer $k = k_t$ and q denotes the actual total well production rate, lbs $H_2O$ per day. The flowing wellbore pressure in layer k is denoted by

$$p_{wbk} = p_{wb} + \Delta p_{wbk} \tag{13}$$

From Equations (12) and (13) the production rates of water phase, gas (steam) phase, total $H_2O$ and enthalpy from layer k are

$$\begin{aligned} q_{wk} &= a_{wk}(p_k - p_{wb} - \Delta p_{wbk}) \\ q_{gk} &= a_{gk}(p_k - p_{wb} - \Delta p_{wbk}) \\ q_k &= q_{wk} + q_{gk} = a_k(p_k - p_{wb} \\ &\quad - \Delta p_{wbk}) \\ q_{Hk} &= q_{wk}H_{wk} + q_{gk}H_{gk} \end{aligned} \tag{14}$$

where

$$a_{wk} = PI_k(k_{rw}\rho_w/\mu_w)_k$$

$$a_{gk} = PI_k(k_{rg}\rho_g/\mu_g)_k$$

$$a_k = a_{wk} + a_{gk}$$

and $\rho_w$, $\rho_g$ are phase densities in units of lbs $H_2O$ per cubic foot.

[5]

As discussed above, the interblock flow rates and heat loss and conduction terms are all treated implicitly in the simulator described herein. If, in addition, the well sink or source terms are implicit, then the entire simulator is implicit. The logic and coding necessary for implicit well treatment is rather simple for the case of a well completed in a single layer of the reservoir grid. Implicit treatment can be extremely difficult for a producing well completed in several layers.

In this section we describe an implicit treatment for multilayer well completion and present several semi-implicit simplifications. Note that $a_k$ in Equations (14) is a function of pressure, temperature and, due to relative permeabilities, saturation $S_g$. Enthalpies $H_w$, $H_g$ are functions of pressure and temperature. Total well production rate q is the sum of $q_k$ over layers $k_1$ - $k_2$ or

$$q = \Sigma a_k(p_k - \Delta p_{wbk}) - p_{wb}\Sigma a_k \tag{15}$$

where the summation term $\Sigma$ denotes summation from $k_1$ to $k_2$. Rearranging Equation (15) gives

$$p_{wb} = (\Sigma a_k(p_k - \Delta p_{wbk}) - \bar{q})/\Sigma a_k \tag{16}$$

as the flowing bottomhole wellbore pressure at center of layer $k_t$ necessary to produce the well target rate $\bar{q}$ lbs $H_2O$ per day. The well is on deliverability if $p_{wb}$ from Equation (16) is less than the specified minimum value $\bar{p}_{wb}$. In any event, the production rates of water, steam and $H_2O$ are given by Equations (14a) - (14c) with $p_{wb}$ equal to the larger of $\bar{p}_{wb}$ and the value given by Equation (16).

Implicit well treatment requires that water phase production rate given by Equation (14a) be expressed as

$$q_{wk} = q^{\ell}_{wk} + \Sigma\frac{\partial q_{wk}}{\partial T_m}\delta T_m + \Sigma\frac{\partial q_{wk}}{\partial S_{gm}}\delta S_{gm} + \Sigma\frac{\partial q_{wk}}{\partial p_m}\delta p_m + \frac{\partial q_{wk}}{\partial p_{wb}}\delta p_{wb} \tag{17}$$

where summation here is over m from $k_1$ to $k_2$, superscript $\ell$ denotes evaluation at latest iterate values of all variables, all partial derivatives are evaluated at latest iterate conditions, $\delta T_m$, $\delta S_{gm}$, $\delta p_m$ are changes in layer m over the coming iteration and $q_{wk}$ is an approximation to the end-of-time step (implicit) value $q_{wk,n+1}$. The gas

phase production rate $q_{gk}$ in Equation (14b) is represented in an analogous fashion. If the producing cell is two-phase ($0<S_g<1$), then $\delta T_m = (dT/dp)_s \delta p_m$ where $(dT/dp)_s$ is the slope of saturated temperature vs. saturated pressure at the latest iterate pressure value. If the producing cell is single-phase ($S_g=0$ or $S_g=1$), then $\delta S_g = 0$. Thus only two of the three unknowns $\delta T_m$, $\delta S_{gm}$, $\delta p_m$ are independent in any case.

The implicit expressions for $q_{wk}$, $q_{gk}$, $q_{Hk}$ of type shown in Equation (17) introduce one additional unknown $\delta p_{wb}$ for each well. The additional required equation corresponding to this unknown is the constraint equation stating that the summation over k $\Sigma(q_{wk} + q_{gk})$ equals target well rate $\bar{q}$ lbs $H_2O$/day:

$$\sum_{k=k_1}^{k_2} \Big\{ \sum_{m=k_1}^{k_2} \Big[ \Big(\frac{\partial q_{wk}}{\partial T_m} + \frac{\partial q_{gk}}{\partial T_m}\Big)\delta T_m + \Big(\frac{\partial q_{wk}}{\partial S_{gm}} + \frac{\partial q_{gk}}{\partial S_{gm}}\Big)\delta S_{gm} + \Big(\frac{\partial q_{wk}}{\partial p_m} + \frac{\partial q_{gk}}{\partial p_m}\Big)\delta p_m \Big] + \Big(\frac{\partial q_{wk}}{\partial p_{wb}} + \frac{\partial q_{gk}}{\partial p_{wb}}\Big)\delta p_{wb} \Big\} = 0 \quad (18)$$

This Equation (18) guarantees that $\Sigma(q_{wk} + q_{gk}) = \bar{q}$ because $q^{\ell}_{wk}$, $q^{\ell}_{gk}$ are calculated using latest iterate values in Equations (14) and $p^{\ell}_{wb}$ from Equation (16). That is, $\Sigma(q^{\ell}_{wk} + q^{\ell}_{gk}) = \bar{q}$. If the well is on deliverability (i.e. $p^{\ell}_{wb}$ from Equation (16) is $\leq \bar{p}_{wb}$), then $\delta p_{wb} = 0$ and Equation (18) is not required.

The implicit well treatment consisting of Equations (17) (and similar equations for $q_{gk}$, $q_{Hk}$) and (18) is extremely difficult to implament due to the derivatives involved. The derivatives $\partial q_{wk}/\partial p_m$, $\partial q_{gk}/\partial S_{gm}$, etc., where $k \neq m$ arise from the wellbore pressure gradient term $\Delta p_{wbk}$ which is $p_{wbk} - p_{wb}$. This term must be obtained by calculating the horizontal flow rates of water and steam phases from each open layer into the well, cumulating these flow rates upward from layers $k > k_t$, downward from layers $k < k_t$, performing an energy balance in each wellbore layer by flashing the total flowing stream to obtain quality, and then calculating density (psi/ft) in each wellbore layer by volumetrically averaging steam and water densities. At a given iteration, this calculation is laborious and iterative in itself.

61

A significant simplification results if we evaluate the term $\Delta p_{wbk}$ in Equations (14) at time level n. This, of course, results in a semi-implicit well treatment and can result in a time step restriction or conditional stability. Using $\Delta p_{wbk,n}$ in Equations (14) and employing an implicit approach to the remaining terms, we have

$$q_{wk} = q^{\ell}_{wk} + \frac{\partial q_{wk}}{\partial T_k}\delta T_k + \frac{\partial q_{wk}}{\partial S_{gk}}\delta S_{gk} + \frac{\partial q_{wk}}{\partial p_k}\delta p_k + \frac{\partial q_{wk}}{\partial p_{wb}}\delta p_{wb} \quad (19)$$

and similar equations for $q_{gk}$, $q_{Hk}$, where $q^{\ell}_{wk}$ and all partial derivatives are evaluated at latest iterate conditions (except for $\Delta p_{wbk,n}$). The impact of taking $\Delta p_{wbk}$ at time level n is that all derivatives of type $\partial Y_k/\partial X_m$ are zero unless $m = k$. Again, the constraint Equation (18) applies (with $\partial Y_k/\partial X_m = 0$ if $m \neq k$) if the well is not on deliverability ($p^{\ell}_{wb} > \bar{p}_{wb}$) and Equation (18) is inactive with $\delta p_{wb} = 0$ if the well is on deliverability ($p^{\ell}_{wb} = \bar{p}_{wb}$).

A further simplification, for the case where the well is not on deliverability, is

$$q_{wk} = q^{\ell}_{wk} + q^{\ell}_k\Big(\frac{\partial f_{wk}}{\partial T_k}\delta T_k + \frac{\partial f_{wk}}{\partial p_k}\delta p_k + \frac{\partial f_{wk}}{\partial S_{gk}}\delta S_{gk}\Big) + \frac{\partial q_{wk}}{\partial p_k}\delta p_k + \frac{\partial q_{wk}}{\partial p_{wb}}\delta p_{wb} \quad (20)$$

where $\partial q_{wk}/\partial p_k$ is simply $a_{wk}$ and $f_{wk}$ is mass fractional flow of water phase from layer k,

$$f_{wk} = a_{wk}/(a_{wk} + a_{gk}) \quad (21)$$

This simplification automatically holds constant over the coming iteration the $q^{\ell}_k$ lbs $H_2O$/day from each layer, as well as the sum $\Sigma(q^{\ell}_{wk} + q^{\ell}_{gk}) = \bar{q}$. This constancy of $q^{\ell}_k$ eliminates the need for terms involving $\delta S_{gk}$, $\delta T_k$ in the constraint Equation (18) and the constraint equation becomes simply

$$\Sigma\left(\frac{\partial q_{wk}}{\partial p_k} + \frac{\partial q_{gk}}{\partial p_k}\right)\delta p_k + \Sigma\left(\frac{\partial q_{wk}}{\partial p_{wb}} + \frac{\partial q_{gk}}{\partial p_{wb}}\right)\delta p_{wb} = 0 \quad (22)$$

or

$$\Sigma(a_{wk} + a_{gk})\delta p_k = [\Sigma(a_{wk} + a_{gk})]\delta p_{wb} \quad (23)$$

Thus the constraint equation involves only pressures and if a single-variable pressure equation is solved in a simulator, then Equation (23) is compatible in that no saturation unknowns appear. We used this latter type of constraint equation four years ago in a black oil coning simulation and found that addition of the $\delta p_{wb}$ unknown considerably improved stability and increased time step size.

If the well is on deliverability, no constraint equation or additional variable $p_{wb}$ is involved and the simplification of evaluating $\Delta p_{wbk}$ at time level n is generally satisfactory in geothermal simulations. The incorporation of terms of type $\partial Y_k/\partial X_m$ where $m \neq k$ in expressions for $q_{wk}$, $q_{gk}$, $q_{Hk}$ or incorporation of the constraint equation is often difficult from a coding point of view. The difficulty is minimized if z-line SOR or vertical-plane block SOR or direct solution is used, but even in these cases the storage and/or computing time requirements for many-well problems can rise appreciably. If the well is on deliverability, then the first simplification of $\Delta p_{wbk,n}$ requires only $\partial Y_k/\partial X_k$ derivatives and no constraint equation applies. Therefore, we use this simplification for the deliverability case.

If the well is not on deliverability, we use a simplification even more explicit than those described above. We express

$$q_{wk} = q^{\ell}_{wk} + q^{\ell}_k\left(\frac{\partial f_{wk}}{\partial T_k}\delta T_k + \frac{\partial f_{wk}}{\partial S_{gk}}\delta S_{gk} + \frac{\partial f_{wk}}{\partial p_k}\delta p_k\right) \quad (24a)$$

$$q_{gk} = q^{\ell}_{gk} + q^{\ell}_k\left(\frac{\partial f_{gk}}{\partial T_k}\delta T_k + \frac{\partial f_{gk}}{\partial S_{gk}}\delta S_{gk} + \frac{\partial f_{gk}}{\partial p_k}\delta p_k\right) \quad (24b)$$

$$q_{Hk} = q^{\ell}_{wk}\left(\frac{\partial H_{wk}}{\partial T_k}\delta T_k + \frac{\partial H_{wk}}{\partial p_k}\delta p_k\right) + q^{\ell}_{gk}\left(\frac{\partial H_{gk}}{\partial T_k}\delta T_k + \frac{\partial H_{gk}}{\partial p_k}\delta p_k\right) + H^{\ell}_{wk}\delta q_{wk} + H^{\ell}_{gk}\delta q_{gk} \quad (24c)$$

where $q^{\ell}_{wk}$ and $q^{\ell}_{gk}$ are computed from Equations (14) using $\Delta p_{wbk,n}$ and $p^{\ell}_{wb}$ from Equation (16). Thus, $\Sigma(q^{\ell}_{wk} + q^{\ell}_{gk}) = \bar{q}$. The derivatives $\partial f_{wk}/\partial T_k$, etc., are evaluated at latest iterate conditions. This simplification runs the risk of pressure instability since no $\partial q_{wk}/\partial p_k = a_{wk}$, etc., terms are used. This instability increases as well productivity index PI increases and as rate $\bar{q}$ decreases. In two-dimensional areal calculations, no such instability exists since there is no pressure allocation among layers. In many three-dimensional and two-dimensional cross-sectional problems, the PI is sufficiently low that the instability is not significant. In many radial-z single-well problems, the instability is severe and we return to implicit procedures.

In radial-z single-well problems, we achieve implicit well treatment by simply incorporating the wellbore in the reservoir grid system. The result of this inclusion is an even more rigorous well treatment than the implicit treatment described in Equations (17) - (18). For inclusion of the wellbore results in transient mass and energy balances applied within the wellbore. Also, reverse flow in any layers from wellbore to the formation is automatically modelled whereas this injection in a producing well is very difficult to account for if the wellbore is not modeled by inclusion in the grid. An apparent disadvantage of wellbore modelling is the very small volume grid blocks giving rise to very large throughput ratios (defined below) for reasonable time step sizes. Our hope at the outset of this work was that the implicit treatment throughout the wellbore and reservoir would eliminate instabilities regardless of very high throughput ratios.

The multiphase flow vertically within or laterally from the column of wellbore grid blocks cannot be modeled by the usual multiphase Darcy flow expressions. The large gas-liquid density difference and high effective vertical "permeability" of the wellbore results in domination by gravity forces even at very high producing rates. This gravity dominance gives low calculated steam saturations in the wellbore resulting in a liquid pressure gradient and high back pressure on the lower formation. At normal rates of geothermal wells, the Reynolds number is so high that assumption of fully developed turbulent flow in the wellbore is usually a good one and assumption of no-slip two-phase flow is an even better one. This no-slip condition is equivalent to volumetric fractional flow equalling saturation.

We programmed this no-slip flow in lieu of usual Darcy flow logic for the wellbore. Alternatively, we could use the Darcy flow logic but calculate wellbore pseudo relative permeabilities which result in volumetric fractional flow $f_g = S_g$. This approach would

require two sets of pseudo relative permeabilities since gravity enters for vertical but not for lateral flow. The vertical wellbore effective permeability used in calculations described below was sufficiently large to hold viscous pressure drops over 500 feet of wellbore to less than 3 psi.

This inclusion of the wellbore in the grid system allows radial-z or r-θ-z simulation of the entire wellbore and overburden from the formation to the surface (wellhead). A problem arises here in altering the no-slip wellbore two-phase flow calculation so that agreement is obtained with two-phase vertical pipe flow correlations. Apart from this problem, the model allows simulation of transient wellbore flow conditions and wellbore heat loss, in addition to the transient multiphase heat and fluid flow in the reservoir. Vertical grid definition in this case would extend from ground surface down to and through the permeable formation.

## EFFECT OF STEAM FLASHING ON WELL DELIVERABILITY

A problem in use of Equations (14) arises even in an areal simulation where NZ = 1, k = 1 and $\Delta p_{wbk} = 0$. The mobilities and specific volumes in Equations (14) are generally evaluated at average (exterior) grid block conditions. If flashing of steam occurs between $r_e$ and $r_w$, then Equations (14) can give considerable error since they do not account for the increasing volumetric flow rate (at constant mass flow rate) toward the well due to water flashing and steam expansion accompanying pressure decline.

Deliverability of a single layer can be corrected to account for water flashing and steam expansion by inserting a fraction f, equal to or less than 1, as

$$q = f(a_w + a_g)(p - p_{wb}) \qquad (25)$$

where, as before, $a_w$ and $a_g$ are evaluated at known block average (exterior) conditions. The factor f is a calculable function of $p_{wb}$, p and $S_{ge}$ where $S_{ge}$ is gas saturation at $r = r_e$, which in turn is generally very close to average grid block saturation. Equation (25) presumes that the average grid block condition is saturated. The Appendix describes the calculation of f and gives a revision of Equation (25) for the case where the saturation point lies between $r_w$ and $r_e$. The calculation of f ignores capillary pressure and assumes steady-state radial flow from pressure p at $r_e$ to pressure $p_{wb}$ at $r_w$.



In addition to $p_{wb}$, p and $S_{ge}$, f is also dependent upon the relative permeability curves.[7] Therefore, a completely general representation of f is not possible. Figure 1 gives f as a function of $p_{wb}$, $p(= p_e)$ and $S_{ge}$ for relative permeability curves

$$k_{rw} = [(S_w - S_{wc})/(1 - S_{wc})]^{n_w} \qquad (26a)$$

$$k_{rg} = k_{rgcw}[(S_g - S_{gc})/(1 - S_{wc} - S_{gc})]^{n_g} \qquad (26b)$$

with $S_{wc} = .2$, $S_{gc} = 0$, $n_w = n_g = 2$ and $k_{rgcw} = .5$.

Figure 1 shows that the deliverability reduction factor is 1 for minimal drawdowns $(p_e - p_{wb})$, decreases with increasing drawdown and, for a given drawdown, it increases with increasing grid block steam saturation, $S_{ge}$. The factor can reach values of .25 or lower for low $S_{ge}$, high drawdown and/or low reservoir pressure $p_e$. This means that deliverabilities calculated using Equation (14) can be erroneously high by a factor of four or more.

### Comparison of Numerical Model and Analytical Deliverabilities

A radial test problem was used to compare the simulator's calculated deliverability with that of Equation (25). This problem was also used as a preliminary test of simulator stability and time-truncation error. Reservoir and fluid property data for this problem are given in Table 1. A 9x1 radial grid was employed with the well producing on deliverability against a wellbore pressure of 160 psia.

In the past, we have performed radial gridding by specifying $r_w$, $r_e$ and an arbitrary first block "center" radius $r_1$. Geometric block center spacing gives $r_i = \alpha r_{i-1}$ where i is r-direction grid block index. Thus, $r_N = \alpha^{N-1} r_1$ and $r_{N+1} = \alpha^N r_1$ where N is the number of radial reservoir grid blocks. Demanding that $r_e$ be the log mean radius between $r_N$ and $r_{N+1}$ gives the equation

$$\frac{\alpha^{N-1}(\alpha - 1) r_1}{\ln \alpha} = r_e \qquad (27)$$

which is solved for $\alpha$ by the Newton-Raphson technique. Generally $r_1$ values of at least 3 feet or more have been used to avoid excessively small grid blocks adjoining the wellbore.

In this work we retain the geometric spacing $r_i = \alpha r_{i-1}$ but eliminate the arbitrary specification of $r_1$. Rather we invoke an imaginary radius $r_0$ within the wellbore in addition to radius $r_{N+1}$ outside $r_e$ and require $r_w$ be the log mean radius of $r_0$ and $r_1$ and $r_e$ be the log mean of $r_N$ and $r_{N+1}$. This gives

$$\frac{(\alpha - 1)r_0}{\ln\alpha} = r_w \qquad (28a)$$

$$\frac{\alpha^N(\alpha - 1)r_0}{\ln\alpha} = r_e \qquad (28b)$$

and division of Equation (28b) by Equation (28a) gives a direct solution for $\alpha$ as

$$\alpha = (r_e/r_w)^{1/N} \qquad (29)$$

Grid block boundary radii used to calculate block pore volumes are calculated as log mean values of adjacent block center radii. Table 1 gives the resulting block center and boundary radii for the case of nine radial increments. The pore volume of the first grid block is 22.27 RB corresponding to 500 feet of formation thickness.

The simulator was run in one-dimensional radial mode using constant 250-day time steps to 16,000 days. Zero capillary pressure was used and the well was on deliverability against the 160 psia flowing bottomhole pressure. The solid curve in Figure 2 shows the calculated flow rates, expressed per-foot of formation thickness, vs. average formation steam saturation. This saturation is close to the exterior grid block 9 saturation, but was calculated as a volume weighted average of all blocks. Figure 2 shows an initial deliverability decline followed by a temporary increase. This behavior was unaffected by time step size, closure tolerances, number of radial blocks and inclusion or exclusion of heat conduction and heat loss in the calculation.

The dotted lines in Figure 2 show deliverability from the steady-state Equation (25) for $p_{wb} = 160$, $p = p_e = 251$. The agreement between model production rate and Equation (25) is good considering that

64

(a) the model used a closed exterior boundary, (b) the model is in a transient decline exhibiting semi-steady-state neither in pressure nor saturation, (c) Equation (25) assumes steady-state with an open exterior boundary. Further, the deliverability factor f varies from .3428 at $S_{ge} = 0$ to .78 at $S_{ge} = .5$ and the discrepancy between the two curves is much less than the error which would occur using Equation (25) with f = 1.

The one-dimensional radial test problem was run to a large time to reach steady-state with an exterior-block well injecting 400°F water at a bottomhole pressure of 251.08 psia at $r = r_e$. Following several time steps to 100 days to allow pressure in grid block 9 to fall below 251 psia (to activate the injection well), two 60,000-day time steps (these steps required 7 and 2 iterations) were taken. The steady-state flow rate calculated was 130,000 lbs $H_2O$/hour. Equation (37) gives for $p_{wb} = 160$, $p_e = 251$ and $S_{ge} = 0$ (corresponding to injection of saturated 100% liquid water),

$$q_{H_2O} = \frac{2\pi k A z_I}{\ln\frac{r_e}{r_w}} = \frac{2\pi(100)(500)(.00633)}{\ln\frac{2000}{.25}} \cdot \frac{12,728}{24}\ \frac{\text{lbs}}{\text{hr}} = 117,349\ \text{lbs/hr}$$

The discrepancy between 130,000 and 117,349 lbs/hour is believed due to the model's upstream weighting of mobilities as opposed to the integration of mobility in Equation (37). In any event, since f = .3428 for $p_e = 251$, $p_{wb} = 160$ and $S_{ge} = 0$, the discrepancy of about 13,000 lbs/hour is small in comparison with the error in using Equation (25) with no correcting f factor. Equations (14) used for an areal grid block of 2,000 feet equivalent exterior radius would give a deliverability of 343,000 lbs/hour. Use of the f factor and Equation (25) would give a calculated deliverability of 117,349 lbs/hour.

## THROUGHPUT RATIO

Evaluation of any term in the interblock flow rates explicitly (at time level n) with respect to any of the dependent variables (p, T, $S_q$) in general will result in a conditional stability. This conditional stability takes the form of an expression giving a maximum time step. Use of a time step size exceeding this maximum will result in divergence of the calculations. The expression for maximum time step generally involves, at least in part, a throughput ratio defined in some manner.

One of the most severe instabilities in multiphase flow simulation is that arising from explicit evaluation of saturation-dependent relative permeabilities in the interblock transmissibilities. The throughput ratio that arises in analysis of this instability is

$$R_{Ti} = \frac{q_i \Delta t}{V_p S_i} \qquad (30)$$

where i denotes phase (e.g., water, gas or oil), $q_i$ is volumetric phase flow rate through the grid block, $S_i$ is grid block saturation of phase i and $V_p$ is grid block pore volume. Thus $R_{Ti}$ is the ratio of total volume of phase i passing through the grid block in one time step divided by the volume of phase i in the block.

Actually, this ratio appears with a multiplier equal to fractional flow derivative, but we are not concerned here with detailed derivations or presentations of stability analysis results. As a practical matter, we have rated the stability of a multiphase flow formulation or model by the cruder ratio

$$R_T = \frac{q_v \Delta t}{V_p} \qquad (31)$$

where $q_v$ is total (all phases) volumetric flow rate through the grid block.

In the geothermal case we can express the above ratio in terms of total mass flow rate of $H_2O$ and quality X of the flowing stream. Many of the results discussed below involve a well producing on deliverability at a flowing bottomhole pressure of 160 psia. Using corresponding water and steam densities of 55 and .355 lbs/cu.ft., respectively, we can express $R_T$ as

$$R_T = 4.27(2.8X + .018)q\Delta t/V_p \qquad (32)$$

where q is total mass flow rate in lbs $H_2O$/hour, $\Delta t$ is time step in days and $V_p$ is reservoir barrels (RB).

Our previous experience with a variety of semi-implicit isothermal and thermal simulators, producing under multiphase flow conditions, has indicated instability or time step restriction at throughput ratios in the range of 1,000 to 20,000. We will return to Equation (32) in connection with results discussed below.

## TIME TRUNCATION ERROR AND STABILITY FOR ONE-DIMENSIONAL RADIAL PROBLEM

Time truncation error and model stability were examined in the one-dimensional radial case by repeating the 16,000-day run described above with time steps of 500, 1,000, 2,000, 4,000, 8,000 and 16,000 days. Table 2 shows the effect of time step size on calculated recovery, producing quality and rate at 4,000, 8,000 and 16,000 days. The time truncation error is quite acceptable for time steps up to 1,000 days.

All these runs converged each time step with two to three iterations per step except for the first step when steam saturation increased from zero to about .45 at the well and 0 - .39 at the 9th block. The first time step required 20-23 iterations, the 23 iterations corresponding to the 16,000-day time step run. The largest throughput ratio occurred for the 16,000-day time step which, from Equation (32), is

$$R_T = 4.27(2.8(.0835) + .018)(67,900)(16,000)/22.27$$
$$= 52.45 \times 10^6$$

This ratio is more than three orders of magnitude larger than the 20,000 ratios of our previous experience mentioned earlier. However, one-dimensional problems are generally poor tests or indicators of true model competence and ratios from two-dimensional results presented below will be given more emphasis.

## TWO-DIMENSIONAL SINGLE-WELL PROBLEM RESULTS

We simulated the radial flow problem described in Table 1 using a two-dimensional 10 x 5 radial-z grid. The five layers were each 100 feet thick. The 10 radial grid blocks included the wellbore. Table 1 gives the grid block center radii, boundary radii and pore volumes calculated using Equation (29). Note that the first reservoir grid block has a center radius of only .40 feet and a pore volume of only 4.45 RB. The pore volume of each wellbore grid block is 3.5 RB so that the throughput ratio, Equation (32), becomes

$$R_T = 1.22(2.8Q + .018)q\Delta t \qquad (33)$$

Rock capillary pressure was assumed negligible in this problem and a pseudo straight-line capillary pressure curve [8, 9] corresponding to layer thickness of 100 feet was employed. Use of saturated steam-water densities at 400°F gives a density difference of .369 psi/foot which translates, for 100-foot layer thickness, to a pseudo capillary pressure equalling 18.45 psi at $S_w = S_{wc} = .2$ and -18.45 at $S_w = 1.0$.

A number of 10,000-day model runs were performed for different well completion intervals. We assumed a tubing/casing configuration so that an additional variable was the layer in which the tubing bottom or withdrawal point was located. For example, with all layers 1-5 perforated, the tubing bottom could be placed in any one of the layers. A packer was assumed placed at top of formation.

A well target rate of 300,000 lbs/hour was specified for all runs with a minimum flowing wellbore pressure at tubing bottom of 160 psia. For all runs, time step was specified as 500 days. Table 3 summarizes model results at 10,000 days. The listed mass fraction produced, producing bottomhole quality, producing rate and produced Btu/lb all apply at the 10,000-day point in time. Average Btu/lb produced is cumulative energy produced over 10,000 days divided by cumulative mass produced. Energy produced is enthalpy, defined as U + pv at producing cell conditions. Internal energy U is relative to a zero value for U of saturated water at 60°F.

Table 3 shows that the location of a single-layer (100 feet) completion is very important. Comparing runs 1-3 shows that cumulative mass fraction recovered at 10,000 days varies from 11.7% to 47.4% as a 100-foot producing interval is lowered from the top 100 feet to the bottom 100 feet of the 500-foot formation.

Runs 4-11 in Table 3 indicate that the perforated or open interval location is important while the location of the tubing bottom or withdrawal point within a given open interval is relatively unimportant. For example, Runs 4 and 5 show about equal recovery values for their top 300 feet open interval regardless of whether the tubing withdrew from the top 100 feet or bottom 100 feet of the interval. Runs 6-7 show the same result for a bottom 300-foot open interval regardless of the tubing position within the open interval. The best recoveries occur for a completely penetrated or open formation -- Runs 9-11 -- and performance is nearly independent of whether the tubing is set at top or bottom of the formation.

In Runs 1-5 the well was on deliverability in the first 500-day time step. Runs 6-7 and 9-11 produced the target 300,000 lbs/hour rate for 1,500 days and Run 8 produced the target rate for 500 days.

Taken together, Runs 1-11 indicate that a partial completion interval effectively drains the portion of the reservoir formation opposite and above the interval, but inefficiently drains the formation below it.

Spatial truncation errors in the results of Table 3 are very small as indicated by several runs we made using a 10 x 10 grid with ten 50-foot thick layers. Time truncation error was examined by repeating Run No. 10 using time steps of 250, 1,000, 2,000 and 5,000 days. Figure 3 shows producing rate and bottomhole producing quality vs. time calculated using the various time steps. The results with $\Delta t = 250$ and $\Delta t = 500$ days are virtually identical. The error with $\Delta t = 1{,}000$ days is significant but not large while $\Delta t = 2{,}000$ days causes an error bordering on acceptability. The surprising feature of these results is the small time truncation error for steps of 1,000 days or less in light of the large changes in saturation which occur in a single step.

The saturation changes stably computed in a single step are illustrated in Table 4 which shows saturations and pressures at the end of the first 2,000-day time step (all layers open, tubing at layer 3). Maximum saturation change was .9989 in grid block (i=1,k=1) and maximum pressure change was -441.4 psi in grid block (i=1,k=5). Initial pressures ranged from 469 to 618 psia from formation top to bottom, some 200 to 350 psi above saturation pressure corresponding to 400°F. That is, the model in this single step proceeded from a highly undersaturated, 100% liquid configuration to that shown in Table 4. Note, also, from Figure 3 that time truncation error for this first time step is virtually negligible. The reader should recall in viewing Table 4 that the first column of cells is the wellbore.

The calculated producing rate for this first 2,000-day step was 286,400 lbs/hour and bottomhole quality was .05794. Using Equation (33), the throughput ratio for withdrawal cell (i=1,k=3) was

$$R_T = 1.22(286,400)(2.8(.05794) + .018)(2,000) = 126 \times 10^6$$

This throughput ratio was achieved with the producing cell steam saturation changing from 0 to .8993. That is, it is not a throughput ratio corresponding to stabilized conditions

with small changes per time step. This ratio is three to four orders of magnitude larger than the 20,000 ratios we have previously achieved with semi-implicit models under high rate-of-change conditions.

Table 5 shows the number of required iterations per time step for each step for the three runs using $\Delta t$ = 500, 1,000 and 2,000 days. The numbers in parentheses in Table 5 are the maximum grid block saturation changes over the grid during each time step.

Table 6 shows calculated pressures and saturations after the first 500-day time step of Run No. 8. Producing rate and quality were 300,000 lbs/hour and .04, respectively, so that the throughput ratio from Equation (33) was

$$R_T = 1.22(300,000)[2.8(.04) + .018](500) = 23.8 \times 10^6$$

This ratio was achieved with a high steam saturation change in the producing cell from 0 to .8481. Required iterations for this first step were 30. The iterations declined to 24 when initial pressure at formation top was reduced to 270 rather than 450 psia. The throughput ratio at 10,000 days for this run was $11.5 \times 10^6$ corresponding to a producing rate and quality of 53,100 lbs/hour and .1208, respectively.

Run 12 in Table 3 is identical to Run 10, except that permeability is 500 md rather than 100 md. The higher permeability resulted in a greater recovery of .7459 compared to .5656 at 10,000 days and gave a considerably higher producing quality of .7058 at 10,000 days. Run 12 produced the target 300,000 lbs/hour rate until 5,000 days. Figure 4 shows the effect of permeability on producing rate and quality vs. mass fraction produced. Producing quality in Figure 4 is calculated at a separator condition of 100 psia. The curves of average reservoir pressure (volumetrically weighted average of all grid blocks) vs. mass fraction produced are not plotted, but are identical for the two runs. Figure 4 shows that produced stream quality at the fixed separator condition is nearly a single-valued function of mass fraction produced and independent of permeability level.

Figure 5 shows average reservoir pressure vs. mass fraction produced calculated for 10,000-day runs using k = 100 and 500 md and $\phi$ = .05 and .35. The figure indicates that permeability level has a negligible effect on average pressure vs. mass fraction produced. The large porosity results in a very slightly lower average reservoir pressure. The small effect is due to the lower rock heat capacity (i.e. less rock) in a higher porosity formation. This small effect of porosity on pressure decline is in contradiction to results reported elsewhere [4].

The average computer time per run for Runs 1-11 was 16 CDC 6600 CPU seconds. For the 10x5 grid and 20 steps per run this translates to .016 seconds per grid block-time step. This figure compares to a rough value of .01 seconds* per grid block-time step for our semi-implicit models.

## SIMULATION OF A FRACTURED-MATRIX RESERVOIR

Many geothermal reservoirs are known or believed to be fractured-matrix systems. Conventional simulation is often used where extensive fractures are known to exist. Such simulation employs an assumption that flow in the matrix-fissure system can be adequately modeled by assuming an unfractured matrix formation with a high effective permeability reflecting the fracture system conductivity.

Here we examine the difference in simulated performances of a fractured reservoir sector modelled first as an unfractured formation, and second as a matrix-fissure system. While nature seldom provides near-uniformity in spacing of fractures, we must employ some semblance of uniform spacing to perform any calculations. We consider a fractured system consisting on the average of 40x40x40 feet matrix blocks separated by a three-dimensional orthogonal planar system of vertical and horizontal fractures.

To reduce the dimensionality of the matrix calculation, we treat the matrix cubes as cylinders of equivalent radius 22.5676 feet ($\pi r^2$ = 40 x 40) and height of 40 feet. We have used this cylindrical approximation for several years in black oil fractured matrix simulation; it is partially justified since the physically real irregularity of fracture spacing and angles undoubtedly yields a variety of matrix block shapes deviating considerably from rectangular parallelepipeds.

Use of a fracture volume equal to 1% of combined fracture plus matrix volume leads to a fracture width of .029 feet. This figure assumes equal widths of horizontal and vertical fractures. From Muskat [10], fracture permeability for width w in cm, is

*This number can vary considerably. For "easy" multiphase flow problems (we omit definitions of "easy" for brevity), we have achieved times as low as .0018 seconds per block-step.

$$k = 10^8 w^2/12 = .6.5 \times 10^6 \text{ Darcies} \quad (14)$$

for the .029 feet width. In simulating flow in fracture grid blocks, it is only necessary to use fracture permeabilities large enough to render viscous forces negligible in comparison with gravitational forces. In previous black oil fractured matrix reservoir work and in this work, we have found results insensitive to use of fracture permeabilities higher than 10 to 20 Darcies.

For the purpose of computations described here, the fracture system conductivity is assumed sufficiently large that the reservoir behavior is dominated by vertical transients in pressure, temperature and saturation. The fracture conductivity is assumed sufficient to maintain negligible areal gradients of these quantities. For example, by this assumption any steam-water contact in the fractures will be nearly rizontal over a wide areal expanse.

The withdrawal rate used for computations was based on a well spacing of about 300 acres with rates of 300,000 lbs $H_2O$/hour per well. This translates to a rate of about 40 lbs/hour for a 1,240-foot vertical column section of the reservoir with areal dimensions 40x40 feet. The vertical gridding consisted of six matrix blocks each subdivided vertically into 10-foot grid blocks and one last deep 1,000-foot matrix grid block. Calculations were terminated before steam-water contacts reached the deep block so that its lack of gridding is immaterial.

In the matrix-fissure simulation, the vertical and horizontal fractures were included in the grid system. Vertically, then, six additional grid blocks each .029 feet thick separated the six matrix blocks and the total number of vertical blocks was 6 x 4 + 6 + 1 or 31. We obtained nearly identical esults using three and two grid blocks adially for the matrix-fissure system. Results given here are for the case of two radial grid blocks. The first radial block was matrix with an inner boundary radius of 0, an outer boundary radius of 22.5676 feet and a "center" radius equal to the volume mean value of 15.96 feet. The second radial grid block was vertical fracture with inner radius of 22.5676 feet and outer radius of 22.5676 + .029/2 feet. Figure 6 illustrates this radial-z grid for the fissure-matrix simulation. Fluid was withdrawn from the bottom 1,000-foot thick vertical fracture block.

Matrix permeability and porosity were 1 md and 0.2, respectively. Grid block pore volumes for the matrix-fissure system illustrated in Figure 6 were

68

| Grid Block | Pore Volume, Res. Bbls. |
|---|---|
| 10-foot matrix | 569.9 |
| .029-foot horizontal fracture radial block #1 | 8.26 |
| .029 x .0145-foot fracture intersection block | .0106 |
| 10-foot vertical fracture | 3.66 |

Initial reservoir pressure was 270 psia at top of formation and temperature was 400°F. Overburden heat loss (gain) had a small effect and was ignored. Heat conduction in the matrix was modeled using a thermal conductivity of 38 Btu/ft-day-°F. Matrix rock heat capacity was 35 Btu/cu.ft. rock-°F. Relative permeabilities of Equations (26) and a linear rock capillary pressure curve of $P_c = 0$ at $S_w = 1$, $P_c = 10$ psi at $S_w = 0$ were used for matrix and zero capillary pressure and linear $k_r = S$ curves were used for the fractures.

The 2 x 31 (radial-z) matrix-fissure simulation was run to 1,500 days for a rate of 40 lbs/hour and to 4,200 days for a rate of 10 lbs/hour. Two runs were made for the 40 lbs/hour rate, the first with a constant 30-day time step, the second with a constant 60-day time step.

Figure 7 shows calculated water saturation vs. depth from top of formation at 1,500 days for the 40 lbs/hour production rate. The solid lines correspond to the 30-day time step while the circles and dashed line show results for the 60-day step. The vertical tic marks indicate water saturations in the first radial horizontal fracture blocks.

This figure shows the poor recovery of water from the matrix blocks due to the capillary discontinuities imposed by the horizontal fractures. Each matrix block above the (vertical fracture) steam-water contact transiently drains toward an equilibrium final saturation vs. depth distribution determined by the rock capillary pressure curve and the zero $P_c$ condition at each matrix block bottom imposed by the horizontal fracture. The significant transient effect is indicated by the decrease in water recovery with matrix block depth. This is due, of course, to the longer times of drainage experienced by higher located matrix blocks.

The horizontal fracture blocks opposite the 100% steam saturated vertical fracture grid blocks rapidly rise toward 100% steam saturation. Above the steam-water contact, the water draining from the bottom of a matrix block enters the horizontal fracture block and then preferentially flows vertically down into the top of the next lower matrix block rather than laterally into the vertical fracture. This preference is very close to 100%. These latter results are shown by model printouts of water and steam interblock flow rate magnitudes and directions at selected times.

Table 7 summarizes average iterations per time step, average saturation change (maximum over grid) per time step and computing times for the three fractured-matrix simulation runs. The negligible time truncation error for 30- and 60-day time steps shown in Figure 7 is somewhat surprising in light of the average saturation change rising from .38 for the 30-day step to .66 for the 60-day step. The .66 figure is actually conservative since 27 vertical fracture grid blocks were swept from 0 to 100% steam saturation in only 25 steps in Run 2. No time steps were repeated due to divergence in any of these runs in spite of nearly 100% saturation changes in one step for the .01 RB pore volume fracture-intersection grid blocks. Both Runs 1 and 2 experienced a number of time steps of 90-100% saturation change. Run No. 1 computing time corresponds to a time per block-step of about .01 seconds.

Figure 8 compares the effect of producing rate on matrix-fissure simulation results. The calculated saturations for Run 1 at 40 lbs/hour and Run 3 at 10 lbs/hour are compared at times of equal cumulative production. The steam-water contact for the higher rate is 40% (140 feet vs. 101 feet) deeper due to the shorter time available for transient water drainage from the matrix blocks above the contact.

Conventional simulation results were generated by running the model in one-dimensional vertical mode using 24 10-foot blocks and one 1,000-foot block. The dashed line in Figure 9 shows resulting calculated water saturation vs. depth at 1,500 days for an "effective" permeability of 50 md and a producing rate of 40 lbs/hour. Gravity forces dominate and the conventional results show a sharp transition zone from a drained ($S_w=S_{wc}=.2$) upper region to the 100% water zone. The transition zone is considerably higher than the matrix-fissure simulation results viewing either the matrix or the vertical fracture steam-water contact.



We can achieve somewhat greater realism in the conventional simulation by utilizing the fact that the capillary discontinuities each 40 feet impose a maximum final recovery of water (by flow alone) which can be predetermined using the rock capillary pressure curve, the 40-foot matrix block height and the .369 psi/foot water-steam density (gradient) difference. Following Reference [8] we integrate the $S_w - P_c$ relation over the 40 feet using the fact that $P_c = 0$ at matrix block bottom and find that final minimum average matrix block water saturation is .417. Using this value for $S_{wc}$ in the relative permeability equations, the conventional simulation gives the water saturation profile indicated by the larger dashed line in Figure 9.

Further adjustments in various data might be made to narrow the difference between matrix-fissure and conventional simulation results. Considering the basic difference in mechanisms for the conventional and more correct matrix-fissure calculations, we hold little hope for forcing accuracy from a conventional simulation. In particular, the above described rate effect (Figure 8) is shown by the more rigorous matrix-fissure simulation, but not by conventional simulation (unless the permeability used is very low).

A full three-dimensional simulation of a fractured-matrix reservoir will require tying in this vertical two-dimensional R-Z matrix-fissure calculation to a two-dimensional areal calculation where the areal blocks communicate through the fracture system and the interblock flows reflect the different "sector" or areal block steam-water contacts. This task will involve a significant effort in logic and coding and will in many cases require disking on fixed memory machines. The two-dimensional R-Z matrix-fissure calculation described here is adequate only if the areal gradients within the reservoir are assumed small due to high fracture conductivity.

## Interpretation of Pressure Drawdown Tests

The major differences between conventional and matrix-fissure simulation results just described arose because of the two-phase flow in a system having capillary discontinuities. Here we illustrate difficulties which can arise in using conventional simulation to interpret pressure drawdown tests in fractured-matrix, hot water systems with single-phase water flow.

Simulation of a well test in a system having a three-dimensional network of orthogonal fracture planes would require a full three-dimensional Cartesian grid. To simplify for the purpose of illustration, we consider a system of 44-foot matrix layers separated by horizontal fractures. A 10x5 radial-z grid was used to model a horizontal disk of matrix beneath a horizontal fracture. The disk dimensions were exterior radius $r_e$ = 10,000 feet and thickness = 22 feet. The five layer thicknesses were w/2, 2, 4, 8, 8 feet where w is horizontal fracture thickness. This disk is a symmetrical element for the case where the well penetrates the entire formation thickness.

The radial spacing was calculated using Equation (29) with the wellbore included in the grid. Wellbore radius was .25 and the 10 block "center" radii were .25, .43, 1.38, 4.48, 14.55, . . ., 5,242.37 feet. Pore volumes of the wellbore cells varied from .0...014 to .2798 RB in layers 1-5 for a small fracture width w = .245 mm.

Matrix and fracture layer porosities were .2 and 1.0, respectively. Initial temperature was uniformly 350°F and initial pressure was 2800 psia at top of formation. The illustrative pressure drawdown test consisted of producing 10,000 lbs/hour from a well open in all five layers for ten days. Fracture conductivity and matrix permeability were varied in five simulation runs as tabulated in Figure 10. The fracture permeabilities were related to fracture width by the relationship $k = 10^8 w^2/12$ where k is in Darcies and w in cm. The homogeneous (no fracture) case, Run 4, has a permeability of 90.9 md, which gives a total md-ft product for the 22-foot thickness equal to that of the fracture cases.

Figure 10 shows calculated pressure drawdown (initial pressure-flowing wellbore pressure) vs. time on a semi-log plot for five cases. The homogeneous case (Run 4) gives a straight-line and use of the well-known relationship, slope = $Qu/4\pi kh$, gives k = 90.9 md, in agreement with the value used. Arbitrary use of the average slope from .1 to 1 days with the relation slope = $Qu/4\pi kh$ gives k = 247, 188 and 157 md for Runs 1-3, respectively. These permeabilities bear little resemblance to either fracture or matrix permeabilities.

The semi-log plots of pressure drawdown vs. time actually are not linear for the fracture cases, but are rather concave upward. This results from the fact that the reservoir transient is primarily a crossflow (vertical) bleeding of fluid into the fracture rather than the radial transient of a homogeneous unfractured formation. The degree of upward curvature of the drawdown curve increases as matrix permeability decreases.

710

The cases of small fracture width, Runs 1-3, exhibit a rapid initial drawdown of 60-80 psia in the first few minutes of flow. The calculated effect of a fivefold larger fracture width is one of reducing this early drawdown to 2-3 psi. However, for times after the first few minutes, the larger fracture gives a calculated, concave upward drawdown curve of shape virtually identical to that for the smaller fracture. This is illustrated by the curves for Runs 1 and 5 in Figure 10.

Figure 11 shows calculated drawdowns for a tenfold larger horizontal fracture spacing of 440 feet. The simulations used a 10 x 8 grid with the eight layer thicknesses equal to .0004, 2, 4, 8, 16, 32, 64 and 94 feet (a total thickness of 220 feet). The kw product for the total fracture width of .0008 feet (.245 mm) is 4 Darcy-feet. A drawdown test flow rate of 100,000 lbs/hour was specified. The curve for this Run 6 in Figure 11 shows a linearity of drawdown vs. ln(t) past 10 days to about 30 days. The upward concave curve shape from 100 to 1,000 days is due to establishment of semi-steady-state conditions throughout the reservoir.

The curve labeled Run 7 in Figure 11 was calculated for a 220-foot homogeneous reservoir with k = 9.09 md corresponding to an equivalent total md-feet product of 2,000. The slopes of the curves for Runs 6 and 7 on Figure 11 give formation permeabilities of 18 md and 9.09 md, respectively. If the 10-day test portion of the Run 6 curve were analyzed by conventional radial flow theory, then a permeability of 18 md and a skin factor of 9.65 would be determined. The circles of Run 8 in Figure 11 show the simulator results for a homogeneous reservoir with this permeability and skin factor. Figure 11 shows that calculated drawdowns for the fractured formation (Run 6) and for an 18 md, homogeneous formation with skin (Run 8) agree well through 1,000 days.

These results of Figure 11 indicate that for the particular fracture spacing and width of 440 feet and .245 mm, respectively, conventional radial flow analysis would (a) yield erroneous permeability and skin but (b) give accurate long-term deliverability predictions. This conclusion does not hold for the previously discussed results of Figure 10 corresponding to the smaller fracture spacing of 44 feet. For this spacing, the short-term drawdown test can fail to yield any linearity from which conventional analysis can determine effective permeability and skin.

Several additional complexities that may exist in practice need mentioning in connection with the results just discussed. A naturally fractured formation will generally have vertical as well as horizontal fractures. Accounting for a three-dimensional network of fracture planes with the model

described herein would require a three-dimensional simulation. If fracture spacing were the order of 100 feet or less, a very large number of grid blocks would be required. A better modelling approach in this case would be a dual porosity formulation where interblock flow is assumed to occur only in the fracture system. The matrix would be accounted for by zero-dimensional, one-dimensional spherical or two-dimensional cylindrical subcalculations tied into the fracture porosity in each grid block. The heat-loss calculation described in Reference [3] is an example of this type of formulation.

The model described here may apply well to an artificially fractured formation since in this case the vertical fractures will intersect the well. An r-θ-z grid representing a symmetrical element in this case may accurately model well performance with a reasonably low number of grid blocks.

An upward concave deviation from linearity in a drawdown test curve may result from factors other than formation fractures. Geothermal reservoirs with brines of high salinity may precipitate salt with pressure drawdown near the well. This can cause a skin factor increasing with time and the mentioned deviation from linearity. It is well-known that faults or other flow barriers near a well can cause upward curvature. Short-term drawdown tests on wells which partially penetrate thick formations, especially where the ratio of vertical to horizontal permeability is small, can result in deviation from linearity. Regardless of penetration, a formation consisting of alternating tight and permeable streaks of large permeability contrast can yield deviation from linearity through the same vertical, crossflow type of transient treated above in the horizontally fractured formation calculations. Quoting from Reference [11], which treated simulation of single-phase gas flow, ". . . The reservoir picture finally employed with success stemmed from the hypothesis that the well communicated with a number of thin permeable stringers . . . fed by severely limited crossflow from large sand volumes. . . .". In that work, for such reservoirs, the calculated and observed drawdown/buildup curves failed to yield the linearity of conventional analysis.

Finally, the fractured formation, drawdown test illustrative calculations and interpretations presented here are not unique to geothermal reservoirs, but apply to any formation subject to single-phase flow of a low compressibility fluid -- oil, water or high pressure gas.

## 71 HEAT EXTRACTION FROM HOT DRY ROCK

We consider a vertical fracture in a hot dry rock initially at 500°F. A 5x5x5 three-dimensional grid describes a rectangular parallelepiped with $\Delta x = \Delta z = 80$ feet and $\Delta y = .01$, 30, 120, 160, 320. These dimensions resulted from combining blocks in a comparison run which used y-direction increments of .01, 10, 20, 40, 80, 160 and 320 feet. The overall dimensions are a 400x400-foot vertical crack of .02-foot width with 630 feet of rock either side of it. The 630 feet of rock in the y-direction is sufficiently large that the system acts as infinite for the 3,000 days of simulation. Different grids were used to determine the acceptably low spatial truncation error of the 5x5x5 grid.

Since the system is symmetrical about the vertical midplane of the crack, this 5x5x5 grid represents half the system. Crack width is of no consequence except in its relation to the kw product where k is fracture permeability and w is fracture total width. In the grid plane j = 1 (the crack) an x-z thermal conductivity of 3.8 Btu/ft-day-°F was used, porosity was 1.0 and permeability was varied over a number of runs from 10 Darcies to 800,000 Darcies. In the planes, j = 2-5 (hard rock) thermal conductivity was 38 Btu/ft-day-°F, rock specific heat was 35 Btu/cu.ft.rock-°F and porosity and permeability were zero.

100°F cold water injection rate was specified as 25,000 lbs/hour into the bottom left corner of the crack (cell i=1,j=1,k=5). A withdrawal well at the upper right corner of the crack (cell i=5,j=1,k=1) maintained pressure at 800 psia due to a large specified productivity index. This withdrawal well produced on deliverability against the 800 psia pressure. The 25,000 lbs/hour injection rate corresponds to actual injection well rate of 50,000 lbs/hour since the grid represents a symmetrical half of the total system.

Figure 12 shows calculated energy recovery and producing well bottomhole temperature vs. time. Energy recovery is defined as cumulative enthalpy produced divided by the sensible heat above 100°F initially contained in a portion of the rock. The portion used is the first 310 feet since the last 320 feet experienced essentially no recovery (temperature decline) at 3,000 days. The initial energy in place on these bases is $6.944 \times 10^{11}$ Btu. Enthalpy of produced water is U + pv where internal energy U is zero at 100°F.

Figure 12 shows a rapid decline of produced water temperature from 500°F to less than 300°F in the first few days followed by a very flat decline from 170°F to 137°F from 1,000 to 3,000 days. Fractional energy recovery is 0.1663 at 3,000 days, equivalent to $1.155 \times 10^{11}$ Btu or an average of 64 Btu/lb water produced (enthalpy relative to zero U at 100°F). The average temperature corresponding to this average enthalpy is about 162°F.

The fracture width w controls system conductivity or throughput. The corresponding parameter or group of importance is the kw Darcy-feet product, which is proportional to $w^3$ since fracture permeability is proportional to $w^2$. We used permeabilities up to 800,000 Darcies with the .02-foot model dimension for the fracture. This 16,000 Darcy-foot kw product corresponds to a fracture width of 4 mm using the fracture permeability equation $k = 10^8 w^2/12$ (w in cm). Fracture width, i.e. the kw product, had no effect on the calculated recovery and temperature shown in Figure 12.

Model runs were made with the injection well located higher, 200 feet from top of formation in cell i=1,j=1,k=3. The change of injection location had no effect on calculated recovery and producing temperature.

Figure 12 also shows calculated recovery and temperature for a larger fracture of dimension 800x800 feet. Again, the above described kw product and injection well location variations had no effect on the calculated recovery and producing temperature. The larger fracture resulted in a considerably higher bottomhole producing temperature vs. time and a lower fractional energy recovery. Calculated absolute energy recovery at 3,000 days was higher for the larger fracture -- $3.53 \times 10^{11}$ Btu vs. $1.155 \times 10^{11}$ Btu for the 400x400 foot fracture. Thus, a fourfold increase in fracture area caused a threefold increase in energy recovery. Average enthalpy of produced water was 196 Btu/lb corresponding to an average temperature of produced water of 292°F.

The runs were performed using automatic time step control due to the rapid initial transients. With a first time step of .1 days, a subsequent minimum $\Delta t$ of .2 days, control by 150°F maximum grid block temperature change per time step and a maximum time step of 500 days, the model took 13 time steps to 3,000 days for the 100,000 Darcy permeability. Computer time for this run was 46 CDC 6600 CPU seconds. Twenty of these seconds were required for the first two time steps.

72

Calculated results for permeabilities less than 100,000 Darcies exhibited no circulatory "free" convection type cells in the vertical fracture plane. Table 8 shows an example of these results at 3,000 days for the case of a 400x400 foot fracture, and 100,000 Darcies fracture permeability which corresponds to a 2 mm fracture width. The table shows calculated pressures in the fracture plane, temperatures in all planes and interblock flow rates (positive to the right and vertically downward). Water flow is uniformly to the right and upwards away from the injection in grid cell i=1,j=1,k=5. Temperature uniformly increases to the right and upward (in the directions of water flow) except in the top row.

Results for the 800,000 Darcy permeability differed markedly from those just described. Table 9 shows pressure, temperature and flow rate distributions at 75 days for the 800x800 foot fracture with 800,000 Darcies. y-direction spacing was altered in this run to .01, 10, 30, 50, 180 feet. The flow rates in Table 9 show extremely strong "free" convection cells in the 5x5 grid of the vertical fracture plane. Water is in fact flowing downward into the injecting cell i=1,j=1,k=5. The flow distribution is complex and the temperature change from left to right alternates in sign in alternate rows corresponding to alternation in direction of horizontal flow rate.

Table 10 shows pressure, temperature and flow rate distributions for this 800,000 Darcy case at 3,000 days. While the flow rates are much more uniform with flow uniformly upward, the free convection still exists with some horizontal flow from right to left. Deviations from a pattern of uniform temperature increase to the right and upward are small but exist and are complex. This 800,000 Darcy run was much more difficult than the runs for 100,000 or fewer Darcies. The number of time steps increased to 21 and computer time increased to 144 CDC 6600 CPU seconds, largely due to divergence and repeat of one of the time steps.

These fractured hot rock simulations did not employ any enhanced heat conduction to the fracture due to thermal cracking induced by temperature decrease. A functional relationship between thermal conductivity and temperature or temperature change can be included in the model. Such a relationship and associated parameters might be deduced from laboratory or field experimental data.

## SUMMARY

An implicit, three-dimensional geothermal model is described and partially evaluated in respect to stability or time step tolerance. The model is only partly implicit in certain applications where various terms associated with allocation of well rates among open layers are treated explicitly.

The implicit model stably accommodated time steps corresponding to 80-100% saturation change in a grid block and throughput ratios the order of $10^8$ in several illustrative multiphase flow problems. This compares with our experience of limits of 3-10% saturation change and throughput ratio of roughly 20,000 with semi-implicit geothermal and oil reservoir models. The implicit model stability allowed inclusion of fractures and wellbores as small-volume grid blocks in several multiphase flow test problems.

An analytical derivation is presented for a well deliverability reduction factor which can be used in simulations using large grid blocks. The factor accounts for increased pressure drop near the well due to hot water flashing and steam expansion.

The model was used to simulate two-phase depletion of a fractured matrix reservoir with horizontal and vertical fractures included as grid blocks. The results were poorly matched by conventional simulation which treats the reservoir as an unfractured formation with high effective permeability.

Simulation of a single-phase flow, pressure drawdown test in a tight formation with horizontal fractures showed upward concave curvature of the pressure drawdown vs. ln(t) plot. The degree of calculated curvature and attendant interpretation difficulty increased with decreasing matrix permeability level and decreasing horizontal fracture spacing.

The final illustrative application treated heat extraction from a fractured, hot dry rock system. For a given cold water injection rate, the calculated energy recovery and production well water temperature vs. time were not affected by fracture permeability-width product or injection well location. The fracture conductance was varied from 2 to 16,000 Darcy-ft, while injection well location was varied only from the bottom corner to the mid-depth of the fracture plane. A fourfold increase in fracture area from 400x400 to 800x800 square feet resulted in a threefold increase in calculated energy recovery at 3,000 days for the same cold water injection rate.

A limited investigation of time truncation error indicates that acceptably low levels can occur in spite of average maximum (over grid) saturation changes per time step as high as 60%.


## NOMENCLATURE

| | |
|---|---|
| $A$ | cross-sectional area normal to flow, $ft^2$ |
| $c$ | compressibility, 1/psi |
| $C_p$ | specific heat, Btu/lb-°F |
| $(\rho C_p)_R$ | rock specific heat, Btu/cu.ft rock-°F |
| $f_w$ | water phase volumetric fractional flow |
| $f_g$ | gas phase volumetric fractional flow |
| $f$ | well deliverability factor, fraction |
| $H$ | enthalpy, U + pv, Btu/lb |
| $k$ | absolute permeability, md |
| $k_r$ | relative permeability, fraction |
| $k_{rgcw}$ | relative permeability to gas at irreducible water saturation $S_{wc}$ |
| $K$ | thermal conductivity, Btu/ft-day-°F |
| $N_x, N_y, N_z$ | numbers of grid blocks in reservoir grid system, in x, y, z directions, respectively |
| $\bar{q}$ | desired or target production rate, lbs $H_2O$/day |
| $q$ | production rate, lbs $H_2O$/day |
| $q_H$ | enthalpy production rate, Btu/day |
| $q_{HL}$ | heat loss rate, Btu/day |
| $p_s(T)$ | water vapor pressure |
| $p$ | gas phase pressure, psia |
| $p_{wb}$ | wellbore flowing pressure, psia |
| $p_c$ | capillary pressure, $p_g - p_w$, psi |
| $R_T$ | throughput ratio, Equation (31) |
| $r$ | radius, feet |

Figure 12 shows a rapid decline of produced water temperature from 500°F to less than 300°F in the first few days followed by a very flat decline from 170°F to 137°F from 1,000 to 3,000 days. Fractional energy recovery is 0.166 at 3,000 days, equivalent to $1.155 \times 10^{11}$ Btu or an average of 64 Btu/lb water produced (enthalpy relative to zero U at 100°F). The average temperature corresponding to this average enthalpy is about 162°F.

The fracture width w controls system conductivity or throughput. The corresponding parameter or group of importance is the kw Darcy-feet product, which is proportional to $w^3$ since fracture permeability is proportional to $w^2$. We used permeabilities up to 800,000 Darcies with the .02-foot model dimension for the fracture. This 16,000 Darcy-foot kw product corresponds to a fracture width of 4 mm using the fracture permeability equation $k = 10^8 w^2/12$ (w in cm). Fracture width, i.e. the kw product, had no effect on the calculated recovery and temperature shown in Figure 12.

Model runs were made with the injection well located higher, 200 feet from top of formation in cell i=1,j=1,k=3. The change of injection location had no effect on calculated recovery and producing temperature.

Figure 12 also shows calculated recovery and temperature for a larger fracture of dimension 800x800 feet. Again, the above described kw product and injection well location variations had no effect on the calculated recovery and producing temperature. The larger fracture resulted in a considerably higher bottomhole producing temperature vs. time and a lower fractional energy recovery. Calculated absolute energy recovery at 3,000 days was higher for the larger fracture -- $3.53 \times 10^{11}$ Btu vs. $1.155 \times 10^{11}$ Btu for the 400x400 foot fracture. Thus, a fourfold increase in fracture area caused a threefold increase in energy recovery. Average enthalpy of produced water was 196 Btu/lb corresponding to an average temperature of produced water of 292°F.

The runs were performed using automatic time step control due to the rapid initial transients. With a first time step of .1 days, a subsequent minimum $\Delta t$ of .2 days, control by 150°F maximum grid block temperature change per time step and a maximum time step of 500 days, the model took 13 time steps to 3,000 days for the 100,000 Darcy permeability. Computer time for this run was 46 CDC 6600 CPU seconds. Twenty of these seconds were required for the first two time steps.

74

Calculated results for permeabilities less than 100,000 Darcies exhibited no circulatory "free" convection type cells in the vertical fracture plane. Table 8 shows an example of these results at 3,000 days for the case of a 400x400 foot fracture, and 100,000 Darcies fracture permeability which corresponds to a 2 mm fracture width. The table shows calculated pressures in the fracture plane, temperatures in all planes and interblock flow rates (positive to the right and vertically downward). Water flow is uniformly to the right and upwards away from the injection in grid cell i=1,j=1,k=5. Temperature uniformly increases to the right and upward (in the directions of water flow) except in the top row.

Results for the 800,000 Darcy permeability differed markedly from those just described. Table 9 shows pressure, temperature and flow rate distributions at 75 days for the 800x800 foot fracture with 800,000 Darcies. y-direction spacing was altered in this run to .01, 10, 30, 50, 180 feet. The flow rates in Table 9 show extremely strong "free" convection cells in the 5x5 grid of the vertical fracture plane. Water is in fact flowing downward into the injecting cell i=1,j=1,k=5. The flow distribution is complex and the temperature change from left to right alternates in sign in alternate rows corresponding to alternation in direction of horizontal flow rate.

Table 10 shows pressure, temperature and flow rate distributions for this 800,000 Darcy case at 3,000 days. While the flow rates are much more uniform with flow uniformly upward, the free convection still exists with some horizontal flow from right to left. Deviations from a pattern of uniform temperature increase to the right and upward are small but exist and are complex. This 800,000 Darcy run was much more difficult than the runs for 100,000 or fewer Darcies. The number of time steps increased to 21 and computer time increased to 144 CDC 6600 CPU seconds, largely due to divergence and repeat of one of the time steps.

These fractured hot rock simulations did not employ any enhanced heat conduction to the fracture due to thermal cracking induced by temperature decrease. A functional relationship between thermal conductivity and temperature or temperature change can be included in the model. Such a relationship and associated parameters might be deduced from laboratory or field experimental data.

## SUMMARY

An implicit, three-dimensional geothermal model is described and partially evaluated in respect to stability or time step tolerance. The model is only partly implicit in certain applications where various terms associated with allocation of well rates among open layers are treated explicitly.

The implicit model stably accommodated time steps corresponding to 80-100% saturation change in a grid block and throughput ratios the order of $10^8$ in several illustrative multiphase flow problems. This compares with our experience of limits of 3-10% saturation change and throughput ratio of roughly 20,000 with semi-implicit geothermal and oil reservoir models. The implicit model stability allowed inclusion of fractures and wellbores as small-volume grid blocks in several multiphase flow test problems.

An analytical derivation is presented for a well deliverability reduction factor which can be used in simulations using large grid blocks. The factor accounts for increased pressure drop near the well due to hot water flashing and steam expansion.

The model was used to simulate two-phase depletion of a fractured matrix reservoir with horizontal and vertical fractures included as grid blocks. The results were poorly matched by conventional simulation which treats the reservoir as an unfractured formation with high effective permeability.

Simulation of a single-phase flow, pressure drawdown test in a tight formation with horizontal fractures showed upward concave curvature of the pressure drawdown vs. ln(t) plot. The degree of calculated curvature and attendant interpretation difficulty increased with decreasing matrix permeability level and decreasing horizontal fracture spacing.

The final illustrative application treated heat extraction from a fractured, hot dry rock system. For a given cold water injection rate, the calculated energy recovery and production well water temperature vs. time were not affected by fracture permeability-width product or injection well location. The fracture conductance was varied from 2 to 16,000 Darcy-ft, while injection well location was varied only from the bottom corner to the mid-depth of the fracture plane. A fourfold increase in fracture area from 400x400 to 800x800 square feet resulted in a threefold increase in calculated energy recovery at 3,000 days for the same cold water injection rate.

A limited investigation of time truncation error indicates that acceptably low levels can occur in spite of average maximum (over grid) saturation changes per time step as high as 60%.


## NOMENCLATURE

| | |
|---|---|
| $A$ | cross-sectional area normal to flow, $ft^2$ |
| $c$ | compressibility, 1/psi |
| $C_p$ | specific heat, Btu/lb-°F |
| $(\rho C_p)_R$ | rock specific heat, Btu/cu.ft rock-°F |
| $f_w$ | water phase volumetric fractional flow |
| $f_g$ | gas phase volumetric fractional flow |
| $f$ | well deliverability factor, fraction |
| $H$ | enthalpy, $U + pv$, Btu/lb |
| $k$ | absolute permeability, md |
| $k_r$ | relative permeability, fraction |
| $k_{rgcw}$ | relative permeability to gas at irreducible water saturation $S_{wc}$ |
| $K$ | thermal conductivity, Btu/ft-day-°F |
| $N_x, N_y, N_z$ | numbers of grid blocks in reservoir grid system, in x, y, z directions, respectively |
| $\bar{q}$ | desired or target production rate, lbs $H_2O$/day |
| $q$ | production rate, lbs $H_2O$/day |
| $q_H$ | enthalpy production rate, Btu/day |
| $q_{HL}$ | heat loss rate, Btu/day |
| $p_s(T)$ | water vapor pressure |
| $p$ | gas phase pressure, psia |
| $p_{wb}$ | wellbore flowing pressure, psia |
| $p_c$ | capillary pressure, $p_g - p_w$, psi |
| $R_T$ | throughput ratio, Equation (31) |
| $r$ | radius, feet |

| | |
|---|---|
| $r_e$ | exterior radius |
| $r_w$ | wellbore radius |
| RB | Reservoir Barrels |
| S | skin factor |
| $S_w$ | water phase saturation, fraction |
| $S_g$ | gas phase saturation, fraction |
| $S_{ge}$ | gas saturation at $r = r_e$ |
| $S_{wc}$ | irreducible water saturation |
| $S_{gc}$ | critical gas saturation |
| t | time, days |
| $\Delta t$ | time step, $t_{n+1} - t_n$, days |
| T | temperature, °F |
| | water saturation temperature, $T_s(p)$, °F |
| U | internal energy, Btu/lb |
| $V_p$ | grid block pore volume, $V\phi$ |
| V | grid block bulk volume, $\Delta x\Delta y\Delta z$, cubic feet |
| v | specific volume, cu.ft/lb |
| w | fraction width |
| X | quality, mass fraction steam |
| x,y,z | Cartesian coordinates, feet, z measured positively vertically downward |
| $\Delta x, \Delta y, \Delta z$ | grid block dimensions, feet |

GREEK

| | |
|---|---|
| $\bar{\delta}$ | time difference operator, $\bar{\delta}X \equiv X_{n+1} - X_n$ |
| $\delta$ | iteration difference operator, $\delta X \equiv X^{\ell+1} - X^{\ell}$ |
| $\phi$ | porosity, fraction |
| $\rho$ | density, lbs/cu.ft |
| $\gamma$ | specific weight or gradient, psi/ft ($\gamma_w = \rho_w/144$) |
| $\lambda$ | mobility, $k_r/\mu$ |

| | |
|---|---|
| $T_c$ | reservoir heat conduction transmissibility $KA/\ell$, where $\ell$ = distance between grid block centers, Btu/day-°F |
| $T_g$ | gas phase transmissibility, $(kA/\ell)(k_{rg}\rho_g/\mu_g) \times .00633$, lbs gas phase/day-psi |
| $T_w$ | water phase transmissibility, $(kA/\ell)(k_{rw}\rho_w/\mu_w) \times .00633$, lbs water phase/day-psi |
| $\Delta(T\Delta P)$ | $= \Delta_x(T_x\Delta_x P) + \Delta_y(T_y\Delta_y P) + \Delta_z(T_z\Delta_z P)$, defined as indicated above Equation (5) |
| $\mu$ | viscosity, cp |

SUBSCRIPTS

| | |
|---|---|
| e | exterior |
| g | gas (steam) phase |
| i,j,k | grid block indices, $x_i, y_j, z_k$ |
| k | grid layer number or index |
| $\ell$ | (superscript) iteration number |
| n | time level, $t_n$ |
| s | saturation condition |
| x,y,z | denotes x, y or z direction, respectively |
| w | water phase |
| wb | wellbore |

## REFERENCES


1. Coats, K. H., and Ramesh, A. B., "Numerical Modeling of Thermal Reservoir Behavior", Preprint presented at the 28th Annual Technical Meeting of the Petroleum Society of C.I.M., Edmonton, Alberta, May 27-June 6, 1977.

2. Carter, R. D., and Tracy, G. W., "An Improved Method for Calculating Water Influx", Trans. AIME (1960), 219, 415-417.

3. Coats, K. H., George, W. D., Chu, Chieh, and Marcum, B. E., "Three-Dimensional Simulation of Steamflooding", Trans. AIME (1974), 257, 573.

4. Toronyi, R. M., and Ali, S. M. Farouq, "Two-Phase, Two-Dimensional Simulation of a Geothermal Reservoir", Soc. Pet. Eng. J. (June, 1977), 171-183.

5. Blair, P. M., and Weinaug, C. F., "Solution of Two-Phase Flow Problems Using Implicit Difference Equations", Trans. AIME (1969), 246, 417.

6. Price, H. S., and Coats, K. H., "Direct Method in Reservoir Simulation", Trans. AIME (1974), 257, 295.

7. Steam Tables, Keenan, J. H., and Keyes, F. G., Hill, P. G., and Moore, J. G., John Wiley & Sons, 1969.

8. Coats, K. H., Nielsen, R. L., Terhune, M. H., and Weber, A. G., "Simulation of Three-Dimensional Two-Phase Flow in Oil and Gas Reservoirs", Soc. Pet. Eng. J. (December, 1967), 377-388.

9. Coats, K. H., Dempsey, J. R., and Henderson, J. H., "The Use of Vertical Equilibrium in Two-Dimensional Simulation of Three-Dimensional Reservoir Performance", Trans. AIME (1971), 251, 63-71.

10. Flow of Homogeneous Fluids, Muskat, M., J. W. Edwards, Ann Arbor, Michigan, 1946.

11. Coats, K. H., Dempsey, J. R., Ancell, K. L., and Gibbs, D. E., "Analysis and Prediction of Gas Well Performance", SPE 3474 presented at 46th Annual Meeting of SPE, New Orleans, Louisiana, October 3-6, 1971.

## APPENDIX

## CALCULATION OF DELIVERABILITY FACTOR f

We consider two-phase, steady-state steam-water flow from some exterior radius R to wellbore radius $r_w$. The point R is assumed to be saturated, and pressure is P at R and $p_{wb}$ at $r_w$.

Darcy's law gives liquid water phase flow rate at any radius as

$$q_w = q(1 - X) = -2\pi k\Delta z \lambda_w \rho_w r dp/dr \quad (35)$$

where X is flowing steam quality, q is total flow rate, lbs $H_2O$/day, $k\Delta z$ is md-ft product x .00633, $\lambda_w$ is $k_{rw}/\mu_w$ and $\rho_w$ is water density in lbs/cu.ft. Integration using the fact that q is constant gives

$$q = \frac{2\pi k\Delta z}{\ln\frac{R}{r_w}} \int_{p_{wb}}^{P} \frac{\lambda_w \rho_w}{1-X} dp \quad (36)$$

or

$$q = \frac{2\pi k\Delta z}{\ln\frac{R}{r_w}} I(P, p_{wb}, S_g) \quad (37)$$

where the integral I is a function only of the integration limits $p_{wb}$, P and of steam saturation $S_g$ at R because, as we will now show, the integrand $\lambda_w \rho_w/(1-X)$ is a single-valued calculable function of pressure p.

Flowing quality X is related to fractional flow by

$$X = 1/(1 + f_w \rho_w/(1-f_w)\rho_g) \quad (38)$$

and enthalpy per lb of flowing stream is

$$H = XH_g + (1 - X)H_w \quad (39)$$

At steady-state, flowing stream enthalpy is constant and from (39),

$$X = (H-H_w)/(H_g-H_w) = X(p), \quad (40)$$

where the dependence upon pressure alone follows from the fact that H is constant and saturated water and steam enthalpies are single-valued functions of pressure. From Equation (38),

$$f_w = 1/[1 + X\rho_w/(1 - X)\rho_g] = f_w(p) \quad (41)$$

where the dependence upon pressure alone follows from the fact that saturated water and steam densities are single-valued functions of pressure.

If p and $S_g$ at R are given, then enthalpy H can be calculated from Equations (38) and (39). Given H, we can calculate the values of X(p) and $f_w(p)$ at any pressure from Equations (40) and (41). Thus, the integral in Equation (36) can be numerically integrated for any given values of P, $p_{wb}$ and $S_g$.

We now consider a grid block of large dimensions, $\Delta x * \Delta y$, with equivalent exterior radius $r_e$ determined by $\pi r_e^2 = \Delta x \Delta y$. Assuming steady-state single-phase water flow from an undersaturated condition at $r_e$ to saturation point R, Darcy's law gives

$$q = \frac{2\pi k \Delta z}{\ln \frac{r_e}{R}} (\lambda_{we}\rho_{we} + \lambda_{ge}\rho_{ge})(p_e - P) \quad (42)$$

where P is pressure at saturation point radius R and $\lambda_{ge}$ is zero if $R < r_e$. Equation (37) describes flow from saturation point R to $r_w$ and can be written

$$q = \frac{2\pi k \Delta z}{\ln \frac{R}{r_w}} \frac{I(\lambda_{we}\rho_{we} + \lambda_{ge}\rho_{ge})}{(\lambda_{we}\rho_{we} + \lambda_{ge}\rho_{ge})(P - p_{wb})} (P - p_{wb}) \quad (43)$$

Solving for $p_e - P$ from (42) and $P - p_{wb}$ from (43) and adding the results gives

$$q = \frac{2\pi k \Delta z (\lambda_{we}\rho_{we} + \lambda_{ge}\rho_{ge})}{\ln \frac{r_e}{R} + \frac{1}{f} \ln \frac{R}{r_w}} (p_e - p_{wb}) \quad (44)$$

where

$$f = \frac{I(P, p_{wb}, S_{ge})}{(\lambda_{we}\rho_{we} + \lambda_{ge}\rho_{ge})(P - p_{wb})} \quad (45)$$

In Equations (44), (45), if the exterior radius $r_e$ is undersaturated, $\lambda_{ge} = 0$ and R must be calculated by trial and error if $p_e$ and $p_{wb}$ are given. P is, of course, equal to saturation pressure corresponding to temperature at $r_e$. If q is given, then R can be calculated directly from (42).

If the exterior radius $r_e$ is saturated, then $R = r_e$, $P = p_e$ and Equation (44) becomes

$$q = \frac{2\pi k \Delta z}{\ln \frac{r_e}{r_w}} f(\lambda_{we}\rho_{we} + \lambda_{ge}\rho_{ge})(p_e - p_w) \quad (46)$$

where f is given by (45) with $P = p_e$.

We have used an analysis similar to that given here to calculate reduced deliverability of oil wells due to release and expansion of solution gas accompanying pressure decline near the well.

TABLE 1

SINGLE-WELL RADIAL FLOW TEST PROBLEM

| | | |
|---|---|---|
| Formation Thickness | = | 500 ft |
| Permeability | = | 100 md |
| Porosity | = | 0.2 |
| Wellbore Radius | = | 0.25 ft |
| Exterior Radius | = | 2,000 ft |
| Initial Pressure at Formation Top | = | 450 psia |
| Initial Temperature | = | 400°F |
| Initial Saturation $S_w$ | = | 1.0 |
| Capillary Pressure | = | 0 |
| $k_{rw}$, $k_{rg}$ from Equations (26) | | |
| Res. and Overburden K | = | 38 Btu/ft-D-°F |
| Res. and Overburden Cp | = | 35 Btu/cu.ft Rock-°F |
| Rock Compressibility | = | $4 \times 10^{-6}$ 1/psi |
| Minimum Wellbore Pressure | = | 160 psia |

| | WELLBORE NOT INCLUDED IN GRID GRID BLOCK RADIUS, FEET | | WELLBORE INCLUDED IN GRID GRID BLOCK RADIUS, FEET | | |
|---|---|---|---|---|---|
| BLOCK | CENTER | INNER BOUNDARY | CENTER | INNER BOUNDARY | BLOCK PORE VOLUME RES. BBLS* |
| 1 | .4 | .25 | .25 | 0 | 3.50 |
| 2 | 1.07 | .68 | .40 | .25 | 4.45 |
| 3 | 2.91 | 1.84 | 1.07 | .68 | $3.28 \times 10$ |
| 4 | 7.91 | 5.00 | 2.91 | 1.84 | $2.42 \times 10^2$ |
| 5 | 21.46 | 13.57 | 7.91 | 5.00 | $1.78 \times 10^3$ |
| 6 | 58.25 | 36.84 | 21.46 | 13.57 | $1.31 \times 10^4$ |
| 7 | 158.10 | 100.00 | 58.25 | 36.84 | $9.67 \times 10^4$ |
| 8 | 429.16 | 271.44 | 158.10 | 100.00 | $7.13 \times 10^5$ |
| 9 | 1164.92 | 736.81 | 429.16 | 271.44 | $5.25 \times 10^6$ |
| 10 | - | - | 1164.92 | 736.81 | $3.87 \times 10^7$ |

*THESE PORE VOLUMES ARE FOR BLOCKS IN ONE 100-FOOT LAYER.

TABLE 2

EFFECT OF TIME STEP SIZE ON
ONE-DIMENSIONAL RADIAL FLOW RESULTS

| TIME, DAYS | TIME STEP SIZE, DAYS | | | | | | |
|---|---|---|---|---|---|---|---|
| 4000 | 250 | 500 | 1000 | 2000 | 4000 | | |
| MASS FRACTION PRODUCED | .1670 | .1669 | .1669 | .1665 | .1642 | | |
| BOTTOMHOLE QUALITY | .0559 | .0566 | .0576 | .0583 | .0576 | | |
| RATE, 1000's LBS/HR | 115.3 | 113.8 | 111.9 | 111.6 | 115.4 | | |
| 8000 | 250 | 500 | 1000 | 2000 | 4000 | 8000 | |
| MASS FRACTION PRODUCED | .3150 | .3133 | .3102 | .3048 | .2950 | .2756 | |
| BOTTOMHOLE QUALITY | .0674 | .0673 | .0668 | .0667 | .0665 | .0638 | |
| RATE, 1000's LBS/HR | 90.5 | 90.9 | 91.2 | 91.3 | 92 | 96.9 | |
| 16000 | 250 | 500 | 1000 | 2000 | 4000 | 8000 | 16000 |
| MASS FRACTION PRODUCED | .4959 | .4935 | .4889 | .4803 | .4644 | .4357 | .3865 |
| BOTTOMHOLE QUALITY | .1442 | .1420 | .1380 | .1310 | .1197 | .1039 | .0835 |
| RATE, 1000's LBS/HR | 43.5 | 44 | 45 | 46.9 | 50.2 | 56.3 | 67.9 |

TABLE 3

2D RADIAL-Z RESULTS AT 10,000 DAYS

| RUN NO. | OPEN LAYERS | TUBING BOTTOM | MASS FRACTION PRODUCED | BOTTOMHOLE PRODUCING QUALITY | BTU/LB PRODUCED AT 10,000 DAYS | RATE 1000's LBS/HR | AVERAGE BTU/LB PRODUCED |
|---|---|---|---|---|---|---|---|
| 1 | 1-1 | 1 | .1167 | .0769 | 371 | 21 | 354 |
| 2 | 3-3 | 3 | .3001 | .0518 | 349 | 46.7 | 347 |
| 3 | 5-5 | 5 | .4741 | .0486 | 346 | 77.4 | 347 |
| 4 | 1-3 | 1 | .3395 | .1305 | 417 | 44.6 | 369 |
| 5 | 1-3 | 3 | .3461 | .1343 | 421 | 44.9 | 368 |
| 6 | 3-5 | 3 | .5565 | .1085 | 398 | 60 | 356 |
| 7 | 3-5 | 5 | .5622 | .1101 | 399 | 60.6 | 359 |
| 8 | 2-4 | 3 | .4579 | .1208 | 409 | 53.1 | 362 |
| 9 | 1-5 | 1 | .5574 | .1485 | 432 | 59.9 | 370 |
| 10 | 1-5 | 3 | .5656 | .1537 | 437 | 59.7 | 371 |
| 11 | 1-5 | 5 | .5709 | .1546 | 439 | 59.9 | 371 |
| 12* | 1-5 | 3 | .7459 | .7058 | 915 | 38.7 | 423 |

*k = 500 md

TABLE 4

CALCULATED PRESSURES, TEMPERATURES AND SATURATIONS AFTER FIRST 2000-DAY TIME STEP

TWO-DIMENSIONAL RADIAL-Z RESULTS; ALL LAYERS OPEN; TUBING AT LAYER 3

PRESSURE AT GRID BLOCK CENTER (psia)

| | 1 | 2 | 3 | 4 | 5 | 6 | 7 | 8 | 9 | 10 |
|---|---|---|---|---|---|---|---|---|---|---|
| 1 | 161.5 | 167.4 | 179.7 | 191.4 | 202.5 | 213.2 | 223.5 | 233.1 | 241.5 | 247.0 |
| 2 | 162.0 | 167.2 | 180.1 | 192.4 | 204.0 | 214.8 | 224.7 | 233.6 | 242.0 | 247.5 |
| 3 | 164.2 | 175.2 | 197.3 | 215.2 | 228.9 | 238.5 | 244.3 | 249.0 | 260.7 | 271.1 |
| 4 | 170.1 | 188.2 | 219.4 | 239.4 | 248.6 | 258.2 | 271.6 | 285.0 | 297.7 | 308.2 |
| 5 | 176.4 | 200.7 | 235.9 | 250.7 | 266.7 | 285.9 | 304.5 | 321.3 | 334.8 | 345.4 |

TEMPERATURE, DEGREES FAHRENHEIT

| | | | | | | | | | | |
|---|---|---|---|---|---|---|---|---|---|---|
| 1 | 361.1273 | 364.3070 | 370.9480 | 377.2541 | 381.6283 | 385.6721 | 389.5429 | 393.1817 | 396.3912 | 398.4668 |
| 2 | 361.3719 | 364.2135 | 371.1780 | 377.8018 | 382.1824 | 386.2585 | 390.0038 | 393.3936 | 396.5752 | 398.6500 |
| 3 | 362.5504 | 368.5034 | 379.6426 | 386.4313 | 391.5900 | 395.2240 | 397.4500 | 398.5491 | 399.0535 | 399.6062 |
| 4 | 365.7484 | 375.5500 | 388.0089 | 395.5828 | 399.0524 | 399.2727 | 399.3217 | 399.5255 | 399.7558 | 399.8914 |
| 5 | 369.1330 | 380.9194 | 394.2408 | 399.8457 | 399.9718 | 399.9165 | 399.8785 | 399.8967 | 399.9551 | 399.9751 |

STEAM SATURATION

| | | | | | | | | | | |
|---|---|---|---|---|---|---|---|---|---|---|
| 1 | .9989 | .7452 | .7379 | .7363 | .7354 | .7339 | .7325 | .7303 | .7272 | .7210 |
| 2 | .9761 | .5917 | .5158 | .4886 | .4734 | .4607 | .4475 | .4300 | .3833 | .2872 |
| 3 | .8993 | .4812 | .3776 | .3195 | .2613 | .1920 | .1017 | 0.0000 | 0.0000 | 0.0000 |
| 4 | .8668 | .4386 | .3208 | .2191 | .0746 | 0.0000 | 0.0000 | 0.0000 | 0.0000 | 0.0000 |
| 5 | .8510 | .4052 | .2565 | .0715 | 0.0000 | 0.0000 | 0.0000 | 0.0000 | 0.0000 | 0.0000 |

TABLE 5

NUMBER OF ITERATIONS PER TIME STEP
ALL LAYERS OPEN; TUNING IN LAYER 3

| Δt, DAYS | | |
|---|---|---|
| 500 | 1000* | 2000 |
| 25 (.9164) | 29 (.9891) | 41 (.9589) |
| 7 (.5446) | 4 (.2000) | 22 (.4297) |
| 8 (.7186) | 14 (.6517) | 6 (.4101) |
| 8 (.2142) | 9 (.3229) | 5 (.1813) |
| 10 (.2012) | 5 (.2239) | 5 (.2705) |
| 6 (.1571) | 6 (.2273) | |
| 5 (.1064) | 4 (.1826) | |
| 5 (.1329) | 5 (.0948) | |
| 9 (.1211) | 4 (.1334) | |
| 3 (.1200) | 4 (.1176) | |
| 4 (.1040) | 2 (.0973) | |
| 5 (.0645) | | |
| 6 (.0481) | | |
| 4 (.0589) | | |
| 4 (.0681) | | |
| 3 (.0672) | | |
| 3 (.0624) | | |
| 2 (.0591) | | |
| 2 (.0551) | | |
| 2 (.0529) | | |

*THE SECOND TIME STEP AUTOMATICALLY CUT TO 100 DAYS DUE TO DIVERGENCE; THE 11TH STEP WAS 900 DAYS; ALL OTHER STEPS WERE 1,000 DAYS.

TABLE 6

CALCULATED RESULTS AFTER FIRST 500-DAY TIME STEP
TWO-DIMENSIONAL RADIAL-Z RESULTS; LAYERS 2-4 OPEN; TUNING AT LAYER 3

PRESSURE AT GRID BLOCK CENTER (psia)

| | 1 | 2 | 3 | 4 | 5 | 6 | 7 | 8 | 9 | 10 |
|---|---|---|---|---|---|---|---|---|---|---|
| 1 | | 248.1 | 248.1 | 248.1 | 248.2 | 248.3 | 248.5 | 248.8 | 249.2 | 249.9 |
| 2 | 172.2 | 181.5 | 206.4 | 224.6 | 238.2 | 247.0 | 250.5 | 251.9 | 267.9 | 275.7 |
| 3 | 177.6 | 196.1 | 227.3 | 245.5 | 251.8 | 266.4 | 280.9 | 294.1 | 304.8 | 312.8 |
| 4 | 184.7 | 209.5 | 242.5 | 254.4 | 276.1 | 297.4 | 316.7 | 331.2 | 341.9 | 350.0 |
| 5 | | 360.8 | 360.8 | 360.8 | 360.9 | 361.4 | 363.4 | 369.6 | 379.1 | 387.2 |

TEMPERATURE, DEGREES FAHRENHEIT

| | | | | | | | | | | |
|---|---|---|---|---|---|---|---|---|---|---|
| 1 | | 398.8822 | 398.8827 | 398.8855 | 398.8981 | 398.9421 | 399.0276 | 399.1101 | 399.3082 | 399.5559 |
| 2 | 366.8782 | 372.9751 | 381.0746 | 389.9853 | 395.1166 | 398.4603 | 399.7671 | 399.8136 | 399.8979 | 399.9522 |
| 3 | 369.8058 | 379.2011 | 390.0953 | 397.9063 | 399.9886 | 399.9776 | 399.9721 | 399.9694 | 399.9802 | 399.9904 |
| 4 | 373.6334 | 384.2601 | 394.7470 | 400.2618 | 400.7151 | 400.1472 | 400.0841 | 400.0282 | 399.9943 | 399.9954 |
| 5 | | 400.0292 | 400.0296 | 400.0304 | 400.0311 | 400.0312 | 400.0275 | 400.0141 | 399.9995 | 399.9978 |

STEAM SATURATION

| | | | | | | | | | | |
|---|---|---|---|---|---|---|---|---|---|---|
| 1 | | .5693 | .5692 | .5692 | .5686 | .5654 | .5489 | .4935 | .3755 | .2414 |
| 2 | .8640 | .4688 | .3697 | .3098 | .2471 | .1669 | .0444 | 0.0000 | 0.0000 | 0.0000 |
| 3 | .8481 | .4225 | .2978 | .1972 | 0.0000 | 0.0000 | 0.0000 | 0.0000 | 0.0000 | 0.0000 |
| 4 | .8249 | .3840 | .2147 | 0.0000 | 0.0000 | 0.0000 | 0.0000 | 0.0000 | 0.0000 | 0.0000 |
| 5 | | 0.0000 | 0.0000 | 0.0000 | 0.0000 | 0.0000 | 0.0000 | 0.0000 | 0.0000 | 0.0000 |

TABLE 7

SUMMARY OF FRACTURED MATRIX RUN CHARACTERISTICS

| RUN NO. | PRODUCTION RATE, LBS/HR | TIME STEP, DAYS | TOTAL TIME, DAYS | AVERAGE NUMBER OF ITERATIONS PER STEP | AVERAGE MAXIMUM SATURATION CHANGE/STEP | TOTAL RUN TIME, CDC 6600 CPU SECONDS |
|---|---|---|---|---|---|---|
| 1 | 40 | 10 | 1500 | 5.1 | 0.38 | 32.3 |
| 2 | 40 | 60 | 1500 | 8.5 | 0.66 | 26.5 |
| 3 | 10 | 120 | 4200 | 6.4 | 0.31 | 20.7 |

## TABLE 8

### HOT DRY ROCK RESULTS AT 1,000 DAYS
### 400 x 400 FEET, 100,000 DARCY FRACTURE

#### PRESSURE, PSIA

J = 1

| | 1 | 2 | 3 | 4 | 5 |
|---|---|---|---|---|---|
| 1 | 801.8 | 801.7 | 801.6 | 801.4 | 801.0 |
| 2 | 836.1 | 836.0 | 835.9 | 835.7 | 835.6 |
| 3 | 870.6 | 870.4 | 870.3 | 870.1 | 870.0 |
| 4 | 905.2 | 905.0 | 904.8 | 904.6 | 904.5 |
| 5 | 940.2 | 939.6 | 939.2 | 939.0 | 938.8 |

#### TEMPERATURE, °F

J = 1

| | 1 | 2 | 3 | 4 | 5 |
|---|---|---|---|---|---|
| 1 | 138.4375 | 139.1442 | 139.1278 | 137.9985 | 137.4555 |
| 2 | 120.3707 | 123.2967 | 126.2684 | 129.1460 | 134.0118 |
| 3 | 110.5972 | 114.3772 | 118.9110 | 924.1954 | 132.1117 |
| 4 | 104.7869 | 108.3930 | 113.2686 | 119.6754 | 129.3627 |
| 5 | 101.5197 | 104.4184 | 108.9581 | 115.5032 | 126.0568 |

J = 2

| | | | | | |
|---|---|---|---|---|---|
| 1 | 192.0262 | 192.6029 | 192.6152 | 191.7483 | 191.3081 |
| 2 | 176.3268 | 178.7883 | 181.4228 | 184.0100 | 187.8308 |
| 3 | 166.5993 | 169.9373 | 174.1229 | 178.9975 | 185.4905 |
| 4 | 160.7664 | 164.0263 | 168.6004 | 174.5594 | 182.6227 |
| 5 | 157.5881 | 160.3054 | 164.6232 | 170.7594 | 179.5778 |

J = 3

| | | | | | |
|---|---|---|---|---|---|
| 1 | 429.3812 | 429.4605 | 429.4268 | 429.2234 | 429.0697 |
| 2 | 425.2453 | 425.7926 | 426.4512 | 427.0833 | 427.7481 |
| 3 | 421.5898 | 422.5007 | 423.7477 | 425.1202 | 426.4752 |
| 4 | 419.1658 | 420.1519 | 421.6267 | 423.4105 | 425.2228 |
| 5 | 417.9100 | 418.8160 | 420.2795 | 422.1785 | 424.2129 |

J = 4

| | | | | | |
|---|---|---|---|---|---|
| 1 | 494.8779 | 494.8820 | 494.8786 | 494.8643 | 494.8519 |
| 2 | 494.5635 | 494.6016 | 494.6501 | 494.6957 | 494.7357 |
| 3 | 494.2421 | 494.3122 | 494.4119 | 494.5182 | 494.6096 |
| 4 | 494.0161 | 494.0965 | 494.2197 | 494.3629 | 494.4906 |
| 5 | 493.8991 | 493.9765 | 494.1023 | 494.2578 | 494.4033 |

J = 5

| | | | | | |
|---|---|---|---|---|---|
| 1 | 499.9092 | 499.9092 | 499.9092 | 499.9090 | 499.9088 |
| 2 | 499.9036 | 499.9042 | 499.9051 | 499.9059 | 499.9065 |
| 3 | 499.8974 | 499.8986 | 499.9005 | 499.9024 | 499.9039 |
| 4 | 499.8928 | 499.8943 | 499.8966 | 499.8993 | 499.9014 |
| 5 | 499.8905 | 499.8919 | 499.8944 | 499.8973 | 499.8998 |

#### X-DIRECTION FLOW RATE, LBS/HR

J = 1

| | 1 | 2 | 3 | 4 | 5 |
|---|---|---|---|---|---|
| 1 | 0.0000 | 2016.3670 | 4220.8752 | 7060.5410 | 12124.8302 |
| 2 | 0.0000 | 1894.5775 | 3315.5218 | 4256.6210 | 4316.0297 |
| 3 | 0.0000 | 2721.4537 | 3732.2798 | 3633.6808 | 2548.8300 |
| 4 | 0.0000 | 5329.2430 | 5442.0878 | 1342.7514 | 2582.6891 |
| 5 | 0.0000 | 13038.3583 | 8289.2342 | 5706.4035 | 3427.6178 |

#### Z-DIRECTION FLOW RATE, LBS/HR

J = 1

| | 1 | 2 | 3 | 4 | 5 |
|---|---|---|---|---|---|
| 1 | 0.0000 | 0.0000 | 0.0000 | 0.0000 | 0.0000 |
| 2 | -2016.1674 | -2204.5087 | -2839.6660 | -5064.2894 | -12875.1657 |
| 3 | -3910.9451 | -3625.4529 | -3780.7657 | -5123.6984 | -8559.1363 |
| 4 | -6632.3988 | -4636.2794 | -3682.1667 | -4038.8478 | -6010.3065 |
| 5 | -11961.6419 | -4749.1240 | -2582.8306 | -2278.7858 | -3427.6175 |

TABLE 9

HOT DRY ROCK RESULTS AT 75 DAYS

800 x 800 FEET, 800,000 DARCY FRACTURE

PRESSURE, PSIA

J = 1

| | 1 | 2 | 3 | 4 | 5 |
|---|---|---|---|---|---|
| 1 | 800.3 | 800.3 | 800.3 | 800.3 | 800.2 |
| 2 | 856.7 | 856.8 | 856.8 | 856.8 | 856.9 |
| 3 | 914.9 | 914.9 | 914.8 | 914.8 | 914.8 |
| 4 | 975.2 | 975.3 | 975.3 | 975.4 | 975.4 |
| 5 | 1039.3 | 1039.2 | 1039.1 | 1039.1 | 1039.0 |

TEMPERATURE, °F

J = 1

| | 1 | 2 | 3 | 4 | 5 |
|---|---|---|---|---|---|
| 1 | 468.3370 | 471.2789 | 474.2237 | 477.2610 | 479.9644 |
| 2 | 462.7538 | 457.2984 | 452.0257 | 446.7013 | 441.5233 |
| 3 | 399.0010 | 407.6237 | 416.3509 | 425.0627 | 433.5945 |
| 4 | 375.0946 | 361.0486 | 347.2332 | 333.1667 | 318.6657 |
| 5 | 189.6355 | 220.9219 | 247.4867 | 271.6548 | 295.6675 |

J = 2

| | | | | | |
|---|---|---|---|---|---|
| 1 | 483.8634 | 485.4144 | 486.9969 | 488.4728 | 489.6844 |
| 2 | 480.5561 | 477.4840 | 474.5136 | 471.6448 | 469.0360 |
| 3 | 444.7546 | 449.7848 | 454.8366 | 459.6667 | 464.3795 |
| 4 | 427.2917 | 419.0025 | 410.6463 | 402.3857 | 394.1028 |
| 5 | 318.5235 | 336.7667 | 352.4652 | 366.8352 | 380.9695 |

J = 3

| | | | | | |
|---|---|---|---|---|---|
| 1 | 498.8198 | 498.9383 | 499.0600 | 499.1664 | 499.2459 |
| 2 | 498.5441 | 498.2961 | 498.0542 | 497.8271 | 497.6309 |
| 3 | 495.6178 | 496.0138 | 496.4561 | 496.8485 | 497.2234 |
| 4 | 493.9525 | 493.2536 | 492.5389 | 491.8134 | 491.1513 |
| 5 | 484.7310 | 486.2680 | 487.6116 | 488.8412 | 490.0439 |

J = 4

| | | | | | |
|---|---|---|---|---|---|
| 1 | 499.9913 | 499.9922 | 499.9931 | 499.9939 | 499.9944 |
| 2 | 499.9891 | 499.9871 | 499.9852 | 499.9835 | 499.9820 |
| 3 | 499.9660 | 499.9693 | 499.9726 | 499.9757 | 499.9786 |
| 4 | 499.9520 | 499.9464 | 499.9407 | 499.9350 | 499.9296 |
| 5 | 499.8779 | 299.8902 | 499.9011 | 499.9110 | 499.9207 |

J = 5

| | | | | | |
|---|---|---|---|---|---|
| 1 | 500.0000 | 500.0000 | 500.0000 | 500.0000 | 500.0000 |
| 2 | 500.0000 | 500.0000 | 500.0000 | 500.0000 | 500.0000 |
| 3 | 499.9999 | 500.0000 | 500.0000 | 500.0000 | 500.0000 |
| 4 | 499.9999 | 499.9999 | 499.9999 | 499.9999 | 499.9999 |
| 5 | 499.9998 | 499.9998 | 499.9998 | 499.9999 | 499.9999 |

X-DIRECTION FLOW RATE, LBS/HR

J = 1

| | 1 | 2 | 3 | 4 | 5 |
|---|---|---|---|---|---|
| 1 | 0.0000 | 20882.9777 | 23901.9082 | 24797.3057 | 24949.6943 |
| 2 | 0.0000 | -23698.1287 | -27798.6156 | -28318.0482 | -26240.1155 |
| 3 | 0.0000 | 25170.5939 | 29614.1274 | 29702.3133 | 26689.1928 |
| 4 | 0.0000 | -28661.3533 | -32354.1902 | -32389.5505 | -28477.6646 |
| 5 | 0.0000 | 31305.4018 | 31635.7540 | 31226.4479 | 28076.8419 |

Z-DIRECTION FLOW RATE, LBS/HR

J = 1

| | 1 | 2 | 3 | 4 | 5 |
|---|---|---|---|---|---|
| 1 | 0.0000 | 0.0000 | 0.0000 | 0.0000 | 0.0000 |
| 2 | -20883.0478 | -3018.9908 | -895.4625 | -152.4403 | -47.8279 |
| 3 | 3815.0101 | 1081.4271 | -356.1180 | -2250.4712 | -26288.0461 |
| 4 | -22355.7418 | -3362.2535 | -444.4305 | 762.5207 | 401.0460 |
| 5 | 6305.5481 | 330.4875 | -409.1554 | -3149.4712 | -28076.7050 |

TABLE 10

HOT DRY ROCK RESULTS AT 1,000 DAYS

800 x 800 FEET, 800,000 DARCY FRACTURE

PRESSURE, PSIA

J = 1

| | 1 | 2 | 3 | 4 | 5 |
|---|---|---|---|---|---|
| 1 | 800.5 | 800.5 | 800.5 | 800.5 | 800.4 |
| 2 | 866.5 | 866.5 | 866.5 | 866.5 | 866.5 |
| 3 | 933.3 | 933.4 | 933.4 | 933.4 | 933.4 |
| 4 | 1000.9 | 1000.9 | 1000.9 | 1001.0 | 1001.0 |
| 5 | 1069.4 | 1069.3 | 1069.2 | 1069.1 | 1069.1 |

TEMPERATURE, °F

J = 1

| | 1 | 2 | 3 | 4 | 5 |
|---|---|---|---|---|---|
| 1 | 249.9689 | 248.0220 | 246.8847 | 245.8461 | 244.6164 |
| 2 | 216.5695 | 218.9366 | 219.5740 | 219.3443 | 218.4954 |
| 3 | 194.9029 | 190.9242 | 188.9332 | 188.3424 | 188.9908 |
| 4 | 153.6767 | 160.1790 | 163.8029 | 164.3298 | 161.8779 |
| 5 | 106.4226 | 113.7653 | 122.3591 | 132.9277 | 147.4336 |

J = 2

| | | | | | |
|---|---|---|---|---|---|
| 1 | 265.8360 | 263.9998 | 262.9122 | 261.9491 | 260.8865 |
| 2 | 233.9842 | 236.1508 | 236.7515 | 236.5108 | 235.6197 |
| 3 | 212.3962 | 208.7877 | 206.9809 | 206.5027 | 207.2386 |
| 4 | 172.9634 | 178.9138 | 182.1814 | 182.5563 | 180.1299 |
| 5 | 126.2235 | 133.4061 | 141.8190 | 152.1030 | 165.9797 |

J = 3

| | | | | | |
|---|---|---|---|---|---|
| 1 | 324.7246 | 323.3435 | 322.4850 | 321.8252 | 321.3318 |
| 2 | 299.2753 | 300.7499 | 301.1835 | 300.8914 | 299.8991 |
| 3 | 279.0948 | 276.7346 | 275.5776 | 275.4845 | 276.4692 |
| 4 | 246.9943 | 251.0076 | 253.0511 | 252.9464 | 250.6793 |
| 5 | 204.0660 | 210.4347 | 217.8984 | 226.8161 | 238.1241 |

J = 4

| | | | | | |
|---|---|---|---|---|---|
| 1 | 451.0672 | 450.7327 | 450.5302 | 450.4661 | 450.5618 |
| 2 | 443.0764 | 443.3598 | 443.3921 | 443.1553 | 442.6485 |
| 3 | 434.2412 | 433.8323 | 433.7200 | 433.9624 | 434.5498 |
| 4 | 423.0384 | 423.8462 | 424.1298 | 423.7657 | 422.7861 |
| 5 | 404.4443 | 407.1044 | 410.1953 | 413.6774 | 417.5579 |

J = 5

| | | | | | |
|---|---|---|---|---|---|
| 1 | 497.0347 | 497.0183 | 497.0098 | 497.0131 | 497.0286 |
| 2 | 496.5171 | 496.5274 | 496.5235 | 496.5012 | 496.4625 |
| 3 | 496.8260 | 495.8133 | 495.8179 | 495.8454 | 495.8922 |
| 4 | 495.0225 | 495.0594 | 495.0655 | 495.0298 | 494.9592 |
| 5 | 493.5814 | 493.7861 | 494.0234 | 494.2813 | 494.5475 |

X-DIRECTION FLOW RATE, LBS/HR

J = 1

| | 1 | 2 | 3 | 4 | 5 |
|---|---|---|---|---|---|
| 1 | 0.0000 | 3823.3153 | 8511.9081 | 13606.8777 | 19054.8352 |
| 2 | 0.0000 | 2706.8557 | 2765.7626 | 2153.8488 | 1207.0827 |
| 3 | 0.0000 | -3422.8521 | -3693.5112 | -2396.7712 | -729.3971 |
| 4 | 0.0000 | 214.0614 | -935.5022 | -3068.0366 | -4893.8505 |
| 5 | 0.0000 | 21678.6244 | 18351.3309 | 14704.0595 | 10361.3012 |

Z-DIRECTION FLOW RATE, LBS/HR

J = 1

| | 1 | 2 | 3 | 4 | 5 |
|---|---|---|---|---|---|
| 1 | 0.0000 | 0.0000 | 0.0000 | 0.0000 | 0.0000 |
| 2 | -3823.8456 | -4688.5961 | -5094.9711 | -5447.9598 | -5945.1321 |
| 3 | -6530.4336 | -4748.0656 | -4483.0575 | -4501.1982 | -4738.0462 |
| 4 | -3107.2900 | -4477.0181 | -5779.8014 | -6168.5727 | -5467.4493 |
| 5 | -3321.3739 | -3327.2930 | -3647.2701 | -4342.7575 | -10361.3018 |

FIGURE 1
DELIVERABILITY FACTOR I VS. $P_w$ FOR RELATIVE PERMEABILITY CURVES OF EON (25)

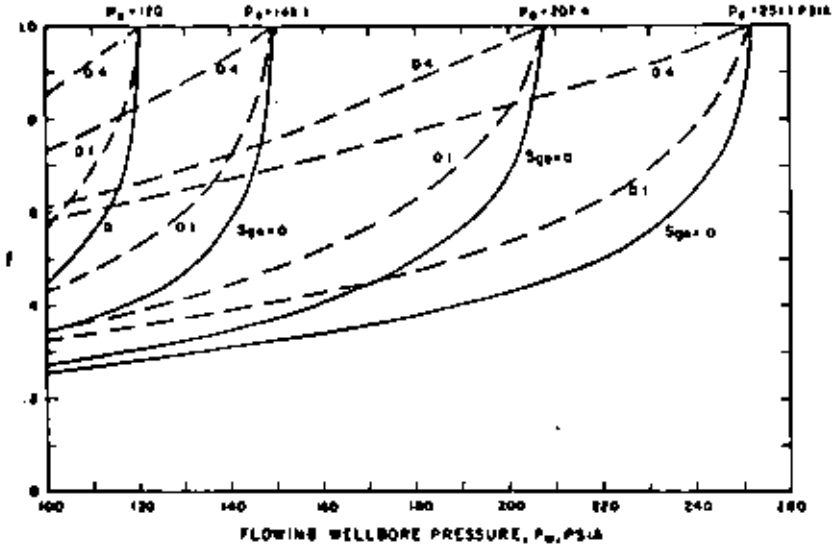


FIGURE 2
PRODUCTION RATE VS Sgc FOR RADIAL WATER-STEAM FLOW

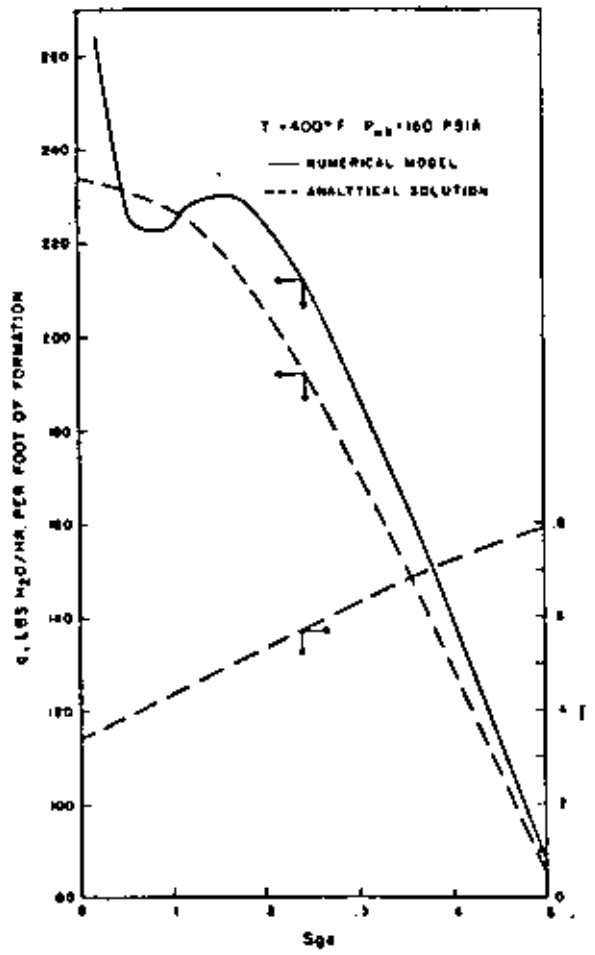

FIGURE 3
TIME TRUNCATION ERROR

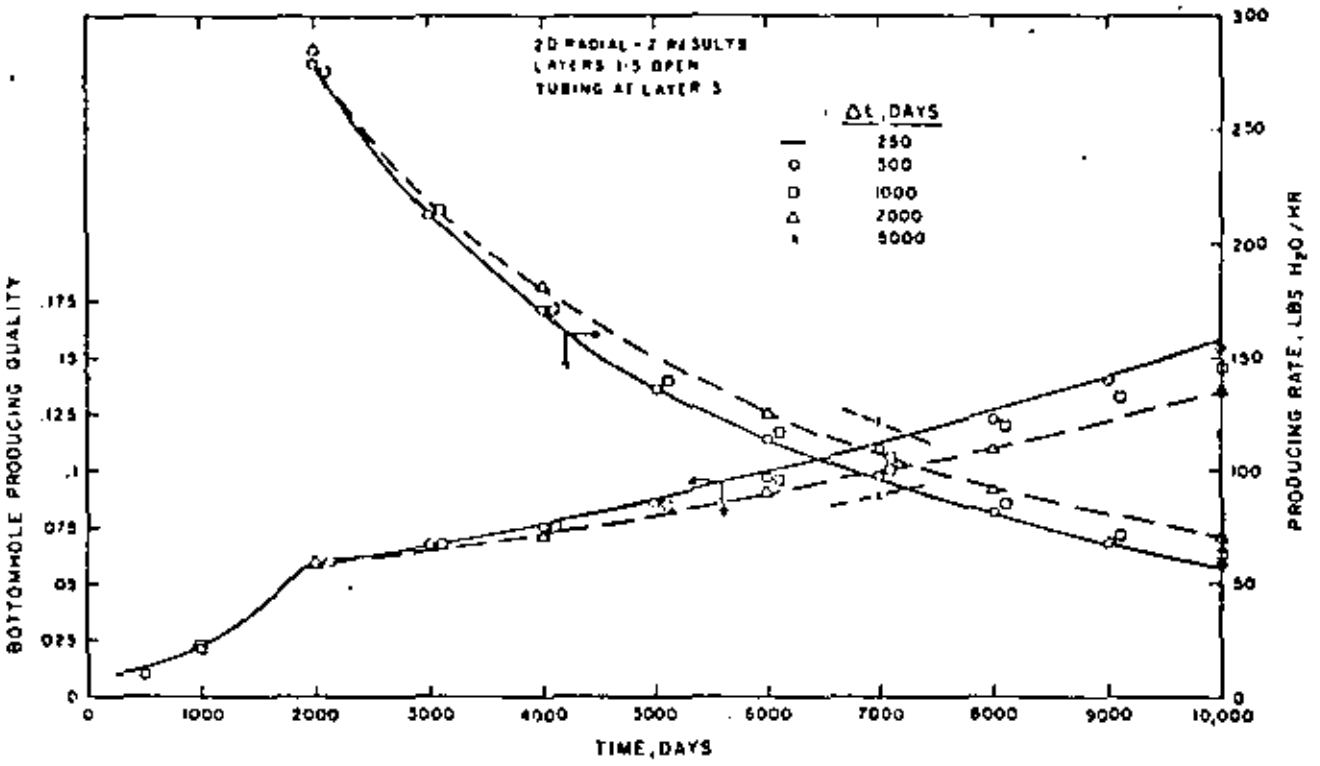


FIGURE 4
EFFECT OF PERMEABILITY ON PRODUCTION RATE AND QUALITY

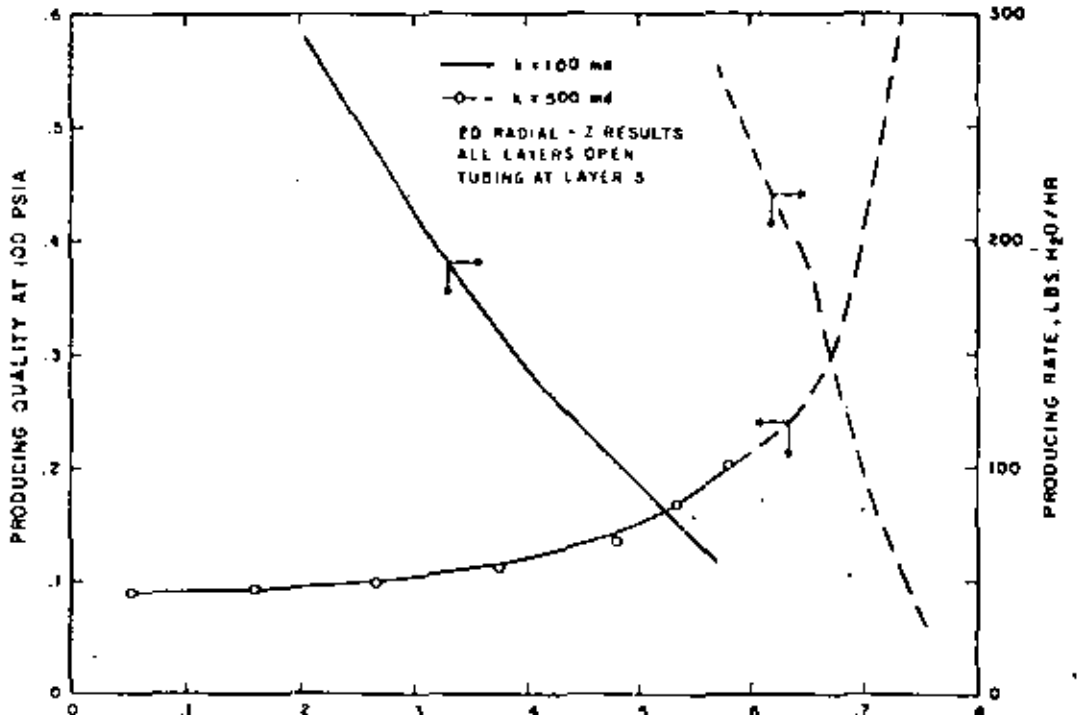

FIGURE 5

EFFECT OF PERMEABILITY AND POROSITY ON AVERAGE RESERVOIR PRESSURE DECLINE

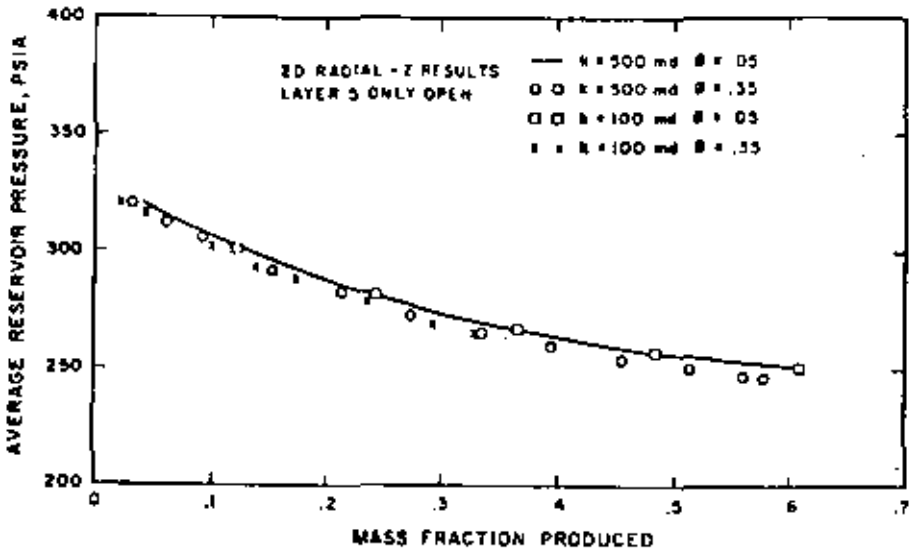


FIGURE 6

RADIAL-Z GRID FOR MATRIX-FISSURE SYSTEM

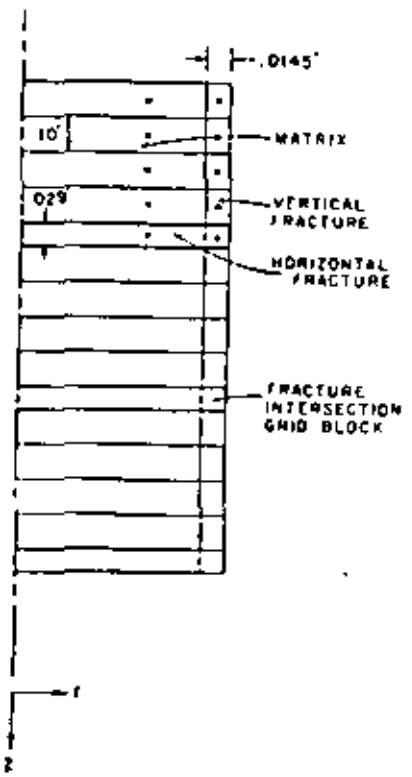

FIGURE 7

MATRIX-FISSURE SIMULATION RESULTS
AT 1500 DAYS

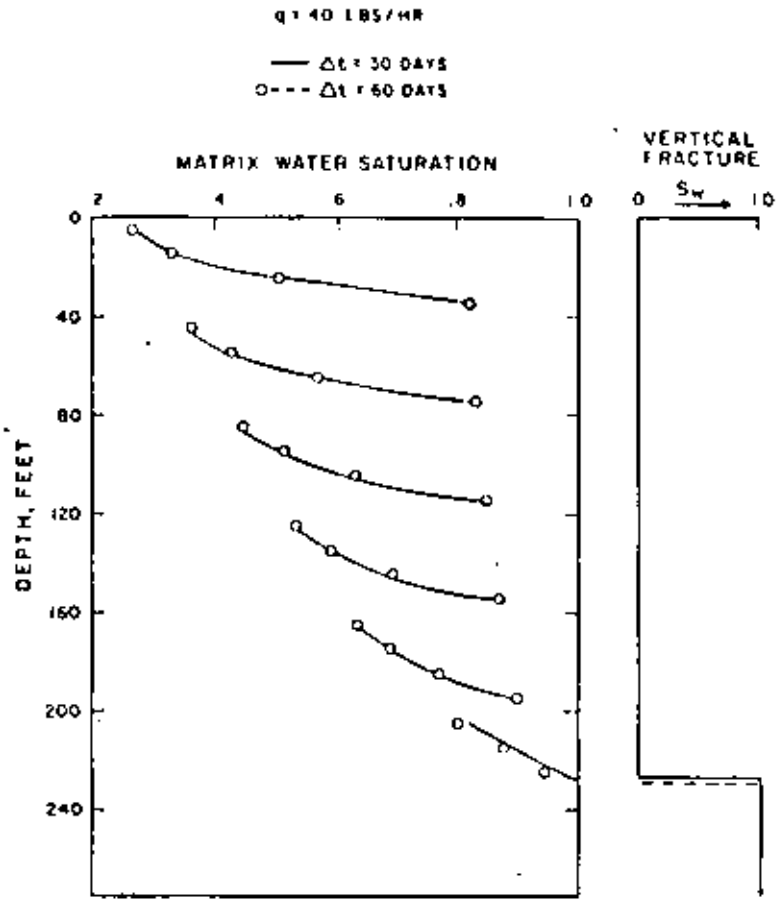


FIGURE 8

EFFECT OF PRODUCTION RATE ON
MATRIX-FISSURE SIMULATION RESULTS

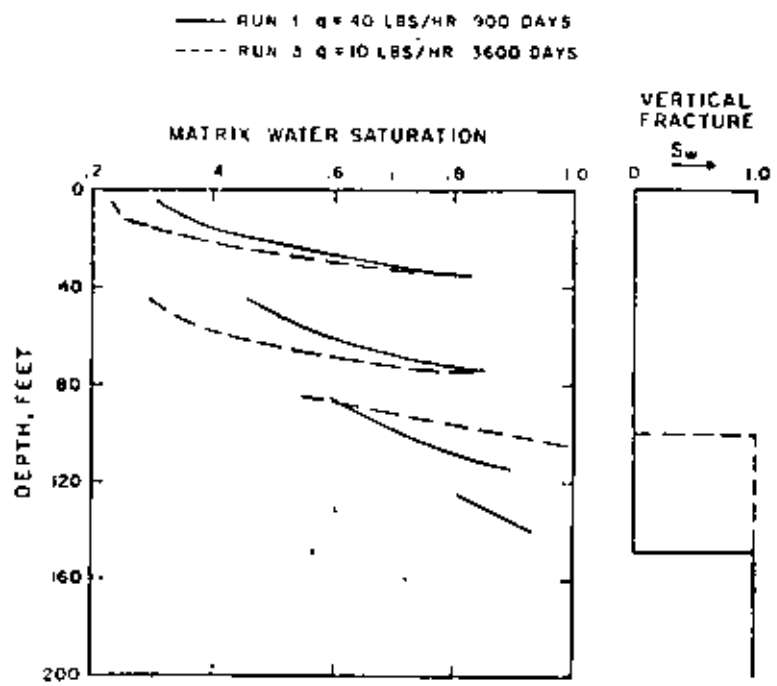

## FIGURE 9
COMPARISON OF MATRIX-FISSURE AND CONVENTIONAL SIMULATION RESULTS

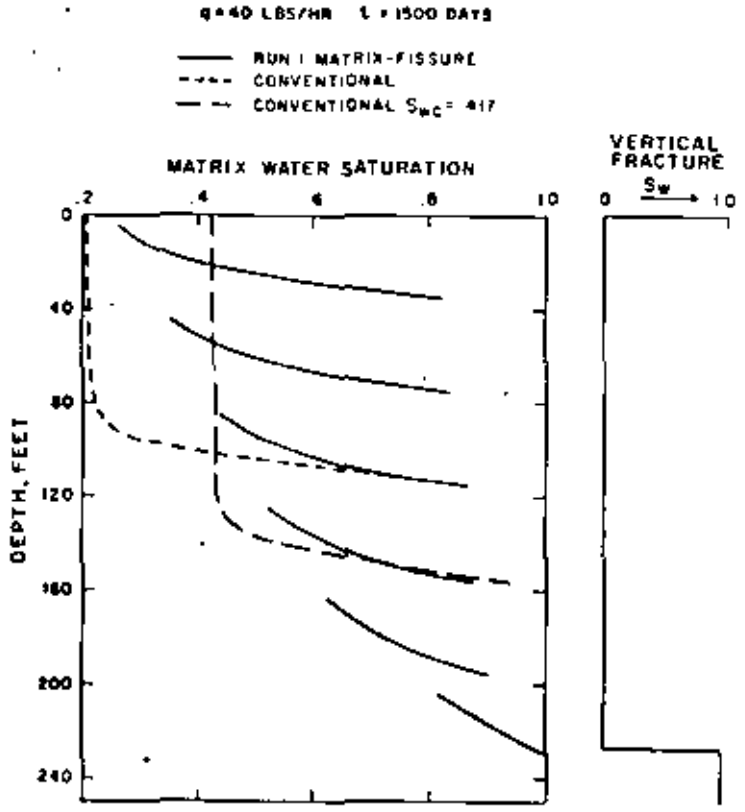


## FIGURE 10
CALCULATED PRESSURE DRAWDOWN, Δp VS. TIME

HORIZONTAL FRACTURE SPACING = 44 FT.

RATE = 10,000 LBS/HR

| RUN | FRACTURE $k_w$, DARCY-FT. | w, MM | MATRIX PERMEABILITY, MD |
|---|---|---|---|
| 1 | 4 | .245 | .0001 |
| 2 | 4 | .245 | .001 |
| 3 | 4 | .245 | .01 |
| 4 | HOMOGENEOUS, k = 90.9 MD | | |
| 5 | 546.4 | 1.26 | .0001 |

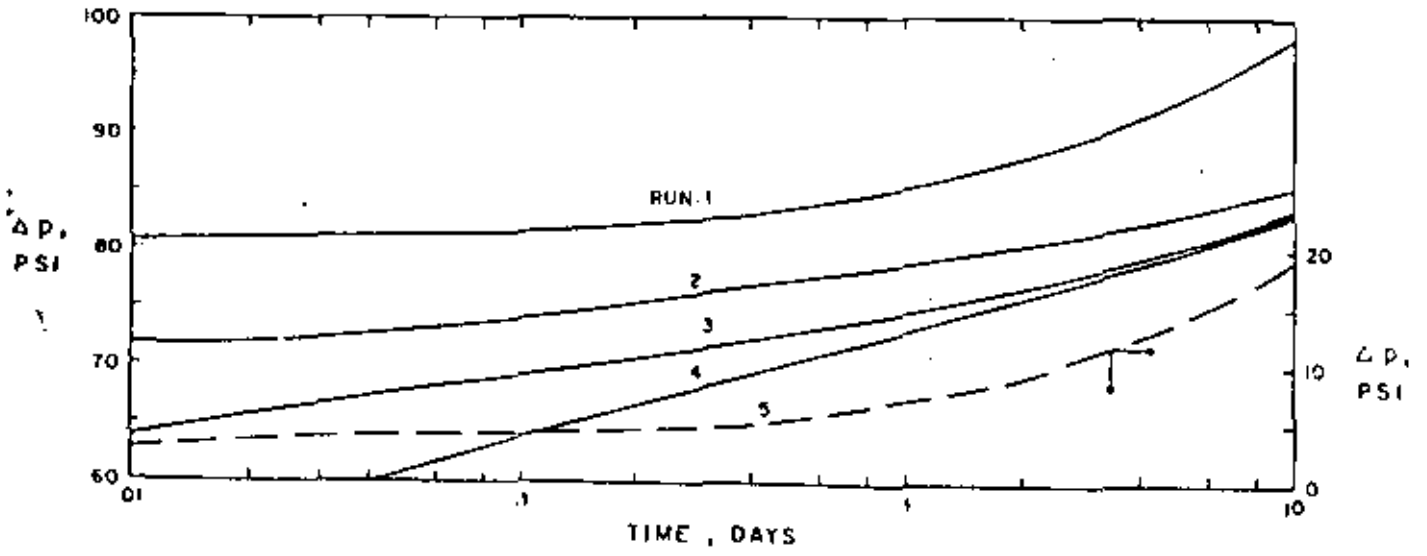

## FIGURE 11

CALCULATED PRESSURE DRAWDOWN, Δp VS. TIME

HORIZONTAL FRACTURE SPACING = 440 FT.

RATE = 100,000 LBS/HR

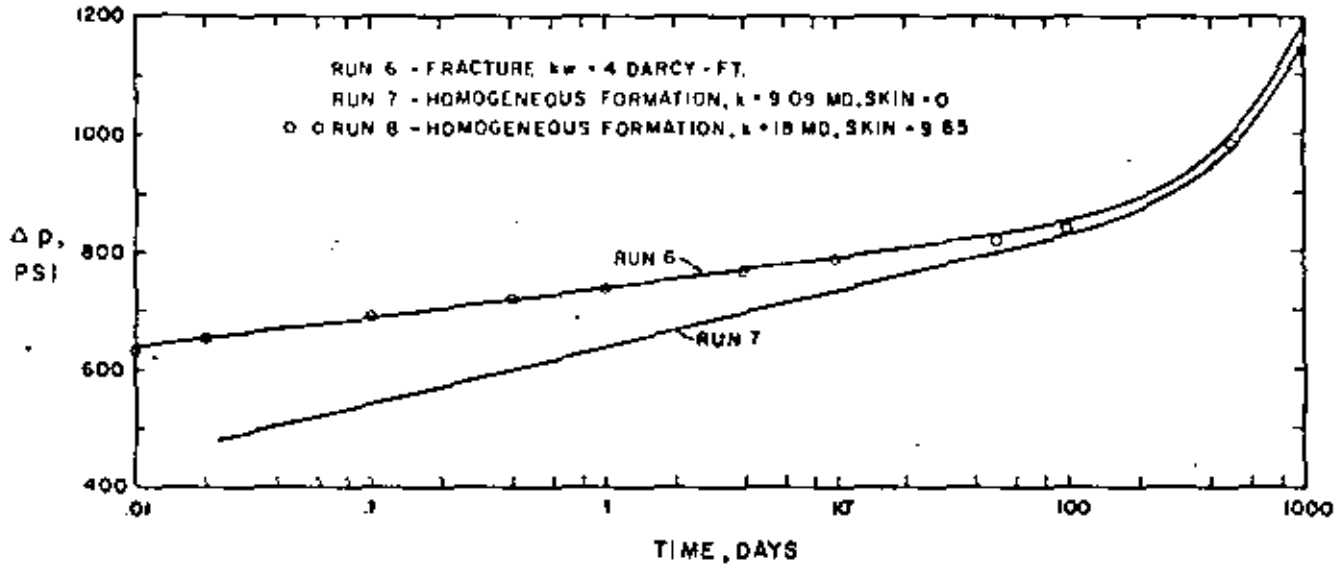


## FIGURE 12

CALCULATED ENERGY RECOVERY AND PRODUCED WATER TEMPERATURE VS. TIME FOR HOT DRY ROCK SYSTEM

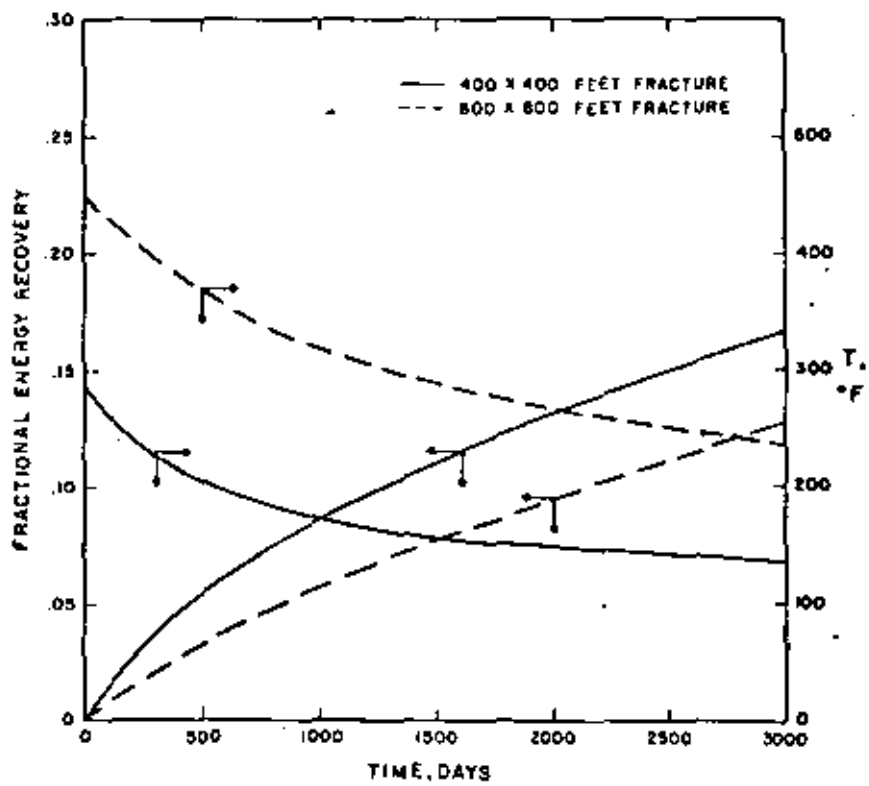

# THEORY OF HEAT EXTRACTION FROM FRACTURED HOT DRY ROCK

by

A. C. Gringarten, Bureau Recherches Géologique et Minères, Orleans, France

P. A. Witherspoon, University of California, Berkeley,

and

Yuzo Ohnishi, Kyoto University, Kyoto, Japan

## ABSTRACT

A theory of heat extraction from fractured hot dry rock is presented based on an infinite series of parallel vertical fractures of uniform aperture. Fractures are uniformly spaced and drain heat from blocks of homogeneous and isotropic impermeable rock. Cold water enters at the bottom of each fracture and solutions are given in terms of dimensionless parameters from which the exiting water temperatures at the top of the fractures can be determined. An example of the application of the theory demonstrates how a multiple-fractured system provides a more efficient mechanism for heat extraction than a single fracture in hot dry rock.

INTRODUCTION

Utilization of geothermal energy is currently limited to a small number of naturally occurring geothermal steam and hot water reservoirs. The growing interest in this new source of energy has also stimulated attempts to develop a method of extracting thermal energy from the numerous regions of the earth's crust containing deposits of hot dry rock, which may constitute a resource at least ten times as large as that permeated by groundwater. The basis of this concept is to develop an adequate fracture surface to be used for heat transfer purposes. Because of the low thermal conductivity of rock, a very large heat-transfer area must be provided, otherwise meaningful amounts of energy cannot be extracted at practical rates.

One proposal (American Oil Shale Corporation, et al., 1971) describes a method for recovering heat through a closed loop cycle of surface water, from dry geothermal sites previously fractured by a suitable array of sequentially fired, fully contained nuclear explosives. Results from a preliminary analysis forecast operation of a 200 megawatt power plant for 30 years (Burnham and Stewart, 1973). Soviet workers have also been considering the use of in-situ explosions to create a highly fractured rock system so that circulating water could extract geothermal heat (Diadkin, et al., 1973).

Another technique, developed by Robinson, et al. (1971), of the Los Alamos Scientific Laboratory requires drilling two parallel deep boreholes, the second of which is directed so as to intersect a vertically oriented crack produced by hydraulic fracturing in the first hole. Water circulating down one well, through the crack, and up the other well would carry off heat from the hot rock to the surface. A supporting theoretical analysis was presented by Harlow and Pracht (1972), which indicates that many tens of

megawatts of thermal power could be supplied for several decades, provided that the initial fracture zone could be extended through the effects of thermal stress cracking in the adjacent hot rocks. A field experiment, conducted in a test well drilled to a depth of 780 m at one edge of a volcanic caldera in the Jemez Mountains of Northern New Mexico, has shown that granite could indeed be fractured hydraulically and was impermeable enough in this region to hold water tightly (Hammond, 1973). The propagation of the fracture from thermal stress effects, however, has not yet been demonstrated.

A third concept that could greatly increase the economic life of hot rock geothermal systems is that proposed by Raleigh et al. (1974). Observing that in many regions the stresses in subsurface rock are reasonably constant over large areas, they suggest that geothermal wells be drilled at an angle, in a direction perpendicular to the expected orientation of fractures, and that a series of parallel, vertical cracks be created from a single well. The horizontal distance between cracks can be controlled and might be of the order of a few tens of meters (Figure 1).

It is the purpose of this paper to present the results of a mathematical analysis of this third method.

## MATHEMATICAL MODEL

The following discussion will be based on a linear model involving an infinite series of parallel, equidistant, vertical fractures of uniform thickness, separated by blocks of homogeneous and isotropic, impermeable rock, the width of the individual fracture being assumed to be negligible when compared to the spacing between the fractures.

Owing to the spatial periodicity of the temperature field, it is possible to replace the infinite system by a finite one, consisting of a single vertical

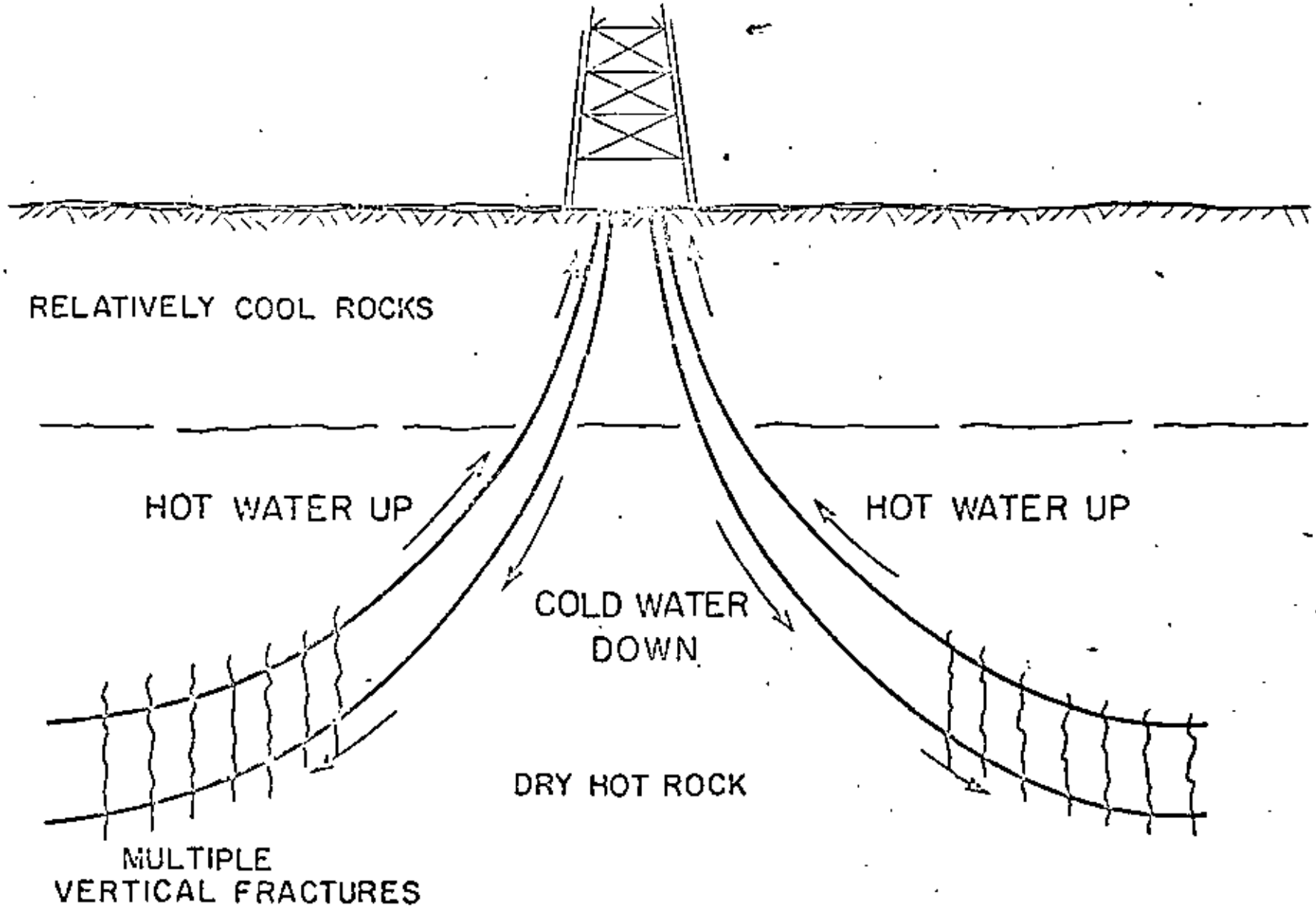


Fig. 1. Schematic diagram of heat extraction from multiple fractures in hot dry rock.

fracture of thickness 2b, between two matrix blocks with an adiabatic outer boundary at a distance from the mid-plane of the fracture equal to half the fracture spacing. As illustrated in Figure 2, a rectilinear coordinate system is placed such that the x=0 plane coincides with the mid-plane of the fracture. Water is injected at z=0, and is flowing upward in the fracture.

The following simplifying assumptions are made:

(1) The product of the density and heat capacity for both the water and the formation, and the formation thermal conductivity are constant. The linear volumetric and mass flow rate of the water is constant in the fracture.

(2) The water temperature, $T_W(z,t)$, is uniform in any cross section of the fracture, and equal, for all z, to the formation temperature at x=b.

(3) There is no heat transfer by radiation within the fracture, nor by conduction in the vertical direction within the fracture or the formation. All heat transport is by horizontal conduction in the rock, and forced convection along the z axis within the fracture.

(4) Initially, both the water in the fracture and the formation are at the same temperature, given by the initial rock temperature at the point of injection, $T_{RO}$, minus the product of distance z above injection point, and geothermal gradient $\omega$, assumed constant. At time t=0, water is injected at constant injection temperature $T_{WO}$. No heat flux is assumed across the boundary at $x=x_E$.

The differential equation governing the water temperature, $T_W(z,t)$, is obtained by writing a heat balance on an element of fracture volume, $(2b\cdot dz\cdot 1)$, between the elevations z and z+dz above the injection point. Because of the symmetry with respect to the fracture mid-plane, this can be written as:

$$b\rho_W c_W \left[\frac{\partial T_W(z,t)}{\partial t} + v\,\frac{\partial T_W(z,t)}{\partial z}\right] = K_R \left.\frac{\partial T_R(x,z,t)}{\partial x}\right|_{x=b} \qquad (1)$$

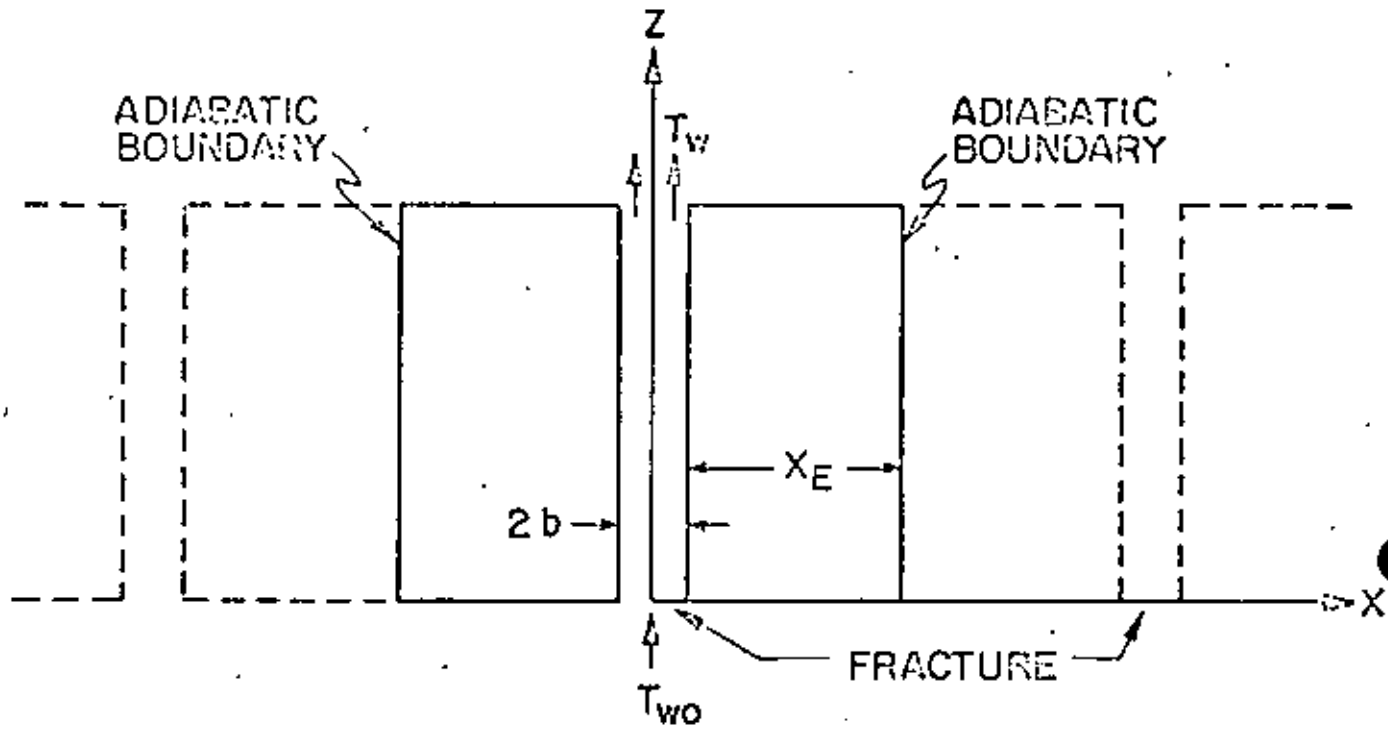


Fig. 2. Mathematical model for fractured hot dry rock.

where v is the water velocity, $\rho_W$ and $c_W$ the water density and specific heat, and $K_R$ is the rock thermal conductivity. $T_R(x,z,t)$ is the rock temperature, which is governed by the heat conduction equation:

$$\frac{\partial^2 T_R(x,z,t)}{\partial x^2} = \frac{\rho_R c_R}{K_R} \frac{\partial T_R(x,z,t)}{\partial t} \tag{2}$$

The temperatures must also satisfy the following initial and boundary conditions:

$$T_R(x,z,t) = T_W(z,t) = T_{RO} - \omega z, \qquad t < \frac{z}{v} \tag{3}$$

$$T_R(x,0,t) = T_W(0,t) = \begin{cases} T_{RO} & \text{if } t < 0 \\ T_{WO} & \text{if } t \geq 0 \end{cases} \tag{4}$$

$$T_W(z,t) = T_R(b,z,t) \text{ for all } z \text{ and } t \tag{5}$$

$$\left.\frac{\partial T_R(x,z,t)}{\partial x}\right|_{x=x_E} = 0 \tag{6}$$

The simultaneous solution of Eqs. 1 and 2, subject to conditions 3 through 6, is derived in Appendix A. The result for the outlet water temperature, at a distance z from the injection point, can be expressed in a general form as a function, $T_{WD}(\beta, X_{ED}, t_D')$ of dimensionless parameters, such that:

$$T_{WD} = \frac{T_{RO} - T_W(z,t)}{T_{RO} - T_{WO}} \tag{7}$$

$$\beta = \frac{\omega z}{T_{RO} - T_{WO}} \tag{8}$$

$$X_{ED} = \frac{\rho_W c_W}{K_R} \left(\frac{Q}{z}\right) x_E \tag{9}$$

$$t_D' = \frac{(\rho_W c_W)^2}{K_R \rho_R c_R} \left(\frac{Q}{z}\right)^2 t' \tag{10}$$

where Q is the volumetric flow rate per fracture per unit thickness of the system in the y direction, and $t' = t - \frac{z}{v}$. $\frac{z}{v}$ is the time lag between the departure of the water from the injection point and the arrival at point z. Because this time lag is very small in comparison with the lengths of time involved in our problem, t' is practically identical to t.

The dimensionless parameter $\beta$ was found to have little effect on the time variation of the outlet water dimensionless temperature, except at small $t'_D$ values, even in the case of a high geothermal gradient. The geothermal gradient can thus safely be neglected, $T_{RO}$ being now taken as the average rock temperature over the zone of interest. The results for this case are shown in Figure 3, where $T_{WD}$ is plotted as a function of $t'_D$, for various values of the dimensionless half-fracture spacing $X_{ED}$.

The ratio of the amount of heat extracted by the water flowing through the fracture to the initial total heat available in the rock was also computed and is shown in Figure 4.

Although the model presented in this paper is strictly valid only for an infinite number of fractures, it can also be used as a good approximation when the number of fractures is finite, but large enough, which should be the case in most practical applications.

## EXAMPLE OF CALCULATION

When designing a geothermal power plant that uses this concept, a number of parameters are imposed and others have to be adjusted. In the system under consideration, the rock and water properties are given, and the total volumetric flow rate, minimum usable outlet temperature, and useful reservoir life are fixed by technical and economical considerations. What has to be chosen is the number of fractures, the dimensions of the individual fracture, and the

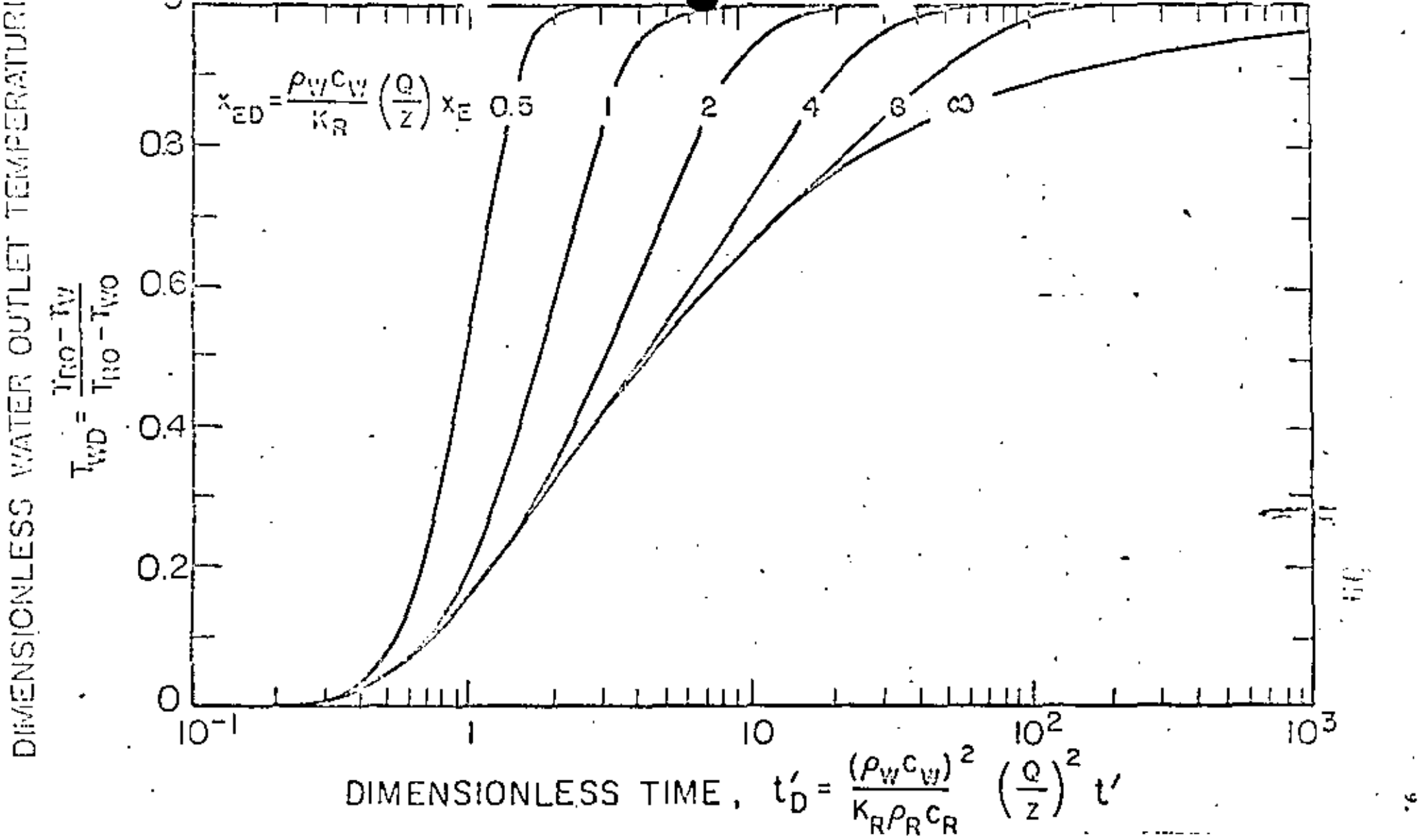


Fig. 3. Dimensionless water outlet temperature versus dimensionless time showing effect of fracture spacing.

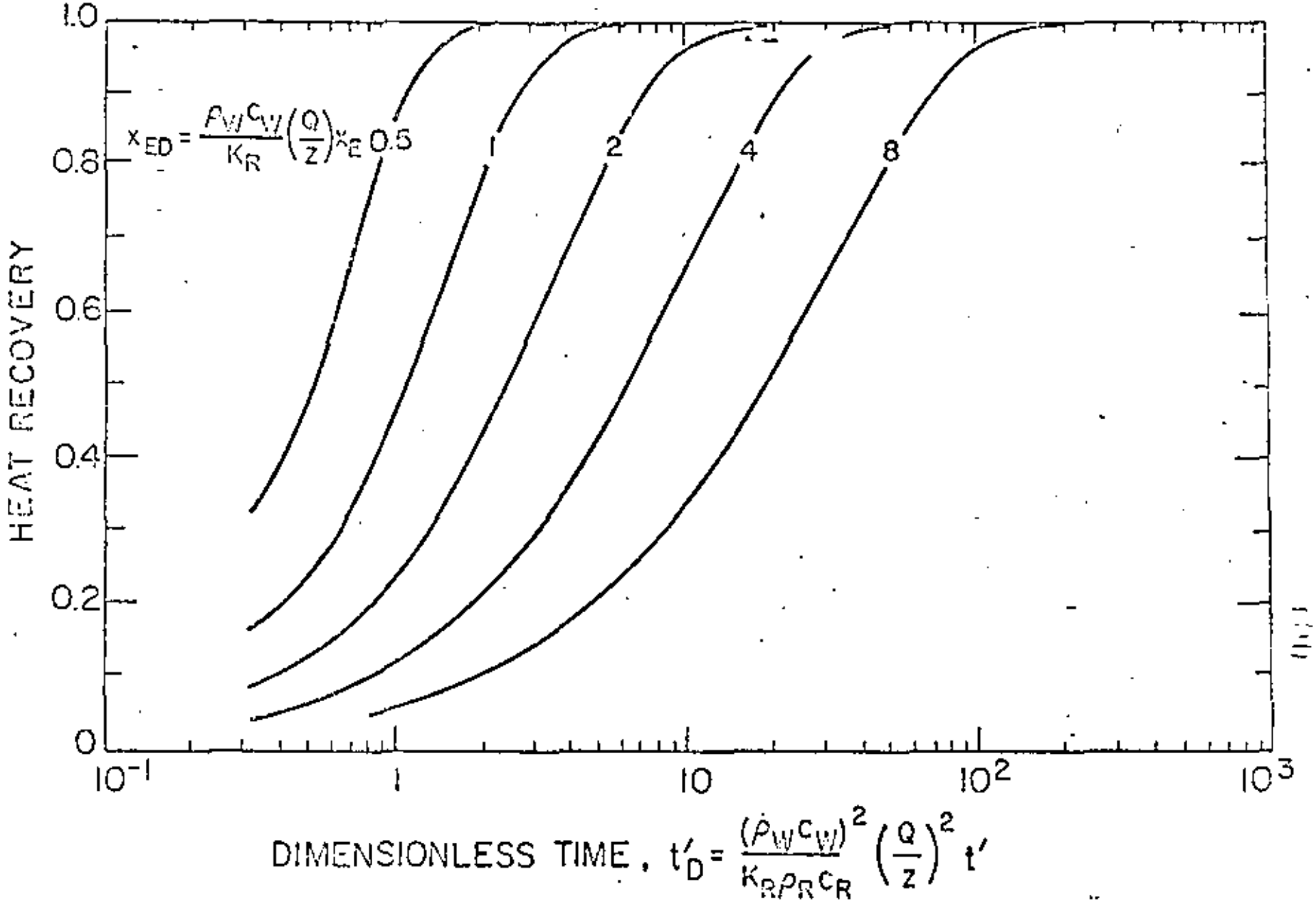


Fig. 4. Fractional heat recovery versus dimensionless time.

spacing between the fractures. These can be determined from Figure 3. An example of this type of calculation is described below.

In order to allow comparison with the system proposed by the Los Alamos group, the data given by Harlow and Pracht (1972) were used in the computations. They assumed a single fracture with a height of 1 km and a length (y direction) of 1 km and used a volumetric flow rate of $1.45 \times 10^5$ cm$^3$/sec. They adopted a rock temperature of 300°C and an inlet water temperature of 65°C. Their remaining material properties were: $K_R = 6.2 \times 10^{-3}$ cal/cm sec °C, $\rho_R = 2.65$ g/cm$^3$, $c_R = 0.25$ cal/g °C, $\rho_W = 1.0$ g/cm$^3$, and $c_W = 1.0$ cal/g °C. Resulting temperatures are shown in Figure 5. With a single fracture, the water outlet temperature drops very quickly after only a few years. This shouldbe the case in Harlow and Pracht's model if thermal fracture propagation turns out to be negligible. On the other hand, if ten fractures are used, the water outlet temperature will drop at a much lower rate, depending on the fracture spacing.

The number of fractures in this example was determined by the requirement of a 297°C water outlet temperature ($T_{WD} = 0.013$) after 20 years. It can be seen from Figure 3 that this temperature corresponds to $t'_D = 0.325$ and $X_{ED} > 0.5$, which, for $t' = 20$ years, yields $Q = 0.145$ cm$^3$/sec. Since this number by definition, is also equal to the total volumetric flow rate ($1.45 \times 10^5$ cm$^3$/sec) divided by the number of fractures, N, and by the fracture length (1 km), the number of fractures follows immediately. The result is $N = 10$.

The spacing between the fractures is determined by the value of the dimensionless spacing parameter $X_{ED}$, which for this example would be $> 0.5$. It is obvious from Figure 3 that temperature will drop at a faster rate for smaller $X_{ED}$. On the other hand, one can see from Figure 4 that the fraction of energy recovered from the rock will be higher. For example, if one were to increase the time period to 100 years ($t_D = 1.6$), it can be seen from

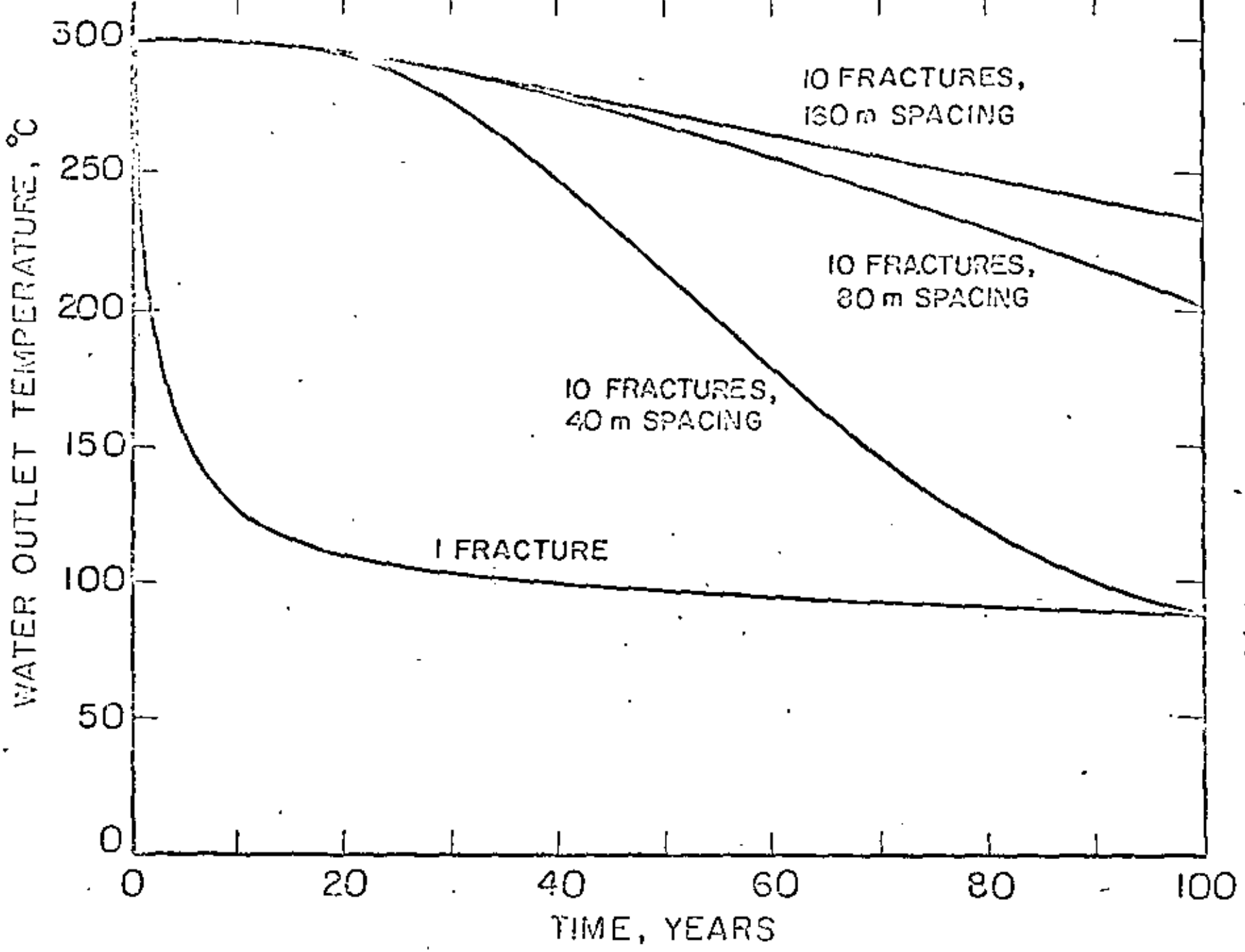


Fig. 5. Water outlet temperature versus time for 1 $km^2$ fractures with $T_{RO}$ = 300°C and $T_{IO}$ = 40°C.

Figures 3 and 4 that there is no advantage in taking $X_{ED}$ greater than 2 (which corresponds to a fracture spacing of 160 m) because a lower heat recovery would result and the drilling costs would be increased with no improvement in the outlet temperatures.

Obviously, the best choice for the fracture spacing is that which would yield the highest electrical power output for the longest period of time. The formulas for computing the electrical power output are given in Appendix B. The results are shown in Figure 6. It can be seen that electrical power output is highest for 10 fractures with a 160 m spacing, and this spacing is capable of producing many times the power output of a single fracture. If 20 fractures were used instead of ten, the maximum output of about 30 MW could be maintained for a century.

## CONCLUSION

Although much simplified, the mathematical model used in this study shows that the multi-fracture concept could greatly increase the economic utilization of hot dry rock geothermal systems. If fracture propagation occurs through the effects of thermal stress cracking, as expected by some authors, geothermal energy extraction will even be greater than that reported in the present study.

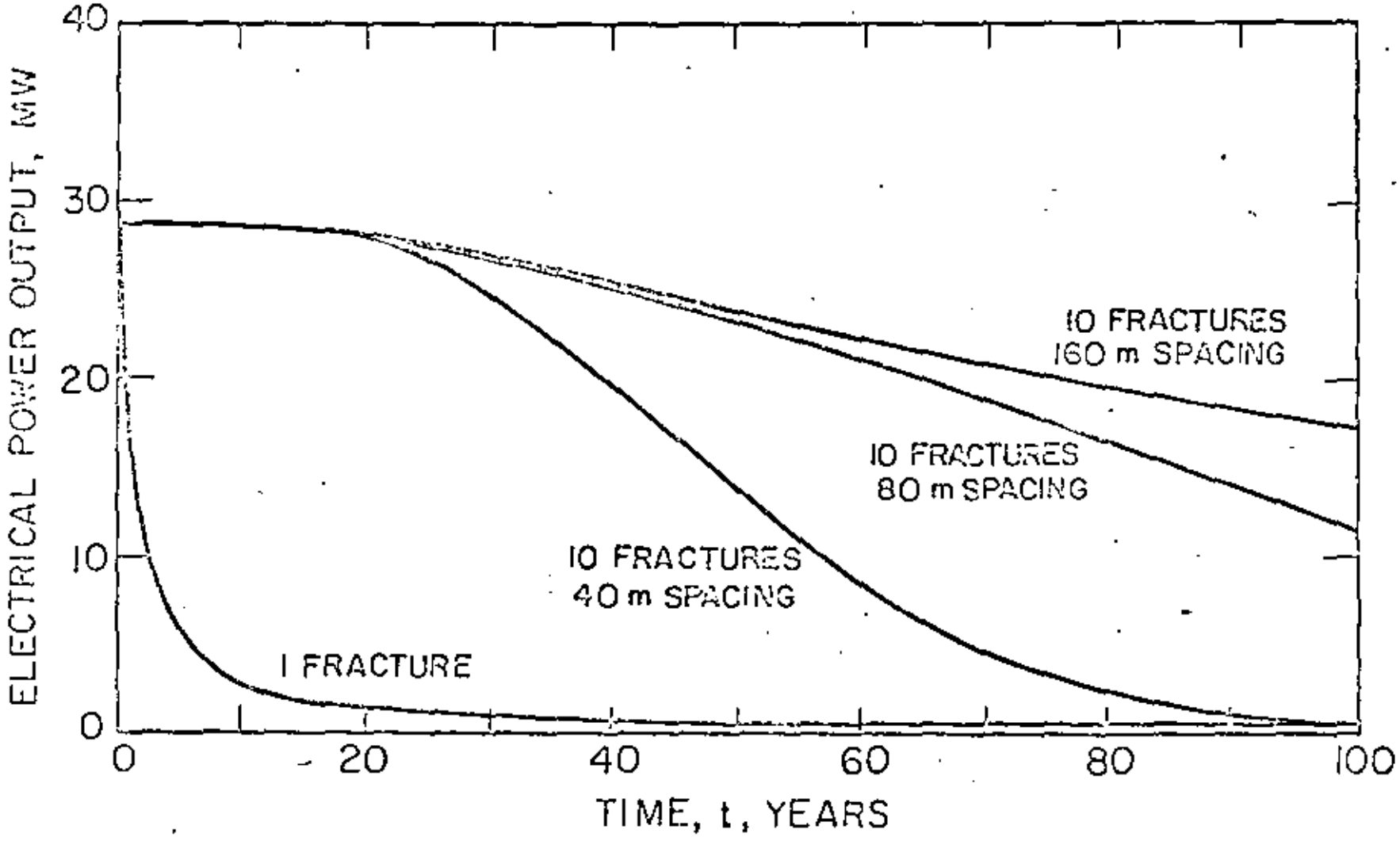


Fig. 6. Electrical power output from 1 $km^2$ fractures at 50% Carnot efficiency.

## APPENDIX A. DERIVATION OF WATER OUTLET TEMPERATURE

Special cases of the mathematical problem considered in the present paper have been studied by previous authors. Bodvarsson (1969) solved the problem of constant flow with sinusoidal temperature through laminated solid, and solutions for $x_E = \infty$ were published by Lauwerier (1955) and Carslaw and Jaeger (1959).

An exact analytical solution for finite $x_E$ was recently presented by Romm (1972). In the present paper, the problem is solved in a slightly different way, and the results for infinite and finite $x_E$ values are presented on the same graph in terms of suitable dimensionless quantities.

A solution is obtained as follows: we first substitute t' in place of t into Eqs. 1 to 4:

$$\rho_W c_W b v \frac{\partial T_W(z,t')}{\partial z} = K_R \frac{\partial T_R(x,z,t')}{\partial x}\bigg|_{x=b} \tag{A-1}$$

$$\frac{\partial^2 T_R(x,t')}{\partial x^2} = \frac{\rho_R c_R}{K_R} \frac{\partial T_R(x,z,t')}{\partial t'} \tag{A-2}$$

$$\lim_{t'\to 0} T_R(x,z,t') = \lim_{t'\to 0} T_W(z,t') = T_{RO} - \omega z \tag{A-3}$$

$$\lim_{z\to 0} T_W(z,t') = T_{WO}, \quad t' > 0 \tag{A-4}$$

We then introduce the following dimensionless quantities:

$$\alpha = \frac{2K_R H}{\rho_W c_W Q b} \tag{A-5}$$

where H is an arbitrary length, and Q is the volumetric flow rate per fracture, per unit length of the system in the y direction;

$$\beta^* = \frac{\omega H}{T_{RO} - T_{WO}} \tag{A-6}$$

$$x_D = x/b \tag{A-7}$$

$$z_D = z/H \tag{A-8}$$

$$t_D^* = \frac{(\rho_W c_W)^2}{4K_R \rho_R c_R} \left(\frac{Q}{H}\right)^2 t' \tag{A-9}$$

$$T_{RD}(x_D, z_D, t_D') = \frac{T_{RO} - T_R(x,z,t')}{T_{RO} - T_{WO}} \tag{A-10}$$

Eqs. A-1 to A-4, and 5 and 6 thus become:

$$\frac{1}{\alpha} \frac{\partial T_{WD}(x_D, t_D^*)}{\partial z_D} = \left.\frac{\partial T_{RD}(x_D, z_D, t_D^*)}{\partial x_D}\right|_{x_D=1} \tag{A-11}$$

$$\frac{\partial^2 T_{RD}(x_D, z_D, t_D^*)}{\partial x_D^2} = \frac{1}{\alpha^2} \frac{\partial T_{RD}(x_D, z_D, t_D^*)}{\partial t_D^*} \tag{A-12}$$

$$\lim_{t_D^* \to 0} T_{RD}(x_D, z_D, t_D^*) = \lim_{t_D^* \to 0} T_{WD}(z_D, t_D^*) = \beta^* z_D \tag{A-13}$$

$$T_{WD}(z_D, t_D^*) = T_{RD}(1, z_D, t_D^*) \tag{A-14}$$

$$\lim_{z_D \to 0} T_{WD}(z_D, t_D^*) = 1, \quad t_D^* \geq 0 \tag{A-15}$$

$$\left.\frac{\partial T_{RD}(x_D, z_D, t_D^*)}{\partial x_D}\right|_{x_D = x_{ED}} = 0 \tag{A-16}$$

Applying the Laplace transform with respect to $t_D^*$ and solving for the water outlet temperature yields:

$$\overline{T_{WD}}(z_D, s) = \frac{1}{s}\left[1 + \left(\frac{\beta^*}{\sqrt{s}\tanh\frac{x_{ED}-1}{\alpha}\sqrt{s}}\right)\right] \exp\left(-z_D \sqrt{s} \tanh \frac{x_{ED}-1}{\alpha} \sqrt{s}\right) + \frac{\beta^* z_D}{s} - \frac{\beta^*}{s^{3/2} \tanh \frac{x_{ED}-1}{\alpha}\sqrt{s}} \tag{A-17}$$

where $\bar{T}_{WD}(z_D,s)$ is the Laplace transform of the dimensionless water outlet temperature.

Eq. A-17 is most difficult to invert analytically, except in the case of a single fracture ($x_E = \infty$), where inversion of Eq. A-17 shows that $T_{WD}$ can be expressed as a function of $\beta$ (Eq. 8) and $t_D'$ (Eq. 10) only:

$$T_{WD}(t_D') = 1-2\beta(t_D'/\pi)^{1/2}[1-\exp(-1/4t_D')] - (1-\beta)\mathrm{erf}(1/2\sqrt{t_D'}) \qquad (A-18)$$

$T_{WD}$ has been plotted versus $t_D'$ in Figure A-1, for various $\beta$ values. The curves are very similar, except at early $t_D'$ values. This indicates that the geothermal gradient can be safely neglected as a first approximation, if $T_{RO}$ is taken as the average temperature along the fracture height. Setting $\beta$=0 into Eq. A-17 and neglecting 1 in front of $x_{ED}$ yields:

$$\bar{T}_{WD}(z_D,s) = \frac{1}{s}\exp(-z_D\sqrt{s}\,\tanh\frac{\rho_W c_W Q x_E}{2K_R H}\sqrt{s}) \qquad (A-19)$$

Eq. A-19 was inverted by means of a numerical method (Papoulis, 1957) and the result expressed as a function of $x_{ED}$ (Eq. 9) and $t_D'$ (Eq. 10) is plotted in Figure 3.

## APPENDIX B. ELECTRICAL POWER OUTPUT

The total amount of heat in the hot rock per unit length of the system in the y direction, which could be recovered by cooling from $T_{RO}$ to $T_{WO}$ is:

$$H_R = 2\rho_R c_R z x_E (T_{RO} - T_{WO}) \qquad (B-1)$$

The heat extraction rate or thermal power output by the water between $T_W$ and $T_{WO}$ is:

$$\rho_W c_W Q(T_W - T_{WO}) \text{ or } \rho_W c_W Q(T_{RO} - T_{WO})\left(1 - \frac{T_{RO} - T_W}{T_{RO} - T_{WO}}\right)$$

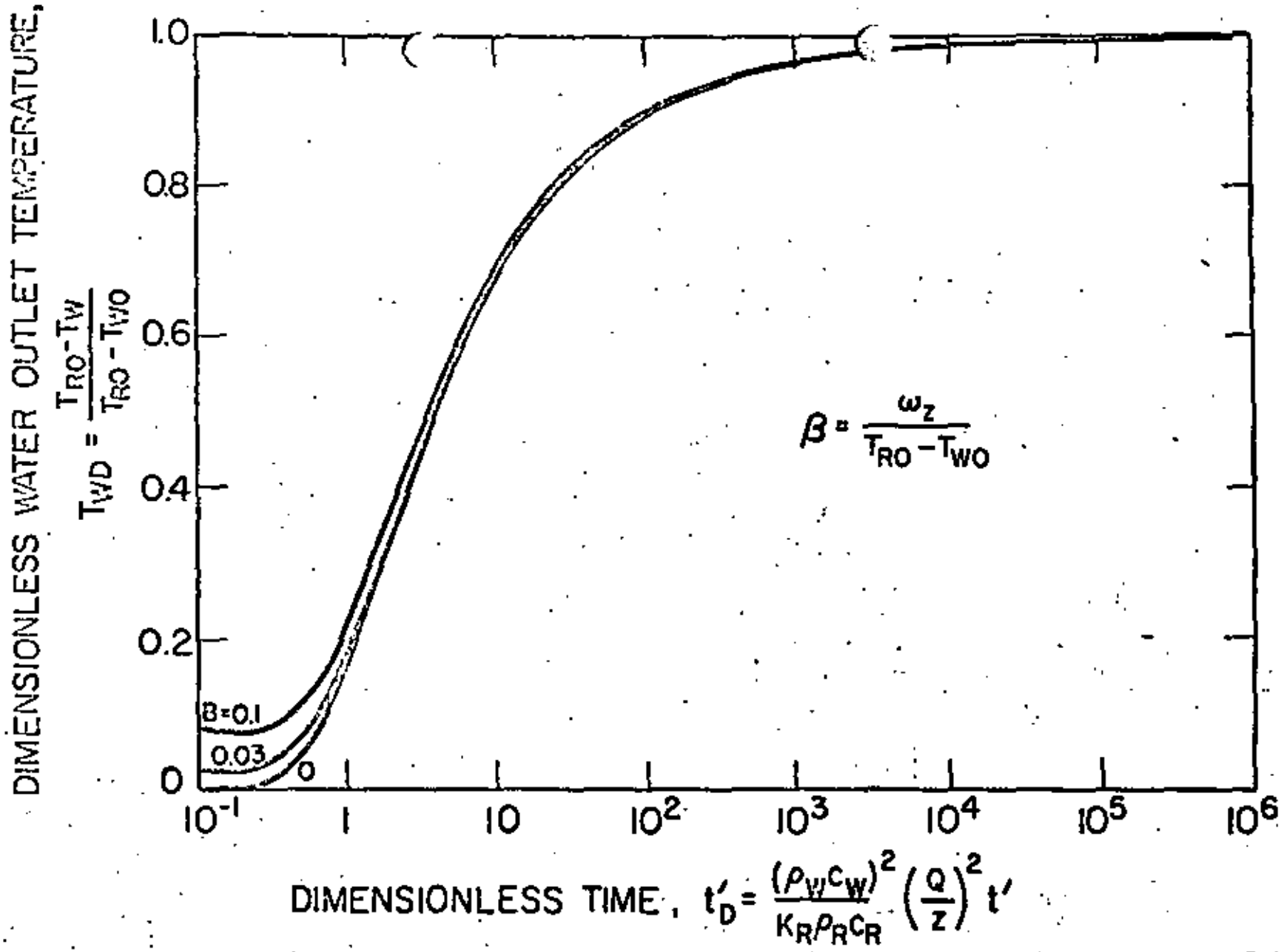


Fig. A1. Dimensionless water outlet temperature versus dimensionless time for a single fracture ($X_{ED} = \infty$) showing effect of geothermal gradient.

Use of this water in a power plant working between $T_W$ and $T_{WO}$ at 50% of the Carnot efficiency would yield an electric power output equal to:

$$h_W = 0.50 \ \rho_W c_W Q \frac{(T_W - T_{WO})^2}{T_W + 273} \qquad (B-2)$$

The cumulative heat extraction by water over a period t' is given by:

$$H_W = \int_0^{t'} \rho_W c_W Q (T_{RO} - T_{WO}) \left(1 - \frac{T_{RO} - T_W}{T_{RO} - T_{WO}}\right) dt' \qquad (B-3)$$

The ratio of the amount of heat extracted by the water to the initial heat content in the rock is thus equal to:

$$\frac{H_W}{H_R} = \int_0^{t'} \frac{\rho_W c_W Q}{2\rho_R c_R z x_E} \left(1 - \frac{T_{RO} - T_W}{T_{RO} - T_{WO}}\right) dt'$$

or

$$\frac{H_W}{H_R} = \frac{1}{2X_{ED}} \int_0^{t_D'} [1 - T_{WD}(t_D')] \, dt_D' \qquad (B-4)$$

American Oil Shale Corporation - U. S. Atomic Energy Commission, "A Feasibility Study of a Geothermal Power Plant" PNE-1550, 1971.

Bodvarsson, G. "On the Temperature of Water Flowing through Fractures", J. Geo. Res., v. 74, no. 8, p. 1987, April 5, 1969.

Burnham, J. B. and Stewart, D. H. "Recovery of Geothermal Energy from Hot, Dry Rock with Nuclear Explosives", Geothermal Energy, ed. by Kruger and Otte, Stanford University Press, Stanford, California, p. 223, 1973.

Carslaw, H. S. and Jaeger, J. C. Conduction of Heat in Solids, 2nd ed. Oxford at the Clarendon Press, p. 396, 1959.

Diadkin, Yu. D., Pariiskii, Yu. M., Vainblat, A. B., and Romanov, B. A., "Issledovanie i razrabotka ratsional'nykh sistem izvlecheniya i ispol'zovaniya tepla, akkumulirovannogo glubinnymi sloyami zemnoi kory v raionakh Krainego Severa i Severo-Vostoka SSSR", (Investigation and development of rational systems of extraction and utilization of heat accumulated in deep layers of the earth in the extreme north and northeast regions of the USSR) Izuchenie i Ispol'zovanie Glubinnogo Tepla Zemli, Izdatel'stvo Nauka, Moscow, p. 43, 1973.

Hammond, A. L. "Dry Geothermal Wells: Promising Experimental Results", Science, vol. 182, p. 43, October 5, 1973.

Harlow, F. H. and Pracht, W. E. "A Theoretical Study of Geothermal Energy Extraction", J. Geo. Res., v. 77, no. 35, p. 7038, December, 1972.

Lauwerier, H. A. "The Transport of Heat in an Oil Layer Caused by the Injection of Hot Fluid", Appl. Sci. Res., Sec. A, v. 5, p. 145, 1955.

Papoulis, A. "A New Method of Inversion of the Laplace Transform", Quart. Appl. Math., v. 14, pp. 405-414, 1957.

Robinson, E. S., Potter, R. M., McInteer, B. B., Rowley, J. C., Armstrong, D. E., Mills, R. L. and Smith, M. C. "A Preliminary Study of the Nuclear Subterrane" Rep. LA-4547, Los Alamos Scientific Lab., 1971.

Romm, E. S. "Ob Odnom Sluchae Teploperenosa v Treshchinovatoi Gornoi Porode" (On one case of heat transfer in fractured rock) Problemy Razrabotki Mestorozhdenii Poleznykh Iskopaemykh Severa, Leningrad Mining Institute, pp. 92-96, 1972.

Raleigh, C. B., Witherspoon, P. A., Gringarten, A. C., and Ohnishi, Y., "Multiple Hydraulic Fracturing for the Recovery of Geothermal Energy," EOS Trans. AGU, v. 55, no. 4, p. 4026, 1974.

DR. HEBER CINCO LEY

111

PAPER NUMBER SPE 5382

THIS IS A REPRINT - SUBJECT TO CORRECTION

# Analysis of Internal Steam Drive in Geothermal Reservoirs

J. C. Martin, Chevron Oil Field Research Company, Member SPE-AIME



This paper was prepared for the 46th Annual California Regional Meeting of the Society of Petroleum Engineers of AIME, to be held in Ventura, Calif., April 2-4, 1975. Permission to copy is restricted to an abstract of not more than 300 words. Illustrations may not be copied. The abstract should contain conspicuous acknowledgment of where and by whom the paper is presented. Publication elsewhere after publication in the JOURNAL OF PETROLEUM TECHNOLOGY or the SOCIETY OF PETROLEUM ENGINEERS JOURNAL is usually granted upon request to the Editor of the appropriate journal, provided agreement to give proper credit is made.

Discussion of this paper is invited. Three copies of any discussion should be sent to the Society of Petroleum Engineers office. Such discussion may be presented at the above meeting and, after review, may be considered for publication in one of the two SPE magazines.

ABSTRACT

Reservoir analysis methods are applied to simple closed geothermal reservoirs that produce by internal steam drive. Relations are presented for the reservoir temperature, pressure, and fluid saturations, with the assumption that the fluids are produced according to their respective relative permeabilities. Calculated performances are given for various types of reservoirs. Results indicate that hot-water reservoirs can have complicated behaviors, including changing from production of hot water to dry steam.

## INTRODUCTION

Recovering of geothermal energy has been accelerated in recent years. Increased understanding is needed of the fundamental heat and fluid flows involved in geothermal reservoir production. Techniques used by petroleum production researchers are particularly well suited to the study of these fundamentals, and to geothermal reservoir engineering in general.

[illegible] appendix, and illustrations [illegible].

Some geothermal reservoirs are similar to oil and gas reservoirs. The reservoir is a porous media, through which the fluids flow according to Darcy's law. Furthermore, some geothermal reservoirs have the equivalent of cap rocks.

The analogy between oil and gas reservoirs is the basis for the fundamental assumption of this paper: fluid flow in a geothermal reservoir can be treated as the flow through a porous medium, and Darcy's law and relative permeabilities are applicable.

There are many analogies between petroleum and geothermal reservoir engineering. For example, a number of the drives which supply reservoir energy are similar. The edge water drive in a petroleum reservoir is analogous to influx from cooler aquifers in geothermal reservoirs. Solution gas drive in petroleum reservoirs is analogous to two-phase internal steam drive in geothermal reservoirs. Compaction drive can occur in both. Waterflooding an oil reservoir is analogous to water cycling in a hot-water geothermal reservoir.

Methods of analysis similar to those used in petroleum reservoir engineering can be used for geothermal reservoirs as illustrated by the development of the material and heat balances in Reference 1. The present paper presents an analysis of internal steam drive, using methods analogous to those used for solution gas drive in Reference 2. The analysis presented herein is based on the following assumptions: the temperature, pressure, and fluid saturation gradients are small; the steam and hot water are produced according to their respective mobilities as determined by relative permeabilities and viscosities; and the effects of capillary pressure and gravity can be neglected. Some gravitational effects however, are treated qualitatively in the discussion. Throughout the analysis and discussion the produced steam and hot water are calculated neglecting the pressure and temperature drops near the wells and in the wellbores. The effects of these additional changes must be introduced to obtain steam and hot water production rates at the wellhead.

## DISCUSSION

### Temperature-Pressure Behavior

As pointed out in Reference 1, initial temperature and pressure in a geothermal reservoir determine its reservoir type. The solid line in Figure 1 presents the boiling curve for pure water. (Curves for actual geothermal brines will be modified by the dissolved salts[3].) Points to the right of the curve and below the critical temperature represent hot water reservoirs. Points to the left of the curve and also points above the critical temperature represent single-phase or steam reservoirs.

The mathematical analysis is presented in the Appendix. Ordinary differential equations are derived for the fluid saturations and reservoir pressure (for two-phase flow) and for the pressure and temperature (for single-phase flow). Equations 13 and 16 of the Appendix were solved numerically for the temperature-pressure behavior of closed geothermal reservoirs containing fresh water and having the relative permeability curves presented in Figure 2. Other values used in the calculations are: 162 lbs/ft$^3$ rock grain density, 0.20 Btu/°F-lb specific heat of rock, 40 Btu/ft-day-°F thermal conductivity, and 1.0 Darcy's permeability. Results of these calculations for a porosity of .25 are presented by the dashed lines in Figure 1.

As production causes the reservoir pressure to decline, the temperature follows the dashed line that passes through initial temperature and pressure. Several such lines are presented in Figure 1. For example, from initial conditions corresponding to Point A in Figure 1, the temperature will move to the left along line 1 as the pressure declines. This case (reservoir A) corresponds to a single-phase (essentially steam) reservoir with initial temperature and pressure above the critical values. No hot water is formed during pressure depletion, since line 1 does not intersect the boiling curve. The reservoir temperature remains high after the pressure is depleted. Thus, additional energy could be extracted by water injection, beginning at any point along line 1.

The initial conditions corresponding to Point B (reservoir B) in Figure 1 represent a dry-steam reservoir in which no hot water is formed during pressure depletion and much heat would remain unproduced if the pressure were depleted. The temperature would move along line 3 as the pressure declines.

Point C (reservoir C) in Figure 1 corresponds to an initial hot water reservoir with pressure above the boiling curve. Unless a strong rock drive exists, initially the pressure declines rapidly with production, since only liquid expansion and rock compaction supply the driving energy. The reservoir performs essentially isothermally along line 4 until the boiling curve is reached. Then steam begins to be generated within the reservoir and a steam phase begins to build up within the rock pores. This supplies a gas drive similar to a solution gas drive in a petroleum reservoir. As production continues, the temperature and pressure decline along the boiling curve. The steam saturation increases with production and when it reaches its equilibrium saturation the reservoir begins to produce steam along with hot water.

The produced steam-hot water ratio continues to increase until the water saturation is reduced to its maximum immobile saturation. Then only saturated steam is produced. Water saturation continues to decline until all the water has been boiled away. The temperature then departs from the boiling curve and its decline essentially stops. The produced steam becomes increasingly superheated, as indicated by line 4 in Figure 1.

Point D (reservoir D) in Figure 1 corresponds to a relatively low-temperature hot water reservoir. Except for those cases with strong rock drives, rapid pressure decline with production should occur, since only liquid expansion and rock drive supply the driving energy above the boiling curve. Two-phase internal steam drive does not begin until the reservoir pressure has declined to a small fraction of its initial value. There is sufficient water in the pores that some water will remain even if the pressure reaches atmospheric. Most of the steam produced through pressure depletion of this type of reservoir will be at low pressures. These low pressures result in low efficiencies if used in steam turbines to produce power. For this reason power production from such reservoirs is perhaps best accomplished by cycling hot water through the reservoirs and using a binary cycle power plant (Reference 4).

## Fluid and Heat Production Performance

Figures 3 and 4 present the variations of the reservoir pressure and temperature with the percent of initial fluid mass produced. Reservoirs A and B perform essentially by isothermal steam expansion; reservoirs C and D involve two-phase internal steam drive. Almost all of the initial fluid is produced from reservoirs A, B and C and much of it is produced from reservoir D. Reservoirs A and B experience little temperature drop during production and in reservoir C the temperature declines from 550 to 530°F. Thus, in these cases much heat remains in the reservoir rock at the end of pressure depletion.

Figure 5 presents the pressure versus steam saturation for reservoirs C and D. The increasing negative slope of the reservoir C curve with steam saturation reflects the increasing produced steam-hot water ratios as the steam saturation increases with pressure depletion.

Figure 6 presents the variation of pressure with the amount of heat produced which is over and above the amount of heat that would be in the reservoir if it contained only saturated steam at atmospheric pressure and 212°F. Results for reservoirs A and B indicate that relatively small amounts of the total heat are produced during pressure depletion. Figure 7 presents the pressure versus heat recovered in the form of steam and in the form of hot water for reservoirs C and D. These results indicate that more heat is produced in the form of steam than hot water. This reflects the higher heat content and the lower viscosity of the steam as compared to the hot water. Figure 8 presents the pressure versus heat produced for six hot water reservoirs with three different porosities. The increase in heat recovered with porosity for the higher initial pressure cases results from the larger volume of initial water present relative to the reservoir rock volume.

## Gravity Segregation

The results presented to this point are based on the assumption that the fluids are uniformly distributed throughout the reservoir. In reality gravity segregation of the steam and hot water will begin as soon as the steam phase becomes mobile. Reservoir performance and gravity segregation studies of oil and gas in oil reservoirs indicate that in many cases segregation occurs rapidly (References 5, 6 and 7). Similar segregation of the steam and hot water should occur in geothermal reservoirs.

The results for uniformly distributed fluids are useful in visualizing the behavior of reservoirs in which rapid gravity segregation takes place and in which heat conduction, natural convection, and capillarity, can be neglected to a first approximation. Steam accumulation at the top of a reservoir resulting from gravity segregation can greatly reduce the amount of water available there to generate steam. Similarly the drainage of hot water to the lower portion of the reservoir increases the amount of water

available there for steam generation. Under gravity segregation reservoir C should perform the same as given in Figures 1 and 3 through 8 until the steam saturation reaches its equilibrium value. Then the steam phase becomes mobile and gravity segregation begins. Steam saturation will increase rapidly near the top of the reservoir. If the wells are completed high in the reservoir or significant steam coning occurs, the produced steam-hot water ratio will increase rapidly. The hot water saturation will decrease rapidly until the water in the region is exhausted. Thus this region will depart from the boiling curve at considerably higher temperatures and pressures than for reservoir C. Points low in the reservoir will have high water saturations longer than if the fluid were to remain uniformly distributed, and these points will remain on the boiling curve to lower temperatures and pressures.

If the wells are completed low in the reservoir and significant steam coning does not take place, the produced steam-hot water ratio will remain low until the steam zone has expanded sufficiently to cause production from the steam zone. Points in the steam zone will depart from the boiling curve at higher pressures and temperatures than in the uniform saturation case and the lower portion of the reservoir will remain on the boiling curve to lower pressures and temperatures.

Thus the relative amounts of steam and hot water produced will depend upon, among other things, the amount of gravity segregation, the relative permeability curves, the structural position of the completion intervals, and the amount of steam and water coning. For many conditions the amount of water initially present is so limited that much usable heat should remain in the reservoir after the water is exhausted. This heat may be distributed in a highly nonuniform manner, with generally higher temperatures in the upper portion of the reservoir. In most cases the produced steam contains much more heat than an equal mass of produced water. Thus for many conditions more total heat can be produced by completing the wells high in the reservoir, to enhance steam production and suppress water production. This should result in more of the dissolved salts being left in the reservoir. This would be an additional advantage provided problems associated with salt deposition are not too severe.

## CONCLUSIONS

1. Reservoir analysis methods can be applied to those geothermal reservoirs that involve the flow of steam or hot water through porous media.

2. Hot-water reservoirs can have complicated producing characteristics including changing from hot water to steam as they are produced.

3. Under certain conditions only a relatively small amount of the heat initially contained in a geothermal reservoir will be produced during pressure depletion. Much of this heat may be contained in the produced steam even though initially the reservoir contains only hot water.

4. For many conditions where gravity segregation of the steam and hot water occur during depletion, more of the total heat can be produced by completing wells high in the reservoir to enhance steam production and suppress water production.

## REFERENCES

1. Whiting, R. L. and Ramey, H. J.: "Application of Material and Energy Balances to Geothermal Steam Production", J. Pet. Tech. (July 1969) pp. 893-900.

2. Martin, J. C.: "Simplified Equations of Flow in Gas Drive Reservoirs and the Theoretical Foundation of Multiphase Pressure Buildup Analyses", Trans AIME (1959) vol. 216, pp. 309-311.

3. Hass, J. L.: "The Effect of Salinity on the Maximum Thermal Gradient of a Hydrothermal System at Hydrostatic Pressure", Econ. Geology, Vol. 66 (1971) pp. 940-946.

4. Kruger, P. and Otte, Carel: Geothermal Energy, Stanford Univ. Press, Stanford, Calif. (1973).

5. Spivak, A.: "Gravity Segregation in Two-Phase Displacement Processes", SPEJ (Dec. 1974) Vol. 14, No. 6, pp. 619-632.

6. Martin, J. C.: "Reservoir Analysis for Pressure Maintenance Operations Based on Complete Segregation of Mobile Fluids", Trans. AIME (1958) Vol. 213, pp. 220-227.

7. Martin, J. C.: "Some Mathematical Aspects of Two-Phase Flow with Applications to Flooding and Gravity Segregation Problems", Prod. Monthly (April 1958), pp. 22-35.

## APPENDIX

The mathematical relations for both two-phase (boiling) and single phase flow are derived in this appendix.

### Two Phase Relations

The basic equations for conditions along the boiling curve are:

Darcy's law for hot water:

$$u_w = - \frac{k\, k_{rw}}{\mu_w} \nabla p \qquad (1)$$

Darcy's law for steam:

$$u_s = - \frac{k\, k_{rs}}{\mu_s} \nabla p \qquad (2)$$

The equation of continuity for mass:

$$\nabla \cdot (\rho_w u_w + \rho_s u_s) = - \frac{\partial}{\partial t} \left[\phi(\rho_w S_w + \rho_s S_s)\right] \qquad (3)$$

The equation of continuity for heat:

$$\nabla \cdot (\rho_w h_w u_w + \rho_s h_s u_s - k_h \nabla T) = - \frac{\partial}{\partial t} \left\{\phi[\rho_w h_w S_w + \rho_s h_s S_s + (\tfrac{1-\phi}{\phi})\rho_r C_r T]\right\} \qquad (4)$$

saturations:

$$S_w + S_s = 1 \qquad (5)$$

Substituting equations 1 and 2 into 3 yields:



$$\nabla \cdot \lambda_f \nabla p = \frac{\partial M_f}{\partial t} \qquad (6)$$

$$\nabla \cdot \lambda_h \nabla p = \frac{\partial M_h}{\partial t} \qquad (7)$$

where

$$\lambda_f = \frac{\rho_w k\, k_{rw}}{\mu_w} + \frac{\rho_s k\, k_{rs}}{\mu_s}$$

$$\lambda_h = \frac{\rho_w h_w k\, k_{rw}}{\mu_w} + \frac{\rho_s h_s k\, k_{rs}}{\mu_s} + k_h \psi'$$

$$M_f = \phi(\rho_w S_w + \rho_s S_s)$$

$$M_h = \phi[\rho_w h_w S_w + \rho_s h_s S_s + (\tfrac{1-\phi}{\phi})\rho_r C_r \psi]$$

$$T = \psi(p) \qquad (8)$$

and

$$\psi' = \frac{d\psi}{dp}$$

The symbol $\lambda_f$ denotes the mobility of the fluids in terms of mass; $\lambda_h$, the mobility of the heat; $M_f$, the mass of fluid per unit volume of reservoir rock; and $M_h$, the total heat per unit volume of rock.

Equations 5 and 6 can be written as

$$\frac{\partial \lambda_f}{\partial p} \nabla p \cdot \nabla p + \frac{\partial \lambda_f}{\partial T} \nabla T \cdot \nabla p + \frac{\partial \lambda_f}{\partial S_w} \nabla S_w \cdot \nabla p + \frac{\partial \lambda_f}{\partial S_s} \nabla S_s \cdot \nabla p + \lambda_f \nabla^2 p = \frac{\partial M_f}{\partial t} \qquad (9)$$

$$\frac{\partial \lambda_h}{\partial p} \nabla p \cdot \nabla p + \frac{\partial \lambda_h}{\partial T} \nabla T \cdot \nabla p + \frac{\partial \lambda_h}{\partial S_w} \nabla S_w \cdot \nabla p + \frac{\partial \lambda_h}{\partial S_s} \nabla S_s \cdot \nabla p + \lambda_h \nabla^2 p = \frac{\partial M_h}{\partial t} \qquad (10)$$

In those cases where the saturation gradient, temperature gradient, and pressure gradients are small, the vector products $\nabla p \cdot \nabla p$, $\nabla T \cdot \nabla p$, $\nabla S_w \cdot \nabla p$ and $\nabla S_s \cdot \nabla p$ are small compared to the magnitudes of $\nabla^2 p$, $\frac{\partial M_f}{\partial t}$, and $\frac{\partial M_h}{\partial t}$, and the terms containing the vector products can be neglected to a first approximation.

Equations 9 and 10 reduce to:

$$\nabla^2 p = \frac{1}{\lambda_f} \frac{\partial M_f}{\partial t} \tag{11}$$

$$\nabla^2 p = \frac{1}{\lambda_h} \frac{\partial M_h}{\partial t} \tag{12}$$

Equations 11 and 12 require that the variations of P, $S_w$, $S_s$, and T are small with distance. Fortunately the variations of these quantities with time need not be small.

The elimination of $\nabla^2 p$ from Equations 11 and 12 yield (replacing T by $\psi(p)$ and $S_s$ by $1-S_w$):

$$\frac{\partial M_f}{\partial p}\frac{\partial p}{\partial t} + \frac{\partial M_f}{\partial S_w}\frac{\partial S_w}{\partial t} = \frac{\lambda_f}{\lambda_h}\left(\frac{\partial M_h}{\partial p}\frac{\partial p}{\partial t} + \frac{\partial M_h}{\partial S_w}\frac{\partial S_w}{\partial t}\right)$$

This equation reduces to the following ordinary differential equation:

$$\frac{dS_w}{dp} = \frac{\lambda_h \frac{\partial M_f}{\partial p} - \lambda_f \frac{\partial M_h}{\partial p}}{\lambda_f \frac{\partial M_h}{\partial S_w} - \lambda_h \frac{\partial M_f}{\partial S_w}} \tag{13}$$

Equation 13 can be integrated numerically to obtain $S_w$ as a function of P. This relation is similar to the Muskat solution gas relation which relates oil or gas saturation to reservoir pressure.

The relation between $S_w$ and P obtained from Equation 13 can be used to eliminate $S_w$ from $\lambda_f$, $\lambda_h$, $M_f$, and $M_h$. This allows Equations 11 and 12 to be expressed in terms of pressure, thereby obtaining a partial differential equation for pressure that can be used in the analysis of transient well pressure data which involve two-phase flow in the reservoir.

Single Phase Flow **116**

The temperature and pressure are not related to the boiling curve for single-phase flow. Equation 11, however, is valid and the equivalent of Equation 12 is:

$$\nabla^2 p + \frac{k_h}{\rho h \lambda}\nabla^2 T = \frac{1}{\rho h \lambda}\frac{\partial M_h}{\partial t} \tag{14}$$

where h is the enthalpy, $\lambda$ is the mobility, and $M_h$ is the single phase equivalent of $M_h$.

In the case of two phase flow it was possible to obtain an ordinary differential equation for the water saturation versus pressure without neglecting the effects of heat conduction, because temperature and pressure are related by the boiling curve. Unfortunately, this is not the case for single phase flow; however, if we neglect the effects of heat conduction, Equation 14 reduces to:

$$\nabla^2 p = \frac{1}{\rho h \lambda}\frac{\partial M_h}{\partial t}$$

Eliminating $\nabla^2 p$ from Equations 11 and 15 leads to the following differential equation for P and T:

$$\frac{dT}{dp} = \frac{\frac{\partial M_h}{\partial p} - h\frac{\partial M_f}{\partial p}}{h\frac{\partial M_f}{\partial T} - \frac{\partial M_h}{\partial T}} \tag{16}$$

This equation was used to calculate T versus P for single phase flow. As expected, numerical results reveal small values of $\frac{dT}{dp}$ indicating essentially isothermal behavior.

Additional Relations

Solutions of Equations 13 and 16 yield the temperature and fluid saturations as functions of reservoir pressure. Heat and mass balances can be used to obtain the fluid and heat productions as functions of pressure. These relations are:

$$G_f = 1 - \frac{M_f}{M_{fi}}$$

where $Q_f$ is the fraction of the original fluid mass that has been produced and the subscipt i refers to initial conditions.

$$Q_h = \frac{M_{hi} - M_h}{M_{hi} - M_{ha}}$$

where $Q_h$ is the fraction of the original heat that has been produced which is above the heat contained in the reservoir at atmospheric pressure and 212°F containing only saturated steam. The subscript a refers to these conditions.

Expressions for the relative amounts of heat produced in the steam and in the hot water can be obtained by integration. These relations are:

$$Q_{hw} = \left(\frac{1}{M_{hi} - M_h}\right)\int_{p_1}^{p}\left(\frac{\rho_w h_w k\, k_{rw}}{\lambda_h\, \mu_w}\right)\frac{dH_h}{dp}\,dp$$

$$Q_{hs} = \left(\frac{1}{M_{hi} - M_h}\right)\int_{p_1}^{p}\left(\frac{\rho_s h_s k\, k_{rs}}{\lambda_h\, \mu_s}\right)\frac{dH_h}{dp}\,dp$$

where $Q_{hw}$ and $Q_{hs}$ are the fractions of the produced heat contained in the hot water production and in the steam production respectively.

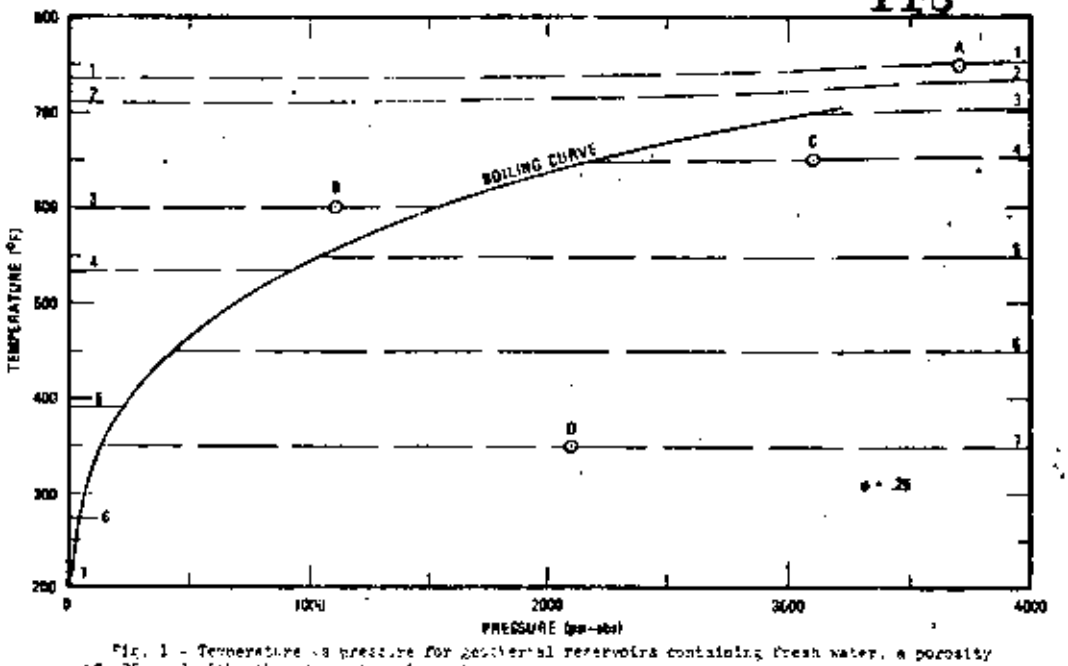


Fig. 1 - Temperature vs pressure for geothermal reservoirs containing fresh water, a porosity of .25, and with other rock-water properties.

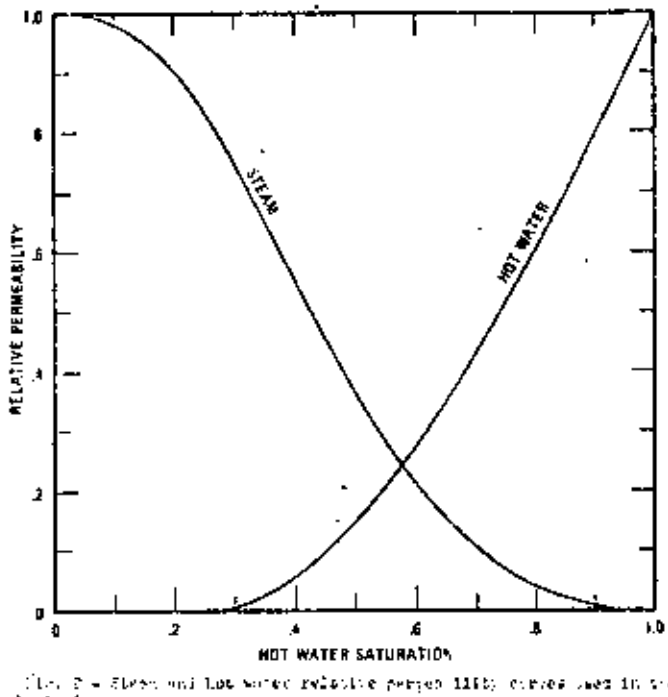


Fig. 2 - Steam and hot water relative permeability curves used in the calculations.

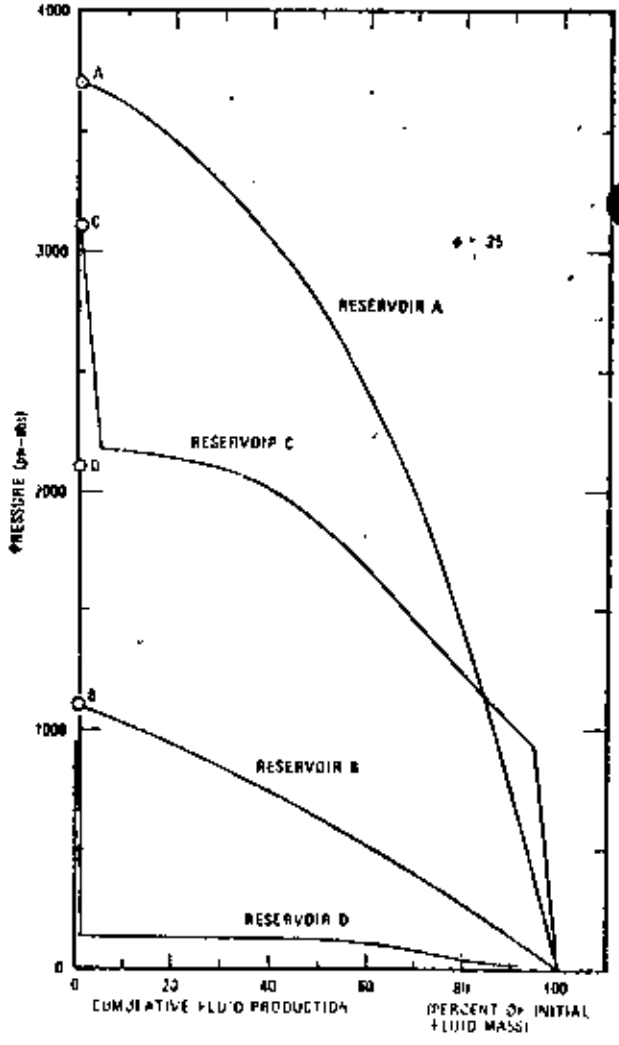


Fig. [illegible] - [illegible] fluid production for reservoirs A, [illegible]

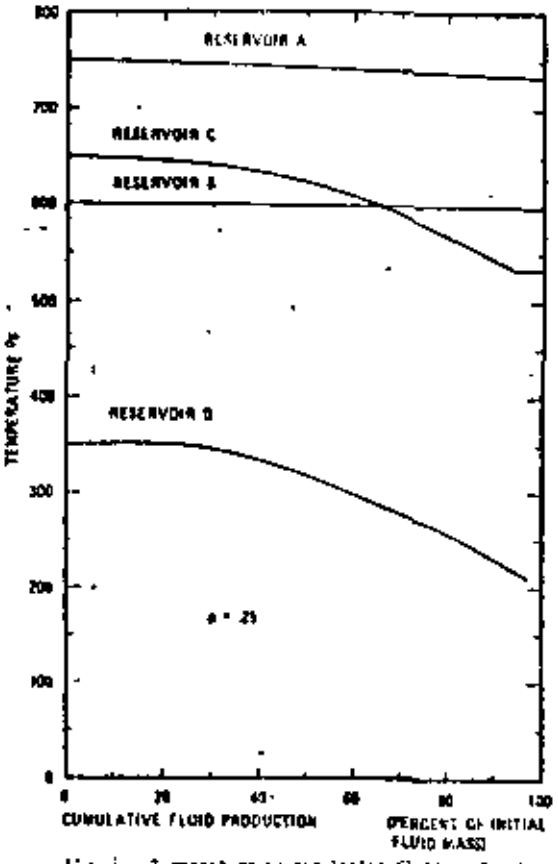


Fig. 4 - Temperature vs cumulative fluid production for reservoirs A, B, C, and D.

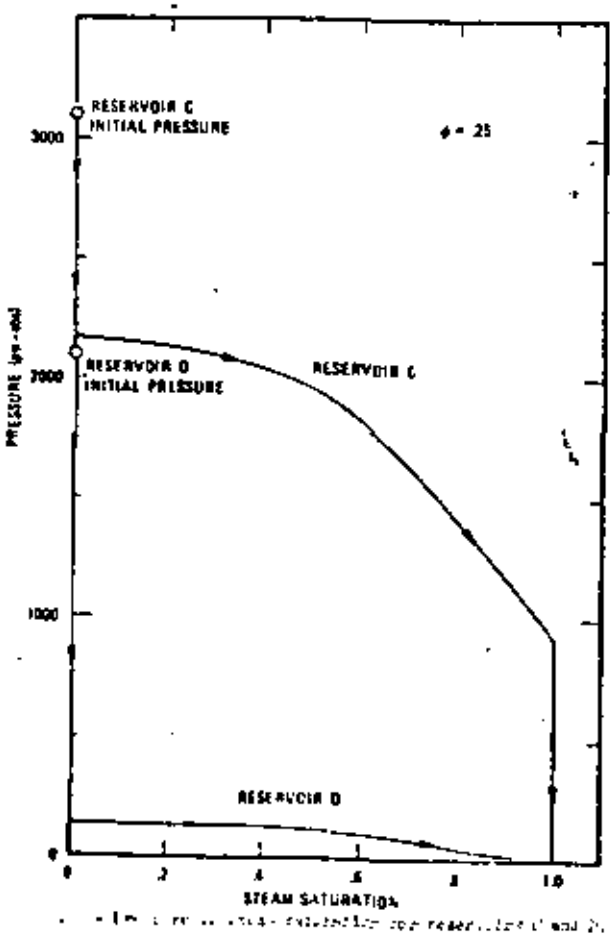

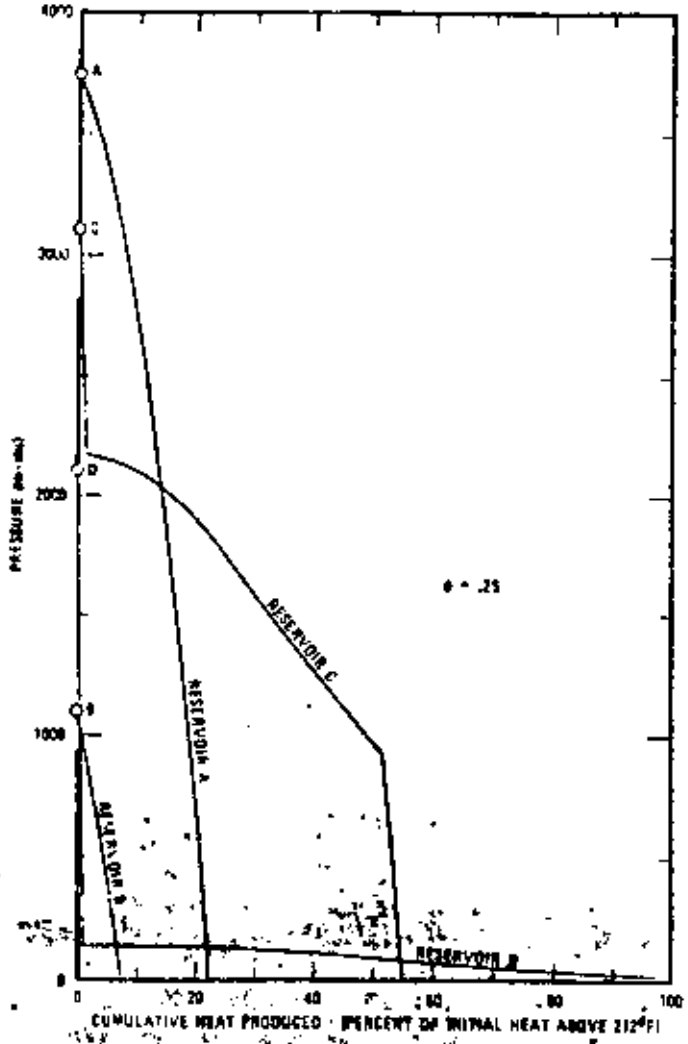


Fig. 1 - Pressure vs cumulative heat produced for reservoirs A, B, C, and D.

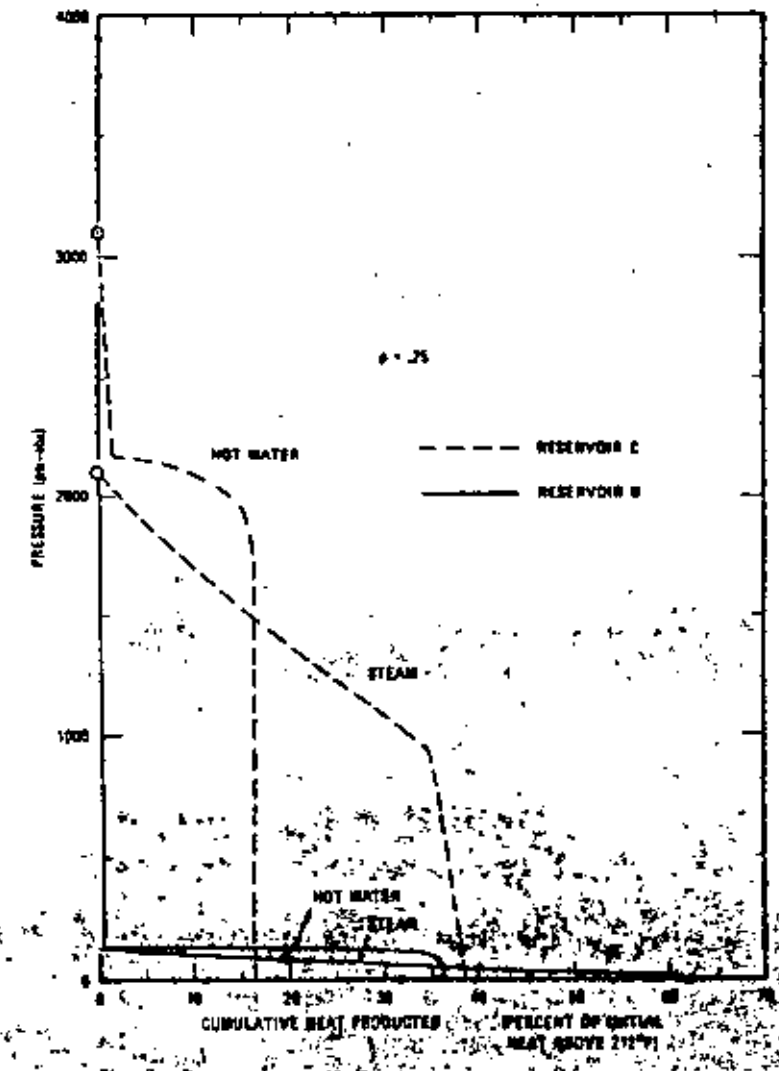


Fig. 2 - Pressure vs cumulative heat produced as steam and as hot water for reservoirs C and D.

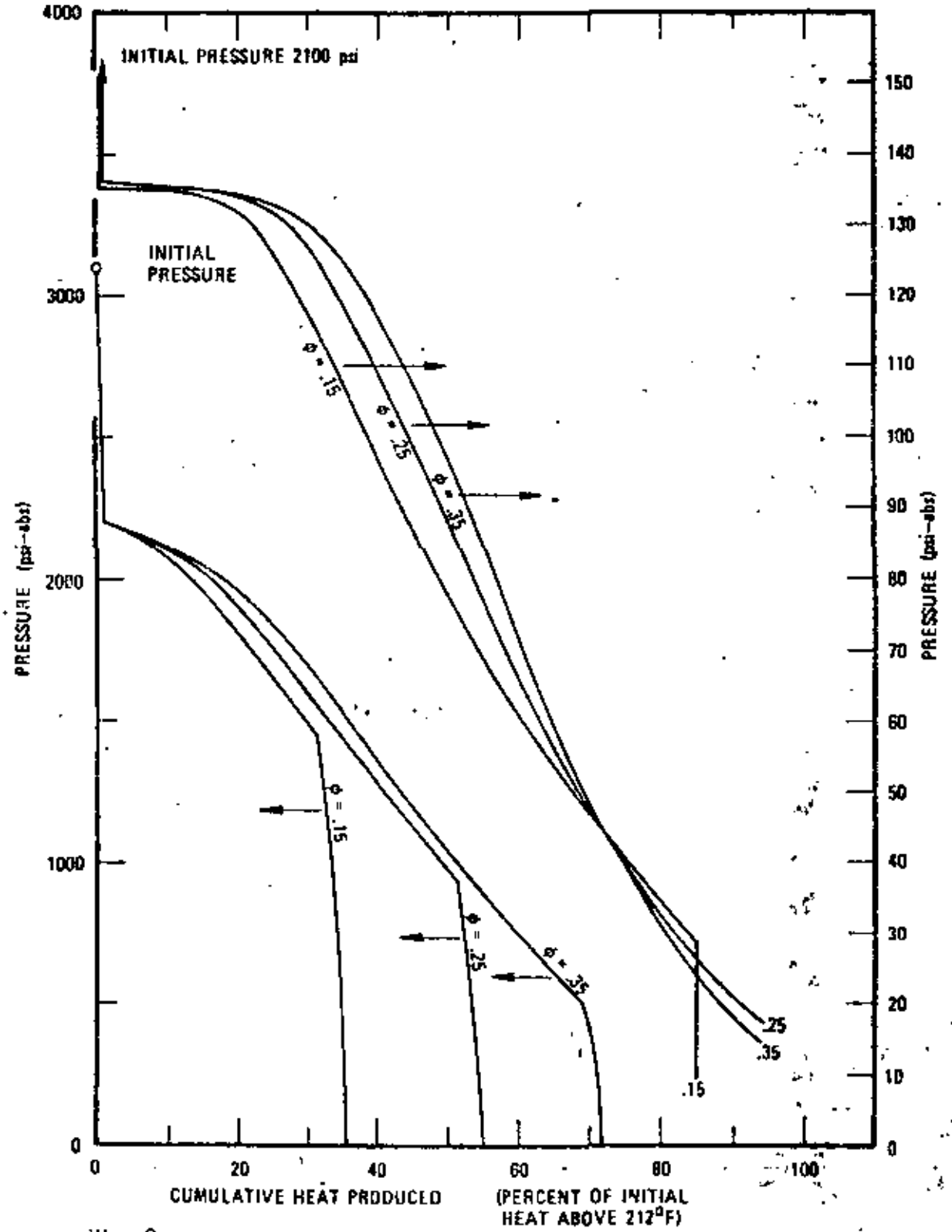


Fig. 8 - Pressure vs cumulative heat produced for three different porosities and two different initial conditions (3100 psi, 650 °F and 2100 psi, 350°F).

# MODELING GEOTHERMAL SYSTEMS

by

P. A. Witherspoon,[1] S. P. Neuman,[1] M. L. Sorey[2]
and M. J. Lippmann[3]

## ABSTRACT

Geothermal systems are receiving more and more attention as an alternative source of energy and, consequently, there is growing interest in attempting to understand their nature and behavior. One approach to this problem is to attempt to deduce the physical behavior of such systems using a mathematical model. This paper presents the governing equations for energy and mass transfer in porous media that must be solved in using such models. Fundamental concepts that have been developed for factors that affect the development of free and forced convection in geothermal systems under natural conditions are reviewed. The results of modeling geothermal systems during exploitation using lumped-parameter and distributed-parameter models are also presented.

---

[1] Lawrence Berkeley Laboratory and Department of Civil Engineering, University of California, Berkeley.

[2] U. S. Geological Survey, Menlo Park, California.

[3] Department of Civil Engineering, University of California, Berkeley.

## INTRODUCTION

Geothermal systems are receiving more and more attention as an alternative source of energy and, consequently, there is growing interest in attempting to understand their nature and behavior. One approach to this problem is to attempt to deduce the physical behavior of such systems using a mathematical model. Such a model consists of a set of equations that describe the processes occurring within the system and the solution to these equations subject to conditions that prevail at a particular site.

The model approach has two important applications: (1) the geothermal system under natural conditions before being disturbed by man, and (2) the geothermal system during exploitation. Natural geothermal systems have been investigated by a great many workers. The main thrust of such studies has been to understand how geothermal systems can form and persist within the earth's crust.

The mathematical model can also be applied to the problem of evaluating the behavior of a geothermal system during exploitation. One of the most critical problems in developing such systems as a viable source of energy is that of determining that a particular reservoir once discovered is capable of producing significant quantities of energy over meaningful periods of time. The model is one of several tools that can be used to analyze this problem. During the early stages, the model may be crude, but its application in parametric analysis of the field data can provide valuable limits as to what can be expected. As more data become available, the model can be refined and such engineering questions as well spacing, optimum rates of fluid withdrawal and effects of reinjection can be studied.

In this review, we shall restrict our attention to hydrothermal systems, i.e., to geothermal systems involving water. We shall pay particular attention

to hydrothermal-convection systems, in which most of the heat is transferred in circulating fluids rather than by heat conduction. Two broad types of hydrothermal systems are recognized: (1) hot-water, and (2) vapor-dominated (White 1973).

In the hot-water type, water is the continuous phase throughout the system and thus provides the pressure control. Continuity of the liquid phase is evident from reservoir pressures that are near hydrostatic and the presence of soluble salts that are not found to any significant degree in low-pressure steam. In the vapor-dominated type, steam is the continuous, pressure-controlling phase, although there is general agreement that liquid water must also be present (Facca and Tonani 1964, Elder, 1965; Craig, 1966; James, 1968; Marinelli, 1969; Sestini, 1970; White et al., 1971).

An intriguing question arises concerning the initial conditions of vapor-dominated systems. At depths below 350 m, they all tend to have temperatures near 240°C and pressures near 35 kg/cm$^2$, which usually means well below hydrostatic (White, 1973). This uniformity in the initial conditions is believed to be strongly influenced by the maximum enthalpy of saturated steam (James, 1968; Sestini, 1970; White at al., 1971).

The material and thermodynamic properties of the different components of geothermal systems are an important consideration in any attempt to develop realistic models of such systems. Fig. 1 presents a pressure-enthalpy diagram for pure water at pressures up to 700 kg/cm$^2$ and temperatures up to 500°C. Dissolved salts are, of course, common in geothermal waters and studies on the effect of salinity on heat capacity (Nevens and Pool, 1964; Likke and Bromley, 1973), density (Haas, 1970), viscosity (Matthews and Russell, 1967, Fig. G4), and maximum thermal gradient (Haas, 1971) of brines are available. Helgeson (1968) has investigated the thermodynamic characteristics of the Salton Sea geothermal system where the highest concentrations, approaching 300,000 ppm, have been found.

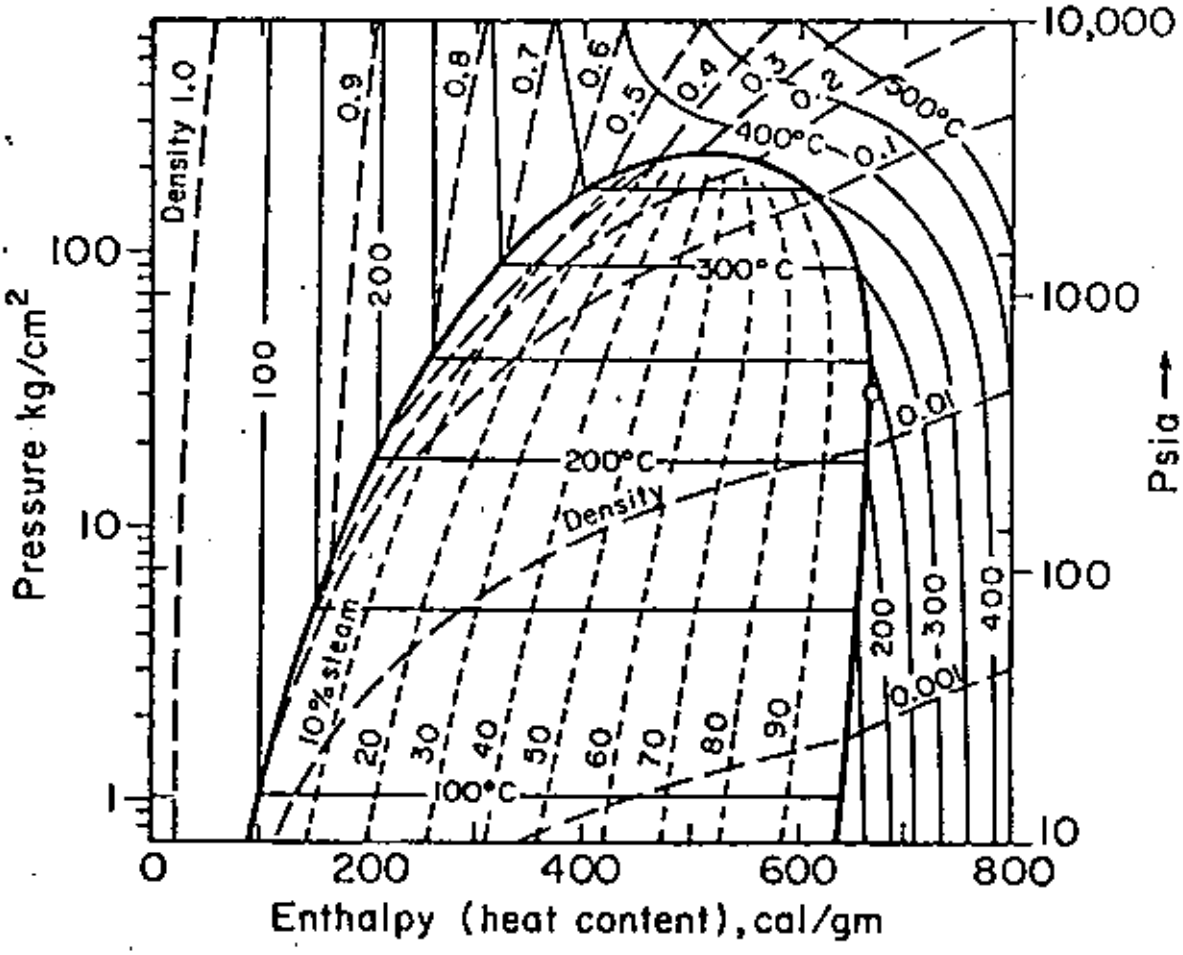


Fig. 1. Pressure–enthalpy diagram for pure water and vapor, showing contours of equal temperature, density and mass proportions of steam to water. Open circle indicates maximum enthalpy of saturated steam, 670 cal/gm at 236°C and 31.8 kg/cm$^2$ (after White et al., 1971).

The thermal properties of rocks are very important since the dominant fraction of the total energy in a geothermal system is in the solid matrix. Comprehensive tables of these properties for dry rocks have recently been compiled by Kappelmeyer and Haenel (1974). Thermal conductivities for most dry rocks range from 4 to 10 mcal/cm sec $^{o}$C; specific heats are approximately 0.2 cal/g $^{o}$C; and thermal diffusivities range from 5 to 15 cm$^2$/sec. Kappelmeyer and Haenel also include the effects on these thermal properties of temperature and pressure.

The thermal conductivity of fluid-saturated rocks is dependent on the conductivities of the dry rock and the saturating fluid as well as the physical properties of the rock. Anand et al. (1973) and Somerton et al. (1974) have shown how thermal conductivities increase with brine saturation and become more sensitive to temperature change. They discuss correlations for predicting thermal conductivity from other rock properties.

The hydraulic properties of the rocks are also important since they control the fluid movement. The absolute values of permeability and porosity for rocks vary considerably and must be measured or estimated for any given system. A few workers have studied the thermal effects and report that the absolute permeability tends to decrease, sometimes significantly, with increasing temperature (Greenberg et al., 1968; Sanyal et al., 1972; Casse, 1974). There are also important effects of temperature on relative permeability (Edmonson, 1965; Davidson, 1969; Poston et al., 1970; Weinbrandt et al., 1972; Lo and Mungan, 1973; Ramey et al., 1974). In studying the effects of pressure, a number of workers (Knutson and Bohor, 1963; Brace et al., 1968; Vairogs et al., 1971) have suggested that permeability depends only on effective stress; that is, permeability is dependent only on the difference between hydrostatic confining pressure and internal pore pressure. However, Zoback and Byerlee (1975), have recently shown that pore pressure has a significantly larger effect on permeability under isothermal conditions than does confining pressure.

In this review of the problems involved in modeling geothermal reservoirs, we shall first present the governing equations for energy and mass transfer in porous media. Then we shall consider some of the fundamental concepts that have been developed for factors that affect the development of free and forced convection in geothermal systems under natural conditions. Lastly, we shall review the results of several efforts that have been made to model geothermal systems during exploitation.

## GOVERNING EQUATIONS

Let us consider a porous medium completely saturated with a single-component homogeneous fluid which can be either in a liquid or gaseous state. The liquid and gas phases are assumed to be separated locally by a distinct interface due to capillarity. Since mass may be transferred from one phase to another across the interface by vaporization or condensation, it is convenient to write a single mass balance equation for both phases

$$\frac{\partial}{\partial t}\left(\phi S^L \rho^L + \phi S^G \rho^G\right) = -\frac{\partial}{\partial x_i}\left(\rho^L v_i^L + \rho^G v_i^G\right) \tag{1}$$

Rate of mass accumulation — Convective mass flux

All mathematical symbols appearing in the text are macroscopic quantities defined over a representative elementary volume of the porous medium. For a definition of these symbols the reader is referred to the Nomenclature.

It is generally believed that capillary pressure between the phases is small relative to absolute pressure, and as each phase may flow independently, we shall assume Darcy's law in the form

$$v_i^L = -\frac{k_{ij} k_r^L}{\mu^L}\left(\frac{\partial p}{\partial x_j} - \rho^L g_j\right) \tag{2}$$

$$v_i^G = -\frac{k_{ij} k_r^G}{\mu^G}\left(\frac{\partial p}{\partial x_j} - \rho^G g_j\right) \tag{3}$$

The relative permeabilities $k_r^L$ and $k_r^G$ are functions of fluid saturation and, as mentioned earlier, they may also be functions of temperature. Recent studies (Coats et al., 1974) indicate the latter effect is important and should be taken into account.

An energy balance equation must also be considered, and one way to derive such an equation in terms of macroscopic quantities is to follow an averaging procedure (see Appendix). Equation A21 is a general form of the macroscopic energy balance for the case where irreversible viscous dissipation of mechanical energy and transfer of kinetic energy between fluid and rock are neglected. An attempt to derive a set of more general equations considering mechanical interaction between rock and fluid has been reported recently by Brownell et al. (1975). It is customary to assume that not only is the capillary pressure zero, but also that the solid, liquid, and gas are locally in thermal equilibrium. In this case (A21) reduces to (A22) which can be written more conveniently without the angular brackets as

$$\underbrace{\frac{\partial}{\partial t}\left[\phi\, S^L \rho^L e^L + \phi\, S^G \rho^G e^G + (1-\phi)\, \rho^S e^S\right]}_{\text{Rate of internal energy accumulation}} = \underbrace{\frac{\partial}{\partial x_i}\left(\kappa_{ij}^{eff} \frac{\partial T}{\partial x_j}\right)}_{\text{Conductive and dispersive internal energy flux}}$$

$$- \underbrace{\frac{\partial}{\partial x_i}\left(\rho^L e^L v_i^L + \rho^G e^G v_i^G\right)}_{\text{Convective internal energy flux}} - \underbrace{p\, \frac{\partial}{\partial x_i}\left(v_i^L + v_i^G\right)}_{\text{Rate of reversible mechanical energy (work) conversion to internal energy}} \qquad (4)$$

Our mathematical analysis indicates that

$$\kappa_{ij}^{eff} = \phi\, S^L \kappa_{ij}^L + \phi\, S^G \kappa_{ij}^G + (1-\phi)\, \kappa^S \delta_{ij} \qquad (5)$$

Laboratory experiments show that $\kappa_{ij}^{eff}$ is not always given by (5) (Combarnous and Bories, 1973, Fig. 6), thus implying that the assumption of local thermal equilibrium may not always hold. Moreover, as mentioned earlier, thermal conductivity may also be a function of temperature.

Equation 4 can be reformulated in terms of enthalpy by writing $h - p/\rho$

instead of e and, as shown in (A25), one then has

$$\frac{\partial}{\partial t}\left[\phi\, S^L\, \rho^L\, h^L + \phi\, S^G\, \rho^G\, h^G + (1-\phi)\overset{0}{\rho^S}\, h^S\right] = \frac{\partial}{\partial x_i}\left(\kappa^{eff}_{ij}\, \frac{\partial T}{\partial x_j}\right)$$

$$- \frac{\partial}{\partial x_i}\left(\rho^L\, h^L\, v_i^L + \rho^G\, h^G\, v_i^G\right) + \frac{\partial(\phi p)}{\partial t} + \left(v_i^L + v_i^G\right)\frac{\partial p}{\partial x_i} \qquad (6)$$

This is identical with an expression reported earlier by Mercer et al. (1974) except that we have omitted source terms.

In the particular case where only one fluid phase is present, the energy equation can be conveniently expressed in terms of temperature and, as shown in (A31), one obtains for a liquid saturated medium

$$\left[\phi\, \rho^L\, c_v^L + (1-\phi)\, \rho^S\, c_v^S\right]\frac{\partial T}{\partial t} = \frac{\partial}{\partial x_i}\left(\kappa^{eff}_{ij}\, \frac{\partial T}{\partial x_j}\right)$$

$$- \rho^L\, v_i^L\, c_v^L\, \frac{\partial T}{\partial x_i} - T\left(\frac{\partial p}{\partial T}\right)_v \frac{\partial v_i^L}{\partial x_i} \qquad (7)$$

A similar expression holds for a medium saturated with gas.

The above equations must be supplemented by equations of state relating the thermodynamic variables e, h, $\rho$, $\mu$, S, p, T. Here it is customary to assume that all phases are in equilibrium and that thermodynamic relationships between macroscopic quantities remain the same as those between the equivalent point quantities. In particular, the macroscopic saturations $S^L$ and $S^G$ are assumed to be uniquely determined by the pressure and total energy or enthalpy of the fluid (both phases combined). In other words, whenever two phases occur simultaneously at a point in the system, their p-T relationship is uniquely determined by conditions at the vapor pressure.

Although capillary pressure is neglected in the governing equations, it may still have an important effect on thermodynamic properties. Ramey et al. (1973) explain that the vapor-pressure curve in the presence of uneven capillary surfaces may be lower than that quoted in steam tables. Calhoun et al. (1949) showed that in consolidated sandstones the vapor-pressure curve at 36°C is significantly

affected by a decreasing liquid saturation. However, Cady (1969) and Silhartz (1971) were unable to confirm this effect on unconsolidated sands with temperatures between 121°C and 240°C. The effect of capillary pressure therefore remains unclear.

Some geothermal systems such as those in Imperial Valley (California) involve waters of high salinity which cannot be treated as a homogeneous fluid because salt concentrations are not uniform. In this case the mass as well as energy balance equations (see Appendix) may have to be modified to include a term for dispersive mass flux and an additional equation for mass balance of the solute. Another complication may arise due to coupling between thermal and chemical gradients which modifies the form of Fourier's law of heat conduction (Dufour effect) and Fick's first law of diffusion (Soret effect). The presence of salts may also cause a slight lowering of the vapor-pressure curve (Haas, 1971; Ramey et al., 1973) and this effect becomes progressively more important as boiling proceeds, due to the increasing salt concentration (White, 1973). Very little is known about the behavior of these so-called thermohaline systems, but a few theoretical analyses have appeared (Nield, 1968, 1974; Rubin, 1973, 1975 a,b,c). The discussion that follows will be concerned solely with homogeneous fluids.

## GEOTHERMAL SYSTEMS UNDER NATURAL CONDITIONS

### Fundamental Characteristics of Free Convection

Mathematical modeling related to geothermal systems has long centered on problems of convective heat transfer in a homogeneous porous layer heated from below. Pioneering work on this subject has been performed independently by Horton and Rogers (1945), Lapwood (1948), and Goguel (1953). Their efforts were directed primarily toward developing criteria for the onset of convection currents in a horizontal and laterally infinite layer. These analyses followed the pattern of earlier work by Rayleigh (1916), Jeffreys (1930), and others who showed that in a static layer of viscous fluid the critical temperature gradient (i.e., the

gradient at which cellular or Bénard convection is formed) depends on thermal conductivity, thermal coefficient of expansion, kinematic viscosity, thickness of the layer, and the boundary conditions. When fluid cannot enter or leave the system, the resulting flow pattern is referred to as "natural" or "free" convection. When fluid flow is entirely due to hydraulic forces acting at the boundaries, the result is known as "forced" convection, whereas "mixed" convection includes a combination of both phenomena. Early work on the subject was restricted to free convection.

In reviewing the mathematical approach to free convection in porous media, we find it instructive to follow a recent development by Beck (1972). Consider a rectangular box of porous material resting on a horizontal surface and saturated by a homogeneous liquid (see Fig. 2). The vertical sides are thermally insulated (i.e., adiabatic), and the lower ($z = 0$) and upper ($z = D$) surfaces are isothermal. Temperature $T_1$ at the bottom is greater than $T_o$ at the top, and all boundaries are impermeable to fluid.

In most analytical studies of thermal convection, it is customary to invoke the Boussinesq approximation that spatial as well as temporal variations in fluid density can be neglected except for buoyancy effects (i.e., everywhere except in the gravity term in the equation of motion). In addition, all coefficients in the governing equations are assumed to be constant scalars. Under these conditions the mass balance equation 1 reduces to

$$\frac{\partial v_i}{\partial x_i} = 0 \tag{8}$$

In writing Darcy's law, it is customary to replace $\rho$ by $\rho_o [1 - \beta(T - T_o)]$ in the gravity term and add a term including the time derivative of velocity (compare with Eq. 2),

$$\frac{1}{\phi}\frac{\partial v_i}{\partial t} + \frac{\mu}{k\rho_o} v_i = [1 - \beta (T - T_o)]\, g_i - \frac{1}{\rho_o}\frac{\partial p}{\partial x_i} \tag{9}$$

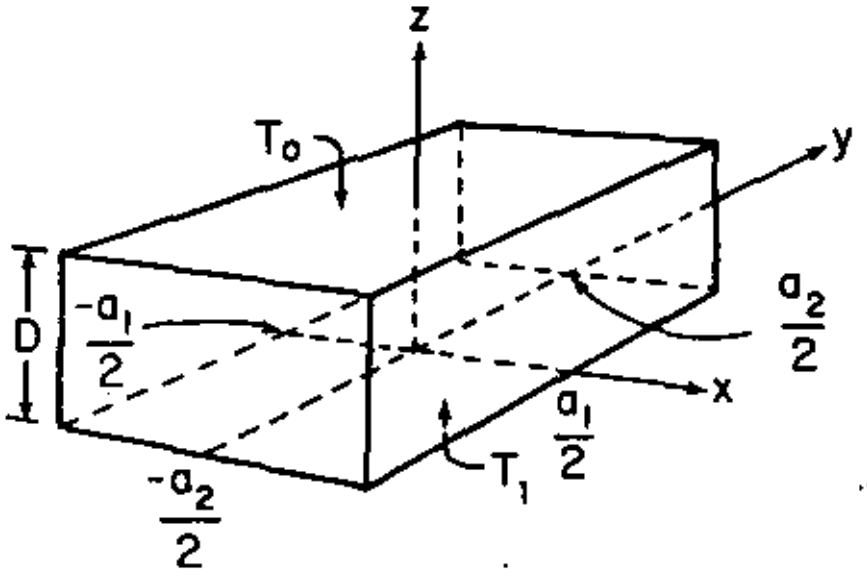


XBL755-2915

Fig. 2. Rectangular box of porous media saturated with a homogeneous liquid.

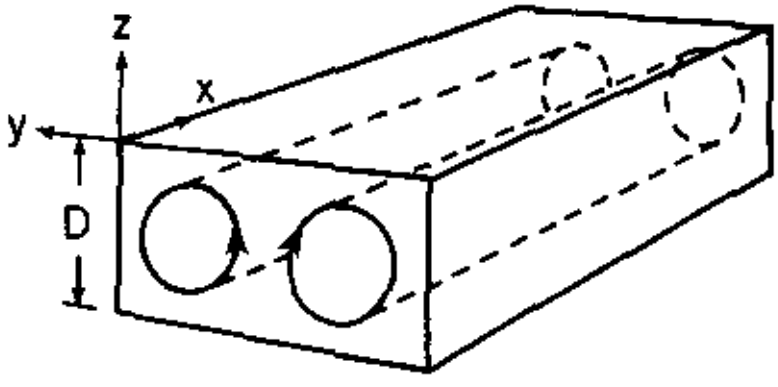


XBL755-2916

Fig. 3. Two convective rolls in rectangular box heated from below.

$$\theta = 0 \qquad \text{at} \quad Z = 0,\ 1 \tag{28}$$

$$\frac{\partial \theta}{\partial X_i} n_i = 0 \quad \text{at} \quad X = \pm \tfrac{1}{2} D_1;\ \ Y = \pm \tfrac{1}{2} D_2 \tag{29}$$

The dynamic stability of this system can be investigated by a linear method or by an energy approach. In the linear approach the disturbances are assumed to be small enough for second-order terms to be neglected. The conditions for marginal stability (i.e., stability just at the onset of convection) can thus be determined from the above equations after reducing (25) and (26) to

$$- Ra^{\frac{1}{2}} \theta \, \delta_{i3} + v_i = - \frac{\partial p_D}{\partial X_i} \tag{30}$$

$$Ra^{\frac{1}{2}} v_i \, \delta_{i3} = - \frac{\partial^2 \theta}{\partial X_i^2} \tag{31}$$

According to the linear theory, the critical Rayleigh number, $Ra_c^{\text{linear}}$, is the smallest eigenvalue of the resulting problem. However, this theory indicates only a necessary condition for stability, and the true critical Rayleigh number may therefore be smaller, $Ra_c^{\text{true}} \leq Ra_c^{\text{linear}}$.

The energy method was first applied to porous media by Westbrook (1969) and was later extended by Wankat and Schowalter (1970) and Beck (1972). Stability is established relative to arbitrary disturbances subject only to the equation of continuity and corresponding boundary conditions. Since stability actually depends on a more restricted class of disturbances satisfying (24) - (29), the critical Rayleigh number obtained may be too conservative and we therefore have $Ra_c^{\text{energy}} \leq Ra_c^{\text{true}}$. However, in the particular case considered here, both methods lead to the same eigenvalue problem and therefore $Ra_c^{\text{linear}} = Ra_c^{\text{energy}}$.

Beck showed that the eigenvalue problem has separable eigenfunctions, the velocity components of which are

$$v_1 = \sin\left[(\tfrac{1}{2}m\pi)(1 + 2X/D_1)\right] \cos\left[(\tfrac{1}{2}n\pi)(1 + 2Y/D_2)\right] U(Z)$$

$$v_2 = \cos\left[(\tfrac{1}{2}m\pi)(1 + 2X/D_1)\right] \sin\left[(\tfrac{1}{2}n\pi)(1 + 2Y/D_2)\right] V(Z) \qquad (32)$$

$$v_3 = \cos\left[(\tfrac{1}{2}m\pi)(1 + 2X/D_1)\right] \cos\left[(\tfrac{1}{2}n\pi)(1 + 2Y/D_2)\right] \sin(\ell\pi Z)$$

$$m,n = 0, 1, 2, \ldots; \quad \ell = 1, 2, \ldots$$

where U(Z) and V(Z) are functions of Z only. The corresponding critical Rayleigh numbers are

$$Ra_c = \pi^2 \min_{\ell,m,n} (b + \ell^2/b)^2 = \pi^2 \min_{m,n} (b + b^{-1})^2 \qquad (33)$$

where $b = \left[(m^2/D_1^2) + (n^2/D_2^2)\right]^{1/2}$ and $\ell = 1$.

Equation 33 shows that the critical Rayleigh number depends entirely on aspect ratios $D_1$ and $D_2$. The minimum possible value of $Ra_c$ is $4\pi^2$ corresponding to $b = 1$. Lapwood (1948) obtained $Ra_c = 4\pi^2$ for the case of a laterally infinite layer, thus indicating that vertical walls tend to stabilize the system. However, $Ra_c$ remains nearly equal to $4\pi^2$ unless $D_1$ or $D_2$ are less than about 0.8, as may happen in a narrow and tall box.

Geometry becomes more important when one considers the mode of convection. It is evident from (32) that when $m = 0$, the horizontal velocity $v_1$ vanishes, which gives rise to n convective cells known as "rolls" (see Fig. 3). Since $Ra_c$ corresponds to $\ell = 1$, $v_3$ in (32) is identically zero only at $Z = 0$ and $Z = 1$, and thus the vertical extent of each roll is equal to the height of the box. A typical temperature profile in a plane perpendicular to the axis of such a roll is shown in Fig. 4. Rolls are invariably preferred over three-dimensional cells whenever the height D is not the smallest dimension. When rolls do form, they are usually parallel to the shorter side, although the overriding rule is for the number of rolls and the direction of their axes to be such that each roll has the closest approximation to a square cross-section as possible. Three-dimensional cells are preferred when $a_1$, $a_2$, and D are nearly the same size (i.e., a cube)

Energy balance is usually expressed by a simplified version of equation 7, and Beck writes, using our notation

$$(\rho c_v)^{eff} \frac{\partial T}{\partial t} = - \rho_o c_v v_i \frac{\partial T}{\partial x_i} + \kappa^{eff} \frac{\partial^2 T}{\partial x_i^2} \tag{10}$$

where $(\rho c_v)^{eff} = \phi \rho_o c_v + (1-\phi) \rho^S c_v^S$ .

Initially, the system is assumed to be in static equilibrium so that the pressure is hydrostatic. Thus,

$$v_i^o = (0, 0, 0) \text{ and } T^o = T_1 + (T_o - T_1) \frac{z}{D} \tag{11}$$

Under these conditions, there are no convective currents and the system is said to be "statically stable." Let a small volume of fluid suddenly be brought from elevation $z = 0$ to a higher elevation $z > 0$, thus superimposing a disturbance ($v_i'$, $T'$, $p'$) upon the "basic state" ($v_i^o$, $T^o$, $p^o$). We now want to determine whether or not the system is "dynamically stable," i.e., whether this disturbance will die out or build up to the level of a discernible convective current. Equations 8 - 11 as well as the boundary conditions must be satisfied by the disturbed state as well as by the basic state. Thus, by writing these equations first in terms of ($v_i^o + v_i'$, $T^o + T'$, $p^o + p'$) and then in terms of ($v_i^o$, $T^o$, $p^o$), we can subtract the second set from the first to obtain

$$\frac{\partial v_i'}{\partial x_i} = 0 \tag{12}$$

$$\frac{1}{\phi} \frac{\partial v_i'}{\partial t} + \frac{\mu}{k\rho_o} v_i' = - \beta T' g_i - \frac{1}{\rho_o} \frac{\partial p'}{\partial x_i} \tag{13}$$

$$(\rho c_v)^{eff} \frac{\partial T'}{\partial t} = - \rho_o c_v v_i' \frac{\partial (T^o + T')}{\partial x_i} + \kappa^{eff} \frac{\partial^2 T'}{\partial x_i^2} \tag{14}$$

subject to the boundary conditions

$$v_i' n_i = 0 \quad \text{at} \quad x = \pm \tfrac{1}{2} a_1;\ y = \pm \tfrac{1}{2} a_2;\ z = 0, D \tag{15}$$

$$T' = 0 \quad \text{at} \quad z = 0, D \tag{16}$$

$$\frac{\partial T'}{\partial x_i} n_i = 0 \quad \text{at} \quad x = \pm \tfrac{1}{2} a_1; \quad y = \pm \tfrac{1}{2} a_2 \tag{17}$$

where $n_i$ is the unit outward normal to the boundaries of the box.

To reduce these equations to a dimensionless form it is helpful to use the following dimensionless groups:

$$\text{Thermal diffusivity:} \quad \alpha = \kappa^{eff}/(\rho_o c_v) \tag{18}$$

$$\text{Rayleigh number:} \quad Ra = k \rho_o g \beta (T_1 - T_o) D/(\mu\alpha) \tag{19}$$

$$\text{Prandtl number:} \quad Pr = k\alpha\rho_o/(\mu D^2 \phi) \tag{20}$$

$$\text{Heat capacity ratio:} \quad H = (\rho c_v)^{eff}/(\rho_o c_v) \tag{21}$$

$$\text{Aspect ratios:} \quad D_1 = a_1/D; \quad D_2 = a_2/D \ . \tag{22}$$

The Rayleigh number relates buoyancy to viscous retardation, whereas the Prandtl number relates thermal diffusivity to viscous retardation. If we also define a set of dimensionless variables

$$\left.\begin{aligned} v_i &= D v_i'/(\alpha Ra^{\frac{1}{2}}) \quad \theta = T'/(T_1 - T_o) \quad p_D = k p'/(\mu \alpha Ra^{\frac{1}{2}}) \\ \tau &= t\alpha/D^2 \qquad X = x/D \qquad Y = y/D \qquad Z = z/D \end{aligned}\right\} \tag{23}$$

we can rewrite (12) - (17) as

$$\frac{\partial v_i}{\partial X_i} = 0 \tag{24}$$

$$Pr \frac{\partial v_i}{\partial \tau} + v_i = \underbrace{Ra^{\frac{1}{2}} \theta \delta_{i3}}_{\substack{\text{zero for} \\ i = 1,2}} - \frac{\partial p_D}{\partial X_i} \tag{25}$$

$$H \frac{\partial \theta}{\partial \tau} = - Ra^{\frac{1}{2}} v_1 \frac{\partial \theta}{\partial X_i} + \underbrace{Ra^{\frac{1}{2}} v_i \delta_{i3}}_{\substack{\text{zero for} \\ i = 1,2}} + \frac{\partial^2 \theta}{\partial X_i^2} \tag{26}$$

$$v_i n_i = 0 \quad \text{at} \quad X = \pm \tfrac{1}{2} D_1; \quad Y = \pm \tfrac{1}{2} D_2; \quad Z = 0, 1 \tag{27}$$

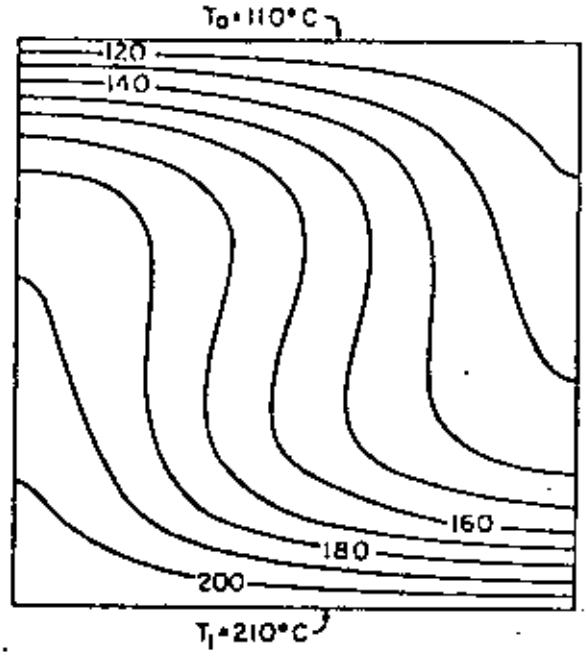


Fig. 4. Typical temperature distribution in plane perpendicular to axis of single convective roll with Ra = 100 (after Sorey, 1975).

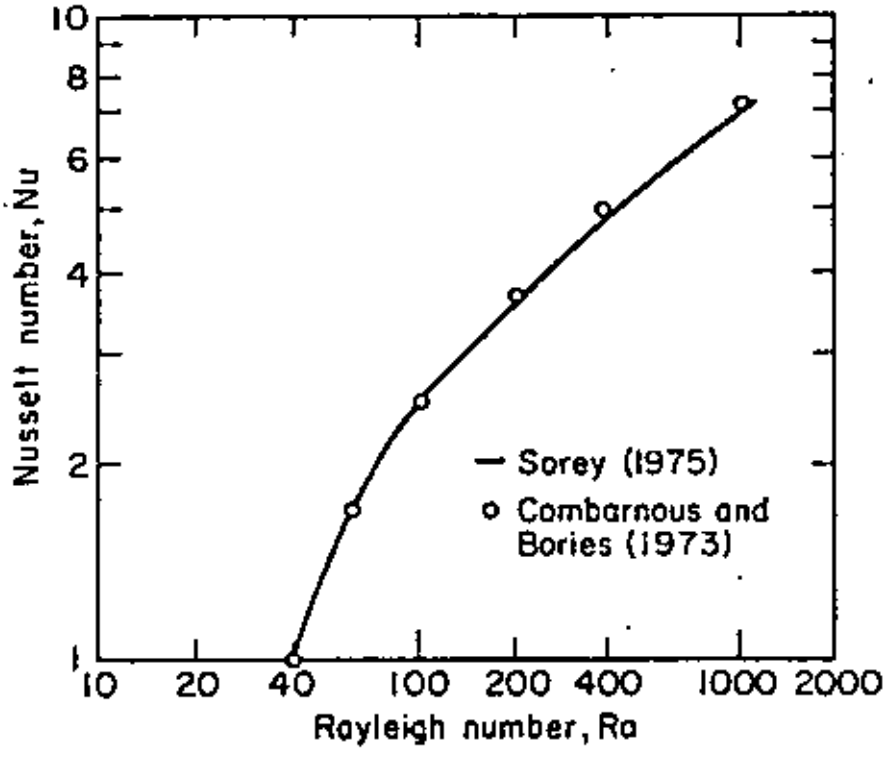


Fig. 5. Maximum Nusselt number versus Rayleigh number for cellular convection in a laterally infinite layer (after Sorey, 1975).

or when the height is less than both lateral dimensions. For a cube, the motion resembles a toroid with vertical axis through the center of the box. For further details regarding these conclusions, the reader is referred to Beck (1972).

It is important to recognize that all of these results have been obtained from an analysis of marginal stability and are therefore limited to Rayleigh numbers in the immediate neighborhood of $Ra_c$. In order to obtain results for higher Rayleigh numbers one must either perform experiments or solve the governing equations by an appropriate analytical or numerical technique. A large number of such studies concerned with both steady and nonsteady state situations have been reported in the literature and we shall try to summarize briefly some of the most important aspects of this work.

One effect of convective motion is to increase the rate of vertical heat transfer through the system. This is measured by the Nusselt number, Nu, which is defined as the ratio of total heat flow in the presence of convection to that by conduction only. For Rayleigh numbers less than the critical value, $Nu = 1$; otherwise $Nu \geq 1$. Fig. 4 shows the steady state temperature distribution corresponding to a roll at $Ra = 100$ for which $Nu = 2.6$.

According to the criterion of Platzman (1965), a system will tend to establish a mode of convection which maximizes the rate of heat transfer. At Rayleigh numbers near $Ra_c$, this means that cells with nearly square cross sections are preferred. However, at large Rayleigh numbers, Combarnous and Bories (1973) and Horne and O'Sullivan (1974) show that the preferred cell width depends on Ra, with aspect ratios of 0.5, .33, and .25 corresponding to Rayleigh numbers of 280, 400 and 700, for layers with no restraining side walls. Similar effects of reduced cell width with increased Ra are observed for box models with restraining side walls. Combarnous and Bories (1973), Holst and Aziz (1972b), and Sorey (1975) found that Nusselt numbers are nearly the same for two- and three-dimensional motions in stable

convection states. The relationship between Ra and the maximum Nusselt number for a laterally infinite layer is plotted in Fig. 5.

Sorey (1975) further indicates that the cellular pattern and Nusselt number at steady state may depend on the initial conditions in the box. Using uniform initial temperature and pressure distributions in a square (two-dimensional problem) with Ra = 100 led to development of two cells with Nu = 2.2. With a non-uniform temperature distribution, the result was a single cell with Nu = 2.6. Horne and O'Sullivan (1974) report from numerical as well as laboratory experiments that for a uniform initial temperature distribution, heating the lower boundary slowly instead of instantaneously results in unicellular rather than multicellular motion. In other words, the mode of convection is not necessarily unique but may depend on the past history of the system. A hysteresis effect has also been noted by Elder (1967) and Karra (1968).

As Ra increases to 280, the system tends to develop a more favorable mode of convection and, as a result, the fluid may start fluctuating. These fluctuations will be irregular when the boundary conditions are uniform, but may develop into stable oscillations when the boundaries are heated in a nonuniform fashion. Horne and O'Sullivan (1974) report isotherms during a single oscillation when half of the bottom boundary has an elevated uniform temperature as shown in Fig. 6. A rough calculation for the Wairakei geothermal region indicates that, if the depth is 5 km, the oscillations would have a time constant on the order of 1000 years, and it would therefore be practically impossible to detect them.

Free Convection Models

Numerous authors have attempted to extend the analysis of free convection to more realistic systems. There are, however, several complicating factors. The concept of a critical Rayleigh number may not apply in geothermal reservoirs where horizontal temperature variations undoubtedly exist along bounding surfaces. Free convection is then set up for any value of Ra > 0, although its effect on the

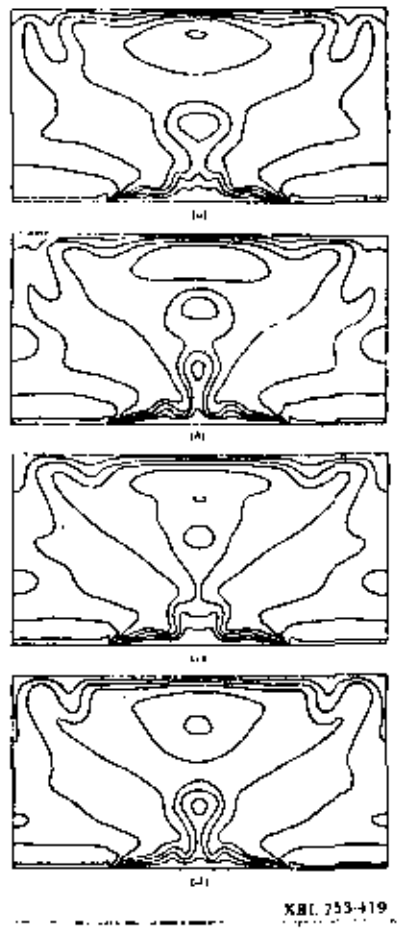

Fig. 6. Isotherm plots at equal intervals of time during a single stable oscillation with Ra = 750 (after Horne and O'Sullivan, 1974).

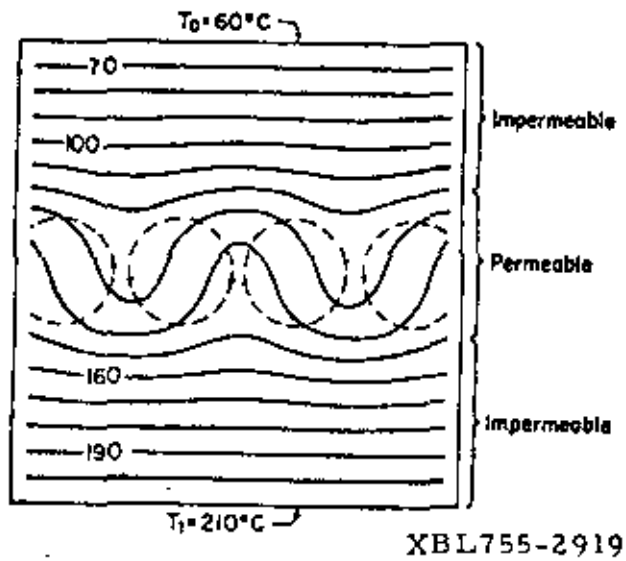


Fig. 7. Distortion of isotherms due to convection in central permeable layer (after Sorey, 1975).

thermal and hydrologic regimes should be negligible unless Ra is large. Donaldson (1968b) estimates that in geothermal areas Ra is in the range of 500-5000. Caltagirone et al. (1971) suggest the concept of a local Rayleigh number which varies spatially within the reservoir to account for the fluctuating convective motions observed.

Combarnous and Bories (1973) evaluated the effects of assuming thermal equilibrium between solid and fluid phases (Eqs. 4-7) for systems with Rayleigh numbers well above theoretical critical values. Comparisons of experimental and numerical results for the relationship between Ra and Nu numbers using various combinations of porous media and fluid types indicate that the assumption of thermal equilibrium between solid and fluid phases is adequate for Ra at least as high as 2000.

Holst and Aziz (1972a) and Sorey (1975) investigated effects of temperature and pressure-dependent parameters on heat transfer in convecting systems. For water, the dominant influence is the viscosity variation such that as the temperature difference across the permeable layer $T_1-T_o$ increases, the effective Rayleigh number increases over the value calculated from equation 19 using parameters computed at $T = T_o$. The Nusselt number would be correspondingly greater and the critical Rayleigh number, lower than for the constant parameter case. Alternatively, if parameters are evaluated at $T = (T_1 + T_o)/2$, values of $Ra_c$ and the Ra versus Nu relationship still vary with $T_1 - T_o$ due to the nonlinearity in the temperature dependence of $c_v$, $\rho$, and $\mu$ (Sorey, 1975). In contrast, realistic variations in fluid density with pressure were found to have negligible effects on the cellular convection problem.

Studies have also been made on the effect of various uniform boundary conditions at the surfaces of the homogeneous region on $Ra_c$. Lapwood (1948) investigated a laterally infinite layer in which the lower boundary is impermeable and the upper boundary is maintained at constant pressure and found that $Ra_c = 27.1$. Lapwood also found that when the upper boundary is a perfectly conducting free

surface, then $Ra_c = 4\pi^2$; but when it becomes an imperfect conductor, then $27.1 \leq Ra_c \leq 4\pi^2$. A table of $Ra_c$ values for a variety of uniform boundary conditions is given by Nield (1968) and in all cases, $Ra_c \leq 4\pi^2$.

Donaldson (1962) analyzed free convection in a two-layer system in which a permeable layer was underlain by an impermeable but thermally conductive layer of equal thickness. This removes the assumption of an isothermal surface at the bottom of the convecting layer. Sorey (1975) extended the analysis to a three-layer system with impermeable zones above and below the reservoir and found, in agreement with Donaldson's results, that vertical heat transfer rates in the multilayer systems were significantly less than in the single-layer system for the same values of Ra. The critical Rayleigh number was also less for the multilayer systems. Fig. 7 shows how temperatures within the impermeable layers are distorted by convection in the central layer.

Some work has also been done on the problem of an inclined system bounded by isothermal surfaces (Combarnous and Bories, 1973; Kaneko et al., 1974). Combarnous and Bories show that, since the temperature gradient and gravity are no longer colinear, the fluid is constantly moving regardless of the Rayleigh number. In a layer of infinite lateral extent, the tendency at low Rayleigh numbers is to develop unicellular convection parallel to the slope. If this is considered the stable state, instabilities develop at critical Rayleigh numbers which depend on the angle of inclination. When this angle is less than $15^\circ$, $Ra_c = 40$ and the mode of convection is similar to that observed in a horizontal layer. Above this lower limit, $Ra_c$ increases rapidly with the angle of inclination and convective movements take the form of adjacent coils climbing upslope. Fluctuating conditions develop at higher and higher Rayleigh numbers ($Ra \geq 240 - 280$ for horizontal layer) as the angle of inclination increases. The case of the inclined box is more complex (Holst and Aziz, 1972a; Kaneko et al., 1974).

Wooding (1963) and McNabb(1965) have studied the effect of localized heat sources on the formation of vertical jet flows. McNabb developed a boundary layer theory for convective flow over a finite circular "hot plate" at the bottom of a semi-infinite porous medium. He estimated the amount of heat convected from the hot plate as a function of its temperature and suggested that a similar approach could be used to evaluate the rate of cooling of a magma chamber beneath a water saturated porous formation.

Cheng and Lau (1974) have investigated steady state free convection in a vertical cross section of an unconfined aquifer in which the position of the water table is not known a priori. The aquifer is assumed to rest on an impermeable horizontal heat source of variable temperature and is bounded on its sides by vertical isothermal surfaces of constant hydraulic head, representing contact with the ocean on a volcanic island. Dispersion and gravity effects due to variations in salt content between fresh water and sea water (mixing occurs by virtue of the vertical boundary conditions) are implicitly neglected. By solving a linearized version of the governing equations, the authors show that pressure in the aquifer remains nearly hydrostatic. Temperature is greatly affected by the size of the heat source but its location is less important. There is a noticeable upwelling of the water table directly above the heat source, which depends primarily on vertical temperature gradients and nature of the heat source.

Much additional literature on various theoretical and experimental aspects of free convection in homogeneous media is available. Holst (1970) has published an extensive review of the literature and the state of the art has been summarized more recently by Combarnous and Bories (1973). For subsequent developments, the reader should consult the works of Fernandez (1972), Holst and Aziz (1972 a,b), Masuoka (1972), Palm et al. (1972), Sun et al. (1972), Gupta and Joseph (1973), Cheng and Lau (1974), Combarnous and Bories (1974), Horne and O'Sullivan (1974), Kaneko et al. (1974), Straus (1974), Yen (1974), Weber (1975 a,b), and Sorey (1975).

Pipe Models

An alternative concept for convection in geothermal areas is the pipe system in which the fluid no longer flows through a homogeneous layer but is channeled through zones of relatively high permeability. Such zones may be caused by fissures or fractures which are known to control local phenomena such as springs, fumaroles, and geysers. As discussed by Einarsson (1942), Bodvarsson (1961), and Donaldson (1970), the occurrence and distribution of thermal areas in Iceland and Ne Zealand could be controlled by variations in permeability as well as by spatial distribution of the heat source.

Einarsson (1942) and Bodvarsson (1961) discuss the thermal areas of Iceland in terms of pipe systems involving deep circulation of water (2 to 3 km) and discharge in hot springs. Elder (1966) analyzed hydrothermal systems in Iceland and New Zealand using lumped parameter and multi-dimensional models to quantify the general features of heat and mass transfer. White (1957, 1961) used pipe systems to explai the chemical composition of waters associated with volcanic and hydrothermal systems

Donaldson (1968b, 1970) suggests the model in Fig. 8 for a hot-water geothermal system. The model consists of cold reservoirs recharged from the surface, a vertical column through which hot water flows, and a permeable horizontal channel connecting the two. The surrounding medium is assumed impermeable, and heat supplied at the lower boundary maintains the density imbalance and resulting convective motion. Though the model is oversimplified, Donaldson's analysis allows for throughflow from recharge to discharge areas and secondary (circulatory) convection in the upflow column. Gross characteristics of hydrothermal systems are simulated by adjusting temperatures at the base of the model, dimensions and permeability of the vertical column, and resistance to flow in the remainder of the pipe system.

Mathematical description of the model involves the single phase, steady state equivalents of (1) and (7) which are solved by numerical relaxation for the boundary conditions shown in Fig. 8. Uniform thermal properties are assumed throughout

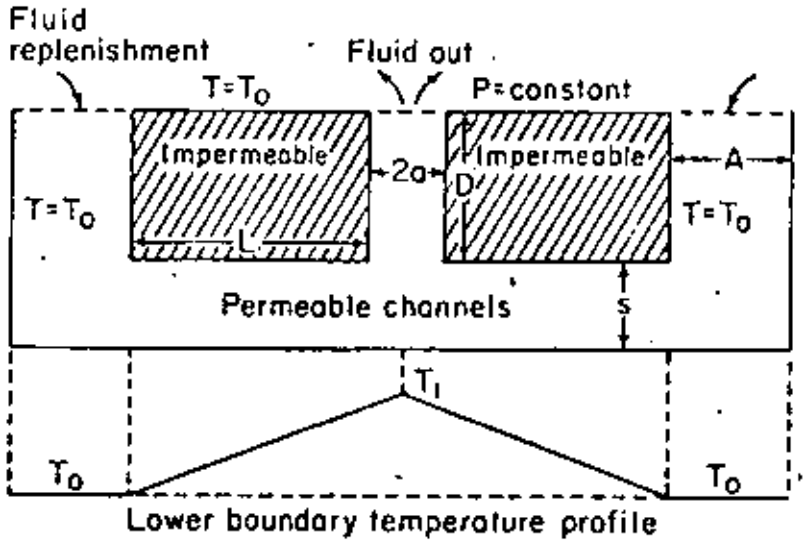


Fig. 8. Pipe model for hot-water geothermal system (after Donaldson, 1968b).

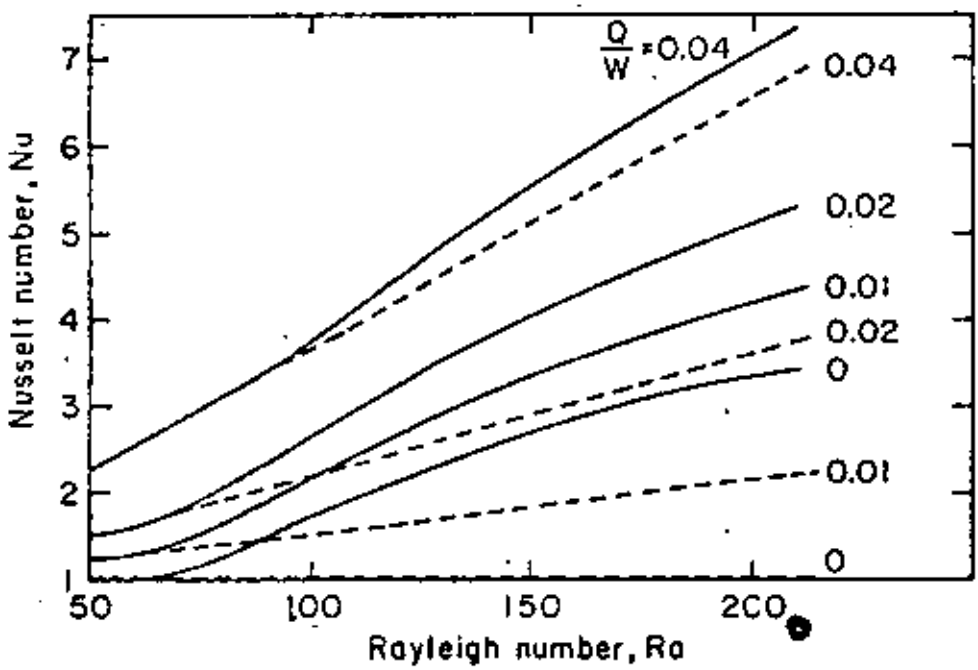


Fig. 9. Nusselt number versus Rayleigh number for combined through and circulatory flows in vertical column with 2a/D = 0.5. Solid lines show combined effect, dashed lines show throughflow effect only (after Donaldson, 1970).

and constant values for k and μ are used in each of the permeable channels. In the absence of secondary convection in the upflow column, the mean mass flow rate is given by

$$Q = \frac{\rho_o \, k \, \beta \, g \, (T_m - T_o)}{(\mu/\rho) \, b} \qquad (34)$$

where $T_m$ = mean temperature in the column and $b = 1 + aL/aD + A/D$. It is not clear from Donaldson's analysis whether $\mu/\rho$ is determined at $T_o$ or $T_m$. Fig. 9 illustrates the relationship between Ra and Nu with throughflow and secondary convection for a column aspect ratio $2a/D = 0.5$. Here $W = \rho_o \, k \, \beta \, g \, (T_1 - T_o)/(\mu/\rho)$ is a measure of the maximum possible throughflow from buoyancy unbalance alone. Hence, $Q/W = [(T_m - T_o)/(T_1 - T_o)] \, (1/b)$. It is seen from Fig. 9 that the heat transferred by circulatory flow decreases markedly as the throughflow increases. Fig. 10 illustrates how throughflow in a column with $2a/D = 0.2$ and $Q/W = 0.05$ tends to sweep the circulatory motion up the channel.

Sorey (1975) modeled heat and liquid mass transfer in hot spring systems using the two-dimensional models shown in Fig. 11. Transient and steady state conditions were simulated numerically to determine conductive heat losses from the vertical conduit and its effect on temperature $T_{sp}$ of water discharging at the spring. The lower boundary was formed by the top of a reservoir with water at temperature $T_b$, and the upper boundary was the land surface at temperature $T_s$. The relationships between dimensionless temperature drop, $1 - \theta_{sp}$, and the dimensionless mass flow rates for the circular conduit, $m_c$, and the fault plane conduit, $m_p$, are plotted in Fig. 12.

Expressions for the total conductive heat loss are $[2\pi \, \kappa^{eff} \, D \, (T_b - T_s) \, m_c \, (1 - \theta_{sp})]$ for the cylinder and $[2 \, \kappa^{eff} \, D \, (T_b - T_s) \, m_p \, (1 - \theta_{sp}) \, L/a]$ for the plane. The plane model applies where fluid rises in a fault zone whose lateral extent is considerably greater than the discharge area of the hot springs. Comparing the two models for the same total mass flow, the fault plane model has greater

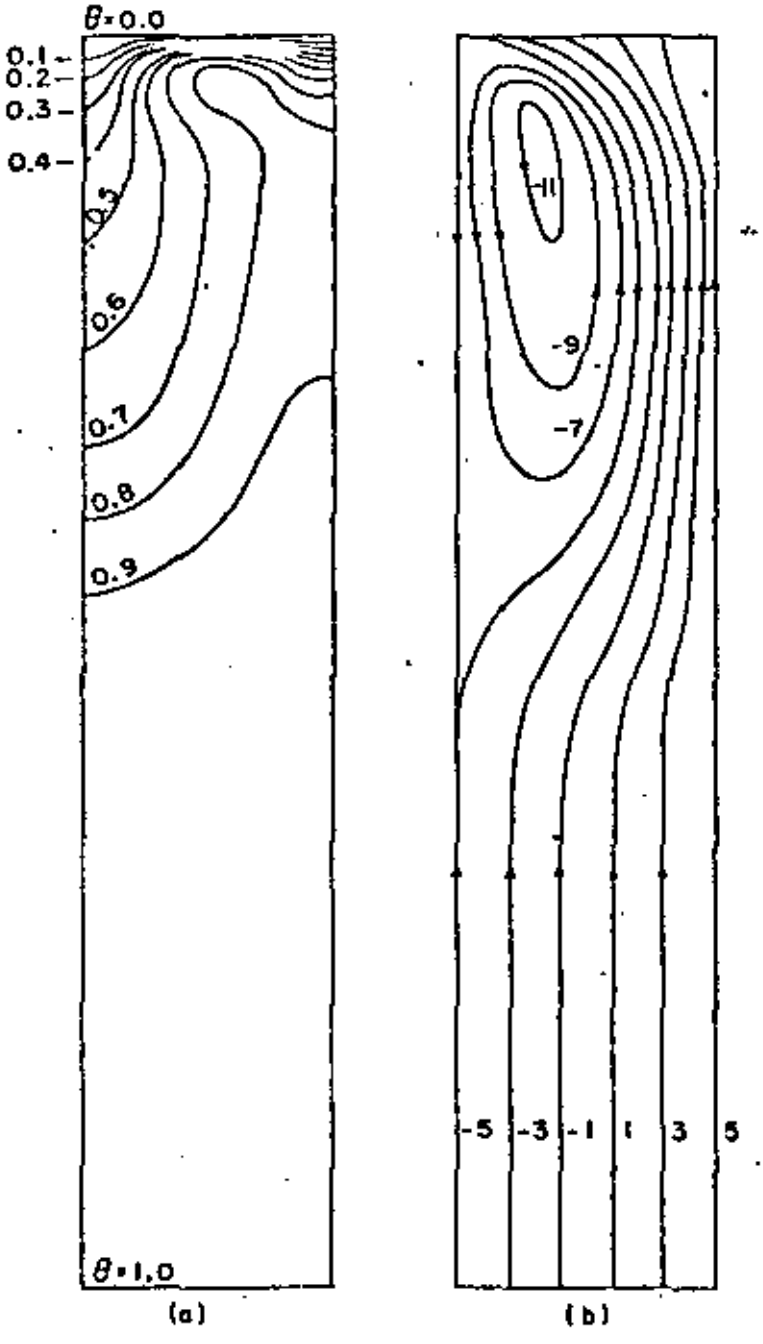


Fig. 10. Effect of throughflow on circulatory convection with Ra = 420, 2a/D = 0.2, Q/W = 0.05; (a) isotherms normalized such that $0 \leq \theta \leq 1.0$, (b) streamlines in arbitrary units (after Donaldson, 1970).

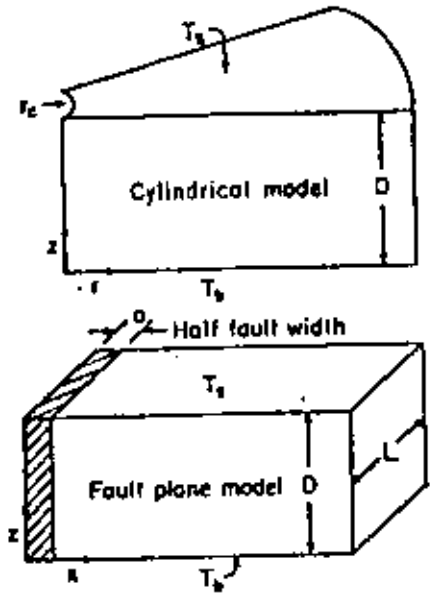


Fig. 11. Two-dimensional models for hot spring systems (after Sorey, 1975).

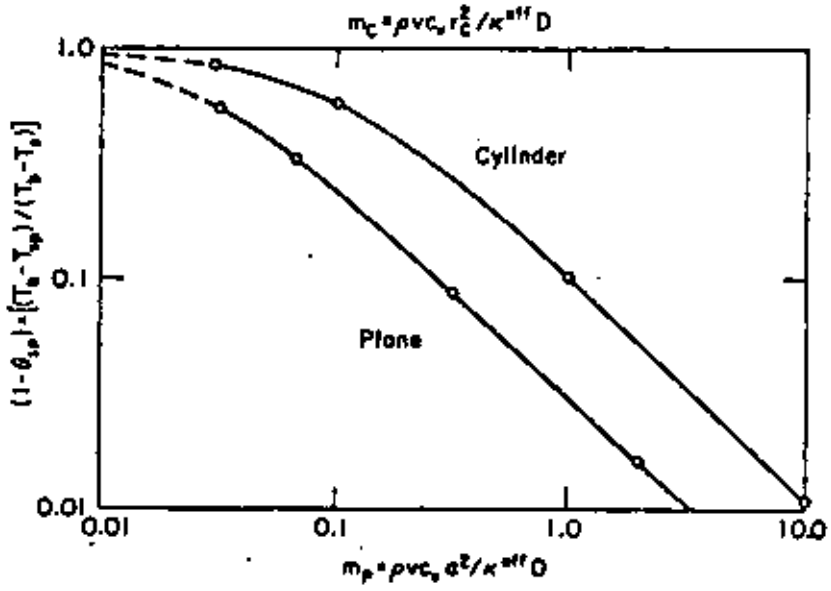


Fig. 12. Dimensionless temperature drop, $1-\theta_{sp}$, versus dimensionless mass flow rates for circular conduit, $m_c$, and fault plane conduit, $m_p$, in hot spring systems (after Sorey, 1975).

heat loss and more temperature drop than the cylindrical conduit model.

The steady-state temperature distribution in a fault plane model with a spring discharge of 100 lpm is shown in Fig. 13. Distortion of the temperatures due to convective motion in the conduit is confined to a zone of about 1 km on either side of the fault. At the land surface, the conductive heat flux near the spring is approximately 50 heat flow units (50 μcal/sec $cm^2$) and decreases to about 3.4 heat flow units as distance exceeds 1 km. These results were obtained using $\kappa^{eff}$ = $2 \times 10^{-3}$ cal/cm sec $^{o}C$ and $c_v$ = 1 cal/gm $^{o}C$.

Analysis of the transient behavior of these systems (Sorey, 1975) shows that periods of 30,000 years or more are required for the conductive thermal regime to reach equilibrium following the geologic development of the spring system. Somewhat shorter time periods are required if convective motions in the rock surrounding the spring conduit are considered. Simulations under these conditions are described by Sorey (1975).

Analysis of pipe models has been extended by Elder (1966) and Donaldson (1968a, 1970) to include boiling in the upflow channel. Elder has developed relationships between mass flow rate, fluid enthalpy, resistance to flow, and the energy supplied by a heat source for channeled circulation caused by buoyancy differences between recharge and discharge areas. He concludes that for systems with large energy input or large resistance, the discharge (mass flow) is not sufficient to transport the energy unless the fluid moves in the form of steam. With low energy inputs or small resistance, the circulating fluid should remain a liquid except for a shallow zone which may contain steam. This approach has been applied to the Tuscany thermal areas near Lardarello, Italy, and the Taupo systems in New Zealand.

Donaldson's (1968a) work involves steady flow of a boiling liquid in a vertical channel. The remainder of the circulation system including the heat source is considered only as controlling temperature, pressure, and mass flux at the bottom of the discharge channel. Lateral heat conduction is neglected so that the

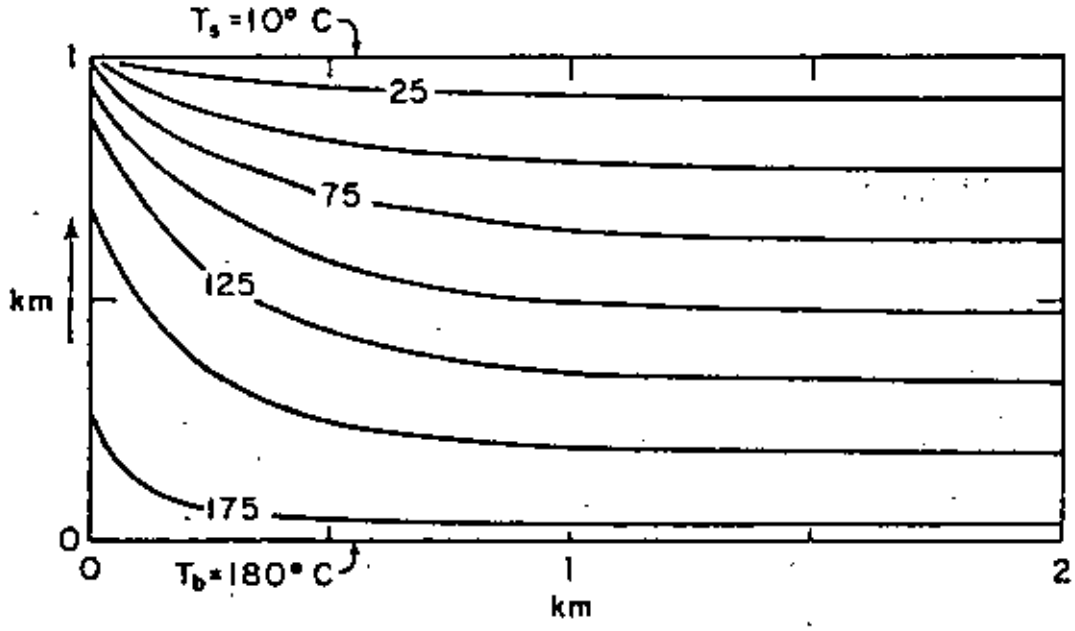


XBL755-2924

Fig. 13. Distortion of steady-state isotherms in vertical fault plane model with discharge = 100 lpm, a = 10 m, L = 1 km, and Ra = 0 (after Sorey, 1975).

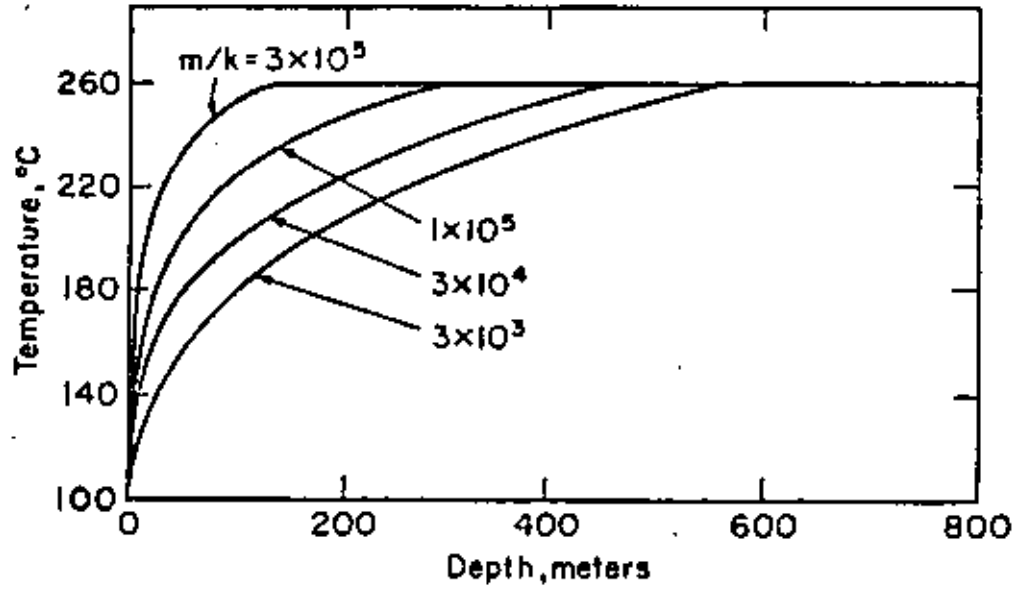


XBL755-2925

Fig. 14. Temperature versus depth in a boiling system as a function of m/k (after Donaldson, 1968a).

equations are one-dimensional. For the case of uniform permeability and small mass flow rate, only liquid flow is considered. Comparison of the resultant pressure-depth relations with saturation pressure curves indicates that boiling will not occur for systems with $c_v\, m/\kappa^{eff} \leq 7 \times 10^{-5}$ cm$^{-1}$, where m is mass flux per unit area. When this critical value is exceeded, boiling must occur in the upper section of the channel.

Two-phase flow in this upper region is described by the one-dimensional, steady state forms of equations 1 - 3 and 6 without the pressure terms. At the interface between the two-phase and liquid-saturated regions, the boundary conditions are constant mass flux and constant temperature equal to that at the channel base. Thus, the lower region is treated as isothermal, and in the upper region, temperature and pressure are related by the vapor pressure curve for water. The equations are solved analytically to yield temperature and pressure, water fraction, and water and steam flow rates as functions of depth. The controlling parameter in these relationships is m/k as seen in Fig. 14. Thus, the onset of boiling is indicated by the value of $c_v\, m/\kappa^{eff}$, whereas when two-phase conditions exist, the controlling parameter is m/k. Effects of vertical heat conduction are significant only if $\kappa^{eff}/k$ is greater than $3 \times 10^8$ cal/cm$^3$ sec $^\circ$C. Donaldson concludes that once boiling commences, it must extend some 200 - 500 meters downward and hence this two-phase region must be considered in studying geothermal systems. Two-phase conditions in columns with variations in vertical permeability have also been discussed by Donaldson (1968a, 1970).

## GEOTHERMAL SYSTEMS DURING EXPLOITATION

### Lumped-Parameter Models

The concept of a lumped-parameter model provides one of the simplest means for describing behavior of a geothermal system during exploitation. The basic idea is to view the entire system as a perfect mixing cell for both mass and energy so that spatial variations in concentration can be neglected. Instead of

considering the internal distribution of mass and energy, attention is restricted to the total amounts generated within the system as well as that crossing the boundaries. Since time is the only independent variable, the system can be characterized mathematically by a set of ordinary differential equations or an equivalent set of algebraic expressions representing total mass and energy balance.

The first and best known lumped-parameter model of a producing geothermal reservoir was developed by Whiting and Ramey (1969). Their system has a bulk volume V and contains vapor, water, and rock. Figure 15 is a schematic diagram of the system from which a simple mass balance yields

$$M_c - M_o = M_e - M_p - M_\ell \tag{35}$$

where $M_c$ = current mass of water (vapor + liquid) in place, $M_o$ = initial mass of water in place, $M_e$ = influx of liquid (no vapor is assumed to enter the system), $M_p$ = mass of water (vapor + liquid) produced, and $M_\ell$ = mass of water (vapor + liquid) lost by leakage. Water may flow in from an adjacent aquifer or leak out of the system via steam vents, springs, wild wells, etc. The water influx, $M_e$, is represented by a linear combination of terms each of which is the product of a theoretical time-dependent response function characterizing a certain aquifer flow geometry (hemispherical, linear, or radial) and pressure. These calculations further assume that the liquid inflow is isothermal with constant enthalpy, $h_e$.

In the energy balance calculation the system is assumed to be in complete thermodynamic equilibrium. According to the first law of thermodynamics one then has

$$\underbrace{M_c\, e_c - M_o\, e_o + V\,(1-\phi)(\rho c_v)^{eff}\,(T_c - T_o)}_{\substack{\text{Internal energy change in fluid} \\ \text{Internal energy change in solid rock}}} = \underbrace{-Q}_{\substack{\text{Net conductive heat influx}}} + \underbrace{M_e\, h_e - M_p\, h_p - M_\ell h_\ell}_{\substack{\text{Net convective enthalpy influx}}} \tag{36}$$

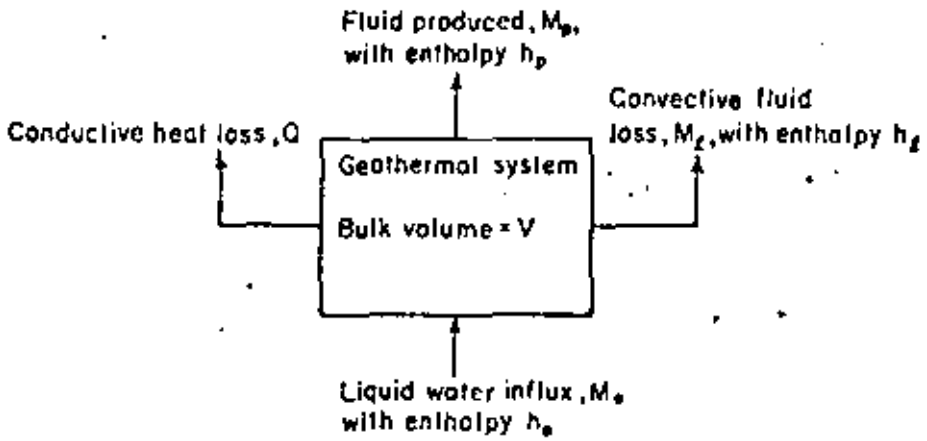


Fig. 15. Schematic diagram of lumped-parameter model for geothermal systems (after Whiting and Ramey, 1969).

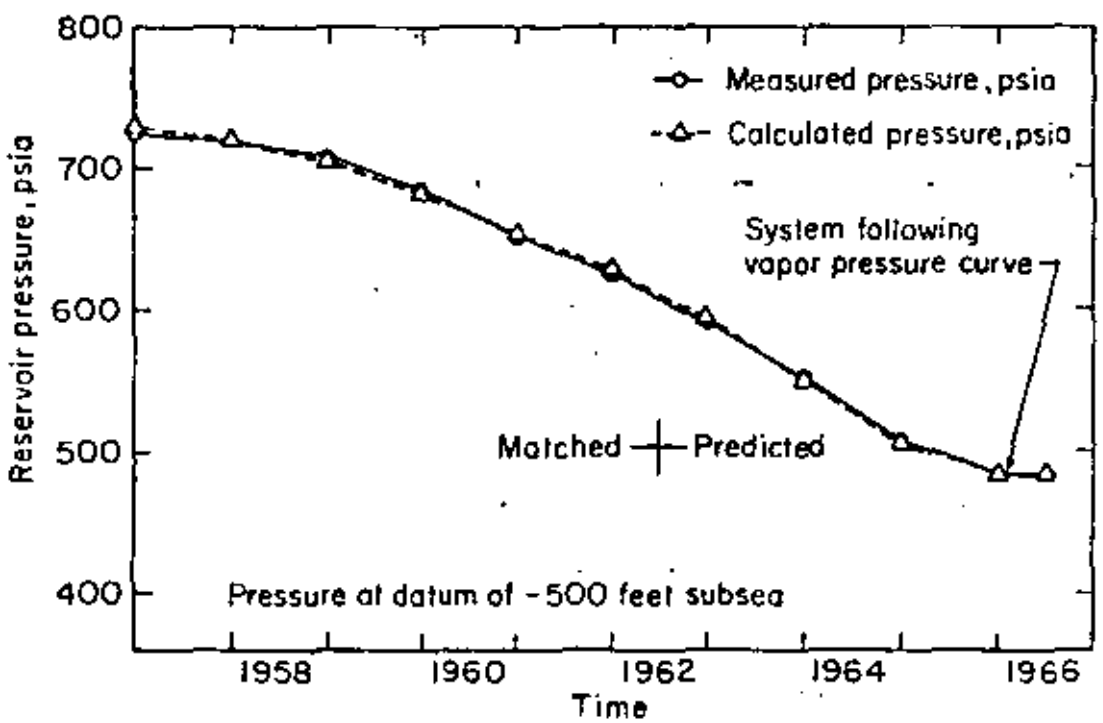


Fig. 16. Comparison of calculated with measured pressures for Wairakei geothermal system (after Whiting and Ramey, 1969).

The volume V can be expressed as

$$V\phi = M_o \left[S_o^G v_o^G + (1-S_o^G)\, v_o^L\right] = M_c \left[S_c^G v_c^G + (1-S_c^G)\, v_c^L\right] \qquad (37)$$

where $S^G$ is vapor (gas) saturation and $v^G$ and $v^L$ are specific volumes of vapor and liquid, respectively. The phase diagram for water (see Fig. 1) indicates that in the particular case where the system contains only compressed liquid, the thermodynamic path of decreasing pressure due to production will be essentially isothermal and isoenthalpic. Equations 35-37 then lead to a mass-volumetric balance similar to that employed for petroleum production above the bubble-point.

$$M_o\,(v^L - v_o^L) + M_e\, v^L - (M_p + M_\ell)\, v^L = 0 \qquad (38)$$

Additional working hypotheses made by Whiting and Ramey are that Q is negligibly small relative to other terms in (36) and that $h_p = h_\ell$ (i.e., the enthalpy of produced and lost fluid is the same).

The compressed liquid version of this lumped-parameter model was applied by Whiting and Ramey to the Wairakei geothermal system in New Zealand. The initial temperature and enthalpy were estimated from field data, and a least-square fit to the production history from 1956 to 1961 was used to determine the initial water in place and the initial pressure. The model was then used to predict performance through 1965 and agreement with measured data was excellent (see Fig. 16). Prediction of future performance from 1966 to the year 2000 took into account two-phase conditions and indicated that pressure and temperature would decrease very little during this period. Recent field data from Wairakei have shown this prediction to be incorrect. The model was also used by Cady (1969) to simulate a laboratory setup but had to be applied separately to the two-phase and dry steam regions that developed.

Brigham and Morrow (1974) have adapted the lumped-parameter approach to vapor-dominated systems (i.e., systems with a significant dry steam region) by considering three different distributions of vapor and liquid. In each case

the system is assumed to be completely closed (i.e., the boundaries are impermeable and adiabatic) and energy is derived only from the rock mass itself.

Their first model concerns a single-phase system completely saturated with vapor. They assume that since the heat capacity of solid rock is much greater than that of steam, the system is essentially isothermal. Thus, there is no need for an energy equation and one can use a mass balance approach similar to that commonly employed in natural gas reservoirs. This approach leads to a linear relationship between p/Z and cumulative production $\Delta M^G$ according to the equation of state for a real gas,

$$\frac{p_1}{Z_1} = \frac{p_o}{Z_o}\,\frac{M_1^G}{M_o^G} = \frac{p_o}{Z_o}\left(\frac{M_o^G - \Delta M^G}{M_o^G}\right) \tag{39}$$

where Z is compressibility factor, $M^G$ is mass of steam in place, and the subscripts indicate different values of time. The intercept of this line on the abscissa is equal to the original fluid in place, $M_o^G$.

In the second model the vapor phase is separated from an underlying layer of liquid by a horizontal interface at which boiling takes place. Since the vapor phase is again assumed to be isothermal, its treatment is similar to that in the previous model. The liquid phase changes its volume continuously and the corresponding lumped system is therefore defined as the pore space filled with liquid at the beginning of each pressure decrement. For this system the mass balance is simply

$$\Delta M^G = -\Delta M^L \tag{40}$$

whereas the energy balance for the fluid is expressed as

$$\underbrace{M_1^L e_1^L + M_1^G \bar{e}^G - M_o^L e_o^L}_{\text{Internal energy change}} = \underbrace{M_1^S c_p^S \left(T_o - T_1\right)}_{\text{Heat transferred from rock to liquid}}$$

$$+ \underbrace{\left(M_o^S - M_1^S\right) c_p^R \left(T_o - \frac{T_o + T_1}{2}\right)}_{\text{Heat transferred from rock to steam}} - \underbrace{\left(M_o^L - M_1^L - M_1^G\right) \bar{h}^G}_{\text{Enthalpy of vapor leaving system}} \tag{41}$$

where $M^S$ is mass of rock in contact with liquid, $\bar{h}^G$ is average enthalpy of vapor leaving system and $\bar{e}^G$ is average internal energy of vapor (both calculated at the average temperature $(T_o + T_1)/2$) and the subscripts o and 1 indicate the beginning and end of a depletion step, respectively. Brigham and Morrow further simplified this equation by reformulating it in terms of enthalpy and neglecting the resulting pressure terms and obtained

$$M_1^L h_1^L - M_o^L h_o^L = M_1^S c_p^S \left(T_o - T_1\right) + \left(M_o^S - M_1^S\right) c_p^S \left(\frac{T_o - T_1}{2}\right) - \left(M_o^L - M_1^L\right) \bar{h}^G \quad (42)$$

Given a rate of production, the resulting system of nonlinear equations can be solved in an iterative manner.

The third model considers a vapor phase overlying a layer of liquid except that now boiling occurs throughout the entire thickness of this layer and its depth remains fixed in time. The resulting energy equation is essentially similar to that of Whiting and Ramey (1969) with the exception that only steam is allowed to leave the system.

Application of these models to various hypothetical reservoirs has shown that in estimating available reserves by extrapolation of early p/Z behavior, the results will tend to be optimistic when porosity is low, but pessimistic when porosity is high. The constant liquid level model was found to predict higher recovery for a given pressure depletion than the falling liquid level model. The presence of even a small amount of liquid in the lower part of a geothermal system was shown to be extremely important because it can account for a large fraction of the total fluid mass and can significantly affect the results of a p/Z analysis. Finally, Brigham and Morrow conclude that "the steam portion of a reservoir will always remain isothermal whether or not there is boiling water below the steam. Thus pressure, temperature, and enthalpy measurements will not be completely diagnostic for determining the original state of the reservoir

fluid system. Because the steam remains essentially isothermal, it gradually increases in enthalpy and becomes superheated as the pressure declines."

An interesting lumped-parameter model based on the assumption that the liquid and gas phases are uniformly distributed throughout the system has been proposed recently by Martin (1975). The system is assumed to be completely closed and each phase is produced at a rate which is related to its relative permeability. His approach is based on a simplified form of equations 1-3 and 6. If we neglect the gravity term in Darcy's law and substitute (2) and (3) into (1), we can write for an isotropic medium

$$\frac{\partial}{\partial x_i}\left(\lambda^f \frac{\partial p}{\partial x_i}\right) = \frac{\partial M^f}{\partial t} \tag{43}$$

where

$$\lambda^f = k\left(\frac{\rho^L k_r^L}{\mu^L} + \frac{\rho^G k_r^G}{\mu^G}\right)$$

$$M^f = \phi\,(\rho^L S^L + \rho^G S^G)$$

Neglecting heat dispersion and the pressure terms in (6) we obtain by the same procedure

$$\frac{\partial}{\partial x_i}\left(\lambda^h \frac{\partial p}{\partial x_i}\right) = \frac{\partial M^h}{\partial t} \tag{44}$$

where

$$\lambda^h = \frac{\rho^L h^L k k_r^L}{\mu^L} + \frac{\rho^G h^G k k_r^G}{\mu^G} + \kappa^{eff}\frac{dT}{dp}$$

$$M^h = \phi S^L \rho^L h^L + \phi S^G \rho^G h^G + (1-\phi)\rho^S c_v^S T$$

since T and p are uniquely related by the boiling curve. The notion of a lumped-parameter model implies that gradients of pressure, temperature, and saturation are small. Expanding (43) and (44) and neglecting the products of these gradients leads to

$$\frac{1}{\lambda^f}\frac{\partial M^f}{\partial t} = \frac{\partial^2 p}{\partial x_i^2} = \frac{1}{\lambda^h}\frac{\partial M^h}{\partial t} \tag{45}$$

Expanding the time derivatives with respect to p and S yields the nonlinear ordinary differential equation

$$\frac{dS^L}{dp} = \frac{\lambda^h \frac{\partial M^f}{\partial p} - \lambda^f \frac{\partial M^h}{\partial p}}{\lambda^f \frac{\partial M^h}{\partial S^L} - \lambda^h \frac{\partial M^f}{\partial S^L}} \qquad (46)$$

In the case of single-phase flow, T and p are not related uniquely to each other, and the above procedure must therefore be modified. If we neglect heat conduction as well as dispersion, we obtain the single-phase equivalent of (45) with $\lambda^h = h\lambda^f$. Expanding the time derivatives with respect to p and T leads to the following nonlinear ordinary differential equation,

$$\frac{dT}{dp} = \frac{\frac{\partial M^h}{\partial p} - h \frac{\partial M^f}{\partial p}}{h \frac{\partial M^f}{\partial T} - \frac{\partial M^h}{\partial T}} \qquad (47)$$

Equations 46 and 47 were used by Martin to calculate numerically the relationships between T, p and S in a hypothetical system free of gravity effects. Integration of (47) showed that in the case of a single phase, dT/dp is very small and the exploitation process is essentially isothermal. This is clearly illustrated in Fig. 17 which shows the thermodynamic paths for various initial p-T conditions in a system with $\phi = 0.25$, $\rho^S = 162$ lb/ft$^3$ (2.6 gm/cm$^3$), $c_v^S = 0.2$ Btu/lb °F (0.2 cal/gm °C), $\kappa^{eff} = 40$ Btu/ft day °F (0.0069 cal/cm sec °C), k = 1 darcy (9.87 x 10$^{-9}$ cm$^2$), and typical $k_r$ values. For example, from initial conditions corresponding to point A, the temperature will drop slightly along line 1 as pressure declines. This corresponds to a single phase (essentially steam) reservoir with temperature and pressure above the critical point. However, if the system is initially saturated with liquid water at point C, production causes an isothermal decrease in pressure until the boiling curve is reached. At this stage p and T begin to follow the boiling curve with a gradual increase in steam saturation. Production of

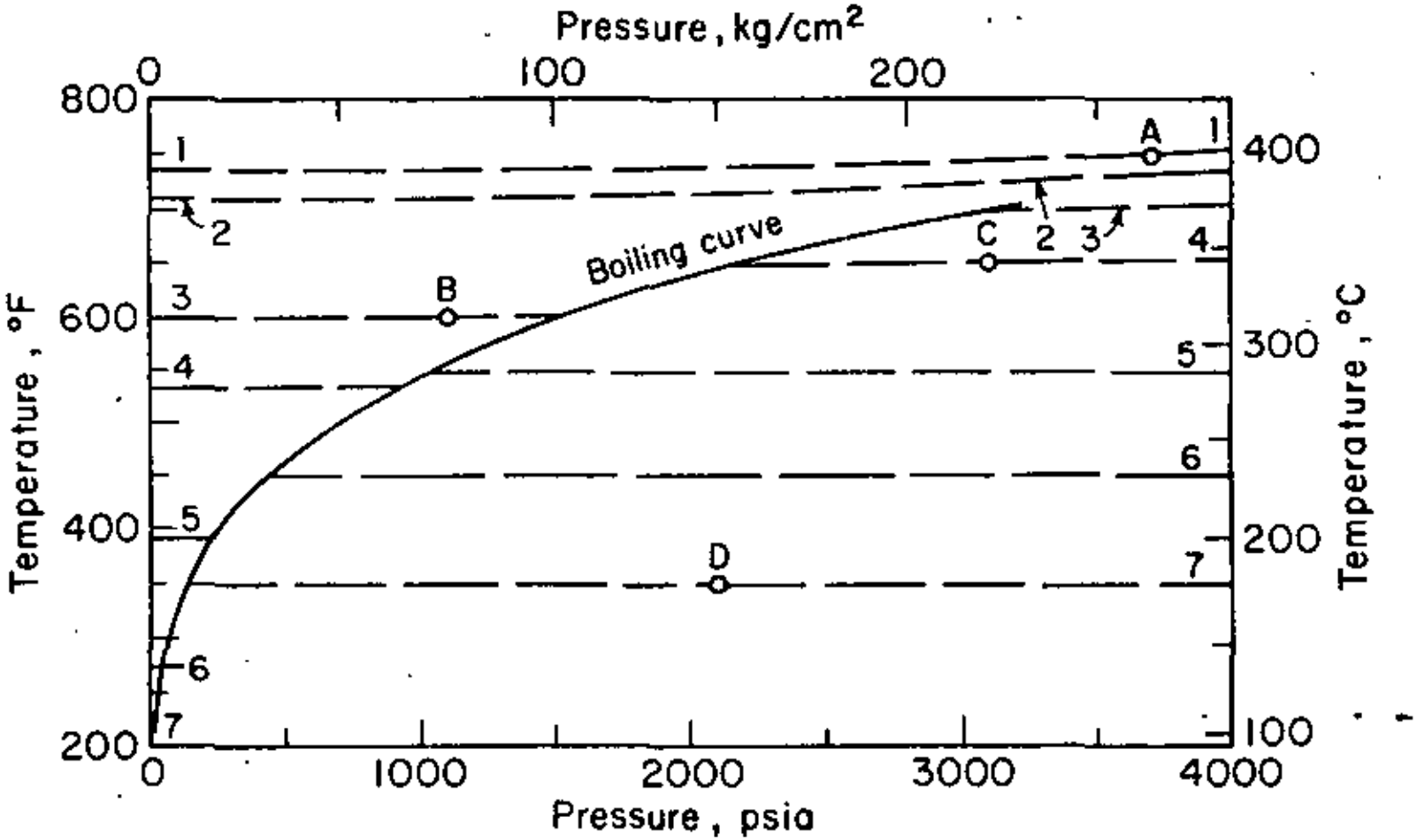


Fig. 17. Pressure-temperature diagram for pure water and vapor showing various thermodynamic paths for depleting a geothermal system (after Martin, 1975).

steam, however, starts only when $S^G$ reaches its so-called equilibrium value at which the vapor phase becomes mobile (below this value $k_r^G = 0$). The ratio between produced steam and liquid water continues to increase until $S^L$ is reduced to a stage where the liquid becomes immobile and production is restricted to saturated steam. When all the water has been boiled away and $S^L = 0$, the temperature departs from the boiling curve and superheated steam is produced under essentially isothermal conditions.

From his study Martin further concluded that "under certain conditions only a relatively small amount of the heat initially contained in a geothermal reservoir will be produced during pressure depletion. Much of this heat may be contained in the produced steam even though initially the reservoir contains only hot water." This is due to the higher heat content and lower viscosity of steam as compared with liquid water. A similar reasoning also led Martin to conclude that "for many conditions where gravity segregation of the steam and hot water occurs during depletion, more of the total heat can be produced by completing wells high in the reservoir to enhance steam production and suppress water production." When gravity effects are important, system C should follow the path shown in Fig. 17 until the steam phase becomes mobile and gravity segregation begins. Since $S^G$ increases rapidly in the upper portion of the system, departure from the boiling curve will occur at considerably higher p and T values than is shown in the figure. In the lower portion of the system $S^L$ decreases slowly and therefore departure from the boiling curve will occur at lower p and T values than in Fig. 17.

Distributed-Parameter Models

A model in which the properties of the rock and/or the fluid (e.g., saturation, viscosity, pressure, etc.) are allowed to vary in space will be called a distributed-parameter model. By taking into account spatial variations of these properties the resulting problem may become too complex to be treated analytically.

An alternative approach is to replace the governing partial differential equations by an equivalent set of algebraic equations and then solve the problem numerically with the aid of a computer. The purpose of the following discussion is to acquaint the reader with some of the results obtained to date by numerical simulation of relatively complex geothermal systems.

A considerable degree of sophistication in the numerical simulation of immiscible, multiphase and multicomponent fluid flow problems under nonisothermal conditions has been achieved in recent years by petroleum engineers. A brief review of this work has been included in a recent paper by Coats et al. (1974). Most of this effort, however, was not concerned with geothermal systems but was directed toward the problem of oil recovery by steamflooding, hot waterflooding, steam stimulation, and other thermal processes which are of immediate concern to the petroleum industry. For example, Spillette and Nielsen (1968) have studied the response of an oil reservoir to hot water injection by assuming that the hydrocarbons and the water will appear only as a liquid phase. Their model consists of a vertical cross-section including a horizontal layer of sand enclosed between two impermeable shale strata. Energy is transported by conduction and convection in the sand layer and by conduction in the shale layers. Fluid densities and viscosities are taken to be temperature dependent and capillary pressure between the two fluid components is taken into account. The equations governing mass transport are solved by an alternating direction implicit (ADI) iterative finite difference procedure whereas the energy equation is solved by the method of characteristics. One of the conclusions of this study was that fluid segregation due to gravity has a significant effect on the system considered.

Another two-dimensional vertical model consisting of a sand layer sandwiched between two impermeable strata has been developed more recently by Weinstein et al. (1974). In this model fluid flow is allowed to take place only in one horizontal direction whereas energy may be transferred by conduction both

horizontally and vertically through the entire system. However, the hydrocarbons and water can coexist both in the liquid and vapor states, so that one must now deal with three distinct phases: oil, water, and gas. The gas phase is a mixture of steam and hydrocarbon vapor. Interphase mass transfer within each component is allowed to account for processes such as water vaporization, steam condensation, hydrocarbon distillation, solvent extraction, and solution-gas drive. The energy equation is expressed in terms of enthalpy, rock compressibility is taken into account, but capillary pressure effects are neglected. A finite difference approach is employed with an implicit pressure-explicit saturation formulation of the mass balance equation, which is solved simultaneously with the energy equation. The authors also discuss various improved numerical techniques for invoking phase constraints and calculating mass transfer terms.

A three-dimensional finite difference model describing nonisothermal, three-phase flow of oil, liquid water, and steam has been described by Coats et al. (1974) for the purpose of simulating oil recovery by steam and hot water injection. In this model fluid densities are taken to be linear functions of temperature and pressure, and the effect of pressure on porosity is also taken into account. The mass and energy balance equations are solved simultaneously by a direct method. A comparison of calculated results with experimental data indicated that the simulation process is sensitive to temperature effects on relative permeability. The authors concluded that such data, especially the temperature dependence of water relative permeabilities, must be taken into account.

The first application of a distributed-parameter model to a geothermal system was made by Mercer (1973) and Mercer and Pinder (1974). A comprehensive account of this work has been described more recently by Mercer et al. (1975). The model consists of a single-phase, two-dimensional areal (horizontal) representation of the hot-water Waiora aquifer in the Wairakei hydrothermal system of New Zealand. The mass and energy balance (Eq. 7 without the pressure term)

are solved in the horizontal plane of the aquifer by the Galerkin finite element approach, using isoparametric elements as shown in Fig. 18. Since the governing equations are averaged over the thickness of the aquifer, cellular convection does not play a role in the resulting model.

However, vertical flow of fluid as well as energy is allowed to take place between the Waiora formation and the overlying Wairakei breccia aquifer through the intervening Huka Falls shale (see Fig. 19). The rate of this vertical leakage is taken to be proportional to the differences in head and temperature between the two aquifers, the values of p and T in the upper aquifer being kept constant. Inflows of heat from the underlying ignimbrites into the Waiora aquifer are treated as unknown source terms to be determined by model calibration. The lateral boundaries of the Waiora aquifer are assumed to be impermeable and isothermal. Viscosity is allowed to vary with temperature whereas fluid density is calculated as a linear function of temperature and pressure. The model is also capable of treating the heat dispersion term in its proper tensorial form.

The first step in applying the model to Wairakei was to adjust the parameters so as to reproduce the steady state conditions existing in 1955, prior to exploitation. The parameters that were adjusted at this stage included element configuration, heat sources at the bottom of the aquifer, dispersion coefficients, and permeabilities. A sensitivity analysis was performed indicating that dispersion had little influence on the results, whereas the permeability of the Huka Falls formation had an important effect on the temperature distribution in the thermal reservoir.

The second step was to simulate the response of the geothermal field to withdrawal of hot water from a series of wells during the period between 1955 and 1962, using time steps of 30 days. The parameters of the model were again adjusted so as to bring about a fit between calculated and observed data. The results showed only a slight change in the configuration of the isotherms during

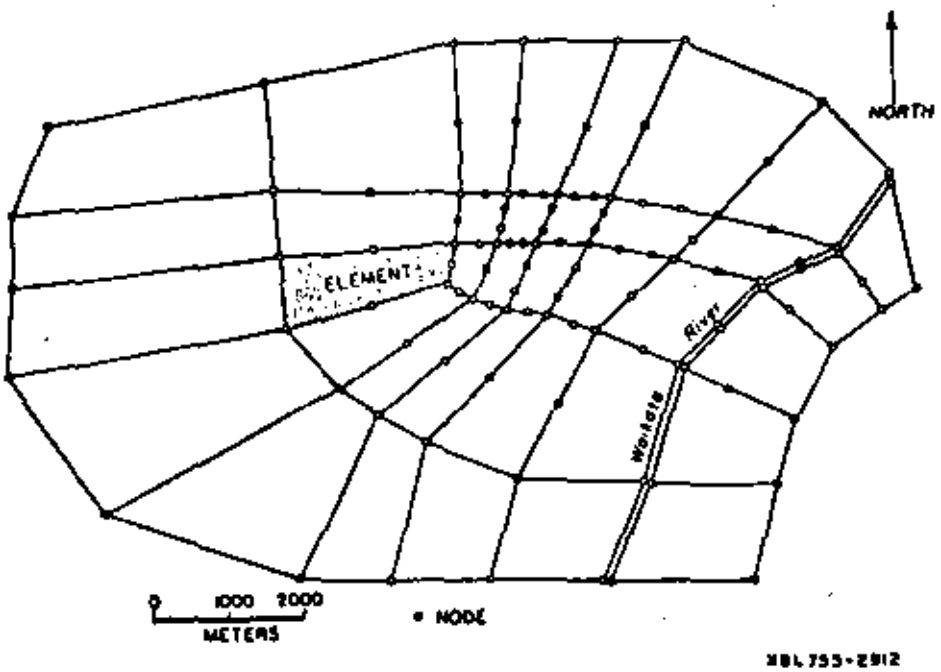


Fig. 18. Network of isoparametric elements used in distributed-parameter model of Wairakei geothermal system (after Mercer et al., 1975).

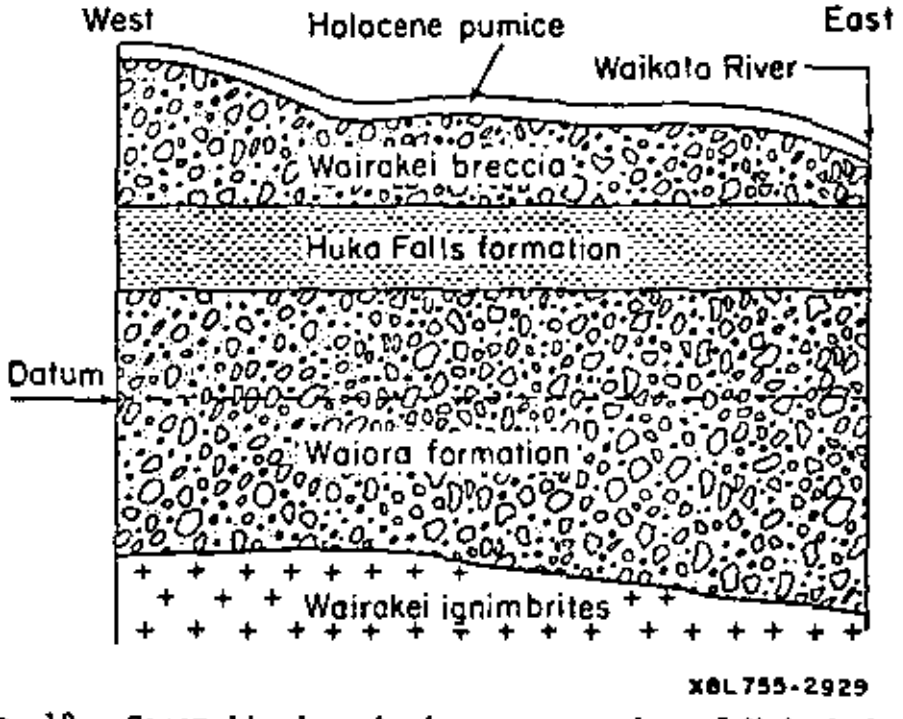


Fig. 19. Generalized geologic cross-section of Wairakei geothermal system. Datum plane 152.4 m above sea level (after Mercer et al., 1975).

the period investigated. Fig. 20 is a comparison of computed and observed potentiometric surfaces in the Waiora aquifer for 1958 and 1962. The single-phase model failed to reproduce historical data after the calibration period of 1955-1962 due to a considerable quantity of steam that had formed in the Waiora aquifer as a result of exploitation. Faust and Mercer (1975) are now developing a two-phase model to handle such problems.

A two-dimensional model of transient single-component, two-phase flow in a geothermal system has been developed by Toronyi (1974). The model is based on Equations 1-3 and 6 (without the last two terms involving pressure) and utilizes a block-centered rectangular finite difference grid capable of simulating flow in either a horizontal or vertical plane. The resulting equations are expressed in an implicit backward difference form and are solved simultaneously by a line iterative quasi-linearization (Newton-Raphson) scheme. Anisotropy is taken into account with the restriction that principal permeabilities and heat conductivities must remain parallel to the coordinates. Thermal conductivity is calculated according to (5) but dispersion is not taken into account. The fluids are assumed to have temperatures and pressures that are always on the vapor pressure curve implying that liquid and vapor co-exist at every point in the system. Consequently p and S are the two dependent variables for which a solution is sought simultaneously.

The external boundaries are impermeable and adiabatic with the understanding that forced convection due to production is much greater than conduction across these boundaries. The distributed-parameter model is coupled to a one-dimensional steady state model of a producing well in which the fluid is assumed to form a homogeneous two-phase mixture. The well is treated as a point source in the finite difference model which, in turn, provides boundary values of p and S for the steady state wellbore model. The wellbore model is represented mathematically by first order ordinary differential equations which are solved by the Runge-Kutta method.

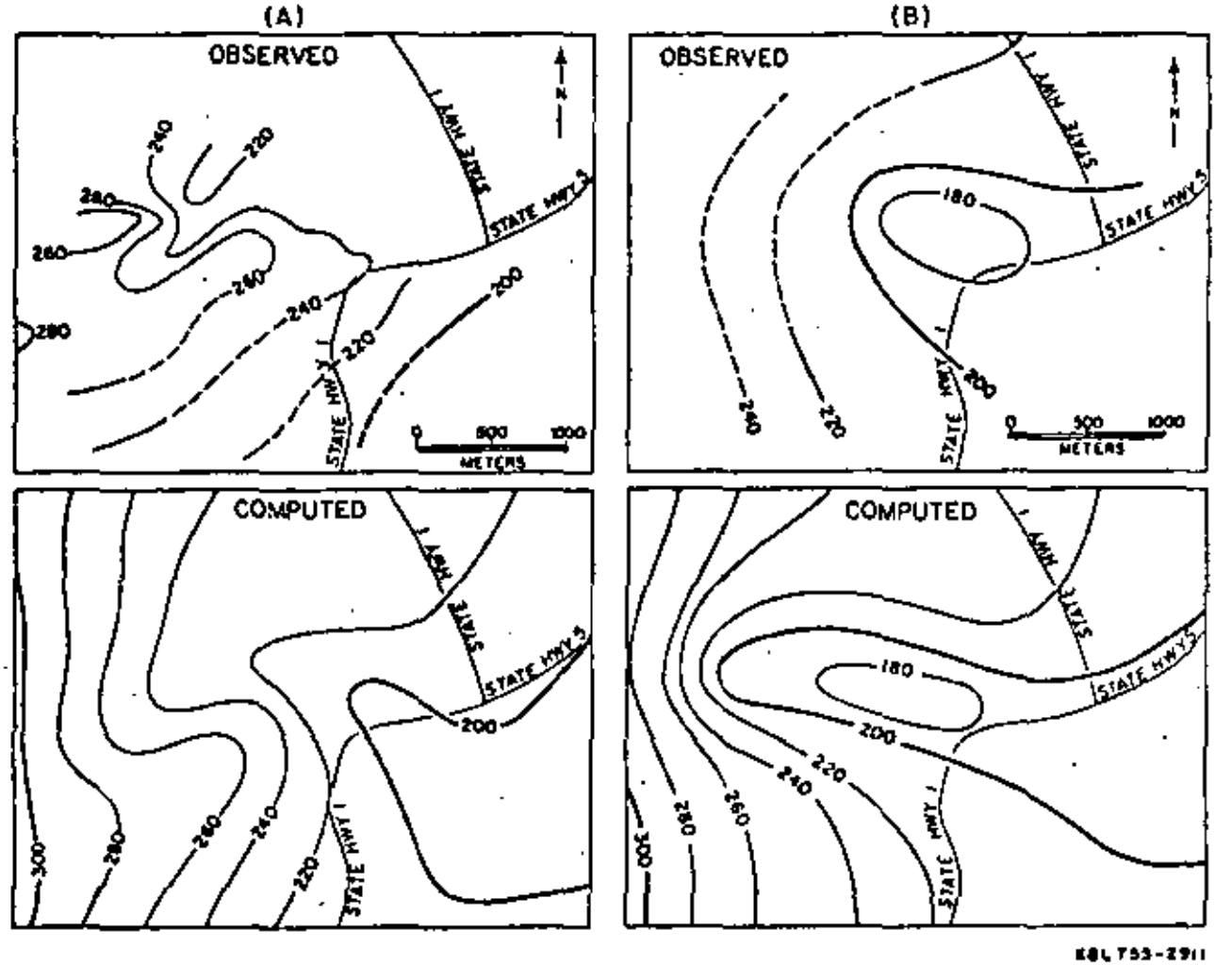


Fig. 20. Comparison of computed with observed potentiometric surfaces in Waiora hot-water aquifer for (A) 1958 and (B) 1962. Values in meters from datum 152.4 m above sea level (after Mercer et al., 1975).

Toronyi applied his model only to a homogeneous and isotropic geothermal system by using a 6 x 6 rectangular finite difference grid. His purpose was to investigate the effects of porosity, permeability, and various uniform initial p and S distributions on the production of geothermal fluid in a horizontal and vertical plane. On the basis of these studies, Toronyi classified the behavior of two-phase geothermal systems into three types in terms of initial liquid saturation: (1) vapor dominated, with initial $S^L < 40\%$; (2) liquid dominated, with initial $S^L > 60\%$, and (3) mixed or intermediate, with initial $S^L$ within the range 40 - 60%. Condensation and vaporization were found to be very important phenomena that could create exceedingly high liquid saturations near a wellbore and disrupt gravitational equilibrium by causing more liquid to occur at the top of the system than at the bottom. Toronyi also found that superheated regions form faster in rocks having relatively low porosity and permeability values. The quality of the produced fluid (in terms of percent steam) was always found to be greater at the wellhead than at the bottom, although the maximum change in quality was small.

A two-phase, multi-dimensional model for geothermal systems has recently been developed by Lasseter et al. (1975) based on an extension of an earlier investigation of single-phase flow under nonisothermal conditions (Lasseter and Witherspoon, 1974). This model utilizes Equations 1 through 4. In the numerical process, Equations 1 through 3 are combined into a flow equation which is then solved in conjunction with the energy equation (Eq. 4). These two equations expressed in an integrated finite difference form (Narasimhan and Witherspoon, 1975) are solved for the two dependent variables, density and energy of the fluids, as a function of time and position within the system. Advantage can be taken of the fact that the time constants for the energy equation are typically several orders of magnitude larger than the time constants of the flow equation, which permits one to decouple the governing equations and still handle the

non-linearities satisfactorily. Thus, while it is necessary to take relatively small time steps to accurately solve the flow equation, the energy field time steps can be much larger.

Some preliminary results for a model of a vapor-dominated geothermal system are shown in Fig. 21. A vertical cross-section of a cylindrical system with a height of 3000 m and a radius of 2000 m was set up using 150 elements. The vapor column had an average initial temperature and pressure of 250°C and 40 kg/cm$^2$ throughout, and an attempt was also made to simulate a 200 m bottom layer that was essentially liquid saturated. The lower boundary of the boiling water layer was maintained at 250°C while the other boundaries were arbitrarily made impermeable to both heat and fluid. Typical values for thermal and flow properties of the materials were assumed. Relative permeability data were temperature independent.

Figure 21 shows reproductions of computer plots after about 1500 days at a steam withdrawal rate from the producing interval of $3 \times 10^7$ kg/day (1380 t/h). As a result of this high rate of production, the pressure in the vapor column dropped to about 25 kg/cm$^2$ (Fig. 21A) and the temperature decreased to about 225°C (Fig. 21B). Figure 21C is a vector plot of the vapor flux showing how vigorous boiling at the bottom of the system is producing substantial steam. Figure 21D is a vector plot of the liquid flux and shows how water is separating from the steam at the base of the system. These preliminary results serve to illustrate the power of this numerical approach in analyzing such complex systems.

Gringarten and Sauty (1975) have developed an analytical model for nonsteady temperature behavior of production wells during reinjection of heat-depleted water into a horizontal aquifer with uniform regional flow. The aquifer is of infinite lateral extent and is confined between two impermeable semi-infinite layers. Initially, the system has a uniform temperature, $T_o$. At time $t = 0$, a well starts producing water at rate Q and injection of relatively cold water starts in a second well in the same aquifer at the same rate. The temperature

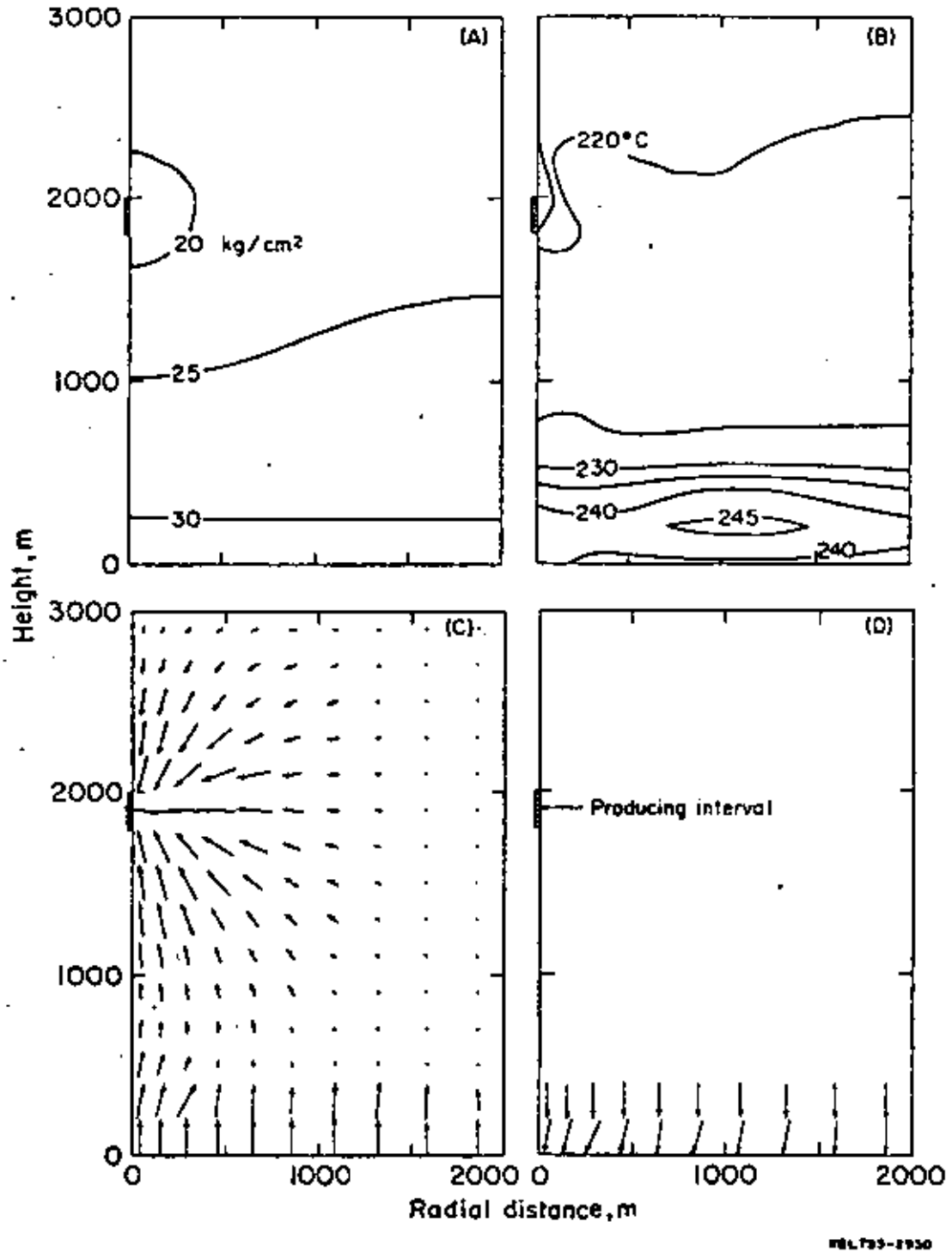


Fig. 21. Distributed-parameter model of vapor-dominated geothermal system showing reservoir conditions after 1500 days of production: (A) pressure field, (B) temperature field, (C) vapor flux, (D) liquid flux.

of the injected water is set equal to $T_1$ and maintained constant thereafter. Such a pair of wells is known as a "doublet."

The authors assume that steady state fluid flow is established much faster than thermal equilibrium and that temperature transfer occurs only by forced horizontal convection in the aquifer and vertical conduction in the confining beds. Assuming further that the waters at temperatures $T_o$ and $T_1$ do not mix (piston displacement), they have arrived at a simple closed form mathematical relationship between temperature, certain dimensionless parameters, and the stream function characterizing water flow. Gringarten and Sauty used their solution to calculate the optimum spacing of isolated doublets to be drilled for space heating purposes in the 1800 m deep Dogger aquifer around Paris, under the requirement that the cold front does not reach the producing well in less than 30 years when Q = 100 $m^3/h$. By introducing a safety factor into their calculations, the optimum spacing was found to be about 900 m for an aquifer 50 m thick.

## NOMENCLATURE

| Symbol | Description | Dimensions |
|---|---|---|
| $a$, $a_1$, $a_2$ | width | L |
| $c_p$ | specific heat at constant pressure | $L^2t^{-2}T^{-1}$ |
| $c_v$ | specific heat at constant volume | $L^2t^{-2}T^{-1}$ |
| D | depth | L |
| $D_1$, $D_2$ | aspect ratio | - |
| $D_{ij}$ | mechanical heat dispersion tensor | $MLt^{-3}T^{-1}$ |
| e | specific internal energy | $L^2t^{-2}$ |
| f | fluid property | arbitrary |
| g | acceleration due to gravity | $Lt^{-2}$ |
| $g_i$ | gravity vector (0, 0, -g) | $Lt^{-2}$ |

| Symbol | Description | Dimensions |
|---|---|---|
| $h$ | specific enthalpy | $L^2t^{-2}$ |
| $H$ | heat capacity ratio | - |
| $k$ | intrinsic permeability | $L^2$ |
| $k_{ij}$ | intrinsic permeability tensor | $L^2$ |
| $k_r$ | relative permeability | - |
| $L$ | length | $L$ |
| $m$ | specific mass flux | $ML^{-2}t^{-1}$ |
| $M$ | mass | $M$ |
| $n_i$ | outward unit normal vector on $\Gamma$ | - |
| $Nu$ | Nusselt number | - |
| $p$ | pressure | $ML^{-1}t^{-2}$ |
| $p_D$ | dimensionless pressure | - |
| $Pr$ | Prandtl number | - |
| $q_i$ | specific conductive heat flux vector | $Mt^{-3}$ |
| $Q$ | heat flux | $ML^2t^{-3}$ |
| $r$ | radius | $L$ |
| $R$ | representative elementary volume | $L^3$ |
| $Ra$ | Rayleigh number | - |
| $Ra_c$ | critical Rayleigh number | - |
| $S$ | fluid saturation | - |
| $t$ | time | $t$ |
| $T$ | temperature | $T$ |
| $v$ | specific volume | $L^3M^{-1}$ |
| $v_i$ | darcy velocity vector | $LT^{-1}$ |
| $V$ | volume | $L^3$ |
| $w_i$ | velocity vector of solid fluid interface | $Lt^{-1}$ |

| Symbol | Description | Dimensions |
|---|---|---|
| $x_i$ | vector of space coordinates (x,y,z) z being the vertical | L |
| Z | compressibility factor for real gas | - |
| $\alpha$ | thermal diffusivity | $L^2t^{-1}$ |
| $\beta$ | coefficient of volumetric thermal expansion | $T^{-1}$ |
| $\Gamma^{LS}$ | liquid-solid interface in R | $L^2$ |
| $\Gamma^{LG}$ | liquid-gas interface in R | $L^2$ |
| $\Gamma^{GS}$ | gas-solid interface in R | $L^2$ |
| $\delta_{ij}$ | kronecker delta (1 if i = j and 0 if i ≠ j) | - |
| $\theta$ | dimensionless temperature | - |
| $\kappa$ | thermal conductivity | $MLt^{-3}T^{-1}$ |
| $\kappa_{ij}$ | thermal dispersion tensor | $MLt^{-3}T^{-1}$ |
| $\mu$ | viscosity | $ML^{-1}t^{-1}$ |
| $v_i$ | dimensionless velocity vector | - |
| $\rho$ | density | $ML^{-3}$ |
| $\tau$ | dimensionless time | - |
| $\phi$ | porosity | - |
| $\langle\ \rangle$ | average over R | arbitrary |
| $\langle\ \rangle^*$ | average over pore space of R | arbitrary |
| $\langle\ \rangle^{L,G,S}$ | average over liquid, gas, or solid phases in R | arbitrary |
| **Subscripts** | | |
| o | reference quantity | |
| **Superscripts** | | |
| eff | effective quantity for fluid-filled rock | |
| G | gas phase | |

| Symbol | Description | Dimensions |
|---|---|---|
| L | liquid phase | |
| S | solid phase | |
| o | deviation from average over R | |

ACKNOWLEDGMENTS

We would like to acknowledge the support for this work provided by the U. S. Atomic Energy Commission, the U. S. Geological Survey, and the University of California.

## APPENDIX

The purpose of this appendix is to derive a macroscopic form of the energy balance equation for a two-phase, single component fluid in a porous medium. This is accomplished by averaging the microscopic equations over a representative elementary volume (Bear, 1972, p. 19) of the medium. The particular method of averaging that is used here has been applied by Lee et al. (1975) to the energy equation and, in this context, was brought to our attention by Gray and Pinder (1974, personal communication). We recognize that the macroscopic energy equation can be derived directly from macroscopic balance considerations, without resorting to an averaging process. However, the formal averaging procedure is helpful in gaining insight into the numerous assumptions that one must make in order to arrive at a manageable macroscopic expression. Such assumptions are implicitly inherent in every macroscopic equation and, by facing them explicitly, one should be able to appreciate some of the limitations of the differential equations used to describe geothermal systems.

### Mathematical Preliminaries

Let R be a representative elementary volume of the porous medium and let $\phi$ be the porosity of R. Whitaker (1969) demonstrated that the averaging procedure used below will lead to meaningful results if the characteristic length of R is much greater than the characteristic length of the pores, and is much smaller than the characteristic length of the entire porous medium. An obvious requirement is that R be large enough to provide a fair representation of all the statistical properties of the pore space. Our analysis is restricted to homogeneous porous media which means that the porosity, $\phi$, as well as all other statistical properties of the pore space, must remain unchanged as one focuses his attention on different elementary representative volumes in the medium. Furthermore, the size and shape of R must be constant and its orientation must remain unchanged.

Let $f^L(x_i)$ be some property of the liquid (e.g., density, temperature, etc.) which, by definition, is zero in the gas phase and in the solids. Then the "liquid phase average" of $f^L$ is defined as

$$\langle f^L \rangle^L = \frac{1}{\phi S^L R} \int_R f^L \, dR \tag{A1}$$

Similarly, the "pore volume average" of $f^L$ is defined as

$$\langle f^L \rangle^* = \frac{1}{\phi R} \int_R f^L \, dR \tag{A2}$$

and the "bulk volume average" as

$$\langle f^L \rangle = \frac{1}{R} \int_R f^L \, dR \tag{A3}$$

From (A1) - (A3) it is evident that

$$\langle f^L \rangle = \phi \langle f^L \rangle^* = \phi S^L \langle f^L \rangle^L \tag{A4}$$

These averages can be viewed as point macroscopic quantities associated with the centroid of R. Thus, there is an average associated with each point in R (each such point being the centroid of another R), and it therefore makes sense to talk about the average value of these averages over R. Whitaker (1969) showed that

$$\langle\langle f^L \rangle\rangle = \langle f^L \rangle \tag{A5}$$

i.e., the average of the average is equal to the average (note that this is by no means self evident).

At any point in the liquid phase within R, $f^L$ can be expressed as

$$f^L = \langle f^L \rangle^L + \tilde{f}^L \tag{A6}$$

where $\tilde{f}^L$ is simply the deviation from the phase average of $f^L$. From (A5) and (A6) it follows that

$$\langle \overset{\circ}{f}{}^{L} \rangle^{L} \equiv 0 \tag{A7}$$

Note that just like $f^L$, the function of $\overset{\circ}{f}{}^{L}$ is taken to be zero everywhere outside the liquid phase.

According to the general transport theorem (c.f. Whitaker, 1968) one has

$$\langle \frac{\partial f^L}{\partial t} \rangle = \frac{\partial \langle f^L \rangle}{\partial t_i} - \frac{1}{R} \int_{\Gamma^{LS}, \Gamma^{LG}} f^L w_i n_i \, d\Gamma \tag{A8}$$

where $n_i$ is a unit normal pointing out of the liquid phase. Another useful relationship known as the "averaging theorem" (Whitaker, 1969; Slattery, 1972, pp. 192-196) states that

$$\langle \frac{\partial f^L}{\partial x_i} \rangle = \frac{\partial \langle f^L \rangle}{\partial x_i} + \frac{1}{R} \int_{\Gamma^{LS}, \Gamma^{LG}} f^L n_i \, d\Gamma \tag{A9}$$

Similar relationships will hold for properties of the solid phase, $f^S$, and the gas phase, $f^G$.

Derivation of Energy Equation for Two-Phase Fluid

In the following analysis, the pore space is assumed to be saturated by a single-component fluid which can be either in a liquid or gaseous state. The liquid and gas phases are assumed to be separated by a distinct interface, $\Gamma^{LG}$, across which there may be a finite change in pressure. If one neglects viscous dissipation, then the energy equation at a point within the liquid can be written (c.f., Currie, 1974, p. 17) as

$$\frac{\partial}{\partial t} (\rho^L e^L) = - \frac{\partial}{\partial x_i} (\rho^L e^L v_i{}^L) - p^L \frac{\partial v_i{}^L}{\partial x_i} - \frac{\partial q_i{}^L}{\partial x_i} \tag{A10}$$

Taking the average of (A10) over a representative elementary volume, R, and using (A8) and (A9), the result (after rearrangement) is

$$\frac{\partial}{\partial t}\langle \rho^L e^L \rangle = -\frac{\partial}{\partial x_i}\langle \rho^L e^L v_i^L \rangle - \frac{1}{R}\int_{\Gamma^{LG}} \rho^L e^L (v_i^L - w_i)\, n_i\, d\Gamma$$

$$- \phi S^L \langle p^L \rangle^L \frac{\partial \langle v_i^L \rangle^L}{\partial x_i} - S^L \langle p^L \rangle^L \frac{1}{R}\int_{\Gamma^{LG}} v_i^L\, n_i\, d\Gamma$$

$$- \frac{\partial \langle q_i^L \rangle}{\partial x_i} - \frac{1}{R}\int_{\Gamma^{LS},\Gamma^{LG}} q_i^L\, n_i\, d\Gamma \qquad \text{(A11)}$$

Equation A11 is based on the assumption that fluid velocity normal to a solid-fluid interface is zero (i.e., there is no transfer of kinetic energy between the fluid and the solid). Furthermore, in order to replace the term $p^L(\partial v_i^L/\partial x_i)$ in (A10) by its macroscopic equivalent in (A11), it is necessary to assume that $\overset{*}{p}{}^L$ and $\partial \overset{*}{v}{}_i^L/\partial x_i$ are uncorrelated so that the average of their product is zero. A possible physical justification for this is to say that local variations in fluid velocity within a pore are controlled primarily by viscous stresses and can therefore be assumed to be independent of pressure.

The energy equation for the gas phase at a point within R has the same form as (A11). When this equation is averaged over R, the result is

$$\frac{\partial}{\partial t}\langle \rho^G e^G \rangle = -\frac{\partial}{\partial x_i}\langle \rho^G e^G v_i^G \rangle + \frac{1}{R}\int_{\Gamma^{LG}} \rho^G e^G (v_i^G - w_i)\, n_i\, d\Gamma$$

$$- \phi S^G \langle p^G \rangle^G \frac{\partial \langle v_i^G \rangle^G}{\partial x_i} + S^G \langle p^G \rangle^G \frac{1}{R}\int_{\Gamma^{LG}} v_i^G n_i\, d\Gamma$$

$$- \frac{\partial \langle q_i^G \rangle}{\partial x_i} - \frac{1}{R}\int_{\Gamma^{GS}} q_i^G\, n_i\, d\Gamma + \frac{1}{R}\int_{\Gamma^{LG}} q_i^G\, n_i\, d\Gamma \qquad \text{(A12)}$$

Here $n_i$ points into the gas along $\Gamma^{LG}$ and into the solid along $\Gamma^{GS}$.

The energy equation at a point within the solid is simply

57

$$\frac{\partial}{\partial t}(\rho^S e^S) = -\frac{\partial q_i^S}{\partial x_i} \tag{A13}$$

Integrating over R gives

$$\rho^S \frac{\partial \langle e^S \rangle}{\partial t} = -\frac{\partial \langle q_i^S \rangle}{\partial x_i} + \frac{1}{R}\int_{\Gamma^{LS},\Gamma^{GS}} q_i^S n_i \, d\Gamma \tag{A14}$$

where $n_i$ points into the solid.

From the requirement of energy continuity at a liquid-gas interface, it can be shown that

$$\int_{\Gamma^{LG}} [q_i^L + \rho^L e^L (v_i^L - w_i)] n_i d\Gamma = \int_{\Gamma^{LG}} [q_i^G + \rho^G e^G (v_i^G - w_i)] n_i d\Gamma \tag{A15}$$

A similar condition must also hold for the conductive energy flux $q_i n_i$ at any solid-fluid interface. Thus, by adding (A11), (A12), and (A14) and using (A4) we obtain

$$\begin{aligned}
&\frac{\partial}{\partial t}[\phi S^L \langle \rho^L e^L \rangle^L + \phi S^G \langle \rho^G e^G \rangle^G + (1-\phi)\rho^S \langle e^S \rangle^S] \\
&= -\frac{\partial}{\partial x_i}[\phi S^L \langle \rho^L e^L v_i^L \rangle^L + \phi S^G \langle \rho^G e^G v_i^G \rangle^G] \\
&- \frac{\partial}{\partial x_i}[\phi S^L \langle q_i^L \rangle^L + \phi S^G \langle q_i^G \rangle^G + (1-\phi)\langle q_i^S \rangle^S] \\
&- \phi S^L \langle p^L \rangle^L \frac{\partial \langle v_i^L \rangle^L}{\partial x_i} - \phi S^G \langle p^G \rangle^G \frac{\partial \langle v_i^G \rangle^G}{\partial x_i} \\
&- S^L \langle p^L \rangle^L \frac{1}{R}\int_{\Gamma^{LG}} v_i^L n_i \, d\Gamma + S^G \langle p^G \rangle^G \frac{1}{R}\int_{\Gamma^{LG}} v_i^G n_i \, d\Gamma
\end{aligned} \tag{A16}$$

We now introduce another assumption that thermodynamic relationships between average (macroscopic) quantities remain exactly the same as those between the equivalent point (microscopic) quantities. This assumption is implicit in all macroscopic equations that we have encountered in the literature. Its implication is that $\rho$ and $e$ are uncorrelated and one can thus replace $\langle \rho^L e^L \rangle^L$ by $\langle \rho^L \rangle^L \langle e^L \rangle^L$ and $\langle \rho^G e^G \rangle^G$ by $\langle \rho^G \rangle^G \langle e^G \rangle^G$. Since mass dispersion is not considered in the

present analysis, $\dot{\rho}$ and $\dot{v}_i$ are also uncorrelated and we can therefore write

$$\phi S^L \langle \rho^L \, e^L \, v_i^L \rangle^L = \phi S^L \left( \langle \rho^L \rangle^L \langle e^L \rangle^L \langle v_i^L \rangle^L + \langle \rho^L \, \overset{\circ}{e}{}^L \, \overset{\circ}{v}_i{}^L \rangle^L \right)$$

$$= \langle \rho^L \rangle^L \langle e^L \rangle^L \langle v_i^L \rangle + \phi S^L \langle \rho^L \, \overset{\circ}{e}{}^L \, \overset{\circ}{v}_i{}^L \rangle^L \tag{A17}$$

where the second term represents mechanical dispersion of energy. Following the current trend in the literature (c.f., Bear, 1972; Gray, 1975) we assume that dispersion is mathematically equivalent to a diffusion process, so that one can write

$$\langle \rho^L \, \overset{\circ}{e}{}^L \, \overset{\circ}{v}_i{}^L \rangle^L = - D_{ij}^L \frac{\partial \langle T^L \rangle^L}{\partial x_j} \tag{A18}$$

where $D_{ij}^L$ is known as the mechanical (or convective) dispersion tensor. The conductive flux, $q_i^L$, is expressed by Fourier's law using a scalar thermal conductivity,

$$q_i^L = - \kappa^L \frac{\partial T^L}{\partial x_i} \tag{A19}$$

the average of which is given by (A9) as

$$\langle q_i{}^L \rangle = - \kappa^L \frac{\partial \langle T^L \rangle}{\partial x_i} - \frac{\kappa^L}{R} \int_{\Gamma^{LG}, \Gamma^{LS}} T^L \, n_i \, d\Gamma \tag{A20}$$

In order to eliminate the surface integral from (A20) we assume that the orientation vector $n_i$ is symmetrically distributed about a zero average value (this is true if the orientations of $\Gamma^{LG}$ and $\Gamma^{LS}$ are random). Then, since temperature is independent of interface orientation (i.e., random temperatures may exist at various points along $\Gamma$ having a given orientation) $T^L$ and $n_i$ are uncorrelated and the surface integral in (A20) can be neglected. In a similar manner, it may appear reasonable to assume that $v_i{}^L n_i$ is symmetrically distributed about a zero average value along $\Gamma^{LG}$ so that the first surface integral in (A16) vanishes. Similar considerations hold for the gas phase. If we further assume that $\phi$, $S^L$, and $S^G$ remain practically constant for any averaging volume whose centroid is

inside R, then (A16) can finally be reduced to

$$\frac{\partial}{\partial t}\left[\phi S^L \langle \rho^L \rangle^L \langle e^L \rangle^L + \phi S^G \langle \rho^G \rangle^G \langle e^G \rangle^G + (1-\phi)\rho^S \langle e^S \rangle^S\right]$$

$$= -\frac{\partial}{\partial x_i}\left(\langle \rho^L \rangle^L \langle e^L \rangle^L \langle v_i^L \rangle + \langle \rho^G \rangle^G \langle e^G \rangle^G \langle v_i^G \rangle\right)$$

$$+ \frac{\partial}{\partial x_i}\left[\phi S^L \kappa_{ij}^L \frac{\partial \langle T^L \rangle^L}{\partial x_j} + \phi S^G \kappa_{ij}^G \frac{\partial \langle T^G \rangle^G}{\partial x_j} + (1-\phi)\kappa^S \frac{\partial \langle T^S \rangle^S}{\partial x_i}\right]$$

$$- \langle p^L \rangle^L \frac{\partial \langle v_i^L \rangle}{\partial x_i} - \langle p^G \rangle^G \frac{\partial \langle v_i^G \rangle}{\partial x_i} \qquad \text{(A21)}$$

where $\kappa_{ij} = \kappa\delta_{ij} + D_{ij}$ is the combined conductive and mechanical dispersion tensor.

In the literature it is customary to assume that all phases are in thermal equilibrium and that capillary pressure differences between the fluid phases are negligible. In this case (A21) reduces to

$$\frac{\partial}{\partial t}\left[\phi S^L \langle \rho^L \rangle^L \langle e^L \rangle^L + \phi S^G \langle \rho^G \rangle^G \langle e^G \rangle^G + (1-\phi)\rho^S \langle e^S \rangle^S\right]$$

$$= -\frac{\partial}{\partial x_i}\left(\langle \rho^L \rangle^L \langle e^L \rangle^L \langle v_i^L \rangle + \langle \rho^G \rangle^G \langle e^G \rangle^G \langle v_i^G \rangle\right)$$

$$+ \frac{\partial}{\partial x_i}\left(\kappa_{ij}^{eff} \frac{\partial \langle T \rangle^*}{\partial x_j}\right) - \langle p \rangle^* \frac{\partial}{\partial x_i}\left(\langle v_i^L \rangle + \langle v_i^G \rangle\right) \qquad \text{(A22)}$$

where

$$\kappa_{ij}^{eff} = \phi S^L \kappa_{ij}^L + \phi S^G \kappa_{ij}^G + (1-\phi)\kappa^S \delta_{ij}$$

This shows that the assumption of thermal equilibrium implies viewing the solid, liquid, and gas as three anisotropic conductors arranged parallel to the direction of heat flow.

Recalling our assumption that thermodynamic relationships between average fluid properties are the same as between the equivalent point properties, we can define the average (macroscopic) enthalpy of the liquid as

$$\langle h^L \rangle^L = \langle e^L \rangle^L + \frac{\langle p^L \rangle^L}{\langle \rho^L \rangle^L} \qquad \text{(A24)}$$

Similar definitions will hold for the gas and the solid. If we now replace each <e> in (A22) by <h> - <p>/<ρ>, we obtain a macroscopic energy equation in terms of enthalpy.

$$\frac{\partial}{\partial t}\left[\phi S^{L}\langle\rho^{L}\rangle^{L}\langle h^{L}\rangle^{L} + \phi S^{G}\langle\rho^{G}\rangle^{G}\langle h^{G}\rangle^{G} + (1-\phi)\rho^{S}\langle h^{S}\rangle^{S}\right]$$

$$= -\frac{\partial}{\partial x_i}\left(\langle\rho^{L}\rangle^{L}\langle h^{L}\rangle^{L}\langle v_i^{L}\rangle + \langle\rho^{G}\rangle^{G}\langle h^{G}\rangle^{G}\langle v_i^{G}\rangle\right)$$

$$+ \frac{\partial}{\partial x_i}\left(\kappa_{ij}^{eff}\frac{\partial\langle T\rangle^{*}}{\partial x_j}\right) + \frac{\partial(\phi\langle p\rangle^{*})}{\partial t} + (\langle v_i^{L}\rangle + \langle v_i^{G}\rangle)\frac{\partial\langle p\rangle^{*}}{\partial x_i} \qquad \text{(A25)}$$

Temperature Equation for a Single Phase

In the particular case where the pores are completely saturated by a single fluid phase (say liquid), one can use the equation of mass continuity to rewrite (A21) in the form

$$\phi\langle\rho^{L}\rangle^{*}\frac{\partial\langle e^{L}\rangle^{*}}{\partial t} + (1-\phi)\rho^{S}\frac{\partial\langle e^{S}\rangle^{S}}{\partial t} = -\langle\rho^{L}\rangle^{*}\langle v_i^{L}\rangle\frac{\partial\langle e^{L}\rangle^{*}}{\partial x_i}$$

$$+ \frac{\partial}{\partial x_i}\left[\phi\kappa_{ij}^{L}\frac{\partial\langle T^{L}\rangle^{*}}{\partial x_j} + (1-\phi)\kappa^{S}\frac{\partial\langle T^{S}\rangle^{S}}{\partial x_i}\right] - \langle p^{L}\rangle^{*}\frac{\partial\langle v_i\rangle^{L}}{\partial x_i} \qquad \text{(A26)}$$

Assuming that the thermodynamic relationships

$$\frac{\partial e}{\partial *} = \left(\frac{\partial e}{\partial v}\right)_T\frac{\partial v}{\partial *} + c_v\frac{\partial T}{\partial *} \qquad \text{(A27)}$$

$$p = T\left(\frac{\partial p}{\partial T}\right)_v - \left(\frac{\partial e}{\partial v}\right)_T \qquad \text{(A28)}$$

hold for the average quantities appearing in (A26), this latter equation can be rewritten as

$$\left(\frac{\partial e^L}{\partial v}\right)_T \left[\phi<\rho^L>^* \frac{\partial(<\rho^L>^*)^{-1}}{\partial t} + <\rho^L>^* <v_i^L> \frac{\partial(<\rho^L>^*)^{-1}}{\partial x_i} - \frac{\partial <v_i^L>}{\partial x_i}\right]$$

$$+ \phi<\rho^L>^* c_v^L \frac{\partial <T^L>^*}{\partial t} + (1-\phi)\rho^S c_v^S \frac{\partial <T^S>^S}{\partial t}$$

$$= - <\rho^L>^* <v_i^L> c_v^L \frac{\partial <T^L>^*}{\partial x_i} + \frac{\partial}{\partial x_i}\left[\phi\kappa_{ij}^L \frac{\partial <T^L>^*}{\partial x_j} + (1-\phi)\kappa^S \frac{\partial <T^S>^S}{\partial x_i}\right]$$

$$- <T^L>^* \left(\frac{\partial \rho}{\partial T}\right)_v \frac{\partial <v_i^L>}{\partial x_i} \qquad \text{(A29)}$$

The first term in brackets can be reformulated as

$$- \frac{1}{<\rho^L>^*}\left[\phi \frac{\partial <\rho^L>^*}{\partial t} + \frac{\partial}{\partial x_i}(<\rho^L>^* <v_i^L>)\right]$$

which vanishes by virtue of mass continuity. Thus, the energy equation for the liquid phase can be expressed entirely in terms of temperature,

$$\phi<\rho^L>^* c_v^L \frac{\partial <T^L>^*}{\partial t} + (1-\phi)\rho^S c_v^S \frac{\partial <T^S>^S}{\partial t} = - <\rho^L>^* <v_i^L> c_v^L \frac{\partial <T^L>^*}{\partial x_i}$$

$$+ \frac{\partial}{\partial x_i}\left[\phi\kappa_{ij}^L \frac{\partial <T^L>^*}{\partial x_j} + (1-\phi)\kappa^S \frac{\partial <T^S>^S}{\partial x_i}\right] - <T^L>^* \left(\frac{\partial \rho}{\partial T}\right)_v \frac{\partial <v_i^L>}{\partial x_i}$$

(A30)

If the solid and the liquid are assumed to be in thermal equilibrium, (A30) reduces to

$$\left[\phi<\rho^L>^* c_v^L + (1-\phi)\rho^S c_v^S\right] \frac{\partial <T>^*}{\partial t} = - <\rho^L>^* <v_i^L> c_v^L \frac{\partial <T>^*}{\partial x_i}$$

$$+ \frac{\partial}{\partial x_i}\left(\kappa_{ij}^{eff} \frac{\partial <T>^*}{\partial x_j}\right) - <T>^* \left(\frac{\partial \rho}{\partial T}\right)_v \frac{\partial <v_i^L>}{\partial x_i} \qquad \text{(A31)}$$

where $\kappa_{ij}^{eff} = \phi\kappa_{ij}^L + (1-\phi)\kappa^S \delta_{ij}$.

Equations A30 and A31 are also applicable when the pores are completely saturated by the gas phase, provided that the superscript L is replaced by G.

181

REFERENCES

Anand, J., W. H. Somerton and E. Gomaa, 1973, Predicting thermal conductivities of formations from other known properties, Soc. Petrol. Engr. Jour., v. 13, no. 5, pp. 267-273.

Bear, J., 1972, Dynamics of Fluids in Porous Media, Am. Elsevier, New York.

Beck, J. L., 1972, Convection in a box of porous material saturated with fluid, Phys. of Fluids, v. 15, no. 8, pp. 1377-1383.

Billhartz, H. L., Jr., 1971, Fluid Production from Geothermal Steam Reservoirs, M. S. thesis, Stanford Univ., Calif.

Bodvarsson, G., 1961, Physical characteristics of natural heat resources in Iceland, paper G.6, U. N. Conf. on New Sources of Energy, Rome, August 21-31.

Brace, W. F., J. B. Walsh and W. T. Francos, 1968, Permeability of granite under high pressure, Jour. Geophys. Research, v. 73, no. 6, pp. 2225-2236.

Brigham, W. E. and W. B. Morrow, 1974, P/Z behavior for geothermal steam reservoirs, paper SPE 4899, 44th Annual Calif. Regional Meeting SPE-AIME, San Francisco, April 4-5.

Brownell, D. H., Jr., S. K. Garg and J. W. Pritchett, 1975, Computer simulation of geothermal reservoirs, paper SPE 5381, 45th Annual Calif. Regional Meeting SPE-AIME, Ventura, Calif. April 2-4.

Cady, G. V., 1969, Model Studies of Geothermal Fluid Production, Ph.D. dissertation, Stanford Univ., Calif.

Calhoun, J. C., M. Lewis, Jr. and R. C. Newman, 1949, Experiments on the capillary properties of porous solids, Trans. AIME, v. 186, pp. 189-196.

Caltagirone, J. P., M. Cloupeau and M. Combarnous, 1971, Convection naturelle fluctuante dans une couche poreuse horizontale, Comptes Rendus, Acad. Sci., Paris, B273, pp. 833-836.

Casse, F. J., 1974, The Effect of Temperature and Confining Pressure on Fluid Flow Properties of Consolidated Rocks, Stanford Geothermal Program, Rep. SGP-TR3, Stanford Univ., Calif.

Cheng, P. and K. H. Lau, 1974, Steady state free convection in an unconfined geothermal reservoir, Jour. Geophys. Res., v. 79, no. 29, pp. 4425-4431.

Coats, K. H., W. D. George, C. Chu and B. E. Marcum, 1974, Three-dimensional simulation of steamflooding, Soc. Petrol. Engr. Jour., v. 15, no. 6, pp. 573-592.

Combarnous, M. A. and S. A. Bories, 1973, Thermal Convection in Saturated Porous Media, Report prepared for Advances in Hydroscience, Institut Francais du Petrole and Institute de Mecanique des Fluides de Toulouse.

Combarnous, M. and S. Bories, 1974, Modelisation de la convection naturelle au sein d'une couche poreuse horizontale a l'aide d'un coefficient de transfert solide-fluide, Int. Jour. Heat Mass Transfer, v. 17, pp. 505-515.

Craig, H., 1966, Superheated steam and mineral-water interactions in geothermal areas, Trans. Am. Geophys. Union, v. 47, pp. 204-205 (abstract).

Currie, I. G., 1974, Fundamental Mechanics of Fluids, McGraw-Hill, New York.

Davidson, L. B., 1969, The effect of temperature on the permeability ratio of different fluid pairs in two-phase systems, Jour. Petrol. Tech., Aug. 1969, pp. 1037-1046.

Donaldson, I. G., 1962, Temperature gradients in the upper layers of the earth's crust due to convective water flows, Jour. Geophys. Res., v. 67, no. 9, pp. 3449-3459.

Donaldson, I. G., 1968a, The flow of steam water mixtures through permeable beds: A simple simulation of a natural undisturbed hydrothermal region, New Zealand Jour. Sci., v. 11, pp. 3-23.

Donaldson, I. G., 1968b, A possible model for hydrothermal systems and methods of studying such a model, paper 2580, Third Australian Conf. on Hydraulics and Fluid Mechanics, Nov. 25-29.

Donaldson, I. G., 1970, The simulation of geothermal systems with a simple convective model, Geothermics, Special issue 2, v. 2, part 1, pp. 649-654.

Edmonson, J. A., 1965, Effect of temperature on waterflooding, Jour. Canadian Petrol. Tech., v. 4, no. 4, pp. 236-242.

Einarsson, T., 1942, Ueber das Wesen der heissen Quellen Islands, Rit. Vísind. Ísl., v. 26, 91 p.

Elder, J. W., 1965, Physical processes in geothermal areas in Terrestrial Heat Flow, W. H. K. Lee, ed., Am. Geophys. Union Mon., ser. 8, pp. 211-239.

Elder, J. W., 1966, Heat and mass transfer in the earth: Hydrothermal systems, New Zealand D.S.I.R. Bull. 169, 115 p.

Elder, J. W., 1967, Transient convection in a porous medium, Jour. Fluid Mech., v. 27, part 3, pp. 609-623.

Facca, G. and F. Tonani, 1964, Theory and technology of a geothermal field, Bull. Volcanol., v. 27, part 1, pp. 143-189,

Faust, C. F. and J. W. Mercer, 1975, Mathematical modeling of geothermal systems, paper to be presented at Second United Nations Symposium on the Development and Use of Geothermal Resources, San Francisco, May 20-29.

Fernandez, R. T., 1972, Natural Convection from Cylinders Buried in Porous Media, Ph.D. dissertation, Univ. of Calif., Berkeley.

Goguel, J., 1953, Le regime thermique de l'eau souterraine, Annales des Mines, v. 10, pp. 3-32.

Gray, W. G., 1975, A derivation of the equations for multi-phase transport, paper submitted to Chem. Engr. Sci.

Greenberg, D. B., R. S. Cresap and T. A. Malone, 1968, Intrinsic permeability of hydrological porous mediums: Variation with temperature, Water Resour. Res., v. 4, no. 4, pp. 791-800.

Gringarten, A. C. and J. P. Sauty, 1975, A theoretical study of heat extraction from aquifers with uniform regional flow, paper submitted to Jour. Geophys. Res.

Gupta, V. P. and D. D. Joseph, 1973, Bounds for heat transport in a porous layer, Jour. Fluid Mech., v. 57, part 3, pp. 491-514.

Haas, J. L., Jr., 1970, An equation for the density of vapor-saturated NaCl-$H_2O$ solutions from 75° to 325°C, Am. Jour. Sci., v. 269, pp. 489-493.

Haas, J. L., Jr., 1971, The effect of salinity on the maximum thermal gradient of a hydrothermal system at hydrostatic pressure, Econ. Geol., v. 66, pp. 940-946.

Helgeson, H. C., 1968, Geologic and thermodynamic characteristics of the Salton Sea geothermal system, Am. Jour. Sci., v. 266, pp. 129-166.

Holst, P. H., 1970, A Theoretical and Experimental Investigation of Natural Convection in Porous Media, Ph.D. dissertation, Univ. of Calgary, Alberta, Canada.

Holst, P. H. and K. Aziz, 1972a, A theoretical and experimental study of natural convection in a confined porous medium, Canadian Jour. Chem. Engr., v. 50, pp. 232-241.

Holst, P. H. and K. Aziz, 1972b, Transient three-dimensional natural convection in confined porous media, Jour. Heat and Mass Transfer, v. 15, pp. 73-90.

Horne, R. N. and M. J. O'Sullivan, 1974, Oscillatory convection in a porous medium heated from below, Jour. Fluid Mech., v. 66, part 2, pp. 339-352.

Horton, C. W. and F. T. Rogers, Jr., 1945, Convection currents in a porous medium, Jour. Appl. Phys., v. 16, no. 6, pp. 367-370.

James, R., 1968, Wairakei and Lardarello geothermal power systems compared, New Zealand Jour. Sci. and Tech., v. 11, pp. 706-719.

Jeffreys, H., 1930, The instability of a compressible fluid heated below, Proc. Cambridge Phil. Soc., v. 26, pp. 170-172.

Kaneko, T., M. F. Mohtadi and K. Aziz, 1974, An experimental study of natural convection in inclined porous media, Int. Jour. Heat Mass Transfer, v. 17, pp. 485-496.

Kapplemeyer, O. and R. Haenel, 1974, Geothermics with Special Reference to Application, Geopublication Associates, Berlin, tables 6.3-6.6, pp. 208-218.

Karra, P. S., 1968, A numerical Study of Natural Convection in Porous Media, M. S. thesis, Univ. of Calgary, Alberta, Canada.

Knutson, C. F. and B. F. Bohor, 1963, Reservoir rock behavior under moderate confining pressure in Symposium on Rock Mechanics, Univ. Minnesota, MacMillan, New York, pp. 627-659.

Lapwood, E. R., 1948, Convection of a fluid in a porous medium, Proc. Cambridge Phil. Soc., v. 44, pp. 508-521.

Lasseter, T. J. and P. A. Witherspoon, 1974, Underground Storage of Liquified Natural Gas in Cavities Created by Nuclear Explosives, Geotechnical Engineering Pub. No. 74-1, Univ. Calif., Berkeley.

Lasseter, T. J., P. A. Witherspoon and M. J. Lippmann, 1975, Multiphase multi-dimensional simulation of geothermal reservoirs, paper submitted to Second United Nations Symposium on the Development and Use of Geothermal Resources, San Francisco, May 20-29.

Lee, P. C. Y., W. G. Gray and G. F. Pinder, 1975, Thermoenergy transport in porous media, paper in preparation.

Likke, S. and L. A. Bromley, 1973, Heat capacities of aqueous NaCl, KCl, $MgCl_2$ $MgSO_4$, and $Na_2SO_4$ solutions between 80° and 200°C, Jour. Chem. Engr. Data, v. 18, no. 2, pp. 189-195.

Lo, H. Y. and N. Mungan, 1973, Effect of temperature on water-oil relative permeabilities in oil-wet and water-wet systems, paper SPE 4505, 48th Annual Meeting SPE-AIME, Las Vegas, Nev., Sept. 30-Oct. 3.

Marinelli, G., 1969, Some geological data on the geothermal areas of Tuscany, Bull. Volcanol., v. 33, no. 1, pp. 319-334.

Martin, J. C., 1975, Analysis of internal steam drive in geothermal reservoirs, paper SPE 5382, 45th Annual Calif. Regional Meeting SPE-AIME, Ventura, Calif., April 2-4.

Masouka, T., 1972, Heat transfer by free convection in a porous layer heated from below, Heat Transfer-Japan Res., v. 1, no. 1, pp. 39-45.

Matthews, C. S. and D. G. Russell, 1967, Pressure Buildup and Flow Tests in Wells, Soc. Petr. Engr. AIME Mon., v. 1.

McNabb, A., 1965, On convection in a porous medium, Proc. Australasian Conf. on Hydraulics and Fluid Mechanics, v. 2, pp. C161-C171.

Mercer, J. W., Jr., 1973, Finite Element Approach to the Modeling of Hydrothermal Systems, Ph.D. dissertation, Univ. of Illinois, Urbana-Champaign.

Mercer, J. W., Jr., C. F. Faust and G. F. Pinder, 1974, Geothermal reservoir simulation, Proc. NSF Conference on Research for the Development of Geothermal Energy Resources, Pasadena, Calif., Sept. 23-25, pp. 256-267.

Mercer, J. W. and G. F. Pinder, 1974, Finite element analysis of hydrothermal systems, in Finite Elements in Fluid Flow, J. T. Oden, et al., eds., Univ. Alabama Huntsville Press, pp. 401-414.

Mercer, J. W., G. F. Pinder and I. G. Donaldson, 1975, A Galerkin-finite element analysis of the hydrothermal system at Wairakei, New Zealand, Jour. Geophys. Res., in press.

Narasimhan, T. N. and P. A. Witherspoon, 1975, An integrated finite difference method for analyzing fluid flow in porous media, paper submitted to Water Resour. Res.

Nevens, T. O. and M. J. Pool, 1964, Determination of Thermodynamic Properties of Brines, Denver Research Inst., Contract Research Report 2151.

Nield, D. A., 1968, Onset of thermohaline convection in a porous medium, Water Resour. Res., v. 4, no. 3, pp. 553-560.

Nield, D. A., 1974, Comments on 'Effect of solute dispersion on thermal convection in a porous medium layer' by H. Rubin, Water Resour. Res., v. 10, no. 4, p. 889.

Palm, E., J. E. Weber and O. Kvernvold, 1972, On steady convection in a porous medium, Jour. Fluid Mech., v. 54, part 1, pp. 153-161.

Platzman, G. W., 1965, The spectral dynamics of laminar convection, Jour. Fluid Mech., v. 23, part 3, pp. 481-510.

Poston, S. W., S. C. Yarael, A. K. M. S. Hossain, E. F. Montgomery, III and H. J. Ramey, Jr., 1970, The effect of temperature on irreducible water saturation and relative permeability of unconsolidated sands, Soc. Petrol. Eng. Jour., v. 10, no. 2, pp. 171-180.

Ramey, H. J., Jr., W. E. Brigham, H. K. Chen, P. G. Atkinson and N. Arihara, 1974, Thermodynamic and hydrodynamic properties of hydrothermal systems, in The Utilization of Volcano Energy, J. L. Colp and A. S. Furumoto, eds., Proc. of Converence, Hilo, Hawaii, Feb. 4-8.

Ramey, H. J., Jr., P. Kruger and R. Raghavan, 1973, Explosive stimulation of hydrothermal reservoirs in Geothermal Energy, P. Kruger and C. Otte, eds., Stanford Univ. Press, pp. 231-249.

Rayleigh, Lord, 1916, On convection currents in a horizontal layer of fluid when the higher temperature is on the underside, Phil. Mag., Ser. 6, v. 32, pp. 529-246.

Rubin, H., 1973, Effect of solute dispersion on thermal convection in a porous medium layer, Water Resour. Res., v. 9, no. 4, pp. 968-974.

Rubin, H., 1975a, Effect of solute dispersion on thermal convection in a porous medium layer, 2, Water Resour. Res., v. 11, no. 1, pp. 154-158.

Rubin, H., 1975b, On the analysis of cellular convection in porous media, Unpublished manuscript.

Rubin, H., 1975c, Effect of hydrodynamic dispersion on thermohaline convection in a porous medium, Unpublished manuscript.

Sanyal, S. K., S. S. Marsden and H. J. Ramey, Jr., 1972, The effect of temperature on electrical resistivity of porous media, Soc. Prof. Well Logging Assoc., 13th Annual Logging Symposium, May 1972.

Sestini, G., 1970, Superheating of geothermal steam, Geothermics, Special issue 2, v. 2, pt. 1, pp. 622-648.

Slattery, J. C., 1972, Momentum, Energy and Mass Transfer in Continua, McGraw-Hill, New York.

Somerton, W. H., J. A. Keese and S. L. Chu, 1974, Thermal behavior of unconsolidated oil sands, Soc. Petrol. Engr. Jour., v. 14, no. 5, pp. 513-521.

Sorey, M. L., 1975, Numerical Modeling of Liquid Geothermal Systems, Ph.D. dissertation, Univ. of Calif., Berkeley (in preparation).

Spillette, A. G. and R. L. Nielsen, 1968, Two-dimensional method for predicting hot waterflood recovery behavior, Jour. Petrol. Tech., v. 20, no. 6, pp. 627-638.

Straus, J. M., 1974, Large amplitude convection in porous media, Jour. Fluid Mech., v. 64, part 1, pp. 51-63.

Sun, Z. S., C. Tien and Y. C. Yen, 1972, Onset of convection in a porous medium containing liquid with a density maximum, paper NC2-11, Fourth Intern. Heat Transfer Conf., Paris-Versailles, v. 4.

Toronyi, R. M., 1974, Two-Phase, Two-Dimensional Simulation of a Geothermal Reservoir and the Wellbore System, Ph.D. dissertation, Pennsylvania State Univ., University Park.

Vairogs, J., C. L. Hearn, D. W. Dareing and V. W. Rhoades, 1971, Effect of rock stress on gas production from low-permeability reservoirs, Jour. Petrol. Tech., Sept. 1971, pp. 1161-1167.

Wankat, P. C. and W. R. Schowalter, 1970, Stability of combined heat and mass transfer in a porous medium, Phys. of Fluids, v. 13, no. 9, pp. 2418-2420.

Weber, J. E., 1975a, Thermal convection in a tilted porous layer, Int. Jour. Heat Mass Transfer, v. 18, pp. 474-475.

Weber, J. E., 1975b, The boundary-layer regime for convection in a vertical porous layer, Int. Jour. Heat Mass Transfer, v. 18, pp. 659-573.

Weinbrandt, R. M., H. J. Ramey, Jr. and F. J. Casse, 1972, The effect of temperature on relative and absolute permeability of sandstones, 47th Annual Meeting SPE-AIME, San Antonio, Texas, Oct. 1972.

Weinstein, H. G., J. A. Wheeler and E. G. Woods, 1974, Numerical model for steam stimulation, paper SPE 4759, SPE-AIME Improved Oil Recovery Symposium, Tulsa, Oklahoma, April 22-24.

Weatbrook, D. R., 1969, Stability of convective flow in a porous medium, Phys. of Fluids, v. 12, no. 8, pp. 1547-1551.

Whitaker, S., 1968, Introduction to Fluid Mechanics, Prentice-Hall, Englewood Cliffs, N. J.

Whitaker, S., 1969, Advances in theory of fluid motion in porous media, Ind. Engr. Chem., v. 61, no. 12, pp. 14-28.

White, D. E., 1957, Thermal waters of volcanic origin, Bull. Geol. Soc. Am., v. 68, pp. 1637-1658.

White, D. E., 1961, Preliminary evaluation of geothermal areas, paper G.2, U. N. Conf. on New Sources of Energy, Rome, August 21-31.

White, D. E., 1973, Characteristics of geothermal resources, in Geothermal Energy, P. Kruger and C. Otte, eds., Stanford Univ. Press, pp. 69-94.

White, D. E., L. J. P. Muffler and A. H. Truesdell, 1971, Vapor-dominated hydrothermal systems compared with hot-water systems, Econ. Geol., v. 66, pp. 75-97.

Whiting, R. L. and H. J. Ramey, Jr., 1969, Application of material and energy balances to geothermal steam production, Jour. Petrol. Tech., v. 21, no. 7, pp. 893-900.

Wooding, R. A., 1963, Convection in a saturated porous medium at large Rayleigh number or Péclet number, Jour. Fluid Mech., v. 15, part 4, pp. 527-544.

Yen, Y. C., 1974, Effects of density inversion on free convective heat transfer in porous layer heated from below, Int. Jour. Heat Mass Transfer, v. 17, pp. 1349-1356.

Zoback, M. D. and J. D. Byerlee, 1975, Permeability and effective stress, AAPG Bull., v. 59, no. 1, pp. 154-158.

Heber Cinco Ley

188

# STEAM TRANSPORT IN POROUS MEDIA

A. F. Moench
U. S. Geological Survey
Water Resources Division
345 Middlefield Road
Menlo Park, CA 94025

Numerous investigators have pursued development of large-scale two-phase digital simulation models of vapor-dominated geothermal systems. These represent significant advances in the capability to numerically simulate complex systems. However, the basic physical phenomena which are being modeled are still under investigation. The purpose of this discussion is to present the results of a numerical study in which some of the physical phenomena which may occur in vapor-dominated geothermal reservoirs are examined. These phenomena include: (1) superheating of discharging steam, (2) energy changes due to compressible work, (3) conductive heat transport, and (4) gravitational effects of the steam column. Further details pertaining to this study are available in a report by Moench (1976).

The numerical model used in this study draws upon the concepts of White and others (1971) for a vapor-dominated geothermal system, though of necessity some simplifications have been made. The physical system is idealized as a one-dimensional column of porous or highly fractured rock filled with a mixture of steam and liquid water under high pressure. This reservoir is overlaid by a "cap rock" that has low permeability. At the bottom of the reservoir there is a zone where liquid water saturates the pores. Heat is supplied by a magma chamber at depth and transferred upward through the liquid-saturated zone by conduction and convection. The primary mechanisms for heat transfer through the vapor-dominated zone are vaporization and condensation. Figure 1 illustrates the distributions of temperature and pressure to be expected in this idealized natural system.

The model is designed to determine the time-varying distributions of liquid-water saturation, pressure, and temperature within the vapor-dominated region. These distributions may be due to the withdrawal of steam at either constant pressure or constant discharge. Basic assumptions of the model include the following: (1) liquid water within the vapor zone is stationary, but subject to vaporization, (2) Darcy's law is valid for two fluids, (3) the rock matrix is rigid, (4) local thermal equilibrium occurs between the fluids and rock, (5) negligible viscous dissipation, (6) negligible thermal dispersion, and (7) negligible surface tension effects.

To simulate the vertical flow of steam through variably saturated porous media, two controlling equations are used (see Appendix): a

fluid-flow equation and an energy equation. These equations contain parameters which are dependent upon pressure, temperature, and liquid-water saturation. The energy equation accounts for heat conduction, convection, vaporization, compressible work, and heat storage. These partial differential equations are coupled through the velocity terms, the vaporization terms, the liquid saturation, and the pressure- and temperature-dependent parameters. The equations are solved simultaneously at discrete time intervals by a finite-difference technique.

## Results

Figure 2 shows the pressure, temperature, and liquid-water saturation after $10^9$ sec (31.6 years) of steam production from the top of a one kilometer column of reservoir rock. This represents the effect of removing about 70% of the mass that was initially available. Steam is produced at a rate which declines with time due to withdrawal at constant pressure. All the liquid water in the top 300 m has been vaporized and steam in this region is superheated.

Temperature distributions "A" and "B" in Figure 2 show the influence of heat conduction and compressible work (as defined by the second term on the righthand side of the energy equation). Distribution "A" shows the temperature profile obtained using the complete energy equation. Distribution "B" shows the temperature profile obtained when the compressible work term is omitted from the calculations. It is clear that compressible work is significant only where superheated steam is present. Both profiles show the temperature increase at the top of the reservoir brought about by conduction from the base of the cap rock at a distance of approximately 50 m. Conduction from the cap rock or other nearby rocks not cooled by the vaporization process may be responsible for the temperature increase of produced steam observed in some wells (Sestini, 1970). The time variation in temperature at the top of the reservoir is shown in Figure 3 for curves "A" and "B". In the early part of the production history, the cooling effect of compressible work counteracts the heating due to conduction from the cap rock.

The effect of eliminating gravity from the calculations upon the pressure and temperature distributions is shown by the dashed lines in Figure 2. Apart from its possible influence upon the vertical distribution of liquid water (not included in this study) the effect of gravity can be safely neglected. The weight of the steam column has little, if any, effect upon reservoir production characteristics.

## References

Moench, A.F., 1976, Simulation of steam transport in vapor-dominated geothermal reservoirs, U. S. Geol. Survey open-file report 76-607, 43 p.

Sestini, G., 1970, Superheating of geothermal steam, Geothermics Special Issue, v. 2, pt. 1, p. 622-648.

White, D.E., Muffler, L.J.P., and Truesdell, A.H., 1971, Vapor-dominated hydrothermal systems compared with hot-water systems, Econ. Geology, v. 66, p. 75-97.

## APPENDIX

The basic equations used in this study are reproduced here for convenience. Additional details and constitutive relationships are given in the report by Moench (1976).

Flow Equation

$$\frac{\partial}{\partial z}[\rho_v \frac{k\, k_r}{\mu_v} (\frac{\partial P}{\partial z} - \rho_v g)] + q + q' = \phi(1-S)\rho_v \kappa \frac{\partial P}{\partial t} - \phi(1-S)\rho_v \beta \frac{\partial T}{\partial t} - \phi \rho_v \frac{\partial S}{\partial t}$$

where

| | |
|---|---|
| $\rho_v$ | density of the water vapor |
| $\mu_v$ | dynamic viscosity of the water vapor |
| $k$ | intrinsic permeability |
| $k_r$ | relative permeability to water vapor |
| $g$ | acceleration of gravity |
| $\phi$ | porosity |
| $S$ | liquid-water saturation |
| $P$ | pressure |
| $q$ | source or sink of steam through wells (positive if source of steam) |
| $q'$ | source or sink of steam by vaporization or condensation (positive if source of steam) |
| $z$ | vertical coordinate (positive downward) |
| $t$ | time |
| $\kappa$ | compressibility of water, $\frac{1}{\rho_v} (\frac{\partial \rho_v}{\partial P})_T$ |
| $\beta$ | thermal expansibility of water vapor, $-\frac{1}{\rho_v} (\frac{\partial \rho_v}{\partial T})_P$ |
| $T$ | temperature |

Energy Equation

$$\frac{\partial}{\partial z}\left(K\frac{\partial T}{\partial z}\right)-c_1 v\frac{\partial T}{\partial z}-Lq'+Q=[c_1+c_2+c_3]\frac{\partial T}{\partial t}$$
$$-\phi(1-S)\,T\,\beta\frac{DP}{Dt}$$

where

| | |
|---|---|
| $K$ | effective thermal conductivity |
| $v$ | average interstitial velocity |
| $c_1$ | heat capacity of vapor, $\phi(1-S)\rho_v c_{pv}$ |
| $c_2$ | heat capacity of liquid, $\phi S\rho_\ell c_{p\ell}$ |
| $c_3$ | heat capacity of solid, $(1-\phi)\rho_s c_{ps}$ |
| $\rho_\ell$ | density of liquid water, |
| $\rho_s$ | density of solid rock particles |
| $c_{pv}$ | specific heat at constant pressure of vapor |
| $c_{p\ell}$ | specific heat at constant pessure of liquid |
| $c_{ps}$ | specific heat at constant pressure of solid |
| $L$ | latent heat of vaporization |
| $Q$ | energy source or sink by means other than condensation or vaporization (positive if source of heat) |
| $\frac{D}{Dt}$ | substantial derivative, $\frac{\partial}{\partial t}+v\frac{\partial}{\partial z}$ |

Liquid-Water Saturation Equation

$$\frac{\partial S}{\partial t}=-\frac{q'}{\phi\rho_\ell}$$

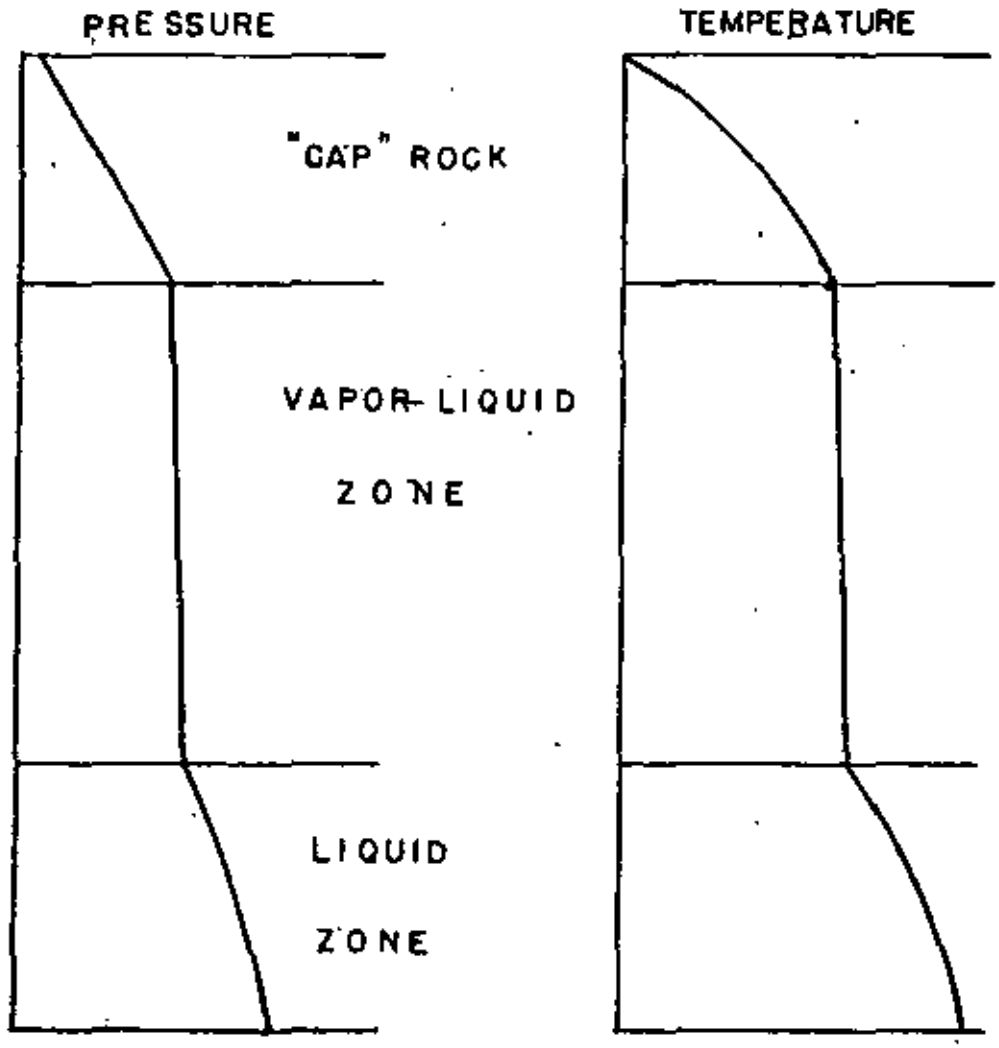


Figure 1. Vertical temperature and pressure distributions in an idealized natural vapor-dominated system.

FIGURE 2. Pressure, temperature and liquid water saturation distributions in a one-kilometer column of reservoir rock which has been producing steam at a pressure of 10 bars for $10^9$ sec. 500 m of cap rock overlie the reservoir. Dashed lines indicate effect of eliminating gravity.

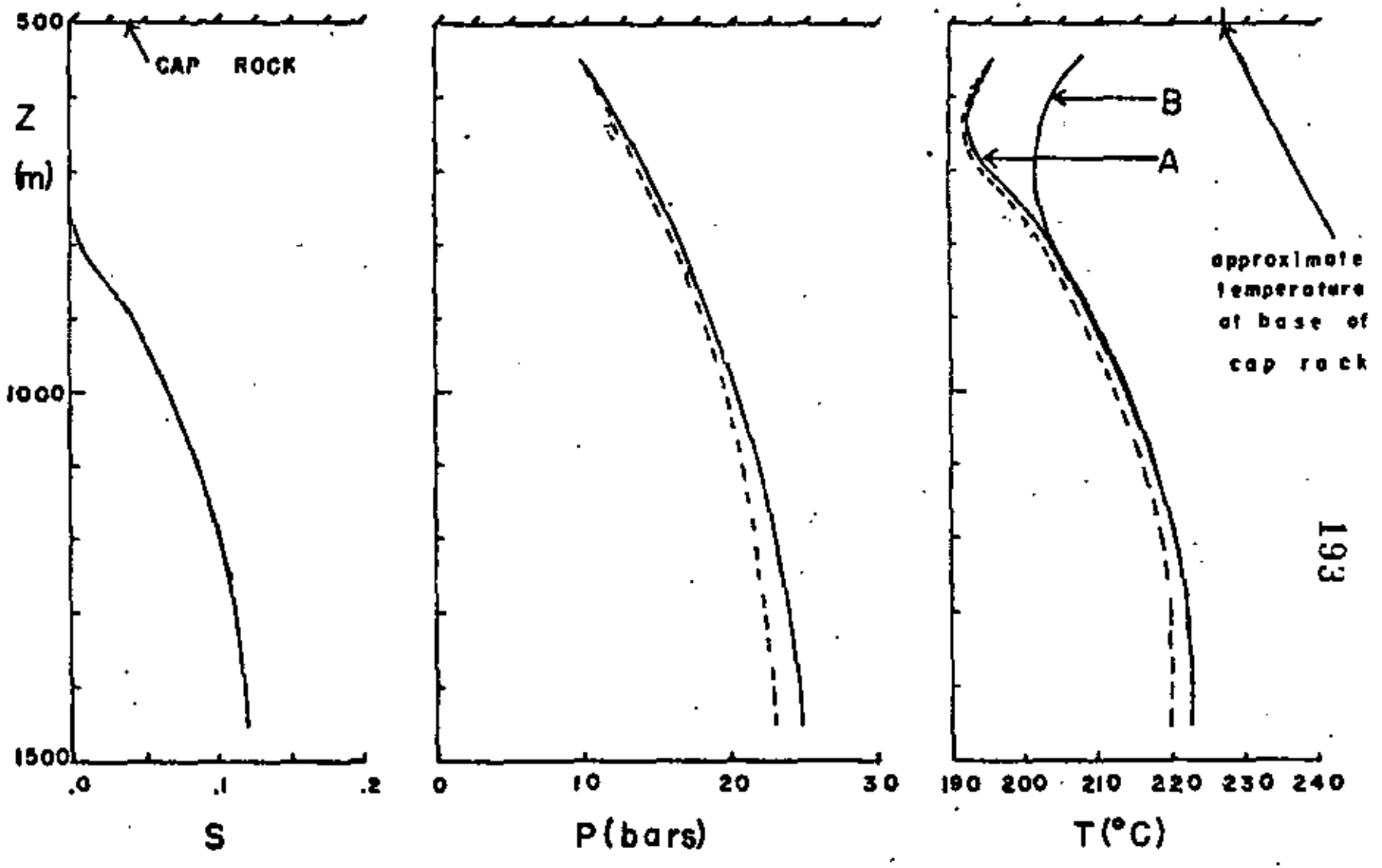


Initial pressure at top = 30 bars
Initial saturation = 0.2
porosity = 0.2
permeability = 10 md

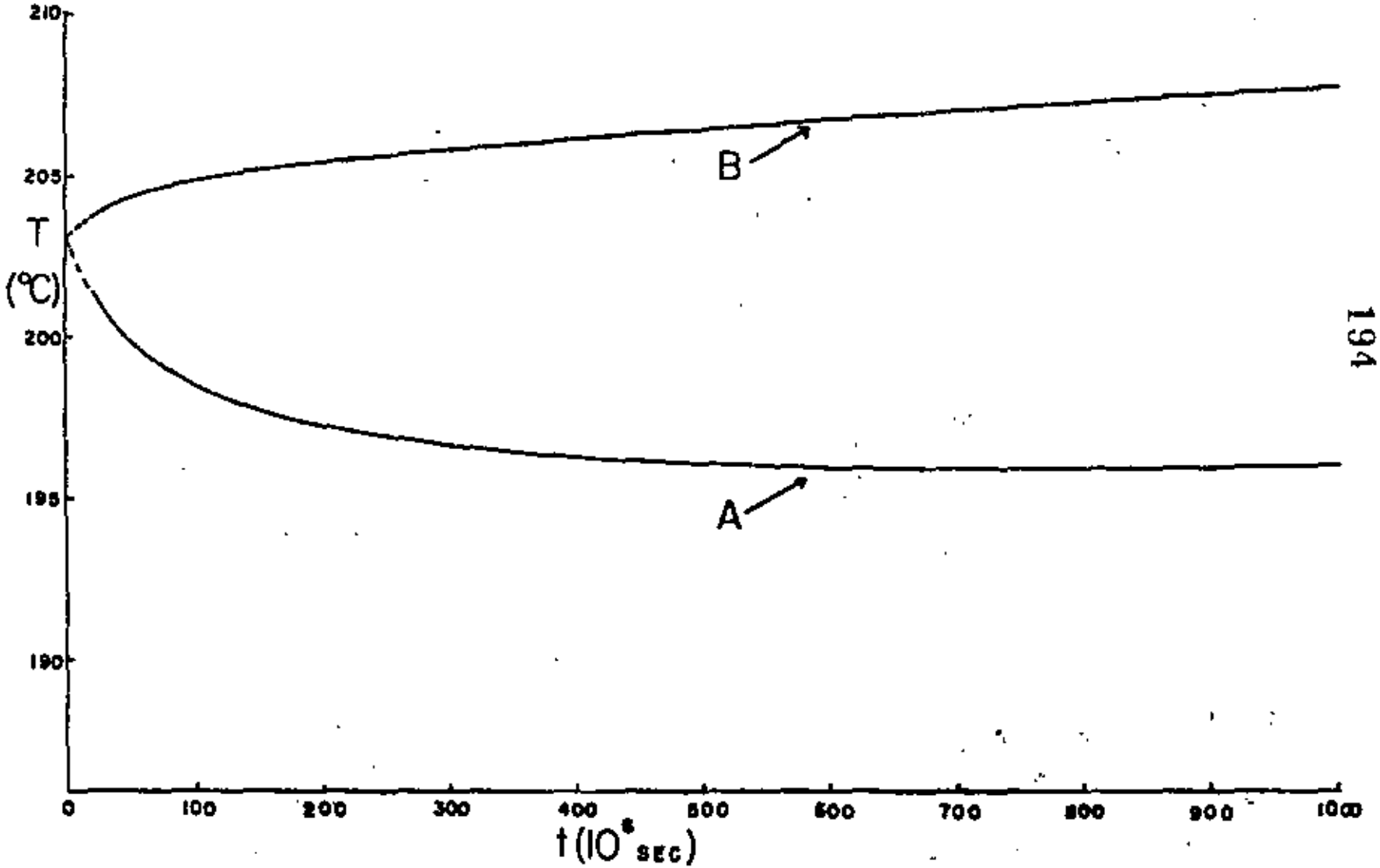


Figure 3. Temperature versus time at top of reservoir for conditions shown in Figure 2.

CURSO: INGENIERIA DE RESERVORIOS GEOTERMICOS.

# FLUJO DE FLUIDOS Y CALOR EN POZOS GEOTERMICOS

PROF. DR. FRANCISCO CORDOVA.

9 de OCTUBRE de 1981.

*Geothermics* (1970) - SPECIAL ISSUE 2

U. N. Symposium on the Development and Utilization of Geothermal Resources, Pisa 1970 Vol. 2, Part 2

VII/6

# Factors Controlling Borehole Performance

R. JAMES *

## ABSTRACT

Geothermal boreholes have been studied to estimate maximum discharges when drawing on (a) a source of pressurized hot water, (b) a source of dry or superheated steam.

The case is initially considered where infinite permeability exists at depth (which is common in areas similar to that at Wairakei, New Zealand) and in which only geometry of the hole controls the flow-rate.

Also investigated was the effect on discharge of increased hole size throughout the depth or over fractions of the depth, with resultant flow increases quantitively established. The relationships derived, enable fall in borefield discharge to be predicted for known decline in temperature and pressure within the reservoir; conversely the actual decline in field discharges can be used to confirm such changes.

For boreholes such as (a) above, the enthalpy may be accurately determined by a method using the maximum running pressure, the wellhead pressure at which imminent collapse of the steam-water mixture occurs, and the bottom hole pressure. A critical discharge pressure tapping located at the pipe outlet face may then measure flow-rates direct over a range of wellhead pressures and hence supply the data required to plot the borehole characteristic curve.

The conditions were also considered where rock permeability controls the flow into the bottom of boreholes either (c) from radial fissures or (d) from permeable-porous media. Because "draw-down" (drop in bottom hole pressure under discharge) is proportional to the square of flow for case (c) and directly as the flow for case (d), it appears that nearly all boreholes operate with discharge supplied from fissures even if these are often very narrow.

## General

Geothermal boreholes can generally be divided into two types: those producing a single-phase discharge such as the dry or superheated steam found in the fields of Larderello and California, and those typified by wells in New Zealand which emit steam-water mixtures, usually, but not always, derived from a deep single-phase all-water source.

Test information required from a borehole includes flow-rate, enthalpy, draw-down (downhole pressure fall under discharge), pressure recovery, downhole temperature variations, quantity and quality of chemicals dissolved in the water phase and of non-condensible gases in the steam phase. These data are necessary not only to evaluate the performance for power potential but are useful for comparison purposes when measurements are taken at timed intervals; this may lead to predictions of the field life under exploitation and to estimates of the volumetric capacity of the reservoir. Non-condensible gases in the steam have an influence on the designed condenser pressure and therefore on the power output, while knowledge of dissolved chemicals can be used to estimate the temperature prevailing in the deep reservoir and also whether deposition of calcite or silica will take place within the borehole or in the source rocks, either of which could be most important for the economics of a scheme.

## Measurement of flow and enthalpy

The measurement of the flow and enthalpy of dry steam bores has presented no difficulty, as conventional means are available which have long been developed in industry (ASME 1959). The density of the steam can be determined from pressure and temperature figures and the flow then metered using a nozzle when discharging to the atmosphere, or an orifice meter if the fluid is being transmitted by pipeline to a power house or process. In the case of bores discharging steam-water mixtures, however, no such equally simple devices were available, and the development of new ones had to be undertaken specifically for two-phase flow.

In the meantime, cumbersome conventional practice, involving calorimeters or phase separators, were the only alternatives which could be used. It was found, however, that the discharge from powerful bores could not be measured using calorimeters in which the whole mixture was condensed to form one phase because the size of the equipment required together with the amounts of cooling water, was prohibitively large. Instead, the mixture was passed into a separator and the discrete phases measured by orifice meters. Although there was no difficulty in measuring the steam phase, the water phase presented some problems as it left the separator at boiling point under the appropriate pressure and it was believed that the intrusion of an orifice plate into the flow would lead to local steam flashing at the plate, hence falsifying the meter readings. To suppress this local boiling, cooling of the hot water pipeline had to be introduced intermediate between the separator and the metering orifice which would reduce the water temperature by about 20-30°C and hence permit single-phase flow through the plate with reasonable accuracy in measurement. Since then; it has been found that the trouble at hot water orifices is due not to local flashing

* D.S.I.R., Taupo, New Zealand.

but to a small percentage of steam being carried over from the separator with the water phase. Even very small quantities of the order of ½% would cause relatively large errors in the estimated flow (at 180 psig this would result in an over-estimation in the water flow by 30%). This occurred even with a level-control tank introduced into the pipeline after the separator, and is due to vortex formation within the exit water pipe; a condition which is rather difficult to eliminate with certainty, as this can take place even when sight gauges on the vessel indicate a high water level, above the water exit point.

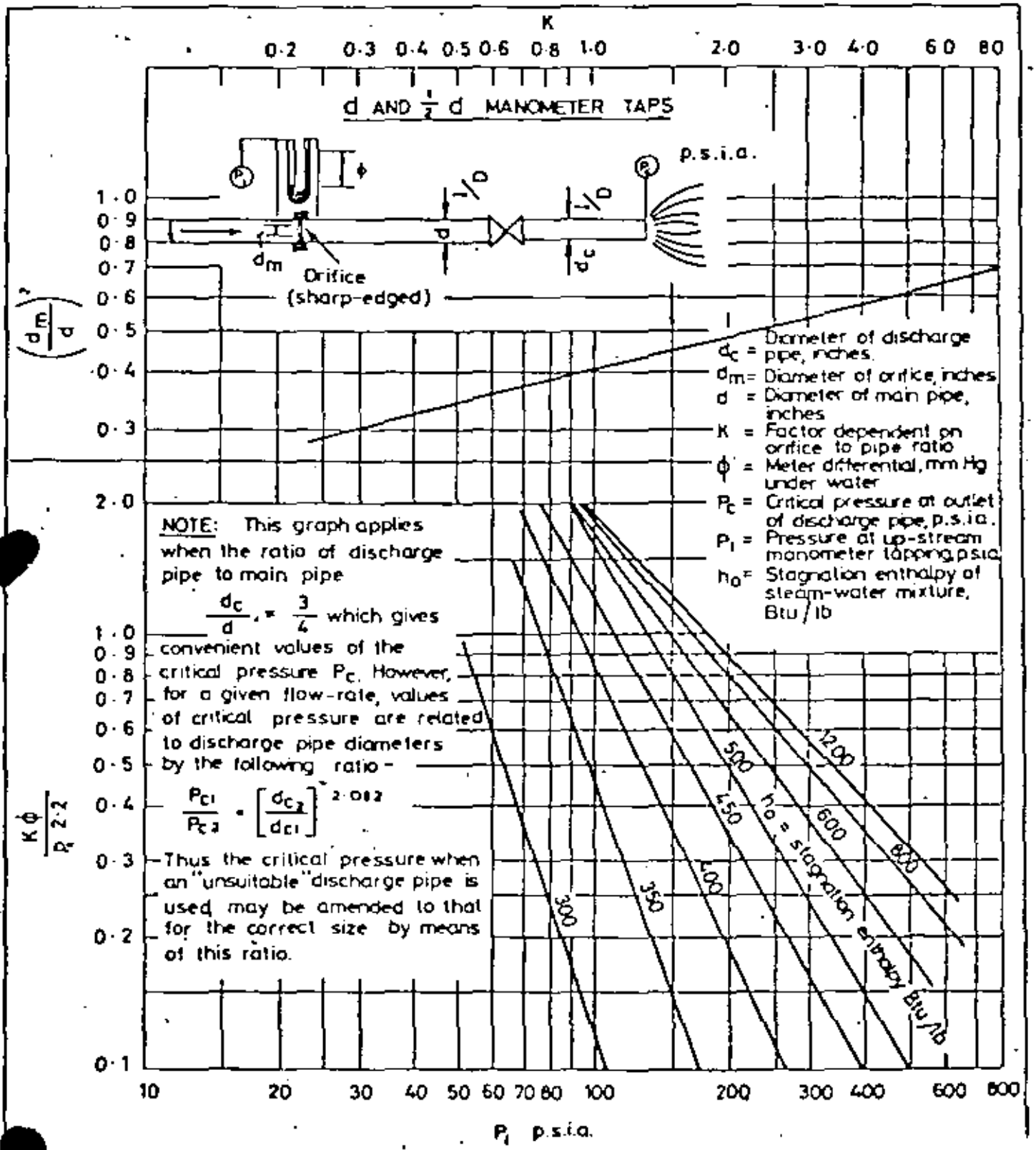


*Fig. 1. — Graph used to evaluate stagnation enthalpy of steam water mixtures.*

Besides these inherent difficulties, the disadvantages using heavy equipment are obvious, especially when it has to be transported to the site of new bores when these are ready for test, or alternatively, full separation, cooling and metering facilities built at each bore.

The technique finally adopted and now in use, avoids the problems mentioned and has the benefit of being applicable without modification to both dry steam as well as steam-water bores. Based upon the fact that when a large flow of a compressible fluid such as steam (or a steam-water mixture) flows along a pipe towards a region of low pressure, in this case, the atmosphere, sonic velocity is attained at the exit and the pressure along the pipe falls to a value at the discharge point which is above atmospheric and which is directly related to the flow-rate and stagnation enthalpy of the flowing fluid. Tests conducted by JAMES (1962) on 3", 6" and 8" diameter commercial pipes, have led to the following empirical equation:

$$\frac{G\, h_o^{1.102}}{P_c^{0.96}} = 11{,}400 \qquad (1)$$

where $G$ = flow in lb/ft² sec: $h_o$ = stagnation enthalpy BTU/lb. $P_c$ = critical discharge pressure, psia.

This equation applies where the critical discharge pressure is taken from a 1/4" hole drilled at a centreline distance of 1/4" from the discharge outlet face of the pipe.

This formula was found immediately applicable for measuring the flow of hot water at known enthalpy rejected from the separators of Wairakei production bores, but could not on its own be used to measure the discharge from new bores not having a separation plant. However, when used in conjunction with an orifice meter, it was found (JAMES 1965) to be capable of solving for both flow and enthalpy for bores discharging horizontally to the atmosphere. A graphical solution for enthalpy is shown in Figure1; equation (1) may then be used to calculate the flow.

Blowing a bore horizontally to the atmosphere is not altogether suitable, however, because of its adverse effect on vegetation (chemical coating of leaves leads to loss in transpiration followed by death), hence most New Zealand bores now have permanent concrete silencers designed in the form of twin vertical towers as shown in Figure 2. These not only silence the noise and save the vegetation but also separate the mixture at atmospheric pressure and allow the water to be measured by a conventional weir situated in the silencer outlet. Coupled with a critical discharge pressure, it can be used (JAMES 1966) to determine both the enthalpy and flow as in the arrangement employing an orifice meter, but is simpler and more convenient than the latter system. The curve of Figure 2 is used to evaluate the enthalpy which is then inserted in the equation for total flow (also on Figure 2). Of course, if the bore is

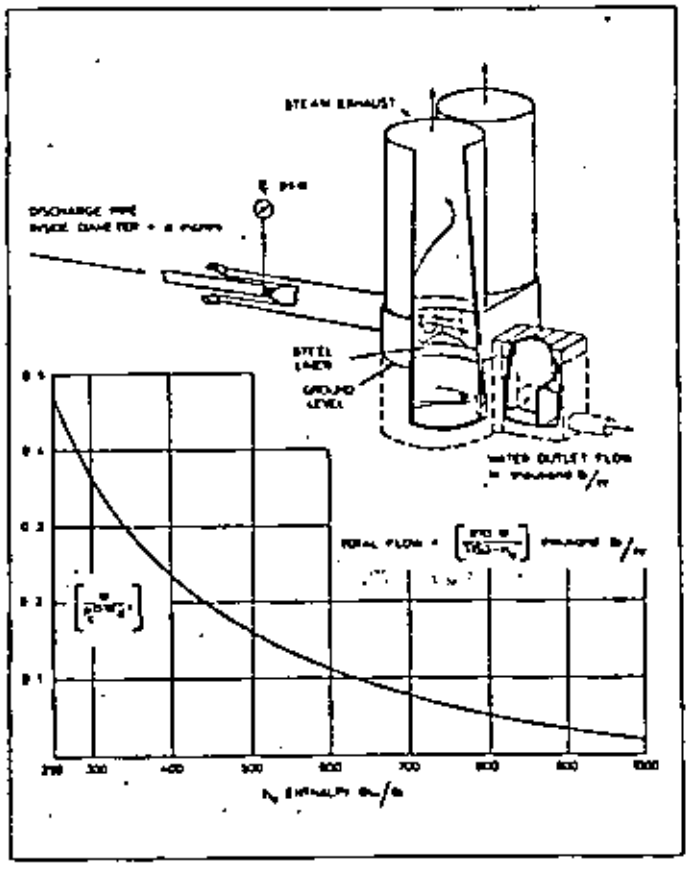


FIG. 2. — *Enthalpy and flow from critical discharge pressure and weir readings.*

dry, neither an orifice meter nor a weir box measurement would be necessary as the critical discharge pressure alone would suffice so long as a thermometer is used at the wellhead to ascertain the steam temperature (and hence, the enthalpy) in case it is superheated.

As the critical discharge pressure is fundamental to these devices, a correction has to be introduced when employed on bores having a high gas content (up to about 0.20 by weight). To correct $P_c$ in Figures 1 and 2, the gauge reading is first amended to absolute pressure, psia, and then multiplied by $(1 + \frac{y}{3.2})$ where y is the $CO_2$ content in lb gas/lb steam, as determined by analysis of an extracted sample.

Another method of finding the enthalpy of steam-water bores is to use the « gas method » as described by MAHON (1966), which relies upon the ratio in gas concentrations of two steam samples each taken at widely different pressures on either side of a throttle on the discharge pipe. This method is fairly reliable on bores with high gas content when the tapping points are selected with care. It can be used in association with the critical discharge pressure $P_c$ and here it may be preferable to sample at the wellhead at pressure $P_w$ and at the location of $P_c$ as these give a maximum difference in pressure and hence greater accuracy. If steam-water samples are taken at these positions and the gas

content analysed, then the following relationships are found to hold:

$$\frac{m_w}{m_c} = \frac{x_c}{x_w} \tag{2}$$

$$h_w = (w_w + x_w L_w) = (w_c + x_c L_c) + \left(\frac{G}{224}\right)^2 (V_c^2 - V_w^2) \tag{3}$$

where:

$m$ = gas concentration, lb gas/lb steam
$x$ = steam dryness fraction, lb steam/lb mixture
$w$ = sensible heat of water, BTU/lb
$L$ = latent heat of steam, BTU/lb
$V$ = specific volume of steam-water mixture, homogeneous, ft³/lb, suffices: w and c at wellhead and critical pressure tapping respectively.

By using equations (1), (2) and (3), the stagnation enthalpy $h_w$ and flow $G$ may be determined. As a first trial, it is necessary to neglect the kinetic energy term $\left(\frac{G}{224}\right)^2 (V_c^2 - V_w^2)$ to gain an approximate figure for the $h_w$.

When taking a steam sample at the wellhead, a water sample should also be retained for analysis of the dissolved chemical. It will be found difficult to do this at the critical discharge pressure tapping because the velocity is very high (Mach 1) which results in stripping of the water from the pipe wall leading to steam dilution of the water sample. The gas method when used correctly should give not only enthalpy and flow but also chemical and gas analyses of the bore fluids. As these data are often required at the same time (to avoid transients in enthalpies), this technique has potential advantages which have been marred somewhat by difficulties in obtaining consistent test results under apparently constant conditions.

### Enthalpy determined by maximum discharge pressure

When the discharge from a borehole is being progressively reduced by throttling of the wellhead valve, the wellhead pressure rises until any further closure of the valve results in the collapse of the suspended steam-water mixture over the vertical extent of the bore: at this point the wellhead pressure passes through a maximum. This is known as the maximum discharge pressure (MDP) and occurs when the pressure difference between the bottom and the top of the borehole just balances the weight of the column of mixture. If the MDP is fairly sharply defined and is reproducible, with a swift recovery (order of a day), then its value may be used to estimate the bore enthalpy. For many wells which tap an all-water source, the enthalpy remains constant throughout the range of discharge as indicated in Figure 3 which shows the characteristic

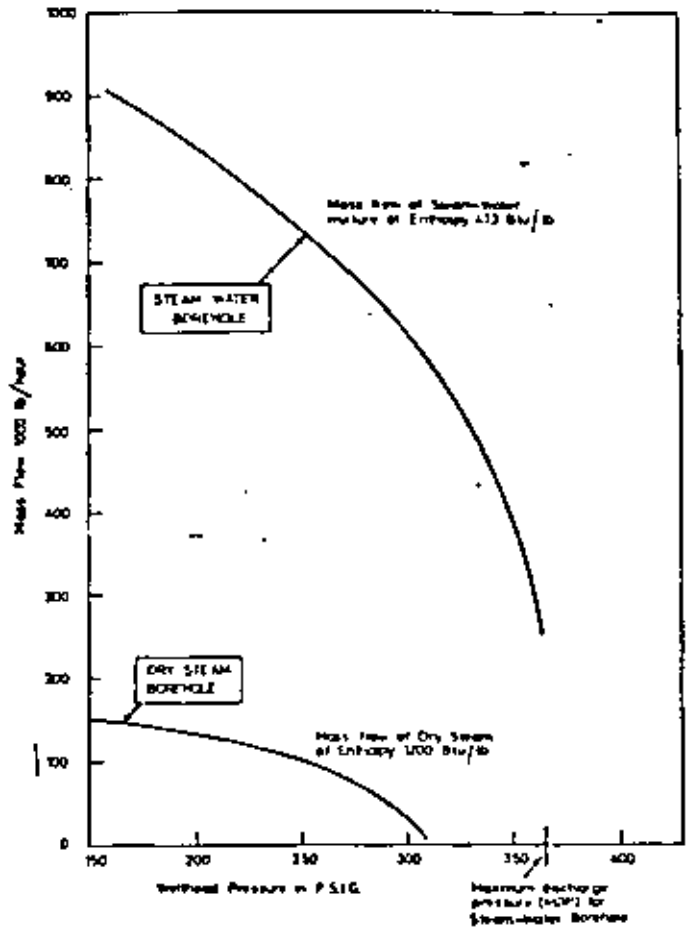


FIG. 3. — *Comparative discharges from specimen 8" boreholes.*

curve of such a hole (together with that of a dry steam hole). Hence, once the enthalpy is known, discharge at various wellhead pressures may be estimated by noting the appropriate values of $P_c$ and using equation (1).

In order to find the enthalpy, it is necessary to close the bore and to measure the stagnation pressure $P_w$ at depth $L$ near the hole bottom, below the water surface (this is usually accomplished by lowering a recording instrument on a long wire through a sealing gland at the wellhead). The bore can now be discharged and the MDP noted; at this point the flow is assumed to be zero (this is discussed later) which eliminates frictional pressure-drops from the calculations. Figure 4 shows the conditions prevailing within the borehole under MDP with only water existing over a distance $L_1$. At the flash point, the pressure would be the saturated steam pressure $P_s$ which is associated with the bore stagnation enthalpy $h_w$; for example, at enthalpy of 467.4 BTU/lb, $P_s = 580$ psia from the steam tables of KEENAN, KEYS, HILL, MOORE (1969). It is seen that the only data required are $P_w$ at depth $L$ and the wellhead pressure $P_c$ at MDP in order to calculate the bore enthalpy, as will be shown.

Over the length $L_1$ only water exists and under essentially static conditions the pressure difference be-

tween the ends of the column are due to the weight f the fluid alone, hence

$$P_b - P_s = \frac{L_1}{144\ V_w} \qquad (4)$$

here $V_w$ is the specific volume of water at enthalpy $h_w$. Similarly, over the length $L_2$ only a steam-water mixture exists, and

$$P_s - P_w = \frac{L_2}{144\ V_{sw}} \qquad (5)$$

here $V_{sw}$ is the unknown specific volume of the mixture at enthalpy $h_w$ and average pressure (over length $L_2$) of $\frac{P_s + P_w}{2}$. As $L_1 + L_2 = L$, which is known, equation (4) and (5) may be used to derive:

$$V_{sw} = \frac{L - 144\ V_w(P_b - P_s)}{144\ (P_s - P_w)} \qquad (6)$$

To determine the enthalpy, a trial calculation is employed using equation (6). The procedure is to assume n enthalpy $h_w$ and from the steam tables take the associated saturated steam pressure, $P_s$ and water specific volume, $V_w$. Using these values, $V_{sw}$ can be estimated and if the assumed enthalpy was the correct one, should agree with the steam-water specific volume calculated at average pressure $\frac{P_s + P_w}{2}$ and at the assumed enthalpy. (To simplify this latter calculation, Figure 5 may be used which correlates $V_{sw}$ at various average ressures and over a range of enthalpies). If these two alues of $V_{sw}$ do not agree, then a new figure for enthalpy has to be chosen and the calculation repeated. This is continued until agreement is reached.

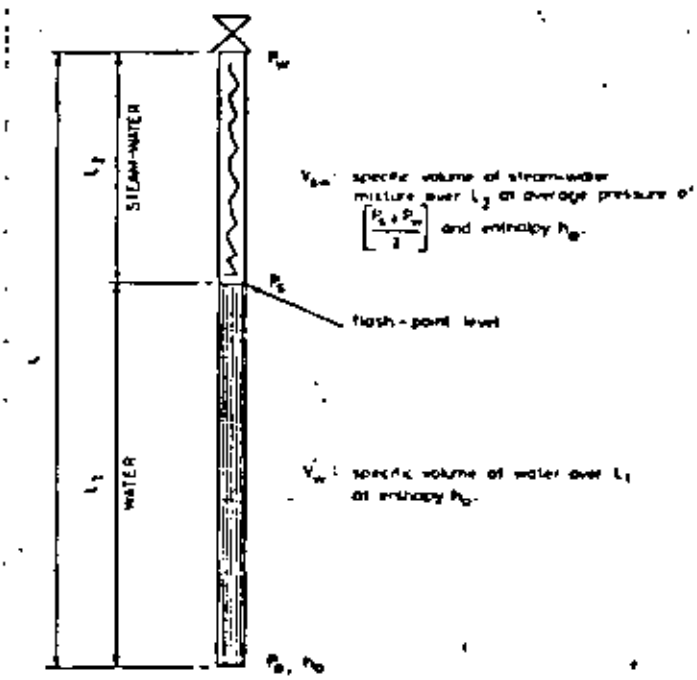


IG. 4. — *Borehole at brink of collapse: discharging with maximum wellhead pressure.*

Actual test results indicate that MDP does not strictly occur at zero flow, flows of 200,000 lb/h in 8 inch pipe have been usually registered, but correcting the above method by the introduction of frictional pressure-drops due to such flows only raises the calculated enthalpies by as little as 1 BTU/lb and can therefore be considered as negligible.

### Downhole temperatures

— When drilling a borehole, water (from the drilling mud used) can spread outwards into fissures or into porous-permeable media and hence reduce the surrounding rock temperatures below their original values. In fact, the very act of drilling alters the whole thermal pattern in the neighbourhood of the hole.

— The hole may intercept different permeable horizons with different fluid temperatures and when the hole is closed, the cooler and denser fluid at the higher horizon will flow down the hole in the uncased region and outwards at the lower temperature horizon. This results in complete distortion of the true thermal situation in the ground which existed prior to drilling and which probably still exists at some distance from the hole. This flow within a closed-in bore may attain quite high values (a few gallons/minute) so that on being closed for a time of say 6 months, can result in an enormous quantity of cooler water flooding into warmer regions. Days or even weeks of discharge may be required to eject this fluid, and to heat up the surroundings to a more truly representative condition.

One method of dealing with this situation is to blow the bore for a while, then close it and lower an electric resistance thermometer (or similar instrument) to the bottom. The hole is then filled with drilling mud, thick enough to inhibit convection between horizons within the closed-in bore, but not thick enough to be baked hard at the temperatures estimated to exist in the ground, otherwise it will be difficult, if not impossible, to withdraw the instrument.

It is clear that it is not easy without taking considerable care to obtain reliable temperatures particularly in steam-water holes; hence the difficulty in obtaining an enthalpy which matches that of the discharging bore even when it is drawing from an apparently all-water source surrounding the uncased lower portion of the hole.

### Maximum flow from boreholes

The maximum discharge from a borehole takes place when the well is flowing vertically, without restriction at the wellhead or at the well bottom, in other words, the flow is dependent only on the bore geometry, such as length and diameter, and not upon limitations imposed by the impermeability of the rock in the uncased hole, or to the tightness of fissures supplying

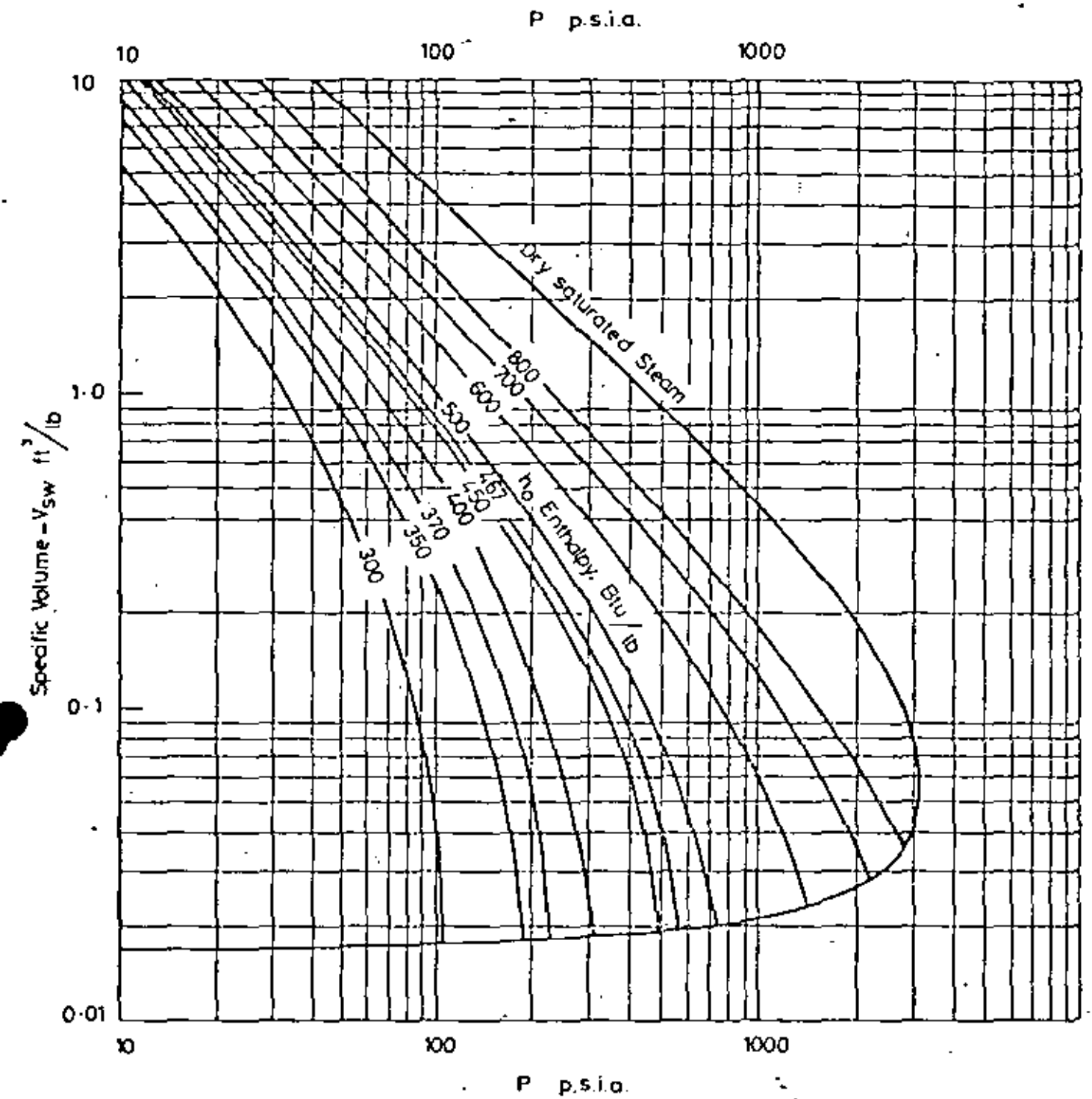


FIG. 5. — *Specific volume of homogeneous steam-water mixture.*

the flow. (These effects will be discussed later). If the pressure and enthalpy are taken below the water surface, at a measured depth near the bottom of a closed borehole it is possible to estimate the maximum possible flow which the well can discharge. Also, the ef- on maximum discharge due to falling bottom hole peratures or pressures can be evaluated and trends predicted.

### MAXIMUM FLOW FROM DRY STEAM BORES

To estimate the maximum flow possible from a free flowing vertical bore which taps a source of dry or superheated steam, the curve of Figure 6 gives the best solution. This is derived from the theoretical study of LAPLE (1943) and its applicability for dry steam was experimentally confirmed over a large range of pipe diameters and lengths by JAMES (1964). With the pres-

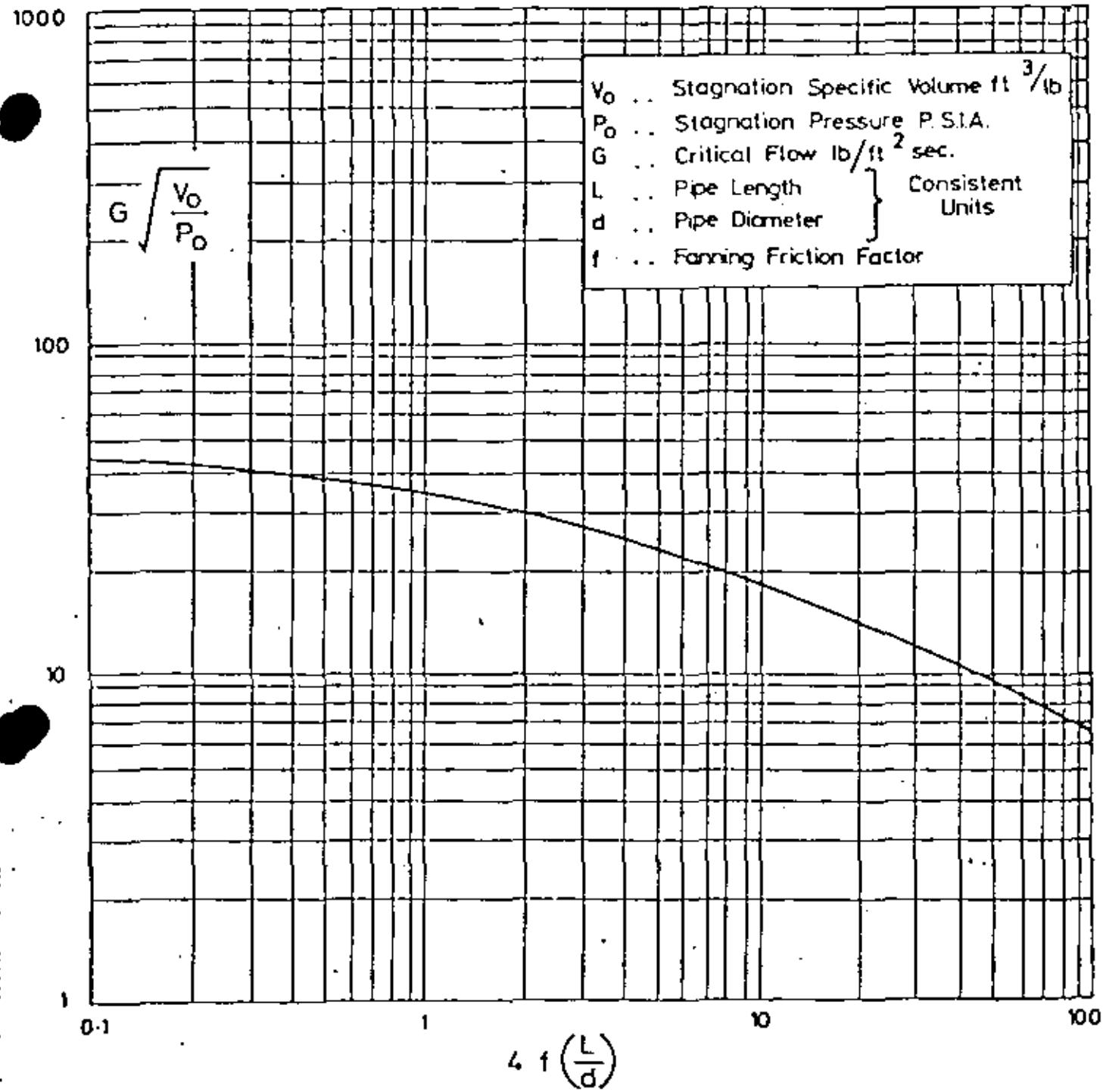


FIG. 6. — *Single-phase, critical flow, capacity curve.*

sure $P_o$ and temperature measured at depth $L$ in a closed bore, the stagnation specific volume $V_o$ is derived from steam tables. The Fanning friction factor $f$ is taken initially at 0.003 for a first trial, in order to estimate $4\,f\frac{L}{d}$ which is used in the figure to evaluate $G\sqrt{\frac{V_o}{P_o}}$ and hence $G$. The flow-rate $G$ is then used to correct the value of friction factor assumed, by first evaluating the Reynold's number

$$R_e = \frac{124\ G\,d}{\mu} \tag{7}$$

where $d$ is in inches and $\mu$ is the viscosity of dry steam in centipoise taken from Figure 7b. The friction factor can now be calculated from an equation derived from the Moody chart as given by PERRY (1963)

$$f = \frac{0.0344}{R_e^{0.184}} \tag{8}$$

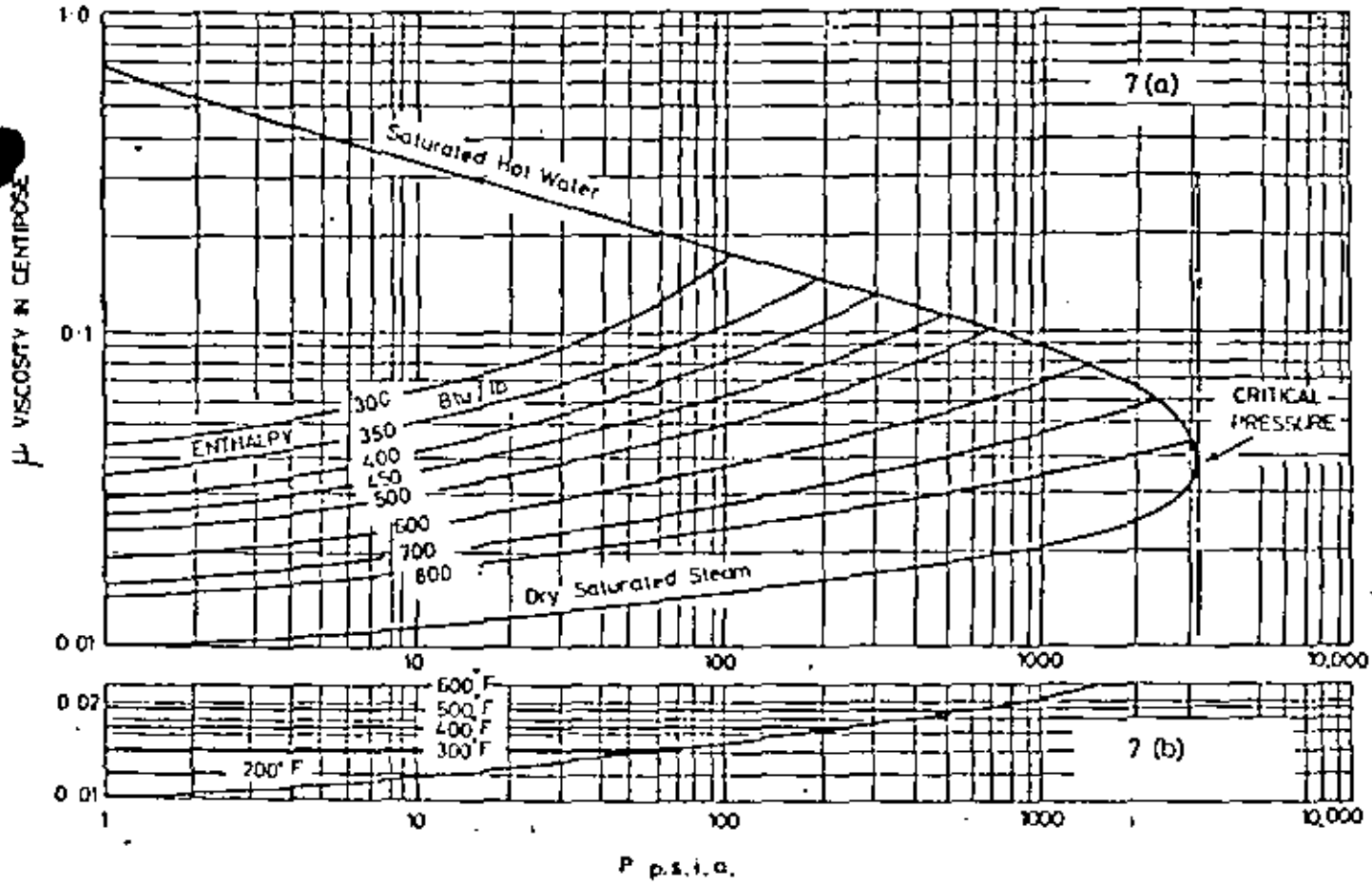


FIG. 7 (a, b). — a) *Viscosity of steam-water mixtures.* b) *Viscosity of superheated steam.*

which applies to commercial steel pipe. Only the one trial is required. The value of $G$ so determined can be compared with that on a vertically discharging dry steam bore by attaching a critical discharge tapping at the pipe outlet face and measuring the actual critical discharge pressure $P_c$ which is related to $G$ by equation (1). If the measured flow is significantly less than that calculated from Figure 6, then draw-down will be taking place at the bottom of the hole where the pressure will be falling below the reservoir value of $P_o$. This assumes, of course, that bottom pressure recovery occurs on closing the bore and that the fall in pressure is not due to gross depletion within the reservoir, but is caused only by the restrictive effect of the surrounding media. As this can be checked by downhole measurements of pressure recovery, there is no difficulty in differentiating between these two conditions.

## MAXIMUM FLOW FROM STEAM-WATER BORES

This is a more difficult problem than for dry steam, particularly where two flow regimes operate within a borehole, namely all-water vertical flow over the lower portion of the hole followed by steam-water two-phase flow over the higher fraction. As this case is quite common in fields tapping hot water aquifers, the following method is very useful in that, not only can it be used to estimate the maximum possible flow for known downhole conditions, but fall-off in field discharge can be related to changes in the aquifer. Alternatively, changes in the maximum discharge can be used to estimate pressure and temperature changes in the aquifer or to confirm instrument measurements of bottom hole conditions.

Figure 8 is a diagrammatic sketch of a borehole of length $L$ ft discharging without restriction vertically from a source at the bottom of the hole of pressure $P_o$ and enthalpy $h_o$ which are considered as unvarying stagnation conditions supplied by an infinitely permeable reservoir. This is usual at Wairakei and elsewhere where it is found that continuous measurements of the bottom hole pressure indicate no significant fall over the range of flows that it is possible to test with an instrument in position.

Over the lower length $L_1$ the flow is of water and it is only when this has risen to a level where the pressure has declined to the saturated pressure $P_s$ that steam can exist. This is known as the flash point and above this point the flow is of a steam-water mixture with increasing steam fraction as the fluid rises to higher

levels at lower pressures. The mixture velocity increases along the pipe until it discharges at the exit with sonic velocity and at a critical discharge pressure $P_c$ just within the outlet face.

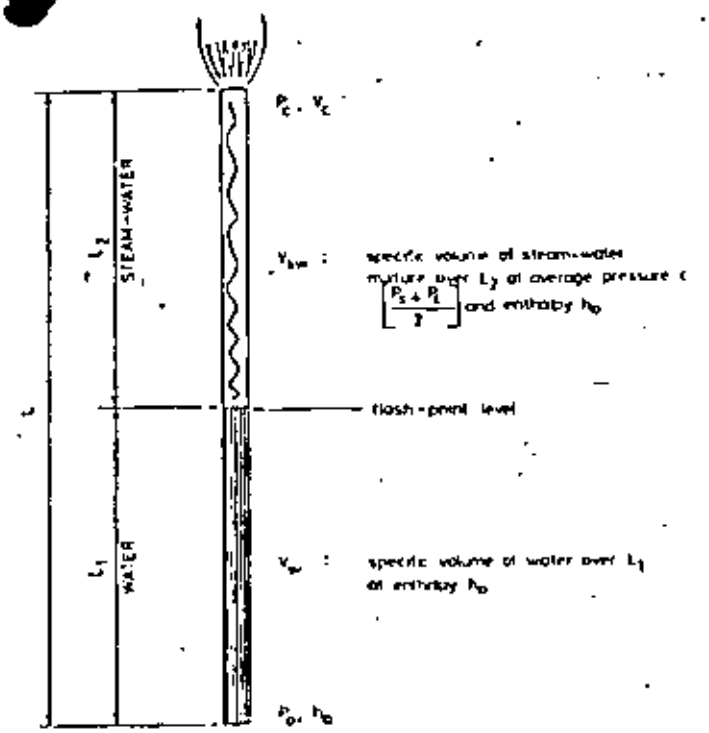


FIG. 8. — *Borehole with unrestricted discharge to the atmosphere: infinite permeability at the bottom.*

### Water flow of length $L_1$

For vertical flow, the pressure-drop $(P_s - P_o)$ equals the sum of the hydrostatic pressure-drop, the frictional pressure-drop and the pressure-drop due to the increase in kinetic energy within the pipe. The hydrostatic pressure-drop is $\frac{L_1}{144\,V_w}$ psi where $V_w$ is the specific volume of the water. The frictional pressure-drop can be transposed from the Fanning equation to the following more convenient form $\left(\frac{G}{13.92}\right)^2 \frac{f_w L_1 V_w}{d}$ where $f_w$ is the Fanning friction factor, $G$ the flow, lb/ft² sec, and $d$ the pipe diameter, inches. The pressure-drop due to the kinetic energy increase at the pipe entrance, is transposed to the form $\left(\frac{G}{96.2}\right)^2 V_w$. The overall pressure-drop equation can now be given as:

$$P_s - P_o = \frac{L_1}{144\,V_w} + \left(\frac{G}{13.92}\right)^2 \frac{f_w L_1 V_w}{d} + \left(\frac{G}{96.2}\right)^2 V_w$$

$$L_1 = \frac{(P_s - P_o) - \left(\frac{G}{96.2}\right)^2 V_w}{\left(\frac{G}{13.92}\right)^2 \frac{f_w V_w}{d} + \frac{1}{144\,V_w}} \qquad (9)$$

The kinetic energy term $\left(\frac{G}{96.2}\right)^2 V_w$ is only of the order of 1 psi so may be ignored, while the Fanning friction factor is found to be close to 0.003 for boreholes at high flows and may be safely taken at this figure (the value of $L_1$ calculated in equation (9) is not sensitive to its value).

### Steam-water flow over length $L_2$

As in the above case of single-phase flow, the overall pressure-drop $P_s - P_c$ equals the sum of the hydrostatic, frictional and kinetic energy pressure drops. The hydrostatic pressure-drop is $\frac{L_2}{144\,V_{sw}}$ where $V_{sw}$ is the homogeneous steam-water specific volume taken at the average pressure of $\frac{P_s + P_c}{2}$ over the flashing length $L_2$ and at enthalpy $h_o$. The frictional pressure-drop is $\left(\frac{G}{13.92}\right)^2 \frac{f_{sw} L_2 V_{sw}}{d}$ where $f_{sw}$ is the Fanning friction factor for homogeneous steam-water mixtures. The pressure equivalent of the change in kinetic energy between $P_s$ and $P_c$ is $\left(\frac{G}{96.2}\right)^2 (V_c - V_w)$ where $V_c$ is the homogeneous specific volume of steam-water mixtures at pressure $P_c$ and enthalpy $h_o$. $L_2$ may now be given as for equation (9):

$$L_2 = \frac{(P_s - P_c) - \left(\frac{G}{96.2}\right)^2 (V_c - V_w)}{\left(\frac{G}{13.92}\right)^2 \frac{f_{sw} V_{sw}}{d} + \frac{1}{144\,V_{sw}}} \qquad (10)$$

The value of $f_{sw}$ is found to be close to 0.003 as for the single-phase portion of the hole and will be initially assumed at this figure. It may be checked finally by calculation from equations (7) and (8) where the two-phase viscosity $\mu_{sw}$ is used in the former equation and taken from Figure 7a at enthalpy $h_o$ and average pressure $\frac{P_s + P_c}{2}$. These plotted values of two-phase viscosity are based on the following equation for homogeneous conditions:

$$\frac{1}{\mu_{sw}} = \frac{x}{\mu_s} + \frac{(1 - x)}{\mu_w} \qquad (11)$$

where $\mu_s$ and $\mu_w$ are the single-phase viscosities of steam and water taken from ASME (1959), $x$ is the steam dryness fraction (weight basis) at enthalpy $h_o$ and pressure $\frac{P_s + P_c}{2}$. It will be noted that $L_1 + L_2 = L$ (the bore depth, which is known); hence from equations (9) and

(10) and ignoring the negligible kinetic energy term in the former:

$$\frac{P_o - P_s}{\left(\frac{G}{13.92}\right)^2 \frac{0.003\,V_w}{d} + \frac{1}{144\,V_w}} + \frac{(P_s - P_c) - \left(\frac{G}{96.2}\right)^2 (V_c - V_w)}{\left(\frac{G}{13.92}\right)^2 \frac{0.003\,V_{ww}}{d} + \frac{1}{144\,V_{ww}}} = L \qquad (12)$$

To solve this equation for maximum flow, we require to know the pipe diameter $d$, the stagnation pressure $P_o$ at known depth, and the stagnation enthalpy $h_o$. The pressure can be obtained down a closed bore by lowering an instrument through a wellhead sealing gland with depth $L$ measured from the casing head flange. The enthalpy can be determined by one of the methods already described. With this information, steam tables give $P_s$ and $V_w$ leaving unknown $G$, $P_c$, and $V_c$. The procedure is to first assume a figure for $P_c$ which permits $G$ to be calculated from equation (1). From Figure 5, $V_{ww}$ and $V_c$ are identified at enthalpy $h_o$ and pressures $\frac{P_s + P_c}{2}$ and $P_c$ respectively. With these values inserted in equation (12), $L$ may be obtained and should be equal to the actual depth taken when measuring $P_o$. If agreement is not met, then a new value of $P_c$ must be tried and the calculation repeated until equality is attained. Although equation (12) looks formidable, it can be solved in about 30 minutes using a slide rule.

It will be noted that these calculations depend on the assumption of homogeneous steam-water flow in the flashing length of pipe and this, in fact, gives good agreement with test results for maximum vertical flow through boreholes. It has not been found necessary to take into account the concept of 'slip' (differential velocity between the phases) postulated by some workers operating with two-phase mixtures flowing horizontally in small diameter pipes, hence the method adopted here is less complicated than it was at one time thought likely to be. In order to study the effect of bottom hole pressures and temperatures on the discharge from bores tapping a source of pressurised hot water under conditions of maximum flow, the dimensions of a typical Wairakei bore are taken as an example. With an internal diameter of 7.825 inches and a depth from the casing head flange of 2200 ft, bottom hole temperatures are taken as 220, 240 and 260°C with bottom hole pressures either at the saturated point or pressurised to an amount $\Delta P$ above this, with values of 0, 200, 400 and 600 psi (the value of $\Delta P = 0$ psi coincides with the ordinate through $L_1 = 0$, where $L_1$ is the single phase length as given on Figure 8). Using these data, the critical discharge pressure has been calculated for conditions of maximum flow and the results plotted on the chart of Figure 9. As an example of the use of this chart, suppose the temperature and the pressure measured at depth of 2200 ft is found to be 240°C and 885 psi, then the steam tables give a water enthalpy of 446 BTU/lb and a saturated steam pressure of 485 psia, hence the amount of pressurisation, $\Delta P$, is 400 psi. From the chart, $P_c = 75$ psia and the flow may be determined from equation (1) to be $G = 855$ lb/ft²sec and through a pipe of 7.825 inches diameter, flow = $= 1.02\ (10)^6$ lb/h. Suppose that after a number of years, this hypothetical bore has been found to decline in bottom hole temperature and pressure to 220°C and 536 psia, with associated water enthalpy of 405.4 BTU/lb and saturated steam pressure of 336 psia, then $\Delta P = 200$ psi and from the chart, $P_c = 43$ psia. From equation (1), the new value of $G = 562$ lb/ft²sec and the maximum discharge has declined to $0.675\ (10)^6$ lb/h. It is clear, therefore, that the chart may be used to predict the effect on discharge of various combinations of bottom hole temperature and pressure; this is particularly important where measurements indicate decline in these factors as it permits future estimates of discharge in time to consider remedial action.

Figure 9 is suitable for geothermal fields which are of the pressurised hot water type so long as the average pipe size does not vary from the Wairakei average of 7.825 inches internal diameter by more than about ± 0.2 inches, in determining the value of $P_c$. And, of course, the measurements of temperature and pressure should be taken at the same depth of 2200 ft outside the cased portion of the hole (i.e. within the region of slotted casing); this is to make sure that the values truly represent reservoir conditions at this level.

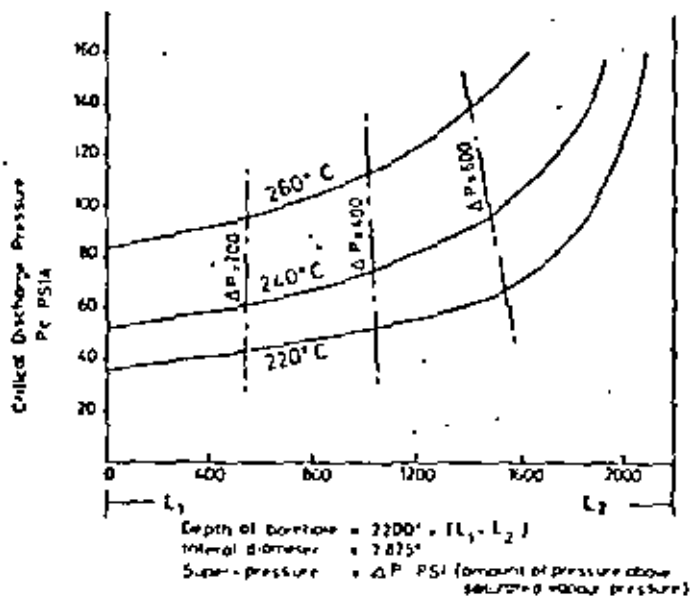


FIG. 9. — *Discharge of borehole related to reservoir temperature and super - pressure.*

Figure 9 indicates the primary importance of water temperature, rather than the amount of pressurisation, on the flow of energy from boreholes. This is reflected in the higher values of critical discharge pressure $P_c$ which from equation (1) is seen to be roughly proportional to $(Gh_w)$ which has units of BTU/ft²sec. The depth of the flash-point from the wellhead (as shown in Figure 8) may also be obtained from the chart where $L_2 = 2200 - L_1$. In the numerical example given, the depth of the flash-point has increased from $L_2 = 1170$ to $L_2 = 1670$ ft during the period while the temperature and pressure at the hole bottom declined.

### Influence of diminishing well casing diameter with depth

Where bores tap a source of dry steam at a horizon of infinite permeability, the hole diameter and length alone limit the flow. For a fixed wellhead pressure and fixed source pressure, the flow is proportional to $d^{2.42}$ when the effect on the friction factor of average steam velocity and pipe diameter is taken into account. Obviously, therefore, in these circumstances it is economically preferable to have as large a pipe diameter as is possible over the whole length of the hole down to the permeable horizon.

In the case of a bore tapping a source of pressurised hot water at a horizon of infinite permeability (as occurs in the Wairakei field), it is of interest to see if the same relationship is obtained or whether it would be preferable to have a large diameter hole over the flashing portion of the hole ($L_2$ of Figure 8) and a rather smaller diameter hole over the portion $L_1$ where only single phase all-water flow takes place. It was found possible to solve this problem using equation (12) by increasing the borehole internal diameter over the whole length $(L_1 + L_2)$ and also by increasing the diameter only over the flashing length $L_2$.

It was found that increasing the diameter from $d_1$ to $d_2$ over the whole pipe length resulted in an increase in the flow according to the relationship:

$$\frac{W_2}{W_1} = \left[\frac{d_2}{d_1}\right]^{2.36} \qquad (13)$$

whereas increasing the diameter over the flashing length to $d_2$ while the diameter of the single phase portion $L_1$ remains at $d_1$ results in the following relationship between $W_{12}$ (the flow through the two-diameter arrangement) and $W_1$ (the flow through the single-diameter arrangement):

$$\frac{W_{12}}{W_1} = \left[\frac{d_2}{d_1}\right]^{1.36} \qquad (14)$$

It is clear that it is preferable to increase the well diameter over the whole of the depth down to the permeable horizon rather that to estimate the length to the flash point $L_2$ and only increase the diameter over that portion. However, even the latter is preferable to the case where the smaller diameter extends over the whole depth $(L_1 + L_2)$. Obviously, drilling rather large diameter boreholes would only be undertaken when there is considerable confidence in the extent and depth of a permeable reservoir either of the dry steam type or of the pressurised hot water type.

It should be mentioned that to be on the side of conservatism, these calculations were performed on a bore with a low enthalpy of 418 BTU/lb and it is expected that the exponents of equations (13) and (14) would increase slightly for higher enthalpies with that of equation (13) finally attaining the value of 2.62 when the bore enthalpy becomes that of dry steam.

### Boiling point with depth curve (B.P.D.)

There is a great deal of circumstantial evidence that hot water reservoirs are "once through" systems in which a uniform column of high temperature water rises slowly from depth towards the ground surface, passing as it does through regions of decreasing hydrostatic pressure. It is only when this ambient pressure exactly matches the vapour pressure associated with the temperature of the column that steam can appear in the water. From this point upwards the water is at boiling point with a temperature associated with the hydrostatic pressure which in turn is controlled by the depth of the water from its surface at 100°C. This water surface, when extrapolated from the reservoir conditions, is estimated to be quite often very close to the ground surface as at Wairakei, but it can be much lower, and at Ahuachapan No. 1 borehole in El Salvador it is found to be about 600 ft below the ground surface. An integrated B.P.D. curve has been calculated and the following equation derived:

$$C = 54.3\, H^{0.305} \qquad (15)$$

where $C$ is the temperature in °C when boiling point exists over a depth $H$ ft from a surface at 100°C. The equation applies over the depth range $H = 100$ to 10,000 ft.

It also appears likely that when the deep column of hot water rises through a broken rock zone, steam can only appear when a horizontal permeable region is reached; this is because the generation of steam would result in a large increase in the specific volume, which in an approximately parallel-sided column would bring the flow to a halt. On entering a permeable horizon, however, there would be no such restriction as the water of the column can now expand radially outwards without restriction. Hence the temperature of the water column may largely be influenced by the presence

of a geologically permeable layer with a depth which can be evaluated from equation (15) if the temperature of the water column is known and if the B.P.D. curve intercepts the ground surface. At Wairakei, the temperature of the water column is now estimated to be 257°C and using this in the equation above, the depth at which boiling commences is 1750 ft which is very close to the depth of the major permeable region at 1800 ft. Recent results from the Broadlands geothermal

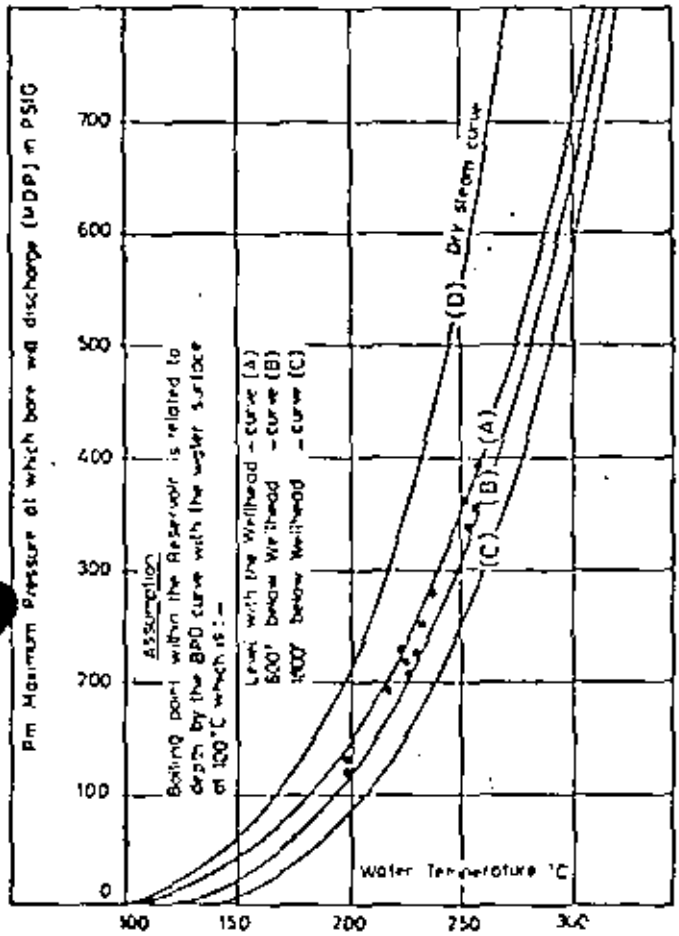


FIG. 10. — *Maximum discharge pressure (MDP) as a function of reservoir water temperature.*

region, which is about 18 miles from Wairakei, indicate that the rising water column temperature there is at abouth 300 °C which, when used in equation (15), gives a depth of 3600 ft to boiling at the permeable layer. Evidence from the Broadlands investigation pores indicate that the permeable horizon is close to that depth, for the deep reservoir.

Employing equations (5) and (15) with $H = L_2$, a curve can be plotted which correlates the maximum discharge pressure (M.D.P.) of a borehole with the temperature of the supply water at the bottom of the well. This is drawn on Figure 10 as curve (A). Also drawn is curve (B) where the B.P.D. relationship is considered as displaced downwards by 600 ft (as at Ahuachapan in El Salvador). For comparison purposes, curve (C) is drawn with the B.P.D. relationship displaced 1800 ft downwards. A selection of Wairakei borehole test results are shown plotted, which are considered to be only roughly accurate because it has, in the past, been found difficult to be sure of the source water temperature supplying a borehole at M.D.P. Because of this difficulty, it is probable that the curves of Figure 10 will be used to determine the source temperature of bores rather than the other way around and particularly after the vertical displacement of the B.P.D. curve has been established by early investigation holes. Deep holes penetrating below the reservoir water surface should result in an estimate of the rising water column temperature and equation (15) will then give the depth to the lower permeable horizon.

For dry steam fields, curve (D) is given which can also apply to pressurised hot water systems when bores are bleeding (severely throttled condition) and in which the depth of the borehole is filled with steam or gas.

For bores which are drilled to shallower depths over which the B.P.D. curve operates, Figure 10 will give temperature of the water supplying the bore but this will be less than that of the rising water column. Such shallow bores are liable to fill with steam and gas when closed as they are often tapping water which is closed to the boiling point and is not pressurised to any marked extent.

As an example of the use of Figure 10, the case of an actual shallow Wairakei borehole is considered which had an M.D.P. of 220 psig when discharging a steam-water mixture. Complete closure of the wellhead valve led to steam and gas filling of the well so that over a time period of 1 day the wellhead pressure rose from 220 psig to a final figure of 325 psig. Plotting of these pressures on Figure 10 indicate that the source water temperature is 222°C and that curve (A) is applicable showing that the B.P.D. curve starts at ground level. Later tests confirmed these results. If the B.P.D. curve was downwards by, say, 600 ft, then curve (B) would have applied, and for the same source water temperature of 222°C the wellhead pressure would have been 190 psig at M.D.P. with an unchanged value of 325 psig for the final closed-in pressure.

As an example of a bore penetrating deep into the pressurised hot water, we may take the case of Ahuachapan No. 1 of which measurements of the bottom hole pressure and temperature indicate has a B.P.D. curve displaced downwards by 600 ft. With a M.D.P. of 202 psig, the rising water column temperature is 226°C. from Figure 10. Equation (15) gives $H = 950$ ft which with the addition of the 600 ft displacement, results in a depth to the permeable horizon of 1550 ft at its highest point. Actual depth to the top very permeable layer has been given in the U.N. Progress Report (1968) as from 1640-1800 ft which is reasonably good agree-

ment.. It should perhaps be mentioned that the maximum discharge of a bore is only slightly reduced by drilling deeper into a hot water permeable aquifer of constant temperature. This because increasing the depth as given in Figure 8 results in a nearly similar increase in $L_1$ and only a small increase in $L_2$. Doubling the depth $L$ can result in a decrease in flow of only about 5%.

With successes in predicting the temperature of the rising deep water column from chemical analyses of geyser fluids, it appears that the approximate depth to permeable horizons may be estimated before actual drilling commences. If the maximum displacement downwards of the B.P.D. curve is assumed as not likely to exceed 1000 ft, then drilling to, say, 5000 ft (about 1.5 km) should locate any *available* permeable horizons in hot water reservoirs with temperatures up to 307°C. Of course, there is no guarantee that such horizons will be successfully pieced as they may present an elusive target, but they should exist somewhere within that depth range at a level where the imposed hydrostatic pressure matches the vapour pressure corresponding to the water temperature, and where the permeability provides room for the steam expansion.

For mathematical and extrapolation purposes, the respective equations for curves (A), (B) and (D) are given below (curve (C) has been neglected as outside the normal range expected).

Curve (A), $$C = 46.8\, P_m^{0.28} \qquad (16)$$

Curve (B), $$C = 63.4\, P_m^{0.24} \qquad (17)$$

Curve (D), $$C = 51.3\, P_m^{0.205} \qquad (18)$$

It should be noted that for convenience, the pressures of Figure 10 are given in psig (gauge pressure), but in the above equations, the maximum discharge pressure is given in psia (absolute pressure). $C$ is the water temperature in °C.

### Flow from hot water reservoir to borehole

The relationship between the flow of a borehole and the pressure gradient surrounding it can be calculated from Darcy's law of linear filtration according to which the flow is proportional to the pressure-gradient and inversely proportional to the viscosity of the fluid. The equation derived from this relationship and commonly applied to the radial flow of homogenous fluid into a borehole is:

$$Q = \frac{2\pi k L\,(P_e - P_b)}{\mu \log_e \left(\frac{R}{r_w}\right)} \qquad (19)$$

where:

$Q$ = borehole flow, cm³/sec;

$k$ = rock permeability, darcies;

$L$ = thickness of permeable horizon, cm;

$\mu$ = viscosity of fluid, centipoise;

$P_e$ and $P_b$ = reservoir and bottom hole pressure, atm

$R$ and $r_w$ = radii of the drainage boundary and the well bore

Test results on Wairakei bores which have flows up to a million lb/h indicate that there is no measurable draw-down, i.e. $(P_e - P_b)$ is probably less than about 4 psi; it is also believed from geological evidence that the wells do not draw from porous-permeable media but instead tap fissures of generous proportions which radially supply the pressurised hot water existing at depth. Recent tests on Broadlands bores indicate that flows are less than those at Wairakei and values of drawn-down attain hundreds of psi. But the relationship established by tests between the flow $Q$, and draw-down $(P_e - P_b)$ is not a linear one as in equation (19), and $Q$ is in fact found to be approximately proportional to $(P_e - P_b)^{0.5}$. This strongly suggests that fissure flow is taking place because an equation suitable for boreholes and based upon radial flow through fissures is:

$$W = 7500\, dt \left[\frac{\Delta P}{V_w}\right]^{0.5} \qquad (20)$$

where:

$W$ = borehole flow, lb/h

$d$ = diameter of well bore, inches

$t$ = thickness of fissure, inches

$\Delta P$ = draw-down, psi, (= difference between reservoir and bottom hole pressure)

$V_w$ = specific volume of fluid, ft³/lb.

For New Zealand wells of about 8 inches diameter, drawing on hot water with a specific volume of approximately 0.02 ft³/lb, equation (20) simplifies to:

$$W = 424000\, t(\Delta P)^{0.5} \qquad (21)$$

Applying equation (21) to Wairakei bores indicates that the fissures there are about 1 inch in width, while for the Broadlands bores, they would be more than an order of magnitude smaller (i.e. less than about 0.1 inches). It would appear, therefore, that the concept of flow through porous-permeable media must be rejected for these fields, and probably elsewhere, and problems involving the identification of reservoir permeability in equation (19) need not be pursued. This is substantiated by two facts; (a) a deep hole has been drilled at each of the Wairakei and Broadlands fields,

neither of which produced any flow from thousands of ft of uncased hole. It appears then, that unless a fissure is penetrated, flows are virtually non-existent, hence it can be concluded that the rock is grossly impermeable from the viewpoint of geothermal exploration. (b) Although the top 2000 ft of the Wairakei field has declined in pressure over the last decade under the combined draw-off of 60 production boreholes, the field output enthalpy has not changed in any significant degree, hence there has been very little heat contributed by the rock in the regions of falling pressure. This is in accordance with the concept of flow through fissures, with minimum fluid contact with the rock. Conductive heat flow through rock is very slow and requires a large and intimate surface contact to make a substantial contribution, and this has apparently not happened.

### Effect of bore size on flow from fissures

As fissures appear to dominate the mode of flow in geothermal reservoirs, it is worth noting that flow-rate is directly proportional to the bore diameter when a fissure is intercepted, as given by equation (20). For fissures of a width of the order of 1 inch however, or greater, the geometry of the bore controls the flow (because draw-down is negligible) and as has been mentioned earlier, the discharge is proportional to $d^{2.36}$ for pressurised hot water, and proportional to $d^{2.62}$ for dry steam. Where the fissure thickness is much less than this, the fissure itself increasingly controls the flow to a point where the discharge is completely dependant on the fissure thickness. When this occurs the flow-rate is proportional to $d$.

From either point of view, improved flows are obtained with larger diameter bores.

### REFERENCES


ASME 1950 — Fluid meters, their theory and application. *Amer. Soc. mech. Engrs. New York.*

KEENAN J. H., KEYES F. G., HILL P. G., MOORE J. G. 1969 — Steam Tables. *John Wiley & Sons.*

LAPPLE C. E. 1943 — Isothermal and adiabatic flow of compressible fluids. *Trans. amer. Inst. chem. Engrs.*, 39, *385.*

MAHON W. A. J. 1966 — A method for determining the enthalpy of a steam-water mixture discharged from a geothermal drillhole. *N. Z. J. Sci.*, 9, *791.*

JAMES R. 1962 — Steam-water critical flow through pipes. *Proc. Inst. mech. Engrs.*, 743.

JAMES R. 1964 — Maximum steam flow through pipes to the atmosphere. *Proc. Inst. mech. Engrs.*, 178, *473.*

JAMES R. 1965 — Metering of steam-water two-phase flow by sharp edged orifices. *Proc. Inst. mech. Engrs.*, 180, *549.*

JAMES R. 1966 — Measurement of steam-water mixtures discharging at the speed of sound to the atmosphere. *N. Z. Engng.*, 21, *437.*

PERRY R. H. 1963 — Chemical Engineers Handbook. *McGraw-Hill.*

1968 — El Salvador. Survey of geothermal resources. *United Nations. Progress Rep.*

# Rapid Estimation of Electric Power Potential of Discharging Geothermal Wells

RUSSELL JAMES
*Department of Scientific and Industrial Research, Taupo, New Zealand*

## ABSTRACT

By means of a lip pressure tapping at the end of the pipe discharging geothermal fluid to the atmosphere under the usual conditions of critical flow (mixture at sonic velocity), it is shown that a fairly accurate estimate can be made of the amount of electric power of which the well is capable. This applies both to wells deriving their flows from a dry steam reservoir and to those based on a pressurized hot-water system.

## INTRODUCTION

When a newly drilled well is first discharged vertically, it usually takes some hours before the flow and pressures are stabilized. After this point is reached, it may be weeks, or even months, before the necessary equipment is assembled to measure the flow and enthalpy so as to estimate the electrical energy which the well could contribute to a power project. However, an estimate of adequate accuracy can be made right from the start with the stabilized well discharging vertically. The method merely entails attaching a lip pressure gauge at the extreme end of the discharge pipe (whose internal diameter must be measured). This simple device is all that is required, and it has been described in an earlier paper (James, 1962). It is now in common use in many geothermal fields in conjunction with twin-tower silencers for measuring the flow and enthalpy of steam-water mixtures.

In order to use this method, the efflux jet must be cursorily examined to see whether the discharge is fairly dry steam or an obvious steam-water mixture: the former is fairly transparent, whereas the latter is opaque. Slightly wet steam usually becomes dry after a few days of discharge if the well penetrates one source of fluid, whereas a steam-water jet indicates that the flowing enthalpy is most likely in the range of 400 to 600 Btu/lb, based on experience of actual well discharges.

## WELLHEAD PRESSURE

If a turbine inlet pressure of 50 psig is required (James, 1967) and if a pressure-drop of 25 psi is allowed between the turbine entrance and the wellheads of supplying boreholes, then obviously the least acceptable wellhead pressure must be 75 psig, to be realistic under test conditions. But because of the decline in reservoir pressures under exploitation which progressively lowers the wellhead pressure over the life of the field, it would appear prudent to throttle the flow initially and hence start with a wellhead pressure of not less than, say, 175 psig. This excess pressure at the wellhead of 100 psi "in hand" can be lowered with time by releasing the amount of throttling, in order to sustain the discharge. For instance, if the pressure declines at a rate of 10 psi/yr, then 10 years would pass before the wellhead pressure had dropped to a value of 75 psig. A further pressure fall would drop the turbine inlet pressure below its design pressure of 50 psig, and hence reduce electric energy output.

It was not found necessary to throttle the Wairakei wells because in the early days of the project the wellhead pressures were quite high. For example, Well 67 had a wellhead pressure of 156 psig when discharging wide-open vertically through an 8-in. diameter discharge pipe. When switched to horizontal discharge—also through an 8-in. pipe—the wellhead pressure rose to 220 psig while the lip pressure fell from the vertical value of 70 psig to the horizontal value of 46 psig. These values show the effect on the flow of passing through a 90° angle when discharging horizontally. The resulting discharge is reduced to 0.73 of the vertical (as flow is proportional to lip pressure in absolute terms at a constant enthalpy). Similarly, the absolute wellhead pressure rose in inverse proportion from 156 + 14.5 = 170.5 psia to $0.73^{-1} \times 170.5 = 233.5$ psia = 219 psig. Absolute pressure at Wairakei averages 14.5 psia (1400 ft above sea level).

## PROCEDURE

With the well discharging vertically under stable conditions and with the flow throttled so that the wellhead pressure is 175 psig, the value of lip pressure, $P_l$, is noted. Figure 1 shows a typical wellhead arrangement—the horizontal by-pass is often extended into a silencer. Figure 2 indicates the geometry of the lip pressure hole, which is drilled into the discharge pipe near its end-face. A socket is welded externally at this location and connected to a pressure gauge.

If the discharging jet is a steam-water mixture, Equation (A) from the appendix is used with English units where $P_l$ is in psia and $d_l$ is in inches. The metric equivalent is Equation (B) where $P_l$ is in bars (absolute) and $d_l$ is in centimeters. Where the jet is obviously dry steam, Equation (C) is used or its metric equivalent, Equation (D),

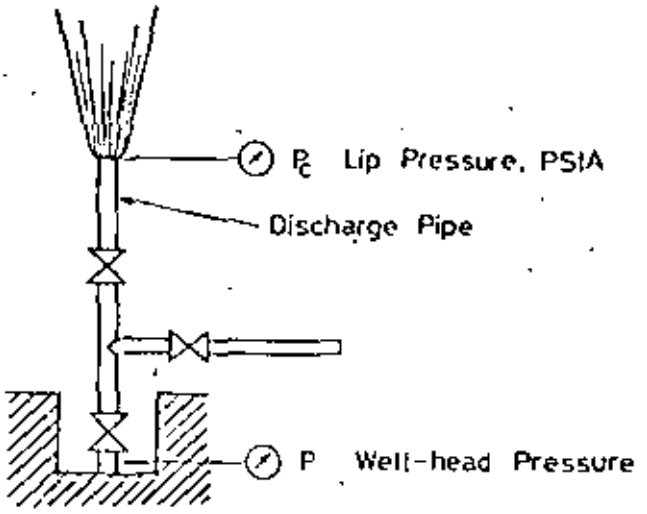


Figure 1. Geothermal well discharging to atmosphere.

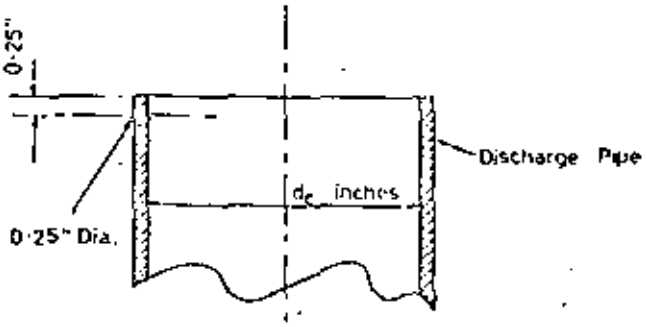


Figure 2. Lip pressure tapping dimensions in discharge pipe.

## ILLUSTRATIVE EXAMPLE

The well shown in Figure 1 is discharging a steam-water mixture under stable flow with a lip pressure, $P_c$, of 45 psig. The internal diameter of the discharge pipe is 8 in., and atmospheric pressure is 14.7 psia. Calculate the electric power in megawatts which the well can produce

$$\text{electric power} = P_c^{0.96}\left(\frac{d_c}{16.94}\right)^2$$

$$= (45 + 14.7)^{0.96}\left(\frac{8}{16.94}\right)^2$$

$$= 11.31$$

If metric units are used, $P_c = (45 + 14.7)/14.5 = 4.12$ bar and $d_c = 8 \times 2.54 = 20.32$ cm. Using Equation (B)

$$\text{electric power} = P_c^{0.96}\left(\frac{d_c}{11.92}\right)^2$$

$$= 4.12^{0.96}\left(\frac{20.32}{11.92}\right)^2$$

$$= 11.31$$

For the same values but if the discharging jet is dry steam, Equation (C) is employed for English units as follows:

$$\text{electric power} = P_c^{0.96}\left(\frac{d_c}{14.48}\right)^2$$

$$= (45 + 14.7)^{0.96}\left(\frac{8}{14.48}\right)^2$$

$$= 15.47$$

Using metric units, Equation (D) is employed.

$$\text{electric power} = P_c^{0.96}\left(\frac{d_c}{10.19}\right)^2$$

$$= 4.12^{0.96}\left(\frac{20.32}{10.19}\right)^2$$

$$= 15.47$$

## CONCLUSIONS

For discharges composed of steam-water mixtures within the enthalpy range 400 to 600 Btu/lb, it is probable that the electric power potential of a well can be estimated to within ±5%, assuming that the thermal efficiency of converting heat energy to electric energy is 0.10. It is likely that with careful design of a power project, this value of thermal efficiency can be somewhat exceeded when employing separation of the phases in two pressure stages: hence the estimated power will be slightly conservative.

For the discharge of dry steam, the accuracy will be improved as the enthalpy is less prone to wide variation, according to data from existing steam fields.

Power-house auxiliaries (cooling-water pumps, gas extractors, and so on) usually impose a toll of up to 5% in geothermal stations; hence the electric power calculated by this method would have to be reduced by that amount to gain a first estimate of net power.

## APPENDIX

The basic formula connecting flow rate, enthalpy, and lip pressure (James 1962) is:

$$\frac{Gh_0^{1.102}}{P_c^{0.96}} = 11400$$

where $G$ is in lb/ft²·sec, $P_c$ = psia, $h_0$ = Btu/lb (enthalpy), and the specific heat flow is $(Gh_0)$ in Btu/ft²·sec = $(11400\ P_c^{0.96}/h_0^{1.102}$. If the internal diameter of the discharge pipe is $d_c$ (in.), then the heat flow in Btu/hr is

$$(Gh_0)\frac{\pi}{4}\left(\frac{d_c}{12}\right)^2 60^2 = (Gh_0)\,19.6d_c^2$$

$$= \frac{11400\ P_c^{0.96}\,19.6\ d_c^2}{h_0^{1.102}}$$

Converting heat flow to megawatts of heat MW(H), where $3.412 \times 10^6$ Btu/hr = 1 MW(H)

$$\text{MW(H)} = \frac{11400 P_c^{0.96} d_c^2\,19.6}{h_0^{1.102}\,3.412 \times 10^6} = \frac{P_c^{0.96}\,d_c^2}{15.27\,h_0^{1.102}}$$

To convert heat energy, MW(H), to electric energy, MW(e),

the thermal efficiency $\eta_t$ is used: hence $MW(e) = \eta_t MW(H)$. In the case of dry-steam systems such as Larderello and The Geysers, the thermal efficiency $\eta_t = 0.15$. For systems discharging steam-water mixtures and which use steam [illegible] d in two pressure stages, $\eta_t = 0.10$. The difference is due to the large quantity of hot water rejected at the wellheads or from surface equipment when a hot-water system discharges mixtures from the wells. At Wairakei, where only one stage of separation was employed, the thermal efficiency was 0.075, whereas a study of the El Tario geothermal field in Chile showed that a thermal efficiency of 0.1054 could be obtained when separation was in two pressure stages. As we are considering a field prior to a feasibility study, a thermal efficiency rounded to 0.10 was considered quite adequate for present estimates and is somewhat on the conservative side.

$$MW(e) = \frac{\eta_t P_c^{0.96} d_c^2}{15.27\, h_0^{0.102}}$$

For steam-water discharges within the enthalpy range 400 to 600 Btu/lb,

$400^{0.102} = 1.843$
$600^{0.102} = 1.920$
average = 1.881 accurate to ±2%

thermal efficiency, $\eta_t = 0.10$

$$MW(e) = \frac{P_c^{0.96} d_c^2}{287.08} = P_c^{0.96} \left(\frac{d_c}{16.94}\right)^2 \qquad (A)$$

Hence the only data required to obtain an estimate of the electric power potential of a geothermal well are the lip pressure and the internal diameter of the discharge pipe. For metric units where the lip pressure is in bars (absolute) and the internal diameter of the discharge pipe in centimeters, the formula is:

$$MW(e) = P_c^{0.96} \left(\frac{d_c}{11.92}\right)^2 \qquad (B)$$

For wells discharging dry steam, the enthalpy $h_0 = 1200$ Btu/lb and $1200^{0.102} = 2.061$. Also thermal efficiency $\eta_t = 0.15$.

$$MW(e) = \frac{P_c^{0.96} d_c^2}{209.81} = P_c^{0.96} \left(\frac{d_c}{14.48}\right)^2 \qquad (C)$$

For metric units where $P_c$ is in bars (absolute) and $d_c$ is in centimeters

$$MW(e) = P_c^{0.96} \left(\frac{d_c}{10.19}\right)^2 \qquad (D)$$

## REFERENCES CITED

James R., 1962, Steam-water critical flow through pipes: Inst. Mech. Engrs. Proc., v. 176, no. 26, p. 741.

——, 1967, Optimum wellhead pressure for geothermal power: New Zealand Engineering, v. 22, p. 221.

# Optimum Wellhead Pressure for Geothermal Power

RUSSELL JAMES*
C.ENG., A.M.I.MECH.E., (MEMBER)

*When a power scheme is being considered for the exploitation of a geothermal region, both fluid flow-rates and economics are shown to be primarily dependent on the value of wellhead pressure chosen for the borefield; differences in such a choice may be reflected in large variations in the capital involved. Curves are presented which indicate that the optimum wellhead pressure is within a relatively narrow range that gives not only close to minimum capital costs but a maximum life for the scheme. This applies where the system enthalpy is not less than about 400 Btu/lb. It is also shown that this result applies not only to fields which derive power from boiling water, as in Mexico and New Zealand, but also to superheated steam fields as in Italy and California. The optimum wellhead pressure is used to determine the turbine stop valve pressure when a pressure drop of 25 lb/in² and a heat loss of 5% is assumed through the long pipeline and ancillary equipment connecting the boreholes to the turbines at the power station.*

## 1. INTRODUCTION

GEOTHERMAL power stations are operating in many countries, including Italy (370 MW), New Zealand (192 MW), California, U.S.A. (25 MW) with other smaller stations in Japan, the U.S.S.R., and the Republic of the Congo. Feasibility studies have been made for Iceland and Mexico, and initial scientific surveys are under review in El Salvador, Chile, and elsewhere.

The geothermal papers presented to the United Nations Conference on New Sources of Energy in Rome, 1961, published as Volumes 2 and 3 of the *Proceedings*, provided a useful guide to the existing knowledge on the subject of geothermal exploration and exploitation. Since then, there have been advances made in theory and practice with the urge to exploit this natural asset.

Geothermal energy may be conveniently divided into two subjects:

(1) Scientific study of the phenomena with its origin, and relationships with other geophysical manifestations such as seismic activity, convection currents in the earth's mantle and continental drift. Some aspects of these have been given by Runcorn (1), Holmes (2), and Lee (3).

(2) Exploitation with power stations built or contemplated and descriptive papers by Einarsson (4); Bruce (5), di Mario (6) and Haldane and Armstead (7). Studies have also been made into the exploitation potential of hot regions by Banwell (8, 9), White (10) and Grindley (11).

Up to the present, there has been no publication primarily concerned with the influence on a geothermal field of the choice of wellhead pressure when exploited for power, although a recent paper (12), comparing the drawing of top steam from a hot water aquifer with the alternative method of tapping deep water, showed that for wellhead pressures within the range 65 to 80 lb/in² gauge, top stream draw-off resulted in a power-life of about double that for deep water removal as practised at Wairakei. Because the hot water level at Wairakei is high compared with that at Larderello, Italy, and The Geysers, U.S.A., there has not been much success here in drilling solely for dry steam; the physical factors inhibiting such exploitation may change, however, with time, under the present draw-off of the deep hot water (order of $70 \times 10^6$ ton per year).

Table 1 shows the wellhead pressures designed and contemplated for various geothermal power stations. The table shows the locality, approximate wellhead pressure, and type of field—that is, whether the power is derived by drilling into a pressurised hot water aquifer or whether steam only is taken.

The range of wellhead pressures is from 60 to 210 lb/in² gauge, and the Larderello field, which has the lowest operating pressure, also has the highest closed-in wellhead pressures (order of 435 lb/in² gauge). This has not passed unquestioned by Contini (15), who recomends a wellhead pressure of about 50% of the closed-in pressure, which would be for Larderello about 210 lb/in² gauge and would be the same as for the Wairakei high pressure boreholes. He lists among the advantages of such higher pressures: (a) there will be a great economy of steam per kilowatt-hour; (b) the borehole will be of small diameter; (c) the transmission pipeline connecting the wellhead to the station will be of small diameter; and (d) the turbine will be smaller.

*Senior scientific officer, Chemistry Division, Department of Scientific and Industrial Research. This paper was first received on 29 September 1966 and this revised version was received on 28 February 1967.

Reprinted from *New Zealand Engineering*, 22 (6): 221-8 (June 1967).

TABLE 1

*Wellhead Pressures for Different Geothermal Fields*

| *Region and reference* | *Type of field* | *Wellhead pressure* (lb/in² gauge) |
|---|---|---|
| Larderello, Italy (13) | superheated steam | 60 |
| Iceland (contemplated) (4) | hot water | 75 |
| Wairakei intermediate pressure (14) | hot water | 80 |
| The Geysers, California (5) | superheated steam | 110 |
| New Zealand (contemplated) (not published) | hot water | 140 |
| Wairakei high pressure (14) | hot water | 210 |

A different viewpoint is advanced by Hansen (16), who mentions that for the first 12.5 MW station at The Geysers, the turbine stop valve pressure was designed at 100 lb/in² gauge but that "subsequent tests have indicated that more power can be developed from The Geysers at reduced pressure, perhaps as low as 65 lb/in² gauge (wellhead pressure)".

For power derived from flashing hot water, Einarsson (4) writes that an analysis of the output of boreholes at Hveragerdi, Iceland, shows that power generated increases with reduction of the wellhead pressure but that a lower limit is set by the size and cost of the wellhead separators and steam transmission pipeline, etc.

Although no region has been finally chosen for a second New Zealand geothermal power station, a wellhead pressure of approximately 140 lb/in² gauge has been recommended as a possibility for a station of 150 MW installed capacity. This pressure is about halfway between the two operating pressures in the Wairakei field, and the system would be a single pressure one, that is, it would not make use of secondary flash steam, owing to New Zealand experience with a pilot hot water line which became redundant with falling water flows from the supplying boreholes.

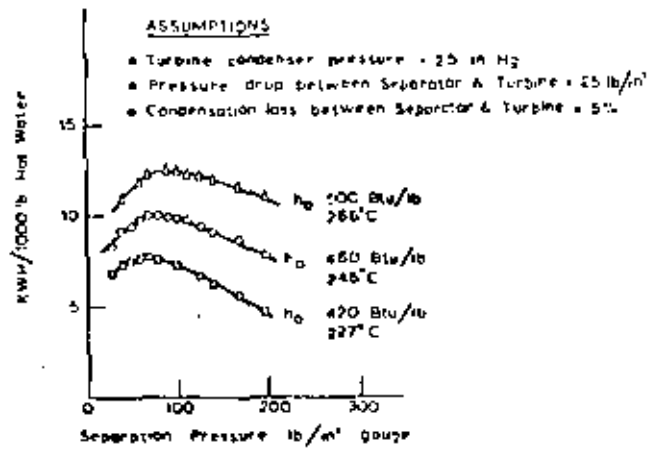


*Fig. 1: Energy derived from flashing water of enthalpy $h_0$.*

## 2. SYSTEMS

### 2.1. Power from Flashing Water

When the pressure on a mass of hot water is reduced to below the saturated pressure associated with the water temperature, a quantity of steam appears which may be separated from the remaining water and passed through a turbine for power. The lower the pressure of separation, the greater the amount of flash steam produced but the less its intrinsic power potential at the turbine. These two opposing effects result in an optimisation curve where the maximum energy obtainable from hot water depends on some unique value of the pressure of separation. The low enthalpy water remaining after separation is considered as rejected and is not used again for secondary flashing.

For a geothermal station deriving its power from a pressurised hot water aquifer, the steam separated at the wellheads of boreholes would have to be piped a considerable distance (order of a mile) resulting in both a pressure-drop and a certain condensation or heat loss even with good insulation. In order, therefore, to present results which can be compared with actual borefield conditions, the curves of Fig. 1 take into account a pressure-drop of 25 lb/in² and a condensation loss of 5% between separators and power house turbines. The turbine condenser pressure is taken as 2.5 inHg, which was the value used by Haldane, Wood and Armstead (17) to determine the steam rate curve reproduced as Fig. 2. The amounts of energy calculated in kilowatt-hours are gross values taken at the turbine; to calculate net values, a certain amount would have to be deducted (at Wairakei, about 4%) to allow for generator efficiency and for

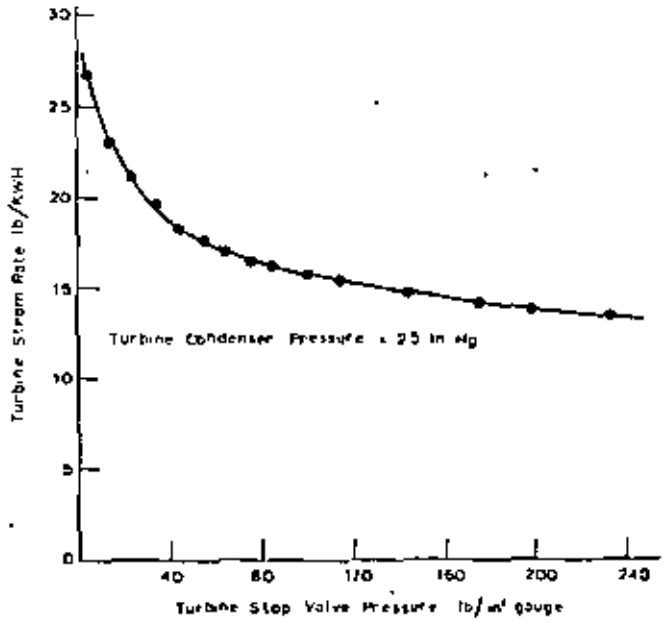


*Fig. 2: Pressure v. dry saturated steam rate; from Haldane, Wood, and Armstead (17).*

such auxiliaries as cooling water and gas removal pumps.

Curves are given for three values of enthalpy—420, 460 and 500 Btu/lb—which cover the usual range of hot water in geothermal regions; higher enthalpies from some boreholes are not uncommon, but it is generally agreed (11) that these take their flows from free underground steam associated with flashing hot water.

Figure 1, which does not depend on the performance of boreholes, is determined only from the steam tables and the steam rate curve of Fig. 2.

As the next New Zealand geothermal power station will possibly be designed for an installed capacity of 150 MW, the curves of Fig. 1 are recalculated and transferred to Fig. 3 where fluid draw-off is given in millions of pounds per hour ($10^6$lb/h). (As a comparison, the Wairakei double pressure system with 192 MW installed capacity, is operating between 15 and 20 $10^6$lb/h depending on output). Curves of high enthalpy are also given, and these show the required flow-rates at different wellhead pressures; these can be misleading, however, in appearing to advocate higher wellhead pressures with reduced flow rates for a given power output. In fact, the actual output characteristics of boreholes have a first order effect which is not obvious at lower enthalpies but which dominates at higher ones. This is shown in Figs. 4 and 5. Figure 4 applies to a typical Wairakei borehole of enthalpy 460 Btu/lb whose output is plotted against wellhead pressure together with the curve of power in MW; the optimum power is obtained at a wellhead pressure of 80 lb/in² gauge, which is close to that given in Fig. 1. It can also be shown that boreholes of enthalpy 420 Btu/lb give good agreement with the appropriate curve of Fig. 1 with an optimum pressure of about 70 lb/in² gauge. For the case of higher enthalpies, Fig. 5 gives the mass and power output versus wellhead pressure of a dry steam borehole (number 216, Wairakei) showing the maximum power of 10 MW at a wellhead pressure of 100 lb/in² gauge.

For boreholes with enthalpies higher than that derived from a flashing all-water phase due to the presence of free steam, the optimum pressure for

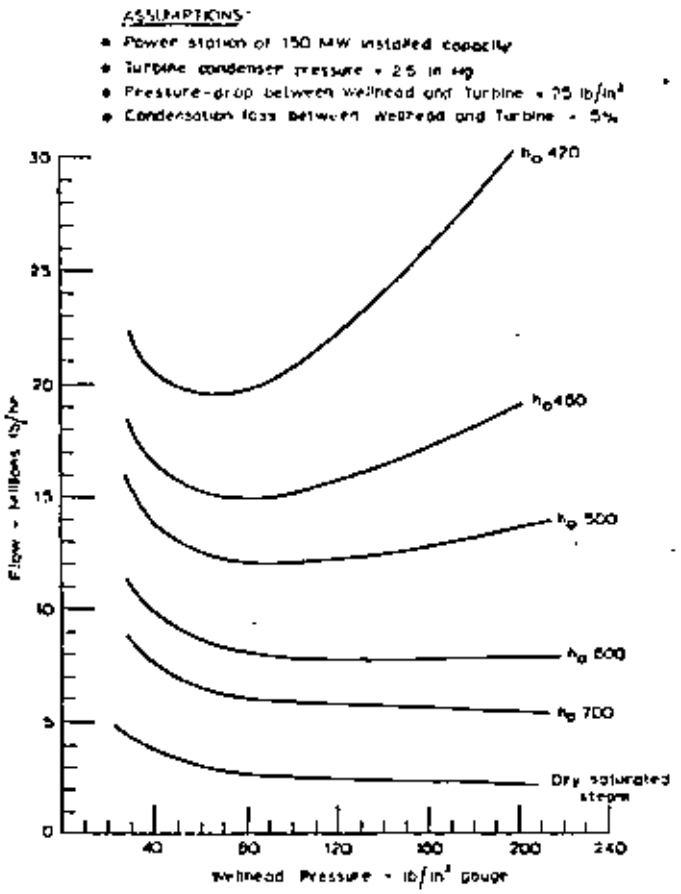


*Fig. 3: Required flow of steam-water mixture of enthalpy $h_0$ for 150 MW scheme.*

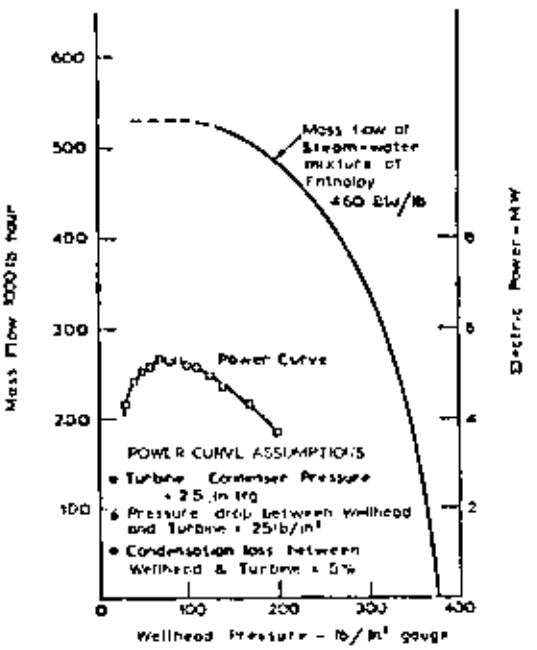


*Fig. 4: Output and power potential of typical high pressure borehole.*

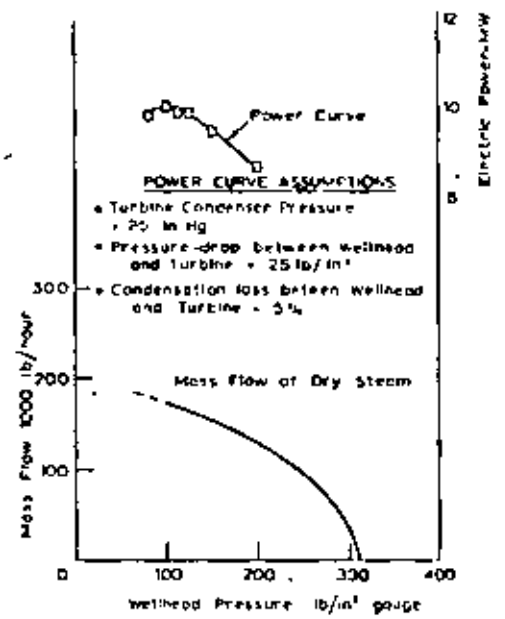


*Fig. 5: Output and power potential of dry steam borehole No. 216, Wairakei.*

power would be intermediate between the value for a "wet" borehole (80 lb/in² gauge at an enthalpy of 460 Btu/lb) and the value for a dry steam borehole (100 lb/in² gauge at about 1,200 Btu/lb).

At this point, then, it can be inferred that for boreholes with enthalpies from 420 to 1,200 Btu/lb (the approximate value for dry saturated steam), the optimum separator pressure is from 70 to 100 lb/in² gauge, giving turbine stop valve pressures from 45 to 75 lb/in² gauge.

### 2.2. Power from Steam-filled Aquifer

Although it is likely that dry steam fields such as those in California and Italy produce by evaporation from the surface of a deep water aquifer (18) with a depth of the order of 6,000 ft, the case is now considered where steam alone exists within a finite aquifer without an associated water phase.

A first approach to determine the optimum pressure of such a field would be to assume that the steam is obtained as if by drilling into a "vessel" of finite dimensions whose initial pressure equals the closed-in pressure of boreholes. Here again, we are faced with an optimisation problem where two contradictory effects operate, one being the increased steam consumption rate of turbines working at lower pressures as given in Fig. 2, and the other being the larger amount of steam taken from the vessel on being drawn-down to a lower final pressure.

The two curves given in Fig. 6a are based on a vessel of initial pressure 435 lb/in² gauge (as for the closed-in pressure at Larderello) initially containing dry saturated steam. The top curve is considered where the vessel is filled with volcanic rock with the steam occupying 10% of the volume; that is, the porosity is 0.1. For this case, the heat content of the rock is roughly 50 times that of the steam, so that the temperature of the vessel's contents, with draw-off, will only drop a few degrees. As the pressure in the vessel decreases, the amount of superheating* of the steam increases with constant temperature. The greatest amount of energy drawn is obtained where the final vessel pressure is reduced to about 75 lb/in² gauge, which fixes the turbine inlet pressure at 50 lb/in² gauge. This result can be compared with that of the lower curve, which is calculated for the case where the vessel contains steam only without volcanic rock, and which therefore remains in a state of constant enthalpy for all pressures throughout draw-off, thus leading to slight superheating with falling vessel pressure. It was considered that these two curves would provide the limiting cases for where the porosity of volcanic rock ranges from 0.1 to 1.0 (10% to 100% voids). The optimum pressure for the lower curve is also approximately 75 lb/in² gauge and shows that the presence of volcanic rock increases the energy output of a steam-reservoir without affecting the optimum design pressure. For comparison, Fig. 6b shows two similar curves where the initial aquifer pressure is taken as 310 lb/in² gauge, which approximates to the value of the closed-in pressure of some dry steam boreholes at Wairakei. Both these curves show an optimum pressure of 70 lb/in² gauge for maximum energy draw-off.

For dry steam aquifers, therefore, these results indicate that the values of optimum pressure are neither sensitive to the initial closed-in pressure nor to the amount of volcanic rock associated with the steam.

### 2.3. Wairakei Type System

In the case of Wairakei, steam is produced from a hot water aquifer either by underground phase separation leading to the few dry steam

*At Larderello, over the last 50 years of intensive exploitation, the degree of superheat has steadily risen (18) by as much at 70° F.

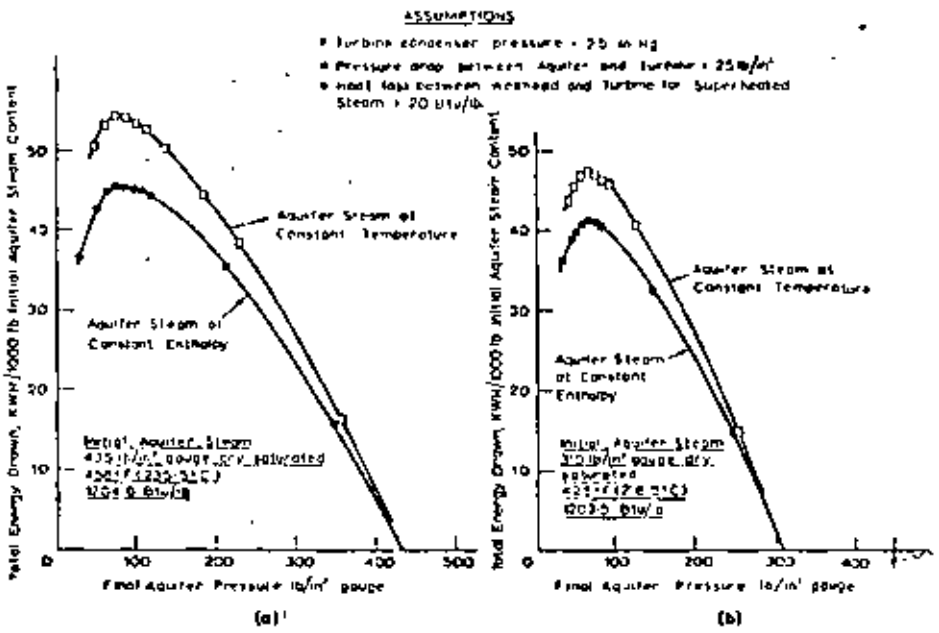


*Fig. 6: Energy derived from steam filled aquifers of finite content.*

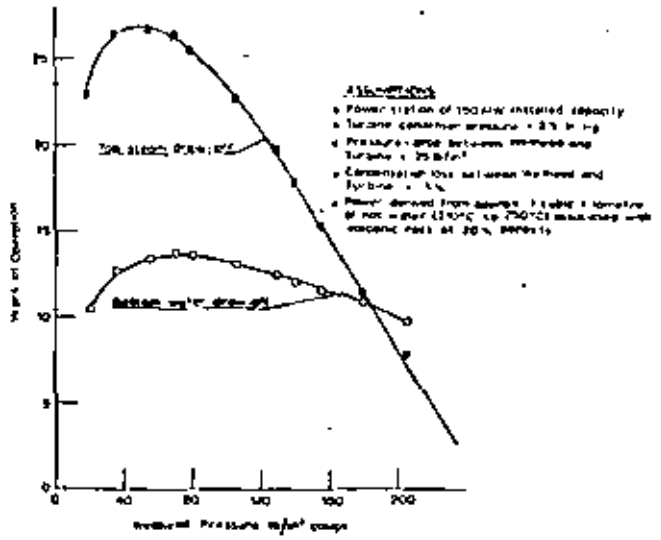

*Fig. 7: Effect on life of field of mode of draw-off and wellhead pressure.*

boreholes, or by the usual method of tapping the deep pressurised hot water and separating the flashing steam-water mixtures at the wellheads. Calculations using a theoretical model of the Wairakei system (12) indicate both the advantages of low wellhead pressures and the drawing of top steam as compared with tapping the deep hot water. These results, which were determined for two pressures only, have been extended in the present paper over a range of wellhead pressures and plotted as Fig. 7. They are based upon an aquifer of approximately one cubic kilometre of hot water associated with volcanic rock of porosity 0.2; the depth of the water is taken as 1,500 ft with temperatures of 210° C at the top surface and 250° C at the bottom. Assuming that steam is required for a power station of 150 MW installed capacity, the number of years of operation are determined for both methods of draw-off at different wellhead pressures. The pressures that give maximum operational life are 50 lb/in² gauge for top steam draw-off and 70 lb/in² gauge when bottom water is removed.

### 2.4. Optimum Wellhead Pressure

Summarising the evidence on wellhead pressures using these various approaches, it is apparent that there is little disagreement on the optimum value either for the case of a dry steam aquifer with steam taken either superheated at constant temperature or at constant enthalpy, or for the case of a hot water aquifer with either steam taken from the top or separated from flashed bottom water. Optima appear to lie within the range 50 to 80 lb/in² gauge, although if the output of dry steam borehole number 216 as given in Fig. 5 was assumed to remain constant throughout the life of a geothermal power scheme (order of 20 years) then such dry boreholes would optimise at 100 lb/in² gauge. However, the output of this borehole has been progressively falling since the 1961 output curve of Fig. 5, and no such guarantee could be entertained for any borehole based on current experience.

## 3. CAPITAL COSTS

A provisional cost estimate of a particular 150 MW geothermal scheme was undertaken in 1964 and is held by the Ministry of Works, Wellington. As the results were of a tentative nature, only relative figures are presented here in Fig. 8. Involved in the costing were only those factors which were influenced by wellhead pressure, such as the number of boreholes drilled, with associated silencers and branch lines, as well as size of main transmission pipeline and cooling towers. These various factors produced an optimisation curve of costs with minimum values within the wellhead range 80 to 100 lb/in² gauge. Below 80 lb/in² gauge, it is expected that the influence of increasing specific volume of the steam used would prevail and that the cost curve would once again increase.

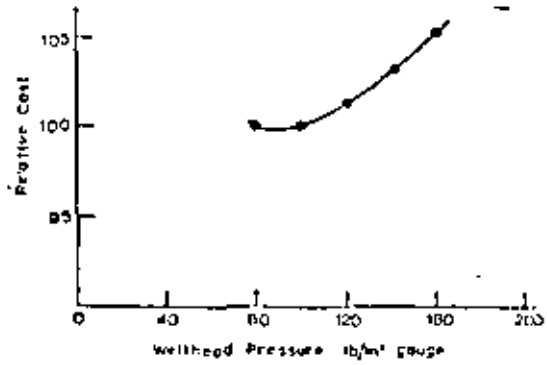


*Fig. 8: Relative capital cost of 150 MW scheme related to wellhead pressure.*

## 4. WELLHEAD PRESSURES OF HIGH PRODUCTION BOREHOLES

Some large output boreholes at Wairakei and elsewhere have wellhead pressures that exceed 150 lb/in² gauge even when passing without restriction to the atmosphere. Such boreholes could not, therefore, initially operate at wellhead pressures as low as 75 lb/in² gauge. However, by means of a throttling orifice placed between the wellhead and the cyclone separator, the pressure of the latter can be adjusted to a value of 75 lb/in² gauge and the flow rate controlled so that the velocity of the cyclone inlet mixture does not exceed that of effective separation (order of 150 ft/s). For a 36 in diameter cyclone with a throughput of 450,000 lb/h at 75 lb/in² gauge and enthalpy 460 Btu/lb, and a throttling orifice as shown in Fig. 9, then when the cyclone is operating, the wellhead pressure has to be adjusted to 235 lb/in² gauge, thus giving a pressure excess of 160 lb/in² above the separator pressure. The power output as supplied to the station (assuming a pressure-drop of 25 lb/in² and a condensation loss of 5%) is 4.4 MW, which is a reasonable figure for a moderate borehole of average enthalpy where steam only is utilised (11). When the borehole as shown is on production, the excess pressure may be gradually reduced with falling flow rates owing to chemical deposition within the bore casing or other causes. For example, if the output of the borehole de-

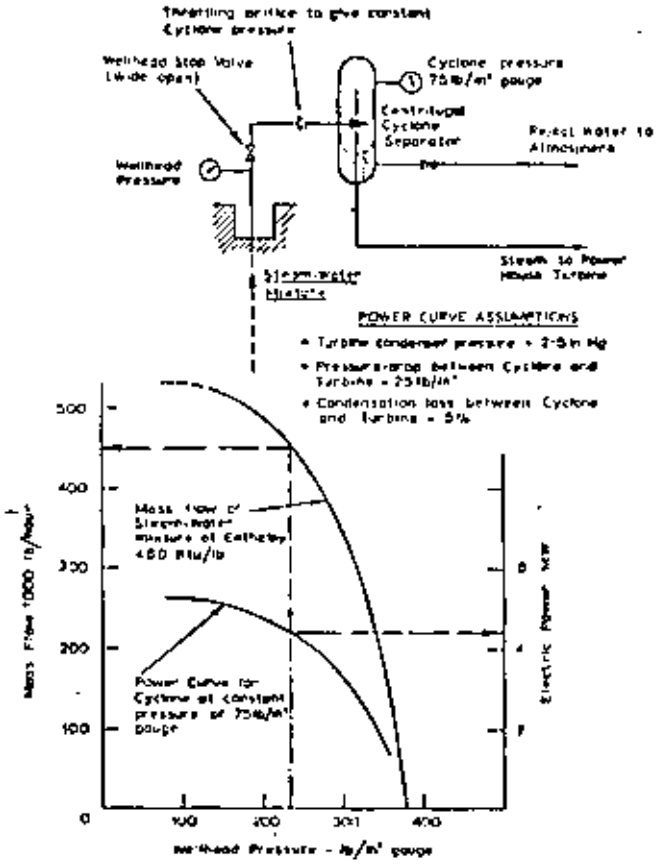


*Fig. 9: Power output (at station) of geothermal borehole with constant cyclone separator pressure of 75 lb/in² gauge.*

creases at a rate which requires a drop in the wellhead pressure of 20 lb/in² per year to sustain the discharge, then by progressively reducing the amount of throttling, production could be continued for eight years before general servicing and reaming out was necessary. For very large output boreholes, an even greater excess pressure may be used, or alternatively two cyclones may be employed with a lesser excess. The largest Wairakei borehole discharged about 900,000 lb/h of steam-water at an enthalpy of 480 Btu/lb and at a wellhead pressure of 220 lb/in² gauge; this could be accommodated by using two cyclones of 36 in diameter with a total power output at the station of 8.8 MW and still give an excess pressure of 145 lb/in². In fact, it may be advisable to drill a sufficient number of boreholes so that as many as possible can be throttled to wellhead pressures initially greater than 200 lb/in² gauge. This will have the added advantage of reducing the amount or likelihood of chemical deposition within the bore casing and should further increase the time before servicing is required. It is possible that with this approach, calcite and silica would deposit only downstream of the wellhead throttling orifice, and most probably within the pipe rejecting the low enthalpy cyclone water to the atmosphere as it is here that the greatest concentration of chemicals occurs. The removal of deposited chemicals from such wellhead equipment should be much easier than from deep down in the production casing.

With boreholes containing very large amounts of chemicals in solution (19), this approach is probably mandatory.

As the excess pressure is taken up over the years, there will be an increasing tendency for chemical deposition within the borepipe, but this problem has to be faced within such a borefield at some time, if the designed final wellhead pressure is low enough to efficiently utilise the resources of the field.

## 5. NON-CONDENSIBLE GASES

The quantity of non-condensible gases to be pumped from the barometric condensers of a geothermal power station has two origins. One portion, mainly carbon dioxide, enters with the turbine steam, while another smaller amount, mainly oxygen and nitrogen, is liberated at the low condenser pressure from the cooling water sprays. An amount of gas is entrained, however, in the coolant and condensate mixture passing downwards and out of the condenser. The amount of pumping power for gas removal may therefore be considered as roughly proportional to the amount of gas in the entering steam for a given vacuum pressure and pumping efficiency.

For a system deriving its steam from a hot water aquifer, as at Wairakei, the amount of non-condensible gas that enters the turbines is related not to the pressure of the steam or its quantity for a given turbine power output, but to the quantity of water taken from the aquifer in which the gas is dissolved at pressure. This is because nearly all the gas in the draw-off water passes into the steam phase when flashing occurs and very little is left in the retaining reject water. For example, Fig. 3 shows that for a borefield of average enthalpy 460 Btu/lb, the amounts of hot water taken for a 150 MW scheme for wellhead pressures of 75 and 140 lb/in² gauge is 14.9 and 16.4 $10^6$ lb/h respectively, an increase in flow at the latter pressure of 10%, which also gives the same percentage increase in gas flow and pumping power for the same vacuum pressure.

Taking as an example the gas concentration in the deep hot water at Wairakei, which is 0.032% by weight, the amount of gas to be pumped from the barometric condensers when a system operates at 75 lb/in² gauge wellhead pressure is (14.9 $10^6$ lb/h) (0.032/100) lb/h, giving a gas flow of 4,760 lb/h. In the early days of the Wairakei development, it seemed possible that the gas concentration in the entering steam might increase with time if the proportion of magmatic (volcanic) steam increased. However, it now appears that the preponderance of these gases originates in the hot water phase owing to accumulation over a time of the order of a million years, and with draw-off of the hot water in the aquifer, the actual concentration of such gases will decrease. A slow trend in this direction has been detected* over the years; it therefore appears that the number of gas exhausters initially

*The gas concentration (by weight) in the aquifer has decreased from 0.045% in 1959 to 0.032% in 1966 (R. B. Glover, pers.com).

designed for a power station similar to Wairakei would not have to be increased throughout the life of the field—rather the reverse.

Operating a hot water geothermal field, therefore, at the optimum wellhead pressure for a maximum power-life, not only reduces the draw-off rate of water fluid to a minimum but also of non-condensible gases, thus resulting in minimum gas pumping power.

## 6. EFFECT OF SOURCE FEEDS TO RESERVOIRS

The various optimisation curves have been determined for finite reservoirs; they are equally applicable, however, to fields where large mass draw-off leads to slow changes in the overall enthalpy of the system owing to possible variation in energy feeds from the volcanic source. These source fluctuations may be triggered by falling aquifer pressures (owing to draw-off) or, more likely, may be the result of a slow fall in fluid temperatures with time leading to a gradual increase in conductive heat flow from the lower volcanic rocks; for physical reasons, however, this latter effect is regarded as slight.

At Wairakei, of recent years, it has been found that there has been a decrease in enthalpy of the aquifer hot water together with a paradoxical increase in the average enthalpy of the boreholes. This is explained by falling water levels leading to a proportion of top steam being tapped by these boreholes through preferential fissures.

Changes in enthalpy from say 460 Btu/lb downwards (Fig. 1) have little effect on the optimum wellhead pressure, whereas changes in enthalpy upwards, although finally tending to a dry borehole optimum wellhead pressure as high as 100 lb/in² gauge (Fig. 5), would be drawing top steam from the aquifer, and Fig. 7 indicates that under this regime the wellhead should be designed for a final pressure as low as 50 lb/in² gauge.

Balancing these slightly different possible results leads to a reasonable terminal wellhead pressure of 75 lb/in² gauge as the final design criterion for all systems of enthalpy greater than 400 Btu/lb.

The effect of a feed into the system would be to increase the power-life without significantly affecting the optimum design pressure as determined for a finite "closed" system.

## 7. CONVENTIONAL COMPARED WITH GEOTHERMAL STATIONS

A comparison between the choice of turbine stop valve pressures adopted by modern power stations that use fuel fired boilers with that of geothermal stations that draw their steam from underground strata shows that a fundamentally different approach has to be made.

In conventional plant—fossil fuel fired or nuclear—the higher the turbine pressure the less steam used per kilowatt and therefore the less fuel used. This has led power station designers to strike a balance between the capital costs of technically advanced plant and the savings in fuel. Over the last 50 years, turbine pressures for coal fired plant have risen through a range from about 200 lb/in² gauge to that of a few supercritical stations, with a fall in fuel requirements from 3 to 0.56 lb/kWh. An advanced example of the latter type, such as the 5,000 lb/in² gauge, 1,200° F, supercritical plant at Eddystone, U.S.A., as described by Harlow (20) has a thermal efficiency of 42%. This is nearly equalled by the latest of nuclear reactors such as the advanced gas-cooled reactor of the U.K. Atomic Energy Authority, which operates* at 2,300 lb/in² gauge, 1,050° F, with a thermal efficiency of 41%. Broadly-speaking, the design of such "conventional" plant has tended towards maximum power output per unit mass of fuel used, commensurate with reasonable capital costs and interest rates.

The important point to notice with conventional plant is that higher turbine pressures give lower fuel consumption for a given power output.

With geothermal plants, where fuel costs are not involved, the important factor is the life of the aquifer from which the steam is taken; and this has been shown to be related to the choice of wellhead pressure. Wellhead pressure may be considered as the independent variable for a geothermal field, and where it is optimised for a maximum power-life, yearly drilling costs (which may be considered as analogous to the fuel costs of conventional plant) should be a minimum, as the least number of boreholes is needed for a given power output.

## 8. CONCLUSIONS

Taking into account the tentative capital costs of a geothermal scheme and the influence of wellhead pressure on the amount of energy derived from a reservoir of finite proportions (and it should be borne in mind that infinite systems do not exist), it is found that the optimum pressure for both superheated steam and hot water aquifers whose enthalpy exceeds 400 Btu/lb is within the narrow range 70 to 80 lb/in² gauge. This is close to the operating wellhead pressures employed at the superheated steam field at Larderello, Italy, and for the "low" pressure wet boreholes of Wairakei, New Zealand, and should not provide any startling new problems, technical or otherwise.

For large output wet boreholes, the optimum pressure of, say, 75 lb/in² gauge would be that of the cyclone separator and a throttling orifice would be necessary between the wellhead and the separator inlet to reduce the velocity of the steam-water mixture to that for efficient separation. This would result in the wellhead pressure being at some higher figure, which would provide a reserve amount at the wellhead for gradual reduction as the borehole pressure declines with time.

## 9. REFERENCES


(1) RUNCORN, S. K. (ed) (1961): *Continental Drift*. Academic Press, New York.

(2) HOLMES, A. (1965): *Principles of Physical Geology*. Nelson, London.

(3) LEE, W. H. K. (ed) (1965): *Monograph No. 8*. Am. Geophys. Union.


*According to a U.K.A.E.A. advertisement in *Scientific American*, March 1966.

(4) EINARSSON, S. S. (1961): Paper G.9. *Proc. U.N. Conf. New Sources of Power*, Rome.

(5) BRUCE, A. W. (1961): Paper G.8. *Proc. U.N. Conf. New Sources of Power*, Rome.

(6) MARIO, P. di (1961): Paper G.68. *Proc. U.N. Conf. New Sources of Power*, Rome.

(7) HALDANE, T. G. N., and ARMSTEAD, H. C. H. (1962): *Proc. Inst. Mech. Engrs, 176*, 603-48.

(8) BANWELL, C. J. (1963): *New Zealand J. Geol Geophys., 6*: 52-69.

(9) BANWELL, C. J. (1964): *New Zealand J. Geol. Geophys., 7*: 585-93.

(10) WHITE, D. E. (1965): *Circular 519*. U.S. Geological Survey.

(11) GRINDLEY, G. W. (1965): *Bulletin n.s. 75*. New Zealand Geological Survey.

(12) JAMES, R. (1965): Power-Life of a Hydrothermal System. *Proc. 2nd Austr. Conf. Hydraulics and Fluid Mech.*, Auckland.

(13) BURGASSI, R. (1961): Paper G.65. *Proc. U.N. Conf. New Sources of Power*, Rome.

(14) Smith, J. H. (1958): Production and Utilisation of Geothermal Steam. *New Zealand Engineering, 13* (10): 354-75.

(15) CONTINI, R. (1961): Paper G.71. *Proc. U.N. Conf. New Sources of Power*, Rome.

(16) HANSEN, A. (1961): Paper G.41. *Proc. U.N. Conf. New Sources of Power*, Rome.

(17) HALDANE, T. G. N., WOOD, B., and ARMSTEAD, H. C. H. (1958): Paper 21 C/1. *Proc. World Power Conf.*, Montreal.

(18) ELDER, J. W. (1965): *Monograph No. 8* (ed. W. H. K. Lee) pp. 211-39. Am. Geophys. Union.

(19) WHITE, D. E. (1963): *Science, 139*: 919-22.

(20) HARLOW, J. M. (1957): Paper 56-A165. *Trans. A.S.M.E.*

# AN EVALUATION OF JAMES' EMPIRICAL FORMULAE FOR THE DETERMINATION OF TWO-PHASE FLOW CHARACTERISTICS IN GEOTHERMAL WELL TESTING

P. Cheng and M. Karmarkar
University of Hawaii
Honolulu, Hawaii 96822

## Introduction

One of the most economical and simple methods of determination of two-phase flow parameters in geothermal well testing is the so-called James' method [1,2]. The method consists of the measurements of lip pressure (p), and the flow rate of water (w) by a conventional weir. The stagnation enthalpy ($h_o$) is then determined from a plot showing $h_o$ versus $w/p^{0.96}$ which is empirically determined by James [1,2]. The mass flow rate is then determined from the following empirical formula

$$G = 11{,}400 \frac{p^{0.96}}{h_o^{1.12}} \qquad (1)$$

where G is the total mass flow rate in $lb_m/sec\text{-}ft^2$, p is the lip pressure in psia, and $h_o$ is the specific enthalpy in $BTU/lb_m$. The above relation is empirically determined for discharge pressure up to 64 psia and pipe diameters up to 8". For pipe diameters smaller than 0.2", it has been suggested that the value of 11,400 be replaced by 12,800. Although the James' method has been widely used in many of the geothermal well testing programs, its accuracy and the range of applicability has never been assessed from a theoretical point of view.

## Two-Phase Critical Flow Theory

In this paper the accuracy of James' method will be assessed in the light of Fauske's two-phase critical flow theory [3]. Fauske suggested that in two-phase flow the maximum discharge rate may not necessarily be accomplished by a shock front. He proposed that at the critical flow condition the absolute value of the pressure gradient at a given location is maximum but finite for a given flow rate or quality, i.e.,

$$(dp/dz)_{G,x} = \text{maximum and finite} \quad . \qquad (2)$$

where z is the coordinate along the streamwise direction, and x the quality of the saturated mixture.

Under the assumptions of (i) annular flow pattern, (ii) two-phases in thermal equilibrium, (iii) negligible frictional loss, and (iv) one-dimensional steady flow, Fauske [3] obtained the following analytical expression for the critical flow rate of a saturated mixture:

$$G_{critical} = \left[-g_c k/((1-x+kx)\ x\ (dv_g/dp) + (v_g(1+2kx-2x) + v_f(2xk-2k-2xk^2+k^2))dx/dp\right]^{1/2} \quad (3)$$

where $g_c = 32.2\ \frac{lb_m\text{-}ft}{lb_f\text{-}sec^2}$ and $k = (v_g/v_f)^{1/2}$ with $v_g$ and $v_f$ denoting the specific volume of the saturated vapor and liquid respectively. Thus, the critical flow rate can be calculated from Eq.(3) if the steam quality and the lip pressure are known.

The corresponding stagnation enthalpy can be determined from

$$h_o = h_f(1-x) + h_g x + (G^2/2g_c)((x^3 v_g^2/Rg^2) + (1-x)^3 v_f^2/(1-Rg)^2)/J \quad , \quad (4)$$

where $R_g$ is the gas void fraction which is related to steam quality[4]. In comparison with experimental data, Levy [4] found, however, that using Eq.(4) for the computation of $h_o$ would lead to under-prediction of the mass flow rate. For this reason we shall compute the stagnation enthalpy on the basis of a homogeneous model, i.e.,

$$h_o = h_f(1-x) + h_g x + G^2 v_h^2/2g_c J \quad , \quad (5)$$

where $v_h = v_f(1-x) + v_g x$ and $J = 778$ ft-$lb_m$/BTU.

The weir flow rate is then determined from

$$w = G(1 - x) \quad . \quad (6)$$

## Results and Discussion

For a given set of values of lip pressure and steam quality and with the data of saturated steam-water properties [5], Eq.(3) can be used for the computation of total mass flow rate G. The stagnation enthalpy and the weir flow rate are then determined from Eqs.(5) and (6). The results of the computations for the lip pressure from 14.7 psia to 200 psia for geothermal well testing applications are plotted in Figs. 1 and 2. When the lip pressure and the weir flow rate are measured in a geothermal well test, the stagnation enthalpy of the reservoir, the steam quality at the well head, and the total mass flow rate can easily be determined from these plots.

To assess the accuracy of the James' method, calculations were carried out for five different sets of lip pressure and weir flow rate using James' empirical formulae and Fauske's theoretical prediction (i.e., Figs. 1 and 2). The results for total mass flow rate, the stagnation enthalpy, and the steam quality are tabulated in Table 1 for comparison. It is shown that the results based on the two methods differ within 2%.

## References


1. James, R., "Measurement of Steam Water Mixtures Discharging at the Speed of Sound to the Atmosphere," New Zealand Engineering, pp. 437-441 (1966).

2. James, R., "Steam-Water Critical Flow Through Pipes," Proc. Inst. Mech. Engrs., v. 176, pp. 741-748 (1962).

3. Fauske, H., "Contribution to the Theory of Two-Phase, One Component Critical Flow," Argonal National Laboratory, Rept. No. ANL-6633 (1962).

4. Levy, S., "Prediction of Two-Phase Critical Flow Rate," A.S.M.E. Paper 64-HT-8.

5. Keenan, J. and Kays, Keys, F. G., Steam Tables, John Wiley and Sons, Inc., New York, N. Y. (1969).

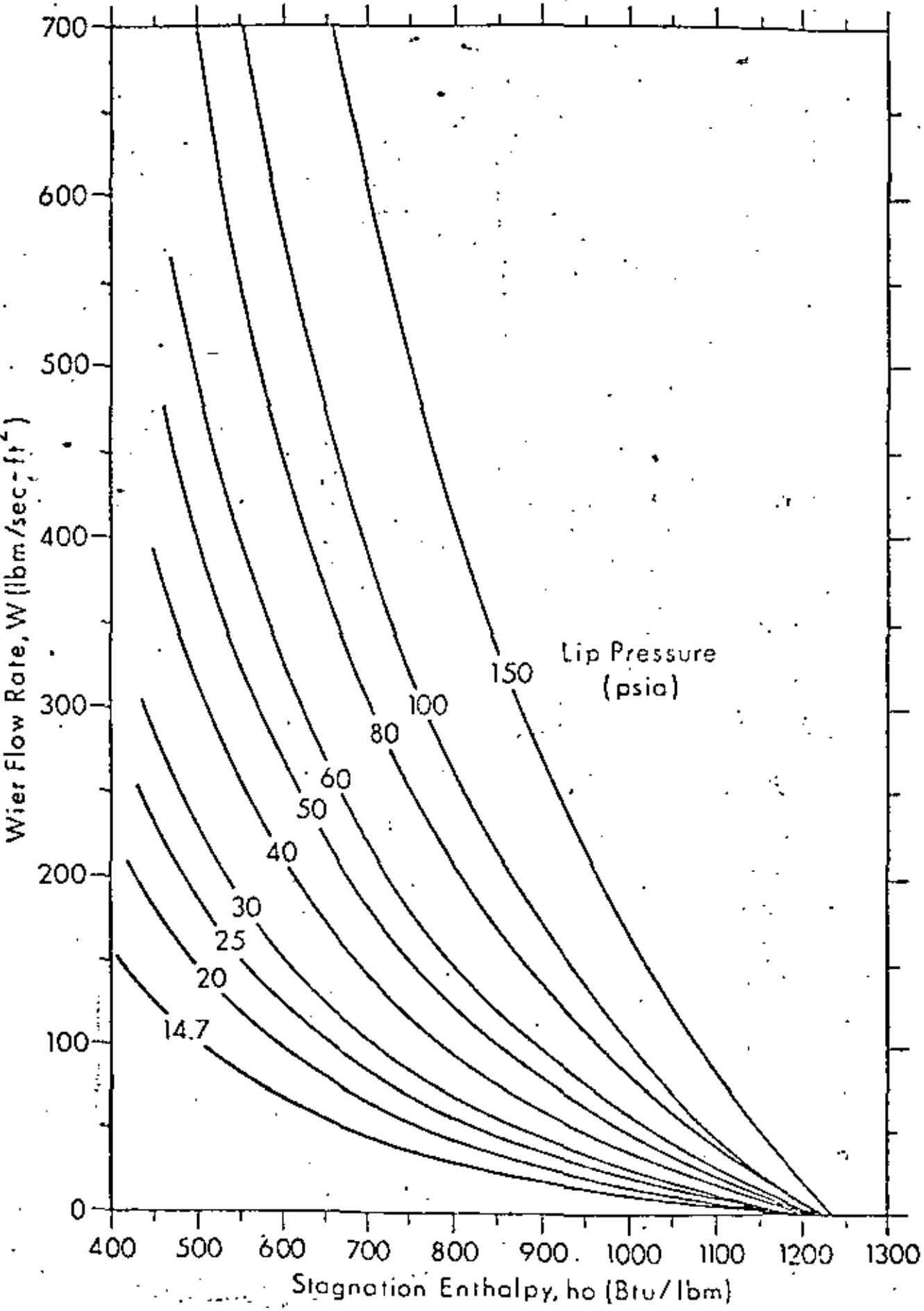


Figure 1. Weir Flow Rate vs Stagnation Enthalpy at Selected Values of Lip Pressure According to Fauske's Theory

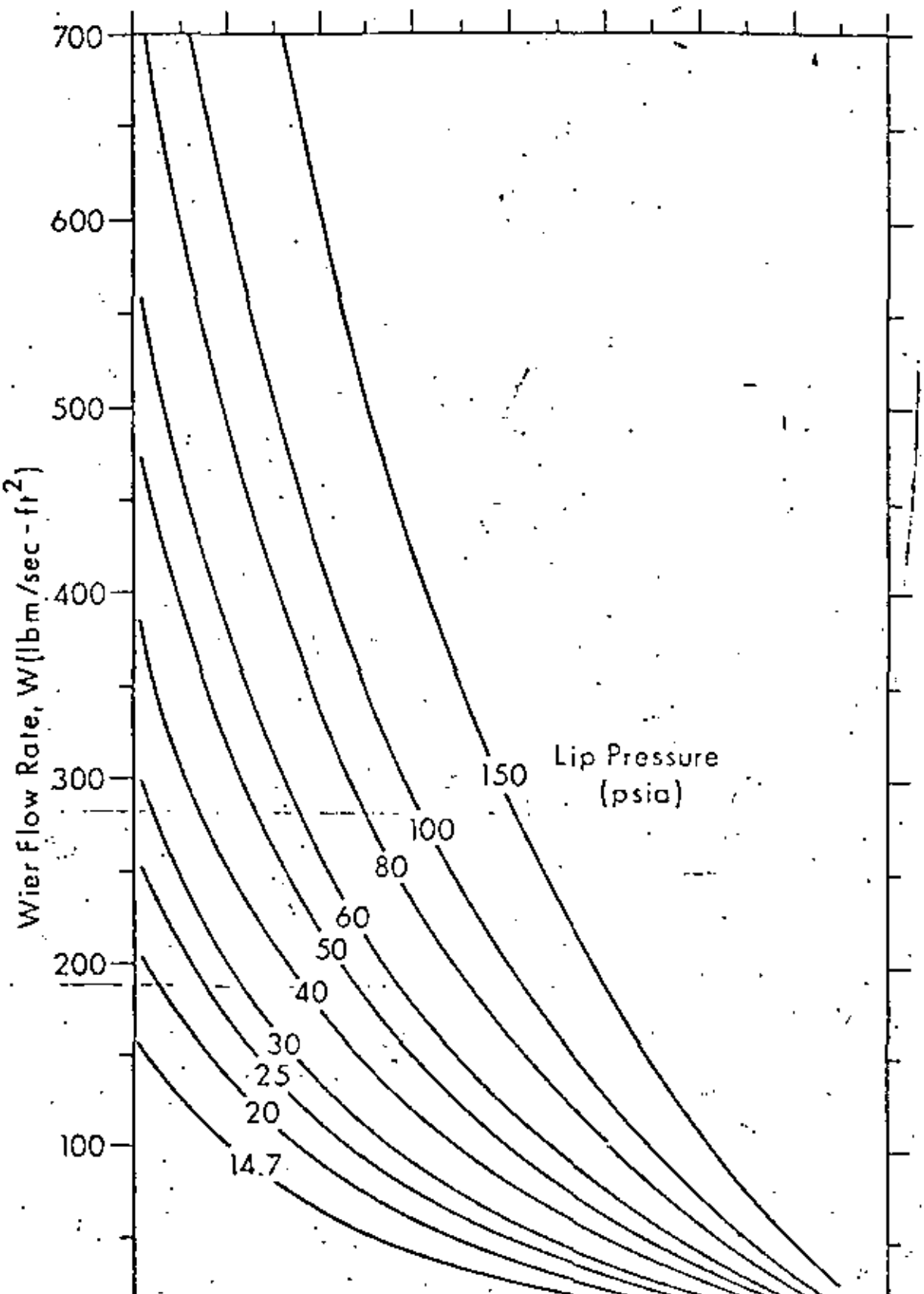


Figure 2. Weir Flow Rate vs Steam Quality at Selected Values of Lip Pressure According to Fauske's Theory

Table 1. COMPARISON OF RESULTS BASED ON THE JAMES' METHOD AND FAUSKE'S ANALYTICAL MODEL

| Case | p (psia) | w ($lb_m/sec\text{-}ft^2$) | $h_o$ BTU/$lb_m$ | G $lb_m/sec\text{-}ft^2$ | x | Method |
|---|---|---|---|---|---|---|
| 1 | 14.7 | 40 | 736.90 | 88.44 | .54 | Fauske (F) |
| | | | 800.00 | 95.13 | .58 | James (J) |
| 2 | 25.0 | 85.5 | 698.78 | 164.59 | .48 | F |
| | | | 750.00 | 170.06 | .50 | J |
| 3 | 60.0 | 226.0 | 697.79 | 403.39 | .44 | F |
| | | | 715.00 | 415.42 | .46 | J |
| 4 | 100.0 | 105.0 | 1004.52 | 419.84 | .75 | F |
| | | | 985.00 | 476.60 | .78 | J |
| 5 | 150.0 | 53.0 | 1148.87 | 523.41 | .90 | F |
| | | | 1130.00 | 590.00 | .90 | J |

Part 6

# Vertical and Inclined-Flow Correlations

Engineering judgment is necessary to adapt two-phase vertical and inclined-flow pressure-drop correlations to situations not covered by them. Existing vertical-flow correlations cover only small-diameter pipes, while for inclined flow the inclination range encompassed is narrow.

ANTHONY E. DeGANCE and ROBERT W. ATHERTON, Brown & Root, Inc.*

In Part 4 of this series, the available methods of calculating the pressure gradient in two-phase, horizontal flow were discussed. Part 5 then presented a mechanical-energy balance by means of which a general theoretical pressure-gradient expression—valid for any conduit orientation and independent of flow regime—was derived. Now we will consider inclined two-phase flow and its variation of vertical flow.

We will not merely present design equations into which numbers may be substituted, but will show how the equations may be modified and applied better to unusual physical situations. The relations presented are for computing the pressure gradient, $\partial P/\partial Z$. To compute a line profile, the algorithm discussed in Part 1 (*Chem. Eng.*, Mar. 23, 1970, p. 139) must be used.

The need for design information on inclined flow can be quickly appreciated by noting that last year a total of 917 mi. of pipeline was installed off the U.S. coast alone for oil-gas gathering systems. Since the flow in these lines is neither vertical nor horizontal, the development by Bonnecaze is of value because it covers a relatively important, though small, range of angles of inclination (−10 to 10°). Most, if not all offshore pipelines fall within this range. In process design, however, a greater variety of angles are encountered, for which a more general correlation is necessary.

Unfortunately, in contrast to horizontal and vertical flow, there are only two correlations for inclined flow with which to compare: Flanigan's and Bonnecaze's. Flanigan proposed a correlation—independent of pipeline inclination—for liquid-head efficiency in an inclined column, as a function of superficial gas velocity. The liquid-head efficiency (or factor), when multiplied by the pressure head of a full column of liquid, yields the static-pressure loss in the column. Flanigan's efficiency is a form of holdup.

Effort has not been spent equally over the entire possible angles of inclination ($\theta$ values from −90 to + 90°). Instead, attention has been devoted almost exclusively to upward vertical flow ($\theta = 90°$).

To engineers in petroleum production,[2,7] such focusing of attention will not seem improper because of the vertical upward flow of petroleum through an oil-well bore. But to other engineers, it is unfortunate that general conduit orientations have received little study, and that there is no good correlation for the entire range of inclined flow.

Faced with preparing estimates for conduit orientations other than vertical upward, we have provided pressure-loss computation methods based on mechanical-energy balances. These methods parallel the development by Dukler of his equations for horizontal flow, Case I and Case II, but their accuracy has yet to be rigorously determined.

For vertical two-phase flow ($\theta = 90°$), large amounts of experimental data are available, which have been correlated. Petroleum production engineers, working with such correlations in conjunction with oil-well data, obtain accuracy to within 10% for their physical systems. However, these methods are restricted to pipe diameters found in oil wells. A "large" diameter for such correlations is 3.5 in.

The best vertical-flow correlation, Orkiszewski's,

* To meet the authors, see *Chem. Eng.*, Mar. 23, 1970, p. 139.

## Nomenclature

| | |
|---|---|
| $AC$ | Acceleration term, $G_t V_{sg}/g_c P$ |
| $C_n$ | Parameter, defined by Eq. (62) |
| $D$ | Conduit hydraulic dia., ft. |
| $f$ | Friction factor of flowing fluid phase |
| $f_o$ | Friction factor, defined by table Eq. (4-B) |
| $Fr_B$ | Bonnecaze's Froude number, Eq. (10) |
| $g$ | Local acceleration, ft./(sec.) (sec.) |
| $g_c$ | Gravitational constant, 32.174(lb.)$_{mass}$ (ft.)/(lb.)$_{force}$ (sec.)$^2$ |
| $G_t$ | Total superficial mass flux, lb./(sq.ft.) (sec.) |
| $N_{gv}$ | Gas-velocity number, Eq. (57) |
| $N_{lv}$ | Liquid-velocity number, Eq. (58) |
| $P$ | Pressure, lb./sq.ft. |
| $P'$ | Pressure, psia. |
| $Re_B$ | Bonnecaze's Reynolds number, Eq. (9) |
| $Re_t$ | Bubble-rise Reynolds number, Eq. (31) |
| $Re_{tt}$ | Bubble-rise, slug-flow Reynolds number, Eq. (34) |
| $R_l$ | Inplace liquid holdup |
| $R_{lB}$ | Bonnecaze's liquid holdup, Eq. (6) |
| $R_{lo}$ | Orkiszewski's liquid holdup, Eq. (26) |
| $t_t$ | Transition-flow parameter, Eq. (44) |
| $V$ | Velocity, ft./sec. |
| $V_t$ | Bubble rise-velocity, ft./sec. |
| $Z$ | Conduit length, ft. |
| $\partial P/\partial Z$ | Pressure gradient, (lb./sq.ft.)/ft. |
| **Greek Letters** | |
| $\alpha$ | Conduit slope, sine $\theta$ |
| $\gamma$ | Parameter, defined by Eq. (37) |
| $\epsilon$ | Absolute roughness, Eq. (47) to (49) |
| $\theta$ | Conduit horizontal angle of inclination |
| $\lambda$ | Flowing volume holdup of liquid |
| $\mu$ | Viscosity, (lb.)$_{mass}$/(sec.)/sq.ft. |
| $\rho$ | Density, lb./cu.ft. |
| $\sigma$ | Surface tension, dynes/sq.cm. |
| $\tau_f$ | Partial derivative of pressure with respect to $Z$ of friction contributions |
| $\psi$ | Parameter, defined by Eq. (61) |
| **Subscripts** | |
| $A$ | Arrhenius |
| $abs$ | Absolute |
| $B$ | Bonnecaze |
| $cs$ | Constant slip |
| $f$ | Friction |
| $g$ | Gas |
| $gV$ | Gas velocity |
| $l$ | Liquid |
| $ns$ | No-slip or homogeneous |
| $hold$ | Holdup |
| $lV$ | Liquid velocity |
| $obs$ | Observed |
| $Ob$ | Orkiszewski's bubble flow |
| $Om$ | Orkiszewski's mist flow |
| $Os$ | Orkiszewski's slug flow |
| $Ot$ | Orkiszewski's transition flow |
| $sec$ | Secondary |
| $t$ | Total |
| $Sg$ | Superficial gas |
| $Sl$ | Superficial liquid |
| $tp$ | Two-phase constant slip |

is twice as accurate as the best one for horizontal flow (Dukler's constant slip) because of the tremendous amount of data used in the correlation, and because accurate flow-regime boundaries could be defined. But for diameters greater than 5 in., oil-well data correlations should not be expected to retain their accuracy; thus, a general correlation is needed for conduits having larger diameters.

We will first present the general correlations (independent of flow regime) for inclined flow, and then the Bonnecaze method for slug flow, with $\theta$ in the range of −10 to 10°. The most-accurate methods for vertical flow (Hagedorn-Brown's and Orkiszewski's) are presented next. Part 7 of the series will contain sample calculations for all the methods presented in Parts 4, 5 and 6.

The following conventions will be used:

The angle $\theta$ is the acute horizontal angle of inclination, positive when the direction of flow is upward, negative when downward. Therefore, the parameter $\alpha = \sin\theta$ has the proper sign to account for the effect of change in elevation on the total pressure gradient.

## TOTAL PRESSURE-GRADIENT CALCULATION METHODS

This section of the article discusses: (1) the equations applicable to the homogeneous and constant-slip types of inclined and vertical flow; and (2) equations applicable for various flow regimes, also for vertical or inclined flow.

*Homogeneous Flow*—In Part 4 of the series, this equation was derived for homogeneous flow:

$$\partial P/\partial Z = -[(\tau_f)_{ns} + \alpha\rho_{ns}g/g_c]/(1 - AC_{ns}) \quad (1)$$

The relations for evaluating the equation, derived in previous installments, are shown in the table.

Eq. (1) is the simplest one for pressure gradient in this installment, and the only one simple enough for hand use. It is adequate for any orientation: horizontal flow, $\alpha = 0$; vertical upward, $\alpha = 1$; vertical downward, $\alpha = -1$; and inclined, $\alpha = \sin\theta$, where the angle sign determines the sign of $\alpha$.

Since homogeneous flow provides the most conservative estimate of pressure for a given configuration, Eq. (1) is useful for a check or first estimate, as well as for accurate estimates of $\partial P/\partial Z$.

The easiest way of obtaining variations of Eq. (1) is by choosing friction factors in the calculation of $\tau_{ns}$, as in Eq. (4-B), in the table. This equation has the major advantage of being an explicit expression for $f_o$, although this term is a "smooth-tube" friction factor that does not correct for roughness. An equation that does consider roughness (table, 6-B) was presented in Part 4, and may be used just as consistently, although its solution requires iteration.

*The Extended Homogeneous Case*—As indicated in Part 5, Eq. (1) may be easily modified, to provide a more accurate estimate, by using a different definition of density. The main reason for using a model

## Summary of Correlations for Two-Phase Vertical and Inclined Flow

### A—DUKLER'S RESULTS AND APPLICATIONS

**Case I, No-Slip**

$$\mu_{ns} = \mu_l\lambda + \mu_g(1-\lambda) \quad (1\text{-A})$$

$$\rho_{ns} = \lambda\rho_l + \rho_g(1-\lambda) \quad (3\text{-A})$$

$$Re_{ns} = G_t D/\mu_{ns} \quad (5\text{-A})$$

$$Eu_{ns} = \frac{(\partial P/\partial Z)_{fg}\,\rho_{ns}\,D}{G_t^2} \quad (7\text{-A})$$

$$(\tau_f)_{ns} = f_{ns}G_t^2/2g_c\rho_{ns}D \quad (9\text{-A})$$

**Case II, Constant-Slip**

$$\mu_{ls} = \mu_l\lambda + \mu_g(1-\lambda) \quad (2\text{-A})$$

$$\rho_{ls} = \rho_l(\lambda^2/R_l) + \rho_g[(1-\lambda)^2/(1-R_l)] \quad (4\text{-A})$$

$$Re_{ls} = \rho_{ls}DV_{ns}/\mu_{ls} \quad (6\text{-A})$$

$$Eu_{ls} = \frac{(\partial P/\partial Z)_{fg}\,\rho_{ns}\,D}{G_t^2[(\rho_l/\rho_{ns})(\lambda^2/R_l) + (\rho_g/\rho_{ns})(1-\lambda)^2/R_g} \quad (8\text{-A})$$

$$(\tau_f)_{ns} = \frac{f_{ls}G_t^2[(\rho_l/\rho_{ns})(\lambda^2/R_l) + (\rho_g/\rho_{ns})(1-\lambda)^2/R_g}{2g_c\rho_{ns}D} \quad (10\text{-A})$$

### B—RELATIONS FOR CALCULATING $f_{ls}$

$$f_{ls} = a(\lambda)f_n \quad (1\text{-B})$$

$$a = 1.281 + 0.4781\log\lambda + 0.444(\log\lambda)^2 + 0.094(\log\lambda)^3 + 0.00843(\log\lambda)^4 \quad (3\text{-B})$$

$$f_{ns} = \left[2\log\left(\frac{Re_{ns}}{4.5223\log Re_{ns} - 3.8215}\right)\right]^{-2} \quad (5\text{-B})$$

$$a(\lambda) = 1.0 - (\log\lambda/a) \quad (2\text{-B})$$

$$f_n = \left[2\log\left(\frac{Re_{ls}}{4.5223\log Re_{ls} - 3.8215}\right)\right]^{-2} \quad (4\text{-B})$$

$$1/f_n^{1/2} = -2\log[(\epsilon/3.7D) + (2.51/Re_{ls}f^{1/2})] \quad (6\text{-B})$$

### C—TOTAL PRESSURE GRADIENT FROM MECHANICAL-ENERGY BALANCE

**Case I, No-Slip**

$$\partial P/\partial Z = -[(\tau_f)_{ns} + a\rho_{ns}(g/g_c)]/(1 - AC_{ns}) \quad (1\text{-C})$$

$$AC_{ns} = G_tV_{sg}/g_cP \quad (3\text{-C})$$

**Case II, Constant-Slip**

$$\partial P/\partial Z = -[(\tau_f)_{ns} + a\rho_{ns}(g/g_c)]/(1 - AC_{ns}) \quad (2\text{-C})$$

$$AC_{ns} = -G_x^2/(g_cR_gP\rho_g) \quad (4\text{-C})$$

$$AC_{ns} = \left[\frac{G_lV_{sl}}{R_l} + \left(\frac{G_gV_{sg}}{R_g}\right)\left(1 - \frac{R_l}{R_g}\right)\right]\left(\frac{1}{g_cP}\right) \quad (5\text{-C})$$

such as homogeneous flow is to gain an estimate of the pressure gradient. Even though using an expression for two-phase-flow density other than $\rho_{ns}$ is inconsistent with the model, such an expression does represent an extrapolation based upon engineering insight, and can greatly improve the accuracy of the equation.

Rewriting Eq. (1) with an improved density $\rho_{ls}$:

$$\partial P/\partial Z = -[(\tau_f)_{ns} + a\rho_{ls}g/g_c]/(1 - AC_{ns}) \quad (2)$$

Physically, $\rho_{ls}$ represents the fluid density necessary to obtain a given pressure change, less the change due to friction and acceleration. For inclined or vertical pipe, $\rho_{ls}$ is nearly always significantly greater than $\tau_f$, and only at high gas velocities—where friction and acceleration loss predominates—is the reverse true.

The simplest definition of $\rho_{ls}$ is analogous to $\rho_{ns}$, replacing $\lambda$ with the *in situ* holdup $R_l$:

$$\rho_{ls} = R_l\rho_l + (1 - R_l)\rho_g \quad (3)$$

To compute $\rho_{ls}$, a reliable holdup correlation for the given flow configuration is needed. One method for determining $R_l$ empirically is to measure the pressure gradient $\partial P/\partial Z$, define friction and acceleration terms, and then back-calculate holdup from the data. This method, which shows the significance of the extended case, is explained in the discussion of Hagedorn-Brown's holdup correlation. Combined with Eq. (2) and (3), this correlation should give very good results.

A holdup correlation should be chosen carefully. Holdup is correlated by flow properties and, usually, is a function of conduit configuration. A correlation for vertical flow upward, such as gas lift, may not be useful for flow downward at 15° ($\theta = -15°$). However, if a holdup correlation representing the proper flow configuration is found, Eq. (2) and (3) should give an improved estimate of the pressure derivative.

*Constant-Slip Case*—As derived in previous installments, the equation for the total pressure gradient consistent with the assumption of constant slip is:

$$\partial P/\partial Z = -[(\tau_f)_{ns} + a\rho_{ns}g/g_c]/(1 - AC_{ns}) \quad (4)$$

The equations that allow use of this relation are presented in the table, parts A, B and C. Again, judgment may be exercised in choosing friction-factor equations, holdup correlations and acceleration terms. The discussion of friction factor in the homogeneous-flow section still applies. Any of the three acceleration terms in the table may be used, although the homogeneous acceleration term provides the most conservative estimate. Eq. (5-C), in the table, yields the most accurate estimate of the effect of acceleration on the total pressure gradient. The acceleration term is most significant for mist flow.

Eq. (4) is more accurate than the previous homogeneous expression. We do not have a precise estimate of its accuracy, which should vary with the application. However, with holdup equations such as Hughmark's or Bonnecaze's, the expression may have

an accuracy of the same order as Dukler's equation for horizontal flow. Dukler's Case II (constant slip) relation is accurate to within ±20%.

## Bonnecaze's Correlation

Bonnecaze[1] and coworkers have developed a correlation for inclined flow for angles from −10 to +10°. The researchers' development is based upon the premise that the slug-flow regime predominates; and their expressions for holdup and pressure gradient take advantage of that fact (slug flow is discussed ahead). In general, the correlation appears reasonably founded and suitable for use with moderate inclinations. This expression is given:

$$\partial P/\partial Z = R_{ls}(\rho_{ns}/g_c + \rho_s f_s V_{ss}^2/2g_c D) \quad (5)$$

where $R_{ls} = (n - n_f)/(1 - n_f) \sim l_s/l_t$ (6)

$l_s$ = liquid-slug length; $l_t$ = total slug length, gas-pocket plus liquid-slug lengths:

$$n = 1 - (1 - \lambda)/\left[1.20 + 0.35\left(1 - \frac{\rho_s}{\rho_l}\right)\delta/Fr_s^{1/2}\right] \quad (7)$$

where $\delta$ is 0 for horizontal flow, 1 for upward inclined flow, and −1 for downward inclined flow.

$$f_s = 0.0192 + 15{,}920/Re_s^{1.155} \quad (8)$$

The liquid Reynolds and Froude numbers are:

$$Re_s = 1{,}488\rho_l D V_{ss}/\mu_l \text{ and } Fr_s = V_{ss}^2/gD \quad (9),(10)$$

where $y$ and $n_f$ must satisfy the equations when $\delta \neq 0$:

$$n_f = (1/\pi)[\cos^{-1}(1 - y) - (1 - y)y^{1/2}(2 - y)^{1/2}] \quad (11)$$

$$2\pi(\sin\theta)_{ns}n_f^2 - f_s Fr_s(0.2 - 1.2n_f)^2\cos^{-1}(1 - y) = 0 \quad (12)$$

Here, $y = 2s/D$, where $s$ = height of liquid in the gas pocket; $s/D$ is therefore physically restricted to lie between 0 and 1. For the special case of $\delta = 0$, Eq. (12) does not apply. Bonnecaze suggests setting $R_l = \lambda$, a reasonable assumption in view of the Hubbard analysis on slug flow (p. 93).

Despite the formidable appearance of Eq. (5) to (12), the Bonnecaze equation is merely a special case of Eq. (3), with a new empirical holdup equation specifically for slug flow. By neglecting the vapor density, the two-phase density of Eq. (2) becomes, according to Bonnecaze:

$$\rho_s = R_{ls}\rho_l \quad (13)$$

By considering only the contribution of the liquid slug to the frictional pressure drop, and defining a new slug friction factor, $\tau$ becomes:

$$(\tau_f)_s = \rho_s f_s V_{ss}^2/2g_c D \quad (14)$$

Eq. (10) is seen to be merely Eq. (2-C) in the table, with Bonnecaze's simplified terms. Finally, since acceleration is important only in the mist-flow regime, the acceleration term is neglected; Eq. (5) is then a special case of Eq. (3).

The significance of Bonnecaze's work is the development of empirical holdup- and friction-factor correlations from actual inclined-flow data. Eq. (5) predicts well both the original data and field data for the values of $\theta$ studied.

Hubbard[10] has shown that the contribution of $n_f$ to holdup is negligible for horizontal flow. Because neglecting this term—whose contribution to holdup may indeed be small—the authors prefer to equate $n$ to $R_l$.

$$R_{ls} = 1 - V_{sg}/[1.20V_m + 1.98\sqrt{gD(\rho_l - \rho_g)/\rho_l\delta}] \quad (15)$$

Eq. (5) to (15) completely define the Bonnecaze expression for the total pressure gradient, $\partial P/\partial Z$.

## Orkiszewski's Correlation

J. Orkiszewski has presented the most accurate method of calculating the pressure gradient for pure vertical flow upward in small-diameter pipes. The experimental work upon which the correlation is based included data up to 3-in.-dia. pipe, and some 8-in. Thus, the Orkiszewski correlaton is valid for pipe diameters greater than 3.5 in.

In general, this section follows Orkiszewski's work. We have rearranged the equations in many cases to simplify computation and make them consistent with previous developments. Orkiszewski's approach is to take the basic mechanical-energy balance equation:

$$\partial P/\partial Z = (\tau_f + \rho_{ns}g/g_c)/(1 - AC) \quad (16)$$

and make use of flow-regime knowledge and a great deal of empirical data to establish his relations for $\tau_f$, $\rho_{ns}$ and $AC$.

The large amount of data enables the establishment of reliable flow-regime boundaries, for Orkiszewski combined the results of Griffith and Wallis, Duns and Ros, and Nicklin et al. He compared the results of each pressure-drop formulation with his bank of petroleum-production data, and then chose the best method to include in his correlation; or if none was accurate enough, he developed relations of his own.

## Flow-Regime Boundaries, Pressure Gradients

Orkiszewski defines these flow-regime parameters:

$$N_{lb} = 1.071 - 0.2218V_m^2/D \quad (17)$$

$$N_{lv} = 50 + 70V_{sl}(\rho_l/\sigma)^{1/4} \quad (18)$$

$$N_{lm} = 75 + 138[V_{sl}(\rho_l/\sigma)^{1/4}]^{0.75} \quad (19)$$

where $N_{lb}$, $N_{lv}$ and $N_{lm}$ are bubble, slug- and mist-flow numbers. The gas-velocity-number equation is:

$$N_{gv} = 1.938V_{sg}(\rho_l/\sigma)^{1/4} \quad (20)$$

The flow regimes are then defined as follows:

*Bubble flow* exists when $V_{sg}/V_m < N_{lb}$ (21)

*Slug flow* when $V_{sg}/V_m > N_{lb}$ and $N_{gv} < N_{lv}$ (22)

*Transition flow* when $N_{lv} > N_{gv} > N_{lb}$ (23)

*Mist flow* when $N_{gv} > N_{lm}$ (24)

For calculating vertical pressure gradients, different Orkiszewski equations apply for each regime:

*Vertical Bubble Flow*—For this regime, the two-phase density is

$$\rho_{ns} = R_{wl} + (1 - R_l) \quad (25)$$

with $R_l$ given by:

$$R_l = 0.5 - 0.625V_m + [(0.5 + 0.625V_m)^2 - 1.25V_{sl}]^{1/2} \quad (26)$$

then,

$$Re_m = 1{,}488\rho_l D V_{sl}/\mu_l R_l \quad (27)$$

and

$$(\tau_f)_m = f_{lp}\rho_l(V_{sl}/R_l)^2/2g_c D \quad (28)$$

where $f_{tp}$ is calculated from Eq. (6-B) in the table, using $Re_{Os}$ as defined above.

*Vertical Slug Flow*—The complicated slug-flow pressure-gradient calculations involve more empirical constants than bubble flow. Slug-flow density is:

$$\rho_{Ol} = (G_l + \rho_l V_r)/(V_m + V_r) + \rho_{gl} \quad (29)$$

where $V_r$ is the bubble-rise velocity. The slug-flow Reynolds number is: $Re_{Ol} = 1{,}488\rho_{ll}DV_m/\mu_l$ (30)

and the bubble-rise $Re$: $Re_t = 1{,}488V_rD\rho_{ll}/\mu_l$ (31)

Defining the quantities $N_1$ and $N_2$ as:

$$N_1 = (0.372 \times 10^6)[-0.35 + (0.1225 + 0.04931V_m/D^{0.5})] \quad (32)$$

$$N_2 = (0.3721 \times 10^6)[-0.546 + (0.2931 + 0.01849V_m/D^{0.5})] \quad (33)$$

then $V_r$ is calculated as follows:

if $Re_{Ol} > N_1$, $V_r = (1.985 + 4.985 \times 10^{-4}Re_{Ol})D^{0.5}$ (34)

if $Re_{Ol} < N_1$, $V_r = (3.097 + 4.958 \times 10^{-5}Re_{Ol})D^{0.5}$ (35)

if $N_2 > Re_{Ol} > N_1$, then:

$$V_r = 0.5[\gamma + (\gamma^2 + 13.59\mu_l)/\rho_l D^{0.5})^{0.5}] \quad (36)$$

$$\gamma = (1.423 + 4.958 \times 10^{-4}Re_{Ol})D^{0.5} \quad (37)$$

The parameter $\Gamma$ is evaluated from these relations:

if $V_m < 10$, $\Gamma = [0.0127 \log(\mu_l + 1)]/D^{1.415} - 0.284 + 0.167 \log V_m + 0.113 \log D$ (38)

if $V_m > 10$, $\Gamma = [0.0274 \log(\mu_l + 1)]/D^{1.371} + 0.161 + 0.569 \log D - [[0.01 \log(\mu_l + 1)]/D^{1.571} + 0.397 - 0.63 \log D]\log V_m$ (39)

The limiting values of $\Gamma$ for the above cases are: for $V_m < 10$, $\Gamma \geqq -0.065\ V_m$; and for $V_m > 10$, $\Gamma \geqq V_r(G_l - V_m)/[(V_r + V_m)(V_r + V_m + 1)]$

These constraints eliminate pressure discontinuity between flow regimes. Finally, $(\tau_f)_{Ol}$ is computed:

$$(\tau_f)_{Ol} = (f_{tp}\rho_l V_m^2/2g_cD)[(V_{sl} + V_r)/(V_m + V_r) + \Gamma] \quad (40)$$

where $f_{tp}$ is again obtained from a conventional Colebrook friction-factor equation using $Re_{Os}$ as defined above.

*Transition Flow*—For this regime, Orkiszewski suggested the averaging procedure:

$$\rho_{ol} = f_{tl}\rho_{Ol} + (1 - f_{tl})\rho_{Om} \quad (41)$$

$$(\tau_f)_{ol} = f_{tl}(\tau_f)_{Ol} + (1 - f_{tl})(\tau_f)_{Om} \quad (42)$$

That is, the density and friction-gradient terms for transition flow are an average of the respective terms for the slug and mist-flow regimes. The equations above, however, are equivalent to averaging the pressure gradient for each flow regime:

$$(\partial P/\partial Z)_{ol} = f_{tl}(\partial P/\partial Z)_{Ol} + (1 - f_{tl})(\partial P/\partial Z)_{Om} \quad (43)$$

where $f_{tl} = (N_{lm} - N_{ll})/(N_{lm} - N_{ll})$ (44)

*Mist Flow*—The calculation of $(\partial P/\partial Z)$ for mist flow is analogous to that for bubble flow, with the density term defined to be the no-slip density, $\rho_m$. The frictional pressure gradient is defined as a gas friction-loss term:

$$(\tau_f)_{Om} = f_{tp}\rho_g V_{sg}^2/2g_cD \quad (45)$$

with the friction factor calculated from the gas Reynolds number:

$$Re_{sg} = 1{,}488\rho_g DV_{sg}/\mu_g \quad (46)$$

A correction term for relative roughness, $\epsilon/D$, is applied where $\epsilon$ is the absolute roughness developed by Duns and Ros: $10^{-3} \leqq \epsilon/D \leqq 0.5$.

Defining $N_{\sigma} = (4.52 \times 10^{-5})(V_{sg}\rho_l/\sigma)^{0.5}(\rho_g/\rho_l)$ (47)

if $N_{\sigma} > 0.005$, $\epsilon/D = 4.15\sigma(N_{\sigma})^{0.302}/(\rho_g V_{sg}^2 D)$ (48)

if $N_{\sigma} < 0.005$, $\epsilon/D = 0.504\sigma/(\rho_g V_{sg}^2 D)$ (49)

where $f_{tp}$ is calculated using $\epsilon/D$, $Re_{sg}$ and the Colebrook equation.

## The Correlation of Hagedorn and Brown

This correlation, which represents a very large amount of data collected for pipe between 1 and 2-in. dia., is not flow-regime dependent, but it is accurate over the range of conditions of the data.[2, 3, 7]

While the Hagedorn and Brown calculation procedure represents years of work, the correlation does not reflect a detailed analysis of two-phase flow. Basically, their calculation procedure is the extended homogeneous case. They have assumed the homogeneous expression for the total pressure gradient, Eq. (3), except that an Arrhenius viscosity is not defined.

Hagedorn and Brown's major contribution is their holdup correlation for vertical flow. They did not measure holdup experimentally; rather, they measured the pressure gradient, and calculated the holdup necessary for the total pressure gradient to give the observed value. The procedure is analogous to the following development. Using the expression for the total pressure gradient:

$$\partial P/\partial Z = [\tau_f + (\rho/g_c)(R_l\rho_l) + (1 - R_l)\rho_g]/(1 - AC_m) \quad (50)$$

let $(\partial P/\partial Z)_{ol}$ be an experimentally observed value; then $R_l = [(\Delta P/\Delta Z)_{ol}(1 - AC_m) - \tau_f - \rho_g]/(\rho_l - \rho_g)$ (51)

The holdup is then calculated from the observed pressure gradient and the assumed behavior of friction and acceleration. The calculated holdup is not the volume fraction occupied by liquid, but an empirical term that accounts for energy losses other than through friction and acceleration. Such a holdup is exactly that described under the extended homogeneous case.

In trying to improve the results of the homogeneous model, Hagedorn and Brown proposed the expression for Arrhenius viscosity $\mu_A$, based solely on Uren's data:

$$\mu_A = (\mu_l^{R_l})(\mu_g^{R_g})(\text{where } R_l = R_l \text{ and } R_g = R_g) \quad (52)$$

This viscosity is used for the computation of the Reynolds number:

$$Re = 1{,}488\ G_tD/\mu_A \quad (53)$$

from which the friction factor is evaluated using the Colebrook Eq. (6-B). The frictional pressure gradient can then be evaluated from Eq. (9-A), or from:

$$(\tau_f)_m = f_{tp}\rho_n V_m^2/2g_cD \quad (54)$$

Numerical comparisons, however, show there is little difference between the results obtained by using $\mu_A$ from those obtained by means of $\mu_m$. Therefore, we suggest that the homogeneous Reynolds number $Re_m$, table Eq. (5-A), be used for calculating frictional factors.

## HOLDUP CORRELATION FOR VERTICAL FLOW

As is often the case, the calculation of holdup from an empirical correlation is very laborious, involving many dimensionless groups raised to noninteger powers. Hagedorn and Brown's correlation is no exception.

## Hagedorn and Brown's Holdup Correlation

This correlation is generally adequate for holdup greater than approximately 0.01 to 0.05, but invalid for lower ranges; therefore, it may not be accurate for mist flow. Hagedorn and Brown correlated holdup, $R_l$, with these dimensionless groups developed by Ros[15] from the Buckingham pi theorem:

$$N_d = 120.9\,D(\rho_l/\sigma)^{1/2}, \quad N_l = 0.1573\mu_l(1/\rho_l\sigma^3)^{1/4} \quad (55),(56)$$

$$N_{gv} = 1.938\,V_{sg}(\rho_l/\sigma)^{1/4}, \quad N_{lv} = 1.938V_{sl}(\rho_l/\sigma)^{1/4} \quad (57),(58)$$

The following correlation parameters are defined:

$$N_{vm} = N_{gv}N_l^{0.38}/N_d^{2.14} \quad (59)$$

$$N_{hold} = (N_{lv}/N_{gv}^{0.575})(P/14.65)^{0.1}C_n(10^4/N_d) \quad (60)$$

The following procedure then gives $R_l$:

1. Compute factor $\Psi$ shown in Graph (a):

$$\Psi = 1 + \exp[0.6559 + 8.8173\ln N_{vm} + 3.7603(\ln N_{vm})^2 + 0.5359(\ln N_{vm})^3] \quad (61)$$

For $N_{vm} < 0.01$, $\Psi = 1.00$; for $N_{vm} > 0.09$, $\Psi = 1.82$.

2. Compute factor $C_n$ shown in Graph (b):

$$C_n = \exp[-4.895 - 1.0775\ln N_l - 0.80822(\ln N_l)^2 - 0.1597(\ln N_l)^3 - 0.01019(\ln N_l)^4] \quad (62)$$

for $N_l > 0.4$, $C_n = 0.0115$; for $N_l > 0.002$, $C_n = 0.00195$.

3. Compute $N_{hold}$ from Eq. (60).

4. Compute $R_l/\Psi$ as shown in Graph (c):

$$R_l = \Psi[\exp(-3.6372 + 0.8913(\ln N_{hold}) - 0.1335(\ln N_{hold})^2 + 0.01853(\ln N_{hold})^3 - 0.001066(\ln N_{hold})^4]$$

for $N_{hold} > 4{,}000$, $R_l = \Psi$; for $N_{hold} < 0.1$, $R_l = 0.02633$.

5. If $R_l < \lambda$, then $R_l = \lambda$.

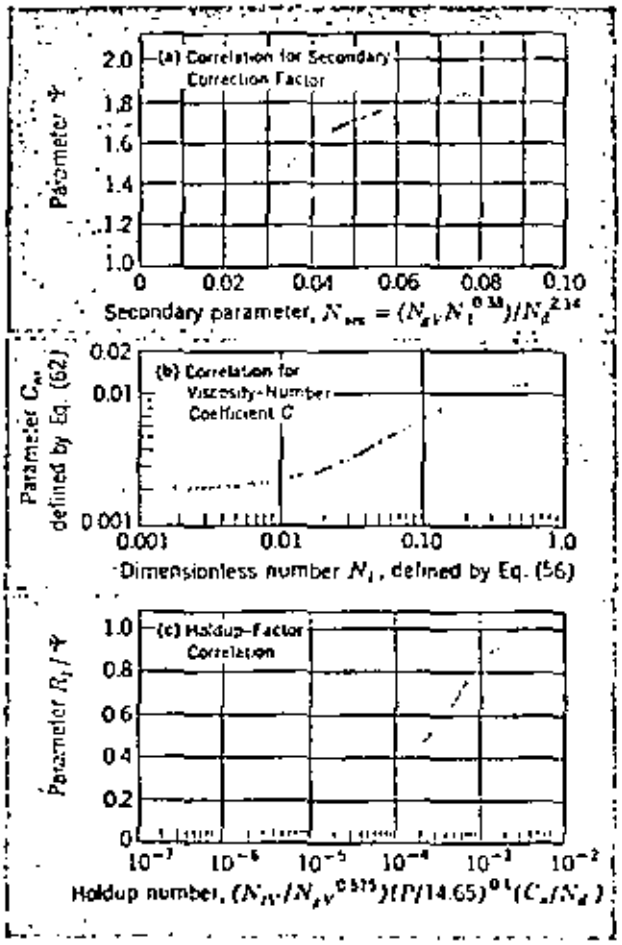


PARAMETER CORRELATIONS of Hagedorn and Brown

Our presentation of Hagedorn and Brown's procedure differs from the original in these ways: (1) their report presents variables familiar mainly to petroleum engineers; here, mass-velocity and phase-relationship variables have been redefined to make the correlation easier to use; (2) empirical functions are given for functions originally depicted as graphs; (3) engineering limits have been placed on holdup functions where they give meaningless results; and (4) the Arrhenius viscosity has been discarded.

## Holdup and the Angle of Inclination

Some general aspects of holdup—horizontal holdup in particular—have already been discussed. What must be emphasized now is that holdup is a function of conduit orientation. Holdup correlations accurate for horizontal flow are, in general, invalid for vertical flow. To date, however, no holdup correlation explicitly attempts to correct for variations in $\theta$, although there are some valid ones for the range $-10$ to $+10°$.

Choosing a holdup correlation for pressure-gradient equations is a major problem. Horizontal or Bonneceaze's can probably be used for small values of $\theta$; for large values, vertical holdup correlations can be used. The choice is more difficult in the intermediate range. We feel that vertical holdup correlations are the best to use.

Of the several holdup correlations presented for inclined flow, Bonneceaze's has perhaps the best approach as it is based upon Froude and Reynolds numbers. This approach has been suggested before.[17] The Froude number, $V^2/g_cD$, contains a gravitational term, which is intuitively appealing because gravity must affect holdup in some manner. At the other extreme, Hagedorn and Brown use the same dimensionless groups for vertical flow that Eaton used for horizontal flow:

$$N_{lv} = V_{sl}(\rho_l/g\sigma)^{1/4}, \quad N_{gv} = V_{sg}(\rho_l/g\sigma)^{1/4}$$
$$N_l = \mu_l(g/\rho_l\sigma^3)^{1/4}, \quad N_d = (\sigma/g\rho)^{1/2}$$

Four correlation groups are perhaps too many; this contributes to the complexity of Eaton's and Hagedorn's computations, the results of which may not represent physical reality any more accurately.

## SLUG-FLOW CONSIDERATIONS

Slugging is particularly important in inclined flow. Orkiszewski[3] reported that slug flow occurred in 95% of the situations covered by his accumulated data bank, and Bonneceaze[2] and coworkers, in their analysis, observed that slug flow predominated. Knowledge of this regime is a great aid in formulating expressions for the total pressure gradient.

Knowledge of slug flow in any orientation is also important from the operating standpoint, because large slugs of liquid tend to overload equipment and destabilize operations. Since slug flow must be predicted and considered in design, the concept of slug length and slug frequency have been introduced.[10]

In two-phase slug flow, the liquid phase bridges the pipe and is then accelerated to the velocity of the gas that follows.[10] This results in alternating liquid-gas flow with large pressure pulsations due to the high-velocity slugs. Although this regime has been noted in horizontal, inclined and vertical flow, very little effort has been devoted to horizontal slug flow, and almost none to the inclined case.

In vertical slug flow, the point of interest is not the liquid slug itself but rather the intervening gas bubbles. Early investigators noted that the bubble shape was that of the one described by G. I. Taylor[16] (bubbles rising in a stagnant-liquid-filled pipe under the influence of a uniform gravity field). These researchers applied Taylor's bubble-rise relations to the vertical-flowing system so as to model the mechanism of slug flow and to predict liquid holdup, pressure drop, and bubble or slug velocity.

In horizontal slug flow, the primary concern is not with the gas zones—or with bubbles separating the slugs—but with the liquid slugs themselves. No longer do gas bubbles rise up through the liquid; instead, liquid has bridged the pipe and moves at a higher velocity than the liquid in the gas zone.

Despite the absence of analytical work, a large amount of holdup and pressure-drop data has been collected for horizontal slug flow. This is mainly because slug flow occupies a rather large segment of liquid-gas space for common fluids in conduits. But, since similarities in mechanisms between horizontal and slug flow appear to be the exception rather than the rule, one fails to understand how an analysis of inclined slug flow can systematically be performed by combining the work of previous investigators in vertical and horizontal slug flow.

## Hubbard's Analysis of Horizontal Slug Flow

Hubbard[10] has provided the best analysis of the slug flow mechanism and associated flow-regime transitions. This description is taken from his thesis:

"Liquid and gas flow concurrently into the pipe. At gas velocities where slug flow takes place, the gas velocity is sufficient to generate waves on the surface of the liquid. These waves grow in amplitude as they travel along the pipe and in a short distance they bridge the pipe, blocking gas flow.

"As soon as bridging occurs, the liquid in the bridge is accelerated to the gas velocity. The liquid appears to be accelerated uniformly across its cross-section, thereby acting as a scoop, picking up all the slow moving liquid in the liquid film ahead of it and accelerating it to slug velocity. As the slug is formed and moves down the pipe, the liquid in the slug establishes a velocity profile similar to that in normal pipe flow. The liquid near the walls of the pipe is moving slower than the average velocity of the slug, thus the liquid is continuously shed from the back of the slug.

"Shortly after a slug is formed, it sweeps up all the excess liquid which entered the pipe since the last slug was formed. At this time, the liquid film which is about to be picked up by the slug is only that liquid which has been shed from the preceding slug. Since the slug is picking up liquid at the same rate that it is shedding it, the slug's length stabilizes.

"Due to the fact that the slug has a higher kinetic energy than the liquid film, the film penetrates a distance into the slug before it is finally assimilated at the slug velocity. This over-running phenomenon creates an eddy at the front of the slug which is essentially a mixing vortex and, therefore, exists without a pressure gradient. As the gas rate, and consequently the slug velocity, increase, the degree of aeration of the slug increases. Ultimately the gas forms a continuous phase along the top of the slug. When this point is reached, the slug no longer maintains a competent bridge to block the gas flow, so the character of the flow changes. This point is referred to as the beginning of "blow-through," or the beginning of the transition to dispersed annular flow.

"Thus, according to the basic model for slug flow, there are two significant contributions to the pressure drop across a slug. The first is the pressure drop that results from the acceleration of the flow, moving liquid film to slug velocity. The second is the pressure drop required to overcome wall friction due to the viscous dissipation in the slug itself. The sum of these two terms is the total pressure drop across a slug."

Hubbard developed a very detailed model for the slug-flow mechanism stating precise definitions of concepts to describe the regime. He first noted that there are two distinct types of slug flow. *Primary slug flow* exists when there is no gas "flow-through," and the entire energy of the gas phase works directly on the slug. *Transition slug flow* exists after gas flow-through has occurred and part of the gas—and its associated energy—is bypassed through the slug.

The key concept of Hubbard's analysis is that of a slug unit composed of the liquid slug and an associated gas pocket. Hubbard's model expresses the velocity of the slug in terms of the no-slip velocity, $V_{sv} = C_1 V_m$.

The parameter $C_1$ is constant over wide ranges of flow conditions. Hubbard obtained the value 1.25 for $C_1$. Another key parameter used by him is the slug frequency, $V_n$, as the number of slugs passing a given point per unit time. The slug frequency is a very important parameter in stabilizing equipment operation.

Hubbard's model will not be discussed further at this time. Given proper correlations for slug frequency and two-phase slug density, the model allows computation of pressure gradients and other characteristic parameters of flow. It can then be extended to develop mechanisms for the prediction of heat and mass transfer in the slug-flow regime.

## Bonnecaze's Analysis of Inclined Slug Flow

As mentioned in the section on inclined correlations, Bonnecaze and coworkers developed their correla-

tion by assuming the presence of slug flow. Their analysis proceeded along the following lines of reasoning.

Assuming the slug length does stabilize in inclined flow, a steady-state momentum balance for a slug unit can be obtained. The pressure loss is credited to three general areas: the mixing zone of the slug, the friction loss of the liquid, and the friction loss in the gas.

While the friction loss in the gas may be safely neglected (an experimentally verified result), it is fallacious to assume that the pressure drop in the mixing zone is zero (in light of Hubbard's horizontal-slug analysis). As previously pointed out, the acceleration of the liquid film to slug velocity is a major contributor to the total pressure-drop of the slug flow mechanism.

Bonnecaze *et al.* obtain their results for slug pressure-loss in Eq. (5). The equation is fundamental because it arises in the flow of nonhorizontal incompressible fluids. However, the friction factor is necessarily a friction factor obtained from single-phase flow, because it arises primarily from wall shear, not interfacial shear. The flow of a liquid slug is necessarily equivalent to single-phase incompressible flow as pointed out previously.

The value of correlating a friction factor for slugging is obviously a way to allow the one degree of freedom in the model to help the most. Thus, by using experimental data to generate the friction factor, the model becomes limited only to the experimental conditions. How can one expect to obtain a universal friction factor relationship from one pipeline?

For all but horizontal pipelines, friction loss plays a role of secondary importance. A pipeline with an inclination angle of only 1 deg. can yield a ratio of gravity to friction forces of approximately 1. Therefore, for large angles of inclination, the friction loss (except for the largest flowrates) is an order of magnitude less than gravity loss.

With only a suitable holdup correlation, the pressure loss may be estimated as being equal to the static-head loss. This is equivalent to calculating $\rho_{tp}$ as in Eq. (3), neglecting $\tau_f$, and computing $(\partial P/\partial Z)_{tp}$. It has been pointed out (Ros, Brown) that there is a liquid film that rides along, contributing nothing to the pressure loss.

Bonnecaze's holdup correlation for moderate pipeline inclination appears to be suitable and reasonably founded. By treating the gas-bubble velocity as the sum of two components, he and his coworkers rely a great deal on physical intuition. The components are buoyancy and no-slip velocity. They developed this concept further by including a buoyancy direction, such that for flow downhill the velocity of the slug decreases, while for uphill flow, it increases. It is interesting to note that this result is experimentally observed.

Bonnecaze's work appears to be a thoughtful analysis of the mechanism of inclined slug flow. However, because of the neglect of the mixing zone and the dubious approach to the friction-factor correlation, its usefulness may be only limited.

## Slug-Frequency and Slug-Velocity Correlations

There are many values in the literature for the parameter $C_o$ for various values of $\theta$. Bonnecaze used the value of 1.2 developed by Nicklin for vertical flow. Hubbard found the value of 1.25 for horizontal flow experimentally. Subsequently, Gregory and Scott[11] determined a horizontal value of $C_o = 1.35$.

In Hubbard's thesis, the factor $C_o$ is shown to be a function of the smooth-tube friction factor. For a smooth friction factor, $C_o$ remained constant for Reynolds numbers from $5.10^4$ to $6.10^5$. If we were to use the Colebrook equation, where the friction factor is a function of relative roughness also, we would suspect $C_o$ to likewise be a function of relative roughness. Subsequent investigators used a pipe half the size of Hubbard's. The difference between constants at low $V_m$ was indistinguishable; only at high $V_m$ values could a least-squares analysis show differences.

Hubbard was unable to develop a correlation for slug frequency. Gregory and Scott,[11] however, have presented a slug frequency correlation in terms of the Froude number. This is an interesting approach, but the correlation appears to have slight application because it is based only on a small amount of $CO_2$-water data, at atmospheric pressure. ■

## References


1. Bonnecaze, R. H., et al., "Holdup and Pressure Drop for Two-Phase Slug Flow in Inclined Pipelines," AIChE, Fifty-Second Annual Meeting, Washington, D.C. 1959.
2. Brown, Kermit E., "Gas Lift Theory and Practice," Prentice-Hall, Englewood Cliffs, N.J. (1967).
3. Orkiszewski, J., "Predicting Two-Phase Pressure Drops in Vertical Pipe," *J. Petrol. Technol.*, July, 1967, p. 829-838.
4. Duns, H., Jr., and Ros, N. C. J., "Vertical Flow of Gas and Liquid Mixtures From Boreholes," Paper 22-PD6, Proceedings of World Petroleum Congress, Section II, Frankfurt, Germany, June 19-26, 1963.
5. Poettmann, F. H., and Carpenter, R. G., "The Multiphase Flow of Gas, Oil and Water Through Vertical Flow Strings, Drill and Prod Practice," p. 257, American Petroleum Institute (1952).
6. Tek, M. R., Multiphase Flow of Water, Oil and Natural Gas Through Vertical Flow Strings, *J. Petrol. Technol.*, Oct. 1961, p. 1029.
7. Hagedorn, A. R., and Brown, K. E., "Experimental Study of Pressure Gradients Occurring During Continuous Flow in Small Diameter Vertical Conduits," Paper SPE940 presented at 39th Meeting of Soc. of Petroleum Engineers, Houston, Tex., Oct. 1964.
8. Griffith, P., and Wallis, G. B., Two-Phase Slug Flow, *J. Heat Transfer*, Aug. 1961, p. 307.
9. Griffith, P., "Two-Phase Flow in Pipes," Special Summer Program, Massachusetts Institute of Technology, Cambridge, Mass. (1965).
10. Hubbard, M. G., "An Analysis of Horizontal Gas-Liquid Slug Flow," Ph.D. thesis, University of Houston, Houston, Tex. (1965).
11. Gregory, G. A., and Scott, D. S., Correlation of Liquid Slug Velocity and Frequency in Horizontal Concurrent Gas-Liquid Slug Flow," *AIChE J.*, Nov. 1969, pp. 933-935.
12. Nicklin, D. J., et al., Two-Phase Flow in Vertical Tubes, *Trans. AIChE*, 40, pp. 61-68 (1962).
13. Hughmark, G. A., Holdup in Gas-Liquid Flow, *Chem. Eng. Progr.*, 58, pp. 62-65 (1962).
14. Hughmark, G. A., *Chem. Eng. Sci.*, 20, p. 1007.
15. Ros, N. C. J., Simultaneous Flow of Gas and Liquid as Encountered in Well Tubing, *J. Petrol. Technol.*, 13, p. 1037 (1961).
16. Taylor, G. I., and Davies, R. M., The Mechanics of Large Bubbles Rising Through External Liquid and Liquids in Tubes, *Proc. Roy. Soc. (London)*, A200, pp. 375-390 (1950).
17. Greskowitch, A. L., et al., True Gas Content for Horizontal Gas-Liquid Flow, *Ind. Eng. Chem. Fundamentals*, Aug. 1969, pp. 531-533.
18. Flanigan, O., Effect of Uphill Flow on Pressure Drop in Design of Two-Phase Systems, *Oil Gas J.*, Mar. 10, 1958, p. 132.

SPE

SPE 6766

# COMPARISON OF CALCULATED AND OBSERVED PRESSURE DROPS IN GEOTHERMAL WELLS PRODUCING STEAM-WATER MIXTURES

by R.N. Upadhyay, J.D. Hartz, B.N. Tomkoria and M.S. Gulati, Members
SPE-AIME, Union Oil Company of California



This paper was presented at the 52nd Annual Fall Technical Conference and Exhibition of the Society of Petroleum Engineers of AIME, held in Denver, Colorado, Oct. 9-12, 1977. The material is subject to correction by the author. Permission to copy is restricted to an abstract of not more than 300 words. Write: 1200 N. Central Expy., Dallas, Texas 75206.

## ABSTRACT

This paper contains comparisons of calculated and observed flowing pressure profiles from geothermal wells located in the United States and the Philippines. Comparisons are included for tubular flow as well as flow through the casing-tubing annulus. Our comparison shows that for tubular flow, the Orkiszewski correlation makes the best prediction, whereas for annular flow, no clear-cut choice of a correlation can be made.

## INTRODUCTION

The capability to accurately predict flowing pressures in a geothermal well producing steam-water mixtures under various operating conditions is of value for several reasons: general engineering essential to evaluation of the geothermal reservoir and proper reservoir management; optimization of wellbore design from well deliverability considerations; and minimization of scale deposits in the wellbore.

This predictive capability is especially important because of the difficulty of running flowing pressure surveys in geothermal wells. These wells are characterized by very high fluid velocities, which sometimes make it impractical for the pressure recorder to traverse downward in the well. There have been cases of pressure recorders thrown out of the wellbore due to high fluid velocities.

In calculating flowing pressure profiles for oil wells, phase transfer between oil and gas requires a rather simple treatment, and is accomplished through the use of solution gas-oil ratio relationships. In geothermal wells, however, phase transfer between water and steam attains critical importance, and calculations must incorporate the steam tables accurately. Pressure profile calculations for geothermal wells vary from those for oil wells in another important aspect in that the temperature of the fluid must be computed precisely.

For calculations included in this paper, a computer program incorporating three previously published correlations for predicting two-phase flow in vertical pipes—coupled with equations for phase transfer and wellbore heat loss—was used to calculate pressures in a number of geothermal wells in which flowing pressure surveys had been run. The paper contains comparisons between the calculated and the observed pressure profiles.

This comparison encompasses a wide range of flow rates and wellhead pressures, and includes tubular as well as annular (between casing and tubing) flow. The three correlations used are: Orkiszewski;[1] Hagedorn and Brown;[2] and Duns and Ros.[3]

The phase behavior relationships used in this work are for pure water,[4] and do not include the effects of dissolved salts. However, the waters in the wells we studied were of low salinity. Also not considered is the effect of non-condensible gases present in the fluid. We do not consider this to be a significant limitation, because in our observation wells, non-condensible gases, consisting almost entirely of carbon dioxide, constituted a small fraction of the steam phase.

This comparison of computed and observed pressure drops in flowing geothermal wells can help determine the degree of confidence an engineer should have in results predicted by the three correlations evaluated. The best correlation does a satisfactory job of predicting pressure drops, and can be used in deliverability prediction calculations. Optimization of wellbore design of future wells in a partially developed field can be accomplished by calculating production rates for different flow string diameters at a given wellhead pressure, and comparing the benefit of increased flow rates against the higher cost of drilling and completing larger diameter wells.

Since the precipitation of calcium carbonate scales, encountered in many hot water wells, is related to the pressure and temperature conditions in the wellbore, calculations can be made to estimate the depth at which scale precipitation would commence for various wellbore diameters and mass flow rates. This can assist the engineer in the selection of operating conditions that will tend to cause scaling at shallower depths, thus requiring easier clean-up operations

* References and illustrations at end of paper.

## CORRELATIONS FOR TWO-PHASE VERTICAL FLOW

For calculations of flowing pressure profiles were made with three correlations: Orkiszewski; Hagedorn and Brown; and Beggs and Brill. Each of these is a well-known correlation for two-phase vertical flow. We chose the first two correlations because they have been widely used by petroleum engineers, and have, in our own experience, done a satisfactory job of predicting pressure drops in oil wells. We included the Beggs and Brill correlation in our study because it is probably the most recently published method.

The following is a brief description of these three correlations; for a more detailed analysis, the reader should refer to the original articles describing the correlations.[1,2,3]

### Orkiszewski Correlation

This correlation takes into consideration the slip between liquid and vapor phases, and therefore includes a correlation to calculate liquid holdup, i.e., the fraction of the pipe cross-sectional area occupied by liquid. It also takes into account the flow regime that exists in any section of the pipe; the flow regimes considered are shown in FIGURE 1. The Orkiszewski correlation is hybrid in that it uses different published correlations for different flow regimes: Griffith and Wallis[5] correlation for bubble flow regime, and Duns and Ros[6] correlation for transition and mist flow regimes. For slug flow, Orkiszewski developed a new correlation based upon the experimental data of Hagedorn and Brown.[2] Orkiszewski defines the various flow regimes by the following limits:

Bubble flow: $v_{sg}/v_m < L_B$

Slug flow: $v_{sg}/v_m > L_B$, $N_{GV} < L_S$

Transition flow: $L_M > N_{GV} > L_S$

Annular mist flow: $N_{GV} > L_M$

where $L_B = 1.071 - (0.2218\ v_m^2/d) \geq 0.13$

$L_S = 50 + 36\ N_{LV}$

$L_M = 75 + 84\ (N_{LV})^{0.75}$

### Bubble Flow

Liquid holdup in this flow regime is given by the following equation:

$$H_L = 1 - \frac{1}{2}\left[1 + \frac{v_m}{v_s} - \sqrt{\left(1 + \frac{v_m}{v_s}\right)^2 - 4\,\frac{v_{sg}}{v_s}}\right] \quad \ldots\ldots(1)$$

In equation (1), $v_s$ is assumed to have a constant value of 0.8 ft/sec.

The pressure drop due to friction is given by

$$\left(\frac{dp}{dz}\right)_f = \frac{f\rho_L\,(v_{sl}/H_L)^2}{2g_c d} \quad \ldots\ldots(2)$$

The Reynolds Number for the calculation of friction factor is given by the following relationship:

$$N_{Re} = \frac{1488\ \rho_L\ d\ v_{sl}}{H_L\ \mu_L} \quad \ldots\ldots(3)$$

The friction factor, f, in equation (2) is calculated by using the Reynolds Number and the standard Moody diagram.[7] In this flow regime, pressure drop due to acceleration is neglected.

### Slug Flow

Orkiszewski uses the following relationship to calculate two-phase density in this flow regime:

$$\rho_m = \frac{\rho_L(v_{sl} + v_b) + \rho_g v_{sg}}{v_m + v_b} + \rho_L\,\delta \quad \ldots\ldots(4)$$

where $v_b = C_1 C_2 \sqrt{gd}$

$C_1$ is a function of bubble Reynolds Number, $N_{Reb}$, and $C_2$ is a function of both $N_{Reb}$ and liquid Reynolds Number, $N_{ReL}$, defined below:

$$N_{Reb} = \frac{1488\ \rho_L v_b d}{\mu_L} \quad \ldots\ldots(5)$$

$$N_{ReL} = \frac{1488\ \rho_L v_m d}{\mu_L} \quad \ldots\ldots(6)$$

Because of the interdependence of $v_b$ and $N_{Reb}$, the calculation of $v_b$ requires an iterative procedure. For $v_m < 10$,

$$\delta = (0.013 \log \mu_L)/d^{1.38} - 0.681 + 0.232 \log v_m - 0.428 \log d \quad \ldots\ldots(7)$$

with the limit $\delta \geq -0.065\ v_m$

For $v_m > 10$

$$\delta = (0.045 \log \mu_L)/d^{0.799} - 0.709 - 0.162 \log v_m - 0.888 \log d \quad \ldots\ldots(8)$$

with the limit $\delta \geq \frac{-v_b}{v_m + v_b}\,(1 - \rho_m/\rho_L)$

Pressure drop due to friction is given by

$$\left(\frac{dp}{dz}\right)_f = \frac{f\rho_L v_m^2}{2g_c d}\left[\left(\frac{v_{sl} + v_b}{v_m + v_b}\right) + \delta\right] \quad \ldots\ldots(9)$$

The friction factor, f, in equation (9) is calculated from the Moody diagram using the following definition of Reynolds Number:

$$N_{Re} = \frac{1488\ \rho_L\ d\ v_m}{\mu_L} \quad \ldots\ldots(10)$$

Pressure drop due to acceleration in the slug flow regime is too small, and is neglected.

### Transition Flow

This flow regime provides a transition from slug flow to annular mist flow. The pressure drop in this regime is calculated by linear interpolation between the

pressure drops for slug and mist flow regimes. Mixture density and frictional pressure drop terms are calculated for both slug flow and mist flow; they are then linearly weighted with respect to a dimensionless gas velocity term and the limits of the transition zone in order to arrive at the terms applicable to this flow regime.

Mist Flow

In this flow regime, the gas phase is continuous, and is the controlling factor. Because of high gas flow rates, it is assumed that there is no slip between gas and liquid phases, and the mixture density is given as

$$\rho_m = \rho_L \frac{v_{sl}}{v_m} + \rho_g \frac{v_{sg}}{v_m} \quad \ldots\ldots\ldots\ldots (11)$$

The frictional pressure drop is based on gas phase only, and is given as

$$\left(\frac{dp}{dz}\right)_f = \frac{f \rho_g v_{sg}^2}{2 g_c d} \quad \ldots\ldots\ldots\ldots (12)$$

The friction factor, f, is obtained from the Moody diagram and the gas Reynolds Number, defined below:

$$N_{Re} = \frac{1488 \rho_g v_{sg} d}{\mu_g} \quad \ldots\ldots\ldots\ldots (13)$$

A modified form of relative roughness factor (e/D) is calculated for use with the Moody diagram; this is done to take into account the effect of the liquid film on the pipe. The modified e/D is limited to values between $10^{-3}$ and 0.5, both inclusive.

Pressure drop due to acceleration can be given by the following equation:

$$\left(\frac{dp}{dz}\right)_{acc} = \frac{v_m v_{sg} \rho_m}{g_c p} \cdot \frac{dp}{dz} \quad \ldots\ldots\ldots\ldots (14)$$

Hagedorn and Brown Correlation

This method considers slip between liquid and gas phases, but does not divide flow into different regimes. The correlation was developed from a study of flowing pressure gradients in a 1500-foot experimental well. Pressure drops were measured for two-phase flow through 1-in., 1 1/4-in., and 1 1/2-in. nominal diameter tubing. Although liquid holdup was not measured, it was calculated to satisfy the total pressure drop measured after the contribution of friction and acceleration had been calculated. These calculated values of liquid holdup were then correlated with flow rates, pipe diameters, and fluid properties. It was found that the liquid holdup is related primarily to the following four dimensionless terms:

Liquid velocity number,

$$N_{LV} = 1.938 \, v_{sl} \left(\frac{\rho_L}{\sigma}\right)^{1/4} \quad \ldots\ldots\ldots\ldots (15)$$

Gas velocity number,

$$N_{GV} = 1.938 \, v_{sg} \left(\frac{\rho_L}{\sigma}\right)^{1/4} \quad \ldots\ldots\ldots\ldots (16)$$

Pipe diameter number,

$$N_D = 120.872 \, d \left(\frac{\rho_L}{\sigma}\right)^{1/2} \quad \ldots\ldots\ldots\ldots (17)$$

Liquid viscosity number,

$$N_L = 0.15726 \, \mu_L \left(\frac{1}{\rho_L \sigma^3}\right)^{1/4} \quad \ldots\ldots\ldots\ldots (18)$$

The calculation of liquid holdup using this correlation requires a three-step process: (1) From the liquid viscosity number, $N_L$, a quantity $CN_L$ is evaluated; (2) The value of $CN_L$, together with $N_{LV}$ and $N_{GV}$, is used to calculate $H_L/\psi$, i.e., liquid holdup divided by a secondary correlation factor; (3) An expression containing $N_{GV}$, $N_L$ and $N_D$ is used to evaluate the secondary correlation factor, $\psi$, and thence $H_L$.

From the calculated value of liquid holdup, the mixture density can be calculated using the following equation:

$$\rho_m = \rho_L H_L + \rho_g (1 - H_L) \quad \ldots\ldots\ldots\ldots (19)$$

The frictional pressure drop is given by

$$\left(\frac{dp}{dz}\right)_f = \frac{f w^2}{7.116 \times 10^{12} \times \rho_m \times d^5} \quad \ldots\ldots\ldots\ldots (20)$$

In equation (20), the density, $\rho_m$, is based upon liquid holdup. The friction factor, f, is read from the Moody diagram using a two-phase Reynolds Number defined below:

$$N_{Re} = \frac{1488 \rho_m v_m d}{\mu_m} \quad \ldots\ldots\ldots\ldots (21)$$

where $v_m = v_{sl} + v_{sg}$

and $\mu_m = \mu_L^{H_L} \mu_g^{(1-H_L)}$

The pressure gradient due to acceleration is given by

$$\left(\frac{dp}{dz}\right)_{acc.} = \frac{\rho_m}{2 g_c} \cdot \frac{d(v_m^2)}{dz} \quad \ldots\ldots\ldots\ldots (22)$$

Beggs and Brill Correlation

This is the newest of the three correlations. Like the Orkiszewski correlation, it takes into account the slip between liquid and vapor phases, and recognizes the existence of different flow regimes. The correlation contains a relationship to calculate liquid holdup at all pipe angles. Beggs and Brill developed their correlation from flow experiments in 90-ft long acrylic pipe, 1 in. and 1.5 in. in diameter, which could be inclined at any angle.

This correlation assumes the flow in a horizontal pipe to exist in one of three major flow patterns: segregated, intermittent, and distributed, as shown in FIGURE 2. Even for non-horizontal flow, the method first calculates the flow regime that would exist if the flow were horizontal. Separate equations are used to calculate the liquid holdup for different "horizontal" flow regimes; the liquid holdup is then corrected for pipe angle of deviation from horizontal.

The "horizontal" flow regime limits are defined by the Froude Number ($N_{FR}$) and various functions of $\lambda_L$ where

$$N_{FR} = \frac{v_m^2}{gd}$$

and

$$\lambda_L = \frac{v_{sl}}{v_m}$$

The "horizontal" liquid holdup is corrected for pipe inclination by using a multiplier, which, for vertical flow, reduces to (1 + 0.3C). Values of C differ with the calculated "horizontal" flow regime, and are different for uphill and downhill flow. (Refer to Beggs and Brill[3] for calculation of C.)

The frictional pressure gradient is given by

$$\left(\frac{dp}{dz}\right)_f = \frac{f_{tp}\rho_n v_m^2}{2g_c d} \quad \ldots\ldots\ldots\ldots\ldots\ldots (23)$$

where $\rho_n = \rho_L\lambda_L + \rho_g(1 - \lambda_L)$

and $f_{tp} = f_n e^s$

The non-slip friction factor, $f_n$, is calculated from the Moody diagram using the following definition of Reynolds Number:

$$N_{Ren} = \frac{1488\,\rho_n v_m d}{\mu_L\lambda_L + \mu_g(1 - \lambda_L)} \quad \ldots\ldots\ldots\ldots\ldots\ldots (24)$$

The exponent s is a function of input liquid fraction, and the calculated liquid holdup, corrected for vertical flow.

Pressure gradient due to acceleration is given by

$$\left(\frac{dp}{dz}\right)_{acc.} = \frac{[\rho_L H_L + \rho_g(1 - H_L)]}{g_c}\frac{v_m v_{sg}}{p}\cdot\frac{dp}{dz} \quad \ldots\ldots (25)$$

## COMPUTER PROGRAM FOR CALCULATING PRESSURE PROFILES

The computer program we used in this study follows the procedure outlined below in calculating the pressure profile in a flowing geothermal well:

1. Wellhead flowing pressure (p), and steam and water flow rates at wellhead conditions act as the starting point. (Although bottomhole conditions can just as easily be treated as the starting point, the information is usually available for wellhead conditions, and needs to be calculated for bottomhole conditions.)

2. A small pressure increment ($\Delta P$) is selected, and the depth interval ($\Delta Z$) over which this increment would occur is calculated following these steps:

   a. A new steam fraction (i.e., fraction of total mass flow rate that is steam) is assumed to exist at p + $\Delta p$. Using an average pressure and average steam fraction over the interval, the specified two-phase flow correlation is used to calculate the pressure gradient ($\Delta p/\Delta Z$) over the interval. If flow is in single phase, the pressure gradient is calculated by using single-phase density and Reynolds Number, and the Moody diagram.

   b. From the calculated pressure gradient $\frac{\Delta p}{\Delta Z}$, and pressure increment $\Delta p$, the depth interval $\Delta Z$ is calculated. Heat loss from the well-bore into the surrounding formation over the depth interval $\Delta Z$ is now calculated using a transient heat transfer relationship. This takes into account the time for which the well has been producing, and the overall heat transfer coefficient for the wellbore. Energy losses due to potential energy and kinetic energy changes are calculated and combined with the heat loss calculated above. A new fluid enthalpy is thus computed. Using this new enthalpy, and pressure p + $\Delta p$, the steam fraction at depth $\Delta Z$ is calculated. If the difference between calculated and assumed steam fractions is within a specified tolerance, calculation proceeds to the next pressure increment. If not, the average of the two is assumed to be the steam fraction for the second iteration. This iterative procedure is continued until assumed and calculated steam fractions converge. The pressure gradient calculated in the last iteration is used to calculate the depth increment $\Delta Z$ corresponding to the pressure increment $\Delta p$. For single-phase flow, iterations are made to achieve fluid temperature convergence rather than steam fraction convergence.

3. The pressure is increased again by increment $\Delta p$, and the corresponding $\Delta Z$ is calculated following the procedure outlined in step 2 above. This procedure is continued until the total depth of the well is reached.

Properties of pure water and steam were used in our calculations. Improvements in calculations can be made by taking into consideration the effects of salt concentration on the phase behavior of water, and also the effect of non-condensible gas content.

For heat transfer calculations, ground temperature and a geothermal gradient are used; this gradient is used to calculate the rock temperature up to the top of the producing formation. The temperature within the producing formation itself is assumed to have no vertical gradient. This has been found to be generally true in our experience.

The computer program calculates heat transfer from the wellbore into the surrounding rock formation using the following relationship:

$$Q = \frac{U_w d\Delta Z(T_f - T_r)}{Wf(t)} \quad \ldots\ldots\ldots\ldots\ldots\ldots (26)$$

where

$$f(t) = -\ln\left(\frac{r_c}{2\sqrt{\alpha t}}\right) - 0.29$$

Ramey[8] has found equation (26) to be valid for flow periods in excess of a week. Because of high flow rates encountered during our surveys, heat transfer between the wellbore and the surrounding rock did not affect results appreciably. We used a heat transfer coefficient of 10 Btu/(hr. °F ft$^2$) in our calculations.

## OBSERVED PRESSURE PROFILES

Our flowing surveys were conducted during tubular as well as annular flow; the annular flow surveys will be discussed later. For tubular flow, the typical wellbore configuration consisted of a 9 5/8-in. casing in the upper half of the well, and a 7-in. slotted liner

in the bottom half. A typical wellbore diagram appears in FIGURE 3.

Flowing wellhead pressures in these surveys varied between 39 and 160 psia; measured bottomhole pressures ween 240 and 1100 psia. Mass flow rates ranged be..een 90,000 lb/hr and 389,000 lb/hr. Steam fraction at wellhead conditions varied from 0.15 to 0.46 by weight. The shallowest survey was 1600 ft deep; the deepest, 5000 ft. Wellbore and flow rate data for these surveys are summarized in TABLE 1 (surveys 1 through 5).

The total dissolved solids in the produced fluids varied from a low of 6100 ppm to a high of 9700 ppm. Non-condensible gases, composed almost entirely of carbon dioxide, ranged from a low of 0.2% to a high of 4.3% by weight of steam.

## COMPARISON OF OBSERVED AND CALCULATED PRESSURE PROFILES

The comparison of observed and computed pressure profiles appears in FIGURES 4 through 8. In FIGURE 7, it can be seen that the observed pressure profile starts deviating from the calculated values at a depth of 1500 ft; this deviation becomes considerable below 2000 ft. There is a simple explanation for this, however. The observed pressure gradient in this well below 2000 ft is 0.376 psi/ft, and temperature surveys indicate the reservoir temperature to be 383°F. From steam tables, water density at 383°F is 54.76 lb/ft,$^3$ which results in a static pressure gradient of 0.380 psi/ft. This shows that the observed pressure gradient below 2000 ft is a static gradient, and that there is no ...w entering the wellbore below that depth. Between ...00 ft and 2000 ft depth, fluid enters the well at different points, and therefore there is divergence between the calculated and the observed pressures.

An examination of FIGURES 4 through 8 immediately reveals that the Orkiszewski correlation calculates pressures that are closest to the observed pressures; the Hagedorn and Brown method is a close second. In FIGURES 6 and 7, both Orkiszewski and Hagedorn and Brown predict approximately the same pressure profile; however, in FIGURE 6, it is noteworthy that below 4500 ft the Orkiszewski correlation follows a change in the observed pressure gradient, whereas the Hagedorn and Brown correlation does not. In our work, the Beggs and Brill correlation did not do a satisfactory job of predicting pressure profiles in geothermal wells producing steam-water mixtures.

It should be noted that in our calculation of pressure profiles, we assumed that all the fluid flows through the inside of the slotted liner, i.e., there is no flow through the open hole-liner annulus.

## ANNULAR FLOW

We ran several pressure surveys in a well in which flow took place through the 9 5/8-in. casing—2 3/8-in. tubing annulus. The tubing was closed at the top and open at the bottom; it had several perforations at different intervals to allow pressure communication be...en the casing and the tubing. A bottomhole pressure ...order was moved up and down the tubing to conduct ... surveys. Although some flow obviously occurred through the tubing because of the perforations, we feel that it was not an appreciable part of the total flow, and we assumed the total flow to be through the annulus.

The annular surveys can be generally classified into two groups: One with wellhead pressures close to 135 psia, the other with wellhead pressures in the vicinity of 220 psia. Wellbore and flow rate data pertinent to these surveys are summarized in TABLE 1 (surveys 6 and 7). Two comparisons of observed and calculated pressure profiles, representing the two survey groups, appear in FIGURES 9 and 10.

In calculating the annular flow pressure profile, we used the hydraulic diameter, defined below as the pipe diameter.

Hydraulic diameter,

$$d_h = \frac{4 \times \text{cross-sectional area of flow}}{\text{wetted perimeter}}$$

If the casing inside diameter is $d_1$ and tubing outside diameter is $d_2$,

$$d_h = \frac{4(\pi/4)(d_1^2 - d_2^2)}{\pi(d_1 + d_2)} = d_1 - d_2 \quad \ldots\ldots\ldots (27)$$

For a 9 5/8-in. nominal casing and 2 3/8-in. nominal tubing, $d_h$ is calculated to be 0.545 ft.

The hydraulic diameter was used in calculating Reynolds Number and pipe relative roughness. For calculating fluid velocities, we used the actual cross-sectional area of the annulus.

An examination of FIGURES 9 and 10 shows that no clear-cut choice can be made as to the best correlation for annular flow. This statement can be made for all the annular flow pressure surveys conducted by us. We find that while Orkiszewski and Hagedorn and Brown tend to under-predict the pressure drop, the Beggs and Brill correlation has a tendency to over-predict it. However, since all the annular flow surveys were run in a single well, we do not know if our finding will be generally true. We find ourselves in agreement with the conclusion of Sanchez[9] that no sufficiently accurate and precise method exists for annular flow.

## CONCLUSIONS

Based upon the limited number of flowing pressure surveys conducted, we come to the following conclusions:

1. For predicting flowing pressure profiles in geothermal wells producing steam and hot water mixtures, the Orkiszewski correlation does a satisfactory job; the Hagedorn and Brown correlation comes a close second.

2. The Beggs and Brill correlation did not adequately predict pressure loss in these flowing geothermal wells.

3. For annular flow in geothermal wells, we cannot make a definite choice of a correlation. Our results show that while the Orkiszewski and the Hagedorn and Brown correlations under-predict the pressure drop, the Beggs and Brill correlation over-predicts it.

4. The Orkiszewski correlation has been used with success in predicting geothermal well deliverability under different wellbore designs. Together with appropriate treatment of solubility characteristics of $CO_2$ in water, the Orkiszewski correlation

can be used to approximate the depth at which scale deposits will take place in a well as a function of wellbore diameter.

Our calculations did not include the effect of dissolved solids in the water, nor the non-condensible gas content of the steam. However, the wellbore fluids in our wells were not high in dissolved solids content.

## NOMENCLATURE

$C_1$, $C_2$ = Parameters used to calculate bubble rise velocity in the Orkiszewski correlation

$CN_L$ = A function of liquid viscosity number, $N_L$

$d$ = Pipe inside diameter, ft

$d_1$ = Casing inside diameter, ft

$d_2$ = Tubing outside diameter, ft

$d_h$ = Hydraulic diameter, ft

$e$ = Absolute pipe roughness, ft

$f$ = Darcy-Weisbach or Moody friction factor

$f_n$ = Non-slip friction factor

$f(t)$ = A function of time, t (days), since well was open to flow

$f_{tp}$ = Two-phase friction factor

$g$ = Acceleration due to gravity, 32.2 ft/sec$^2$

$g_c$ = Conversion constant, 32.2 lbm-ft/lbf-sec$^2$

$H_L$ = Liquid holdup, fraction

$L_B$ = Bubble-slug boundary term

$L_M$ = Transition-mist boundary term

$L_S$ = Slug-transition boundary term

$N_D$ = Pipe diameter number

$N_{FR}$ = Froude Number

$N_{GV}$ = Gas Velocity Number

$N_L$ = Liquid Viscosity Number

$N_{LV}$ = Liquid Velocity Number

$N_{Re}$ = Reynolds Number

$N_{Reb}$ = Bubble Reynolds Number

$N_{Rel}$ = Liquid Reynolds Number

$N_{Ren}$ = Non-slip Reynolds Number

$P$ = Pressure, psf

$\left(\frac{dp}{dz}\right)_{acc}$ = Acceleration pressure gradient, psf/ft

$\left(\frac{dp}{dz}\right)_f$ = Frictional pressure, gradient, psf/ft

$Q$ = Heat lost to surroundings, Btu/lb

$r_c$ = Outer radius of casing, ft

$s$ = Exponent used in relating no-slip friction factor to two-phase friction factor

$t$ = Time since well was open for flow, days

$T_f$ = Fluid temperature in a segment of wellbore; °F

$T_r$ = Rock temperature surrounding a segment of wellbore, °F

$U$ = Overall heat transfer coefficient, Btu/(hr-ft$^2$-°F)

$v_b$ = Bubble rise velocity, ft/sec

$v_m$ = Mixture velocity, ft/sec

$v_s$ = Slip velocity (difference between average gas and liquid velocities), ft/sec

$v_{sg}$ = Superficial gas velocity, ft/sec

$v_{sl}$ = Superficial liquid velocity, ft/sec

$W$ = Mass flow rate, lbm/hr

$Z$ = vertical length, ft

### Greek Symbols

$\alpha$ = Thermal diffusivity of earth, ft$^2$/day

$\delta$ = Liquid distribution coefficient

$\lambda_L$ = Input liquid fraction, or no-slip liquid holdup

$\mu_g$ = Gas viscosity, cp

$\mu_L$ = Liquid viscosity, cp

$\mu_m$ = Mixture viscosity, cp

$\rho_g$ = Gas density, lbm/ft$^3$

$\rho_L$ = Liquid density, lbm/ft$^3$

$\rho_m$ = Mixture density, lbm/ft$^3$

$\rho_n$ = No-slip mixture density, lbm/ft$^3$

$\sigma$ = Interfacial tension, dynes/cm

$\psi$ = Secondary correlation factor

## ACKNOWLEDGMENTS

We thank the Management of Union Oil Company of California for permission to present this paper. The computer program used in our work was originally written at the Petroleum Engineering Department of the University of Tulsa under a contract from Union Oil Company of California.

## REFERENCES

1. Orkiszewski, J.: "Predicting Two-Phase Pressure Drop in Vertical Pipe", J. Pet. Tech. (June, 1967) 829-838.

2. Hagedorn, A.R. and Brown, K.E.: "Experimental Study of Pressure Gradients Occurring During Continuous Two-Phase Flow in Small Diameter Vertical Conduits", J. Pet. Tech. (April, 1965) 475-484.

3. Beggs, H.D. and Brill, J.P.: "A Study of Two-Phase Flow in Inclined Pipes", J. Pet. Tech. (May, 1973) 607-617.

4. Argonne National Laboratory: "STEAM67"--A Subroutine package incorporating 1967 ASME Steam Tables.

5. Griffith, P. and Wallis, G.B.: "Two Phase Slug Flow", J. Heat Transfer; Trans., AIME (Aug., 1961) 307-320.

6. Duns, H., Jr. and Ros, N.C.J.: "Vertical Flow of Gas and Liquid Mixtures from Boreholes", Proc., Sixth World Pet. Congress, Frankfurt (June 19-26, 1963) Section II, Paper 22-PD6.

7. Moody, L.F.: "Friction Factors in Pipe Flow", Trans., ASME (1944) 66, 671-684.

8. Ramey, H. J., Jr.: "Wellbore Heat Transmission" J. Pet. Tech. (April, 1962) 427-435.

9. Sanchez, M. J.: "Comparison of Correlations for Predicting Pressure Losses in Vertical Multiphase Annular Flow", M.S. Thesis, The University of Tulsa, 1972.

TABLE 1

WELLBORE AND FLOW RATE DATA FOR PRESSURE SURVEYS

| Survey | Tubular Flow | | | | | Annular Flow | |
|---|---|---|---|---|---|---|---|
| | 1 | 2 | 3 | 4 | 5 | 6 | 7 |
| Flowing Wellhead Pressure, psia | 160 | 129 | 80 | 39 | 151 | 138 | 219 |
| Total Mass Flow Rate, lb/hr | 281,174 | 271,395 | 89,608 | 120,175 | 389,000 | 149,700 | 133,700 |
| Steam Fraction at Wellhead | 0.162 | 0.157 | 0.463 | 0.149 | 0.211 | 0.643 | 0.530 |
| Casing Inside Diameter, inches | 8.921 | 8.921 | 8.801 | 8.758 | 8.921 | 8.921 | 8.921 |
| Casing Depth, feet | 1621 | 1621 | 2290 | 1783 | 1621 | 2371 | 2371 |
| Liner Inside Diameter, inches | 6.276 | 6.276 | 6.276 | 6.276 | 6.276 | 2.375[a] | 2.375[a] |
| Liner Depth, feet | 4976 | 4976 | 6060 | 4805 | 4976 | 2371[b] | 2371[b] |
| Formation Temperature, °F | 540 | 540 | 540 | 383 | 540 | 525 | 525 |

a Tubing outside diameter. Flow takes place in the annulus between casing and tubing.
b Tubing depth.

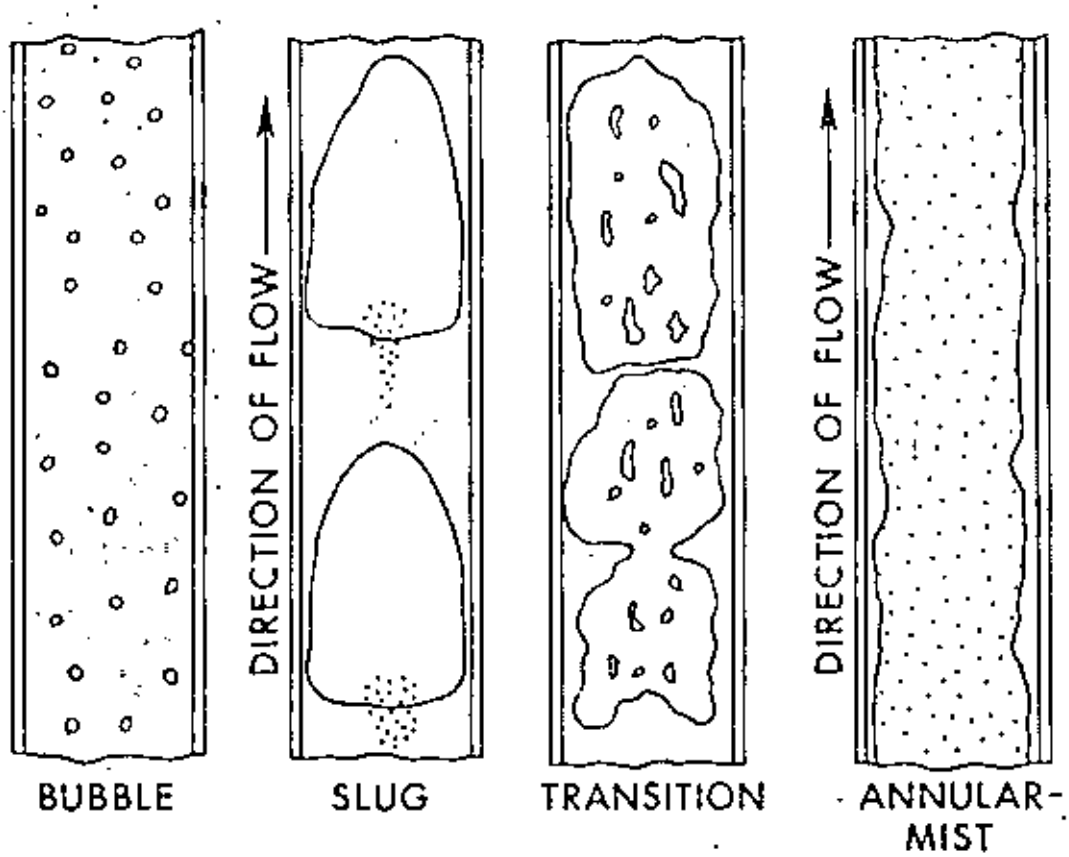


Fig. 1 - Flow regimes for the Orkiszewski correlation.

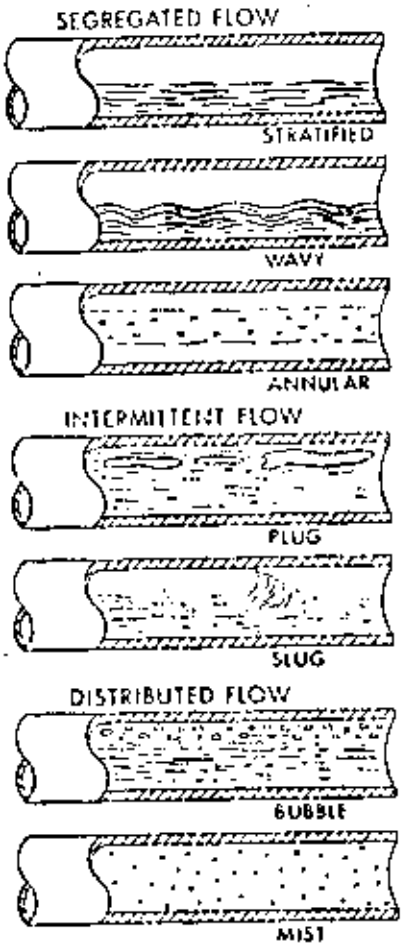


FIG. 2 - FLOW REGIMES FOR THE BEGGS AND BRILL CORRELATION.

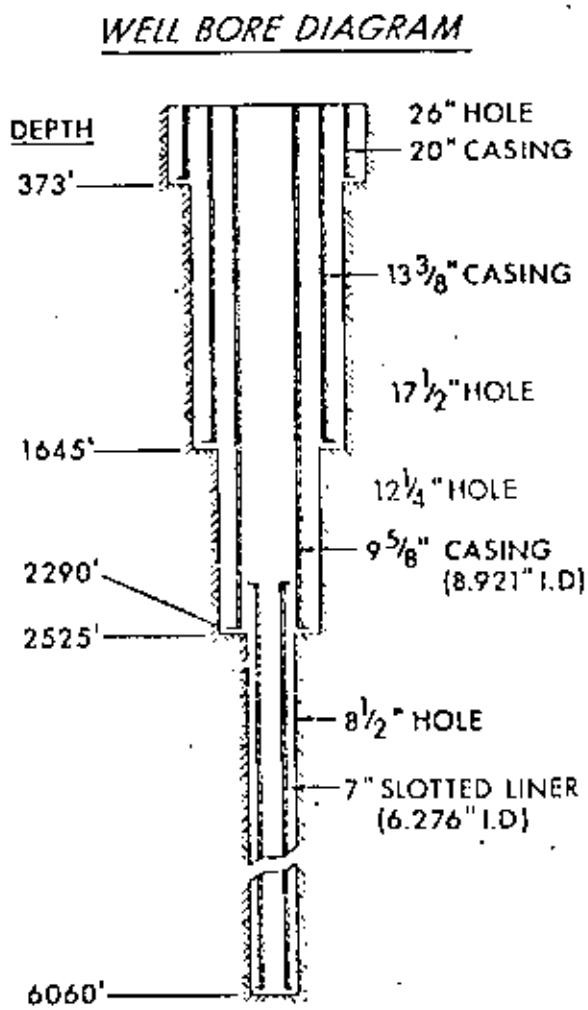


FIG. 3 - A TYPICAL GEOTHERMAL WELLBORE DIAGRAM.

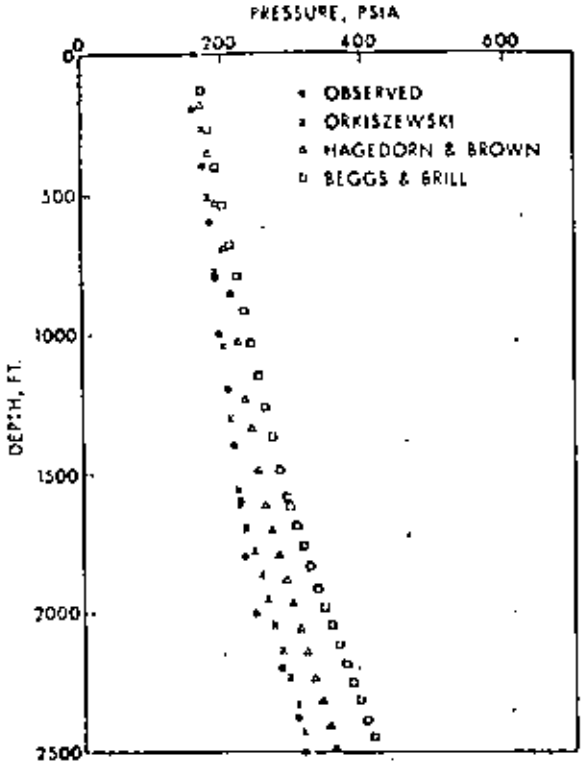


Fig. 4 – Comparison of calculated and observed pressure profiles for survey 1.

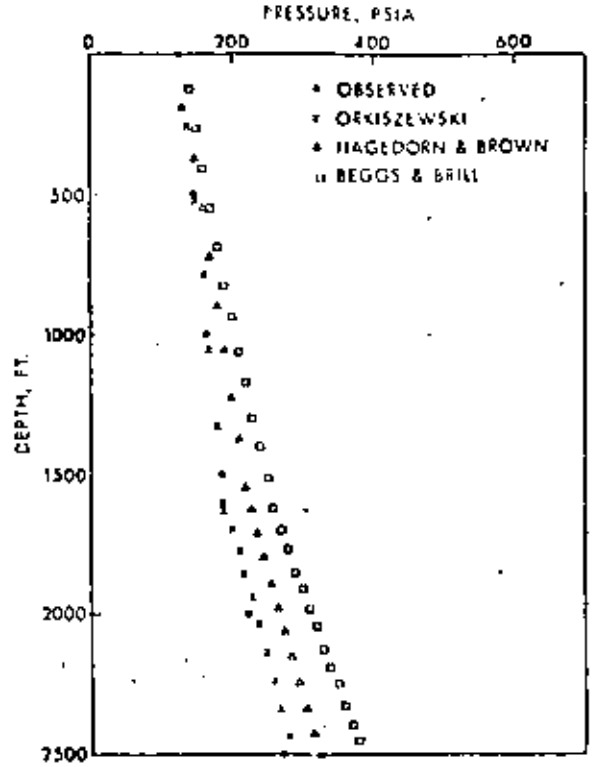


Fig. 5 – Comparison of calculated and observed pressure profiles for survey 2.

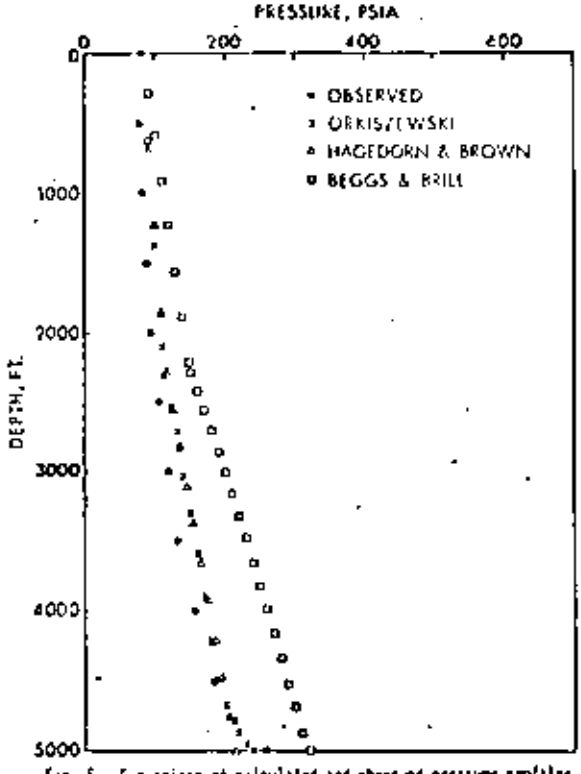


Fig. 6 – Comparison of calculated and observed pressure profiles for survey 3.

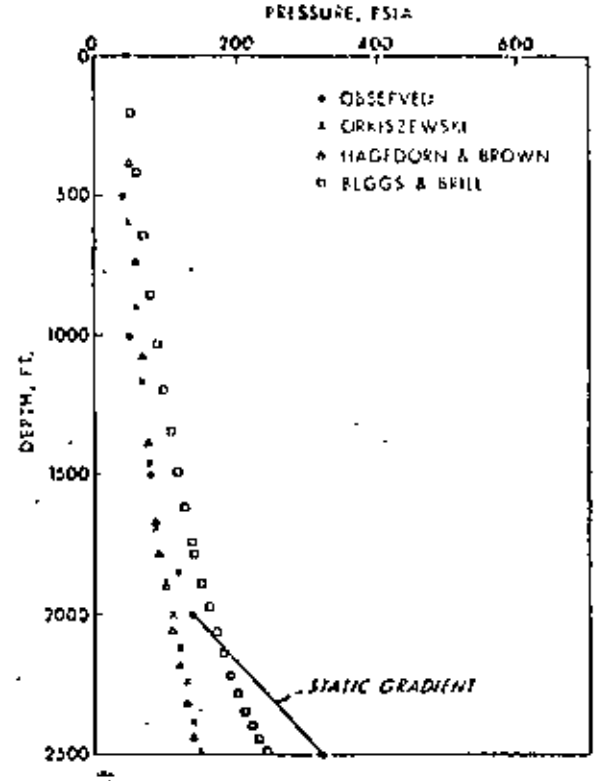


Fig. 7 – Comparison of calculated and observed pressure profiles for survey 4.

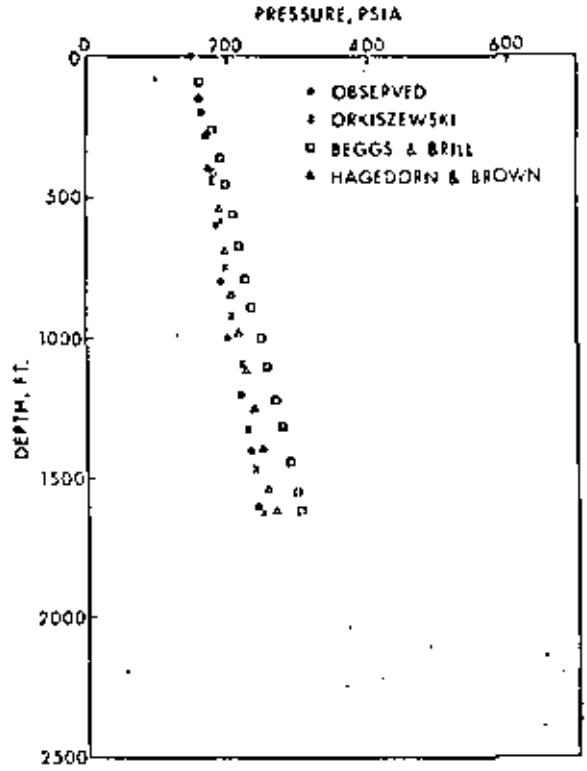


Fig. 8 - Comparison of calculated and observed pressure profiles for survey 5.

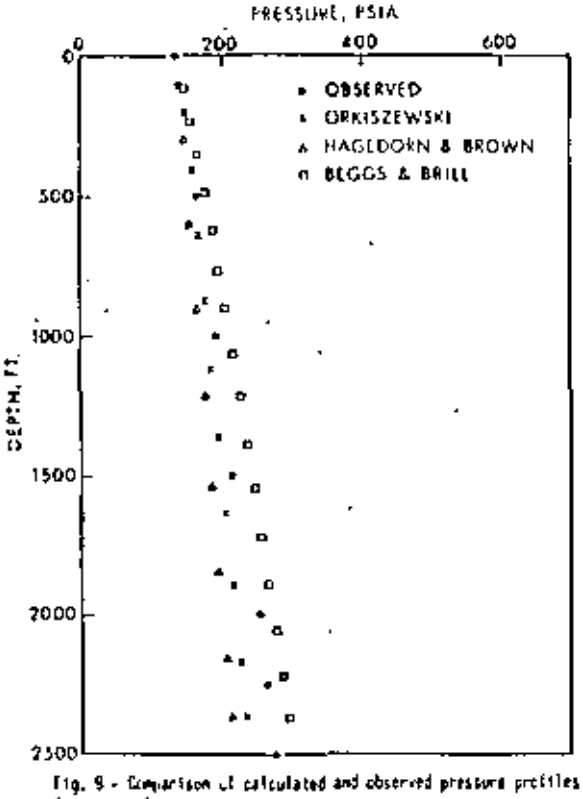


Fig. 9 - Comparison of calculated and observed pressure profiles for survey 6.

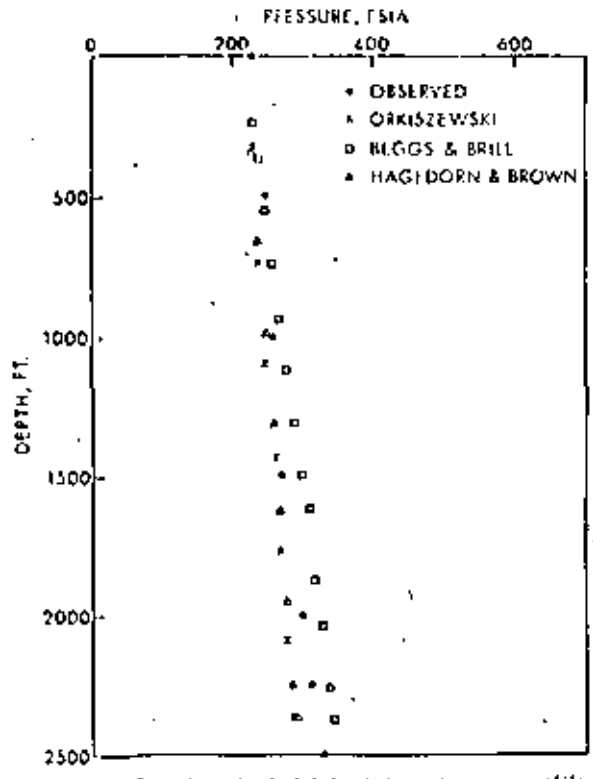


Fig. 10 - Comparison of calculated and observed pressure profiles for survey 7.

THERMODYNAMICS AND FLUID MECHANICS GROUP



# STEAM–WATER CRITICAL FLOW THROUGH PIPES

By Russell James*

Steam and steam-water flashing flow were used to obtain critical† discharge pressures for pipes over the stagnation enthalpy range 230 to 1200 Btu/lb and for the critical pressure range 14 to 61 lb/in² abs.

Pipe sizes used were 3, 6 and 8 in. in diameter. The following empirical equation covers the data with an accuracy of ±3 per cent:

$$\frac{GA^{1.102}}{P^{0.98}} = 11\,400$$

where $G$ is mass-velocity, lb/sec.ft², $h$ is specific stagnation enthalpy, Btu/lb, and $P$ is the critical discharge pressure, lb/in² abs.

It is also shown that the amount of energy flowing along a pipe can be obtained accurately to within ±10 per cent if the critical pressure only is known; that is, the stagnation enthalpy is not known.

## INTRODUCTION

When a moderate flow of a compressible fluid passes along a pipe to the atmosphere, the pressure drops continuously along the pipe but much more rapidly near the pipe outlet, where the fluid velocity increases to a maximum; also the flow issuing from the pipe outlet is seen to be roughly parallel to the pipe wall.

The pressure just inside the pipe outlet would be the same as that of the atmosphere, that is, a pressure gauge at this position would register zero. However, if the flow is progressively increased there will eventually appear a pressure on this gauge and when this occurs the flow no longer leaves the pipe as before but takes on the shape of a paraboloid with a size proportional to the outlet pressure (Fig. 1). The fluid leaves the pipe with this shape because of the sudden expansion which takes place in passing from the higher pressure within the pipe outlet to the surrounding atmosphere.

The indication of a pressure on the gauge shows that the fluid velocity has reached the maximum possible—a limit such as is imposed by the speed of sound in the fluid—and that the only inherent adjustment left to enable greater flows to pass is for the density to increase; to effect this the outlet pressure must increase.

The flow of flashing water through pipes has been studied (1)–(5) (7) (9) (10) (11)‡ and critical pressures examined (1)–(4) (7) (10). The only investigation to specifically measure critical flows over a wide range of dryness-fraction is that by Isbin, Moy and da Cruz (6) 1957, whose valuable series of tests applied to pipes up to 1 in. in diameter.

The present series of tests was conducted using a geothermal bore at Wairakei, New Zealand, where large flows are available. Thus, pipe sizes used were 3, 6 and 8 in. diameter. The purpose of the tests was to obtain the relation between mass-velocity, stagnation enthalpy and critical pressure over as wide a range as possible and to use the critical pressure as a means of measuring the flow-rate of two-phase flashing flow passing to the atmosphere, when the stagnation enthalpy is known.

## EXPERIMENTAL

Fig. 2 is a diagrammatic sketch of the equipment used in these tests.

Steam–water mixtures were obtained by two methods:

(1) By flashing pressurized water through throttle valve A into the discharge pipe. This applied to the range of stagnation enthalpies 230 to 390.

*The MS. of this paper was first received at the Institution on 14th August 1961, and in its revised form, as accepted by the Council for publication, on 23th November 1961.*

* *Department of Scientific and Industrial Research, Dominion Laboratory, Lower Hutt, New Zealand.*

† *Critical pressure is associated with critical flow which occurs when a fluid is travelling at the velocity of sound.*

‡ *A numerical list of references is given in Appendix II.*

*Fig. 1. 56 000 lb/h of steam discharging to the atmosphere from a 3-in. diameter pipe*

(2) By injecting pressurized hot water through valve C into the steam pipe. This applied to the range of stagnation enthalpies 500 to 1100.

The source of steam-water used was a geothermal bore producing up to 900 000 lb/h at an enthalpy of 475. The flow was separated at the well-head by means of a cyclone, and the water and steam passed separately through 8-in. pipes, throttle valves, and discharge pipes to the atmosphere. The method of measuring the flow-rates was by means of orifice meters.

In the case of the water which was at the saturation temperature, a large cooling tank was necessary in the line in order to suppress local flashing at the orifice. The amount of undercooling was approximately 10° to 30°F and was measured by a temperature socket inserted in the line between the cooling tank and the orifice. The level-control tank was used to eliminate the possibility of steam from the cyclone escaping into the low enthalpy line during tests. A sight glass was provided in this tank for indication of the water level.

Because of the large quantities tested, both discharge pipes entered a concrete silencer before releasing their flows to the atmosphere.

Critical pressures were taken by drilling a $\frac{1}{4}$-in. hole at a centre distance of $\frac{1}{4}$ in. from the extreme end of the pipe (see Appendix 1). A $\frac{1}{4}$-in. socket was welded in position externally and a small-bore connecting pipe brought outside the silencer to a pressure point. To the pressure point was attached a goose-neck syphon, needle valve and glycerine-damped gauge. The ends of the pipe were clean, square, and free from internal burrs and the break-through of the $\frac{1}{4}$-in. hole was deburred.

The selection of a glycerine gauge was dictated by the need to dampen the vibrations normally associated with two-phase flow in pipes. The effect of the high frequency, low-amplitude vibration mechanically transmitted along the pipe was thus eliminated and the low-frequency, high-amplitude vibration due to surging (probably projected along the pipeline by flow-pattern changes upstream of the measuring point) was reduced considerably. The needle valve served to reduce further the amplitude of this second vibration sufficiently to enable precise pressure readings to be taken.

Provision for mechanical mixing of the flows after the point of injection of water into the steam was considered unnecessary because of several features inherent to the system (Fig. 2).

(*a*) The flashing of the pressurized water through valve C into the steam line.
(*b*) The turbulence promoted at the change in pipe cross-section from 8 to 6 in. diameter.
(*c*) The rapid acceleration of the mixture along the 12-ft length of the outlet pipe tended to disperse the water into minute droplets.

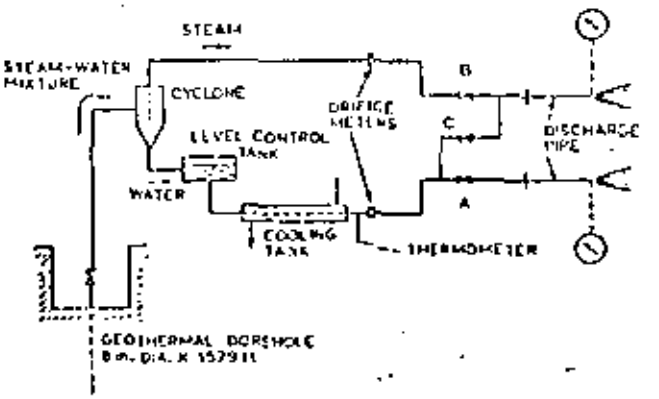


*Fig. 2. Equipment used for tests*

### Stagnation enthalpy range 230 to 390

For a series of constant values of stagnation enthalpy, the flow rates of pressurized water were regulated by valve A and the corresponding values of the critical pressure developed at the outlet were measured.

An 8-in. discharge pipe was used up to a critical pressure of 30 lb/in² abs., a 6-in. pipe until 47 lb/in² abs. was reached and a 3-in. pipe up to a pressure of 61 lb/in² abs.

### Stagnation enthalpy range 500 to 1100

Adjustment of valves B and C permitted the attainment of steam-water mixtures of the required stagnation enthalpy and of the required total mass flow. The critical outlet pressures were measured for a series of values of stagnation enthalpy between 500 and 1100 at different values of mass flow. A 6-in. discharge pipe was used.

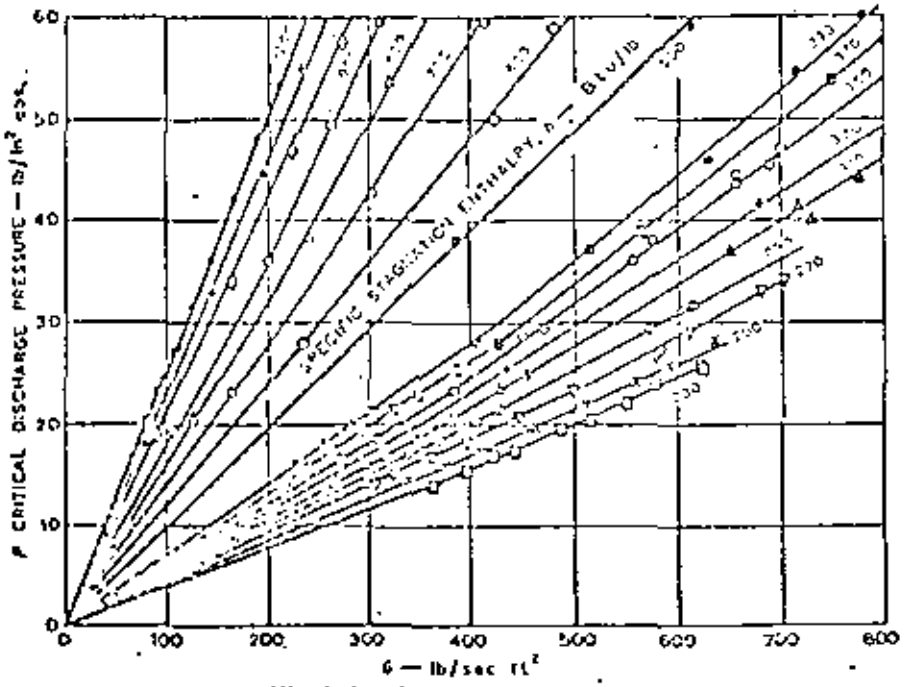


*Fig. 3. Results of experimental tests*

### Stagnation enthalpy 1200

The values of critical pressure at different values of mass flow were measured at a stagnation enthalpy of 1200. This value of stagnation enthalpy was obtained by passing dry st[illegible] through 6 in. and 3 in. discharge pipes. A few [illegible]minations were also made with an 8 in. discharge pipe.

## RESULTS

The experimental results of the tests are shown in Fig. 3 where the mass flows measured in the different discharge pipes are expressed as mass-velocities (lb/sec.ft²) and are plotted against the measured values of critical pressure for various values of stagnation enthalpy between 230 and 1200.

It is important to note that stagnation enthalpy in this context is the total specific energy of the flow and is derived from up-stream conditions where the kinetic energy of the fluid is negligible compared with the critical flow conditions prevailing at the pipe outlet.

Values of the parameter $G/P^{0.96}$ are calculated from these results and plotted against stagnation enthalpy in Fig. 4. This parameter was used by Isbin, Moy and da Cruz (6) for their empirical correlation with the dryness fraction of steam-water mixtures.

The following empirical equation has been derived from the straight-line graph of Fig. 4.

$$\frac{Gh^{1.102}}{P^{0.96}} = 11\,400 \quad . \quad . \quad . \quad . \quad (1)$$

Values of $G$ calculated by this equation from the appropriate values of $h$ and $P$ (for critical pressures below 61 lb/in² abs.) agree with the experimental results for steam-water mixtures with an error less than ±3 per cent.

For dry steam, the plot in Fig. 3 is a straight line and the equation in this case can be more simply expressed as

$$G = 4P \quad . \quad . \quad . \quad . \quad . \quad (2)$$

Equation (1) can be modified in order to calculate $E$, the rate of energy flowing per ft² of cross-sectional area, where $E = Gh$ Btu/sec.ft².

$$\frac{Eh^{0.102}}{P^{0.96}} = 11\,400 \quad . \quad . \quad . \quad . \quad (3)$$

It is obvious from this equation that the relation between $E$ and $P$ is little affected by variations in the stagnation

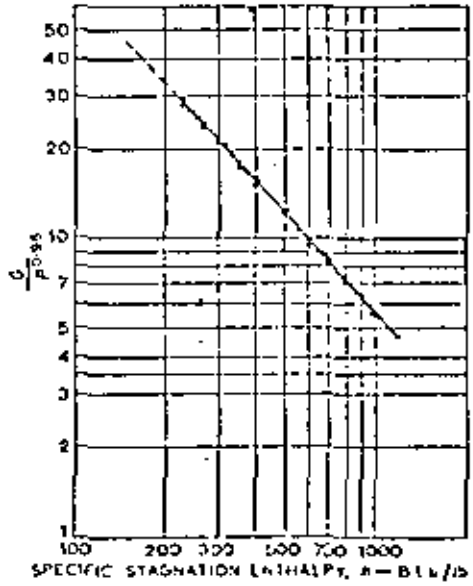


*Fig. 4. $G/P^{0.96}$ against stagnation enthalpy*

enthalpy—calculations show that within the range 300–1200, the use of the geometric mean of these limiting stagnation enthalpies in equation (3) introduces errors no larger than 7 per cent.

The error introduced thus by using this mean value of $h$ of 600, together with the possible error of ±3 per cent applying to equation (1) gives a total possible error of 10 per cent in the value of $H$ determined by equation (3) for any stagnation enthalpy within the range 300–1200 and for a given critical pressure.

Equation (3) has a significant practical application in the measurement of the energy flow from New Zealand geothermal bores which are generally derived from pressurized water sources. The stagnation enthalpy of the steam–water mixtures generally lie within the relatively narrow limits 350 to 600 Btu/lb, and thus an accuracy within ±6 per cent can be obtained for the value of energy flow.

### Comparison with the results of Isbin, Moy and da Cruz (6)

The experimental results of Isbin, Moy and da Cruz produce flow-rates approximately 10 per cent less than those presented here. Although their tests applied to pipes of small diameter (¼, ½, ¾ and 1 in.) compared with the present series, it seems unlikely that the difference is attributable to a size effect (such as a greater relative pipe roughness) and is more probably due to their nearest pressure tapping to the outlet being no closer than one pipe diameter. This rendered it necessary to extrapolate in order to obtain values of critical pressure.

The difficulty in performing such an extrapolation is shown in Fig. 5, which gives the pressure profile near the outlet of a 0·44-in. diameter pipe passing steam to the atmosphere. It is evident that extrapolation from a distance of one pipe diameter from the outlet would give a value of critical pressure higher than the true one. This, in turn, would lead to a lower flow-rate for a given critical pressure.

It seems probable, therefore, that owing to extrapolation, consistently high critical pressures relative to the true ones were obtained over the whole range of enthalpies tested and that this is the most likely explanation for the difference in results obtained.

### Flashing fluids other than steam-water

For establishing a similar relation for such substances with the minimum of tests, a suggested approach is to assume that the following equation applies:

$$\frac{G^x h^y}{P^y} = K$$

where $x$ and $y$ are unknown exponents and $K$ is an unknown constant. This equation can be solved by taking four test runs; two at constant stagnation enthalpy and two at constant critical pressure.

The critical pressure tapping geometry recommended is $D/d = 16$, where $D$ is the diameter of the discharge pipe, $d$ the diameter of the critical pressure tapping, and also

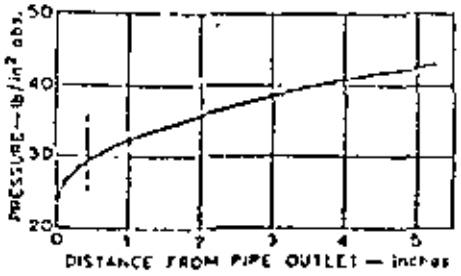


*Fig. 5. Pressure profile near outlet of 0·44-in. pipe passing steam to atmosphere*

equals the distance from the centre-line of the tapping to the end of the discharge pipe.

As pipe sizes would presumably be small, it is further recommended that the material be non-corrodible (such as stainless steel) and that the pressure tapping be into the side of the pipe for horizontal discharge. This should minimize possible blockage by corrosion products or foreign matter.

## CONCLUSIONS

It has been shown that the critical discharge pressure can be used to measure the mass flow or the energy flow of steam–water mixtures passing to the atmosphere through pipes. This has a useful application where water of known stagnation enthalpy flashes to a low-pressure receiver as it gives a simple and direct means of obtaining the flow rate.

For such an application where the stagnation enthalpy is constant, the dial of the gauge reading the critical pressure can be replaced by one reading the flow rate direct. Because of the pressure pulsations natural to flashing flow, a damped gauge will be necessary; a glycerine or oil-damped gauge was found to be quite suitable when used in conjunction with a needle valve.

Care must be taken to obtain a critical pressure tapping as near to the pipe outlet as possible and thus to avoid values obtained by extrapolation.

This method of obtaining flow-rates is already finding application on geothermal boreholes at Wairakei, New Zealand.

## ACKNOWLEDGEMENT

The author wishes to thank the engineers of the Ministry of Works, Wairakei, for their co-operation.

## APPENDIX 1

### LOCATION OF CRITICAL PRESSURE TAPPING ON 3 IN., 6 IN. AND 8 IN. PIPES

The shortest distance which could conveniently be used between the centre-line of a critical pressure tapping and the end of a discharge pipe was ¾ in. A hole of ⅛ in. diameter was drilled at this point. The possibility of blockage of the hole by foreign matter from the pipeline prevented the use of holes of diameter less than ¼ in.

To check the effect of variations in the distance between the tapping and the end of the pipe, mixed flows were passed through 5 in. and 8 in. discharge pipes attached to geothermal boreholes, and the critical pressures developed at points ¾ in. and ⅛ in. from

the pipe ends were measured. The results are shown in the following table.

| | 8-in. pipe, centre-line distance from pipe face, in. | | 5-in. pipe, centre-line distance from pipe face, in. | |
|---|---|---|---|---|
| | ¼ | ½ | ¼ | ½ |
| Critical pressures, lb/in² abs. | 81<br>73<br>65<br>41<br>24·25 | 86<br>75<br>66·75<br>42<br>24·5 | 40<br>20 | 41<br>20·5 |

As a result of these investigations, the distance between the pressure tapping and the pipe end was fixed at ¼ in. Comparison of the results obtained with 3 in. and 8 in. pipes indicated that the ratio of this distance to the pipe diameter was not critical but obviously if the pipe diameter is decreased further then the increasing departure from geometric similarity may eventually produce different results.

## APPENDIX II

### REFERENCES


(1) ALLEN, W. P., Jun. 1951 *Trans. Amer. Soc. mech. Engrs*, vol. 73, p. 297.
(2) BENJAMIN, M. W. and MILLER, J. G. 1942 *Trans. Amer. Soc. mech. Engrs*, vol. 64, p. 657.
(3) BOTTOMLEY, W. T. 1956–57 *Trans. N.-E. Cst Instn Engrs Shipb.*, vol. 53, p. 65.
(4) BURNELL, J. G. 1916 *Engineering, Lond.*, vol. 101, p. 572.
(5) HODGINSON, B. 1937 *Engineering, Lond.*, vol. 143, p. 629.
(6) ISBIN, H. S., MOY, J. E. and DA CRUZ, A. J. R. 1957 *Amer. Inst. Chem. Engrs J.*, vol. 3, p. 361.
(7) LINNING, D. L. 1952 *Proc. Instn mech. Engrs, Lond.*, B, vol. 1B, p. 64.
(8) MARTINELLI, R. C. and LOCKHART, R. W. 1949 *Chem. Engng Progr.*, vol. 45, No. 1, p. 39.
(9) SILVER, R. S. 1938 *Proc. Roy. Soc.* A, vol. 164, p. 464.
(10) SILVER, R. S. and MITCHELL, J. A. 1945–46 *Trans. N.-E. Cst Instn Engrs Shipb.*, vol. 62, p. 51, D15–30.
(11) STUART, M. D. and YARNELL, D. R. 1936 *Mech. Engng*, vol. 58, p. 481; 1944 *Trans. Amer. Soc. mech. Engrs*, vol. 66, p. 387.


# Communications

Mr C. J. Banwell (Wellington, N.Z.) wrote that the method of measuring the discharge rates of steam-water mixtures described in the paper promised to be of much value for the rapid determination of geothermal bore characteristics and similar purposes during field development and exploitation. Although the mass and heat flows could not be determined separately, a study of two-phase flow in geothermal bores he had himself carried out had shown that a satisfactory estimate of the enthalpy of the discharge could be made in many cases from the form of the curve of heat output versus wellhead pressure, so that at least preliminary measurements by a simple method became possible.

The limiting curve for dry steam shown in Fig. 3 agreed very closely with that calculated on the assumption of sonic velocity at the pipe exit. If the steam was considered to behave as a perfect gas with a ratio of specific heats of 1·32, the theoretical relation between mass-velocity and pressure was

$$G = 4{\cdot}42P^{0{\cdot}97},$$

which agreed with Mr James's equation (2) and the steam line of Fig. 3 within ±2 per cent over the pressure range between 15 and 50 lb/in² abs. The value of the exponent of $P$ was also close to the empirical value (0·96) given in equation (1), so that the shape of all the curves of the family seemed to be related to some common critical flow condition. However, the experimental values for the mass flow of the steam-water mixtures were appreciably greater than those calculated from the sonic velocity in a homogeneous mixture, except near the upper and lower limits of the enthalpy range. Thus if the steam in the mixture was assumed to have the same elastic properties as dry saturated steam at the same temperature and pressure, and only the increased density due to the water was considered, the ratio of observed to calculated mass flows at a constant pressure of 25 lb/in² abs. was about unity near 230 Btu/lb, rose steeply to a maximum of nearly 1·5 at about 360 Btu/lb, and fell more gradually to unity again for dry steam. If the velocity was calculated on the assumption of instantaneous equilibrium between the vapour and liquid phases, the disagreement was still greater.

There could be little doubt that much, if not all of this difference was due to departure from homogeneous conditions. Apart from possible velocity difference between steam and water droplets in accelerated flows, gross separation of the phases into layers was often evident from direct observation of bore discharges. He had himself confirmed this separation in the course of measurements with a sampling nozzle*, and it was also confirmed by the later beta ray absorption measurements in flow nozzles described by Belin and Bainbridge†. The nozzle observations showed that some layering of the water near the pipe wall occurred in both vertical and horizontal flows, and with several different forms of upstream throttling. Also, momentum near the walls was found to be generally higher than over the middle part of the flow, indicating a high rate of mass transport in the liquid layer. The beta ray

* BANWELL, C. J. 1957 *Trans. Amer. Soc. mech. Engrs*, vol. 79, p. 269, 'Flow sampling and discharge measurement in geothermal bores'.

† BELIN, R. E. and BAINBRIDGE, A. E. 1957 *Proc. Instn mech. Engrs*, vol. 171, p. 907, 'Estimation of dryness fraction and mass discharge of geothermal bores'.

# Measurement of Steam-water Mixtures Discharging at the Speed of Sound to the Atmosphere

RUSSELL JAMES*
C.ENG., A.M.I.MECH.E.

*The flow of steam or steam-water mixtures discharging to the atmosphere through pipes can be measured by merely taking the pressure on a gauge at the extreme end of the pipe, provided the mixture attains the speed of sound at the outlet. As such speeds are usual at the Wairakei geothermal borefield, this technique has immediate practical application. The influence of the three major variables—flow rate, enthalpy, and the end-of-pipe pressure—were studied by passing steam and steam-water mixtures through small stainless steel tubes and comparing the results with those previously obtained on large commercial steel pipes. The effect of the precise location of the end-of-pipe pressure tapping was also investigated for various pipe sizes; from these studies, a formula has been derived relating mass flow rate to enthalpy, discharge pressure, pipe diameter, and tapping location. The relationship holds for discharge pressures ranging up to 64 lb/in²abs and pipe diameters of up to 8 in.*

## 1. INTRODUCTION

WHEN a moderate flow of a compressible fluid passes along a length of pipe to the atmosphere, the pressure falls progressively until within the pipe outlet it is equal to the atmospheric pressure. At the same time, the velocity has increased from an upstream approximately stagnant condition to its highest value within the pipe outlet.

When very large flows are achieved by increasing the up-stream pressure, eventually the pressure within the pipe outlet will be higher than atmospheric, and can be measured by a pressure gauge at the extreme end of the pipe. This pressure is known as the critical discharge pressure, and it is associated with the so-called critical flow, which occurs when a compressible fluid attains the speed of sound. When critical flow takes place at the pipe outlet, increasing the up-stream pressure not only increases the flow rate but increases the critical discharge pressure. The last two factors are indeed linearly related and the gauge reading may be used to measure the flow-rate direct.

Provided the back pressure does not exceed the critical discharge pressure, its variation has no significant effect on the system because pressure fluctuations that may travel at the speed of sound cannot be transmitted up-stream of a fluid already at that velocity. This is well attested by those familiar with the use of critical flow meters (1).

Although compressible flow is generally regarded as that of a single-phase fluid such as air or steam, it may also be applied to a two-phase fluid such as a steam-water mixture if one of the phases can be considered as compressible within the usual meaning of the term. This is confirmed by the existence of critical flow at the end of pipes passing such steam-water mixtures to the atmosphere at the geothermal borefield at Wairakei, where it has been noticed that change in flow rate is faithfully followed by change in the critical discharge pressure.

It was realised that this phenomenon could be used to measure the outputs of geothermal boreholes if the relationship between the flow-rate, the enthalpy (total heat) of the mixture, and the critical discharge pressure could be determined. As overseas workers using relatively small pipes had not attained conclusive results, a test series was undertaken at Wairakei (2) to investigate the critical flow of steam-water mixtures to the atmosphere through horizontal 3, 6, and 8 in diameter pipes over the enthalpy range 270 to 1,200 Btu/lb and over the critical discharge pressure range 14 to 64 lb/in²abs. The position of the critical pressure tapping was fixed for all three pipe sizes at 4 in from the pipe

*Senior scientific officer, Chemistry Division, Department of Scientific and Industrial Research.

Reprinted from *New Zealand Engineering*, 21 (10) : 437-41 (October 1966).

discharge face where a hole of ¼ in diameter was drilled. It was found that formula 1 below covered the data with an accuracy of ±3%.

$$Gh^{1.102}/P^{0.96} = 11{,}400 \qquad \text{.....(1)}$$

where:

$G$ = mass velocity of flow, lb/s.ft²
$h$ = specific stagnation enthalpy, Btu/lb
$P$ = critical discharge pressure, lb/in² abs

The term "stagnation enthalpy" is used because when a compressible fluid approaches the speed of sound, the increase in velocity is at the expense of the energy content of the fluid and can result in an enthalpy drop of about 50 Btu/lb in the case of dry steam. To avoid using such locally reduced values of enthalpy at the point of critical flow—which could not be calculated for steam-water mixtures—the enthalpy values were taken from upstream conditions where the velocity was negligible compared with that at the outlet.

Formula 1 was found immediately useful in the measurement of the pressurised hot water of known enthalpy that is separated at the production wellheads of geothermal bores and is flashed to the atmosphere through horizontal discharge pipes.

If the enthalpy of the flowing fluid is unknown, the value of the critical discharge pressure cannot be used to give a direct solution of the flow rate. However, this presents no great difficulty at Wairakei where nearly all production boreholes discharge into vertical twin-tower concrete silencers from which the residual water, which has lost its flash steam, is measured at atmospheric pressure and 100° C by means of a rectangular weir, before it passes to the main draining culvert. Using a critical pressure tapping at the end of a pipe discharging an unknown mixture into such a silencer, it is possible to calculate both flow and enthalpy using merely the values of the critical discharge pressure and the flow rate at the weir. Figure 1 shows a diagrammatic sketch of the arrangement and presents the solution of enthalpy in the form of a graph; the enthalpy value so determined is then used in formula 1 to obtain the flow rate. An illustrative example is given in the Appendix.

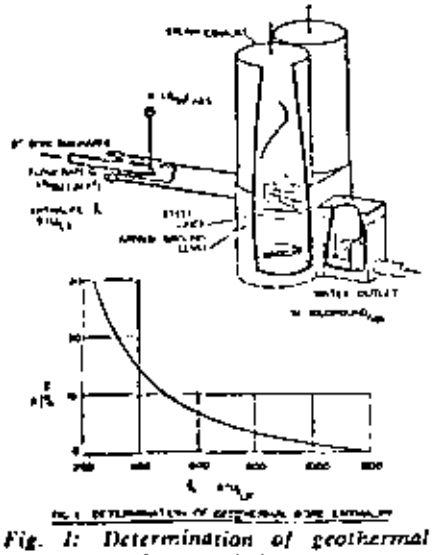

*Fig. 1: Determination of geothermal bore enthalpy.*

The derivation of formula 1 from the results of the test series on large pipes was surprisingly good considering that the same pressure tapping geometry was used on pipes as different in diameter as 3 and 8 inches. However, it raised a number of questions:

(a) Would a relationship as simple as that given in formula 1 be forthcoming for critical steam-water flow through small pipes?

(b) How important is the critical pressure tapping distance from the pipe outlet face?

(c) Does formula 1 also apply to the vertical critical flow of steam-water mixtures (such as occurs when a newly opened bore-hole is discharged to the atmosphere)?

To resolve these questions, the three test series described below were undertaken as part of the long-term research on steam-water flow phenomena conducted by representatives of the chemical engineering section, Chemistry Division, Department of Scientific and Industrial Research, who have a permanent station at borehole 203, Wairakei.

## 2. EXPERIMENTS AND RESULTS

### 2.1. Test 1: Flow Through Small Tubes

The experimental equipment for passing steam-water mixtures at maximum discharge through small diameter tubes is shown in Fig. 2. Two stainless steel tubes were tested, of 0.067 and 0.17 in inside diameter. Steam from a geothermal borehole and water at 70° F were mixed in a manifold before passing through the tube being tested, to a heat exchanger. The end of the tube was sealed within the heat exchanger entrance, as was a small pipe connecting the critical pressure tapping (close to the tube discharge face) to an outside gauge. The pressure tapping geometry used for both sizes of tube, was a 0.04 in diameter hole drilled at a centreline distance of 0.04 in from the discharge face. A pressure tapping was also made within the entrance of the heat exchanger to ensure that the back pressure induced did not attain the value of the critical discharge pressure at the end of the test tube. By taking flow rates and temperatures, of the cooling water and condensate of the heat exchanger, the values of stagnation enthalpy and mass velocity in the test tube were determined.

Using these values and the value of critical discharge pressure, the value of the parameter $Gh^{1.102}/P^{0.96}$ was calculated and plotted against stagnation enthalpy for all test results obtained in both test

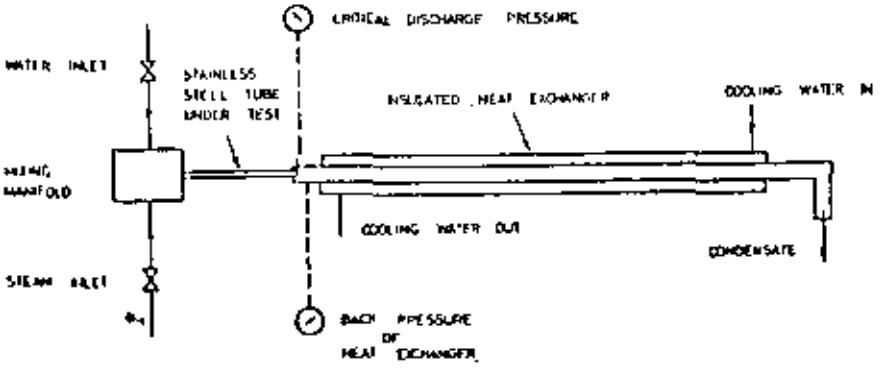


*Fig. 2: Equipment used for tests on small tubes.*

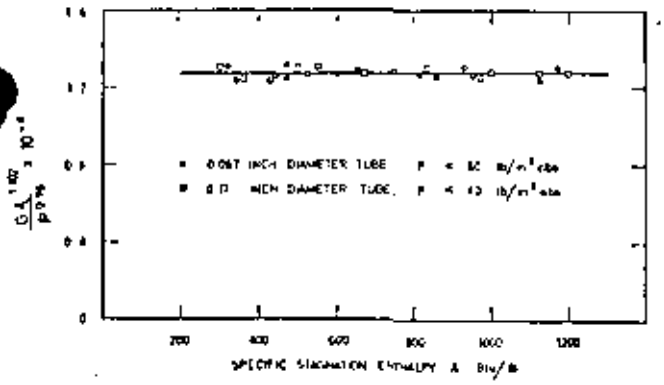

*Fig. 3: Results of experimental tests on small tubes.*

tubes. This is shown in Fig. 3, where the line drawn at 12,800 covers the data accurately to ±3%.

The relationship established for the two stainless steel tubes tested was therefore

$$Gh^{1.102}/P^{0.04} = 12{,}800 \qquad \text{.....(2)}$$

## 2.2. Test 2: Critical Pressure Related to Tapping Position

To study the pressure profile for different pipe sizes and for various values of enthalpy, a series of 0.031 in diameter holes was drilled at various distances from the outlet face of a number of pipes. Using dry steam initially and pipe sizes 0.23, 0.44, 1.07, and 4 in diameter, flow rates were adjusted to give a pressure at the tapping nearest to the outlet face of 20 lb/in²abs. The values of pressure at all the other tapping points were then plotted (see Fig. 4) for these sizes of pipe. It is seen that at a distance of less than approximately half an inch from the discharge face, the same curve suits all sizes of pipe, and the same value of pressure would be obtained independent of the diameter of pipe (over the range 0.23 to 4 in).

Two pipe sizes were then taken of 0.23 and 1.07 in diameter, and steam-water mixtures passed through of stagnation enthalpies 900, 725, 650, 520, and 395 Btu/lb. For comparative purposes, the flow rates were adjusted to give pressures at the tappings nearest the outlet faces in the region of 20 to 30 lb/in²abs. The pressures at all tapping positions are shown plotted in Fig. 5. Separation of the curves occurs in the region of approximately 0.6 to 1 in from the pipe face; at distances closer to the outlet face than this, it is apparent that one curve would suit both sizes of pipe tested.

The results of these tests indicate that within a close distance of the pipe outlet face, the pressure

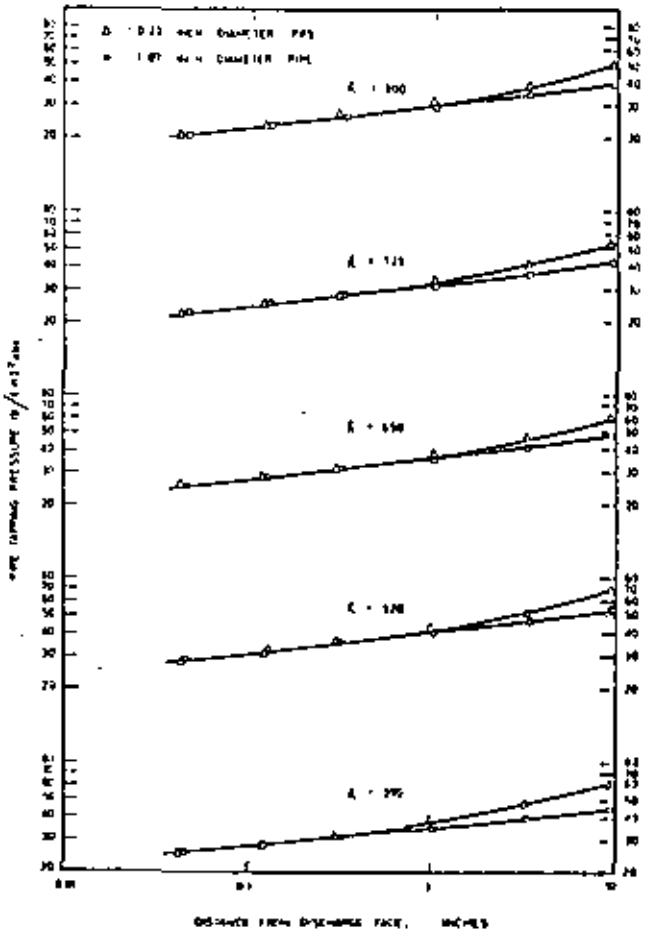

*Fig. 5: Pressure profile for steam-water flow through pipes.*

at a given position is independent of pipe diameter. For ease of comparison between pipes of different diameters it is therefore important to keep the pressure tapping diameter and absolute distance from the pipe face the same on all pipe sizes; if that is not possible then the distances of the pressure tappings should be kept to the minimum from the pipe face and due allowance made for different pressures at different distances from the face. For large pipes of 3, 6, and 8 in diameter, with (tapping diameter)/(face distance) ratios of 0.25/0.25, the numerical constant in the flow equation (formula 1) is 13,400; for small pipes 0.067 and 0.17 in with ratios of 0.04/0.04, it is (formula 2) 12,800.

To obtain a flow relation applicable to the range of pipe diameters considered, this constant is as-

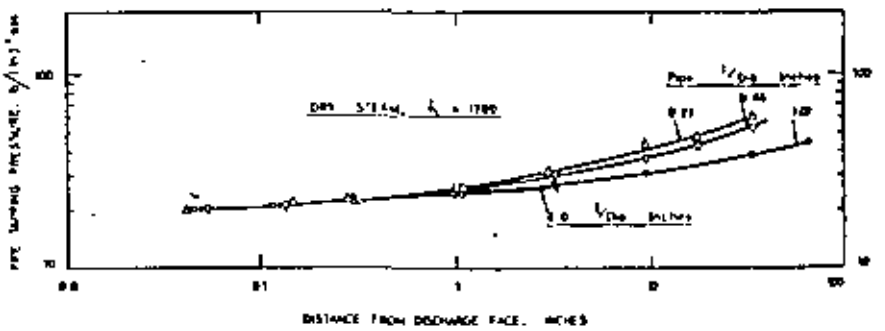

*Fig. 4: Pressure profile for steam flow through pipes.*

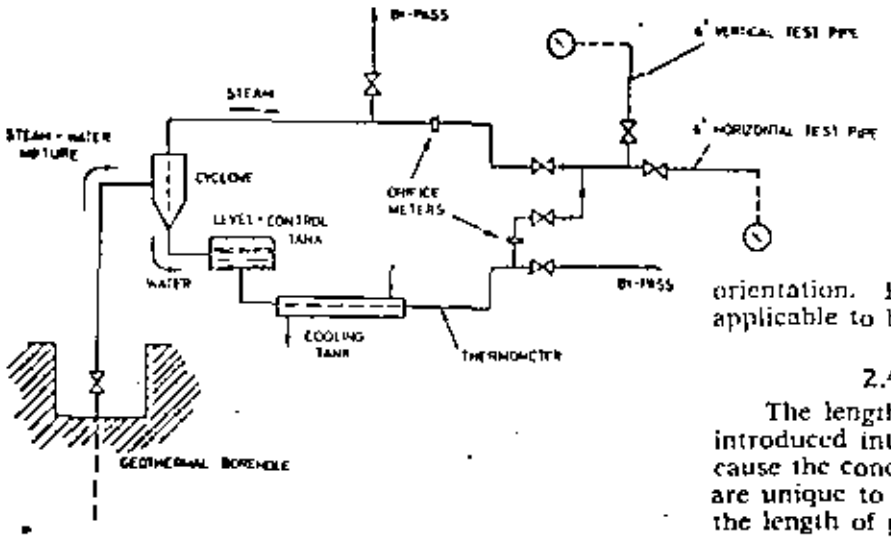


*Fig. 6: Equipment used to compare vertical flow with horizontal flow.*

sumed equal to $K/y^n$, and is independent of pipe diameter for distances close to the pipe discharge face. $K$ and $n$ are constants and $y$ is the distance from the pipe discharge face to the centre of the pressure tapping hole.
That is:

$K/0.25^n = 11{,}400$ for the 3, 6, and 8 in pipes, and
$K/0.04^n = 12{,}800$ for the 0.067 and 0.17 in tubes.

The formula derived to suit both test series is therefore:

$$G/P^{1.107}/P_{0.08} = 10{,}450/y^{0.045} \qquad \ldots\ldots (3)$$

This formula strictly applies where the size of hole used as a critical pressure tapping is dimensionally equal to the value of $y$; also from an extrapolation of the data of test 2, it is suggested that $y$ be restricted to a value not exceeding 0.3 in over the range of pipes diameters 0.067 to 8 in.

### 2.3. Test 3: Vertical Compared with Horizontal Flow

Both the earlier test series on large pipes and the present series on small tubes were conducted with the steam-water mixtures passing horizontally to the atmosphere. During some testing of geothermal boreholes, the discharge to the atmosphere takes place in a vertical direction; it is therefore of importance to determine if the relationship between mass flow, stagnation enthalpy and critical discharge pressure is the same as for horizontal flow or whether the effect of gravity produces a different correlation. To study this relationship, equipment was assembled (see Fig. 6) in which steam-water mixtures of known stagnation enthapy and flow-rate could be passed successively through a horizontal and a vertical 6 in diameter test pipe. Both pipes had identical critical pressure tappings of a $\frac{1}{4}$ in diameter hole at a distance of $\frac{1}{4}$ in from the pipe discharge face. Figure 7 shows the comparison between critical discharge pressures for vertical and horizontal flow over the stagnation enthalpy range 271 to 1,200 Btu/lb and over the critical discharge pressure range 15 to 67 lb/in²abs. There is no significant difference between the pressure values, and therefore it can be assumed that there is no material difference attributable to pipe orientation. Hence formula 3 can be accepted as applicable to both cases.

### 2.4. Effect of Pipe Length

The length of the discharge pipe has not been introduced into the tests and equations; this is because the conditions at the extreme end of the pipe are unique to that location and are independent of the length of parallel pipe up-stream.

The longer the pipe for given conditions of upstream pressure and enthalpy, the smaller the flow-rate and therefore the lower the critical discharge pressure, but this does not invalidate the equations.

The effect of pipe length on flow-rate has been studied for dry saturated steam with critical flow occurring at the outlet face in a previous series of tests (3) using eight pipe sizes with length/diameter ratios ranging from 2.27 to 3,000. For very short pipes of length/diameter less than 3 discharging to the atmosphere from a pressure vessel, the pressure at the outlet face begins to approach that at the throat of a similarly discharging convergent nozzle, where it is well known that the throat pressure is approximately half the vessel pressure.

Some tests at Wairakei on steam-water critical flow through very short pipes discharging to the atmosphere from a pressure vessel gave results approximating to that for dry steam, in that the discharge pressure was roughly half the vessel pressure.

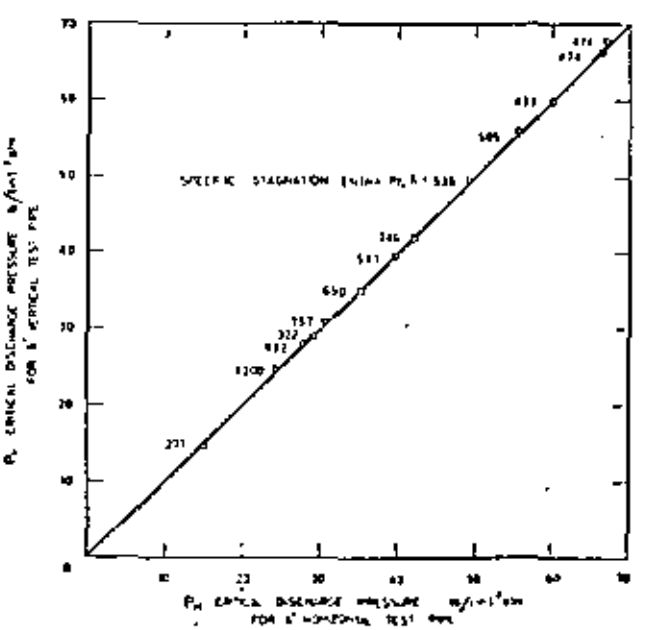


*Fig. 7: Results of tests comparing vertical with horizontal flow.*

## 3. CONCLUSIONS

All the relevant factors involved in measuring the flow of steam-water mixtures discharging to the atmosphere at the speed of sound have been studied, and the derived formula is applicable over a very large range of pipe sizes and steam-water mixture ratios.

Although the tests were conducted with values of critical discharge pressures no greater than 70 lb/in²abs, this is sufficiently high for use at the Wairakei geothermal borefield, where pressures at the outlet of 8 in pipes rarely exceed this. Other borefields, however, may attain higher values—in Mexico, for example, a value of 140 lb/in²abs has been reported for a 6 in discharge pipe—in which case it would seem desirable to continue tests into higher pressure regions. Spot values taken at Wairakei with critical discharge pressures as high as 135 lb/in²abs in 3 in pipe indicate that the relationship given in the formulas is still valid.

This technique is now in use both in New Zealand and overseas, and is proving to be one of the few methods existing for the measurement of two-phase critical flow with reasonable accuracy.

## 4. REFERENCES


(1) BRITISH STANDARDS INSTITUTION (1964): *B.S. 1042 : 1964, Part 1.*

(2) JAMES, R. (1962): Steam-water Critical Flow through Pipes. *Proc. Inst. Mech. Engrs., 176* (26) : 741.

(3) JAMES, R. (1964): Maximum Steam Flow through Pipes to the Atmosphere. *Proc. Inst. Mech. Engrs., 178, Part 1* (18) : 473.


## APPENDIX

### Illustrative Example

The flow of hot water from the silencer of a geothermal borehole is measured as 350,000 lb/h by using a rectangular weir, while the pressure at the end of the 8 in discharge pipe is 20 lb/in²gauge. Find the enthalpy and flow from the bore.

$W = 350$ klb/h; $P = (20 + 14.2) = 34.2$ lb/in²abs

(where the average atmospheric pressure at Wairakei is 13.2 lb/in²abs at 1,300 ft above sea level).

$$W/P^{0.96} = 350/34.2^{0.96} = 11.67$$

From Fig. 1, the bore enthalpy = 460 Btu/lb.

From formula 1, $G = (11{,}400 \times 34.2^{0.96})/460^{1.393}$

$= 398$ lb/s.ft²

Flow in pounds per hour through 8 in discharge pipe

$= (398)\ (\pi/4)\ (8/12)^2\ 63^2 = 505{,}000$ lb/h

Note: It is assumed in the above example that the critical pressure tapping geometry is a ¼ in diameter hole drilled at ¾ in from the pipe discharge face, which is a convenient arrangement for pipe sizes greater than 3 in; where, however, the tapping geometry differs from this, formula 3 should be used. It should also be noted that Fig. 1 applies for 8 in inside diameter discharge pipes such as are used at Wairakei; where discharge pipe sizes differ from this, $W/P^{0.96}$ should be amended to $(8/d)^2(W/P^{0.96})$ where $d$ is the inside diameter of the discharge pipe in inches.

# A HAND COMPUTER PROGRAM FOR JAMES' LIP PRESSURE STEAM-WATER FLOW RATE

HENRY J. RAMEY, JR.

PETROLEUM ENGINEERING DEPT., STANFORD UNIVERSITY, STANFORD, CA 94305

Programmable hand computers are rapidly becoming the engineer's slide rule of the future. Read-write recording programmable hand computers offer a capability not available through computer terminals. These hand computers will have a massive impact on engineering. There is currently a resistance on the part of both technologists and management to accept the role of the hand computer. Programming hand computers elevates the level of logic and computing ability of technologists. Problems will be solved without error that were previously avoided. Management hesitance to invest in hand computers because of obsolescence or duplication of large computer facilities should be reconsidered. One way to meet the current engineer shortage is by upgrading the capabilities of existing staff. The hand computer is one means to this end. The purpose of this report is to present a useful program which may be reprogrammed on other hand computers, the James' Lip pressure method for finding steam mixture flow rates.

An important geothermal fluid production problem is measuring the flow rates from wells in liquid-dominated steam reservoirs. One such method is the James' Lip Pressure method[1]. In this method, a steam-liquid mixture is passed from a well head through a horizontal pipe of constant diameter, d inches, and exhausted to a muffler. The "lip" pressure is measured through a 1/4" hole drilled 1/4 inch from the end of the pipe. The liquid collected from the muffler is measured in a weir. The liquid height in H inches is recorded. From this information, it is desired to compute the following: (1) the liquid rate, $W_L$, kilo lbs/hr, (2) the total mass rate, $W_t$, kilo lbs/hr, (3) the mixture enthalpy, BTU/lb, and (4) the steam quality, mass fraction vapor.

A hand computer program capable of making the necessary computations is presented in Tables 1-3. This program is written in reverse polish logic for the HP-67/97 hand computers. The program description including equations is given in Table 1. The equations are sufficient for the program to be rewritten for other hand computers. The program runs in about 5 seconds, and is a useful aid for making flow rate calculations for liquid-dominated steam wells. The mixture enthalpy equation is a curve fit of graphical data presented by James. The User Instructions are presented in Table 2. The program commands are presented in Table 3.

## Example Calculation

Given H = 3.5 inches
p = 5 psig
d = 6 inches

Answers $W_L$ = 24.09 K lbs/hr
$W_t$ = 81.70 K lbs/hr
h = 865.18 Btu/lb
x = 0.71 weight fraction
$d^2p$ = 629.49 $in^2$-psia

## Reference

James, R.: "Steam-Water Critical Flow Through Pipes," Proc. Inst. Mech. Engrs. (1962), 176, No. 26, p. 741.

## TABLE 1. Program Description

Program Title: GEOTHERMAL STEAM RATE BY JAMES' LIP PRESSURE
Name: HENRY J. RAMEY JR. Date: 11-10-76
Address: PETROLEUM ENGINGERING DEPT., STANFORD UNIV.
City: STANFORD State: CA Zip Code: 94305

Program Description, Equations, Variables etc.: PROGRAM CALCULATES: (1) WEIR LIQUID RATE, (2) STEAM-LIQUID MIXTURE ENTHALPY, (3) TOTAL MASS RATE, & (4) STEAM QUALITY BY RUSSELL JAMES LIP PRESSURE METHOD. EQUATIONS ARE:

WEIR LIQUID RATE: $W_L = 1.051(H)^{2.5}$

MIXTURE ENTHALPY: $y = (c-y) + b(\ln h) + a(\ln h)^2$

$$y = \left(\frac{B}{d}\right)^2 \left(\frac{W_L}{P^{.96}}\right)$$

WHERE: $y \le 4.78$: $c-y = 295.46$; $b = -75.157$; $a = 4.5155$; $700 \le h \le 1100$
$y > 4.78$: $c-y = 627.24$; $b = -178.76$; $a = 12.787$; $250 \le h \le 700$

LIP PRESSURE: $W_L = 225.84 \frac{d^2 P^{.96}}{h^{1.82}}$

SYMBOLS: $W_L$ = WEIR LIQ. RATE, K LBS/HR; $h$ = MIXTURE ENTHALPY, BTU/LB
$W_t$ = STM-LIQ. RATE, K LBS/HR
$P$ = LIP PRES., PSIA; $x$ = STEAM QUALITY, MASS FRACTION
$d$ = PIPE I.D., INCHES; $H$ = LIQ. HT IN WEIR, IN.

REFERENCE: JAMES, R.: "STEAM-WATER CRITICAL FLOW THROUGH PIPES," PROC. INST. MECH. ENGRS., VOL. 176, NO. 26, P. 741, 1962.

Operating Limits and Warnings: ERROR IN ENTHALPY CALC. IS ± 2% AT MOST; FOR $h \le 700$, ± 0.6%. RUN TIME ON HP-67 IS 5 SEC. NOTE: IF BAROMETRIC PRESSURE IS OTHER THAN 14.7, CORRECT PRESSURE SHOULD REPLACE 14.7 ON STEPS 021 TO 024.

## TABLE 2. User Instructions

JAMES LIP PRES. 11-10-76 HJR

H=>$W_L$ = d, IN P=> h W$_t$ X

| STEP | INSTRUCTIONS | INPUT DATA UNITS | KEYS | | OUTPUT DATA UNITS |
|---|---|---|---|---|---|
| 01 | ENTER PROGRAM | | | | |
| 02 | TO SEE MIXTURE ENTHALPY | | | | |
| 03 | ENTER LIQUID HEIGHT IN WEIR, IN. | H, IN. | A | | $W_L$, K LB/HR |
| 04 | ENTER PIPE DIAMETER, IN. | d, IN. | B | | $d^2$, IN$^2$ |
| 05 | ENTER LIP PRES., PSIG | P, PSIG | C | | h, BTU/LB |
| 06 | PRESS D TO SEE TOT. MASS RATE, $W_t$ | | D | | $W_t$, K LB/HR |
| 07 | PRESS E TO SEE STEAM QUALITY | | E | | X, MASS FR. |
| 08 | ENTER NEW LIP PRES., GO TO 04 | | | | |
| | | | | | |

Table 3 Forsell Jones Hip Pinecone Computer Program for AT 62,47

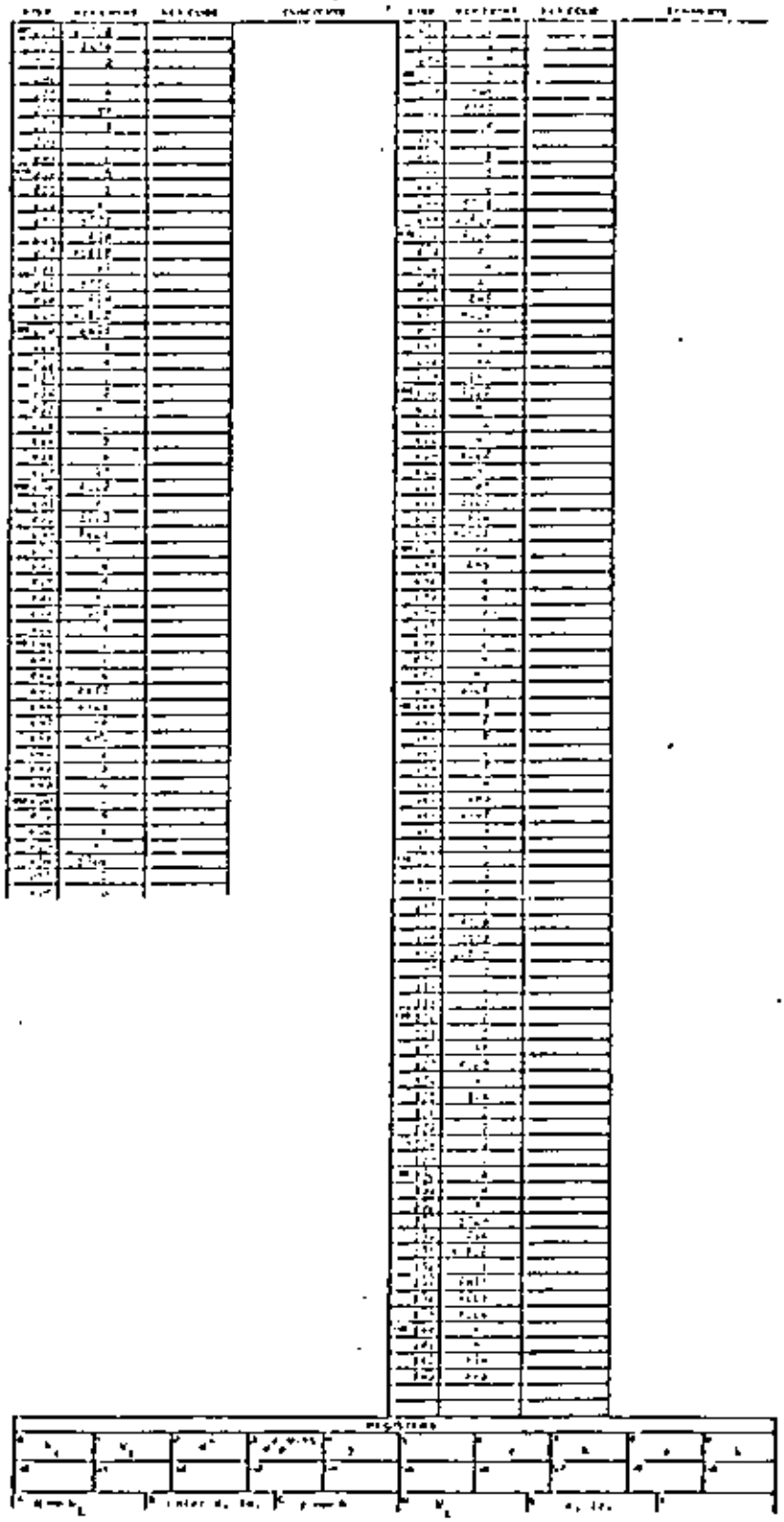

# Choke Design for Geothermal Bores

RUSSELL JAMES
*Department of Scientific and Industrial Research, Taupo, New Zealand*

## ABSTRACT

To control long-term discharges from the wellheads of geothermal bores, chokes are preferable to control valves, which are expensive and liable to be damaged by erosion or chemical deposits.

The type of choke recommended is a steel plate with a hole machined in it. This is inserted between the flanges of the horizontal discharge pipe, which terminates in a lip pressure tapping.

A simple equation is used to obtain the choke diameter for a given flow rate at the appropriate wellhead pressure.

## INTRODUCTION

Before a power scheme is given final approval for a geothermal field, it is usual for wells to be discharged horizontally to the atmosphere for periods of more than six months. Wellhead pressures are set at a value estimated to be that employed when the wells are on production. But even if this estimate proves to be incorrect, it is very useful to discharge at some definite wellhead pressure, in order to measure change in this important factor with long running times. At the Broadlands geothermal field, New Zealand, for example, a wellhead pressure of 160 psig has been selected.

It is preferable to control long-term discharges by means of a choke, rather than by using an expensive valve which would have to be severely throttled to obtain the same effect. Under such conditions, a steam-water mixture is deflected by the gate of the valve and is extremely erosive to the surrounding metalwork. A choke, on the other hand, produces a symmetrical jet which has very little erosive effect even when sand is carried with the mixture. Another factor to be considered is that some wells deposit chemicals at or below the valve gate and this is difficult to remove, whereas it is relatively easy with a choke where it nearly always appears on the downstream face and in the discharge pipe.

Perhaps the only objection to a choke is the difficulty in estimating its diameter for a given flow condition; this results in a tedious trial-and-error test procedure before a satisfactory size is installed in a pipeline, as shown in Figure 1.

## TYPE OF CHOKE AND LOCATION

The simplest kind of choke has been found most useful and consists merely of a mild steel plate about 1 in. thick with a hole machined in it. The plate is trapped between flanges on the horizontal discharge pipeline and for reasons which will be made clear, it should be close up against the downstream face of the throttle valve.

## THEORY

Taking critical flow (sonic velocity) as occurring just within the rim at the downstream face of the orifice of the choke and also at the lip of the discharge pipe, the following relationship can be established with the location given as suffices O and C (James, 1962), and pressure at the rim outlet, $P_1$.

$$\frac{G_o h_o^{1.102}}{P_1^{0.96}} = 11\,400 = \frac{G_c h_c^{1.102}}{P_c^{0.96}}$$

$G$ = specific flow rate, lb/(ft)$^2$ (sec)
$h$ = stagnation enthalpy, Btu/lb
$P$ = critical discharge pressure, psia

As the stagnation enthalpy is constant, $h_o = h_c$

Hence, $$\frac{G_o}{P_1^{0.96}} = \frac{G_c}{P_c^{0.96}}$$

Taking $d_o$ = orifice diameter, inches
$d_c$ = discharge pipe diameter, inches
$W$ = mass flow rate, lb/hr

$$W = G_o \frac{\pi}{4}\left(\frac{d_o}{12}\right)^2 60^2 = G_c \frac{\pi}{4}\left(\frac{d_c}{12}\right)^2 60^2$$

Therefore, $$\frac{G_o}{G_c} = \left(\frac{d_c}{d_o}\right)^2 = \left(\frac{P_1}{P_c}\right)^{0.96}$$

For flows of steam and steam-water mixtures through pipes of varying lengths (James 1963, 1966), it has been found that for very short lengths approximating to orifices, $P_c = 2P_1$, where $P_c$ is the pressure just upstream of the orifice as shown in Figure 2.

Hence $$\left(\frac{P_o}{2P_1}\right)^{0.96} = \left(\frac{d_c}{d_o}\right)^2$$

and $$d_o = \frac{1.4\, d_c}{\left(\frac{P_o}{P_1}\right)^{0.48}}$$

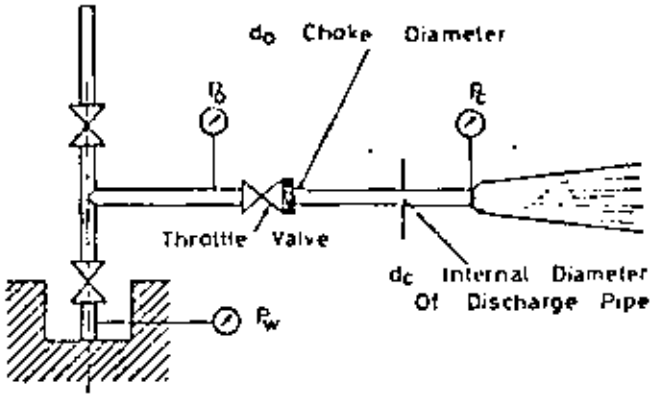


Figure 1. Choke controlling flow of steam-water mixture.

It will be noted that although English units have been used, this equation is strictly nondimensional, with the reminder that pressures are, of course, in absolute terms.

## TEST PROCEDURE

A lip pressure tapping is located at the outlet face of the discharge pipe as described in James (1962, 1975), and a pressure tapping to measure $P_b$ is located within a meter of the upstream face of the horizontal throttle valve as shown in Figure 1. The well is discharged horizontally with the valve throttled to give the required wellhead pressure (at production operating conditions). With the flow stabilized, pressures $P_b$ and $P_t$ are used together with the internal diameter of the discharge pipe $d_c$ in the formula above—which is also given in Figure 2—to determine the diameter of the choke. The throttle valve is now closed and a choke of the calculated diameter is installed between the throttle valve and the flange of the discharge pipe. The throttle valve is now opened fully so that the choke is then controlling the discharge under the required operating conditions.

## ILLUSTRATIVE EXAMPLE

A well is discharged horizontally with the valve throttled to give a wellhead pressure of 175 psig. Values of $P_b$ and $P_t$ are noted to be 160 psig and 20 psig respectively. The internal diameter of the discharge pipe is measured as 8 in. and the barometric pressure is 14.7 psia. Calculate the choke diameter.

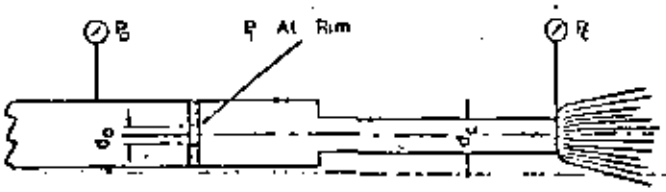


$$d_o = \frac{1.4\ d_c}{\left(\frac{P_b}{P_t}\right)^{0.48}}$$

Figure 2. Non-dimensional relationship for estimating choke size.

$$d_o = \frac{1.4\ d_c}{\left(\frac{P_b}{P_t}\right)^{0.48}} = \frac{1.4\,(8.0)}{\left(\frac{160 + 14.7}{20 + 14.7}\right)^{0.48}}$$

$$= 5.36 \text{ inches diameter}$$

It will be noted that Figure 1 shows the same diameter used for the discharge pipe as for the pipe upstream of the throttle valve, while Figure 2 shows different sizes. This is of no importance for calculating the choke size, and either condition can be used.

## OPERATING FLUID

The above procedure has been used on the steam-water mixtures of the El Tatio geothermal field in Chile with good results, and should also be suitable for dry steam discharges, as the same theory applies. However, for the case of separated hot water which is either under-cooled or at the boiling point, the formula would not be appropriate. This is because flashing of the water only takes place immediately after passing through the choke, and critical flow does not take place there. It does, of course, take place at the outlet of the discharge pipe, at the lip pressure location where a steam-water mixture is evident, but the conditions are not the same at the choke. For flows of saturated hot water, the choke diameter would have to be calculated by use of cold-water theory but with the appropriate hot-water density and viscosity values.

## CONCLUSIONS

The method outlined here will ease the work of test engineers by eliminating (or at any rate reducing) the trial and error procedure usually required to obtain a satisfactory choke size for controlling the horizontal discharge from geothermal wells. It is important that either dry steam or a genuine steam-water mixture exists upstream of the choke as the derived formula does not apply for pressurized hot water, which flashes only after passing through the choke.

Also, the formula would not apply very accurately to fluids where the noncondensable gas fraction of the steam phase exceeded, say, 1% by weight at the lip pressure. However, an allowance can be made for this in a particular field and correction factors added.

## REFERENCES CITED

James, R., 1962, Steam-water critical flow through pipes: Proc. Inst. Mech. Engrs., v. 176, no. 26, p. 741.

——, 1963, Maximum steam flow through pipes to the atmosphere: Proc. Inst. Mech. Engrs., v. 178, no. 18, p. 473.

——, 1966, Measurement of steam-water mixtures at the speed of sound: New Zealand Engineering, v. 21, no. 10, p. 437.

——, 1975, Rapid estimate of electric power potential of discharging geothermal wells: Second UN Symposium on the Development and Use of Geothermal Resources, San Francisco, Proceedings, Lawrence Berkeley Lab., Univ. of California.

INGENIERIA DE RESERVORIOS GEOTERMICOS

# VI. FLUJO DE FLUIDOS Y CALOR EN POZOS GEOTERMICOS

PROF. DR. FRANCISCO CORDOBA M.

SEPTIEMBRE 1981.

# FLUJO DE FLUIDOS Y CALOR EN POZOS GEOTERMICOS

## 1. INTRODUCCION

Cuando el agua caliente fluye en el pozo geotérmico ésta llega a una cierta altura donde la presión hidrostática es igual a la presión de vapor del agua a la temperatura dada del agua. De este punto en adelante vapor de agua empieza a formarse y la calidad de éste aumenta a medida que la mezcla se mueve hacia el cabezal del pozo. En esta región tenemos lo que comúnmente se conoce como flujo de dos fases o flujo bifásico (Fig. 1).

El comportamiento del pozo está controlado en gran parte por la zona de flujo de dos fases ya que ésta determina en la mayoría de los casos el flujo máximo posible a través del pozo. También es importante conocer el comportamiento de flujo de dos fases para determinar caídas de presión y temperatura a lo largo del pozo así como para llevar a cabo mediciones de flujo y otros parámetros necesarios para evaluar el potencial geotérmico del pozo.

## 2. TIPOS DE FLUJO DE DOS FASES

El flujo de dos fases normalmente se clasifica de acuerdo con los aspectos morfológicos del flujo como por ejemplo: de burbuja, de pistón, anular y de rocío en sistemas líquido-vapor. Tipos de flujo híbridos que representan la transición entre un tipo de flujo y otro se representan como pistón-anular, anular-rocío, etc.

Como un ejemplo de la complejidad de flujos de dos fases la Fig. 2 muestra una secuencia de flujos de dos fases como podría presentarse en un pozo geotérmico a medida que más y más agua se transforma en vapor. Obviamente, diferentes partes del pozo requieren métodos diferentes de análisis y el problema de cómo un tipo de flujo cambia otro tipo también tiene que considerarse.

## 3. FLUJO HOMOGENEO

La teoría de flujo homogéneo nos proporciona una de las técnicas más simples para analizar flujos de dos fases. Propiedades promedio adecuadas para la mezcla se definen y la mezcla es tratada como un pseudofluído que obedece las ecuaciones de mecánica de fluidos aplicables a un fluído puro. Todas las técnicas normales de mecánica de fluídos se pueden aplicar en este caso.

Las propiedades promedio que se requieren son velocidad, propiedades termodinámicas (temperatura y densidad por ejemplo), y propiedades de transporte (viscosidad por ejemplo). Estas

pseudopropiedades son promedios ponderados para la mezcla y no son necesariamente los mismos que las propiedades de cada fase. El método para determinar qué tipo de propiedades promedio se van a usar es comenzar con ecuaciones más complejas que se aplican a cada fase individual y combinarlas de tal forma que las ecuaciones resultantes se reduzcan a ecuaciones equivalentes para flujos de un solo componente.

Diferencias en velocidad, temperatura y potencial químico entre las fases provocara una transferencia mutua de momentum, calor y masa. Frecuentemente, estos procesos ocurren rapidamente, especialmente cuando una fase está finamente devidida, y se puede suponer que se alcanza un estado de equilibrio. En este caso los valores promedio de velocidad, temperatura y potencial químico son los mismos que los valores individuales para cada fase y se puede suponer que tenemos flujo homogéneo en equilibrio.

Las ecuaciones resultantes cuando suponemos flujo homogéneo en equilibrio son simples de usar, sin embargo, es necesario corroborar la validez de esta suposición. Para flujo en pozos geotérmicos normalmente se supone que existe flujo homogéneo en equilibrio y parece existir cierta evidencia experimental que tiende a corroborar esta suposición.



## 4. BALANCE DE MASA PARA FLUJO UNIDIMENSIONAL Y HOMOGENEO

La ecuación básica para el balance de masa es:

$$\partial\rho/\partial t = -\partial(\rho v)/\partial z \qquad (4.1)$$

Donde $\rho$ es la densidad promedio de la mezcla y v es la velocidad de la mezcla. En flujo homogéneo ambas fases se mueven a la misma velocidad y no existe deslizamiento entre ellas, por lo tanto el valor de v es único y no es necesario distinguir entre velocidades de las fases. La densidad promedio $\rho$ de la mezcla está dada por:

$$\rho = (1-a)\rho_a + a\rho_v \qquad (4.2)$$

Donde a es la fracción volumétrica de vapor en la mezcla y $\rho_a$, $\rho_v$ son las densidades del agua y vapor respectivamente. Nótese que $\rho_v \leq \rho \leq \rho_a$, esto es la densidad promedio de la mezcla está entre la densidad del vapor y la densidad del agua. Si definimos el volumen específico de la mezcla, agua y vapor de agua como $\nu$, $\nu_a$ y $\nu_v$ respectivamente, tenemos que:

$$\begin{aligned} \nu &= 1/\rho \\ \nu_a &= 1/\rho_a \\ \nu_v &= 1/\rho_v \end{aligned} \qquad (4.3)$$

y el volumen específico promedio de la mezcla está dado por:

$$\nu = (1-x)\nu_a + x\nu_v \qquad (4.4)$$

Donde x es la calidad del vapor (fracción masa de vapor en la mezcla). Note que la ecuación (4.4) también la podemos escribir como:

$$\frac{1}{\rho} = \frac{(1-x)}{\rho_a} + \frac{x}{\rho_v} \qquad (4.5)$$

La masa de cada componente por unidad de volumen de mezcla se puede obtener en función de α ó x por medio de las siguientes ecuaciones:

$$x\rho = \alpha\rho_v \qquad (4.6)$$

$$(1-x)\rho = (1-\alpha)\rho_a \qquad (4.7)$$

Para flujo en estado estacionario (independiente del tiempo), el balance de masa dada por la ecuación (4.1) se reduce a:

$$\frac{\partial(\rho v)}{\partial z} = 0 \qquad (4.8)$$

lo cual nos dá como resultado:

$$G = \rho_v = \text{CONSTANTE} \qquad (4.9)$$

Suponiendo que el área de la sección transversal del pozo es constante. Esto significa que el flujo de masa total por unidad de área, el cual denominamos G, es constante.

Para propósitos de cálculo para flujos de dos fases es conveniente definir el flujo volumétrico total, el flujo volumétrico de agua y el flujo volumétrico de vapor (en litros por segundo)



como Q, $Q_a$ y $Q_v$ respectivamente. Similarmente definimos los flujos de masa por unidad de área (en kilogramos por segundo por centímetro cuadrado) para agua y vapor como $G_a$ y $G_v$ respectivamente. Las siguientes relaciones se aplican en estos casos.

$$G = G_a + G_v \qquad (4.10)$$

$$Q = Q_a + Q_v \qquad (4.11)$$

$$\alpha = Q_v/Q \qquad (4.12)$$

$$x = G_v/G \qquad (4.13)$$

## 5. BALANCE DE MOMENTUM PARA FLUJO UNIDIMENSIONAL Y HOMOGENEO

El balance de momentum está dado por:

$$\rho\left(\frac{\partial v}{\partial t} + v\frac{\partial v}{\partial z}\right) = -\frac{\partial p}{\partial z} - \rho g - \frac{L}{A}\tau_p \qquad (5.1)$$

Suponiendo que el flujo es vertical ascendente y en contra de la dirección de la aceleración de la gravedad. En esta ecuación A y L representan el área de la sección transversal y el perímetro del pozo respectivamente, $\tau_p$ es el esfuerzo cortante promedio sobre la pared (fricción), g es la aceleración de la gravedad y p la presión. Los términos restantes tienen el mismo significado que en la ecuación de balance de masa.

Suponiendo flujo en estado estacionario ($\partial v/\partial t = 0$), podemos escribir la ecuación (5.1) como:

$$G \frac{\partial v}{\partial z} = - \frac{\partial P}{\partial z} - \rho g - \frac{L}{A} \pi_p \qquad (5.2)$$

La ecuación (5.2) se puede resolver en forma explícita para la caída de presión $\partial P/\partial z$, donde como resultado:

$$\frac{\partial P}{\partial z} = - \frac{L}{A} \pi_p - G \frac{\partial v}{\partial z} - \rho g \qquad (5.3)$$

Los tres términos en el lado derecho de la ecuación se consideran como los componentes de la caída de presión debidos a fricción, aceleración y gravedad (caída de presión hidrostática). Desde el punto de vista de ingeniería estamos interesados comúnmente en caídas de presión por lo tanto definiremos:

$$- \left(\frac{\partial P}{\partial z}\right)_f = \frac{L}{A} \pi_p \qquad \text{Caída de presión debida a fricción} \qquad (5.4)$$

$$- \left(\frac{\partial P}{\partial z}\right)_a = G \frac{\partial v}{\partial z} \qquad \text{Caída de presión debida a aceleración} \qquad (5.5)$$

$$- \left[\frac{\partial P}{\partial z}\right]_g = \rho g \qquad \text{Caída de presión hidrostática} \qquad (5.6)$$

La caída de presión total es la suma de cada uno de estos componentes. Por lo tanto podemos escribir la ecuación (5.3) como:

$$\frac{\partial P}{\partial z} = \left(\frac{\partial P}{\partial z}\right)_f + \left(\frac{\partial P}{\partial z}\right)_a + \left(\frac{\partial P}{\partial z}\right)_g \qquad (5.7)$$



Como podemos ver, este análisis nos lleva directamente a la conclusión que la caída de presión total es la suma de tres caídas de presión independientes: Fricción, aceleración e hidrostática. En la mayoría de los casos en pozos geotérmicos la caída de presión por aceleración es despreciable cuando el flujo es en estado estacionario (independiente del tiempo). Sin embargo, en estado transiente (que depende del tiempo) los términos de aceleración se deben considerar.

## 6. DESARROLLO DEL BALANCE DE MOMENTUM

El balance de momentum se puede desarrollar expresando el esfuerzo cortante promedio sobre la pared en función de un factor de fricción y un radio hidráulico. El esfuerzo promedio sobre la pared se da como:

$$\pi_p = C_f \ (\rho v^2/2) \qquad (6.1)$$

Donde $C_f$ es el factor de fricción y el radio hidráulico $R_h$ está dado por:

$$R_h = A/L \qquad (6.2)$$

Para un pozo de sección transversal circular tenemos que el radio hidráulico:

$$R_h = A/L = \frac{(\pi/4)D^2}{\pi D} = \frac{D}{4} \qquad (6.3)$$

Donde D es el diámetro del pozo. Substituyendo las ecuaciones (6.3) y (6.1) en la ecuación (5.4) resulta en:

$$-\left(\frac{\partial P}{\partial Z}\right)_f = \frac{C_f \rho\, v^2}{2\, R_h} = \frac{2C_f \rho\, v^2}{D} \qquad (6.4)$$

Trabajando con volúmenes específicos en lugar de densidades y usando las ecuaciones (4.4) y (4.9) podemos escribir la ecuación (6.4) como:

$$-\left(\frac{\partial P}{\partial Z}\right)_f = \frac{2C_f G^2}{D} v = \frac{2C_f G^2}{D}\left[(1-x)\nu_a + x\nu_v\right] \qquad (6.5)$$

Para simplificar la notación, definiremos el volumen específico de vaporización $\nu_{av} = \nu_v - \nu_a$ y escribiremos la ecuación (6.5) como:

$$-\left(\frac{\partial P}{\partial Z}\right)_f = 2\,\frac{C_f G^2}{D}\left(\nu_a + x\nu_{av}\right) \qquad (6.6)$$

Debido a que el flujo masa es constante y cada fase tiene la misma velocidad, la caída de presión por aceleración (5.5) la podemos escribir como:

$$-\left(\frac{\partial P}{\partial Z}\right)_a = G\,\frac{\partial(G\nu)}{\partial Z} = G^2\,\frac{\partial \nu}{\partial Z} = G^2\,\frac{\partial}{\partial Z}\left(\nu_a + x\nu_{av}\right) \qquad (6.7)$$

suponiendo que el área de la sección transversal del pozo es constante. La caída de presión hidrostática la podemos expresar como:

$$-\left(\frac{\partial P}{\partial Z}\right)_g = g/\nu = \frac{g}{(\nu_a + x\nu_{av})} \qquad (6.8)$$

Substituyendo las ecuaciones (6.6), (6.7) y (6.8) en la ecuación (5.7) resulta en:

$$-\left(\frac{\partial P}{\partial Z}\right) = 2\,\frac{2C_f G^2}{D}\left(\nu_a + x\nu_{av}\right) + G^2\,\frac{\partial}{\partial Z}\left(\nu_a + x\nu_{av}\right) + \frac{g}{(\nu_a + x\nu_{av})} \qquad (6.9)$$

En la región de dos-fases para agua y vapor de agua, tenemos que $\nu_a$ y $\nu_v$ son funciones de la presión solamente. Por lo tanto tenemos que:

$$\frac{\partial}{\partial Z}\left(\nu_a + x\nu_{av}\right) = \frac{\partial \nu_a}{\partial Z} + \nu_{av}\frac{\partial x}{\partial Z} + x\left(\frac{\partial \nu_v}{\partial Z} - \frac{\partial \nu_a}{\partial Z}\right)$$

$$= \nu_{av}\frac{\partial x}{\partial Z} + \frac{\partial P}{\partial Z}\left(x\,\frac{\partial \nu_v}{\partial P} + (1-x)\,\frac{\partial \nu_a}{\partial P}\right) \qquad (6.10)$$

Por lo tanto substituyendo la ecuación (6.10) en la ecuación (6.9) y despejando para $\partial P/\partial Z$ resulta en:

$$-\frac{\partial P}{\partial Z} = \frac{2\,\frac{C_f G^2}{D}\left(\nu_a + x\nu_{av}\right) + G^2\nu_{av}\frac{\partial x}{\partial Z} + \frac{g}{(\nu_a + x\nu_{av})}}{1 + G^2\left(x\,\frac{\partial \nu_v}{\partial P} + (1-x)\,\frac{\partial \nu_a}{\partial P}\right)} \qquad (6.11)$$

Esta ecuación se puede poner en función de otras variables como por ejemplo la densidad, sin embargo, la forma de la ecuación será la misma y el significado físico de cada término será el mismo. Cualquier análisis unidimensional dará eventualmente como resultado una ecuación de la forma:

$$-\frac{\partial P}{\partial z} = \frac{K_f + K_x \frac{\partial x}{\partial z} + K_g \quad g}{1 - M^2} \qquad (6.12)$$

Donde $K_f$, $K_x$ y $K_g$ son coeficientes de influencia similares a las que se usan en flujo compresible y que expresan los efectos de fricción, cambio de fase y gravedad sobre la caída de presión. El término $M^2$ en el denominador tiene el mismo significado que el número de Mach al cuadrado el cual es un parámetro en flujo compresible.

## 7. VELOCIDAD DEL SONIDO EN FLUJO DE DOS FASES

Comparando las ecuaciones (6.11) y (6.12) y usando la relación $G = \rho v$ podemos deducir que la velocidad del sonido C de una mezcla homogénea de dos fases está dada por:

$$C = \left[ -\rho^2 \left( x \frac{\partial v_v}{\partial p} + (1-x) \frac{\partial v_a}{\partial p} \right) \right]^{-1/2} \qquad (7.1)$$



La velocidad del sonido en cada uno de los componentes por sí solo está dada por:

$$C_v = \left(-\rho_v^2 \frac{\partial v_v}{\partial p}\right)^{-1/2} \qquad (7.2)$$

$$C_a = \left(-\rho_a^2 \frac{\partial v_a}{\partial p}\right)^{-1/2} \qquad (7.3)$$

Usando estas ecuaciones en la ecuación (7.1) obtenemos:

$$\frac{1}{C^2} = \rho^2 \left( \frac{x}{C_v^2 \rho_v^2} + \frac{(1-x)}{C_a^2 \rho_a^2} \right) \qquad (7.4)$$

Usando la definición de densidad promedio (4.2) y las ecuaciones (4.6) y (4.7) podemos escribir la ecuación (7.4) como:

$$\frac{1}{C^2} = \left( (1-\alpha) \rho_a + \alpha \rho_v \right) \left( \frac{\alpha}{C_v^2 \rho_v} + \frac{(1-\alpha)}{C_a^2 \rho_a} \right) \qquad (7.5)$$

En los casos en donde $C_a^2 \rho_a >> C_v^2 \rho_v$ y $\rho_a >> \rho_v$

(por ejemplo mezclas agua-vapor de agua a bajas presiones) esta ecuación se reduce a:

$$C^2 = \frac{\rho v}{\rho_a} \frac{C_v^2}{\alpha(1-\alpha)} \qquad (7.6)$$

Lo cual nos demuestra que la velocidad del sonido en una mezcla homogénea puede ser mucho menor que la velocidad del sonido en vapor de agua solamente. La ecuación (7.6) tiene un mínimo a

una fracción volumétrica $\alpha = 0.5$ y para agua y vapor de agua a presión atmosférica esto dá una velocidad sónica mínima de aproximadamente 2lm/s. Para agua y vapor de agua en equilibrio y en el rango de temperaturas de 100 a 300°C podemos usar como valores aproximados $C_v = 430$ m/s y $C_a = 1490$ m/s.

Si en la ecuación (7.4) hacemos la aproximación

$\rho_a^2 C_a^2 \gg \alpha_a \gg \rho_v$ ésta se reduce a:

$$C^2 = x C_v^2 \qquad (7.7)$$

La cual de nuevo nos indica que la velocidad del sonido en la mezcla es menor que la velocidad del sonido en vapor de agua solamente. Sin embargo en esta ecuación no existe un mínimo y la velocidad del sonido de la mezcla aumenta linealmente con la calidad del vapor. La diferencia estriba en la naturaleza de las diferentes aproximaciones empleadas en las ecuaciones (7.6) y (7.7). En general fracciones volumétricas de vapor relativamente elevadas corresponden a calidades de vapor muy bajas debido al gran volumen que por unidad de masa ocupa el vapor relativo al que ocupa el agua líquida. Por ejemplo para agua y vapor de agua en condiciones de equilibrio a 100°C, cuando la fracción volumétrica de vapor es 50% encontramos que la calidad del vapor es del orden del 0.06% mientras que a 300°C una calidad de vapor de aproximadamente 7% corresponde a una fracción volumétrica de 50%.



Si asumimos que el vapor de agua se comporta como un gas ideal y para un proceso isotérmico (este proceso el que se aproxima más en la realidad a medidas experimentales de velocidad del sonido en mezclas) obtenemos:

$$C_v^2 = P/\rho_v \qquad (7.8)$$

Usando la aproximación (7.7) y la definición del número de Mach $M^2 = v^2/C^2$ obtenemos:

$$M^2 = \frac{\rho_v v^2}{xP} \qquad (7.9)$$

Debido a la aproximación $\rho_a \gg \rho_v$ tenemos que $1/\rho \simeq x/\rho_v$, por lo tanto:

$$M^2 = \frac{\rho v^2}{P} = \frac{G^2}{\rho P} \qquad (7.10)$$

Otro tipo de aproximaciones pueden emplearse para calcular el número de Mach, sin embargo, la aproximación (7.10) es la que comúnmente se utiliza en la literatura sobre dos fases.

## 8. SIMPLIFICACION DEL BALANCE DE MOMENTUM

Como se había mencionado en la sección 5, la caida de presión por aceleración en pozos geotérmicos es despreciable cuando

el flujo es en estado estacionario. Por lo tanto el balance de momentum (6.12) se vuelve:

$$-\frac{\partial p}{\partial z} = \frac{K_f + K_g \, G}{1 - x^2} \qquad (8.1)$$

Es decir $\partial x/\partial z$ es despreciable. Con esta simplificación y usando las ecuaciones (6.11), (6.12) y (7.10) podemos escribir (8.1) como:

$$-\frac{\partial p}{\partial z} = \frac{\dfrac{2 C_f G^2}{\rho D} + \rho g}{1 - \dfrac{G^2}{\rho p}} \qquad (8.2)$$

Esta es la forma en que el balance de momentum normalmente aparece en el tratamiento de flujo de dos fases. Algunas veces se escribe simplemente como:

$$\frac{\partial p}{\partial z} = \frac{-\left(\frac{\partial p}{\partial z}\right)_f - \rho g}{1 - x^2} \qquad (8.3)$$

Donde $(\partial p/\partial z)_f = 2 C_f G^2/\rho D$ se usa para indicar la caida de presión por fricción, $\rho g$ es la caida de presión hidrostática y $x$ es el número de Mach. Todas las correlaciones empíricas existentes presentan métodos para evaluar $(\partial p/\partial z)_f$ ó equivalente a esto $C_f$.



## 9. FACTOR DE FRICCION EN FLUJO HOMOGENEO.

Muchos métodos han sido propuestos para evaluar el factor de fricción para dos fases, $C_f$, el cual es el único parámetro empírico en la ecuación (8.2). Excepto en casos extremos el factor de fricción en flujo turbulento no varía mas que por un solo factor de 2 del valor aproximado $C_f \simeq 0.005$. En la práctica, cuando las tuberías están sujetas a corrosión, precipitación de sales, etc., la precisión con que las caidas de presión pueden ser calculadas en flujo de una sola fase no es mejor que un 25% y sería esperar demasiado el tratar de obtener una correlación mejor que ésta para el caso de dos fases.

Las tres alternativas que comúnmente se utilizan para estimar los factores de fricción para flujo turbulento de dos fases son:

1. Usar un valor constante en todos los casos. Un buen valor es:

$$C_f = 0.005 \qquad (8.4)$$

2. Para mezclas de baja calidad de vapor se puede suponer que el factor de fricción es el mismo que el que se obtendrá si el flujo total (agua mas vapor de agua) fuera líquido solamente. El número de Reynolds apropiado para este caso es:

$$Re_{,a} = \frac{GD}{\mu_a} \qquad (8.5)$$

Donde $\mu_a$ es la viscosidad del agua y el factor de fricción se puede leer directamente de gráficas que normalmente se proporcionan en textos de mecánica de fluídos para fluídos de una sola fase.

3. Usar una expresión para la viscosidad equivalente de la mezcla en el número de Reynolds.

$$R_e = \frac{GD}{\mu} \qquad (8.6)$$

Donde $\mu$ es la viscosidad equivalente de la mezcla y usar las gráficas para factores de fricción de fluídos de una sola fase.

Por ejemplo, para flujo en tuberías perfectamente lisas la ecuación de Blasius, es:

$$C_f = 0.079\ R_e^{-0.25} \qquad (8.7)$$

La viscosidad equivalente de la mezcla se puede estimar usando:

$$\frac{1}{\mu} = \frac{x}{\mu_v} + \frac{(1-x)}{\mu_a} \qquad (8.8)$$

ó

$$\mu = x\mu_v + (1-x)\mu_a \qquad (8.9)$$

Existen otras expresiones para calcular la viscosidad equivalente. La razón para esto es que frecuentemente los detalles de la distribución de agua y vapor en el flujo de



dos fases no se conocen y un modelo reológico idealizado de la mezcla no se puede definir. Debido a que existe la necesidad de escoger algún tipo de expresión para la viscosidad equivalente de la mezcla, muchos investigadores han escogido promedios que se aproximan a las condiciones límite cuando alguna de las fases no está presente. Las ecuaciones (8.8) y (8.9) son dos ejemplos de este tipo de promedios.

## 9. BALANCE DE ENERGIA PARA FLUJO UNIDIMENSIONAL Y HOMOGENEO.

El balance de energía está dado por:

$$\frac{\partial}{\partial t}\left[\rho\left(E + \frac{v^2}{2}\right)\right] = -\frac{\partial}{\partial z}\left[\rho v\left(h + \frac{v^2}{2}\right)\right] + \frac{\partial q}{\partial z} - \rho v g \qquad (9.1)$$

Donde E es la energía interna, h la entalpía y q el flujo de calor por unidad de área. En estado estacionario esta ecuación se reduce a:

$$-\frac{\partial}{\partial z}\left[\rho v\left(h + \frac{v^2}{2}\right)\right] + \frac{\partial q}{\partial z} - \rho v g = 0 \qquad (9.2)$$

Usando el balance de masa (4.8), podemos escribir la ecuación (9.2) como:

$$\frac{\partial}{\partial z}\left(h + \frac{v^2}{2} + gz\right) = \frac{1}{q}\cdot\frac{\partial q}{\partial z} \qquad (9.3)$$

Para flujo adiabático en el pozo tenemos que $\partial q/\partial z = 0$ y la ecuación (9.3) nos dá:

$$h + \frac{v^2}{2} + gz = \text{constante} \qquad (9.4)$$

Por lo cual podemos escribir para dos secciones del pozo

$$(h_2 - h_1) + \frac{(v_2^2 - v_1^2)}{2} + g(z_2 - z_1) = 0 \qquad (9.5)$$



De esta ecuación se puede deducir que la disminución de entalpía de la mezcla en el caso adiabático es igual al aumento de energía cinética y potencial. Para pozos geotérmicos la contribución del término de energía cinética se puede despreciar en la ecuación de energía. Por ejemplo un pozo geotérmico con un flujo de 300 ton/hr y un diámetro de 15 cm (aproximadamente 6 pulgadas) que descarga una mezcla de agua-vapor con una calidad de 30% a la velocidad del sonido en el cabezal nos dá un aumento en energía cinética $V^2/2$ equivalente a 6.6 cal/gm, debido a que $h > 200$ cal/gm podemos despreciar el aumento de energía cinética. Este es un caso extremo, en la mayoría de los casos el aumento de energía cinética es menor.

Por lo tanto la ecuación (9.4) se vuelve:

$$h + gz = \text{constante} \qquad (9.6)$$

La cual nos indica que la disminución en entalpía es igual al aumento en energía potencial a medida que la mezcla fluye hacia el cabezal del pozo. Por ejemplo, en una diferencia de altura de 1 km el aumento de energía potencial gz es equivalente a 2.3 cal/gm y en 3 Km es simplemente 3(2.3) = 6.9 cal/gm. Debido a que $h > 200$ cal/gm en la mayoría de los casos en pozos geotérmicos vemos que podemos aproximar:

$$h = \text{constante} \qquad (9.10)$$

Este resultado indica que el flujo en el pozo geotérmico es isoentalpico cuando no hay transferencia de calor hacia el

pozo. Esto se ha observado frecuentemente en la práctica en el caso de pozos completamente desarrollados y cuando la transferencia de calor del yacimiento hacia el pozo ha disminuido considerablemente. Durante la etapa de calentamiento hay que tomar en consideración la transferencia de calor hacia el pozo.

# INGENIERIA DE RESERVORIOS GEOTERMICOS

MODELOS MATEMATICOS DE SIMULACION

PROF. DR. ISMAEL HERRERA..

12 de Octubre de 1981.

# Multiphase Multidimensional Simulation of Geothermal Reservoirs

T. J. LASSETER

*Geonuclear Nobel Paso, Paris, France; currently with Intercomp Inc., The Hague, The Netherlands*

P. A. WITHERSPOON

M. J. LIPPMANN

*Lawrence Berkeley Laboratory and Department of Civil Engineering, University of California, Berkeley, California 94720, USA*

## ABSTRACT

A mathematical method of modeling geothermal reservoirs has been developed using a computer program called SHAFT (Simultaneous Heat and Fluid Transport). This program numerically solves the coupled equations describing the simultaneous transport of mass and energy by a one- or two-phase fluid in porous media for transient or steady-state systems in one, two, or three dimensions. The governing equations are set up in terms of two expressions, one for flow and one for internal energy. Solutions are obtained by solving for two unknowns, density and internal energy, as a function of time and position within the system. Details of the development of flow and energy equations are presented. Two examples of the application of SHAFT to two-phase geothermal reservoirs are included.

## INTRODUCTION

Geothermal systems are receiving an increasing amount of attention, and consequently it is important to understand the behavior of these complex systems. One approach is to simulate their behavior by use of mathematical models, and a recent review (Witherspoon et al., 1975) reveals the growing interest in such methods. As part of our research effort in this field we have developed a computer program called SHAFT, which stands for simultaneous heat and fluid transport. This program is an extension of an earlier code developed by Lasseter and Witherspoon (1974) to handle nonisothermal flow of gases in porous media.

SHAFT numerically solves the coupled equations describing the simultaneous transport of mass and energy by a one- or two-phase fluid in porous media for transient or steady-state systems in one, two, or three dimensions. The fluid must be pure or of uniform composition in both phases, although different fluids can be handled as long as they are confined to separate regions of the system. The equation of state which describes the thermodynamic behavior of the fluid is a function not only of the fluid's inherent properties but also of the position of the fluid within the system. This is particularly important for flow in porous media where interactions between the fluid and solid matrix mean that the thermodynamic behavior of the fluid is dependent on the nature of the matrix as well as of the fluid.

## GENERAL APPROACH

The classical behavior of matter can be fully described in terms of three equations for the conservation of mass, momentum, and energy. For a multicomponent fluid, we must have a conservation-of-mass equation for each component, but in the present approach we have assumed that the fluid is pure water. We therefore have only one equation for conservation of mass. This approach may also be applicable to mixtures whose composition is essentially the same in both liquid and vapor phases.

For flow in porous media, it is customary to describe the behavior of the system on a macroscopic scale and to replace the momentum equation by the empirical equation known as Darcy's Law. Darcy (1856) determined that the flow of water through a bed of sand was proportional to the pressure gradient. His law has since been extended to other fluids in many different kinds of porous and fractured media. Deviations from Darcy behavior have also been observed, but in most practical field problems Darcy's law is perfectly acceptable. Since we shall be dealing with two-phase flow, we must have separate Darcy equations for each phase.

Thus, the basic governing equations in the present version of SHAFT consist of one equation for conservation of mass, two Darcy equations, and one energy equation. We will show how the conservation-of-mass equation and the two Darcy equations can be combined into a single equation, which will be called the "flow" equation. The resulting flow and energy equations can be solved numerically for two unknowns, the density and internal energy of the fluid as a function of time and position within the system.

The most rigorously correct procedure is to solve these two equations in a completely coupled manner. To do this, one would estimate the energy field and solve for the density distribution at a particular time. By substituting the density distribution back into the energy equation, one could obtain

a better estimate of the energy field, which could then be used in the flow equation to obtain a second solution for the density distribution. This process could be continued until the differences between successive estimates of the energy and density distributions are within acceptable limits. This procedure would have to be repeated for each time step and becomes expensive and time-consuming for large problems.

Direct methods of solving the coupled flow and energy equations are also possible. However, the nonlinearities in the equations and the large differences in time constants between the two governing equations make such a technique less efficient than the one we use.

The SHAFT program uses a standard technique that has been found acceptable in many applications and involves decoupling the governing equations. In this method, one starts with the initial energy distribution and assumes that this distribution remains relatively constant over a short interval of time. We then solve for the new density distribution at the end of the time step. Using this new density distribution, we solve for the energy field at the end of a second time interval, and so on.

What makes this approach possible is that the energy field varies much more slowly than the density field, that is the energy time constants of the system are much larger than the corresponding density time constants. Thus, while it is necessary to take relatively small time steps to accurately solve the density equation, the energy field time steps can be much larger. Selecting the appropriate time steps so that the solution procedure is both accurate and efficient is one of the most important parts of this numerical method.

## Basic Numerical Method

The basic numerical method can be most easily demonstrated by developing the finite difference equation for the simple transient conductive heat flow equation:

$$\rho c \frac{\partial T}{\partial t} = \nabla \cdot k \nabla T \qquad (1)$$

where $\rho$ is the density of the material, $c$ is the heat capacity, $T$ is the temperature, $t$ is time, and $k$ is the thermal conductivity (see Table 1 for a complete nomenclature list).

Integrating Equation (1) over a region $R$ having a volume $V$ and a surface $S$ having an area $A$, and applying the divergence theorem to the right-hand side, we have:

$$\int_R \left(\rho c \frac{\partial T}{\partial t}\right) dv = \oint_S (k \nabla T \cdot \hat{n})\, da \qquad (2)$$

where $\hat{n}$ is the outward-directed unit normal to the surface $S$.

To derive the corresponding finite difference equation, we will make the following assumptions: (1) the volume integral on the left-hand side can be represented by an average value times the volume of region $R$; and (2) the surface $S$ of the region can be broken into a series of subsections, $A_m$, over which the normal component of the conductive energy flux vector can be approximated with an average value.

We can therefore rewrite Equation (2) as

$$V\left(\rho c \frac{\partial T}{\partial t}\right) = \sum_m A_m k_m (\nabla T)_m \qquad (3)$$

where $k_m$ is the effective thermal conductivity over surface subsection $m$ and $(\nabla T)_m$ is the normal component of the temperature gradient vector over the surface subsection $m$. We will now consider a general region which we have subdivided into many subregions. We will refer to these subregions as nodes. Figure 1 shows a typical node $n$ connected to an adjacent node $m$. The area of the interface between these nodes is denoted as $A_{n,m}$. The distance $d_{n,m}$ between nodal point $n$ and the interface between nodes $n$ and $m$ is measured along a line perpendicular to that surface (Fig. 1). The numerical method used as well as the algorithm developed for the program are such that node $n$ can be connected to any number of nodes desired by the user.

Equation (3) can be immediately applied to the solution of the energy balance for node $n$ once we have defined the normal component of the temperature gradient vector and the effective conductivity over the surface subsection $m$.

Determining the normal component of the temperature gradient vector would be conceptually easy if we had some idea of the temperature variation within the nodes. Since the temperature distribution within the nodes is represented only by an average value, this is not possible. We therefore assume that the normal component of the temperature gradient vector is equal to the temperature difference between the nodes divided by the distance between the geometric centers of the nodes (or some other distance if more appropriate), where we define the distance as the sum of the two normal distances from the geometric centers of the nodes to the interface. While this may seem a gross simplification, it is clear that as the nodes become smaller and smaller, this approximation approaches the mathematically correct solution. The advantage of this approach is the fact that the numerical method used in solving the system of equations of this form is very fast and can solve systems containing a large number of nodes.

To solve this equation numerically, we must also replace

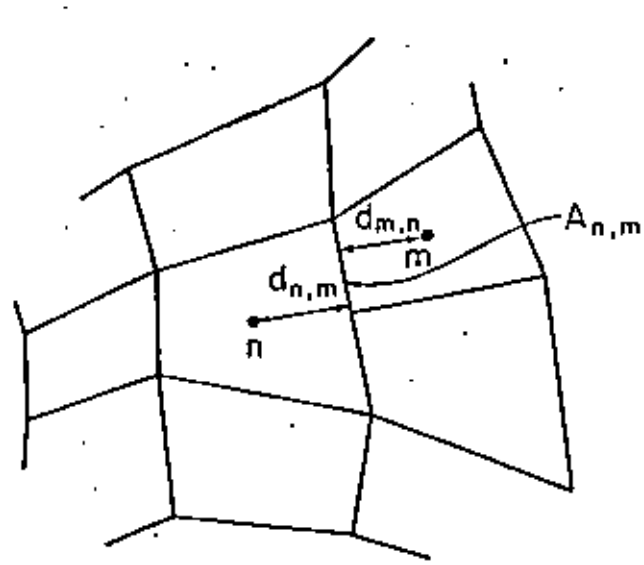


Figure 1. Typical node connection network and nomenclature.

Table V. Nomenclature. Dimensions are mass (M), length (L), time (t), and temperature (T).

| Symbol | Meaning | Dimensions |
|---|---|---|
| $A$ | area | $L^2$ |
| $c$ | specific heat at constant volume | $L^2 t^{-2} T^{-1}$ |
| $C$ | heat capacity | $ML^2 t^{-2} T^{-1}$ |
| $d_{n,m}$ | distance between nodal point $n$ and interface between nodes $n$ and $m$ | $L$ |
| $D_{n,m}$ | distance between nodal points $n$ and $m$ ($D_{n,m} = d_{n,m} + d_{m,n}$) | $L$ |
| $E$ | specific internal energy | $L^2 t^{-2}$ |
| $f$ | fraction of net mass flux rate which is vapor | – |
| $F$ | mass flux | $ML^{-2}t^{-1}$ |
| $g$ | acceleration parameter ($g \geq 0$) | – |
| $\mathbf{g}$ | acceleration due to gravity | $Lt^{-2}$ |
| $k$ | thermal (or effective thermal) conductivity | $MLt^{-3}T^{-1}$ |
| $K$ | intrinsic permeability | $L^2$ |
| $m$ | mass | $M$ |
| $M$ | mobility | $M^{-1}L^3t$ |
| $\hat{n}$ | outward directed normal to surface | – |
| $P$ | fluid pressure | $ML^{-1}t^{-2}$ |
| $q$ | energy flux across surface | $ML^2t^{-3}$ |
| $Q$ | energy injection rate from sources within node (or volume $V$) | $ML^2t^{-3}$ |
| $R$ | relative permeability | – |
| $S$ | mass injection rate per unit volume from sources within node (or volume $V$) | $ML^{-3}t^{-1}$ |
| $t$ | time | $t$ |
| $T$ | temperature | $T$ |
| $\bar{T}$ | average temperature | $T$ |
| $\mathbf{v}$ | Darcy fluid velocity | $Lt^{-1}$ |
| $V$ | volume | $L^3$ |
| $Z$ | sum of transductances | $ML^2t^{-3}T^{-1}$ |
| $\beta_{n,m}$ | direction cosine between the normal from node $n$ to $m$ and the gravitational acceleration vector | – |
| $\epsilon$ | energy content of volume $V$ | $ML^2t^{-2}$ |
| $\theta$ | interpolation factor ($0.5 \leq \theta \leq 1.0$) | – |
| $\lambda$ | weighting factor ($0.5 \leq \lambda \leq 1.0$) | – |
| $\mu$ | viscosity | $ML^{-1}t^{-1}$ |
| $\rho$ | density | $ML^{-3}$ |
| $\phi$ | porosity | – |
| $\Omega$ | transductance | $ML^2t^{-3}T^{-1}$ |
| $(\nabla T)_m$ | normal component of the temperature gradient vector over the surface subsection $m$ | $TL^{-1}$ |
| $\Gamma$ | lumped parameter | arbitrary |
| **Subscripts** | | |
| $c$ | convective | |
| down | at downstream node | |
| $e$ | fluid-solid mixture | |
| ex | explicit | |
| $f$ | fluid | |
| $l$ | liquid | |
| $m$ | at node (or surface subsection) $m$ | |
| $n$ | at node (or time step) $n$ | |
| $n,m$ | at interface between nodes $n$ and $m$ | |
| $s$ | solid | |
| up | at upstream node | |
| $v$ | vapor | |
| **Superscripts** | | |
| $a$ | at surface $A$ | |
| $l$ | liquid | |
| $p$ | iteration number | |
| $v$ | vapor | |

the infinitely small time change $dt$ with a finite time change or time-step $\Delta t$. We can now write the difference equation form of Equation (3):

$$V_n \rho_n c_n \frac{\Delta T_n}{\Delta t} = \sum_m \frac{A_{n,m} k_{n,m}}{D_{n,m}} (\bar{T}_m - \bar{T}_n) \qquad (4)$$

Here we have put a bar over $T_m$ and $T_n$ because, for the maximum accuracy, they must be values of the temperatures between those at the beginning and at the end of the time step. If we know the exact form of the temperature change during the time step, this intermediate value can be selected so that it exactly equals the time integrated average of the temperature over the time step. If this could be done with complete accuracy, absolutely no error would be introduced by the time step procedure. Unfortunately, however, we can only estimate what the form of the temperature change is. But for sufficiently small time steps, little error should be introduced. One of the important sophistications of the numerical procedure used is the manner in which it estimates the average temperature for the time step. The average temperature for each node, then, can be written as

$$\bar{T}_n = T_n + \theta \Delta T_n \qquad (5)$$

where $T_n$ is the temperature at the beginning of the time step, $\Delta T_n$ is the change in temperature during the time step, and $\theta$ is a value between 0.5 and 1.0. The value of $\theta$ is determined every time step and is the same for all nodes for that time step.

We also have the problem of defining the effective thermal conductivity, $k_{n,m}$. Without going into detail, it can be shown (Lasseter and Witherspoon, 1974) that continuity of temperature and energy flux is maintained at the interface if the effective conductivity is written in terms of the conductivities of the material in each node as

$$\frac{D_{n,m}}{k_{n,m}} = \frac{d_{n,m}}{k_n} + \frac{d_{m,n}}{k_m} \tag{6}$$

where

$$D_{n,m} = d_{n,m} + d_{m,n}.$$

We can now rewrite Equation (4) as

$$V_n \rho_n c_n \frac{\Delta T_n}{\Delta t} = \sum_m \frac{A_{n,m} k_{n,m}}{D_{n,m}} [(T_m - T_n) + \theta (\Delta T_m - \Delta T_n)]. \tag{7}$$

The first term in the brackets of Equation (7) is the "explicit" part, since these values are known at the beginning of the time step. The second term is the "implicit" part since it contains the temperature changes for which we are solving.

For a system of $n$ nodes, we have a system of $n$ equations like Equation (7) to solve. The SHAFT program, like the TRUMP program on which it is based (Edwards, 1972), uses an iterative technique to solve these equations. We first rewrite Equation (7) for simplicity as

$$\Delta T_n = \Delta T_{n,ex} + \frac{\theta \Delta t}{C_n} \sum_m \Omega_{n,m} (\Delta T_m - \Delta T_n) \tag{8}$$

where

$$C_n = \rho_n c_n V_n$$

$$\Delta T_{n,ex} = \frac{\Delta t}{C_n} \sum_m \Omega_{n,m} (T_m - T_n)$$

$$\Omega_{n,m} = A_{n,m} k_{n,m} / D_{n,m}.$$

Defining $Z_n = \sum_m \Omega_{n,m}$, we can solve Equation (8) for $\Delta T_n$:

$$\Delta T_n = \frac{\Delta T_{n,ex} + \frac{\theta \Delta t}{C_n} \sum_m \Omega_{n,m} \Delta T_m}{1 + \frac{\theta \Delta t}{C_n} Z_n} \tag{9}$$

This iterative procedure was first derived by Evans, Brousseau, and Keirstead (1954) and is called an acceleration method; it is similar to, but different from, the successive over-relaxation method often used. To implement this technique, we substitute in the left side of Equation (8) $\Delta T_n = \Delta T_n^{(p+1)}$, and in the right side we substitute $\Delta T_n = (1 + g)\Delta T_n^{(p+1)} - g\Delta T_n^{(p)}$ and $\Delta T_m = \Delta T_m^{(p)}$, where $g$ is the acceleration parameter ($g \geq 0$), and $p$ is the iteration number in the superscript. Making these substitutions, Equation (8) can be rewritten:

$$\Delta T_n^{(p+1)} = \Delta T_{n,ex} + \frac{\theta \Delta t}{C_n} \left( \sum_m \Omega_{n,m} \Delta T_m^{(p)} - (1 + g) Z_n \Delta T_n^{(p+1)} + g Z_n \Delta T_n^{(p)} \right). \tag{10}$$

We can then solve Equation (10) for $\Delta T_n$ at the $p + 1$ iteration in terms of $\Delta T_n$ and $\Delta T_m$ at the $p$ iteration:

$$\Delta T_n^{(p+1)} = \frac{\Delta T_{n,ex} + \frac{\theta \Delta t}{C_n} \left( \sum_m \Omega_{n,m} \Delta T_m^{(p)} + g Z_n \Delta T_n^{(p)} \right)}{1 + (1 + g) \frac{\theta \Delta t}{C_n} Z_n} \tag{11}$$

The iteration procedure would begin with an estimate of the temperature changes in each of the nodes which we will call the "zeroth" iteration. We then compute the values at the first iteration using Equation (11) and the zeroth iteration values, and so on. The iteration procedure is stopped when the maximum change in temperature between successive iterations is less than some prescribed value.

The stability and convergence for this iterative procedure are discussed by Lasseter (1975). For this difference equation as well as those to be developed describing multiphase convective heat and mass transfer, stability and convergence are guaranteed regardless of node size and shape and of the contrast in material properties between nodes.

This is the basic numerical method that will be used in solving the more complete energy and mass transport equations to be discussed in the following sections. The advantages of this method are discussed in detail by Edwards (1972) and Lasseter (1975).

## The Internal Energy Equation

Numerous authors have developed the form of the internal energy equation appropriate for convective and conductive energy transport in porous media. Rather than reproduce one of these more rigorous derivations, we prefer to present a derivation which is simpler and more "physical" than most. In the succeeding discussion we will refer to the internal energy simply as energy.

The energy equation is a simple balance equation. It can best be described by considering a small volume $V$. The energy equation keeps track of the energy content of $V$ and the fluxes of energy in and out of $V$. In words, it can be written:

[the time rate-of-change of energy in $V$] = [the flux of energy in and out of $V$] + [energy sources within $V$]

The corresponding mathematical equation is written:

$$\frac{\partial \epsilon}{\partial t} = -\oint_A \mathbf{q}\cdot\hat{n}\,da + Q \qquad (12)$$

where $\epsilon$ is the energy content of $V$, $\mathbf{q}$ is the flux of energy (units of energy per unit area per unit time across the surface $A$ of the volume $V$, $\hat{n}$ is the unit vector normal to $A$ in the outward direction from $V$, and $Q$ is the energy injection rate from sources within $V$.

For a porous medium, we will consider a volume $V$ which contains fluid, designated by the subscript $f$, and solid, designated by the subscript $s$. Properties of the fluid-solid mixture will be designated by the subscript, $r$.

The energy content of the volume is then given by

$$\epsilon_r = m_f E_f + m_s E_s \qquad (13)$$

where $m$ is the mass and $E$ is the energy per unit mass.

For convenience, we will assume that the volume $V$ expands and contracts with the solid "skeleton" of the porous media. Thus the solid mass is always the same since no mass moves across the surface of the volume. The fluid mass will, in general, change with time as the fluid flows in and out of the volume.

The energy balance, Equation (12) can then be written:

$$E_f\frac{dm_f}{dt} + m_f\frac{dE_f}{dt} + m_s\frac{dE_s}{dt} = -\oint_A \mathbf{q}\cdot\hat{n}\,da + Q. \qquad (14)$$

The energy flux, $\mathbf{q}$, consists of the conduction and convection components, which for a single-phase fluid can be written:

$$\mathbf{q} = F_f^* E_f^* - k_r^*(\nabla T)_r^* \qquad (15)$$

where $F_f^*$ is the mass flux of fluid across the surface $A$, $k_r^*$ is the effective thermal conductivity of the fluid-solid matrix evaluated at $A$, $(\nabla T)_r^*$ is the temperature gradient in the matrix at $A$ (we assume the fluid and solid are in thermal equilibrium), and $E_f^*$ is the energy of the fluid crossing $A$.

For completeness a compressible work term (reversible conversion of internal energy to kinetic energy) and a viscous dissipation term (irreversible conversion of kinetic energy to internal energy by frictional forces at the fluid-solid interfaces) should be included in the balance equation. Even though these terms could be added to the program, at the present time, they have been neglected because it is believed these phenomena are probably not important in most geothermal reservoir systems.

We can now rewrite the first term on the left-hand side of Equation (14) as:

$$E_f\frac{dm_f}{dt} = -E_f\oint_A F_f^*\cdot\hat{n}\,da + E_f SV \qquad (16)$$

where $S$ is the mass injection rate, per unit volume, from sources within $V$. Substituting Equations (15) and (16) into (14), we have:

$$V_f\rho_f\frac{dE_f}{dt} + m_s\frac{dE_s}{dt} = \oint_A (E_f - E_f^*)\,F_f^*\cdot\hat{n}\,da + \oint_A k_r^*(\nabla T)_r^*\cdot\hat{n}\,da + Q - E_f SV. \qquad (17)$$

Note that if the system is deforming, the volume of fluid originally within the volume $V$ may be changing with time. Thus, $V_f$ must be specified as a function of time, pressure, and/or temperature.

## Difference Form of Energy Equation

Before writing the difference form of the energy equation, several points should be discussed. It is obvious that Equation (17) consists of several unknowns: $E_f$, $E_s$, $F_f$, $T_r$, and $\rho_f$. It is assumed that the conductivity, $k_r$, and the source terms, $Q$ and $S$, are defined. For a two-phase homogeneous fluid, one can show that the thermodynamic state of the fluid can be uniquely defined in terms of its internal energy and density. Temperature and pressure do not uniquely define the fluid state since, during phase change, these two variables may be constant while the fluid energy is changing. We could also solve the two equations in terms of internal energy and pressure, but in order to guarantee strict conservation of mass, we solve the flow equation in terms of density rather than pressure.

We will assume that the solid and fluid are in thermodynamic equilibrium; that is, in each node we assume that they are at the same temperature and pressure. Knowing the temperature of the fluid will tell us the energy of the solid. We can therefore define the solid energy as a function of the fluid energy and density. Thus we can write

$$\frac{dE_s}{dt} = \left[\left(\frac{\partial E_s}{\partial E_f}\right)_\rho + \left(\frac{\partial E_s}{\partial \rho}\right)_{E_f}\frac{d\rho}{dE_f}\right]\frac{dE_f}{dt} \qquad (18)$$

We evaluate $d\rho/dE_f$ from computed values of the time derivatives:

$$\frac{d\rho}{dE_f} = \frac{d\rho/dt}{dE_f/dt} \qquad (19)$$

In deriving the difference equations, a similar situation arises in the evaluation of $\Delta T$ and $\Delta P$ in terms of our dependent variables $E$ and $\rho$. We can write $\Delta T$ for example as

$$\Delta T = \left[\left(\frac{\partial T}{\partial E_f}\right)_\rho + \left(\frac{\partial T}{\partial \rho}\right)_{E_f}\frac{d\rho}{dE_f}\right]\Delta E_f = \frac{dT}{dE_f}\Delta E_f. \qquad (20)$$

In deriving the finite difference form of the energy equation, we will use "upwind" differencing in the convective transport term to determine the interface energy. That is, the interface energy is not determined by a spatial interpolation of the energies of the two adjacent nodes, but is "weighted" in the direction from which the fluid crossing that interface is coming. This weighting is intuitively correct as well as being required for numerical stability. Thus the energy of the fluid at the interface between nodes $n$ and $m$ is written:

$$E_{n,m} = \lambda E_{up} + (1-\lambda)E_{down} \qquad (21)$$

where $E_{up}$ is the energy of the upstream node, $E_{down}$ is

the energy of the downstream node, and $\lambda$ is the weighting factor and must be between 0.5 and 1.0.

To guarantee stability, the change in the interface energy must be equal to the change in the energy of the upstream node, $\Delta E_{n,m} = \Delta E_{up}$.

With these points in mind, and dropping the subscript $\phi$, we can write the difference form of the single-phase energy equation as

$$\left(V_n \rho + m_n \frac{dE_n}{dE}\right)_{\tau} \frac{\Delta E_n}{\Delta t} \tag{22}$$

$$= \sum_m \left\{ [\lambda E_{up} + (1-\lambda) E_{down} - E_n] F_{n,m} + \frac{A_{n,m}}{D_{n,m}} k_{n,m} (T_m - T_n) \right\} + Q_n - E_n S_n V_n + \theta \sum_m \left[ \Delta E_{up} F_{n,m} + \frac{A_{n,m}}{D_{n,m}} k_{n,m} \left( \frac{dT_m}{dE_m} \Delta E_m - \frac{dT_n}{dE_n} \Delta E_n \right) \right]$$

where $E_n$ is the fluid energy of node $n$, $F_{n,m}$ is the fluid flow rate between the nodes $m$ and $n$ (positive if into $n$), $A_{n,m}$ is the area connecting nodes $m$ and $n$, $D_{n,m}$ is the distance between nodal points $n$ and $m$, $T_n$ is the temperature of node $n$, $\rho_{n,m}$ is the density of the fluid crossing the boundary between nodes $m$ and $n$, $Q_n$ is the energy injection rate into node $n$, and $S_n$ is the mass injection rate, per unit volume, into node $n$.

To derive the difference form of the two-phase energy equation, we need only recognize that the convective transport term in Equation (15) must be replaced by two terms describing the convective transport of liquid and vapor. Defining the convective transport term as $q_t$, the two-phase convective transport term can be written:

$$q_t = F_v^* E_v + F_l^* E_l = [E_l + (E_v - E_l) f] F_l^* \tag{23}$$

where $F_v^*$ is the mass flux rate of vapor in units of mass per unit area per unit time, $F_l^*$ is the mass flux rate of liquid, $E_v$ is the internal energy of the vapor, $E_l$ is the internal energy of the liquid, $F_l^*$ is the net mass flux rate of fluid, and $f$ is the fraction of the net mass flux rate of fluid which is vapor.

Note that if the liquid and vapor are moving in opposite directions, the vapor fraction, $f$, need not be positive nor must its magnitude be less than one. The two-phase energy equation can then be written:

$$\left(V_n \rho + m_n \frac{dE_n}{dE}\right)_{\tau} \frac{\Delta E_n}{\Delta t} \tag{24}$$

$$= \sum_m \left\{ [E_{n,m}^l + (E_{n,m}^v - E_{n,m}^l) f_{n,m} - E_n] F_{n,m} + \frac{A_{n,m}}{D_{n,m}} k_{n,m} (T_m - T_n) \right\} + Q_n - E_n S_n V_n + \theta \sum_m \left[ \Delta E_{up} F_{n,m} + \frac{A_{n,m}}{D_{n,m}} k_{n,m} \left( \frac{dT_m}{dE_m} \Delta E_m - \frac{dT_n}{dE_n} \Delta E_n \right) \right].$$

Here we have approximated the change in the vapor fraction of the flux in terms of the change in the vapor fraction of the upstream node. This is only an approximation, but we feel it is acceptable for a number of reasons. First of all, the time steps for energy are typically much smaller than the energy time constants, so that the implicit correction represented by this term is very small. Secondly, this assumption says physically that the change in the fraction of vapor crossing the interface is approximated by the change in the upstream node which seems reasonable. A final pragmatic argument is that stability can be guaranteed only if the change in the interface energy is weighted towards the upstream node.

## The Flow Equation

The flow equation will be developed by combining the conservation-of-mass equation, often termed the continuity equation, with the conservation-of-momentum equation which, in porous media, is given by Darcy's law.

The conservation of mass is given by

$$\frac{\partial}{\partial t} (\phi \rho) = -\nabla \cdot \rho \mathbf{v} + S \tag{25}$$

where $\phi$ is the porosity, $\rho$ is the fluid density, $\mathbf{v}$ is the Darcy velocity of the fluid, and $S$ is the mass injection rate per unit volume.

The conservation of momentum is given by Darcy's law which in effect assumes that the momentum of the fluid can be ignored. Darcy's law is then only a force balance. It is given as

$$\mathbf{v} = -\frac{K}{\mu} (\nabla P - \rho \mathbf{g}) \tag{26}$$

where $K$ is the intrinsic permeability, $\mu$ is the fluid viscosity, $P$ is the fluid pressure, and $\mathbf{g}$ is the acceleration due to gravity.

Equation (26) can be substituted into (25), yielding

$$\frac{\partial}{\partial t} (\phi \rho) = \nabla \cdot \left[ \frac{K}{\mu} (\nabla P - \rho \mathbf{g}) \right] + S. \tag{27}$$

Integrating this equation over the volume, we have

$$\int_v \left[ \frac{\partial}{\partial t} (\phi \rho) \right] dv = \oint_A \left[ \frac{K}{\mu} \rho (\nabla P - \rho \mathbf{g}) \cdot \hat{n} \right] da + \int_v S \, dv. \tag{28}$$

If we assume that the left-hand side of Equation (28) can be represented by an average value times the region volume, and the right-hand side can be represented by an average value over each of the $m$ surface subsections, we have

$$V\left[\frac{\partial}{\partial t}(\phi\rho)\right] = \sum_m \left[\frac{K}{\mu}\rho(\nabla P - \rho g)\cdot\hat{n}\right]_m A_m + SV. \quad (29)$$

For a two-phase fluid, we have separate Darcy equations for vapor and liquid. The mobilities of each phase are highly nonlinear.

Darcy's law for each phase is given by

$$v_v = -M_v[\nabla P - \rho_v g] \quad (30)$$

$$v_l = -M_l[\nabla P - \rho_l g] \quad (31)$$

where the mobilities are defined as:

$$M_v = \frac{K}{\mu_v} R_v \quad (32)$$

$$M_l = \frac{K}{\mu_l} R_l \quad (33)$$

where $R_v$ is the vapor relative permeability and $R_l$ is the liquid relative permeability.

In general, the intrinsic permeability for each phase is the same, but this is not an essential assumption for the derivation or solution method.

The corresponding mass fluxes are

$$F_v = \rho_v v_v = -M_v\rho_v(\nabla P - \rho_v g) \quad (34)$$

$$F_l = \rho_l v_l = -M_l\rho_l(\nabla P - \rho_l g). \quad (35)$$

The total flux is

$$F = F_v + F_l = -(M_v\rho_v + M_l\rho_l)\nabla P + (M_v\rho_v^2 + M_l\rho_l^2)g. \quad (36)$$

We will substitute this fluid flux for $\rho v$ in Equation (25). We can justify doing this rather than writing separate mass conservation equations for each phase because the total amount of each phase is not being conserved, but only the total amount of fluid. We must, however, know what fraction of the flux is vapor to properly compute the conservation of energy as we have shown. We are implicitly assuming that the two phases are in thermodynamic equilibrium. This means that the characteristic time for the equilibrium process between phases in a given node is small compared to the typical time step used in modelling the system numerically. We feel intuitively that this characteristic time is small, but this assumption may perhaps be incorrect under some conditions.

Following the suggestion of S. K. Garg (personal comm., 1974), we can write a combined form of the fluid flow equation:

$$F = -(M\rho)^*\nabla P + (M\rho^2)^* g \quad (37)$$

where $(M\rho)^* = M_v\rho_v + M_l\rho_l$ and $(M\rho^2)^* = M_v\rho_v^2 + M_l\rho_l^2$.

The two-phase flow equation corresponding to the single-phase flow Equation (29) can therefore be written:

$$V\left[\frac{\partial}{\partial t}(\phi\rho)\right] = \sum_m \left[(M\rho)^*\nabla P\cdot\hat{n} - (M\rho^2)^* g\cdot\hat{n}\right]_m A_m + SV. \quad (38)$$

## Difference Form of Flow Equation

Both the one- and two-phase flow equations can be written in the form of the two-phase flow equation given as Equation (38). Using the general numerical method developed in the section above, we can write the corresponding difference equation for Equation (38) as

$$\left(\phi + \rho\frac{\partial\phi}{\partial\rho}\right)_n V_n \frac{\Delta\rho_n}{\Delta t} = \sum_m A_{n,m}\left[(M\rho)^*_{n,m}\left(\frac{P_m - P_n}{D_{n,m}}\right) - (M\rho^2)^*_{n,m}\beta_{n,m}g\right] + S_n V_n \quad (39)$$

where $\beta_{n,m}$ is the direction cosine between the normal from node $n$ to $m$ and the gravitational acceleration vector.

The complete difference equation can now be written:

$$\left(\phi + \rho\frac{\partial\phi}{\partial\rho}\right)_n V_n \frac{\Delta\rho_n}{\Delta t} = \sum_m A_{n,m}\left[(M\rho)^*_{n,m}\left(\frac{P_m - P_n}{D_{n,m}}\right) - (M\rho^2)^*_{n,m}\beta_{n,m}g\right] + \theta\sum_m A_{n,m}\left\{\left[X_{n,m}\frac{d_{n,m}}{D_{n,m}} - \frac{(M\rho)^*_{n,m}}{D_{n,m}}\frac{\partial P_n}{\partial\rho_n}\right]\Delta\rho_n + \left[X_{n,m}\frac{d_{n,m}}{D_{n,m}} + \frac{(M\rho)^*_{n,m}}{D_{n,m}}\frac{\partial P_m}{\partial\rho_m}\right]\Delta\rho_m\right\} + S_n V_n \quad (40)$$

where

$$X_{n,m} = \left(\frac{\partial(M\rho)^*}{\partial\rho}\right)_{n,m}\left(\frac{P_m - P_n}{D_{n,m}}\right)' - \left(\frac{\partial(M\rho^2)^*}{\partial\rho}\right)_{n,m}\beta_{n,m}g$$

$$(M\rho)^*_{n,m} = \frac{D_{n,m}(M\rho)^*_n(M\rho)^*_m}{d_{n,m}(M\rho)^*_m + d_{m,n}(M\rho)^*_n}$$

$$(M\rho^2)^*_{n,m} = \frac{(M\rho^2)^*_n(M\rho)^*_m d_{n,m} + (M\rho^2)^*_m(M\rho)^*_n d_{m,n}}{d_{n,m}(M\rho)^*_m + d_{m,n}(M\rho)^*_n}$$

The values of $(M\rho)^*_{n,m}$ and $(M\rho^2)^*_{n,m}$ have been derived in terms of the values in nodes $n$ and $m$ in order to guarantee the continuity of fluid flux and pressure at the interface.

We have now developed the flow difference equation which is solved together with the energy difference equation by the SHAFT program.

## EXAMPLES OF RESULTS

To illustrate some capabilities of the SHAFT program, preliminary results from two two-phase geothermal reservoir simulations will be given. Examples of one phase problems solved by use of an earlier version of SHAFT have already been discussed by Lasseter and Witherspoon (1974). The results described here demonstrate the application of the program to liquid-dominated and vapor-dominated geothermal systems. While these examples are similar in some

Table 2. Assumed reservoir properties.

| | |
|---|---|
| Porosity | 0.2 |
| Permeability | 5.0 millidarcies |
| Fluid conductivity | 0.65 J/m·°C·sec |
| Solid conductivity | 2.18 J/m·°C·sec |
| Solid heat capacity | 1000 J/kg·°C |
| Solid density | 2.5 g/cm³ |

respects to existing geothermal systems, they are intended primarily as demonstrations of the program's capabilities and no attempt has been made to model actual field behavior.

## Liquid-Dominated System

For a liquid-dominated system, we have selected an axisymmetric model 2000 m high and 5000 m in radius. The zoning consists of 10 evenly spaced vertical nodes and 25 evenly spaced horizontal nodes. Hot water at a temperature of 250°C is upwelling into the bottom node on the axis at a rate of 100 tons per day. The bottom boundary is otherwise a no-flow boundary held at a constant temperature of 100°C. The top boundary is permeable and adiabatic with the pressure at the boundary being held at 1 kg/cm². The other boundaries have no flow of heat or fluid across them. The constant material properties are given in Table 2. Input tables give the internal energy, density, viscosity, and phase of the fluid as a function of temperature and pressure. Relative permeability values are tabulated as a function of volumetric vapor saturation.

For simplicity, the problem was started with a uniform temperature and pressure everywhere and was allowed to run until a steady state was reached. This necessitated running the problem for approximately one million days of physical time, which required about 100 seconds of computer time. The temperature, density, and flow fields are shown in Figure 2.

Having established the steady-state flow field, field production was simulated by withdrawing fluid from the node on the axis at a depth of 700 m at a daily rate of 100 tons (4167 kg/hr). The flow field under these conditions after 20 years is shown in Figure 2D. We see that the flow is no longer moving to the surface as before, but now is directed towards the well. The temperature and density distributions are not appreciably changed from their initial values, even after 20 years. It was thought that some phase change might occur by this time, but this did not happen. It is possible that with a higher bottom-boundary temperature and with finer zones near the well some phase transitions will develop.

## Vapor-Dominated System

To study a vapor-dominated system, a model based loosely on The Geysers field was selected. The model consists of an axisymmetric system 2000 m in radius and 3000 m high. The zoning consists of 15 evenly spaced nodes in the vertical direction and 10 nodes in the horizontal direction whose spacing increases with radius. The same material properties as given in Table 1 were used except that the permeability is 1 darcy and the system is almost completely filled with steam. The bottom boundary is a no-fluid-flow boundary

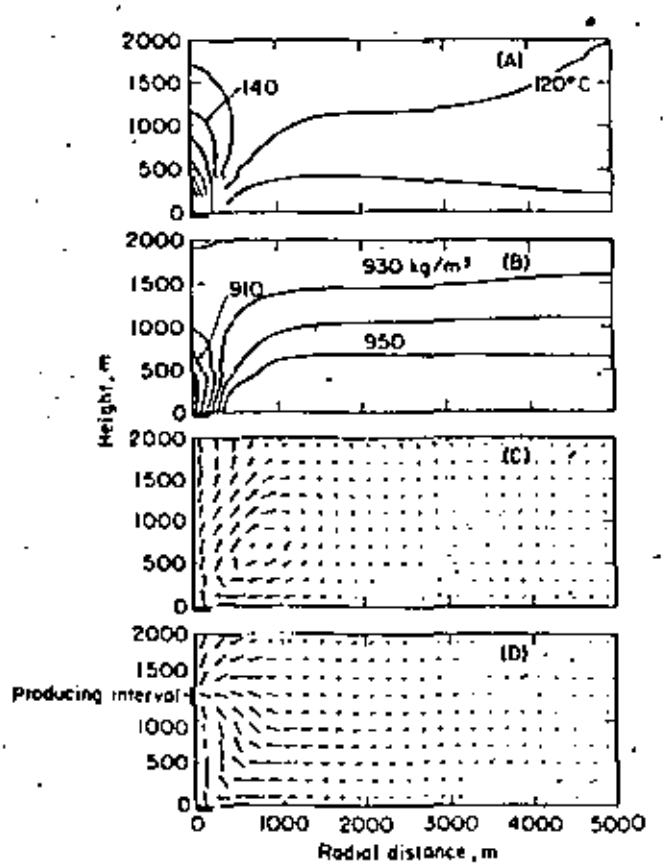


Figure 2. Liquid-dominated system showing (A) temperature field, (B) density field, (C) mass flux for initial steady state conditions, and (D) mass flux after 20 years of production.

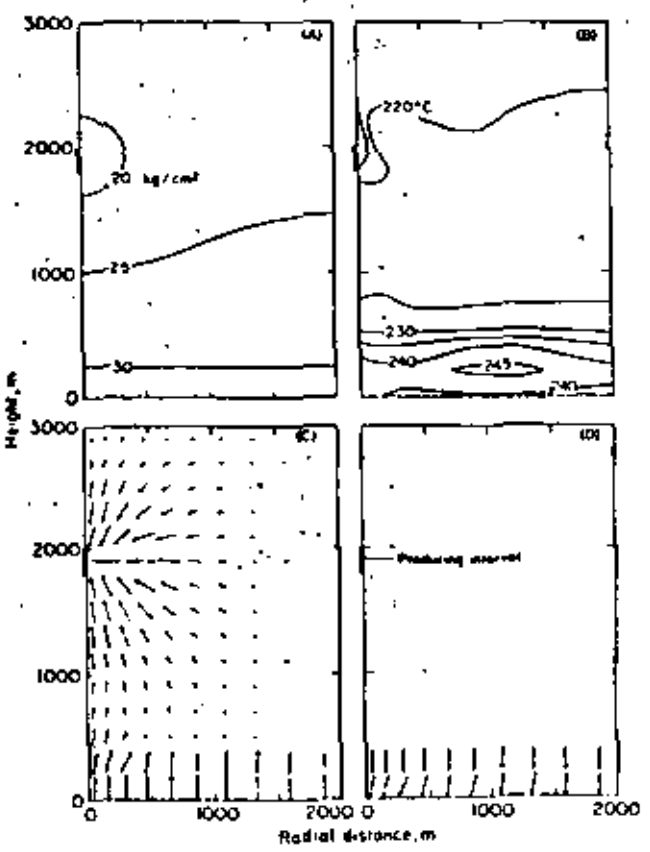


Figure 3. Vapor-dominated system showing reservoir conditions after 1500 days of production: (A) pressure field, (B) temperature field, (C) vapor flux, (D) liquid flux.

fixed at a temperature of 250°C. The other boundaries have no flow of heat or fluid across them. Steam is being withdrawn from the three nodes nearest the axis at a depth 100 m at a total rate of $3 \times 10^4$ ton/day ($1.25 \times 10^6$ kg/hr). This flow rate is probably unreasonably high, but was selected to examine the problem of total system depletion and the effect on a boiling layer of water that was assumed to exist in the bottom 200 m of the vertical column. The system begins at a temperature of 250°C and an average pressure of 35 kg/cm$^2$.

Plots of temperature, pressure, liquid flux, and vapor flux after 1500 days of production are shown in Figure 3. The boiling at the bottom of the system is clearly seen from the vector plots (Fig. 3 C and D). As the steam rises, the liquid moves downward to replace it. The average system temperature decreased to about 225°C and the mean pressure of the steam column decreased to about 25 kg/cm$^2$. Vapor-dominated systems usually remain isothermal, and we suspect that the input convergence criterion for this problem was not adequate. We are currently investigating this.

## ACKNOWLEDGMENT

This work was performed under the auspices of the U.S. Energy Research and Development Administration.

## REFERENCES CITED

Darcy, H., 1856, Les fontaines publiques de la ville de Dijon: Paris, Victor Dalmont.

Edwards, A. L., 1972, TRUMP: A computer program for transient and steady state temperature distribution in multidimensional systems: Livermore, California, Lawrence Livermore Lab. Rept. UCRL-14754, Rev. 3.

Evans, G. W., Brousseau, R. J., and Kelrstead, R., 1954, Instability considerations for various difference equations derived from the diffusion equation: Livermore, California, Lawrence Livermore Lab. Rept. UCRL-4476.

Lasseter, T. J., 1975, SHAFT: A computer program for the numerical simulation of heat and mass transfer in multidimensional two-phase geothermal reservoirs: Prelim. rept. by Geonuclear Nobel Paso, Geneva, Switzerland, to the Lawrence Berkeley Lab., Berkeley, California.

Lasseter, T. J., and Witherspoon, P. A., 1974, Underground storage of liquified natural gas in cavities created by nuclear explosives: Berkeley, California, Univ. of California, Dept. of Civil Engineering, Pub. no. 74-1.

Witherspoon, P. A., Neuman, S. P., Sorey, M. L., and Lippmann, M. J., 1975, Modeling geothermal systems: Presented at the International Meeting on Geothermal Phenomena and Its Applications, Accademia Nazionale dei Lincei, Rome (Berkeley, California, Lawrence Berkeley Lab. reprint LBL-3263).

ACCADEMIA NAZIONALE DEI LINCEI

ATTI DEI CONVEGNI LINCEI

30

Convegno internazionale

# IL FENOMENO GEOTERMICO E SUE APPLICAZIONI

(Roma–Pisa, 3–5 marzo 1975)

*(ESTRATTO)*

ROMA

ACCADEMIA NAZIONALE DEI LINCEI

P. A. WITHERSPOON, S. P. NEUMAN, M. L. SOREY and M. J. LIPPMANN

## MODELING GEOTHERMAL SYSTEMS

### INTRODUCTION

Geothermal systems are receiving more and more attention as an alternative source of energy and, consequently, there is growing interest in attempting to understand their nature and behavior. One approach to this problem is to attempt to deduce the physical behavior of such systems using a mathematical model. Such a model consists of a set of equations that describe the processes occurring within the system and the solution to these equations subject to conditions that prevail at a particular site.

The model approach has two important applications: 1) the geothermal system under natural conditions before being disturbed by man, and 2) the geothermal system during exploitation. Natural geothermal systems have been investigated by a great many workers. The main thrust of such studies has been to understand how geothermal systems can form and persist within the earth's crust.

The mathematical model can also be applied to the problem of evaluating the behavior of a geothermal system during exploitation. One of the most critical problems in developing such systems as a viable source of energy is that of determining that a particular reservoir once discovered is capable of producing significant quantities of energy over meaningful periods of time. The model is one of several tools that can be used to analyze this problem. During the early stages, the model may be crude, but its application in parametric analysis of the field data can provide valuable limits as to what can be expected. As more data become available, the model can be refined and such engineering questions as well spacing, optimum rates of fluid withdrawal and effects of reinjection can be studied.

In this review, we shall restrict our attention to hydrothermal systems, i.e., to geothermal systems involving water. We shall pay particular attention to hydrothermal-convection systems, in which most of the heat is transferred in circulating fluids rather than by heat conduction. Two broad types of hydrothermal systems are recognized: 1) hot-water, and 2) vapor-dominated (White, 1973).

In the hot-water type, water is the continuous phase throughout the system and the pressure provides the pressure control. Continuity of the liquid phase is evident from reservoir pressures that are near hydrostatic and the presence of soluble salts that are not found to any significant degree in low-pressure steam. In the vapor-dominated type, steam is the continuous, pressure-controlling phase, although there is general agreement that liquid water must also be present (Facca and Tonani, 1964; Elder, 1965; Craig, 1966; James, 1968; Marinelli, 1969; Sestini, 1970; White *et al.*, 1971).

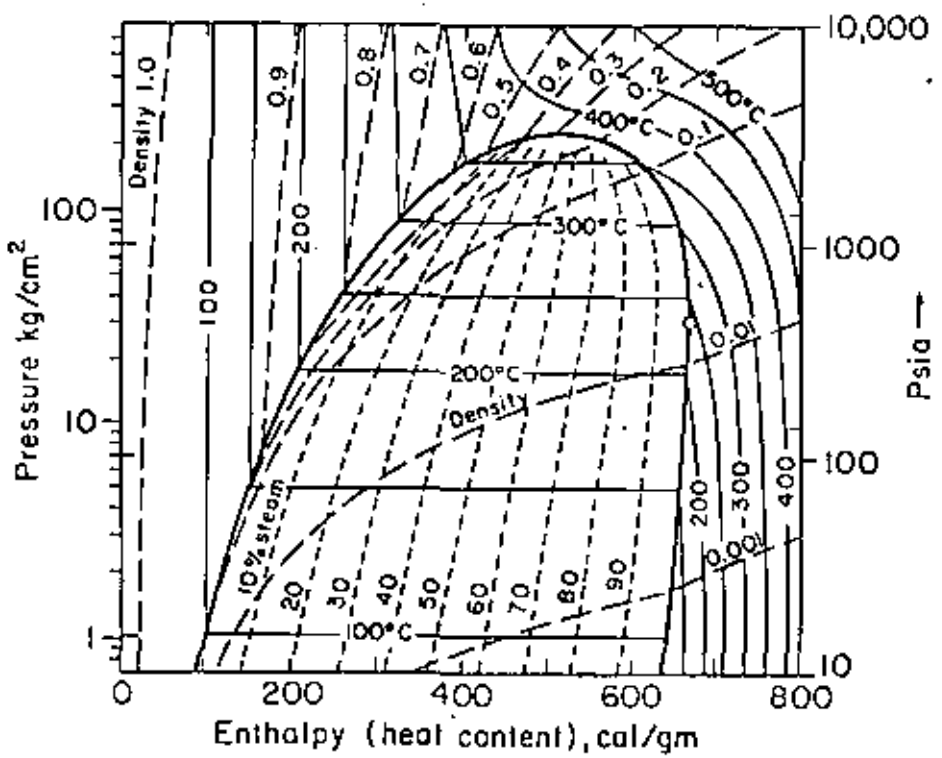


Fig. 1. – Pressure–enthalpy diagram for pure water and vapor, showing contours of equal temperature, density and mass proportions of steam to water. Open circle indicates maximum enthalpy of saturated steam, 670 cal/gm at 236 °C and 31.8 kg/cm² (after Worra *et al.*, 1971).

An intriguing question arises concerning the initial conditions of vapor-dominated systems. At depths below 350 m, they all tend to have temperatures near 240 °C and pressures near 35 kg/cm², which usually means well below hydrostatic (White, 1973). This uniformity in the initial conditions is believed to be strongly influenced by the maximum enthalpy of saturated steam (James, 1968; Sestini, 1970; White *et al.*, 1971).

The material and thermodynamic properties of the different components of geothermal systems are an important consideration in any attempt to develop realistic models of such systems. Fig. 1 presents a pressure-enthalpy



diagram for pure water at pressures up to 700 kg/cm² and temperatures up to 700 °C. Dissolved salts are, of course, common in geothermal waters and studies on the effect of salinity on heat capacity (Nevens and Pool, 1964; Likke and Bromley, 1973), density (Haas, 1970), viscosity (Matthews and Russell, 1967, fig. G 4), and maximum thermal gradient (Haas, 1971) of brines are available. Helgeson (1968) has investigated the thermodynamic characteristics of the Salton Sea geothermal system where the highest concentrations, approaching 300,000 ppm, have been found.

The thermal properties of rocks are very important since the dominant fraction of the total energy in a geothermal system is in the solid matrix. Comprehensive tables of these properties for dry rocks have recently been compiled by Kappelmeyer and Haenel (1974). Thermal conductivities for most dry rocks range from 4 to 10 meal/cm sec °C; specific heats are approximately 0.2 cal/g °C; and thermal diffusivities range from 5 to $15 \times 10^{-3}$ cm²/sec. Kappelmeyer and Haenel also include the effects on these thermal properties of temperature and pressure.

The thermal conductivity of fluid-saturated rocks is dependent on the conductivities of the dry rock and the saturating fluid as well as the physical properties of the rock. Anand *et al.* (1973) and Somerton *et al.* (1974) have shown how thermal conductivities increase with brine saturation and become more sensitive to temperature change. They discuss correlations for predicting thermal conductivity from other rock properties.

The hydraulic properties of the rocks are also important since they control the fluid movement. The absolute values of permeability and porosity for rocks vary considerably and must be measured or estimated for any given system. A few workers have studied the thermal effects and report that the absolute permeability tends to decrease, sometimes significantly, with increasing temperature (Greenberg *et al.*, 1968; Sanyal *et al.*, 1972; Casse, 1974). There are also important effects of temperature on relative permeability (Edmonson, 1965; Davidson, 1969; Poston *et al.*, 1970; Weinbrandt *et al.*, 1972; Lo and Mungan, 1973; Ramey *et al.*, 1974). In studying the effects of pressure, a number of workers (Knutson and Bohor, 1963; Brace *et al.*, 1968; Vairogs *et al.*, 1971) have suggested that permeability depends only on effective stress; that is, permeability is dependent only on the difference between hydrostatic confining pressure and internal pore pressure. However, Zoback and Byerlee (1975), have recently shown that pore pressure has a significantly larger effect on permeability under isothermal conditions than does confining pressure.

In this review of the problems involved in modeling geothermal reservoirs, we shall first present the governing equations for energy and mass transfer in porous media. Then we shall consider some of the fundamental concepts that have been developed for factors that affect the development of free and forced convection in geothermal systems under natural conditions. Lastly, we shall review the results of several efforts that have been made to model geothermal systems during exploitation.

## GOVERNING EQUATIONS

Let us consider a porous medium completely saturated with a single-component homogeneous fluid which can be either in a liquid or gaseous state. The liquid and gas phases are assumed to be separated locally by a distinct interface due to capillarity. Since mass may be transferred from one phase to another across the interface by vaporization or condensation, it is convenient to write a single mass balance equation for both phases

$$(1)\qquad \frac{\partial}{\partial t}(\varphi S^L \rho^L + \varphi S^G \rho^G) = -\frac{\partial}{\partial x_i}(\rho^L v_i^L + \rho^G v_i^G)$$

Rate of mass accumulation — Convective mass flux

All mathematical symbols appearing in the text are macroscopic quantities defined over a representative elementary volume of the porous medium. For a definition of these symbols the reader is referred to the Nomenclature.

It is generally believed that capillary pressure between the phases is small relative to absolute pressure, and as each phase may flow independently, we shall assume Darcy's law in the form

$$(2)\qquad v_i^L = -\frac{k_{ij}k_r^L}{\mu^L}\left(\frac{\partial p}{\partial x_j} - \rho^L g_j\right)$$

$$(3)\qquad v_i^G = -\frac{k_{ij}k_r^G}{\mu^G}\left(\frac{\partial p}{\partial x_j} - \rho^G g_j\right)$$

The relative permeabilities $k_r^L$ and $k_r^G$ are functions of fluid saturation and, as mentioned earlier, they may also be functions of temperature. Recent studies (Coats *et al.*, 1974) indicate the latter effect is important and should be taken into account.

An energy balance equation must also be considered, and one way to derive such an equation in terms of macroscopic quantities is to follow an averaging procedure (see Appendix). Equation A 21 is a general form of the macroscopic energy balance for the case where irreversible viscous dissipation of mechanical energy and transfer of kinetic energy between fluid and rock are neglected. An attempt to derive a set of more general equations considering mechanical interaction between rock and fluid has been reported recently by Brownell *et al.* (1975). It is customary to assume that not only is the capillary pressure zero, but also that the solid, liquid, and gas are locally in thermal equilibrium. In this case (A 21) reduces to (A 22) which can be



written more conveniently without the angular brackets as

$$(4)\qquad \frac{\partial}{\partial t}[\varphi S^L \rho^L e^L + \varphi S^G \rho^G e^G + (1-\varphi)\rho^S e^S] = \frac{\partial}{\partial x_i}\left(\kappa_{ij}^{\text{eff}}\frac{\partial T}{\partial x_j}\right) -$$

Rate of internal energy accumulation — Conductive and dispersive internal energy flux

$$- \frac{\partial}{\partial x_i}(\rho^L e^L v_i^L + \rho^G e^G v_i^G) - p\frac{\partial}{\partial x_i}(v_i^L + v_i^G)$$

Convective internal energy flux — Rate of reversible mechanical energy (work) conversion to internal energy

Our mathematical analysis indicates that

$$(5)\qquad \kappa_{ij}^{\text{eff}} = \varphi S^L \kappa_{ij}^L + \varphi S^G \kappa_{ij}^G + (1-\varphi)\kappa^S \delta_{ij}$$

Laboratory experiments show that $\kappa_{ij}^{\text{eff}}$ is not always given by (5) (Combarnous and Bories, 1973, fig. 6), thus implying that the assumption of local thermal equilibrium may not always hold. Moreover, as mentioned earlier, thermal conductivity may also be a function of temperature.

Equation 4 can be reformulated in terms of enthalpy by writing $h = p/\rho$ instead of $e$ and, as shown in (A 25), one then has

$$(6)\qquad \frac{\partial}{\partial t}[\varphi S^L \rho^L h^L + \varphi S^G \rho^G h^G + (1-\varphi)\rho^S h^S] = \frac{\partial}{\partial x_i}\left(\kappa_{ij}^{\text{eff}}\frac{\partial T}{\partial x_j}\right) -$$

$$- \frac{\partial}{\partial x_i}(\rho^L h^L v_i^L + \rho^G h^G v_i^G) + \frac{\partial(\varphi p)}{\partial t} + (v_i^L + v_i^G)\frac{\partial p}{\partial x_i}$$

This is identical with an expression reported earlier by Mercer *et al.* (1974) except that we have omitted source terms.

In the particular case where only one fluid phase is present, the energy equation can be conveniently expressed in terms of temperature and, as shown in (A 31), one obtains for a liquid saturated medium

$$(7)\qquad [\varphi\rho^L c_v^L + (1-\varphi)\rho^S c_v^S]\frac{\partial T}{\partial t} = \frac{\partial}{\partial x_i}\left(\kappa_{ij}^{\text{eff}}\frac{\partial T}{\partial x_j}\right) -$$

$$- \rho^L v_i^L c_v^L \frac{\partial T}{\partial x_i} - T\left(\frac{\partial p}{\partial T}\right)_v \frac{\partial v_i^L}{\partial x_i}$$

A similar expression holds for a medium saturated with gas.

The above equations must be supplemented by equations of state relating the thermodynamic variables $e, h, \rho, \mu, S, p, T$. Here it is customary to

assume that all phases are in equilibrium and that thermodynamic relationships between macroscopic quantities remain the same as those between the equivalent point quantities. In particular, the macroscopic saturations $S^l$ and $S^g$ are assumed to be uniquely determined by the pressure and total energy or enthalpy of the fluid (both phases combined). In other words, whenever two phases occur simultaneously at a point in the system, their $p$-T relationship is uniquely determined by conditions at the vapor pressure.

Although capillary pressure is neglected in the governing equations, it may still have an important effect on thermodynamic properties. Ramey *et al.* (1973) explain that the vapor-pressure curve in the presence of uneven capillary surfaces may be lower than that quoted in steam tables. Calhoun *et al* (1949) showed that in consolidated sandstones the vapor-pressure curve at 36 °C is significantly affected by a decreasing liquid saturation. However, Cady (1969) and Bilhartz (1971) were unable to confirm this effect on unconsolidated sands with temperatures between 121 °C and 240 °C. The effect of capillary pressure therefore remains unclear.

Some geothermal systems such as those in Imperial Valley (California) involve waters of high salinity which cannot be treated as a homogeneous fluid because salt concentrations are not uniform. In this case the mass as well as energy balance equations (see Appendix) may have to be modified to include a term for dispersive mass flux and an additional equation for mass balance of the solute. Another complication may arise due to coupling between thermal and chemical gradients which modifies the form of Fourier's law of heat conduction (Dufour effect) and Fick's first law of diffusion (Soret effect). The presence of salts may also cause a slight lowering of the vapor-pressure curve (Haas, 1971; Ramey *et al.*, 1973), and this effect becomes progressively more important as boiling proceeds, due to the increasing salt concentration (White, 1973). Very little is known about the behavior of these so-called thermohaline systems, but a few theoretical analyses have appeared (Nield, 1968, 1974; Rubin, 1973, 1975, a, b, c). The discussion that follows will be concerned solely with homogeneous fluids.

## Geothermal Systems under Natural Conditions

### *Fundamental Characteristics of Free Convection.*

Mathematical modeling related to geothermal systems has long centered on problems of convective heat transfer in a homogeneous porous layer heated from below. Pioneering work on this subject has been performed independently by Horton and Rogers (1945), Lapwood (1948), and Goguel (1953). Their efforts were directed primarily toward developing criteria for the onset of convection currents in a horizontal and laterally infinite layer. These analyses followed the pattern of earlier work by Rayleigh (1916), Jeffreys (1930), and others who showed that in a static layer of viscous fluid the critical temperature gradient (i.e., the gradient at which cellular or Bénard convection is formed) depends on thermal conductivity, thermal coefficient of expansion, kinematic viscosity, thickness of the layer, and the boundary conditions. When fluid cannot enter or leave the system, the resulting flow pattern is referred to as "natural" or "free" convection. When fluid flow is entirely due to hydraulic forces acting at the boundaries, the result is known as "forced" convection, whereas "mixed" convection includes a combination of both phenomena. Early work on the subject was restricted to free convection.

In reviewing the mathematical approach to free convection in porous media, we find it instructive to follow a recent development by Bock (1972). Consider a rectangular box of porous material resting on a horizontal surface and saturated by a homogeneous liquid (see fig. 2). The vertical sides are thermally insulated (i.e., adiabatic), and the lower ($z = 0$) and upper ($z = D$) surfaces are isothermal. Temperature $T_1$ at the bottom is greater than $T_0$ at the top, and all boundaries are impermeable to fluid.

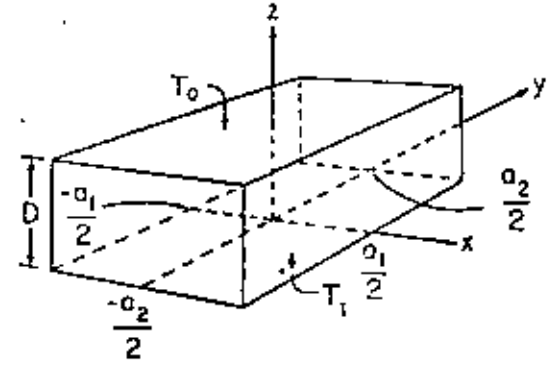


Fig. 2. – Rectangular box of porous media saturated with a homogeneous liquid.

In most analytical studies of thermal convection, it is customary to invoke the Boussinesq approximation that spatial as well as temporal variations in fluid density can be neglected except for buoyancy effects (i.e., everywhere except in the gravity term in the equation of motion). In addition, all coefficients in the governing equations are assumed to be constant scalars. Under these conditions the mass balance equation 1 reduces to

$$\frac{\partial v_i}{\partial x_i} = 0 \tag{3}$$

In writing Darcy's law, it is customary to replace $\rho$ by $\rho_0 [1 - \beta (T - T_0)]$ in the gravity term and add a term including the time derivative of velocity (compare with Eq. 2),

$$\frac{1}{\varphi} \frac{\partial v_i}{\partial t} + \frac{\mu}{k \rho_0} v_i = [1 - \beta (T - T_0)] g_i - \frac{1}{\rho_0} \frac{\partial p}{\partial x_i} \tag{9}$$

Energy balance is usually expressed by a simplified version of equation 7 and Beck uses our notation

$$(\rho c_v)^{*\theta} \frac{\partial T}{\partial t} = -\rho_0 c_v v_i \frac{\partial T}{\partial x_i} + \kappa^{*\theta} \frac{\partial^2 T}{\partial x_i^2} \tag{10}$$

where

$$(\rho c_v)^{*\theta} = \varphi \rho_0 c_v + (1 - \varphi) \rho^s c_v^s .$$

Initially, the system is assumed to be in static equilibrium so that the pressure is hydrostatic. Thus,

$$v_i^0 = (0, 0, 0) \quad \text{and} \quad T^0 = T_1 + (T_0 - T_1) \frac{z}{D} \tag{11}$$

Under these conditions, there are no convective currents and the system is said to be "statically stable". Let a small volume of fluid suddenly be brought from elevation $z = 0$ to a higher elevation $z > 0$, thus superimposing a disturbance $(v_i', T', p')$ upon the "basic state" $(v_i^0, T^0, p^0)$. We now want to determine whether or not the system is "dynamically stable", i.e., whether this disturbance will die out or build up to the level of a discernible convective current. Equations 8–11 as well as the boundary conditions must be satisfied by the disturbed state as well as by the basic state. Thus, by writing these equations first in terms of $(v_i^0 + v_i', T^0 + T', p^0 + p')$ and then in terms of $(v_i^0, T^0, p^0)$, we can subtract the second set from the first to obtain

$$\frac{\partial v_i'}{\partial x_i} = 0 \tag{12}$$

$$\frac{1}{\varphi} \frac{\partial v_i'}{\partial t} + \frac{\mu}{k \rho_0} v_i' = -\beta T' g_i - \frac{1}{\rho_0} \frac{\partial p'}{\partial x_i} \tag{13}$$

$$(\rho c_v)^{*\theta} \frac{\partial T'}{\partial t} = -\rho_0 c_v v_i' \frac{\partial (T^0 + T')}{\partial x_i} + \kappa^{*\theta} \frac{\partial^2 T'}{\partial x_i^2} \tag{14}$$

subject to the boundary conditions

$$v_i' n_i = 0 \quad \text{at} \quad x = \pm \frac{1}{2} a_1 ; \quad y = \pm \frac{1}{2} a_2 ; \quad z = 0, D \tag{15}$$

$$T' = 0 \quad \text{at} \quad z = 0, D \tag{16}$$

$$\frac{\partial T'}{\partial x_i} n_i = 0 \quad \text{at} \quad x = \pm \frac{1}{2} a_1 ; \quad y = \pm \frac{1}{2} a_2 \tag{17}$$

where $n_i$ is the unit outward normal to the boundaries of the box.

To reduce these equations to a dimensionless form it is helpful to use the following dimensionless groups:



Thermal diffusivity:

$$\alpha = \kappa^{*\theta} / (\rho_0 c_v) \tag{18}$$

Rayleigh number:

$$\mathrm{Ra} = k \rho_0 g \beta (T_1 - T_0) D / (\mu \alpha) \tag{19}$$

Prandtl number:

$$Pr = k \alpha \rho_0 / (\mu D^2 \varphi) \tag{20}$$

Heat capacity ratio:

$$H = (\rho c_v)^{*\theta} / (\rho_0 c_v) \tag{21}$$

Aspect ratios:

$$D_1 = a_1 / D ; \qquad D_2 = a_2 / D . \tag{22}$$

The Rayleigh number relates buoyancy to viscous retardation, whereas the Prandtl number relates thermal diffusivity to viscous retardation. If we also define a set of dimensionless variables

$$\begin{array}{llll} v_i = D v_i' / (\alpha \mathrm{Ra}^{\frac{1}{2}}) & \theta = T' / (T_1 - T_0) & p_D = k p' / (\mu \alpha \mathrm{Ra}^{\frac{1}{2}}) & \\ \tau = t \alpha / D^2 & X = x / D & Y = y / D & Z = z / D \end{array} \tag{23}$$

we can rewrite (12)–(17) as

$$\frac{\partial v_i}{\partial X_i} = 0 \tag{24}$$

$$Pr \frac{\partial v_i}{\partial \tau} + v_i = \underbrace{\mathrm{Ra}^{\frac{1}{2}} \theta \delta_{i2}}_{\text{zero for } i = 1, 2} - \frac{\partial p_D}{\partial X_i} \tag{25}$$

$$H \frac{\partial \theta}{\partial \tau} = -\mathrm{Ra}^{\frac{1}{2}} v_i \frac{\partial \theta}{\partial X_i} + \underbrace{\mathrm{Ra}^{\frac{1}{2}} v_i \delta_{i2}}_{\text{zero for } i = 1, 2} + \frac{\partial^2 \theta}{\partial X_i^2} \tag{26}$$

$$v_i n_i = 0 \quad \text{at} \quad X = \pm \frac{1}{2} D_1 ; \quad Y = \pm \frac{1}{2} D_2 ; \quad Z = 0, 1 \tag{27}$$

$$\theta = 0 \quad \text{at} \quad Z = 0, 1 \tag{28}$$

$$\frac{\partial \theta}{\partial X_i} n_i = 0 \quad \text{at} \quad X = \pm \frac{1}{2} D_1 ; \quad Y = \pm \frac{1}{2} D_2 \tag{29}$$

The dynamic stability of this system can be investigated by a linear method or energy approach. In the linear approach the disturbances are assumed so small enough for second-order terms to be neglected. The conditions for marginal stability (i.e., stability just at the onset of convection) can thus be determined from the above equations after reducing (25) and (26) to

$$(30) \qquad -\mathrm{Ra}^{\frac{1}{2}}\theta\delta_{ij} + v_i = -\frac{\partial p_D}{\partial X_i}$$

$$(31) \qquad \mathrm{Ra}^{\frac{1}{2}} v_i \delta_{ij} = -\frac{\partial^2 \theta}{\partial X_j^2}$$

According to the linear theory, the critical Rayleigh number, $\mathrm{Ra}_c^{\text{linear}}$, is the smallest eigenvalue of the resulting problem. However, this theory indicates only a necessary condition for stability, and the true critical Rayleigh number may therefore be smaller, $\mathrm{Ra}_c^{\text{true}} \leq \mathrm{Ra}_c^{\text{linear}}$.

The energy method was first applied to porous media by Westbrook (1969) and was later extended by Wankat and Schowalter (1970) and Beck (1972). Stability is established relative to arbitrary disturbances subject only to the equation of continuity and corresponding boundary conditions. Since stability actually depends on a more restricted class of disturbances satisfying (24)–(29), the critical Rayleigh number obtained may be too conservative and we therefore have $\mathrm{Ra}_c^{\text{energy}} \leq \mathrm{Ra}_c^{\text{true}}$. However, in the particular case considered here, both methods lead to the same eigenvalue problem and therefore $\mathrm{Ra}_c^{\text{linear}} = \mathrm{Ra}_c^{\text{energy}}$.

Beck showed that the eigenvalue problem has separable eigenfunctions, the velocity components of which are

$$(32) \quad \begin{aligned} v_1 &= \sin\left[\left(\frac{1}{2}m\pi\right)(1 + 2X/D_1)\right]\cos\left[\left(\frac{1}{2}n\pi\right)(1 + 2Y/D_2)\right]U(Z) \\ v_2 &= \cos\left[\left(\frac{1}{2}m\pi\right)(1 + 2X/D_1)\right]\sin\left[\left(\frac{1}{2}n\pi\right)(1 + 2Y/D_2)\right]V(Z) \\ v_3 &= \cos\left[\left(\frac{1}{2}m\pi\right)(1 + 2X/D_1)\right]\cos\left[\left(\frac{1}{2}n\pi\right)(1 + 2Y/D_2)\right]\sin(l\pi Z) \end{aligned}$$

$$m, n = 0, 1, 2, \cdots; \qquad l = 1, 2, \cdots$$

where $U(Z)$ and $V(Z)$ are functions of Z only. The corresponding critical Rayleigh numbers are

$$(33) \qquad \mathrm{Ra}_c = \pi^2 \min_{l,m,n} (b + l^2/b)^2 = \pi^2 \min_{m,n} (b + b^{-1})^2$$

where

$$b = [(m^2/D_1^2) + (n^2/D_2^2)]^{\frac{1}{2}} \text{ and } l = 1.$$



Equation 33 shows that the critical Rayleigh number d[illegible] is entirely [illegible] aspect ratios $D_1$ and $D_2$. The minimum possible value of $4\pi^2$ corresponding to $b = 1$. Lapwood (1948) obtained $\mathrm{Ra}_c = 4\pi^2$ for the case of a laterally infinite layer, thus indicating that vertical walls tend to stabilize the system. However, $\mathrm{Ra}_c$ remains nearly equal to $4\pi^2$ unless $D_1$ or $D_2$ are less than about 0.8, as may happen in a narrow and tall box.

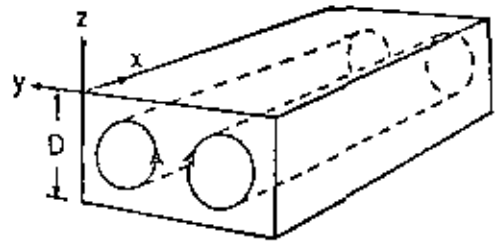


Fig. 3. – Two convective rolls in rectangular box heated from below.

Geometry becomes more important when one considers the mode of convection. It is evident from (32) that when $m = 0$, the horizontal velocity $v_1$ vanishes, which gives rise to $n$ convective cells known as "rolls" (see fig. 3). Since $\mathrm{Ra}_c$ corresponds to $l = 1$, $v_3$ in (32) is identically zero only at $Z = 0$ and $Z = 1$, and thus the vertical extent of each roll is equal to the height

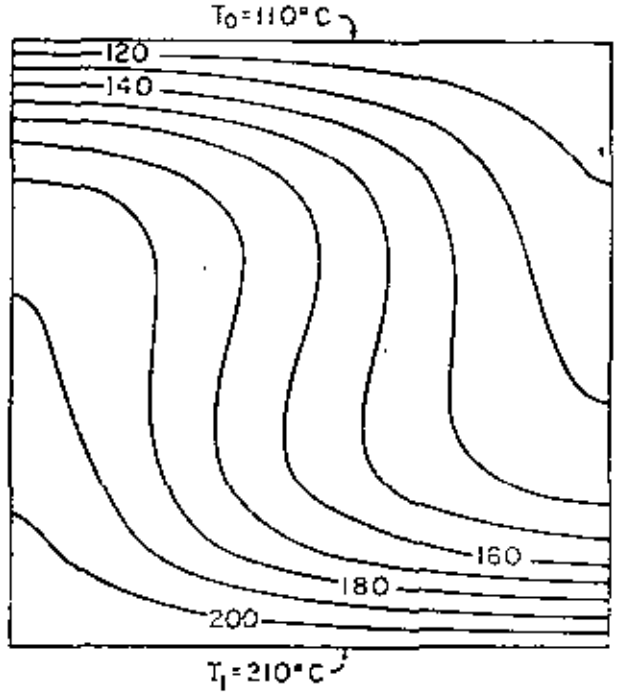


Fig. 4. – Typical temperature distribution in plane perpendicular to axis of single convective roll with $\mathrm{Ra} = 100$.

of the box. ypical temperature profile in a plane perpendicular to the axi of such a r shown in fig. 4. Rolls are invariably preferred over three-dimensional cells whenever the height D is not the smallest dimension. When rolls do form, they are usually parallel to the shorter side, although the overriding rule is for the number of rolls and the direction of their axes to be such that each roll has the closest approximation to a square cross-section as possible. Three-dimensional cells are preferred when $a_1$, $a_2$, and D are nearly the same size (i.e., a cube) or when the height is less than both lateral dimensions. For a cube, the motion resembles a toroid with vertical axis through the center of the box. For further details regarding these conclusions, the reader is referred to Beek (1972).

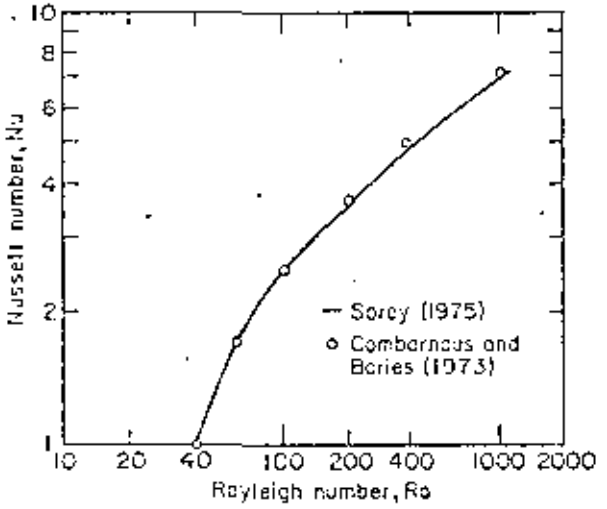


Fig. 5. – Maximum Nusselt number versus Rayleigh number for cellular convection in a laterally infinite layer.

(after Sorey, 1975).

It is important to recognize that all of these results have been obtained from an analysis of marginal stability and are therefore limited to Rayleigh numbers in the immediate neighborhood of $Ra_c$. In order to obtain results for higher Rayleigh numbers one must either perform experiments or solve the governing equations by an appropriate analytical or numerical technique. A large number of such studies concerned with both steady and nonsteady state situations have been reported in the literature and we shall try to summarize briefly some of the most important aspects of this work.

One effect of convective motion is to increase the rate of vertical heat transfer through the system. This is measured by the Nusselt number, Nu, which is defined as the ratio of total heat flow in the presence of convection to that by conduction only. For Rayleigh numbers less than the critical value, Nu = 1; otherwise Nu > 1. Fig. 4 shows the steady state temperature distribution corresponding to a roll at Ra = 100 for which Nu = 2.6.



According to the criterion of Platzman (1965), a system will tend to establish a mode of convection which maximizes the rate of heat transfer. At Rayleigh numbers near $Ra_c$, this means that cells with nearly square cross sections are preferred. However, at large Rayleigh numbers, Combarnous and Bories (1973) and Horne and O'Sullivan (1974) show that the preferred cell width depends on Ra, with aspect ratios of 0.5, .33, and .25 corresponding to Rayleigh numbers of 280, 400 and 700, for layers with no restraining side walls. Similar effects of reduced cell width with increased Ra are observed for box models with restraining side walls. Combarnous and Bories (1973), Holst and Aziz (1972 b), and Sorey (1975) found that Nusselt numbers are nearly the same for two-and three-dimensional motions in stable convection states. The relationship between Ra and the maximum Nusselt number for a laterally infinite layer is plotted in fig. 5.

Sorey (1975) further indicates that the cellular pattern and Nusselt number at steady state may depend on the initial conditions in the box. Using uniform initial temperature and pressure distributions in a square (two-dimensional problem) with Ra = 100 led to development of two cells with Nu = 2.2. With a non-uniform temperature distribution, the result was a single cell with Nu = 2.6. Horne and O'Sullivan (1974) report from numerical as well as laboratory experiments that for a uniform initial temperature distribution, heating the lower boundary slowly instead of instantaneously results in unicellular rather than multicellular motion. In other words, the mode of convection is not necessarily unique but may depend on the past history of the system. A hysteresis effect has also been noted by Elder (1967) and Karra (1968).

As Ra increases to 280, the system tends to develop a more favorable mode of convection and, as a result, the fluid may start fluctuating. These fluctuations will be irregular when the boundary conditions are uniform, but may develop into stable oscillations when the boundaries are heated in a non-uniform fashion. Horne and O'Sullivan (1974) report isotherms during a single oscillation when half of the bottom boundary has an elevated uniform temperature as shown in fig. 6. A rough calculation for the Wairakei geothermal region indicates that, if the depth is 3 km, the oscillations would have a time constant on the order of 1,000 years, and it would therefore be practically impossible to detect them.

*Free Convection Models.*

Numerous authors have attempted to extend the analysis of free convection to more realistic systems. There are, however, several complicating factors. The concept of a critical Rayleigh number may not apply in geothermal reservoirs where horizontal temperature variations undoubtedly exist along bounding surfaces. Free convection is then set up for any value of Ra > 0, although its effect on the thermal and hydrologic regimes should be negli-

gilde unless Ra is large. Donaldson (1968 b) estimates that in geothermal areas Ra i the range of 500–5,000. Caltagirone *et al.* (1971) suggest ti concept of al Rayleigh number which varies spatially within the reservoir to account for the fluctuating convective motions observed.

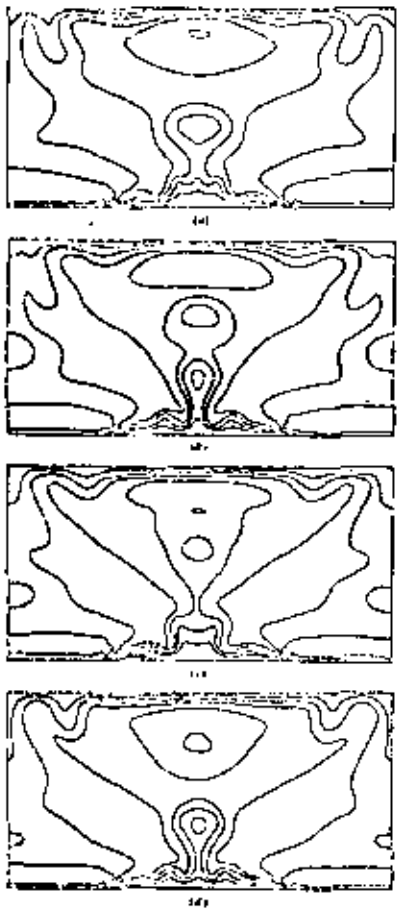

Fig. 6. – Isotherm plots at equal intervals of time during a single stable oscillation with Ra = 750. (after Holst and Aziz, 1972).

Combarnous and Bories (1973) evaluated the effects of assuming thermal equilibrium between solid and fluid phases (Eqs. 4–7) for systems with Rayleigh numbers well above theoretical critical values. Comparisons of experimental and numerical results for the relationship between Ra and Nu numbers using various combinations of porous media and fluid types indicate that the assumption of thermal equilibrium between solid and fluid phases is adequate for Ra at least as high as 2,000.

Holst and Aziz (1972 a) and Sorey (1975) investigated effects of temperature and pressure-dependent parameters on heat transfer in convecting systems. For water, the dominant influence is the viscosity variation such that as the temperature difference across the permeable layer $T_1 - T_0$ increases, the effective Rayleigh number increases over the value calculated from equation 19 using parameters computed at $T = T_0$. The Nusselt number would be correspondingly greater and the critical Rayleigh number lower than for the constant parameter case. Alternatively, if parameters evaluated at $T = (T_1 + T_0)/2$, values of $Ra_c$ and the Ra versus Nu relationship still vary with $T_1 - T_0$ due to the nonlinearity in the temperature dependence of $c_r$, $\rho$, and $\mu$ (Sorey, 1975). In contrast, realistic variations in fluid density with pressure were found to have negligible effects on the cellular convection problem.

Studies have also been made on the effect of various uniform boundary conditions at the surfaces of the homogeneous region on $Ra_c$. Lapwood (1948) investigated a laterally infinite layer in which the lower boundary is impermeable and the upper boundary is maintained at constant pressure and found that $Ra_c = 27.1$. Lapwood also found that when the upper boundary is a perfectly conducting free surface, then $Ra_c = 4\pi^2$; but when it becomes an imperfect conductor, then $27.1 \leq Ra_c \leq 4\pi^2$. A table of $Ra_c$ values for a variety of uniform boundary conditions is given by Nield (1968) and in all cases, $Ra_c \leq 4\pi^2$.

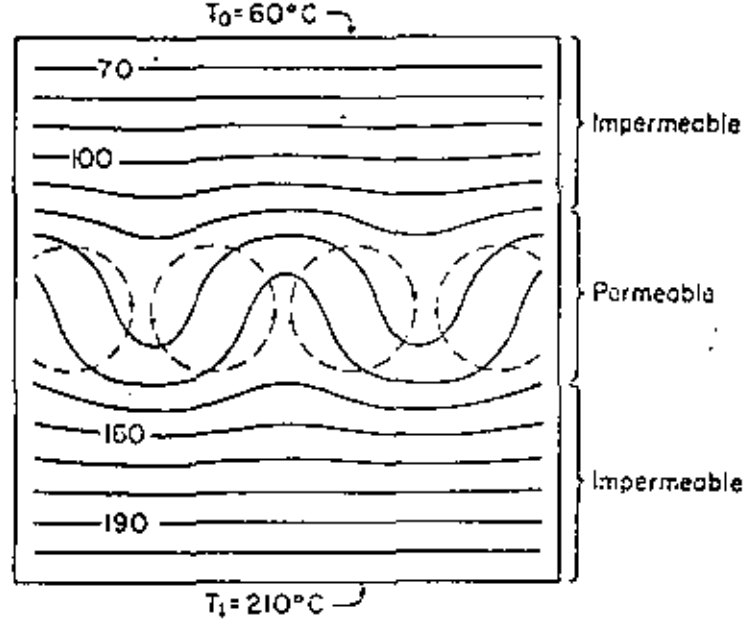


Fig. 7. – Distortion of isotherms due to convection in central permeable layer. (after Sorey, 1975).

Donaldson (1962) analyzed free convection in a two-layer system in which a permeable layer was underlain by an impermeable but thermally conductive layer of equal thickness. This removes the assumption of an isothermal surface at the bottom of the convecting layer. Sorey (1975) extended the analysis to a three-layer system with impermeable zones above and below the reservoir and found, in agreement with Donaldson's results, that vertical heat transfer rates in the multilayer systems were significantly less than in the single-layer system for the same values of Ra. The critical Rayleigh number

was also less [illegible] the multilayer systems. Fig. 7 shows how temperatures within the impert [illegible] layers are distorted by convection in the central layer.

Some work has also been done on the problem of an inclined system bounded by isothermal surfaces (Combarnous and Bories, 1973; Kaneko *et al.*, 1974). Combarnous and Bories show that, since the temperature gradient and gravity are no longer colinear, the fluid is constantly moving regardless of the Rayleigh number. In a layer of infinite lateral extent, the tendency at low Rayleigh numbers is to develop unicellular convection parallel to the slope. If this is considered the stable state, instabilities develop at critical Rayleigh numbers which depend on the angle of inclination. When this angle is less than 15°, $Ra_c \approx 40$ and the mode of convection is similar to that observed in a horizontal layer. Above this lower limit, $Ra_c$ increases rapidly with the angle of inclination and convective movements take the form of adjacent coils climbing upslope. Fluctuating conditions develop at higher and higher Rayleigh numbers ($Ra \geq 240$-$280$ for horizontal layer) as the angle of inclination increases. The case of the inclined box is more complex (Holst and Aziz, 1972 a; Kaneko *et al.*, 1974).

Wooding (1963) and McNabb (1965) have studied the effect of localized heat sources on the formation of vertical jet flows. McNabb developed a boundary layer theory for convective flow over a finite circular "hot plate" at the bottom of a semi-infinite porous medium. He estimated the amount of heat convected from the hot plate as a function of its temperature and suggested that a similar approach could be used to evaluate the rate of cooling of a magma chamber beneath a water saturated porous formation.

Cheng and Lau (1974) have investigated steady state free convection in a vertical cross section of an unconfined aquifer in which the position of the water table is not known a priori. The aquifer is assumed to rest on an impermeable horizontal heat source of variable temperature and is bounded on its sides by vertical isothermal surfaces of constant hydraulic head, representing contact with the ocean on a volcanic island. Dispersion and gravity effects due to variations in salt content between fresh water and sea water (mixing occurs by virtue of the vertical boundary conditions) are implicitly neglected. By solving a linearized version of the governing equations, the authors show that pressure in the aquifer remains nearly hydrostatic. Temperature is greatly affected by the size of the heat source but its location is less important. There is a noticeable upwelling of the water table directly above the heat source, which depends primarily on vertical temperature gradients and nature of the heat source.

Much additional literature on various theoretical and experimental aspects of free convection in homogeneous media is available. Holst (1970) has published an extensive review of the literature and the state of the art has been summarized more recently by Combarnous and Bories (1973). For subsequent developments, the reader should consult the works of Fernandez (1972), Holst and Aziz (1972 a, b), Masuoka (1972), Palm *et al.* (1972), Sun *et al.* (1972), Gupta and Joseph (1973), Cheng and Lau (1974), Combarnous and Bories (1974), Horne and O'Sullivan (1974), Kaneko *et al.* (1974), Straus (1974), Yen (1974), Weber (1975 a, b), and Sorey (1975).



*Pipe Models.*

An alternative concept for convection in geothermal areas is the pipe system in which the fluid no longer flows through a homogeneous layer but is channeled through zones of relatively high permeability. Such zones may be caused by fissures or fractures which are known to control local phenomena such as springs, fumaroles, and geysers. As discussed by Einarsson (1942), Bodvarsson (1961), and Donaldson (1970), the occurrence and distribution of thermal areas in Iceland and New Zealand could be controlled by variations in permeability as well as by spatial distribution of the heat source.

Einarsson (1942) and Bodvarsson (1961) discuss the thermal areas of Iceland in terms of pipe systems involving deep circulation of water (2 to 3 km) and discharge in hot springs. Elder (1966) analyzed hydrothermal systems in Iceland and New Zealand using lumped parameter and multi-dimensional models to quantify the general features of heat and mass transfer. White (1957, 1961) used pipe systems to explain the chemical composition of waters associated with volcanic and hydrothermal systems.

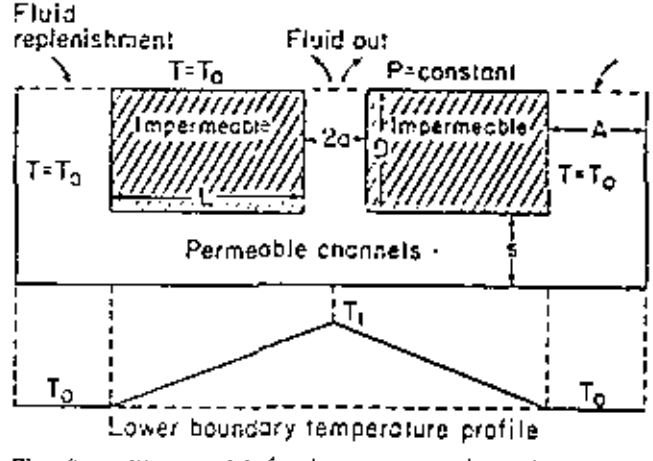


Fig. 8. – Pipe model for hot-water geothermal system.
(after Donaldson, 1968 b).

Donaldson (1968 b, 1970) suggests the model in fig. 8 for a hot-water geothermal system. The model consists of cold reservoirs recharged from the surface, a vertical column through which hot water flows, and a permeable horizontal channel connecting the two. The surrounding medium is assumed impermeable, and heat supplied at the lower boundary maintains the density imbalance and resulting convective motion. Though the model is oversimplified, Donaldson's analysis allows for throughflow from recharge to discharge areas

and secondary (circulatory) convection in the upflow column. Gross characteristics of [illegible] thermal systems are simulated by adjusting temperatures at the base [illegible] model, dimensions and permeability of the vertical column, and resistance to flow in the remainder of the pipe system.

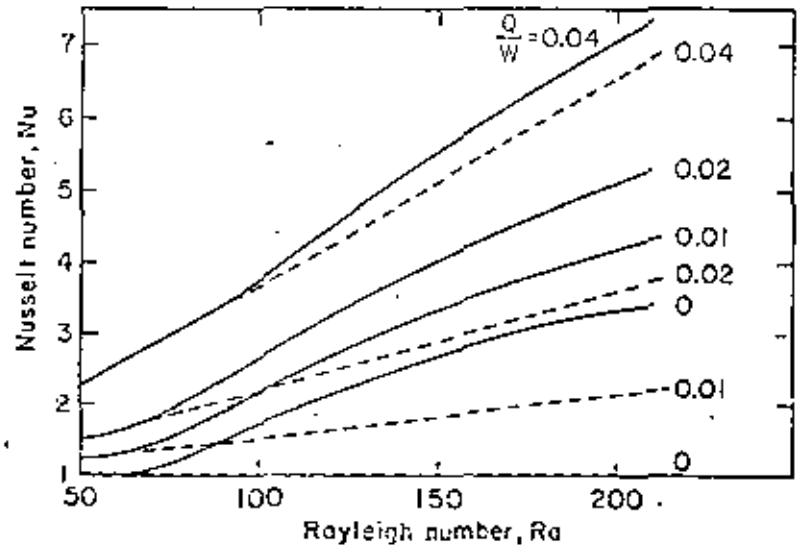


Fig. 9. – Nusselt number versus Rayleigh number for combined through and circulatory flows in vertical column with $2a/D = 0.5$. Solid lines show combined effect, dashed lines show throughflow effect only.

(after Donaldson, 1970).

Mathematical description of the model involves the single phase, steady state equivalents of (1) and (7) which are solved by numerical relaxation for the boundary conditions shown in fig. 8. Uniform thermal properties are assumed throughout and constant values for $k$ and $\mu$ are used in each of the permeable channels. In the absence of secondary convection in the upflow column, the mean mass flow rate is given by

$$Q = \frac{\rho_0 k \beta g (T_m - T_0)}{(\mu/\rho)\, b} \tag{34}$$

where $T_m$ = mean temperature in the column and $b = 1 + aL/sD + \Lambda/D$. It is not clear from Donaldson's analysis whether $\mu/\rho$ is determined at $T_0$ or $T_m$. Fig. 9 illustrates the relationship between Ra and Nu with throughflow and secondary convection for a column aspect ratio $2a/D = 0.5$. Here $W = \rho_0 k \beta g (T_1 - T_0)/(\mu/\rho)$ is a measure of the maximum possible throughflow from buoyancy unbalance alone. Hence, $Q/W = [(T_m - T_0)/(T_1 - T_0)]\,(1/b)$. It is seen from fig. 9 that the heat transferred by circulatory flow decreases markedly as the throughflow increases. Fig. 10 illustrates how throughflow in a column with $2a/D = 0.2$ and $Q/W = 0.05$ tends to sweep the circulatory motion up the channel.



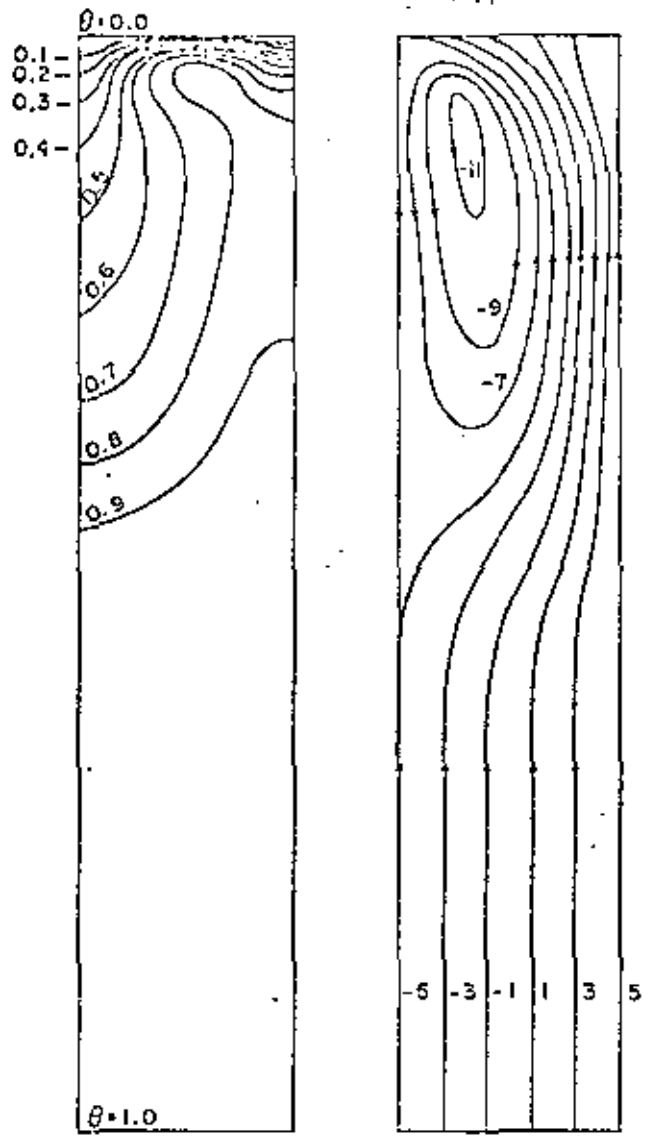


Fig. 10. – Effect of throughflow on circulatory convection with $Ra = 420$, $2a/D = 0.2$, $Q/W = 0.05$; (a) isotherms normalized such that $0 \leq \theta \leq 1.0$, (b) streamlines in arbitrary units.

(after Donaldson, 1970).

Sorey (1975) modeled heat and liquid mass transfer in hot spring systems using the two-dimensional models shown in fig. 11. Transient and steady state conditions were simulated numerically to determine conductive heat losses from the vertical conduit and its effect on temperature $T_w$ of water discharging at the spring. The lower boundary was formed by the top of a reservoir with water at temperature $T_b$, and the upper boundary was the land surface at temperature $T_s$. The relationships between dimensionless temperature drop, $1 - \theta_w$, and the dimensionless mass flow rates for the circular conduit, $m_c$, and the fault plane conduit, $m_p$, are plotted in fig. 12.

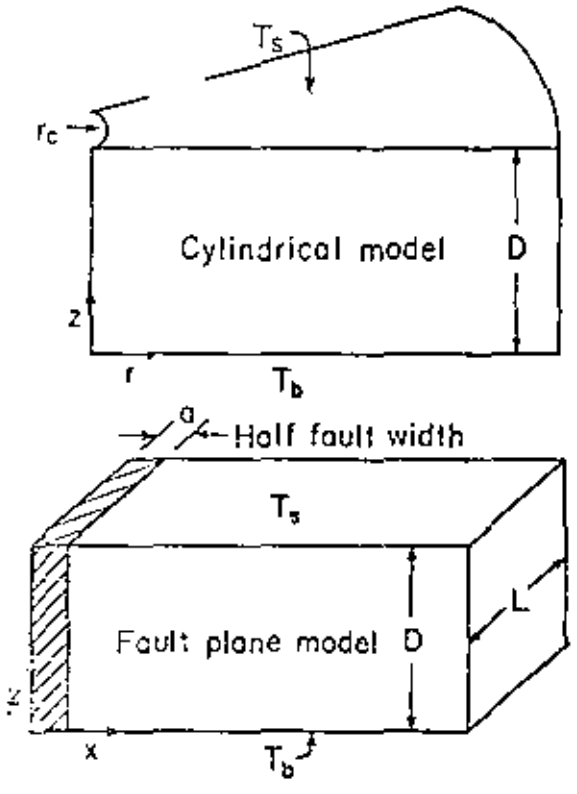


Fig. 11. – Two-dimensional models for hot spring systems.

(after Sorey, 1975).

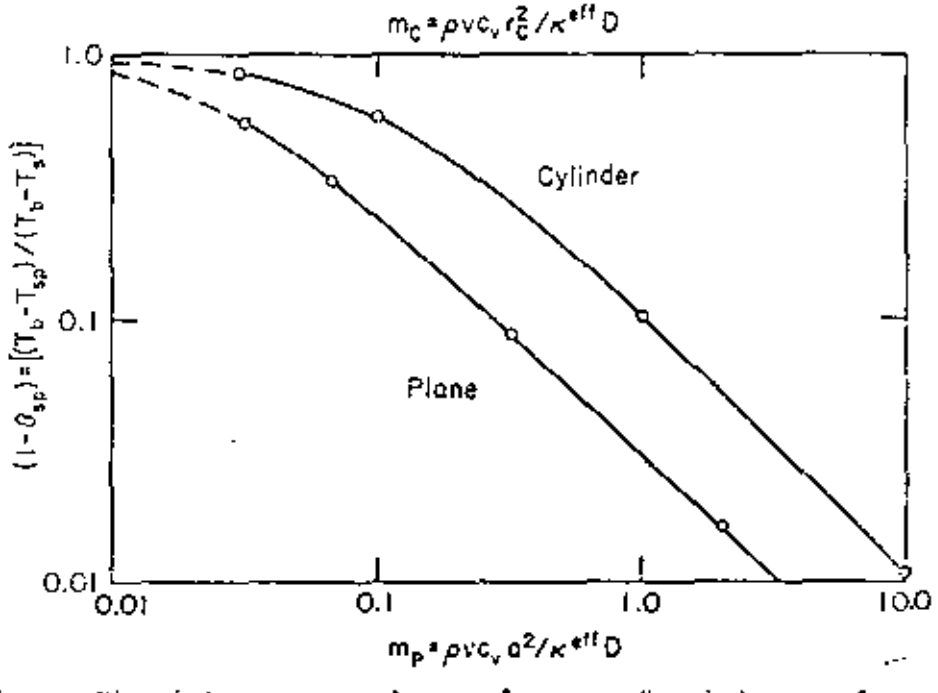


Fig. 12. – Dimensionless temperature drop, $1 - \theta_{sp}$, versus dimensionless mass flow rates for circular conduit, $m_c$, and fault plane conduit, $m_p$, in hot spring systems.

(after Sorey, 1975).

Expressions for the total conductive heat loss are $[2\pi\kappa^{eff} D (T_b - T_s) m_c (1 - \theta_{sp})]$ for the cylinder and $[2\kappa^{eff} D (T_b - T_s) m_p (1 - \theta_{sp})]$ for the plane. The plane model applies where fluid rises in a fault zone whose lateral extent is considerably greater than the discharge area of the hot springs. Comparing the two models for the same total mass flow, the fault plane model has greater heat loss and more temperature drop than the cylindrical conduit model.

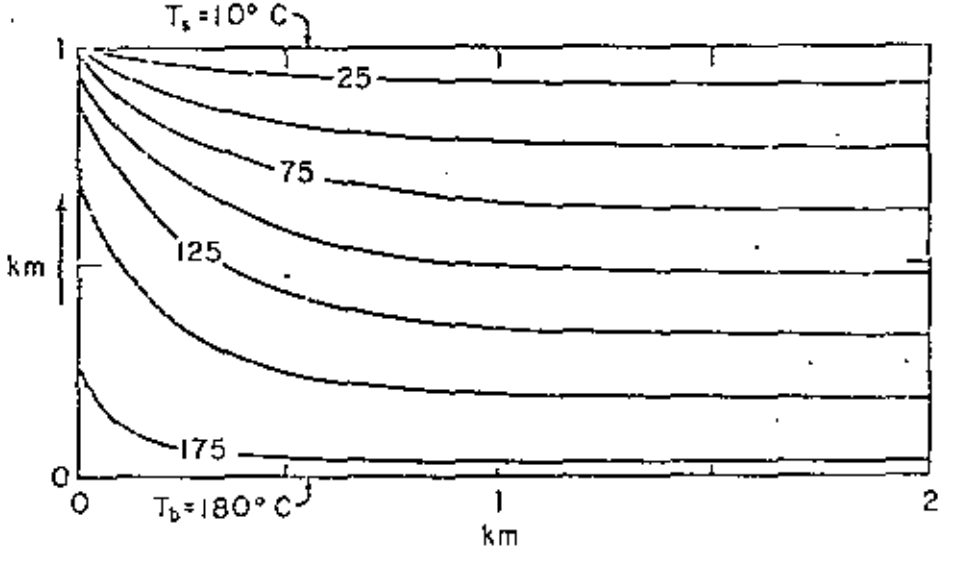


Fig. 13. – Distortion of steady-state isotherms in vertical fault plane model with discharge = 100 lpm, $a$ = 10 m, $L$ = 1 km, and Ra = 0.

(after Sorey, 1975).

The steady-state temperature distribution in a fault plane model with a spring discharge of 100 lpm is shown in fig. 13. Distortion of the temperatures due to convective motion in the conduit is confined to a zone of about 1 km on either side of the fault. At the land surface, the conductive heat flux near the spring is approximately 50 heat flow units (50 μcal/sec cm²) and decreases to about 3.4 heat flow units as distance exceeds 1 km. These results were obtained using $\kappa_{sa} = 2 \times 10^{-3}$ cal/cm sec °C and $c_v = 1$ cal/gm °C.

Analysis of the transient behavior of these systems (Sorey, 1975) shows that periods of 30,000 years or more are required for the conductive thermal regime to reach equilibrium following the geologic development of the spring system. Somewhat shorter time periods are required if convective motions in the rock surrounding the spring conduit are considered. Simulations under these conditions are described by Sorey (1975).

Analysis of pipe models has been extended by Elder (1966) and Donaldson (1968 a, 1970) to include boiling in the upflow channel. Elder has developed relationships between mass flow rate, fluid enthalpy, resistance to flow, and the energy supplied by a heat source for channeled circulation caused by buoyancy differences between recharge and discharge areas. He concludes

that for systems with large energy input or large resistance, the discharge (mass flow) [illegible] sufficient to transport the energy unless the fluid moves in the form of [illegible]. With low energy inputs or small resistance, the circulating fluid should remain a liquid except for a shallow zone which may contain steam. This approach has been applied to the Tuscany thermal areas near Larderello, Italy, and the Taupo systems in New Zealand.

Donaldson's (1968 a) work involves steady flow of a boiling liquid in a vertical channel. The remainder of the circulation system including the heat source is considered only as controlling temperature, pressure, and mass flux at the bottom of the discharge channel. Lateral heat conduction is neglected so that the equations are one-dimensional. For the case of uniform permeability and small mass flow rate, only liquid flow is considered. Comparison of the resultant pressure-depth relations with saturation pressure curves indicates that boiling will not occur for systems with $c_p m/\kappa^{ff} \leq 7 \times 10^{-5}$ cm$^{-1}$, where $m$ is mass flux per unit area. When this critical value is exceeded, boiling must occur in the upper section of the channel.

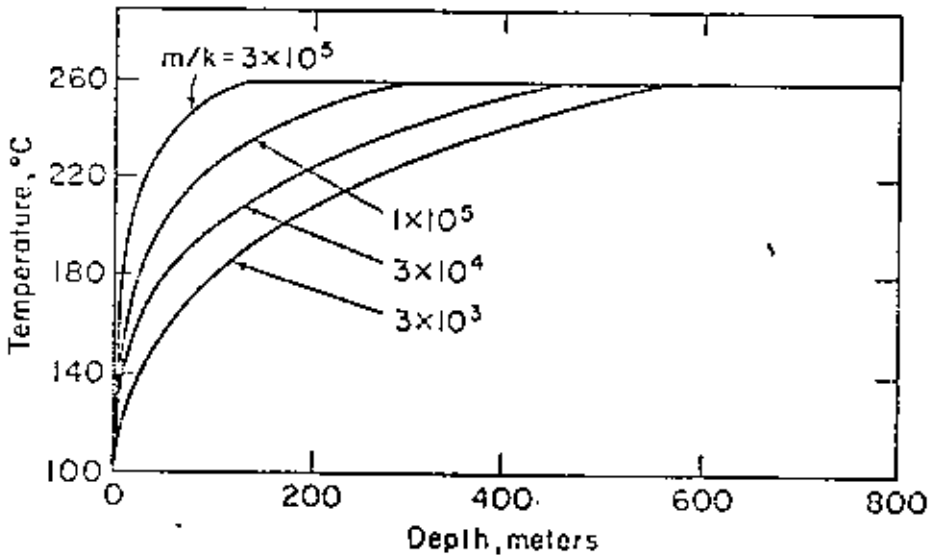


Fig. 14. – Temperature versus depth in a boiling system as a function of $m/k$.

(after Donaldson, 1968 a).

Two-phase flow in this upper region is described by the one-dimensional, steady state forms of equations 1–3 and 6 without the pressure terms. At the interface between the two-phase and liquid-saturated regions, the boundary conditions are constant mass flux and constant temperature equal to that at the channel base. Thus, the lower region is treated as isothermal, and in the upper region, temperature and pressure are related by the vapor pressure curve for water. The equations are solved analytically to yield temperature and pressure, water fraction, and water and steam flow rates as functions of depth. The controlling parameter in these relationships is $m/k$ as seen in fig. 14. Thus, the onset of boiling is indicated by the value of $c_p m/\kappa^{ff}$, whereas, when two-phase conditions exist, the controlling parameter i[illegible]. Effects of vertical heat conduction are significant only if $\kappa^{ff}/k$ is great[illegible]an $3 \times 10^{-3}$ cal/cm$^3$ sec °C. Donaldson concludes that once boiling commences, it must extend some 200–500 meters downward and hence this two-phase region must be considered in studying geothermal systems. Two-phase conditions in columns with variations in vertical permeability have also been discussed by Donaldson (1968 a, 1970).

## Geothermal systems during exploitation

### *Lumped-Parameter Models.*

The concept of a lumped-parameter model provides one of the simplest means for describing behavior of a geothermal system during exploitation. The basic idea is to view the entire system as a perfect mixing cell for both mass and energy so that spatial variations in concentration can be neglected. Instead of considering the internal distribution of mass and energy, attention is restricted to the total amounts generated within the system as well as that crossing the boundaries. Since time is the only independent variable, the system can be characterized mathematically by a set of ordinary differential equations or an equivalent set of algebraic expressions representing total mass and energy balance.

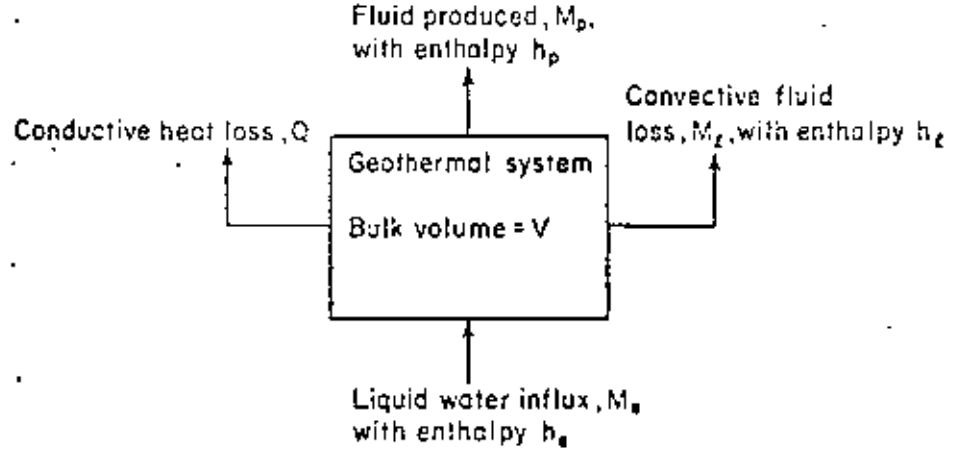


Fig. 15. – Schematic diagram of lumped-parameter model for geothermal systems.

(after Whiting and Ramey, 1969).

The first and best known lumped-parameter model of a producing geothermal reservoir was developed by Whiting and Ramey (1969). Their system has a bulk volume V and contains vapor, water, and rock. Fig. 15 is a schematic diagram of the system from which a simple mass balance yields

$$M_\ell - M_0 = M_\ell - M_p - M_i \tag{35}$$

where $M_e$ = current mass of water (vapor + liquid) in place, $M_0$ = initial mass of water in place, $M_r$ = influx of liquid (no vapor is assumed to enter the system), $M_p$ = mass of water (vapor + liquid) produced, and $M_l$ = mass of water (vapor + liquid) lost by leakage. Water may flow in from an adjacent aquifer or leak out of the system via steam vents, springs, wild wells, etc. The water influx, $M_r$, is represented by a linear combination of terms each of which is the product of a theoretical time-dependent response function characterizing a certain aquifer flow geometry (hemispherical, linear, or radial) and pressure. These calculations further assume that the liquid inflow is isothermal with constant enthalpy, $h_r$.

In the energy balance calculation the system is assumed to be in complete thermodynamic equilibrium. According to the first law of thermodynamics one then has

$$\underbrace{M_e u_e - M_0 u_0}_{\text{Internal energy change in fluid}} + \underbrace{V(1-\varphi)(\rho c)^{rr}(T_e - T_0)}_{\text{Internal energy change in solid rock}} = \tag{36}$$

$$= \underbrace{-Q}_{\text{Net conductive heat influx}} + \underbrace{M_r h_r - M_p h_p - M_l h_l}_{\text{Net convective enthalpy influx}}$$

The volume V can be expressed as

$$V\varphi = M_0 [S_0^G v_0^G + (1 - S_0^G) v_0^L] = M_e [S_e^G v_e^G + (1 - S_e^G) v_e^L] \tag{37}$$

where $S^G$ is vapor (gas) saturation and $v^G$ and $v^L$ are specific volumes of vapor and liquid, respectively. The phase diagram for water (see fig. 1) indicates that in the particular case where the system contains only compressed liquid, the thermodynamic path of decreasing pressure due to production will be essentially isothermal and isoenthalpic. Equations 35–37 then lead to a mass-volumetric balance similar to that employed for petroleum production above the bubble-point,

$$M_0 (v^L - v_0^L) + M_e v^L - (M_p + M_l) v^L = 0 \tag{38}$$

Additional working hypotheses made by Whiting and Ramey are that Q is negligibly small relative to other terms in (36) and that $h_p = h_l$ (i.e., the enthalpy of produced and lost fluid is the same).

The compressed liquid version of this lumped-parameter model was applied by Whiting and Ramey to the Wairakei geothermal system in New Zealand. The initial temperature and enthalpy were estimated from field data, and a least-square fit to the production history from 1956 to 1961 was used to determine the initial water in place and the initial pressure. The model was then used to predict performance through 1965 and agreement with measured data was excellent (see fig. 16). Prediction of future performance from 1966 to the year 2000 took into account two-phase conditions and indicated that pressure and temperature would decrease very little during this period. Recent field data from Wairakei have shown this prediction to be incorrect. The model was also used by Cady (1969) to simulate a laboratory setup but had to be applied separately to the two-phase and dry steam regions that developed.



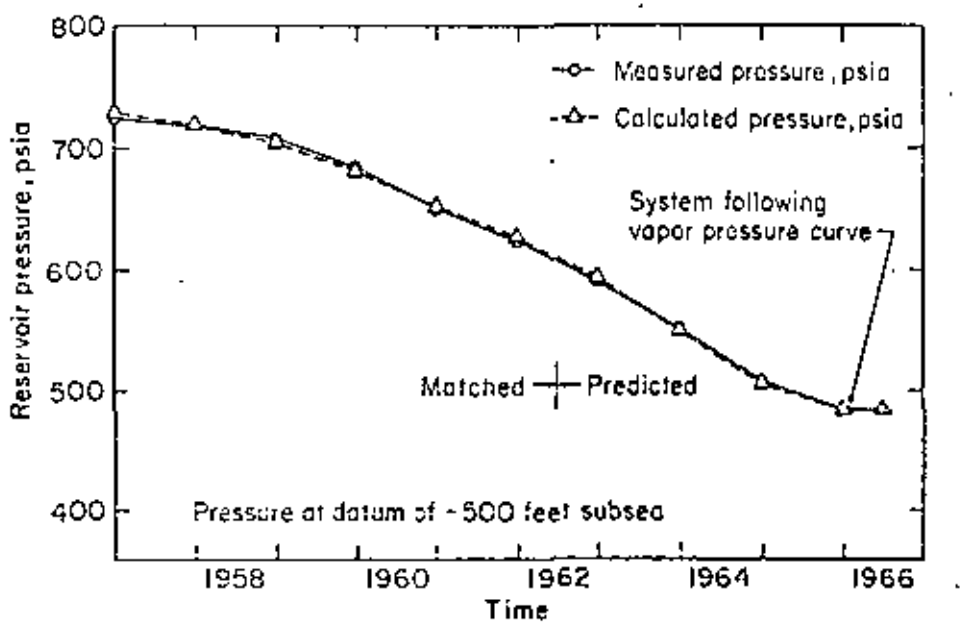


Fig. 16. – Comparison of calculated with measured pressures for Wairakei geothermal system. (after Whiting and Ramey, 1969).

Brigham and Morrow (1974) have adapted the lumped-parameter approach to vapor-dominated systems (i.e., systems with a significant dry steam region) by considering three different distributions of vapor and liquid. In each case the system is assumed to be completely closed (i.e., the boundaries are impermeable and adiabatic) and energy is derived only from the rock mass itself.

Their first model concerns a single-phase system completely saturated with vapor. They assume that since the heat capacity of solid rock is much greater than that of steam, the system is essentially isothermal. Thus, there is no need for an energy equation and one can use a mass balance approach similar to that commonly employed in natural gas reservoir. This approach leads to a linear relationship between $p/Z$ and cumulative production $\Delta M^G$ according to the equation of state for a real gas,

$$\frac{p_1}{Z_1} = \frac{p_0}{Z_0}\frac{M_1^G}{M_0^G} = \frac{p_0}{Z_0}\left(\frac{M_0^G - \Delta M^G}{M_0^G}\right) \tag{39}$$

where Z is compressibility factor, $M^G$ is mass of steam in place, and the subscripts indicate different values of time. The intercept of this line on the abscissa is equal to the original fluid in place, $M_0^G$.

In the second model the vapor phase is separated from an underlying layer of l[illegible] by a horizontal interface at which boiling takes place. Sin[illegible] the vapor [illegible]se is again assumed to be isothermal, its treatment is similar to that in the previous model. The liquid phase changes its volume continuously and the corresponding lumped system is therefore defined as the pore space filled with liquid at the beginning of each pressure decrement. For this system the mass balance is simply

$$\Delta M^G = -\Delta M^L \tag{40}$$

whereas the energy balance for the fluid is expressed as

$$\underbrace{M_1^L e_1^L + M_1^G e^G - M_0^L e_0^L}_{\text{Internal energy change}} = \underbrace{M_1^S c_p^S (T_0 - T_1)}_{\text{Heat transferred from rock to liquid}} + \tag{41}$$

$$+ (M_0^S - M_1^S) c_p^R \left(T_0 - \frac{T_0 + T_1}{2}\right) - \underbrace{(M_0^L - M_1^L - M_1^G) h^G}_{\text{Enthalpy of vapor leaving system}}$$

Heat transferred from rock to steam

where $M^S$ is mass of rock in contact with liquid, $h^G$ is average enthalpy of vapor leaving system and $e^G$ is average internal energy of vapor (both calculated at the average temperature $(T_0 + T_1)/2$ and the subscripts 0 and 1 indicate the beginning and end of a depletion step, respectively. Brigham and Morrow further simplified this equation by reformulating it in terms of enthalpy and neglecting the resulting pressure terms and obtained

$$M_1^L h_1^L - M_0^L h_0^L = M_1^S c_p^S (T_0 - T_1) + \tag{42}$$

$$+ (M_0^S - M_1^S) c_p^S \left(\frac{T_0 - T_1}{2}\right) - (M_0^L - M_1^L) h^G$$

Given a rate of production, the resulting system of nonlinear equations can be solved in an iterative manner.

The third model considers a vapor phase overlying a layer of liquid except that now boiling occurs throughout the entire thickness of this layer and its depth remains fixed in time. The resulting energy equation is essentially similar to that of Whiting and Ramey (1969) with the exception that only steam is allowed to leave the system.

Application of these models to various hypothetical reservoirs has shown that in estimating available reserves by extrapolation of early $p/Z$ behavior the results will tend to be optimistic when porosity is low, but pessimistic when porosity is high. The constant liquid level model was found to predict higher recovery for a given pressure depletion than the falling liquid level model. The presence of even a small amount of liquid in the lower part of a geothermal system was shown to be extremely important because it can account for a large fraction of the total fluid mass and can significantly affect



the results of a $p/Z$ analysis. Finally, Brigham and Morrow conclude that "the steam portion of a reservoir will always remain isothermal whether or not there is boiling water below the steam. Thus pressure, temperature, and enthalpy measurements will not be completely diagnostic for determining the original state of the reservoir fluid system. Because the steam remains essentially isothermal, it gradually increases in enthalpy and becomes superheated as the pressure declines".

An interesting lumped-parameter model based on the assumption that the liquid and gas phases are uniformly distributed throughout the system has been proposed recently by Martin (1975). The system is assumed to be completely closed and each phase is produced at a rate which is related to its relative permeability. His approach is based on a simplified form of equations 1–3 and 6. If we neglect the gravity term in Darcy's law and substitute (2) and (3) into (1), we can write for an isotropic medium

$$\frac{\partial}{\partial x_i}\left(\chi' \frac{\partial p}{\partial x_i}\right) = \frac{\partial M'}{\partial t} \tag{43}$$

where

$$\chi' = k\left(\frac{\rho^L k_r^L}{\mu^L} + \frac{\rho^G k_r^G}{\mu^G}\right)$$

$$M' = \varphi(\rho^L S^L + \rho^G S^G)$$

Neglecting heat dispersion and the pressure terms in (6) we obtain by the same procedure

$$\frac{\partial}{\partial x_i}\left(\chi^h \frac{\partial p}{\partial x_i}\right) = \frac{\partial M^h}{\partial t} \tag{44}$$

where

$$\chi^h = \frac{\rho^L h^L k k_r^L}{\mu^L} + \frac{\rho^G h^G k k_r^G}{\mu^G} + \varkappa^* \frac{dT}{dp}$$

$$M^h = \varphi S^L \rho^L h^L + \varphi S^G \rho^G h^G + (1 - \varphi)\rho^S c_p^S T$$

since $T$ and $p$ are uniquely related by the boiling curve. The notion of a lumped-parameter model implies that gradients of pressure, temperature, and saturation are small. Expanding (43) and (44) and neglecting the products of these gradients leads to

$$\frac{1}{\chi'}\frac{\partial M'}{\partial t} = \frac{\partial^2 p}{\partial x_i^2} = \frac{1}{\chi^h}\frac{\partial M^h}{\partial t} \tag{45}$$

Expanding the time derivatives with respect to $p$ and S yields the nonlinear ordinary differential equation

$$\frac{dS^L}{dp} = \frac{\chi^h \dfrac{\partial M'}{\partial p} - \chi' \dfrac{\partial M^h}{\partial p}}{\chi' \dfrac{\partial M^h}{\partial S^L} - \chi^h \dfrac{\partial M'}{\partial S^L}} \tag{46}$$

In the case of single-phase flow, T and $p$ are not related uniquely to each other, and the above procedure must therefore be modified. If we neglect heat conduction as well as dispersion, we obtain the single-phase equivalent of (45) with $\lambda^{\phi} = \lambda^{l}$. Expanding the time derivatives with respect to $p$ and T leads to the following nonlinear ordinary differential equation,

$$\frac{dT}{dp} = \frac{\frac{\partial M^{\phi}}{\partial p} - h\frac{\partial M^{l}}{\partial p}}{h\frac{\partial M^{l}}{\partial T} - \frac{\partial M^{\phi}}{\partial T}} \qquad (47)$$

Equations 46 and 47 were used by Martin to calculate numerically the relationships between T, $p$ and S in a hypothetical system free of gravity effects. Integration of (47) showed that in the case of a single phase, $dT/dp$ is very small and the exploitation process is essentially isothermal. This is clearly illustrated in fig. 17 which shows the thermodynamic paths for various initial

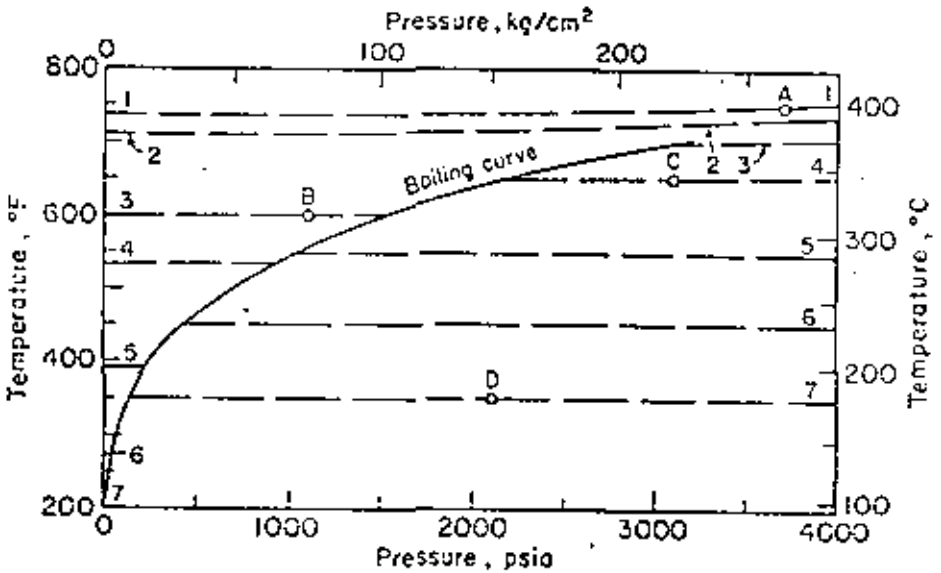


Fig. 17 – Pressure-temperature diagram for pure water and vapor showing various thermodynamic paths for depleting a geothermal system.

(after Martin, 1968).

$p$-T conditions in a system with $\varphi = 0.25$, $\rho^{s} = 162$ lb/ft³ (2.6 gm/cm³), $c^{s} = 0.2$ Btu/lb °F (0.2 cal/gm °C), $\kappa^{eff} = 40$ Btu/ft day °F (0.0069 cal/cm sec °C), $k = 1$ darcy ($9.87 \times 10^{-9}$ cm²), and typical $k_r$ values. For example, from initial conditions corresponding to point A, the temperature will drop slightly along line 1 as pressure declines. This corresponds to a single phase (essentially steam) reservoir with temperature and pressure above the critical point. However, if the system is initially saturated with liquid water at point C, production causes an isothermal decrease in pressure until the boiling



curve is reached. At this stage $p$ and T begin to follow the boiling curve with a gradual increase in steam saturation. Production of steam however, starts only when $S^{\phi}$ reaches its so-called equilibrium value at which the vapor phase becomes mobile (below this vale $k_r^{\phi} = 0$). The ratio between produced steam and liquid water continues to increase until $S^{l}$ is reduced to a stage where the liquid becomes immobile and production is restricted to saturated steam. When all the water has been boiled away and $S^{l} = 0$, the temperature departs from the boiling curve and superheated steam is produced under essentially isothermal conditions.

From his study Martin further concluded that " under certain conditions only a relatively small amount of the heat initially contained in a geothermal reservoir will be produced during pressure depletion. Much of this heat may be contained in the produced steam even though initially the reservoir contains only hot water ". This is due to the higher heat content and lower viscosity of steam as compared with liquid water. A similar reasoning also led Martin to conclude that " for many conditions where gravity segregation of the steam and hot water occurs during depletion, more of the total heat can be produced by completing wells high in the reservoir to enhance steam production and suppress water production ". When gravity effects are important, system C should follow the path shown in fig. 17 until the steam phase becomes mobile and gravity segregation begins. Since $S^{\phi}$ increases rapidly in the upper portion of the system, departure from the boiling curve will occur at considerably higher $p$ and T values than is shown in the figure. In the lower portion of the system $S^{l}$ decreases slowly and therefore departure from the boiling curve will occur at lower $p$ and T values than in fig. 17.

*Distributed-Parameter Models.*

A model in which the properties of the rock and/or the fluid (e.g., saturation, viscosity, pressure, etc.) are allowed to vary in space will be called a distributed-parameter model. By taking into account spatial variations of these properties the resulting problem may become too complex to be treated analytically. An alternative approach is to replace the governing partial differential equations by an equivalent set of algebraic equations and then solve the problem numerically with the aid of a computer. The purpose of the following discussion is to acquaint the reader with some of the results obtained to date by numerical simulation of relatively complex geothermal systems.

A considerable degree of sophistication in the numerical simulation of immiscible, multiphase and multicomponent fluid flow problems under non-isothermal conditions has been achieved in recent years by petroleum engineers. A brief review of this work has been included in a recent paper by Coats *et al.* (1974). Most of this effort, however, was not concerned with geothermal systems but was directed toward the problem of oil recovery by steamflooding, hot waterflooding, steam stimulation, and other thermal pro-

cesses which are of immediate concern to the petroleum industry. For example, Spillette and [illegible]en (1968) have studied the response of an oil reservoir to hot water injection by assuming that the hydrocarbons and the water will appear only as a liquid phase. Their model consists of a vertical cross-section including a horizontal layer of sand enclosed between two impermeable shale strata. Energy is transported by conduction and convection in the sand layer and by conduction in the shale layers. Fluid densities and viscosities are taken to be temperature dependent and capillary pressure between the two fluid components is taken into account. The equations governing mass transport are solved by an alternating direction implicit (ADI) iterative finite difference procedure whereas the energy equation is solved by the method of characteristics. One of the conclusions of this study was that fluid segregation due to gravity has a significant effect on the system considered.

Another two-dimensional vertical model consisting of a sand layer sandwiched between two impermeable strata has been developed more recently by Weinstein *et al.* (1974). In this model fluid flow is allowed to take place only in one horizontal direction whereas energy may be transferred by conduction both horizontally and vertically through the entire system. However, the hydrocarbons and water can coexist both in the liquid and vapor states, so that one must now deal with three distinct phases: oil, water, and gas. The gas phase is a mixture of steam and hydrocarbon vapor. Interphase mass transfer within each component is allowed to account for processes such as water vaporization, steam condensation, hydrocarbon distillation, solvent extraction, and solution-gas drive. The energy equation is expressed in terms of enthalpy, rock compressibility is taken into account, but capillary pressure effects are neglected. A finite difference approach is employed with an implicit pressure-explicit saturation formulation of the mass balance equation, which is solved simultaneously with the energy equation. The authors also discuss various improved numerical techniques for invoking phase constraints and calculating mass transfer terms.

A three-dimensional finite difference model describing nonisothermal, three-phase flow of oil, liquid water, and steam has been described by Coats *et al.* (1974) for the purpose of simulating oil recovery by steam and hot water injection. In this model fluid densities are taken to be linear functions of temperature and pressure, and the effect of pressure on porosity is also taken into account. The mass and energy balance equations are solved simultaneously by a direct method. A comparison of calculated results with experimental data indicated that the simulation process is sensitive to temperature effects on relative permeability. The authors conclude that such data, especially the temperature dependence of water relative permeabilities, must be taken into account.

The first application of a distributed-parameter model to a geothermal system was made by Mercer (1973) and Mercer and Pinder (1974). A comprehensive account of this work has been described more recently by Mercer *et al.* (1975). The model consists of a single-phase, two-dimensional areal



(horizontal) representation of the hot-water Waiora aquifer in [illegible] Wairakei hydrothermal system of New Zealand. The mass and energy [illegible]re (Eq. 7 without the pressure term) are solved in the horizontal plane of the aquifer by the Galerkin finite element approach, using isoparametric elements as shown in fig. 18. Since the governing equations are averaged over the thickness of the aquifer, cellular convection does not play a role in the resulting model.

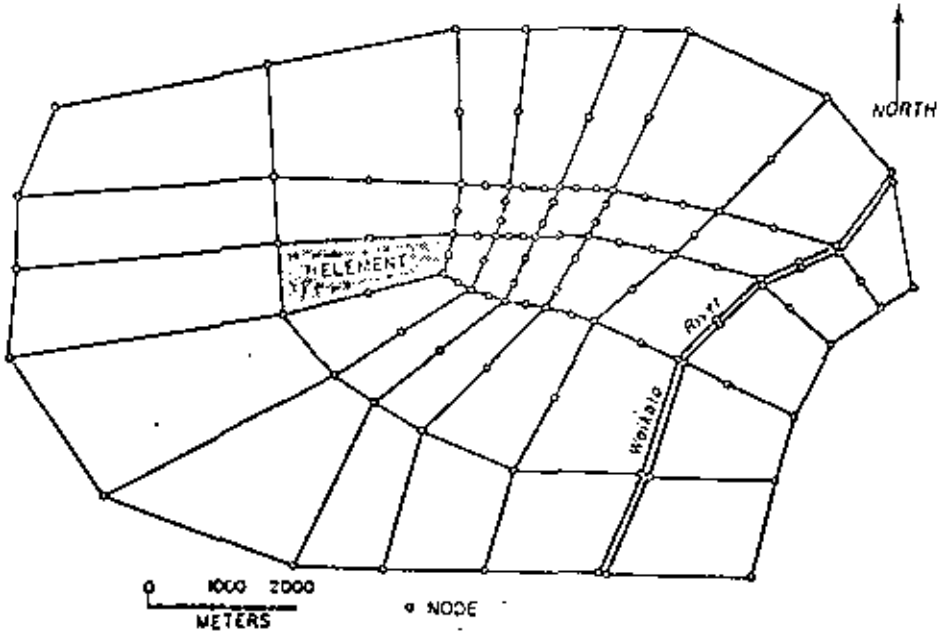


Fig. 18 – Network of isoparametric elements used in distributed-parameter model of Wairakei geothermal system.

(after Mercer *et al.*, 1975).

However, vertical flow of fluid as well as energy is allowed to take place between the Waiora formation and the overlying Wairakei breccia aquifer through the intervening Huka Falls shale (see fig. 19). The rate of this vertical leakage is taken to be proportional to the differences in head and temperature between the two aquifers, the values of $p$ and T in the upper aquifer being kept constant. Inflows of heat from the underlying ignimbrites into the Waiora aquifer are treated as unknown source terms to be determined by model calibration. The lateral boundaries of the Waiora aquifer are assumed to be impermeable and isothermal. Viscosity is allowed to vary with temperature whereas fluid density is calculated as a linear function of temperature and pressure. The model is also capable of treating the heat dispersion term in its proper tensorial form.

The first step in applying the model to Wairakei was to adjust the parameters so as to reproduce the steady state conditions existing in 1955, prior to exploitation. The parameters that were adjusted at this stage included

element configuration, heat sources at the bottom of the aquifer, dispersion coefficients, and permeabilities. A sensitivity analysis was performed indicating that dispersion had little influence on the results, whereas the permeability of the Huka Falls formation had an important effect on the temperature distribution in the thermal reservoir.

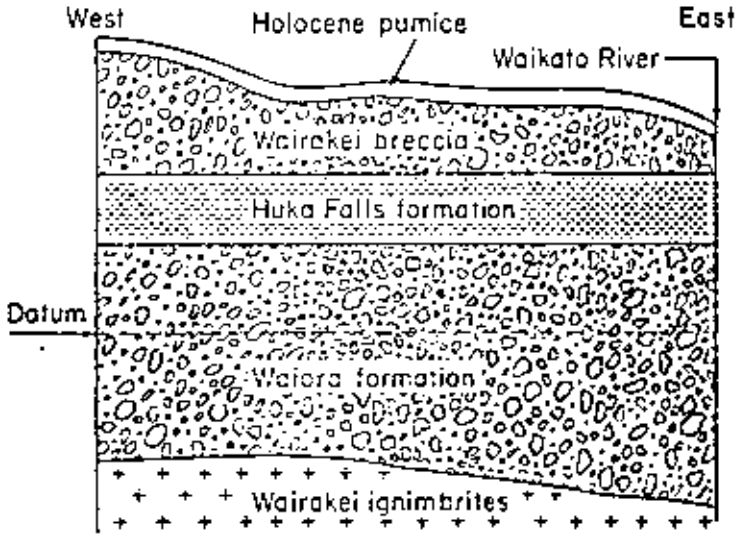


Fig. 19. – Generalized geologic cross-section of Wairakei geothermal system. Datum plane 152.4 m above sea level.

(after Mercer et al., 1975)

The second step was to simulate the response of the geothermal field to withdrawal of hot water from a series of wells during the period between 1955 and 1962, using time steps of 30 days. The parameters of the model were again adjusted so as to bring about a fit between calculated and observed data. The results showed only a slight change in the configuration of the isotherms during the period investigated. Fig. 20 is a comparison of computed and observed potentiometric surfaces in the Waiora aquifer for 1958 and 1962. The single-phase model failed to reproduce historical data after the calibration period of 1955–1962 due to a considerable quantity of steam that had formed in the Waiora aquifer as a result of exploitation. Faust and Mercer (1975) are now developing a two-phase model to handle such problems.

A two-dimensional model of transient single-component, two-phase flow in a geothermal system has been developed by Toronyi (1974). The model is based on Equations 1–3 and 6 (without the last two terms involving pressure) and utilizes a block-centered rectangular finite difference grid capable of simulating flow in either a horizontal or vertical plane. The resulting equations are expressed in an implicit backward difference form and are solved simultaneously by a line iterative quasi-linearization (Newton–Raphson) scheme. Anisotropy is taken into account with the restriction that principal permeabilities



and heat conductivities must remain parallel to the coordinates. Thermal conductivity is calculated according to (5) but dispersion is not taken into account. The fluids are assumed to have temperatures and pressures that are always on the vapor pressure curve implying that liquid and vapor co-exist at every point in the system. Consequently $p$ and S are the two dependent variables for which a solution is sought simultaneously.

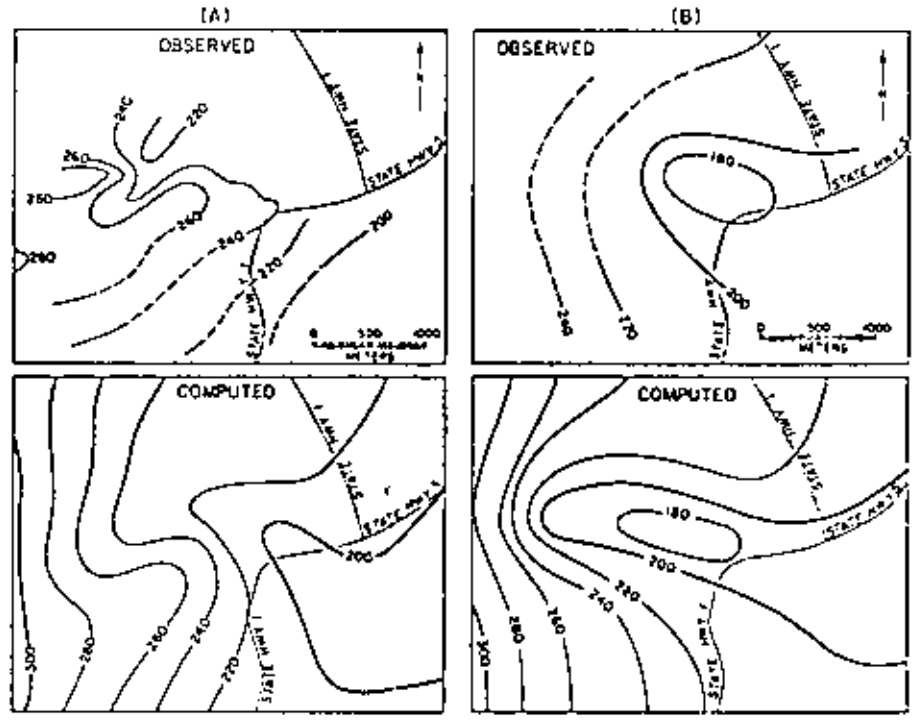


Fig. 20. – Comparison of computed with observed potentiometric surfaces in Waiora hot-water aquifer for (A) 1958 and (B) 1962. Values in meters from datum 152.4 m above sea level.

(after Mercer et al., 1975)

The external boundaries are impermeable and adiabatic with the understanding that forced convection due to production is much greater than conduction across these boundaries. The distributed-parameter model is coupled to a one-dimensional steady state model of a producing well in which the fluid is assumed to form a homogeneous two-phase mixture. The well is treated as a point source in the finite difference model which, in turn, provides boundary values of $p$ and S for the steady state wellbore model. The wellbore model is represented mathematically by first order ordinary differential equations which are solved by the Runge-Kutta method.

Toronyi applied his model only to a homogeneous and isotropic geothermal system by using a 6×6 rectangular finite difference grid. His purpose was to investigate the effects of porosity, permeability, and various uniform initial $p$ and S distributions on the production of geothermal fluid in a hori-

zontal and vertical plane. On the basis of these studies, Toronyi classified the behavior of two-phase geothermal systems into three types in terms of initial liquid saturation: 1) vapor dominated, with initial $S^l < 40\%$; 2) liquid dominated, with initial $S^l > 60\%$, and 3) mixed or intermediate, with initial $S^l$ within the range 40–60 %. Condensation and vaporization were found to be very important phenomena that could create exceedingly high liquid saturations near a wellbore and disrupt gravitational equilibrium by causing more liquid to occur at the top of the system than at the bottom. Toronyi also found that superheated regions form faster in rocks having relatively low porosity and permeability values. The quality of the produced fluid (in terms of percent steam) was always found to be greater at the wellhead than at the bottom, although the maximum change in quality was small.

A two-phase, multi-dimensional model for geothermal systems has recently been developed by Lasseter *et al.* (1975) based on an extension of an earlier investigation of single-phase flow under nonisothermal conditions (Lasseter and Witherspoon, 1974). This model utilizes Equations 1 through 4. In the numerical process, Equations 1 through 3 are combined into a flow equation which is then solved in conjunction with the energy equation (Eq. 4). These two equations expressed in an integrated finite difference form (Narasimhan and Witherspoon, 1975) are solved for the two dependent variables, density and energy of the fluids, as a function of time and position within the system. Advantage can be taken of the fact that the time constants for the energy equation are typically several orders of magnitude larger than the time constants of the flow equation, which permits one to decouple the governing equations and still handle the non-linearities satisfactorily. Thus, while it is necessary to take relatively small time steps to accurately solve the flow equation, the energy field time steps can be much larger.

Some preliminary results for a model of a vapor-dominated geothermal system are shown in fig. 21. A vertical cross-section of a cylindrical system with a height of 3,000 m and a radius of 2,000 m was set up using 150 elements. The vapor column had an average initial temperature and pressure of 250 °C and 40 kg/cm² throughout, and an attempt was also made to simulate a 200 m bottom layer that was essentially liquid saturated. The lower boundary of the boiling water layer was maintained at 250 °C while the other boundaries were arbitrarily made impermeable to both heat and fluid. Typical values for thermal and flow properties of the materials were assumed. Relative permeability data were temperature independent.

Fig. 21 shows reproductions of computer plots after about 1,500 days at a steam withdrawal rate from the producing interval of $3 \times 10^7$ kg/day (1,380 *t/h*). As a result of this high rate of production, the pressure in the vapor column dropped to about 25 kg/cm² (fig. 21 A) and the temperature decreased to about 225 °C (fig. 21 B). Fig. 21 C is a vector plot of the vapor flux showing how vigorous boiling at the bottom of the system is producing substantial steam. Fig. 21 D is a vector plot of the liquid flux and shows how water is separating from the steam at the base of the system. These preliminary results serve to illustrate the power of this numerical approach in analyzing such complex systems.

Gringarten and Sauty (1975) have developed an analytical model for nonsteady temperature behavior of production wells during reinjection of heat-depleted water into a horizontal aquifer with uniform regional flow. The aquifer is of infinite lateral extent and is confined between two impermeable semi-infinite layers. Initially, the system has a uniform temperature, $T_0$. At time $t = 0$, a well starts producing water at rate Q and injection of relatively cold water starts in a second well in the same aquifer at the same rate. The temperature of the injected water is set equal to $T_i$ and maintained constant thereafter. Such a pair of wells is known as a "doublet".

The authors assume that steady state fluid flow is established much faster than thermal equilibrium and that temperature transfer occurs only by forced

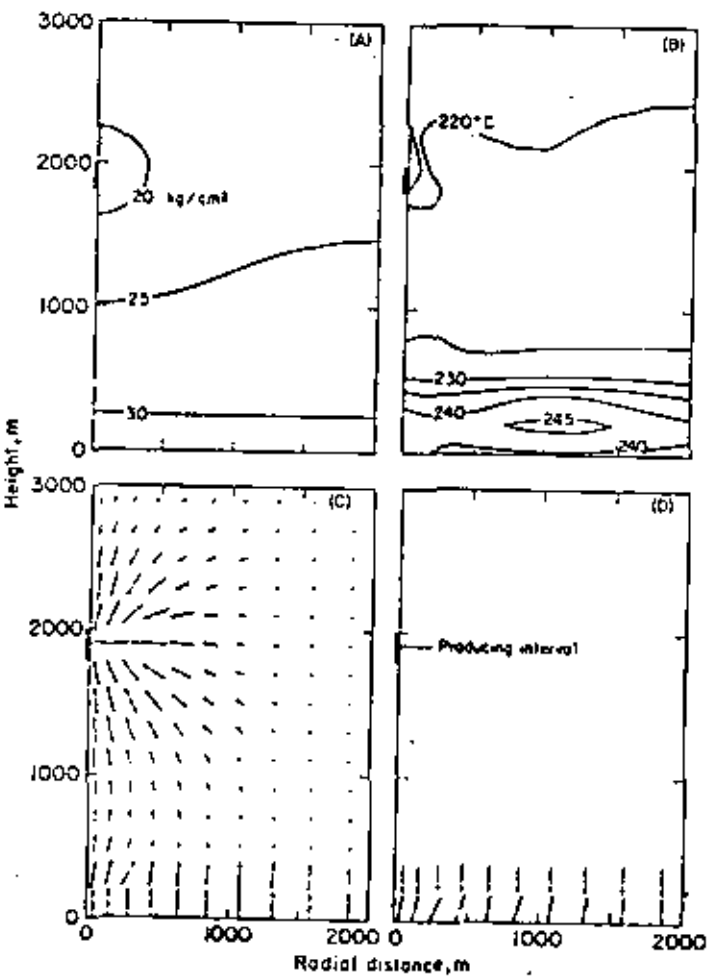


Fig. 21. – Distributed-parameter model of vapor-dominated geothermal system showing reservoir conditions after 1,500 days of production: (A) pressure field, (B) temperature field, (C) vapor flux, (D) liquid flux.

horizontal convection in the aquifer and vertical conduction in the confining beds. [redacted]ing further that the waters at temperatures $T_0$ and $T_1$ do not mix (piston displacement), they have arrived at a simple closed form mathematical relationship between temperature, certain dimensionless parameters, and the stream function characterizing water flow. Gringarten and Sauty used their solution to calculate the optimum spacing of isolated doublets to be drilled for space heating purposes in the 1,800 m deep Dogger aquifer around Paris, under the requirement that the cold front does not reach the producing well in less than 30 years when Q = 100 m³/h. By introducing a safety factor into their calculations, the optimum spacing was found to be about 900 m for an aquifer 50 m thick.

## NOMENCLATURE

| Symbol | Description | Dimensions |
|---|---|---|
| $a$, $a_1$, $a_2$ | width | L |
| $c_p$ | specific heat at constant pressure | $L^2 t^{-2} T^{-1}$ |
| $c_v$ | specific heat at constant volume | $L^2 t^{-2} T^{-1}$ |
| D | depth | L |
| $D_1$, $D_2$ | aspect ratio | — |
| $D_{ij}$ | mechanical heat dispersion tensor | $ML t^{-3} T^{-1}$ |
| $e$ | specific internal energy | $L^2 t^{-2}$ |
| $f$ | fluid property | arbitrary |
| $g$ | acceleration due to gravity | $L t^{-2}$ |
| $g_i$ | gravity vector (0, 0, $-g$) | $L t^{-2}$ |
| $h$ | specific enthalpy | $L^2 t^{-2}$ |
| H | heat capacity ratio | — |
| $k$ | intrinsic permeability | $L^2$ |
| $k_{ij}$ | intrinsic permeability tensor | $L^2$ |
| $k_r$ | relative permeability | — |
| L | length | L |
| $m$ | specific mass flux | $ML^{-2} t^{-1}$ |
| M | mass | M |
| $n_i$ | outward unit normal vector on $\Gamma$ | — |
| Nu | Nusselt number | — |
| $p$ | pressure | $ML^{-1} t^{-2}$ |
| $p_n$ | dimensionless pressure | — |
| Pr | Prandtl number | — |
| $q_i$ | specific conductive heat flux vector | $Mt^{-3}$ |
| Q | heat flux | $ML^2 t^{-3}$ |
| $r$ | radius | L |
| R | representative elementary volume | $L^3$ |
| Ra | Rayleigh number | — |
| $Ra_c$ | critical Rayleigh number | — |
| S | fluid saturation | — |
| $t$ | time | $t$ |



| Symbol | Description | Dimensions |
|---|---|---|
| T | temperature | T |
| $v$ | specific volume | $L^3 M^{-1}$ |
| $v_i$ | darcy velocity vector | $LT^{-1}$ |
| V | volume | $L^3$ |
| $w_i$ | velocity vector of solid fluid interface | $Lt^{-1}$ |
| $x_i$ | vector of space coordinates ($x$, $y$, $z$) $z$ being the vertical | L |
| Z | compressibility factor for real gas | — |
| $\alpha$ | thermal diffusivity | $L^2 t^{-1}$ |
| $\beta$ | coefficient of volumetric thermal expansion | $T^{-1}$ |
| $\Gamma^{LS}$ | liquid-solid interface in R | $L^2$ |
| $\Gamma^{LG}$ | liquid-gas interface in R | $L^2$ |
| $\Gamma^{GS}$ | gas-solid interface in R | $L^2$ |
| $\delta_{ij}$ | kronecker delta (1 if $i = j$ and 0 if $i \neq j$) | — |
| $\theta$ | dimensionless temperature | — |
| $\kappa$ | thermal conductivity | $MLt^{-3} T^{-1}$ |
| $\kappa_{ij}$ | thermal dispersion tensor | $MLt^{-3} T^{-1}$ |
| $\mu$ | viscosity | $ML^{-1} t^{-1}$ |
| $\nu_i$ | dimensionless velocity vector | — |
| $\rho$ | density | $ML^{-3}$ |
| $\tau$ | dimensionless time | — |
| $\varphi$ | porosity | — |
| $\langle\rangle$ | average over R | arbitrary |
| $\langle\rangle^*$ | average over pore space of R | arbitrary |
| $\langle\rangle^{L,G,S}$ | average over liquid, gas, or solid phases in R | arbitrary |
| *Subscripts* | | |
| $o$ | reference quantity | |
| *Superscripts* | | |
| *eff* | effective quantity for fluid-filled rock | |
| G | gas phase | |
| L | liquid phase | |
| S | solid phase | |
| $\circ$ | deviation from average over R | |

*Acknowledgments.* – We would like to acknowledge the support for this work provided by the U. S. Atomic Energy Commission, the U. S. Geological Survey and the University of California.

# APPENDIX

The purpose of this appendix is to derive a macroscopic form of the energy balance equation for a two-phase, single component fluid in a porous medium. This is accomplished by averaging the microscopic equations over a representative elementary volume (Bear, 1972, p. 19) of the medium. The particular method of averaging that is used here has been applied by Lee *et al.* (1975) to the energy equation and, in this context, was brought to our attention by Gray and Pinder (1974, personal communication). We recognize that the macroscopic energy equation can be derived directly from macroscopic balance considerations, without resorting to an averaging process. However, the formal averaging procedure is helpful in gaining insight into the numerous assumptions that one must make in order to arrive at a manageable macroscopic expression. Such assumptions are implicitly inherent in every macroscopic equation and, by facing them explicitly, one should be able to appreciate some of the limitations of the differential equations used to describe geothermal systems.

*Mathematical Preliminaries.*

Let R be a representative elementary volume of the porous medium and let $\varphi$ be the porosity of R. Whitaker (1969) demonstrated that the averaging procedure used below will lead to meaningful results if the characteristic length of R is much greater than the characteristic length of the pores, and is much smaller than the characteristic length of the entire porous medium. An obvious requirement is that R be large enough to provide a fair representation of all the statistical properties of the pore space. Our analysis is restricted to homogeneous porous media which means that the porosity, $\varphi$, as well as all other statistical properties of the pore space, must remain unchanged as one focuses his attention on different elementary representative volumes in the medium. Furthermore, the size and shape of R must be constant and its orientation must remain unchanged.

Let $f^L(x_i)$ be some property of the liquid (e.g., density, temperature, etc.) which, by definition, is zero in the gas phase and in the solids. Then the "liquid phase average" of $f^L$ is defined as

$$\langle f^L \rangle^L = \frac{1}{\varphi S^L R} \int_R f^L \, dR \tag{A1}$$

Similarly, the "pore volume average" of $f^L$ is defined as

$$\langle f^L \rangle^* = \frac{1}{\varphi R} \int_R f^L \, dR \tag{A2}$$

and the "bulk volume average" as

$$\langle f^L \rangle = \frac{1}{R} \int_R f^L \, dR \tag{A3}$$

From (A1)-(A3) it is evident that

$$\langle f^L \rangle = \varphi \langle f^L \rangle^* = \varphi S^L \langle f^L \rangle^L \tag{A4}$$

These averages can be viewed as point macroscopic quantities associated with the centroid of R. Thus, there is an average associated with each point in R (each such point being the centroid of another R), and it therefore makes sense to talk about the average value of these averages over R. Whitaker (1969) showed that

$$\langle \langle f^L \rangle \rangle = \langle f^L \rangle \tag{A5}$$

i.e., the average of the average is equal to the average (note that this is by no means self evident).

At any point in the liquid phase within R, $f^L$ can be expressed as

$$f^L = \langle f^L \rangle^L + f^{L} \tag{A6}$$

where $f^{L}$ is simply the deviation from the phase average of $f^L$. From (A5) and (A6) it follows that

$$\langle f^{L} \rangle^L \equiv 0 \tag{A7}$$

Note that just like $f^L$, the function of $f^{L}$ is taken to be zero everywhere outside the liquid phase.

According to the general transport theorem (c.f., Whitaker, 1968) one has

$$\left\langle \frac{\partial f^L}{\partial t} \right\rangle = \frac{\partial \langle f^L \rangle}{\partial t_i} - \frac{1}{R} \int_{A^{LS}, A^{LG}} f^L w_i n_i \, d\Gamma \tag{A8}$$

where $n_i$ is a unit normal pointing out of the liquid phase. Another useful relationship known as the "averaging theorem" (Whitaker, 1969; Slattery, 1972, pp. 192-196) states that

$$\left\langle \frac{\partial f^L}{\partial x_i} \right\rangle = \frac{\partial \langle f^L \rangle}{\partial x_i} + \frac{1}{R} \int_{A^{LS}, A^{LG}} f^L n_i \, d\Gamma \tag{A9}$$

Similar relationships will hold for properties of the solid phase, $f^S$, and the gas phase, $f^G$.

*Derivation of Energy Equation for Two-Phase Fluid.*

In the following analysis, the pore space is assumed to be saturated by a single-component fluid which can be either in a liquid or gaseous state. The liquid and gas phases are assumed to be separated by a distinct interface, $\Gamma^{LG}$, across which there may be a finite change in pressure. If one neglects viscous dissipation, then the energy equation at a point within the liquid can be written (e.f., Currie, 1974, p. 17) as

$$\frac{\partial}{\partial t}(\rho^L e^L) = -\frac{\partial}{\partial x_i}(\rho^L e^L v_i^L) - p^L \frac{\partial v_i^L}{\partial x_i} - \frac{\partial q_i^L}{\partial x_i} \tag{A10}$$

Taking the average of (A10) over a representative elementary volume, R, and using (A8) and (A9), the result (after rearrangement) is

$$\begin{aligned}\frac{\partial}{\partial t}(\rho^L e^L) = &-\frac{\partial}{\partial x_i}(\rho^L e^L v_i^L) - \frac{1}{R}\int_{\Gamma^{LG}} \rho^L e^L (v_i^L - w_i)\, n_i\, d\Gamma - \\ &- \varphi S^L (p^L)^L \frac{\partial (v_i^L)^L}{\partial x_i} - S^L (p^L)^L \frac{1}{R}\int_{\Gamma^{LG}} v_i^L n_i\, d\Gamma - \\ &- \frac{\partial (q_i^L)}{\partial x_i} - \frac{1}{R}\int_{\Gamma^{LS},\Gamma^{LG}} q_i^L n_i\, d\Gamma\end{aligned} \tag{A11}$$

Equation A11 is based on the assumption that fluid velocity normal to a solid-fluid interface is zero (i.e., there is no transfer of kinetic energy between the fluid and the solid). Furthermore, in order to replace the term $p^L(\partial v_i^L/\partial x_i)$ in (A10) by its macroscopic equivalent in (A11), it is necessary to assume that $\overset{\circ}{p}{}^L$ and $\partial \overset{\circ}{v}{}_i^L/\partial x_i$ are uncorrelated so that the average of their product is zero. A possible physical justification for this is to say that local variations in fluid velocity within a pore are controlled primarily by viscous stresses and can therefore be assumed to be independent of pressure.

The energy equation for the gas phase at a point within R has the same form as (A11). When this equation is averaged over R, the result is

$$\begin{aligned}\frac{\partial}{\partial t}(\rho^G e^G) = &-\frac{\partial}{\partial x_i}(\rho^G e^G v_i^G) + \frac{1}{R}\int_{\Gamma^{LG}} \rho^G e^G (v_i^G - w_i)\, n_i\, d\Gamma - \\ &- \varphi S^G (p^G)^G \frac{\partial (v_i^G)^G}{\partial x_i} + S^G (p^G)^G \frac{1}{R}\int_{\Gamma^{LG}} v_i^G n_i\, d\Gamma - \\ &- \frac{\partial (q_i^G)}{\partial x_i} - \frac{1}{R}\int_{\Gamma^{GS}} q_i^G n_i\, d\Gamma + \frac{1}{R}\int_{\Gamma^{GI}} q_i^G n_i\, d\Gamma\end{aligned} \tag{A12}$$

Here $n_i$ points into the gas along $\Gamma^{LG}$ and into the solid along $\Gamma^{GS}$.



The energy equation at a point within the solid is simply

$$\frac{\partial}{\partial t}(\rho^S e^S) = -\frac{\partial q_i^S}{\partial x_i} \tag{A13}$$

Integrating over R gives

$$\rho^S \frac{\partial (e^S)}{\partial t} = -\frac{\partial (q_i^S)}{\partial x_i} + \frac{1}{R}\int_{\Gamma^{LS},\Gamma^{GS}} q_i^S n_i\, d\Gamma \tag{A14}$$

where $n_i$ points into the solid.

From the requirement of energy continuity at a liquid-gas interface, it can be shown that

$$\int_{\Gamma^{LG}} [q_i^L + \rho^L e^L (v_i^L - w_i)]\, n_i\, d\Gamma = \int_{\Gamma^{LG}} [q_i^G + \rho^G e^G (v_i^G - w_i)]\, n_i\, d\Gamma \tag{A15}$$

A similar condition must also hold for the conductive energy flux $q_i n_i$ at any solid-fluid interface. Thus, by adding (A11), (A12), and (A14) and using A4) we obtain

$$\begin{aligned}\frac{\partial}{\partial t}[&\varphi S^L (\rho^L e^L)^L + \varphi S^G (\rho^G e^G)^G + (1-\varphi)\rho^S (e^S)^S] = \\ &= -\frac{\partial}{\partial x_i}[\varphi S^L (\rho^L e^L v_i^L)^L + \varphi S^G (\rho^G e^G v_i^G)^G] - \\ &- \frac{\partial}{\partial x_i}[\varphi S^L (q_i^L)^L + \varphi S^G (q_i^G)^G + (1-\varphi)(q_i^S)^S] - \\ &- \varphi S^L (p^L)^L \frac{\partial (v_i^L)^L}{\partial x_i} - \varphi S^G (p^G)^G \frac{\partial (v_i^G)^G}{\partial x_i} - \\ &- S^L (p^L)^L \frac{1}{R}\int_{\Gamma^{LG}} v_i^L n_i\, d\Gamma + S^G (p^G)^G \frac{1}{R}\int_{\Gamma^{LG}} v_i^G n_i\, d\Gamma\end{aligned} \tag{A16}$$

We now introduce another assumption that thermodynamic relationships between average (macroscopic) quantities remain exactly the same as those between the equivalent point (microscopic) quantities. This assumption is implicit in all macroscopic equations that we have encountered in the literature. Its implication is that $\overset{\circ}{p}$ and $\overset{\circ}{e}$ are uncorrelated and one can thus replaces $(\rho^L e^L)^L$ by $(\rho^L)^L (e^L)^L$ and $(\rho^G e^G)^G$ by $(\rho^G)^G (e^G)^G$. Since mass dispersion is not considered in the present analysis, $\overset{\circ}{p}$ and $\overset{\circ}{v}_i$ are also uncorrelated and we can therefore write

$$\begin{aligned}\varphi S^L (\rho^L e^L v_i^L)^L &= \varphi S^L [(\rho^L)^L (e^L)^L (v_i^L)^L + (\rho^L \overset{\circ}{e}{}^L \overset{\circ}{v}{}_i^L)^L] = \\ &= (\rho^L)^L (e^L)^L (v_i^L) + \varphi S^L (\rho^L \overset{\circ}{e}{}^L \overset{\circ}{v}{}_i^L)^L\end{aligned} \tag{A17}$$

where the second term represents mechanical dispersion of energy. Following the current [illegible] dispersion [illegible] mathematically equivalent to a diffusion process, so that one can write

$$(A18) \qquad (\rho^L \epsilon^L \delta v_i)^L = -D_{ij}^L \frac{\partial (T^L)^L}{\partial x_j}$$

where $D_{ij}^L$ is known as the mechanical (or convective) dispersion tensor. The conductive flux, $q_i^L$, is expressed by Fourier's law using a scalar thermal conductivity,

$$(A19) \qquad q_i^L = -\kappa^L \frac{\partial T^L}{\partial x_i}$$

the average of which is given by (A9) as

$$(A20) \qquad (q_i^L) = -\kappa^L \frac{\partial (T^L)}{\partial x_i} - \frac{\kappa^L}{R} \int_{\Gamma^{LG}, \Gamma^{LS}} T^L n_i \, d\Gamma$$

In order to eliminate the surface integral from (A20) we assume that the orientation vector $n_i$ is symmetrically distributed about a zero average value (this is true if the orientations of $\Gamma^{LG}$ and $\Gamma^{LS}$ are random). Then, since temperature is independent of interface orientation (i.e., random temperatures may exist at various points along $\Gamma$ having a given orientation) $T^L$ and $n_i$ are uncorrelated and the surface integral in (A20) can be neglected. In a similar manner, it may appear reasonable to assume that $v_i^L n_i$ is symmetrically distributed about a zero average value along $\Gamma^{LG}$ so that the first surface integral in (A16) vanishes. Similar considerations hold for the gas phase. If we further assume that $\varphi$, $S^L$, and $S^G$ remain practically constant for any averaging volume whose centroid is inside R, then (A16) can finally be reduced to

$$(A21) \qquad \frac{\partial}{\partial t} [\varphi S^L (\rho^L)^L (\epsilon^L)^L + \varphi S^G (\rho^G)^G (\epsilon^G)^G + (1-\varphi) \rho^S (\epsilon^S)^S] =$$
$$= -\frac{\partial}{\partial x_i} ((\rho^L)^L (\epsilon^L)^L (v_i^L) + (\rho^G)^G (\epsilon^G)^G (v_i^G)) +$$
$$+ \frac{\partial}{\partial x_i} \left[ \varphi S^L \kappa_{ij}^L \frac{\partial (T^L)^L}{\partial x_j} + \varphi S^G \kappa_{ij}^G \frac{\partial (T^G)^G}{\partial x_j} + (1-\varphi) \kappa^S \frac{\partial (T^S)^S}{\partial x_i} \right] -$$
$$- (\rho^L)^L \frac{\partial (v_i^L)}{\partial x_i} - (\rho^G)^G \frac{\partial (v_i^G)}{\partial x_i}$$

where $\kappa_{ij} = \kappa \delta_{ij} + D_{ij}$ is the combined conductive and mechanical dispersion tensor.



In the literature it is customary to assume that all phases are in thermal equilibrium and that capillary pressure differences between fluid phases are negligible. In this case (A21) reduces to

$$(A22) \qquad \frac{\partial}{\partial t} [\varphi S^L (\rho^L)^L (\epsilon^L)^L + \varphi S^G (\rho^G)^G (\epsilon^G)^G + (1-\varphi) \rho^S (\epsilon^S)^S] =$$
$$= -\frac{\partial}{\partial x_i} ((\rho^L)^L (\epsilon^L)^L (v_i^L) + (\rho^G)^G (\epsilon^G)^G (v_i^G)) +$$
$$+ \frac{\partial}{\partial x_i} \left( \kappa_{ij}^{eff} \frac{\partial (T)^*}{\partial x_j} \right) - (p)^* \frac{\partial}{\partial x_i} ((v_i^L) + (v_i^G))$$

where

$$(A23) \qquad \kappa_{ij}^{eff} = \varphi S^L \kappa_{ij}^L + \varphi S^G \kappa_{ij}^G + (1-\varphi) \kappa^S \delta_{ij}$$

This shows that the assumption of thermal equilibrium implies viewing the solid, liquid, and gas as three anisotropic conductors arranged parallel to the direction of heat flow.

Recalling our assumption that thermodynamic relationships between average fluid properties are the same as between the equivalent point properties, we can define the average (macroscopic) enthalpy of the liquid as

$$(A24) \qquad (h^L)^L = (\epsilon^L)^L + \frac{(p^L)^L}{(\rho^L)^L}$$

Similar definitions will hold for the gas and the solid. If we now replace each $(\epsilon)$ in (A22) by $(h) - (p)/(\rho)$, we obtain a macroscopic energy equation in terms of enthalpy.

$$(A25) \qquad \frac{\partial}{\partial t} [\varphi S^L (\rho^L)^L (h^L)^L + \varphi S^G (\rho^G)^G (h^G)^G + (1-\varphi) \rho^S (h^S)^S] =$$
$$= -\frac{\partial}{\partial x_i} ((\rho^L)^L (h^L)^L (v_i^L) + (\rho^G)^G (h^G)^G (v_i^G)) +$$
$$+ \frac{\partial}{\partial x_i} \left( \kappa_{ij}^{eff} \frac{\partial (T)^*}{\partial x_j} \right) + \frac{\partial (\varphi (p)^*)}{\partial t} + ((v_i^L) + (v_i^G)) \frac{\partial (p)^*}{\partial x_i}$$

*Temperature Equation for a Single Phase.*

In the particular case where the pores are completely saturated by a single fluid phase (say liquid), one can use the equation of mass continuity to rewrite (A21) in the form

$$(A26) \qquad \varphi (\rho^L)^* \frac{\partial (\epsilon^L)^*}{\partial t} + (1-\varphi) \rho^S \frac{\partial (\epsilon^S)^S}{\partial t} = -(\rho^L)^* (v_i^L) \frac{\partial (\epsilon^L)^*}{\partial x_i} +$$
$$+ \frac{\partial}{\partial x_i} \left[ \varphi \kappa_{ij}^L \frac{\partial (T^L)^*}{\partial x_j} + (1-\varphi) \kappa^S \frac{\partial (T^S)^S}{\partial x_i} \right] - (\rho^L)^* \frac{\partial (v_i)^L}{\partial x_i}$$

Assuming that the thermodynamic relationships

$$\frac{\partial e}{\partial \cdot} = \left(\frac{\partial e}{\partial v}\right)_T \frac{\partial v}{\partial \cdot} + c_v \frac{\partial T}{\partial \cdot} \tag{A27}$$

$$p = T\left(\frac{\partial p}{\partial T}\right)_v - \left(\frac{\partial e}{\partial v}\right)_T \tag{A28}$$

hold for the average quantities appearing in (A26), this latter equation can be rewritten as

$$\left(\frac{\partial e^L}{\partial v}\right)_T \left[\varphi (\rho^L)^* \frac{\partial ((\rho^L)^*)^{-1}}{\partial t} + (\rho^L)^* (v_i^L) \frac{\partial ((\rho^L)^*)^{-1}}{\partial x_i} - \frac{\partial (\Gamma_i^L)}{\partial x_i}\right] +$$

$$+ \varphi (\rho^L)^* c_v^L \frac{\partial (T^L)^*}{\partial t} + (1-\varphi)\rho^S c_v^S \frac{\partial (T^S)^S}{\partial t} =$$

$$= -(\rho^L)^* (v_i^L) c_v^L \frac{\partial (T^L)^*}{\partial x_i} + \frac{\partial}{\partial x_i}\left[\varphi \kappa_{ij}^L \frac{\partial (T^L)^*}{\partial x_j} + (1-\varphi)\kappa^S \frac{\partial (T^S)^S}{\partial x_i}\right] -$$

$$- (T^L)^* \left(\frac{\partial p}{\partial T}\right)_v \frac{\partial (v_i^L)}{\partial x_i} \tag{A29}$$

The first term in brackets can be reformulated as

$$-\frac{1}{(\rho^L)^*}\left[\varphi \frac{\partial (\rho^L)^*}{\partial t} + \frac{\partial}{\partial x_i}((\rho^L)^* (v_i^L))\right]$$

which vanishes by virtue of mass continuity. Thus, the energy equation for the liquid phase can be expressed entirely in terms of temperature,

$$\varphi (\rho^L)^* c_v^L \frac{\partial (T^L)^*}{\partial t} + (1-\varphi)\rho^S c_v^S \frac{\partial (T^S)^S}{\partial t} = -(\rho^L)^* (v_i^L) c_v^L \frac{\partial (T^L)^*}{\partial x_i} +$$

$$+ \frac{\partial}{\partial x_i}\left[\varphi \kappa_{ij}^L \frac{\partial (T^L)^*}{\partial x_j} + (1-\varphi)\kappa^S \frac{\partial (T^S)^S}{\partial x_i}\right] - (T^L)^* \left(\frac{\partial p}{\partial T}\right)_v \frac{\partial (v_i^L)}{\partial x_i} \tag{A30}$$

If the solid and the liquid are assumed to be in thermal equilibrium, (A30) reduces to

$$[\varphi (\rho^L)^* c_v^L + (1-\varphi)\rho^S c_v^S] \frac{\partial (T)^*}{\partial t} = -(\rho^L)^* (v_i^L) c_v^L \frac{\partial (T)^*}{\partial x_i} +$$

$$+ \frac{\partial}{\partial x_i}\left(\kappa_{ij}^{eff} \frac{\partial (T)^*}{\partial x_j}\right) - (T)^* \left(\frac{\partial p}{\partial T}\right)_v \frac{\partial (v_i^L)}{\partial x_i} \tag{A31}$$

where $\kappa_{ij}^{eff} = \varphi \kappa_{ij}^L + (1-\varphi)\kappa^S \delta_{ij}$.

Equations A30 and A31 are also applicable when the pores are completely saturated by the gas phase, provided that the superscript L is replaced by G.

## References


Bland J., Sosserton W. H. and Gonan E. (1973) – *Predicting thermal conductivities of formations from other known properties*, «Soc. Petrol. Engr. Jour.», 13, 5, 267-273.

Bear J. (1972) – *Dynamics of Fluids in Porous Media*, Am. Elsevier, New York.

Beck J. L. (1972) – *Convection in a box of porous material saturated with fluid*, «Phys. of Fluids», 15, 8, 1377-1383.

Bielhartz H. L. Jr. (1971) – *Fluid Production from Geothermal Steam Reservoirs*, M. S. thesis, Stanford Univ., Calif.

Bodvarsson G. (1961) – *Physical characteristics of natural heat resources in Iceland*, paper G. 6. U. N. Conf. on New Sources of Energy, Rome, August 21-31.

Brace W. F., Walsh J. B. and Frangos W. T. (1968) – *Permeability of granite under high pressure*, «Jour. Geophys. Res.», 73, 6, 2225-2236.

Brigham W. E. and Morrow W. B. (1974) – *P/Z behavior for geothermal steam reservoirs*, paper SPE 4899, 44th Annual Calif. Regional Meeting SPE-AIME, San Francisco, April 4-5.

Brownell D. H. Jr., Garg S. K. and Pritchett J. W. (1975) – *Computer simulation of geothermal reservoirs*, paper SPE 5381, 45th Annual Calif. Regional Meeting SPE-AIME, Ventura, Calif., April 2-4.

Cady G. V. (1969) – *Model Studies of Geothermal Fluid Production*, Ph. D. dissertation, Stanford Univ., Calif.

Calhoun J. C., Lewis M. Jr. and Newman R. C. (1949) – *Experiments on the capillary properties of porous solids*, «Trans. AIME», 186, 189-196.

Caltagirone J. P., Cloupeau M. and Combarnous M. (1971) – *Convection naturelle fluctuante dans une couche poreuse horizontale*, «Comptes Rendus, Acad. Sci.», Paris, B 273, 833-836.

Casse F. J. (1974) – *The Effect of Temperature and Confining Pressure on Fluid Flow Properties of Consolidated Rocks*, Stanford Geothermal Program, Rep. SGP-TR 3, Stanford Univ., Calif.

Cheng P. and Lau K. H. (1974) – *Steady state free convention in an unconfined geothermal reservoir*, «Jour. Geophys. Res.», 79, 29, 4425-4431.

Coats K. H., George W. D., Chu C. and Marcum B. E. (1974) – *Three-dimensional simulation of steamflooding*, «Soc. Petrol. Engr. Jour.», 15, 6, 573-592.

Combarnous M. A. and Bories S. A. (1973) – *Thermal Convection in Saturated Porous Media*, Report prepared for Advances in Hydroscience, Institut Français du Petrole and Institute de Mecanique des Fluides de Toulouse.

Combarnous M. and Bories S. (1974) – *Modelisation de la convection naturelle au sein d'une couche poreuse horizontale a l'aide d'un coefficient de transfert solide-fluide*, «Int. Jour. Heat Mass Transfer», 17, 505-515.

Craig H. (1966) – *Superheated steam and mineral water interactions in geothermal areas*, «Trans Am. Geophys. Union», 47, 204-205 (abstract).

Currie I. G. (1974) – *Fundamental Mechanics of Fluids*, McGraw-Hill, New York.

Davidson L. B. (1969) – *The effect of temperature on the permeability ratio of different fluid pairs in two-phase systems*, «Jour. Petrol. Tech.», Aug. 1969, 1037-1046.

Donaldson I. G. (1962) – *Temperature gradients in the upper layers of the earth's crust due to convective water flows*, «Jour. Geophys. Res.», 67, 9, 3449-3459.

Donaldson I. G. (1968 a) – *The flow of steam water mixtures through permeable beds: A simple simulation of a natural undisturbed hydrothermal region*, «New Zealand Jour. Sci.», 11, 3-23.

Donaldson I. G. (1968 b) – *A possible model for hydrothermal systems and methods of studying such a model*, paper 2580, Third Australian Conf. on Hydraulics and Fluid Mechanics, Nov. 25-29.

DONALDSON I. G. (1970) – *The simulation of geothermal systems with a simple convective mod[illegible]*, « Geothe[illegible] », Special Issue 2, 2, part 1, 649-654.

EDMONSON J. [illegible] (1965) – *Effect of temperature on waterflooding*, « Jour. Canadian Petrol. Tech. », 4, 236-242.

EINARSSON T. (1942) – *Ueber das Wesen der heissen Quellen Islands*, « Rit. Visind. Isl. », 26, 91.

ELDER J. W. (1965) – *Physical processes in geothermal areas*, in « Terrestrial Heat Flow », W. H. K. Lee, ed., « Am. Geophys. Union Mon. », Ser. 8, 211-239.

ELDER J. W. (1966) – *Heat and mass transfer in the earth: Hydrothermal systems*, « New Zealand D. S. I. R. Bull. », 169, 115.

ELDER J. W. (1967) – *Transient convection in a porous medium*, « Jour. Fluid Mech. », 27, part 3, 609-623.

FACCA G. and TONANI F. (1964) – *Theory and technology of a geothermal field*, « Bull. Volcanol. », 27, part 1, 143-198.

FAUST C. F. and MERCER J. W. (1975) – *Mathematical modeling of geothermal systems*, paper to be presented at Second United Nations Symposium on the Development and Use of Geothermal Resources, San Francisco, May 20-29.

FERNANDEZ R. T. (1972) – *Natural Convection from Cylinders Buried in Porous Media*, Ph. D. dissertation, Univ. of Calif., Berkeley.

GOGUEL J. (1953) – *Le regime thermique de l'eau souterraine*, « Annales des Mines », 10, 1-32.

GRAY W. G. (1975) – *A derivation of the equations for multi-phase transport*, paper submitted to « Chem. Engr. Sci. ».

GREENBERG D. B., CRESAP R. S. and MALONE T. A. (1968) – *Intrinsic permeability of hydrological porous mediums: Variation with temperature*, « Water Resour. Res. », 4, 4, 791-800.

GRINGARTEN A. C. and SAUTY J. P. (1975) – *A theoretical study of heat extraction from aquifers with uniform regional flow*, paper submitted to « Jour. Geophys. Res. ».

GUPTA V. P. and JOSEPH D. D. (1973) – *Bounds for heat transport in a porous layers*, « Jour. Fluid Mech. », 57, part 3, 491-514.

HAAS J. L. Jr. (1970) – *An equation for the density of vapor-saturated* NaCl—$H_2O$ *solutions from 75° to 325 °C*, « Am. Jour. Sci. », 269, 489-493.

HAAS J. L. Jr. (1971) – *The effect of salinity on the maximum thermal gradient of a hydrothermal system at hydrostatic pressure*, « Econ. Geol. », 66, 940-946.

HELGESON H. C. (1968) – *Geologic and thermodynamic characteristics of the Salton Sea geothermal system*, « Am. Jour. Sci. », 266, 129-166.

HOLST P. H. (1970) – *A Theoretical and Experimental Investigation of Natural Convection in Porous Media*, Ph. D. dissertation, Univ. of Calgary, Alberta, Canada.

HOLST P. H. and AZIZ K. (1972 a) – *A theoretical and experimental study of natural convection in a confined porous medium*, « Canadian Jour. Chem. Engr. », 50, 232-241.

HOLST P. H. and AZIZ K. (1972 b) – *Transient three-dimensional natural convection in confined porous media*, « Jour. Heat and Mass Transfer. », 15, 73-90.

HORNE R. N. and O'SULLIVAN M. J. (1974) – *Oscillatory convection in a porous medium heated from below*, « Jour. Fluid Mech. », 66, part 2, 339-352.

HORTON C. W. and ROGERS F. T. Jr. (1945) – *Convection currents in a porous medium*, « Jour. Appl. Phys. », 16, 367-370.

JAMES R. (1968) – *Wairakei and Larderello geothermal power systems compared*, « New Zealand Jour. Sci. and Tech. », 11, 706-719.

JEFFREYS H. (1930) – *The instability of a compressible fluid heated below*, « Proc. Cambridge Phil. Soc. », 26, 170-172.

KANEKO T., MOHTADI M. F. and AZIZ K. (1974) – *An experimental study of natural convection in inclined porous media*, « Int. Jour. Heat Mass Transfer », 17, 485-496.

KAPPELMEYER O. and HAENEL R. (1974) – *Geothermics with Special Reference to Application*, Geopublication Associates, Berlin, Tables 6.3-6.6, 208-218.



KARRA P. S. (1968) – *A numerical Study of Natural Convection in Porous Media*, M. S. thesis, Univ. of Calgary, Alberta, Canada.

KNUTSON C. F. and BOHOR B. F. (1963) – *Reservoir rock behavior under moderate confining pressure*, in « Symposium on Rock Mechanics, Univ. Minnesota », MacMillan, New York, 627-659.

LAPWOOD E. R. (1948) – *Convection of a fluid in a porous medium*, « Proc. Cambridge Phil. Soc. », 44, 508-521.

LASSETER T. J. and WITHERSPOON P. A. (1974) – *Underground Storage of Liquified Natural Gas in Cavities Created by Nuclear Explosives*, Geotechnical Engineering Pub. No. 74-1, Univ. Calif., Berkeley.

LASSETER T. J., WITHERSPOON P. A. and LIPPMANN M. J. (1975) – *Multiphase multidimensional simulation of geothermal reservoirs*, paper submitted to Second United Nations Symposium on the Development and Use of Geothermal Resources, San Francisco, May 20-29.

LEE P. C. Y., GRAY W. G. and PINDER G. F. (1975) – *Thermoenergy transport in porous media*, paper in preparation.

LIKKE S. and BROMLEY L. A. (1973) – *Heat capacities of aqueous* NaCl, KCl, $MgCl_2$, $MgSO_4$, and $Na_2SO_4$ *solutions between 80° and 200 °C*, « Jour. Chem. Engr. Data », 18, 189-195.

LO H. Y. and MUNGAN N. (1973) – *Effect of temperature on water-oil relative permeabilities in oil-wet and water-wet systems*, paper SPE 4505, 48th Annual Meeting SPE-AIME, Las Vegas, Nev., Sept. 30-Oct. 3.

MARINELLI G. (1969) – *Some geological data on the geothermal areas of Tuscany*, « Bull. Volcanol. », 33, 1, 319-334.

MARTIN J. C. (1973) – *Analysis of internal steam drive in geothermal reservoirs*, paper SPE 5382, 45th Annual Calif. Regional Meeting SPE-AIME, Ventura, Calif., April 2-4.

MASUOKA T. (1972) – *Heat transfer by free convection in a porous layer heated from below*, « Heat Transfer-Japan Res. », 1, 39-45.

MATTHEWS C. S. and RUSSELL D. G. (1967) – *Pressure Buildup and Flow Tests in Wells*, « Soc. Petr. Engr. AIME Mon. », 1.

MCNABB A. (1965) – *On convection in a porous medium* « Proc. Australasian Conf. on Hydraulics and Fluid Mechanics », 2, C 161-C 171.

MERCER J. W. Jr. (1973) – *Finite Element Approach to the Modeling of Hydrothermal Systems*, Ph. D. dissertation, Univ. of Illinois, Urbana-Champaign.

MERCER J. W. Jr., FAUST C. F. and PINDER G. F. (1974) – *Geothermal reservoir simulation*, Proc. NSF Conference on Research for the Development of Geothermal Energy Resources, Pasadena, Calif., Sept. 23-25, 256-267.

MERCER J. W. and PINDER G. F. (1974) – *Finite element analysis of hydrothermal systems*, in « Finite Elements in Fluid Flow », J. T. Oden, *et al.*, eds., Univ. Alabama Huntsville Press, 401-414.

MERCER J. W., PINDER G. F. and DONALDSON I. G. (1975) – *A Galerkin-finite element analysis of the hydrothermal system at Wairakei, New Zealand*, « Jour Geophys. Res. », in press.

NARASIMHAN T. N. and WITHERSPOON P. A. (1975) – *An integrated finite difference method for analyzing fluid flow in porous media*, paper submitted to « Water Resour. Res. »

NEVENS T. O. and POOL M. J. (1964) – *Determination of Thermodynamic Properties of Brines*, Denver Research Inst., Contract Research Report 2151.

NIELD D. A. (1968) – *Onset of thermohaline convection in a porous medium*, « Water Resour. Res. », 4, 3, 553-560.

NIELD D. A. (1974) – *Comments on, Effect of solute dispersion on thermal convection in a porous medium layer' by H. Rubin*, « Water Resour. Res. », 10, 4, 889.

PALM E., WEBER J. E. and KVERNVOLD O. (1972) – *On steady convection in a porous medium*, « Jour. Fluid Mech. », 54, part 1, 153-161.

PLATZMAN G. W. (1965) – *The spectral dynamics of laminar convection*, « Jour. Fluid Mech. », 23, part 3, 481-510.

POSTON S. W[illiam] ALI S. C., HOSSAIN A. K. M. S., MONTGOMERY E. F. III and RAMEY H. J. Jr. (1970) – *The effect of temperature on irreducible water saturation and relative permeability of unconsolidated sands*, « Soc. Petrol. Eng. Jour. », *10*, 2, 171-180.

RAMEY H. J. Jr., BRIGHAM W. E., CHEN H. K., ATKINSON P. G. and ARIHARA N. (1974) – *Thermodynamic and hydrodynamic properties of hydrothermal systems*, in « The Utilization of Volcano Energy », J. L. Colp and A. S. Furumoto, eds., Proc. of Conference, Hilo, Hawaii, Feb. 4-8.

RAMEY H. J. Jr., KRUGER P. and RAGHAVAN R. (1973) – *Explosive stimulation of hydrothermal reservoirs* in « Geothermal Energy », P. Kruger and C. Otte, eds., Stanford Univ. Press, 231-249.

RAYLEIGH LORD (1916) – *On convection currents in a horizontal layer of fluid when the higher temperature is on the underside*, « Phil. Mag. », Ser. 6, *32*, 529-546.

RUBIN H. (1973) – *Effect of solute dispersion on thermal convection in a porous medium layer*, « Water Resour. Res. », 9, 4, 968-974.

RUBIN H. (1975 a) – *Effect of solute dispersion on thermal convection in a porous medium layer*, 2, « Water Resour. Res. », *11*, 1, 154-158.

RUBIN H. (1975 b) – *On then analysis of cellular convection in porous media*, Unpublished manuscript.

RUBIN H. (1975 c) – *Effect of hydrodynamic dispersion on thermohaline convection in a porous medium*, Unpublished manuscript.

SANYAL S. K., MARSDEN S. S. and RAMEY H. J. Jr. (1973) – *The effect of temperature on electrical resistivity of porous media*, « Soc. Prof. Well Logging Assoc., 13th Annual Logging Symposium, May.

SESTINI G. (1970) – *Superheating of geothermal steam*, « Geothermics », Special issue 2, 2, pt. 1 622-648.

SLATTERY J. C. (1972) – *Momentum, Energy and Mass Transfer in Continua*, McGraw-Hill New York.

SOMERTON W. H., KEESE J. A. and CHU S. L. (1974) – *Thermal behavior of unconsolidated oil sands*, « Soc. Petrol. Engr. Jour. », *14*, 5, 513-521.

SOREY M. L. (1975) – *Numerical Modeling of Liquid Geothermal Systems*, Ph. D. dissertation' Univ. of Calif., Berkeley (in preparation).

SPILLETTE A. G. and NIELSEN R. L. (1968) – *Two-dimentional method for predicting hot waterflood recovery behavior*, « Jour. Petrol. Tech. », *20*, 6, 627-638.

STRAUS J. M. (1974) – *Large amplitude convection in porous media*, « Jour. Fluid Mech. », *64*, part 1, 51-63.

SUN Z. S., TIEN C. and YEN Y. C. (1972) – *Onset of convection in a porous media, containing liquid with a density maximum*, paper NC2-11, Fourth Interm. Heat Transfer Conf., Paris-Versailles, *4*.

TORGNYI R. M. (1974) – *Two-Phase, Two Dimensional Simulation of a Geothermal Reservoir and the Wellbore System*, Ph. D. dissertation, Pennsylvania State Univ., University Park.

VAIROGS J., HEARN C. L., DARLING D. W. and RHOADES V. W. (1971) – *Effect of rock stress on gas production from low-permeability reservoirs*, « Jour. Petrol. Tech. », Sept., 1161-1167.

WANKAT P. C. and SCHOWALTER W. R. (1970) – *Stability of combined heat and mass transfer in a porous medium*, « Phys. of Fluids », *13*, 9, 2418-2420.

WEBER J. E. (1975 a) – *Thermal convection in a tilted porous layer*, « Int. Jour. Heat Mass Transfer », *18*, 474-475.

WEBER J. E. (1975 b) – *The boundary-layer regime for convection in a vertical porous layer*, « Int. Jour. Heat Mass Transfer », *18*, 569-573.

WEINBRANDT R. M., RAMEY H. J. Jr. and CASSE F. J. (1972) – *The effect of temperature on relative and absolute permeability of sandstones*, 47th Annual Meeting SPE-AIME, San Antonio, Texas, Oct.



WEINSTEIN H. G., WHEELER J. A. and WOODS E. G. (1974) – *Numerical [illegible] for steam stimulation*, paper SPE 4759, SPE-AIME Improved Oil Recov[illegible] Symposium, Tulsa, Oklahoma, April 22-24.

WESTBROOK D. R. (1969) – *Stability of convective flow in a porous medium*, « Phys. of Fluids », *12*, 8, 1547-1551.

WHITAKER S. (1968) – *Introduction to Fluid Mechanics*, Prentice-Hall, Englewood Cliffs, N. J.

WHITAKER S. (1969) – *Advances in theory of fluid motion in porous media*, « Ind. Engr. Chem. », *61*, 12, 14-28.

WHITE D. E. (1957) – *Thermal waters of volcanic origin*, « Bull. Geol. Soc. Am. », 68, 1637-1658.

WHITE D. E. (1961) – *Preliminary evaluation of geothermal areas*, paper G. 2, U. N. Conf. on New Sources of Energy, Rome, August 21-31.

WHITE D. E. (1973) – *Characteristics of geothermal resources*, in « Geothermal Energy », P. Kruger and C. Otte, eds., Stanford Univ. Press, 69-94.

WHITE D. E., MUFFLER L. J. P. and TRUESDELL A. H. (1971) – *Vapor-dominated hydrothermal systems compared with hot-water systems*, « Econ. Geol. », 66, 75-97.

WHITING R. L. and RAMEY H. J. Jr. (1969) – *Application of material and energy balances to geothermal steam production*, « Jour. Petrol. Tech. », *21*, 7, 893-900.

WOODING R. A. (1963) – *Convection in a saturated porous medium at large Rayleigh number or Peclet number*, « Jour. Fluid Mech. », *15*, part 4, 527-544.

YEN Y. C. (1974) – *Effects of density inversion on free convective heat transfer in porous layer heated from below*, « Int. Jour. Heat Mass Transfer », *17*, 1349-1356.

ZOBACK M. D. and BYERLEE J. D. (1975) – *Permeability and effective stress*, « AAPG Bull. », 59, 1, 154-158.

# An Integrated Finite Difference Method for Analyzing Fluid Flow in Porous Media

T. N. NARASIMHAN

*Department of Civil Engineering, University of California, Berkeley, California 94720*

P. A. WITHERSPOON

*Lawrence Berkeley Laboratory, University of California, Berkeley, California 94720*

The theoretical basis for the integrated finite difference method (IFDM) is presented to describe a powerful numerical technique for solving problems of groundwater flow in porous media. The method combines the advantages of an integral formulation with the simplicity of finite difference gradients and is very convenient for handling multidimensional heterogeneous systems composed of isotropic materials. Three illustrative problems are solved to demonstrate that two- and three-dimensional problems are handled with equal ease. Comparison of IFDM with the well-known finite element method (FEM) indicates that both are conceptually similar and differ mainly in the procedure adopted for measuring spatial gradients. The IFDM includes a simple criterion for local stability and an efficient explicit-implicit iterative scheme for marching in the time domain. If such a scheme can be incorporated in a new version of FEM, it should be possible to develop an improved numerical technique that combines the inherent advantages of both methods.

## INTRODUCTION

Numerical analysis of fluid flow through porous media in problems with complex geometry is greatly facilitated by the use of integral formulations. Perhaps the most widely used integral method is the finite element method (FEM), which can be based on variational principles or the Galerkin approach.

In this paper we will describe another integral formulation which has been successfully used to solve heat transfer problems in heterogeneous isotropic multidimensional flow regions. For reasons that will become clear later, we shall call this method the 'integrated finite difference method' (IFDM). Although the method has been used in studying groundwater systems [*Todd*, 1959; *Tyson and Weber*, 1964; *Cooley*, 1971], it does not appear to have been widely employed in the field of hydrogeology. It is our opinion, however, that the IFDM can be a very powerful tool in analyzing heterogeneous groundwater systems with complex geometries. Furthermore, in comparing the conceptual bases of IFDM and FEM we find that they have much in common.

The purpose of this paper is first to develop the IFDM equations and demonstrate the power of the method with three different problems. We will then examine the conceptual bases of both IFDM and FEM and attempt to identify those features which give each of these techniques unique advantages in handling specific classes of problems. Finally, we will consider the possibility of developing a new technique which could combine some of the unique advantages of each method.

## INTEGRATED FINITE DIFFERENCE METHOD

*MacNeal* [1953] is apparently the first worker to use the IFDM approach, and he classified it as an 'asymmetric finite difference network.' He used this approach in solving second-order boundary value problems. Subsequently, the method has been used successfully for solving heat transfer problems, and a good description of the approach and related aspects can be found in *Dusinberre* [1961]. *Edwards* [1972] used the IFDM in developing a powerful computer code called Trump for calculating transient and steady state temperature distributions in multidimensional systems, and the following discussion will be based in large measure on the Trump program. Although Trump can handle conductive, convective, and radiative heat transfer, we will restrict our attention to the heat conduction part of the program, since conductive heat transfer is conceptually similar to fluid flow in porous media.

Consider the partial differential equation for groundwater flow

$$\text{div } K \text{ grad } \phi + g = c\, \partial\phi/\partial t \qquad (1)$$

For the sake of simplicity, we shall assume $K$ and $c$ in (1) to be constant and independent of $\phi$, so that (1) is a linear equation.

We can spatially integrate (1) over a conveniently small finite subregion $V$ of the flow region and write [*Encyclopedia of Science and Technology*, 1960]

$$\int_V (\text{div } K \text{ grad } \phi + g)\, dV = \frac{\partial}{\partial t} \int_V c\phi\, dV \qquad (2)$$

We now use the divergence theorem to convert the first term on the left-hand side to a surface integral, and on the right-hand side we assume that $c$ and $\phi$ are average values over $V$. Then

$$\int_S K \text{ grad } \phi \cdot \mathbf{n}\, dS + gV = cV \frac{\partial \phi}{\partial t} \qquad (3)$$

The central concept of IFDM is to discretize the total flow domain into conveniently small subdomains or 'elements' and evaluate the mass balance in each element as indicated in (3). Physically, the surface integral on the left-hand side of (3) is the summation of fluxes over the surface $S$ and thus measures the rate at which mass is accumulating in the element, as governed by initial and boundary conditions. The right-hand side converts the rate of accumulation of fluid into the corresponding average time rate of change in potential over the element.

To illustrate the IFDM, let the shaded region in Figure 1 be an element whose average properties are associated with a representative nodal point $m = 6$, which may be located anywhere within or on the boundaries of the element. For maximum accuracy, interfaces between elements should be perpendicular to the line joining the two nodal points and intersect that line at an appropriate mean position (arithmetic mean of nondivergent coordinates, log mean of cylindrical radii, or geometric mean of spherical radii). This ideal situation may be difficult to achieve in practice but should be approximated as closely as possible [*Edwards*, 1972]. In Figure 1, element $m$ is connected to adjoining elements $n = 1$–5. Under these conditions the finite difference approximation for (3) can be written

$$g_m V_m + \sum_n K_{m,n} \frac{\phi_n - \phi_m}{D_{m,n}} A_{m,n} = c_m V_m \frac{\Delta\phi_m}{\Delta t} \qquad (4)$$

where $K_{m,n}$ is the harmonic mean permeability when elements $m$ and $n$ are composed of different materials.

For appropriately small values of $\Delta t$, (4) can be written in a stable explicit form as

$$\frac{\Delta t}{c_m V_m} [g_m V_m + \sum_n U_{m,n}(\phi_n^0 - \phi_m^0)] = \Delta\phi_m \qquad (5)$$

Here, $U_{m,n} = (K_{m,n} A_{m,n})/D_{m,n}$ is the 'conductance' of the interface separating elements $m$ and $n$ and represents the rate of fluid transfer per unit difference in potential between nodal points $m$ and $n$. The terms $\phi_m^0$ and $\phi_n^0$ represent the initial values of potentials at the beginning of the interval $\Delta t$. Equation (5) can be directly used to solve for $\Delta\phi_m$ if the geometric parameters $A_{m,n}$, $D_{m,n}$, and $V_m$ are provided as input data, in addition to the material properties $K$ and $c$.

If it is desired to use large values of $\Delta t$, then (4) can be expressed implicitly as

$$\frac{\Delta t}{c_m V_m} [g_m V_m + \sum_n U_{m,n}[(\phi_n^0 + \lambda\Delta\phi_n) - (\phi_m^0 + \lambda\Delta\phi_m)]] = \Delta\phi_m \qquad (6)$$

where $0 \leq \lambda \leq 1$. When $\lambda = 0$, (6) reduces to the forward-differencing scheme (5). When $\lambda = 1$, (6) becomes a fully implicit backward-differencing scheme, while $\lambda = \frac{1}{2}$ yields the well-known central-differencing, or Crank-Nicholson, procedure. For unconditional stability, $\lambda \geq \frac{1}{2}$. Both prescribed potential and prescribed flux boundaries or even mixed boundary conditions can be suitably handled as described by *Edwards* [1972] and *Narasimhan* [1975].

It can be shown either from simple reasoning [*Duinberre*, 1961] or on the basis of an analysis of error propagation [*O'Brien et al.*, 1951; *Evans et al.*, 1954; *Narasimhan*, 1975] that for each element $m$, there is a critical time constant $\Delta t_m$ such that (5) is unstable if $\Delta t > \Delta t_m$. The magnitude of this critical time constant is given by

$$\Delta t_m = c_m V_m / \sum_n U_{m,n} \qquad (7)$$

where $n$ now stands for all elements connected to element $m$. Physically, $\Delta t_m$ represents the approximate time required for element $m$ to react significantly to changes in potential in the adjacent elements to which $m$ is connected [*Edwards*, 1972]. Obviously, if $\Delta t > \Delta t_m$ for any element $m$, one would have to use (6) instead of (5) for that particular element with $\frac{1}{2} \leq \lambda \leq 1$.

The implicit calculations inherent in the application of (6) can be carried out either with the help of matrix inversion techniques or with the help of iterative techniques. The Trump computer program [*Edwards*, 1972] employs an iterative technique based on the generalization of a method suggested by *Evans et al.* [1954]. Using this approach and recognizing the fact that the critical time step $\Delta t_m$ is defined for each element, *Edwards* [1972] has successfully incorporated in Trump a technique by which explicit calculations are carried out for those elements where $\Delta t < \Delta t_m$ and implicit calculations for the balance where $\Delta t > \Delta t_m$, with $\frac{1}{2} \leq \lambda \leq 1$. When the IFDM is combined with the explicit-implicit iterative scheme developed in Trump, it provides a very useful tool in analyzing fluid flow problems in heterogeneous systems.

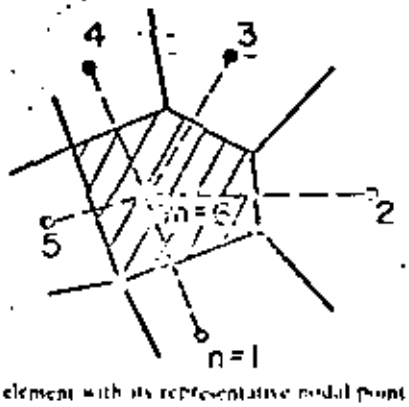


Fig. 1. An element with its representative nodal point in the IFDM network.

## Solutions to Illustrative Problems

To illustrate the utility of the IFDM, we shall consider three problems for which analytical solutions are available. The first of these has been chosen to demonstrate the accuracy that can be expected from IFDM. The second is designed to demonstrate the ability of IFDM to solve three-dimensional problems. The last example serves to illustrate the use of the method in approaching systems with radially symmetric geometry, in which the material distribution can be asymmetric.

*Theis problem.* A classical problem in the field of groundwater hydrology is that of nonsteady radial flow to a well discharging at a constant rate $Q$ and piercing a horizontally infinite homogeneous and isotropic aquifer. The solution to this problem is the well-known *Theis* [1935] equation

$$s = \frac{Q}{4\pi T} \int_{r^2 S/4Tt}^{\infty} \frac{e^{-u}}{u} du \qquad (8)$$

*Pinder and Frind* [1972] have shown how the FEM developed from the Galerkin formulation can be used to simulate the Theis solution. They verified the accuracy of their FEM results in comparison with the analytical solution using linear as well as isoparametric elements. Their FEM mesh consisted of only nine nodal points along any radial line from the well. To check the accuracy of IFDM, we set up a mesh with nine nodal points along a radial line such that the distances from the origin were identical to those of *Pinder and Frind* [1972]. They report their results for the node at $r = 12.7$ feet as shown in Figure 2, but they do not indicate the magnitude of the time steps used in obtaining these results. We solved the same problem, using IFDM and the mixed explicit-implicit scheme of *Edwards* [1972] with time steps that varied from an initial value of $\Delta t = 3.6 \times 10^{-4}$ s to a maximum value of $\Delta t = 50.0$ s in reaching a total time of $10^5$ s. In Figure 2 we give our results at $r = 12.7$ feet. It can be seen that over the time period

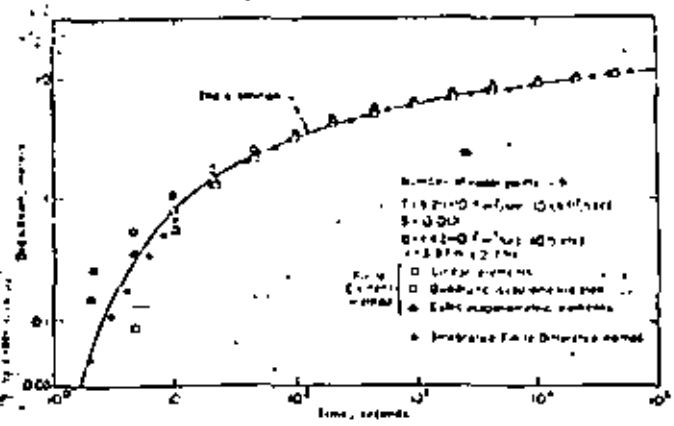

Fig. 2. A comparison of numerical results with the analytical solution for the Theis problem.

studied, the IFDM results compare very favorably with the analytical solution.

*Continuous point source problem.* An advantage of formulating the governing equation in the form of (5) or (6) is that these equations are equally valid in one, two, or three dimensions. Therefore the IFDM can handle one-, two-, or three-dimensional problems with equal ease. To verify the ability of IFDM to handle three-dimensional flow, we applied the method to the problem of a continuous point source in an isotropic medium. The analytical solution is given by *Carslaw and Jaeger* [1959] as

$$\phi(r, t) - \phi_0(r, t_0) = \frac{Q}{4\pi\kappa r} \operatorname{erfc}\left[\frac{r}{(4\kappa t)^{1/2}}\right] \qquad (9)$$

To solve the above problem in three dimensions by using the IFDM, the flow region was visualized as a sphere enclosed in a cube. Thus the spherical elements near the point source gradually lost their curvature in grading outward to cubic-shaped elements at the outer boundary (Figure 3). This was done so that one could accurately simulate spherical symmetry close to the source and at the same time allow for more general conditions of flow near the outer limits. The flow region was everywhere subdivided into three-dimensional elements. From considerations of symmetry (eight octants in a cube and three Cartesian axes) a wedge-shaped portion of the flow region, whose volume is 1/24 of a cube, was chosen for actual modeling, as is illustrated in Figure 3.

The shortest distance from the point source to the outer boundary of the wedge was 400 m. The mesh consisted of 47 three-dimensional elements and 87 interfaces between elements. Owing to the curvilinear nature of the elements, different nodal points were located along different radial lines from the point source. Distances from the source to nodal points varied from 1 m for the closest to 593 m for the farthest, while element volumes ranged from $9.1 \times 10^{-3}$ to $1.09 \times 10^{8}$ m$^3$. The problem was solved with the following arbitrary parameters: $Q = 10^3$ m$^3$/s, $K = 10^{-1}$ m/s, and $c = 10^{-3}$ m$^{-1}$. Impermeable conditions were assumed on all faces of the wedge-shaped flow region.

The results of the computations are shown in Figure 4. Instead of presenting the data in dimensionless form we can demonstrate the overall accuracy in more detail by plotting drawdown as a function of time for various distances (Figure 4*a*) and drawdown as a function of distance for various times (Figure 4*b*) in comparison to the analytical solution. The problem was solved from 0 to $10^8$ s in 683 time cycles by using

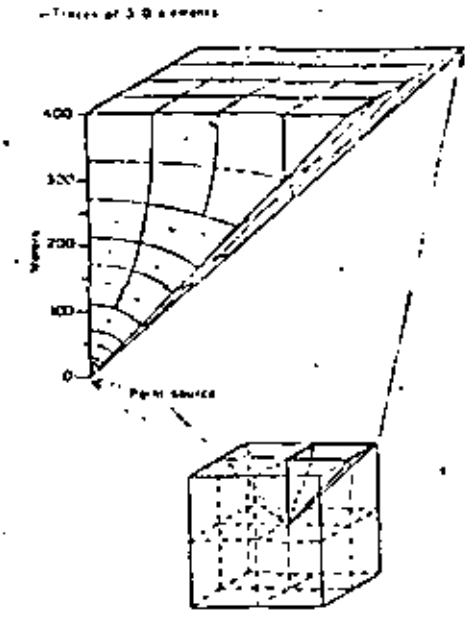


Fig. 3. A three-dimensional IFDM network of elements for the point source problem.

the mixed explicit-implicit scheme. The magnitude of the time steps varied from $1 \times 10^{-1}$ to $8.5 \times 10^{6}$ s. The simulation took 8.5 s of CDC 7600 machine time.

Figures 4*a* and 4*b* show that the computed results deviate from the analytical solution for small values of time and at small radial distances. However, we believe that the overall agreement with the analytical solution is quite good, and we conclude that the IFDM has successfully been used in solving this three-dimensional problem.

***Fracture flow problem.*** The parallel plate formulation for flow in a fracture is widely used by many workers [*Snow*, 1965; *Romm*, 1966; *Louis*, 1969; *Sharp and Maini*, 1972; *Wilson and Witherspoon*, 1974; *Gale et al.*, 1974] and leads to a fracture permeability defined as

$$k = \rho g b^2 / 12\mu \qquad (10)$$

However, when the fracture closes, the surfaces do not neces-

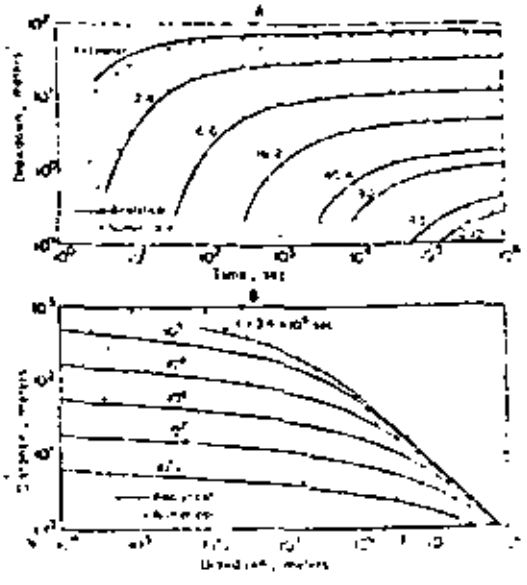

Fig. 4. A comparison of the numerical results with the analytical solution for the point source problem: (*a*) time drawdown and (*b*) distance drawdown.

...y much at every point, and this becomes quite obvious when any natural fracture is examined in detail. This has led some investigators [*Louis*, 1969; *Sharp and Maini*, 1972] to suggest that the exponent in (10) is some value less than 2 for a fracture that is being closed under normal stress.

In other work in this laboratory we are currently investigating this problem using a single horizontal fracture under conditions of radial flow. The fracture is formed by two cylindrical blocks of impermeable rock, 0.152 m in diameter, each having smooth faces. Flow originates at a 0.0254-m-diameter hole in the center that is concentric with the external boundary. If the circular fracture is open and the planar surfaces are parallel, then the steady state flow is given by

$$Q = (2\pi\rho g b^3 \Delta\phi)/[12\mu \ln (r_e/r_i)] \qquad (11)$$

To investigate this problem, we have used the IFDM and set up a flow net of elements as shown in Figure 5. The flow region has been discretized into 264 elements with 456 interfaces, and permeability within each element is given by (10).

As a practical problem of interest in the laboratory work we solved an arbitrary case where $\Delta\phi = 21.09$ m of water (30 psi), $\rho = 1000$ kg/m$^3$, $\mu = 0.001$ kg/m s, and $b = 1.27 \times 10^{-4}$ m. From (11) one can quickly compute

$$Q = \frac{2\pi(1000)(9.8)(1.27 \times 10^{-4})^3(21.09)}{12(0.001) \ln (0.076/0.0127)}$$

$$= 1.237 \times 10^{-4} \text{ m}^3/\text{s}$$

We then solved the same problem, using IFDM and the network shown in Figure 5 and obtained $Q = 1.227 \times 10^{-4}$ m$^3$/s. Pressures should be a linear function of $\ln r$, and a comparison of IFDM results with those from the analytical solution is shown in Figure 6. The agreement is very good.

Of considerably more interest is the case where the fracture partially closes and the areas of contact are impermeable. This kind of heterogeneity can be handled with the IFDM by assuming that certain elements within the network of Figure 5 have zero permeability. The results of a hypothetical problem with a random distribution of impermeable elements are given in Figure 7. Here the pressure head has been normalized in terms of percent of the injection pressure. The pressure profile along line AB of Figure 7 is shown in Figure 6. For the same aperture and flow conditions as were given above, the flow was

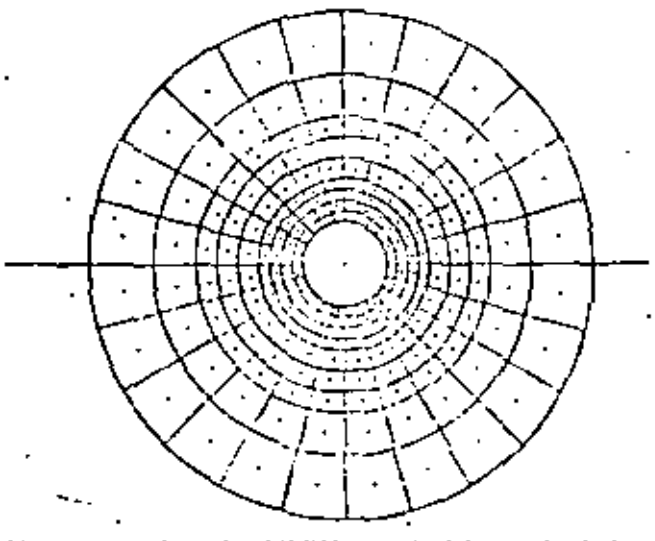

Fig. 5. A two-dimensional IFDM network of elements for the fracture flow problem.

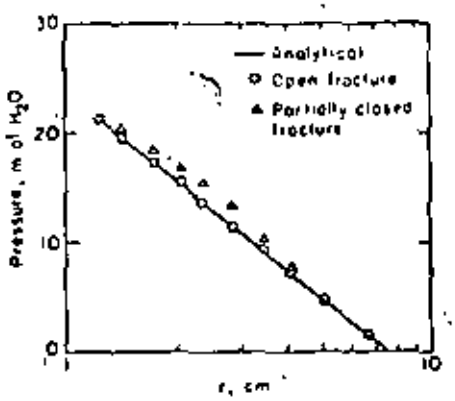


Fig. 6. A comparison of the numerical results with the analytical solution for the fracture flow problem.

found to be $8.032 \times 10^{-5}$ m$^3$/s. In other words, the impermeable contact area that amounts to about 15% of the total fracture surface caused a reduction in flow of approximately 35%. Computer simulations of carefully chosen hypothetical situations for this kind of fracture flow can provide valuable assistance in analyzing laboratory data.

## Comparison of IFDM and FEM

From the above discussion we have seen how the IFDM can be used to analyze transient fluid flow problems in multidimensional systems with complex geometry. The FEM is also well suited to such problems, and the question will arise as to how the two methods compare. A detailed analysis is not an easy task, and only a comparison of the overall features will be attempted here. Our purpose is to provide some clues for choosing an approach to certain classes of problems and also to provide an insight into the development of new techniques of analysis that will combine the inherent advantages of both IFDM and FEM.

Although FEM equations can be developed from variational principles [*Javandel and Witherspoon*, 1968] or physical considerations [*Winslow*, 1966; *Wilson*, 1968], mathematically, the most direct method is the Galerkin approach [*Zienkiewicz*

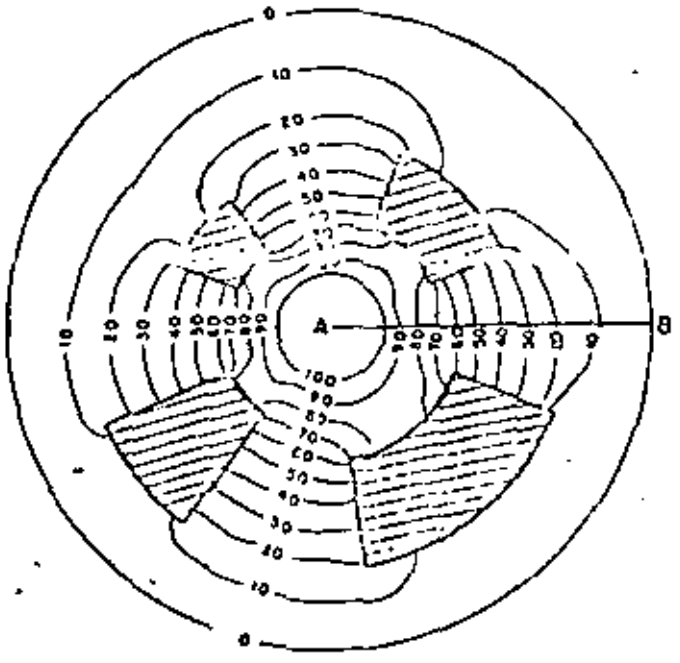


Fig. 7. The pressure distribution in a partially closed fracture.

*...and Pinder, 1970; Pinder and Frind, 1972; Neuman, 1973, 1975]*. In the following we will analyze the Galerkin formulation of the FEM, and since the IFDM uses a linear approximation for potential gradient, we will restrict our analysis of FEM to triangular elements where a linear approximation is used.

In the Galerkin scheme the partial differential equation is first weighted with an appropriate weighting function and then integrated. Thus after neglecting the source term in (2), we have

$$\int_V \xi_m \left( \nabla \cdot K \nabla \xi_n \phi_n - c \frac{\partial \xi_n \phi_n}{\partial t} \right) dV = 0 \qquad (12)$$

In writing (12) we have replaced $\phi$ by the approximate relation $\phi \approx \xi_n \phi_n$, where the repetition of $n$ denotes summation over $n$ nodal points. The particular feature of the Galerkin procedure is that the weighting function $\xi_m(x_i)$ is the same as the coordinate function $\xi_n(x_i)$ that is used to approximate $\phi$. In the FEM, which is a subdomain scheme, $\xi_m$ is defined as unity at nodal point $m$ and zero at all other nodal points.

In the simplest case involving linear elements the FEM flow region is discretized into a series of appropriately small triangles, within each of which $\phi$ is assumed to vary linearly. Thus $\xi_m$ also varies linearly from a value of 1 at nodal point $m$ to zero along the line connecting the remaining two nodal points of the triangular element. For isotropic media, $K$ in (12) is a scalar, and for anisotropic media, $K$ is a second-rank symmetrical tensor.

Assuming $K$ and $c$ to be constant within each triangular element and making use of Green's first identity [*Sokolnikoff and Redheffer*, 1966], we can rewrite (12) as

$$\sum_{\text{all } e} \left( -\int_{V^e} \nabla \xi_m \cdot K \nabla \xi_n \phi_n \, dV + \int_{A^e} \xi_m K \nabla \xi_n \phi_n \cdot \mathbf{n} \, dS - \int_{V^e} \xi_m c \frac{\partial \xi_n \phi_n}{\partial t} \, dV \right) = 0 \qquad (13)$$

In (13) the superscript $e$ denotes a triangular element, and the summation denotes integration over all elements of the flow region. One equation such as (13) is set up for each nodal point $m$ at which the time rate of change of potential is to be determined. Furthermore, the nature of the weighting function $\xi_m$ is such that the surface integral is zero for all interior nodal points. If $m$ lies on a boundary of the flow region where the flux is prescribed, the surface integral becomes a known quantity.

Hence we need to concern ourselves only with the two volume integrals in (13). Moreover, by definition, $\xi_m$ has nonzero values only in those elements that include nodal point $m$. Thus the summation implied in (13) actually means summation only over those triangular elements at whose apex $m$ lies. We shall call the subdomain composed of these triangles the 'primary' element of $m$, while each triangular element will be called a 'secondary' element (Figure 8).

Let us now consider the first volume integral in (13) as applied to secondary element II in Figure 8. It can be shown [*Narasimhan, 1975*] that the integral $\int \nabla \xi_m \cdot K \nabla \xi_n \phi_n \, dV$, evaluated with respect to nodal point $m$, is simply the flux normal to the line connecting the midpoints A and B of the sides adjacent to $m$, as is shown in Figure 9. Furthermore, if G is the centroid of secondary element II, then because of the constant gradient of $\phi$ within the element the flux across the line AB is exactly equal to the flux across the line AGB. Hence extending this approach to all secondary elements shown in Figure 8 leads to the conclusion that $\sum_e \int \nabla \xi_m \cdot K \nabla \xi_n \phi_n \, dV$ is a summation of fluxes across the surface enclosing the subregion around nodal point $m$, as is shown in Figure 10.

Comparison of Figures 10 and 1 shows that the weighted integration of the spatial integral in the Galerkin scheme and the evaluation of the surface integral in the IFDM both lead to a summation of fluxes across the surface of a subdomain associated exclusively with the nodal point of interest. This summation can therefore be interpreted as the net rate at which fluid is accumulating within the exclusive subdomain associated with nodal point $m$.

The other volume integral in (13), $\int \xi_m c \, \partial \xi_n \phi_n / \partial t \, dV$, determines how the fluid accumulating in the exclusive subdomain of nodal point $m$ (Figure 10) is distributed within the subdomain so as to cause $\phi_m$ to change with time. We will consider two possible ways of interpreting this integral.

First, let us review the conventional Galerkin procedure (12) in which $\xi_n \phi_n$ ($= \phi$) is substituted for $\phi$ in the time derivative. Assuming that $c$ is constant within $e$ and recognizing that $\xi_m(x_i)$ is independent of time, we get

$$\sum_e \int_{V^e} \xi_m c \frac{\partial \phi_n}{\partial t} \, dV = \sum_e c^e \int_{V^e} \xi_m \xi_n \frac{\partial \phi_n}{\partial t} \, dV \qquad (14)$$

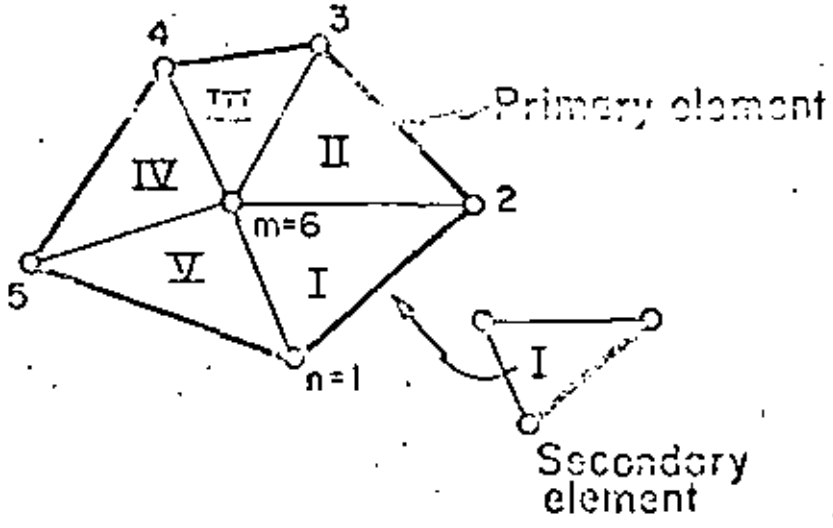


Fig. 8. Primary and secondary elements of a FEM network.

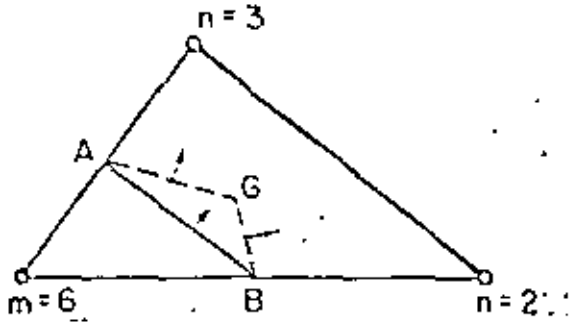


Fig. 9. An expanded view of secondary element II in Figure 8.

Using *Felippa's* [1966] evaluation of $\int_{V_e} \xi_m \xi_n \, dV$ for triangular elements, we can rewrite (14) as

$$\sum_e \int_{V_e} \xi_m c \frac{\partial \xi_n \phi_n}{\partial t} \, dV = \sum_e c^e \left[ \frac{\Delta^e}{6} \frac{\partial \phi_m}{\partial t} + \frac{\Delta^e}{12} \left( \frac{\partial \phi_n^1}{\partial t} + \frac{\partial \phi_n^2}{\partial t} \right) \right] \quad (15)$$

where $\partial \phi_n^1 / \partial t$ and $\partial \phi_n^2 / \partial t$ are time derivatives at the remaining two nodal points of element $e$. If we recognize that the exclusive subdomain associated with nodal point $m$ in Figure 10 is one third of the area of the entire pentagon, (15) may be taken to imply that $\partial \phi_m / \partial t$, which is an average value representative of one sixth of the area of the pentagon, can be interpreted as the mean rate of change in potential over one half of the shaded subregion in Figure 10. Over the remaining half of this subregion the accumulating fluid is assumed to be distributed in accordance with the average time rates $\partial \phi_n / \partial t$ at the neighboring nodal points of $m$.

The second way to interpret the integral $\int_{V_e} \xi_m c \, \partial \xi_n \phi_n / \partial t \, dV$ is to consider that the net rate of fluid accumulation arising out of the first volume integral in (13) is distributed in such a fashion within the shaded subregion in Figure 10 that the time rate of change in potential is uniform throughout the exclusive subdomain. This would imply that in the second volume integral in (13) we should replace $\partial \xi_n \phi_n / \partial t$ by $\partial \phi^m / \partial t$, which is now the mean rate of change in potential over the exclusive subdomain of nodal point $m$. According to this interpretation we get instead of (15)

$$\sum_e \int_{V_e} \xi_m c \frac{\partial \phi^m}{\partial t} \, dV = \frac{\partial \phi^m}{\partial t} \sum_e c^e \int_{V_e} \xi_m \, dV = \frac{\partial \phi^m}{\partial t} \sum_e \frac{\Delta^e c^e}{3} \quad (16)$$

The right-hand side of (15) leads to a nondiagonal capacity matrix, while the right-hand side of (16) leads to a diagonal form. In attempting to extend the conventional Galerkin approach in (15) to the quasi-linear problem of unsaturated-saturated groundwater flow, *Neuman* [1973, 1975] found that he could not get a convergent solution unless he diagonalized the capacity matrix as was done in (16). He reasoned that since the Galerkin approximation applies only at a given instant of time, the time derivative in the governing equation should be determined independently of the orthogonalization process. *Ericksen and Carson* [1973] also indicate a preference for an FEM approach in which the time derivative is treated as it is in the finite difference (IFDM) equation (15). Equation (16) also conforms to the purely physical development of the FEM equations of *Wilson* [1966] and *Wilson* [1968]. It may be noted here that the nondiagonal capacity matrix of (15) leads to an algorithm requiring both a larger computer storage requirement and a larger number of computational operations than the algorithm derived from the diagonal capacity matrix resulting from (16).

In summary, when $m$ is an interior nodal point, the surface integral in (13) disappears, and depending on the choice of (15) or (16) the FEM equations can be written in either of the following two forms:

The conventional Galerkin form

$$-\sum_e \int_{V_e} \nabla \xi_m \cdot K \nabla \xi_n \phi_n \, dV = \sum_e c^e \left[ \frac{\Delta^e}{6} \frac{\partial \phi_m}{\partial t} + \frac{\Delta^e}{12} \left( \frac{\partial \phi_n^1}{\partial t} + \frac{\partial \phi_n^2}{\partial t} \right) \right] \quad (17)$$

The modified Galerkin form

$$-\sum_e \int_{V_e} \nabla \xi_m \cdot K \nabla \xi_n \phi_n \, dV = \frac{\partial \phi^m}{\partial t} \sum_e \frac{\Delta^e c^e}{3} \quad (18)$$

Comparison of (18) with (5) or (6) shows that the modified Galerkin form is similar to the IFDM except for the difference in the procedure used for evaluating the gradient of $\phi$. Comparison of (17) with (5) or (6) shows that the conventional Galerkin procedure is conceptually similar to IFDM in associating an exclusive subdomain with each nodal point of interest and summing the surface fluxes to evaluate the effect of the rate of fluid accumulation within the subdomain.

The interesting fact that emerges out of a comparison of IFDM with FEM is that the chief difference between the two methods lies in the manner in which the spatial gradients in $\phi$ are evaluated. The IFDM employs the simple finite difference approximation and is thus constrained to a measurement of gradients normal to a given surface and restricted to first-order approximations. As a result it cannot handle general tensorial quantities, since they require evaluation of tangential gradients along the reference surface in addition to the normal gradient. Moreover, when the spatial variation of $\phi$ is rapid, the IFDM would require a large number of mesh points to simulate accurately the rapid variation of $\phi$ in terms of successive linear segments.

The FEM, on the other hand, by setting up a surface $\phi = \xi_n \phi_n$ for the variation of potential over an elemental region, achieves a very general and powerful form of expressing the spatial variation of $\phi$. As a result, the FEM is not only well suited for handling general tensorial parameters (e.g., stress, permeability, dispersion) but is also well suited to the utilization of higher-order surfaces, which can approximate the rapid spatial variation of $\phi$ with greater accuracy.

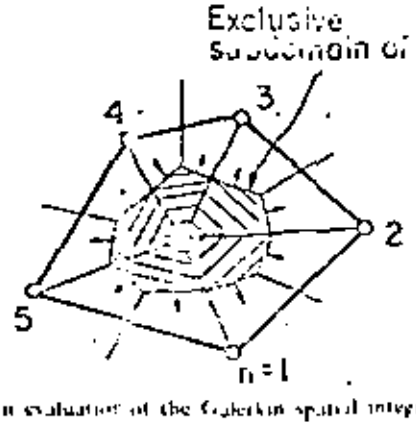


Fig. 10. An evaluation of the Galerkin spatial integral for nodal point $m$.

The basic integration scheme in the FEM involves evaluation of volume integrals. Hence the FEM has to choose, at the outset, a coordinate system of known symmetry, usually Cartesian. In addition, to facilitate evaluation of the volume integral, the elemental volume has to have a simple shape the volume of which can be expressed as a simple function of its dimensions. As a result, when the flow domain has a complex geometry with mixed symmetry, the FEM has to approximate the domain by using fundamental shapes such as triangles or squares, which may not always be easy. To some extent, this difficulty can be overcome by resorting to higher-order isoparametric elements.

In the case of IFDM, which basically evaluates surface fluxes and in which geometrical parameters are provided as input information, there is no restriction on choosing any basic elemental shape. Therefore arbitrarily shaped elements can be chosen judiciously not only to handle mixed symmetries (as was done in Figure 3) but also to fit complex boundaries with a small number of elements. A very desirable feature of the IFDM is that it can, in a simple way, handle complex boundaries and still retain a linear approximation for potential variation.

In the IFDM, care must be taken to design the mesh so that the lines joining nodal points coincide with the normals to the interfaces between the points. This restriction, as well as the requirement for providing geometrical parameters as input data, may require added effort in the design of networks for complex problems. To some extent, this effort can be minimized by developing auxiliary computer programs for mesh and input data generation. On the other hand, the design of the FEM mesh may be less restrictive, since the geometric parameters are generated implicitly in the volume integration. However, even in the FEM it may be necessary to have basic elements with some regularity of shape (e.g., to avoid obtuse-angled triangles) in order to avoid undesirable matrix properties that affect the efficiency of the solution process [*Neuman and Narasimhan*, 1976; *Narasimhan et al.*, 1976].

Certain apparent differences between IFDM and FEM arise mostly owing to the conventions and customary procedures that are followed. If we look at the conventional Galerkin form of the FEM equation (17), we note that the equation for nodal point $n$ also contains the unknown time derivatives at the neighboring nodal points $n$. Hence the set of equations arising out of (17) would have to be solved as a set of simultaneous equations involving these unknowns. In other words, (17) cannot be solved explicitly, even for small time steps. On the other hand, the modified Galerkin equation in (18), which is similar to the IFDM (5) or (6), can be solved explicitly or implicitly as required.

In addition to their simplicity, an added advantage of IFDM equations is that local stability conditions are easier to define (7), and this has enabled the development of an optimal explicit-implicit procedure used in the program Trump. The IFDM has also been amenable to the development of a successful iterative scheme that has produced satisfactory results for a wide class of problems [*Edwards*, 1972; *Narasimhan*, 1975]. The result of using such a scheme is that IFDM is not constrained by the need for optimal numbering of nodal points, as is the case in some FEM schemes. Furthermore, a single computer program is able to handle one-, two- or three-dimensional problems, and the size of a problem does not necessarily depend on its dimensionality.

From the above discussion of IFDM and FEM we have seen that some of the differences are intrinsic in the methods used, while others are mainly a matter of convention. If suitable changes in convention could be made, it appears that one could combine the advantages of both methods and develop an improved numerical process.

As was discussed earlier, the modified Galerkin approach (18) is conceptually similar to (5) or (6) of the IFDM. An analysis of (18) has shown [*Neuman and Narasimhan*, 1976] that for this equation, not only is it possible to define a local stability criterion similar to (7) of the IFDM, but it is also possible to establish local convergence criteria for the numerical equation. Furthermore, (18) has also been found to be amenable to the iterative solution scheme of *Evans et al.* [1954] on which the explicit-implicit procedure of Trump is based. Therefore by incorporating (18) into the Trump algorithm we have been able to develop a new mixed explicit-implicit computer scheme for solving diffusion-type problems [*Neuman and Narasimhan*, 1976; *Narasimhan et al.*, 1976].

## Conclusions

The theoretical basis for the integrated finite difference method reveals a rather simple but powerful numerical technique for solving groundwater flow problems. Examples have been provided to demonstrate that the IFDM as incorporated in Trump can handle two- or three-dimensional problems with ease.

A comparison of IFDM and FEM indicates that each of these integral methods has distinct advantages in handling certain classes of problems. The modified Galerkin form of the FEM is conceptually almost the same as the IFDM except for the difference in the procedure used in evaluating the gradient of $\phi$. This suggests the possibility of developing a new FEM code that can incorporate the explicit-implicit iterative solution scheme in Trump and thus combine the advantages that are inherent in both IFDM and FEM.

## Notation

$A_{m,n}$ area of interface between elements $m$ and $n$ in IFDM ($L^2$).
$b$ fracture aperture ($L$).
$c$ specific fluid capacity or specific storage ($1/L$).
$D_{m,n}$ distance between nodal points $m$ and $n$ in IFDM.
$g$ flow rate per unit volume ($1/T$) or acceleration due to gravity in the fracture flow problem ($L/T^2$).
$g_m$ flow rate per unit volume of element $m$ ($1/T$).
$K$ hydraulic conductivity ($L/T$).
$K'_{m,n}$ mean hydraulic conductivity between elements $m$ and $n$ ($L/T$).
$m$ subscript used to denote an element or a nodal point (1).
$n$ subscript used to denote an element or a nodal point (1).
$\mathbf{n}$ unit outer normal to a surface (1).
$Q$ flow rate ($L^3/T$).
$r$ radial distance ($L$).
$r_e$ radial distance to external boundary in fracture flow problem ($L$).
$r_i$ radial distance to internal boundary in fracture flow problem ($L$).
$S$ storage coefficient in Theis equation (1) or surface of integration.
$t$ time ($T$).
$T$ coefficient of transmissibility in Theis equation ($L^2/T$).
$U_{m,n}$ conductance between elements $m$ and $n$ ($L^2/T$).
$V$ volume ($L^3$).

$V_m$ volume of element $m$ ($L^3$)
$\Delta^e$ area of triangular element $e$,
$\alpha$ diffusivity ($L^2/t$).
$\lambda$ weight given to the backward-differencing operation in the implicit scheme (1).
$\mu$ viscosity of fluid ($M/LT$).
$\xi$ function to express the variation of potential over an element $e$ in the FEM or the Galerkin weighting function (1).
$\xi_m$ weighting function pertaining to nodal point $m$.
$\rho$ density of fluid ($M/L^3$).
$\phi$ fluid potential or hydraulic head ($L$).

*Acknowledgments.* We would like to thank T. J. Lasseter and S. P. Neuman for many fruitful discussions during the preparation of this paper. We also appreciate the assistance of Katsuhiko Iwai in providing the solution for the fracture flow problem. This work was partially supported by the U.S. Energy Research and Development Administration.

## References

Carslaw, H. S., and J. C. Jaeger, *Conduction of Heat in Solids*, p. 261, Oxford at the Clarendon Press, London, 1959.

Cooley, R. L., A finite difference method for variably saturated porous media: Application to a single pumping well, *Water Resour. Res.*, *7*(6), 1607–1625, 1971.

Dusinberre, G. M., *Heat Transfer Calculations by Finite Differences*, International Textbooks, Scranton, Pa., 1961.

Edwards, A. L., *Trump: A Computer Program for Transient and Steady State Temperature Distributions in Multidimensional Systems*, National Technical Information Service, National Bureau of Standards, Springfield, Va., 1972.

Emery, A. F., and W. W. Carson, An evaluation of the use of the finite-element method in the computation of temperature, *J. Heat Transfer*, *93*, 136–145, 1971.

*Encyclopedia of Science and Technology*, vol. 5, p. 45, McGraw-Hill, New York, 1960.

Evans, G. W., R. J. Brousseau, and R. Keirstead, Instability considerations for various difference equations derived from the diffusion equation, *Rep. UCRL-6476*, Lawrence Radiat. Lab., Livermore, Calif., 1954.

Felippa, C. A., Refined finite element analysis of linear and nonlinear two-dimensional structures, *Rep. SESM 66-22*, Dep. of Civil Eng., Univ. of Calif., Berkeley, 1965.

Gale, J. E., R. L. Taylor, P. A. Witherspoon, and M. S. Ayatollahi, Flow in rocks with deformable fractures, in *Finite Element Methods in Flow Problems*, edited by J. T. Oden et al., pp. 583–598, UAH Press, Huntsville, Ala., 1974.

Javandel, I., and P. A. Witherspoon, Application of the finite element method to transient flow in porous media, *Soc. Petrol. Eng. J.*, *8*(3), 241–250, 1968.

Louis, C., A study of groundwater flow in jointed rock and its influence on the stability of rock masses, *Rock Mech. Res. Rep. 10*, Imp. Coll., Univ. of London, London, 1969.

MacNeal, R. H., An asymmetric finite difference network, *Quart. Appl. Math.*, *2*, 295–310, 1953.

Narasimhan, T. N., A unified numerical model for saturated-unsaturated groundwater flow, Ph.D. thesis, Dep. of Civil Eng., Univ. of Calif., Berkeley, 1975.

Narasimhan, T. N., S. P. Neuman, and A. L. Edwards, Mixed explicit-implicit iterative finite element scheme for diffusion-type problems, 2, Solution strategy and examples, submitted to *Int. J. Numer. Methods Eng.*, 1976.

Neuman, S. P., Saturated-unsaturated seepage by finite elements, *J. Hydraul. Div. Amer. Soc. Civil Eng.*, *99*(HY 12), 2233–2250, 1973.

Neuman, S. P., Galerkin approach to saturated-unsaturated flow in porous media, in *Finite Elements in Fluids*, vol. 1, edited by R. H. Gallagher, chap. 10, John Wiley, New York, 1975.

Neuman, S. P., and T. N. Narasimhan, Mixed explicit-implicit iterative finite element scheme for diffusion-type problems, I, Theory, submitted to *Int. J. Numer. Methods Eng.*, 1976.

O'Brien, G. G., M. A. Hyman, and S. Kaplen, A study of the numerical solution of partial differential equations, *J. Math. Phys.*, *29*, 223–251, 1951.

Pinder, G. F., and E. O. Frind, Application of Galerkin procedure to aquifer analysis, *Water Resour. Res.*, *8*(1), 108–120, 1972.

Romm, E. S., *Flow Phenomena in Fractured Rocks* (in Russian), Nedra, Moscow, 1966.

Sharp, J. C., and Y. N. T. Maini, Fundamental considerations on the hydraulic characteristics of joints in rock, in *Proceedings of Symposium on Percolation Through Fissured Rock*, pp. T-1-5, Deutsche Gesellschaft für Erd-und-Grundbau, Essen, Germany, 1972.

Snow, D. T., A parallel plate model of fractured permeable media, Ph.D. thesis, Dep. of Civil Eng., Univ. of Calif., Berkeley, 1965.

Sokolnikoff, I. S., and R. M. Redheffer, *Mathematics of Physics and Modern Engineering*, McGraw-Hill, New York, 1966.

Theis, C. V., The relation between the lowering of the piezometric surface and the rate of duration and discharge of a well using groundwater storage, *Eos Trans. AGU*, *16*, 519–524, 1935.

Todd, D. K., *Ground Water Hydrology*, John Wiley, New York, 1959.

Tyson, H. N., and E. M. Weber, Groundwater management for the nations future—Computer simulation of groundwater basins, *J. Hydraul. Div. Amer. Soc. Civil Eng.*, *90*(HY4), 59–77, 1964.

Wilson, C. R., and P. A. Witherspoon, Steady state flow in rigid networks of fractures, *Water Resour. Res.*, *10*(2), 328–335, 1974.

Wilson, E. L., The determination of temperatures within mass concrete structures, *SESM Rep. 68-17*, Dep. of Civil Eng., Univ. of Calif., Berkeley, 1968.

Winslow, A. M., Numerical solution of the quasilinear Poisson equation in a non-uniform triangle mesh, *J. Comput. Phys.*, *1*, 149–172, 1966.

Zienkiewicz, O. C., and C. J. Parekh, Transient field problems: Two-dimensional and three-dimensional analysis by isoparametric finite elements, *Int. J. Numer. Methods Eng.*, *2*, 61–71, 1970.

(Received May 5, 1975;
revised September 15, 1975;
accepted September 15, 1975.)

UNITED STATES
DEPARTMENT OF THE INTERIOR
GEOLOGICAL SUSVEY

# SIMULATION OF STEAM TRANSPORT IN VAPOR-DOMINATED GEOTHERMAL RESERVOIRS

OPEN-FILE REPORT 76-607



*Menlo Park, California*
*1976*

UNITED STATES
DEPARTMENT OF THE INTERIOR
GEOLOGICAL SURVEY

SIMULATION OF STEAM TRANSPORT IN
VAPOR-DOMINATED GEOTHERMAL RESERVOIRS

By
Allen F. Moench

Open-File Report 76-607
Menlo Park, California
1976

CONTENTS



LIST OF TABLES



LIST OF ILLUSTRATIONS

Vapor-dominated Geothermal Reservoirs

By

Allen F. Moench

ABSTRACT

A numerical model of steam transport through a porous medium is presented and applied to a hypothetical geothermal reservoir in order to explain observed production characteristics. A vapor-dominated geothermal reservoir is conceptualized as a one-dimensional column of porous or highly fractured rock initially filled with a mixture of saturated steam and liquid water under high pressure. A simple finite-difference technique is used to solve the flow and energy equations simultaneously for temperature and pressure. Analysis involves evaluation of pressure, temperature, and liquid-water saturation distributions when steam is produced at either constant discharge or constant pressure. Constant pressure is considered to be a more realistic condition for geothermal systems and permits computation of the discharge-versus-time relation.

Comparisons of computed saturation profiles with previously published results lead to the conclusion that movement in the liquid phase can be neglected at low moisture contents. Production characteristics that can be explained with this model include: temperature and pressure changes when steam is produced at constant or variable discharge, temperature- and discharge-versus-time variations when steam is produced at constant pressure, and the existence of superheated steam. Results also demonstrate that temperature changes due to fluid expansion or compression may be significant when dealing with superheated steam.



INTRODUCTION

Hydrothermal convection systems are classified as either vapor-dominated systems or hot water systems. Vapor-dominated systems occur in the United States at The Geysers, California, in Japan at Matsukawa, and in Italy at Larderello. Such systems are relatively uncommon, but it is probable that some high-temperature, hot-water systems will convert to steam upon development as appears to be the case in the Wairakei, New Zealand geothermal system (Boulton, 1970). Hence, present investigations of vapor-dominated systems may have future application to present-day hot-water systems.

The reservoir characteristics and production characteristics of vapor-dominated geothermal systems have been described by numerous investigators. A summary and synthesis of these characteristics has been given by Truesdell and White (1973). Truesdell and White argue convincingly that the model proposed by White, and others, (1971) provides the best basis for explaining initial and production characteristics of steam reservoirs. The model used in this report draws heavily upon the concepts of White, and others (1971), though of necessity some simplifications have been made.

Recent expanded interest in the exploitation of hydrothermal systems has led several investigators to pursue development of large-scale, distributed-parameter, two-phase digital simulation models (e.g., Toronyi, 1974; Garg, and others, 1975; Lasseter, 1975; Mercer and Faust, 1975; Faust, 1976). These represent significant advances in the numerical capability to simulate complex systems, however, the basic physical

phenomena which are being modeled are not completely understood. The purpose of this report is to present a simple alternative model of a hypothetical vapor-dominated geothermal system and to use this model to examine some of the physical processes which have been assumed to occur in such systems. In addition, this model is used to explain certain of the production characteristics of real systems.

## CONCEPTUAL MODEL

A vapor-dominated geothermal system is conceptualized as a one-dimensional column of porous or highly fractured rock initially filled with a mixture of saturated steam and liquid water under high pressure. Steam is transported under pressure gradients and liquid water, which is distributed in the small pores and crevices, acts as a source of steam. The reservoir is overlain by a "cap rock" that is assumed to have low permeability and which, prior to development, allows for release of some of the reservoir steam through small vents. In areas far from natural vents, the temperature in the cap rock increases with depth to the top of the reservoir. (This has been observed at The Geysers by Urban, and others, 1975). Prior to development, temperature and pressure in the vapor-dominated region are essentially constant with depth. At the bottom of the reservoir there is assumed to be a zone where liquid water saturates the pores. Heat is supplied by a magma chamber at depth and transferred upward through the liquid-saturated zone by conduction and convection. The topmost part of this zone serves as a source of steam for the system. Vaporization from this zone and condensation at the top of the reservoir results in the vertical transfer of large quantities of latent heat to the base of the cap rock. (Anomalously large heat flows have been observed in the rocks overlying the reservoir at The Geysers; Urban and others, 1975). Liquid condensate in excess of that which can be held by surface tension in the porous matrix, flows downward under the influence of gravity.

Wells drilled for production of steam from the undeveloped reservoir penetrate the cap rock and encounter saturated steam at a high pressure and temperature (usually around 31 bars at 235°C). If a well is opened to the atmosphere, the sudden pressure decline will cause flashing of the liquid water distributed in the rock in the vicinity of the well bottom. This will result in cooling around the well and a large initial discharge rate, the magnitude of which will depend largely upon the well characteristics. As drying occurs in the rock around the well bottom, discharge becomes increasingly dependent upon the reservoir characteristics. With continued discharge, the liquid water in the vapor-dominated zone becomes depleted by vaporization and the discharge then becomes dependent upon the location and temperature of the deep-seated "water table", hereafter referred to as the liquid-vapor interface.

The digital simulation model presented here makes many of the same assumptions used by other investigators (Mercer and Faust, 1975; Faust 1976; Toronyi, 1974; Weinstein, and others, 1974). The essential features of this model that make it different from many previously published models are:

1) Temperature and pressure are used as the independent variables.
2) Liquid-water saturation is computed directly from the amount of liquid evolved by boiling due to pressure reduction.
3) The energy changes due to fluid expansion and contraction are not neglected.
4) Liquid water distributed in the small interstices of the vapor-dominated reservoir is assumed not to move under pressure gradients.
5) The solution technique is simple to use and rapid computationally.

## THEORY

To simulate the vertical flow of steam through variably saturated porous media two controlling equations, a fluid flow equation and an energy equation, are used. These coupled partial differential equations are written in terms of the directly-measured, intensive fluid properties, temperature and pressure. The liquid-water phase is treated as a source or sink for steam and does not move in response to pressure gradients.

The energy equation is coupled to the flow equation through the velocity term, the vaporization term, the liquid saturation, and the pressure and temperature dependent parameters. The two partial differential equations are solved simultaneously at discrete time levels.

### Flow Equation

The equation for steam transport is obtained by combining the mass balance with the momentum balance for the motion of steam in porous media. The momentum balance can be approximated by Darcy's law for two fluids and the flow equation in the vertical dimension can be written as:

$$\frac{\partial}{\partial z}\left[\rho_v \frac{k\, k_r}{\mu_v}\left(\frac{\partial P}{\partial z} - \rho_v g\right)\right] + q + q' = \frac{\partial}{\partial t}\left[\rho_v (1-S)\right] \qquad (1)$$

where

| | | |
|---|---|---|
| $\rho_v$ | density of the water vapor | $M/L^3$ |
| $\mu_v$ | dynamic viscosity of the water vapor | $M/Lt$ |
| $k$ | intrinsic permeability | $L^2$ |
| $k_r$ | relative permeability to water vapor | |
| $g$ | acceleration of gravity | $L/t^2$ |
| $\phi$ | porosity | |
| $S$ | liquid-water saturation | |
| $P$ | pressure | $M/t^2L$ |
| $q$ | source or sink of steam through wells (positive if source of steam) | $M/tL^3$ |
| $q'$ | source or sink of steam by vaporization or condensation (positive if source of steam) | $M/tL^3$ |
| $z$ | vertical coordinate (positive downward) | $L$ |
| $t$ | time | $t$ |

The density as defined by the equation of state for pure steam is a function of temperature and pressure. Accordingly, the right-hand side of equation (1) can be expanded and equation (1) may be rewritten as follows:

$$\frac{\partial}{\partial z}\left[\rho_v \frac{k\, k_r}{\mu_v}\left(\frac{\partial P}{\partial z} - \rho_v g\right)\right] + q + q' = \phi(1-S)\rho_v \kappa \frac{\partial P}{\partial t} \qquad (2)$$

$$-\phi(1-S)\rho_v \beta \frac{\partial T}{\partial t} - \phi \rho_v \frac{\partial S}{\partial t}$$

where

$\kappa$ compressibility of water, $\frac{1}{\rho_v}\left(\frac{\partial \rho_v}{\partial P}\right)_T$ ----------$Lt^2/M$

$\beta$ thermal expansivity of water vapor, $-\frac{1}{\rho_v}\left(\frac{\partial \rho_v}{\partial T}\right)_P$ --------$1/T$

$T$ Temperature----------$T$

In the above equation, the coefficients $\kappa$ and $\beta$ are derived from the equation of state for pure steam (Appendix) and hence are dependent upon temperature and pressure. The dynamic viscosity is a function of temperature. The intrinsic permeability is spatially dependent and the relative permeability is assumed to be a function of the liquid-water saturation. Definition of these quantities is given in the Appendix.

Equation (1) makes the assumption that the rock matrix is rigid, hence the porosity does not change with pressure. (In vapor-dominated geothermal reservoirs, this is a valid approximation because the compressibility of reservoir rocks is negligible compared with the compressibility of steam.) The effect of gravity will be neglected in the remainder of this report because of its small influence upon production characteristics in the cases studied.

The boundary conditions for the flow equations are zero-flow. Mass transfer at those boundaries is treated as a source or sink.

## Energy Equation

The equation used in this report for energy transport is derived by combining the equation of change for pure steam, written in terms of temperature and specific heat at constant pressure (Bird, and others, 1960, p. 322), with the diffusion equation for heat transport through the solid-liquid matrix. Adding the appropriate source terms, the equation for energy transport is given by:

$$\frac{\partial}{\partial z}\left(K\frac{\partial T}{\partial z}\right)-c_1 v\frac{\partial T}{\partial z}-Lq'+Q=[c_1+c_2+c_3]\frac{\partial T}{\partial t}-\phi(1-S)\,T\,\beta\,\frac{DP}{Dt} \qquad (3)$$

where

$K$ effective thermal conductivity----------$M/t^3T$

$v$ average interstitial velocity----------$L/t$

$c_1$ heat capacity of vapor, $\phi(1-S)\rho_v c_{pv}$----------$M/t^2TL$

$c_2$ heat capacity of liquid, $\phi S\rho_\ell c_{p\ell}$----------$M/t^2TL$

$c_3$ heat capacity of solid, $(1-\phi)\rho_s c_{ps}$----------$M/t^2TL$

$\rho_\ell$ density of liquid water----------$M/L^3$

$\rho_s$ density of solid rock particles----------$M/L^3$

$c_{pv}$ specific heat at constant pressure of vapor----------$L^2/t^2T$

$c_{p\ell}$ specific heat at constant pressure of liquid----------$L^2/t^2T$

$c_{ps}$ specific heat at constant pressure of solid----------$L^2/t^2T$

$L$ latent heat of vaporization----------$L^2/t^2$



$Q$ energy source or sink by means other than condensation or vaporization (positive if source of heat)----------$M/t^3L$

$\frac{D}{Dt}$ substantial derivative, $\frac{\partial}{\partial t}+v\frac{\partial}{\partial z}$----------$1/t$

The terms in equation (3) have the following physical interpretations:

| | |
|---|---|
| $\frac{\partial}{\partial z}K\frac{\partial T}{\partial z}$ | rate of change of thermal energy by Fourier conduction. |
| $c_1 v\frac{\partial T}{\partial z}$ | rate of change of thermal energy by vapor movement. |
| $Lq'$ | source or sink of thermal energy by condensation or vaporization. |
| $Q$ | source or sink due to fluid withdrawal or conduction through boundaries. |
| $[c_1+c_2+c_3]\frac{\partial T}{\partial t}$ | rate of change of thermal energy stored in the vapor, liquid, and solid components. |
| $\phi(1-S)T\beta\frac{DP}{Dt}$ | rate of change of thermal energy due to compressible work. |

Equation (3) is an approximate equation for the transport of energy in a steam-filled porous medium. Major assumptions used in the development of this equation can be summarized as follows: 1) local thermal equilibrium exists between the vapor and solid-liquid matrix; 2) the dispersive component of heat transport is negligible; and 3) surface tension effects are negligible.

The latent heat of vaporization is a function of the vapor pressure of saturated steam. It is evaluated by taking the difference between the enthalpy of the liquid and the enthalpy of the vapor (see Appendix). Other parameters such as thermal conductivity, specific heats of the vapor, liquid, and solid components, and densities of the liquid and solid components are assumed to be constant.

The upper boundary for the energy equation is assumed to be insulating. This is justifiable because of the short time scale in the cases studied. Some discussion will be devoted to the case where it is not insulating. The lower boundary, defined by the liquid-vapor interface, is a variable temperature boundary. Temperature reductions at this boundary are assumed to be due to vaporization.



Boiling Mechanism

Liquid water may be distributed throughout a vapor-dominated reservoir in greater or lesser amounts. In the vapor region it will occupy only a small fraction of the available pore space and it will provide a source of steam under proper conditions of temperature and pressure. In the region below the liquid-vapor interface, liquid will fill or nearly fill the available pore space and will provide a source of steam at the lower boundary of the vapor zone. It is assumed that vaporization at the interface will not occur until the liquid water overlying the interface has been depleted.

In regions where liquid and vapor exist together, steam will be produced by boiling in response to pressure reductions or temperature increases. Condensation will occur in these regions in response to pressure increases or temperature reductions. The criterion under which one or the other of these effects will occur is established by the saturation pressure or temperature which is taken to be that of pure water for a flat-surface interface (Appendix). If the pressure should fall below saturated-vapor pressure for the prevailing temperature, steam will evolve until either the pressure is brought up to the vapor pressure of saturated steam, or no more liquid water exists. Likewise, if temperature should increase above the temperature for saturated steam, steam will evolve until pressure is brought up to saturated-vapor pressure, or no more liquid water exists. The source term for vaporization is obtained by satisfying equation (1) through an iterative procedure described in the next section.

The final equation required for solution of equations (2) and (3) involves changes in the degree of liquid-water saturation by vaporization or condensation and is expressed as:

$$\frac{\partial S}{\partial t} = -\frac{q'}{\phi \rho_L} \qquad (4)$$

When liquid-water saturation becomes zero at a point there can be no further vaporization (though condensation can occur). Further reductions in pressure result in superheating.





Equations (2) and (3) are solved using a space-centered fully-implicit, finite-difference technique. The method is second-order correct in space, but is only first-order correct in time. This makes it less accurate than other techniques, but it yields numerically stable results, regardless of the size of the time increment, when applied to diffusive-type equations (fluid flow equation) or sufficiently parabolic, convective-diffusion equations (energy equation). Truncation error introduced by the method can be minimized by reducing the time increment. If the energy equation becomes strongly hyperbolic (convective component overwhelms the diffusive component) small space increments may be required to prevent instability (Rosenberg, 1969, p. 25). This has not been found to be a difficulty in this study. The finite-difference forms of equations (2) and (3) are written in terms of changes in pressure and temperature rather than absolute values. This helps to reduce roundoff errors. The equations are solved using a direct technique (Thomas algorithm).

At the start of a time step, the energy equation is solved for the temperature distribution using pressures, velocities, and sources and sinks computed in the previous time step. Next, the temperature dependent parameters such as viscosity, density, and saturated-vapor pressure are updated and the flow equation is solved for the pressure distribution. Iteration on the flow equation is necessary because of adjustments required for evaluating the vaporization term. The rate of vaporization (or condensation) is computed from an equation of the form:

$$q' = \frac{\phi(1-S)}{\Delta t} \sum_{n=1}^{m} [\rho_v(T^*,P^*) - \rho_v(T^*,P_n)] \qquad (5)$$

where ,

| | | |
|---|---|---|
| n | iteration number | |
| m | total number of iterations | |
| $T^*$ | temperature of saturated steam at pressure $P^*$ | T |
| $P^*$ | pressure of saturated steam at temperature $T^*$ | $M/t^2L$ |
| $\Delta t$ | time interval | t |

Density is reevaluated with each iteration and iteration is continued until the vapor pressure approaches saturation, and further additions to or subtractions from the vaporization term become less than a prescribed tolerance. Finally, liquid-water saturations and steam velocities are computed and all parameters are updated before going on to the next time step. Iteration on the energy equation is not necessary because temperature changes within each time step are small.



Steam extraction can be simulated for any point in the vertical column by assuming either a constant discharge rate or a constant pressure. Simulation with constant discharge requires less computation than simulation in which pressure is held constant, however, the constant pressure condition is more realistic for geothermal reservoirs under development and allows for prediction of the discharge-versus-time relationship. Simulation with constant pressure is accomplished by computing the discharge necessary to hold the pressure constant from one iteration to the next.

## MODEL RESULTS

### Constant Discharge

In order to demonstrate that the model operates in the desired fashion, a comparison is made with results of a constant discharge, finite-difference model published by Toronyi (1974). In this test case the flow of steam is horizontal instead of vertical and there is no liquid-saturated zone. Because gravitational effects have been neglected, the present model applies to both vertical and horizontal steam flow. In Toronyi's model, pressure and liquid-phase saturation are the independent variables. Toronyi's model accounts for flow in both the liquid and vapor phases, however, the model is valid only where the two phases exist together. With these exceptions, the assumptions and relationships for computing coefficients are similar to those given in this report. Compressible work is not included in Toronyi's model, so it is omitted from the computations. Parameters and initial conditions are shown in Table 1. The reservoir is closed to flow of mass and energy.

Although Toronyi's model is designed for two-dimensional flow, his results for areal flow are essentially one-dimensional. This is because of the nodal configuration and the reservoir parameters used. Figure 1a shows the nodal distribution used in this model with the constant discharge sink indicated by shading.

Figure 1b shows saturation profiles for 0.19 and 0.58 mass fractions produced. These are compared with Toronyi's results. Results for 0.19 mass fraction produced are further corroborated by the finite element model of Mercer and Faust (1975) where pressure and enthalpy were used as the independent variables. The close agreement in the results obtained suggests that liquid movement, under the conditions of Table 1, is negligible and that changes in saturation can be accounted for almost entirely by vaporization alone.



Figures 2a, 2b, and 2c illustrate the declines in liquid-wa saturation, temperature and pressure, respectively, at the producing node when production is continued at a constant rate until liquid water becomes totally depleted. The temperature decline is due primarily to vaporization of the liquid water, hence it is not surprising that the temperature decrease is nearly proportional to the decrease in liquid-water saturation. The change in temperature at any point in a reservoir due to vaporization of a known quantity of water can be easily calculated (Nathenson, 1975a). The temperature change of 5.6°C, shown in figure 2b, is within 0.1°C of the temperature change obtained using the method described by Nathenson. After the liquid water at the producing node has been totally vaporized, there is no further significant decline in temperature. This is primarily because the effect of compressible work has been neglected.

The pressure decline at the producing node up to a mass fraction of 0.72, shown in figure 2c, is simply the decline in saturated-vapor pressure due to temperature reduction. At this point, the liquid water at the producing node has been completely vaporized. As the pressure continues to decline, the produced steam becomes superheated. When all the liquid water present in the reservoir has vaporized at a mass fraction of 0.90, the pressure declines very rapidly until the remaining steam is depleted. The pressure change shown here is similar in shape to that of the lumped parameter system given by Brigham and Morrow (1974).

A time step of 1000 sec yields sufficiently accurate results. 350 time steps are required to produce a mass fraction of 0.98. With an average of six iterations per time step this uses 25 seconds CPU time on an IBM 370/168 computer.

## Constant Pressure

A constant discharge boundary condition (i.e. constant within a time step) is not particularly useful for simulating geothermal systems because it cannot be used for predictive purposes without some *a priori* knowledge of how the discharge will change in the future. The constant pressure condition is more realistic because the reservoir steam ultimately reaches atmospheric pressure after passing through wells, pipes and turbines. In addition, the constant pressure condition allows for prediction of the discharge-versus-time relationship and provides a means for estimating reservoir life.

The parameters and initial conditions used to illustrate the effects of fluid production at constant pressure are shown in Table 2. The values of the parameters given should be realistic for geothermal systems. A constant well bottom pressure of 10 bars is chosen so that there is sufficient pressure to drive the turbines after allowing for pressure losses in the well bore and associated piping. The liquid-vapor interface is assumed to be stationary at a depth of one kilometer.

Figure 3 shows the results obtained at different times. Figure 3a gives the arrangement of the nodes with the producing node indicated by shading. The liquid-water saturation, pressure, and temperature are given in figures 3b, 3c, and 3d, respectively, for each of these nodes.



Figure 3d shows the effect of compressible work upon the temperature distribution near the producing node. By way of comparison, a computer run was made neglecting compressible work and some of the results are plotted in Figure 3d. The temperature difference in the two sets of data shown for $3 \times 10^5$ sec can be accounted for by adiabatic cooling of the expanding steam.

Adiabatic expansion or contraction of an ideal gas can be described by (see e.g., Zemansky, 1957, p. 124):

$$P \hat{v}^{\gamma} = \text{constant} \qquad (6)$$

where

$\hat{v}$ specific volume, $1/\rho_v$ ---------- $L^3/M$

$\gamma$ ratio of specific heat at constant pressure to specific heat at constant volume ----------

Incorporating the ideal gas law and rearranging equation (6), the change in temperature in bringing an ideal gas from state 1 to state 2 can be expressed as:

$$T_2 = T_1 \left(\frac{P_1}{P_2}\right)^{\frac{1-\gamma}{\gamma}} \qquad (7)$$

For comparison with the numerical approach, temperature changes computed using equation (7) were adjusted for heat transfer from the rock matrix and for fluid travel time to the node of interest from the upstream node. This procedure resulted in temperature changes which were within 55 percent of the temperature change which occurs when the ideal gas assumption ($\gamma_s = 1$) is used in the compressible work term of equation (3). When

steam properties are used in the compressible work term instead of ideal gas properties, the temperature change is increased. Some 20 percent of the temperature change due to compressible work in Figure 3d is due to the non-ideal nature of steam.



Compressible work is clearly unimportant when liquid and vapor exist together in the porous medium (see the bottom 3 nodes in Figure 3d). This is because pressure changes are small when vaporization is taking place. It is possible that in real systems where pressure changes are more gradual, the effect of adiabatic cooling or heating may not be important even for superheated systems. This requires further study.

The discharge versus time relationship is shown in Figure 4. At any point, this represents the mass of steam that must leave the producing node per unit cross-sectional area in order to maintain constant pressure. The actual discharge in kilograms per second is dependant upon the areal dimension chosen.

The discharge in Figure 4 declines with time as the distance increases to the zone of partial liquid-water saturation, and as the temperature declines in the zone of vaporization. The scalloped shape of the early part of Figure 4 is caused by the finite distance between nodes. When all the liquid water in the vapor-dominated region has vaporized (at about $4 \times 10^6$ sec), further decline in discharge will depend upon the temperature of the liquid-vapor interface and the distance of the interface from the producing node. These quantities determine the pressure gradient in the reservoir.

As little is known about the phenomenon of boiling in liquid-saturated parts of vapor-dominated systems, it is difficult to determine just how the discharge will continue to decline. If the temperature were to remain constant and location of the interface fixed, it is clear that the discharge rate would be constant. Constant temperature at the interface is unlikely, however, because of boiling within a

zone immediately below the interface. Temperature reduction due to vaporization will result in a decline in vapor pressure, and consequently a decline in discharge. The temperature decline depends upon the thickness of the boiling zone. Figure 4 shows cases of how the discharge would decline if boiling should occur throughout a 500 m depth (curve A) or thoroughout a 100 m depth (curve B). The rate, $V_f$ at which liquid must move to replace that lost by vaporization is easily calculated using the continuity of mass at the interface,

$$V_f = \rho_v \frac{v}{\rho_\ell} \qquad (8)$$

At $7 \times 10^6$ sec, this rate is about 0.001 cm/s using the date for curve B

More computation is required in the constant pressure case than in the constant discharge case. A time step of 10,000 seconds yields sufficiently accurate results. 700 time steps with a minimum of 10 iterations per time step, requires 110 seconds of computation time on an IBM 370/168 computer.



## DISCUSSION AND CONCLUSIONS

It is possible to use the results of the previous section in a qualitative way to give insight into the behavior of vapor-dominated systems, or for that matter, liquid-dominated systems that, upon development, have converted to steam systems. Within a time frame short enough that heat conduction effects are negligible, most realistic combinations of pertinent parameters (see Table 2) would give results similar to those shown in Figures 3 and 4; only the magnitude of the numbers would change. Reducing intrinsic permeability, for example, by a factor of 10 lengthens the time required to obtain saturation, pressure and temperature distributions similar to Figure 3 by a factor of 10. Reducing initial liquid-water saturation causes a more rapid decline in discharge than shown in Figure 4.

Comparisons of saturation distributions and temperature distributions in Figures 2 and 3 show that temperature changes are primarily a function of the amount of varporization that has occurred at any particular location. If the initial liquid-water saturation is variably distributed, regions in the reservoir that have the highest water contents will attain the lowest temperatures as boiling goes on. This is especially important at the surface of the hypothesized deep "water table" where reduced temperatures result in reduced vapor pressures and consequently reduced well discharge (Figure 4).

vertical movement of the liquid-vapor interface will alter the discharge-versus-time relationship. As the model described in this report does not consider movement in the liquid-saturated zone it can not predict changes in position of the interface. It is likely that movement either up or down will cause the interface to move into zones of higher temperature not yet cooled greatly by vaporization. This will result in the maintenance of high discharge rates and will help to uniformly extract energy from the rock.

The temperature of produced steam, as used in this report, is the temperature of the production node. No account is taken of pressure and temperature changes of the steam in transit up the well bore. The temperature difference between the pre-production temperature and the steam temperature when superheating starts, gives an indication of the original liquid-water content of the reservoir, at least in the vicinity of the well.

Continued temperature reduction of the produced steam, after it becomes superheated, is due primarily to adiabatic cooling of the expanding steam. This quantity, which is significant in Figure 3d, has generally been assumed to be negligible by modelers of two-phase systems (Mercer and Faust, 1975; Faust 1976; Toronyi, 1974; Brownell, and others, 1975; Weinstein, and others, 1974). This assumption is probably valid for the cases studied by these investigators as long as the system does not become superheated.

As time goes on and production declines, pressure gradients become small, and conductive transport of heat becomes important. Steam produced from several wells in the Larderello field has been observed



to have an increasing temperature over the years (Sestini, 1970 and Ferrara, and others, 1970). When corrections are made for energy losses during fluid transit up the well bore, the temperature of the fluid at the well bottom can be either increasing, decreasing, or constant with time (Mathenson, 1975b). These differences can be explained by the location of the well bottom within the reservoir and the amount of liquid water originally in the vicinity of the well bottom. Increasing temperatures can be explained by heat conduction from overlying impermeable rocks which have not been cooled by vaporization. The closer the well bottom to the overlying rocks, the more rapid the temperature rise. This provides an alternative to the explanation given by Truesdell and White (1973), where increasing temperatures are attributed to boiling from greater depths and from more concentrated brines; and, in addition, could account for the reduction of this temperature increase (Sestini, 1970) as heat in the overlying rocks is depleted.

It is of interest to consider what goes on at and below the liquid-vapor interface as boiling occurs there. Cooling due to vaporization at a stationary interface causes a pressure reduction. Consequently, liquid in the saturated zone below the interface may become superheated. It is unlikely that convection in this zone could be rapid enough to provide uniform cooling, hence it is possible that flashing may be initiated below the interface. If this actually happens, it may explain the occasional explosive-type microearthquakes which are observed (C. Bufe, personal communication, 1976) below zones of production at The Geysers.

In future studies, it is planned to incorporate conditions in the model that will allow long-term effects to be studied. The computer runs shown in Figures 3 and 4 show the reservoir to be essentially depeleted in a few months. This is too short for conductive effects to be important with 100 m spacing between nodes. Under the specified conditions, lower permeability and a higher porosity would result in a longer-lasting reservoir. The model will also be modified to allow for conduction with the cap rock as this will have a bearing upon the temperature of the produced steam.

The sudden initial reduction in pressure at the production node is a rather severe condition. This approximation can be refined by using a constant or variable discharge initially, until all the liquid in the production node is vaporized, followed by the constant-pressure condition.



Within the limitations imposed by a one-dimensional model and the assumptions involved, the "well-bottom" production characteristics of vapor-dominated geothermal systems that can be explained with this model include: 1) temperature and pressure changes when steam is produced at constant or variable discharge; 2) temperature and discharge-versus-time variations when steam is produced at constant pressure; and 3) existence of superheated steam. The relationships concerned with discharge provide a means for estimating reservoir life and potential yield.

Agreement in the liquid-water saturation distributions obtained by various investigators helps to validate the different numerical and mathematical approaches. In addition, under the assumption of negligible capillary effects, this agreement suggests that liquid movement due to pressure gradients can be ignored in rock with relatively low liquid-water saturation. Results obtained with this model also indicate that the effect of compressible work in the energy balance may be significant when steam is superheated.

## ACKNOWLEDGEMENTS

Appreciation is extended to the author's colleagues: William Herkelrath, Akio Ogata, Michael Sorey and Manuel Nathenson for the many profitable discussions pertaining to vapor-dominated geothermal systems and comments on the manuscript.



## REFERENCES

Bird, R.B., Stewart, W.E., and Lightfoot, E.N., 1960, Transport phenomena: John Wiley and Sons, Inc., New York.

Boulton, R.S., 1970, The behavior of the Wairakei geothermal field during exploitation: Geothermics Special Issue 2, v. 2, pt. 2, p. 1426-1439.

Brownell, D.H., Jr., Garg, S.K., and Pritchett, J.W., 1975, Computer simulation of geothermal reservoirs: Paper SPE 5381 presented at the 45th Annual California Regional Meeting of the Society of Petroleum Engineers of AIME, Ventura, Calif., Apr. 2-4.

Brigham, W.E., and Morrow, W.B., 1974, P/Z behavior for geothermal steam reservoirs: Paper SPE 4899 presented at 44th Annual California Regional Meeting of the Society of Petroleum Engineers of AIME, San Francisco, Calif., Apr. 4-5.

Corey, A.T., 1954, The interrelation between gas and oil relative permeabilities: Producers Monthly, v. 19, p. 38-41.

Dorsey, N.E., 1968, Properties of ordinary water-substance: (facsimile of the 1940 edition) Hafner Publishing Co., New York, 673 pp.

Faust, C.R., 1976, Numerical simulation of fluid flow and energy transport in liquid- and vapor-dominated hydrothermal systems: Ph.D. thesis, Pennsylvania State University, University Park, Pa.

Ferrara, G.C., Panichi, C., and Stefani, G., 1970, Remarks on the geothermal phenomenon in an intensively exploited field. Results of an experimental well: Geothermics Special Issue 2, v. 2, pt. 1, p. 578-586.

Garg, S.K., Pritchett, J.W., and Brownell, D.H., Jr., 1975, Transport of mass and energy in porous media: Proceedings of the Second United Nations Symposium on the Development and Use of Geothermal Resources, San Francisco, Calif., May 19-29 (in press).

Keenan, J. nd Keyes, F.G., 1936, Thermodynamic properties of steam: John Wiley and Sons, New York.

Lasseter, T.J., Witherspoon, P.A., and Lippman, M. J., 1975, Numerical simulation of heat and mass transfer in multi-dimensional two-phase geothermal reservoirs (abs): *in* Second United Nations Symposium on the Development and Use of Geothermal Resources, San Francisco, Calif., May 19-29.

Mercer, J.W., and Faust, C.R., 1975, Simulation of water- and vapor-dominated hydrothermal reservoirs: Paper SPE 5520 presented at the 50th Annual Fall Meeting of the Society of Petroleum Engineers of AIME, Dallas, Texas, Sept. 28- Oct. 1.

Nathenson, M., 1975a, Physical factors determining the fraction of stored energy recoverable from hydrothermal convection systems and conduction-dominated areas: U.S. Geological Survey, open-file report, 75-525.

_____, 1975b, Some reservoir engineering calculations for the vapor-dominated system at Larderello, Italy: U.S. Geological Survey, open-file report, 75-142.

Rosenberg, D.U., von, 1969, Methods for the numerical solution of partial differential equations: American Elsevier Publishing Co., Inc., New York, 128 pp.

Sestini, G., 1970, Superheating of geothermal steam: Geothermics Special Issue 2, v. 2, pt. 1, p. 622-648.

Toronyi, R.M., 1974, Two-phase, two-dimensional simulation of a geothermal reservoir and the wellbore system: Ph. D. thesis, Pennsylvania State University, University Park, Pa.

Truesdell, A.H., and White, D.E., 1973, Production of superheated steam from vapor-dominated geothermal reservoirs: Geothermics, v. 2, no. 3, p. 154-175.

Urban, T.C., Jamieson, T.M., Diment, W.H., and Sass, J.H., 1975, Heat-flow at the Geysers, California (abs): *in* Second United Nations Symposium on the Development and Use of Geothermal Resources, San Francisco, Calif., May 19-20.



Weinstein, H.G., Wheeler, J.A., and Woods, E.G., 1974, Numerical model for steam simulation: Paper SPE 4759 presented at the Society of Petroleum Engineers - AIME Improved Oil Recovery Symposium, Tulsa, Okla., Apr. 22-24.

White, D.E., Muffler, L.J.P., and Truesdell, A.H. 1971, Vapor-dominated, hydrothermal systems compared with hot-water systems: Econ. Geology, v. 66, p. 75-97.

## APPENDIX

A. Equation of state for pure steam published by Keyes, Smith and Gerry in 1935 (see Dorsey, 1940, p. 78):

$$\frac{1}{\rho_v} = \frac{4.55504\ T}{P} + B$$

Where B represents the departure from an ideal gas.

$$B = B_o + B_o^2 g_1 \frac{P}{T} + B_o^4 g_2 \left(\frac{P}{T}\right)^3 - B_o^{13} g_3 \left(\frac{P}{T}\right)^{12}$$

$$B_o = 1.89 - 2641.62 \left(\frac{1}{T}\right) 10^A$$

$$A = \frac{80870}{T^2}$$

$$g_1 = \frac{82.546}{T} - \frac{1.6246 \times 10^5}{T^2}$$

$$g_2 = 0.21828 - \frac{1.2697 \times 10^5}{T^2}$$

$$g_3 = 3.635 \times 10^{-4} - \frac{6.768 \times 10^{64}}{T^{24}}$$

The units of density, $\rho_v$, are $g/cm^3$, the units of temperature, T, are degrees Kelvin and the units of pressure, P, are atmospheres (one atmosphere = $1.01325 \times 10^6$ dynes/$cm^2$).

B. Saturated vapor pressure for pure steam published by Osborne and Meyer in 1934 (see Dorsey, 1940, p. 574):

$$\text{Log}_{10} P = A + \frac{B}{T} + C \frac{x}{T} \left(10^{Dx^2} - 1\right) + E\ 10^{Fy^{5/4}}$$

A = 5.4266514

B = -2005.1

$C = 1.3869 \times 10^{-4}$

$D = 1.1965 \times 10^{-11}$



E = -0.0044

F = -0.0057148

$x = T^2 - 293700.$

$y = 647.27 - T$

The units of temperature, T, are degrees Kelvin and the units of pressure, P, are atmospheres.

C. The latent heat of vaporization, L, for pure steam is obtained using polynomial approximations for the enthalpies of saturated steam, $h_v$, and liquid water, $h_l$ (Mercer and Faust, 1975). These approximations are valid for a pressure range of 1 to 175 bars.

$$L = h_v - h_l$$

$$h_v = A_1\ 10^7$$

$$h_l = A_2\ 10^7$$

$$A_1 = 2822.82 - 39.952/PP + 2.54342/PP^2 - 0.938879\ PP^2$$

$$A_2 = 809.674 + 94.4665\ PP - 4.50247\ PP^2 + 0.120265\ PP^3 - 162.7/PP + 29.8163/PP^2 - 1.72623/PP^3$$

Where $PP = P\ 10^{-7}$ and the units of pressure, P, are dynes/$cm^2$ and the units of enthalpy are ergs/g.

The relative permeability to steam is a modification of an equation given by Corey (1954):

$$k_r = (1-S)^2\ (1-S^2)$$

E. The dynamic viscosity for pure steam is given by Keenan and Keyes (1936):

$$\mu_v = \frac{A\,T^{1.5}}{T + B}$$

$A = 1.501 \times 10^{-5}$

$B = 446.8$

The units of temperature are degrees Kelvin and the units of viscosity are poisies.



Table 1.--Quantities used for constant discharge results.

| Parameters: | Symbols | Value |
|---|---|---|
| porosity | $\phi$ | 0.05 |
| permeability | k | $1 \times 10^{-8}$ cm$^2$ |
| thermal conductivity | K | $4.1 \times 10^{-3}$ cal/(cm $^{o}$C s) |
| rock density | $\rho_r$ | 2.56 g/cm$^3$ |
| rock specific heat | $c_{pr}$ | 0.23 (cal/g)/$^{o}$C |
| liquid specific heat | $c_{p\ell}$ | 1.06 (cal/g)/$^{o}$C |
| vapor specific heat | $c_{pv}$ | 0.6 (cal/g)/$^{o}$C |
| liquid density | $\rho_\ell$ | 0.79 g/cm$^3$ |
| nodal spacing | $\Delta z$ | 3048 cm |
| nodal volume | | $1.7 \times 10^{11}$ cm$^3$ |
| number of nodes | | 6 |
| discharge rate | q | $2.52 \times 10^4$ g/s |
| Initial Conditions: | | |
| temperature | T | 257.3$^{o}$C |
| pressure | P | 44.9 bars |
| saturation | S | 0.2 |

Table 2.--Quantities used for constant pressure results.

| Parameters: | Symbol | Value |
|---|---|---|
| porosity | $\phi$ | 0.05 |
| permeability | k | $1 \times 10^{-8}$ cm$^2$ |
| thermal conductivity | K | $4 \times 10^{-3}$ cal/(cm °C s) |
| rock density | $\rho_r$ | 2.3 g/cm$^3$ |
| rock specific heat | $c_{pr}$ | 0.23 (cal/g)/°C |
| liquid specific heat | $c_{pl}$ | 1.06 (cal/g)/°C |
| vapor specific heat | $c_{pv}$ | 0.6(cal/g)/°C |
| liquid density | $\rho_l$ | 0.82 g/cm$^3$ |
| nodal spacing | $\Delta z$ | $1 \times 10^4$ cm |
| number of nodes | | 10 |
| well bottom pressure | $P_w$ | 10 bars |
| Initial Conditions: | | |
| temperature | T | 233.83 °C |
| pressure | P | 30 bars |
| liquid water saturation | S | 0.2 |



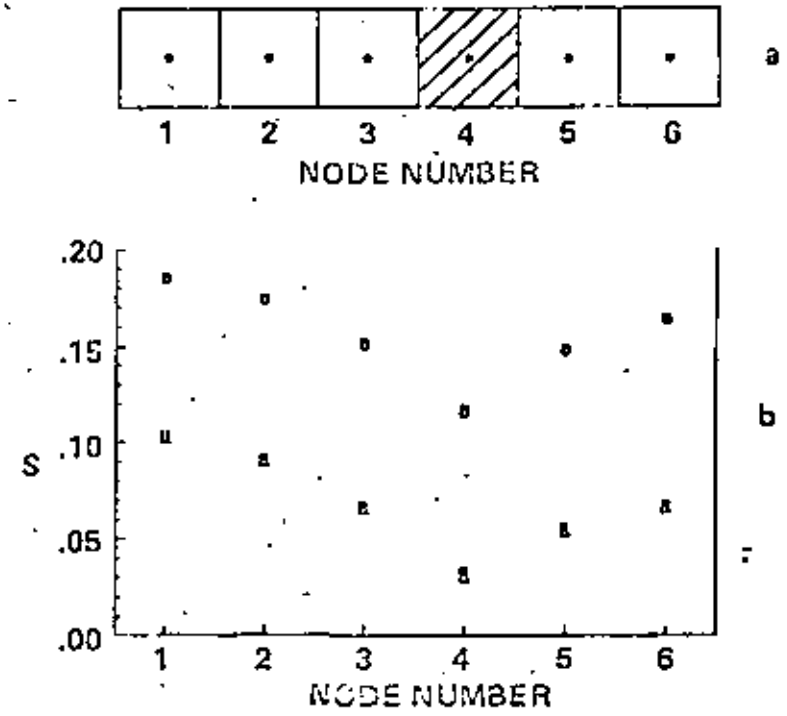


Figure 1.--Nodal configuration(a) and saturation distribution due to constant discharge from node 4(b).

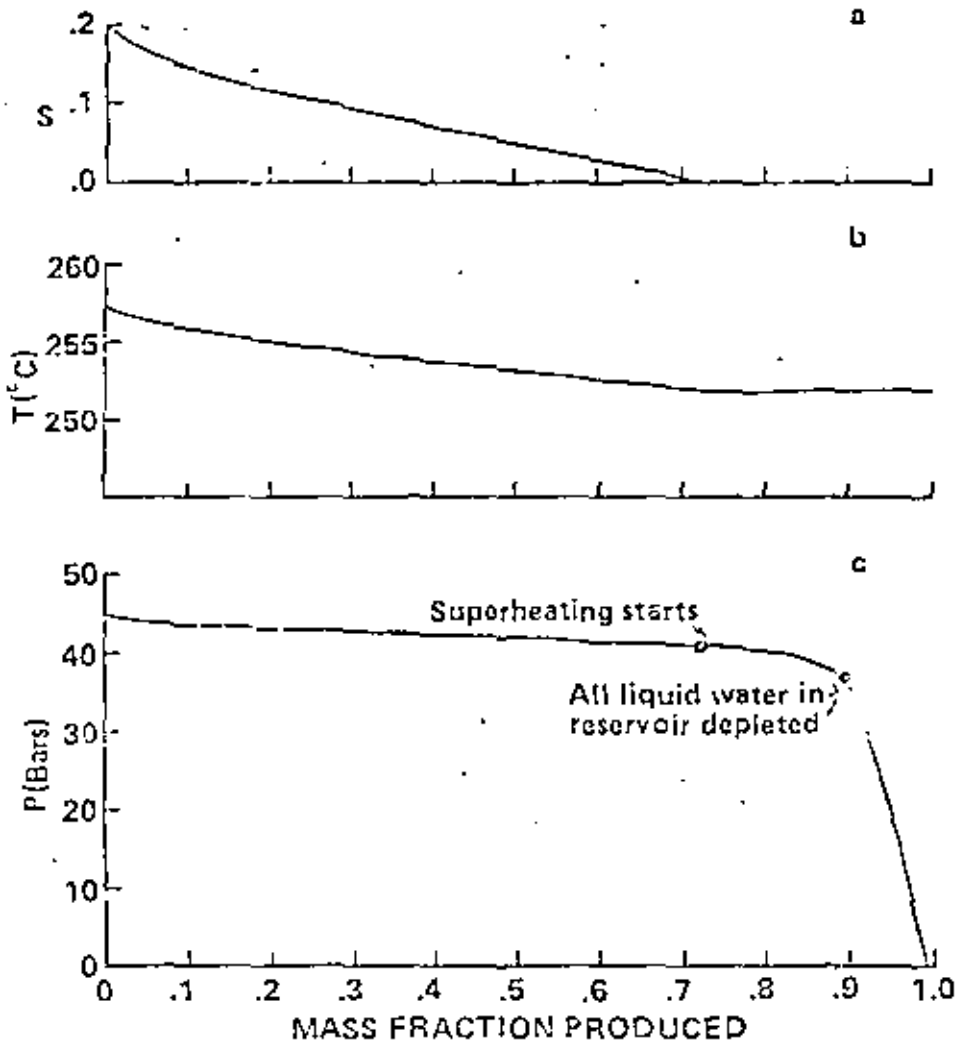


Figure 2.--Saturation (a), temperature (b), and pressure (c) at the discharge node of Figure 1 as a function of mass fraction produced.

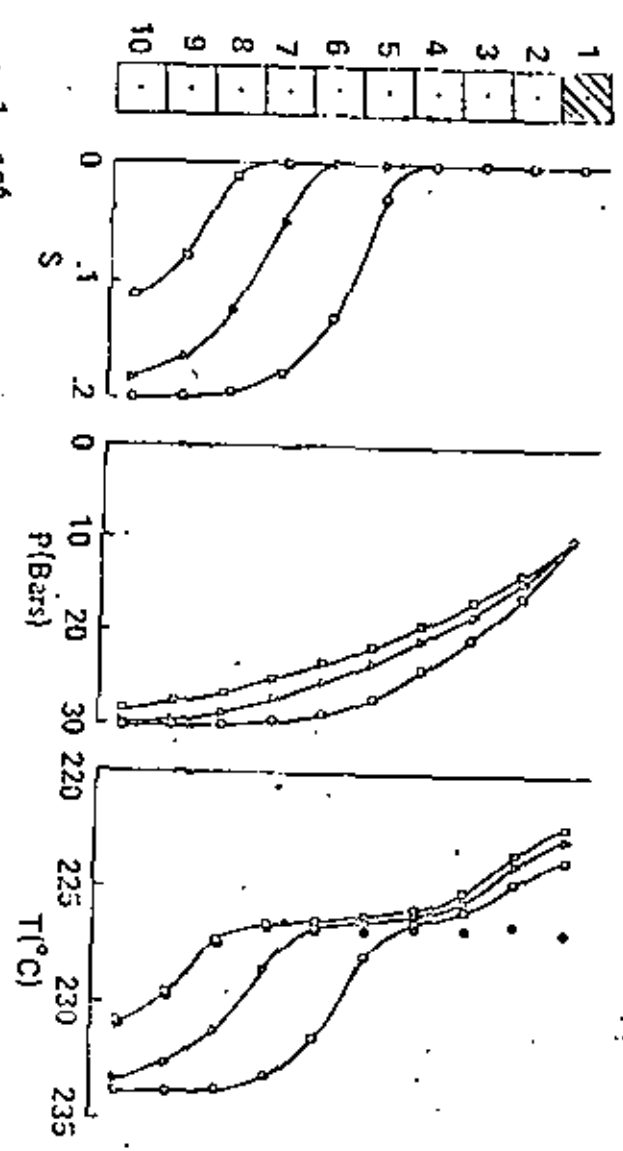


Figure 3.--Nodal configuration (a) and saturation (b), pressure (c), and temperature (d) distributions due to fluid withdrawal from node 1 at constant pressure.

- ∘ $1 \times 10^6$ sec
- ▲ $2 \times 10^6$ sec
- ○ $3 \times 10^6$ sec
- • $3 \times 10^6$ sec neglecting compressible work

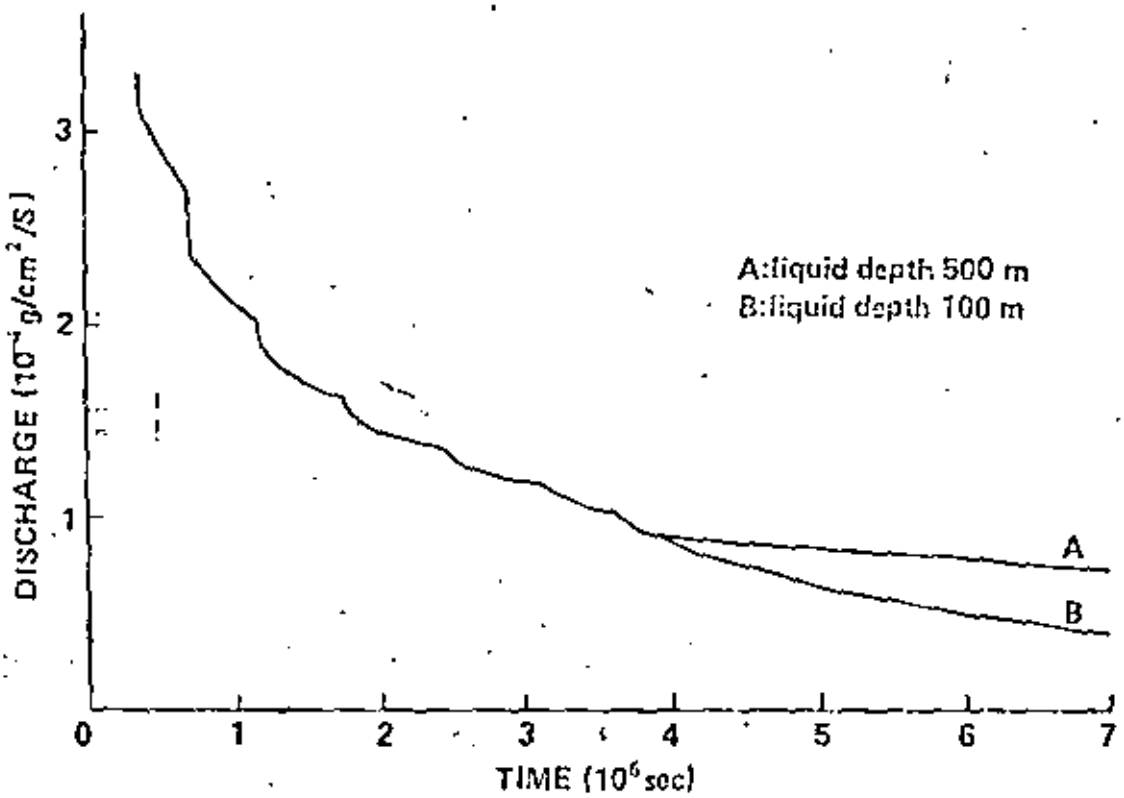


Figure 4.--Discharge-versus-time relation due to fluid withdrawal from the discharge node of Figure 3 at constant pressure.

Publication n°121 of the International Association of Hydrological Sciences
Proceedings of the Anaheim Symposium, December 1976

LBL 4462

# NUMERICAL SIMULATION OF RESERVOIR COMPACTION IN LIQUID DOMINATED GEOTHERMAL SYSTEMS

Marcelo J. Lippmann, T. N. Narasimhan and P. A. Witherspoon
Lawrence Berkeley Laboratory
University of California
Berkeley, California 94720

## Abstract

Recently much attention has been focused on the development of geothermal systems. A large number of geothermal fields are of the hot water type, dominated by circulating liquid that transfers most of the heat and largely controls subsurface pressures. During the exploitation of such systems, a reduction of pressures is inevitable which, in some areas may lead to land subsidence.

A numerical model is introduced which simulates the effects of fluid production as well as reinjection on the vertical deformation of water dominated geothermal reservoirs. This program, based on an Integrated Finite Difference technique and Terzaghi's one-dimensional consolidation model, computes the transport of heat and water through porous media, and resulting pore volume changes. Examples are presented to show the effects of reservoir heterogeneities on the compaction of these hot water systems, as well as the effects of different production-injection schemes. The use of isothermal models to simulate the deformation of non-isothermal systems is also investigated.

## Introduction

The production of fluids from geothermal systems may result in ground surface displacements due to the lowering of pressures in the reservoir and surrounding rocks. These displacements may not only affect installations directly related to the geothermal field (e.g., well casings, steam transmission lines, power plant) but also nearby roads, buildings, and irrigation canals. Therefore it is important to foresee the magnitude and location of the so-called "subsidence bowl" as soon as adequate data on the geologic structure, stratigraphy, rock properties, and proposed development program become available. A number of models to simulate the vertical and horizontal ground deformations in geothermal systems have been or are being developed. These are reviewed in another paper presented at this meeting (Finnemore and Gillam, 1976).

Here, we introduce a mathematical model to simulate the transport of heat and water through a porous geothermal system, including the vertical deformations produced by effective stress changes. This code named "CCC" (for Conduction-Convection-Consolidation) is restricted to one-phase water dominated geothermal fields. At the present time, these systems have the largest potential for developing geothermal energy for electrical and non-electrical uses. They are characterized by circulating liquid that transfers most of the heat and largely controls subsurface pressures (Renner, et al., 1975).

A number of examples are presented below to illustrate some of the capabilities of our computer program. We shall demonstrate the effect of geologic heterogeneities on the behavior of the geothermal system as well as the effect of the location of production and injection wells. A comparison of results will also be made when the system is analyzed under isothermal and non-isothermal conditions.

## Method and Governing Equations

Program CCC is based on the numerical models SCHAFF (Sorey, 1975) for

mass and heat transport through saturated porous media, and TRUST (Narasimhan, 1975) for one-dimensional isothermal consolidation. The code can simulate one, two or three-dimensional, heterogeneous, isotropic, non-isothermal systems. Deformation parameters may be non-linear and non-elastic; the thermal and hydraulic properties can be temperature and/or pressure dependent.

An integrated finite difference method (Narasimhan and Witherspoon, 1976) is used to solve the energy and fluid flow equations. In integral form the flow equation for a slightly compressible fluid (e.g., water) is given by:

$$\frac{\partial}{\partial t}\int_V \frac{\rho}{1+e}\left(e\kappa + \frac{de}{d\sigma'}\right) P\,dV = \int_S \frac{k\rho}{\mu}\left(\nabla P - \rho\vec{g}\right)\cdot\hat{n}\,dS + \int_V Q\,dV \qquad (1)$$

and the energy equation is given by:

$$\left(\frac{\partial}{\partial t}\int_V (\rho c)_M T\,dV = \int_S K_M \nabla T\cdot\hat{n}\,dS - \int_S \rho c_p \delta T \vec{v}_d\cdot\hat{n}\,dS + \int_V q\,dV \qquad (2)$$

where, t is time, $\rho$ fluid density, e void ratio, $\kappa$ fluid compressibility, $\sigma'$ effective stress, P pore pressure, V volume, k intrinsic permeability, $\mu$ viscosity, $\vec{g}$ gravitational acceleration, $\hat{n}$ outward unit normal on surface S, Q mass injection rate per unit volume, $(\rho c)_M$ heat capacity per unit volume of the solid-fluid mixture, $K_M$ thermal conductivity of the solid-fluid mixture, $c_p$ fluid specific heat capacity at constant volume, $\delta T$ difference between the mean temperature within the volume element and that on the surface element dS, $\vec{v}_d$ Darcy velocity, and q heat injection rate per unit volume. Details of the method used to solve these equations are given by Sorey (1975) and Narasimhan (1975), and will not be repeated here.

Concurrent with the mass and energy flow, the vertical deformation of the geothermal system is simulated based on the one-dimensional consolidation theory of Terzaghi. The void ratio at each nodal point is computed by using "e-log $\sigma'$" curves (Figure 1). According to the preconsolidation and effective stresses at the point, the program calculates the void ratio by using either the virgin curve (of slope $C_c$) or swelling-recompression curves (of slope $C_s$). The model neglects the hysteresis between swelling and recompression curves. While the pore volume changes with effective stress, the solid volume is defined to remain constant; the thermal expansion of the rock skeleton is not considered. Because of

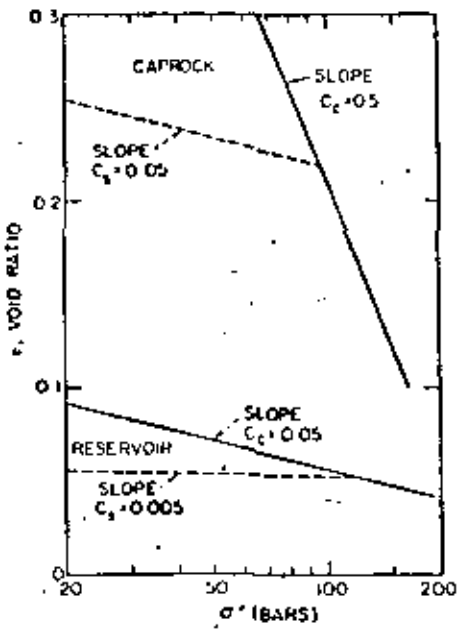


Figure 1. Plot of void ratio (e) versus effective stress ($\sigma'$) for caprock and reservoir of example 4.

the one-dimensional nature of the consolidation model the pore volume changes caused by void ratio changes are directly reflected in a vertical deformation of the individual volumetric nodes.

The deformations computed by this model are restricted to those of the reservoir and neighboring saturated formations which release water from storage to partly or wholly compensate for the fluid withdrawn. These vertical displacements may or may not be directly expressed at the ground surface. The external loading of the overburden, caused by the vertical deformation of the deeper geothermal system, may result in displacements at the surface that may be different in magnitude and direction. Future versions of this model will include the computation of vertical and horizontal displacements at the ground surface itself.

The flow and energy equations (1) and (2) are interconnected by (a) the second order equation of state for the fluid,

$$\rho = \rho_0[1 - \beta(T-T_0) - \gamma(T-T_0)^2] \quad (3)$$

where, $\beta$ and $\gamma$ are coefficients of thermal expansion, and $\rho_0$ and $T_0$ are the reference density and temperature, respectively, for the fluid, (b) the Darcy velocity used in the convection term of the energy equation, and (c) the temperature and/or pressure dependence of certain parameters.

Because these interrelations, equations 1 and 2 are solved alternatively by interlacing their solutions in time; this is shown schematically on Figure 2. The flow equation solves for P, $\vec{v}_f$ and e assuming that the temperature dependent properties of the fluid and rock remain constant. Then, the energy equation is used to obtain T assuming that $\vec{v}_f$ and pressure dependent properties remain constant. Since the temperature varies much more slowly than the pressure, much smaller time steps have to be taken in the flow cycles than in the energy cycles (Figure 2) in order to compute pressure variations accurately.

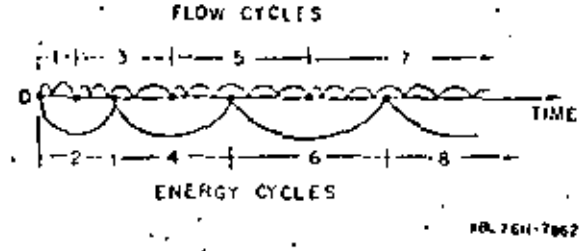


Figure 2. Interlacing of flow and energy calculations

Examples and Results

Four examples are presented below. In all cases it is assumed that, (a) the systems are normally consolidated (i.e., initial effective stresses and preconsolidation stresses are equal), (b) total stresses do not change in time, and (c) the intrinsic permeability (k), thermal conductivity ($K_R$), and heat capacity of the rock ($c_R$), as well as the compressibility ($\alpha$) and coefficients of thermal expansion ($\beta$,$\gamma$) of the water are constant. These assumptions are made to simplify the examples presented here, although the program can consider more complex conditions and relationships. The fluid density ($\rho$), heat capacity ($c_f$) and viscosity ($\mu$) are temperature dependent, while the void ratio (e) is dependent on pore pressure and previous stress history.

Example 1. System with caprock of variable thickness

This case shows a totally penetrating well placed at the center of an axisymmetric system which has a caprock of variable thickness. The well withdraws $2.8 \times 10^6$ kg/day of water uniformly along the thickness of the reservoir. Figure 3 shows the dimensions, boundary conditions and initial temperature distribution for this system. At $t = 0$, only heat conduction occurs between the boundaries, since the Rayleigh number (Ra) in the reservoir is less than 20. This dimensionless number is equal to the ratio between the buoyant and viscous forces acting in the reservoir, and at this low Ra, free convection is not expected to occur.

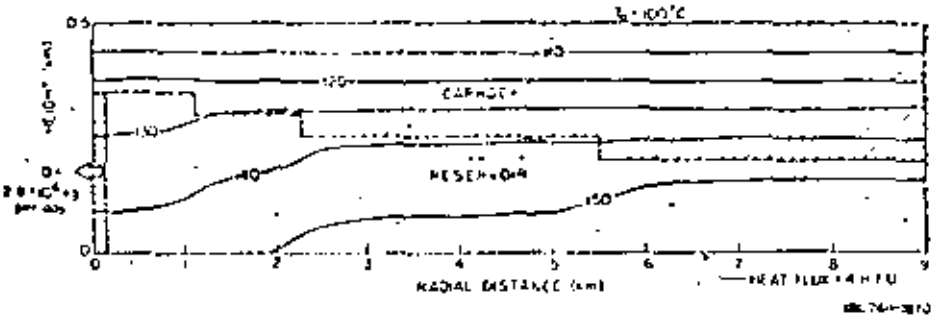


Figure 3. Example 1. Geometry, initial temperature and boundary conditions

The shape of the initial isotherms reflects the non-uniform thicknesses of materials of different thermal conductivities under the prevailing boundary conditions. The lower boundary is impermeable with a constant influx of $4 \times 10^{-6}$ cal cm$^{-2}$ sec$^{-1}$ (1 H.F.U.). The upper boundary is isothermal (100°C) and impermeable. The outer radial boundary is closed both to heat and fluid flow. The overburden (not shown) is 1000 m thick and its average density is 2.5 g.cm$^{-3}$. The rock and fluid properties used in this example are given in Tables 1 and 2.

When production starts, water in the reservoir flows essentially radially towards the well and vertically downward in the caprock. The resulting consolidation after 2400 days is shown on Figure 4. Near the well a maximum compaction of 29.2 cm was determined, of which about 70% occurred in the caprock.

The same system was also investigated under isothermal

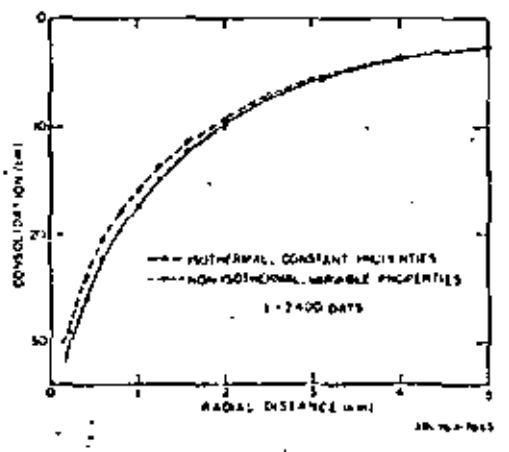


Figure 4. Example 1. Consolidation versus distance under isothermal and non-isothermal conditions.

Table 1. Material properties of rocks used in examples 1 to 3

| | Caprock | Reservoir |
|---|---|---|
| Thermal conductivity ($K_H$) (mcal $cm^{-1}$ $sec^{-1}$ $°C^{-1}$) | 2.52 | 6.64 |
| Rock heat capacity ($c_R$) (cal $g^{-1}$ $°C^{-1}$) | 0.222 | 0.232 |
| Rock density ($\rho_R$) (g $cm^{-3}$) | 2.70 | 2.65 |
| Intrinsic permeability (k) ($cm^2$) | $1 \times 10^{-12}$ | $5 \times 10^{-10}$ |
| Reference void ratio ($e_o$) | 0.250 | 0.053 |
| Reference effective stress ($\sigma'_o$) (bars) | 185 | 185 |
| Slope of virgin curve ($C_c$) | 0.5 | 0.05 |
| Slope of swelling-recompression curve ($C_s$) | 0.05 | 0.005 |

Table 2. Fluid properties of water used in all examples

| | |
|---|---|
| Compressibility ($\gamma$) | $5.5 \times 10^{-5}$ $bars^{-1}$ |
| Coefficient of thermal expansion ($\beta$) | $3.17 \times 10^{-4}$ $°C^{-1}$ |
| Coefficient of thermal expansion ($\gamma$) | $2.56 \times 10^{-6}$ $°C^{-2}$ |
| Reference temperature ($T_o$) | 25°C |
| Reference density ($\rho_o$) | 0.997 g $cm^{-3}$ |
| Viscosity ($\mu$) and heat capacity ($c_f$) | f(T) for P = 100 bars |

conditions using fluid properties corresponding to 135°C, which is the average temperature for example 1. In this case, the consolidation within 2 km from the well was between 7 and 9% larger than under non-isothermal conditions (Figure 4). The larger computed compaction for the isothermal case is apparently to be attributed to the viscosity effects; in the isothermal system a constant viscosity of 0.284 cp was used, whereas in the non-isothermal case the viscosity varied between 0.202 cp and 0.315 cp across the system.

From this example, we conclude that in order to use an isothermal model to simulate the behavior of a non-isothermal system, periodic adjustments of model properties may have to be made to account for the temperature variations that can occur as the simulation progresses in time.

Example 2. System with low permeability lens in reservoir

The system considered here differs from that of example 1 in that a lens of the same material as the caprock has been incorporated into the reservoir. This lens increases the tortuosity of the flow lines, resulting in more pressure drop near the well and less drop further away. This is shown on Figure 5 where lines of equal pressure reduction at t=2400 days are plotted for examples 1 and 2. The effects of these differences in pore pressure change produce different consolidation patterns as shown on Figure 6. These results indicate that it is possible to have a larger compaction away from the producing well due to a heterogeneity in the

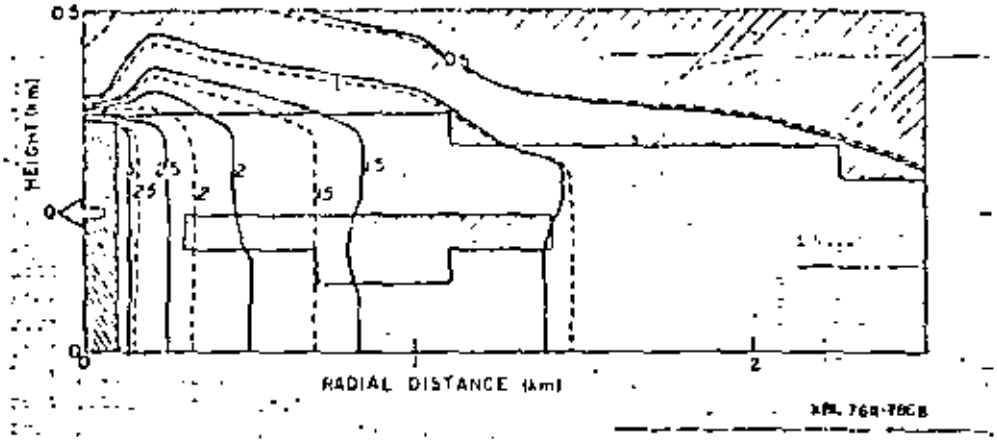


Figure 5. Pore pressure drop, in bars, after 2400 days of water withdrawal. Dashed lines: Example 1 (without lens); Solid lines: Example 2 (with lens).

reservoir. The lens provides a larger volume of more compressible material at locations where large pressure changes are occurring.

This type of heterogeneity in the reservoir could explain why in the Wairakei geothermal field of New Zealand, the maximum ground displacements occur in an area distant from the more intensively developed well field (Stilwell et al., 1976). This idea needs further investigation using three dimensional systems with non-uniform caprocks and differently shaped lenticular structures.

Example 3. System with intercalated layer in reservoir

This example is intended to show that even when all the produced water is reinjected, some amount of compaction cannot be avoided. The geometry, properties, initial and boundary conditions used here are similar to those of example 1. A layer of the same material as the caprock is intercalated in the reservoir as shown in figure 7. The layer might be an aquitard partially dividing the reservoir in two parts. The separation is

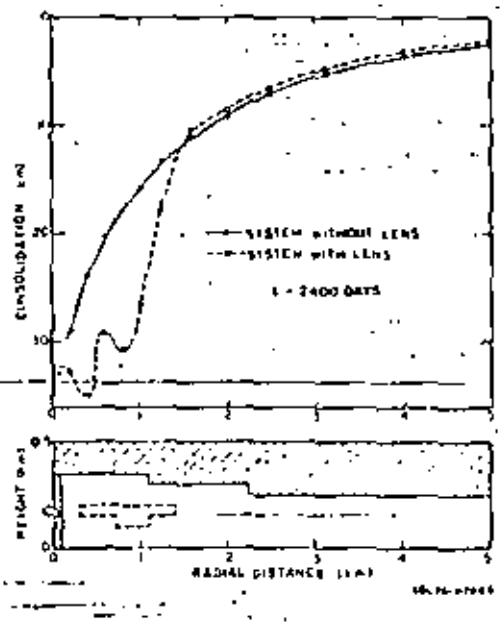


Figure 6. Consolidation versus distance after 2400 days of water withdrawal. Solid lines: Example 1; Dashed lines: Example 2

not complete since the layer only extends radially 1750 m from the well. A production rate of $1.2 \times 10^6$ kg/day of hot water is maintained from the upper 150 m of the reservoir. The same mass is reinjected into the lower 100 m of the reservoir, but the temperature of the injected water is only 25°C. The total pressure changes after 15 years of simulation time are shown in Figure 8. Note that pressures decrease in the upper part and increase in the lower part. As shown in Figure 7, the consolidation of the system is restricted to the first 1500 m out from the well. Negligible effects occurred beyond this distance from the well which agrees with the location of the curve for zero pressure change (see Figure 8). The development of consolidation with time is depicted on Figure 7. At the beginning, the compaction rate of the system is significant, but it falls off rapidly with time.

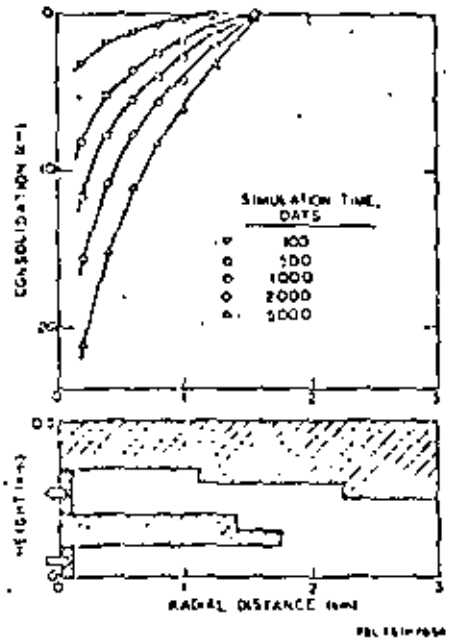


Figure 7. Example 3. Geometry and consolidation versus time and distance.

Because of the injection of colder waters, the lower part of the reservoir slowly cools. After 15 years, the thermal front separating the colder and warmer waters is located at a radial distance of about 175 m from the well. The hydrodynamic front, indicating the position of the reinjected water which largely has been warmed up by the heat stored in the reservoir rock skeleton, has advanced to about 650 m from the well. The approximate location of the hydrodynamic front has been calculated by assuming that the water has flowed only radially away from the injection well. This is only a simplification since some of the water actually has seeped upward through the layer separating the reservoir.

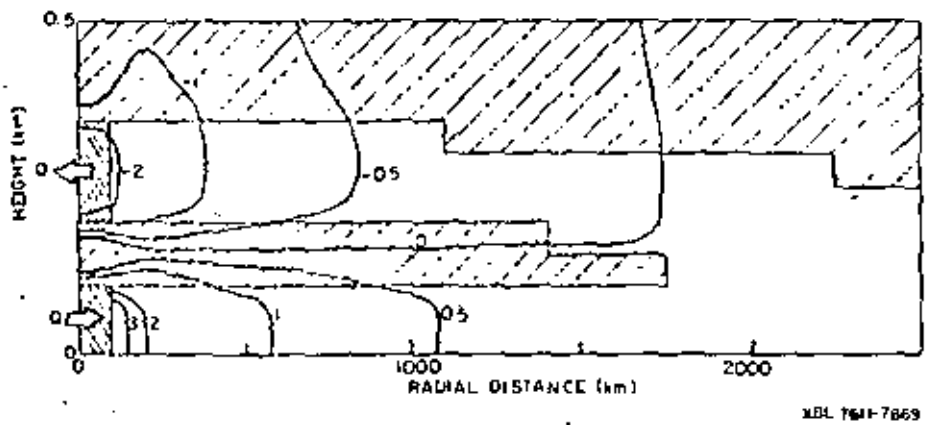


Figure 8. Example 3. Pressure changes, in bars, after 15 years of simulation.

Due to the colder temperature near the well and the higher mass flow rate per unit injectrd area of the well, large increases of pressure occur in the lower part of the reservoir, which are greater in magnitude than the pressure reductions in the upper reservoir. Even under these conditions, a net compaction still occurs around the well. This suggests that it may be necessary to have rates of reinjection that are larger than the production rates in order to minimize the effects of consolidation. Further work along these lines is needed.

Example 4. Convecting system with three layers

This last example is intended to describe the response of a free convecting system to two different production and reinjection schemes. The system is a parallelepiped 550 m high, 750 m wide and 50 m deep and contains three different layers (Figure 9). The caprock and reservoir are deformable, their "e-log σ'" curves are given in Figure 1, but the baserock is incompressible. Tables 2 and 3 list the fluid and material properties used in this example. Because of the large temperature difference between the top and bottom boundaries (260°C), the heat flow across this system is much larger than in the previous cases. It is approximately 37 H.F.U. The Rayleigh number for the reservoir is about 93, which exceeds the critical Ra = 40. Indeed, free convection is established in the reservoir as is shown schematically in Figure 9 by the dashed circles and reflected by the shapes of the isotherms. Two production-injection schemes were considered. In both cases a total of $4 \times 10^4$ kg/day of water were produced and $3.2 \times 10^4$ kg/day of 100°C water were reinjected

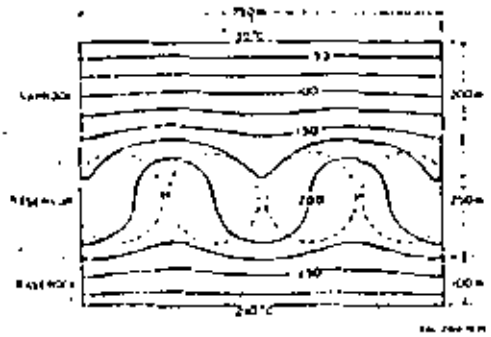

Figure 9. Example 4. Geometry and initial temperature distribution. Dashed circles: Convection cells (schematic representation).

Table 3. Material properties of rocks used in example 4

| | Caprock | Reservoir | Baserock |
|---|---|---|---|
| Thermal conductivity ($K_R$) (meal $cm^{-1}$ $sec^{-1}$ $°C^{-1}$) | 4.98 | 4.98 | 5.53 |
| Rock heat capacity ($c_R$) (cal $g^{-1}$ $°C^{-1}$) | 0.222 | 0.232 | 0.222 |
| Rock density ($\rho_R$) (g $cm^{-3}$) | 2.70 | 2.65 | 2.70 |
| Intrinsic permeability (k) ($cm^2$) | $1 \times 10^{-12}$ | $5 \times 10^{-10}$ | $1 \times 10^{-13}$ |

(80% reinjection). The amount of water involved is rather small, and the rates used in this example were such as to avoid "overpowering" the natural convection cells, each of which transported about 7000 kg/day of water through the system. In the first case (example 4a) water is removed at the top of the ascending columns of convection and injection is at the bottom of the descending columns (Figure 10A). In example 4b water is removed at the bottom of the ascending columns and injection is at the top of the descending columns (Figure 11A). A symmetrical arrangement of sources and sinks was used to retain the symmetry implied by the impermeable side boundaries.

Figures 10B and 11B show the resulting temperature distribution for both cases after 20 years of simulation. A general cooling of the system is observed. There was no significant difference in the amount of consolidation occurring in either case. A difference might possibly be detected after longer period of time because the cooling patterns are not the same in both cases. The consolidation is fairly uniform across the system being slightly larger (2%) over the pumping areas. Figure 12 shows the development of consolidation in time for example 4a. The compaction increases almost linearly with time, and the contribution of the reservoir to the total consolidation is important only at early time. Later, most of the compaction occurs in the caprock. This may be explained by the delayed lowering of pore pressure in the caprock (see Figure 13).

For comparison purposes, example 4a was also modelled as a 175°C isothermal system. Pore pressures, total and preconsolidation stresses were the same. The resulting compaction was 4-6% higher than that of the non-isothermal case. When pressure changes are compared (Figure 14), it is evident that in the isothermal system, the pore pressure decreased more in the upper part of the caprock and less in the lower part as well as in the reservoir.

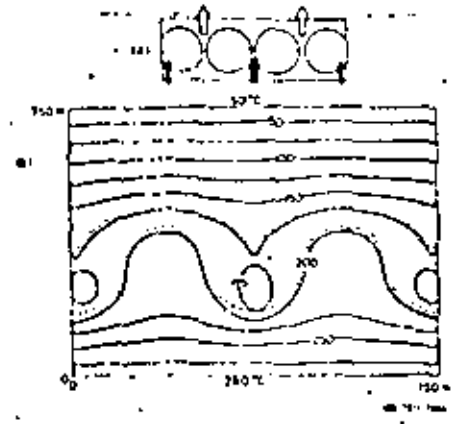

Figure 10. Example 4a. (A) Dark arrows: injection; light arrows: production. (B) Temperature distribution after 20 years of simulation. Dashed lines: initial 175° and 200°C isotherms.

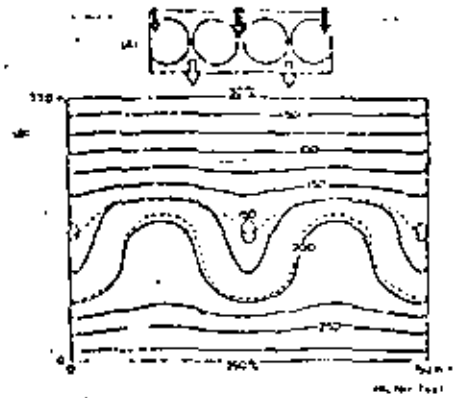

Figure 11. Example 4b. (A) Dark arrows: injection; light arrows: production. (B) Temperature distribution after 20 years of simulation. Dashed lines: initial 175° and 200°C isotherms.

As in example 1, the unequal response to the withdrawal of fluids can be attributed to the viscosity differences in the two cases. In the isothermal system, the viscosity is uniform (0.212 cp), but in the non-isothermal case it varies from 0.150 cp at the bottom of the reservoir, to 0.446 cp at the top of caprock. The differences in the distribution of fluid density in the isothermal and non-isothermal cases will also have similar effects on pressure distribution and compaction as the viscosity variation, but the magnitudes will be smaller relative to viscosity effects.

The final example suggests that compaction of water dominated geothermal fields with large temperature differences and complex fluid patterns will be difficult to model as isothermal systems. This is especially the case if one is interested in the pressure and compaction history at particular parts of the system.

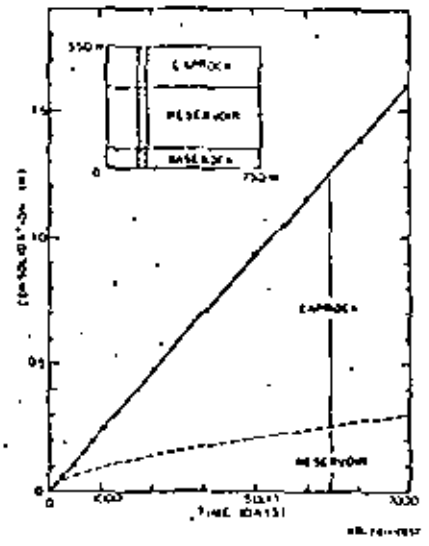

Figure 12. Example 4a. Consolidation versus time (corresonds to the column indicated in the insert).

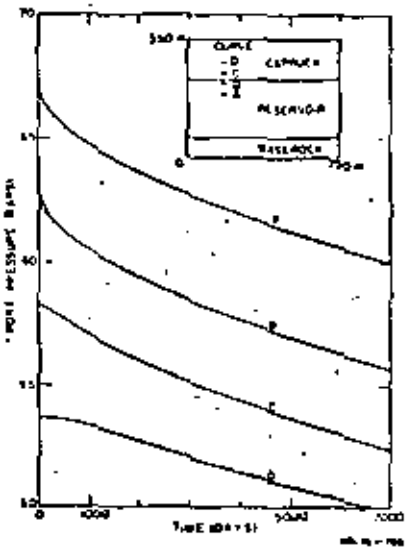

Figure 13. Example 4a. Pore pressure change with time at different points in the caprock and reservoir.

## References


Finnemore, E. J. and M. L. Gillam, 1976. Compaction processes and mathematical models of land subsidence in geothermal areas: Proc. 2nd Int. Symp. Land Subsidence, Anaheim, Ca., Dec. 13-17, 1976.

Narasimhan, T. N., 1975. A unified numerical model for saturated -unsaturated groundwater flow: Ph.D. thesis, Univ. California, Berkeley, 244 p.

Narasimhan, T. N. and P. A. Witherspoon, 1976. An integrated finite difference method for analyzing fluid flow in porous media: Water Resour. Res., 12(1), p. 57-64.

Renner, J. L., D. E. White and D. L. Williams, 1975. Hydrothermal convection systems: U. S. Geol. Survey Circ. 726, p. 5-57.

Sorey, M. L., 1975. Numerical modeling of liquid geothermal systems: Ph.D. thesis, Univ. California, Berkeley, 65 p.

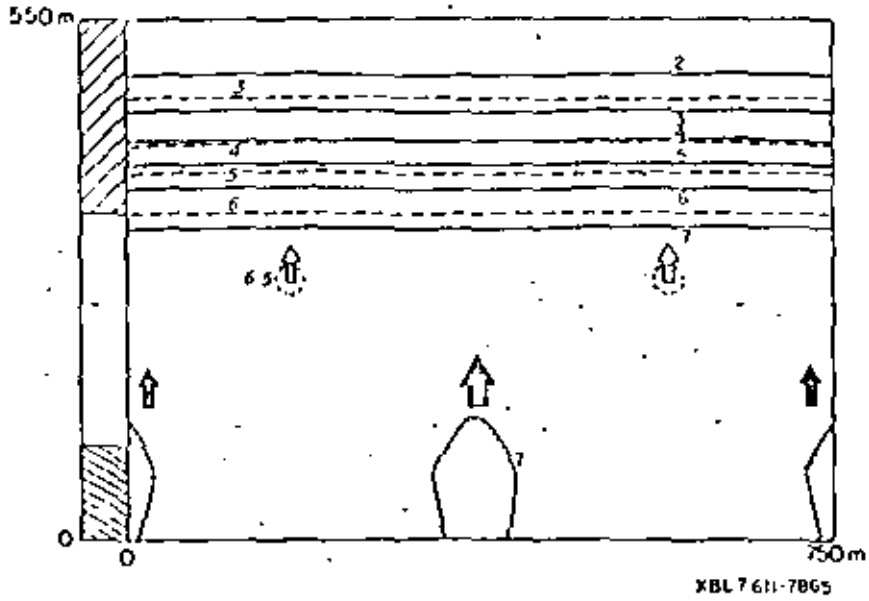


Figure 14. Example 4a. Pressure drop, in bars, after 20 years of simulation. Solid lines: non-isothermal case; Dashed lines: isothermal case; Dark arrows: injection; Light arrows: production (not to scale).

Stilwell, W. B., W. K. Hall and J. Tauhai, 1976. Ground movement in New Zealand geothermal fields: Proc. 2nd U. N. Symp. Development and Use of Geothermal Resources, San Francisco, Ca., May 20-29, 1975, p. 1427-1434.

Acknowledgement

This work was done with support from the U. S. Energy Research and Development Administration.

# Governing Equations for Geothermal Reservoirs

D. H. Bradley, Jr., S. K. Garg, and J. W. Pritchett

*Systems, Science and Software, La Jolla, California 92038*

Balance laws and constitutive relations are developed for convective hydrothermal (liquid water and liquid water-steam) geothermal reservoirs. A fully interactive theory is used to describe rock-fluid interactions involving momentum and energy transfer and the dependence of rock porosity (and permeability) upon the fluid and rock stresses. The viscous stress-strain behavior treatment permits the nonlinear and history-dependent constitutive behavior of the material to be properly taken into account.

## Introduction

In order to study problems characterized by essential alterations in the porous matrix itself, it is necessary to consider fully interacting rock-fluid systems. Particular examples of these problems include the interaction between pore collapse (subsidence) and fluid extraction rates, the reinjection of collapsed pores by condensate injection, and the effects of variations in natural mechanical forces (e.g., overburden stress) on the state of the geothermal system. In these cases there would appear to be significant interactions between the porous matrix and the fluid. Thus it appears necessary to consider the general interaction theories in order to assess the effect of the motion of the matrix on the motion of the fluid and vice versa.

General balance laws and constitutive relations incorporating the various interactions in a solid-fluid mixture have previously been developed by *Morland* [1972] and by *Garg* [1971], *Garg and Nur* [1973], and *Garg et al.* [1975*a*]. For geothermal reservoir applications where fluid velocities are low and times of interest are long, it is possible to simplify considerably the general balance laws. In this paper we will first present the fully interactive equations for a single-phase system and then indicate possible simplifications for single-phase (liquid water) geothermal applications. Extension to two-phase (liquid water and steam) systems is discussed next. This is followed by constitutive relations. The simplified system of governing equations presented herein is similar to the previous formulations of two-phase flow (excluding solid motion) developed by *Donaldson* [1968] and *Mercer et al.* [1974].

## Balance Laws (Single Phase—Liquid Water)

General equations expressing balance of mass, momentum, and energy for a solid-liquid mixture [*Garg*, 1971; *Garg and Nur*, 1973; *Garg et al.*, 1975*a*] are given below.

Solid mass

$$[\partial(1-\phi)\rho_s/\partial t] + \nabla\cdot[(1-\phi)\rho_s\mathbf{v}_s] = 0 \tag{1}$$

Liquid mass

$$(\partial\phi\rho_l/\partial t) + \nabla\cdot(\phi\rho_l\mathbf{v}_l) = 0 \tag{2}$$

Solid momentum

$$(1-\phi)\rho_s[(\partial\mathbf{v}_s/\partial t) + \mathbf{v}_s\cdot\nabla\mathbf{v}_s] = -\nabla(1-\phi)p_s + \nabla\cdot\mathbf{S} + (1-\phi)\rho_s\mathbf{g} + \rho_s\hat{\mathbf{p}} \tag{3}$$

Liquid momentum

$$\phi\rho_l[(\partial\mathbf{v}_l/\partial t) + \mathbf{v}_l\cdot\nabla\mathbf{v}_l] = -\nabla\phi p_l + \phi\rho_l\mathbf{g} - \rho_s\hat{\mathbf{p}} \tag{4}$$

Here $\rho_s\hat{\mathbf{p}}$ is the momentum supply to the solid due to interaction with the liquid [*Garg et al.*, 1975*a*]:

$$\rho_s\hat{\mathbf{p}} = -p_l\nabla\phi + (\phi^2\mu_l/k)(\mathbf{v}_l - \mathbf{v}_s) \tag{5}$$

Some authors (see, for example, *Morland* [1972]) ignore the first term in (5); this is, in general, unjustified. For a complete discussion of this question, reference is made to *Garg* [1971] and *Garg et al.* [1975*a*].

The liquid viscosity $\mu_l$ will, in general, vary with liquid pressure ($p_l$) and temperature ($T_l$):

$$\mu_l = \mu_l(p_l, T_l) \tag{6a}$$

The rock permeability $k$ is a complex function of rock and liquid stresses (see, for example, *Brace* [1972]). For the sake of computational tractability (without perhaps much geologic justification) it is often postulated that this dependence is primarily exhibited through changes in porosity or:

$$k = k(\phi) \tag{6b}$$

To continue with the balance laws,

Solid energy

$$(1-\phi)\rho_s(D_sE_s/Dt) = -(1-\phi)p_s\nabla\cdot\mathbf{v}_s + \mathbf{S}:\nabla\mathbf{v}_s + \rho\hat{\psi}_s - \nabla\cdot\mathbf{q}_s - \nabla\cdot\mathbf{Q} \tag{7}$$

Liquid energy

$$\phi\rho_l(D_lE_l/Dt) = -\phi p_l\nabla\cdot\mathbf{v}_l + \rho\hat{\psi}_l - \nabla\cdot\mathbf{q}_l + \nabla\cdot\mathbf{Q} \tag{8}$$

where $D_i/Dt = \partial/\partial t + \mathbf{v}_i\cdot\nabla$, $i = s, l$.

In (7), $\mathbf{S}:\nabla\mathbf{v}_s$ denotes the scalar product ($S^{ij}v_{s_{i,j}}$) of two second-order tensors $\mathbf{S}$ and $\nabla\mathbf{v}_s$. Here $\rho\hat{\psi}_s$ ($\rho\hat{\psi}_l$) denotes the mechanical interaction energy supply to solid (liquid) [*Garg et al.*, 1975*a*]:

$$\rho\hat{\psi}_s = p_l[(\partial\phi/\partial t) + \mathbf{v}_s\cdot\nabla\phi] \tag{9}$$

$$\rho\hat{\psi}_l = -p_l[(\partial\phi/\partial t) + \mathbf{v}_l\cdot\nabla\phi] + (\phi^2\mu_l/k)\mathbf{v}_l^2 \tag{10}$$

In (7) and (8), $\nabla\cdot\mathbf{Q}$ is the thermal interaction energy supply to the liquid.

## Balance Equations for Passive Reservoir

The balance equations (1)–(10) are quite complex. Fortunately, for geothermal reservoir applications it is possible to simplify these equations. For the sake of simplicity, first consider a passive reservoir ($\mathbf{v}_s = 0$, $\partial\phi/\partial t = 0$, and $\nabla\phi \neq 0$). For such a reservoir the mass and momentum balance equations for the solid are satisfied trivially. The governing system of equations thus reduces to the following:



Paper number 7WR0389.

Liquid mass

$$\phi(\partial\rho_l/\partial t) + \nabla\cdot(\phi\rho_l\mathbf{v}_l) = 0 \qquad (11)$$

Liquid momentum

$$\rho_l[\partial\mathbf{v}_l/\partial t + \mathbf{v}_l\cdot\nabla\mathbf{v}_l] = -\nabla p_l + \rho_l\mathbf{g} - (\phi\mu_l/k)(\mathbf{v}_l) \qquad (12)$$

Solid energy

$$(1-\phi)\rho_s(\partial E_s/\partial t) = -\nabla\cdot\mathbf{q}_s - \nabla\cdot\mathbf{Q} \qquad (13)$$

Liquid energy

$$\phi\rho_l(\partial E_l/\partial t) = -\rho_l\nabla\cdot(\phi\mathbf{v}_l) - \nabla\cdot\mathbf{q}_l + \nabla\cdot\mathbf{Q} + (\phi^2\mu_l/k)|\mathbf{v}_l|^2 \qquad (14)$$

For the present discussion it will suffice to consider only the mixture energy balance. We will furthermore assume that $T_l = T_s = T$. The mixture energy balance is therefore given by

$$[(1-\phi)\rho_s(\partial E_s/\partial t) + \phi\rho_l(\partial E_l/\partial t)] + \phi\rho_l\mathbf{v}_l\cdot\nabla E_l = -p_l\nabla\cdot(\phi\mathbf{v}_l) - \nabla\cdot\mathbf{q} + (\phi^2\mu_l/k)|\mathbf{v}_l|^2 \qquad (15)$$

where $\mathbf{q} = \mathbf{q}_l + \mathbf{q}_s$.

To make the following discussion more concrete, we will assume that heat conduction in the rock-liquid composite is governed by Fourier's law:

$$\mathbf{q} = -\kappa_m\nabla T \qquad (16)$$

where $\kappa_m$ denotes the mixture (rock-liquid) thermal conductivity.

By eliminating $\nabla\cdot(\phi\mathbf{v}_l)$ between (11) and (15) the mixture energy balance can be expressed in the following alternate form:

$$\left((1-\phi)\rho_s\frac{\partial E_s}{\partial t} + \phi\rho_l\frac{\partial E_l}{\partial t}\right) + \phi\rho_l\mathbf{v}_l\cdot\nabla E_l = \frac{\phi p_l}{\rho_l}\left(\frac{\partial\rho_l}{\partial t} + \mathbf{v}_l\cdot\nabla\rho_l\right) + \nabla\cdot(\kappa_m\nabla T) + \frac{\phi^2\mu_l}{k}|\mathbf{v}_l|^2 \qquad (17)$$

The passive reservoir is thus described by (11), (12), and (17).

## Nondimensional Analysis

It is convenient to reduce (11), (12), and (17) to a nondimensional form. For this purpose it is essential to choose certain characteristic parameters. We will use the following set of quantities:

- $\rho_0$ density (e.g., initial liquid density);
- $C_V$ specific heat (e.g., mixture specific heat);
- $T_0$ temperature (e.g., temperature difference across reservoir);
- $L$ length (e.g., linear reservoir dimension);
- $v_0$ velocity (e.g., average liquid velocity).

We next introduce the following nondimensional quantities:

$$\rho_l' = \rho_l/\rho_0 \qquad \rho_s' = \rho_s/\rho_0 \qquad s' = x/L$$
$$\mathbf{v}_l' = \mathbf{v}_l/v_0 \qquad p_l' = p_l/(\rho_0 Lg) \qquad T' = T/T_0 \qquad (18)$$
$$E_l' = E_l/C_V T_0 \qquad E_s' = E_s/C_V T_0 \qquad t' = tv_0/L.$$

Substituting from (18) into (11), (12), and (17) and dropping primes, we obtain the following set of nondimensional equations:

$$\phi(\partial\rho_l/\partial t) + \nabla\cdot(\phi\rho_l\mathbf{v}_l) = 0 \qquad (19)$$

$$\rho_l\left(\frac{\partial\mathbf{v}_l}{\partial t} + \mathbf{v}_l\cdot\nabla\mathbf{v}_l\right) = -\left(\frac{gL}{v_0^2}\right)(\nabla p_l - \rho_l\mathbf{g}) - \left(\frac{\phi\mu_l L}{k\rho_0 v_0}\right)\mathbf{v}_l \qquad (20)$$

$$\left((1-\phi)\rho_s\frac{\partial E_s}{\partial t} + \phi\rho_l\frac{\partial E_l}{\partial t}\right) + \phi\rho_l\mathbf{v}_l\cdot\nabla E_l = \left(\frac{\phi gL}{C_V T_0}\right)\frac{\rho_l}{\rho_l}\left(\frac{\partial\rho_l}{\partial t} + \mathbf{v}_l\cdot\nabla\rho_l\right) + \nabla\cdot\left[\left(\frac{\kappa_m}{\rho_0 C_V v_0 L}\right)\nabla T\right] + \phi^2\left(\frac{\mu_l v_0 L}{k\rho_0 C_V T_0}\right)|\mathbf{v}_l|^2 \qquad (21)$$

In (20), $\mathbf{g}$ is the unit vector in the direction of gravity.

The system of (19)-(21) involves five nondimensional groups, i.e.,

$$\frac{gL}{v_0^2} \quad \frac{\phi\mu_l L}{k\rho_0 v_0} \quad \frac{\phi gL}{C_V T_0} \quad \frac{\kappa_m}{\rho_0 C_V v_0 L} \quad \frac{\mu_l v_0 L\phi^2}{k\rho_0 C_V T_0} \qquad (22)$$

There are, however, only four independent dimensionless quantities, since

$$\frac{\phi^2\mu_l v_0 L}{k\rho_0 C_V T_0} = \left(\frac{\phi\mu_l L}{k\rho_0 v_0}\right)\left(\frac{\phi gL}{C_V T_0}\right)\Big/\left(\frac{gL}{v_0^2}\right)$$

We shall now examine the importance of various terms in (19)-(21) to find out if it is possible to make any simplifications. For a typical geothermal (liquid water) reservoir, we have

$$g \sim 10^3\ \text{cm/s}^2 \qquad L \sim 10^5\ \text{cm} \qquad \mu_l \sim 10^{-3}\ \text{dyn s/cm}^2$$
$$k \sim 10^{-9}\ \text{cm}^2 \qquad \phi \sim 10^{-1} \qquad \rho_0 \sim 1\ \text{gm/cm}^3$$
$$T_0 \sim 100°\text{C} \qquad \kappa_m \sim 10^5\ \text{dyn/s °C}$$

Therefore we have

$$\frac{gL}{v_0^2} \sim \frac{10^5}{v_0^2} \qquad \frac{\phi\mu_l L}{k\rho_0 v_0} \sim \frac{10^{11}}{v_0} \qquad \frac{\phi gL}{C_V T_0} \sim \frac{10^5}{C_V}$$
$$\frac{\kappa_m}{\rho_0 C_V v_0 L} \sim \frac{1}{v_0 C_V} \qquad \frac{\phi^2\mu_l v_0 L}{k\rho_0 C_V T_0} \sim \frac{10^6 v_0}{C_V}$$

On noting that

$$\rho_l \sim O(1) \qquad \mathbf{v}_l \sim O(1) \qquad \nabla\cdot\mathbf{v}_l \sim \partial\rho_l/\partial t \sim O(1)$$
$$(\nabla p_l - \rho_l\mathbf{g}) \sim O(1)$$

we have the following from momentum balance equation (20):

$$O(1) = -(10^5/v_0^2)O(1) - (10^{11}/v_0)O(1)$$

or

$$v_0^2 O(1) = 10^6 O(1) - 10^{11} v_0 O(1)$$

Thus unless $v_0 \sim O(10^6)$ (highly unlikely in geothermal reservoirs), we are safe in ignoring inertia terms (left-hand side) in momentum equation (20). Furthermore, we have

$$v_0 \sim (\rho_0 gk/\phi\mu_l) \sim O(10^{-3}\ \text{cm/s})$$

By putting $v_0 = \rho_0 gk/\phi\mu_l$ and ignoring inertia terms, the momentum and energy equations (20) and (21) become

$$\mathbf{v}_l = -(\nabla p_l - \rho_l\mathbf{g}) \qquad (20')$$

$$\left((1-\phi)\rho_s\frac{\partial E_s}{\partial t}+\phi\rho_l\frac{\partial E_l}{\partial t}\right)+\phi\rho_l\mathbf{v}_l\cdot\nabla E_l$$
$$=\left(\frac{\phi gL}{C_vT_0}\right)\left[\frac{p_l}{\rho_l}\left(\frac{\partial\rho_l}{\partial t}+\mathbf{v}_l\cdot\nabla\rho_l\right)+|\mathbf{v}_l|^2\right]+\nabla\cdot\left[\left(\frac{\kappa_m\phi\rho_l}{\rho_0^2C_vLgk}\right)\nabla T\right] \quad (21')$$

Note that this leaves us with only two dimensionless groups:

$$\phi gL/C_vT_0 \qquad \kappa_m\phi\rho_l/\rho_0^2C_vLgk$$

Furthermore,

$$\phi gL/C_vT_0 \sim (10^2/C_v) \qquad \kappa_m\phi\rho_l/\rho_0^2C_vLgk \sim O(10^2/C_v)$$

We are now ready to examine the magnitude of various terms in the energy equation. Assuming that $E_s \sim O(E_l)$, we have

$$O\left(\frac{\partial E_l}{\partial t}\right)+\nabla E_l O(10^{-4})=\frac{10^2}{C_v}\left[O\left(\frac{\partial\rho_l}{\partial t}\right)+O(\nabla p_l)+O(1)\right]+\frac{10^2}{C_v}\left[O(\nabla^2T)\right]$$

If we, furthermore, assume that $E_l \sim C_vT$, the order of various terms in the energy equation becomes

$$O\left(\frac{\partial T}{\partial t}\right)+\underbrace{\nabla TO(10^{-4})}_{\text{convection}}=\frac{10^2}{C_v}\left[\underbrace{O(\partial\rho_l/\partial t)+O(\nabla p_l)}_{\text{pressure work}}+\underbrace{O(1)}_{\text{viscous dissipation}}+\underbrace{O(10^{-2}\nabla^2T)}_{\text{thermal diffusion}}\right]$$

Since $\nabla T \sim O(1)$, the left-hand side is at least of $O(10^{-4})$. Thus for any term on the right-hand side of the energy equation to be retained, it must be of $O(C_v^2/10^2)$, i.e., of $O(10^2)$ if $C_v \sim O(10^3)$. In view of the latter result we are certainly justified in ignoring the viscous dissipation term. Furthermore, for the pressure work term we have

$$\partial p_l/\partial t \sim O(\nabla p_l) \sim O[\nabla\cdot(\mathbf{v}_l)] \ll O(10^2)$$

Thus the pressure work term is also likely to be unimportant.

On the basis of the preceding discussion it is possible to draw the following conclusions for a passive liquid-dominated geothermal reservoir:

1. The general system of balance equations for liquid flow in a porous medium is characterized by four independent dimensionless quantities, i.e., $gL/\varepsilon_0^2$, $\phi\mu_lL/kp_0\varepsilon_0$, $\phi gL/C_vT_0$, and $\kappa_m/\rho_0C_v\varepsilon_0L$.

2. In geothermal applications it is possible to ignore inertia terms in the momentum equation. The number of independent dimensionless parameters is two, i.e., $\phi gL/C_vT_0$ and $\kappa_m\phi\mu_l/\rho_0^2C_vLgk$.

3. Pressure work and viscous dissipation terms in the energy equation may be ignored. This implies that the liquid flow can be described by a single dimensionless parameter, i.e., $\kappa_m\phi\mu_l/\rho_0^2C_vLgk$.

## Simplified Balance Laws for a Single-Phase (Liquid) Fully Interactive System

Let us now consider a fully interactive system. In a geothermal reservoir, rock matrix strains are likely to be quite small. (At Wairakei, New Zealand, maximum strains are of the order of $10^{-3}$ [*Pritchett et al.*, 1976].) Furthermore, it is permissible to assume that the solid velocity $\mathbf{v}_s$ is much smaller than the liquid velocity $\mathbf{v}_l$. (As a matter of fact, we need only to postulate that $\mathbf{v}_s \sim O(\mathbf{v}_l)$.) The last assumption enables us to ignore inertia terms in the solid momentum equation (3) and all mechanical work and mechanical interaction energy terms in the energy equations (7) and (8). Thus we obtain the following simplified system of balance equations (in dimensional form) for the fully interactive geothermal reservoir:

Solid mass

$$\dot{\varepsilon}=\nabla\cdot\mathbf{v}_s \quad (23)$$

Liquid mass

$$[\partial/\partial\varepsilon+\phi/K_l](\phi\rho_l)+\phi\rho_l\nabla\cdot\mathbf{v}_l=0 \quad (24)$$

Solid momentum

$$-\nabla[(1-\phi)p_s+\phi p_l]+\nabla\cdot\mathbf{S}+[(1-\phi)\rho_s+\phi\rho_l]\mathbf{g}=0 \quad (25)$$

Liquid momentum

$$\mathbf{v}_l=(k/\phi\mu_l)(-\nabla p_l+\rho_l\mathbf{g}) \quad (26)$$

Solid energy

$$(1-\phi)\rho_s(\partial E_s/\partial t)=-\nabla\cdot\mathbf{q}_s-\nabla\cdot\mathbf{Q} \quad (27)$$

Liquid energy

$$\phi\rho_l[(\partial E_l/\partial t)+\mathbf{v}_l\cdot\nabla E_l]=-\nabla\cdot\mathbf{q}_l+\nabla\cdot\mathbf{Q} \quad (28)$$

The momentum balance relation for the solid matrix (25), obtained by summing (3) and (4) and dropping inertia terms, merely states that the liquid-saturated rock aggregate behaves in a quasi-static manner. It is also appropriate to note here that in geothermal applications it is permissible to regard the liquid and the solid matrix to be in local thermal equilibrium. Justification for this is given in a paper by *Nayfeh et al.* [1975]. Assumption of local thermal equilibrium ($T_s = T_l = T$) implies that one need consider only the mixture energy balance obtained by summing (27) and (28).

## Extension to Two-Phase (Liquid-Vapor) Flow

Theoretical considerations for two-phase (liquid-vapor) flow through porous media are considerably more complicated than those for single-phase (liquid water) flow discussed in the preceding sections. *Garg and Pritchett* [1977] have recently examined the conditions under which the pressure work and viscous dissipation terms can be neglected in two-phase fluid flow. In the following, we will not delve into a detailed order of magnitude analysis for two-phase flows; we shall merely present a system of balance equations which has been found adequate (see, for example, *Garg et al.* [1975b, 1976] and *Garg and Pritchett* [1977]) to describe two-phase fluid flow in many laboratory and field situations.

Assuming that (1) inertia (momentum balance), pressure work, and viscous dissipation (energy balance) terms are negligible, (2) water and water vapor are in local pressure and thermal equilibrium, and (3) fluid (water and water vapor) and rock matrix are in local thermal equilibrium, the equations expressing mass, momentum, and energy balance are

Liquid mass

$$(\partial/\partial t)[\phi(1-S)\rho_l]=-\nabla\cdot[\phi(1-S)\rho_l\mathbf{v}_l]-\dot{m} \quad (29)$$

Vapor mass

$$(\partial/\partial t)(\phi S\rho_v) = -\nabla \cdot [\phi S\rho_v \mathbf{v}_v] + \dot{m} \tag{30}$$

where $\dot{m}$ is the mass transfer rate from liquid to vapor due to phase change.

Liquid momentum

$$\mathbf{v}_l = -[R_l k/[\phi(1 - S)\mu_l]](\nabla p_l - \rho_l g) \tag{31}$$

Vapor momentum

$$\mathbf{v}_v = -(R_v k/\phi S\mu_v)(\nabla p_l - \rho_v g) \tag{32}$$

where $p_l$ denotes the fluid (= liquid = vapor) pressure. Assumption of pressure equilibrium is tantamount to assuming that the capillary pressure is negligible. For water-steam systems the capillary pressure is less than 1 bar (see, for example, *Ramey et al.* [1974]) and is therefore likely to be insignificant in comparison with the pressure changes induced by production/injection. Capillary pressure may be included in the balance laws by modifying the pressure equilibrium relation ($p_l = p_v = p_l$).

Rock-liquid-vapor mixture energy

$$(\partial/\partial t)[(1 - \phi)\rho_r E_r + \phi(1 - S)\rho_l E_l + \phi S\rho_v E_v] + \nabla \cdot [\phi(1 - S)\rho_l E_l \mathbf{v}_l + \phi S\rho_v E_v \mathbf{v}_v] = \nabla \cdot (\kappa_m \nabla T) \tag{33}$$

where $\kappa_m$ denotes the mixture (solid and fluid) conductivity and $T(= T_r = T_l = T_v)$ is the mixture temperature.

The system of (29)–(33) is similar to the formulations of two-phase flow developed by *Donaldson* [1968] and *Mercer et al.* [1974]. For the fully interactive rock-fluid system it is necessary to supplement (29)–(33) with the solid mass and momentum balance relations.

## Constitutive Relations for Geothermal Fluids (Water-Steam)

The mass transfer term $\dot{m}$ in the mass balance laws for the liquid and vapor components may be eliminated by summing (29) and (30). For computational purposes it is also convenient to eliminate the separate density ($\rho_l$, $\rho_v$) and energy ($E_l$, $E_v$) fields for liquid and vapor and to employ instead mixture (liquid-vapor) density $\rho_f$ and energy $E_f$ fields:

$$\rho_f = S\rho_v + (1 - S)\rho_l \tag{34}$$

$$E_f = [(1 - S)\rho_l E_l + S\rho_v E_v]/\rho_f \tag{35}$$

After introducing the 'steam quality' $Q$,

$$Q = M_v/(M_l + M_v) \tag{36}$$

$\rho_l$, $\rho_v$, $E_l$, and $E_v$ can be expressed in terms of $\rho_f$, $E_f$, $Q$, $S$, and $\delta$:

$$\rho_l = \rho_f\left(\frac{1 - Q}{1 - S}\right) \qquad \rho_v = \rho_f\left(\frac{Q}{S}\right)$$

$$\rho_l E_l = \rho_f E_f\left[\frac{(1 - Q)(1 - \psi Q)}{1 - S}\right] \tag{37}$$

$$\rho_v E_v = \rho_f E_f\left\{\frac{Q[1 + \psi(1 - Q)]}{S}\right\}$$

where $\psi = \delta/E_f$, $M_l(M_v)$ is the liquid (vapor) mass per unit volume, and $\delta (= E_v - E_l)$ is the heat of vaporization. Substituting for $\rho_l$, $\rho_v$, $E_l$, and $E_v$ from (37) into (29), (30), and (33) gives the balance relations in the desired form.

The modified system of balance equations contains liquid and vapor viscosities, relative vapor volume, steam quality, and latent heat of vaporization in addition to fluid density $\rho_f$, internal energy $E_f$, and pressure $p_f$. Furthermore, specification of mixture (solid-liquid-vapor) thermal conductivity $\kappa_m$ requires the knowledge of liquid $\kappa_l$ and vapor $\kappa_v$ conductivities. It was therefore necessary to construct a fairly general tabular equation of state for water. Given fluid density $\rho_f$ and internal energy $E_f$, the equation of state subroutines used in the simulation code yield pressure $p_f$, derivatives of pressure with respect to $\rho_f$ and $E_f$, steam volume fraction $S$, quality $Q$, fluid temperature $T$, derivatives of temperature with respect to $\rho_f$ and $E_f$, and latent heat of vaporization $\delta$ and its derivatives with respect to $\rho_f$ and $E_f$. This description is valid up to ultrahigh pressures (several megabars) and temperatures up to 3000°C. The equation of state subroutine also gives liquid and vapor viscosities ($\mu_l$, $\mu_v$) and thermal conductivities ($\kappa_l$, $\kappa_v$) as functions of $\rho_f$ and $E_f$; these data are, however, valid up to only pressures less than 1 kbar and temperatures less than 800°C.

## Constitutive Relations for the Rock Matrix

We need to prescribe the following functions for the rock matrix:

| | |
|---|---|
| $T_r(E_r)$ | dependence of rock temperature on rock internal energy; |
| $\kappa_m(\kappa_r, \phi, S)$ | dependence of the mixture (solid-liquid-vapor) conductivity on $\kappa_r$, $\phi$, and $S$; |
| $\kappa_r(T)$ | dependence of thermal conductivity on temperature; |
| $k(\phi)$ | dependence of permeability on porosity $\phi$; |
| $R_{l,v}(S, T)$ | dependence of relative liquid and vapor permeabilities on steam saturation and temperature; |
| $\sigma'(\varepsilon, T_r)$ | dependence of rock matrix stress tensor upon rock strain tensor $\varepsilon$ and temperature, equal to $-(1 - \phi)p_f I + S$; |
| $\phi(\sigma', p_f, T)$ | dependence of rock porosity upon the stress state and temperature. |

For geothermal applications it will suffice to assume that

$$E_r = C_{vr}T_r \tag{38}$$

where $C_{vr}$ is the constant volume heat capacity of the solid. *Ramey et al.* [1974] present a review of the measurements and empirical formulas for the thermal conductivities of dry and fluid-saturated rocks. The thermal conductivity of most rocks decreases with an increase in temperature. Thermal conductivities of fluid-saturated rocks are 2–5 times greater than those of dry rocks. Where detailed experimental data are unavailable, the mixture thermal conductivity $\kappa_m$ may be approximated by the following relationship due to *Budiansky* [1970]:

$$(1 - \phi)\left[\frac{2}{3} + \frac{1}{3}\left(\frac{\kappa_r}{\kappa_m}\right)\right]^{-1} + \phi\left\{(1 - S)\left[\frac{2}{3} + \frac{1}{3}\left(\frac{\kappa_l}{\kappa_m}\right)\right]^{-1} + S\left[\frac{2}{3} + \frac{1}{3}\left(\frac{\kappa_v}{\kappa_m}\right)\right]^{-1}\right\} = 1 \tag{39}$$

As was mentioned in the preceding, the rock permeability $k$ may be regarded as a function of porosity $\phi$. For many rocks, $k(\phi)$ can be adequately approximated by the following relation:

$$k = k_0\left(\frac{\phi}{\phi_0}\right)^n\left(\frac{1 - \phi_0}{1 - \phi}\right)^m \tag{40}$$

where $n$ and $m$ are empirically determined constants. Note that $n = 3$, $m = 2$ yields the classical Carman-Kozeny relation (see, for example, *Scheidegger* [1963]). Sufficient data are usually unavailable to determine the dependence of relative permeabilities ($R_{r,s}$) on temperature; it will be therefore assumed that the relative permeabilities are functions only of vapor saturation $S_v$. In particular, the relative permeabilities may be represented by the equations of *Corey et al.* [1956]:

$$R_l = (S_l^*)^4 \qquad R_v = (1 - S_l^{*2})(1 - S_l^{*2}) \tag{41}$$

where

$$S_l^* = (S_l - S_{lr})/(1 - S_{lr} - S_{vr}) \qquad S_l = (1 - S) \tag{42}$$

Here $S_{lr}(S_{vr})$ is the irreducible liquid (vapor) saturation, and $S_l^*$ is the volumetric liquid saturation normalized with respect to the mobile fluid saturation in the pore space. Note that for $S_l < S_{lr}$, $R_l = 0$ and $R_v = 1$; and for $S_l > (1 - S_{vr})$, $R_l = 1$ and $R_v = 0$. In the remainder of this subsection we shall consider the constitutive relations for $\sigma^*$ and $\rho$.

The bulk strain rate tensor for rock is given by

$$\dot{\varepsilon} = (1/2)[\nabla \mathbf{v}_s + (\nabla \mathbf{v}_s)^T] = (\dot{\varepsilon}/3)\,\mathbf{I} + \dot{\mathbf{E}} \tag{43}$$

where $\dot{\mathbf{E}}$ denotes the deviatoric part of the strain rate tensor. Bulk volumetric strain $\varepsilon$ is related to the rock grain (or effective) volumetric strain $\varepsilon^*$ through the relation [*Garg and Nur*, 1973]:

$$\varepsilon^* = (\rho_{s0}/\rho_s) - 1 = [(1 - \phi)/(1 - \phi_0)](1 + \varepsilon) - 1 \tag{44}$$

The rock grain may be assumed to be a linear thermoelastic material over the range of temperature and pressure encountered in geothermal reservoirs:

$$p_s = -K_s(\varepsilon^* - 3\alpha_s T_s) \tag{45}$$

Additionally, we will postulate that the shear stresses $\mathbf{S}$ are linearly related to shear strains $\mathbf{E}$ through Hooke's law:

$$\mathbf{S} = 2\mu_s \mathbf{E} \tag{46}$$

Equation (46) should be adequate to describe the relatively small shear stress changes expected in geothermal systems. In case the shear stress changes are large (in relation to yield and/or fracture strengths), it would be necessary to consider more general (e.g., elastic-plastic) material models (see, for example, *Garg et al.* [1977]).

Porosity $\phi$ depends in a complex manner on the current state of stress ($\sigma^*$, $p_f$), stress history, temperature, and the rock type. Consolidated rocks generally exhibit greater compaction at elevated temperatures than they do at lower temperatures; the effect of temperature is not, however, so significant in loose or unconsolidated sands. Shear stresses $\mathbf{S}$, depending upon the rock type and the stress level, may contribute to compaction, may lead to dilatancy, or may have no significant effect on $\phi$ [*Garg et al.*, 1977]. We will here restrict ourselves to the case when $\phi$ does not appreciably depend upon $\mathbf{S}$; in this case, $\phi$ (small deformations being assumed) can be expressed as a function of $(p_c - p_f)$ and $T$ [*Garg*, 1976]:

$$\frac{\partial}{\partial t}\phi = A\,\frac{\partial}{\partial t}(p_c - p_f) + B\,\frac{\partial T}{\partial t} \tag{47}$$

where

$$A = [(1/K_s) - [(1 - \phi)/K]] \qquad B = 3(1 - \phi)(\alpha - \alpha_s)$$

Here $K$ is the bulk modulus of the porous rock and depends upon $(p_c - p_f)$, the loading direction (i.e., increase or decrease in $p_c - p_f$), and the past stress history. This dependence of $K$ on the loading direction and history is responsible for the hysteretic effects observed in ground subsidence uplift due to changes in subsurface pore pressures. In many field applications it is either not possible to measure $K$ and $\alpha$ separately or it is sufficient to consider the reservoir compaction to be primarily uniaxial. The uniaxial compaction coefficient $C_m$ ($= (K + \frac{4}{3}\mu)^{-1}$) like $K$ depends upon $(p_c - p_f)$, the loading direction, and the past stress history; in field applications, small changes in $(p_c - p_f)$ can often result in extremely large changes in $C_m$. Thus for example at Wairakei (New Zealand) an average reservoir pressure drop of less than 30 bars has resulted in a fifteenfold change in $C_m$ [*Pritchett et al.*, 1976].

The theoretical model discussed above requires $C_m$, $\alpha_s$, $k$, $R_{r,s}$, $\phi_0$, $\mu_s$, $K_s$, $K$, $\eta$, and $\eta_s$ as empirically determined input functions. Most of these properties can be determined from standard laboratory tests on cores obtained from the reservoir in question. The reservoir behavior is, however, frequently governed by fractures, formation inhomogeneities, and other large-scale features such as faults. In particular, the productibility and compaction behavior of a geothermal reservoir will be profoundly influenced by the presence of fractured rock masses. It therefore becomes important to supplement the laboratory measurements by suitable field data. Permeability $k$ and relative permeabilities $R_{r,s}$ are best determined from well flow data (this is a standard practice in petroleum reservoir engineering). Also bulk and shear moduli ($K$, $\mu_s$) of reservoir rocks should be obtained from either seismic measurements or field subsidence data.

## Concluding Remarks

The system of governing equations outlined in the preceding sections is quite complex and must be solved numerically. A numerical procedure for solving the transport of heat and fluid mass in a "quasi-active" geothermal reservoir has previously been presented by *Garg et al.* [1975*b*]. The method is applicable to the two phase case and properly treats the effects of phase changes (liquid $\rightleftharpoons$ vapor) within the pores of the reservoir rock. The quasi-active case is midway in sophistication between the "rigid matrix" model in which all rock properties (porosity, permeability, thermal conductivity, etc.) are treated as functions of position only and the "fully interactive" case in which the entire rock stress and deformation fields are calculated, along with the heat and fluid flow. In the quasi-active model the rock thermal properties (heat capacity and thermal conductivity) may be functions of temperature as well as position; the permeability may change with porosity, and the porosity may also vary with position and time, but at a particular point the local porosity is assumed to depend only on the local pore pressure. The quasi-active model has recently been extended at Systems, Science and Software to the fully interactive case by supplying constitutive relations for the rock matrix and imposing a static equilibrium condition (where pore pressure contributes to total stress) at each time step [*Garg et al.*, 1977].

## Notation

- $E_i$ internal energy of $i$th phase ($i = s$ (solid), $i = l$ (liquid), $i = v$ (vapor), $i = f$ (fluid)).
- $\mathbf{g}$ acceleration due to gravity.
- $k$ rock permeability.
- $K_s(K)$ rock grain (porous rock) bulk modulus.
- $p_s(p_f)$ solid (fluid) pressure.
- $\mathbf{q}_s(\mathbf{q}_f)$ heat flux vector within porous solid (interspersed fluid).

$k_l(k_r)$ relative permeability for liquid (water).
$S$ relative vapor volume ($= V_v/(V_l + V_v)$).
$s$ deviatoric stress tensor for porous rock.
$T_s(T_f)$ solid (fluid) temperature.
$\mathbf{v}_i$ velocity of $i$th phase ($i = s, l, v, f$).
$V_v(V_l)$ vapor (liquid) volume.
$\delta$ heat of vaporization at a given pressure and temperature ($= E_v - E_l$).
$\dot{\epsilon}$ partial (or bulk) strain rate tensor for rock matrix ($= (\dot{\epsilon}/3)\mathbf{I} + \dot{\mathbf{E}}$).
$\eta_s(\eta_f)$ coefficient of linear thermal expansion for rock grain (porous rock).
$\kappa_s(\kappa_f)$ rock grain (fluid) thermal conductivity.
$\mu_i$ viscosity ($i = f, l, v$).
$\mu_p$ shear modulus of porous rock.
$\rho_i$ density ($i = s, f, l, v$).
$\phi$ porosity.

*Acknowledgments.* This work was sponsored in part by NSF/RANN grant GI-43856 to Systems, Science and Software and also by NSF/RANN grant GI-34212 to the University of Colorado and Systems, Science and Software.

## REFERENCES

Biot, M. A., Pore pressure in geophysics, in *Flow and Fracture of Rocks*, *Geophys. Monogr. Ser.*, vol. 16, edited by H. C. Heard et al., pp. 265–273, American Geophysical Union, Washington, D. C., 1972.

Budiansky, B., Thermal and thermoelastic properties of isotropic composites, *J. Compos. Mater.*, *4*, 286, 1970.

Corey, A. T., et al., Three-phase relative permeability, *Trans. Amer. Inst. Mining Eng.*, *207*, 349, 1956.

Donaldson, I. G., The flow of steam water mixtures through permeable beds. A simple simulation of a natural undisturbed hydrothermal region, *N. Z. J. Sci.*, *11*, 3, 1968.

Garg, S. K., Wave propagation effects in a fluid-saturated porous solid, *J. Geophys. Res.*, *76*, 7947, 1971.

Garg, S. K., Constitutive relations for fluid-saturated porous rocks, *Rep. SSS-IR-76-2445*, Systems, Science and Software, La Jolla, Calif., March 1976.

Garg, S. K., and A. Nur, Effective stress laws for fluid-saturated porous rocks, *J. Geophys. Res.*, *78*, 5911, 1973.

Garg, S. K., and J. W. Pritchett, On pressure-work, viscous dissipation and the energy balance relation for geothermal reservoirs, submitted to *Adv. Water Resour.*, 1977.

Garg, S. K., et al., Shock wave propagation in fluid-saturated porous media, *J. Appl. Phys.*, *45*, 702, 1974a.

Garg, S. K., J. W. Pritchett, and J. D. H. Brownell, Jr., Transport of mass and energy in porous media, in *Proceedings of the Second United Nations Symposium on the Development and Use of Geothermal Resources, San Francisco*, pp. 1651–1656, U.S. Government Printing Office, Washington, D. C., 1975b.

Garg, S. K., et al., Study of the geothermal production and subsidence history of the Wairakei field, in *Proceedings of the 17th U. S. Symposium on Rock Mechanics, Snowbird, Utah*, pp. 3B3-1–3B3-5, University of Utah, Salt Lake City, 1976.

Garg, S. K., D. H. Brownell, Jr., and J. W. Pritchett, Dilatancy-induced fluid migration and the velocity anomaly, *J. Geophys. Res.*, *82*, 855, 1977.

Mercer, J. W., Jr., C. Faust, and G. F. Pinder, Geothermal reservoir simulation, in *Proceedings of NSF/RANN Conference on Research for the Development of Geothermal Energy Resources*, pp. 258–267, Jet Propulsion Laboratory/California Institute of Technology, Pasadena, Calif., 1974.

Morland, L. W., A simple constitutive theory for a fluid-saturated porous solid, *J. Geophys. Res.*, *77*, 890, 1972.

Nayfeh, A. H., D. H. Brownell, Jr., and S. K. Garg, Heat exchange in a fluid percolating through porous media, in *Proceedings of the 12th Annual Meeting of the Society of Engineering Science*, pp. 1125–1137, University of Texas at Austin, Austin, Tex., 1975.

Pritchett, J. W., et al., Geohydrological environmental effects of geothermal power production, phase II-A, *Rep. SSS-R-77-2966*, Systems, Science and Software, La Jolla, Calif., 1976.

Ramey, H. J., et al., Thermodynamic and hydrodynamic properties of hydrothermal systems, *Stanford Geothermal Program Rep. SGP-TR-6*, Stanford Univ., Stanford, Calif., April 1974.

Scheidegger, A. E., Hydrodynamics in porous media, in *Handbuch der Physik*, vol. VIII/2, pp. 625–662, Springer, New York, 1963.

(Received April 1976;
accepted April 26, 1977.)

SOCIETY OF PETROLEUM ENGINEERS
6200 North Central Expressway
Dallas, Texas 75206

PAPER NUMBER SPE 5381

THIS IS A PREPRINT - SUBJECT TO CORRECTION

# Computer Simulation of Geothermal Reservoirs

By

D. H. Brownell, Jr., S. K. Garg, and J. W. Pritchett, Systems, Science and Software



## ABSTRACT

General balance laws and constitutive relations are developed for convective hydrothermal geothermal reservoirs. A fully interacting rock-fluid system is considered; typical rock-fluid interactions involve momentum and energy transfer, and the dependence of rock porosity (and permeability) upon the fluid and rock stresses. The mathematical model also includes multiphase (water/steam) effects. The geologic stress-strain behavior treatment permits the highly nonlinear and history-dependent constitutive behavior of the material to be properly taken into account. Work is presently underway on devising numerical methods for the governing equations, and will be reported in future publications.

## INTRODUCTION

In order to study problems characterized by essential alterations in the porous matrix itself, it is necessary to consider fully interacting rock-fluid systems. Particular examples of these problems include the interaction between pore collapse (subsidence) and fluid extraction rates, the reinjection of collapsed pores by condensate injection, and the effects of variations in natural mechanical forces (e.g., overburden stress) on the state of the geothermal system. In these cases there would appear to be significant interactions between the porous matrix and the fluid. Thus, it appears necessary to consider the general interaction theories in order to assess the effect of the motion of the matrix on the motion of the fluid and vice versa.

General balance laws and constitutive relations incorporating the various interactions in a solid-fluid mixture have previously been developed by Morland,[1] and Garg, et al.[2-7] For geothermal reservoir applications where fluid velocities are low and times of interest are long, it is possible to considerably simplify the general balance laws. In this paper, we will first present the fully interactive equations for a single phase system, and then indicate possible simplifications for geothermal applications. Extension to two-phase systems is discussed next. This is followed by constitutive relations. Work is presently proceeding on the numerical

References at end of paper.

solution of the governing equations, and will be described in subsequent publications.

## BALANCE LAWS (SINGLE PHASE)

General equations expressing balance of mass, momentum and energy, for a solid-fluid mixture are:[2-4,6,7]

Mass:

Solid:

$$\frac{\partial(1-\phi)\rho_s}{\partial t} + \nabla \cdot \left((1-\phi)\rho_s \underline{v}_s\right) = 0. \quad [1]$$

Fluid:

$$\frac{\partial \phi \rho_f}{\partial t} + \nabla \cdot \left(\phi \rho_f \underline{v}_f\right) = 0. \quad [2]$$

Momentum:

Solid:

$$(1-\phi)\rho_s\left[\frac{\partial \underline{v}_s}{\partial t} + v_s \cdot \nabla \underline{v}_s\right] = -\nabla(1-\phi)p_s + \text{div } \underline{\underline{S}} + (1-\phi)\rho_s \underline{g} + \rho \underline{\beta}. \quad [3]$$

Fluid:

$$\phi\rho_f\left[\frac{\partial \underline{v}_f}{\partial t} + \underline{v}_f \cdot \nabla \underline{v}_f\right] = -\nabla \phi p_f + \phi \rho_f \underline{g} - \rho \underline{\beta} \quad [4]$$

Here $\rho\underline{\beta}$ is the momentum supply to the solid due to interaction with the fluid.

$$\rho \underline{\beta} = -p_f \nabla \phi + \frac{\phi^2 \mu_f}{k}(\underline{v}_f - \underline{v}_s) \quad [5]$$

The fluid viscosity $\mu_f$ will in general vary with fluid pressure ($p_f$) and temperature ($T_f$)

$$\mu_f = \mu_f(p_f, T_f). \quad [6a]$$

The rock permeability $k$ is a complex function of rock and fluid stresses (see, e.g., Brace[8]). For the sake of simplicity, we will postulate that this dependence is primarily exhibited through changes in porosity $\phi$

$$k = k(\phi). \quad [6b]$$

Energy:

Solid:

$$(1-\phi)\rho_s \frac{D_s E_s}{Dt} = -(1-\phi)p_s \text{ div } \underline{v}_s + \underline{\underline{S}} : \nabla \underline{v}_s + \rho\psi_s - \nabla \cdot (\kappa_1 \nabla T_s) - \nabla \cdot \underline{Q} \quad [7]$$

Fluid:

$$\phi\rho_f \frac{D_f E_f}{Dt} = -\phi p_f \text{ div } \underline{v}_f + \rho\psi_f - \nabla \cdot (\kappa_2 \nabla T_f) + \nabla \cdot \underline{Q} \quad [8]$$

where

$$D_i/Dt = \partial/\partial t + \underline{v}_i \cdot \text{grad}, \quad i = s, f.$$

In general, $\kappa_1 \neq (1-\phi)\kappa_s$, $\kappa_2 \neq \phi\kappa_f$. Here $\rho\psi_s$ ($\rho\psi_f$) denotes the mechanical interaction energy supply to solid (fluid).

$$\rho\psi_s = p_f\left[\frac{\partial \phi}{\partial t} + \underline{v}_s \cdot \nabla\phi\right] \quad [9]$$

$$\rho\psi_f = -p_f\left[\frac{\partial \phi}{\partial t} + \underline{v}_f \cdot \nabla\phi\right] + \frac{\phi^2 \mu_f}{k}|\underline{v}_f - \underline{v}_s|^2 \quad [10]$$

In Eqs. [7] and [8], $\nabla \cdot \underline{Q}$ is the thermal interaction energy supply to the fluid.

## BALANCE EQUATIONS FOR PASSIVE RESERVOIR

The balance equations [1] - [10] are quite complex. Fortunately for geothermal reservoir applications, it is possible to simplify these equations. For the sake of simplicity, first consider a passive reservoir ($\underline{v}_s \equiv 0$, $\partial\phi/\partial t \equiv 0$, $\nabla\phi \neq 0$). For such a reservoir, the mass and momentum balance equations for the solid are satisfied trivially. The governing system of equations thus reduces to:

Mass:

Fluid:

$$\phi \frac{\partial \rho_f}{\partial t} + \nabla \cdot (\phi \rho_f \underline{v}_f) = 0 \quad [11]$$

Momentum:

Fluid:

$$\rho_f\left[\frac{\partial \underline{v}_f}{\partial t} + \underline{v}_f \cdot \nabla \underline{v}_f\right] = -\nabla p_f + \rho_f \underline{g} - \frac{\phi\mu_f}{k}(\underline{v}_f) \quad \ldots\ldots [12]$$

Energy:

Solid:

$$(1-\phi)\rho_s \frac{\partial E_s}{\partial t} = \nabla \cdot (\kappa_1 \nabla T_s) - \nabla \cdot \underline{Q} \quad [13]$$

Fluid:

$$\phi\rho_f \frac{D_f E_f}{Dt} = -p_f \nabla \cdot (\phi \underline{v}_f) + \nabla \cdot (\kappa_2 \nabla T_f) + \nabla \cdot \underline{Q} + \frac{\phi^2 \mu_f}{k} |\underline{v}_f|^2 \quad \ldots\ldots [14]$$

For the present discussion, it will suffice to consider only the mixture energy balance. We will furthermore assume that $T_s = T_f = T$. The mixture energy balance is therefore given by:

$$\left[(1-\phi)\rho_s \frac{\partial E_s}{\partial t} + \phi\rho_f \frac{\partial E_f}{\partial t}\right] + \phi\rho_f \underline{v}_f \cdot \nabla E_f = -p_f \nabla \cdot (\phi \underline{v}_f) + \nabla \cdot (\kappa_m \nabla T) + \frac{\phi^2 \mu_f}{k} |\underline{v}_f|^2 \quad \ldots\ldots [15]$$

where

$$\kappa_m = \kappa_1 + \kappa_2 \quad \ldots\ldots [16]$$

Eliminating $\nabla \cdot (\phi \underline{v}_f)$ between Eqs. [11] and [15], the mixture energy balance can be expressed in the following alternate form:

$$\left[(1-\phi)\rho_s \frac{\partial E_s}{\partial t} + \phi\rho_f \frac{\partial E_f}{\partial t}\right] + \phi\rho_f \underline{v}_f \cdot \nabla E_f = \frac{\phi p_f}{\rho_f}\left[\frac{\partial \rho_f}{\partial t} + \underline{v}_f \cdot \nabla \rho_f\right] + \nabla \cdot (\kappa_m \nabla T) + \frac{\phi^2 \mu_f}{k} |\underline{v}_f|^2 \quad \ldots\ldots [17]$$

The passive reservoir is thus described by Eqs. [11], [12] and [17].

## NONDIMENSIONAL ANALYSIS

It is convenient to reduce Eqs. [11], [12] and [17] to a nondimensional form. For this purpose, it is essential to choose certain characteristic parameters. We will use the following set of quantities:

$\rho_0$ ~ density (e.g., initial fluid density)

$C_V$ ~ specific heat (e.g., mixture specific heat)

$T_0$ ~ temperature (e.g., temperature difference across reservoir)

$L$ ~ length (e.g., linear reservoir dimension)

$v_0$ ~ velocity (e.g., average fluid velocity)

We next introduce the following nondimensional quantities:

$$\rho_f' = \rho_f/\rho_0;\ \rho_s' = \rho_s/\rho_0;\ x' = x/L;$$

$$\underline{v}_f' = \underline{v}_f/v_0;\ p_f' = p_f/\rho_0 Lg;\ T' = T/T_0;$$

$$E_f' = E_f/C_V T_0;\ E_s' = E_s/C_V T_0;$$

$$t' = tv_0/L \quad \ldots\ldots [18]$$

Substituting from Eqs. [18] into Eqs. [11], [12], and [17], and dropping primes, we obtain the following set of nondimensional equations:

$$\phi \frac{\partial \rho_f}{\partial t} + \nabla \cdot (\phi\rho_f \underline{v}_f) = 0 \quad \ldots\ldots [19]$$

$$\rho_f\left[\frac{\partial \underline{v}_f}{\partial t} + \underline{v}_f \cdot \nabla \underline{v}_f\right] = -\left(\frac{gL}{v_0^2}\right)\left[\nabla p_f - \rho_f \delta_{iz}\right] - \left(\frac{\phi\mu_f L}{k\rho_0 v_0}\right)\underline{v}_f \quad \ldots\ldots [20]$$

$$\left[(1-\phi)\rho_s \frac{\partial E_s}{\partial t} + \phi\rho_f \frac{\partial E_f}{\partial t}\right] + \phi\rho_f \underline{v}_f \cdot \nabla E_f$$

$$= \left(\frac{\phi g L}{C_V T_0}\right) \frac{p_f}{\rho_f}\left[\frac{\partial \rho_f}{\partial t} + \underline{v}_f \cdot \nabla \rho_f\right]$$

$$+ \nabla \cdot \left[\left(\frac{\kappa_m}{\rho_0 C_V v_0 L}\right) \nabla T\right]$$

$$+ \phi^2 \left(\frac{\mu_f v_0 L}{k\rho_0 C_V T_0}\right) |v_f|^2 \quad \ldots\ldots [21]$$

The system of Eqs. [19] - [21] involves five nondimensional groups, i.e.,

$$\frac{gL}{v_0^2} ; \frac{\phi\mu_f L}{k\rho_0 v_0} ; \frac{\phi g L}{C_V T_0} ; \frac{\kappa_m}{\rho_0 C_V v_0 L} ;$$

$$\frac{\mu_f v_0 L \phi^2}{k\rho_0 C_V T_0} \quad \ldots\ldots\ldots\ldots [22]$$

There are, however, only four independent dimensionless quantities since

$$\frac{\phi^2 \mu_f v_0 L}{k\rho_0 C_V T_0} = \left(\frac{\phi\mu_f L}{k\rho_0 v_0}\right)\left(\frac{\phi g L}{C_V T_0}\right) \Big/ \left(\frac{gL}{v_0^2}\right) \quad [23]$$

We shall now examine the importance of various terms in Eqs. [19] - [21] to find out if it is possible to make any simplifications. For a typical geothermal (liquid) reservoir, we have:

$g \sim 10^3$ cm/sec$^2$, $L \sim 10^5$ cm ,

$\mu_f \sim 10^{-2}$ dyne-sec/cm$^2$, $k \sim 10^{-9}$ cm$^2$ ,

$\phi \sim 10^{-1}$, $\rho_0 \sim 1$ gm/cm$^3$, $T_0 \sim 100$°C ,

$\kappa_m \sim 10^5$ dyne/sec°C

Therefore, we have

$$\frac{gL}{v_0^2} \sim 10^8/v_0^2 ; \frac{\phi\mu_f L}{k\rho_0 v_0} \sim 10^{11}/v_0 ;$$

$$\frac{\phi g L}{C_V T_0} \sim 10^5/C_V ; \frac{\kappa_m}{\rho_0 C_V v_0 L} \sim 1/v_0 C_V ;$$

$$\frac{\phi^2 \mu_f v_0 L}{k\rho_0 C_V T_0} \sim 10^8 v_0/C_V$$

On noting that

$$\rho_f \sim 0(1), \underline{v}_f \sim 0(1),$$

$$\nabla \underline{v}_f \sim \frac{\partial \underline{v}_f}{\partial t} \sim 0(1), (\nabla p_f - \rho_f \delta_{iz}) \sim 0(1) .$$

we have from momentum balance Eq. [20]:

$$0(1) = -\frac{10^8}{v_0^2} 0(1) - \frac{10^{11}}{v_0} 0(1)$$

or

$$v_0^2 0(1) = -10^8 0(1) - 10^{11} v_0 0(1)$$

Thus, unless $v_0 \sim 0(10^4)$ [highly unlikely in geothermal reservoirs], we are safe in ignoring inertia terms (left hand side) in momentum Eq. [20]. Furthermore, we have

$$v_0 \sim \frac{\rho_0 g k}{\phi\mu_f} \sim 0(10^{-3} \text{ cm/sec}).$$

Putting

$$v_0 = \frac{\rho_0 g k}{\phi\mu_f} ,$$

and ignoring inertia terms, the momentum and energy equations [20] and [21] become:

$$\underline{v}_f = -[\nabla p_f - \rho_f \delta_{iz}] \quad \ldots\ldots [20']$$

$$\left[(1-\phi)\rho_s \frac{\partial E_s}{\partial t} + \phi\rho_f \frac{\partial E_f}{\partial t}\right]$$

$$+ \phi\rho_f \underline{v}_f \cdot \nabla E_f$$

$$= \left(\frac{\phi g L}{C_V T_0}\right)\left\{\frac{p_f}{\rho_f}\left[\frac{\partial \rho_f}{\partial t} + \underline{v}_f \cdot \nabla \rho_f\right] + |\underline{v}_f|^2\right\}$$

$$+ \nabla \cdot \left\{\left[\frac{\kappa_m \phi \mu_f}{\rho_0^2 C_V L g k}\right] \nabla T\right\} \quad \ldots\ldots [21']$$

Note that this leaves us with only two dimensionless groups:

$$\phi g L/C_V T_0, \kappa_m \phi \mu_f / \rho_0^2 C_V L g k \quad \ldots\ldots [22']$$

Furthermore,

$$\phi gL/C_V T_o \sim (10^3/C_V);$$

$$\kappa_m \phi u_f/\rho_o^2 C_V Lgk \sim O(10^3/C_V) .$$

We are now ready to examine the magnitude of various terms in the energy equation. Assuming that

$$E_s \sim O(E_f) ,$$

we have

$$O\left(\frac{\partial E_f}{\partial t}\right) + \nabla E_f \; O(10^{-1}) = \frac{10^3}{C_V}\left\{O\left(\frac{\partial \rho_f}{\partial t}\right) + O(\nabla \rho_f) + O(1)\right\} + \frac{10^3}{C_V}\left\{O(\nabla^2 T)\right\} .$$

If we, furthermore, assume that $E_f \sim C_V T$, the order of various terms in the energy equation becomes:

$$O\left(\frac{\partial T}{\partial t}\right) + \underbrace{\nabla T \; O(10^{-1})}_{\text{convection}} = \frac{10^3}{C_V^2}\left\{\underbrace{O\left(\frac{\partial \rho_f}{\partial t}\right) + O(\nabla \rho_f)}_{\text{pressure work}} + \underbrace{O(1)}_{\text{viscous diffusion}} + \underbrace{O(10^2 \nabla^2 T)}_{\text{thermal diffusion}}\right\} .$$

Since $\nabla T \sim O(1)$, the left hand side is at least of $O(10^{-1})$. Thus for any term on the right hand side of the energy equation to be retained, it must be of $O(C_V^2/10^4)$, i.e., of $O(10^2)$ if $C_V \sim O(10^3)$. In view of the latter result, we are certainly justified in ignoring the viscous diffusion term. Furthermore, for pressure work term, we have

$$\frac{\partial \rho_f}{\partial t} \sim O(\nabla \rho_f) \sim O[\nabla \cdot (\underline{v}_f)] << O(10^4) .$$

Thus the pressure work term is also likely to be unimportant.

On the basis of the preceding discussion, it is possible to draw the following conclusions for a passive geothermal reservoir:

1. General system of governing equations for fluid flow in a porous medium is characterized by four independent dimensionless quantities, i.e.,

$$\frac{gL}{v_o^2} \; ; \; \frac{\phi \mu_f L}{k \rho_o v_o} \; ; \; \frac{\phi gL}{C_V T_o} \; ; \; \frac{\kappa_m}{\rho_o C_V v_o L}$$

2. In geothermal applications, it is possible to ignore inertia terms in the momentum equation. The number of independent dimensionless parameters is two, i.e.,

$$\phi gL/C_V T_o \; ; \; \kappa_m \phi u_f/\rho_o^2 C_V Lgk .$$

3. Pressure work and viscous diffusion terms in the energy equation may be ignored. This implies that the fluid flow can be described by a single dimensionless parameter, i.e.,

$$\kappa_m \phi u_f/\rho_o^2 C_V Lgk .$$

## SIMPLIFIED BALANCE LAWS FOR A SINGLE PHASE FULLY INTERACTIVE SYSTEM

Let us now consider a fully interactive system. In a geothermal reservoir, rock matrix strains are likely to be quite small; this implies that one need not consider the solid mass balance Eq. [1]. Furthermore, it is permissible to assume that the solid velocity, $v_s$, is much smaller than the fluid velocity, $v_f$ (as a matter of fact, we need only to postulate that $v_s \sim O(v_f)$). The last assumption enables us to ignore inertia terms in the solid momentum Eq. [3], and all mechanical work and mechanical interaction energy terms in the energy Eqs. [7] and [8]. Thus we obtain the following simplified system of balance equations (in dimensional form) for the fully interactive geothermal reservoir (coordinate system attached to the solid matrix):

Mass:

Solid:

None

Fluid:

$$\left[\frac{\partial}{\partial t} + (\underline{v}_f - \underline{v}_s) \cdot \nabla\right](\phi \rho_f) + \phi \rho_f \nabla \cdot \underline{v}_f = 0 \quad \ldots\ldots\ldots [23]$$

Momentum:

Solid:

$$-\nabla\left[(1-\phi)p_s + \phi p_f\right] + \text{div}\,\underline{S} + \left[(1-\phi)\rho_s + \phi\rho_f\right]\underline{g} = 0 \quad \ldots\ldots [24]$$

Fluid:

$$(\underline{v}_f - \underline{v}_s) = \frac{k}{\phi\mu_f}\left[-\nabla p_f + \rho_f \underline{g}\right] \quad \ldots [25]$$

Energy:

Solid:

$$(1-\phi)\rho_s \frac{\partial E_s}{\partial t} = \nabla \cdot (\kappa_1 \nabla T_s) - \nabla \cdot \underline{Q} \quad \ldots [26]$$

Fluid:

$$\phi\rho_f\left[\frac{\partial E_f}{\partial t} + (\underline{v}_f - \underline{v}_s)\cdot\nabla E_f\right] = \nabla\cdot(\kappa_2\nabla T_f) + \nabla\cdot\underline{Q} \quad \ldots\ldots [27]$$

It is appropriate to note here that in geothermal applications, it is permissible to regard the fluid and the solid matrix to be in local thermal equilibrium. Justification for this is given in a paper by Nayfeh, et al.[9] Assumption of local thermal equilibrium ($T_s = T_f = T$) implies that one need consider only the mixture energy balance obtained by summing Eqs. [26] and [27].

## EXTENSION TO TWO-PHASE (LIQUID/VAPOR) FLOW

Assuming that (1) inertia (momentum balance), pressure work and viscous dissipation (energy balance) terms are negligible, (2) water and water vapor are in local pressure and thermal equilibrium, and (3) fluid and rock matrix are in local thermal equilibrium, the equations expressing mass, momentum and energy balance are:

Mass:

Liquid:

$$\frac{\partial}{\partial t}\left[\phi(1-S)\rho_l\right] = -\nabla\cdot\left[\phi(1-S)\rho_l\underline{v}_l\right] - \dot{m} \quad \ldots\ldots [28]$$

Vapor:

$$\frac{\partial}{\partial t}\left[\phi S\rho_v\right] = -\nabla\cdot\left[\phi S\rho_v\underline{v}_v\right] + \dot{m} \quad \ldots [29]$$

where $\dot{m}$ is the mass transfer rate from liquid to vapor due to phase change.

Momentum:

Liquid:

$$\underline{v}_l = -\frac{R_l k}{\phi(1-S)\mu_l}\left[\nabla p_f - \rho_l \underline{g}\right] \quad \ldots\ldots [30]$$

Vapor:

$$\underline{v}_v = -\frac{R_v k}{\phi S\mu_v}\left[\nabla p_f - \rho_v \underline{g}\right] \quad \ldots\ldots [31]$$

where $p_f$ denotes the fluid (= liquid = vapor) pressure.

Energy:

Rock/Liquid/Vapor Mixture:

$$\frac{\partial}{\partial t}\left[(1-\phi)\rho_s E_s + \phi(1-S)\rho_l E_l + \phi S\rho_v E_v\right] + \nabla\cdot\left[\phi(1-S)\rho_l E_l\underline{v}_l + \phi S\rho_v E_v\underline{v}_v\right] = \nabla\cdot\left[\kappa_m\nabla T\right] \quad \ldots\ldots [32]$$

where $\kappa_m$ denotes the mixture (solid and fluid) conductivity, and $T$ ($=T_s = T_l = T_v$) is the mixture temperature.

For computational purposes, it may be convenient to eliminate two velocity fields ($\underline{v}_l$, $\underline{v}_v$) in favor of a single liquid/vapor mixture velocity field ($\underline{v}_f$).

Introducing

$$\rho_f(\text{mixture density}) = S\rho_v + (1-S)\rho_l \quad \ldots [33]$$

and

$$\underline{v}_f(\text{mixture velocity}) = \frac{S\rho_v\underline{v}_v + (1-S)\rho_l\underline{v}_l}{\rho_f} \quad \ldots\ldots [34]$$

and adding Eqs. [28] and [29], the mixture mass balance may be expressed as:

$$\frac{\partial}{\partial t}[\phi\rho_f] = -\nabla \cdot [\phi\rho_f \underline{v}_f] \quad \ldots\ldots [35]$$

To obtain the mixture momentum balance equation, substitute for $\underline{v}_l$ and $\underline{v}_v$ from Eqs. [30] and [31] into Eq. [34]. This yields

$$\underline{v}_f = -\frac{k}{\phi\mu_f}[\nabla p_f - \rho^* \underline{g}] \quad \ldots\ldots [36]$$

where

$$\mu_f = \frac{\mu_l\mu_v\rho_f}{R_l\rho_l\mu_v + R_v\rho_v\mu_l} \quad \ldots\ldots [37]$$

$$\rho^* = \frac{R_l\rho_l^2\mu_v + R_v\rho_v^2\mu_l}{R_l\rho_l\mu_v + R_v\rho_v\mu_l} \quad \ldots\ldots [38]$$

Note that for

S = 1 (all vapor):

$$R_l = 0,\ R_v = 1,\ \rho_f = \rho_v$$

$$\underline{v}_f = \underline{v}_v,\ \mu_f = \mu_v,\ \rho^* = \rho_v \quad \ldots\ldots [39]$$

S = 0 (all liquid):

$$R_l = 1,\ R_v = 0,\ \rho_f = \rho_l$$

$$\underline{v}_f = \underline{v}_l,\ \mu_f = \mu_l,\ \rho^* = \rho_l \quad \ldots\ldots [40]$$

Introducing

$$E_f \equiv \frac{(1-S)\rho_l E_l + S\rho_v E_v}{(1-S)\rho_l + S\rho_v} \quad \ldots\ldots [41]$$

and noting that

$$E_v \equiv E_l + \delta \quad \ldots\ldots [42]$$

$$E_f = E_l + S(\rho_v/\rho_f)\delta \quad \ldots\ldots [43]$$

$$E_l - E_f = -S(\rho_v/\rho_f)\delta \quad \ldots\ldots [44a]$$

$$E_v - E_f = \delta[1-S(\rho_v/\rho_f)] \quad \ldots\ldots [44b]$$

the energy balance relation [32] may be rewritten as:

$$\frac{\partial}{\partial t}[(1-\phi)\rho_s E_s + \phi\rho_f E_f] + \nabla \cdot [\phi\rho_f \underline{v}_f E_f + \underline{X}] = \nabla \cdot [\kappa_m \nabla T] \quad \ldots\ldots [45]$$

where

$$\underline{X} = \phi(1-S)\rho_l \underline{v}_l (E_l - E_f) + \phi S\rho_v \underline{v}_v (E_v - E_f) \quad \ldots\ldots [46]$$

Substituting for $(E_l - E_f)$ and $(E_v - E_f)$ from Eqs. [44] into Eq. [46], we have

$$\underline{X} = \phi\delta S\rho_v [\underline{v}_v - \underline{v}_f] \quad \ldots\ldots [46']$$

Vapor velocity $\underline{v}_v$ can now be eliminated by combining Eqs. [31] and [46']. Thus

$$\underline{X} = -\phi\delta S\rho_v \left[\frac{R_v k}{\phi S\mu_v}(\nabla p_f - \rho_v \underline{g}) + \underline{v}_f\right]. \quad [47]$$

Equations [35], [36] and [45] are the desired mixture mass, momentum and energy balance relations.

## CONSTITUTIVE RELATIONS

The partial strain-rate tensor for rock $\dot{\varepsilon}^r_{ij}$ is given by:

$$\dot{\varepsilon}^r_{ij} = \frac{1}{2}\left[\text{grad } \underline{v}_s + (\text{grad } \underline{v}_s)^t\right] = \frac{\dot{\varepsilon}^r}{3}\delta_{ij} + \dot{e}_{ij} \quad \ldots\ldots [48]$$

where $\dot{\varepsilon}^r$ and $\dot{e}_{ij}$ denote the isotropic (volumetric) and the deviatoric parts of the strain-rate tensor, respectively. Partial volumetric strain is related to the effective volumetric strain $\varepsilon^{re}$ through the relation:[1-7]

$$\varepsilon^{re} = \frac{\rho_{os}}{\rho_s} - 1 = \left(\frac{1-\phi}{1-\phi_o}\right)(1+\varepsilon^r) - 1. \quad [49]$$

The rock grain may be assumed to be a linear thermoelastic material over the range of temperatures and pressures encountered in geothermal reservoirs. Therefore

$$p_s = -K_s\varepsilon^{re}(1-3\eta_s T_s) \quad \ldots\ldots [50]$$

Additionally, we will postulate that the shear stresses $\underline{S}$ are linearly related to shear strains $\underline{e}$ through Hooke's law:

$$\underline{S} = 2\mu_p \underline{e} \quad \ldots\ldots [51]$$

The fluid (water and water vapor) equation of state (constitutive relation) will be taken to be of the form:

$$p_f = p_f(\rho_f, E_f) \quad \ldots\ldots\ldots [52a]$$

$$T_f = T_f(\rho_f, E_f) \quad \ldots\ldots\ldots [52b]$$

To complete the above description, we need to prescribe a constitutive relation for porosity $\phi$ in terms of other field variables. Porosity $\phi$ will, in general, depend upon mixture pressure $p_c$ ($= \phi p_f + (1-\phi) p_s$), fluid pressure $p_f$ and deviatoric stresses $\underset{\sim}{S}$.

$$\phi = \phi(p_c, p_f, S) \quad \ldots\ldots\ldots [53]$$

Specific functional forms for $\phi$ may be developed from the usual laboratory tests on rock specimens (see, e.g., Garg, et al.).[7]

## CONCLUDING REMARKS

The system of governing equations outlined in the preceding sections is quite complex and must be solved numerically. A numerical procedure has been derived for solving the transport of heat and fluid mass in a "quasi-active" geothermal reservoir. The method is applicable to the two-phase case, and properly treats the effects of phase changes (liquid ⇄ vapor) within the pores of the reservoir rock. The quasi-active case is midway in sophistication between the "rigid matrix" model in which all rock properties (porosity, permeability, thermal conductivity, etc.) are treated as functions of position only, and the "fully interactive" case in which the entire rock stress and deformation fields are calculated, along with the heat and fluid flow. In the quasi-active model, the rock thermal properties (heat capacity and thermal conductivity) may be functions of temperature as well as position; the permeability may change with porosity, and the porosity may also vary with position and time, but, at a particular point, the local porosity is assumed to depend only on the local pore pressure. The quasi-active model can be extended to the fully interactive case by supplying constitutive relations for the rock matrix and imposing a static equilibrium condition (where pore pressure contributes to total stress) at each time step. Work along these lines is underway and will be described in future publications.

## NOMENCLATURE

| | |
|---|---|
| $E_i$ | Internal energy of ith phase [i = s (solid), i = l (liquid), i = v (vapor), i = f (fluid)] |
| $g$ | Acceleration due to gravity |
| $k$ | Rock permeability |
| $k_s$ | rock grain bulk modulus |
| $p_s(p_f)$ | Solid (fluid) pressure |
| $R_l(R_v)$ | Relative permeability for liquid (vapor) |
| $S$ | Relative vapor volume [$= V_v/(V_v + V_l)$] |
| $\underset{\sim}{S}$ | Deviatoric stress tensor for porous rock |
| $T_s(T_f)$ | Solid (fluid) temperature |
| $\underline{v}_i$ | Velocity of ith phase (i = s, l, v, f) |
| $V_v(V_l)$ | Vapor (liquid) volume |
| $\delta$ | Heat of vaporization at a given pressure and temperature |
| $\eta_s$ | Coefficient of linear thermal expansion for rock grain |
| $\kappa_l(\kappa_2)$ | Porous solid (interspersed fluid) thermal conductivity |
| $\kappa_s(\kappa_f)$ | Rock grain (fluid) thermal conductivity |
| $\mu_i$ | Viscosity (i = f, l, v) |
| $\mu_p$ | Shear modulus of porous rock |
| $\rho_i$ | Density (i = s, f, l, v) |
| $\phi$ | Porosity |

## ACKNOWLEDGMENT

This work was sponsored in part by NSF/RANN Grant (GI-43884) to Systems, Science and Software, and also by NSF/RANN Grant (GI-44212) to the University of Colorado and Systems, Science and Software.

REFERENCES


1. Morland, L. W.: "A Simple Constitutive Theory for a Fluid-Saturated Porous Solid," J. Geophys. Res. (1972) 77, 890-900.

2. Garg, S. K.: "Wave Propagation Effects in a Fluid-Saturated Porous Solid," J. Geophys. Res. (1971) 76, 7947-7962.

3. Garg, S. K. and Kirsch, J. W.: "Hugoniot Analysis of Composite Materials," J. Composite Materials (1971) 5, 428-445.

4. Garg, S. K. and Kirsch, J. W.: "Steady Shock Waves in Composite Materials," J. Composite Materials (1973) 7, 277-285.

5. Garg, S. K. and Nur, A.: "Effective Stress Laws for Fluid-Saturated Porous Rocks," J. Geophys. Res. (1973) 78, 5911-5921.

6. Garg, S. K., Nayfeh, A. H. and Good, A. J.: "Compressional Waves in Fluid-Saturated Elastic Porous Media," J. Appl. Phys. (1974) 45, 1968 - 1974.

7. Garg, S. K., Brownell, Jr., D. H., Pritchett, J. W. and Herrmann, R. G.: "Shock Wave Propagation in Fluid-Saturated Porous Media," to appear in J. Appl. Phys.

8. Brace, W. F.: "Pore Pressure in Geophysics," in Flow and Fracture of Rocks, American Geophysical Union, Washington, D. C. (1972) 265-273.

9. Nayfeh, A. H., Brownell, Jr., D. H. and Garg, S. K.: "Heat Exchange in a Fluid Percolating Through Porous Media," submitted to Journal of Heat Transfer.

SPE 6892

# GEOTHERMAL RESERVOIR MODELLING

by

K. H. Coats
INTERCOMP Resource Development
and Engineering, Inc.



This paper was presented at the 52nd Annual Fall Technical Conference and Exhibition of the Society of Petroleum Engineers of AIME, held in Denver, Colorado, Oct. 9-12, 1977. The material is subject to correction by the author. Permission to copy is restricted to an abstract of not more than 300 words. Write 6200 N. Central Expy., Dallas, Texas 75206.

## ABSTRACT

This paper describes and partially evaluates an implicit, three-dimensional geothermal reservoir simulation model. The evaluation emphasizes stability or time-step tolerance of the implicit finite-difference formulation. In several illustrative multiphase flow problems, the model stably accomodated time steps corresponding to grid block saturation changes of 80-100% and grid block throughput ratios the order of $10^8$. This compares to our experience of limits of 3 to 10% saturation change and roughly 20,000 throughput ratio with semi-implicit oil and geothermal reservoir models.

The illustrative applications shed some light on practical aspects of geothermal reservoir behavior. Applications include single- and two-phase single-well behavior, fractured-matrix reservoir performance and well test interpretation, and extraction of energy from fractured hot dry rock. Model stability allows inclusion of formation fractures and wellbores as grid blocks.

An analytical derivation is presented for a well deliverability reduction factor which can be used in simulations using large grid blocks. The factor accounts for reduced deliverability due to hot water flashing and steam expansion accompanying pressure decline near the well.

References and illustrations at end of paper.

## INTRODUCTION

This paper describes a numerical model for simulating geothermal well or reservoir performance. The model is considerably more general than any described in the literature to date. It treats transient, three-dimensional, single- or two-phase fluid flow in normal heterogeneous or fractured-matrix formations. Both conductive and convective heat flow are accounted for and fluid states in the reservoir can range from undersaturated liquid to two-phase steam-water mixtures to superheated steam. Aquifer water influx and heat source/sink terms necessary in simulating free convection cells are included in the model formulation.

The primary purpose of the work described here was evaluation of the capability of an implicit model formulation. Our experience with semi-implicit simulation of petroleum and geothermal reservoirs has shown time step restrictions related to conditional stability. In multiphase flow problems, the maximum tolerable time step size generally corresponds to a maximum of 3 to 10 percent saturation change in any grid block in one time step. In some steamflood and geothermal simulations, we have found this to result in very small time steps and correspondingly high computing costs. This work was performed with the hope that the implicit model formulation would give unconditional stability with no time step restriction other than that imposed by time truncation error.

Calculated results are presented for a variety of geothermal well and reservoir illustrative problems. Emphasis in connection with these results is placed on the stability or time step tolerance of the model. However, the applications are also intended to shed some light on practical aspects of geothermal reservoir behavior.

Following description of the implicit model formulation, the paper presents applications including single-well deliverability under two-phase flow conditions, depletion of a fractured-matrix formation with boiling, drawdown test interpretation in single-phase, fractured-matrix formations, and heat extraction from artificially fractured hot dry rock. An analytical expression is derived to represent the effective transient productivity index of a well which experiences hot water flashing due to pressure drawdown from an exterior radius where steam saturation may be zero or small.

We have applied the model extensively in simulation of natural convection cells with zero porosity (hard rock) grid block definition above and below the formation. This definition eliminates the erroneous imposition of constant temperature boundaries at the top and bottom of the convection cell common in many reported studies of natural convection. Another application simulated development over geologic time of a superheated (Geyser's type) reservoir from an early time of magma or heat source intrusion beneath an initial normal gradient cold water aquifer. These natural convection type applications are omitted here due to the significant length of the paper. Some of this convection work is reported in a recent paper [4].

## MODEL DESCRIPTION

The model consists of two equations expressing conservation of mass of $H_2O$ and conservation of energy. These equations account for three-dimensional, single- or two-phase fluid flow, convective and conductive heat flow in the reservoir and conductive heat transfer between the reservoir and overlying and underlying strata. The phase configuration at any time can vary spatially through the formation from single-phase undersaturated water to two-phase steam-water mixture to single-phase superheated steam.

The equations represent water influx from an aquifer extending beyond the reservoir grid using the Carter-Tracy [2] or simpler approximations. Heat source and sink terms in the equations are useful in imposing temperature and/or heat flux boundary conditions in simulation of natural convection. The mass equations do not account for the presence of inert gases or for varying concentration and precipitation of dissolved salts.

The model applies to reservoir grids including one-dimensional, two-dimensional radial-z, x-z or x-y and three-dimensional, either x-y-z Cartesian or r-$\phi$-z cylindrical. In the r-z and r-$\phi$-z case, the wellbore of a well at r = 0 can be included in the grid, resulting in enhanced stability and accuracy as discussed below. The r-z grid can be used in simulating a sector of a fractured-matrix reservoir with the horizontal and vertical fractures represented by grid blocks. The grid can include blocks of zero porosity representing hard rock, with no pressure calculated, and blocks of 100% porosity representing either fractures or wellbores.

The mass balance on $H_2O$ combines in a single equation the steam-phase and liquid water-phase mass balance equations. This combination was proposed in our early steamflood work [3] to eliminate difficulties in handling the mass transfer term. The energy balance is the First Law of Thermodynamics applied to each grid block. The grid block is an open system with fixed boundaries. With potential and kinetic energy terms ignored, the energy balance states that (enthalpy flow rate in) - (enthalpy flow rate out) = rate of gain of internal energy in the grid block. For some reason, considerable confusion exists in the literature regarding this energy balance. Enthalpy is U + pv where U is internal energy. Many modelling papers ignore the pv term, in which case the energy balance erroneously becomes (net flow rate of internal energy into the grid block = rate of gain of internal energy in the block). A recent paper [4] uses an erroneous energy balance stating (net flow rate of enthalpy into the grid block = rate of gain of enthalpy in the block).

The two model equations are*

$$\Delta[T_w(\Delta p_w - \gamma_w \Delta z) + T_g(\Delta p_g - \gamma_g \Delta z)] - q = \frac{V}{\Delta t}\bar{\delta}(\phi\rho_w S_w + \phi\rho_g S_g) \qquad (1a)$$

$$\Delta[T_w H_w(\Delta p_w - \gamma_w \Delta z) + T_g H_g(\Delta p_g - \gamma_g \Delta z)] + \Delta(T_c \Delta T) - q_{HL} - q_H = \frac{V}{\Delta t}\bar{\delta}(\phi\rho_w S_w U_w + \phi\rho_g S_g U_g) + (1-\phi)(\rho c_p)_R T \qquad (1b)$$

For a given grid block (i,j,k), all terms in these equations are single-valued functions of $(T, S_g, p)_{i,j,k}$ and $(T, S_g, p)$ in the six neighboring grid blocks (i±1,j,k), (i,j±1,k), (i,j,k±1). Thus, transposing the right-hand sides, we can write Equations (1) simply as

*See Nomenclature for definition of terms.

$$F_1(\underline{x}) = 0$$
$$F_2(\underline{x}) = 0 \qquad (2)$$

where $\underline{x}$ represents the vector of the above listed 21 unknowns.

Following the totally implicit procedure described by Blair and Weinaug [5], we apply the Newton-Raphson iterative method to (2) as

$$F_1(\underline{x}) \approx F_1(\underline{x}^\ell) + \sum_{i=1}^{21} (\partial F_1/\partial x_i)^\ell \delta x_i = 0$$
$$F_2(\underline{x}) \approx F_2(\underline{x}^\ell) + \sum_{i=1}^{21} (\partial F_2/\partial x_i)^\ell \delta x_i = 0 \qquad (3)$$

where we temporarily use $x_i$ to denote the 21 unknowns and superscript $\ell$ denotes latest iterate value. The operator $\Delta$ in Equations (1) denotes change over time step while $\delta$ in Equations (3) denotes change over the coming iteration. The approximation $\delta x_i \approx x_{i,n+1} - x_i^\ell$ becomes increasingly exact as we near convergence.

The partial derivatives in Equations (3) are all evaluated at latest iterate values of $x_i$. The functions $F_1$, $F_2$ involve three different types of terms: right-hand sides (accumulation terms), sink/source terms and interblock flow terms. Differentiation of accumulation terms is straightforward. The heat loss term and its derivative is evaluated as described in Reference [3]. The well injection/production terms and their derivatives are evaluated as described in some detail below. The interblock flow terms are evaluated as follows: Relative permeabilities and enthalpies are evaluated at upstream grid block conditions, interblock $\rho/\mu$ and $\gamma$ values are evaluated as arithmetic averages of their values in the two grid blocks. Water phase pressure $p_w$ is expressed as $p - P_c$ where $p$ is gas pressure and capillary pressure $P_c$ is a single-valued function of $S_g$.

For all $N_x N_y N_z$ grid blocks taken together, Equations (3) are $2N_x N_y N_z$ equations in $3N_x N_y N_z$ unknowns, ($\delta T$, $\delta S_g$, $\delta p$) for each grid block. Only two of these three unknowns in each block are independent. If the block contains undersaturated water or superheated steam, $\delta S_g = 0$ and $\delta T$, $\delta p$ are the block's two unknowns. If the block is saturated, two-phase, then temperature $T = T_s(p)$ and $\delta T$ is $(dT/dp)_s \delta p$ where subscript s denotes the saturated condition.

Equations (3) can be written for each grid block in the form

$$\Delta(T_{11}\delta P_1) + \Delta(T_{12}\delta P_2) + R_1 = C_{11}P_1 + C_{12}P_2$$
$$\Delta(T_{21}\delta P_1) + \Delta(T_{22}\delta P_2) + R_2 = C_{21}P_1 + C_{22}P_2 \qquad (4)$$

where $P_1$ is either $\delta T$ or $\delta S_g$ and $P_2$ is $\delta p$. The terms $R_1$, $R_2$ are $F_1(\underline{x}^\ell)$, $F_2(\underline{x}^\ell)$, respectively, in Equations (3). The $\Delta(T\Delta P)$ type terms are not true Laplacians but rather are, as illustrated by the x-direction component

$$\Delta_x(T_x\Delta_x P) = T^+_{xi}P_{i+1} + T^0_{xi}P_i + T^-_{xi}P_{i-1}$$

where the center term $T^0_{xi}$ can be combined with the appropriate $C_{ij}$ in Equation (4) and need not be stored. More simply, Equation (4) can be written

$$\Delta(T\Delta\underline{P}) + \underline{R} = C\underline{P} \qquad (5)$$

where T and C are the 2 x 2 matrices $T_{ij}$, $C_{ij}$ and $\underline{R}$ and $\underline{P}$ are column vectors. We use reduced band width direct solution [6] to solve Equation (5) for $P_1$, $P_2$ and obtain new iterate values as $p^{\ell+1} = p^\ell + \delta p$. Convergence is defined by

$$\text{Max}|\delta p_{ijk}| \leq \epsilon_p$$
$$\text{Max}|\delta T_{ijk}| \leq \epsilon_T \qquad (6)$$
$$\text{Max}|\delta S_{gijk}| \leq \epsilon_S$$

where MAX denotes maximum over all grid blocks. We generally use tolerances of .1 psia, 1°F, 1% saturation and have not found sensitivity of results to tighter tolerances.

## PVT TREATMENT

At saturated conditions, $U_w$, $U_g$, $\rho_w$, $\rho_g$ are evaluated as single-valued functions of temperature from the Steam Tables [7]. $U_w$ is assumed a single-valued function of temperature for undersaturated water. Density of undersaturated water is calculated as

$$\rho_w = \rho_{ws}(T)[1 + c_w(T)(p - p_s(T))] \qquad (7)$$

where subscript s denotes saturation condition. The "compressibility" $c_w(T)$ is derived as follows. The Steam Tables [7] include a tabulation of $(v - v_s)$ for undersatufated water as a function of temperature and pressure, where v is specific volume, cubic feet per pound. The tabular values are fit well by the expression

$$v = v_s - s(T)(p - p_s(T))$$

where s(T) is dependent only upon temperature as:

| T, °F | $s(T) \times 10^5$ |
|---|---|
| < 200 | .0054 |
| 300 | .0072 |
| 400 | .0109 |
| 500 | .0205 |
| 600 | .065 |
| 660 | .355 |

This equation can be written

$$\frac{1}{\rho_w} = \frac{1}{\rho_{ws}(T)} - \frac{s(T)\rho_{ws}(T)}{\rho_{ws}(T)}(p - p_s(T))$$

Since $s(T)\rho_{ws}(T)(p - p_s(T))$ is small in comparison to 1 (except at temperatures approaching 700°F), this equation can be written as Equation (7) where $c_w(T)$ is $s(T)\rho_{ws}(T)$.

For superheated steam, internal energy $U_g$ and density $\rho_g$ are approximated by

$$U_g \cong U_{gs}(p) + C_{psteam}(T - T_s(p)) \quad (8)$$

$$\rho_g \cong \rho_{gs}(p)\frac{T_s(p) + 460}{T + 460} \quad (9)$$

where specific heat $C_{psteam}$ is constant. Equation (9) is accurate in proportion to the constancy of steam z-factor from p, $T_s(p)$ to p, T. Water and steam phase viscosities are evaluated as single-valued functions of temperature equal to their respective saturated values. Enthalpies are

$$H_w = U_w + 144/778.2\ p/\rho_w$$

$$H_g = U_g + 144/778.2\ p/\rho_g \quad (10)$$

The model uses steam phase pressure as the pressure variable in all PVT relationships.

Porosity is calculated from

$$\phi = \phi_o(1 + c_r(p - p_o)) \quad (11)$$

where $\phi_o$ is porosity at pressure $p_o$ and $c_r$ is constant. Reservoir thermal conductivity may vary with spatial position, but is treated as independent of pressure, temperature and saturation. Formation rock heat capacity may vary with position but is independent of temperature. Overburden thermal conductivity and heat capacity are constants.

## IMPLICIT AND SEMI-IMPLICIT ALLOCATIONS OF WELL RATE AMONG LAYERS

Numerical simulation of most reservoir processes encounters the problem of representing production rates from wells located in grid blocks of large areal dimensions. The reservoir grid system consists of NZ vertical layers with the layers numbered from top to bottom as k = 1, k = 2, . . ., k = NZ. A producing well located in areal block (i, j) is perforated or open to flow in layers $k = k_1, k_1 + 1, \ldots, k_2$. For example, NZ might be 8 and a well open in layers 3-7, ($k_1 = 3$, $k_2 = 7$). The wellbore radius is denoted by $r_w$. The grid blocks penetrated by the well are of dimensions $\Delta x$, $\Delta y$, $\Delta z_k$ where $\Delta x$ and $\Delta y$ are the areal dimensions. Assuming (a) $\Delta x \cong \Delta y$, b) the well is located areally near the center of the grid block, (c) steady- or semi-steady-state radial flow in each grid block $\Delta x$, $\Delta y$, $\Delta z_k$ open to the well, (d) no vertical crossflow between open layers, we can derive from Darcy's law for single-phase flow of a unit mobility fluid ($k_r/\mu = 1$)

$$Q_k \cong \frac{2\pi(k\Delta z)_k}{\ln(r_e/r_w) + S}(p_k - p_{wbk}) \equiv PI_k(p_k - p_{wbk}) \quad (12)$$

where

- $Q_k$ = rate of radial flow of a unit mobility fluid in layer k from grid block to the wellbore, cubic feet/day,
- $k_k$ = absolute permeability of layer k, md x 0.00633,
- $\Delta z_k$ = layer thickness, feet,
- S = skin factor,
- $r_o$ = $\sqrt{\Delta x \cdot \Delta y/\pi}$ = equivalent radius feet,
- $p_k$ = pressure in grid block i,j,k at $r = r_e$, psia,
- $p_{wbk}$ = flowing wellbore pressure opposite layer k, psia.

In practice, for the case where $r_e >> r_w$, we assume $p_k$ equal to the average grid block pressure calculated in the simulator and, for more rigor, replace S by S - 1/2 or S - 3/4 for steady- or semi-steady-state flow. $PI_k$ denotes the coefficient in Equation (12), a layer productivity index in units of cubic feet/day-psi. All pressures $p_k$, $p_{wbk}$ refer to points vertically centered in the thickness $\Delta z_k$.

In the geothermal reservoir case treated here, $\bar{q}$ denotes the well target or desired production rate, and $\bar{p}_{wb}$ denotes the minimum flowing wellbore pressure in layer $k_t$. If no tubing is in the well, then $k_t$ would normally be specified as $k_1$, the uppermost open layer. If tubing is in the perforated casing, then a minimum (bottomhole tubing) wellbore pressure may be specified at any layer, $k_1 \leq k_t \leq k_2$.

$p_{wb}$ denotes the actual flowing wellbore pressure at the center of layer $k = k_t$ and q denotes the actual total well production rate, lbs $H_2O$ per day. The flowing wellbore pressure in layer k is denoted by

$$p_{wbk} = p_{wb} + \Delta p_{wbk} \qquad (13)$$

From Equations (12) and (13) the production rates of water phase, gas (steam) phase, total $H_2O$ and enthalpy from layer k are

$$\begin{aligned} q_{wk} &= \alpha_{wk}(p_k - p_{wb} - \Delta p_{wbk}) \\ q_{gk} &= \alpha_{gk}(p_k - p_{wb} - \Delta p_{wbk}) \\ q_k &= q_{wk} + q_{gk} = \alpha_k(p_k - p_{wb} - \Delta p_{wbk}) \\ q_{Hk} &= q_{wk}H_{wk} + q_{gk}H_{gk} \end{aligned} \qquad (14)$$

where

$$\begin{aligned} \alpha_{wk} &= PI_k(k_{rw}\rho_w/\mu_w)_k \\ \alpha_{gk} &= PI_k(k_{rg}\rho_g/\mu_g)_k \\ \alpha_k &= \alpha_{wk} + \alpha_{gk} \end{aligned}$$

and $\rho_w$, $\rho_g$ are phase densities in units of lbs $H_2O$ per cubic foot.

As discussed above, the interblock flow rates and heat loss and conduction terms are all treated implicitly in the simulator described herein. If, in addition, the well sink or source terms are implicit, then the entire simulator is implicit. The logic and coding necessary for implicit well treatment is rather simple for the case of a well completed in a single layer of the reservoir grid. Implicit treatment can be extremely difficult for a producing well completed in several layers.

In this section we describe an implicit treatment for multilayer well completion and present several semi-implicit simplifications. Note that $\alpha_k$ in Equations (14) is a function of pressure, temperature and, due to relative permeabilities, saturation $S_g$. Enthalpies $H_w$, $H_g$ are functions of pressure and temperature. Total well production rate q is the sum of $q_k$ over layers $k_1$ - $k_2$ or

$$q = \Sigma\alpha_k(p_k - \Delta p_{wbk}) - p_{wb}\Sigma\alpha_k \qquad (15)$$

where the summation term $\Sigma$ denotes summation from $k_1$ to $k_2$. Rearranging Equation (15) gives

$$p_{wb} = [\Sigma\alpha_k(p_k - \Delta p_{wbk}) - \bar{q}]/\Sigma\alpha_k \qquad (16)$$

as the flowing bottomhole wellbore pressure at center of layer $k_t$ necessary to produce the well target rate $\bar{q}$ lbs $H_2O$ per day. The well is on deliverability if $p_{wb}$ from Equation (16) is less than the specified minimum value $\bar{p}_{wb}$. In any event, the production rates of water, steam and $H_2O$ are given by Equations (14a) - (14c) with $p_{wb}$ equal to the larger of $\bar{p}_{wb}$ and the value given by Equation (16).

Implicit well treatment requires that water phase production rate given by Equation (14a) be expressed as

$$q_{wk} = q^i_{wk} + \Sigma\frac{\partial q_{wk}}{\partial T_m}\delta T_m + \Sigma\frac{\partial q_{wk}}{\partial S_{gm}}\delta S_{gm} + \Sigma\frac{\partial q_{wk}}{\partial p_m}\delta p_m + \frac{\partial q_{wk}}{\partial p_{wb}}\delta p_{wb} \qquad (17)$$

where summation here is over m from $k_1$ to $k_2$, superscript i denotes evaluation at latest iterate values of all variables, all partial derivatives are evaluated at latest iterate conditions, $\delta T_m$, $\delta S_{gm}$, $\delta p_m$ are changes in layer m over the coming iteration and $q_{wk}$ is an approximation to the end-of-time step (implicit) value $q_{wk,n+1}$. The gas

phase production rate $q_{gk}$ in Equation (14b) is represented in an analogous fashion. If the producing cell is two-phase ($0<S_g<1$), then $\delta T_m = (dT/dp)_s \delta p_m$ where $(dT/dp)_s$ is the slope of saturated temperature vs. saturated pressure at the latest iterate pressure value. If the producing cell is single-phase ($S_g=0$ or $S_g=1$), then $\delta S_g = 0$. Thus only two of the three unknowns $\delta T_m$, $\delta S_{gm}$, $\delta p_m$ are independent in any case.

The implicit expressions for $q_{wk}$, $q_{gk}$, $q_{Hk}$ of type shown in Equation (17) introduce one additional unknown $\delta p_{wb}$ for each well. The additional required equation corresponding to this unknown is the constraint equation stating that the summation over k $\Sigma(q_{wk} + q_{gk})$ equals target well rate $\bar{q}$ lbs $H_2O$/day:

$$\sum_{k=k_1}^{k_2} \Big( \sum_{m=k_1}^{k_2} \Big[ \Big(\frac{\partial q_{wk}}{\partial T_m} + \frac{\partial q_{gk}}{\partial T_m}\Big)\delta T_m + \Big(\frac{\partial q_{wk}}{\partial S_{gm}} + \frac{\partial q_{gk}}{\partial S_{gm}}\Big)\delta S_{gm} + \Big(\frac{\partial q_{wk}}{\partial p_m} + \frac{\partial q_{gk}}{\partial p_m}\Big)\delta p_m \Big] + \Big(\frac{\partial q_{wk}}{\partial p_{wb}} + \frac{\partial q_{gk}}{\partial p_{wb}}\Big)\delta p_{wb} \Big) = 0 \quad (18)$$

This Equation (18) guarantees that $\Sigma(q_{wk} + q_{gk}) = \bar{q}$ because $q^i_{wk}$, $q^i_{gk}$ are calculated using latest iterate values in Equations (14) and $p^i_{wb}$ from Equation (16). That is, $\Sigma(q^i_{wk} + q^i_{gk}) = \bar{q}$. If the well is on deliverability (i.e. $p^i_{wb}$ from Equation (16) is $\leq \bar{p}_{wb}$), then $\delta p_{wb} = 0$ and Equation (18) is not required.

The implicit well treatment consisting of Equations (17) (and similar equations for $q_{gk}$, $q_{Hk}$) and (18) is extremely difficult to implement due to the derivatives involved. The derivatives $\partial q_{wk}/\partial p_m$, $\partial q_{gk}/\partial S_{gm}$, etc., where $k \neq m$ arise from the wellbore pressure gradient term $\Delta p_{wbk}$ which is $p_{wbk} - p_{wb}$. This term must be obtained by calculating the horizontal flow rates of water and steam phases from each open layer into the well, cumulating these flow rates upward from layers $k > k_t$, downward from layers $k < k_t$, performing an energy balance in each wellbore layer by flashing the total flowing stream to obtain quality, and then calculating density (psi/ft) in each wellbore layer by volumetrically averaging steam and water densities. At a given iteration, this calculation is laborious and iterative in itself.

A significant simplification results if we evaluate the term $\Delta p_{wbk}$ in Equations (14) at time level n. This, of course, results in a semi-implicit well treatment and can result in a time step restriction or conditional stability. Using $\Delta p_{wbk,n}$ in Equations (14) and employing an implicit approach to the remaining terms, we have

$$q_{wk} = q^i_{wk} + \frac{\partial q_{wk}}{\partial T_k}\delta T_k + \frac{\partial q_{wk}}{\partial S_{gk}}\delta S_{gk} + \frac{\partial q_{wk}}{\partial p_k}\delta p_k + \frac{\partial q_{wk}}{\partial p_{wb}}\delta p_{wb} \quad (19)$$

and similar equations for $q_{gk}$, $q_{Hk}$, where $q^i_{wk}$ and all partial derivatives are evaluated at latest iterate conditions (except for $\Delta p_{whk,n}$). The impact of taking $\Delta p_{wbk}$ at time level n is that all derivatives of type $\partial Y_k/\partial X_m$ are zero unless $m = k$. Again, the constraint Equation (18) applies (with $\partial Y_k/\partial X_m = 0$ if $m \neq k$) if the well is not on deliverability ($p^i_{wb} > \bar{p}_{wb}$) and Equation (18) is inactive with $\delta p_{wb} = 0$ if the well is on deliverability ($p^i_{wb} = \bar{p}_{wb}$).

A further simplification, for the case where the well is not on deliverability, is

$$q_{wk} = q^i_{wk} + q^i_k\Big(\frac{\partial f_{wk}}{\partial T_k}\delta T_k + \frac{\partial f_{wk}}{\partial p_k}\delta p_k + \frac{\partial f_{wk}}{\partial S_{gk}}\delta S_{gk}\Big) + \frac{\partial q_{wk}}{\partial p_k}\delta p_k + \frac{\partial q_{wk}}{\partial p_{wb}}\delta p_{wb} \quad (20)$$

where $\partial q_{wk}/\partial p_k$ is simply $a_{wk}$ and $f_{wk}$ is mass fractional flow of water phase from layer k,

$$f_{wk} = a_{wk}/(a_{wk} + a_{gk}) \quad (21)$$

This simplification automatically holds constant over the coming iteration the $q^i_k$ lbs $H_2O$/day from each layer, as well as the sum $\Sigma(q^i_{wk} + q^i_{gk}) = \bar{q}$. This constancy of $q^i_k$ eliminates the need for terms involving $\delta S_{gk}$, $\delta T_k$ in the constraint Equation (18) and the constraint equation becomes simply

$$\left(\frac{\partial q_{wk}}{\partial p_k} + \frac{\partial q_{gk}}{\partial p_k}\right)\delta p_k + \Sigma\left(\frac{\partial q_{wk}}{\partial p_{wb}} + \frac{\partial q_{nk}}{\partial p_{wb}}\right)\delta p_{wb} = 0 \qquad (22)$$

$$(\alpha_{wk} + \alpha_{gk})\delta p_k = \{\Sigma(\alpha_{wk} + \alpha_{gk})\}\delta p_{wb} \qquad (23)$$

...the constraint equation involves only pressures and if a single-variable pressure equation is solved in a simulator, then equation (23) is compatible in that no saturation unknowns appear. We used this latter type of constraint equation four years ago in a black oil coning simulation and found that addition of the $\delta p_{wb}$ unknown considerably improved stability and increased time step size.

If the well is on deliverability, no constraint equation or additional variable $p_{wb}$ is involved and the simplification of evaluating $\Delta p_{wbk}$ at time level n is generally satisfactory in geothermal simulations. The incorporation of terms of type $\partial Y_k/\partial X_m$ where $m \neq k$ in expressions for $q_{wk}$, $q_{gk}$, $q_{Rk}$ or incorporation of the constraint equation is often difficult from a coding point of view. The difficulty is minimized if z-line SOR or vertical-plane block SOR or direct solution is used, but even in these cases the storage and/or computing time requirements for many-well problems can rise appreciably. If the well is on deliverability, then the first simplification of $\Delta p_{wbk,n}$ requires only $\partial Y_k/\partial X_k$ derivatives and no constraint equation applies. Therefore, we use this simplification for the deliverability case.

If the well is not on deliverability, we use a simplification even more explicit than those described above. We express

$$q_{wk} = q^t_{wk} + q^t_k\left(\frac{\partial f_{wk}}{\partial T_k}\delta T_k + \frac{\partial f_{wk}}{\partial S_{gk}}\delta S_{gk} + \frac{\partial f_{wk}}{\partial p_k}\delta p_k\right) \qquad (24a)$$

$$q_{gk} = q^t_{gk} + q^t_k\left(\frac{\partial f_{gk}}{\partial T_k}\delta T_k + \frac{\partial f_{gk}}{\partial S_{gk}}\delta S_{gk} + \frac{\partial f_{gk}}{\partial p_k}\delta p_k\right) \qquad (24b)$$

$$q_{nk} = q^t_{wk}\left(\frac{\partial H_{wk}}{\partial T_k}\delta T_k + \frac{\partial H_{wk}}{\partial p_k}\delta p_k\right) + q^t_{gk}\left(\frac{\partial H_{gk}}{\partial T_k}\delta T_k + \frac{\partial H_{gk}}{\partial p_k}\delta p_k\right) + H^t_{wk}\delta q_{wk} + H^t_{gk}\delta q_{gk} \qquad (24c)$$

where $q^t_{wk}$ and $q^t_{gk}$ are computed from Equations (14) using $\Delta p_{wbk,n}$ and $p^t_{wb}$ from Equation (16). Thus, $\Sigma(q^t_{wk} + q^t_{gk}) = \bar{q}$. The derivatives $\partial f_{wk}/\partial T_k$, etc., are evaluated at latest iterate conditions. This simplification runs the risk of pressure instability since no $\partial q_{wk}/\partial p_k = \alpha_{wk}$, etc., terms are used. This instability increases as well productivity index PI increases and as rate $\bar{q}$ decreases. In two-dimensional areal calculations, no such instability exists since there is no pressure allocation among layers. In many three-dimensional and two-dimensional cross-sectional problems, the PI is sufficiently low that the instability is not significant. In many radial-z single-well problems, the instability is severe and we return to implicit procedures.

In radial-z single-well problems, we achieve implicit well treatment by simply incorporating the wellbore in the reservoir grid system. The result of this inclusion is an even more rigorous well treatment than the implicit treatment described in Equations (17) - (18). For inclusion of the wellbore results in transient mass and energy balances applied within the wellbore. Also, reverse flow in any layers from wellbore to the formation is automatically modelled whereas this injection in a producing well is very difficult to account for if the wellbore is not modeled by inclusion in the grid. An apparent disadvantage of wellbore modelling is the very small volume grid blocks giving rise to very large throughput ratios (defined below) for reasonable time step sizes. Our hope at the outset of this work was that the implicit treatment throughout the wellbore and reservoir would eliminate instabilities regardless of very high throughput ratios.

The multiphase flow vertically within or laterally thru the column of wellbore grid blocks must be modeled by the usual multiphase Darcy-flow expressions. The large gas-liquid density difference and high effective vertical "permeability" of the wellbore results in domination by gravity forces even at very small producing rates. This gravity dominance gives low calculated steam saturations in the wellbore resulting in a liquid pressure gradient and high back pressure on the lower formation. At normal rates of geothermal wells, the Reynolds number is so high that assumption of fully developed turbulent flow in the wellbore is usually a good one and assumption of no-slip two-phase flow is even better one. This no-slip condition is equivalent to volumetric fractional flow equalling saturation.

We programmed this no-slip flow in lieu of usual Darcy flow logic for the wellbore. Alternatively, we could use the Darcy flow logic to calculate wellbore pseudo relative permeabilities which result in volumetric fractional flow $f_g = S_g$. This approach would

require two sets of pseudo relative permeabilities since gravity enters for vertical but not for lateral flow. The vertical wellbore effective permeability used in calculations described below was sufficiently large to hold viscous pressure drops over 500 feet of wellbore to less than 3 psi.

This inclusion of the wellbore in the grid system allows radial-z or r-θ-z simulation of the entire wellbore and overburden from the formation to the surface (wellhead). A problem arises here in altering the no-slip wellbore two-phase flow calculation so that agreement is obtained with two-phase vertical pipe flow correlations. Apart from this problem, the model allows simulation of transient wellbore flow conditions and wellbore heat loss, in addition to the transient multiphase heat and fluid flow in the reservoir. Vertical grid definition in this case would extend from ground surface down to and through the permeable formation.

## EFFECT OF STEAM FLASHING ON WELL DELIVERABILITY

A problem in use of Equations (14) arises even in an areal simulation where H2 = 1, k = 1 and $\Delta p_{wbk} = 0$. The mobilities and specific volumes in Equations (14) are generally evaluated at average (exterior) grid block conditions. If flashing of steam occurs between $r_e$ and $r_w$, then Equations (14) can give considerable error since they do not account for the increasing volumetric flow rate (at constant mass flow rate) toward the well due to water flashing and steam expansion accompanying pressure decline.

Deliverability of a single layer can be corrected to account for water flashing and steam expansion by inserting a fraction f, equal to or less than 1, as

$$q = f(\alpha_w + \alpha_g)(p - p_{wb}) \qquad (25)$$

where, as before, $\alpha_w$ and $\alpha_g$ are evaluated at known block average (exterior) conditions. The factor f is a calculable function of $p_{wb}$, p, and $S_{ge}$ where $S_{ge}$ is gas saturation at $r = r_e$, which in turn is generally very close to average grid block saturation. Equation (25) presumes that the average grid block condition is saturated. The Appendix describes the calculation of f and gives a revision of Equation (25) for the case where the saturation point lies between $r_w$ and $r_e$. The calculation of f ignores capillary pressure and assumes steady-state radial flow from pressure p at $r_e$ to pressure $p_{wb}$ at $r_w$.

In addition to $p_{wb}$, p and $S_{ge}$, f is also dependent upon the relative permeability curves. Therefore, a completely general representation of f is not possible. Figure 1 gives f as a function of $p_{wb}$, $p(= p_e)$ and $S_{ge}$ for relative permeability curves

$$k_{rw} = [(S_w - S_{wc})/(1 - S_{wc})]^{n_w} \qquad (26a)$$

$$k_{rg} = k_{rgcw}[(S_g - S_{gc})/(1 - S_{wc} - S_{gc})]^{n_g} \qquad (26b)$$

with $S_{wc} = .2$, $S_{gc} = 0$, $n_w = n_g = 2$ and $k_{rgcw} = .5$.

Figure 1 shows that the deliverability reduction factor is 1 for minimal drawdowns $(p_e - p_{wb})$, decreases with increasing drawdown and, for a given drawdown, it increases with increasing grid block steam saturation, $S_{ge}$. The factor can reach values of .25 or lower for low $S_{ge}$, high drawdown and/or low reservoir pressure $p_e$. This means that deliverabilities calculated using Equation (14) can be erroneously high by a factor of four or more.

### Comparison of Numerical Model and Analytical Deliverabilities

A radial test problem was used to compare the simulator's calculated deliverability with that of Equation (25). This problem was also used as a preliminary test of simulator stability and time-truncation error. Reservoir and fluid property data for this problem are given in Table 1. A 9x1 radial grid was employed with the well producing on deliverability against a wellbore pressure of 160 psia.

In the past, we have performed radial gridding by specifying $r_w$, $r_e$ and an arbitrary first block "center" radius $r_1$. Geometric block center spacing gives $r_i = \alpha r_{i-1}$ where i is r-direction grid block index. Thus, $r_N = \alpha^{N-1} r_1$ and $r_{N+1} = \alpha^N r_1$ where N is the number of radial reservoir grid blocks. Demanding that $r_e$ be the log mean radius between $r_N$ and $r_{N+1}$ gives the equation

$$\frac{\alpha^{N-1}(\alpha - 1) r_1}{\ln \alpha} = r_e \qquad (27)$$

which is solved for $a$ by the Newton-Raphson technique. Generally $r_1$ values of at least 3 feet or more have been used to avoid excessively small grid blocks adjoining the wellbore.

In this work we retain the geometric spacing $r_i = ar_{i-1}$ but eliminate the arbitrary specification of $r_1$. Rather we invoke an imaginary radius $r_0$ within the wellbore in addition to radius $r_{N+1}$ outside $r_e$ and require $r_w$ be the log mean radius of $r_0$ and $r_1$ and $r_e$ be the log mean of $r_N$ and $r_{N+1}$. This gives

$$\frac{(a-1)r_0}{\ln a} = r_w \qquad (28a)$$

$$\frac{a^N(a-1)r_0}{\ln a} = r_e \qquad (28b)$$

and division of Equation (28b) by Equation (28a) gives a direct solution for $a$ as

$$a = (r_e/r_w)^{1/N} \qquad (29)$$

Grid block boundary radii used to calculate block pore volumes are calculated as log mean values of adjacent block center radii. Table 1 gives the resulting block center and boundary radii for the case of nine radial increments. The pore volume of the first grid block is 22.27 RB corresponding to 500 feet of formation thickness.

The simulator was run in one-dimensional radial mode using constant 250-day time steps to 16,000 days. Zero capillary pressure was used and the well was on deliverability against the 160 psia flowing bottomhole pressure. The solid curve in Figure 2 shows the calculated flow rates, expressed per foot of formation thickness, vs. average formation steam saturation. This saturation is close to the exterior grid block 9 saturation, but was calculated as a volume weighted average of all blocks. Figure 2 shows an initial deliverability decline followed by a temporary increase. This behavior was unaffected by time step size, closure tolerances, number of radial blocks and inclusion or exclusion of heat conduction and heat loss in the calculation.

The dotted lines in Figure 2 show deliverability from the steady-state Equation (25) for $p_{wb} = 160$, $\bar{p} = p_e = 251$. The agreement between model production rate and Equation (25) is good considering that (a) the model used a closed exterior boundary, (b) the model is in a transient decline exhibiting semi-steady-state neither in pressure nor saturation, (c) Equation (25) assumes steady-state with an open exterior boundary. Further, the deliverability factor f varies from .3428 at $S_{ge} = 0$ to .78 at $S_{ge} = .5$ and the discrepancy between the two curves is much less than the error which would occur using Equation (25) with f = 1.

The one-dimensional radial test problem was run to a large time to reach steady-state with an exterior-block well injecting 400°F water at a bottomhole pressure of 251.09 psia at $r = r_e$. Following several time steps to 100 days to allow pressure in grid block 9 to fall below 251 psia (to activate the injection well), two 60,000-day time steps (these steps required 7 and 2 iterations) were taken. The steady-state flow rate calculated was 130,000 lbs $H_2O$/hour. Equation (37) gives for $p_{wb} = 160$, $p_e = 251$ and $S_{ge} = 0$ (corresponding to injection of saturated 100% liquid water),

$$q_{H_2O} = \frac{2\pi k \Delta z_I}{\ln \frac{r_e}{r_w}} = \frac{2\pi(100)(500)(.00833)}{\ln \frac{2000}{.25}}$$

$$\cdot \frac{12,728}{24}\ \frac{\text{lbs}}{\text{hr}} = 117,349\ \text{lbs/hr}$$

The discrepancy between 130,000 and 117,349 lbs/hour is believed due to the model's upstream weighting of mobilities as opposed to the integration of mobility in Equation (37). In any event, since f = .3428 for $p_e = 251$, $p_{wb} = 160$ and $S_{ge} = 0$, the discrepancy of about 13,000 lbs/hour is small in comparison with the error in using Equation (25) with no correcting f factor. Equations (14) used for an areal grid block of 2,000 feet equivalent exterior radius would give a deliverability of 343,000 lbs/hour. Use of the f factor and Equation (25) would give a calculated deliverability of 117,349 lbs/hour.

## THROUGHPUT RATIO

Evaluation of any term in the interblock flow rates explicitly (at time level n) with respect to any of the dependent variables ($\bar{p}$, T, $S_g$) in general will result in a conditional stability. This conditional stability takes the form of an expression giving a maximum time step. Use of a time step size exceeding this maximum will result in divergence of the calculations. The expression for maximum time step generally involves, at least in part, a throughput ratio defined in some manner.

One of the most severe instabilities in multiphase flow simulation is that arising from explicit evaluation of saturation-dependent relative permeabilities in the interblock transmissibilities. The throughput ratio that arises in analysis of this instability is

$$R_{Ti} = \frac{q_i \Delta t}{V_p S_i} \qquad (30)$$

where i denotes phase (e.g., water, gas or oil), $q_i$ is volumetric phase flow rate through the grid block, $S_i$ is grid block saturation of phase i and $V_p$ is grid block pore volume. Thus $R_{Ti}$ is the ratio of total volume of phase i passing through the grid block in one time step divided by the volume of phase i in the block.

Actually, this ratio appears with a multiplier equal to fractional flow derivative, but we are not concerned here with detailed derivations or presentations of stability analysis results. As a practical matter, we have rated the stability of a multiphase flow formulation or model by the cruder ratio

$$R_T = \frac{q_v \Delta t}{V_p} \qquad (31)$$

where $q_v$ is total (all phases) volumetric flow rate through the grid block.

In the geothermal case we can express the above ratio in terms of total mass flow rate of $H_2O$ and quality X of the flowing stream. Many of the results discussed below involve a well producing on deliverability at a flowing bottomhole pressure of 100 psia. Using corresponding water and steam densities of 55 and .355 lbs/cu.ft., respectively, we can express $R_T$ as

$$R_T = 4.27(2.8X + .018)q\Delta t/V_p \qquad (32)$$

where q is total mass flow rate in lbs $H_2O$/hour, $\Delta t$ is time step in days and $V_p$ is reservoir barrels (RB).

Our previous experience with a variety of semi-implicit isothermal and thermal simulators, producing under multiphase flow conditions, has indicated instability or time step restriction at throughput ratios in the range of 1,000 to 20,000. We will return to Equation (32) in connection with results discussed below.

## TIME TRUNCATION ERROR AND STABILITY FOR ONE-DIMENSIONAL RADIAL PROBLEM

Time truncation error and model stability were examined in the one-dimensional radial case by repeating the 16,000-day run described above with time steps of 500, 1,000, 2,000, 4,000, 8,000 and 16,000 days. Table 2 shows the effect of time step size on calculated recovery, producing quality and rate at 4,000, 8,000 and 16,000 days. The time truncation error is quite acceptable for time steps up to 1,000 days.

All these runs converged each time step with two to three iterations per step except for the first step when steam saturation increased from zero to about .45 at the well and 0 - .39 at the 9th block. The first time step required 20-23 iterations, the 23 iterations corresponding to the 16,000-day time step run. The largest throughput ratio occurred for the 16,000-day time step which, from Equation (32), is

$$R_T = 4.27(2.8(.0835) + .018)(67,900)(16,000)/22.27$$
$$= 52.45 \times 10^6$$

This ratio is more than three orders of magnitude larger than the 20,000 ratios of our previous experience mentioned earlier. However, one-dimensional problems are generally poor tests or indicators of true model competence and ratios from two-dimensional results presented below will be given more emphasis.

## TWO-DIMENSIONAL SINGLE-WELL PROBLEM RESULTS

We simulated the radial flow problem described in Table 1 using a two-dimensional 10 x 5 radial-x grid. The five layers were each 100 feet thick. The 10 radial grid blocks included the wellbore. Table 1 gives the grid block center radii, boundary radii and pore volumes calculated using Equation (29). Note that the first reservoir grid block has a center radius of only .40 feet and a pore volume of only 4.45 RB. The pore volume of each wellbore grid block is 3.5 RB so that the throughput ratio, Equation (32), becomes

$$R_T = .122(2.80 + .018)q\Delta t \qquad (33)$$

Rock capillary pressure was assumed negligible in this problem and a pseudo straight-line capillary pressure curve [8, 9] corresponding to layer thickness of 100 feet was employed. Use of saturated steam-water densities at 400°F gives a density difference of .369 psi/foot which translates, for 100-foot layer thickness, to a pseudo capillary pressure equalling 18.45 psi at $S_w = S_{wc} = .2$ and -18.45 at $S_w = 1.0$.

A number of 10,000-day model runs were performed for different well completion intervals. We assumed a tubing/casing configuration so that an additional variable was the layer in which the tubing bottom or withdrawal point was located. For example, with all layers 1-5 perforated, the tubing bottom could be placed in any one of the layers. A packer was assumed placed at top of formation.

A well target rate of 300,000 lbs/hour was specified for all runs with a minimum flowing wellbore pressure at tubing bottom of 360 psia. For all runs, time step was specified as 500 days. Table 3 summarizes model results at 10,000 days. The listed mass fraction produced, producing bottomhole quality, producing rate and produced Btu/lb all apply at the 10,000-day point in time. Average Btu/lb produced is cumulative energy produced over 10,000 days divided by cumulative mass produced. Energy produced is enthalpy, defined as U + pv at producing cell conditions. Internal energy U is relative to a zero value for U of saturated water at 60°F.

Table 3 shows that the location of a single-layer (100 feet) completion is very important. Comparing runs 1-3 shows that cumulative mass fraction recovered at 10,000 days varies from 11.7% to 47.4% as a 100-foot producing interval is lowered from the top 100 feet to the bottom 100 feet of the 500-foot formation.

Runs 4-11 in Table 3 indicate that the perforated or open interval location is important while the location of the tubing bottom or withdrawal point within a given open interval is relatively unimportant. For example, Runs 4 and 5 show about equal recovery values for their top 300 feet open interval regardless of whether the tubing withdrew from the top 100 feet or bottom 100 feet of the interval. Runs 6-7 show the same result for a bottom 300-foot open interval regardless of the tubing position within the open interval. The best recoveries occur for a completely penetrated or open formation -- Runs 9-11 -- and performance is nearly independent of whether the tubing is set at top or bottom of the formation.

In Runs 1-5 the well was on deliverability in the first 500-day time step. Runs 6-7 and 9-11 produced the target 300,000 lbs/hour rate for 1,500 days and Run 8 produced the target rate for 500 days.

Taken together, Runs 1-11 indicate that a partial completion interval effectively drains the portion of the reservoir formation opposite and above the interval, but inefficiently drains the formation below it.

Spatial truncation errors in the results of Table 3 are very small as indicated by several runs we made using a 10 x 10 grid with ten 50-foot thick layers. Time truncation error was examined by repeating Run No. 10 using time steps of 250, 1,000, 2,000 and 5,000 days. Figure 3 shows producing rate and bottomhole producing quality vs. time calculated using the various time steps. The results with $\Delta t = 250$ and $\Delta t = 500$ days are virtually identical. The error with $\Delta t = 1{,}000$ days is significant but not large while $\Delta t = 2{,}000$ days causes an error bordering on acceptability. The surprising feature of these results is the small time truncation error for steps of 1,000 days or less in light of the large changes in saturation which occur in a single step.

The saturation changes stably computed in a single step are illustrated in Table 4 which shows saturations and pressures at the end of the first 2,000-day time step (all layers open, timing at layer 3). Maximum saturation change was .9939 in grid block (i=1,k=1) and maximum pressure change was -441.4 psi in grid block (i=1,k=5). Initial pressures ranged from 469 to 618 psia from formation top to bottom, some 200 to 350 psi above saturation pressure corresponding to 400°F. That is, the model in this single step proceeded from a highly undersaturated, 100% liquid configuration to that shown in Table 4. Note, also, from Figure 3 that time truncation error for this first time step is virtually negligible. The reader should recall in viewing Table 4 that the first column of cells is the wellbore.

The calculated producing rate for this first 2,000-day step was 286,400 lbs/hour and bottomhole quality was .05794. Using Equation (33), the throughput ratio for withdrawal cell (i=1,k=3) was

$$R_T = 1.2(286,400)(2.8(.05794) + .008)(2,000) = 126 \times 10^6$$

This throughput ratio was achieved with the producing cell steam saturation changing from 0 to .8993. That is, it is not a throughput ratio corresponding to stabilized conditions

with small changes per time step. This ratio is three to four orders of magnitude larger than the 20,000 ratios we have previously achieved with semi-implicit models under high rate-of-change conditions.

Table 5 shows the number of required iterations per time step for each step for the three runs using $\Delta t$ = 500, 1,000 and 2,000 days. The numbers in parentheses in Table 5 are the maximum grid block saturation changes over the grid during each time step.

Table 6 shows calculated pressures and saturations after the first 500-day time step of Run No. 8. Producing rate and quality were 300,000 lbs/hour and .04, respectively, so that the throughput ratio from Equation (33) was

$$R_T = 1.22(300,000)[2.8(.04) + .018](500) = 23.8 \times 10^6$$

This ratio was achieved with a high steam saturation change in the producing cell from 0 to .8481. Required iterations for this first step were 30. The iterations declined to 24 when initial pressure at formation top was reduced to 270 rather than 450 psia. The throughput ratio at 10,000 days for this run was $11.5 \times 10^6$ corresponding to a producing rate and quality of 53,100 lbs/hour and .1200,* respectively.

Run 12 in Table 3 is identical to Run 10, except that permeability is 500 md rather than 100 md. The higher permeability resulted in a greater recovery of .7459 compared to .5656 at 10,000 days and gave a considerably higher producing quality of .7058 at 10,000 days. Run 12 produced the target 300,000 lbs/hour rate until 5,000 days. Figure 4 shows the effect of permeability on producing rate and quality vs. mass fraction produced. Producing quality in Figure 4 is calculated at a separator condition of 100 psia. The curves of average reservoir pressure (volumetrically weighted average of all grid blocks) vs. mass fraction produced are not plotted, but are identical for the two runs. Figure 4 shows that produced stream quality at the fixed separator condition is nearly a single-valued function of mass fraction produced and independent of permeability level.

Figure 5 shows average reservoir pressure vs. mass fraction produced calculated for 10,000-day runs using k = 100 and 500 md and $\phi$ = .05 and .35. The figure indicates that permeability level has a negligible effect on average pressure vs. mass fraction produced. The large porosity results in a very slightly lower average reservoir pressure. The small effect is due to the lower rock heat capacity (i.e. less rock) in a higher porosity formation. This small effect of porosity on pressure decline is in contradiction to results reported elsewhere [4].

The average computer time per run for Runs 1-11 was 16 CDC 6600 CPU seconds. For the 10x5 grid and 20 steps per run this translates to .016 seconds per grid block-time step. This figure compares to a rough value of .01 seconds* per grid block-time step for our semi-implicit models.

## SIMULATION OF A FRACTURED-MATRIX RESERVOIR

Many geothermal reservoirs are known or believed to be fractured-matrix systems. Conventional simulation is often used where extensive fractures are known to exist. Such simulation employs an assumption that flow in the matrix-fissure system can be adequately modeled by assuming an unfractured matrix formation with a high effective permeability reflecting the fracture system conductivity.

Here we examine the difference in simulated performances of a fractured reservoir sector modelled first as an unfractured formation, and second as a matrix-fissure system. While nature seldom provides near-uniformity in spacing of fractures, we must employ some semblance of uniform spacing to perform any calculations. We consider a fractured system consisting on the average of 40x40x40 feet matrix blocks separated by a three-dimensional orthogonal planar system of vertical and horizontal fractures.

To reduce the dimensionality of the matrix calculation, we treat the matrix cubes as cylinders of equivalent radius 22.5676 feet ($\pi r^2 = 40 \times 40$) and height of 40 feet. We have used this cylindrical approximation for several years in black oil fractured matrix simulation; it is partially justified since the physically real irregularity of fracture spacing and angles undoubtedly yields a variety of matrix block shapes deviating considerably from rectangular parallelepipeds.

Use of a fracture volume equal to 1% of combined fracture plus matrix volume leads to a fracture width of .029 feet. This figure assumes equal widths of horizontal and vertical fractures. From Muskat [10], fracture permeability for width w in cm, is

*This number can vary considerably. For "easy" multiphase flow problems (we omit definitions of "easy" for brevity), we have achieved times as low as .0018 seconds per block-step.

$$k = 10^8 w^2/12 = 6.5 \times 10^6 \text{ Darcies} \quad (34)$$

for the .029 feet width. In simulating flow in fracture grid blocks, it is only necessary to use fracture permeabilities large enough to render viscous forces negligible in comparison with gravitational forces. In previous black oil fractured matrix reservoir work and in this work, we have found results insensitive to use of fracture permeabilities higher than 10 to 20 Darcies.

For the purpose of computations described here, the fracture system conductivity is assumed sufficiently large that the reservoir behavior is dominated by vertical transients in pressure, temperature and saturation. The fracture conductivity is assumed sufficient to maintain negligible areal gradients of these quantities. For example, by this assumption any steam-water contact in the fractures will be nearly horizontal over a wide areal expanse.

The withdrawal rate used for computations was based on a well spacing of about 300 acres with rates of 300,000 lbs $H_2O$/hour per well. This translates to a rate of about 40 lbs/hour for a 1,240-foot vertical column section of the reservoir with areal dimensions 40x40 feet. The vertical gridding consisted of six matrix blocks each subdivided vertically into 10-foot grid blocks and one last deep 1,000-foot matrix grid block. Calculations were terminated before steam-water contacts reached the deep block so that its lack of gridding is immaterial.

In the matrix-fissure simulation, the vertical and horizontal fractures were included in the grid system. Vertically, then, six additional grid blocks each .029 feet thick separated the six matrix blocks and the total number of vertical blocks was 6 x 4 + 6 + 1 or 31. We obtained nearly identical results using three and two grid blocks radially for the matrix-fissure system. Results given here are for the case of two radial grid blocks. The first radial block was matrix with an inner boundary radius of 0, an outer boundary radius of 22.5676 feet and a "center" radius equal to the volume mean value of 15.96 feet. The second radial grid block was vertical fracture with inner radius of 22.5676 feet and outer radius of 22.5676 + .029/2 feet. Figure 6 illustrates this radial-z grid for the fissure-matrix simulation. Fluid was withdrawn from the bottom 1,000-foot thick vertical fracture block.

Matrix permeability and porosity were 1 md and 0.2, respectively. Grid block pore volumes for the matrix-fissure system illustrated in Figure 6 were

| Grid Block | Pore Volume, Res. Bbls. |
|---|---|
| 10-foot matrix | 569.9 |
| .029-foot horizontal fracture radial block #1 | 8.26 |
| .029 x .0145-foot fracture intersection block | .0106 |
| 10-foot vertical fracture | 3.66 |

Initial reservoir pressure was 270 psia at top of formation and temperature was 400°F. Overburden heat loss (gain) had a small effect and was ignored. Heat conduction in the matrix was modeled using a thermal conductivity of 38 Btu/ft-day-°F. Matrix rock heat capacity was 35 Btu/cu.ft. rock-°F. Relative permeabilities of Equations (26) and a linear rock capillary pressure curve of $P_c = 0$ at $S_w = 1$, $P_c = 10$ psi at $S_w = 0$ were used for matrix and zero capillary pressure and linear $k_r = S$ curves were used for the fractures.

The 2 x 31 (radial-z) matrix-fissure simulation was run to 1,500 days for a rate of 40 lbs/hour and to 4,200 days for a rate of 10 lbs/hour. Two runs were made for the 40 lbs/hour rate, the first with a constant 30-day time step, the second with a constant 60-day time step.

Figure 7 shows calculated water saturation vs. depth from top of formation at 1,500 days for the 40 lbs/hour production rate. The solid lines correspond to the 30-day time step while the circles and dashed line show results for the 60-day step. The vertical tic marks indicate water saturations in the first radial horizontal fracture blocks.

This figure shows the poor recovery of water from the matrix blocks due to the capillary discontinuities imposed by the horizontal fractures. Each matrix block above the (vertical fracture) steam-water contact transiently drains toward an equilibrium final saturation vs. depth distribution determined by the rock capillary pressure curve and the zero $P_c$ condition at each matrix block bottom imposed by the horizontal fracture. The significant transient effect is indicated by the decrease in water recovery with matrix block depth. This is due, of course, to the longer times of drainage experienced by higher located matrix blocks.

The horizontal fracture blocks opposite the 100% steam saturated vertical fracture grid blocks rapidly rise toward 100% steam saturation. Above the steam-water contact, the water draining from the bottom of a matrix block enters the horizontal fracture block and then preferentially flows vertically down into the top of the next lower matrix block rather than laterally into the vertical fracture. This preference is very close to 100%. These latter results are shown by model printouts of water and steam interblock flow rate magnitudes and directions at selected times.

Table 7 summarizes average iterations per time step, average saturation change (maximum over grid) per time step and computing times for the three fractured-matrix simulation runs. The negligible time truncation error for 30- and 60-day time steps shown in Figure 7 is somewhat surprising in light of the average saturation change rising from .36 for the 30-day step to .66 for the 60-day step. The .66 figure is actually conservative since 27 vertical fracture grid blocks were swept from 0 to 100% steam saturation in only 25 steps in Run 2. No time steps were repeated due to divergence in any of these runs in spite of nearly 100% saturation changes in one step for the .01 RB pore volume fracture-intersection grid blocks. Both Runs 1 and 2 experienced a number of time steps of 90-100% saturation change. Run 3. 1 computing time corresponds to a time per block-step of about .01 seconds.

Figure 8 compares the effect of producing rate on matrix-fissure simulation results. The calculated saturations for Run 1 at 40 lbs/hour and Run 3 at 10 lbs/hour are compared at times of equal cumulative production. The steam-water contact for the higher rate is 40% (140 feet vs. 101 feet) deeper due to the shorter time available for transient water drainage from the matrix blocks above the contact.

Conventional simulation results were generated by running the model in one-dimensional vertical mode using 24 10-foot blocks and one 1,000-foot block. The dashed line in Figure 9 shows resulting calculated water saturation vs. depth at 1,500 days for an "effective" permeability of 50 md and a producing rate of 40 lbs/hour. Gravity forces dominate and the conventional results show a sharp transition zone from a drained ($S_w=S_{wc}=.2$) upper region to the 100% water zone. The transition zone is considerably higher than the matrix-fissure simulation results viewing either the matrix or the vertical fracture steam-water contact.

We can achieve somewhat greater realism in the conventional simulation by utilizing the fact that the capillary discontinuities each 40 feet impose a maximum final recovery of water (by flow alone) which can be predetermined using the rock capillary pressure curve, the 40-foot matrix block height and the .360 psi/foot water-steam density (gradient) difference. Following Reference [8] we integrate the $S_w - P_c$ relation over the 40 feet using the fact that $P_c = 0$ at matrix block bottom and find that final minimum average matrix block water saturation is .417. Using this value for $S_{wc}$ in the relative permeability equations, the conventional simulation gives the water saturation profile indicated by the larger dashed line in Figure 9.

Further adjustments in various data might be made to narrow the difference between matrix-fissure and conventional simulation results. Considering the basic difference in mechanisms for the conventional and more correct matrix-fissure calculations, we hold little hope for forcing accuracy from a conventional simulation. In particular, the above described rate effect (Figure 8) is shown by the more rigorous matrix-fissure simulation, but not by conventional simulation (unless the permeability used is very low).

A full three-dimensional simulation of a fractured-matrix reservoir will require tying in this vertical two-dimensional R-Z matrix-fissure calculation to a two-dimensional areal calculation where the areal blocks communicate through the fracture system and the interblock flows reflect the different "sector" or areal block steam-water contacts. This task will involve a significant effort in logic and coding and will in many cases require disking on fixed memory machines. The two-dimensional R-Z matrix-fissure calculation described here is adequate only if the areal gradients within the reservoir are assumed small due to high fracture conductivity.

## Interpretation of Pressure Drawdown Tests

The major differences between conventional and matrix-fissure simulation results just described arose because of the two-phase flow in a system having capillary discontinuities. Here we illustrate difficulties which can arise in using conventional simulation to interpret pressure drawdown tests in fractured-matrix, hot water systems with single-phase water flow.

Simulation of a well test in a system having a three-dimensional network of orthogonal fracture planes would require a full three-dimensional Cartesian grid. To simplify for the purpose of illustration, we consider a system of 44-foot matrix layers separated by horizontal fractures. A 10x5 radial-x grid was used to model a horizontal disk of matrix beneath a horizontal fracture. The disk dimensions were exterior radius $r_e$ = 37,320 feet and thickness = 22 feet. The five layer thicknesses were w/2, 2, 4, 8, 8 feet where w is horizontal fracture thickness. This disk is a symmetrical element for the case where the well penetrates the entire formation thickness.

The radial spacing was calculated using Equation (29) with the wellbore included in the grid. Wellbore radius was .25 and the 10 block "center" radii were .25, .43, 1.38, 4.44, 14.55, . . ., 5,242.37 feet. Pore volumes of the wellbore cells varied from .266914 to .2798 RB in layers 1-5 for a small fracture width w = .245 mm.

Matrix and fracture layer porosities were .2 and 1.0, respectively. Initial temperature was uniformly 350°F and initial pressure was 3800 psia at top of formation. The illustrative pressure drawdown test consisted of producing 10,000 lbs/hour from a well open in all five layers for ten days. Fracture conductivity and matrix permeability were varied in five simulation runs as tabulated in Figure 10. The fracture permeabilities were related to fracture width by the relationship $k = 10^8 w^2/12$ where k is in darcies and w in cm. The homogeneous (no fracture) case, Run 4, has a permeability of 90.9 md, which gives a total md-ft product for the 22-foot thickness equal to that of the fracture cases.

Figure 10 shows calculated pressure drawdown (initial pressure-flowing wellbore pressure) vs. time on a semi-log plot for five cases. The homogeneous case (Run 4) follows a straight-line and use of the well-known relationship, slope = $Qu/4\pi kh$, gives k = 90.9 md, in agreement with the value used. Arbitrary use of the average slope from .1 to 1 days with the relation slope = $Qu/4\pi kh$ gives k = 247, 188 and 157 md for Runs 1-3, respectively. These permeabilities bear little resemblance to either fracture or matrix permeabilities.

The semi-log plots of pressure drawdown vs. time actually are not linear for the fracture cases, but are rather concave upward. This results from the fact that the reservoir transient is primarily a crossflow (vertical) bleeding of fluid into the fracture rather than the radial transient of a homogeneous unfractured formation. The degree of upward curvature of the drawdown curve increases as matrix permeability increases.

The cases of small fracture width, Runs 1-3, exhibit a rapid initial drawdown of 60-80 psia in the first few minutes of flow. The calculated effect of a fivefold larger fracture width is one of reducing this early drawdown to 2-3 psi. However, for times after the first few minutes, the larger fracture gives a calculated, concave upward drawdown curve of shape virtually identical to that for the smaller fracture. This is illustrated by the curves for Runs 1 and 5 in Figure 10.

Figure 11 shows calculated drawdowns for a tenfold larger horizontal fracture spacing of 440 feet. The simulations used a 10 x 8 grid with the eight layer thicknesses equal to .0004, 7, 4, 8, 16, 32, 64 and 94 feet (a total thickness of 220 feet). The kw product for the total fracture width of .0008 feet (.245 mm) is 4 Darcy-feet. A drawdown test flow rate of 100,000 lbs/hour was specified. The curve for this Run 6 in Figure 11 shows a linearity of drawdown vs. ln(t) past 10 days to about 30 days. The upward concave curve shape from 100 to 1,000 days is due to establishment of semi-steady-state conditions throughout the reservoir.

The curve labeled Run 7 in Figure 11 was calculated for a 220-foot homogeneous reservoir with k = 9.09 md corresponding to an equivalent total md-feet product of 2,000. The slopes of the curves for Runs 6 and 7 on Figure 11 give formation permeabilities of 18 md and 9.09 md, respectively. If the 10-day test portion of the Run 6 curve were analyzed by conventional radial flow theory, then a permeability of 18 md and a skin factor of 9.65 would be determined. The circles of Run 8 in Figure 11 show the simulator results for a homogeneous reservoir with this permeability and skin factor. Figure 11 shows that calculated drawdowns for the fractured formation (Run 6) and for an 18 md, homogeneous formation with skin (Run 8) agree well through 1,000 days.

These results of Figure 11 indicate that for the particular fracture spacing and width of 440 feet and .245 mm, respectively, conventional radial flow analysis would (a) yield erroneous permeability and skin but (b) give accurate long-term deliverability predictions. This conclusion does not hold for the previously discussed results of Figure 10 corresponding to the smaller fracture spacing of 44 feet. For this spacing, the short-term drawdown test can fail to yield any linearity from which conventional analysis can determine effective permeability and skin.

Several additional complexities that may exist in practice need mentioning in connection with the results just discussed. A naturally fractured formation will generally have vertical as well as horizontal fractures. Accounting for a three-dimensional network of fracture planes with the model

described herein would require a three-dimensional simulation. If fracture spacing were the order of 100 feet or less, a very large number of grid blocks would be required. A better modelling approach in this case would be a dual porosity formulation where interblock flow is assumed to occur only in the fracture system. The matrix would be accounted for by zero-dimensional, one-dimensional spherical or two-dimensional cylindrical subcalculations tied into the fracture porosity in each grid block. The heat-loss calculation described in Reference [3] is an example of this type of formulation.

The model described here may apply well to an artificially fractured formation since in this case the vertical fractures will intersect the well. An r-θ-z grid representing a symmetrical element in this case may accurately model well performance with a reasonably low number of grid blocks.

An upward concave deviation from linearity in a drawdown test curve may result from factors other than formation fractures. Geothermal reservoirs with brines of high salinity may precipitate salt with pressure drawdown near the well. This can cause a skin factor increasing with time and the mentioned deviation from linearity. It is well-known that faults or other flow barriers near a well can cause upward curvature. Short-term drawdown tests on wells which partially penetrate thick formations, especially where the ratio of vertical to horizontal permeability is small, can result in deviation from linearity. Regardless of penetration, a formation consisting of alternating tight and permeable streaks of large permeability contrast can yield deviation from linearity through the same vertical, crossflow type of transient treated above in the horizontally fractured formation calculations. Quoting from Reference [11], which treated simulation of single-phase gas flow, ". . . The reservoir picture finally employed with success stemmed from the hypothesis that the well communicated with a number of thin permeable stringers . . . fed by severely limited crossflow from large sand volumes. . . . . In that work, for such reservoirs, the calculated and observed drawdown/buildup curves failed to yield the linearity of conventional analysis.

Finally, the fractured formation, drawdown test illustrative calculations and interpretations presented here are not unique to geothermal reservoirs, but apply to any formation subject to single-phase flow of a low compressibility fluid -- oil, water or high pressure gas.

## HEAT EXTRACTION FROM HOT DRY ROCK

We consider a vertical fracture in a hot dry rock initially at 500°F. A 5x5x5 three-dimensional grid describes a rectangular parallelepiped with $\Delta x = \Delta z = 80$ feet and $\Delta y = .01, 30, 120, 160, 320$. These dimensions resulted from combining blocks in a comparison run which used y-direction increments of .01, 10, 20, 40, 80, 160 and 320 feet. The overall dimensions are a 400x400-foot vertical crack of .02-foot width with 630 feet of rock either side of it. The 630 feet of rock in the y-direction is sufficiently large that the system acts as infinite for the 3,000 days of simulation. Different grids were used to determine the acceptably low spatial truncation error of the 5x5x5 grid.

Since the system is symmetrical about the vertical midplane of the crack, this 5x5x5 grid represents half the system. Crack width is of no consequence except in its relation to the kw product where k is fracture permeability and w is fracture total width. In the grid plane j = 1 (the crack) an x-z thermal conductivity of 3.8 Btu/ft-day-°F was used, porosity was 1.0 and permeability was varied over a number of runs from 10 Darcies to 800,000 Darcies. In the planes, j = 2-5 (hard rock) thermal conductivity was 38 Btu/ft-day-°F, rock specific heat was 35 Btu/cu.ft.rock-°F and porosity and permeability were zero.

100°F cold water injection rate was specified as 25,000 lbs/hour into the bottom left corner of the crack (cell i=1,j=1,k=5). A withdrawal well at the upper right corner of the crack (cell i=5,j=1,k=1) maintained pressure at 800 psia due to a large specified productivity index. This withdrawal well produced on deliverability against the 800 psia pressure. The 25,000 lbs/hour injection rate corresponds to actual injection well rate of 50,000 lbs/hour since the grid represents a symmetrical half of the total system.

Figure 12 shows calculated energy recovery and producing well bottomhole temperature vs. time. Energy recovery is defined as cumulative enthalpy produced divided by the sensible heat above 100°F initially contained in a portion of the rock. The portion used is the first 310 feet since the last 320 feet experienced essentially no recovery (temperature decline) at 3,000 days. The initial energy in place on these bases is $6.944 \times 10^{11}$ Btu. Enthalpy of produced water is U + pv where internal energy U is zero at 100°F.

Figure 12 shows a rapid decline of produced water temperature from 500°F to less than 300°F in the first few days followed by a very flat decline from 170°F to 137°F from 1,000 to 3,000 days. Fractional energy recovery is 0.1663 at 3,000 days, equivalent to $1.155 \times 10^{11}$ Btu or an average of 64 Btu/lb water produced (enthalpy relative to zero U at 100°F). The average temperature corresponding to this average enthalpy is about 162°F.

The fracture width w controls system conductivity or throughput. The corresponding parameter or group of importance is the kw Darcy-feet product, which is proportional to $w^3$ since fracture permeability is proportional to $w^2$. We used permeabilities up to 800,000 Darcies with the .02-foot model dimension for the fracture. This 16,000 Darcy-foot kw product corresponds to a fracture width of 4 mm using the fracture permeability equation $k = 10^8 w^2/12$ (w in cm). Fracture width, i.e. the kw product, had no effect on the calculated recovery and temperature shown in Figure 12.

Model runs were made with the injection well located higher, 200 feet from top of formation in cell i=1,j=1,k=3. The change of injection location had no effect on calculated recovery and producing temperature.

Figure 12 also shows calculated recovery and temperature for a larger fracture of dimension 800x800 feet. Again, the above described kw product and injection well location variations had no effect on the calculated recovery and producing temperature. The larger fracture resulted in a considerably higher bottomhole producing temperature vs. time and a lower fractional energy recovery. Calculated absolute energy recovery at 3,000 days was higher for the larger fracture -- $3.53 \times 10^{11}$ Btu vs. $1.155 \times 10^{11}$ Btu for the 400x400 foot fracture. Thus, a fourfold increase in fracture area caused a threefold increase in energy recovery. Average enthalpy of produced water was 196 Btu/lb corresponding to an average temperature of produced water of 292°F.

The runs were performed using automatic time step control due to the rapid initial transients. With a first time step of .1 days, a subsequent minimum $\Delta t$ of .2 days, control by 150°F maximum grid block temperature change per time step and a maximum time step of 500 days, the model took 13 time steps to 3,000 days for the 100,000 Darcy permeability. Computer time for this run was 46 CDC 6600 CPU seconds. Twenty of these seconds were required for the first two time steps.

Calculated results for permeabilities less than 100,000 Darcies exhibited no circulatory "free" convection type cells in the vertical fracture plane. Table 8 shows an example of these results at 3,000 days for the case of a 400x400 foot fracture, and 100,000 Darcies fracture permeability which corresponds to a 2 mm fracture width. The table shows calculated pressures in the fracture plane, temperatures in all planes and interblock flow rates (positive to the right and vertically downward). Water flow is uniformly to the right and upwards away from the injection in grid cell i=1,j=1,k=5. Temperature uniformly increases to the right and upward (in the directions of water flow) except in the top row.

Results for the 800,000 Darcy permeability differed markedly from those just described. Table 9 shows pressure, temperature and flow rate distributions at 75 days for the 800x800 foot fracture with 800,000 Darcies. y-direction spacing was altered in this run to .01, 10, 30, 50, 180 feet. The flow rates in Table 9 show extremely strong "free" convection cells in the 5x5 grid of the vertical fracture plane. Water is in fact flowing downward into the injecting cell i=1,j=1,k=5. The flow distribution is complex and the temperature change from left to right alternates in sign in alternate rows corresponding to alternation in direction of horizontal flow rate.

Table 10 shows pressure, temperature and flow rate distributions for this 800,000 Darcy case at 3,000 days. While the flow rates are much more uniform with flow uniformly upward, the free convection still exists with some horizontal flow from right to left. Deviations from a pattern of uniform temperature increase to the right and upward are small but exist and are complex. This 800,000 Darcy run was much more difficult than the runs for 100,000 or fewer Darcies. The number of time steps increased to 21 and computer time increased to 144 CDC 6600 CPU seconds, largely due to divergence and repeat of one of the time steps.

These fractured hot rock simulations did not employ any enhanced heat conduction to the fracture due to thermal cracking induced by temperature decrease. A functional relationship between thermal conductivity and temperature or temperature change can be included in the model. Such a relationship and associated parameters might be deduced from laboratory or field experimental data.

## SUMMARY

An implicit, three-dimensional geothermal model is described and partially evaluated in respect to stability or time step tolerance. The model is only partly implicit in certain applications where various terms associated with allocation of well rates among open layers are treated explicitly.

The implicit model stably accommodated time steps corresponding to 80-100% saturation change in a grid block and throughput ratios the order of $10^8$ in several illustrative multiphase flow problems. This compares with our experience of limits of 3-10% saturation change and throughput ratio of roughly 20,000 with semi-implicit geothermal and oil reservoir models. The implicit model stability allowed inclusion of fractures and wellbores as small-volume grid blocks in several multiphase flow test problems.

An analytical derivation is presented for a well deliverability reduction factor which can be used in simulations using large grid blocks. The factor accounts for increased pressure drop near the well due to hot water flashing and steam expansion.

The model was used to simulate two-phase depletion of a fractured matrix reservoir with horizontal and vertical fractures included as grid blocks. The results were poorly matched by conventional simulation which treats the reservoir as an unfractured formation with high effective permeability.

Simulation of a single-phase flow, pressure drawdown test in a tight formation with horizontal fractures showed upward concave curvature of the pressure drawdown vs. ln(t) plot. The degree of calculated curvature and attendant interpretation difficulty increased with decreasing matrix permeability level and decreasing horizontal fracture spacing.

The final illustrative application treated heat extraction from a fractured, hot dry rock system. For a given cold water injection rate, the calculated energy recovery and production well water temperature vs. time were not affected by fracture permeability-width product or injection well location. The fracture conductance was varied from 2 to 16,000 Darcy-ft, while injection well location was varied only from the bottom corner to the mid-depth of the fracture plane. A fourfold increase in fracture area from 400x400 to 800x800 square feet resulted in a threefold increase in calculated energy recovery at 3,000 days for the same cold water injection rate.

A limited investigation of time truncation error indicates that acceptably low levels can occur in spite of average maximum (over grid) saturation changes per time step as high as 60%.


## NOMENCLATURE

| | |
|---|---|
| $A$ | cross-sectional area normal to flow, $ft^2$ |
| $c$ | compressibility, 1/psi |
| $C_p$ | specific heat, Btu/lb-°F |
| $(\rho C_p)_R$ | rock specific heat, Btu/cu.ft rock-°F |
| $f_w$ | water phase volumetric fractional flow |
| $f_g$ | gas phase volumetric fractional flow |
| $f$ | well deliverability factor, fraction |
| $H$ | enthalpy, $U + pv$, Btu/lb |
| $k$ | absolute permeability, md |
| $k_r$ | relative permeability, fraction |
| $k_{rgcw}$ | relative permeability to gas at irreducible water saturation $S_{wc}$ |
| $K$ | thermal conductivity, Btu/ft-day-°F |
| $N_x, N_y, N_z$ | numbers of grid blocks in reservoir grid system, in x, y, z directions, respectively |
| $\bar{q}$ | desired or target production rate, lbs $H_2O$/day |
| $q$ | production rate, lbs $H_2O$/day |
| $q_H$ | enthalpy production rate, Btu/day |
| $q_{HL}$ | heat loss rate, Btu/day |
| $p_s(T)$ | water vapor pressure |
| $p$ | gas phase pressure, psia |
| $p_{wb}$ | wellbore flowing pressure, psia |
| $p_c$ | capillary pressure, $p_g - p_w$, psi |
| $R_T$ | throughput ratio, Equation (31) |
| $r$ | radius, feet |

$r_e$ exterior radius

$r_w$ wellbore radius

RB Reservoir Barrels

S skin factor

$S_w$ water phase saturation, fraction

$S_g$ gas phase saturation, fraction

$S_{ge}$ gas saturation at $r = r_e$

$S_{wc}$ irreducible water saturation

$S_{gc}$ critical gas saturation

t time, days

$\Delta t$ time step, $t_{n+1} - t_n$, days

T temperature, °F

$T_s$ water saturation temperature, $T_s(p)$, °F

U internal energy, Btu/lb

$V_p$ grid block pore volume, $V\phi$

V grid block bulk volume, $\Delta x\Delta y\Delta z$, cubic feet

v specific volume, cu.ft/lb

w fraction width

X quality, mass fraction steam

x,y,z Cartesian coordinates, feet, z measured positively vertically downward

$\Delta x, \Delta y, \Delta z$ grid block dimensions, feet

GREEK

$\bar{\delta}$ time difference operator,

$\bar{\delta}X \equiv X_{n+1} - X_n$

$\delta$ iteration difference operator,

$\delta X \equiv X^{\ell+1} - X^{\ell}$

$\phi$ porosity, fraction

$\rho$ density, lbs/cu.ft

$\gamma$ specific weight or gradient, psi/ft ($\gamma_w = \rho_w/144$)

$\lambda$ mobility, $k_r/\mu$

$T_c$ reservoir heat conduction transmissibility KA/ℓ, where ℓ = distance between grid block centers, Btu/day-°F

$T_g$ gas phase transmissibility, $(kA/\ell)(k_{rg}\rho_g/\mu_g) \times .00633$, lbs gas phase/day-psi

$T_w$ water phase transmissibility, $(kA/\ell)(k_{rw}\rho_w/\mu_w) \times .00633$, lbs water phase/day-psi

$\Delta(T\Delta P) = \Delta_x(T_x\Delta_x P) + \Delta_y(T_y\Delta_y P) + \Delta_z(T_z\Delta_z P)$, defined as indicated above Equation (5)

$\mu$ viscosity, cp

SUBSCRIPTS

e exterior

g gas (steam) phase

i,j,k grid block indices, $x_i, y_j, z_k$

k grid layer number or index

ℓ (superscript) iteration number

n time level, $t_n$

s saturation condition

x,y,z denotes x, y or z direction, respectively

w water phase

wb wellbore

REFERENCES

1. Coats, K. H., and Ramesh, A. B., "Numerical Modeling of Thermal Reservoir Behavior", Preprint presented at the 28th Annual Technical Meeting of the Petroleum Society of C.I.M., Edmonton, Alberta, May 27-June 6, 1977.

2. Carter, R. D., and Tracy, G. W., "An Improved Method for Calculating Water Influx", Trans. AIME (1960), 219, 415-417.

3. Coats, K. H., George, W. D., Chu, Chieh, and Marcum, B. E., "Three-Dimensional Simulation of Steamflooding", Trans. AIME (1974), 257, 573.

4. Toronyi, R. M., and Ali, S. M. Farouq, "Two-Phase, Two-Dimensional Simulation of a Geothermal Reservoir", Soc. Pet. Eng. J. (June, 1977), 171-183.

5. Blair, P. M., and Weinaug, C. F., "Solution of Two-Phase Flow Problems Using Implicit Difference Equations", Trans. AIME (1969), 246, 417.

6. Price, H. S., and Coats, K. H., "Direct Method in Reservoir Simulation", Trans. AIME (1974), 257, 295.

7. Steam Tables, Keenan, J. H., and Keyes, F. G., Hill, P. G., and Moore, J. G., John Wiley & Sons, 1969.

8. Coats, K. H., Nielsen, R. L., Terhune, M. H., and Weber, A. G., "Simulation of Three-Dimensional Two-Phase Flow in Oil and Gas Reservoirs", Soc. Pet. Eng. J. (December, 1967), 377-388.

9. Coats, K. H., Dempsey, J. R., and Henderson, J. H., "The Use of Vertical Equilibrium in Two-Dimensional Simulation of Three-Dimensional Reservoir Performance", Trans. AIME (1971), 251, 63-71.

10. Flow of Homogeneous Fluids, Muskat, M., J. W. Edwards, Ann Arbor, Michigan, 1946.

11. Coats, K. H., Dempsey, J. R., Ancell, K. L., and Gibbs, D. E., "Analysis and Prediction of Gas Well Performance", SPE 3474 presented at 46th Annual Meeting of SPE, New Orleans, Louisiana, October 3-6, 1971.

## APPENDIX

## CALCULATION OF DELIVERABILITY FACTOR f

We consider two-phase, steady-state steam-water flow from some exterior radius R to wellbore radius $r_w$. The point R is assumed to be saturated, and pressure is P at R and $p_{wb}$ at $r_w$.

Darcy's law gives liquid water phase flow rate at any radius as

$$q_w = q(1 - X) = -2\pi k\Delta z \lambda_w \rho_w r dp/dr \quad (35)$$

where X is flowing steam quality, q is total flow rate, lbs $H_2O$/day, $k\Delta z$ is md-ft product x .00633, $\lambda_w$ is $k_{rw}/\mu_w$ and $\rho_w$ is water density in lbs/cu.ft. Integration using the fact that q is constant gives

$$q = \frac{2\pi k\Delta z}{\ln\frac{R}{r_w}} \int_{p_{wb}}^{P} \frac{\lambda_w \rho_w}{1-X} dp \quad (36)$$

or

$$q = \frac{2\pi k\Delta z}{\ln\frac{R}{r_w}} I(P, p_{wb}, S_g) \quad (37)$$

where the integral I is a function only of the integration limits $p_{wb}$, P and of steam saturation $S_g$ at R because, as we will now show, the integrand $\lambda_w\rho_w/(1-X)$ is a single-valued calculable function of pressure p.

Flowing quality X is related to fractional flow by

$$X = 1/(1 + f_w\rho_w/(1-f_w)\rho_g) \quad (38)$$

and enthalpy per lb of flowing stream is

$$H = XH_g + (1 - X)H_w \quad (39)$$

At steady-state, flowing stream enthalpy is constant and from (39),

$$X = (H-H_w)/(H_g-H_w) = X(p), \quad (40)$$

where the dependence upon pressure alone follows from the fact that H is constant and saturated water and steam enthalpies are single-valued functions of pressure. From Equation (38),

$$f_w = 1/[1 + X\rho_w/(1 - X)\rho_g] = f_w(p) \quad (41)$$

where the dependence upon pressure alone follows from the fact that saturated water and steam densities are single-valued functions of pressure.

If p and $S_g$ at R are given, then enthalpy H can be calculated from Equations (38) and (39). Given H, we can calculate the values of X(p) and $f_w(p)$ at any pressure from Equations (40) and (41). Thus, the integral in Equation (36) can be numerically integrated for any given values of P, $p_{wb}$ and $S_g$.

We now consider a grid block of large dimensions, $\Delta x * \Delta y$, with equivalent exterior radius $r_e$ determined by $\pi r_e^2 = \Delta x \Delta y$. Assuming steady-state single-phase water flow from an undersaturated condition at $r_e$ to saturation point R, Darcy's law gives

$$q = \frac{2\pi k \Delta z}{\ln \frac{r_e}{R}} (\lambda_{we}\rho_{we} + \lambda_{ge}\rho_{ge})(p_e - P) \quad (42)$$

where P is pressure at saturation point radius R and $\lambda_{ge}$ is zero if $R < r_e$. Equation (37) describes flow from saturation point R to $r_w$ and can be written

$$q = \frac{2\pi k \Delta z}{\ln \frac{R}{r_w}} \frac{I(\lambda_{we}\rho_{we} + \lambda_{ge}\rho_{ge})}{(\lambda_{we}\rho_{we} + \lambda_{ge}\rho_{ge})(P - P_{wb})} (P - P_{wb}) \quad (43)$$

Solving for $p_e - P$ from (42) and $P - P_{wb}$ from (43) and adding the results gives

$$q = \frac{2\pi k \Delta z (\lambda_{we}\rho_{we} + \lambda_{ge}\rho_{ge})}{\ln \frac{r_e}{R} + \frac{1}{f} \ln \frac{R}{r_w}} (p_e - P_{wb}) \quad (44)$$

where

$$f = \frac{I(P, P_{wb}, S_{ge})}{(\lambda_{we}\rho_{we} + \lambda_{ge}\rho_{ge})(P - P_{wb})} \quad (45)$$

In Equations (44), (45), if the exterior radius $r_e$ is undersaturated, $\lambda_{ge} = 0$ and R must be calculated by trial and error if $p_e$ and $P_{wb}$ are given. P is, of course, equal to saturation pressure corresponding to temperature at $r_e$. If q is given, then R can be calculated directly from (42).

If the exterior radius $r_e$ is saturated, then $R = r_e$, $P = p_e$ and Equation (44) becomes

$$q = \frac{2\pi k \Delta z}{\ln \frac{r_e}{r_w}} f(\lambda_{we}\rho_{we} + \lambda_{ge}\rho_{ge})(p_e - p_w) \quad (46)$$

where f is given by (45) with $P = p_e$.

We have used an analysis similar to that given here to calculate reduced deliverability of oil wells due to release and expansion of solution gas accompanying pressure decline near the well.

## TABLE 1

## SINGLE-WELL RADIAL FLOW TEST PROBLEM

| | | |
|---|---|---|
| Formation Thickness | = | 500 ft |
| Permeability | = | 100 md |
| Porosity | = | 0.2 |
| Wellbore Radius | = | 0.25 ft |
| Exterior Radius | = | 2,000 ft |
| Initial Pressure at Formation Top | = | 450 psia |
| Initial Temperature | = | 400°F |
| Initial Saturation $S_w$ | = | 1.0 |
| Capillary Pressure | = | 0 |
| $k_{rw}$, $k_{rg}$ from Equations (26) | | |
| Res. and Overburden K | = | 38 Btu/ft-D-°F |
| Res. and Overburden Cp | = | 35 Btu/cu.ft Rock-°F |
| Rock Compressibility | = | $4 \times 10^{-6}$ 1/psi |
| Minimum Wellbore Pressure | = | 160 psia |

| | WELLBORE NOT INCLUDED IN GRID | | WELLBORE INCLUDED IN GRID | | |
|---|---|---|---|---|---|
| | GRID BLOCK RADIUS, FEET | | GRID BLOCK RADIUS, FEET | | BLOCK |
| BLOCK | CENTER | INNER BOUNDARY | CENTER | INNER BOUNDARY | PORE VOLUME RES. BBLS* |
| 1 | .4 | .25 | .25 | 0 | 3.50 |
| 2 | 1.07 | .68 | .40 | .25 | 4.45 |
| 3 | 2.91 | 1.84 | 1.07 | .68 | $3.28 \times 10$ |
| 4 | 7.91 | 5.00 | 2.91 | 1.84 | $2.42 \times 10^2$ |
| 5 | 21.46 | 13.57 | 7.91 | 5.00 | $1.78 \times 10^3$ |
| 6 | 58.25 | 36.84 | 21.46 | 13.57 | $1.31 \times 10^4$ |
| 7 | 158.10 | 100.00 | 58.25 | 36.84 | $9.67 \times 10^4$ |
| 8 | 429.16 | 271.44 | 158.10 | 100.00 | $7.13 \times 10^5$ |
| 9 | 1164.92 | 736.81 | 429.16 | 271.44 | $5.25 \times 10^6$ |
| 10 | - | - | 1164.92 | 736.81 | $3.87 \times 10^7$ |

*THESE PORE VOLUMES ARE FOR BLOCKS IN ONE 100-FOOT LAYER.

## TABLE 2

## EFFECT OF TIME STEP SIZE ON ONE-DIMENSIONAL RADIAL FLOW RESULTS

| TIME, DAYS | TIME STEP SIZE, DAYS | | | | |
|---|---|---|---|---|---|
| 4000 | 250 | 500 | 1000 | 2000 | 4000 |
| MASS FRACTION PRODUCED | .1670 | .1669 | .1669 | .1665 | .1642 |
| BOTTOMHOLE QUALITY | .0559 | .0566 | .0576 | .0583 | .0576 |
| RATE, 1000's LBS/HR | 115.3 | 113.8 | 111.9 | 111.4 | 115.4 |

| 8000 | 250 | 500 | 1000 | 2000 | 4000 | 8000 |
|---|---|---|---|---|---|---|
| MASS FRACTION PRODUCED | .3150 | .3133 | .3102 | .3049 | .2950 | .2756 |
| BOTTOMHOLE QUALITY | .0674 | .0671 | .0668 | .0667 | .0665 | .0638 |
| RATE, 1000's LBS/HR | 90.5 | 90.9 | 91.2 | 91.3 | 92 | 96.9 |

| 16000 | 250 | 500 | 1000 | 2000 | 4000 | 8000 | 16000 |
|---|---|---|---|---|---|---|---|
| MASS FRACTION PRODUCED | .4959 | .4935 | .4889 | .4803 | .4644 | .4357 | .3865 |
| BOTTOMHOLE QUALITY | .1442 | .1420 | .1380 | .1310 | .1197 | .1039 | .0835 |
| RATE, 1000's LBS/HR | 43.5 | 44 | 45 | 46.9 | 50.2 | 56.3 | 67.9 |

TABLE 3

2D RADIAL-Z RESULTS AT 10,000 DAYS

| RUN NO. | OPEN LAYERS | TUBING BOTTOM | MASS FRACTION PRODUCED | BOTTOMHOLE PRODUCING QUALITY | BTU/LB PRODUCED AT 10,000 DAYS | RATE 1000's LBS/HR | AVERAGE BTU/LB PRODUCED |
|---|---|---|---|---|---|---|---|
| 1 | 1-1 | 1 | .1167 | .0769 | 371 | 21 | 354 |
| 2 | 3-3 | 3 | .3001 | .0518 | 349 | 46.7 | 347 |
| 3 | 5-5 | 5 | .4741 | .0486 | 346 | 77.4 | 347 |
| 4 | 1-3 | 1 | .3395 | .1305 | 417 | 44.6 | 369 |
| 5 | 1-3 | 3 | .3461 | .1343 | 421 | 44.9 | 368 |
| 6 | 3-5 | 3 | .5565 | .1085 | 398 | 60 | 356 |
| 7 | 3-5 | 5 | .5622 | .1101 | 399 | 60.6 | 359 |
| 8 | 2-4 | 3 | .4579 | .1208 | 409 | 53.1 | 362 |
| 9 | 1-5 | 1 | .5574 | .1485 | 432 | 59.9 | 370 |
| 10 | 1-5 | 3 | .5656 | .1537 | 437 | 59.7 | 371 |
| 11 | 1-5 | 5 | .5709 | .1546 | 439 | 59.9 | 371 |
| 12* | 1-5 | 3 | .7459 | .7058 | 915 | 38.7 | 423 |

*k = 500 md

TABLE 4

CALCULATED PRESSURES, TEMPERATURES AND SATURATIONS AFTER FIRST 2000-DAY TIME STEP

TWO-DIMENSIONAL RADIAL-Z RESULTS; ALL LAYERS OPEN; TUBING AT LAYER 3

PRESSURE AT GRID BLOCK CENTER (psia)

| | 1 | 2 | 3 | 4 | 5 | 6 | 7 | 8 | 9 | 10 |
|---|---|---|---|---|---|---|---|---|---|---|
| 1 | 161.5 | 167.4 | 179.7 | 191.4 | 202.5 | 213.2 | 223.5 | 233.1 | 241.5 | 247.0 |
| 2 | 162.0 | 167.2 | 180.1 | 192.4 | 204.0 | 214.8 | 224.7 | 233.6 | 242.0 | 247.5 |
| 3 | 164.2 | 175.2 | 197.3 | 215.2 | 228.9 | 238.5 | 244.3 | 249.0 | 260.7 | 271.1 |
| 4 | 170.1 | 188.2 | 219.4 | 239.4 | 248.6 | 258.2 | 271.6 | 285.0 | 297.7 | 308.2 |
| 5 | 176.4 | 200.7 | 235.9 | 250.7 | 266.7 | 285.9 | 304.5 | 321.3 | 334.8 | 345.4 |

TEMPERATURE, DEGREES FAHRENHEIT

| | | | | | | | | | | |
|---|---|---|---|---|---|---|---|---|---|---|
| 1 | 361.1273 | 364.3070 | 370.9480 | 377.2541 | 381.6283 | 385.6721 | 389.5429 | 393.1817 | 396.3912 | 398.4668 |
| 2 | 361.3719 | 364.2135 | 371.1780 | 377.8018 | 382.1824 | 386.2585 | 390.0038 | 393.3936 | 396.5752 | 398.6500 |
| 3 | 362.5504 | 368.5034 | 379.6426 | 386.4313 | 391.5900 | 395.2240 | 397.4500 | 398.5491 | 399.0535 | 399.6002 |
| 4 | 365.7484 | 375.5500 | 388.0089 | 395.5828 | 399.0524 | 399.2727 | 399.3217 | 399.5255 | 399.7558 | 399.8914 |
| 5 | 369.1330 | 380.9194 | 394.2408 | 399.8457 | 399.9718 | 399.9165 | 399.8785 | 399.8967 | 399.9551 | 399.9751 |

STEAM SATURATION

| | | | | | | | | | | |
|---|---|---|---|---|---|---|---|---|---|---|
| 1 | .9989 | .7452 | .7379 | .7363 | .7354 | .7339 | .7325 | .7303 | .7272 | .7210 |
| 2 | .9761 | .5917 | .5158 | .4886 | .4734 | .4607 | .4475 | .4300 | .3833 | .2872 |
| 3 | .8993 | .4812 | .3776 | .3195 | .2613 | .1920 | .1017 | 0.0000 | 0.0000 | 0.0000 |
| 4 | .8668 | .4386 | .3208 | .2191 | .0746 | 0.0000 | 0.0000 | 0.0000 | 0.0000 | 0.0000 |
| 5 | .8510 | .4052 | .2565 | .0715 | 0.0000 | 0.0000 | 0.0000 | 0.0000 | 0.0000 | 0.0000 |

TABLE 5

NUMBER OF ITERATIONS PER TIME STEP

ALL LAYERS OPEN; TUBING IN LAYER 1

| $\Delta t$, DAYS | | | | | |
|---|---|---|---|---|---|
| 500 | | 1000* | | 2000 | |
| 25 | (.9164) | 29 | (.9891) | 41 | (.9989) |
| 7 | (.5446) | 4 | (.2000) | 22 | (.4297) |
| 8 | (.7186) | 14 | (.6517) | 6 | (.4101) |
| 8 | (.2142) | 9 | (.3229) | 5 | (.1813) |
| 10 | (.2012) | 5 | (.2239) | 5 | (.2205) |
| 6 | (.1571) | 6 | (.2273) | | |
| 5 | (.1064) | 4 | (.1826) | | |
| 5 | (.1329) | 5 | (.0948) | | |
| 9 | (.1211) | 4 | (.1334) | | |
| 3 | (.1200) | 4 | (.1176) | | |
| 4 | (.1040) | 3 | (.0973) | | |
| 5 | (.0645) | | | | |
| 6 | (.0481) | | | | |
| 4 | (.0589) | | | | |
| 4 | (.0681) | | | | |
| 3 | (.0672) | | | | |
| 3 | (.0624) | | | | |
| 2 | (.0591) | | | | |
| 2 | (.0551) | | | | |
| 2 | (.0529) | | | | |

*THE SECOND TIME STEP AUTOMATICALLY CUT TO 100 DAYS DUE TO DIVERGENCE; THE 11TH STEP WAS 900 DAYS; ALL OTHER STEPS WERE 1,000 DAYS.

TABLE 6

CALCULATED RESULTS AFTER FIRST 500-DAY TIME STEP

TWO-DIMENSIONAL RADIAL-I RESULTS; LAYERS 2-4 OPEN; TUBING AT LAYER 3

PRESSURE AT GRID BLOCK CENTER (psia)

| | 1 | 2 | 3 | 4 | 5 | 6 | 7 | 8 | 9 | 10 |
|---|---|---|---|---|---|---|---|---|---|---|
| 1 | | 248.1 | 248.1 | 248.1 | 248.2 | 248.3 | 248.5 | 248.8 | 249.2 | 249.9 |
| 2 | 172.2 | 183.5 | 206.4 | 224.6 | 238.2 | 247.0 | 250.5 | 257.9 | 267.9 | 275.7 |
| 3 | 177.6 | 196.1 | 227.3 | 245.5 | 251.8 | 266.4 | 280.9 | 294.1 | 304.8 | 312.8 |
| 4 | 184.7 | 209.5 | 242.5 | 254.4 | 276.1 | 297.4 | 316.7 | 331.2 | 341.9 | 350.0 |
| 5 | | 360.8 | 360.8 | 360.8 | 360.9 | 361.4 | 363.4 | 369.6 | 379.1 | 387.2 |

TEMPERATURE, DEGREES FAHRENHEIT

| | | | | | | | | | | |
|---|---|---|---|---|---|---|---|---|---|---|
| 1 | | 398.8822 | 398.8827 | 398.8855 | 398.8981 | 398.9423 | 399.0276 | 399.1301 | 399.3082 | 399.5559 |
| 2 | 366.8782 | 372.9753 | 383.0746 | 389.9853 | 395.1186 | 398.4603 | 399.7631 | 399.8496 | 399.8979 | 399.9522 |
| 3 | 369.8058 | 379.7011 | 390.9933 | 397.9063 | 399.9896 | 399.9776 | 399.9721 | 399.9694 | 399.9802 | 399.9904 |
| 4 | 373.6334 | 384.2601 | 396.7470 | 400.2618 | 400.2153 | 400.1472 | 400.0841 | 400.0282 | 399.9943 | 399.9954 |
| 5 | | 400.0292 | 400.0296 | 400.0304 | 400.0311 | 400.0312 | 400.0275 | 400.0141 | 399.9995 | 399.9978 |

STEAM SATURATION

| | | | | | | | | | | |
|---|---|---|---|---|---|---|---|---|---|---|
| 1 | | .5693 | .5692 | .5692 | .5686 | .5654 | .5489 | .4935 | .3755 | .2414 |
| 2 | .8640 | .4688 | .3697 | .3098 | .2471 | .1669 | .0444 | 0.0000 | 0.0000 | 0.0000 |
| 3 | .8481 | .4225 | .2978 | .1772 | 0.0000 | 0.0000 | 0.0000 | 0.0000 | 0.0000 | 0.0000 |
| 4 | .8249 | .3840 | .2147 | 0.0000 | 0.0000 | 0.0000 | 0.0000 | 0.0000 | 0.0000 | 0.0000 |
| 5 | | 0.0000 | 0.0000 | 0.0000 | 0.0000 | 0.0000 | 0.0000 | 0.0000 | 0.0000 | 0.0000 |

TABLE 7

SUMMARY OF FRACTURED MATRIX RUN CHARACTERISTICS

| RUN NO. | PRODUCTION RATE, LBS/HR | TIME STEP, DAYS | TOTAL TIME, DAYS | AVERAGE NUMBER OF ITERATIONS PER STEP | AVERAGE MAXIMUM SATURATION CHANGE/STEP | TOTAL RUN TIME, CDC 6600 CPU SECONDS |
|---|---|---|---|---|---|---|
| 1 | 40 | 30 | 1500 | 5.1 | 0.38 | 32.3 |
| 2 | 40 | 60 | 1500 | 8.5 | 0.66 | 26.5 |
| 3 | 30 | 120 | 4700 | 4.4 | 0.31 | 20.7 |

TABLE 8

HOT DRY ROCK RESULTS AT 3,000 DAYS

400 x 400 FEET, 100,000 DARCY FRACTURE

PRESSURE, PSIA

J = 1

| | 1 | 2 | 3 | 4 | 5 |
|---|---|---|---|---|---|
| 1 | 801.8 | 801.7 | 801.6 | 801.4 | 801.0 |
| 2 | 836.1 | 836.0 | 835.9 | 835.7 | 835.6 |
| 3 | 870.6 | 870.4 | 870.3 | 870.1 | 870.0 |
| 4 | 905.2 | 905.0 | 904.8 | 904.6 | 904.5 |
| 5 | 940.2 | 939.6 | 939.2 | 939.0 | 938.8 |

TEMPERATURE, °F

J = 1

| | 1 | 2 | 3 | 4 | 5 |
|---|---|---|---|---|---|
| 1 | 138.4375 | 139.1442 | 139.1278 | 137.9985 | 137.4555 |
| 2 | 120.3707 | 123.2967 | 126.2684 | 129.1460 | 134.0118 |
| 3 | 110.5972 | 114.3772 | 118.9110 | 924.1954 | 132.1117 |
| 4 | 104.7869 | 108.3930 | 113.2686 | 119.6754 | 129.3627 |
| 5 | 101.5197 | 104.4184 | 108.9581 | 115.5032 | 126.0568 |

J = 2

| | | | | | |
|---|---|---|---|---|---|
| 1 | 192.0262 | 192.6029 | 192.6152 | 191.7483 | 191.3081 |
| 2 | 176.3268 | 178.7883 | 181.4228 | 184.0100 | 187.8308 |
| 3 | 166.5993 | 169.9173 | 174.1229 | 178.9975 | 185.4905 |
| 4 | 160.7664 | 164.0263 | 168.6004 | 174.5594 | 182.6227 |
| 5 | 157.5881 | 160.3054 | 164.6232 | 170.7594 | 179.5778 |

J = 3

| | | | | | |
|---|---|---|---|---|---|
| 1 | 429.3812 | 429.4605 | 429.4268 | 429.2234 | 429.0697 |
| 2 | 425.2453 | 425.7926 | 426.4512 | 427.0833 | 427.7481 |
| 3 | 421.5898 | 422.5007 | 423.7477 | 425.1202 | 426.4752 |
| 4 | 419.1658 | 420.1519 | 421.6267 | 423.4105 | 425.2228 |
| 5 | 417.9100 | 418.8160 | 420.2795 | 422.1785 | 424.2129 |

J = 4

| | | | | | |
|---|---|---|---|---|---|
| 1 | 494.8779 | 494.8820 | 494.8786 | 494.8643 | 494.8519 |
| 2 | 494.5635 | 494.6016 | 494.6501 | 494.6957 | 494.7357 |
| 3 | 494.2421 | 494.3122 | 494.4119 | 494.5182 | 494.6096 |
| 4 | 494.0161 | 494.0965 | 494.2197 | 494.3629 | 494.4906 |
| 5 | 493.8991 | 493.9765 | 494.1023 | 494.2578 | 494.4033 |

J = 5

| | | | | | |
|---|---|---|---|---|---|
| 1 | 499.9092 | 499.9092 | 499.9092 | 499.9090 | 499.9088 |
| 2 | 499.9036 | 499.9042 | 499.9051 | 499.9059 | 499.9065 |
| 3 | 499.8974 | 499.8986 | 499.9005 | 499.9024 | 499.9039 |
| 4 | 499.8928 | 499.8943 | 499.8966 | 499.8993 | 499.9014 |
| 5 | 499.8905 | 499.8919 | 499.8944 | 499.8973 | 499.8998 |

X-DIRECTION FLOW RATE, LBS/HR

J = 1

| | 1 | 2 | 3 | 4 | 5 |
|---|---|---|---|---|---|
| 1 | 0.0000 | 2016.3670 | 4220.8752 | 7060.5410 | 12124.8102 |
| 2 | 0.0000 | 1894.5775 | 3315.5218 | 4256.6210 | 4316.0297 |
| 3 | 0.0000 | 2721.4537 | 3732.2798 | 3633.6808 | 2548.8300 |
| 4 | 0.0000 | 5329.2430 | 5442.0878 | 4342.7514 | 2582.6891 |
| 5 | 0.0000 | 13038.3583 | 8289.2342 | 5706.4035 | 3427.6178 |

Z-DIRECTION FLOW RATE, LBS/HR

J = 1

| | 1 | 2 | 3 | 4 | 5 |
|---|---|---|---|---|---|
| 1 | 0.0000 | 0.0000 | 0.0000 | 0.0000 | 0.0000 |
| 2 | -2016.3674 | -2204.5087 | -2839.6660 | -5064.2894 | -12875.1657 |
| 3 | -3910.9451 | -3625.4529 | -3780.7657 | -5123.6984 | -8559.1161 |
| 4 | -6632.3988 | -4636.2794 | -3682.1667 | -4038.8478 | -6010.3065 |
| 5 | -11961.6419 | -4749.1240 | -2582.8306 | -2278.7858 | -3427.6175 |

## TABLE 9

### HOT DRY ROCK RESULTS AT 75 DAYS
### 800 x 800 FEET, 800,000 DARCY FRACTURE

### PRESSURE, PSIA

J = 1

| | 1 | 2 | 3 | 4 | 5 |
|---|---|---|---|---|---|
| 1 | 800.3 | 800.3 | 800.3 | 800.3 | 800.2 |
| 2 | 856.7 | 856.8 | 856.8 | 856.8 | 856.9 |
| 3 | 914.9 | 914.9 | 914.8 | 914.8 | 914.8 |
| 4 | 975.2 | 975.3 | 975.3 | 975.4 | 975.4 |
| 5 | 1039.3 | 1039.2 | 1039.1 | 1039.1 | 1039.0 |

### TEMPERATURE, °F

J = 1

| | 1 | 2 | 3 | 4 | 5 |
|---|---|---|---|---|---|
| 1 | 468.3370 | 471.2289 | 474.2237 | 477.2610 | 479.9644 |
| 2 | 462.7538 | 457.2984 | 452.0257 | 446.7013 | 441.5233 |
| 3 | 399.0010 | 407.6237 | 416.3509 | 425.0627 | 433.5945 |
| 4 | 375.0946 | 361.0486 | 347.2332 | 333.3667 | 318.6657 |
| 5 | 189.6355 | 220.9219 | 247.4867 | 271.6548 | 295.6675 |

J = 2

| | | | | | |
|---|---|---|---|---|---|
| 1 | 483.8634 | 485.4144 | 486.9969 | 488.4728 | 489.6844 |
| 2 | 480.5561 | 477.4840 | 474.5136 | 471.6448 | 469.0360 |
| 3 | 444.7546 | 449.7848 | 454.8366 | 459.6667 | 464.3795 |
| 4 | 427.2917 | 419.0025 | 410.6463 | 402.3857 | 394.1028 |
| 5 | 318.5235 | 336.7667 | 352.4652 | 366.8352 | 380.9695 |

J = 3

| | | | | | |
|---|---|---|---|---|---|
| 1 | 498.8198 | 498.9383 | 499.0600 | 499.1664 | 499.2459 |
| 2 | 498.5441 | 498.2961 | 498.0542 | 497.8271 | 497.6309 |
| 3 | 495.6178 | 496.0338 | 496.4561 | 496.8485 | 497.2234 |
| 4 | 493.9525 | 493.2536 | 492.5389 | 491.8334 | 491.1513 |
| 5 | 484.7310 | 486.2680 | 487.6116 | 488.8412 | 490.0439 |

J = 4

| | | | | | |
|---|---|---|---|---|---|
| 1 | 499.9913 | 499.9922 | 499.9931 | 499.9939 | 499.9944 |
| 2 | 499.9891 | 499.9871 | 499.9852 | 499.9835 | 499.9820 |
| 3 | 499.9660 | 499.9693 | 499.9726 | 499.9757 | 499.9786 |
| 4 | 499.9520 | 499.9464 | 499.9407 | 499.9350 | 499.9296 |
| 5 | 499.8779 | 299.8902 | 499.9011 | 499.9110 | 499.9207 |

J = 5

| | | | | | |
|---|---|---|---|---|---|
| 1 | 500.0000 | 500.0000 | 500.0000 | 500.0000 | 500.0000 |
| 2 | 500.0000 | 500.0000 | 500.0000 | 500.0000 | 500.0000 |
| 3 | 499.9999 | 500.0000 | 500.0000 | 500.0000 | 500.0000 |
| 4 | 499.9999 | 499.9999 | 499.9999 | 499.9999 | 499.9999 |
| 5 | 499.9998 | 499.9998 | 499.9998 | 499.9999 | 499.9999 |

### X-DIRECTION FLOW RATE, LBS/HR

J = 1

| | 1 | 2 | 3 | 4 | 5 |
|---|---|---|---|---|---|
| 1 | 0.0000 | 20882.9777 | 23901.9082 | 24797.3057 | 24949.6943 |
| 2 | 0.0000 | -23698.1287 | -27798.6156 | -28338.0482 | -26240.1155 |
| 3 | 0.0000 | 25170.5939 | 29614.1274 | 29782.3133 | 26689.1928 |
| 4 | 0.0000 | -28661.3533 | -32354.1902 | -32369.5505 | -28477.6646 |
| 5 | 0.0000 | 31305.4018 | 31635.7540 | 31226.4479 | 28076.8419 |

### Z-DIRECTION FLOW RATE, LBS/HR

J = 1

| | 1 | 2 | 3 | 4 | 5 |
|---|---|---|---|---|---|
| 1 | 0.0000 | 0.0000 | 0.0000 | 0.0000 | 0.0000 |
| 2 | -2083.0478 | -1018.9908 | -895.4625 | -152.4403 | -47.8279 |
| 3 | 2815.0301 | 1081.4271 | -356.1100 | -2250.4732 | -26288.0461 |
| 4 | -22355.7438 | -3362.2535 | -444.4305 | 762.5207 | 401.0460 |
| 5 | 6305.5481 | 330.4875 | -409.1554 | -3149.4712 | -28076.7050 |

TABLE 10

HOT DRY ROCK RESULTS AT 3,000 DAYS

800 x 800 FEET, 800,000 DARCY FRACTURE

PRESSURE, PSIA

J = 1

| | 1 | 2 | 3 | 4 | 5 |
|---|---|---|---|---|---|
| 1 | 800.5 | 800.5 | 800.5 | 800.5 | 800.4 |
| 2 | 866.5 | 866.5 | 866.5 | 866.5 | 866.5 |
| 3 | 933.3 | 933.4 | 933.4 | 933.4 | 933.4 |
| 4 | 1000.9 | 1000.9 | 1000.9 | 1001.0 | 1001.0 |
| 5 | 1069.4 | 1069.3 | 1069.2 | 1069.1 | 1069.1 |

TEMPERATURE, °F

J = 1

| | 1 | 2 | 3 | 4 | 5 |
|---|---|---|---|---|---|
| 1 | 249.9689 | 248.0220 | 246.8849 | 245.8461 | 244.6164 |
| 2 | 216.5695 | 218.9366 | 219.5740 | 219.3443 | 218.4954 |
| 3 | 194.9029 | 190.9242 | 188.9332 | 188.3424 | 188.9908 |
| 4 | 153.6767 | 160.1790 | 163.8029 | 164.3298 | 161.8779 |
| 5 | 106.4226 | 113.7653 | 122.3591 | 132.9277 | 147.4336 |

J = 2

| | | | | | |
|---|---|---|---|---|---|
| 1 | 265.8360 | 263.9998 | 262.9122 | 261.9491 | 260.8865 |
| 2 | 233.9842 | 236.1508 | 236.7515 | 236.5108 | 235.6197 |
| 3 | 212.3962 | 208.7877 | 206.9809 | 206.5027 | 207.2386 |
| 4 | 172.9634 | 178.9138 | 182.1814 | 182.5563 | 180.1299 |
| 5 | 126.2235 | 133.4061 | 141.8190 | 152.1030 | 165.9797 |

J = 3

| | | | | | |
|---|---|---|---|---|---|
| 1 | 324.7246 | 323.3435 | 322.4850 | 321.8252 | 321.3318 |
| 2 | 299.2753 | 300.7499 | 301.1835 | 300.8914 | 299.8991 |
| 3 | 279.0948 | 276.7346 | 275.5776 | 275.4845 | 276.4692 |
| 4 | 246.9943 | 251.0076 | 253.0511 | 252.9464 | 250.6793 |
| 5 | 204.0660 | 210.4347 | 217.8984 | 226.8161 | 238.1241 |

J = 4

| | | | | | |
|---|---|---|---|---|---|
| 1 | 451.0672 | 450.7327 | 450.5302 | 450.4661 | 450.5618 |
| 2 | 443.0764 | 443.3598 | 443.3921 | 443.1553 | 442.6485 |
| 3 | 434.2412 | 433.8323 | 433.7200 | 433.9624 | 434.5498 |
| 4 | 423.0384 | 423.8462 | 424.1298 | 423.7657 | 422.7861 |
| 5 | 404.4443 | 407.1044 | 410.1953 | 413.6774 | 417.5579 |

J = 5

| | | | | | |
|---|---|---|---|---|---|
| 1 | 497.0347 | 497.0183 | 497.0098 | 497.0131 | 497.0286 |
| 2 | 496.5171 | 496.5274 | 496.5235 | 496.5012 | 496.4625 |
| 3 | 496.8260 | 495.8133 | 495.8179 | 495.8454 | 495.8922 |
| 4 | 495.0225 | 495.0594 | 495.0655 | 495.0298 | 494.9592 |
| 5 | 493.5814 | 493.7861 | 494.0234 | 494.2813 | 494.5475 |

X-DIRECTION FLOW RATE, LBS/HR

J = 1

| | 1 | 2 | 3 | 4 | 5 |
|---|---|---|---|---|---|
| 1 | 0.0000 | 3823.3153 | 8511.9081 | 13616.8777 | 19054.8352 |
| 2 | 0.0000 | 2706.8557 | 2765.7626 | 2153.8488 | 1207.0827 |
| 3 | 0.0000 | -3422.8521 | -3693.5112 | -2316.7712 | -729.3971 |
| 4 | 0.0000 | 214.0614 | -935.5022 | -3018.0366 | -4893.8505 |
| 5 | 0.0000 | 21678.6244 | 18351.3309 | 14714.0595 | 10361.3012 |

Z-DIRECTION FLOW RATE, LBS/HR

J = 1

| | 1 | 2 | 3 | 4 | 5 |
|---|---|---|---|---|---|
| 1 | 0.0000 | 0.0000 | 0.0000 | 0.0000 | 0.0000 |
| 2 | -3823.8456 | -4688.5961 | -5094.9711 | -5447.9598 | -5945.1321 |
| 3 | -6530.4316 | -4748.0656 | -4483.0575 | -4501.1982 | -4738.0462 |
| 4 | -3107.2900 | -4477.0181 | -5779.9014 | -6161.5727 | -5467.4493 |
| 5 | -3321.3739 | -3327.2930 | -3647.2701 | -4343.7575 | -10361.3018 |

FIGURE 1

DELIVERABILITY FACTOR f VS. $P_w$ FOR RELATIVE PERMEABILITY CURVES OF EQN (26)

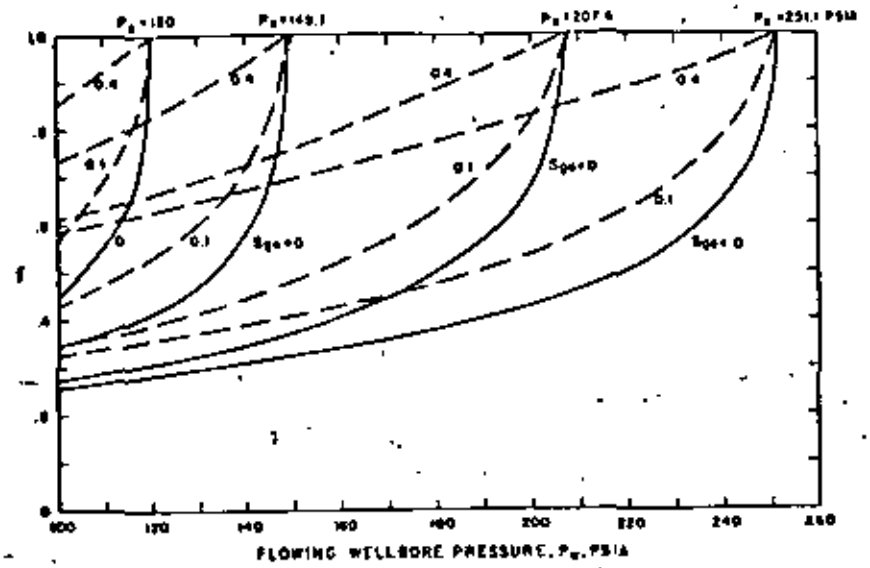


FIGURE 2

PRODUCTION RATE VS. $S_{gs}$ FOR RADIAL WATER-STEAM FLOW

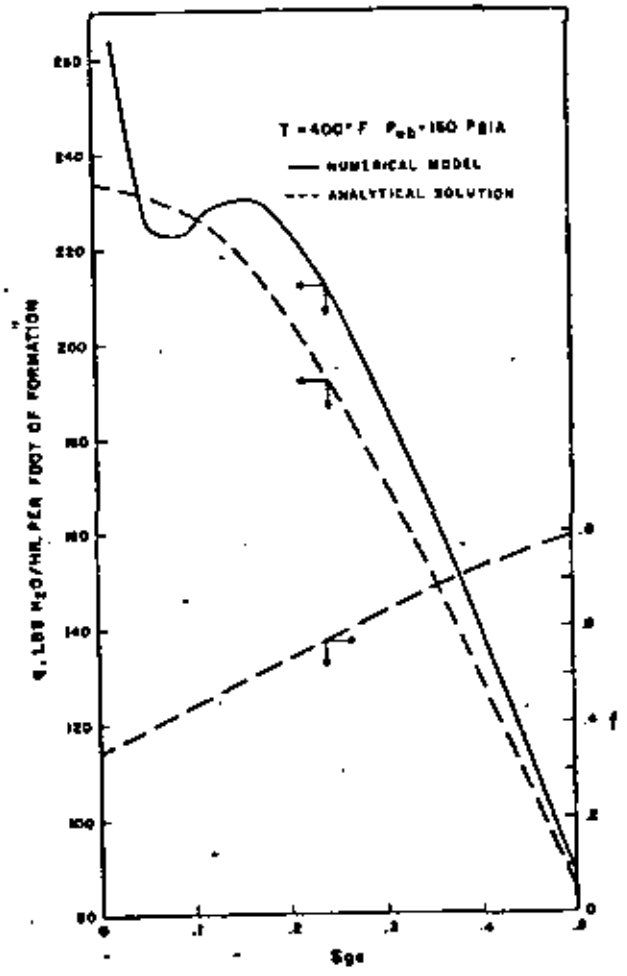

FIGURE 3

TIME TRUNCATION ERROR

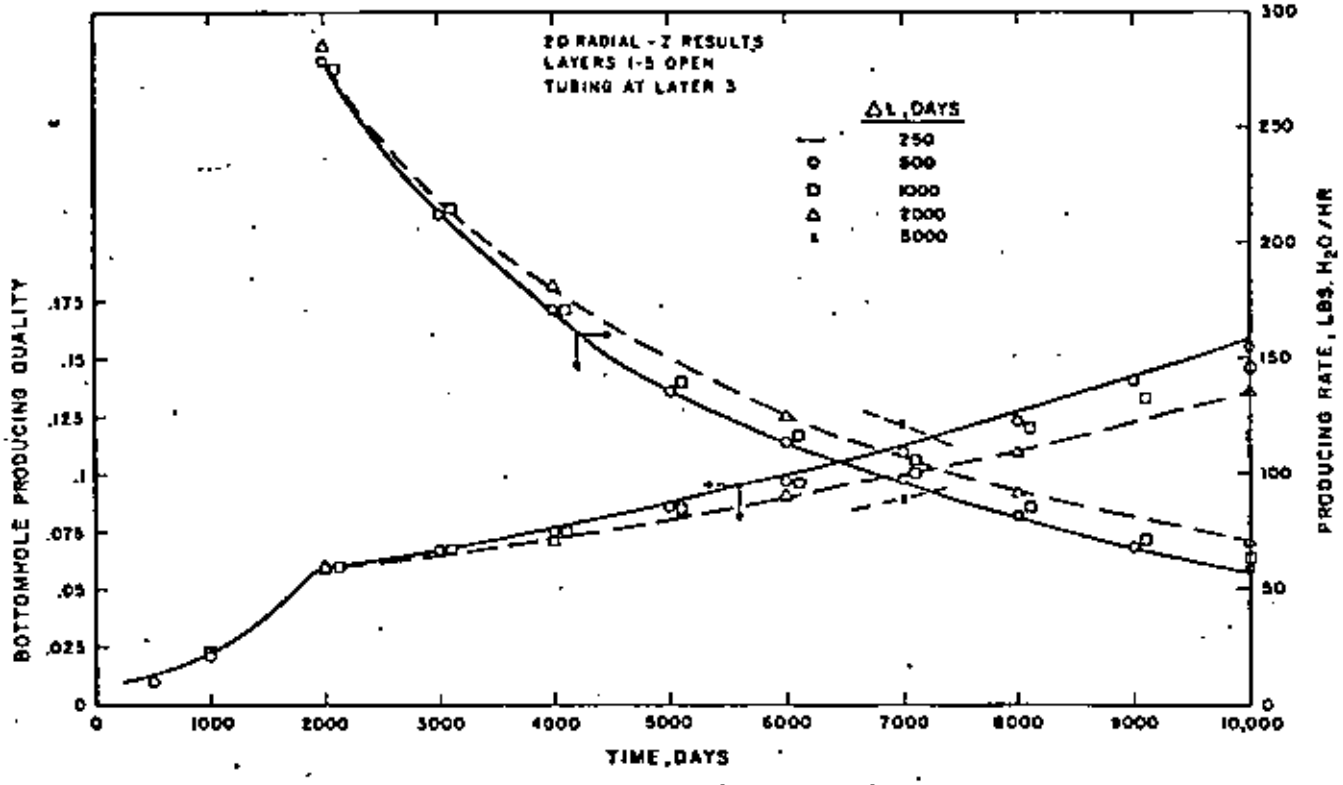


FIGURE 4

EFFECT OF PERMEABILITY ON PRODUCTION RATE AND QUALITY

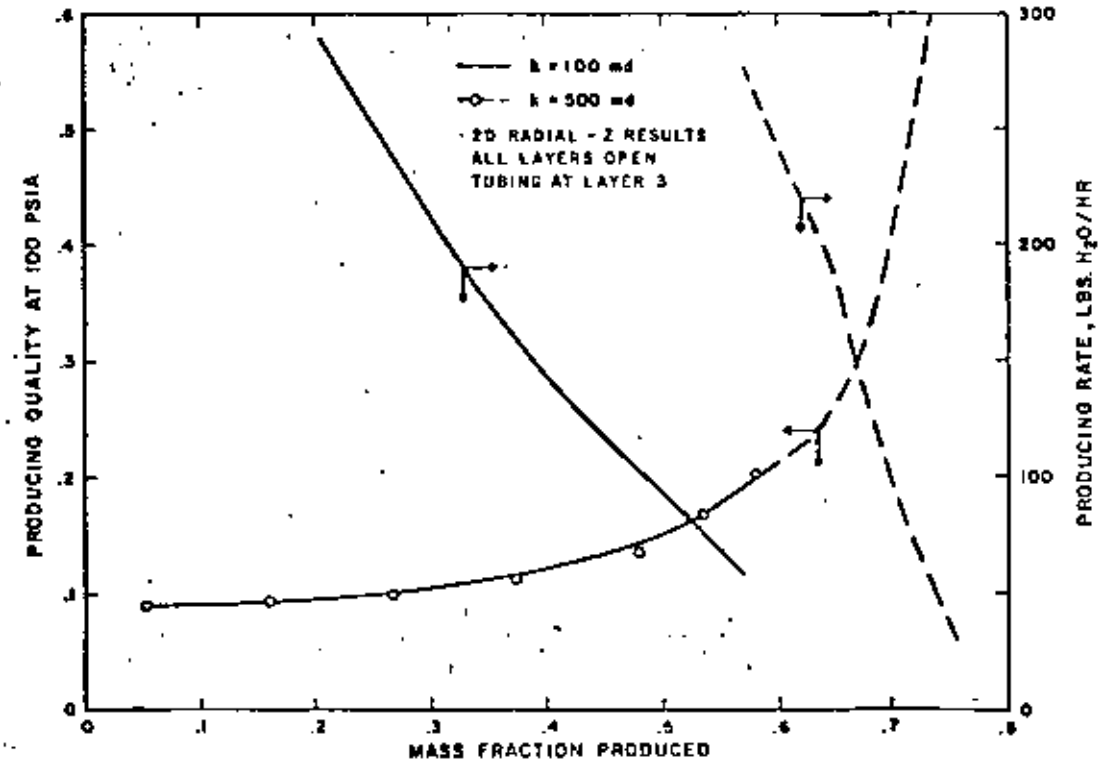

FIGURE 5

EFFECT OF PERMEABILITY AND POROSITY ON AVERAGE RESERVOIR PRESSURE DECLINE

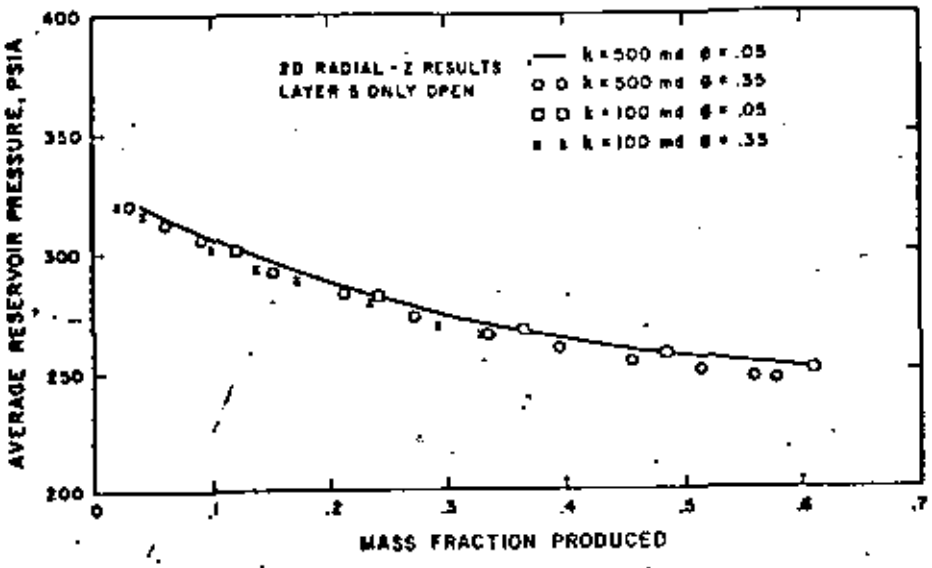


FIGURE 6

RADIAL-Z GRID FOR MATRIX-FISSURE SYSTEM

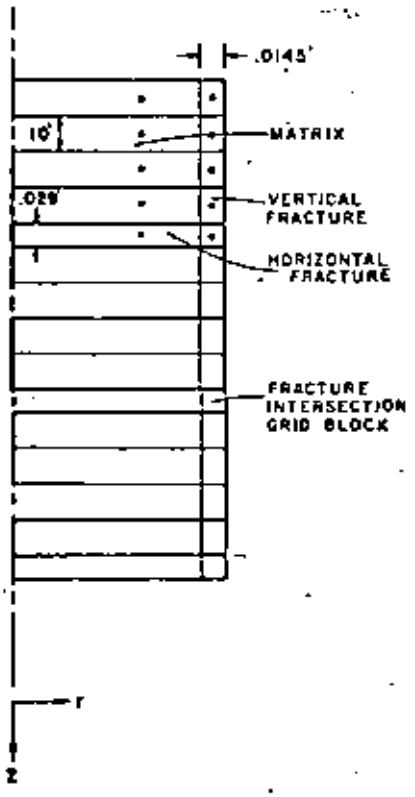

FIGURE 7

MATRIX-FISSURE SIMULATION RESULTS
AT 1500 DAYS

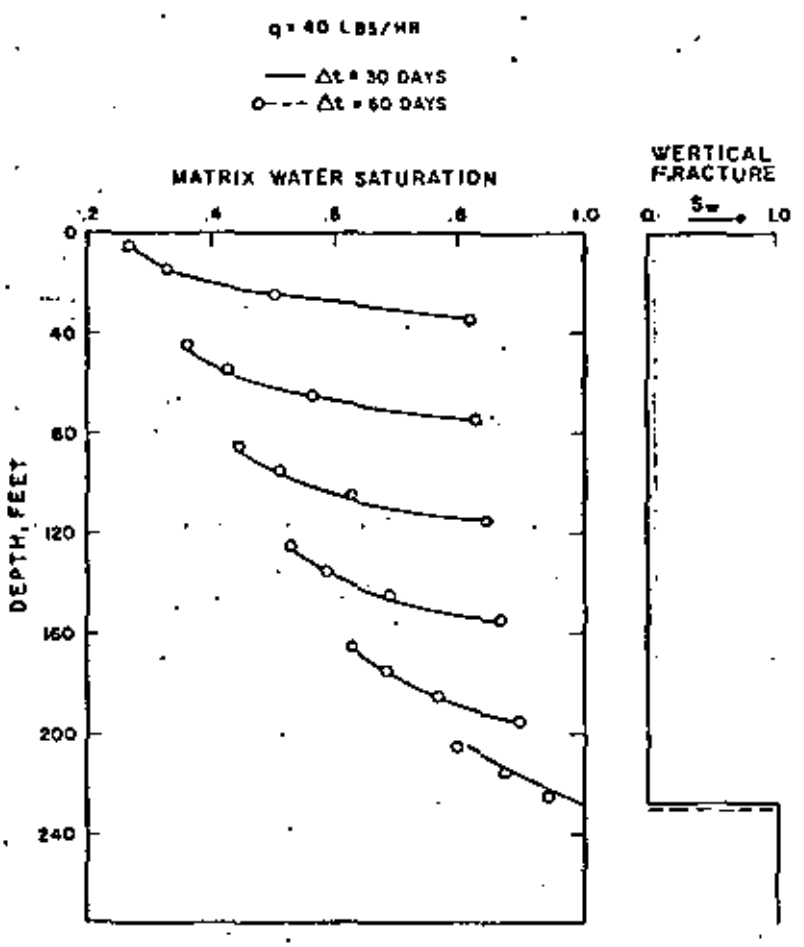


FIGURE 8

EFFECT OF PRODUCTION RATE ON
MATRIX-FISSURE SIMULATION RESULTS

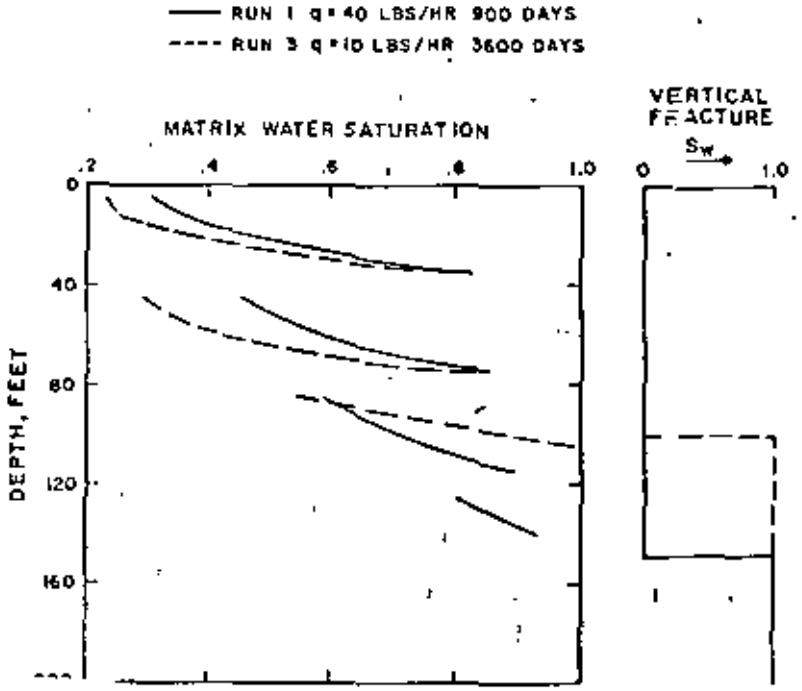

## FIGURE 9

### COMPARISON OF MATRIX-FISSURE AND CONVENTIONAL SIMULATION RESULTS

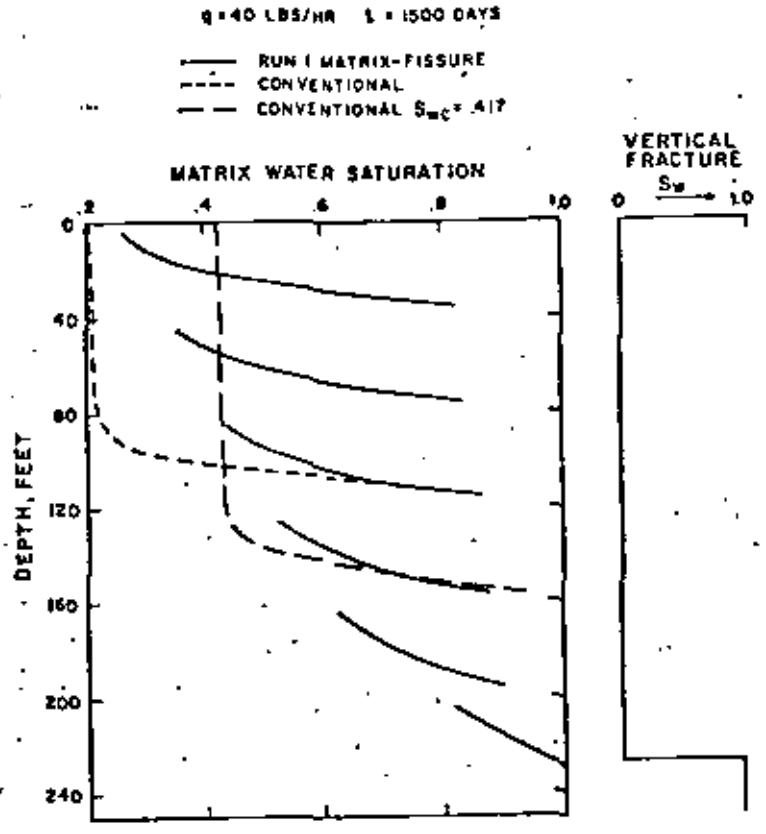


## FIGURE 10

### CALCULATED PRESSURE DRAWDOWN, Δp VS. TIME

HORIZONTAL FRACTURE SPACING = 44 FT.

RATE = 10,000 LBS/HR

| RUN | FRACTURE $k_w$, DARCY-FT. | w, MM | MATRIX PERMEABILITY, MD |
|---|---|---|---|
| 1 | 4 | .245 | .0001 |
| 2 | 4 | .245 | .001 |
| 3 | 4 | .245 | .01 |
| 4 | HOMOGENEOUS, k = 90.9 MD | | |
| 5 | 546.4 | 1.26 | .0001 |

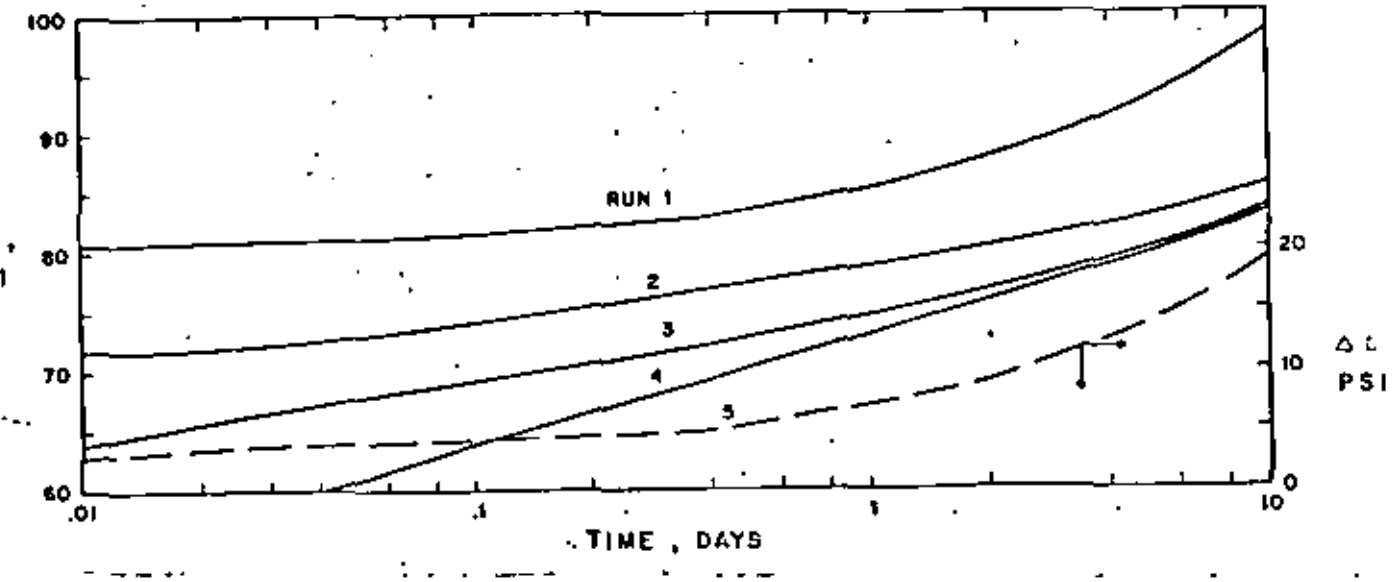

FIGURE 11

CALCULATED PRESSURE DRAWDOWN, Δp VS. TIME

HORIZONTAL FRACTURE SPACING = 440 FT.

RATE = 100,000 LBS/HR

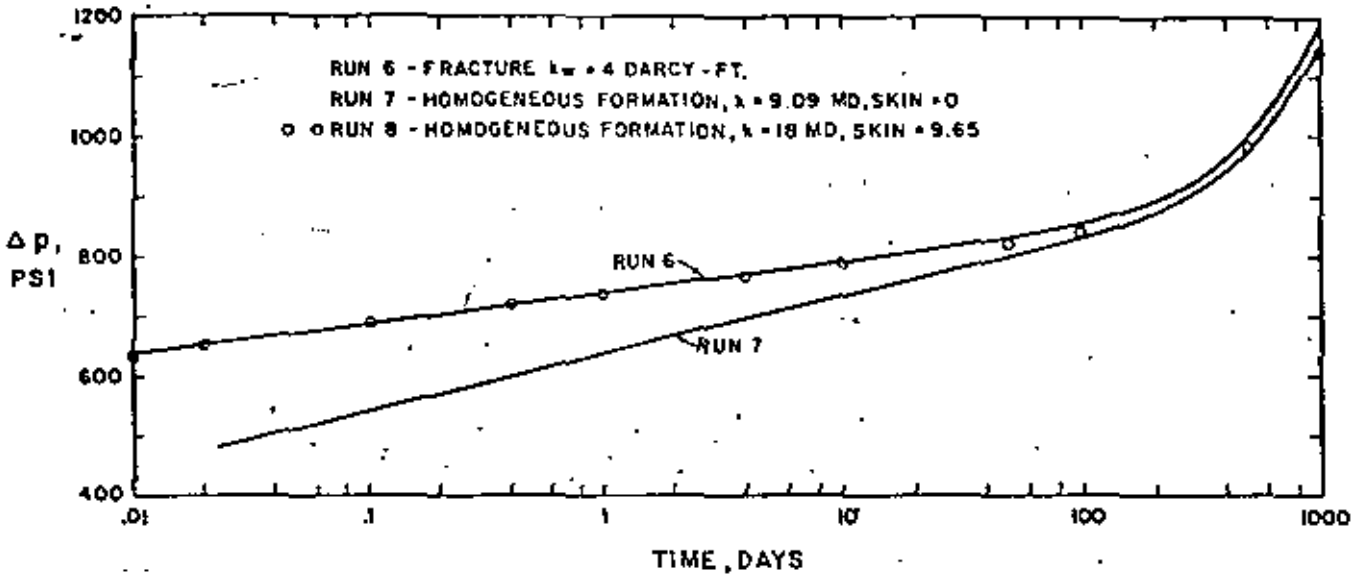


FIGURE 12

CALCULATED ENERGY RECOVERY AND PRODUCED WATER TEMPERATURE VS. TIME FOR HOT DRY ROCK SYSTEM